University of Glasgow

Modular Synthesis of Lanthanide Heterobimetallic Complexes

Samuel Horsewill

Submitted in fulfilment of the requirements for the degree of

Doctor of Philosophy

School of Chemistry

College of Science and Engineering

University of Glasgow

September 2021

Abstract

This thesis presents a modular synthesis of lanthanide heterobimetallics incorporating a redox-active bridging ligand, 1,10-phenanthroline-5,6-dione (pd). Monometallic complexes $Ln(hfac)_3$(*N,N'*-pd) **1-Ln** are synthesised and fully characterised, and it is established that $Ln(hfac)_3$ coordinates selectively to the *N,N'* coordination site of the ligand. The reaction of **1-Ln** with $V(Cp)_2$ results in the two-electron reduction of pd and synthesis of the *d-f* heterobimetallics $Ln(hfac)_3$(*N,N'-O,O'*-pd)$V(Cp)_2$ **2-Ln**.

The pd ligand is reduced using $CoCp_2$ to provide $[CoCp_2]^+[pd]^{-\bullet}$ **3**, the first fully characterised example of the pd radical anion. Reaction of **3** with $Ln(hfac)_3(THF)_2$ **4-Ln** produces the monometallic lanthanide radical compounds $[CoCp_2]^+[Ln(hfac)_3$(*N,N'*-pd)$]^{-\bullet}$ **5-Ln**, in which $Ln(hfac)_3$ again selectively coordinates to the *N,N'* coordination site of the ligand. The photoluminescent properties of the modular system comprising **1-Ln**, **4-Ln** and **5-Ln** are investigated. In this way, the contributions of the different components of the system, including the organic radical, to quenching of lanthanide photoluminescence are identified. Importantly, by using TCSPC to investigate the emission from the ligands, some energy transfer processes from the emissive excited states of the hfac and pd ligands are also observed.

A range of lanthanide reagents are reacted with **3** and **5-Ln** to develop a synthesis of lanthanide heterobimetallics. Organolanthanide transmetallation reagents $Ln(Cp^t)_2(OTf)_2K$ **6-Ln** and lanthanide scorpionates $Ln(Tp)_2(OTf)$ **7-Ln** are synthesised and fully characterised for this purpose. Of **6-Ln**, **7-Ln** and $Ln(Tp^*)_2(OTf)$, **7-Ln** exhibits the best reactivity with **3**, selectively coordinating to the *O,O'* coordination site of the ligand to produce $Ln(Tp)_2$(*O,O'*-pd) **8-Ln**. Reaction of **8-Ln** generated *in situ* with **4-Ln** in toluene solution is shown to successfully produce lanthanide heterobimetallic complexes $Ln(hfac)_3$(*N,N'-O,O'*-pd)Ln'$(Tp)_2$ **9-LnLn'**. Ligand redistribution reactions producing side-products such as $Ln(Tp)_2(hfac)$ are limited by performing the reaction cold and quenching it as quickly as possible. The solid state molecular structures of **9-YY'** and **9-EuYb** are determined and the bond lengths in **9-EuYb** are indicative that lanthanide scrambling has not occurred. Photoluminescence spectroscopy of **9-LnLn'** is also consistent with the selective coordination of the lanthanides to the two different binding sites of the ligand.

Declaration

The work described in this thesis was carried out at the University of Glasgow between 2017 and 2021 under the supervision of Dr Joy H. Farnaby. All the work submitted is my own, unless stated to the contrary and has not been previously submitted for any degree at this or any other university.

Samuel James Horsewill

September 2021

Acknowledgements

I would like to thank my supervisor Dr Joy Farnaby for her consistent insight and dedicated supervision. Throughout my PhD studies she has been unwavering in her dedication to make me the best researcher that I can be, and fully supportive of me completing my thesis in an unprecedented environment.

At work, the laboratory was made an exciting and enjoyable place to work by the other wonderful members of the Farnaby group. Without the conversations and support of the other PhD students (James, Bradley, Tajrian) and undergraduate research students with whom I shared the space I can believe that my research would never have reached the place it did.

I am also incredibly grateful for the work of our fantastic collaborators, who have brought my complexes to life and given them meaning outside of the glovebox. Thank you to Jake and Stephen for the EPR spectroscopy and simulation, and patient explanations of how EPR works. Thank you to Claire for running countless crystals (and even more lumps of powder) on the X-ray diffractometer. Thank you to Nicki and Gordon for letting me shine lasers at my complexes.

Finally, I have been supported by an amazing family throughout the process. I would especially like to thank my parents for being incredibly supportive and generous, despite my decision to move to Scotland nine years ago, and the long periods when we couldn't see each other. My thanks last of all to Ffion, for her constant support, and not least for putting up with me.

Table of Contents

Definitions and abbreviations

acac – acetyl acetonate

Ar – aryl

ATR-IR – attenuated total reflectance infrared

BHT – butylated hydroxytoluene

bipy – bipyridine

Bu – butyl

cat – catecholate

crypt – cryptand, cryptate

Cp – cyclopentadienyl

Cp^{t} – 1,2,3,4-tetramethyl cyclopentadienyl

Cp^{tt} – 1,3-bis-*tert*-butyl cyclopentadienyl

Cp^{ttt} – 1,2,4-tris-*tert*-butyl cyclopentadienyl

Cp* – pentamethyl cyclopentadienyl

Cp'' - 1,3-bis-trimethylsilyl cyclopentadienyl

CT – charge transfer

cyc – cyclic polyimine (eg. porphyrin, pthalocyanine)

d – doublet

DCM – dichloromethane

dike – diketonate

dmpz – dimethyl pyrazolyl

DMSO – dimethyl sulfoxide

DOTA – 1,4,7,10-tetraazacyclododecane-1,4,7,10-tetraacetic acid

DO3A – 1,4,7,10-tetraazacyclododecane-1,4,7-triacetic acid

DTBSQ – 3,5-di-*tert*-butyl semiquinone

DTPA – 1,1,4,7,7-diethylenetriamine pentaacetic acid

EA – elemental analysis

EPR – electron paramagnetic resonance

Et – ethyl

EXAFS – extended X-ray absorption fine structure

Fc – ferrocene

FRET – Förster resonant energy transfer

fwhh – full width at half height

glyme – polyether

hfac – hexafluoroacetyl acetonate

HOMO – highest occupied molecular orbital

ILCT – intra-ligand charge transfer

LMCT – ligand to metal charge transfer

Ln – lanthanoid (Sc, Y, La-Lu)

LUMO – lowest unoccupied molecular orbital

m – multiplet

Me – methyl

MeCN – acetonitrile

MLCT – metal to ligand charge transfer

N”– hexamethyldisilazyl

NIR – near infrared

NMR – nuclear magnetic resonance

OTf – triflate, trifluoromethyl sulfonate

Pc – pthalocyanine

PCS – pseudo-contact shift

pd – 1,10-phenanthroline-5,6-dione

PDA – prodanediamine

Ph – phenyl

phen – phenanthroline

PL – photoluminescence

Por – porphyrin

Pr – propyl

py – pyridine, pyridyl

q – quartet

s – singlet

SOMO – singly occupied molecular orbital

SSCE – sodium-saturated calomel electrode

t – triplet

^{t}Bu – *tert*-butyl

TCSPC – time-correlated single photon counting

TD-DFT – time-dependent density functional theory

THF – tetrahydrofuran

TFA – trifluoro acetic acid

TMEDA – tetramethyl ethylene diamine

Tol – toluene

Tp – *tris*-pyrazolyl borate

Tp* – *tris*-dimethylpyrazolyl borate

tren – tris-2-aminoethyl amine

triflic acid – trifluoromethane sulfonic acid

Trp – tryptophan

tta – thenoyl trifluoroacetone

UV – ultraviolet

vis – visible

XRD – X-ray diffraction

1 Introduction

1.1 Abstract

This chapter reviews the lanthanide heteromultimetallic complexes reported in the literature and conceives a new approach to the synthesis of lanthanide heterobimetallics, which will be the ultimate goal of the work described in this thesis.

The approaches to controlling the synthesis of lanthanide heterometallic complexes may be split into two categories. In syntheses using thermodynamic control, speciation is determined by the relative binding energy of different lanthanides to different binding sites of a ligand. Differences in ionic radius and Lewis acidity of the lanthanides result in preferential coordination to selective binding sites at equilibrium. In syntheses using kinetic control, speciation is controlled by the coordination of lanthanide ions to very strongly binding sites, forming a kinetically inert complex. The complex is then modified to incorporate further metal sites or metal-containing fragments, thus negating any reliance on differences in ionic radius or lewis acidity.

Thermodynamic control has been used to synthesise heterobimetallics based on ligands with size-selective binding sites, both using a single ligand[1-3] and using a trio of functionalised diketonates with multiple, size-selective binding sites for heterobimetallic and -trimetallic complexes.[4-6] Triple-stranded helicates with multiple binding sites preferred differently sized lanthanide ions, though the products underwent some scrambling.[7-10] Heteromultimetallics synthesised by kinetic control typically use strongly-binding ligands as building blocks to form architectures. These strongly-bound units can be linked covalently to synthesise a single ligand with multiple irreversibly bound lanthanides coordinated, as pioneered using DOTA-type complexes (DOTA = 1,4,7,10-tetraazacyclododecane-1,4,7,10-tetraacetic acid).[11, 12] Other binding groups have also been used in this way, such as cryptates[13, 14] or porphyrins and pthalocyanines.[15, 16] Selective demetallation has also been used to synthesise heterobimetallics,[17] as well as coordination of lanthanides to reactive pendant groups.[18-21]

The lanthanide heterobimetallics described exhibit a range of useful and unusual properties. Lanthanide to lanthanide energy transfer is reported, both downconversion[6, 11] and upconversion.[19, 20] Molecules with multiple spin centers have been proposed as potential quantum logic processors,[4, 5] or as single molecule magnets in spintronics.[16] Strategies for linking lanthanide fragments have been presented which themselves introduce functionality

into the complex[22] or which use very well-known facile[23] or versatile[14] reactions in a new way. The methods and complexes synthesised are varied, and the benefits and limitations of the syntheses are discussed.

The 1,10-phenanthroline-5,6-dione (pd) ligand is then presented, and its use as a bridging ligand in transition metal and lanthanide complexes is discussed. A strategy using the bridging nature of the pd ligand and its different and selective binding sites to synthesise radical-bridged lanthanide heterobimetallics is described. It is suggested that lanthanide reagents could be found which are selective to the *N,N'* phenanthroline and *O,O'* semiquinone binding sites. In addition to imbuing selectivity (thermodynamic control), the reagents would be required to be individually kinetically stable under the conditions of the reaction to prevent scrambling (kinetic control). Thus, such a strategy combines kinetic and thermodynamic control to provide a synthetic route to unique radical-bridged lanthanide heterobimetallics.

1.2 Lanthanides: Electronic structure, bonding and applications

The key distinguishing feature of the lanthanides are their f-orbitals, whose unique nature directly result in the various properties of the lanthanides. As such, it is vital to understand these orbitals to understand the chemistry and physics of the lanthanides. The lanthanides are the lightest elements which occupy the 4f orbitals. However, these orbitals do not extend beyond the 5p and 5s orbitals. They are partially-filled core orbitals, and their minimal interactions between the f-orbitals and ligands results in predominant ionic bonding. As electrons are added to the core-like f-orbitals across the series, the lanthanides exhibit a significant and uniform decrease in the ionic radii of the 3+ oxidation state (trivalent ions) across the series. This is known as the lanthanide contraction. This decrease has non-trivial effects on the chemistry, as the larger ions such as Ce(III) (ionic radius 1.143 Å)[24] have higher coordination numbers than the smaller ions such as Yb(III) (ionic radius 0.985 Å).[24] This can result in varying reactivity or may necessitate the use of different supporting ligand sets for different lanthanides.

The general electronic structure of the lanthanides is written as $[Xe]6s^2 5d^1 4f^n$, where n = 1 for Ln = Ce and n = 14 for Ln = Lu. The 4f orbitals are largely inaccessible to oxidation due to their core-like nature, so upon oxidation electrons are first removed from the higher-energy 6s and 5d orbitals. Thus, in the majority of cases, the lanthanides are most stable in the 3+ (trivalent) oxidation state, and the electronic structure of Ln(III) is written as $[Xe]4f^n$. As a result of the negligible interactions with ligands, the lanthanides experience very low crystal-field splitting of their energy levels, affording a tendency towards high-spin electronic structures. This is key to their application in high-strength magnets and single-molecule magnets.[25-29] Importantly, as the f-orbitals are core-like, their electronic states have relatively few vibrational states. There are therefore significant energy gaps between the lowest-lying electronic excited states and the ground state, and this results in the emission of photons in the visible-NIR region (photoluminescence).[30]

The lanthanides are a series of elements with relatively similar radii, and typically have an oxidation state of 3+. They therefore generally exhibit similar reactivity and coordination properties to each other. Trivalent lanthanide ions are hard lewis acids, with the smaller ions being slightly harder than the larger ions. The general picture of lanthanide bonding reflects

that. They are highly oxophilic, and tend to prefer coordination by small, charged, anionic ligands. Their ligands are commonly arranged to fill the coordination space around them (typical coordination numbers range from 8 to 10), with solvent molecules or neutral ligands coordinating to fill any empty space. Therefore, complexes containing softer Lewis base ligands are significantly more sensitive and challenging to work with as they can easily be displaced from the coordination sphere.

However, there are exceptions to the general rules. Other oxidation states than Ln(III) are accessible. When either oxidation or reduction would result in an empty ($4f^0$), half-filled ($4f^7$) or full ($4f^{14}$) set of 4f orbitals, this can stabilise the 2+ or 4+ oxidation states significantly. The lanthanide ions Ce(IV) ($4f^0$), Eu(II) ($4f^7$), Tb(IV) ($4f^7$) and Yb(II) ($4f^{14}$) are all stabilised by this mechanism. However, these are not the only lanthanides that have been shown to exhibit the 2+ or 4+ oxidation states. Lanthanide dihalides have been reported for several other lanthanides (Ln = Sm, Tm, Dy, Ho), due to a relatively high third oxidation potential in the lattice.[30, 31] Of these, Sm(II) is the most stabilised and molecular species containing Sm(II) are therefore (relatively) common. However, depending on the ligand environment the 2+ oxidation state may be stabilised for other lanthanides. For example, the group of Evans were the first to successfully synthesise a homologous series of Ln(II) complexes of every lanthanide La-Yb.[32-34] They discovered that the *tris*-η^5-cyclopentadienyl ligand environment has a stabilising effect on the $5d_z^2$ orbital. Reduction of Ln(III) complexes in a *tris*-cyclopentadienyl environment therefore resulted in the population of the $5d_z^2$ orbital alongside the 4f orbitals. The general electronic structure for these Ln(II) compounds is therefore described by a $[Xe]5d^14f^n$ configuration. In this case, the specific ligand environment has a significant influence on the electronic properties of the lanthanide, in contravention of the typical picture of lanthanide bonding.

1.3 Synthetic strategies for making lanthanide heteromultimetallics

Multimetallic lanthanide complexes have shown a range of behaviours arising from the inclusion of multiple different lanthanides in the complex. For example, exchange coupling of two lanthanide ions through radical ligands has been shown to increase the onset temperature of single molecule magnetism.[25-27, 35] Combination of light emission from different lanthanides, or light emission with MRI (magnetic resonance imaging) contrast agent properties, can have applications in imaging as powerful "multiplex" (multiple channel) imaging agents.[36, 37] Unique behaviours have also been observed, such as in the case of molecular thermometers,[21, 38] or energy transfer between lanthanides in both down- and up-conversion.[11, 19, 20] There are a range of examples of statistically synthesised multimetallic lanthanide materials which use these properties, from nanoparticles[39-41] to doped glasses.[42] These have found many applications, mainly in optics. However, this introduction will be limited to discussion of molecular compounds which have been selectively synthesised to incorporate multiple different lanthanides (heteromultimetallics), as that is the focus of this thesis.

However, as discussed in Section 1.2, the lanthanides are chemically similar and tend to form ionic bonds. Preventing the formation of statistical mixtures of lanthanide heteromultimetallics is therefore a synthetic challenge as many ligands are labile and undergo redistribution reactions. Control must be exerted over the speciation to prevent rearrangement to a statistical occupation of sites (scrambling). This may take the form of either kinetic or thermodynamic control of the synthesis, each of which has its own advantages and limitations. Thermodynamic control utilises ligands with multiple binding sites, each of different size, to selectively coordinate lanthanides based on their ionic radius, using the lanthanide contraction to control the equilibrium speciation. Synthesis by kinetic control uses ligands with strong binding sites to synthesise kinetically inert complexes, from which a multimetallic architecture can be constructed. The lanthanides are prevented from rearrangement by extremely strong binding by multidentate and often macrocyclic ligands.

1.3.1 Thermodynamic control

Speciation of a lanthanide heteromultimetallic compound may be controlled by the use of a ligand or ligands with multiple binding sites of different sizes. Reaction of this type of ligand with an appropriate molar ratio of different lanthanide ions leads to preferential occupation of larger binding sites by larger lanthanides, and vice versa. If the selectivity is sufficiently high, the targeted lanthanide heteromultimetallic is the only species formed. The speciation is therefore controlled by an equilibrium, and the relative binding energies of the lanthanides in the different binding sites of the ligands. As the heteromultimetallic species is therefore the thermodynamic minimum, this is called thermodynamic control of the synthesis.

Synthesis of lanthanide heteromultimetallics by thermodynamic control has been demonstrated using a range of very different ligand systems. The first example of thermodynamic control, and indeed the first structurally authenticated example of a lanthanide heterobimetallic complex, used a three-armed ligand ($tren_{PhO2}$ in Scheme 1.1) with two binding sites, an N_4O_3 site composed of a tertiary amine, three imines and three μ-aryloxide donors, and an O_6 site composed of the same three μ-aryloxide and three methoxy donor atoms.[1] Sequential addition of first one, then a second and larger lanthanide to the ligand resulted in the synthesis of heterobimetallic complexes $[(tren_{PhO2})LnLn'(NO_3)]^{2+}[NO_3]_2$ (Ln = Gd, Yb; Ln' = La, Gd) as shown in Scheme 1.1. The selectivity of the heterobimetallic was confirmed by solid-state molecular structure determination of $[(tren_{PhO2})YbLa(NO_3)_2]_2^{+}[La(NO_3)_5(H_2O)]^{2-}$ and by a thorough mass spectrometric analysis of various other pairings of lanthanide ions.

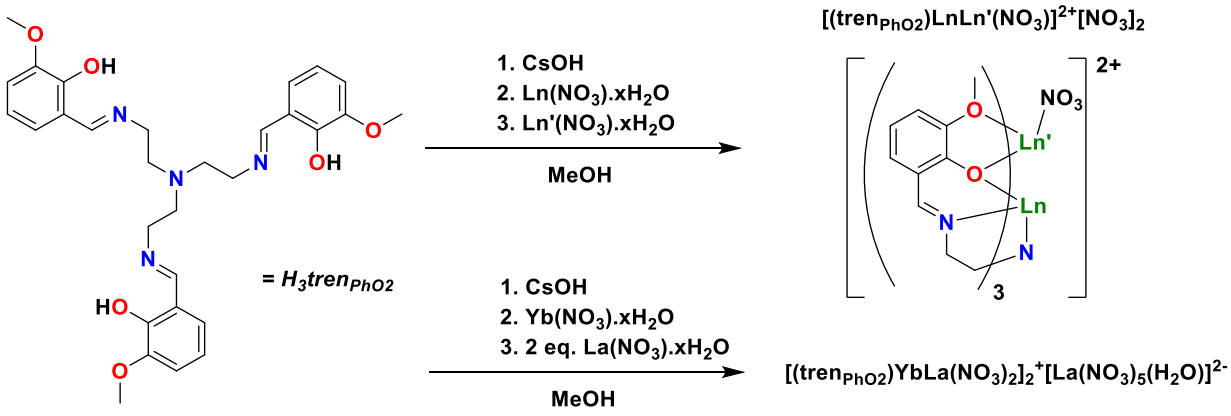

Scheme 1.1: The synthesis of the first structurally authenticated lanthanide heterobimetallic compound $[(tren_{PhO2})YbLa(NO_3)_2]_2^{+}[La(NO_3)_5(H_2O)]^{2-}$ and other bimetallics (Ln = Gd, Yb; Ln' = La, Gd).[1] The synthesis was later extended to a wider range of lanthanide pairings.[2, 3]

Following the initial synthesis of the heterobimetallics, the synthesis was extended to a greater range of lanthanide pairings.[2, 3] It was found that in order to eliminate scrambling of the lanthanide ions and formation of a statistical mixture of products, the order of addition of lanthanide ions to the ligand was important. When a medium to large lanthanide (Ln = La, Dy for example) was already bound in the ligand in the N_4O_3 binding site, addition of a smaller lanthanide (Ln = Gd, Eu, Yb for example) would result in a mixture of the targeted heterobimetallic and the homobimetallic of the smaller lanthanide.[2] This indicates that smaller lanthanide ions preferentially displace larger lanthanides from the N_4O_3 coordination site, demonstrating the difference in the two sites. Analysis of the magnetic properties of the various $(tren_{PhO2})LnLn'(NO_3)_3$ showed that while antiferromagnetic interactions between the lanthanides were typical, in selected pairs (LnLn' = YbGd, GdNd, GdCe) a weak ferromagnetic interaction was observed. The coupling was determined by comparison to heterobimetallics containing the paramagnetic lanthanides individually, and therefore no coupling energies were reported. A thorough study of the mechanism of addition of the two lanthanides to the ligand was carried out, isolating and crystallising a range of intermediates.[3] The synthesis was refined to avoid the use of mineral bases by complexation of the lanthanide to the ligand before deprotonation by NEt_3 as shown in Scheme 1.2.

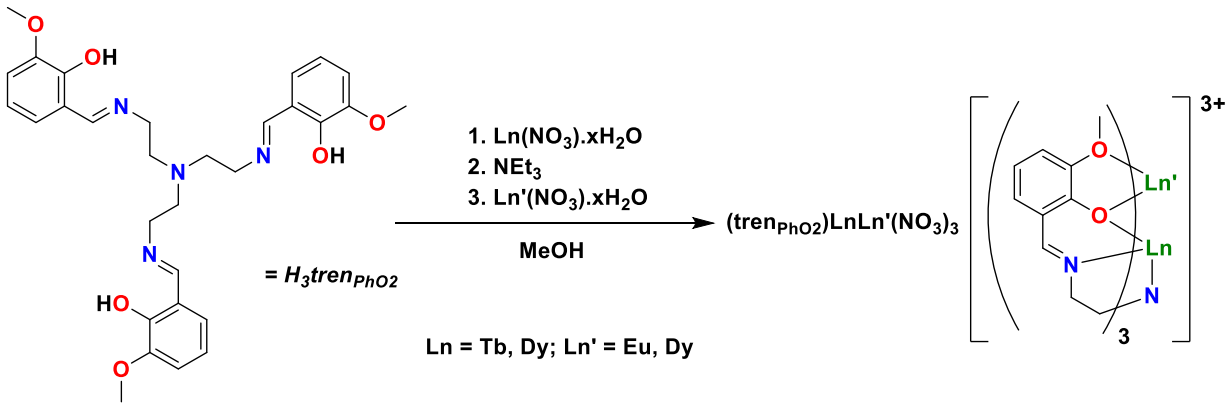

Scheme 1.2: The stepwise synthesis of lanthanide heteromultimetallics $(tren_{PhO2})LnLn'(NO_3)_3$ (Ln = Tb, Dy; Ln' = Eu, Dy) following optimisation.[3]

Another example of thermodynamic control is a series of triple-stranded helicate complexes constructed using chiral multidentate one-dimensional ligands.[7-10] This was a refinement of a system which had previously been applied to the synthesis of homomultimetallic[43, 44] and mixtures of heteromultimetallic compounds.[44, 45] However, by use of ligands which promoted the formation of differently sized binding sites, it was possible to favour certain compositions over others when combining large and small lanthanides. Using a ligand with two binding sites such as that shown in Figure 1.1, selectivity roughly proportional to the difference in ionic radii of the two lanthanides was achieved, up to 90% for the La(III)-Lu(III) pair.[7, 8] It was found that modification of the R group on the pyridyl part of the *N,N',O* binding site had an effect on the ratio of ligand conformations in the products, reducing (R = NEt_2) or enhancing (R = Cl) the selectivity compared to the unsubstituted ligand (R = H).[9]

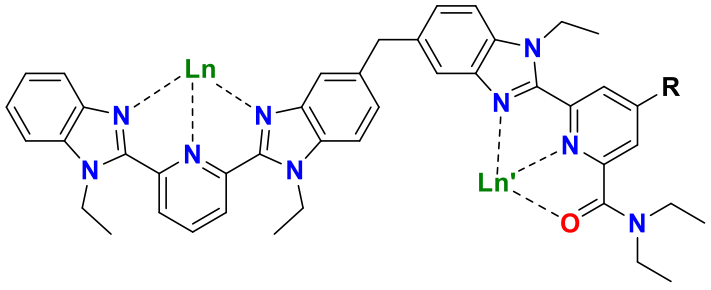

Figure 1.1: A chiral, one-dimensional ligand used to recognise differently sized lanthanides in *bis*-lanthanide triple-stranded helicate complexes. Ln, Ln' are shown in the two binding sites for illustrative purposes. R = H, NEt_2, Cl.[7-9]

The strategy of using helicates to synthesise heterobimetallics has also been extended up to tetrametallic complexes. Using a longer one-dimensional ligand with four binding sites as shown in Scheme 1.3 allowed the assembly of tetrametallic species of Lu and La, the possible

combinations of which are also shown in Scheme 1.3.[10] The authors made an in-depth investigation of the speciation at various relative lanthanide concentrations by titration of the ligand with La(III) and Lu(III) and monitoring by ^{1}H NMR spectroscopy. They found the highest selectivity was achieved for a La_3Lu tetrametallic species, of around 45%. Given the 10 possible species were all present in the solution during the titration, this level of selectivity is remarkable. The persistent issues of mixed species, solvation and electrostatic interactions were identified by the authors as the main causes of scrambling in multimetallic helicates.

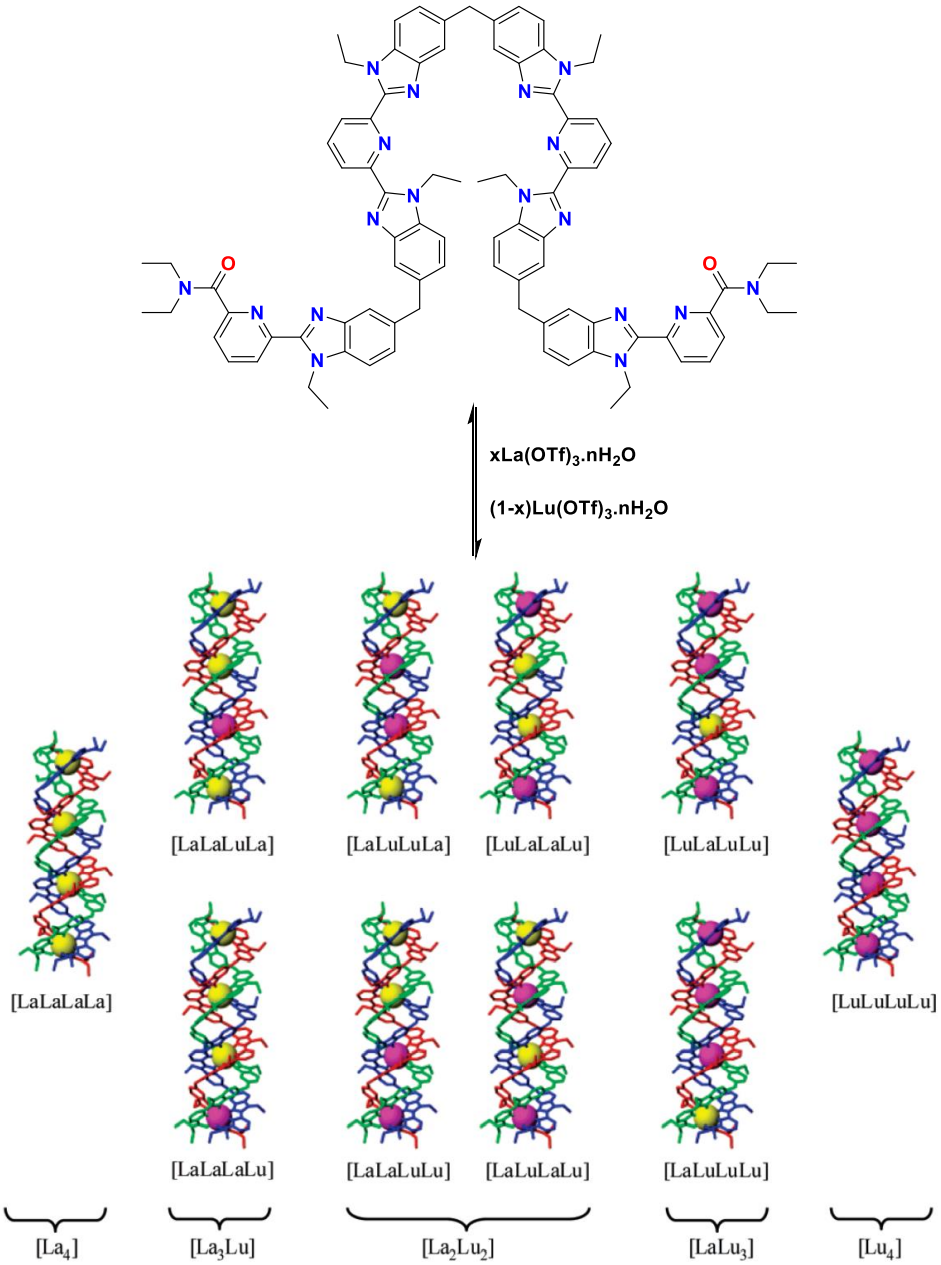

Scheme 1.3: The synthesis of heterotetrametallic lanthanide helicate complexes (Ln = La, Lu). In the 3D representations of the tetrametallic helicates, La atoms are shown as yellow spheres, while

Lu atoms are shown in pink. The three ligand strands forming the helicates are shown in red, blue and green. Image of helicate structures (bottom) reproduced from Dalla-Favera 2007.[10]

More recently, a new class of functionalised *β*-diketonate ligands with multiple, differently sized binding sites has been used to synthesise heterobimetallic and heterotrimetallic complexes. The first of these examples used the ligand 6-(3-oxo-3-(2-hydroxyphenyl)propionyl)pyridine-2-carboxylic acid ($H_3(acac_{pca\text{-}PhOH}$) in Figure 1.2).[4] This ligand has a potential three distinct coordination sites which in homobimetallic complexes were previously shown to result in two very differently sized binding sites.[46] Therefore, the reaction of a 1:1 mixture of cerium and erbium nitrates with 3 eq. $H_3(acac_{pca\text{-}PhOH})$ in pyridine resulted in the isolation of the heterobimetallic complex $CeEr(Hacac_{pca\text{-}PhOH})_2(H_2acac_{pca\text{-}PhOH})(NO_3)(py)(H_2O)$ (py = pyridine) as shown in Scheme 1.4 in good yields. The heterometallic nature of the complex was confirmed by mass spectrometry, which identified solely heterobimetallic fragments. X-ray crystallography of the complex demonstrated that as might be expected the larger Ce(III) (ionic radius 1.143 Å)[24] occupied a larger asymmetric coordination pocket while Er(III) (ionic radius 1.004 Å)[24] occupied a somewhat smaller coordination pocket, with the two metals forming the axle of a wheel of three ligands (shown in Figure 1.3). Additionally, the La/Er and Ce/Y heterobimetallics were synthesised in order to investigate the local magnetic environments of the paramagnets in isolation from each other. These heterobimetallic complexes were conceived for the purpose of using the two paramagnetic lanthanide ions as a component in a quantum computer, performing the function of a qubit logic gate. The complexes were investigated for this purpose, and it was found that the CeEr complex did exhibit the resonant behaviour required for a spin processor, albeit with very fast decoherence times (410 ns).[4]

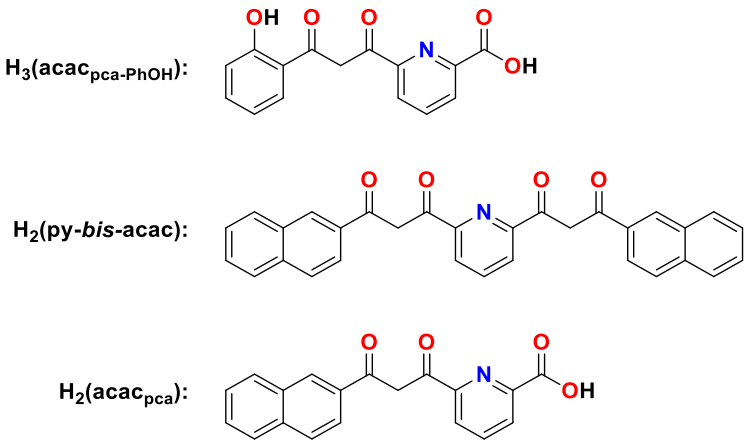

Figure 1.2: Ligands used to synthesise heterobimetallic and heterotrimetallic complexes.[4-6]

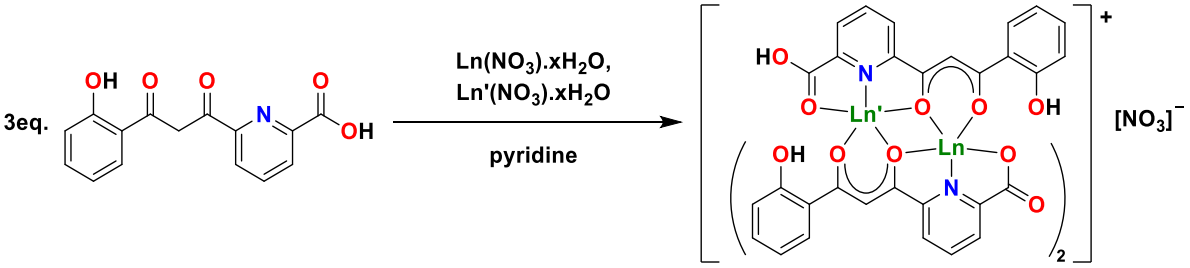

Scheme 1.4: Synthesis of lanthanide heterobimetallic complexes $LnLn'(Hacac_{pca\text{-}PhOH})_2(H_2acac_{pca\text{-}PhOH})(NO_3)(py)(H_2O)$ (Ln = La, Ce; Ln' = Er, Y).[4] Coordinated NO_3 is shown separately and coordinated pyridine and H_2O molecules are omitted for clarity.

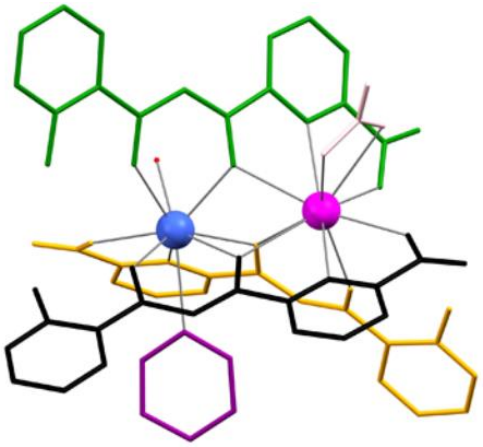

Figure 1.3: The solid-state molecular structure of the thermodynamically controlled heterobimetallic $CeEr(Hacac_{pca\text{-}PhOH})_2(H_2acac_{pca\text{-}PhOH})(NO_3)(py)(H_2O)$. Ce is shown in pink and Er as a blue sphere. Ligands are shown in wireframe and H atoms omitted for clarity. Reproduced from Aguilà 2014.[4]

A similar synthetic route was used to access the isostructural heterobimetallics $(Hpy)\{LnLn'(Hacac_{pca\text{-}PhOH})_3(NO_3)(py)(H_2O)\}$ (Ln = Eu, Nd; Ln' = Yb), with the goal of enhancing lanthanide-lanthanide energy transfer *via* the short intermetallic distances.[6] This allowed a

successful observation of NIR-NIR energy transfer between Yb(III) and Nd(III), though Vis-NIR energy transfer was not observed between Eu(III) and Yb(III).

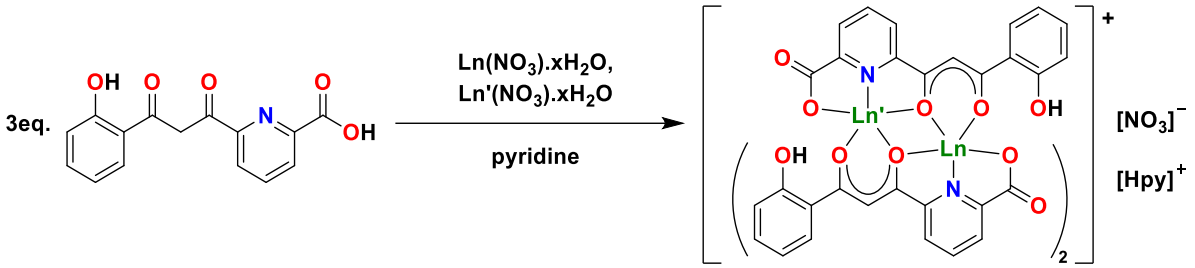

Scheme 1.5: The synthesis of lanthanide heterobimetallics (Hpy){LnLn'(Hacac$_{pca\text{-}PhOH}$)$_3$(NO$_3$)(py)(H$_2$O)} (Ln = Eu, Nd; Ln' = Yb).[6] Coordinated NO$_3$ is shown separately and coordinated pyridine and H$_2$O molecules are omitted for clarity.

This synthetic protocol using modified *β*-diketonate ligands with additional binding sites was also extended to synthesise heterotrimetallic complexes, with the goal of extending the quantum processing properties reported for CeEr(Hacac$_{pca\text{-}PhOH}$)$_2$(H$_2$acac$_{pca\text{-}PhOH}$)(NO$_3$)(py)(H$_2$O).[5] A larger ligand with three binding sites was therefore used, containing two *β*-diketone fragments either side of a pyridine moiety (H$_2$py-*bis*-acac) in Figure 1.2). By reaction of 1 eq. Ce(NO$_3$).xH$_2$O and 2 eq. Ln(NO$_3$)$_3$.xH$_2$O (Ln = Ho, Er, Yb) with 2 eq. H$_2$py-*bis*-acac and 2 eq. H$_2$acac$_{pca}$ (see Figure 1.2) in pyridine, in the presence of Cu(Cl)$_2$.xH$_2$O, three heterotrimetallic compounds formulated as [CeLn$_2$(py-*bis*-acac)$_2$(acac$_{pca}$)$_2$(py)(H$_2$O)$_2$]$^+$[NO$_3$]$^-$ (Ln = Ho, Er, Yb) were synthesised as shown in Scheme 1.6. Again, the larger ionic radius of Ce(III) resulted in its selective occupation of the larger coordination site of the assembly, while the smaller Ln(III) ions occupied the smaller sites, either side of the larger site as shown in Figure 1.4. The heterotrimetallic species were demonstrated by mass spectrometry to be the only trimetallic components in all three cases. This work demonstrates how careful selection and design of ligands can be used to overcome a synthetic challenge, in this case to form highly selective binding sites.

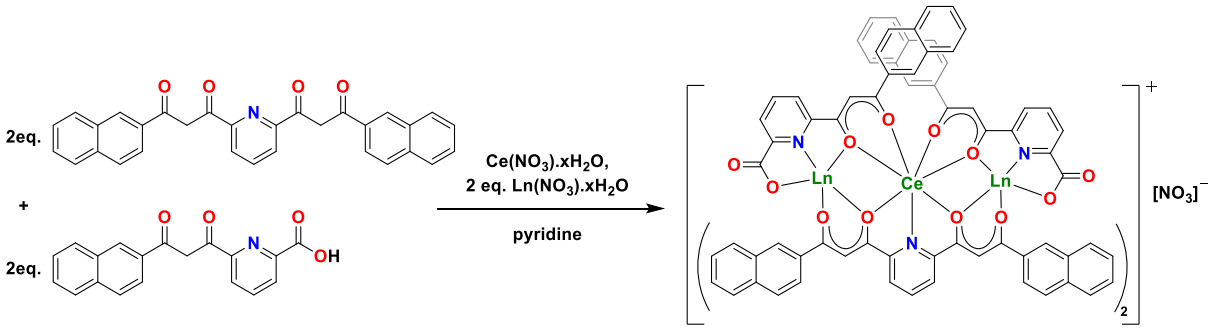

Scheme 1.6: The synthesis of the lanthanide heterotrimetallics $[CeLn_2(py\text{-}\textit{bis}\text{-}acac)_2(acac_{pca})_2(py)(H_2O)_2]^+[NO_3]^-$ (Ln = Ho, Er, Yb). Coordinated pyridine and H_2O molecules are omitted for clarity.[5]

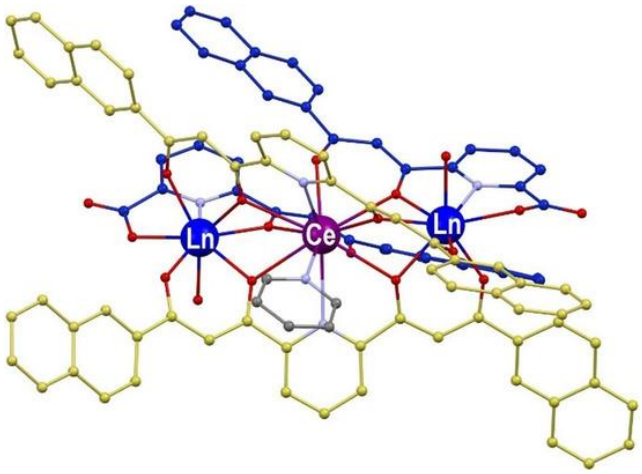

Figure 1.4: A representative solid-state molecular structure of the thermodynamically controlled heterotrimetallic complexes $[CeLn_2(py\text{-}\textit{bis}\text{-}acac)_2(acac_{pca})_2(py)(H_2O)_2]^+[NO_3]^-$ (Ln = Ho, Er, Yb). Ce(III) is shown as a purple sphere, and the sites occupied by other Ln(III) are shown in blue. Ligands are shown as ball-and-stick, with C atoms of $(py\text{-}\textit{bis}\text{-}acac)^{2-}$ shown in lime and C atoms of $(acac_{pca})^{2-}$ shown in navy. H atoms are omitted for clarity. Reproduced from Velasco 2019.[5]

1.3.2 Kinetic control

Control of the speciation of lanthanide heteromultimetallics may be achieved by using a sufficiently strongly binding ligand that the lanthanide is kinetically inert under the conditions of the reaction. In order to achieve the strong binding required, ligands must be multidentate to make use of the chelate effect, and are often preorganised in a macrocycle. The lanthanide, thus coordinated, will not readily dissociate from the ligand. The kinetically inert lanthanides can then be further reacted to form a multimetallic architecture which is not at equilibrium. This is therefore termed kinetic control of the synthesis. These examples fall into two broad categories, kinetically inert complexes with external coordination sites, and the post-synthetic modification of a kinetically inert complex.

1.3.2.1 Kinetically inert complexes with external coordination sites

The first example of kinetic control of the synthesis of lanthanide multimetallics was a sequential synthesis of porphyrin (Por) and phthalocyanine (Pc) stacked complexes.[15] A range of ligands were synthesised, bearing a range of substituents as shown in Figure 1.5. Heteroleptic half-sandwich complexes Eu(acac)(cyc) (cyc = Por, Pc) were reacted with heteroleptic and homoleptic sandwich complexes (cyc')Ln'(cyc") (cyc', cyc" = Por, Pc; Ln' = Eu, Ce). This resulted in one of the ligands in the full sandwich complex reacting to form a bridge between the lanthanide ions with elimination of Hacac to form bimetallic triple-decker complexes (cyc)Ln(cyc')Ln'(cyc") as illustrated in Scheme 1.7. However, scrambling of the lanthanides in the products was generally observed under these conditions. By reaction of the alternative half-sandwich complexes Ce(Por)(N") with double-decker complexes (cyc)Ln(tBPc) (cyc = Por, tBPc; Ln = Ce, Eu) triple-decker heterobimetallics (Por)Ce(tBPc)Eu(cyc) were selectively synthesised. The authors planned to leverage the tunability of the ligands and the variety of functional groups on the ligands in their complexes to develop multimetallic arrays for information storage.

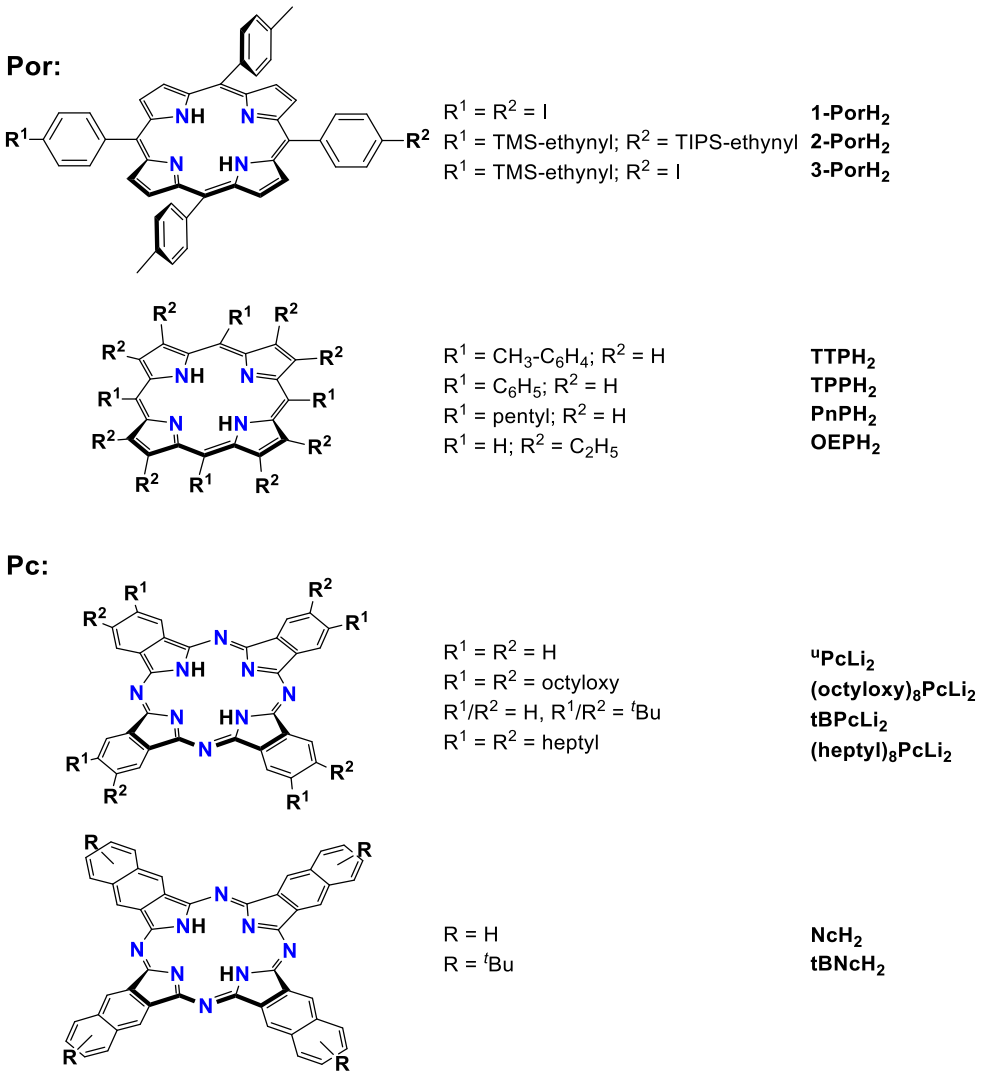

Figure 1.5: Porphyrin (Por) and Pthalocyanine (Pc) ligands used to construct heterometallic arrays.[15]

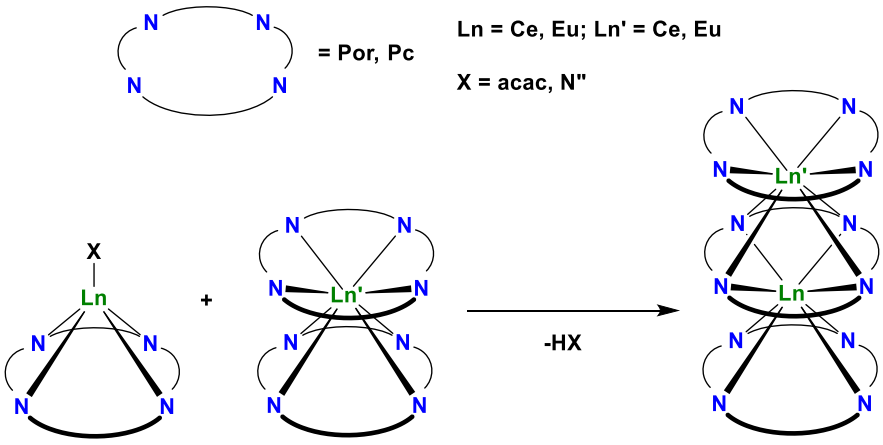

Scheme 1.7: The synthesis of lanthanide heterobimetallic triple-decker complexes using porphyrin and pthalocyanine ligands.[15]

The DOTA ligand is an excellent example of a very strongly binding ligand, and may be relatively easily functionalised. A DOTA-type ligand covalently linked to a DTPA (1,1,4,7,7-diethylenetriamine pentaacetic acid) functional group to form a *bis*-chelate has been used for the synthesis of lanthanide heterobimetallic complexes.[17] The ligand also incorporated a tryptophan group as an antenna group for sensitisation of lanthanide luminescence. First, two equivalents of lanthanide ions were coordinated to the ligand, then the lanthanide ion coordinated to the DTPA fragment was selectively removed by addition of trifluoroacetic acid (TFA) as shown in Scheme 1.8. After work-up to obtain the *mono*-lanthanide complex, addition of one equivalent of a second lanthanide selectively coordinated to the DTPA moiety to form the heterobimetallic product.

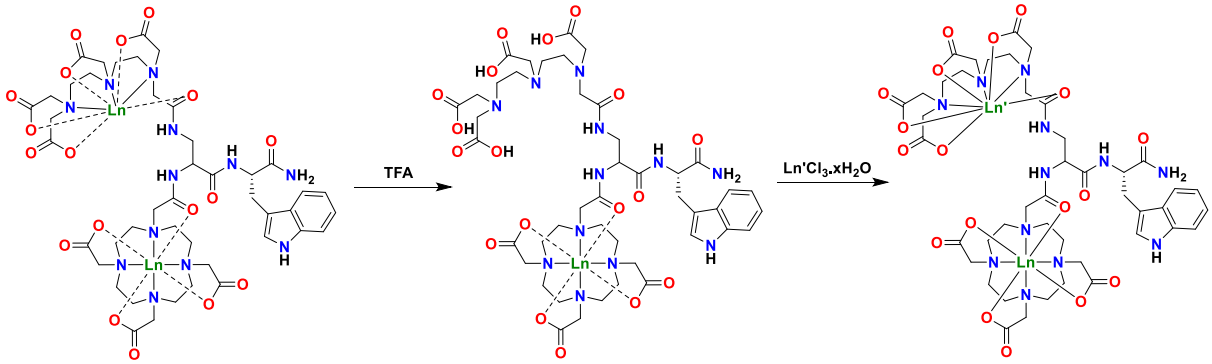

Scheme 1.8: The synthesis of lanthanide DOTA-DTPA heterobimetallic complex (Ln = Tb; Ln' = Eu, Gd) by selective demetallation.[17]

Another example of a DOTA-type ligand appended by a functional group being used for the synthesis of lanthanide heterobimetallics has also been reported. In this case, a pendant phenanthroline ligand was used as a secondary coordination site.[21] Coordination of one equivalent of lanthanide chloride to the ligand resulted in selective and irreversible coordination to the DOTA-type binding site as has been previously described. Addition of one equivalent of lanthanide *tris*-pyrrolidine dithiocarbamate then resulted in the coordination to the *N,N'* binding site of the phenanthroline moiety, forming heterobimetallic complexes Ln(DO3A-phen)Ln'$(S_2CNC_4H_8)_3$ (Ln, Ln' = Eu, Tb) as shown in Scheme 1.9. Perhaps unsurprisingly, energy transfer to Ln(III) from phenanthroline was found to be substantially more efficient when bound to the phenanthroline binding site. The complexes exhibited temperature-dependent lifetimes of luminescence, and the variation in the ratio of emission intensity between the two lanthanide ions in the Tb(III) and Eu(III) heterobimetallics had a clear trend with temperature in a relatively wide range from 0-300K in one isomer. The

heterobimetallic complexes Ln(DO3A-phen)Ln'($S_2CNC_4H_8$)$_3$ (Ln, Ln' = Eu, Tb) (DO3A = 1,4,7,10-tetraazacyclododecane-1,4,7-triacetic acid) therefore demonstrated excellent potential as luminescent thermometers due to the two very different environments of the lanthanide ions.

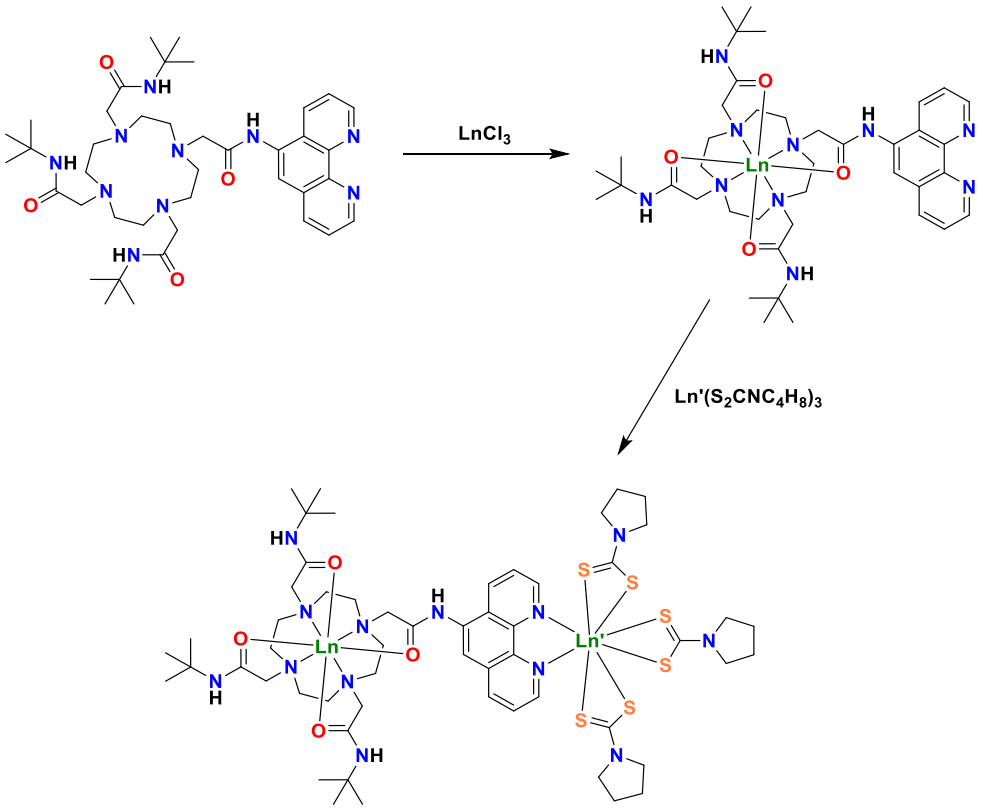

Scheme 1.9: The synthesis of a DOTA-phen based lanthanide heterobimetallic complex (Ln, Ln' = Eu, Tb) used for a molecular luminescent thermometer.[21]

Cyclic polyamine complexes are not the only complexes that have been used as a ligand equivalent for a kinetically controlled synthesis. Ytterbium complexes of the phosphonated bipyridyl ligand bipy$_{phos}$ (see Scheme 1.10) have been reported to accept Tb(III) ions into a dimeric pocket between two Yb(bipy$_{phos}$) units.[20] NIR-visible upconversion was observed upon titration of Tb(III) ions into a solution of Yb(bipy$_{phos}$). Two-photon upconversion from Yb(III) to Tb(III) was reported here for the first time in a molecular species. Three visible-emitting species were identified in the solution, identified by titration to correspond to one, two and three Tb(III) ions coordinated to the Yb(bipy$_{phos}$) dyad as {Yb(bipy$_{phos}$)}$_2$Tb$_x$ (x = 1-3). DFT analysis was used to identify possible structures for these species, shown in Scheme 1.10. These heteromultimetallic species presumably exhibit upconversion properties due to the close approach of the Tb(III) ions to two Yb(III) ions (3.9-4.6 Å), allowing relatively efficient

energy transfer. While the solid-state molecular structure of the monometallic Yb(bipy$_{phos}$) complex was determined, the structure of the heteromultimetallic species has not been identified in the solution or solid state, except by DFT. As a result, it is unclear what the oxidation state of the bipy$_{phos}$ ligand is in the association complexes, along with the identity and quantity of any anions or solvent molecules.

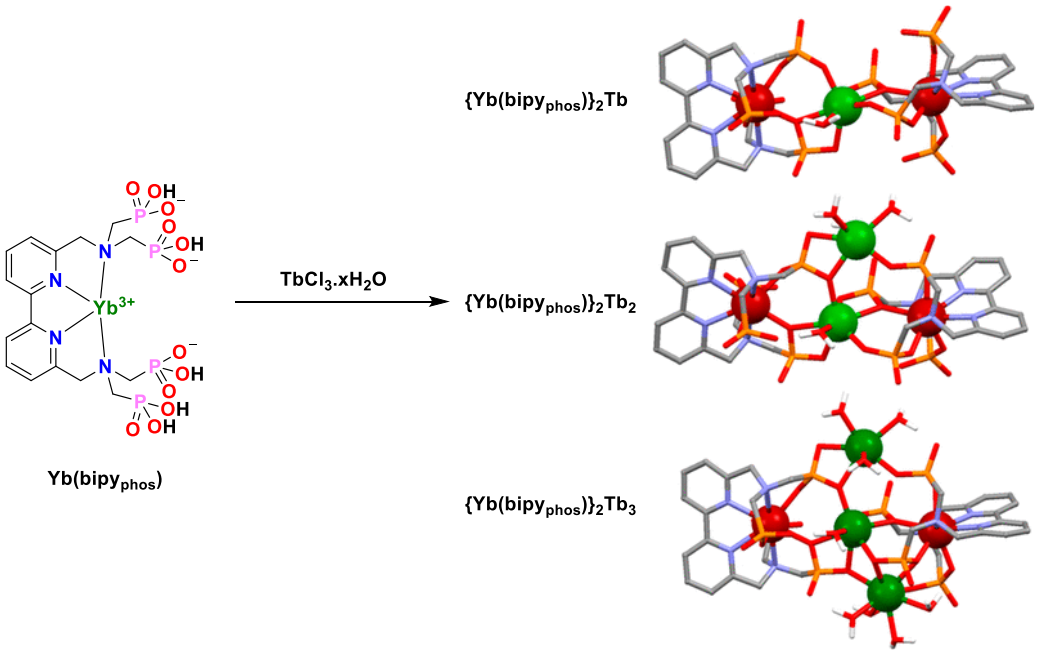

Scheme 1.10: Synthesis of heteromultinuclear lanthanide complexes {Yb(bipy$_{phos}$)}$_2$Tb$_x$ (x = 1-3), with their proposed structures as calculated by DFT.[20]

A similar strategy of phosphonating a strongly chelating ligand was also applied to some cyclic polyamine ligands, following the successful observation of upconversion in the bipyridyl complexes.[18, 19] First, the phosphonated 1,4,7-triazacyclononane (tacn$_{phos}$) ligand was used, which bears three pendant phosphonate arms.[19] The Yb(III) ion in Yb(tacn$_{phos}$) is encapsulated in the pocket formed by the three N donor ligands of the heterocycle and the phosphonate arms. Critically, the Yb(III) ion was found to be sufficiently strongly bound to occupy this space without dissociation, including in aqueous solution. As with Yb(bipy$_{phos}$), addition of Tb(III) ions to the solution resulted in observation of upconversion luminescence following energy transfer from Yb(III) to Tb(III). While the quantum yield of upconversion was very low at around $1x10^{-8}$ in D_2O (less intense emission was observed in H_2O), this was the first report of upconversion in an aqueous solution. The cyclam-based phosphonated ligands (cyclam$_{phos}$) shown in Scheme 1.11 were similarly complexed with Ln(III) (Ln = Eu, Tb, Yb, Lu) to form chelated complexes.[18] The heterobimetallic complexes {Tb(cyclam$_{phos}$)}$_x$Eu$_y$, formed by

addition of Eu(III) to Tb(cyclam$_{phos}$), exhibited high-efficiency (>90%) energy transfer from Tb to Eu. However, titrations of Yb(cyclam$_{phos}$) complexes with Tb(III) did not result in observation of upconversion luminescence under any conditions. The oxidation state of the ligands and the number of counteranions and solvent molecules is not known for either the tacn$_{phos}$ or cyclam$_{phos}$ association complexes.

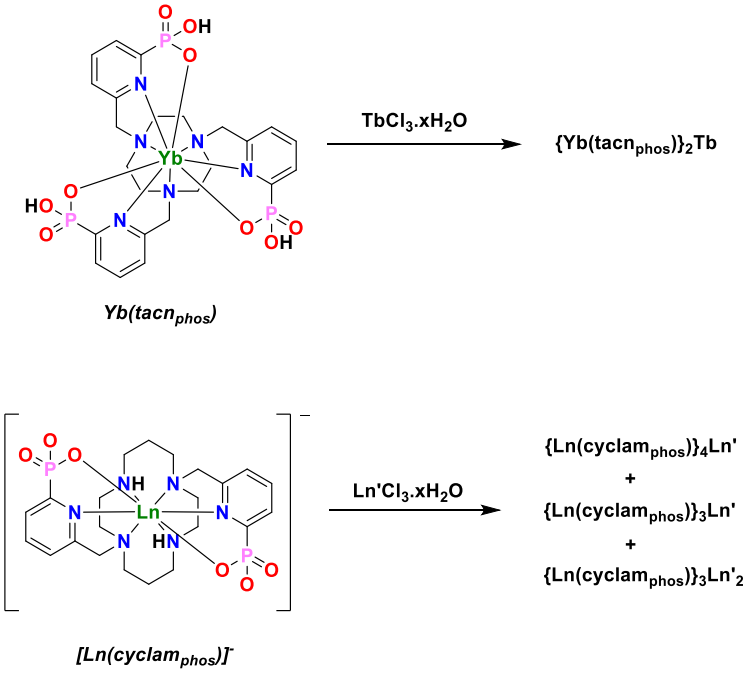

Scheme 1.11: The synthesis of the proposed lanthanide heterobimetallics {Yb(tacn$_{phos}$)}$_2$Tb, and {Ln(cyclam$_{phos}$)}$_x$Ln'$_y$ (x = 4, y = 1; x = 3, y = 1; x = 3, y = 2) (Ln = Tb, Ln' = Eu; Ln = Yb, Ln' = Tb).[18, 19]

1.3.2.2 Post-synthetic modification of kinetically inert complexes

Perhaps the most frequently utilised ligand type used to immobilise lanthanide ions for the synthesis of multimetallic arrays are multidentate polyamides such as those derived from the DOTA ligand.[12] These are often cyclic with pendant carboxylic acids, providing a pre-organised binding pocket for the lanthanide ion where the ligand has at least seven points of coordination to the lanthanide. This results in extremely high association rate constants (K > 10^{10}) even in aqueous solutions, meaning that the lanthanide is kinetically inert and will not decomplex from the binding site except under extreme conditions. If reactive sites are included on the ligand framework these can then be covalently linked to form the multimetallic compound. Sørensen and Faulkner give a complete overview of their work in this field in their 2018 review,[12] and this introduction will give a brief overview of selected papers described therein.

The first example of using a DOTA-type ligand for the synthesis of heteromultimetallic arrays was reported by the group of Faulkner.[11] A DO3A-derived ligand with a pendant aniline group DO3A-PhNH$_3$ (shown in Scheme 1.12) strongly complexed Tb(III) such that the aniline groups of 2 eq. Tb(DO3A-PhNH$_3$) were available to react with DTPA anhydride. This formed the bimetallic complex {Tb(DO3A-PhNH$_3$)}$_2$DTPA containing a DTPA-like binding site. It was confirmed *via* luminescence rate constant determination of the hydration number of Tb(III) that no migration between binding sites had occurred. To this bimetallic complex was complexed 1 eq. Yb(III) to form the heterotrimetallic complexes {Tb(DO3A-PhNH$_3$)}$_2$DTPA(Yb) (as shown in Scheme 1.12). It was found that in the trimetallic complex, following direct excitation of Tb(III), energy transfer to Yb(III) occurred, resulting in the first reported example of NIR photoluminescence sensitised by a lanthanide ion.[11]

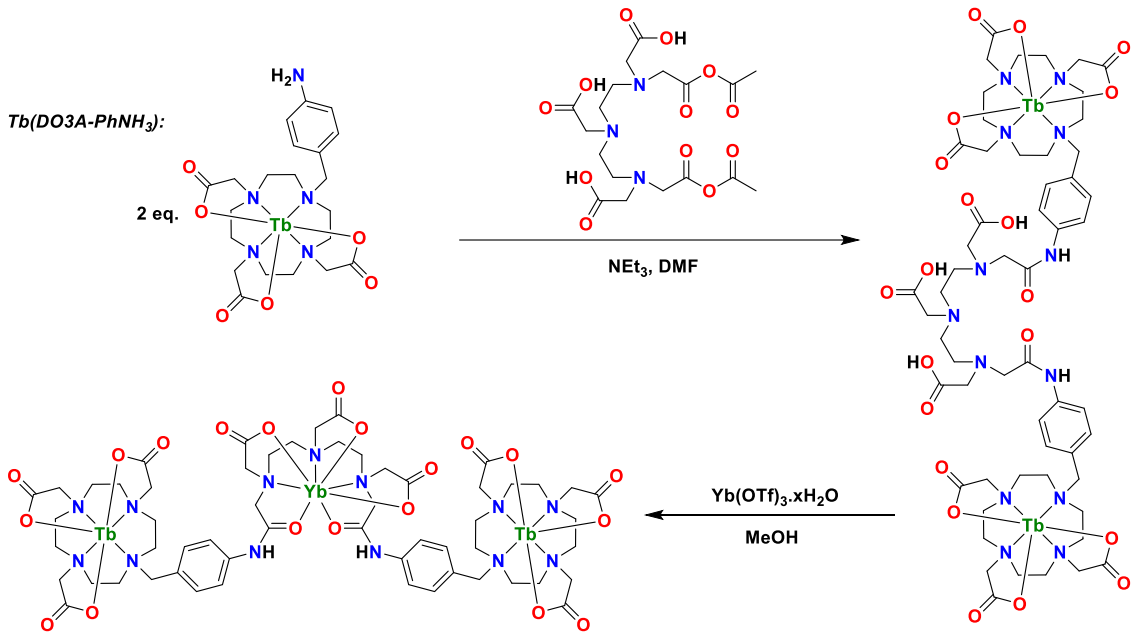

Scheme 1.12: The synthesis of a heterotrimetallic DO3A/DTPA complex of Tb and Yb.

An alternative linkage mechanism of DOTA-chelated lanthanide complexes was explored using diazotisation.[22] The reaction of two different aryl-bridged bimetallic complexes was used to form a heterotetrametallic complex, with an azo dye bridge as shown in Scheme 1.13. This synthesis is particularly notable as it is an example of the coupling reaction being used to introduce a useful functionality, in this case, a sensitising chromophore. Additionally, the complex was found to be stable under the rather forcing conditions required to perform the diazotisation. DOTA-type complexes are well-known to be highly kinetically stable in aqueous

and biological media, and this study demonstrates their stability both in strongly acidic (HCl) and in reducing basic (hydrazine) conditions.

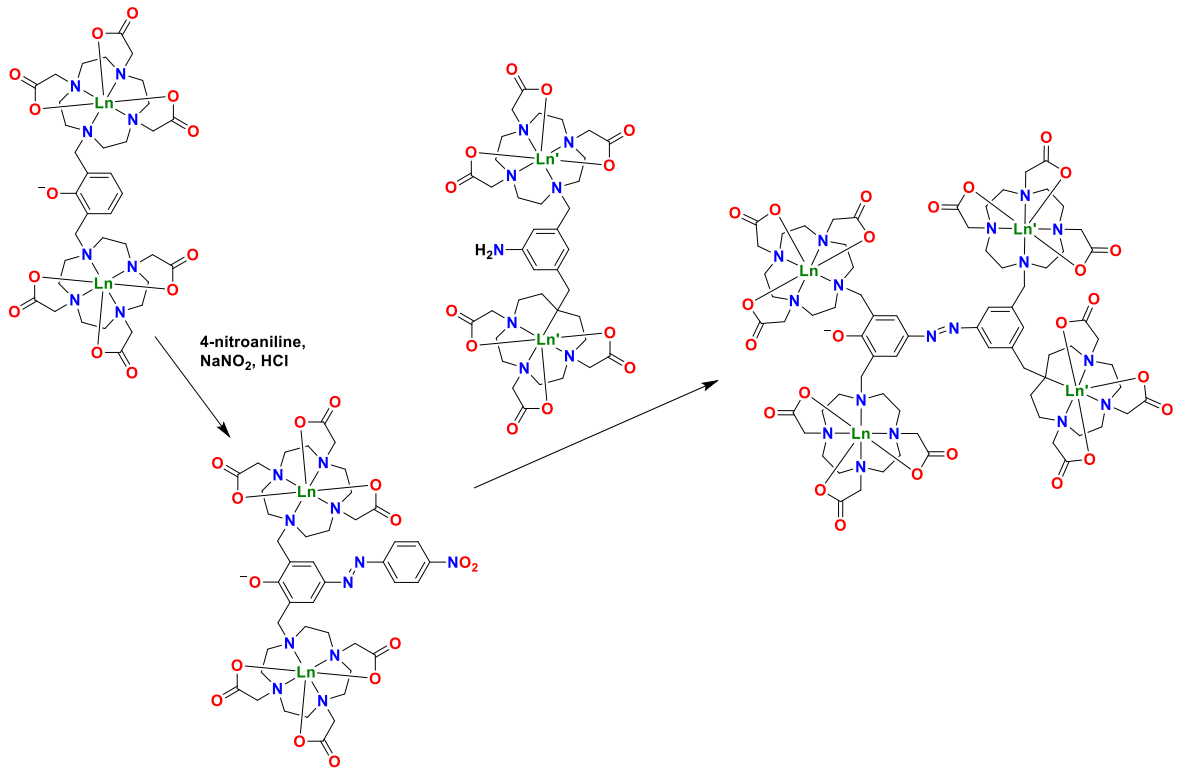

Scheme 1.13: The synthesis of a DOTA-based lanthanide heterotetrametallic complex (Ln, Ln' = Nd, Yb) using a diazotisation linkage reaction.

Another example of a straightforward coupling which has been applied to the synthesis of heteromultimetallic complexes is "click" chemistry, or the facile and high-yielding coupling reaction of azides with carbynes to form a triazole bridge.[23] An azide-appended DOTA-type ligand was first synthesised by reaction of an azide-appended acyl bromide with the protected pro-ligand, followed by deprotection of the carboxylic acid groups. Lanthanide triflates were then used to complex the ligand, and a carbyne-appended DO3A complex was added along with a catalytic quantity of $CuSO_4$ and sodium ascorbate. This rapidly formed heterobimetallic complexes Ln(DOTA-Ph-triazole-DO3A)Ln', incorporating a conjugated bridge as shown in Scheme 1.14. The luminescent properties of Eu(DOTA-Ph-triazole-DO3A)Yb and Yb(DOTA-Ph-triazole-DO3A)Eu varied significantly from each other in relative intensities, which the authors attributed to a LMCT state accessible for the lanthanides in the DO3A site closest to the triazole moiety. Variations in the fine structure of the emission from Yb(III) in the two complexes were also evident, as a result of the differing coordination environments of the two binding sites.

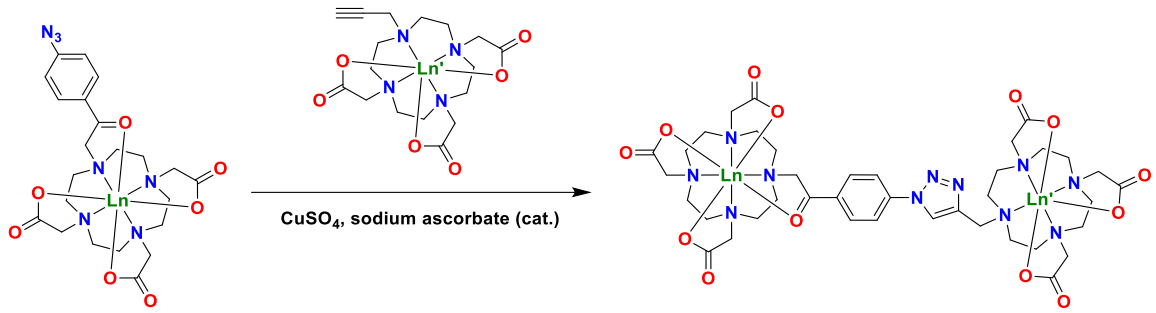

Scheme 1.14: The synthesis of a DOTA-based lanthanide heterobimetallic complex (Ln, Ln' = Eu, Yb) using "click" chemistry.

Another study elected to link two lanthanide coordinated porphyrin complexes.[16] Lanthanide complexes of two alkyne-appended porphyrin ligands, each with a substituted group of different polarity, were capped by a cobalt phosphate tripodal metalloligand $[CpCo\{PO(OEt)_2\}_3]^-$ (CoPO). Alkyne coupling by addition of a palladium catalyst to a 1:1 mixture of the two different porphyrin complexes resulted in the synthesis of a mixture of hetero- and homo-metallic dimers as shown in Scheme 1.15, which were separated by chromatography to obtain the pure heterobimetallic complexes (CoPO)Ln(Por_2)Ln'(CoPO). The Dy-Tb heterobimetallic complex (CoPO)Dy(Por_2)Tb(CoPO) was found to exhibit single-molecule magnet properties, as were the mono-lanthanide porphyrin complexes (CoPO)Ln(Por) (Ln = Dy, Tb) and the homobimetallics (CoPO)Ln(Por_2)Ln(CoPO) (Ln = Dy, Tb). Measurement of the quantum coherence of the mono-Gd porphyrin and Gd_2 dimer complexes revealed a decoherence time in the dimer of around 3.0 μs. In combination with the slow magnetic relaxation of the Dy-Tb dimer, this indicates that the system has potential for use in spintronic applications.

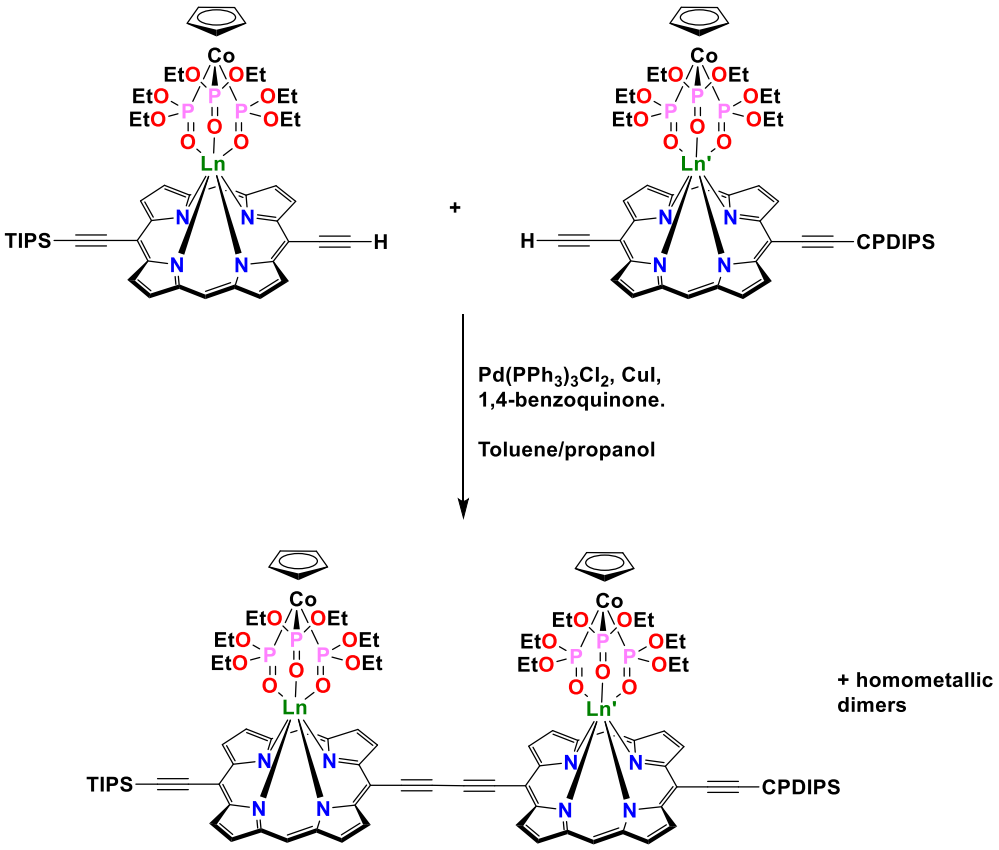

Scheme 1.15: Synthesis of lanthanide porphyrin homo- and hetero-metallic dimers (Ln = Dy, Gd, Tb; Ln' = Dy, Gd, Tb) by alkyne coupling.[16]

A recent study selected cryptates as a kinetically inert unit for the synthesis of lanthanide heterobimetallic complexes.[13] By reaction of *tris*(2-aminoethyl)amine (tren) with 2,6-diformyl-*p*-cresol (dfmp) in the presence of $Ln(OTf)_3(H_2O)_x$ (Ln = Y, Gd, Yb, Lu), the mono-lanthanide cryptate complexes LnL_{crypt} were synthesised as shown in Scheme 1.16.[13, 47] Due to the very strong binding of the multidentate macrocyclic ligand, the lanthanide was kinetically inert in the pyridine solution used for the reaction. Addition of 3-5 molar equivalents (depending on the ionic radius) of $Ln'(OTf)_3(H_2O)_x$ (Ln = Y, Gd, Yb, Lu) to LnL_{crypt} resulted in coordination of a second lanthanide ion, and formation of the lanthanide heterobimetallics $[LnLn'L_{crypt}]^{3+}[OTf]^{-}_3$ (Scheme 1.16). Solid-state molecular structure determination showed that the lanthanide ions each occupy a 7-coordinate binding site in the interior pocket of the cryptate. The lanthanide ions are separated from each other by around 3.5 Å. The anion and the reaction solvent were both vitally important in the prevention of scrambling of the lanthanide ions. Use of lanthanide nitrates as reagents resulted in scrambling, as did using a more weakly Lewis basic solvent such as PrCN in place of pyridine. Based on this, the authors proposed that pyridine played an important role as a base in the

reaction, inhibited by nitrate anions. This was evidenced by pyridinium triflate detected in product mixtures prior to work-up. Mass spectrometry demonstrated that using these conditions and reagents, heterobimetallic pairings were selectively synthesised for pairs of medium-sized lanthanides (Y, Gd), pairs of smaller lanthanides (Yb, Lu) and for combinations of medium and small lanthanides. Determination of the dependence of the magnetic susceptibility on temperature for homobimetallics $[Ln_2L_{crypt}]^{3+}[OTf]^{-}_3$ containing paramagnetic lanthanides (Ln = Gd, Yb) showed antiferromagnetic exchange between the lanthanides with small exchange values ($Ln_2 = Gd_2$, J = -0.194 cm^{-1}; $Ln_2 = Yb_2$, J = -0.0072 cm^{-1}), while the heterobimetallic $[GdYbL_{crypt}]^{3+}[OTf]^{-}_3$ exhibited ferromagnetic exchange (J = 0.01780 cm^{-1}). All exchange values reported were exceedingly small despite the short inter-lanthanide distance, with the largest being the antiferromagnetic Gd-Gd interaction of -0.194 cm^{-1}.

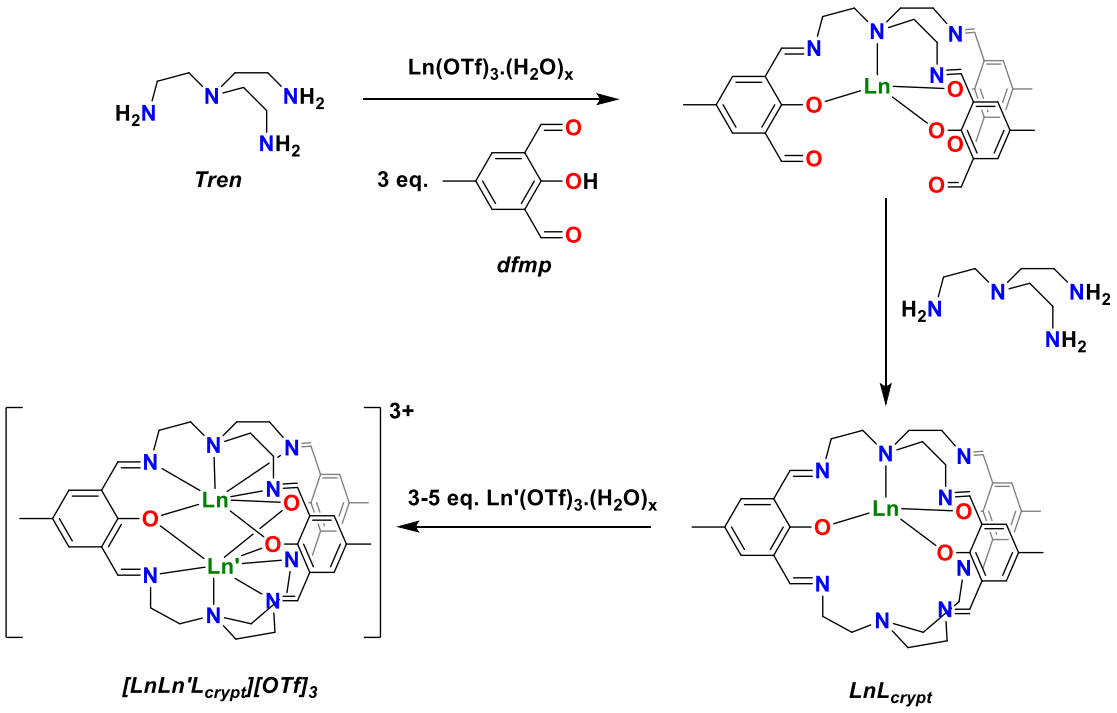

Scheme 1.16: Synthesis of cryptate heterobimetallic lanthanide complexes $[LnLn'L_{crypt}]^{3+}[OTf]^{-}_3$ (Ln, Ln' = Y, Gd, Yb, Lu).[13]

Also taking advantage of the kinetically inert cryptate-style ligands, heteromultinuclear arrays have been successfully synthesised *via* a stepwise peptide synthesis, attached to a solid support.[14] A series of cryptate-appended amino acids were first synthesised, protected by the Fmoc group (Fmoc = fluorenylmethoxycarbonyl). After irreversible coordination of lanthanide ions to the cryptate functionality, these were then successfully used in the same fashion as

any other amino acid in a peptide synthesis, as depicted in Scheme 1.17. A deprotected amino acid attached to a polystyrene support is reacted with a second, protected, amino acid to selectively synthesise a bimetallic peptide chain, and then the protection is removed from the amino acid at the end of the chain for further reactivity, and so on. The most important feature of the cryptate amino acid complexes is that they are stable, and strongly bind the lanthanide ion, even under the strongly acidic (trifluoroacetic acid, TFA) conditions required for the deprotection and coupling of the amino acids. This synthesis therefore takes advantage of the flexibility of the organic peptide chain synthesis, where the sequential protection, deprotection and coupling reliably forms covalent chain polymers. However, the lanthanide ions are by necessity held very far apart from each other, and they will therefore be unlikely to experience any inter-lanthanide interaction in this environment.

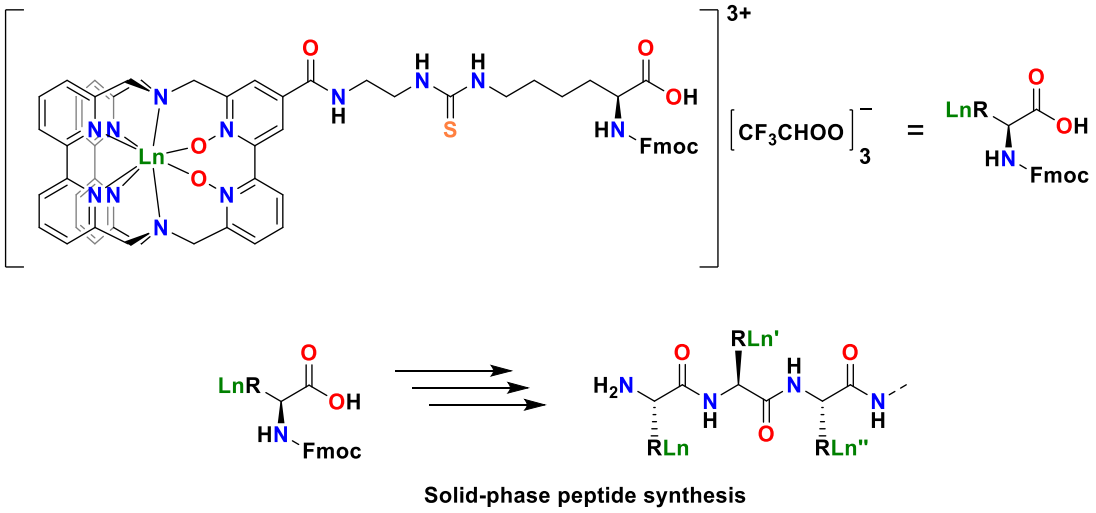

Scheme 1.17: The structure of the amino acid lanthanide cryptate monomer complex and the solid-phase peptide synthesis used to synthesise heteromultimetallic lanthanide arrays.[14]

1.3.3 Summary and Outlook

A wide variety of methods have been used to synthesise lanthanide heteromultimetallic complexes. These range from careful tailoring of the ligand environment to encourage selective coordination of lanthanides, to coupling of strongly bound covalent units by well-known bond-forming reactions, to developing complexes which have external (or internal) binding sites which can be selectively coordinated by a second lanthanide. The lanthanides can be held at a range of distances to each other, from very close to at a great distance. Functional groups on the ligands have been used to introduce functionality or to promote interaction between the lanthanide ions. However, despite the remarkable properties displayed, many of the methods for the synthesis of heteromultimetallics described have limitations of various kinds. Targeting a very strongly bound complex using a DOTA-type ligand, for example, limits the coordination environment of the lanthanide to the amine and carboxylic acid groups. Using a convenient coupling reaction such as a peptide synthesis results in a specific type of linkage between the lanthanide ions. Forming solution state associative complexes, such as in the polyphosphates, which bring the lanthanides into sufficiently close contact to achieve multi-photon absorption upconversion has presented challenges in isolation and characterisation of the molecular species. It is therefore desirable to develop new routes to lanthanide heterobimetallic complexes in new coordination environments. This will allow further investigation of the remarkable properties and applications resulting from the intermolecular interaction of lanthanide ions.

1.4 Aims and Concept

At present, no example of a lanthanide heteromultimetallic complex has been reported where the lanthanide is bridged by a redox-active ligand. Such a system would allow an unprecedented degree of control of the communication between lanthanides, through tuning the oxidation state of the ligand. Lanthanide pairings could be selected to simulate a multiplexing agent combining photoluminescent and magnetic properties of the lanthanides, and to investigate how any interactions between the lanthanides affected the properties of the complex. It is therefore the goal of the work described in this thesis to address this deficit.

The greatest hurdle to the synthesis of lanthanide heteromultimetallics is the chemical similarity of the lanthanides. The various methods used previously to overcome this, and their limitations, have been summarised in Section 1.3.3. However, coordination chemistry might provide an alternative answer. Control of the ancillary ligand environment of a lanthanide might be used to impart selectivity to a vacant coordination site of the lanthanide, tunable to the different coordination sites of an asymmetric bridging ligand. This could be through controlling the available coordination space on the lanthanide, or through the use of more or less strongly donating ligands to tune the electron density of the lanthanide. It should therefore be possible to design lanthanide complexes with vacant and selective coordination sites, which are themselves kinetically inert under the conditions of coordination to a bridging ligand. This would constitute a new strategy combining kinetic and thermodynamic control, to synthesise lanthanide heteromultimetallic complexes with new types of bridging ligand which cannot be synthesised using published methods. In particular, lanthanide reagents will be identified which are selective to the different binding sites of the redox-active ligand 1,10-phenanthroline-5,6-dione (pd), to synthesise lanthanide heterobimetallic complexes bridged by pd.

1.5 The 1,10-phenanthroline-5,6-dione ligand

The 1,10-phenanthroline-5,6-dione (pd) ligand will be a focus of this thesis, and thus it is important to introduce its chemistry. The pd ligand is a redox-active bridging ligand, with two different co-ordination sites: the *N,N'* phenanthroline site and the *O,O'* quinone site which each exhibit different reactivity (Figure 1.6). The *N,N'* phenanthroline site reacts mainly as a Lewis base, while the *O,O'* quinone site is redox active and can react with organometallic transition metal reagents. The ligand may undergo either a 1- or 2-electron reduction, the electronic structures of which are given in Figure 1.7.

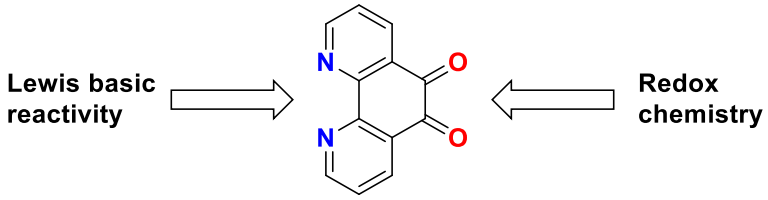

1,10-phenanthroline-5,6-dione, pd

Figure 1.6: The two co-ordination sites of the pd ligand

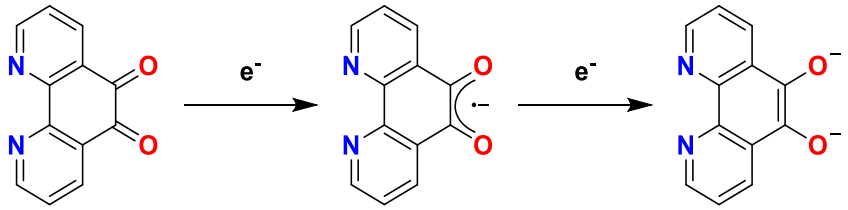

Figure 1.7: The reduction of pd to $pd^{\bullet-}$ and pd^{2-}

1.5.1 Co-ordination Chemistry of 1,10-phenanthroline-5,6-dione

The group of Balch first established the divergent reactivity of the two sites of pd, preparing the complexes $(PPh_3)_2Pt(O,O'\text{-pd})$ and $Cl_2Pd(N,N'\text{-pd})$ by reaction of pd with Pt(0) or Pd(II) precursors respectively.[48] Building on this chemistry, Pierpont and co-workers synthesised the first bimetallic complexes of pd by demonstrating the use of Balch's Pt and Pd complexes as a "bipyridine equivalent" and a "benzoquinone equivalent" (referring to the identity of the available coordination site), as shown in Scheme 1.18, to give bridging complexes.[49] Reaction of $(PPh_3)_2Pt(O,O'\text{-pd})$ with the transition metal halides $Pd(PhCN)_2Cl_2$ and $Ru(PPh_3)_3Cl_2$ provided heterobimetallics $(PPh_3)_2Pt(O,O'\text{-}N,N'\text{-pd})MCl_2$ (M = Pd, Ru), whereas reaction of the bipyridine equivalent complex with $Pt_2(DBA)_3$ (DBA = dibenzylideneacetone), a Pt(0) reagent, provided the mixed-oxidation state Pt bimetallic $(PPh_3)_2Pt^{II}(O,O'\text{-}N,N'\text{-pd})Pt^0(DBA)$.

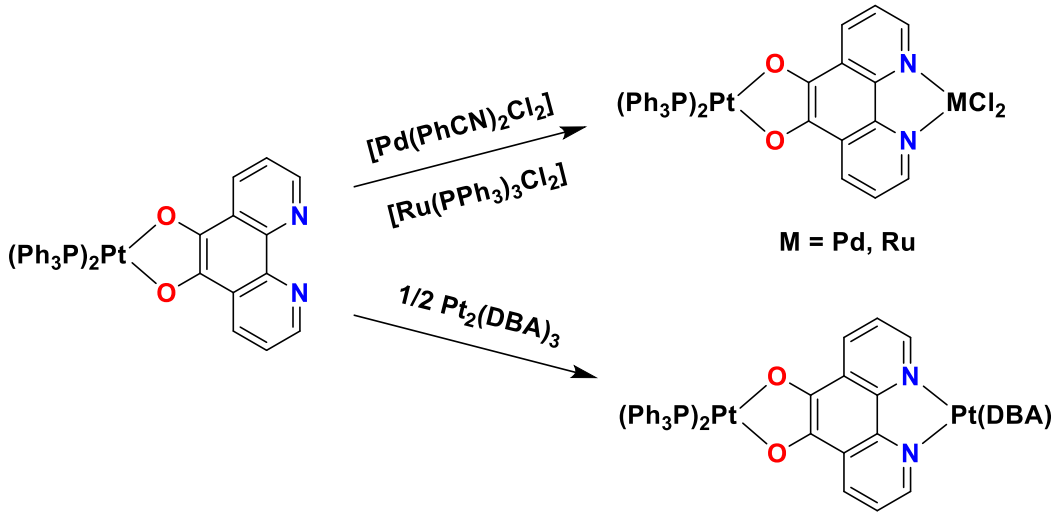

Scheme 1.18: Synthesis of bimetallic complexes by reaction of the "bipyridine equivalent" $(PPh_3)_2Pt(O,O'$-pd) with Lewis acidic transition metal complexes.[49]

Later, Calderazzo *et al.* synthesised further bimetallic complexes, using both "bipyridine equivalent" and "benzoquinone equivalent" starting materials.[50] They reported that the choice of transition metal reagent allowed selective addition of the metal to either the *N,N'* or *O,O'* co-ordination site. Transition metal halides co-ordinated to the *N,N'* site, while organometallic reducing agents such as low-oxidation state metallocenes underwent oxidative addition to the *O,O'* co-ordination site, as shown in Scheme 1.19. Addition of each of VCp_2, $TiCp_2(CO)_2$ and $ZrCp_2(CO)_2$ resulted in a two-electron reduction of the *O,O'* co-ordination site of the ligand.

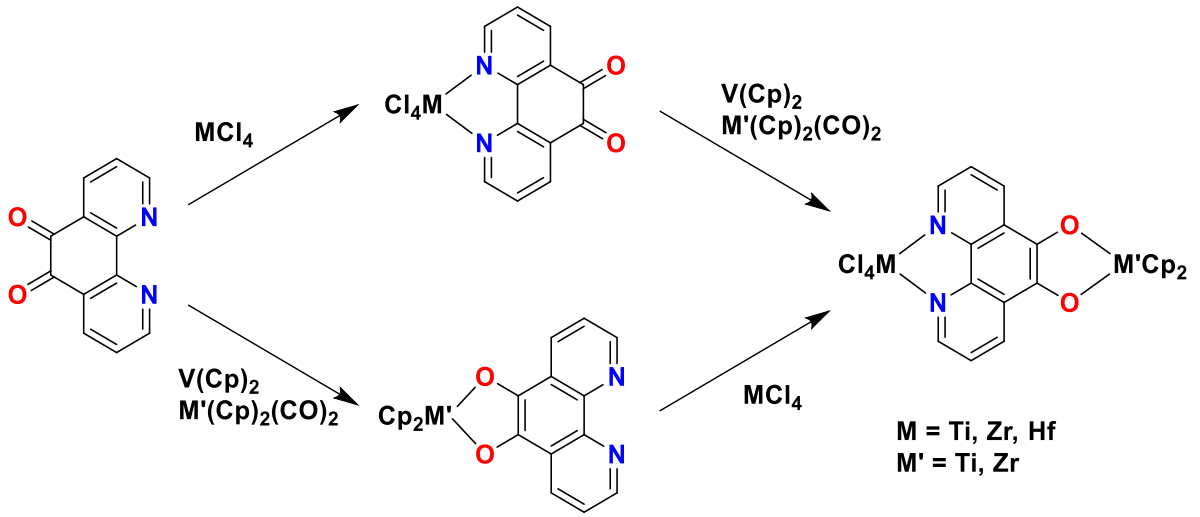

Scheme 1.19: Synthesis of transition metal bimetallic complexes by selective addition to *N,N'* and *O,O'* co-ordination sites of pd, as reported by Calderazzo *et al.*[50]

Calderazzo and co-workers also reported the synthesis of a range of higher nuclearity multimetallic complexes, containing 4-7 metals.[51] Due to the low solubility of these complexes, they were characterised solely using solid-state techniques (IR, EA, μ_{eff}, solid-state molecular structures of some of the mono and bimetallics). By using an arene sandwich complex of Ti(0) or V(0), they synthesised *tris*-*O,O'*-pd "pinwheel" complexes M(*O,O'*-pd)$_3$ (M = Ti, V), formally assigned to a mix of 2- and 1- oxidation states of pd, as shown in Scheme 1.20. They treated these as a *tris*-phenanthroline equivalent, reacting them with three equivalents of a Lewis acidic complex, to give a pinwheel style metal cluster M((*O,O'*-*N,N'*-pd)$_3$M'(Cp)$_2$) (M = Ti, V, M' = Ti), with pd radially arranged around the central metal. They also used an Fe(II) complex to synthesise a *tris*-*N,N'*-pd complex Fe(*N,N'*-pd)$_3$, and which they used as a *tris*-benzoquinone equivalent. In this case, reaction of the *tris*-pd complex with three equivalents of the bimetallic complex TiCl$_2$(*N,N'*-*O,O'*-pd)V(Cp)$_2$ afforded the larger cluster [Fe{(*N,N'*-*O,O'*-pd)TiCl$_2$(*N,N'*-*O,O'*-pd)V(Cp)$_2$}$_3$][PF$_6$]$_2$.

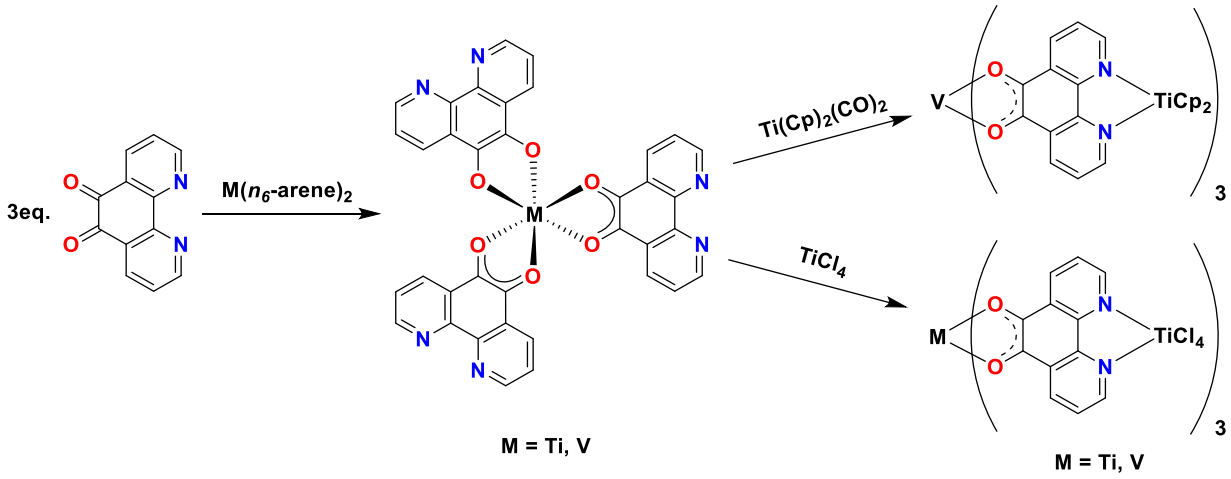

Scheme 1.20: Synthesis of transition metal clusters using pd as a bridging ligand, as reported by Calderazzo *et al.*[51]

An alternative method for the synthesis of multimetallic pd complexes was reported by Eisenberg *et al.*[52] They report the stepwise synthesis of Pt-pd chain complexes, with pd acting as a bridge between Pt atoms, as shown in Scheme 1.21. They performed the reduction of pd to the catechol pdoH$_2$ (1,10-phenanthroline-5,6-diol), which was then deprotonated by Pt(dbbpy)Cl$_2$ (dbbpy = di-*tert*-butylbipyridine) to give the complex Pt(dbbpy)(*O,O'*-pd). Reaction of this monometallic complex with Pt(PhCN)$_2$Cl$_2$ gave the bimetallic complex Pt(dbbpy)(*O,O'*-*N,N'*-pd)PtCl$_2$. This could then undergo a further reaction with Pt(PhCN)$_2$Cl$_2$ and a catechol (pdoH$_2$, dbcatH$_2$ or tdtH$_2$) to form a chain structure with the deprotonation of

the catechol. The chain was capped by reaction with mono-functional groups (see Scheme 1.21). A rapid decrease in solubility was observed on addition of a second metal-pd unit, leading to difficulties extending and characterising the chain beyond 3 metal centres.

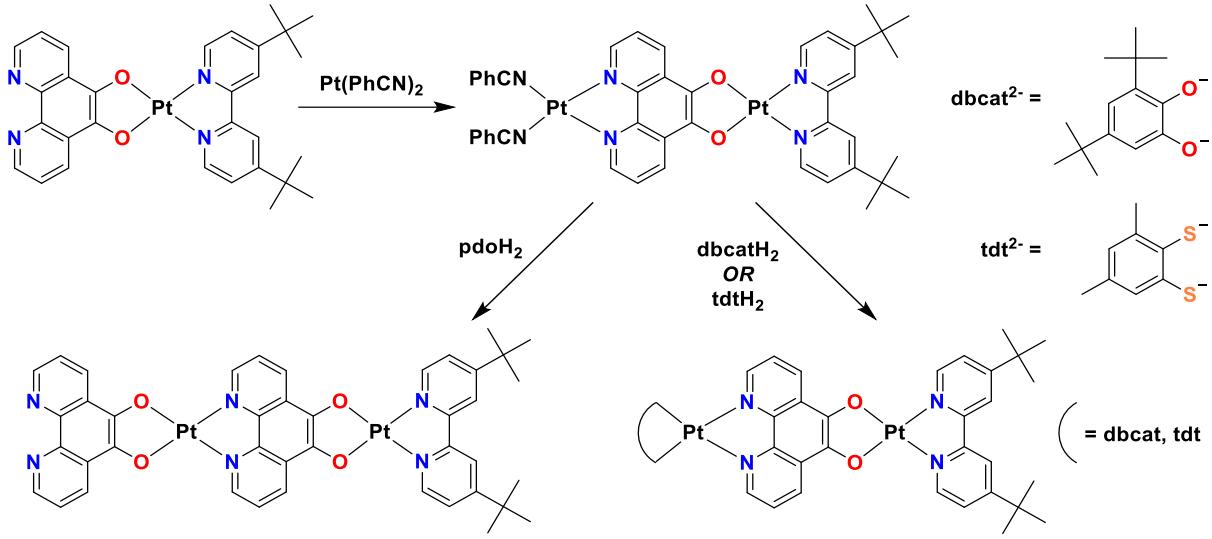

Scheme 1.21: Formation of Pt-pd chain complexes by use of $pdoH_2$. Monofunctional capping ligands: dbcat = di-*tert*-butylcatecholate, tdt = toluenedithiolate.

The reactivity of the pd ligand with the lanthanides was first reported by Faulkner and Ward, who synthesised the lanthanide pd complexes $Ln(tta)_3(N,N'\text{-}O,O'\text{-pd})Pt(PPh_3)_2$ (Htta = thenoyltrifluoroacetone, Ln = La, Nd, Gd, Er, Yb), as shown in Scheme 1.22.[53, 54] In place of the chlorides commonly used for synthesis of transition metal complexes, they used diketonate ligands both in order to satisfy the co-ordination sphere of the lanthanide, and to impart greater solubility to the complexes. In their lanthanide-transition metal heterobimetallic complexes, the *O,O'* coordinated Pt(II) was able to act as a chromophore and sensitise emission from NIR-emitting lanthanide ions (Ln = Nd, Er, Yb). The bridging pd ligand facilitated energy transfer between the two metals, indicating that the conjugated π-system can be used to encourage cooperativity between metals at the two binding sites.

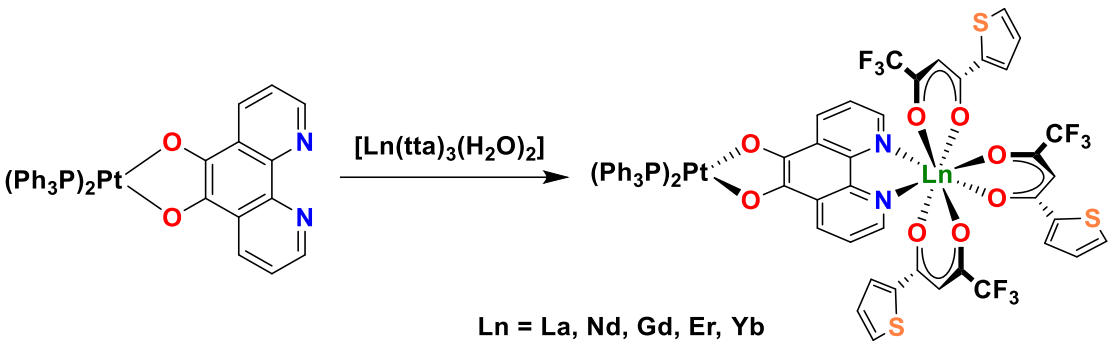

Scheme 1.22: Synthesis of lanthanide-transition metal heterobimetallic complexes, as described by Shavaleev *et al.*[53, 54]

1.5.2 The radical anion of 1,10-phenanthroline-5,6-dione

The radical anion of pd ($pd^{-\bullet}$) is an intriguing target, as radical bridged complexes, particularly of the lanthanides, are a topic of great recent interest.[25-27, 55-59] However, the radical form of the ligand is primarily known as either the free ligand or as complexes that have been electrochemically reduced, with only a single fully characterised example in the literature.[60] Analysis of the electronic structure of Calderazzo's *tris*-pd pinwheel-type complexes for example, which contain a mix of 1- and 2- oxidation states of pd, was not possible due to their insolubility.[51] The synthesis of a fully-characterised, stable example of the radical ligand had not been reported prior to the work described herein.[61]

There are two examples of non-electrochemically generated complexes of $pd^{-\bullet}$ reported in the literature. Fukuzumi *et al.* report the synthesis and thermochromism of Mg^{2+} and Sc^{3+} complexes of $pd^{-\bullet}$.[60] They synthesised the radical complexes by the 1-electron reduction of pd by Me_2Fc (Me_2Fc = dimethylferrocene, $Fe(MeCp)_2$) in presence of Mg^{2+} or Sc^{3+} ions, and recorded EPR and electronic spectra of the resultant solution. The EPR spectra indicated that the radical was coupled both to the protons of the ligand and to the metal, consistent with complex formation, though no isolation of the radical species was carried out. Interestingly, they observed thermochromism of the radical complexes. In the Mg^{2+} complex, a reduction in intensity of the radical charge transfer band was observed as temperature was lowered from 298 K to 203 K, along with a corresponding decrease in intensity of the EPR spectrum. In the Sc^{3+} complex, an increase in intensity of the charge transfer band and EPR spectrum was observed as temperature was decreased from 298 K to 183 K. Fukuzumi and co-workers attributed this by spectral titration to the difference in Lewis acidity of the metal. They proposed that the strong Lewis acid Sc^{3+} facilitates complete electron transfer from Me_2Fc to

pd, and an exothermic disproportionation equilibrium leads to an increase in concentration of the radical at lower temperature. Meanwhile, the weaker Lewis acid Mg^{2+} is suggested to only encourage a partial electron transfer to pd, and the electron transfer equilibrium thus established favours neutral pd at low temperature. This demonstrates the significant effect that the presence of Lewis acidic metals in solution can have on the electronic structure of the pd ligand. Pampaloni and co-workers synthesised the $pd^{-\bullet}$ complex $CrCl_2$(*O,O'*-$pd^{\bullet}$) by reaction of $CrCl_2$ with pd, effecting the mono-reduction, which they characterised by IR analysis.[62] They were unable to obtain the solid-state structure or EPR spectrum of the complex due to very low solubility, but they were able to characterise the structure of a closely related complex of 9,10-phenanthrenesemiquinone.

1.5.3 Electrochemical studies

A number of electrochemical studies have investigated the electronic structure of the pd ligand in all its of oxidation states. Abruña *et al.* performed electrochemical studies on complexes of pd, during which they observed the shift of the two reversible pd-centred reductions from -0.45 and -1.25 V (*vs* sodium-saturated calomel electrode (SSCE)) in the free ligand to higher potentials in transition metal complexes.[63] In the Ru complex $[Ru(bpy)_2$(*N,N'*-pd)$]^{2+}$, the same two potentials shifted to -0.065 and -0.77 V (*vs* SSCE), indicating that complexation has a significant effect on the reduction potential of pd, despite the metal being coordinated to the *N,N'* binding site rather than the redox-active *O,O'* oxidation site. Kaim *et al.* also studied the electrochemistry of the pd complexes M(Cp)Cl(*N,N'*-pd) (M = Rh, Ir), in combination with EPR and electronic spectroscopy.[64] They reported a radical, reversibly generated at -0.55 V (*vs* Fc^+/Fc), with a hyperfine splitting pattern and g-value in accordance with those expected for a semiquinone radical. Yellowlees *et al.* also performed a spectroelectrochemical study of the ligand, providing electrochemical, electronic and EPR spectroscopy and Density Functional Theory (DFT) calculations both for the free ligand and a range of complexes, both *N,N'*- and *O,O'*-coordinated.[65] They report a positive shift in both the first and second oxidative potentials in the *N,N'*-coordinated complexes from the free ligand (-0.4/-1.24 V in pd to -0.12/-0.78 V in Pt(*N,N'*-pd)Cl_2, both *vs* Ag/AgCl). A significantly greater positive shift is reported for the first and second oxidations of pd in Pt(*O,O*-pd)$(PPh_3)_2$ (+0.38/+1.07 V *vs* Ag/AgCl). The coordination of a metal to the ligand, and the binding site in which it resides was therefore very important to the electrochemical properties of the ligand.

Their investigation of the electronic structure also supports a semiquinone-based radical structure, with a small degree of delocalisation over the ligand resulting in coupling of the radical to H and N nuclei of the ligand. The data presented in this study are particularly useful in analysis of the electronic structure of pd complexes.

1.5.4 Conclusions

The pd ligand has been used to synthesise a range of transition metal multimetallic complexes. The selective synthesis of these complexes relies on the divergent reactivity of the *N,N'* and *O,O'* binding sites of the ligand. Using this asymmetric reactivity, multimetallic complexes have been synthesised with a range of structures, from bimetallics[48, 50] to tetrametallic pinwheels[51] to one-dimensional chains,[52] containing the ligand in a variety of oxidation states. The electronic properties of the ligand in various oxidation states have been investigated by several groups.[63-65] Of particular note, it has been shown that the electronic and redox properties of pd are highly dependent on the coordination environment of the ligand.[60, 62] In particular, coordination of a Lewis acidic metal to pd results in a significant decrease in the first and second reduction potentials compared to the free ligand. However, no molecular examples of the radical anion were reported prior to the work presented in this thesis.

The properties of the pd ligand are highly attractive for the synthesis of lanthanide multimetallics, due to the asymmetric nature of its coordination sites, and multiple accessible oxidation states. No examples of lanthanide heteromultimetallic complexes containing a tunable bridging ligand are known. Development of a complex containing such an environment would allow study of how conjugation affects the cooperativity and interactivity of lanthanide ions in the two coordination sites of the ligand.

1.6 Scope of the thesis

The goal of this thesis is to develop a new synthesis of lanthanide heterobimetallics, using lanthanide reagents which are selective to the different binding sites of the pd bridging ligand. This synthesis will select coordination reagents which are designed such that each will only coordinate either the *N,N'* site or the *O,O'* site. If those individual components can be controlled so that they are kinetically inert under the conditions of the reaction, this will constitute a new technique combining kinetic and thermodynamic control. It will be flexible, able to accommodate any combination of lanthanides, and in principle applicable to any asymmetric bridging ligand. This will allow the investigation of a whole range of new systems for magnetic and luminescent properties. For pd specifically, it will allow the first synthesis of a radical-bridged lanthanide heteromultimetallic complex, in which the lanthanides are linked directly for the first time by a partially conjugated ligand.

To this end, Chapter 2 describes the synthesis of a series of monometallic lanthanide complexes of pd $Ln(hfac)_3$(*N,N'*-pd) **1-Ln**, establishing that $Ln(hfac)_3$ selectively coordinates to the *N,N'* coordination site of pd in the neutral oxidation state. A redox process is also performed on the ligand while coordinated to a lanthanide, synthesising *d-f* heterobimetallics $Ln(hfac)_3$(*N,N'-O,O'*-pd)$V(Cp)_2$ **2-Ln**, containing the ligand in the 2- oxidation state. Chapter 3 describes the synthesis of the first molecular example of the radical anion of pd by reaction of pd with $CoCp_2$ to form $[CoCp_2]^+[pd]^{-\bullet}$ **3**. The lanthanide coordination properties of the ligand are investigated in the radical oxidation state. The coordination reagents $Ln(hfac)_3(THF)_2$ **4-Ln** are synthesised, and are shown to be selective to the *N,N'* binding site, forming lanthanide radical compounds $[CoCp_2]^+[Ln(hfac)_3$(*N,N'*-pd)$]^{-\bullet}$ **5-Ln**. In Chapter 4, the photophysical properties of the lanthanide compounds of pd described in Chapters 2 and 3 are investigated. The dependence of their photoluminescent properties on the coordination environment is probed, and initial results indicate that energy transfer processes could be investigated using a modular system. Chapter 5 details preliminary work investigating transmetallation reactivity of $[CoCp_2]^+[pd]^{-\bullet}$ towards the synthesis of lanthanide heterobimetallics. A variety of reagents are investigated with this goal. Organometallic reagents $Ln(Cp^t)_2(OTf)_2K$ **6-Ln** are synthesised and fully characterised, and scorpionates $Ln(Tp^*)_2(OTf)$. Chapter 6 builds on the work in the previous chapter, demonstrating the selectivity of the transmetallation reagent $Ln(Tp)_2(OTf)$ **7-Ln** to the *O,O'* binding site of pd.

Reaction of **7-Ln** with **5-Ln** results in ligand redistribution, producing $Ln(Tp)_2(hfac)$. Some crystallisations of the products produced by this metathesis reaction result in the supramolecular square complex $\{Ln(hfac)_2(N,N'\text{-}O,O'\text{-pd})\}_4$. Reaction of **7-Ln** with **3**, however, selectively coordinates **7-Ln** to the *O,O'* binding site of the pd ligand, synthesising $Ln(Tp)_2(O,O'\text{-pd})$ **8-Ln**. Finally, **8-Ln** is reacted *in situ* with **4-Ln**, which selectively coordinates to the *N,N'* binding site of pd to successfully synthesise lanthanide heterobimetallics $Ln(hfac)_3(N,N'\text{-}O,O'\text{-pd})Ln'(Tp)_2$ **9-LnLn'**.

1.7 References

1. J. P. Costes, F. Dahan, A. Dupuis, S. Lagrave and J. P. Laurent, *Inorg. Chem.*, 1998, **37**, 153-155.
2. J.-P. Costes and F. Nicodème, *Chem. Eur. J.*, 2002, **8**, 3442-3447.
3. J.-P. Costes, F. Dahan and F. Nicodème, *Inorg. Chem.*, 2003, **42**, 6556-6563.
4. D. Aguilà, L. A. Barrios, V. Velasco, O. Roubeau, A. Repollés, P. J. Alonso, J. Sesé, S. J. Teat, F. Luis and G. Aromí, *J. Am. Chem. Soc.*, 2014, **136**, 14215-14222.
5. V. Velasco, L. A. Barrios, M. Schütze, O. Roubeau, F. Luis, S. J. Teat, D. Aguilà and G. Aromí, *Chem. Eur. J.*, 2019, **25**, 15228-15232.
6. L. Abad Galán, D. Aguilà, Y. Guyot, V. Velasco, O. Roubeau, S. J. Teat, M. Massi and G. Aromí, *Chem. Eur. J.*, 2021, **n/a**.
7. N. André, R. Scopelliti, G. Hopfgartner, C. Piguet and J.-C. G. Bünzli, *Chem. Commun.*, 2002, DOI: 10.1039/B109065H, 214-215.
8. N. André, T. B. Jensen, R. Scopelliti, D. Imbert, M. Elhabiri, G. Hopfgartner, C. Piguet and J.-C. G. Bünzli, *Inorg. Chem.*, 2004, **43**, 515-529.
9. T. B. Jensen, R. Scopelliti and J.-C. G. Bünzli, *Inorg. Chem.*, 2006, **45**, 7806-7814.
10. N. Dalla-Favera, J. Hamacek, M. Borkovec, D. Jeannerat, G. Ercolani and C. Piguet, *Inorg. Chem.*, 2007, **46**, 9312-9322.
11. S. Faulkner and S. J. A. Pope, *J. Am. Chem. Soc.*, 2003, **125**, 10526-10527.
12. T. J. Sørensen and S. Faulkner, *Acc. Chem. Res.*, 2018, **51**, 2493-2501.
13. C. D. Buch, S. H. Hansen, D. Mitcov, C. M. Tram, G. S. Nichol, E. K. Brechin and S. Piligkos, *Chem. Sci.*, 2021, **12**, 6983-6991.
14. E. Kreidt, W. Leis and M. Seitz, *Nat. Commun.*, 2020, **11**, 1346.
15. T. Gross, F. Chevalier and J. S. Lindsey, *Inorg. Chem.*, 2001, **40**, 4762-4774.
16. J. J. Le Roy, J. Cremers, I. A. Thomlinson, M. Slota, W. K. Myers, P. H. Horton, S. J. Coles, H. L. Anderson and L. Bogani, *Chem. Sci.*, 2018, **9**, 8474-8481.
17. M. S. Tremblay and D. Sames, *Chem. Commun.*, 2006, **39**, 4116-4118.
18. R. C. Knighton, L. K. Soro, T. Troadec, V. Mazan, A. M. Nonat, M. Elhabiri, N. Saffon-Merceron, S. Djenad, R. Tripier and L. J. Charbonnière, *Inorg. Chem.*, 2020, **59**, 10311-10327.
19. A. Nonat, S. Bahamyirou, A. Lecointre, F. Przybilla, Y. Mély, C. Platas-Iglesias, F. Camerel, O. Jeannin and L. J. Charbonnière, *J. Am. Chem. Soc.*, 2019, **141**, 1568-1576.
20. N. Souri, P. Tian, C. Platas-Iglesias, K.-L. Wong, A. Nonat and L. J. Charbonnière, *J. Am. Chem. Soc.*, 2017, **139**, 1456-1459.
21. G. Bao, K.-L. Wong, D. Jin and P. A. Tanner, *Light Sci. Appl.*, 2018, **7**, 96.
22. M. P. Placidi, A. J. L. Villaraza, L. S. Natrajan, D. Sykes, A. M. Kenwright and S. Faulkner, *J. Am. Chem. Soc.*, 2009, **131**, 9916-9917.

23. M. Tropiano, A. M. Kenwright and S. Faulkner, *Chem. Eur. J.*, 2015, **21**, 5697-5699.

24. R. D. Shannon, *Acta Crystallogr. Sect. A*, 1996, **32**, 751-767.

25. S. Demir, M. I. Gonzalez, L. E. Darago, W. J. Evans and J. R. Long, *Nat. Commun.*, 2017, **8**, 2144.

26. J. D. Rinehart, M. Fang, W. J. Evans and J. R. Long, *J. Am. Chem. Soc.*, 2011, **133**, 14236-14239.

27. J. D. Rinehart, M. Fang, W. J. Evans and J. R. Long, *Nat. Chem.*, 2011, **3**, 538.

28. C. A. P. Goodwin, F. Ortu, D. Reta, N. F. Chilton and D. P. Mills, *Nature*, 2017, **548**, 439.

29. F.-S. Guo, B. M. Day, Y.-C. Chen, M.-L. Tong, A. Mansikkamäki and R. A. Layfield, *Angew. Chem. Int. Ed.*, 2017, **56**, 11445-11449.

30. D. A. Atwood, ed., *The Rare Earth Elements - Fundamentals and Applications*, Wiley, Chichester, 2012.

31. D. W. Smith, *J. Chem. Educ.*, 1986, **63**, 228.

32. M. R. MacDonald, J. E. Bates, M. E. Fieser, J. W. Ziller, F. Furche and W. J. Evans, *J. Am. Chem. Soc.*, 2012, **134**, 8420-8423.

33. M. R. MacDonald, J. E. Bates, J. W. Ziller, F. Furche and W. J. Evans, *J. Am. Chem. Soc.*, 2013, **135**, 9857-9868.

34. M. R. MacDonald, J. W. Ziller and W. J. Evans, *J. Am. Chem. Soc.*, 2011, **133**, 15914-15917.

35. T. Rajeshkumar and G. Rajaraman, *Chem. Commun.*, 2012, **48**, 7856-7858.

36. M. C. Heffern, L. M. Matosziuk and T. J. Meade, *Chem. Rev.*, 2014, **114**, 4496-4539.

37. T. Koullourou, L. S. Natrajan, H. Bhavsar, Pope, J. Feng, J. Narvainen, R. Shaw, E. Scales, R. Kauppinen, A. M. Kenwright and S. Faulkner, *J. Am. Chem. Soc.*, 2008, **130**, 2178-2179.

38. D. Errulat, R. Marin, D. A. Gálico, K. L. M. Harriman, A. Pialat, B. Gabidullin, F. Iikawa, O. D. D. Couto, J. O. Moilanen, E. Hemmer, F. A. Sigoli and M. Murugesu, *ACS Cent. Sci.*, 2019, **5**, 1187-1198.

39. F. Wang, D. Banerjee, Y. Liu, X. Chen and X. Liu, *Analyst*, 2010, **135**, 1839-1854.

40. C. F. Gainer, G. S. Joshua, C. R. De Silva and M. Romanowski, *J. Mater. Chem.*, 2011, **21**, 18530-18533.

41. Y. Lu, J. Zhao, R. Zhang, Y. Liu, D. Liu, E. M. Goldys, X. Yang, P. Xi, A. Sunna, J. Lu, Y. Shi, R. C. Leif, Y. Huo, J. Shen, J. A. Piper, J. P. Robinson and D. Jin, *Nat. Phot.*, 2014, **8**, 32-36.

42. O. Kıbrıslı, N. Vahedigharehchopogh, A. E. Ersundu and M. Çelikbilek Ersundu, *J. of Phys. Chem. C*, 2020, **124**, 10687-10695.

43. C. Piguet, A. F. Williams and G. Bernardinelli, *Angew. Chem. Int. Ed.*, 1992, **31**, 1622-1624.

44. C. Piguet, J. C. G. Buenzli, G. Bernardinelli, G. Hopfgartner and A. F. Williams, *J. Am. Chem. Soc.*, 1993, **115**, 8197-8206.

45. J.-C. G. Bünzli and C. Piguet, *Chem. Rev.*, 2002, **102**, 1897-1928.

46. D. Aguilà, L. A. Barrios, F. Luis, A. Repollés, O. Roubeau, S. J. Teat and G. Aromí, *Inorg. Chem.*, 2010, **49**, 6784-6786.

47. C. D. Buch, D. Mitcov and S. Piligkos, *Dalton Trans.*, 2020, **49**, 13557-13565.

48. A. Y. Girgis, Y. S. Sohn and A. L. Balch, *Inorg. Chem.*, 1975, **14**, 2327-2331.

49. G. A. Fox, S. Bhattacharya and C. G. Pierpont, *Inorg. Chem.*, 1991, **30**, 2895-2899.

50. F. Calderazzo, F. Marchetti, G. Pampaloni and V. Passarelli, *J. Chem. Soc., Dalton Trans.*, 1999, DOI: 10.1039/A906016B, 4389-4396.

51. F. Calderazzo, G. Pampaloni and V. Passarelli, *Inorg. Chim. Acta*, 2002, **330**, 136-142.

52. W. Paw and R. Eisenberg, *Inorg. Chem.*, 1997, **36**, 2287-2293.

53. N. M. Shavaleev, L. P. Moorcraft, S. J. A. Pope, Z. R. Bell, S. Faulkner and M. D. Ward, *Chem. Commun.*, 2003, **10**, 1134-1135.

54. M. Shavaleev Nail, P. Moorcraft Lucy, J. A. Pope Simon, R. Bell Zöe, S. Faulkner and D. Ward Michael, *Chem. Eur. J.*, 2003, **9**, 5283-5291.

55. S. Demir, J. M. Zadrozny, M. Nippe and J. R. Long, *J. Am. Chem. Soc.*, 2012, **134**, 18546-18549.

56. S. Demir, M. Nippe, M. I. Gonzalez and J. R. Long, *Chem. Sci.*, 2014, **5**, 4701-4711.

57. B. S. Dolinar, S. Gomez-Coca, D. I. Alexandropoulos and K. R. Dunbar, *Chem. Commun.*, 2017, **53**, 2283-2286.

58. A. Gould Colin, E. Darago Lucy, I. Gonzalez Miguel, S. Demir and R. Long Jeffrey, *Angew. Chem. Int. Ed.*, 2017, **56**, 10103-10107.

59. S. Hohloch, J. R. Pankhurst, E. E. Jaekel, B. F. Parker, D. J. Lussier, M. E. Garner, C. H. Booth, J. B. Love and J. Arnold, *Dalton Trans.*, 2017, **46**, 11615-11625.

60. J. Yuasa, T. Suenobu and S. Fukuzumi, *J. Phys. Chem. A*, 2005, **109**, 9356-9362.

61. J. R. Hickson, S. J. Horsewill, J. McGuire, C. Wilson, S. Sproules and J. H. Farnaby, *Chem. Commun.*, 2018, **54**, 11284-11287.

62. E. K. Brechin, L. Calucci, U. Englert, L. Margheriti, G. Pampaloni, C. Pinzino and A. Prescimone, *Inorg. Chim. Acta*, 2008, **361**, 2375-2384.

63. C. A. Goss and H. D. Abruna, *Inorg. Chem.*, 1985, **24**, 4263-4267.

64. S. Berger, J. Fiedler, R. Reinhardt and W. Kaim, *Inorg. Chem.*, 2004, **43**, 1530-1538.

65. D. M. Murphy, K. McNamara, P. Richardson, V. Sanchez-Romaguera, R. E. P. Winpenny and L. J. Yellowlees, *Inorg. Chim. Acta*, 2011, **374**, 435-441.

2 The synthesis of lanthanide complexes and d-f heterobimetallic complexes utilising the redox-active ligand 1,10-phenanthroline-5,6-dione.

Publications:

The following publication reports work detailed in this chapter:
J. R. Hickson, S. J. Horsewill, C. Bamforth, J. McGuire, C. Wilson, S. Sproules and J. H. Farnaby, *Dalton Trans.*, 2018, **47**, 10692-10701.

2.1 Abstract

The lanthanide coordination chemistry of the redox active bridging ligand 1,10-phenanthroline-5,6-dione (pd) ligand has been investigated. Compounds Ln(hfac)$_3$(*N,N'*-pd) (**1-Ln**, Ln = Y, Eu, Gd, Tb, Yb) were synthesised by a robust one-pot synthesis and have been fully characterised by ^{1}H and ^{19}F NMR, ATR-IR, UV-vis and EPR spectroscopy and Evans method magnetometry. The solid-state molecular structures of **1-Ln** were determined by X-ray crystallography and except for **1-Yb** display different binding modes when crystallised from Et_2O or from toluene.[1-3] Compounds **1-Ln** are unusually coloured, and analysis of the UV-vis spectra showed that the intensity of a transition with λ_{max} = 600 nm is highly dependent on the lewis acidity and ionic radius of the lanthanide bound to the *N,N'* binding site. Trends in the magnitude and sign of the paramagnetic shift tensors in the ^{1}H and ^{19}F NMR spectra of **1-Ln** were identified. The reactivity of the resulting compounds with reducing vanadocenes was probed. The synthesis of *d-f* bimetallic compounds Ln(hfac)$_3$(*N,N'-O,O'*-pd)V(Cp^R)$_2$ (**2-Ln**: Ln = Y, Gd; Cp^R = Cp. **2a-Gd**: Ln = Gd; Cp^R = Cp^t) by reaction of **1-Ln** with V(Cp)$_2$ was carried out, and **2-Ln** and **2a-Gd** are fully characterised by ATR-IR, UV-vis and EPR spectroscopy and Evans method magnetometry.[1, 2] A combination of ATR-IR, EPR and Evans method magnetometry indicated that the vanadocene undergoes a two-electron oxidative addition to the *O,O'* site of the pd ligand, resulting in the ligand being in the pd^{2-} oxidation state. The solid-state molecular structures of **2-Ln** have also been determined by single crystal X-ray crystallography, confirming the selective coordination of Ln to the *N,N'* site and V to the *O,O'* site.

2.2 Synthesis of $Ln(hfac)_3$(*N,N'*-pd) 1-Ln (Ln = Y, La, Eu, Gd, Tb, Yb)

2.2.1 Starting material selection and synthesis

Early experiments probing the lanthanide coordination chemistry of pd found that coordinating the lanthanide ion with a highly solubilising ancillary ligand was necessary, in order to avoid insoluble coordination polymer formation.[1] The β-diketonate ligand hexafluoro acetylacetonate (hfac) was chosen as it is both highly solubilising and relatively redox inert. The ligand can also be used as a ^{19}F NMR spectroscopic handle. It is well-documented that diketonates form eight-coordinate complexes with the lanthanides.[4-6] In particular, in lanthanide *tris*-diketonate compounds coordinated solvent molecules can be easily displaced by chelating agents such as phenanthroline or bipyridine to form saturated eight-coordinate complexes with lanthanides.[7-10] The synthesis of K(hfac) was performed by the deprotonation of hexafluoroacetyl acetone with potassium hydride in THF at low temperature, obtaining K(hfac) in moderate yield (54%).

The lanthanide triflate salts $Ln(OTf)_3$ are frequently used as Lewis acid catalysts.[11] They were selected as the lanthanide source for this work due to their facile synthesis from the oxide, and their ease of dehydration (10^{-3} mbar, 18 h, 200 °C), when compared to lanthanide chlorides. The most commonly used method for dehydration of lanthanide chlorides involves heating to 300 °C with ammonium chloride under high vacuum, though other methods have been used,[12] and while anhydrous lanthanide chlorides are available commercially they are expensive. The direct synthesis of $Ln(hfac)_3$(glyme) (glyme = a range of chelating polyethers of varied length and denticity, including dimethoxyethane) from Ln_2O_3 has been reported. However, the chelating polyethers used in this synthesis to avoid aggregation might interfere with the coordination chemistry. Lanthanide triflates $Ln(OTf)_3$ were prepared by refluxing Ln_2O_3 (Ln = Y, La, Eu, Gd, Yb) with 6.6 eq. trifluoromethane sulfonic acid (triflic acid) at 100 °C overnight. After removal of water by rotary evaporation, the excess acid was removed by washing with Et_2O (dissolution of a small quantity of the solid in deionised water allowed pH determination by pH paper), and the white solids were finally dehydrated by drying overnight at 200 °C under vacuum (at 10^{-3} mbar) (Ln = Sc, 88%; Y, 88%; La, 83%; Ce, 74%; Eu, 54%; Gd, 71%; Yb, 57%). $Tb(OTf)_3.(H_2O)_x$ was purchased and dehydrated by the same method. In all cases, complete dehydration of $Ln(OTf)_3$ was confirmed by ATR-IR spectroscopy, where no

characteristically intense O-H stretching frequency of H_2O was observed in the region of 3300 cm^{-1}.

The ligand 1,10-phenanthroline-5,6-dione (pd) was synthesised by a modified version of the synthesis described by Yamada and co-workers.[13] In a round-bottomed flask, 1,10-phenanthroline and KBr were mixed with frozen sulfuric acid, then nitric acid was added dropwise through a reflux condenser. The reaction was then gradually warmed to room temperature with stirring, then heated to reflux. Upon heating, bromine gas was evolved, and the reaction was heated until gas evolution was complete. The solution was then cooled to room temperature and poured over ice. Excess acid was neutralised with sodium bicarbonate, keeping the mixture cold by adding further ice if necessary, and pd was extracted into dichloromethane. Solvent was then removed from the yellow dichloromethane solution by rotary evaporation, and pd was obtained as a bright yellow solid. The solid was washed with methanol, then dried *in vacuo* overnight to obtain pd as a yellow solid in good yield (81%).

The characterisation of pd was undertaken by ^{1}H NMR spectroscopy in both *d*-chloroform and in d_3-acetonitrile. In *d*-chloroform, pd exhibits three resonances at δ = 7.69 (dd, J = 7.9, 4.7 Hz), 8.50 (dd, J = 7.9, 1.9 Hz), 9.12 (dd, J = 4.7, 1.8 Hz) ppm, each integrating to 2 protons. Similarly, in d_3-acetonitrile, three resonances are observed at δ = 7.62 (dd, J = 7.8, 4.7 Hz), 8.42 (dd, J = 7.8, 1.8 Hz) and 9.03 (dd, J = 4.7, 1.8 Hz) ppm. The expected dd, dd, dd splitting pattern is observed for the three distinct and adjacent aromatic protons. The most deshielded resonance (9.03 ppm in d_3-acetonitrile) is assigned to the proton environment closer to the diketone moiety of the ligand (C(3,8)), and the second most deshielded proton (8.42 ppm) is assigned to the proton environment adjacent to the diimine moiety (C(1,10)). The resonance at 7.62 ppm is assigned to the middle proton (C(2,9)). These assignments are consistent with the magnitude of the coupling constants observed.

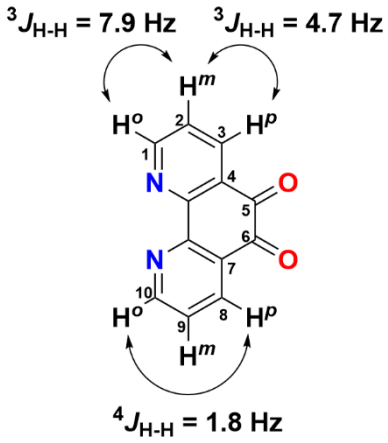

Figure 2.1: Numbering scheme for pd and coupling constants observed by ^{1}H NMR in d_3-MeCN.

2.2.2 Synthesis of Ln(hfac)$_3$(*N,N'*-pd) 1-Ln (Ln = Y, Eu, Gd, Tb, Yb)

Using these starting materials, the *N,N'*-coordinated complexes Ln(hfac)$_3$(*N,N'*-pd) **1-Ln** (Ln = Y, Eu, Gd, Tb, Yb) were synthesised by the one-pot reaction of Ln(OTf)$_3$ (Ln = Y, Eu, Gd, Tb, Yb) with 3 eq. K(hfac) and pd (Scheme 2.1) in good yields.[1-3] The synthesis has been optimised from that reported in our initial publication by the addition of a further purification step by recrystallisation.[2] In a typical preparation, THF was added to a dry mixture of Ln(OTf)$_3$, K(hfac) (3 eq.) and pd (1 eq.) at -78 °C with stirring. An immediate colour change from yellow to green was observed upon addition of THF, and after stirring for 1 hour THF was removed *in vacuo* from the green solution. Toluene was used to extract **1-Ln** from the green solids, with filtration by filter cannula to exclude K(OTf), resulting in a green or yellow solution depending on the lanthanide. The solution was reduced *in vacuo* to saturation and cooled to -15 °C overnight, whereupon small green crystals formed. After decanting the supernatant *via* narrow-bore cannula, it was again concentrated to half volume and cooled to -15 °C to obtain a second crop of crystals. Both sets of crystals were washed with hexanes, then dried *in vacuo*, to attain **1-Ln** as pale green (Ln = Y, Eu, Gd, Tb) or yellow (Ln = Yb) solids in good to excellent yields (Ln = Y, 81%; Eu, 81 %; Gd, 79%; Tb, 67%; Yb; 64%).[1-3] Elemental analysis of **1-Ln** (Ln = Y, Gd, Tb, Yb) was consistent with the 1:1 adduct, formulated as Ln(hfac)$_3$(pd), while analysis of **1-Eu** was consistent with the presence of 1 eq. co-crystallised toluene as Eu(hfac)$_3$(pd).(Tol).

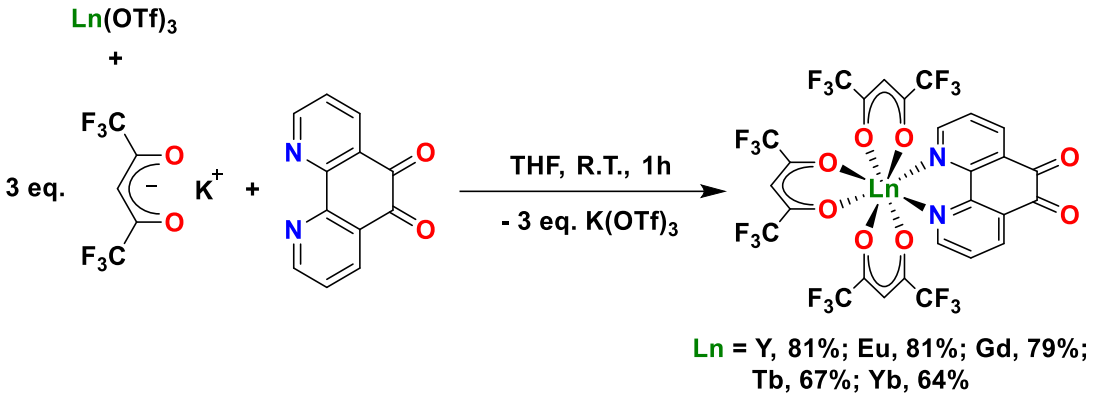

Scheme 2.1: The one-pot synthesis of *N,N'*-coordinated pd complexes 1-Ln Ln(hfac)$_3$(*N,N'*-pd) (Ln = Y, Eu, Gd, Tb, Yb).[1-3]

It is worth noting that the solubility of **1-Ln** is dependent on the solvent from which they were crystallised. Solubility is high for all **1-Ln** in polar solvents such as Et_2O or THF. However, for Ln = Y, Eu and Gd, after crystallisation from toluene, the solid does not readily re-dissolve in toluene. Full dissolution is, however, vital for understanding of solution concentrations, and therefore for investigation of the solution and solid-state behaviour of **1-Ln**, as discussed in Chapter 4. Therefore, if **1-Ln** is first dissolved in Et_2O, then Et_2O is removed entirely *in vacuo*, subsequent solubility in toluene can be increased significantly. This observation may be explained by the observed differences in solid-state molecular structures when crystallised from different solvents (see Section 2.2.7).

2.2.3 NMR spectroscopy of 1-Ln

For interpretation of the paramagnetic NMR spectra of **1-Ln** (Ln = Eu, Tb, Yb), it is useful first to understand the NMR spectra of the diamagnetic **1-Y**.[1, 2] The ^{1}H NMR spectrum of **1-Y** was recorded in d_3-acetonitrile and in d_6-benzene at room temperature, and each spectrum displays four resonances. In d_3-acetonitrile, resonances are observed at δ = 6.22 (s, 3H), 7.93 (dd, J = 7.9, 5.3 Hz, 2H), 8.69 (d, J = 8.0 Hz, 2H) and 9.22 (d, J = 4.3 Hz, 2H) ppm, with an integral ratio of 3:2:2:2 (Figure 2.5). A low intensity resonance is observed at δ = 6.13 ppm. These data are consistent with the 1:1 adduct, containing three hfac ligands and pd. The deprotonated hfac ligand has a single proton, which in the free ligand is observed as a singlet at δ = 5.53 ppm (recorded in d_3-acetonitrile). This is shifted upfield in **1-Y** to the resonance observed at δ = 6.22 ppm, consistent with hfac binding to the metal centre. The ^{19}F{^{1}H} NMR spectrum of **1-Y**, recorded in d_3-acetonitrile at room temperature exhibited a single resonance at δ = -

77.58 ppm (Figure 2.4). This resonance is assigned to the CF_3 groups of the hfac ligand and is shifted slightly compared to the ^{19}F NMR resonance of K(hfac), which is observed in d_3-acetonitrile at δ = -77.36 ppm, again consistent with coordination to yttrium.

The pd ligand has three magnetically inequivalent proton environments. As discussed in Section 2.2.1, these are observed in the free ligand at δ = 7.62 (dd, J = 7.8, 4.7 Hz, 2H, C(2,9)-**H**), 8.42 (dd, J = 7.8, 1.8 Hz, 2H, C(1,10)-**H**), 9.03 (dd, J = 4.7, 1.8 Hz, 2H, C(3,8)-**H**) ppm (recorded in d_3-acetonitrile). The chemical shifts of these resonances are shifted downfield to δ = 7.93 (dd, J = 7.9, 5.2 Hz, 2H, C(2,9)-**H**), 8.69 (d, J = 8.0 Hz, 2H, C(1,10)-**H**) and 9.22 (d, J = 4.5 Hz, 2H, C(3,8)-**H**) ppm on coordination of yttrium to pd in **1-Y**. The coupling constants observed (shown in Figure 2.2) are consistent with the assignment of each resonance, with two $^3J_{H\text{-}H}$ couplings observed for the proton in the C(2,9) position and one $^3J_{H\text{-}H}$ observed for those in the C(1,10) and C(3,8) positions (see Figure 2.2). In the ^1H NMR spectrum of **1-Y** as recorded in d_6-benzene, again four resonances are observed at δ = 6.23 (s, 3H), 6.40 (dd, J = 7.9, 5.3 Hz, 2H, C(2,9)-**H**), 7.54 (dd, J = 7.9, 1.7 Hz, 2H, C(1,10)-**H**) and 9.16 (dd, J = 5.3, 1.7 Hz, 2H, C(3,8)-**H**) ppm, and a single resonance is observed in the $^{19}F\{^1H\}$ NMR spectrum at δ = -76.95 ppm. The resonances assigned to the protons at the C(1,10) and C(2,9) positions are shifted upfield in this spectrum compared to in d_3-acetonitrile. In addition to the $^3J_{H\text{-}H}$ coupling observed in d_3-acetonitrile, $^4J_{H\text{-}H}$ coupling is observed in d_6-benzene.

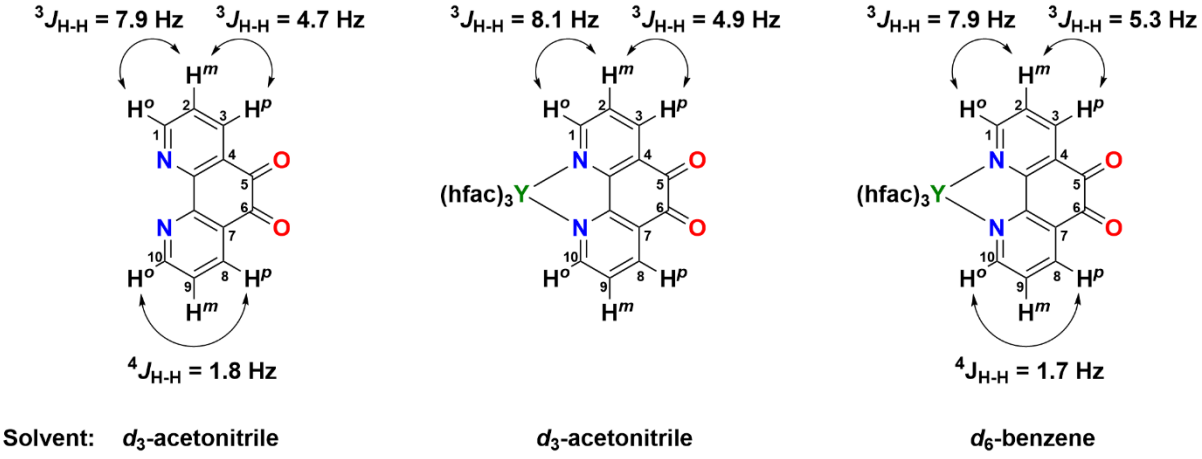

Figure 2.2: The $^3J_{H\text{-}H}$ and $^4J_{H\text{-}H}$ coupling observed in both the free pd ligand and in 1-Y as recorded in d_3-acetonitrile and in 1-Y as recorded in d_6-benzene, showing the various coupling constants between the protons *ortho*, *meta* and *para* to the *N,N'* metal binding site.

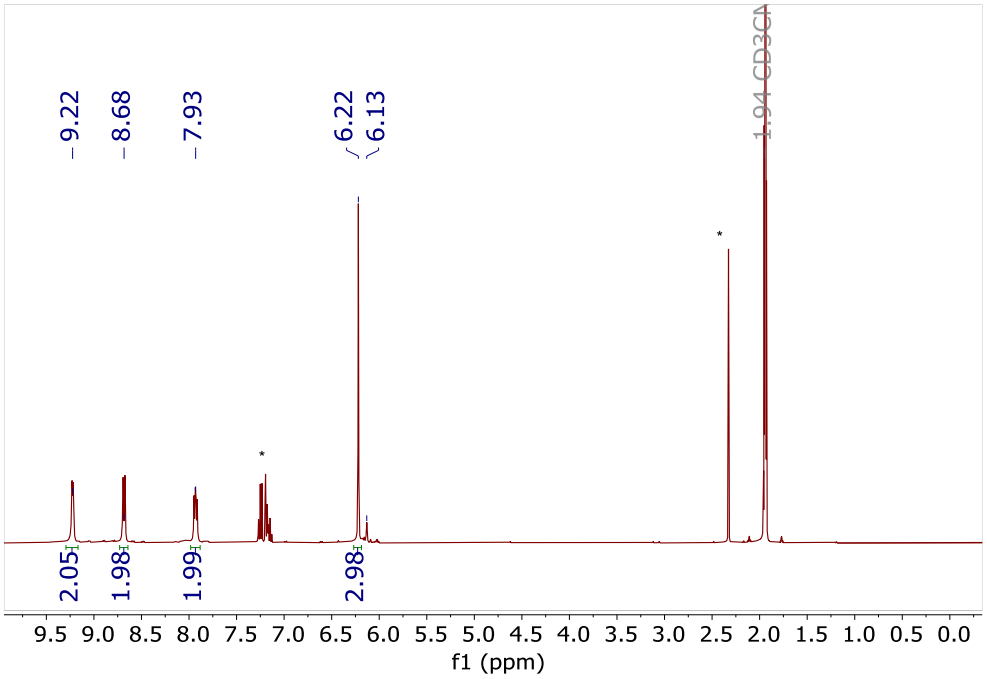

Figure 2.3: The ^{1}H NMR spectrum of 1-Y, recorded in d_3-acetonitrile. Co-crystalised toluene is visible at δ = 2.33 and 7.10-7.25 ppm denoted with *.

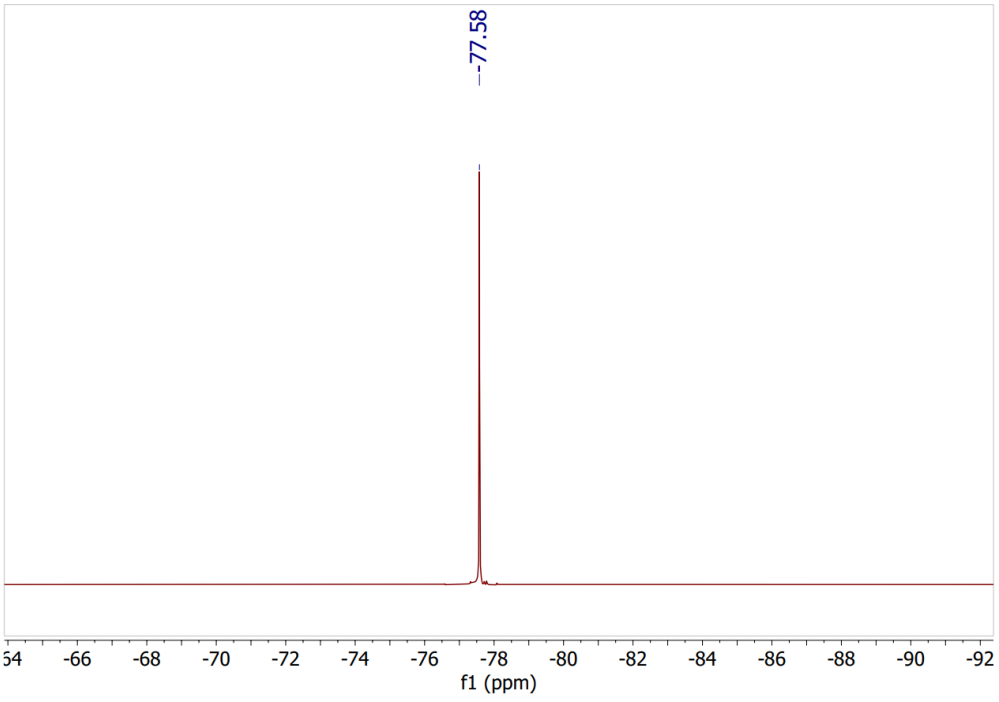

Figure 2.4: The ^{19}F{^{1}H} NMR spectrum of 1-Y, recorded in d_3-acetonitrile.

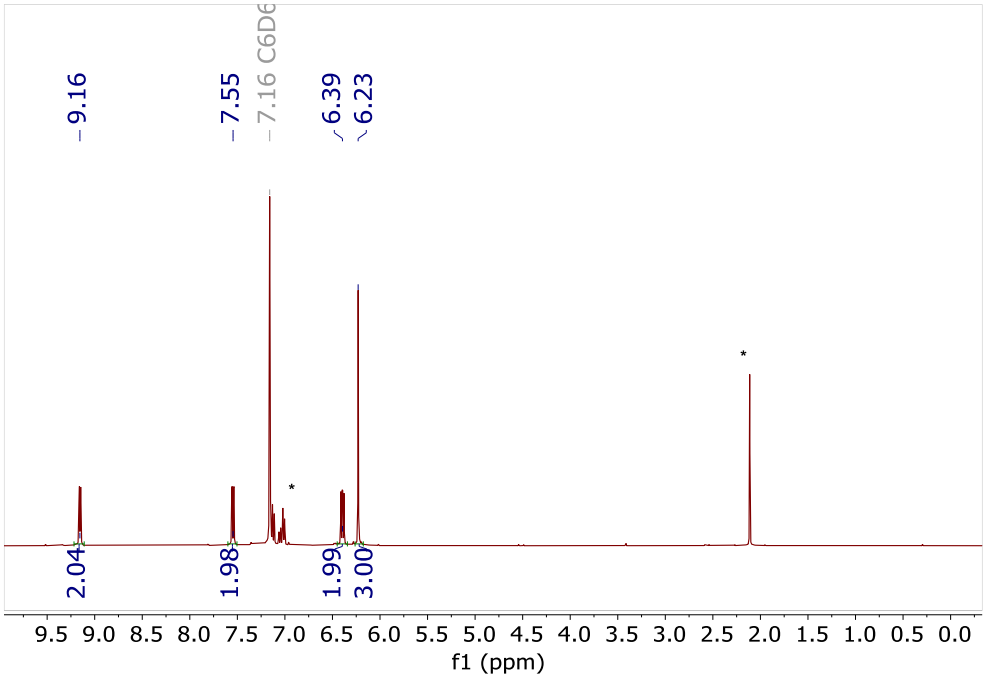

Figure 2.5: The ^{1}H NMR spectrum of 1-Y, recorded in d_6-benzene. Co-crystalised toluene is visible at δ = 2.11 and 7.00-7.12 ppm denoted with *.

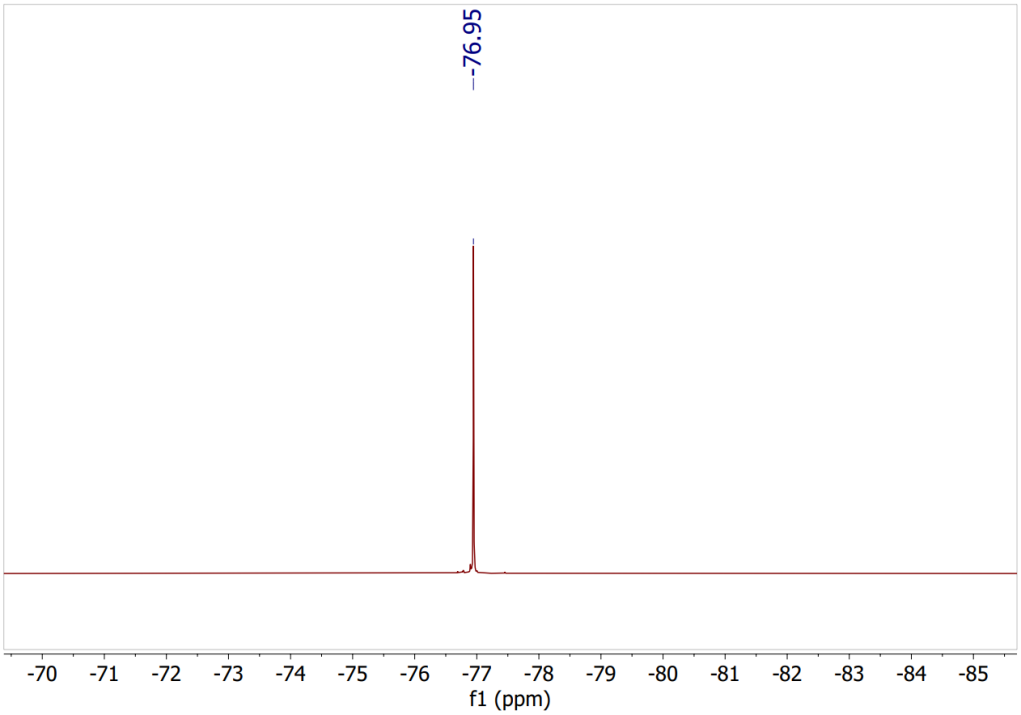

Figure 2.6: The ^{19}F{^{1}H} NMR spectrum of 1-Y, recorded in d_6-benzene.

The paramagnetic lanthanide complexes, **1-Ln** (Ln = Eu, Tb, Yb) were also characterised by ^{1}H and ^{19}F{^{1}H} NMR spectroscopy. Despite the large and complex paramagnetic pseudo-contact shifts (PCS), ^{1}H and ^{19}F NMR spectroscopy are useful tools in analysing the complexation of ligands to lanthanides.[14, 15] The PCS fields of lanthanide complexes have been utilised for the determination of the structures of a variety of large biomolecules in solution.[16-18] Indeed,

recent work combining NMR and either X-ray diffraction (XRD) and extended X-ray absorption fine structure (EXAFS) analysis[15] or photoluminescence spectroscopy[19, 20] with quantum chemical calculations has shown that information such as the crystal field and magnetic easy axis of lanthanide complexes can be extracted with high accuracy from detailed NMR studies. However, it is important to note two points when studying the NMR of paramagnetic compounds. Firstly, that relative integrations may not be quantitative due to the paramagnetically induced relaxation. Secondly and often more noticeably, chemical shifts are dependent on perturbations of the local magnetic field due to the paramagnetic ions (this effect can be described by the PCS field), which can be highly variable depending on the identity of the lanthanide and its coordination environment.

The ^{1}H and ^{19}F{^{1}H} NMR spectra of paramagnetic **1-Ln** (Ln = Eu, Tb, Yb) were recorded in both d_6-benzene and d_3-acetonitrile at room temperature. The ^{1}H NMR spectrum of **1-Eu**, recorded in d_6-benzene, exhibited four resonances at δ = 3.85 (s, 3H), 6.87 (d, 2H), 9.01 (d, 2H), 11.34 (s, 2H) ppm, which integrate in a 3:2:2:2 ratio, consistent with the 1:1 adduct of pd to europium (Figure 2.7). The resonances observed at δ = 6.87, 9.01 and 11.34 ppm are assigned to the pd ligand in **1-Eu**. These resonances are significantly shifted from those observed in the diamagnetic analogue **1-Y** (δ = 6.37 (dd, pd-C(2,9)-**H**), 7.53 (d, pd-C(1,10)-**H**) and 9.16 (d, pd-C(3,8)-**H**) ppm). Interestingly, despite the presence of the paramagnetic Eu(III) ion (ground state $^{7}F_0$), the resonances are still well-defined, and the resonances at δ = 6.87, 9.01 appear resolved as doublets ($^{3}J_{H\text{-}H}$ = 8 Hz). This coupling constant is consistent with that observed for the protons in the C(2,9) and C(3,8) positions of the free pd ligand and of **1-Y** (H^m and H^p in Figure 2.2). The resonances δ = 6.87 and 9.01 are therefore assigned to the protons at the C(2,9) and C(3,8) positions of the pd ligand, though it is not possible to determine which with certainty. Each proton experiences a small paramagnetic shift of between -2.24 and +2.69 ppm (calculated based on the minimum and maximum possible shifts). The resonance at δ = 11.34 ppm is assigned to the proton at the C(1,10) (H^o in Figure 2.2) position, experiencing a slightly larger downfield shift of +3.81 ppm. The resonance observed at δ = 3.85 ppm is a singlet, assigned to the hfac ligand by relative integration, and has been shifted upfield by -2.38 ppm with respect to that observed in **1-Y** (δ = 6.23 (s, 3H, hfac-C**H**) ppm). The ^{19}F{^{1}H} NMR spectrum of **1-Eu**, recorded in d_6-benzene, exhibited a single resonance at δ = -79.30 ppm, consistent with the single hfac environment observed in the ^{1}H NMR spectrum (Figure

2.8). This resonance is shifted upfield by -2.37 ppm compared to the single resonance observed in the $^{19}F\{^{1}H\}$ NMR spectrum of **1-Y** (δ = -76.93 ppm). It is of note that the paramagnetically induced shifts in the NMR spectra of **1-Eu** compared to **1-Y** are not large, this is likely due to the relatively low orbital angular momentum of Eu(III) (Eu(III) is $4f^6$, ground state $^{7}F_0$).

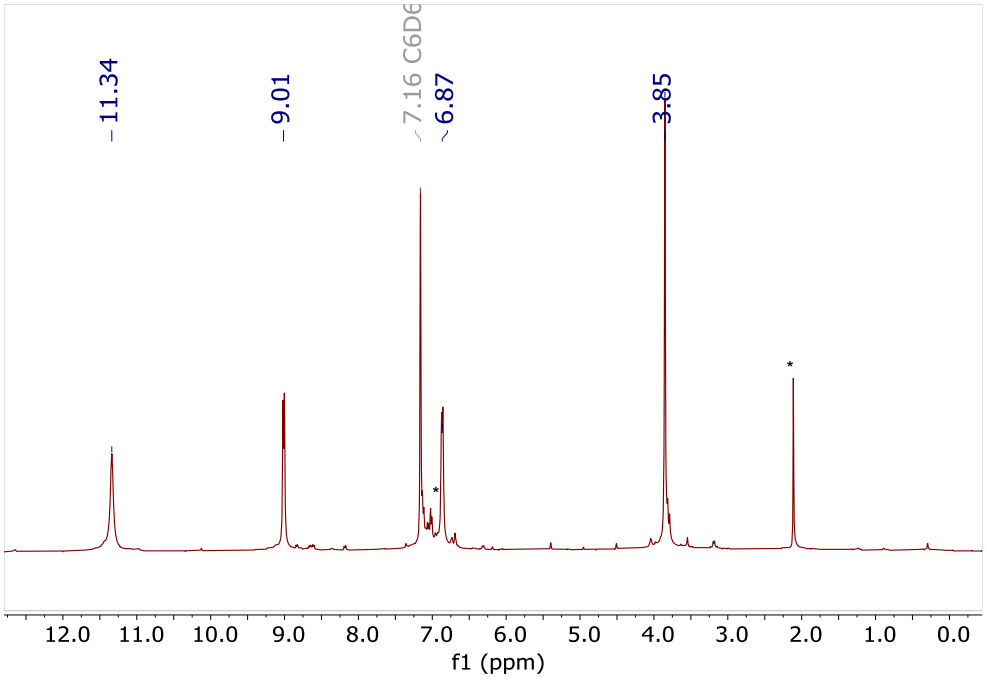

Figure 2.7: ^{1}H NMR spectrum of 1-Eu, recorded in d_6-benzene. Co-crystalised toluene is visible at δ = 2.11 and 7.00-7.12 ppm denoted with *.

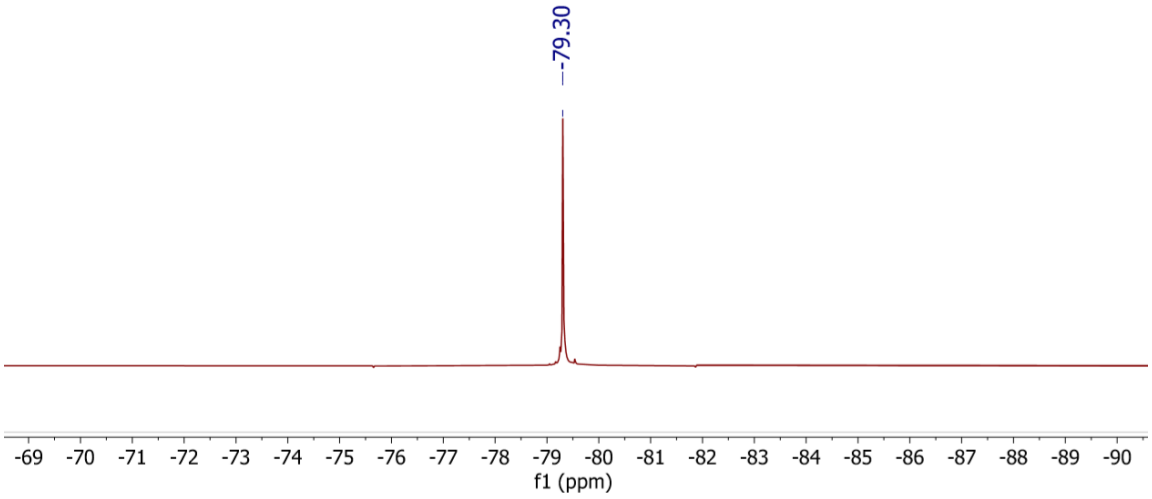

Figure 2.8: $^{19}F\{^{1}H\}$ NMR spectrum of 1-Eu recorded in d_6-benzene.

The ^{1}H and $^{19}F\{^{1}H\}$ NMR spectra of **1-Tb** were recorded in d_6-benzene at room temperature. The ^{1}H NMR spectrum of **1-Tb** (Tb(III) ground state $^{7}F_6$), recorded in d_6-benzene, exhibited four resonances at δ = -178.55, -32.83, -11.68, 103.69 ppm, which integrate in a 2:2:2:3 ratio, consistent with the 1:1 addition of pd to terbium (Figure 2.9). The resonances observed at δ = -178.55, -32.83, -11.68 ppm are assigned on the basis of relative integration to the pd ligand. They are shifted upfield significantly compared to **1-Ln** (Ln = Y, Eu). Unlike in the case of **1-Eu**, no multiplicity is observed due to significant broadening of the resonances induced by the paramagnetic metal centre, which is particularly evident for the resonance observed at δ = -178.55 ppm. The line width at half height of this resonance is difficult to measure due to the low intensity of the resonance, but is in the region of 1000 Hz, compared to 116 and 158 Hz for the resonances at δ = -11.68 and -32.83 ppm respectively. For comparison, the line width at half height for the resonances observed in **1-Y** is between 2 and 2.5 Hz for each resonance. The resonances assigned to the protons of the pd ligand are shifted upfield by between -18 and -186 ppm. The greater paramagnetic shift and broadening indicate a greater interaction with Tb(III), so the resonance at δ = -178.55 ppm is assigned to the proton closest to the *N,N'* binding site, at the C(1,10) positions of pd. The resonances with chemical shifts of δ = -11.68 and -32.83 ppm are assigned to the protons at the C(2,9) and C(3,8) positions and the resonance observed at δ = 103.69 ppm is assigned to the hfac ligands. A significant downfield shift of +96 ppm is observed for the hfac ligands, compared to the resonance assigned to hfac in the ^{1}H NMR spectrum of **1-Y** (δ = 6.23 (s, 3H, hfac-C**H**) ppm). The $^{19}F\{^{1}H\}$ NMR spectrum exhibits a single resonance at δ = -63.32 ppm (Figure 2.10), which is shifted downfield by +14 ppm from the resonance observed in the $^{19}F\{^{1}H\}$ NMR spectrum of **1-Y** (δ = -76.93 ppm).

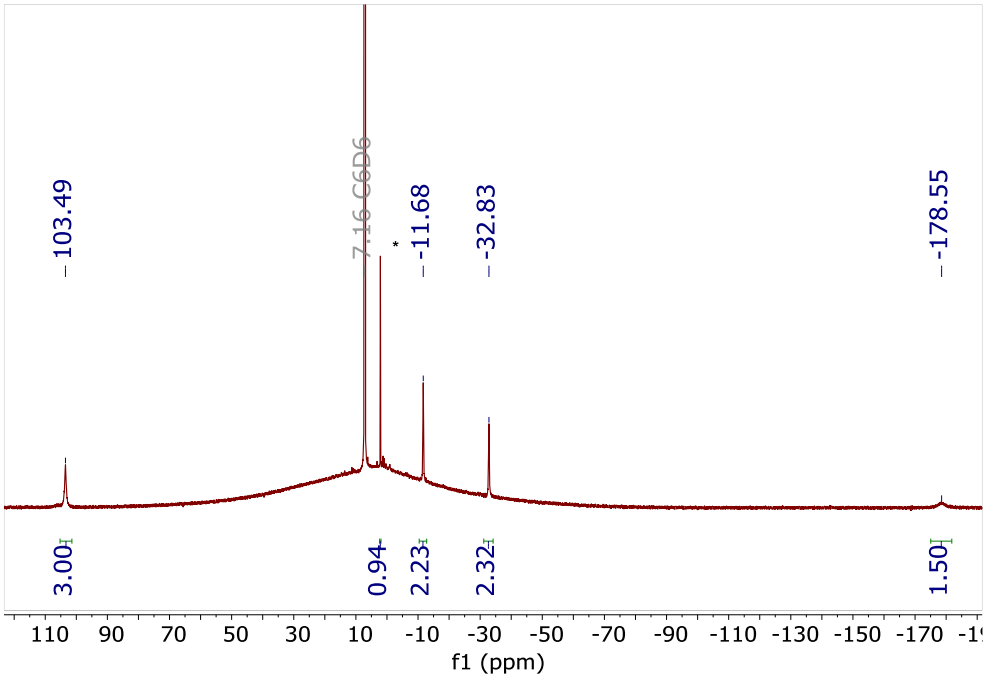

Figure 2.9: The ^{1}H NMR spectrum of 1-Tb recorded in d_6-benzene. Co-crystalised toluene is visible at δ = 2.11 ppm denoted with *.

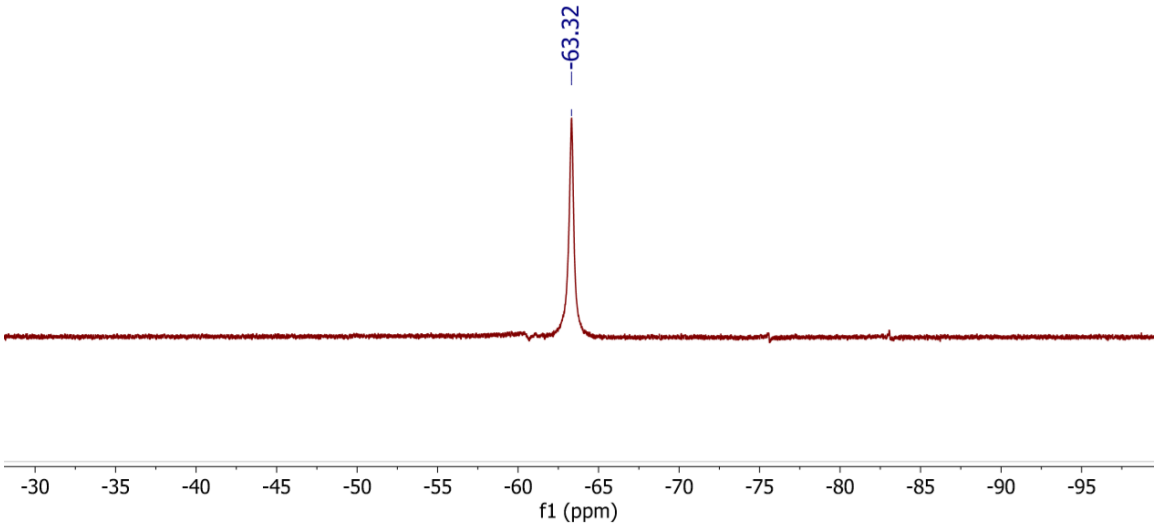

Figure 2.10: The ^{19}F{^{1}H} NMR spectrum of 1-Tb recorded in d_6-benzene.

The ^{1}H NMR spectrum of **1-Yb** (Yb(III) ground state $^{2}F_{7/2}$), recorded in d_6-benzene, exhibited four resonances at δ = -7.00, 9.27, 10.59, 15.19 ppm, which integrate in a 3:2:2:2 ratio, consistent with the 1:1 addition of pd to ytterbium (Figure 2.11). By relative integration, the resonances at δ = 9.27, 10.59, 15.19 ppm are assigned to the pd ligand. A downfield shift of between +1.43 and +8.82 ppm is observed for the protons of the pd ligand, compared to the ^{1}H environments assigned to the pd ligand in **1-Y** (δ = 6.37 (dd, pd-C(2,9)-**H**), 7.53 (d, pd-C(1,10)-**H**) and 9.16 (d, pd-C(3,8)-**H**) ppm). The resonances are so broadened compared to

those in **1-Y** as to preclude any observation of multiplicity. The resonance observed at 9.27 ppm is particularly broad, with a full width at half height of 61 Hz, compared to the resonances at 10.59 and 15.19 ppm, which have a full width at half height of around 12 Hz each. This resonance is therefore tentatively assigned to the proton closest to the *N,N'* binding site, that should be subject to the strongest interaction with the lanthanide ion. The resonances at 10.59 and 15.19 ppm are assigned to the protons of the C(2,9) and C(3,8) positions. The peak observed at δ = -7.00 ppm is assigned to the hfac ligands, and is shifted upfield by -13.00 ppm compared to the hfac ligands in **1-Y** (δ = 6.23 (s, 3H, hfac-C**H**) ppm). The $^{19}F\{^{1}H\}$ NMR spectrum shows a single resonance at δ = -84.42 ppm, which is assigned to the hfac ligands (Figure 2.12). This resonance is shifted upfield by -7.00 ppm compared to that assigned to the hfac ligands in **1-Y** (δ = -76.93 ppm).

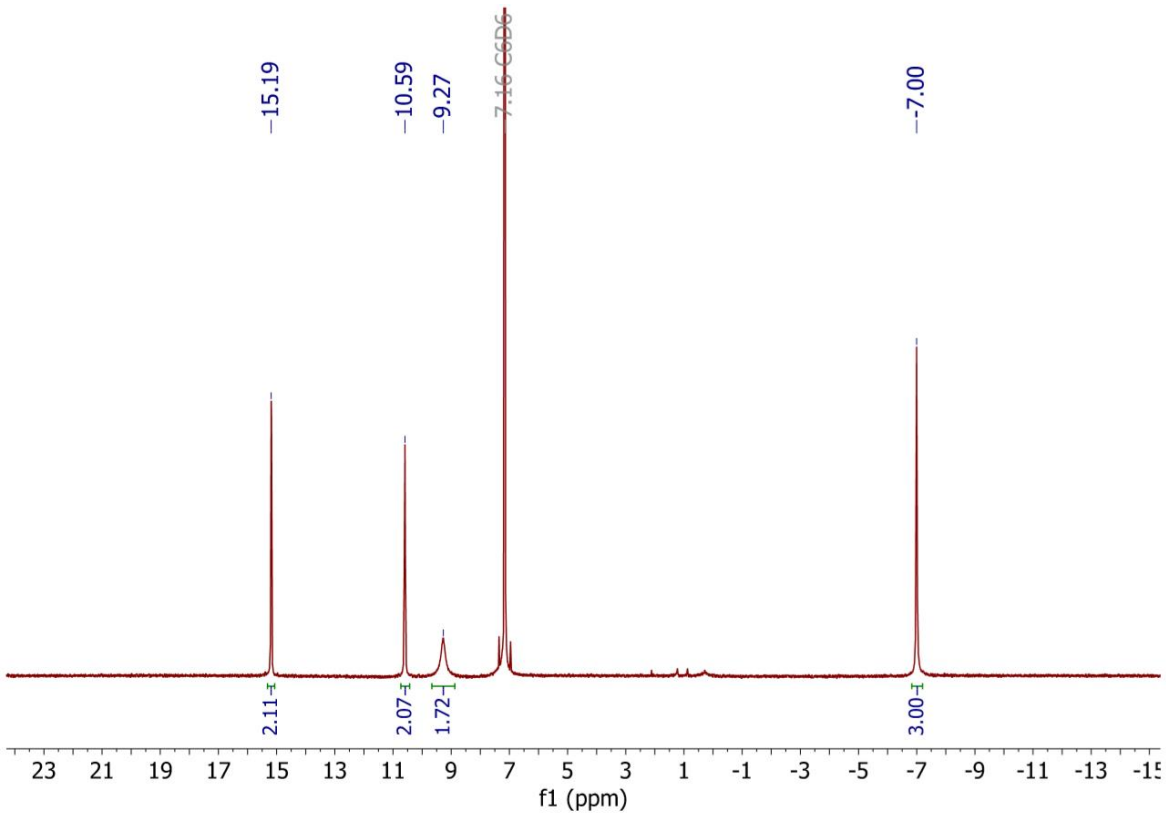

Figure 2.11: The ^{1}H NMR spectrum of 1-Yb recorded in d_6-benzene.

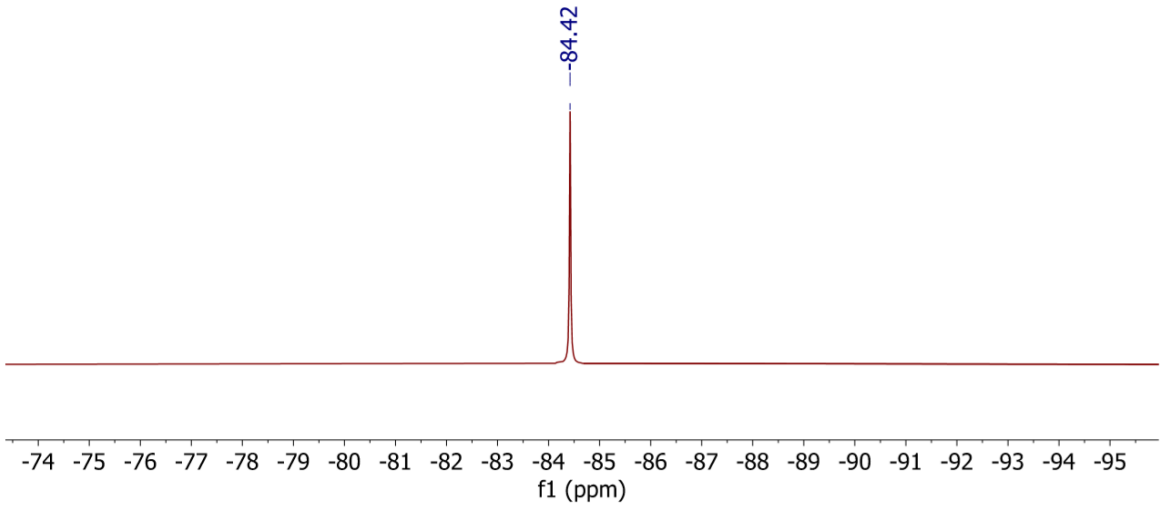

Figure 2.12: The $^{19}F\{^{1}H\}$ NMR spectrum of 1-Yb recorded in d_6-benzene.

Table 2.1 and Table 2.2 list the resonances and the paramagnetically induced shift $\Delta\delta$ as recorded in d_3-acetonitrile, and compared to **1-Y** as a diamagnetic reference for each individual resonance. Since the resonances of the pd-C(2,9) and pd-C(3,8) protons cannot be assigned based on these data, the paramagnetically induced shifts of these protons are given as a range, calculated based on the minimum and maximum possible shifts. Several features are of note in these data. In each **1-Ln**, the paramagnetically induced shifts of the ^{1}H and ^{19}F NMR resonances assigned to the hfac ligands are of the same sign. Additionally, in each **1-Ln**, the sign of the pseudo contact shift, either downfield (positive) or upfield (negative), is opposite for the hfac ligands and for the (1,10) proton resonances of the pd ligand. It is unclear whether this trend holds for the C(2,9) and C(3,8) protons of the pd ligand due to the range of the **1-Eu** stretching between -2.29 and +2.64 ppm. Thirdly, the paramagnetic shifts in **1-Tb** are of a significantly greater magnitude than those in **1-Eu** and **1-Yb**, consistent with the magnitude and anisotropy of the paramagnetic tensor of the Tb(III) ion. Tb(III) has a ground state of $^{7}F_6$, highly anisotropic and with six unpaired electrons, and would therefore be expected to cause significant shifts. The paramagnetic shifts of the various resonances are presented graphically in Figure 2.13. A similar pattern in both the signs and the magnitude of the paramagnetic shift has been observed in the related complexes $Ln(hfac)_3(phen)_2$ (phen = 1,10-phenanthroline) (Ln = Pr, Nd; relative to Ln = La)[21] and $Ln(hfac)_3(phen)$ (Ln = Sm, Eu, Tb, Ho, Er, Yb, relative to Ln = Lu).[21, 22] The authors of that study did note the anomalous behaviour of $Tm(hfac)_3(phen)$, for which the proton environments of the hfac and phenanthroline ligands were both shifted upfield. Similarly again to observations of **1-Ln**,

significantly greater paramagnetic shifts were observed in the spectrum for $Tb(hfac)_3(phen)$ than for $Eu(hfac)_3(phen)$ and $Yb(hfac)_3(phen)$.

Table 2.1: Chemical shift of the various ^1H and ^{19}F NMR resonances in 1-Ln (Ln = Y, Eu, Tb, Yb)

	Chemical Shift (ppm)				
Ln	pd-C(1,10)**H**	pd-C(2,9)**H**, pd-C(3,8)**H**		hfac-C**H**	hfac-C**F**$_3$
Y	7.53	6.37	9.16	6.23	-76.93
Eu	11.34	6.87	9.01	3.85	-79.3
Tb	-178.55	-32.83	-11.68	103.69	-63.32
Yb	9.27	10.59	15.19	-7.00	-84.42

Table 2.2: Paramagnetically induced shift ($\Delta\delta$) for resonances in 1-Eu, 1-Tb, 1-Yb, compared to 1-Y. The shifts of the C(2,9)H and C(3,8)H environments are given as a range.

	$\Delta\delta$ (ppm)			
Ln	pd-C(1,10)**H**	pd-C(2,9)**H**, pd-C(3,8)**H**	hfac-C**H**	hfac-C**F**$_3$
Eu	+3.81	-2.29 to +2.64	-2.38	-2.37
Tb	-186.08	-18.05 to -41.84	+97.46	+13.61
Yb	+1.74	+1.43 to +8.82	-13.23	-7.49

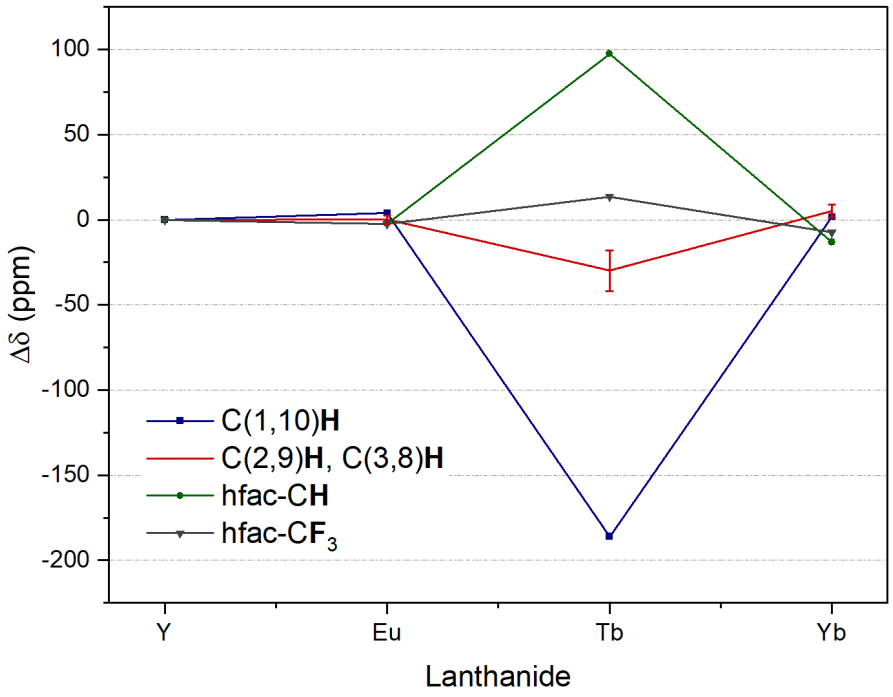

Figure 2.13: Graph illustrating the paramagnetically induced shift ($\Delta\delta$) of each ^1H and ^{19}F resonance in 1-Ln compared to 1-Y. The shift of the resonances of the C(2,9)H and C(3,8)H environments are given as a range.

1-Gd did not exhibit either a ^1H or $^{19}F\{^1H\}$ NMR spectrum, due to the extremely rapid relaxation of the ^1H and ^{19}F nuclear spins caused by the isotropic $4f^7$, S = 7/2 electronic configuration of Gd(III) (ground state $^8S_{7/2}$).[23] This isotropic electronic structure means that

the angular momentum of the Gd(III) ion is zero, and therefore the relatively simple spin-only magnetic moment formula can be applied to compounds of Gd(III). The solution state magnetic moment μ_{eff} of the complex was therefore calculated using the Evans method.*[24] The magnetic moment of **1-Gd** was determined to be in the range of 7.56-7.71 μ_{eff}, consistent with the calculated spin-only magnetic moment of 7.94 μ_{SO} for Gd(III).

2.2.4 X-band EPR spectroscopy of 1-Gd

The X-band EPR spectrum of **1-Gd** was recorded in collaboration with the group of Dr Stephen Sproules in toluene solution at 293 K and is shown in Figure 2.14. The spectrum shows a single, broad line, with a simulated value of g_{iso} = 1.989 close to that of a free electron (g = 2.0023),[25] and is characteristic of Gd(III).[26] Typically for f-block complexes, it is not possible to observe the EPR spectrum at room temperature due to the high degree of orbital angular momentum, and the resulting spin-orbit coupling (along with mixing of the ground and excited states) causing rapid relaxation.[26] However Gd(III) is $4f^7$ and therefore completely isotropic, so the room-temperature X-band EPR spectrum can generally be observed.[26, 27]

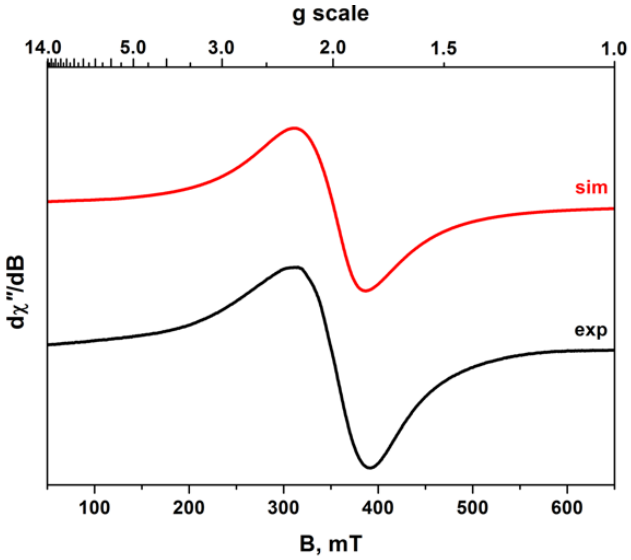

Figure 2.14: X-band EPR spectrum of 1-Gd recorded in toluene solution at 293 K. (Experimental conditions: frequency, 9.8623 GHz; power, 0.63 mW; modulation, 0.3 mT). g_{iso} = 1.989. Experimental data are represented by the black line, simulation by the red trace.

* The Evans method is performed by inserting a sealed capillary of NMR solvent into an NMR tube containing a sample of known concentration, then measuring the difference (in Hz) between the chemical shift of the two solvent signals. This difference in chemical shift can then be used to determine the magnetic moment μ_{eff}.

2.2.5 ATR-IR spectroscopy of 1-Ln

While ATR-IR spectroscopy is not able to provide a definitive assignment of *N,N'- vs O,O'*-pd coordination, it informs on the bond order and thus oxidation state of the *O,O'* site. The pd ligand exhibits significant variation in the carbonyl stretching frequency depending on the oxidation state: pd^0, 1678 cm^{-1}; $pd^{-\bullet}$, 1400-1500 cm^{-1}; pd^{2-}, 1300-1400 cm^{-1} (Figure 2.15).[28, 29]

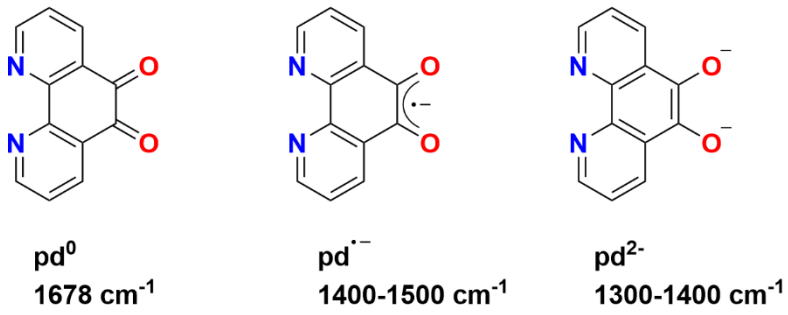

Figure 2.15: The three oxidation states of the pd ligand, showing the change in electronic structure in the *O,O'* binding site, shown with typical carbonyl stretching frequencies from IR .[28, 29]

The ATR-IR spectra of **1-Ln** were recorded on material recrystallised from toluene. The spectra are near-identical, and display three stretching frequencies in the carbonyl region (Figure 2.16) at 1645-1647, 1660-1668 and 1697-1699 cm^{-1}. By comparison to other examples of lanthanide β-diketonate compounds such as $Ln(hfac)_3(glyme)$ and $Ln(hfac)_3(S)_2$ (**4-Ln**, described in Chapter 3), the strong absorption at 1645-1647 cm^{-1} is assigned to the hfac ligands. The carbonyl stretches of beta-diketonates are typically found in the region 1650-1660 cm^{-1}.[4, 30, 31] The absorptions at 1697-1699 cm^{-1} are assigned to pd, and are consistent with other examples of *N,N'*-bound pd such as MCl_4(*N,N'*-pd) (M = Ti, Zr, Hf)[29] and $[Fe(N,N'\text{-pd})_3][PF_6]_2$.[32] It is proposed that the third absorption at 1660-1668 cm^{-1} is due to an intermolecular interaction between the metal centre and one oxygen atom of the neighbouring molecule, or another short contact interaction. This splits the stretching frequency of the *O,O'* site of pd and results in a lower energy stretching frequency being observed. These data are consistent with the intermolecular interactions and *N,N'-O*-pd binding mode observed in the solid-state molecular structures (see Section 2.2.7). The lower frequency is also consistent with the ATR-IR spectra of $(MCl_4)_2$(*N,N'-O,O'*-pd) (M = Ti, Zr, Hf), where the coordination of a metal to the *O,O'* coordination site resulted in a shift of the carbonyl stretching frequency of pd to a lower frequency when compared to $M(Cl)_4$(*N,N'*-pd).[29]

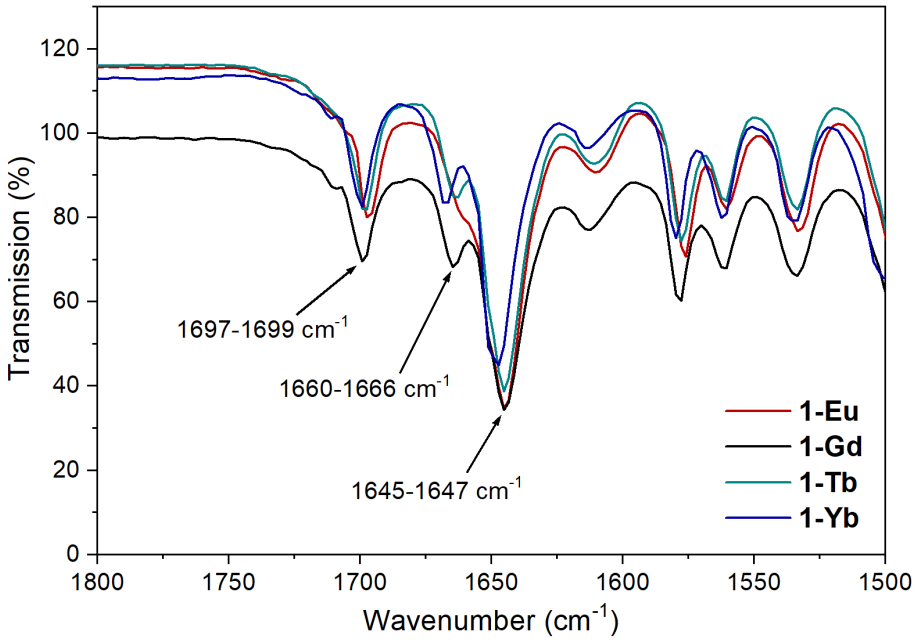

Figure 2.16: The ATR-IR spectra of 1-Ln [Ln(hfac)$_3$(*N,N'*-pd)] (Ln = Eu, Gd, Tb, Yb), showing the region between 1500-1800 cm^{-1}.

2.2.6 UV-vis-NIR spectroscopy of 1-Ln

The deep colour of **1-Ln** is atypical among trivalent lanthanide complexes. The forbidden *f-f* transitions result in extremely low molar extinction coefficients and pale colouration.[33, 34] For example, related lanthanide compounds with similar redox-active phenanthroline and bipyridine ligands are not strongly coloured.[35-37] However, as noted in the synthesis section, upon coordination of pd to lanthanides a significant colour change from yellow to green is observed. The UV-vis-NIR absorption spectra of **1-Ln** as recorded in acetonitrile will be discussed here, but there is significant variance in the UV-vis-NIR spectra of **1-Ln** by solvent, depending on their physical properties. This will be discussed further in Chapter 4, in the context of the photophysical characterisation and light-emitting properties **1-Ln** (Ln = Eu, Gd, Tb, Yb).

1-Ln are intensely absorbing in the UV. Two transition envelopes are visible in the UV spectrum above 250 nm (see Figure 2.17). A high-energy transition is partly visible with a ε maximum close to 250 nm. By comparison to similar energy transitions in transition metal complexes of pd^0,[32, 38, 39] and the UV absorptions of the pd ligand, which exhibits a transition at 257 nm with an extinction coefficient of 37,800 M^{-1} cm^{-1}, this transition is assigned to the π-π* transitions of the pd ligand. A transition is also observed at *ca* 300 nm, with an extinction

coefficient of between 26,400 and 37,800 M^{-1} cm^{-1}, also consistent with a π-π* transition.[40] By comparison to the absorption spectra of $Ln(hfac)_3(S)_2$ **4-Ln** (S = THF, MeCN; Ln = Eu, Gd, Yb; detailed in Chapter 3) and to literature compounds such as the series $Ln(diketonate)_3(OP(Ar^F)_3)$ (Ln = Sm, Eu, Tb, Er, Yb; diketonate = hfac, F_7-acetylacetonate; Ar^F = pentafluorophenyl) and other lanthanide *tris*-diketonate chelates,[6, 41-43] this transition is assigned to the π-π* transitions of the hfac ligands. The hfac ligand and other beta-diketonates are well known for sensitisation of lanthanide luminescence,[6, 34, 41, 44] and Chapter 4 provides an in-depth discussion of the photoluminescence of **1-Ln** (Ln = Eu, Gd, Tb, Yb).

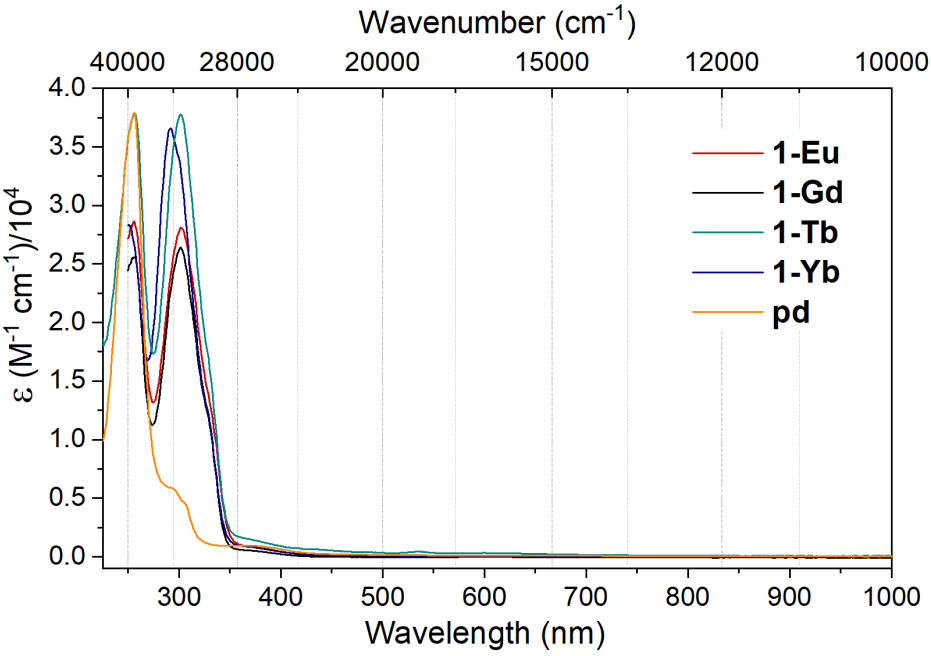

Figure 2.17: The UV-vis-NIR absorption spectra of 1-Ln (Ln = Eu, Gd, Tb, Yb) and pd, recorded in MeCN on 40 µM solutions.

Two distinct transition envelopes are evident in the visible region of the absorption spectra of **1-Ln** (Figure 2.18). A higher-energy transition envelope between 430-500 nm is broad, and in some **1-Ln** shoulder features are evident. Depending on the lanthanide, λ_{max} changes position from 483 nm in **1-Yb**, to a shoulder at *ca* 450 nm in **1-Y**, **1-Eu** and **1-Gd**. The molar extinction coefficient also varies, from 17 M^{-1} cm^{-1} in **1-Yb** to 75 M^{-1} cm^{-1} in **1-Gd** and 117 M^{-1} cm^{-1} in **1-Y**, consistent with charge transfer. The pd ligand also exhibits an absorption in this region, with a maximum of 480 nm and an extinction coefficient of 18 M^{-1} cm^{-1}. This transition envelope is therefore assigned to intra-ligand charge transfer (ILCT) transitions. The transition

occurs at lower energy, and with a lower extinction coefficient, in the smaller and more lewis acidic Yb compared to Y, Eu, Gd and Tb.[45, 46]

A lower energy transition envelope is also observed in the absorption spectrum of **1-Ln**, with maxima at *ca* 600 nm, which is responsible for the green colour of the complexes when dissolved in coordinating solvents (see Chapter 4 for a discussion of the solvent dependence of the absorption spectra of **1-Ln**). The intensity of this transition is highly variable depending on the metal, from 113 M^{-1} cm^{-1} in **1-Y**, to 87 M^{-1} cm^{-1} in **1-Gd** and 21 M^{-1} cm^{-1} in **1-Tb**, and is not observed at all in **1-Yb**. No transitions are observed in this spectral region for either the pd ligand or lanthanide *tris*-hfac compounds (see Chapter 3). The intensity of these transition envelopes are consistent with either ILCT or ligand to metal charge transfer (LMCT).[40] In the case of **1-Y**, this transition has been assigned to LMCT.[2] In general, the smaller and more Lewis acidic the metal, the lower the intensity of this transition. It is notable that Ln = Y, Eu, Gd all show similar extinction coefficients, while **1-Tb** has a significantly lower intensity. This is therefore more likely to be the result of a coordination change in solution rather than the variation in Lewis acidity due to the precipitous change between neighbouring Ln = Gd and Tb.

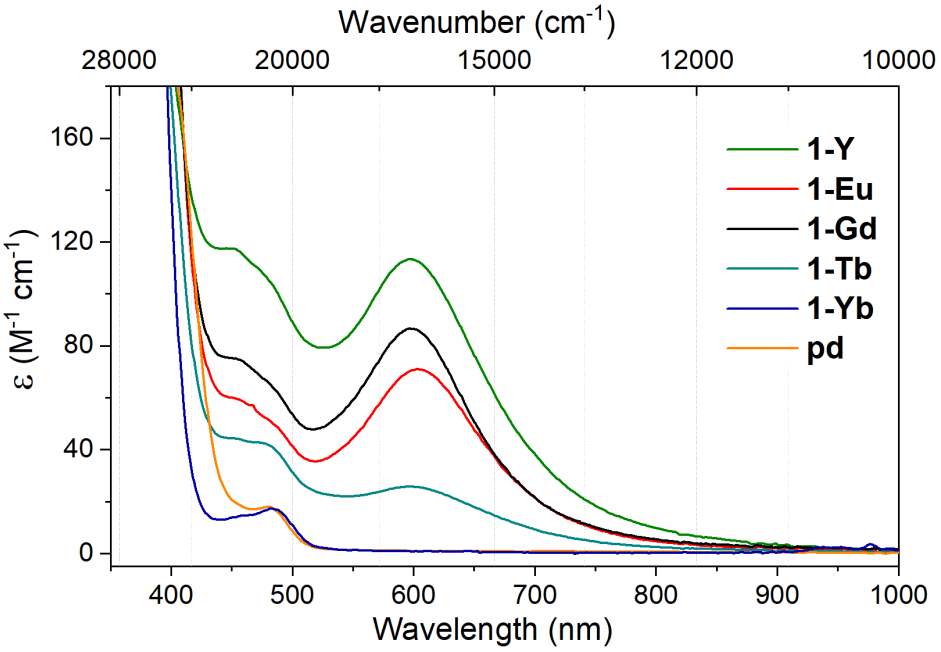

Figure 2.18: The Vis-NIR absorption spectra of 1-Ln (Ln = Y, Eu, Gd, Tb, Yb) and pd, recorded in MeCN on 1 mM solutions.

Several examples of lanthanide compounds of pd are reported in the literature, however their electronic spectra are rarely reported.[47-53] Those spectra that have been reported are not consistent with or comparable to these data. Study of fully characterised compounds of pd in this oxidation state was therefore limited to the transition metals. As mentioned above, other examples of lanthanide *tris*-diketonate *N,N'*-chelate (bipyridine, phenanthroline) compounds have no visible absorption, precluding their use a comparitors.[35-37] The transition metal *N,N'* bound pd complexes whose UV-vis absorption spectra have been reported have highly varied visible absorption profiles. For example, the group 10 complexes $PtCl_2$(*N,N'*-pd) and $PdCl_2$(*N,N'*-pd) are reported to have no features in their visible absorption spectra above 425 nm. At 425 nm, $PtCl_2$(*N,N'*-pd) exhibits a metal-ligand charge transfer (MLCT) transition.[39] Group 8 complexes $[Fe(N,N'\text{-pd})_3]^{2+}$, $[Ru(bipy)_{3-n}(N,N'\text{-pd})_n]^{2+}$ (n = 1-3) and $[Os(L)_2(N,N'\text{-pd})]^{2+}$ (L = bipy, phen; bipy = bipyridine) have complex visible absorption profiles spanning the 400-700 nm region with extinction coefficients in the range 1000-15000 M^{-1} cm^{-1}, consistent with CT but as expected significantly more intense than those in **1-Ln**.[32, 39] The group 9 complexes $[Co(N,N'\text{-pd})_3]^{2+}$ and RhCl(Cp)(*N,N'*-pd) show no spectral features higher than 380 nm, while [IrCl(Cp)(*N,N'*-pd)] exhibits a shoulder at 415 nm.[32, 38] Where reported, the visible absorptions in these complexes are also several orders of magnitude greater than those observed **1-Ln**.

2.2.7 Crystallography of Ln(hfac)$_3$(pd) 1-Ln (Ln = Sc, Y, Ce, Eu, Gd, Tb, Yb)

The solid-state molecular structures of **1-Ln** have been determined by single-crystal X-ray diffraction (XRD). The complexes **1-Ln** can be crystallised from both Et_2O (**1(i)-Ln**) and toluene (**1(ii)-Ln**) solutions. For reference, the solid-state molecular structure of the pd ligand is shown in Figure 2.19 with the numbering scheme for C, N, O atoms.[54]

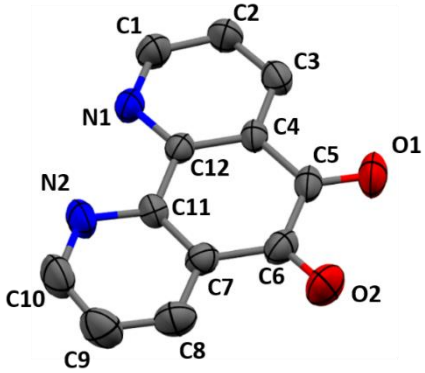

Figure 2.19: The solid-state molecular structure of pd. Thermal ellipsoids drawn at 50% probability. H atoms and a solvent molecule are omitted for clarity. Selected bond distances (Å): C5-C6 1.541(2); C-O 1.213(5)-1.216(5).[1, 54]

Single crystals suitable for X-ray diffraction of **1-Ln** were grown from concentrated solutions at -35 °C in either Et_2O (Ln = Y, Ce, Eu, Gd, Yb) (**1(i)-Ln**) or in toluene (Ln = Sc, Y, Gd, Tb, Yb) (**1(ii)-Ln**).[1-3] The *N,N'* site of pd is occupied by the lanthanide. The solid-state molecular structure of **1-Gd** is typical of **1-Ln** (Ln = Y, Eu, Tb, Yb) (Figure 2.20).[2]

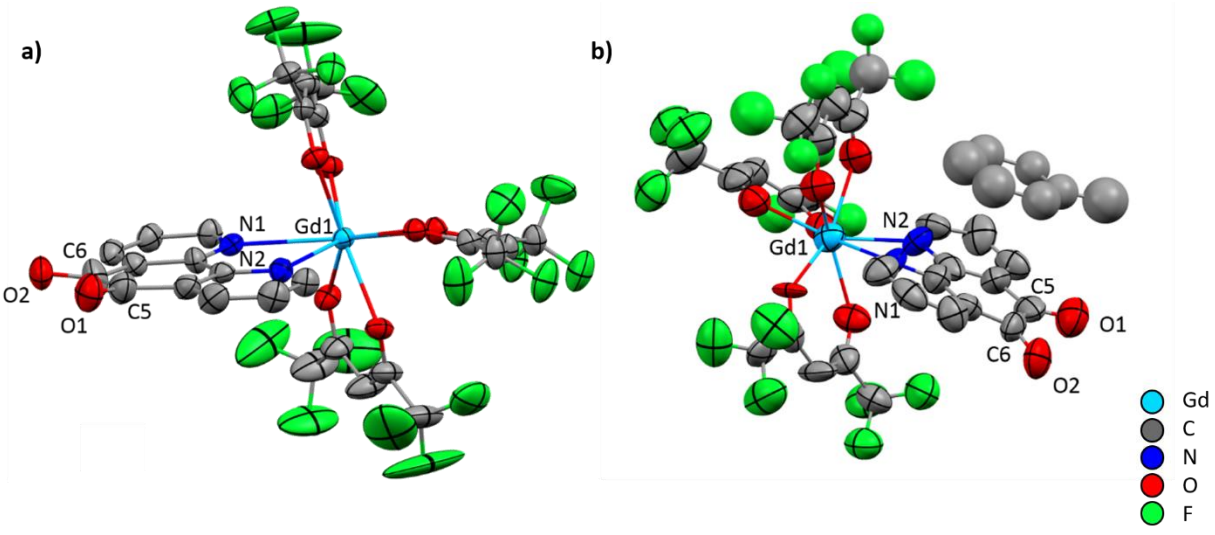

Figure 2.20: Solid state molecular structures of 1(i)-Gd and 1(ii)-Gd. Selected atoms refined isotropically. Thermal ellipsoids drawn at 50% probability. H atoms, and Et_2O molecule in 1(i)-Gd are omitted for clarity. Selected bond distances (Å): a) Gd-O 2.348(7)-2.383(7); Gd-N 2.555(9)-2.585(8); C5-C6 1.54(6); C-O 1.23(2)-1.24(2); b) Gd-O 2.32(2)-2.42(1); Gd-N 2.53(2)-2.58(1); C5-C6 1.53(3); C-O 1.22(3)-1.26(3); Gd-O(pd) 2.830(2). Gd-N-ring angles: a) 177-179°; b) 164-169°.[2]

Single crystals of **1-Gd** suitable for X-ray diffraction were grown by cooling a saturated Et_2O or toluene solution to -35 °C overnight, and both structures show *N,N'* coordinated pd, as shown in Figure 2.20. The Gd-O(hfac) bond distances of 2.348(7)-2.383(7) Å in **1(i)-Gd** and 2.32(2)-2.42(1) Å in **1(ii)-Gd** are consistent with other Gd-O(diketonate) bond distances found in the literature. For example, the Gd-O(diketonate) bonds in $Gd(tta)_3(pd)Pt(PPh_3)_2$ (tta = 2-thenoyl-trifluoro-acetonate) are in the range of 2.335(5)-2.374(5) Å;[9] those in the series $Gd(acac)_3(L)$ (acac = acetylacetonate; L = phen, dpq, dppz; dpq = dipyrido-[3,2-*d*:2'-3'-*f*]quinoxaline; dppz = dipyrido-[3,2-*a*:2'-3'-*c*]phenazine) are in the range of 2.328(4)-2.380(3) Å.[55] Likewise, the Gd-N(pd) bond distances of 2.555(9)-2.585(8) in **1(i)-Gd** and 2.53(2)-2.58(1) Å in **1(ii)-Gd** are consistent with those in $Gd(tta)_3(pd)Pt(PPh_3)_2$ (2.535(6)-2.539(7) Å) and the Gd-N bonds in $Gd(acac)_3(L)$ (2.581(2)-2.631(4) Å).

Single crystals of **1(i)-Eu** suitable for X-ray diffraction were grown from a concentrated Et_2O solution at -35 °C overnight, and the solid state molecular structure is shown in Figure 2.21.[3] Eu-O(hfac) and Eu-N(pd) distances of 2.354(3)-2.389(3) and 2.564(3)-2.569(3) Å are consistent with those in the closely related literature compounds $Eu(tta)_3(phen)$ (2.342(5)-2.408(4) and 2.585(5)-2.590(5) Å), $Eu(acac)_3(phen)$ (2.356(9)-2.409(9) and 2.645(12)-2.641(8) Å) and $Eu(hfac)_3(dmphen)$ (2.386(2)-2.494(2) and 2.590(3)-2.599(3), dmphen = 3,8-dimethyl-1,10-phenanthroline).[7, 56, 57] All attempts to grow crystals of **1-Eu** from a toluene solution resulted in microcrystalline solids which did not give a diffraction pattern.

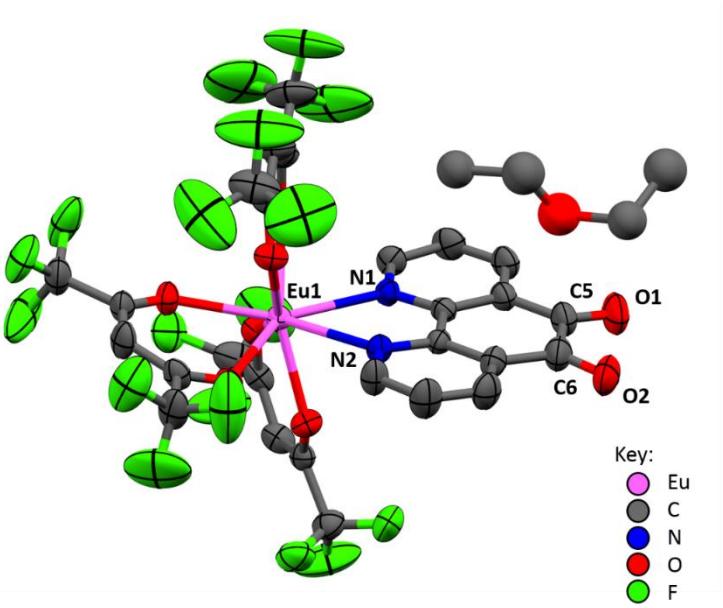

Figure 2.21 Solid State Molecular Structure of 1(i)-Eu, crystallised from an Et_2O solution at -35 °C. Ellipsoids are shown at 50% probability. H atoms are omitted for clarity. Selected bond distances: Eu-O 2.354(3)-2.389(3); Eu-N 2.564(3)-2.569(3); C5-C6 1.534 (8); C5-O1 1.210(6); C6-O2 1.212(6) Å. Eu-N-ring angle: 176-179°.[3]

Single crystals of **1-Tb** suitable for X-ray diffraction were obtained by cooling a concentrated toluene solution to -35 °C, and the solid-state molecular structure is shown in Figure 2.22.[3] The Tb-O(hfac) bonds are in the range 2.318(4)-2.377(3) Å and Tb-N(pd) bonds in the range 2.538(4)-2.566(3) Å. The Tb-O(diketonate) bond distances are consistent with the Tb-O(diketonate) bonds in $Tb(acac)_3(phen)$ of 2.332(1)-2.349(1) and in $Tb(hfac)_3(dmbpy)$ (dmbpy = 4,4'-dimethyl-2,2'-dipyridyl) of 2.337(2)-2.394(2) Å.[10, 58] Similarly, the Tb-N(pd) bonds are consistent with the Tb-N(phen) (2.551(1)-2.588(1) Å) and Tb-N(dmbpy) (2.521(3)-2.543(3) Å) bonds in the same two complexes.

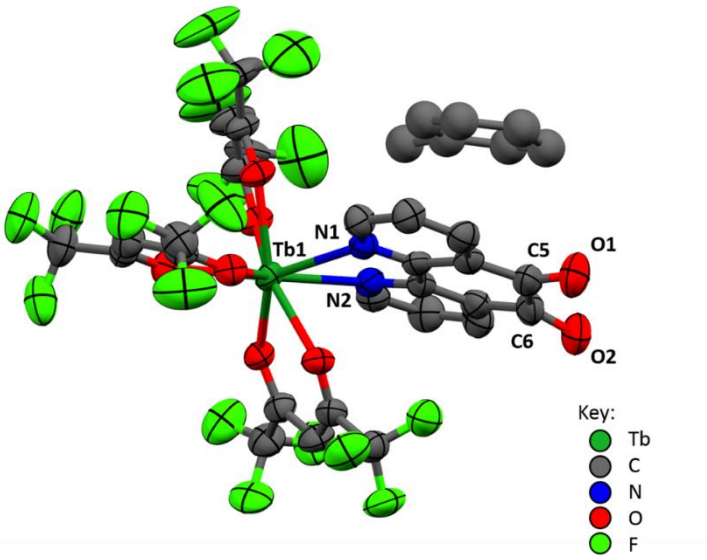

Figure 2.22 Solid State Molecular Structure of 1(ii)-Tb, crystallised from a toluene solution at -15 °C. Thermal ellipsoids are shown at 50% probability. H atoms are omitted for clarity. Selected bond distances: Tb-O 2.318(4)-2.377(3); Tb-N 2.538(4)-2.566(3); C5-C6 1.530(7); C5-O1 1.224(6); C6-O2 1.216(7) Å. Tb-N-ring angle: 166-167°.[3]

Single crystals of **1-Yb** suitable for X-ray diffraction were grown by cooling saturated Et_2O (**1(i)-Yb**) and toluene (**1(ii)-Yb**) solutions to -35 °C overnight. The solid state molecular structures are shown in Figure 2.23.[3] The Yb-O(hfac) bonds of **1(i)-Yb** and **1(ii)-Yb** are in the range of 2.272(2)-2.312(2) and 2.268(4)-2.306(4) Å, respectively, and the Yb-N(pd) bonds are in the range of 2.491(2)-2.492(2) and 2.472(5)-2.488(4) Å, respectively. The Yb-O(diketonate) bonds are consistent with those in the related complexes $Yb(acac)_3(phen)$ of 2.241(2)-2.292(2) Å, $Yb(dpzac)_3(phen)$ (dpzac = 1,3-bis(dimethylpyrazolyl)-propane-1,3-dionate) of 2.252(4)-2.322(4) Å and $Yb(hfth)_3(phen)$ (hfth = 4,4,5,5,6,6,6-heptafluoro-1-(2-thienyl)hexane-1,3-dione) of 2.269(5)-2.294(5) Å.[43, 59, 60] The Yb-N(pd) bonds are significantly shorter than the Yb-N(phen) bonds in $Yb(acac)_3(phen)$ and $Yb(dpzac)_3(phen)$ of 2.527(3)-2.561(3) Å and 2.539(5)-2.555(5) Å respectively. They are, however, consistent with the Ln-N(pd) bonds in $Yb(hfth)_3(phen)$ of 2.495(7)-2.509(6) Å, and with the other **1-Ln**, once the variation in ionic radii is taken into account (see Table 2.3 below).[45]

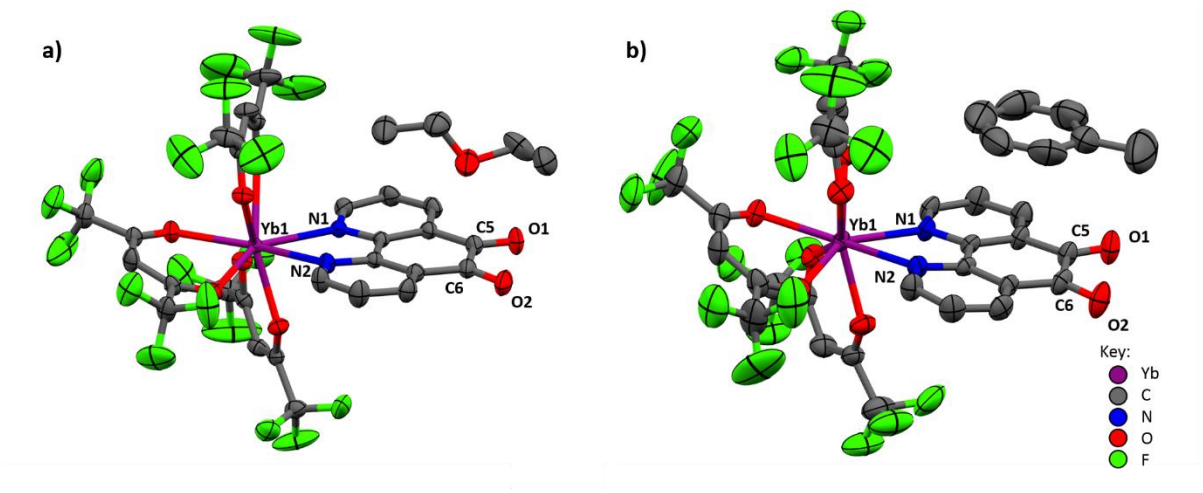

Figure 2.23: Solid State Molecular Structures of 1(i)-Yb and 1(ii)-Yb, crystallised from a concentrated a) Et_2O or b) toluene solution at -35 °C. Thermal ellipsoids are shown at 50% probability. H atoms are omitted for clarity. Selected bond distances (Å): a) Yb-O, 2.272(2)-2.312(2); Yb-N, 2.491(2)-2.492(2); C5-C6, 1.538(5); C-O, 1.209(3)-1.212(4). b) Yb-O, 2.268(4)-2.306(4); Yb-N, 2.472(5)-2.488(4); C5-C6, 1.540(8); C-O, 1.196(7)-1.208(7). Yb-N-ring angles: a) 175-179°; b), 173-179°.[3]

A feature shared by the solid-state molecular structures of **1(i)-Ln** (Ln = Y, Eu, Gd) and **1(ii)-Ln** (Ln = Y, Gd, Tb) is the variance in their solid-state molecular structures depending on the nature of the solvent from which they were crystallised. Interestingly, in the solid-state molecular structures of **1(ii)-Ln** (Ln = Y, Gd, Tb), an interaction is observed between the lanthanide and one oxygen atom of the pd ligand in the neighbouring molecule, resulting in a *N,N'-O* binding mode of the ligand. This interaction varies in magnitude by the ionic radius of the lanthanide (Y(III) 1.019 Å, Gd(III) 1.053 Å, Tb(III) 1.040 Å), from a full bonding interaction in **1(ii)-Gd** of 2.830(2) Å, comparable to the van der Waals radius of Gd(III),[61] to an intermolecular non-bonding interaction in **1(ii)-Tb** and **1(ii)-Y** (of 3.046(4) and 3.154(3) Å, respectively). No such interaction is observed in the structures of **1(i)-Ln**, nor in the solid-state molecular structure of **1(ii)-Yb** where the interaction is likely prevented by the smaller ionic radius of Yb(III) (Yb(III), 0.985 Å; Y(III), 1.019 Å; Tb(III), 1.040 Å; Gd(III), 1.053 Å).[45] This trend also continues to the larger lanthanides. Compounds of the larger lanthanides La and Ce with pd have an even greater interaction between the *O,O'* site of pd. The solid-state molecular structure of compounds of La and Ce with pd and hfac ligands is of a one-dimensional chelating coordination polymer $\{Ln(hfac)_3(N,N'\text{-}O,O'\text{-pd})\}_n$ **1-Ce**, **1-La**. In this structure, La or Ce is ten-coordinate and bonds to both O atoms and both N atoms of pd.[1] The solid-state molecular structure of $\{Ce(hfac)_3(N,N'\text{-}O,O'\text{-pd})\}_n$ is shown in Figure 2.27.

The variance in the solid-state molecular structures of **1-Ln** of the structures also manifests in the angle of coordination of the pd ligand. In each **1(i)-Ln**, pd coordinates to the lanthanide in a planar or linear fashion, with Ln-N-ring angles (measured by the Ln-N(1,2)-C(3,8) angle, shown in Figure 2.24) close to 180°, 177-179° in **1-Y**, 177-179° in **1-Gd**, 176-179° in **1-Eu** and 175-179° in **1-Yb**. In **1(ii)-Yb**, this same angle is again close to linear at 173-179°. In contrast, in the examples of **1(ii)-Ln** (Ln = Y, Gd, Tb) where an intermolecular Ln-O interaction does occur, pd coordinates at an obtuse angle, 163-165° in **1-Y**, 164-169° in **1-Gd**, 166-167° in **1-Tb**. This results in the solid-state molecular structures of **1(ii)-Ln** (Ln = Y, Gd, Tb) containing a one-dimensional zig-zag $Ln(hfac)_3(N,N'\text{-}O\text{-pd})]_n$ coordination (Ln = Gd) or pseudo-coordination (Ln = Y, Tb) polymer, illustrated in Figure 2.25 (**1(ii)-Gd**) and Figure 2.26 (**1(ii)-Tb**).

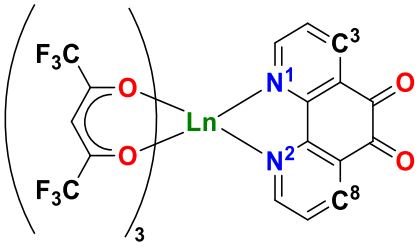

Figure 2.24: Schematic depicting the atoms used to define the Ln-N-ring angle where pd coordinates to Ln.

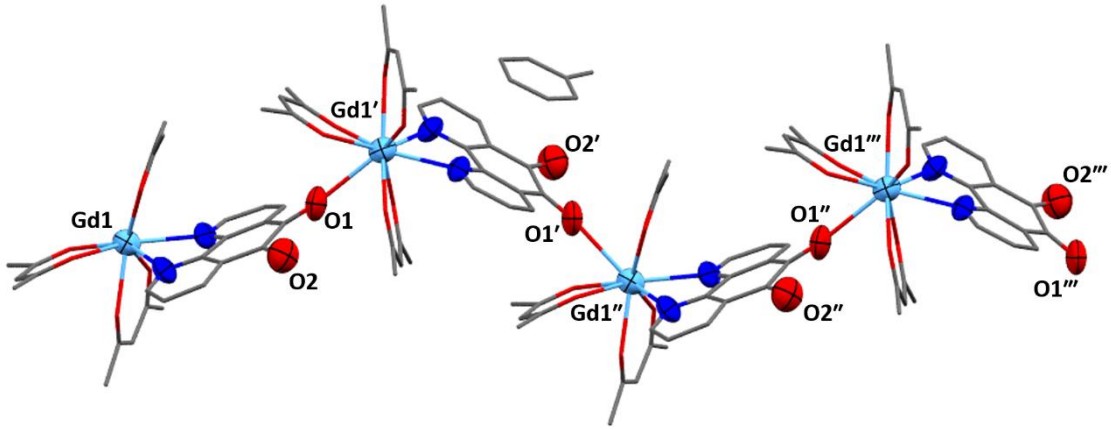

Figure 2.25: The zig-zag polymeric solid-state structure of 1(ii)-Gd. Gd and donor atoms of pd are depicted as thermal ellipsoids of 50% probability, C atoms are depicted as wireframe, and H and F atoms are omitted for clarity. Gd-O1 distance: 2.830(2) Å.[2]

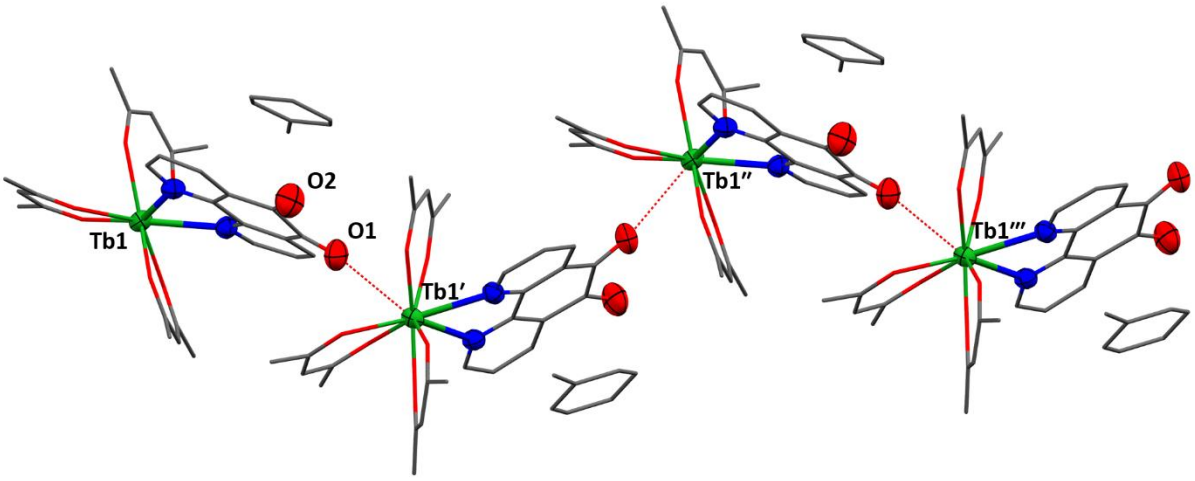

Figure 2.26: The zig-zag pseudo-polymeric structure of 1(ii)-Tb. Tb and donor atoms of pd are depicted as thermal ellipsoids of 50% probability, C atoms are depicted as wireframe, and H and F atoms are omitted for clarity. The non-bonding interaction between Tb and O1 is depicted by a dotted red line. Tb-O1 distance: 3.046(4) Å.[3]

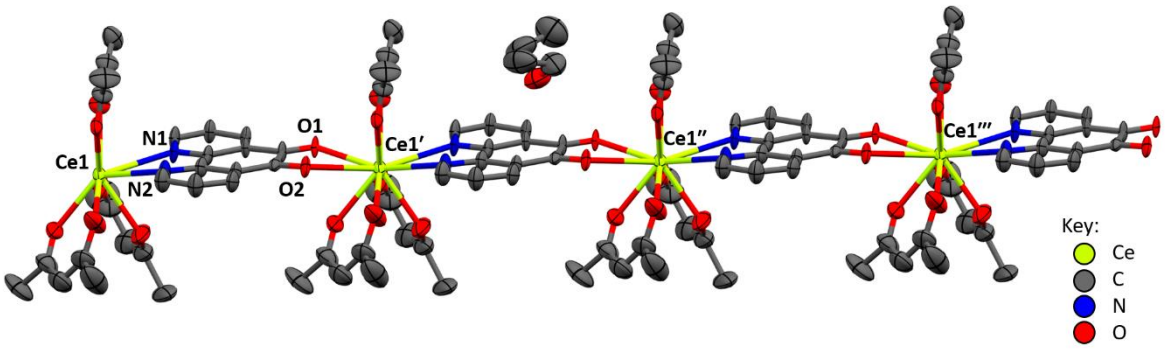

Figure 2.27: Polymeric solid state molecular structure of 1-Ce. Four crystallographically identical repeating units are depicted. Thermal ellipsoids depicted at 50% probability. H and F atoms, and three Et_2O molecules are omitted for clarity. Selected bond distances (Å): Ce-O(hfac), 2.45(1)-2.51(1); Ce-N, 2.682(6)-2.836(8); C5-C6, 1.53(2); C-O 1.21(2)-1.23(2); Ce-O(pd), 2.597(7)-2.867(8). Ce-Ce distance (Å): 9.4396(5). Ce-N-ring angles: 170-1°.

In the solid-state molecular structure of **1(ii)-Yb**, while it does not have Yb-O contacts, some long-range order is observed within the crystal lattice. A plane of pd ligands runs through the structure, illustrated in Figure 2.28. This is facilitated by an attractive but non-covalent interaction between the O atoms of pd and the H atoms of the neighbouring pd ligands, shown in Figure 2.28 in green. The O-H distances of 2.546-2.867 Å, while short, do not constitute hydrogen bonds (H-bonding defined as 1.5-2.5 Å).[62] A similar interaction is also observed in **1-Sc**, where the O-H distances are very similar at 2.534-2.870 Å.[1]

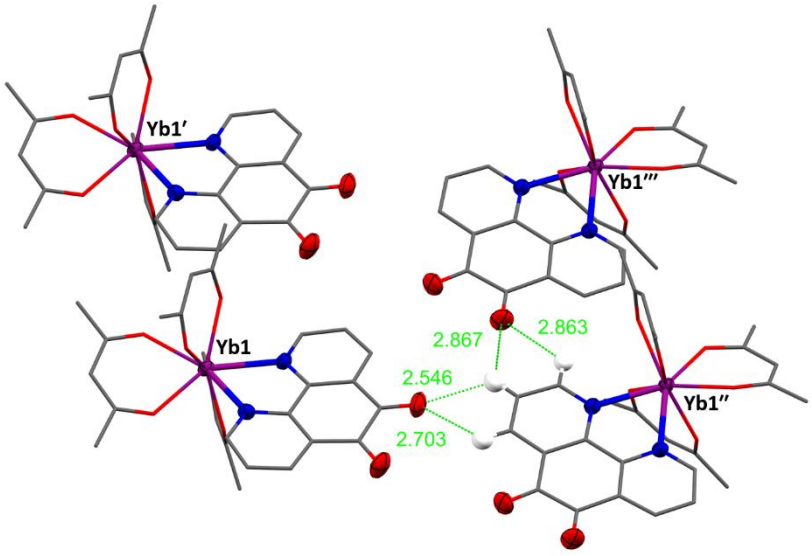

Figure 2.28: The crystal packing of the pd ligands in 1(ii)-Yb, crystallised from toluene. Yb atoms, and N and O atoms of pd are shown as ellipsoids, and selected H atoms are shown in ball-and-stick, while all other atoms are shown in wireframe. Ellipsoids are drawn at 50% probability. F atoms and toluene solvent molecules are omitted for clarity. O-H interactions and distances (Å) are shown in lime.

There are significant π-π interactions between molecules in **1-Ln**. Toluene solvent molecules exhibit face-to-face interactions with the pd ligand in all **1(ii)-Ln**, shown for **1(ii)-Gd** in Figure 2.29. Toluene sits roughly above the central ring of pd (see Figure 2.29), at a distance of between 3.3-3.5 Å, which is in the typical range for a *π*-*π* interaction.[63-65] In **1(i)-Ln**, the molecules pair symmetrically, allowing for *π* interactions between the pd ligands of neighbouring molecules, shown in Figure 2.30 for **1(i)-Eu**. The ligands, rather than overlapping fully, have an offset structure. In this situation, rather than a ring-ring interaction, the dominant interaction is a ring-bond interaction, between each ring system and the C=O double bond. The distance of the interaction in **1(i)-Ln** is between 3.4-3.5 Å, again in the typical range for *π*-*π* interactions.

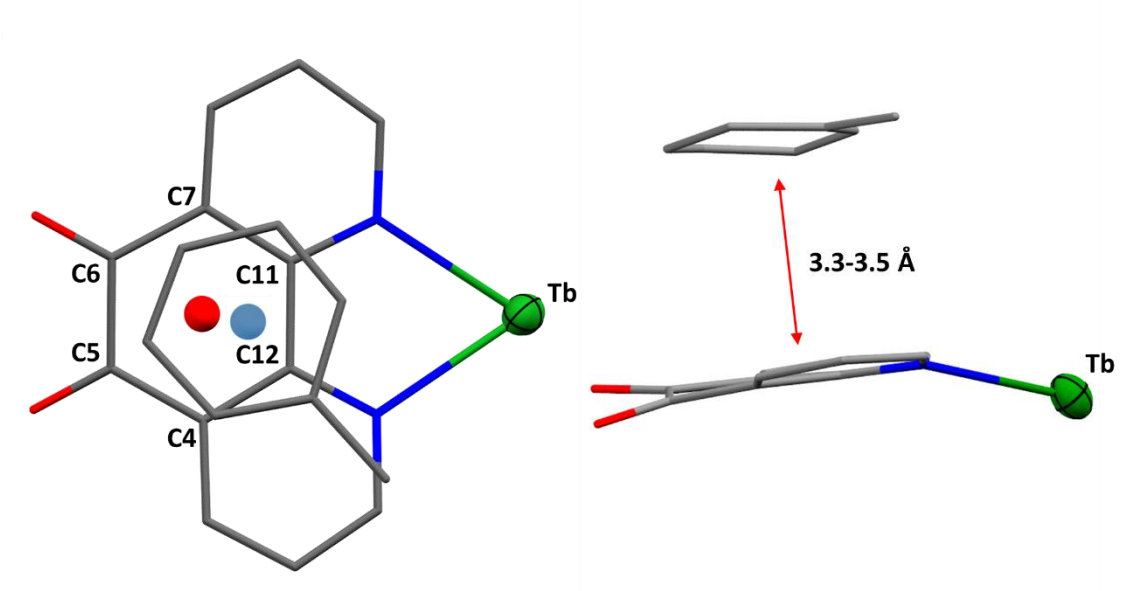

Figure 2.29: The view of the solid-state molecular structure of 1(ii)-Tb perpendicular to and in the plane of the plane of the pd ligand, as an example of the π-π stacking in toluene solvates 1(ii)-Ln. Tb is shown as a thermal ellipsoid of 50% probability, all other atoms displayed in wireframe. The carbon atoms of the central pd ring are numbered, and the centroid is shown as a red sphere. The centroid of the toluene ring is shown as a blue sphere. The hfac ligands are omitted for clarity.

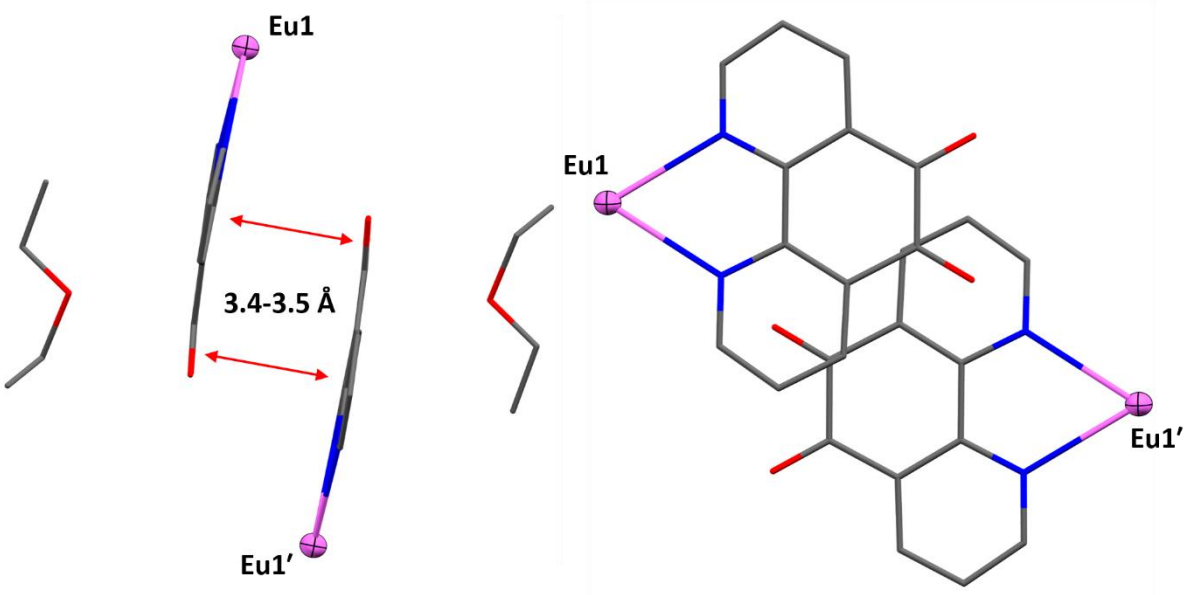

Figure 2.30: The view of the solid-state molecular structure of 1(i)-Eu in the plane and perpendicular to the plane of the pd ligands, as an example of the π-π stacking in Et_2O solvates 1(i)-Ln. Eu is shown as a thermal ellipsoid of 50% probability, all other atoms displayed in wireframe. The hfac ligands are omitted for clarity.

Table 2.3 summarises the key bond distances and angles of **1-Ln**. In all cases, the bond distances of the *O,O'* site of pd (C5-C6 and C-$O_{(pd)}$) are consistent with a single C-C bond and double C=O bonds (see Table 2.3), and are in agreement with those observed in the solid-state molecular structure of the pd ligand (C5-C6, 1.541(2) Å; C-O, 1.213(5)-1.216(5) Å).[54] No significant variation in these bond lengths is observed between **1-Ln**, independent of the coordination mode of the ligand, whether *N,N'* in **1(i)-Ln** (Ln = Y, Eu, Gd, Yb) and **1(ii)-Ln** (Ln = Yb, Sc), or in *N,N'-O* (**1(ii)-Ln** (Ln = Y, Gd, Tb) and *N,N'-O,O'* (**1-Ce**), despite coordination of the Lewis acidic lanthanide to the *O,O'* binding site of pd. The solid-state molecular structures of **1(i)-Y** and **1(ii)-Y** are similar to those of **1(i)-Gd** and **1(ii)-Gd**,[1, 2] and key bond lengths are consistent with the closest structural match in the Cambridge Crystallographic Data Centre (CCDC), $Y(tta)_3(phen)$.[8] The solid-state molecular structure of **1(ii)-Sc** is almost identical to that of **1(ii)-Yb**.[1]

Table 2.3: Key bond distances and angles in 1-Ln (Ln = Sc, Y, Ce, Eu, Gd, Tb, Yb).

1-Ln	Solvent	Bond distances (Å)					Ln-N-ring angle (°)	Ln ionic radius (Å)[45]
		Ln-$O_{(hfac)}$	Ln-$N_{(pd)}$	Ln-$O_{(pd)}$	C5-C6	C-$O_{(pd)}$		
1(ii)-Sc[1]	Tol	2.168(9)-2.21(1)	2.36(1)-2.42(1)	n/a	1.54(2)	1.170(2)-1.250(2)	172-178	0.870
1(i)-Y[1, 2]	Et_2O	2.300(3)-2.341(3)	2.520(3)-2.524(3)	n/a	1.535(7)	1.220(5)-1.224(4)	177-179	1.019
1(ii)-Y[1, 2]	Tol	2.299(3)-2.344(2)	2.501(3)-2.552(3)	3.154(3)	1.524(6)	1.213(5)-1.216(5)	163-165	1.019
1-Ce[1]	Et_2O	2.45(1)-2.51(1)	2.682(6)-2.836(8)	2.597(7)-2.867(8)	1.53(2)	1.21(2)-1.23(2)	170-171	1.143
1(i)-Eu	Et_2O	2.354(3)-2.389(3)	2.564(3)-2.569(3)	n/a	1.534(8)	1.210(6)-1.212(6)	176-179	1.066
1(i)-Gd[2]	Et_2O	2.348(7)-2.383(7)	2.555(9)-2.585(8)	n/a	1.54(6)	1.23(2)-1.24(2)	177-179	1.053
1(ii)-Gd[2]	Tol	2.32(2)-2.42(1)	2.53(2)-2.58(1)	2.830(2)	1.53(3)	1.22(3)-1.26(3)	164-169	1.053
1(ii)-Tb	Tol	2.318(4)-2.377(3)	2.538(4)-2.566(3)	3.046(4)	1.530(7)	1.216(7)-1.224(6)	166-167	1.040
1(i)-Yb	Et_2O	2.272(2)-2.312(2)	2.491(2)-2.492(2)	n/a	1.538(5)	1.209(3)-1.212(4)	175-179	0.985
1(ii)-Yb	Tol	2.268(4)-2.306(4)	2.472(5)-2.488(4)	n/a	1.540(8)	1.196(7)-1.208(7	173-179	0.985

2.3 Synthesis and Characterisation of Ln(hfac)$_3$(*N,N'-O,O'*-pd)V(Cp)$_2$ 2-Ln

One of the key features of the pd ligand is its redox activity localised on the *O,O'* binding site. The pd ligand has three accessible oxidation states: the neutral ligand pd^0, radical anion pd$^{-\bullet}$ (semiquinone) and dianion pd^{2-} (catecholate), shown in Figure 2.31. In pd^0 the reduction potentials are reported as -0.85 and -1.71 eV (vs. Fc/Fc$^+$) for the first and second reductions respectively.[32, 39] As complex **1-Y** was found to be unstable under standard electrochemical conditions, these potentials were used as a guide for the selection of reducing agent. Vanadocene was therefore chosen as an reductant for **1-Ln** as it is a good redox match (V(II)/V(III) = -0.93 eV, vs. Fc/Fc$^+$)[66] for the first reduction of pd. Previously, vanadocene has been reported to react with pd to form (*O,O'*-pd)V(Cp)$_2$,[29] however, in our hands this reaction formed intractable dark green solids.[1]

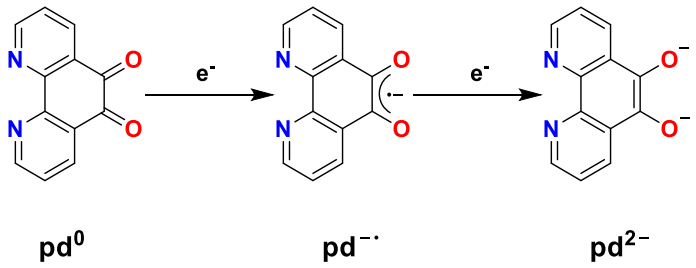

Figure 2.31: The three oxidation states of pd.

The reaction of selected **1-Ln** with the reducing agents vanadocene V(Cp^R)$_2$ was undertaken, forming the *d-f* bimetallic complexes **2-Ln** Ln(hfac)$_3$(*N,N'-O,O'*-pd)V(Cp)$_2$ (Ln = Y, Gd; Cp^R = Cp, $C_5H_5^-$) and **2a-Gd** (Cp^R = Cp^t, $C_5Me_4H^-$).[1, 2] In these complexes, V(Cp)$_2$ underwent a 2 electron oxidative addition to pd resulting in pd being in the 2- oxidation state as shown in Scheme 2.2, rather than a single-electron reduction reaction occurring.

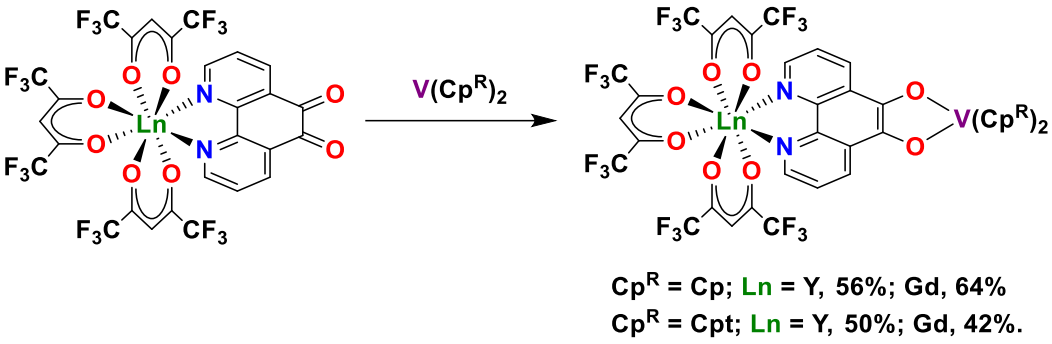

Scheme 2.2: The synthesis of 2-Ln Ln(hfac)$_3$(*N,N'-O,O'*-pd)V(Cp)$_2$ (Ln = Y, Gd) and 2a-Ln Ln(hfac)$_3$(*N,N'-O,O'*-pd)V(Cp^t)$_2$ (Ln = Y, Gd).[1, 2]

In a typical preparation, **1-Ln** and 1 eq. VCp$_2$ or VCp$^t_2$ was cooled to -78 °C and Et$_2$O or THF was added with stirring. The colour of the reaction immediately darkened intensely from green to a very dark green. The solvent was then removed *in vacuo* and recrystallisation from a toluene/hexane mixture at -15 °C yielded **2-Ln** Ln(hfac)$_3$(*N,N'-O,O'*-pd)V(Cp)$_2$ (Ln = Y, 56%; Gd, 64%) and **2a-Ln** Ln(hfac)$_3$(*N,N'-O,O'*-pd)V(Cp^t)$_2$ (Ln = Y, 50%; Ln = Gd, 42%) as dark microcrystalline solids in good yields. Elemental analyses were consistent with the expected Ln(hfac)$_3$(pd)V(Cp^R)$_2$ formulation.

2.3.1 X-band EPR spectroscopy of 2-Ln

The X-band EPR spectrum of 2-Ln (Ln = Y, Gd) and 2a-Ln (Ln = Y, Gd) were recorded in collaboration with the Sproules group. EPR spectroscopy can be used to analyse compounds of V(IV) due to its 3d^1 electronic configuration. The room-temperature X-band EPR spectra of 2-Y and 2a-Y are shown in Figure 2.32, each showing the characteristic eight-line spectrum of the unpaired electron on V(IV) (g_{iso} = 1.9799, A_{iso} = 65.8 x10^{-4} cm^{-1}).[1, 2] The eight-line splitting is caused by the hyperfine coupling of the unpaired *d*-electron to ^{51}V (I = 7/2, 100%[†]), and the g-value determined by simulation is consistent with other examples of non-oxo V(IV) compounds.[67, 68] These data are therefore consistent with the two-electron reduction of pd by vanadocene, with the V(IV) residing in the *O,O'* binding site. The X-band EPR spectrum of 2a-Y exhibits two overlapping octets, well-simulated by two V(IV) environments in a 1:1 ratio (environment A: g_{iso} = 1.9819, A_{iso} = 68.4 x10^{-4} cm^{-1}; B: g_{iso} = 1.9779, A_{iso} = 64.9 x10^{-4} cm^{-1}). These are assigned to two rotational conformers of the Cp^t rings in the [V(Cp^t)$_2$]$^{2+}$ unit.

[†] CIAAW. **Isotopic compositions of the elements 2019**. Available online at www.ciaaw.org.

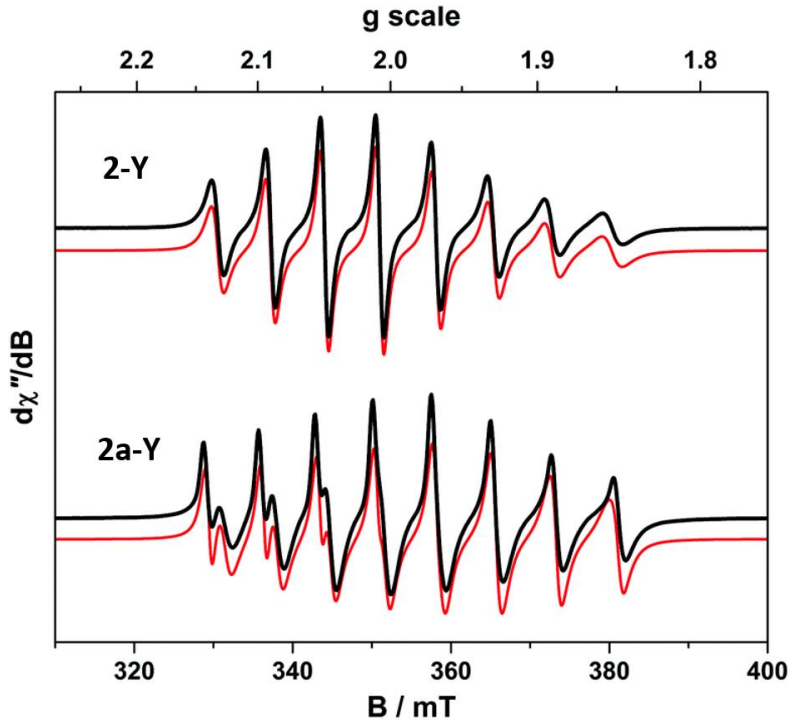

Figure 2.32: X-band EPR spectra of 2-Y and 2a-Y, recorded in toluene at 293 K. (experimental conditions: frequency, 9.8634 GHz; power, 0.63 mW; modulation, 0.2 mT). 2-Y: g_{iso}(V(IV)) = 1.9799, A_{iso} (V(IV)) = 65.8 x 10^{-4} cm^{-1}; 2a-Y a) g_{iso}(V(IV)) = 1.9819, A_{iso}V(IV) = 68.4 x10^{-4} cm^{-1}; b) g_{iso} (V(IV)) = 1.9779, A_{iso} (V(IV)) = 64.9 x10^{-4} cm^{-1}. Experimental data are represented by black lines, simulation by red traces.

The X-band EPR spectrum of **2-Y** was also recorded at 130 K, in a frozen toluene solution, to obtain the anisotropic g parameters (g_x = 1.9657, g_y = 1.9776, g_z = 1.9978; A_x = 106.6, A_y = 78.1, A_z = 11.0 x10^{-4} cm^{-1}) (Figure 2.33).[1, 2] These values are consistent with the unpaired electron residing in the $d_{x^2-y^2}$ orbital in C_{2v} symmetry at V(IV) and the pseudo-tetrahedral geometry observed in the solid-state molecular structure (see Section 2.3.4).

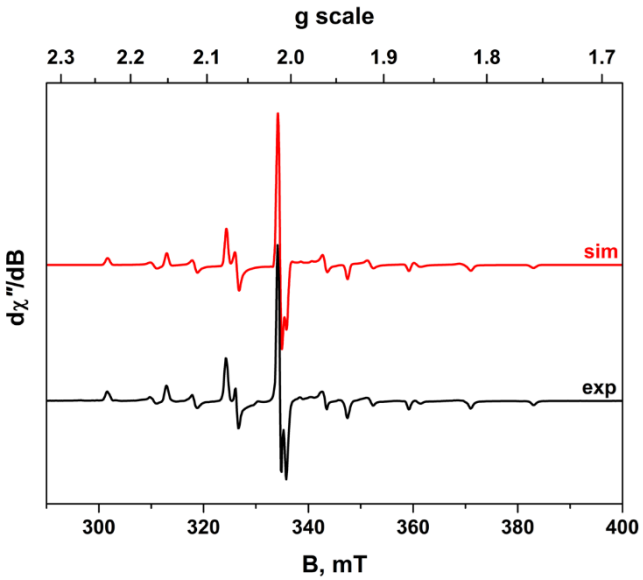

Figure 2.33: X-band EPR spectrum of 2-Y, recorded in a frozen toluene solution at 130 K. (experimental conditions: frequency, 9.4244 GHz; power, 0.2 mW; modulation, 0.1 mT). *g*(V(IV)) = 1.9657, 1.9776, 1.9978; *A*(V(IV)) = (106.6, 78.1, 11.0) × 10^{-4} cm^{-1}. Experimental data are represented by the black line, simulation by the red trace.

The X-band EPR spectrum of **2-Gd** is shown in Figure 2.34. The spectrum is an overlay of the typical broad isotropic Gd(III) signal (see Figure 2.14) and the eight-line spectrum of V(IV), as seen in **2-Y** and **2a-Y**. The intensities of the Gd(III) and V(IV) signals are in the ratio 7:1, as expected for the $4f^7$ electronic configuration of Gd(III) and $3d^1$ electronic configuration of V(IV). Analogously to the EPR spectrum of Y(hfac)$_3$(*N,N'-O,O'*-pd)V(Cp^t)$_2$,[2] two signals are observed for V(IV) with slightly different *g*-values, which are assigned to rotational conformers of the Cp rings (g_{iso} (Gd(III), 87.7%) = 1.9912; g_{iso}(V(IV), 10.5%) = 1.9975; g_{iso}(V(IV)), 1.8%) = 1.9950. A_{iso}(V(IV)), 10.5%) = 72.0 x 10^{-4} cm^{-1}; A_{iso}(V(IV)), 1.8%) = 72.2 x 10^{-4} cm^{-1}). The spectrum is well-reproduced by simulation with J = 0, indicating that there is no exchange coupling observed between Gd(III) and V(IV).

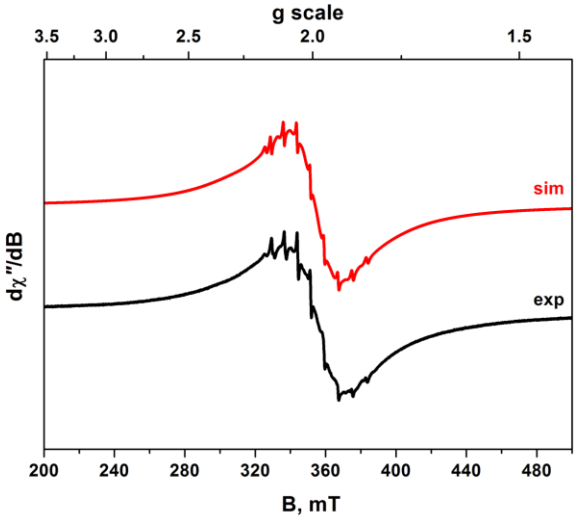

Figure 2.34: X-band EPR spectrum of 2-Gd recorded in THF solution at 293 K (Experimental conditions: frequency, 9.8717 GHz; power 0.63 mW; modulation, 0.3 mT). g_{iso}(Gd(III), 87.7%) = 1.9912; g_{iso}(V(IV), 10.5%) = 1.9975; g_{iso}(V(IV)), 1.8%) = 1.9950. A_{iso}(V(IV)), 10.5%) = 72.0 x 10^{-4}; A_{iso}(V(IV)), 1.8%) = 72.2 x 10^{-4}. Experimental data are represented by the black line, simulation by the red trace.

DFT calculations were performed on **2-Y**. The optimised structure is in good agreement with solid-state molecular structure determined by single-crystal XRD (see Section 2.3.4). The Mulliken spin density analysis of **2-Y** shows that the spin is almost entirely localised on V(IV), with a $d_{x^2-y^2}$ character as shown in

Figure 2.35. This is consistent with the observed frozen solution EPR spectrum of **2-Y** (Figure 2.33). The small amount of opposite spin on the *O,O'* binding site of pd is a result of bond polarisation due to the Lewis acidic V(IV).

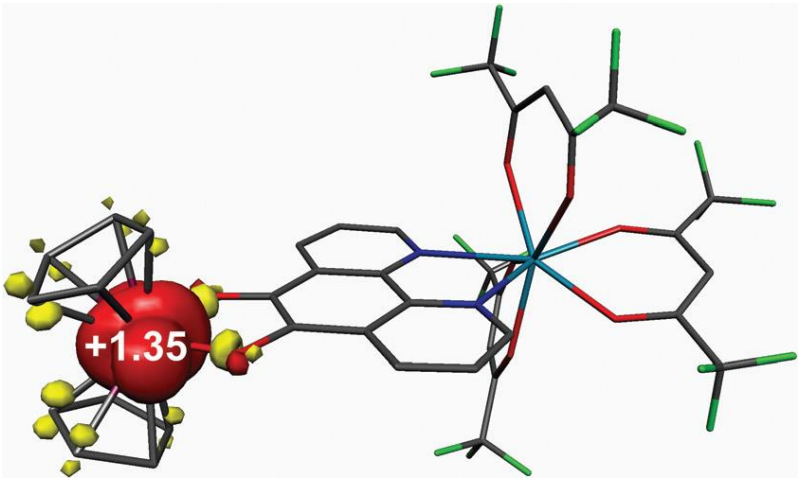

Figure 2.35: DFT-optimised structure of 2-Y, with Mulliken spin density population overlaid. Red regions indicate *α*-spin, yellow indicate *β*-spin.

2.3.2 ATR-IR spectroscopy of 2-Ln (Ln = Y, Gd)

As discussed for **1-Ln**, ATR-IR spectroscopy may inform on the bond order of the ketone moieties of the pd ligand, and thus its oxidation state. The ATR-IR spectra of **2-Ln** and **2a-Ln** (Figure 2.36) have a stretching frequency at *ca* 1650 cm^{-1}, assigned to the hfac ligands, which is consistent with that observed in **1-Ln**. No other absorption is observed in this region, where a stretching frequency is present for the neutral ligand in **1-Ln** (at 1699-1697 cm^{-1} and 1668-1661 cm^{-1}), evidencing the reduction of the ligand. As discussed in Section 2.2.5, the single C-O bonds of pd^{2-} are expected to have a stretching frequency of 1300-1400 cm^{-1}.[28, 29] A stretching frequency is observed in the ATR-IR spectra of **2-Ln** at 1371-1381 cm^{-1} which is not present in **1-Ln**. This is therefore assigned to the pd^{2-} C-O stretching frequency, consistent with the reduction of pd to the dianionic oxidation state.

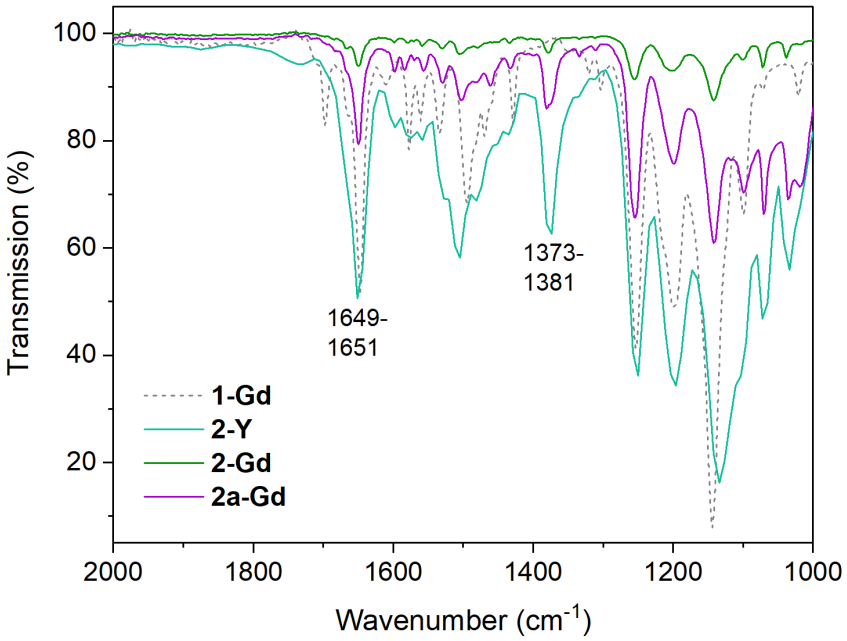

Figure 2.36: The ATR-IR spectra of 2-Ln (Ln = Y, Gd) and 2a-Gd, recorded at R.T. ν_{CO}(hfac) and ν_{CO}(pd) are highlighted at 1649-1651 and 1373-1381 cm^{-1} respectively.[1, 2] 1-Gd is also included for ease of comparison.

2.3.3 UV-vis spectroscopy of 2-Ln (Ln = Sc, Y, Gd)

Compounds **2-Ln** are very strongly coloured, and solutions at millimolar concentrations are very dark green. The electronic spectra of **2-Ln** (Ln = Y, Gd) are shown in Figure 2.37. Each spectrum exhibits three transitions, which in **2-Y** are at 431 (5400), 600 (2630) and 788 nm (1840 M^{-1} cm^{-1}), while in **2-Gd** transitions occur at 425 (4650), 576 (3430) and 797 nm (2740

M^{-1} cm^{-1}). In **2a-Gd**, two maxima are observed in the spectrum at 435 (6250) and 575 nm (2900 M^{-1} cm^{-1}), along with a shoulder at around 800 nm. The spectra of the three complexes are comparable, exhibiting very similar transitions, consistent with a shared electronic structure. The magnitudes of these transitions are consistent with charge transfer, though significantly more intense than those observed in **1-Ln**, which have extinction coefficients in the visible region of up to 100 M^{-1} cm^{-1}. The typical *d-d* transitions observed in pseudo-tetrahedral vanadocenes are not observed in **2-Ln** or **2a-Ln** as they are of significantly lower intensity than the observed transitions.[69, 70] Time-dependent density functional theory calculations were performed on **2-Y**, and the electronic structure analysis is shown in Figure 2.38.[2] The TD-DFT analysis had good agreement with the experimental spectrum, allowing the transitions to be assigned. The maxima at 576 and 797 nm are assigned to a HOMO-1 to LUMO transition, which is a pd^{2-}→V(IV) charge transfer transition. The presence of the unpaired electron of V(IV) polarises the spin states of the ligand, resulting in the splitting of this transition to two energies. The transition at 425 nm, which was also observed in *N,N'* coordinated Pt(*N,N'*-pd)Cl_2,[39] was assigned to an intra-ligand charge transfer (ILCT) transition.

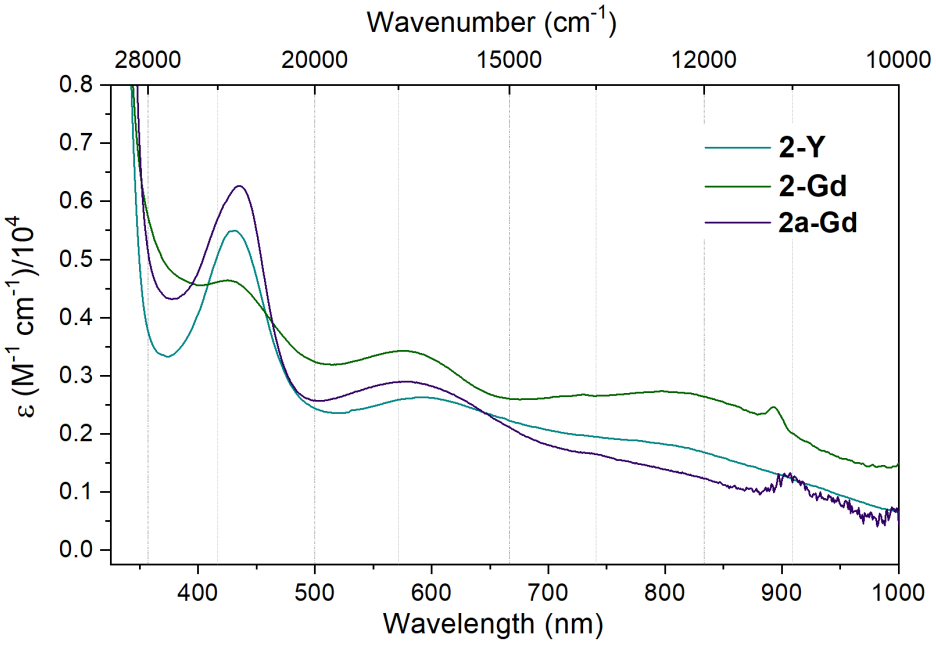

Figure 2.37: Electronic absorption spectra of 2-Ln (Ln = Y, Gd) and 2a-Gd, recorded on 1 μM MeCN solutions at R.T. The bump in the spectrum of 2-Gd and 2a-Gd at 890 nm is an artefact from a spectrometer lamp change.[1, 2]

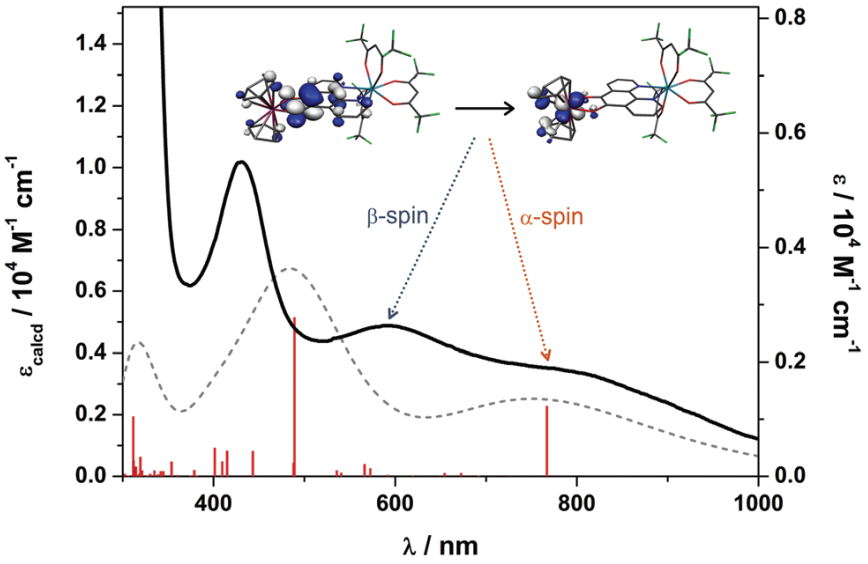

Figure 2.38: Overlaid experimental (solid line, right hand axis) and TD-DFT calculated (dashed line, left hand axis) electronic absorption spectra of 2-Y. Vertical bars show the individually calculated transitions. The inset shows the molecular orbitals involved in the predominant charge transfer transitions.[1]

2.3.4 Crystallography of 2a-Gd

Single crystals of **2a-Gd** suitable for X-ray diffraction were obtained by cooling a concentrated solution of **2a-Gd** in Et_2O to -35 °C overnight, with diffusion of hexane into the solution. The solid-state molecular structure of **2a-Gd** is shown in Figure 2.40. The hfac ligands and pd are arranged around Gd in the same manner as was observed for **1-Ln**, in a distorted square antiprismatic geometry. The vanadium atom is bound to the *O,O* site of pd, with the two oxygen atoms and two cyclopentadienyl ligands in a pseudo-tetrahedral arrangement, which is typical for V(IV) metallocenes.[67, 71] The Gd-O bond distances of 2.355(2)-2.390(2) Å and the Gd-N bond distances of 2.527(2)-2.532(2) Å are consistent with those in **1-Gd**, when crystallised from Et_2O (Gd-O 2.348(7)-2.383(7), Gd-N 2.555(9)-2.585(8) Å) or from toluene (Gd-O 2.32(2)-2.42(1), Gd-N 2.53(2)-2.58(1) Å). Overall, the Gd-N distances are slightly shorter, if not significantly so, due to the negative charge on the ligand.

Comparing the bond distances of the *O,O'* binding site to those observed for **1-Gd**, it is evident that the binding site has undergone an oxidation state change. In **2a-Gd**, the C5-C6 bond distance of 1.387(3) Å is consistent with a double C=C bond. The same bond in **1-Gd** had distances of 1.54(6) and 1.53(3) Å in the solid-state molecular structure as crystallised from Et_2O and toluene respectively, consistent with a single C-C bond. Likewise, in **2a-Gd**, the C-O(pd) bond distances of 1.333(3)-1.333(3) Å are consistent with single C-O bonds, whereas in **1-Gd** the C-O(pd) bond distances of 1.22(3)-1.26(3) Å are consistent with double C=O bonds. These bond assignments are consistent with a change from pd^0 to pd^{2-}, shown in Figure 1.7.

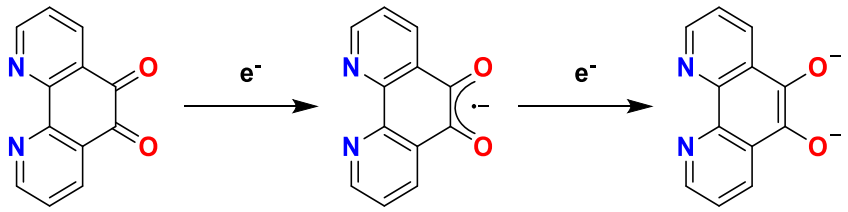

Figure 2.39: The reduction of pd to $pd^{\bullet-}$ and pd^{2-}

The V-O distances of 1.9862(18)-1.9869(18) Å are similar to those in related catecholate complexes $[Et_3NH]_2[V(cat)_3]$.MeCN (cat = catecholate) (V-O(cat) = 1.930(3) Å) and $VO(cat)_2(1,3\text{-HPDA})_2$.MeOH (1,3-PDA = 1,3-propanediamine) (V-O(cat) = 1.948(2)-1.968(2) Å).[68, 72] The bond distances in **2a-Gd** are therefore consistent with the pd ligand being in the pd^{2-} oxidation state, and this charge being localised on the *O,O'* site.

The solid-state molecular structure of **2-Y** is shown in Figure 2.41 for reference, and the key bond distances (C5-C6 1.40(3), C-O(pd) 1.24(2)-1.40(2), V-O 1.97(1)-1.97(2) Å) are consistent with those in **2a-Gd**. For **2-Y**, a significant difference between the two C-O bonds of 1.24(2) and 1.40(2) Å is believed to be due to crystal packing and not chemically significant.

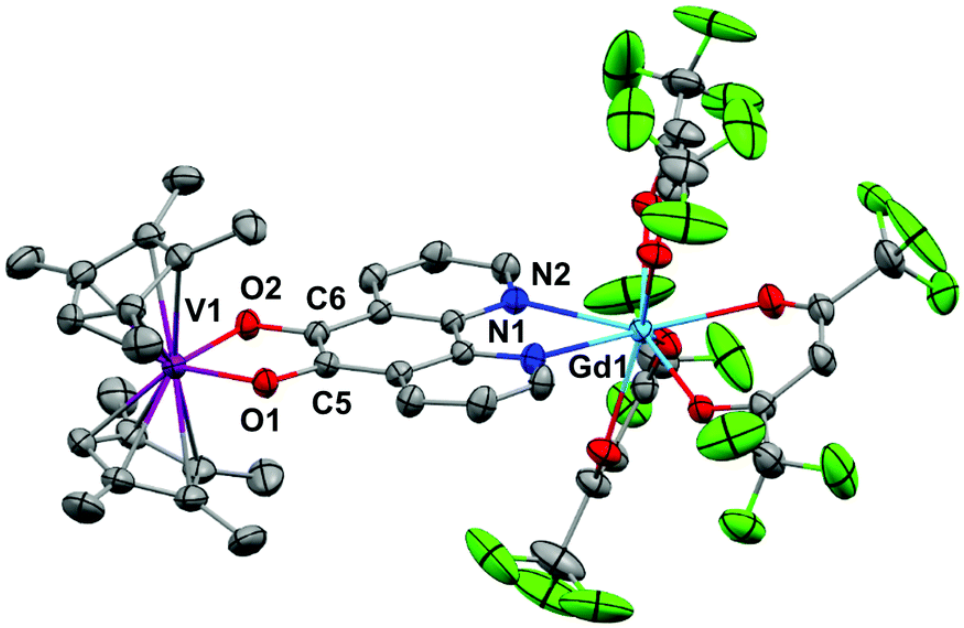

Figure 2.40: Solid-state molecular structure of 2a-Gd. Thermal ellipsoids are drawn at 50% probability. H atoms are omitted for clarity. Selected bond distances: Gd-O 2.355(2)-2.390(2), Gd-N 2.527(2)-2.532(2), C5-C6 1.387(3), C-O(pd) 1.333(3)-1.333(3), V-O 1.9862(18)-1.9869(18).

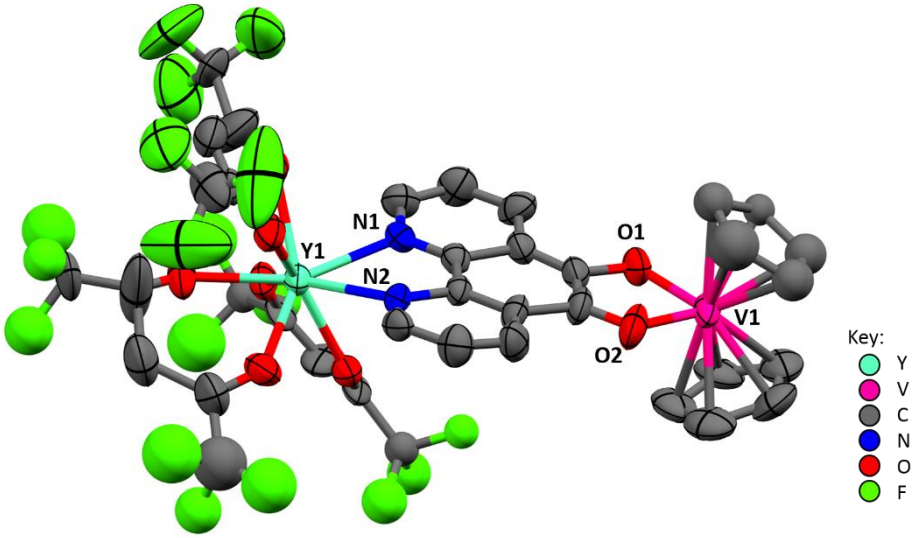

Figure 2.41: Solid-state molecular structure of 2-Y. Thermal ellipsoids are drawn at 50% probability. H atoms are omitted for clarity. Selected C and F atoms are refined isotropically due to disorder. Selected bond distances (Å): Y-O, 2.29(1)-2.37(2); Y-N, 2.47(2)-2.48(2); C5-C6, 1.40(3); C-O(pd), 1.24(2)-1.40(2); V-O, 1.97(1)-1.97(2); V-C, 2.29(1)-2.41(3). Y-V distance: 8.313(2) Å.

2.4 Conclusions

This chapter describes the development of a new and robust synthesis of **1-Ln** Ln(hfac)$_3$(*N,N'*-pd) (Ln = Y, Eu, Gd, Tb, Yb). These compounds are the first monometallic building blocks in the development of a modular multimetallic system which will be described in this thesis. Compounds **1-Ln** were fully characterised by NMR (except **1-Gd**), UV-vis and ATR-IR spectroscopies, and for **1-Gd** EPR spectroscopy and Evans Method magnetometry were employed.

By ^{1}H NMR spectroscopy the composition of the compounds was confirmed to be of a 1:1 adduct of pd to Ln, with three hfac ligands also coordinated in each case, supported by ^{19}F NMR measurements. Both ^{1}H and ^{19}F NMR spectroscopy proved to be of great use in the characterisation of the compounds, including of paramagnetic lanthanide-containing complexes. Trends in the sign and magnitude of the paramagnetic shift tensors were observed, which were consistent with the behaviour observed in a related series of lanthanide *tris*-diketonate phenanthroline compounds. The UV-vis spectra of **1-Ln** were recorded, and the absorptions in the UV region were each assigned to the π-π* transitions of the ligands. The absorptions in the visible region have extinction coefficients consistent with charge transfer, and these transitions displayed a particular dependence on the ionic radius and Lewis acidity of the lanthanides.

The solid-state molecular structures of all **1-Ln** were determined by single crystal X-ray diffractometry, and it was discovered that depending on the solvent of crystallisation, the solid-state molecular structure had significant variation. When Et_2O was used as the solvent for crystallisation, the pd ligand exhibited planar coordination to the lanthanide, with a C-N-Ln angle of close to 180°, and the extended structure was made up of discrete molecules. When toluene was used as the solvent of crystallisation, the pd ligand coordinated to Ln at an angle in medium-to-large **1-Ln** (Ln = Y, Gd, Tb; **1-Eu** was not crystallised from toluene) and in those **1-Ln** an increasingly strong interaction was observed between one O atom of pd and Ln, forming a 1-dimensional zig-zag coordination polymer in **1-Gd** with an *N,N'-O* binding mode. This interaction is more pronounced in **1-Ce** and **1-La**, which exhibit a chelating coordination polymer in the solid state.

The reaction of **1-Ln** with reducing agents $V(Cp^R)_2$ (Cp^R = Cp, Cp^t) was undertaken to investigate the redox properties of the compounds. These reactions produced $Ln(hfac)_3$(*N,N'*-*O,O'*-pd)$V(Cp^R)_2$, **2-Ln** (Ln = Y, Gd; Cp^R = Cp) and **2a-Gd** (Ln = Gd; Cp^R = Cp^t), which were fully characterised by UV-vis, ATR-IR and EPR spectroscopy, and Evans' Method magnetometry.

ATR-IR spectroscopy of **2-Ln** and **2a-Gd** provided evidence for the two-electron oxidative addition of $V(Cp^R)_2$ to the *O,O'* binding site of pd, displaying a characteristic stretching frequency for pd^{2-}. EPR spectroscopy was also consistent with this assignment, clearly indicating the presence of V(IV). Both EPR and Evans' Method magnetometry were consistent with the presence of two uninteracting spin centres in **2-Gd** and **2a-Gd**, in the form of Gd(III) ($4f^7$) and V(IV) ($3d^1$). In combination with TD-DFT analysis, the UV-visible electronic absorption spectra of **2-Ln** and **2a-Gd** were recorded and assigned fully, providing a key spectroscopic signature for pd^{2-}. The solid-state molecular structures of **2-Y** and **2a-Gd** were also determined. In addition to confirming the *N,N'*-coordination of Ln and the *O,O'*-coordination of V, the bond lengths in the redox-active *O,O'* site were consistent with the two-electron reduction of pd.

2.5 Synthetic details for Chapter 2

2.5.1 Starting materials

$V(Cp)_2$ and $V(Cp^t)_2$ were synthesised according to published procedures.[73] Hexafluoroacetyl acetone H(hfac) was purchased from Sigma Aldrich and degassed by three freeze-thaw cycles before use. Potassium hydride under mineral oil was purchased from Sigma Aldrich, the mineral oil was removed by washing with anhydrous hexanes and stored under N_2. Ln_2O_3 (Ln = Y, Eu, Gd, Yb) were purchased from Sigma Aldrich and used without further purification.

2.5.2 Synthesis and dehydration of $Ln(OTf)_3$

The following synthesis is a modification of published routes.[2, 11, 74]

A white powder of Ln_2O_3 was added to a thick-walled ampoule with a stirrer bar. Triflic acid (10 g) was added dropwise by pipette to 10 ml H_2O at 0 °C. Fumes were observed upon triflic acid addition and the diluted triflic acid was added to the ampoule. The ampoule was then sealed under partial vacuum and the suspension was heated to reflux (110 °C) with stirring for 16 h, after which a slightly cloudy solution was obtained. Water was removed by rotary evaporation (40 mbar, 50 °C) until precipitation was observed, then the mixture was filtered by frit to obtain $Ln(OTf)_3(H_2O)_x$ as a white, wet crystalline solid. The solids were washed several times with Et_2O (at least 5 x 5ml) until a sample of solid dissolved in H_2O had neutral pH. The $Ln(OTf)_3$ were then dried by heating to 200 °C overnight under vacuum (5 $x10^{-3}$ mbar) to afford $Ln(OTf)_3$ as a free-flowing white powder. Complete dehydration was confirmed by ATR-IR and ^1H NMR spectroscopy.

$Y(OTf)_3$ was synthesised using the following materials and quantities: Y_2O_3 (2.23 g, 9.88 mmol), HOTf (10 g, 66.6 mmol, 6.6 eq.). Yield: 6.35 g, 11.85 mmol, 60%.

$Eu(OTf)_3$ was synthesised using the following materials and quantities: Eu_2O_3 (3.55 g, 10.1 mmol), HOTf (10 g). Yield: 6.54 g, 10.91 mmol, 54%.

$Gd(OTf)_3$ was synthesised using the following materials and quantities: Gd_2O_3 (3.66 g, 10.1 mmol), HOTf (10 g). Yield: 8.67 g, 14.34 mmol, 71%.

$Yb(OTf)_3$ was synthesised using the following materials and quantities: Yb_2O_3 (4.17 g, 11 mmol), HOTf (10 g). Yield: 7.78 g, 12.54 mmol, 57%.

$Tb(OTf)_3$ was purchased from Sigma Aldrich and dehydrated by heating to 200 °C overnight under vacuum (5 $x10^{-3}$ mbar).

2.5.3 Synthesis of K(hfac)

H(hfac) (5 g, 24 mmol) was freeze-pump-thaw degassed, then added to a slurry of KH (1.0 g, 25 mmol) in THF (30 ml) at -78 °C with stirring. The suspension began to bubble as H_2 gas was evolved. The suspension was allowed to warm slowly to room temperature with a bleed needle to prevent pressure build-up, then stirred for 1 h at room temperature to ensure the reaction was complete. The suspension was filtered *via* a filter cannula, then THF was removed from the yellow solution *in vacuo* to yield a beige solid. The solid was washed with hexane (2x 15 ml) and dried *in vacuo*, yielding K(hfac) as a beige solid (3.13 g, 53%). [1]

2.5.4 Synthesis of 1,10-phenanthroline (pd)

The following synthesis is a modification of a previously published route.[2, 13]

A 3-necked flask was charged with H_2SO_4 (97%, 100 ml, 1.88 mol). The H_2SO_4 was frozen in a dry ice bath, then 1,10-phenanthroline (10 g, 47.6 mmol) and KBr (20 g, 168 mmol) were added. The mixture was warmed to RT over 30 m, to give an orange paste. After fitting a reflux condenser to the reaction flask HNO_3 (65%, 50 ml, 1.20 mol) was added dropwise through the condenser over 30 m. Orange Br_2 gas was evolved during addition. The reaction mixture was then heated to 130 °C and heated for 16 h, until evolution of Br_2 gas was complete. The reflux condenser was then removed and the mixture was poured onto ice (1 L) in a 5 L beaker. $NaHCO_3$ was added gradually with continual stirring until a pH paper test confirmed a neutral pH. The solution turned from a bright green/yellow colour when acidic to yellow/orange when neutral. A further colour change to green/brown would indicate that too much base has been added. Significant quantities of heat were evolved in this process, and ice was added as necessary to prevent the reaction proceeding too rapidly. The mixture was then filtered by using a Büchner funnel and extracted with CH_2Cl_2 (3x 20 ml) to obtain a yellow solution, which was dried by stirring over $MgSO_4$ for 2h. $MgSO_4$ was removed by Büchner filtration and CH_2Cl_2 was removed by rotary evaporation to obtain pd as a bright yellow solid. The solid was washed by stirring in MeOH (50 ml) for 1 h, then pd was dried *in vacuo* to obtain a free-flowing yellow powder (8.1 g, 38.5 mmol, 81%) ^{1}H NMR (*d*-chloroform): δ = 7.69 (dd, *J* = 7.9, 4.7 Hz, 2H, C(2,9)-**H**), 8.50 (dd, *J* = 7.9, 1.9 Hz, 2H, C(1,10)-**H**), 9.12 (dd, *J* = 4.7, 1.8 Hz, 2H, C(3,8)-**H**) ppm.

^{1}H NMR (d_3-acetonitrile): δ = 7.62 (dd, *J* = 7.8, 4.7 Hz, 2H, C(2,9)-**H**), 8.42 (dd, *J* = 7.8, 1.8 Hz, 2H, C(1,10)-**H**), 9.03 (dd, *J* = 4.7, 1.8 Hz, 2H, C(3,8)-**H**) ppm. UV-vis (MeCN) λ_{max}/nm (ε/$M^{-1}cm^{-1}$): 257 (37 800), 480 (18).

2.5.5 Synthesis of 1-Eu Eu(hfac)$_3$(*N,N'*-pd)

This synthesis is a modified and optimised version of a published procedure.

$Eu(OTf)_3$ (0.632 g, 1.06 mmol), K(hfac) (0.814 g, 3.17 mmol, 3 eq.) and pd (0.221 g, 1.05 mmol, 1 eq.) were added to a Schlenk flask, then THF (20 ml) was added with stirring. Upon addition of THF, a characteristic colour change from yellow to deep green was observed. Removal of THF *in vacuo* afforded a dark green solid which was extracted into toluene (2x 15 ml) and filtered by filter cannula to exclude K(OTf). The toluene extract was concentrated to saturation (*ca* 15 ml) *in vacuo*, then cooled to -15 °C overnight, whereupon **1-Eu** precipitated from solution as a microcrystalline green solid. The supernatant was decanted using a narrow-bore cannula and the green solid was washed with hexane (3x 15 ml) then dried *in vacuo*. A second crop of microcrystals was obtained by re-concentration of the supernatant to *circa* half volume. The two recrystallisations yielded **1-Eu** as a green solid (0.8087 g, 0.822 mmol, 78%). Single crystals suitable for X-ray diffraction were obtained by cooling a saturated Et_2O solution to -35 °C overnight. ^{1}H NMR (d_6-benzene): *δ* = 3.85 (s, 3H, hfac-C**H**), 6.87 (d, *J* = 8 Hz, 2H, C(2,9)-**H**), 9.01 (d, *J* = 8 Hz, 2H, C(3,8)-**H**), 11.34 (s, 2H, C(1,10)-**H**) ppm. ^{19}F{^{1}H} NMR (d_6-benzene): *δ* = -79.30 (s, hfac-C**F**$_3$) ppm. IR(ATR)/cm^{-1} (intensity): 1697 (w, pd-ν_{CO}), 1660 (sh, pd-ν_{CO}), 1645 (s, hfac-ν_{CO}), 1611 (m), 1576 (m), 1533 (m), 1491 (s), 1470 (m), 1252 (s), 1194 (s), 1136 (s), 1020 (w). UV-vis (MeCN) λ_{max}/nm (ε/M^{-1} cm^{-1}): 302 (28 100), 453 (60.0), 603 (70.9). Anal. calcd. for $C_{27}H_9N_2EuO_8F_{18}\cdot C_7H_8$: C, 37.79%; H, 1.59%; N, 2.60%. Found: C, 36.58-36.68%; H, 1.30-1.35%; N, 2.47-2.47%.

2.5.6 Synthesis of 1-Gd Gd(hfac)$_3$(*N,N'*-pd)

1-Gd was synthesised using an analogous synthesis to **1-Eu** using the following materials and quantities: $Gd(OTf)_3$ (0.759 g, 1.25 mmol); K(hfac) (0.997 g, 3.77 mmol, 3 eq.); pd (0.263 g, 1.25 mmol, 1 eq.). Yield: 79%. Single crystals suitable for X-ray diffraction were obtained by cooling saturated solutions of both Et_2O and toluene to -35 °C overnight. IR(ATR)/cm^{-1} (intensity): 1697 (w, pd-ν_{CO}) 1661 (w, pd-ν_{CO}) 1647 (s) 1495 (m) 1252 (m) 1202 (m) 1142 (s) 1098 (w) 802 (s) 732 (m) 660 (s). UV-vis (MeCN) λ_{max}/nm (ε/$M^{-1}cm^{-1}$): 302 (26 400), 455 (78.8)

597 (129). **1-Gd** is NMR silent. Anal. calcd for $C_{27}H_9N_2O_8F_{18}Gd \cdot C_7H_8$: C, 37.79%; H, 1.59%; N, 2.59%. Found: C, 37.58%; H, 1.47%; N, 2.54%. μ_{eff} (Evans' method) (d_8-THF) 7.56–7.71 BM.

2.5.7 Synthesis of 1-Tb Tb(hfac)$_3$(*N,N'*-pd)

1-Tb was synthesised using an analogous synthesis to **1-Eu** using the following materials and quantities: $Tb(OTf)_3$ (0.501 g, 0.828 mmol); K(hfac) (0.639 g, 2.49 mmol, 3 eq.); pd (0.175 g, 0.833 mmol, 1 eq.). Yield: 67%. Single crystals suitable for X-Ray diffraction were obtained from a concentrated toluene solution cooled at -15 °C over 3 days. ^{1}H NMR (d_6-benzene): δ = -178.55 (s (br), 2H, C(1,10)-**H**), -32.83 (s, 2H, C(2,9)-**H**), -11.68 (s, 2H, C(3,8)-**H**), 103.69 (s, 3H, hfac-C**H**) ppm. ^{19}F{^{1}H} NMR (d_6-benzene): δ = -63.32 (s, hfac-C**F**$_3$) ppm. IR(ATR)/cm^{-1} (intensity): 1699 (w, pd-ν_{CO}), 1665 (w, pd-ν_{CO}), 1647 (s, hfac-ν_{CO}), 1612 (w), 1570 (w), 1533 (m), 1487 (m), 1429 (w), 1252 (s), 1202 (s), 1134 (s), 1024 (w). UV-vis (MeCN) λ_{max}/nm (ε/M^{-1} cm^{-1}): 256 (37 900), 301 (37 800), 454 (44), 597 (25.7). Anal. calcd. for $C_{27}H_9N_2O_8F_{18}Tb$: C, 32.29%; H, 0.92%; N, 2.83%. Found: C, 32.67-33.55%; H, 0.83-0.83%; N, 2.77-2.85%.

2.5.8 Synthesis of 1-Yb Yb(hfac)$_3$(*N,N'*-pd)

1-Yb was synthesised using an analogous synthesis to **1-Eu** using the following materials and quantities: $Yb(OTf)_3$ (0.9833 g, 1.59 mmol); K(hfac) (1.1714 g, 4.76 mmol, 3 eq.); pd (0.3334 g, 1.59 mmol, 1 eq.). Yield: 64%. Single crystals suitable for X-ray diffraction were obtained by crystallisation from both saturated toluene and Et_2O solutions at -35 °C after 24 hours. ^{1}H NMR (d_6-benzene): δ = -7.00 (s, 3H, hfac-C**H**), 9.27 (s (br), 2H, C(1,10)-**H**), 10.59 (s, 2H, C(2,9)-**H**), 15.19 (s, 2H, C(3,8)-**H**) ppm. ^{19}F{^{1}H} NMR (d_6-benzene): δ = -84.42 ppm (s, hfac-C**F**$_3$). IR(ATR)/cm^{-1} (intensity): 1701 (m, pd-ν_{CO}), 1667 (w, pd-ν_{CO}), 1649 (s, hfac-ν_{CO}), 1612 (m), 1498 (m), 1429 (w), 1252 (s), 1206 (s), 1134 (m), 1026 (w). UV-vis (MeCN) λ_{max}/nm (ε/M^{-1} cm^{-1}): 292 (36 600), 483 (17.2). Anal. calcd. for $C_{27}H_9N_2O_8F_{18}Yb$: C, 32.29%; H, 0.90%; N, 2.79%. Found: C, 33.61%; H, 1.08-1.16%; N, 2.63-2.77%.

2.5.9 Synthesis of 2-Gd Gd(hfac)$_3$(*N,N'-O,O'*-pd)V(Cp)$_2$

THF (15 mL) was added to a dry mixture of **1-Gd** (500 mg, 0.505 mmol) and $V(Cp)_2$ (91.3 mg, 0.504 mmol) and the dark suspension was stirred for 24 h. THF was removed *in vacuo*. Gd(hfac)$_3$(N,N'-O,O'-pd)V(Cp)$_2$ was extracted into toluene with filtration by filter cannula and cooled to -15 °C, whereupon it precipitated as a black powder (378 mg, 0.322 mmol, 64% yield). The solid was ^{1}H NMR and ^{19}F{^{1}H} NMR silent. IR(ATR)/cm^{-1} (intensity): 1651 (m, hfac-

ν_{CO}) 1497 (m) 1381 (w, ν_{CO}) 1258 (m) 1204 (w) 1134 (s) 1018 (s) 795 (s) 656 (m). UV-vis (MeCN) λ_{max}/nm (ε/M^{-1} cm^{-1}): 425 (4 650) 576 (3 430) 797 (2 740). Anal. Calcd. for $C_{37}H_{19}F_{18}N_2O_8VGd$: C, 37.99%; H, 1.64%; N, 2.39%. Found: C, 37.11%; H, 1.70%; N, 2.38%.

2.5.10 Synthesis of 2a-Gd Gd(hfac)$_3$(*N,N'-O,O'*-pd)V(Cp^t)$_2$

Et_2O (30 ml) was added to a dry mixture of **1-Gd** (130 mg, 0.13 mmol) and V(Cp^t)$_2$ (38 mg, 0.13 mmol) at -78 °C and the reaction was stirred at room temperature for 16 h. The suspension was filtered *via* filter cannula and Et_2O was removed *in vacuo*. The solids were recrystallised from a saturated toluene and hexane solution at -15 °C overnight. The mother liquor was decanted and the crystals were washed with hexane (3x 15 ml) and dried *in vacuo* to obtain **2a-Gd** as a dark powder (70 mg, 5.4 mmol, 42%). Crystals suitable for X-ray diffraction were grown by diffusion of hexane vapour into an Et_2O solution at -35 °C over several days. IR(ATR)/cm^{-1} (intensity): 1650 (s, hfac-ν_{CO}), 1500 (m), 1370 (w, ν_{CO}), 1250 (s), 800 (m), 733 (w), 662 (m). UV-vis (MeCN) λ_{max} (ε/M^{-1} cm^{-1})/nm: 440 (4115), 700 (2160). Anal. Calcd. for $C_{45}H_{35}F_{18}N_2O_8VGd$: C, 42.16%; H, 2.75%; N, 2.19%. Found: C, 42.45%; H, 3.18%; N, 2.04%.

2.6 References

1. J. R. Hickson, PhD, Imperial College London, 2018.
2. J. R. Hickson, S. J. Horsewill, C. Bamforth, J. McGuire, C. Wilson, S. Sproules and J. H. Farnaby, *Dalton Trans.*, 2018, **47**, 10692-10701.
3. S. J. Horsewill, D. Phipps, O. Umeano, N. Fairbairn, G. Hedley, B. Wilson, C. Wilson and J. H. Farnaby, *Manuscript in preparation*.
4. G. Malandrino, R. Lo Nigro, L. Fragalà Ignazio and C. Benelli, *Eur. J. Inorg. Chem.*, 2003, **2004**, 500-509.
5. O. L. Malta and F. R. Gonçalves e Silva, *Spectrochim. Acta A Mol. Biomol.*, 1998, **54**, 1593-1599.
6. A. N. Swinburne, M. H. L. Paden, T. L. Chan, S. Randall, F. Ortu, A. M. Kenwright and L. S. Natrajan, *Inorganics*, 2016, **4**, 27.
7. C. R. De Silva, J. R. Maeyer, R. Wang, G. S. Nichol and Z. Zheng, *Inorg. Chim. Acta*, 2007, **360**, 3543-3552.
8. Y. Bi , Y.-N. Guo, L. Zhao, Y. Guo, S.-Y. Lin, S.-D. Jiang, J. Tang, B.-W. Wang and S. Gao, *Chem. Eur. J.*, 2011, **17**, 12476-12481.
9. N. M. Shavaleev, L. P. Moorcraft, S. J. A. Pope, Z. R. Bell, S. Faulkner and M. D. Ward, *Chem. Commun.*, 2003, DOI: 10.1039/B301878D, 1134-1135.
10. B. V. Bukvetskii, A. G. Mirochnik and A. S. Shishov, *J. Lumin.*, 2018, **195**, 44-48.
11. S. Kobayashi, M. Sugiura, H. Kitagawa and W. W. L. Lam, *Chem. Rev.*, 2002, **102**, 2227-2302.
12. M. D. Taylor, *Chem. Rev.*, 1962, **62**, 503-511.
13. M. Yamada, Y. Tanaka, Y. Yoshimoto, S. Kuroda and I. Shimao, *Bull. Chem. Soc. Jpn.*, 1992, **65**, 1006-1011.
14. "Paramagnetic NMR Lanthanide Induced Shifts for Extracting Solution Structures" in *Handbook on Physics and Chemistry of the Rare Earths*, 2005.
15. M. Autillo, L. Guerin, T. Dumas, M. S. Grigoriev, A. M. Fedoseev, S. Cammelli, P. L. Solari, D. Guillaumont, P. Guilbaud, P. Moisy, H. Bolvin and C. Berthon, *Chem. Eur. J.*, 2019, **25**, 4435-4451.
16. C. Nitsche and G. Otting, *Prog. Nucl. Magn. Reson. Spectrosc.*, 2017, **98-99**, 20-49.
17. C. Schmitz, R. Vernon, G. Otting, D. Baker and T. Huber, *J. Mol. Biol.*, 2012, **416**, 668-677.
18. J. Koehler and J. Meiler, *Prog. Nucl. Magn. Reson. Spectrosc.*, 2011, **59**, 360-389.
19. K. Mason, A. C. Harnden, C. W. Patrick, A. W. J. Poh, A. S. Batsanov, E. A. Suturina, M. Vonci, E. J. L. McInnes, N. F. Chilton and D. Parker, *Chem. Commun.*, 2018, **54**, 8486-8489.

20. A. C. Harnden, E. A. Suturina, A. S. Batsanov, P. K. Senanayake, M. A. Fox, K. Mason, M. Vonci, E. J. L. McInnes, N. F. Chilton and D. Parker, *Angew. Chem. Int. Ed.*, 2019, **58**, 10290-10294.

21. Z. Ahmed and K. Iftikhar, *Inorg. Chim. Acta*, 2010, **363**, 2606-2615.

22. Z. Ahmed and K. Iftikhar, *Inorg. Chim. Acta*, 2012, **392**, 165-176.

23. M. C. Heffern, L. M. Matosziuk and T. J. Meade, *Chem. Rev.*, 2014, **114**, 4496-4539.

24. S. K. Sur, *J. Mag. Res. (1969)*, 1989, **82**, 169-173.

25. B. Odom, D. Hanneke, B. D'Urso and G. Gabrielse, *Phys. Rev. Lett.*, 2006, **97**, 030801.

26. P. Bertrand, in *Electron Paramagnetic Resonance Spectroscopy: Fundamentals*, ed. P. Bertrand, Springer International Publishing, Cham, 2020, pp. 289-321.

27. M. Hardiman, J. Pellisson, S. E. Barnes, P. E. Bisson and M. Peter, *Physical Review B*, 1980, **22**, 2175-2194.

28. G. A. Fox, S. Bhattacharya and C. G. Pierpont, *Inorg. Chem.*, 1991, **30**, 2895-2899.

29. F. Calderazzo, F. Marchetti, G. Pampaloni and V. Passarelli, *J. Chem. Soc., Dalton Trans.*, 1999, **24**, 4389-4396.

30. C.-Y. Fu, L. Chen, X. Wang and L.-R. Lin, *ACS Omega*, 2019, **4**, 15530-15538.

31. N. B. D. Lima, A. I. S. Silva, P. C. Gerson, Jr., S. M. C. Gonçalves and A. M. Simas, *PLoS One*, 2015, **10**, e0143998-e0143998.

32. C. A. Goss and H. D. Abruna, *Inorg. Chem.*, 1985, **24**, 4263-4267.

33. J.-C. G. Bünzli, *Chem. Rev.*, 2010, **110**, 2729-2755.

34. J.-C. G. Bunzli and S. V. Eliseeva, in *Lanthanide Luminescence: Photophysical, Analytical and Biological Aspects*, eds. P. Hanninen and H. Harma, Springer, Berlin, 2011, vol. 7, pp. 1-46.

35. I. V. Taidakov, Y. A. Strelenko, R. S. Borisov, A. Z. Temerdashev, N. P. Datskevich and A. G. Vitukhnovskii, *Russ. J. Coord. Chem.*, 2015, **41**, 230-239.

36. D. Roitershtein, Â. Domingos, L. C. J. Pereira, J. R. Ascenso and N. Marques, *Inorg. Chem.*, 2003, **42**, 7666-7673.

37. S. Herzog and K. Gustav, *Z. Anorg. Allg. Chem.*, 1966, **346**, 150-161.

38. S. Berger, J. Fiedler, R. Reinhardt and W. Kaim, *Inorg. Chem.*, 2004, **43**, 1530-1538.

39. D. M. Murphy, K. McNamara, P. Richardson, V. Sanchez-Romaguera, R. E. P. Winpenny and L. J. Yellowlees, *Inorg. Chim. Acta*, 2011, **374**, 435-441.

40. P. Atkins, T. Overton, J. Rourke, M. Weller and F. Armstrong, in *Shriver & Atkins: Inorganic Chemistry*, Oxford University Press, Oxford, 4th edn., 2006, ch. *d*-metal complexes: Electronic Structure and Spectra, pp. 459-490.

41. N. M. Shavaleev, L. P. Moorcraft, S. J. A. Pope, Z. R. Bell, S. Faulkner and M. D. Ward, *Chem. Eur. J.*, 2003, **9**, 5283-5291.

42. M. Yano, K. Matsuhira, M. Tatsumi, Y. Kashiwagi, M. Nakamoto, M. Oyama, K. Ohkubo, S. Fukuzumi, H. Misaki and H. Tsukube, *Chem. Commun.*, 2012, **48**, 4082-4084.

43. I. V. Taydakov, V. M. Korshunov, Y. A. Belousov, Y. V. Nelyubina, F. Marchetti, R. Pettinari and C. Pettinari, *Inorg. Chim. Acta*, 2020, **513**, 119922.

44. K. Binnemans, in *Handbook on the Physics and Chemistry of Rare Earths*, eds. K. A. Schneider, J.-C. Bunzli and V. K. Pecharsky, Elsevier, 2005, vol. 35, ch. 225, pp. 107-272.

45. R. D. Shannon, *Acta Crystallogr. Sect. A*, 1996, **32**, 751-767.

46. S. Cotton, *Lanthanide and Actinide Chemistry*, John Wiley & Sons Ltd., Chichester, 2006.

47. L. Bertolo, S. Tamburini, P. A. Vigato, W. Porzio, G. Macchi and F. Meinardi, *Eur. J. Inorg. Chem.*, 2006, **2006**, 2370-2376.

48. Y.-M. Song, J.-P. Xu, L. Ding, Q. Hou, J.-W. Liu and Z.-L. Zhu, *J. Inorg. Biochem.*, 2009, **103**, 396-400.

49. Y. Li, Y. Li, Y. Chu, X. Tao, H. Xu, Y. Shen and A. Zheng, *J. Lumin.*, 2012, **132**, 1663-1667.

50. Y. Li, Y. Li, H. Xu, X. Tao, D. Zhang and Y. Shen, *J. Rare Earths*, 2010, **28**, 654-659.

51. M. Abdus Subhan, M. Saifur Rahman, K. Alam and M. Mahmud Hasan, *Spectrochim. Acta A Mol. Biomol.*, 2014, **118**, 944-950.

52. X.-F. Zhang, C.-J. Xu and J. Wan, *Monatsh. Chem.*, 2014, **145**, 1913-1917.

53. M. Bortoluzzi, D. Battistel, G. Albertin, S. Daniele, F. Enrichi and R. Rumonato, *Chem. Papers*, 2016, **70**, 43-52.

54. J.-W. Dai, Z.-Y. Li and O. Sato, *Acta Cryst. E*, 2014, **70**, o573.

55. A. Hussain, S. Saha, R. Majumdar, R. R. Dighe and A. R. Chakravarty, *Indian J. Chem., Sect A*, 2011, **50**, 519-530.

56. W. H. Watson, R. J. Williams and N. R. Stemple, *J. Inorg. Nucl. Chem.*, 1972, **34**, 501-508.

57. H.-Y. Wong, W.-S. Lo, W. T. K. Chan and G.-L. Law, *Inorg. Chem.*, 2017, **56**, 5135-5140.

58. P. Hu, F.-P. Xiao, Y. Li, J.-F. Cao, Z.-S. Chen, L.-L. Zhu and W.-P. Huang, *Inorg. Chem. Commun.*, 2017, **84**, 207-211.

59. L.-N. Sun, H.-J. Zhang, Q.-G. Meng, F.-Y. Liu, L.-S. Fu, C.-Y. Peng, J.-B. Yu, G.-L. Zheng and S.-B. Wang, *J. Phys. Chem. B*, 2005, **109**, 6174-6182.

60. L.-N. Sun, J.-B. Yu, G.-L. Zheng, H.-J. Zhang, Q.-G. Meng, C.-Y. Peng, L.-S. Fu, F.-Y. Liu and Y.-N. Yu, *Eur. J. Inorg. Chem.*, 2006, **2006**, 3962-3973.

61. S. Alvarez, *Dalton Trans.*, 2013, **42**, 8617-8636.

62. P. A. Kollman and L. C. Allen, *Chem. Rev.*, 1972, **72**, 283-303.

63. F. Maharaj, V. Russell, H. Chow, M. Page, M. Scudder, D. Craig and I. Dance, *CrystEngComm*, 2003, **5**, 285-293.

64. V. Russell, M. Scudder and I. Dance, *J. Chem. Soc., Dalton Trans.*, 2001, **6**, 789-799.

65. C. Janiak, *J. Chem. Soc., Dalton Trans.*, 2000, **21**, 3885-3896.

66. J. D. L. Holloway and W. E. Geiger, *J. Am. Chem. Soc.*, 1979, **101**, 2038-2044.

67. B. Gleeson, J. Claffey, M. Hogan, H. Müller-Bunz, D. Wallis and M. Tacke, *J. Organomet. Chem.*, 2009, **694**, 1369-1374.

68. S. R. Cooper, Y. B. Koh and K. N. Raymond, *J. Am. Chem. Soc.*, 1982, **104**, 5092-5102.

69. J. L. Petersen and L. F. Dahl, *J. Am. Chem. Soc.*, 1975, **97**, 6422-6433.

70. D. P. Bakalik and R. G. Hayes, *Inorg. Chem.*, 1972, **11**, 1734-1738.

71. J. A. Belot, R. D. McCullough, A. L. Rheingold and G. P. A. Yap, *Organometallics*, 1996, **15**, 5062-5065.

72. Z. Chi, L. Zhu, X. Lu, H. Yu and B. Liu, *Z. Anorg. Allg. Chem.*, 2012, **638**, 1523-1530.

73. L. E. Manzer, E. A. Mintz and T. J. Marks, *Inorg. Synth.*, 1989, **28**, 260-263.

74. S. Fukuzumi, Y. Fujii and T. Suenobu, *J. Am. Chem. Soc.*, 2001, **123**, 10191-10199.

3 Synthesis of the radical anion of 1,10-phenanthroline-5,6-dione and its reactivity with lanthanide coordination compounds

Publications:

The following publications report work detailed in this chapter:
J. R. Hickson, S. J. Horsewill, J. McGuire, C. Wilson, S. Sproules and J. H. Farnaby, *Chem. Commun.*, 2018, **54**, 11284-11287.

3.1 Abstract

The first molecular example of the radical anion of the 1,10-phenanthroline-5,6-dione (pd) ligand, $[CoCp_2]^+[pd]^{-\bullet}$ **3** (Cp^- = cyclopentadienyl) have been synthesised and fully characterised. Its lanthanide coordination chemistry has been investigated by reaction with $Ln(hfac)_3(S)_2$ **4-Ln** (Ln = Y, Eu, Gd, Yb; S = THF, MeCN) and lanthanide radical compounds $[CoCp_2]^+[Ln(hfac)_3(N,N'\text{-pd})]^{-\bullet}$ **5-Ln** (Ln = Y, Eu, Gd, Yb) were synthesised and fully characterised. Compound **3** was synthesised in excellent yields, and the oxidation state of the ligand was confirmed by UV-visible, ATR-IR and EPR spectroscopies and by X-ray crystallography. The electronic structure of the ligand in the radical anion oxidation state was also studied by TD-DFT analysis. The synthesis of lanthanide coordination compounds **4-Ln** was optimised under oxygen- and moisture-free conditions to allow for investigation of their reaction with **3**. Full characterisation of **4-Ln** by NMR, UV-vis and ATR-IR spectroscopy, and X-ray crystallography was undertaken. The reaction of **3** with **4-Ln** was investigated and the resulting compounds **5-Ln** were synthesised in high yields, and fully characterised. NMR, UV-vis, ATR-IR and EPR spectroscopies were carried out in conjunction with TD-DFT analysis on **5-Y**. The data were consistent with the lanthanide being selectively bound to the *N,N'* site of pd, and with the ligand remaining in the radical oxidation state.

3.2 Synthesis of $[CoCp_2]^+[pd]^{-\bullet}$ 3

3.2.1 Starting material choice and synthesis

The chemistry of the pd ligand has been explored, particularly with the transition metals, in both the neutral and the dianionic oxidation states.[1-6] The coordination chemistry of pd to the lanthanides in the neutral oxidation state was explored in the previous chapter, and it was demonstrated that it is possible to perform redox operations on the ligand while coordinated to lanthanides. However, before the work described below was undertaken, the radical anion of the pd ligand had never been isolated in a molecular compound. Spectroelectrochemical studies had successfully generated the radical anion of pd in solution, and probed its properties,[7-9] and one study investigated chemically generated compounds of the radical anion of pd in solution.[10] Additionally, there had also been reports of solid-state materials containing the radical anion of pd.[4] Initial efforts in our laboratory to effect the single electron reduction of pd while coordinated to lanthanides were unsuccessful. The reduction of **1-Ln** with potent single-electron reducing agents resulted in multiple decomposition products being obtained, largely due to breakdown of the hfac ligands.[11] The reduction of pd using KH was also attempted.[11] The spectroscopic data of the product were consistent with $[K]^+[pd]^{-\bullet}$, with the ligand being in the radical anion oxidation state. However, the synthetic utility of $[K]^+[pd]^{-\bullet}$ was limited and another synthon was targeted.

In order to access the radical anion form of the ligand, cobaltocene $CoCp_2$ (Cp^- = cyclopentadienyl) was selected as a potent single-electron reducing agent. For reference, the single-electron reduction potential of $CoCp_2$ is -1.33 V (vs. Fc/Fc^+).[12] Additionally, the cobaltocenium cation typically remains in the outer coordination sphere, and is unlikely to have a close interaction with the ligand. This is desirable both for investigating the electronic properties of the ligand and should not impede the investigation of further coordination and transmetallation reactivity. Cobaltocene $CoCp_2$ was synthesised by the reaction of anhydrous $CoCl_2$ with 2 eq. of the cyclopentadienyl salt NaCp. Purification of $CoCp_2$ was performed by either sublimation or by extraction into hexanes, followed by recrystallisation from a concentrated hexane solution at -35 °C.

3.2.2 Synthesis of $[CoCp_2]^+[pd]^{-\bullet}$ 3

The first molecular example of the radical anion of the pd ligand, $pd^{-\bullet}$, was synthesised by the reaction of pd with cobaltocene $CoCp_2$ as shown in Scheme 3.1. The synthesis of **3** was initially performed in MeCN,[13] though it has since been optimised to that presented here. A yellow solution of pd in THF was then added to a slight excess of $CoCp_2$ (1.1 eq.) in THF with stirring. Immediately, purple solids precipitated from the solution. The suspension was filtered by filter cannula, then the purple solids were washed with THF and hexane to obtain $[CoCp_2]^+[pd]^{-\bullet}$ **3** as a purple solid in excellent yield (93%). Purity was confirmed by elemental analysis.

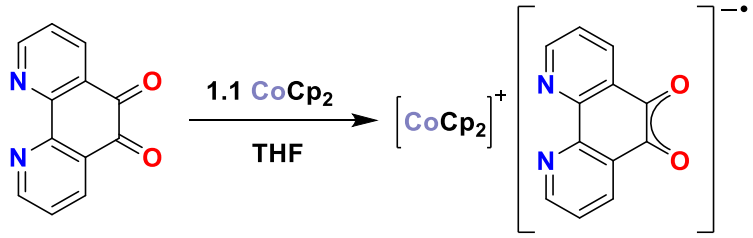

3; 93%

Scheme 3.1: Optimised synthesis of 3

3.2.3 NMR Spectroscopy of 3

In the ^1H NMR spectrum of **3**, recorded in d_3-acetonitrile, only a singlet resonance is observed at δ = 5.67 ppm (with a full width at half height (fwhh) of 10 Hz), which is assigned to the aromatic protons of the $[CoCp_2]^+$ counter cation. The chemical shift is consistent with the resonance of the $[CoCp_2]^+[OTf]^-$ salt, observed at δ = 5.77 ppm in d_2-dichloromethane.[14] As expected, the organic radical in **3** results in the pd ligand being NMR silent.

3.2.4 EPR Spectroscopy of 3

As a radical organic species, **3** has an informative EPR spectrum. The X-band EPR spectrum was recorded of a dilute MeCN solution of **3**, shown in Figure 3.1. It shows an organic radical with a g value of 2.0053, close to that of a free electron (g = 2.0023).[15] Hyperfine coupling is observed to each of the H and N atoms of pd, resulting in a complex spectrum, which nevertheless was well simulated and has good agreement with electrochemically generated examples of the pd radical anion in solution.[7, 8] DFT Mulliken spin density calculations performed on the radical anion $[pd]^{-\bullet}$ found that the radical is localised almost entirely on the

O,O' site (Figure 3.2). A small amount of delocalisation to the C and N atoms of the pd ligand is consistent with the hyperfine coupling observed in the EPR spectrum.[13]

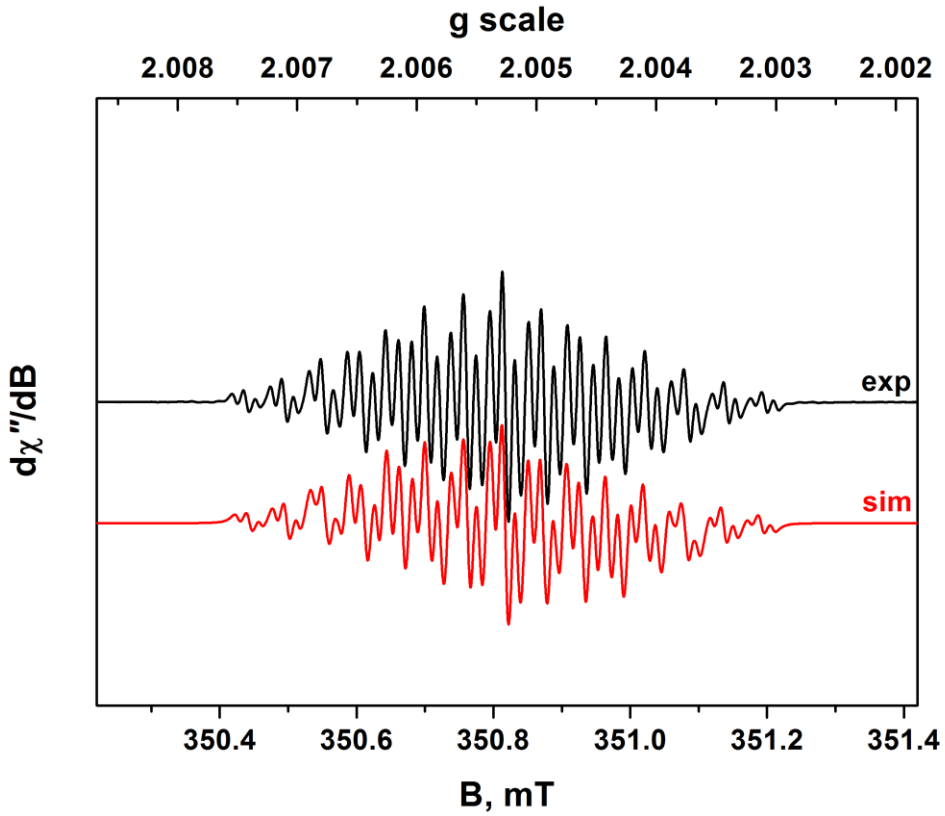

Figure 3.1: X-band EPR spectrum of 3 $[CoCp_2]^+[pd]^{-\bullet}$, recorded in MeCN at R.T. g = 2.0053; $J(^1H)$ = 1.40, 1.08, 1.56 x 10^{-4} cm^{-1}; $J(^{14}N)$ = 0.51 x 10^{-4} cm^{-1} (experimental conditions: frequency, 9.8461 GHz; power, 0.63 mW; modulation, 0.007 mT).

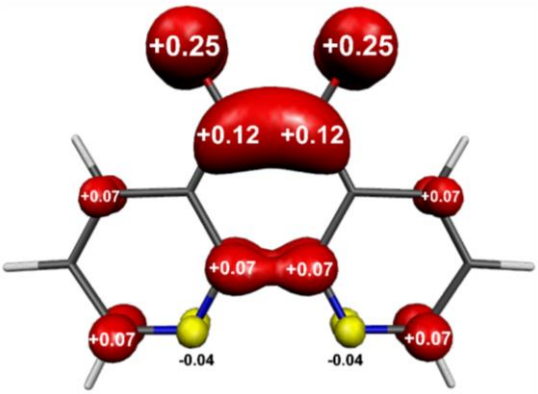

Figure 3.2: Calculated Mulliken spin density distribution for $[pd]^{-\bullet}$ (red: α-spin, yellow: β-spin).

3.2.5 ATR-IR spectroscopy of 3

As discussed in Chapter 2, IR spectroscopy may be used as an indicator of the oxidation state of pd (pd^0, 1678 cm^{-1}; pd$^{-\bullet}$, 1400-1500 cm^{-1}; pd^{2-}, 1300-1400 cm^{-1}).[2, 3] The ATR-IR spectrum (Figure 3.3) of **3** does not exhibit a significant absorption in the carbonyl (1600-1700 cm^{-1}) region, as observed for pd^0 in **1-Ln** (see Section 2.2.6), consistent with the full reduction of the pd ligand. No significant absorptions are observed in the region 1300-1400 cm^{-1}, as would be expected for pd^{2-} (1370-1380 cm^{-1} in **2-Ln**). Assignment of the radical semiquinone stretching frequency is non-trivial as it is expected to exhibit a stretching frequency between 1400-1500 cm^{-1}, which is the same spectral region as the various C-C and C-H stretching frequencies and bending modes of the Cp$^-$ and pd ligands.[3, 4] However, the assignment of 1402 and 1413 cm^{-1} as the semiquinone stretching frequency is made, by comparison to the ATR-IR spectra of **3** to **1-Ln**, **2-Ln** and to [K]$^+$[pd]$^{-\bullet}$.[11, 13, 16]

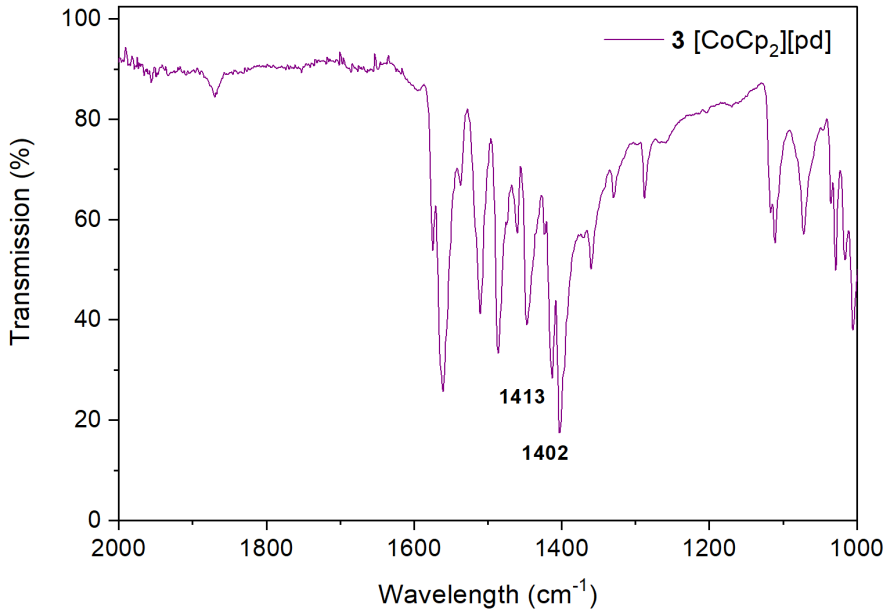

Figure 3.3: The ATR-IR spectrum of 3

3.2.6 UV-vis-NIR spectroscopy of 3

The solid **3** is dark purple, and in solutions of greater than 0.1 mM concentration **3** is an extremely deep purple colour, significantly more coloured than pd or **1-Ln**, as expected for a radical species. The UV-vis-NIR absorption spectrum of **3** shows two maxima, at 558 (3866) and 401 nm (3246 M^{-1} cm^{-1}) (Figure 3.4). The extinction coefficients of these peaks are consistent with π-π* transitions.[17] The peak positions and profile of the absorption spectrum

are consistent with those observed for the radical anion of pd,[8] and its transition metal complexes[7] when generated electrochemically in solution, and the qualitatively obtained spectrum of $[K]^+[pd]^{-\bullet}$.[11] For a more in-depth analysis of the electronic structure of the ligand, TD-DFT simulations were performed on the $[pd]^{-\bullet}$ anion.[13] The calculated absorption spectra are shown in Figure 3.4 as the dotted line, and have excellent agreement with the experimentally obtained spectrum of **3**. The key maxima at 401 and 558 nm were determined by TD-DFT to be due to π-π* transitions of the pd ligand. In particular, the predominant transition at 558 nm was determined to be the SOMO to LUMO+1 transition, illustrated in the inset in Figure 3.4.

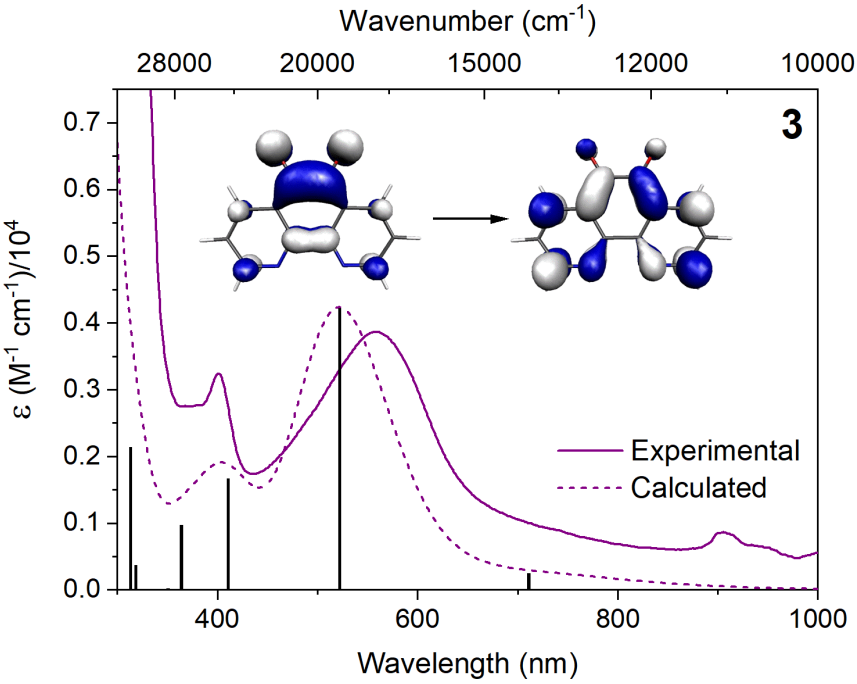

Figure 3.4: Comparison of experimental (solid line, recorded on a 0.1 mM solution in MeCN) and computationally derived (dashed line) UV-vis-NIR spectra of 3 $[CoCp_2]^+[pd]^{-\bullet}$. The inset shows the π-π* molecular orbital transition corresponding to the absorption maximum at 558 nm. The bump at 920 nm in the experimentally obtained spectrum is an artefact due to a lamp change.

3.2.7 Crystallography of 3 $[CoCp_2]^+[pd]^{-\bullet}$

Single crystals of **3** suitable for X-ray diffraction were obtained by cooling a concentrated MeCN solution to -35 °C over two weeks. The solid-state molecular structure of **3** is shown in Figure 3.5. The structure is of a separated ion pair, where there is no non-ionic interaction between $[CoCp_2]^+$ and $[pd]^{-\bullet}$. The solid-state molecular structure can be used as another method of confirming the oxidation state of the ligand, by analysis of the bond lengths in the

O,O' site, as discussed for **1-Ln** and **2-Ln** in Chapter 2. In the case of **3**, the C-C bond distance of 1.456(5) Å and the C-O bond distances of 1.268(4)-1.278(4) Å are intermediate between the equivalent bonds in **1-Ln** (pd^0, C-C 1.524(6)-1.54(6) Å, C=O 1.170(2)-1.250(2) Å) and **2-Gd** (pd^{2-}, C=C 1.387(3) Å, C-O 1.333(3)-1.333(3) Å). This is consistent with the radical semiquinone oxidation state, and with delocalisation of the radical over the *O,O'* site of the ligand.

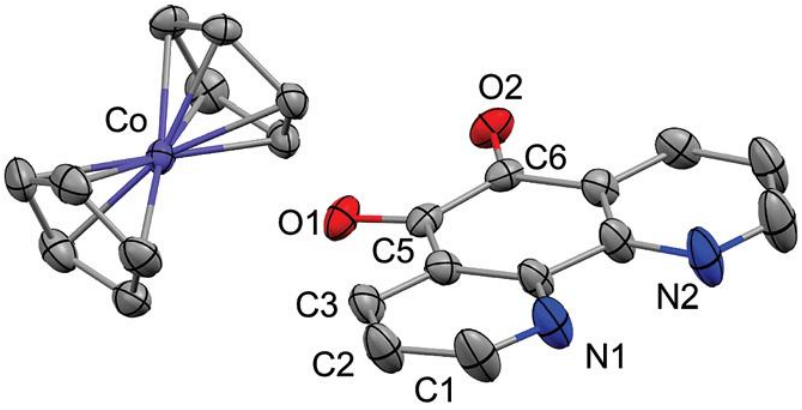

Figure 3.5: The solid state molecular structure of 3 $[CoCp_2]^+[pd]^{-\bullet}$. H atoms are omitted for clarity. Thermal ellipsoids are shown at 50% probability. Key bond distances (Å): C5-C6, 1.456(5); C-O, 1.268(4)-1.278(4).

3.3 Synthesis of $Ln(hfac)_3(S)_2$ (4-Ln)

Lanthanide *tris*-β-diketonate complexes readily accept further chelating ligands such as bipyridines, phenanthrolines or *ortho*-quinones to form coordinatively saturated complexes.[18-22] This makes them ideal for investigation of the coordination properties of **3**. However, most often lanthanide *tris*-β-diketonates are prepared either under ambient atmospheric conditions or *in situ*. Due to the sensitivity of **3** to air and moisture, an air-sensitive synthesis was required. Additionally, for comparative spectroscopy (see photoluminescence data in Chapter 4), it was also desirable to isolate the lanthanide diketonate complexes individually rather than to generate them *in situ*. The synthesis of the compounds $Ln(hfac)_3(S)_2$ **4-Ln** (S = THF, Ln = Y, Eu, Gd, Yb; S = MeCN, Ln = Eu, Gd, Yb) was therefore undertaken as shown in Scheme 3.2.

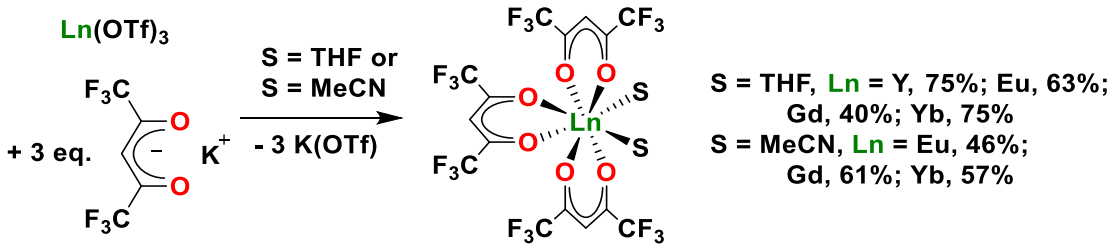

Scheme 3.2: Synthesis of 4-Ln $Ln(hfac)_3(S)_2$ (S = THF; Ln = Y, Eu, Gd, Yb. S = MeCN, Ln = Eu, Gd, Yb)

$Ln(OTf)_3$ were stirred with 3 eq. K(hfac) in THF or MeCN for 1-2 hours, producing an orange solution. The solvent was then removed *in vacuo* to leave a beige solid, which was extracted into toluene with filtration *via* filter cannula to exclude K(OTf). Toluene was removed *in vacuo* and the beige solid was washed with cold (-88 °C) hexanes three times with stirring. The solid was thoroughly dried *in vacuo* to afford **4-Ln** as a beige solid (S = THF: Ln = Y, 75%; Eu, 63%; Gd, 40%; Yb, 75%. S = MeCN: Ln = Eu, 46%; Gd, 61%; Yb, 42%). Due to the low melting point of **4-Ln**, elevating the temperature of the product as a solid inevitably resulted in the product partially melting, and on cooling forming an oily solid which was not easily isolable. Therefore, complete removal of the toluene extractant at room temperature, along with thorough washing with very cold hexane was vital to obtain **4-Ln** as a tractable, free-flowing powder. As **4-Ln** have significant solubility in hexane at -78 °C, it was necessary to undertake the washing with hexane at very cold temperatures at -88 °C to maximise yield. In all cases, though **4-Ln** were isolated with either THF or MeCN solvent coordinated, THF universally produced the most tractable products.

3.3.1 NMR Spectroscopy of 4-Ln (Ln = Y, Eu, Yb)

Compounds **4-Ln** (Ln = Y, Eu, Yb) were characterised by ^{1}H and ^{19}F NMR spectroscopy. As seen in Chapter 2, **4-Y** provides an important diamagnetic handle for analysis of the paramagnetic **4-Ln**. Three singlets are observed in the ^{1}H NMR spectrum of **4-Y** (recorded in d_6-benzene) at δ = 1.16, 3.59 and 6.28 ppm. The integral ratio of the resonances is 8:8:3 and is consistent with two coordinated THF molecules to three hfac ligands. The resonances at δ = 1.16 and 3.59 ppm are assigned to the coordinated THF ligands, and the resonance at δ = 6.28 ppm is assigned to the hfac-C**H**. Supporting this assignment, in **1-Y** the hfac-C**H** resonance occurs at δ = 6.23 ppm, as shown in Section 2.2.3. A single resonance is observed in the ^{19}F NMR spectrum in d_6-benzene, at δ = -76.68 ppm. This is consistent with the resonance observed for the trifluoro groups of hfac in **1-Y**, at δ = -77.58 ppm.

The ^{1}H NMR spectrum of **4-Eu** as recorded in d_6-benzene (Figure 3.6) exhibits three singlets, at δ = 0.08, 7.69 and 20.34 ppm, integrating in a 3:8:8 ratio. The integral ratio is consistent with two THF molecules being coordinated to Eu as in the case of **4-Y**. Due to the paramagnetic shift, these resonances have been assigned by relative integration. The resonance at δ = 0.08 ppm is assigned to the three hfac ligands, and the resonances at δ = 7.69 and 20.34 ppm are assigned to the two THF resonances. In **1-Eu**, the hfac-C**H** resonance occurs at δ = 3.85 ppm, shifted upfield by -2.38 ppm compared to **1-Y**. For **4-Eu**, a slightly larger upfield paramagnetic shift of -6.20 ppm is observed for the hfac-C**H** resonance in comparison to the ^{1}H NMR spectrum of diamagnetic **4-Y**. The resonances assigned to THF are also significantly shifted downfield by between 3.10 and 19.18 ppm, though as the resonances are not assigned to individual ^{1}H environments in the ligand, it is not possible based on these data to assign the paramagnetic shifts of the THF ligand to specific environments. The ^{19}F NMR spectrum of **4-Eu** as recorded in d_6-benzene exhibits a single resonance at δ = -81.62 ppm, assigned to the trifluoro group of hfac (Figure 3.7), and shifted upfield by -4.94 ppm compared to **4-Y**. Similarly to the ^{1}H NMR resonances of the hfac-C**H** group, this is a slightly more significant upfield shift than that observed for **1-Eu** (δ = -79.30 ppm, $\Delta\delta$ = -2.37 ppm).

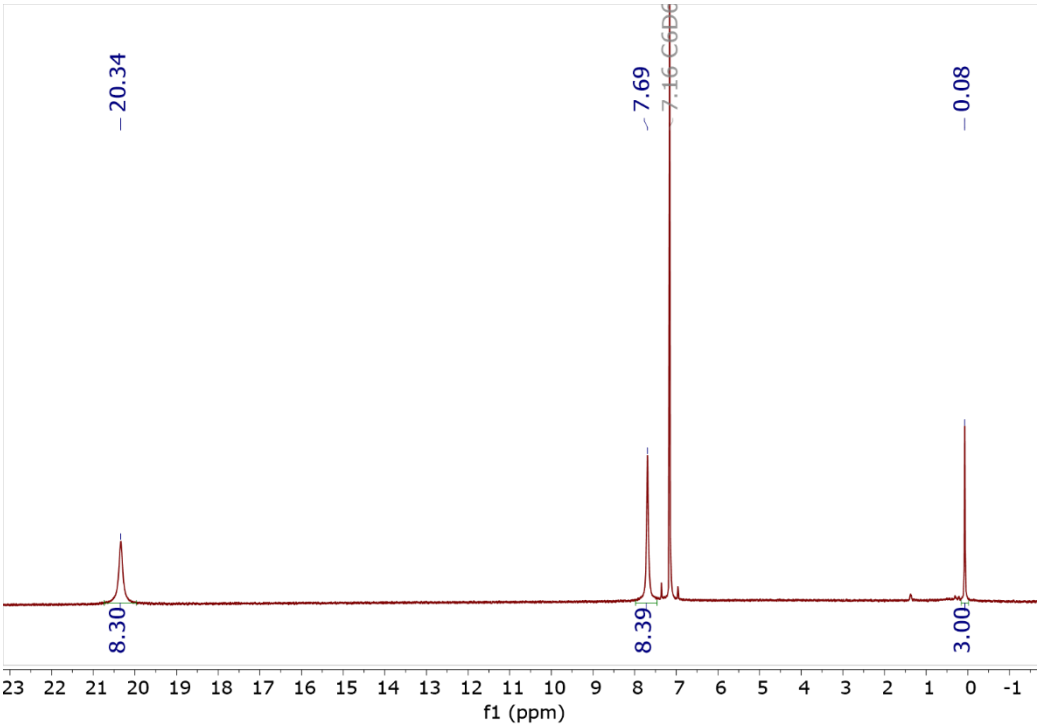

Figure 3.6: ^{1}H NMR spectrum of 4-Eu, recorded in d_6-benzene.

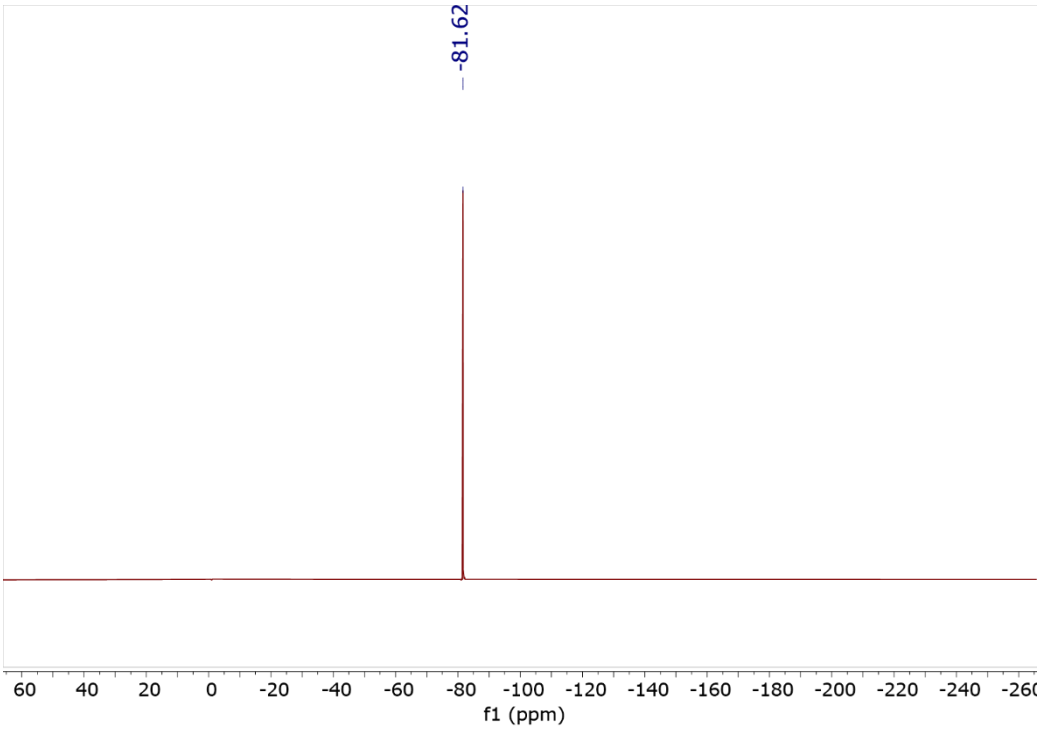

Figure 3.7: ^{19}F{^{1}H} NMR spectrum of 4-Eu, recorded in d_6-benzene.

The ^{1}H NMR spectrum of **4-Yb** as recorded in d_6-benzene (Figure 3.8) likewise exhibits three singlet resonances, at δ = -23.57, 26.50 and 62.82 ppm. The resonances integrate in a 3:8:8 ratio, and by relative integration the resonance at δ = -23.57 ppm is assigned to the hfac ligands (3H) and the resonances at δ = 26.50 and 62.82 ppm are assigned to the two resonances of the THF ligands (8H). The hfac-C**H** resonance experiences a significant upfield paramagnetic shift of -29.95 ppm compared to that in **4-Y**. By comparison, as discussed in Section 2.2.3 in the ^{1}H NMR spectrum of **1-Yb**, the hfac-C**H** group occurs at δ = -7.00 ppm, experiencing a smaller upfield shift of -13.23 ppm. The resonances assigned to THF are shifted upfield from those observed for **4-Y** by between 22.91 and 61.66 ppm, significantly greater than the equivalent shifts observed for **4-Eu**. The ^{19}F NMR spectrum of **4-Yb** as recorded in d_6-benzene exhibits a single resonance at δ = -90.49 ppm, assigned to the trifluoro groups of the hfac ligands (Figure 3.9). This resonance has undergone an upfield paramagnetic shift of -13.81 ppm from the hfac-C**F**$_3$ groups in **4-Y**, again greater than the shift experienced by the hfac-C**F**$_3$ resonance in **1-Yb** from **1-Y** of -7.00 ppm, and more significant than the shift observed for the hfac-C**F**$_3$ groups in **4-Eu**.

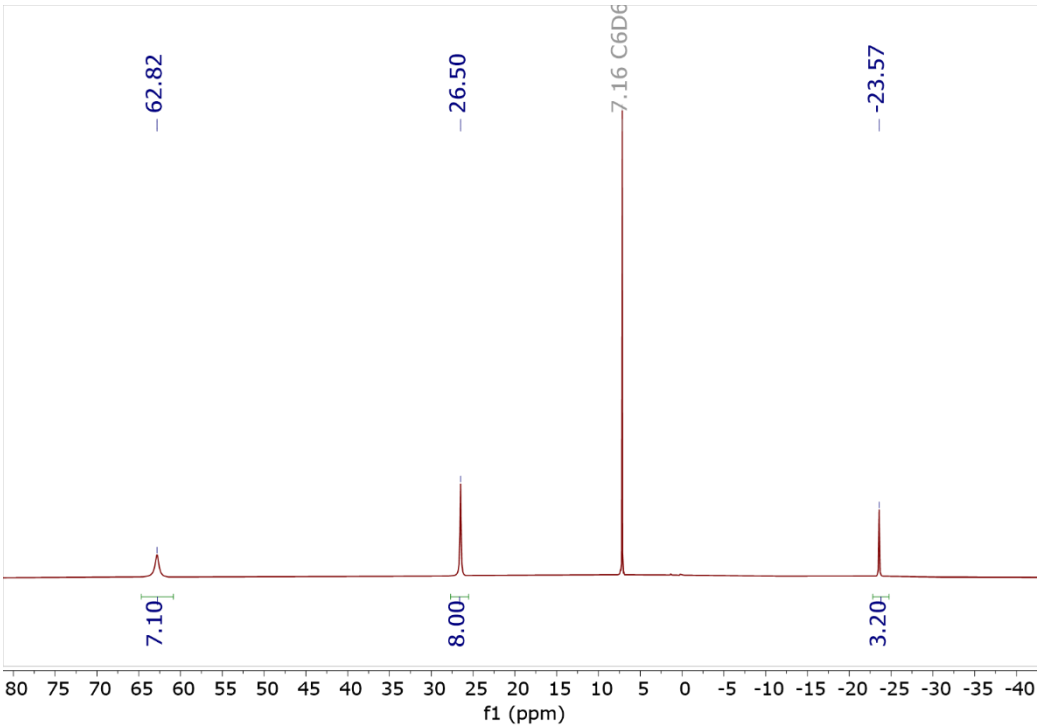

Figure 3.8: ^{1}H NMR spectrum of 4-Yb, recorded in d_6-benzene.

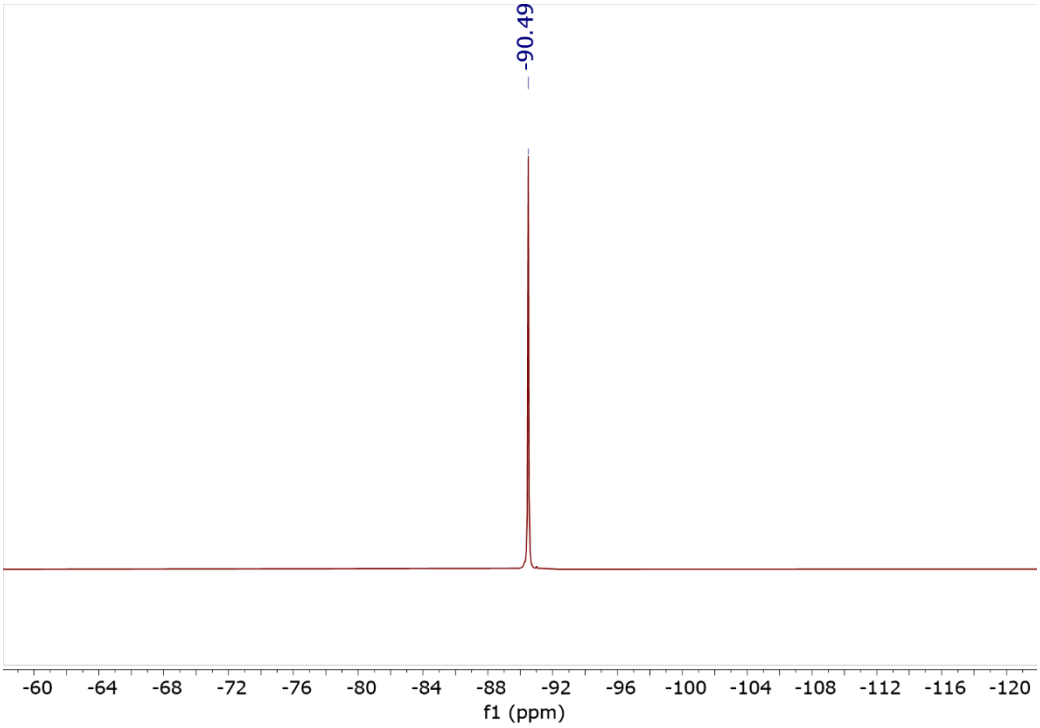

Figure 3.9: $^{19}F\{^{1}H\}$ NMR spectrum of 4-Yb, recorded in d_6-benzene.

The ^{1}H and ^{19}F NMR spectra and the paramagnetic shifts observed in **4-Ln** (summarised in Table 3.1) show similar trends to those of **1-Ln** (see Section 2.2.3 for spectra, also presented in Table 3.1). The shift of the ^{1}H hfac-C**H** and ^{19}F hfac-C**F**$_3$ resonances in **4-Eu** and **4-Yb** is upfield, as are the hfac-C**H** and hfac-C**F**$_3$ shifts in **1-Eu** and **1-Yb**. In **1-Yb**, the hfac-C**H** and hfac-C**F**$_3$ resonances are shifted by more than the equivalent resonances in **1-Eu**, and this pattern is also true in **4-Ln**. The magnitude is however somewhat different, and both the hfac-C**H** and hfac-C**F**$_3$ resonances experience a chemical shift change of between two and three times the magnitude in **4-Ln** as in the corresponding **1-Ln**. In both **4-Eu** and **4-Yb** the resonances of the THF ligands experience a downfield paramagnetic shift, which is of significantly greater magnitude in **4-Yb** than in **4-Eu**. The increased magnitude of the shifts in **4-Yb** compared to **4-Eu** is attributed to the increased angular momentum of the Yb(III) ground state ($^{2}F_{7/2}$) over that of Eu(III) ($^{7}F_{0}$).

Table 3.1: Paramagnetically induced shift (*Δδ*) for resonances in 4-Eu and 4-Yb, compared to 4-Y. The shifts of the THF environments are given as a range and 1-Ln are compared to 1-Y for reference.

	Δδ (ppm)		
Complex	**hfac-CH**	**hfac-CF_3**	**THF-CH_2**
4-Eu	-6.20	-4.94	+3.10 to +19.18
4-Yb	-29.95	-13.81	+22.91 to +61.66
1-Eu	-2.38	-2.37	n/a
1-Tb	+97.46	+13.61	n/a
1-Yb	-13.23	-7.49	n/a

3.3.2 ATR-IR spectroscopy of 4-Ln

The ATR-IR spectra of **4-Ln**, shown in Figure 3.10, exhibit a single strong carbonyl stretching frequency at 1645-1649 cm^{-1}, consistent with the hfac ligand bound to a metal.[19, 23, 24] This absorption was also observed in **1-Ln** and **2-Ln** between 1645-1651 cm^{-1} (see Chapter 2).[16] **4-Ln** also exhibit a number of absorptions in the region 1450-1600 cm^{-1} which are assigned to the C-C and C-H stretching frequencies of the hfac ligands.

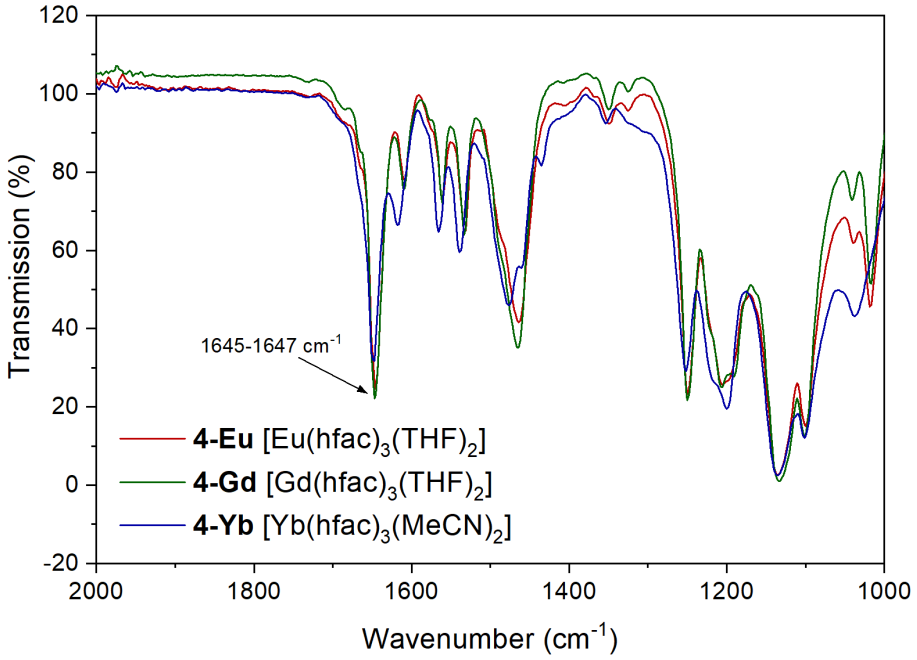

Figure 3.10: ATR-IR spectra of 4-Ln (S = THF; Ln = Eu, Gd. S = MeCN, Ln = Yb).

3.3.3 UV-vis-NIR spectroscopy of 4-Ln (Ln = Eu, Gd, Yb)

The electronic spectra of **4-Ln** (Ln = Eu, Gd, Yb) as recorded in MeCN solution (Figure 3.11) consist of one intense transition envelope with a maximum at 300 nm and an extinction coefficient of around 25 000 M^{-1} cm^{-1}, consistent with a π-π* transition of the hfac ligands.[17] This transition is observed in all hfac-containing compounds studied in this thesis, and has also previously been assigned to the π-π* transition in other diketonate compounds.[25] As mentioned in Chapter 2, this transition is frequently exploited in sensitisation of photoluminescence from lanthanide compounds (see Chapter 4).[6, 18, 25, 26]

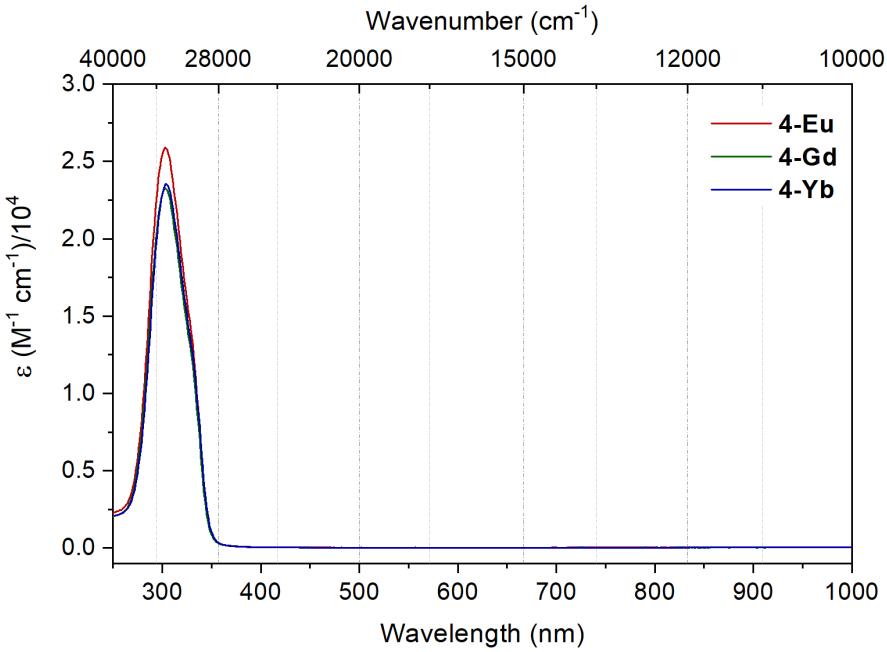

Figure 3.11: UV-vis-NIR spectra of 4-Ln (S = THF, Ln = Eu, Gd. S = MeCN; Ln = Yb) recorded on 70 μM MeCN solutions.

The UV-vis-NIR absorbance spectra of **4-Ln** (Ln = Eu, Yb), recorded at higher concentrations (*ca* 10 mM) are shown in Figure 3.12. In the electronic spectrum of **4-Eu**, and only observable at high concentrations, a weak, sharp transition occurs at 466 nm, with an extinction coefficient of 9.2 M^{-1} cm^{-1}. This transition is assigned to the laporte forbidden $^5D_2 \leftarrow {}^7F_0$ *f-f* transition of Eu(III). Likewise in the electronic spectrum of **4-Yb**, in concentrated solutions a transition is observed at 975 nm with an extinction coefficient of 6.3 M^{-1} cm^{-1}, which is assigned to the $^2F_{5/2} \leftarrow {}^2F_{7/2}$ *f-f* transition of Yb(III).

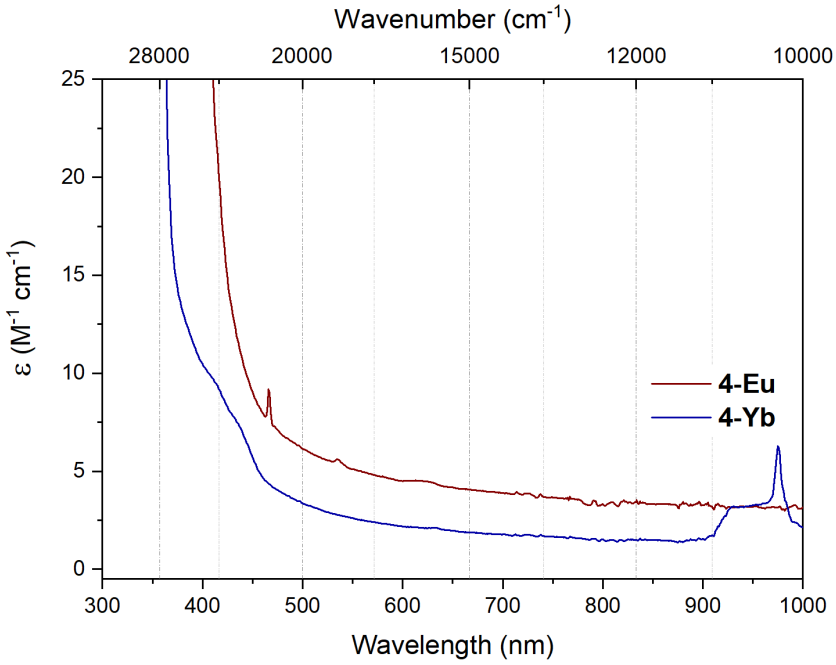

Figure 3.12: UV-vis-NIR spectra of 4-Ln (Ln = Eu, Yb), recorded on 10 mM MeCN solutions.

3.3.4 Crystallography of 4-Ln (Ln = Eu, Gd)

Due to the low-melting nature of **4-Ln**, it was important to prevent the crystals from losing crystallinity before the single-crystal X-ray diffraction (XRD) could be carried out. The Fomblin® oil and a microscope slide were therefore pre-cooled to -35 °C before any manipulations of the crystals were carried out. The crystals were collected into Fomblin® on the slide and the slide was transported to the diffractometer on a bed of dry ice.

Single crystals of **4-Eu** (S = MeCN) suitable for X-ray diffraction were grown from a concentrated hexane solution at -35 °C over several days. The solid-state molecular structure contains an 8-coordinate Eu atom, with three hfac ligands and two MeCN molecules arranged around Eu in a distorted square antiprismatic geometry. The Eu-O bond distances of 2.356(3)-2.400(3) Å are consistent with the same metric in other europium *β*-diketonate compounds such as **1-Eu** (2.354(3)-2.389(3) Å), $Eu(tta)_3(phen)$ (tta = thenoyl trifluoro acetonate) (2.342(5)-2.408(4) Å) and $Eu(acac)_3(phen)$ (acac = acetyl acetonate) (2.356(9)-2.409(9) Å).[27, 28]

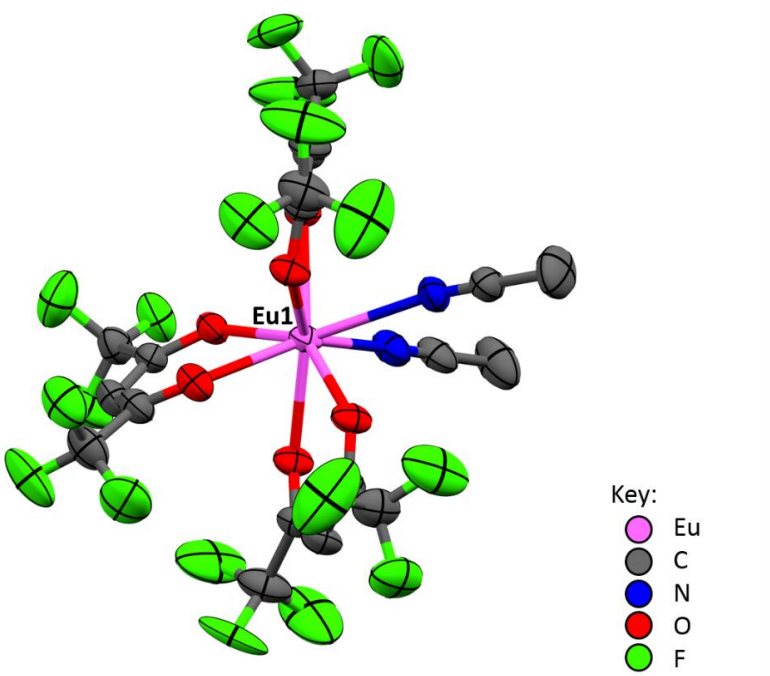

Figure 3.13: Solid State Molecular Structure of 4-Eu (S = MeCN), crystallised from hexane at -35 °C. Thermal ellipsoids are shown at 50% probability. H atoms are omitted for clarity. Selected bond distances: Eu-O, 2.356(3)-2.400(3); Eu-N, 2.506(4)-2.571(4) Å.

Single crystals suitable for X-ray diffraction were obtained by cooling a concentrated toluene solution of **4-Gd** (S = MeCN) to -35 °C for several days. The structure thus obtained was of a dimeric molecule $Gd_2(\mu\text{-hfac})_3(hfac)_3(MeCN)$. Three of the hfac molecules have one bridging oxygen atom, bridging both Gd atoms, resulting in both Gd atoms being 8-coordinate, with MeCN completing the coordination sphere of one Gd atom. The Gd-O bond distances vary slightly based on the coordination mode of the hfac ligand with the Gd-O distances of 2.307(4)-2.394(4) Å of the terminal hfac ligands being shorter than the bridging Gd-(μ-O) distances of 2.407(4)-2.516(3) Å. The shorter Gd-O distances to terminal hfac oxygen atoms are consistent with other gadolinium *β*-diketonate compounds such as **1-Gd** (2.32(2)-2.42(1) Å), **2-Gd** (2.355(2)-2.390(2) Å) or $Gd(acac)_3(L)$ (L = phen, dpq, dppz) (2.328(4)-2.380(3) Å).[16, 29] Other compounds with the same μ-O(diketonate) binding mode also exhibit slightly longer bond lengths for the bridging oxygen atoms. For example, the most appropriate matches in the CCDC for the bridging ligand binding mode, $Gd_2(acac)_4(L)$ and $Gd_4(acac)_8(L)_2$ (H_2L = *N,N'*-bis(salicylidene)-*1,2*-cyclohexanediamine) have Gd-(μ-O) bonds that are 0.1-0.2 Å longer than the terminal Gd-O bonds.[21, 30] It should be noted that the structure of **4-Gd** as determined in the solid state is not believed to be representative of the wider speciation in solution in a coordinating solvent. As discussed above in Section 3.3.1, both **4-Eu** (larger than Gd, with an

ionic radius of 1.066 Å) and **4-Yb** (smaller, with an ionic radius of 0.985 Å)[31] have ^{1}H NMR spectra consistent with the coordination of two THF molecules in solution, and it is therefore expected that **4-Gd** behaves similarly. The structure obtained is due to the partial dissociation of the MeCN solvent in the conditions used for crystallisation.

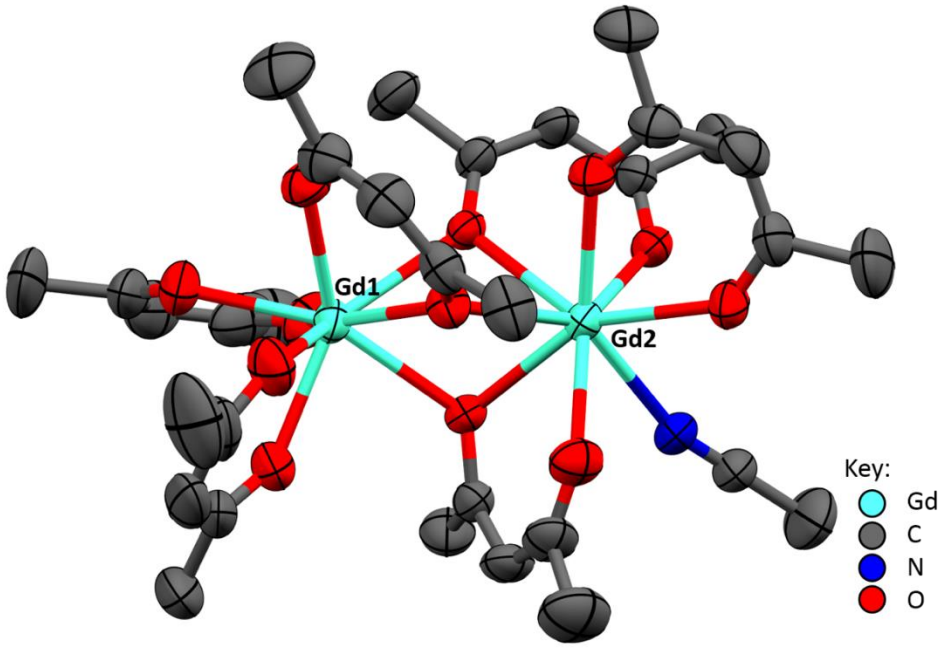

Figure 3.14: Solid State Molecular Structure of $Gd_2(hfac)_6(MeCN)$, crystallised from a toluene solution at -35 °C. Thermal ellipsoids are shown at 50% probability. F and H atoms, and a toluene molecule, are omitted for clarity. Selected bond distances: Gd-O, 2.307(4)-2.394(4); Gd-(μ-O), 2.407(4)-2.516(3); Gd-N, 2.502(4) Å. Gd1-Gd2 distance: 3.7182(5) Å.

3.4 Synthesis of 5-Ln $[CoCp]^+[Ln(hfac)_3(N,N'\text{-pd})]^{-\bullet}$

Following the selective *N,N'* coordination of pd in the neutral oxidation state to lanthanides in **1-Ln** and **2-Ln**, the coordination properties of the radical anion were investigated. The radical anion salt **3** was reacted with **4-Ln** (Ln = Y, Eu, Gd, Yb) and in all cases **4-Ln** reacted readily with **3** to form the radical lanthanide compounds $[CoCp_2]^+[Ln(hfac)_3(N,N'\text{-pd})]^{-\bullet}$ **5-Ln** (Ln = Y, Eu, Gd, Yb) as shown in Scheme 3.1.

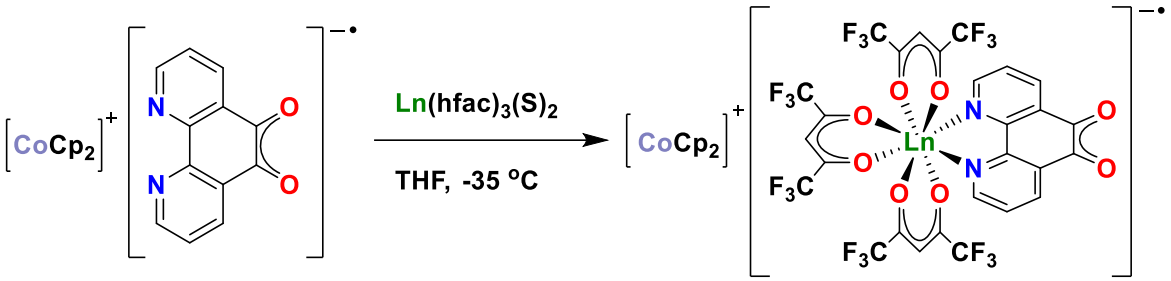

5-Ln; Ln = Y, 63%; Eu, 81%; Gd, 91%; Yb, 78%

Scheme 3.3: Synthesis of 5-Ln $[CoCp_2]^+[Ln(hfac)_3(N,N'\text{-pd})]^{-\bullet}$ (Ln = Y, Eu, Gd, Yb)

At -35 °C, a suspension of **3** in THF was added to a solution of 1 eq. **4-Ln** (Ln = Y, Eu, Gd, Yb) in THF with stirring. Immediately, a colour change from deep purple to dark green was observed. After stirring for 30 m the mixture was filtered through a frit, and THF was removed from the filtrate *in vacuo*. The dark green solids were washed with toluene, then with hexane, then dried *in vacuo* to obtain **5-Ln** (Ln = Y, 65%; Eu, 81%; Gd, 91%; Yb, 78%) as free-flowing green solids. As inorganic salts, the complexes are soluble only in strongly polar solvents such as THF or MeCN. Uniquely **5-Yb** is insoluble in MeCN, and therefore all measurements of **5-Yb** were recorded in THF, d_8-THF, or in the solid state as appropriate.

3.4.1 NMR Spectroscopy of 5-Ln $[CoCp_2]^+[Ln(hfac)_3(N,N'\text{-pd})]^{-\bullet}$ (Ln = Y, Eu, Yb)

As has been seen in Chapter 2, NMR analysis can be used in the characterisation of even highly paramagnetic species containing unpaired f-electrons such as **5-Ln** (Ln = Y, Eu, Yb).[32-34] **5-Y**, which contains only an organic radical, provides a useful handle for analysis. The ^{1}H NMR spectrum of **5-Y** as recorded in d_8-THF shows two resonances, at δ = 5.76 (s, 10H) and 5.99 (s, 3H) ppm, which integrate in a 10:3 ratio. The resonance at δ = 5.76 ppm is therefore assigned to the $[CoCp_2]^+$ fragment and the resonance at δ = 5.99 ppm is assigned to the hfac-C**H**. The resonance assigned to $[CoCp_2]^+$ is consistent with that reported for $[CoCp_2]^+[OTf]^-$ as recorded

in *d*-chloroform of δ = 5.77 ppm.[14] The hfac-C**H** resonance of δ = 5.99 ppm is consistent with the other examples of hfac-C**H** resonances discussed in this thesis (**1-Y**, δ = 6.23 ppm; **4-Y**, δ = 6.28 ppm). The ^{1}H NMR resonances of the pd$^{-\bullet}$ ligand are not observed, due to the organic radical on the *O,O'*-binding site. Early results as published[11, 13] showed an additional set of three resonances, each integrating to *ca* 1H, at δ = 7.57, 8.42 and 9.01 ppm, which were assigned to the resonances of the pd ligand. However, following optimisation of the synthesis to that described in this thesis, these resonances were not observed. These resonances are therefore believed to be the result of decomposition due to reaction with adventitious water. The ^{19}F NMR spectrum of **5-Y** shows a single resonance at δ = -77.75 ppm, in the typical region for a hfac-C**F**$_3$ group as observed in **1-Y** (δ = -76.93 ppm) and in **4-Y** (δ = -76.68 ppm).

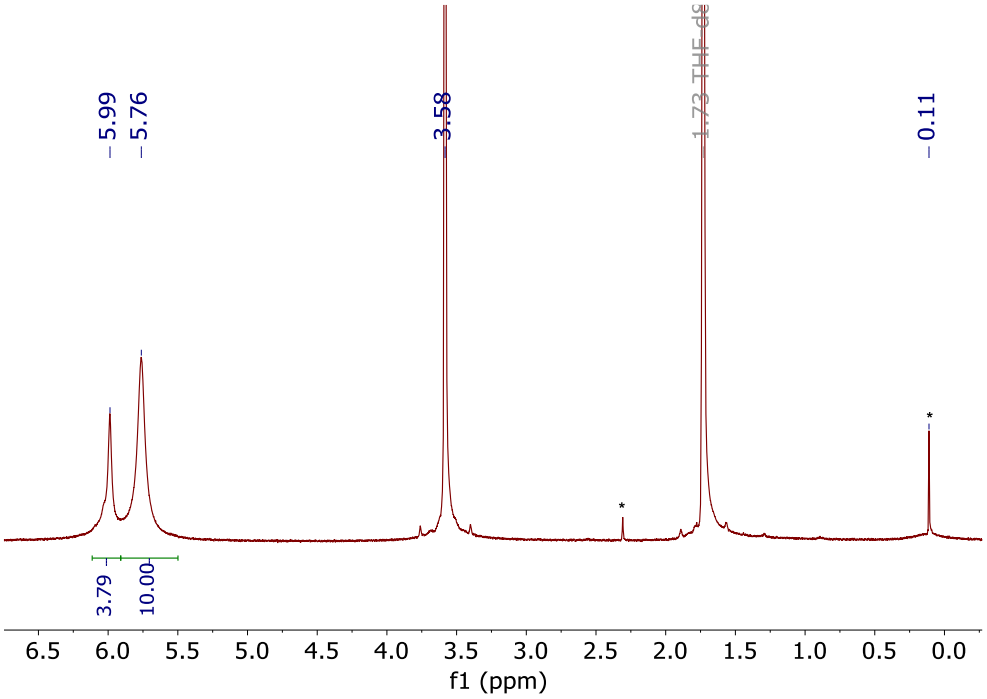

Figure 3.15: The ^{1}H NMR spectrum of 5-Y, recorded in d_8-THF. Resonances assigned to a small quantity of silicone grease and toluene solvent are denoted by *.

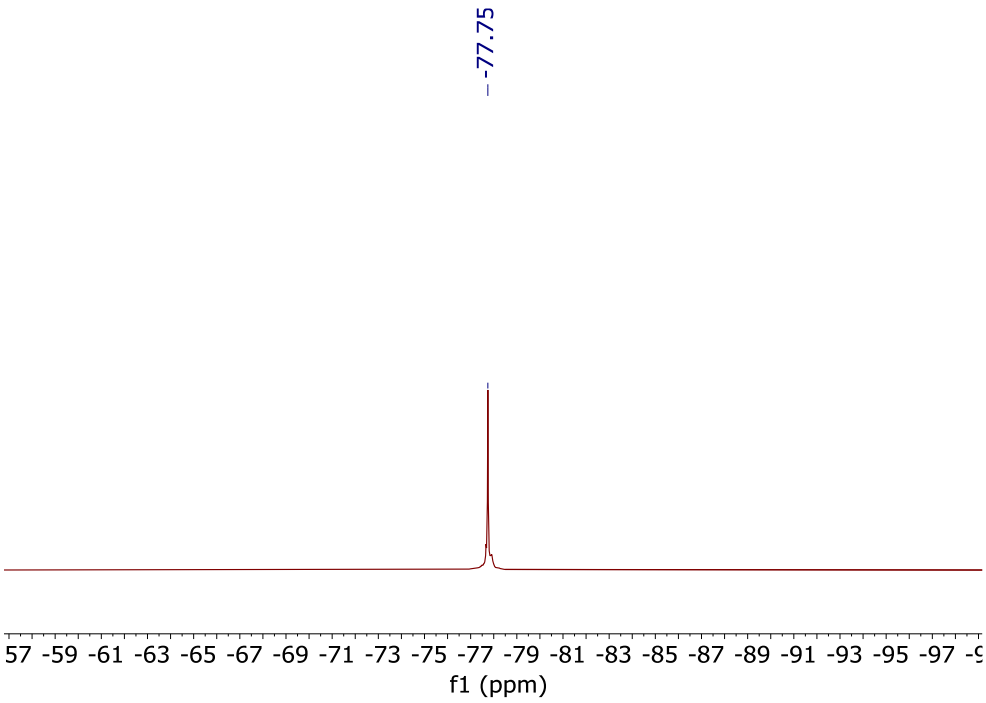

Figure 3.16: The ^{19}F NMR spectrum of 5-Y, recorded in d_8-THF.

The ^{1}H NMR spectrum of **5-Eu** as recorded in d_8-THF (Figure 3.17) shows two resonances at δ = 3.19 and 6.42 ppm, which integrate in a 2:10 ratio. The resonance at δ = 6.42 ppm is assigned to the $[CoCp_2]^+$ counter cation, by relative integration and by comparison to the ^{1}H NMR spectrum of **5-Y**. This $[CoCp_2]^+$ ^{1}H NMR resonance is not significantly shifted from that observed in **5-Y** (δ = 5.82 ppm), consistent with the expected outer sphere nature of the cation. This resonance has a fwhh of 15 Hz, similar to that observed in **5-Y** of 25 Hz. The resonance at δ = 3.20 ppm is assigned by relative integration to the hfac-C**H** groups, which are shifted upfield by 2.76 ppm from the resonance assigned to the hfac-C**H** groups in **5-Y**. The difference in integration from the expected 10:3 ratio likely results from the differing local environments relative to both the Ln paramagnet and the organic radical of the Ln-bound hfac ligand and outer-sphere $[CoCp_2]^+$. As in the case of **5-Y**, no resonances of the $pd^{-\bullet}$ ligand are observed. The ^{19}F{^{1}H} NMR spectrum shows a single resonance at δ = -80.50 ppm, assigned to the trifluoro groups of hfac (Figure 3.18). This resonance has been contact shifted upfield by -2.78 ppm compared to **5-Y**, similarly to the upfield shift in **1-Eu** from **1-Y** of -2.73 ppm and slightly smaller than that observed in **4-Eu** from **4-Y** (see Table 3.1).

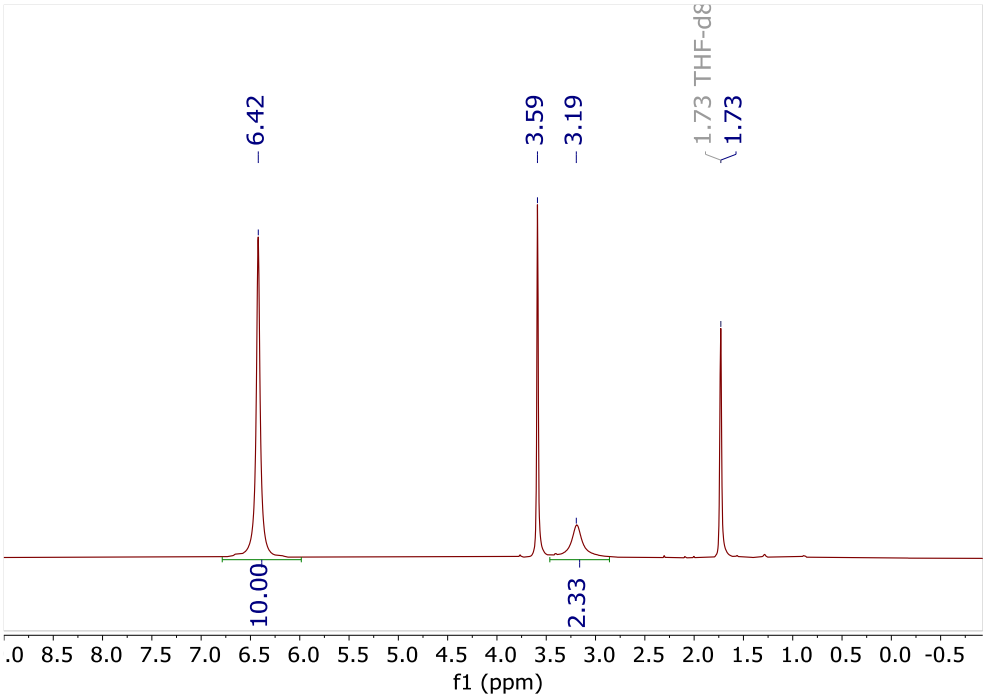

Figure 3.17: ^{1}H NMR spectrum of 5-Eu, recorded in d_8-THF.

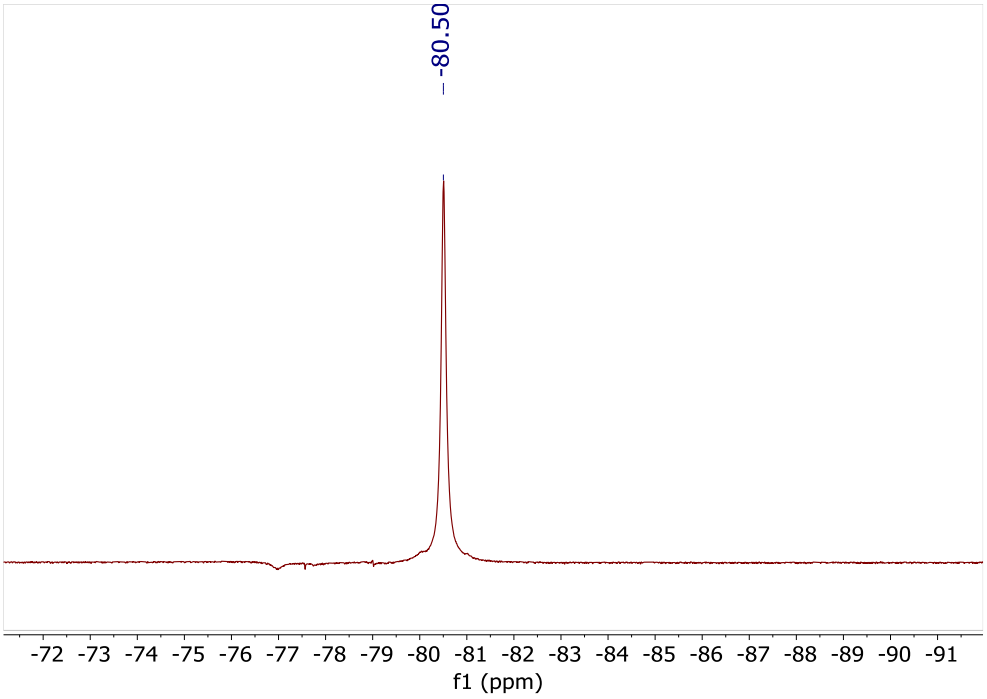

Figure 3.18: ^{19}F{^{1}H} NMR spectrum of 5-Eu, recorded in d_8-THF.

The ^{1}H NMR spectrum of **5-Yb** as recorded in d_8-THF (Figure 3.19) likewise shows two resonances at δ = -10.93 and 8.18 ppm, which integrate in a 2:10 ratio. By relative integration, the resonance at δ = -10.93 ppm is assigned to the hfac-C**H**, while that at δ = 8.18 ppm is assigned to the $[CoCp_2]^+$ fragment. As for **5-Eu**, the integration of the hfac ligands is low compared to $[CoCp_2]^+$ due to the outer sphere nature of the cobaltocenium cation. No

resonances of the $pd^{-\bullet}$ ligand are observed. A greater downfield shift of the $[CoCp_2]^+$ resonance is observed in **5-Yb** than **5-Eu** compared to **5-Y** due to the greater angular momentum of Yb(III) compared to Eu(III). The fwhh of the resonance of 18 Hz is however very similar to that in **5-Eu** (15 Hz) and **5-Y** (25 Hz). Similarly to **5-Eu**, the hfac ligands experience a greater paramagnetic shift than the $[CoCp_2]^+$ resonances, exhibiting an upfield shift (from δ = 5.96 ppm to δ = -10.93 ppm) of -16.89 ppm, which is significantly larger than that observed in **5-Eu** (-2.78 ppm) and similar to that observed in **1-Yb** compared to **1-Y** (-13.23 ppm). The $^{19}F\{^1H\}$ NMR spectrum shows a resonance at δ = -83.14 ppm, assigned to the hfac-C**F**$_3$ groups, which experiences an upfield paramagnetic shift of -5.42 ppm (Figure 3.20) compared to that of **5-Y**.

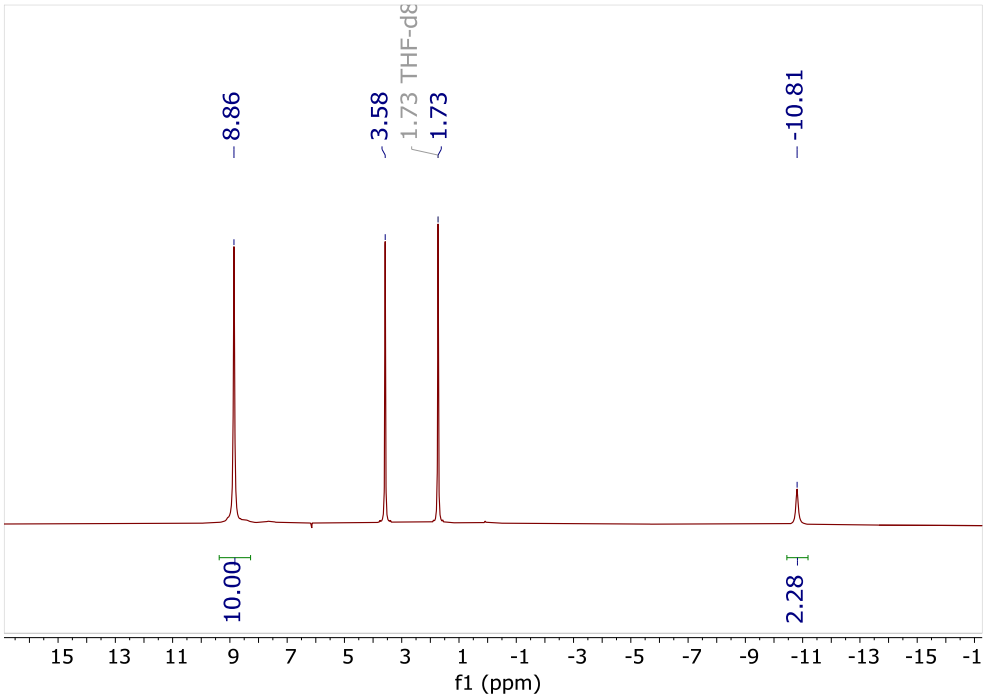

Figure 3.19: ^{1}H NMR spectrum of 5-Yb, recorded in d_8-THF.

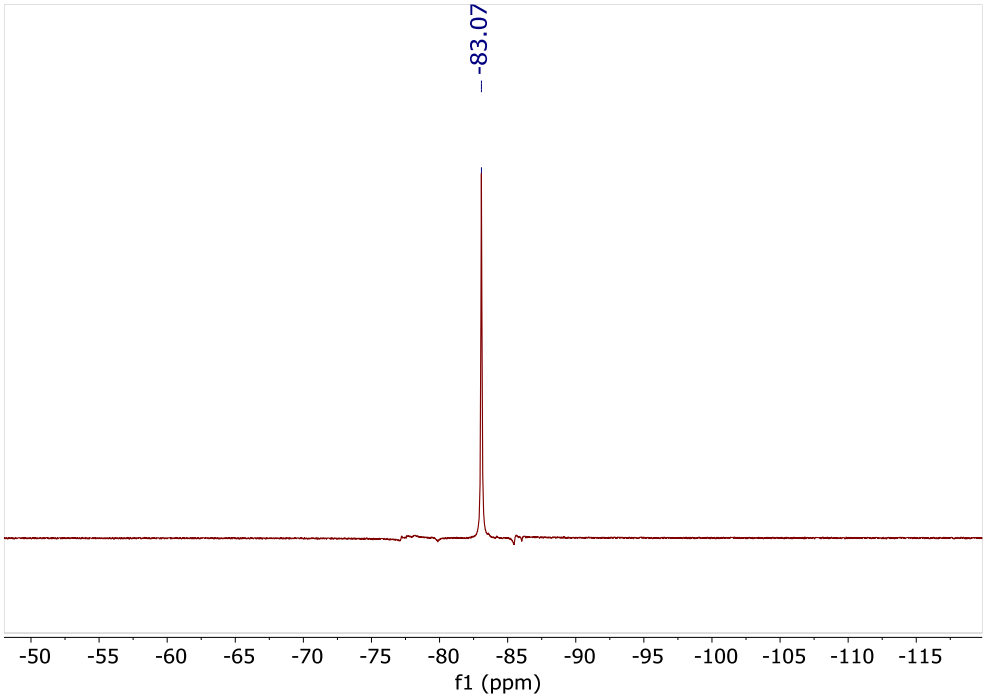

Figure 3.20: $^{19}F\{^{1}H\}$ NMR spectrum of 5-Yb, recorded in d_8-THF.

Similar trends are observed in the paramagnetic shifts of **5-Ln** (Ln = Eu, Yb) compared to **5-Y**, shown in Table 3.2, compared to those observed in **4-Ln** and **1-Ln** (see Table 3.1, Section 3.4.1). As in both **1-Ln** and **4-Ln**, an upfield (negative) shift is observed for both the ^{1}H hfac-C**H** and the ^{19}F hfac-C**F**$_3$ resonances. This paramagnetically induced shift is greater in the case of **5-Yb** than in **5-Eu**, consistent with observations of both **1-Ln** and **4-Ln**. The magnitude of the shift in **5-Ln** is similar to that observed in **1-Ln**, and significantly smaller than that observed in **4-Ln**. This is unsurprising, given the proposed similarities between the molecular structures of **1-Ln** and **5-Ln**, with the three hfac ligands and *N,N'* bound pd ligand. It must be noted, however, that the values for **1-Ln** and for **4-Ln** were recorded in d_6-benzene solution, while those for **5-Ln** were recorded in d_8-THF solution due to their low solubility in non-coordinating solvents. Consistent with the outer-sphere nature of the $[CoCp_2]^+$ cation, while the resonances assigned to this fragment experience a slight downfield (positive) shift in **5-Ln** (Ln = Eu, Yb) compared to **5-Y**, they are significantly less contact shifted by the two paramagnetic species than the hfac ligands. Supporting the assignment of the $[CoCp_2]^+$ ion to the outer sphere, the fwhh of the resonances assigned to hfac-C**H** and to $[CoCp_2]^+$ in **5-Ln** (see Table 3.3) does not change significantly in **5-Ln** (Ln = Eu, Yb) compared to in **5-Y**. A much greater difference is observed in the resonances assigned to the hfac-C**H** resonances.

Table 3.2: Paramagnetically induced shift $\Delta\delta$ for the various resonances in the ^{1}H and ^{19}F NMR spectra of 5-Ln (Ln = Eu, Yb) compared to 5-Y.

	$\Delta\delta$ (ppm)		
Ln	hfac-C**H**	hfac-C**F**$_3$	$[CoCp_2]^+$
Eu	-2.76	-2.78	+0.60
Yb	-16.89	-5.42	+2.37

Table 3.3: Full width at half height in Hz of the various resonances in the ^{1}H NMR spectra of 5-Ln (Ln = Y, Eu, Yb).

	Full width at half height (Hz)	
Ln	hfac-C**H**	$[CoCp_2]^+$
Y	11	25
Eu	58	15
Yb	29	18

As for **1-Gd**, **2-Gd** and **4-Gd**,[13, 16] **5-Gd** is NMR silent, as expected for a compound containing Gd(III), and no signals were observed in the ^{1}H or $^{19}F\{^{1}H\}$ NMR spectrum due to paramagnetically induced relaxation.

3.4.2 Evans' Method magnetic moment determination

Using the Evans' Method, the magnetic moment of **5-Gd** was determined. The magnetic moment was found to be in the range of 7.60-7.67 μ_B based on three measurements. This value is lower than that expected for a system with two uninteracting spin centres (Gd(III), S = 7/2; organic radical, S = 1/2) which is calculated by a modification of the spin-only magnetic moment formula to be 8.12 μ_B.[3] This indicates that the spin centres couple weakly antiferromagnetically. For reference, in **2-Gd** (Gd(III), S = 7/2; V(IV), S = 1/2), the magnetic moment was determined to be 7.99-8.41 μ_B. Typically, examples of coupling between Gd(III) and organic radicals exhibit antiferromagnetic interactions of up to -11 cm^{-1},[35, 36] though there is no evidence for a significant interaction in **5-Gd**. Generally, even coupling between organic

[3] See Appendix two (section 8.2) for the calculation used to determine this value.

radicals and neighbouring Gd(III) ions is vanishingly small (J <5 cm^{-1}) and very challenging to measure experimentally, requiring computational determination along with measurement of the temperature dependence of the magnetic moment at very low temperatures.

3.4.3 X-band EPR spectroscopy of 5-Y

Since **5-Ln** contain an organic radical, it is informative to analyse them by EPR spectroscopy. Therefore, the X-band EPR spectrum of **5-Y** was recorded in MeCN solution, as shown in Figure 3.21. The spectrum exhibits a single organic radical, with a g value of 2.0041, only slightly shifted from that of **3** (g = 2.0053). Hyperfine coupling is once again observed to the H and N atoms of pd, but no hyperfine coupling was observed to the S = 1/2 nucleus of 100% abundant ^{89}Y.[4] Since it might be expected to observe hyperfine coupling between the unpaired electron of the radical anion and the Y atom if the metal was coordinated in the *O,O′* site, this is consistent with *N,N′* coordination of $Y(hfac)_3$ to $pd^{-\bullet}$. However, due to the low nuclear magnetic moment of Y, this coupling may be smaller than the linewidth of the spectrum in any case, as no coupling was observed between the organic radical and the Y atom in $[CoCp_2]^+[\{Y(Tp)_2(dto)\}_2Ni]^{-\bullet}$.[37] The spectrum of **5-Y** covers a wider magnetic field range than the EPR spectrum of **3**, and the linewidth is also greater. This is attributed to the slower tumbling of $[Y(hfac)_3(N,N'\text{-pd})]^{-\bullet}$ in solution compared to $[pd]^{-\bullet}$. Notably, the coupling to the H atom *meta* to the semiquinone is halved compared to the same coupling in **3** (0.52 and 1.08 x 10^{-4} cm^{-1} in **5-Y** and **3** respectively). This reduction in coupling to the *meta* proton is predicted by TD-DFT calculations performed on $[Y(hfac)_3(N,N'\text{-pd})]^{-\bullet}$.[16] The Mulliken spin density plot calculated based on the geometry-optimised structure of the anion $[Y(hfac)_3(N,N'\text{-pd})]^{-\bullet}$ (Figure 3.22) show the radical to be localised on the *O,O′* site, with a small amount of delocalisation to the C and N atoms of pd. In particular, a significantly lower spin density is located on the *meta* carbon in this anion than was observed for **3**, consistent with the lower coupling to the *meta* protons. This is therefore strong evidence for the *N,N′* binding in **5-Y**.

[4] CIAAW. **Isotopic compositions of the elements 2019**. Available online at www.ciaaw.org.

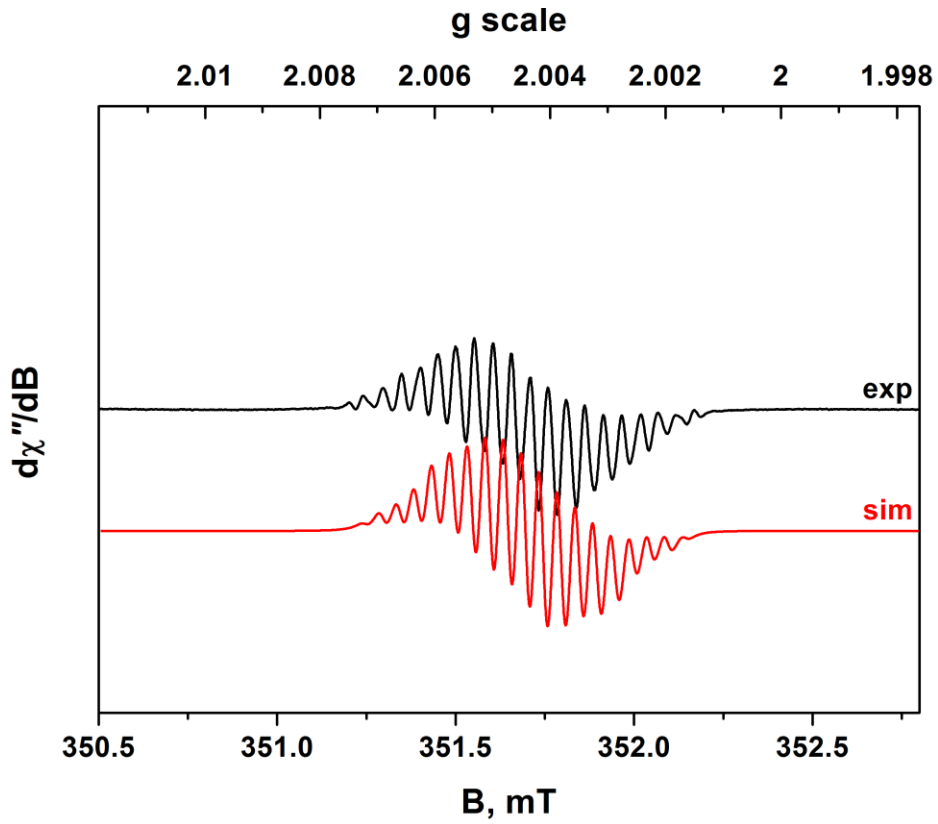

Figure 3.21: X-band EPR spectrum of 5-Y $[CoCp_2]^+[Y(hfac)_3(pd)]^{-\bullet}$, recorded in MeCN at R.T. g = 2.0041; $J(^1H)$ = 1.41, 0.52, 1.56 x 10^{-4} cm^{-1}; $J(^{14}N)$ = 0.45 x 10^{-4} cm^{-1} (experimental conditions: frequency, 9.8653 GHz; power, 0.63 mW; modulation, 0.02 mT).

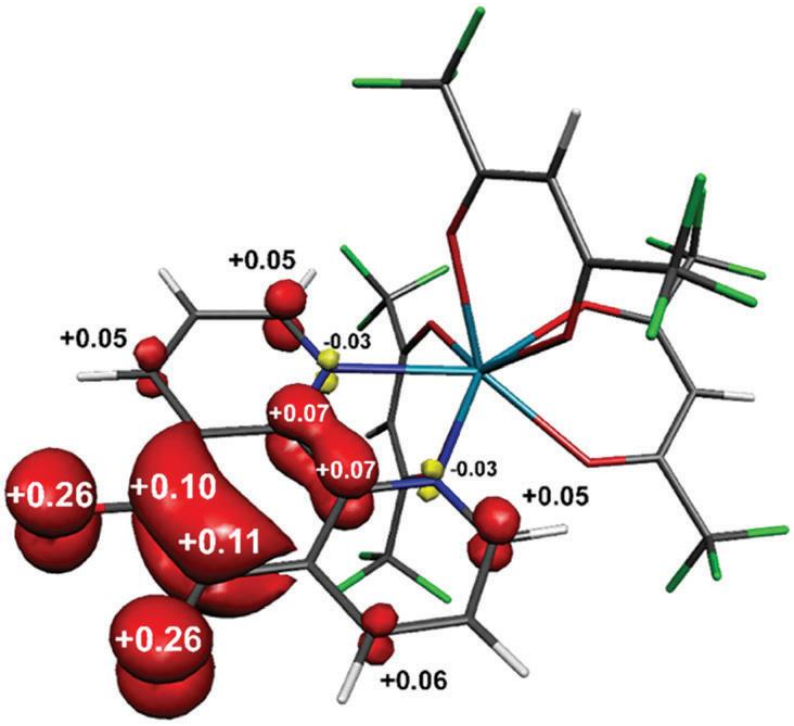

Figure 3.22: Mulliken spin density distribution in the geometry-optimised structure of $[Y(hfac)_3(N,N'\text{-pd})]^{-\bullet}$ (red: α-spin, yellow: β-spin)

The X-band EPR spectra of **5-Ln** (Ln = Eu, Gd), were recorded and are presented in Figure 3.23. However, the quality of the data was very low, and as such the spectra produced were not simulated. In the case of **5-Gd**, the spectrum displays only a very weak, broad signal with g = 1.982, which is consistent with Gd(III). In **1-Gd**, Gd(III) exhibits an EPR signal with g = 1.989, while in **2-Gd**, Gd(III) exhibits an EPR signal with g = 1.9912. These values are consistent with those expected for Gd(III).[38] However, the EPR signal of **5-Gd** was much weaker than that of **1-Gd** and **2-Gd**, (spectra in Sections 2.2.4, 2.3.1), attributed to the presence of the organic radical which is not observed, in contrast to the clear and sharp signal observed in **3** (g = 2.0053). In the case of **5-Eu**, the X-band EPR spectrum exhibited a single identifiable signal with g = 2.001, consistent with an organic radical. However, this signal was very weak, such that it could be attributed to dust in the spectrometer.

The EPR data for **5-Ln** (Ln = Eu, Gd) are surprising. Lanthanides typically couple very weakly to organic radical ligands. Indeed, the strongest lanthanide-organic radical couplings are typically only determined by *ab initio* calculations, even in extremely strongly interacting systems such as the dinitrogen bridged lanthanide dimers $(LnN''_2)_2(N_2^{-\bullet})$ ($|J| \leq 38.2$ cm^{-1}).[39, 40] It would therefore be expected that these spectra would appear either as a summation of a broad signal from Gd(III) and a sharp, intense organic radical (**5-Gd**) or simply as an organic radical similar to **3** (**5-Eu**) as Eu(III) does not give an X-band EPR signal. By comparison to work on similar semiquinonate compounds, couplings of J < -10 cm^{-1} are predicted to be experienced by the lanthanides and the organic radical in **5-Ln**.[41]

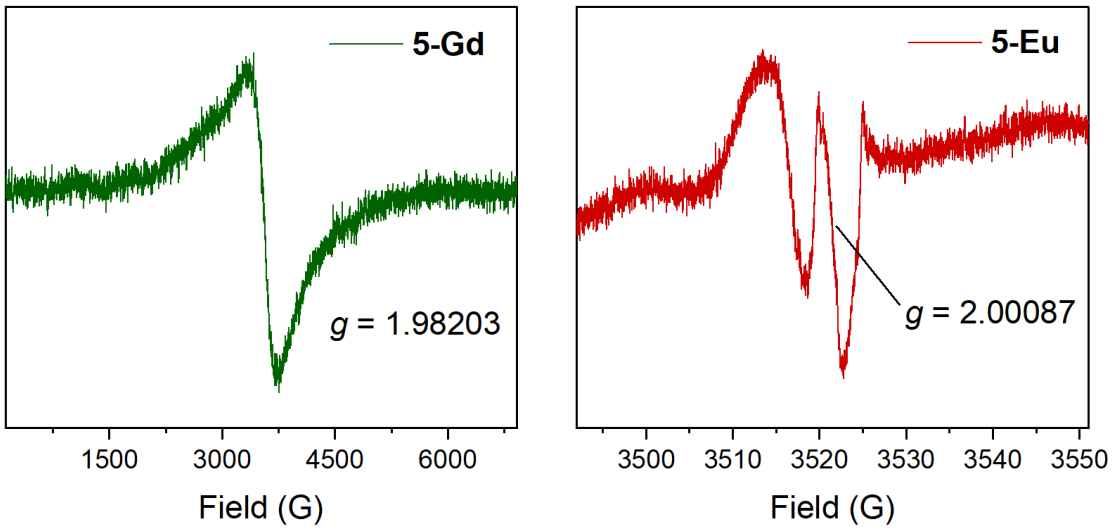

Figure 3.23: X-band EPR spectra of 5-Ln (Ln = Eu, Gd), recorded at 298 K on dilute MeCN solutions.

3.4.4 ATR-IR spectroscopy of 5-Ln

The ATR-IR spectra of **5-Ln** exhibit a stretching frequency at 1649-1653 cm^{-1}, assigned to the carbonyl moiety in the hfac ligand by comparison to **1-Ln**, **4-Ln** and literature compounds such as $Ln(hfac)_3(glyme)$.[19, 23, 24] No other stretching frequencies were observed in the region 1650-1700 cm^{-1} such as are observed for **1-Ln**, consistent with reduction of the pd ligand to $pd^{-\bullet}$ in **5-Ln**. A group of absorbances with a maximum absorption of 1453 to 1557 cm^{-1} is assigned to the various C=C stretching and C-H bending frequencies, as observed in **3**. Similarly to the semiquinone stretching frequency assigned in **3** at 1400-1420 cm^{-1}, an absorbance in **5-Ln** at 1417-1420 cm^{-1} is assigned to the singly reduced pd semiquinone stretching frequency, intermediate between the neutral pd^0 (1660-1700 cm^{-1}) and doubly reduced pd^{2-} (1370-1380 cm^{-1}).[16] This is consistent with a similar stretching frequency observed in radical quinone complexes $[CoCp_2]^+[(Ln(Tp)_2)_2(\mu\text{-}CA)]^{-\bullet}$ (Ln = Dy, Gd; Tp^- = hydro *tris*-pyrazolyl borate; CA^{2-} = chloranilate) at 1450 cm^{-1}, supporting its assignment as the radical semiquinone.[41] The wavenumber of the absorbance assigned to the semiquinone is similar to that of the non-coordinated ligand in **3**, consistent with *N,N'*-coordination. Additionally, the small decrease in frequency compared to the bound semiquinone compounds $[CoCp_2]^+[(Ln(Tp)_2)_2(\mu\text{-}CA)]^{-\bullet}$ (from 1450 cm^{-1} to 1417-1420 cm^{-1}) is consistent with the ligand being coordinated only by the *N,N'* binding site.

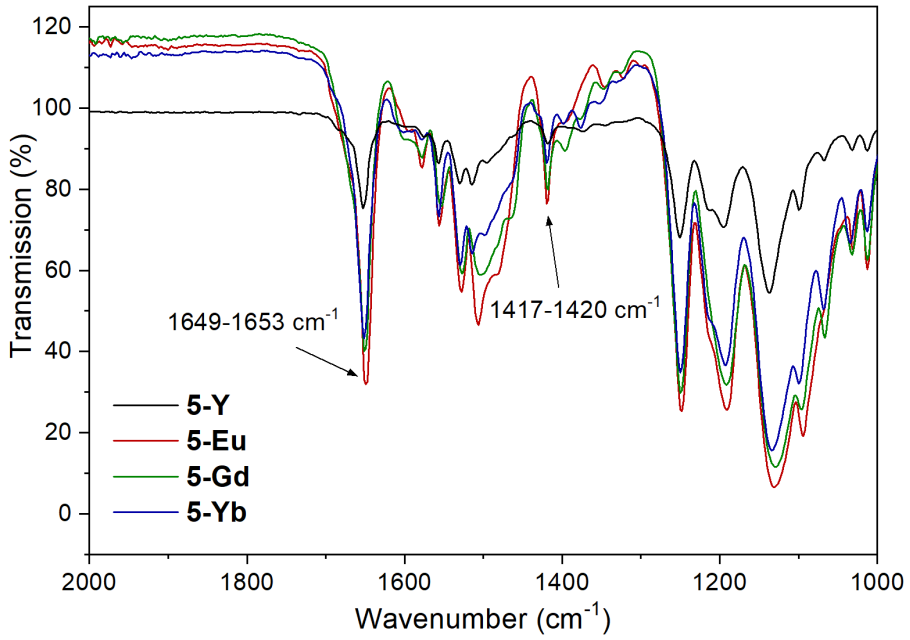

Figure 3.24: ATR-IR spectra of 5-Ln $[CoCp_2]^+[Ln(hfac)_3(N,N'\text{-pd})]^{-\bullet}$ (Ln = Y, Eu, Gd, Yb), recorded at R.T.

3.4.5 UV-vis-NIR spectroscopy of 5-Ln

As with **1-Ln** and **2-Ln**, **5-Ln** have rich absorption spectra, and their UV-vis-NIR spectra have been analysed in combination with TD-DFT calculations to learn about the electronic structure of the radical ligand-containing complex. Figure 3.26 shows a comparison of the experimentally obtained absorption spectrum of **5-Y** and the TD-DFT derived UV-vis-NIR spectrum of the geometry-optimised structure of $[Y(hfac)_3(N,N'\text{-pd})]^{-\bullet}$. There is good agreement between the spectra, supporting the assignment of the coordination of Y to the *N,N'* site of the pd ligand. The experimentally obtained spectrum has two transitions at 387 (6 986) and 642 nm (2 356 M^{-1} cm^{-1}), which have extinction coefficients of a magnitude consistent with charge transfer transitions.[17] The extinction coefficients are significantly larger than those in **1-Ln**, as expected for a radical species,[17] though lower overall than those in **3**, likely as a result of the change in coordination. Both maxima are assigned by TD-DFT calculations to ILCT transitions, and the molecular orbital transition responsible for the absorption maximum at 639 nm is shown inset in Figure 3.25.[13] This transition involves similar molecular orbitals to the dominant π-π^* transition of **3** (λ_{max} = 558 nm, ε = 3 866 M^{-1} cm^{-1}), and therefore the significant shift of this absorption to 642 nm demonstrates that

coordination of the lanthanide to the ligand modulates the electronic structure of the ligand significantly.

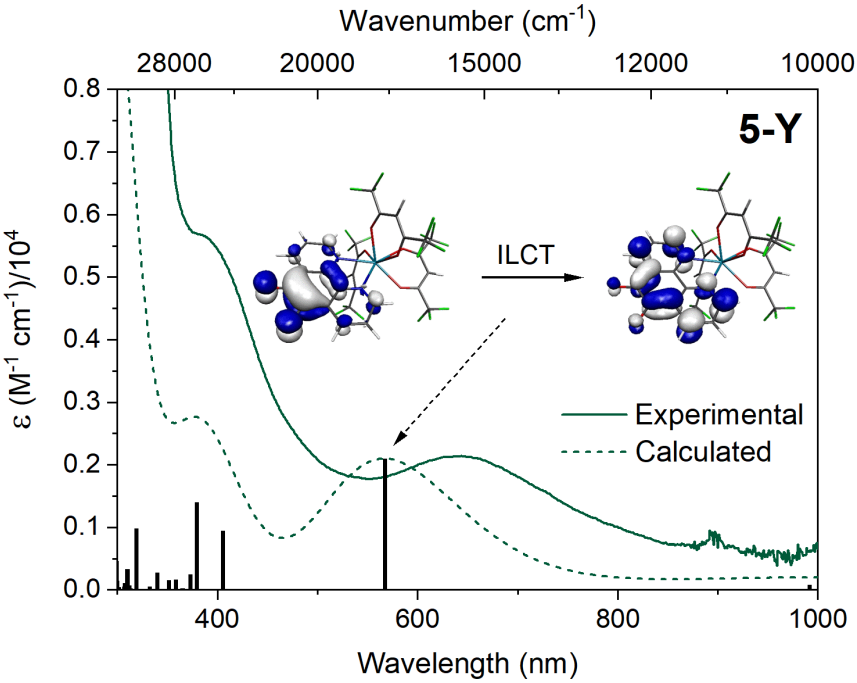

Figure 3.25: Comparison of experimental (solid line, recorded in MeCN at R.T.) and computationally derived (dashed line) UV-vis-NIR spectra of 5-Y $[CoCp_2]^+[Y(hfac)_3(pd)]^{-\bullet}$. The inset shows the ILCT molecular orbital transition corresponding to the absorption maximum at 650 nm.

The visible absorption spectra of **5-Ln** (Ln = Eu, Gd, Yb) are shown in Figure 3.26. The spectra exhibit two transitions of a slightly lower intensity than those in **5-Y**, at 420-440 nm (1400-1850 M^{-1} cm^{-1}) and at 600-620 nm (510 M^{-1} cm^{-1} 670 M^{-1} cm^{-1}). As in **5-Y**, these are assigned as ILCT transitions. In the UV region of the absorption spectrum, two transition envelopes are observed at 263-266 nm and at 299-301 nm, both with extinction coefficients of 40 000 M^{-1} cm^{-1}. In both **1-Ln** and **4-Ln** an absorption with λ_{max} = 300 nm is assigned to the hfac ligands' π-π* transition. The absorption at 299-301 nm is therefore assigned to the π-π* transition of the hfac ligands. Meanwhile, the absorption band at 263-266 nm is assigned to the π-π* transitions of the pd ligand. By comparison with the spectra of **1-Ln**, the UV π-π* transitions of pd in **5-Ln** are shifted only slightly to lower energy (from 250 nm in **1-Ln** to 260 nm in **5-Ln**), and there is no change in molar extinction coefficient.

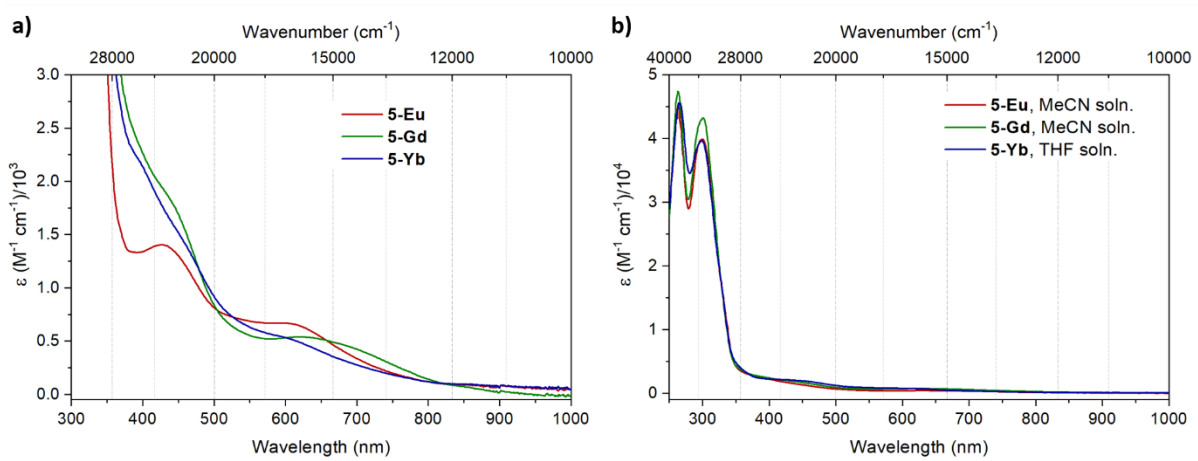

Figure 3.26: UV-vis-NIR spectra of 5-Ln $[CoCp_2]^+[Ln(hfac)_3(N,N'\text{-pd})]^{-\bullet}$(Ln = Eu, Gd, Yb). Spectra were recorded on a) 2 mM THF solutions or b) 40 μM THF or MeCN solutions.

3.5 Conclusions

This chapter describes the synthesis of the first molecular example of the radical anion of pd, **3** $[CoCp_2]^+[pd]^{-\bullet}$, by the one electron reduction of pd by cobaltocene. The isolation of **3** has allowed a full study of the electronic structure of the ligand in the radical anion oxidation state, as **3** has been fully characterised by NMR, UV-vis, ATR-IR and EPR spectroscopy. Compound **3** is an important synthon for incorporating the radical ligand in lanthanide complexes, and its spectroscopic properties are now well-understood. The nature of **3** as a separated ion pair provides the possibility of using metathesis reactions to drive coordination of metals to the radical pd ligand.

In conjunction with TD-DFT calculations, EPR spectroscopy was used to investigate the nature of the radical, and it was found that the unpaired electron resides almost entirely on the *O,O'* site of the ligand. A small percentage occupancy on the C and N atoms of pd results in observable couplings to each of the H and N atoms of pd in the EPR spectrum, which is well simulated. The UV-vis spectrum was also used to determine the electronic structure, with comparison to TD-DFT calculated transitions. The predominant electronic transition was determined to be of a π-π^* transition of the pd radical anion involving the singly occupied molecular orbital. In addition, the solid-state molecular structure of **3** was determined, showing the expected separated ion-pair. The bond lengths of the *O,O'* site in **3** were consistent with the semiquinone oxidation state.

The synthesis and full characterisation of the lanthanide coordination compounds **4-Ln** $Ln(hfac)_3(S)_2$ (Ln = Y, Eu, Gd, Yb; S = THF, MeCN) is also described. The synthesis of these compounds was optimised to obtain anhydrous **4-Ln**, appropriate for reactivity with **3**. The data from NMR, UV-vis and ATR-IR spectroscopy provide the spectroscopic signature for **4-Ln**, and two different solid-state molecular structures provide a useful reference.

The reactions of **3** with **4-Ln** have also been investigated, producing the monometallic lanthanide radical compounds **5-Ln** $[CoCp_2]^+[Ln(hfac)_3(N,N'\text{-pd})]^{-\bullet}$ (Ln = Y, Eu, Gd, Yb). These first examples of lanthanide compounds of the radical anion of pd were obtained in high yields, and were fully characterised by NMR, EPR, UV-vis and ATR-IR spectroscopy. In particular, EPR, UV-vis and ATR-IR spectroscopy indicate that **4-Ln** coordinates selectively to

the *N,N'* site of the radical ligand, consistent with the coordination properties of the ligand in the neutral oxidation state.

The EPR spectrum of **5-Y** was analysed in combination with DFT calculations. Simulation of the EPR spectrum was consistent with the absence of coupling of the *O,O'*-localised organic radical to Y, indicating that Y coordinated to the *N,N'* site of the ligand. Coupling to the other nuclei of the pd ligand is also consistent with Mulliken spin density calculations performed on the geometry-optimised structure of the *N,N'*-coordinated anion $[Y(hfac)_3(N,N'\text{-pd})]^{-\bullet}$. The ATR-IR spectra of **5-Ln** are also consistent with *N-N'* bound Y, exhibiting a stretching frequency at 1417-1420 cm^{-1} which is assigned to the semiquinone moiety. This frequency is similar to the frequency assigned to the semiquinone moiety in non-coordinated **3** and slightly lower in energy than previously reported *O,O'* coordinated semiquinones. The UV-vis absorption spectra of **5-Y** was analysed with comparison to TD-DFT data and it was found that the most salient absorption in the visible region is a π-π^* transition, similar to that observed in the unbound radical ligand. The energy of the transition is shifted by 80 nm to lower energy, from 560 nm to 640 nm, consistent with the coordination of Lewis acidic Y(III). The same transitions as in **5-Y** are observed in the absorption spectra of **5-Ln** (Ln = Eu, Gd, Yb). The selective coordination of **4-Ln** to the *N,N'* site of the ligand is therefore established in both the neutral and radical anion oxidation states. This selectivity is vital for developing a selective synthesis of lanthanide heterobimetallics based on the pd ligand.

3.6 Experimental information for Chapter 3

3.6.1 Starting materials

$CoCl_2$ was dehydrated *in vacuo* before being stored under N_2. Lanthanide triflates, K(hfac), K(Cp), KH and 1,10-phenanthroline-5,6-dione (pd) were prepared as described in Chapter 2.

3.6.2 Synthesis of $CoCp_2$

$CoCp_2$ was prepared by modification of a literature procedure.[42]

K(Cp) (806 mg, 7.69 mmol) and $CoCl_2$ (500 mg, 3.85 mmol) were separately suspended in THF (10 ml each) and K(Cp) was added to $CoCl_2$ at -78 °C with stirring. Immediately upon stirring, a colour change from a yellow solution to a dark suspension was observed. The reaction was warmed to RT with stirring then stirred for 1 h. THF was removed *in vacuo* to leave a dark solid, which was extracted into hexane (3x 10 ml) with filtration by filter cannula to exclude KCl and a dark reddish brown solution was obtained. The solution was reduced to saturation and cooled to -15 °C overnight to crystallise. The mother liquor was decanted by cannula while keeping the reaction vessel at -15 °C and the crystals were dried *in vacuo* to afford $CoCp_2$ as dark shardlike crystals (380.8 mg, 2.05 mmol, 52%).

3.6.3 Synthesis of 3 $[CoCp_2]^+[pd]^{-\bullet}$

To a -78 °C suspension of pd (0.22 g, 1.0 mmol) in THF (5 mL), a solution of $CoCp_2$ (0.21 g, 1.1 mmol, 1.1 eq.) in THF (5 mL) was added dropwise over 10 m, immediately giving a deep purple solution. The reaction was warmed to room temperature with stirring over 15 m, then stirred for 1 h. THF was removed in vacuo, and the dark purple solids washed with toluene (3 x 5 mL) and hexane (2 x 5 mL). The product was dried in vacuo, giving **3** $[CoCp_2]^+[pd]^{-\bullet}$ as a deep purple powder (0.37 g, 0.93 mmol, 93% yield). Crystals of **3** suitable for X-ray diffraction were grown from a saturated MeCN solution at -35 °C over 14 days. ^{1}H NMR (d_3-MeCN): δ = 5.67 (10H, s, Cp**H**) ppm. IR (ATR)/cm^{-1}: 1575 (m), 1561 (s), 1511 (s), 1486 (s), 1446 (m), 1413 (m), 1402 (s, ν_{CO}) cm^{-1}. UV-vis (MeCN) λ_{max}/nm (ε/M^{-1} cm^{-1}): 401 (3 230), 560 (3 830). Anal. Calcd. for $C_{22}H_{16}N_2O_2Co$: C, 66.17%; H, 4.04%; N, 7.02%. Found: C, 66.19%; H, 3.96%; N, 7.46%.

3.6.4 Synthesis of 4-Ln [Ln(hfac)$_3$(S)$_2$] (S = THF; Ln = Y, Eu, Gd. S = MeCN; Ln = Eu, Gd, Yb)

*3.6.4.1 Synthesis of **4-Y***

Y(OTf)$_3$ (0.64 g, 1.18 mmol) was suspended in THF (5 mL) and cooled to -78 °C. With stirring, a solution of K(hfac) (0.88 g, 3.55 mmol) in THF (5 mL) was added. The resultant suspension was warmed to room temperature over 15 m and stirred for 16 h. THF was removed *in vacuo*, and the off-white solids extracted into toluene (2 x 10 mL). Toluene was then removed *in vacuo*, and the solids washed with hexane (2 x 5 mL) to give **4-Y** Y(hfac)$_3$(THF)$_2$ as a low melting off-white solid (0.76 g, 0.89 mmol, 75% yield). ^{1}H NMR (d_6-benzene): δ = 1.16 (8H, s, THF-C**H**$_2$) 3.59 (8H, s, THF-C**H**$_2$) 6.28 (3H, s, hfac-C**H**) ppm. ^{19}F{^{1}H} NMR (d_6-benzene): δ = -76.68 (s, hfac-C**F**$_3$) ppm. IR (ATR)/cm^{-1}: 1668 (w), 1649 (s), 1612 (w), 1558 (w), 1531 (m), 1474 (s), 1250 (s), 1194 (s), 1134 (s), 1101 (m), 1022 (m) cm^{-1}.

*3.6.4.2 Synthesis of **4-Eu** (S = THF)*

K(hfac) (661.9 mg, 2.69 mmol, 3 eq.) was dissolved in THF (20 ml) and added to a suspension of Eu(OTf)$_3$ (537.8 mg, 0.880 mmol, 1 eq.) in THF (5 ml) at -78 °C. The mixture was warmed to room temperature with stirring over 15 m, then stirred for 1 h. THF was removed *in vacuo* and the remaining beige solid was extracted into toluene (3x 15 ml) by filter cannula to exclude K(OTf), then toluene was removed *in vacuo*. After 1h at 10^{-3} mbar the oily solid became a beige powder which was further dried *in vacuo* for 4 h. The solid was then cooled to -78 °C and washed with cold hexanes (3x 5 ml), then dried *in vacuo* for 3.5 h to yield **4-Eu** Eu(hfac)$_3$(THF)$_2$ (507.0 mg, 0.553 mmol, 63%). ^{1}H NMR (d_6-benzene): δ = 0.08 (s, 3H, hfac-C**H**), 7.69 (s, 8H, THF-C**H**$_2$), 20.34 (s, 8H, THF-C**H**$_2$) ppm. ^{19}F{^{1}H} NMR (d_6-benzene): δ = -81.62 ppm (s, hfac-C**F**$_3$). IR (ATR)/cm^{-1} (intensity): 1645 (s, ν_{CO}), 1609 (w), 1560 (m), 1531 (m), 1463 (s), 1350 (w), 1250 (s), 1206 (s), 1134 (s), 1099 (m), 1018 (m). UV-vis (MeCN) λ_{max}/nm (ε/M^{-1} cm^{-1}): 303 (25 900), 466 (9.2). Anal. Calcd. for $C_{23}H_{19}EuF_{18}O_8$: C, 30.11%; H, 1.59%; N, 0%. Found: C, 30.58-31.33%; H, 1.86-1.92%; N, 0%.

*3.6.4.3 Synthesis of **4-Eu** (S = MeCN)*

Eu(OTf)$_3$ (521.3 mg, 0.870 mmol (1 eq.) and K(hfac)(THF)$_{0.15}$ (671.6 mg, 2.614 mmol, 3 eq.) were added to a schlenk. At 0 °C, THF was added with stirring, and the mixture was allowed to warm to R.T., then stirred for 2 h. THF was removed *in vacuo* to give a beige solid and toluene was used to extract the product (20 ml). Toluene was removed *in vacuo* from the

extract and MeCN (15 ml) was added to the beige solid. The solution was filtered, then MeCN was removed *in vacuo* to leave an oily solid, which was dried *in vacuo* overnight, but did not form a tractable powder. The solid was dissolved in Et_2O, following which, removal of the Et_2O *in vacuo* afforded an oily solid (344.6 mg, 0.403 mmol, 46%). Plate-like single crystals suitable for X-ray diffraction were obtained by cooling a saturated solution of $Eu(hfac)_3(MeCN)_2$ in hexane to -35 °C overnight.

*3.6.4.4 Synthesis of **4-Gd** (S = THF)*

$Gd(OTf)_3$ (214.2 mg, 0.354 mmol, 1 eq.) and K(hfac) (264.5 mg, 1.08 mmol, 3 eq.) were added to a schlenk. THF (15 ml) was added and the mixture was stirred for 2 h. THF was removed from the yellow solution *in vacuo* and the beige solid was extracted into toluene (3x 10 ml) with vigorous stirring, and filtered by filter cannula to exclude K(OTf), then toluene was removed *in vacuo* to give a beige solid. The solid was washed with hexane (2x 10 ml) at -88 °C, then dried *in vacuo* (10^{-2} mbar, 1 h) to yield **4-Gd** $Gd(hfac)_3(THF)_2$ (130.7 mg, 0.142 mmol, 40%). IR (ATR)/cm^{-1} (intensity): 1647 (s, ν_{CO}), 1609 (w), 1560 (m), 1533 (m), 1468 (s), 1350 (w), 1249 (s), 1207 (m), 1134 (s), 1101 (m), 1041 (w), 1016 (m). UV-vis (MeCN) λ_{max}/nm (ε/M^{-1} cm^{-1}): 303 (23 300).

*3.6.4.5 Synthesis of **4-Gd** (S = MeCN)*

$Gd(OTf)_3$ (719.5 mg, 1.190 mmol, 1 eq.) and $K(hfac)(THF)_{0.15}$ (920.1 mg, 3.581 mmol, 3 eq.) were added to a schlenk flask. At -78 °C, THF (15 ml) was added. A colour change from yellow to orange was observed and the mixture was stirred to R.T. over 1 h. THF was removed *in vacuo* to leave a beige solid, which was extracted into toluene (25 ml with sonication, then 2x 15 ml). Toluene was removed *in vacuo* to leave a beige, oily solid. MeCN (20 ml) was added and the solution filtered, then MeCN was removed *in vacuo* to leave an oily solid. The solid was dissolved in minimum MeCN (2ml) and cooled to -35 °C, whereupon a beige solid formed. The solid was dried *in vacuo* until it began to melt/redissolve, at which point it was cooled again to -35 °C to precipitate, and this process was repeated until a beige, free-flowing powder of $Gd(hfac)_3(MeCN)_2$ was obtained (623.3 mg, 0.724 mmol, 61%). Plate-like single crystals of $Gd(hfac)_3(\mu\text{-hfac})_3(MeCN)$ suitable for X-ray diffraction were obtained by cooling a saturated solution of $Gd(hfac)_3(MeCN)_2$ in toluene to -35°C.

3.6.4.6 Synthesis of **4-Yb** (S = THF)

$Yb(OTf)_3$ (649.6 mg, 1.047 mmol) and K(hfac) (772.7 mg, 3.141 mmol, 3 eq.) were added to a schlenk, and THF (20 ml) was added with stirring. The mixture was stirred for 1 h, then THF was removed *in vacuo*. The beige solids were extracted into hexane (3x 10 ml) with filtration *via* filter cannula to exclude K(OTf). Hexane was then removed *in vacuo* and the solids were washed with -88 °C hexane (3x 5 ml). The solid was then dried *in vacuo* and weighed to give **4-Yb** $Yb(hfac)_3(THF)_2$ as a beige free-flowing solid (733.6 mg, 0.782 mmol, 75% yield). ^{1}H NMR (d_6-benzene): δ = -23.57 (s, 3H, hfac-C**H**), 26.50 (s, 8H, THF-C**H**$_2$), 62.82 (s, 8H, THF-C**H**$_2$) ppm. ^{19}F{^{1}H} NMR (d_6-benzene): δ = 90.49 (s) ppm. IR (ATR)/cm^{-1} (intensity): 1647 (s, ν_{CO}), 1618 (w), 1566 (m), 1539 (m), 1476 (s), 1460 (w), 1435 (w), 1354 (w), 1252 (s), 1200 (s), 1134 (s), 1101 (m), 1038 (m). UV-vis (MeCN) λ_{max}/nm (ε/M^{-1} cm^{-1}): 304 (23 500), 975 (6.3).

3.6.4.7 Synthesis of **4-Yb** (S = MeCN)

$Yb(OTf)_3$ (0.8322 g, 1.342 mmol, 1 eq.) and K(hfac) (0.9908 g, 4.025 mmol, 3 eq.) were added to a schlenk, which was cooled to -78 °C and MeCN (25 ml) was added with stirring. The yellow solution was warmed to R.T. and stirred for 30 m, then MeCN was removed *in vacuo* to give a beige solid. The solid was extracted into toluene (2x 15 ml, then 20 ml) by cannula filtration. Toluene was removed *in vacuo* to give a beige oily solid. Hexane (30 ml) was added to the solid and the mixture was sonicated for 5 m. Hexane was then removed *in vacuo* and the solid dried *in vacuo* for 2 h to yield $Yb(hfac)_3(MeCN)_2$ (490.2 mg, 0.559 mmol, 42%). ^{1}H NMR (d_8-THF): δ = -0.09 (s, 6H, C**H**$_3$CN), 1.77 (s, 3H, hfac-C**H**) ppm. ^{19}F{^{1}H} NMR (d_8-THF): δ = -91.43 (s, hfac-C**F**$_3$) ppm.

3.6.5 Synthesis of 5-Ln $[CoCp_2]^+[Ln(hfac)_3(N,N'\text{-pd})]^{-\bullet}$ (Ln = Y, Eu, Gd, Yb)

3.6.5.1 Synthesis of **5-Y**

At -78 °C, a solution of **4-Y** $Y(hfac)_3(MeCN)_2$ (543.5 mg, 0.8123 mmol) in THF (20 ml) was added to a suspension of **3** (320.4 mg, 0.8024 mmol) in THF (5 ml) with stirring. The suspension was warmed to room temperature with stirring for 2 h. A colour change was immediately observed from purple to dark green. The solution was filtered *via* filter cannula to obtain a dark green solution, from which THF was removed *in vacuo*. The resultant dark green solids were washed with toluene (3x 15 ml) and hexane (20 ml) then dried *in vacuo* to give **5-Y** as a dark green solid (638.9 mg, 0.5759 mmol, 72% yield). ^{1}H NMR (d_8-THF): δ = 5.76 (10H, s, Cp**H**)

5.99 (3H, s, hfac-C**H**) ppm. $^{19}F\{^{1}H\}$ NMR (d_8-THF): δ = -77.75 (s, hfac-C**F**$_3$) ppm. IR (ATR)/cm^{-1}: 1651 (s) 1579 (w) 1498 (m) 1428 (w, ν_{CO}) 1251 (s) 1136 (s). UV-vis (MeCN) λ_{max}/nm (ε/M^{-1} cm^{-1}): 387 (6 986), 642 (2 356). Anal. Calcd. for $C_{37}H_{19}F_{18}N_2O_8CoY$: C, 40.06%; H, 1.73%; N, 2.53%. Found: C, 39.80%; H, 1.71%; N, 2.90%.

*3.6.5.2 Synthesis of **5-Eu***

In a glovebox, **4-Eu** (S = MeCN) (146.7 mg, 0.172 mmol) was dissolved in THF (5 ml) and was added to a stirred suspension of **3** (68.5 mg, 0.172 mmol) in THF (5 ml). An immediate colour change from purple to green was observed on mixing. The solution was filtered using a frit and the remaining solids were further extracted with THF (2x 2 ml). THF was removed from the filtrate *in vacuo* to obtain dark green solids, which were washed with toluene (3 ml) and dried *in vacuo* to yield **5-Eu** $[CoCp_2]^+[Eu(hfac)_3(N,N'\text{-pd})]^{-\bullet}$ as a dark green solid (163.7 mg, 0.140 mmol, 81%). ^{1}H NMR (d_8-THF): δ = 3.20 (s, hfac-C**H**), 6.19 (s, 10H, Cp-C**H**) ppm. $^{19}F\{^{1}H\}$ NMR (d_8-THF): δ = -80.50 (s, hfac-C**F**$_3$) ppm. IR (ATR)/cm^{-1} (intensity): 1649 (s, hfac-ν_{CO}), 1578 (w), 1557 (m), 1528 (m), 1506 (s), 1483 (w), 1420 (m). UV-vis (MeCN) λ_{max}/nm (ε/M^{-1} cm^{-1}): 263 (45 300), 301 (39 900), 630 (407). UV-vis (THF) λ_{max}/nm (ε/M^{-1} cm^{-1}): 426 (1 403), 594 (669).

*3.6.5.3 Synthesis of **5-Gd***

In a glovebox, **4-Gd** (S = MeCN) (229.3 mg, 0.267 mmol) was dissolved in THF (5 ml) and was added to a suspension of **3** (106.2 mg, 0.266 mmol) in THF (5 ml) with stirring. Immediately a colour change from purple to green was observed and the mixture was stirred for 1 h. The green solution was filtered by frit and THF was removed from the solution *in vacuo*. The solid was washed with toluene (2x 10 ml) and hexane (2x 10 ml), then dried *in vacuo* to yield **5-Gd** $[CoCp_2]^+[Gd(hfac)_3(N,N'\text{-pd})]^{-\bullet}$ as a dark green solid (286.0 mg, 0.243 mmol, 91%). IR(ATR)/cm^{-1} (intensity): 1651 (s, hfac-ν_{CO}), 1578 (w), 1553 (m), 1528 (s), 1503 (s), 1466 (w), 1418 (m). UV-vis (MeCN) λ_{max}/nm (ε/M^{-1} cm^{-1}): 263 (47 400), 301 (43 200), 435 (shoulder), 636 (728). UV-vis (THF) λ_{max}/nm (ε/M^{-1} cm^{-1}): 440 (shoulder), 622 (538). μ_{eff} (Evans method, d_8-THF) = 7.60-7.67 μ_B. Anal. Calcd. for $C_{37}H_{19}CoF_{18}GdN_2O_8$: C, 37.73%; H, 1.63%; N, 2.38%. Found: C, 37.85-38.81%; H, 1.60-1.61%; N, 2.58-2.58%.

*3.6.5.4 Synthesis of **5-Yb***

The same procedure as for **5-Gd** was followed, using the following materials and quantities: **4-Yb** (S = MeCN) (202.1 mg, 0.242 mmol) and **3** (96.0 mg, 0.240 mmol). A dark green solid of **5-Yb** $[CoCp_2]^+[Yb(hfac)_3(N,N'\text{-pd})]^{-\bullet}$ was yielded: (225.7 mg, 0.189 mmol, 78%). ^{1}H NMR (d_8-THF): δ = -10.93 (s, hfac-C**H**), 8.18 (s, Cp-C**H**) ppm. $^{19}F\{^1H\}$ NMR (d_8-THF): δ = -83.14 (s, hfac-C**F**$_3$) ppm. IR (ATR)/cm^{-1} (intensity): 1651 (s, ν_{CO}), 1578 (w), 1557 (m), 1530 (m), 1514 (w), 1499 (w), 1420 (m). UV-vis (THF) λ_{max}/nm (ε/M^{-1} cm^{-1}): 265 (45 600), 298 (39 600), 450 (shoulder), 596 (539).

3.7 References

1. A. Y. Girgis, Y. S. Sohn and A. L. Balch, *Inorg. Chem.*, 1975, **14**, 2327-2331.
2. G. A. Fox, S. Bhattacharya and C. G. Pierpont, *Inorg. Chem.*, 1991, **30**, 2895-2899.
3. F. Calderazzo, F. Marchetti, G. Pampaloni and V. Passarelli, *J. Chem. Soc., Dalton Trans.*, 1999, **24**, 4389-4396.
4. F. Calderazzo, G. Pampaloni and V. Passarelli, *Inorg. Chim. Acta*, 2002, **330**, 136-142.
5. N. M. Shavaleev, L. P. Moorcraft, S. J. A. Pope, Z. R. Bell, S. Faulkner and M. D. Ward, *Chem. Commun.*, 2003, **10**, 1134-1135.
6. N. M. Shavaleev, L. P. Moorcraft, S. J. A. Pope, Z. R. Bell, S. Faulkner and M. D. Ward, *Chem. Eur. J.*, 2003, **9**, 5283-5291.
7. S. Berger, J. Fiedler, R. Reinhardt and W. Kaim, *Inorg. Chem.*, 2004, **43**, 1530-1538.
8. D. M. Murphy, K. McNamara, P. Richardson, V. Sanchez-Romaguera, R. E. P. Winpenny and L. J. Yellowlees, *Inorg. Chim. Acta*, 2011, **374**, 435-441.
9. H. Bock and P. Hänel, *Z. Naturforsch. B*, 1992, **47**, 288-300.
10. J. Yuasa, T. Suenobu and S. Fukuzumi, *J. Phys. Chem. A*, 2005, **109**, 9356-9362.
11. J. R. Hickson, PhD, Imperial College London, 2018.
12. N. G. Connelly and W. E. Geiger, *Chem. Rev.*, 1996, **96**, 877-910.
13. J. R. Hickson, S. J. Horsewill, J. McGuire, C. Wilson, S. Sproules and J. H. Farnaby, *Chem. Commun.*, 2018, **54**, 11284-11287.
14. C. G. Andrews and C. L. B. Macdonald, *J. Organomet. Chem.*, 2005, **690**, 5090-5097.
15. B. Odom, D. Hanneke, B. D'Urso and G. Gabrielse, *Phys. Rev. Lett.*, 2006, **97**, 030801.
16. J. R. Hickson, S. J. Horsewill, C. Bamforth, J. McGuire, C. Wilson, S. Sproules and J. H. Farnaby, *Dalton Trans.*, 2018, **47**, 10692-10701.
17. P. Atkins, T. Overton, J. Rourke, M. Weller and F. Armstrong, in *Shriver & Atkins: Inorganic Chemistry*, Oxford University Press, Oxford, 4th edn., 2006, ch. *d*-metal complexes: Electronic Structure and Spectra, pp. 459-490.
18. K. Binnemans, in *Handbook on the Physics and Chemistry of Rare Earths*, eds. K. A. Schneider, J.-C. Bunzli and V. K. Pecharsky, Elsevier, 2005, vol. 35, ch. 225, pp. 107-272.
19. G. Malandrino, R. Lo Nigro, L. Fragalà Ignazio and C. Benelli, *Eur. J. Inorg. Chem.*, 2003, **2004**, 500-509.
20. C. R. De Silva, J. R. Maeyer, R. Wang, G. S. Nichol and Z. Zheng, *Inorg. Chim. Acta*, 2007, **360**, 3543-3552.
21. P.-F. Yan, P.-H. Lin, F. Habib, T. Aharen, M. Murugesu, Z.-P. Deng, G.-M. Li and W.-B. Sun, *Inorg. Chem.*, 2011, **50**, 7059-7065.
22. B. V. Bukvetskii, A. G. Mirochnik and A. S. Shishov, *J. Lumin.*, 2018, **195**, 44-48.
23. C.-Y. Fu, L. Chen, X. Wang and L.-R. Lin, *ACS Omega*, 2019, **4**, 15530-15538.

24. N. B. D. Lima, A. I. S. Silva, P. C. Gerson, Jr., S. M. C. Gonçalves and A. M. Simas, *PLoS One*, 2015, **10**, e0143998-e0143998.

25. A. N. Swinburne, M. H. L. Paden, T. L. Chan, S. Randall, F. Ortu, A. M. Kenwright and L. S. Natrajan, *Inorganics*, 2016, **4**, 27.

26. J.-C. G. Bunzli and S. V. Eliseeva, in *Lanthanide Luminescence: Photophysical, Analytical and Biological Aspects*, eds. P. Hanninen and H. Harma, Springer, Berlin, 2011, vol. 7, pp. 1-46.

27. W. H. Watson, R. J. Williams and N. R. Stemple, *J. Inorg. Nucl. Chem.*, 1972, **34**, 501-508.

28. H.-Y. Wong, W.-S. Lo, W. T. K. Chan and G.-L. Law, *Inorg. Chem.*, 2017, **56**, 5135-5140.

29. A. Hussain, S. Sahaas, R. Majumdar, R. Dighe and A. Chakravarty, *Indian J. Chem. A*, 2011, **50**, 519-530.

30. Y.-X. Zhang, X.-Y. Cheng, Y.-T. Tang, Y.-H. Zhang, S.-C. Wang, H.-Y. Wei and Z.-L. Wu, *Polyhedron*, 2019, **166**, 23-27.

31. R. D. Shannon, *Acta Crystallogr. Sect. A*, 1996, **32**, 751-767.

32. J. Koehler and J. Meiler, *Prog. Nucl. Magn. Reson. Spectrosc.*, 2011, **59**, 360-389.

33. A. C. Harnden, E. A. Suturina, A. S. Batsanov, P. K. Senanayake, M. A. Fox, K. Mason, M. Vonci, E. J. L. McInnes, N. F. Chilton and D. Parker, *Angew. Chem. Int. Ed.*, 2019, **58**, 10290-10294.

34. K. Mason, A. C. Harnden, C. W. Patrick, A. W. J. Poh, A. S. Batsanov, E. A. Suturina, M. Vonci, E. J. L. McInnes, N. F. Chilton and D. Parker, *Chem. Commun.*, 2018, **54**, 8486-8489.

35. A. Caneschi, A. Dei, D. Gatteschi, L. Sorace and K. Vostrikova, *Angew. Chem. Int. Ed.*, 2000, **39**, 246-248.

36. C. Benelli, A. Caneschi, D. Galleschi, J. Laugier and P. Rey, *Angew. Chem. Int. Ed.*, 1987, **26**, 913-915.

37. J. McGuire, B. Wilson, J. McAllister, H. N. Miras, C. Wilson, S. Sproules and J. H. Farnaby, *Dalton Trans.*, 2019, **48**, 5491-5495.

38. P. Bertrand, in *Electron Paramagnetic Resonance Spectroscopy: Fundamentals*, ed. P. Bertrand, Springer International Publishing, Cham, 2020, pp. 289-321.

39. T. Rajeshkumar and G. Rajaraman, *Chem. Commun.*, 2012, **48**, 7856-7858.

40. Y.-Q. Zhang, C.-L. Luo, B.-W. Wang and S. Gao, *J. Phys. Chem. A*, 2013, **117**, 10873-10880.

41. P. Zhang, M. Perfetti, M. Kern, P. P. Hallmen, L. Ungur, S. Lenz, M. R. Ringenberg, W. Frey, H. Stoll, G. Rauhut and J. van Slageren, *Chem. Sci.*, 2018, **9**, 1221-1230.

42. H. P. Fritz, in *Adv. Organomet. Chem*, eds. F. G. A. Stone and R. West, Academic Press, 1964, vol. 1, pp. 239-316.

4 Investigation of photoluminescence and ultrafast energy transfer in a modular series of monometallic lanthanide compounds

4.1 Abstract

Lanthanide photoluminescence is widely used for a variety of purposes, from consumer electronics to medical imaging and laser technologies.[1, 2] Frequently these applications rely on the phenomenon of sensitisation, where the light emitting properties of the lanthanide are enhanced by the use of a chromophore to harvest light and transfer energy to the lanthanide.[1, 3] However, the mechanisms involved in the sensitisation process are complex, and difficult to observe directly.[4, 5] In this chapter, selected lanthanide compounds from Chapter 2 (**1-Ln** Ln(hfac)$_3$(*N,N'*-pd), Ln = Eu, Gd, Tb, Yb) and Chapter 3 (**4-Ln** Ln(hfac)$_3$(S)$_2$, Ln = Eu, Yb) and **5-Ln** [CoCp$_2$]$^+$[Ln(hfac)$_3$(*N,N'*-pd)]$^{-\bullet}$, Ln = Eu, Gd, Yb) have been studied by steady-state photoluminescence and time-correlated single photon counting (TCSPC) in order to better understand the luminescence sensitisation and quenching processes in this modular system. The effects of solvents of different polarities on the electronic structure of **1-Ln** have been investigated, and a clear dependence of the electronic absorption spectrum on the polarity was observed. The excited state lifetime of **1-Eu** as determined by TCSPC also showed a significant dependence on the solvent. Determination of the excited state decay of the organic ligands in **1-Ln** (Ln = Eu, Gd) demonstrated that the emissive excited state of the pd ligand had a shorter lifetime in **1-Eu** than in **1-Gd**. This indicates that the emissive excited state is involved in the energy transfer during sensitisation and could be used to observe and investigate the sensitisation process further.

4.2 Lanthanide photoluminescence

The lanthanides are frequently utilised for their luminescent properties, from consumer electronics to medical imaging and laser technologies.[1, 2] The light emitted by lanthanide ions is determined by the identity of the emitting lanthanide, and generally not the ligand environment it is in. This is due to the core-like nature of the f-orbitals, which are not significantly perturbed by the ligand field, and therefore the energy states are relatively invariable between different Ln(III) environments (see section 1.2 for discussion of the lanthanide electronic structure). An energy level diagram showing the excited state electronic structures of the lanthanides, highlighting the most important emissive states, is given in Figure 4.1.[2] The core-like nature of the f-orbitals results in a relatively few vibrational excited states.[6] This results in large energy gaps between the lowest lying excited states (the emissive state) and the ground state. Thus, only two routes are available for an excited electron to relax to the ground state: interaction with other atoms or molecules (non-radiative de-excitation), or emission of a photon (photoluminescence). The energy gaps between the emissive and ground states of the trivalent lanthanide ions span the visible-NIR region of the electromagnetic spectrum (Figure 4.2), giving the different lanthanides broad utility in a range of applications. The vibrational states are well-defined due to the core-like nature of the *f*-orbitals, and the emissive transitions therefore typically have small line-widths.

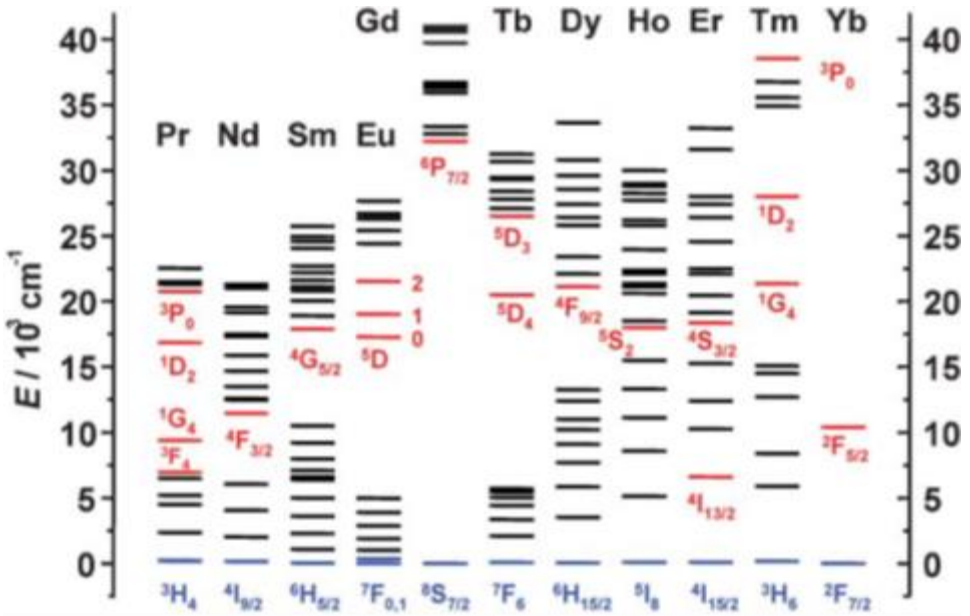

Figure 4.1: The excited state electronic structures of selected lanthanide ions. The ground state is shown in blue, and the most commonly emissive states are shown in red. Image reproduced from Bünzli 2010.[2]

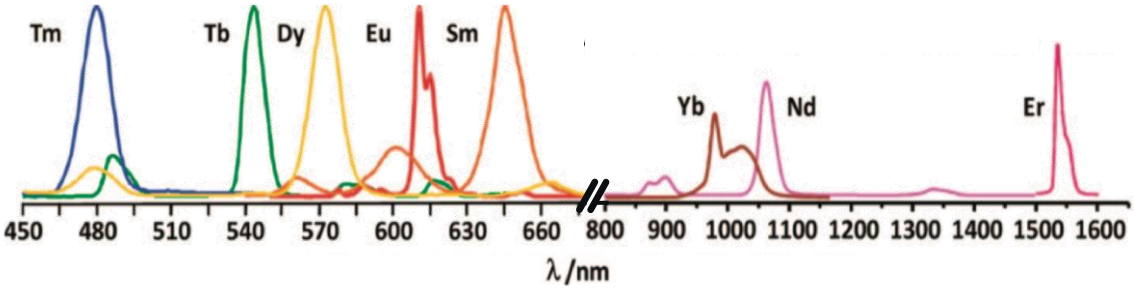

Figure 4.2: The emission spectra of various lanthanide ions. Image reproduced from Bünzli 2010.[2]

The f-f transitions are electric dipole, or symmetry, forbidden transitions, though they are magnetic dipole allowed.[6] This means that the probability of an interaction between a photon of appropriate energy and the f-orbitals resulting in absorption is low. Combined with the discrete energy levels of the lanthanide ions limiting the photon energies to a small range, this means that the number of photons absorbed by a lanthanide ion by direct excitation is very low. To increase the population of the emissive excited state of the lanthanide to produce more light, a different method of populating the excited state is required. Frequently antenna ligands, or sensitising ligands, containing organic chromophores are used to harvest light. Figure 4.3 illustrates the energy transfer processes during sensitisation. Following excitation to the singlet excited states of the ligands, they can undergo intersystem crossing to a triplet excited state. The energy from the excited states of these ligands is then typically

transferred to the lanthanide *via* one of two processes, as shown in Figure 4.3. The most common processes are Förster resonant energy transfer (FRET) and Dexter transfer, though other processes have been observed. FRET is a through-space process from the singlet excited state of the ligand. It involves a dipole-dipole resonance interaction between electrons which results in transfer of energy.[4] Meanwhile, Dexter energy transfer is a through-bond interaction from the triplet excited state of the ligand. Dexter transfer is a process whereby electrons of different energies are exchanged, resulting in the lanthanide being in the excited state.[5] Other reported sensitisation processes include charge transfer (transfer of an excited state electron to the lanthanide, followed by transfer of a ground state electron back to the ligand).[7] This process is typically only observed for complexes of Yb(III), and is frequently a quenching process for Eu(III) complexes.[8]

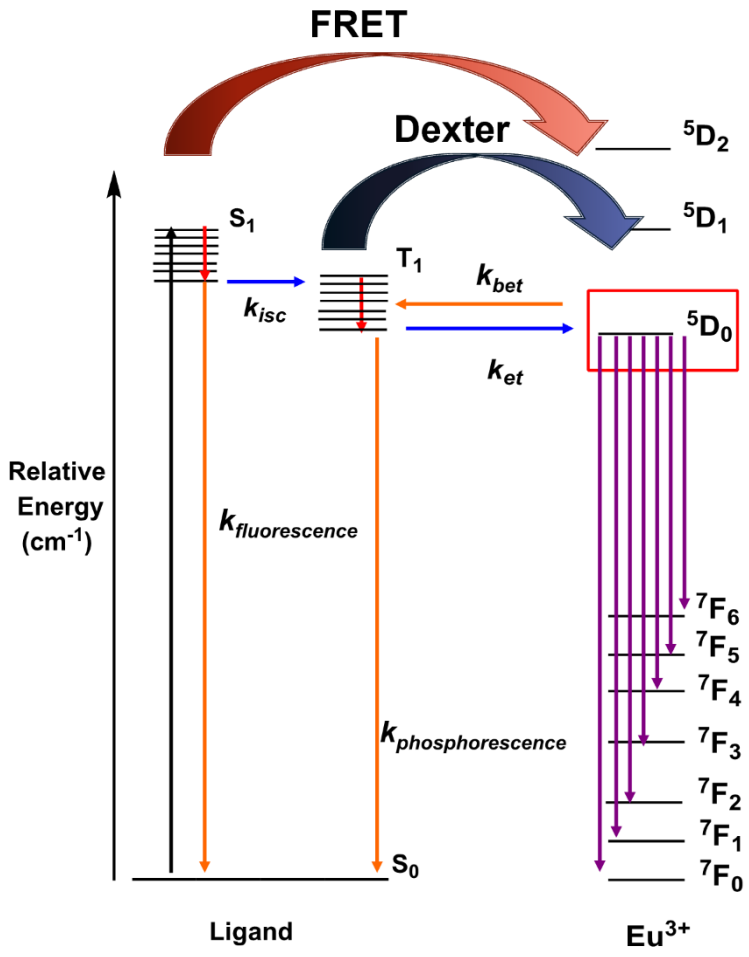

Figure 4.3: Jablonski diagram depicting the sensitisation energy transfer processes in a Eu(III) complex.

Another result of the forbidden nature of the f-f transitions is that once an electron has reached the emissive state, there is a relatively low probability of a radiative de-excitation event (emission of a photon) occurring at any given time. The lanthanides therefore typically have unusually long emission lifetimes, with some complexes of Tb(III) and Eu(III) exhibiting lifetimes of over 1 ms.[1] However, this also means that there is ample time for non-radiative de-excitation events such as energy transfer to the vibrational excited states of ligands and solvent molecules. Ligands with a large number of C-H or O-H groups are therefore particularly effective at quenching lanthanide luminescence.[3] Fluorination or deuteration of ligands and solvent molecules has been found to be effective at increasing quantum yields (the quantum yield is the ratio between the number of photons emitted and absorbed, written as a percentage) and the lifetimes of luminescence by removing this pathway for de-excitation.[3, 6, 9, 10]

4.3 Photoluminescence of 4-Ln Ln(hfac)$_3$(S)$_2$ (Ln = Eu, Yb)

Lanthanide *β*-diketonate compounds are frequently utilised for their photoluminescent properties.[11-14] *β*-diketonate ligands have been shown to be particularly effective sensitising agents for Eu(III) and Tb(III), though they are capable of sensitising emission from other lanthanide ions.[9, 15, 16] Their broad applications are largely due to the high degree of tunability of their electronic structure, achieved by functionalisation of the 1,5-positions of the ligand. Thus, a ligand may be chosen such that the excited state energy levels are appropriate to maximise the efficiency of energy transfer to the lanthanide and minimise loss. The *β*-diketonate ligand hexafluoroacetyl acetonate (hfac) is an effective sensitiser for Eu(III) as its singlet excited state (300 nm, 33 333 cm^{-1}) lies *ca* 15 000 cm^{-1} higher than the emissive $^5D_0$ excited state of Eu(III) (600 nm, 17 000 cm^{-1}), preventing any back energy transfer from Eu(III) to the ligand.

To provide a baseline for the study of pd-containing lanthanide compounds, the photoluminescent properties of **4-Ln** were investigated. Irradiation of **4-Eu** and **4-Yb** by UV light results in sensitisation of lanthanide photoluminescence by the hfac ligands. The excitation and emission spectra of **4-Eu** are shown in the top half of Figure 4.4. The excitation spectrum (recorded at an emission wavelength of 610 nm) has two bands in the UV region: a maximum at 285 nm, and a shoulder up to 320 nm, both in the region of the electronic absorption spectrum assigned to the hfac ligand absorption (see Section 3.3.1). The emission spectrum of **4-Eu** (Figure 4.4, top) is characteristic of Eu *β*-diketonate compounds, and is assigned to the $^5D_0 \rightarrow {}^7F_J$ (J = 0-4) transitions. The emission spectrum is dominated by the $^5D_0 \rightarrow {}^7F_2$ transition at 610 nm, resulting in bright red light emission.[17] The emission spectrum of **4-Eu** when excited by light of either 285 or 320 nm is identical, indicating the excitation bands are not due to the presence of multiple species in solution.

The excitation spectrum of **4-Yb** also has two bands, with a maximum at 280 nm and a shoulder at 320 nm. The emission spectrum of **4-Yb** (Figure 4.4, bottom) is characteristic of Yb(III), with a sharp transition maximum at 974 nm, and broader transitions at 930 nm and up to 1040 nm. These are assigned to the $^2F_{5/2} \rightarrow {}^2F_{7/2}$ transition, relaxing from the excited state to four sub-levels of the $^2F_{7/2}$ ground state.[18] In **4-Yb** as for **4-Eu**, excitation by light of either 280 or 320 nm results in identical emission profiles.

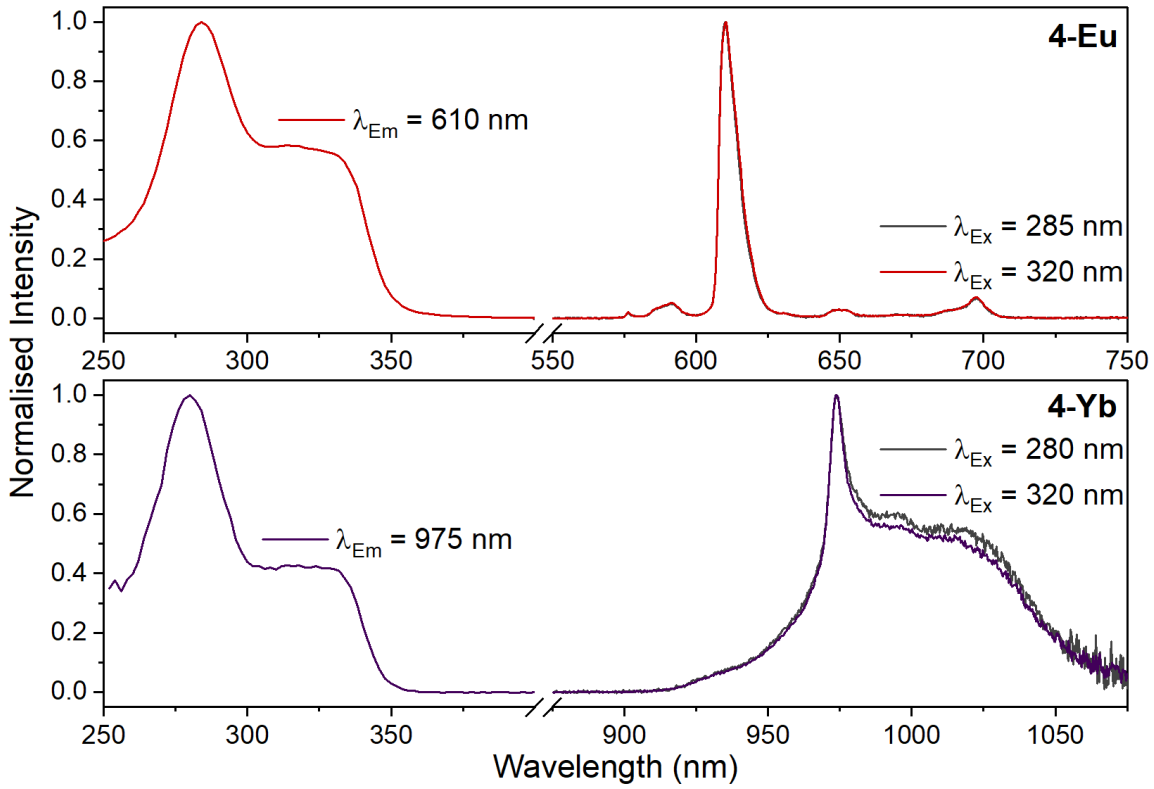

Figure 4.4: Excitation (LHS) and emission (RHS) spectra of 4-Ln (Ln = Eu, Yb), recorded on dilute (4-Eu, 74 μM; 4-Yb, 81 μM) solutions in MeCN. λ_{Ex} and λ_{Em} are depicted in the figure for each 4-Ln.

4.4 UV-vis-NIR solvent dependence and photoluminescence of 1-Ln

Ln(hfac)$_3$(*N,N'*-pd) (Ln = Eu, Gd, Tb, Yb)

4.4.1 Solvent dependence of the UV-vis-NIR spectra of 1-Ln (Ln = Eu, Gd, Yb)

As mentioned in Chapter 2, the solvent has a significant effect on the colour of solutions of **1-Ln**. In order to quantify this effect and identify the causes the electronic absorption spectra of **1-Ln** (Ln = Eu, Gd, Yb) were recorded in a range of solvents (MeCN, THF, Et_2O, dichloromethane (DCM) and toluene), shown in Figure 4.5. As discussed in Section 2.2.6, the visible electronic spectra of **1-Ln** in MeCN have two distinct transition envelopes at 450-500 nm (transition envelope A) and at 600 nm (transition envelope B), both assigned to intra-ligand charge transfer (ILCT) of the pd ligand.

Upon determination of the absorption spectra of **1-Ln** in different solvents, transition envelope A did not exhibit a clear trend, either by solvent polarity or by lanthanide. Transition envelope B, however, was found to have a significant dependence on the solvent in both **1-Eu** and **1-Gd**. The electronic spectrum of **1-Yb** does not exhibit absorbances in the region of transition envelope B in any solvents.

In **1-Eu**, the intensity of transition envelope B is relatively invariable in different solutions (ε between 30 and 70 M^{-1} cm^{-1}), but λ_{max} undergoes a significant shift from 600 nm in polar solvents such as THF and MeCN to 650 nm in less polar solvents such as toluene or DCM. In **1-Gd**, the same trend is observed in the energy of transition envelope B, with λ_{max} close to 600 nm in THF and MeCN and λ_{max} of 650 nm in non-polar toluene. The intensity of transition envelope B, however, varies much more significantly in **1-Gd** than in **1-Eu**. The transition envelope is most intense in MeCN (ε = 85 M^{-1} cm^{-1}), has intermediate intensity in THF (30 M^{-1} cm^{-1}) and toluene (20 M^{-1} cm^{-1}), and is observed only as a tail from 500 nm to 750 nm in Et_2O and in DCM. It is evident that a correlation exists between the solvent polarity and both the energy and intensity of transition envelope B, and that the identity of the lanthanide also has a significant impact on the electronic absorbance spectrum.

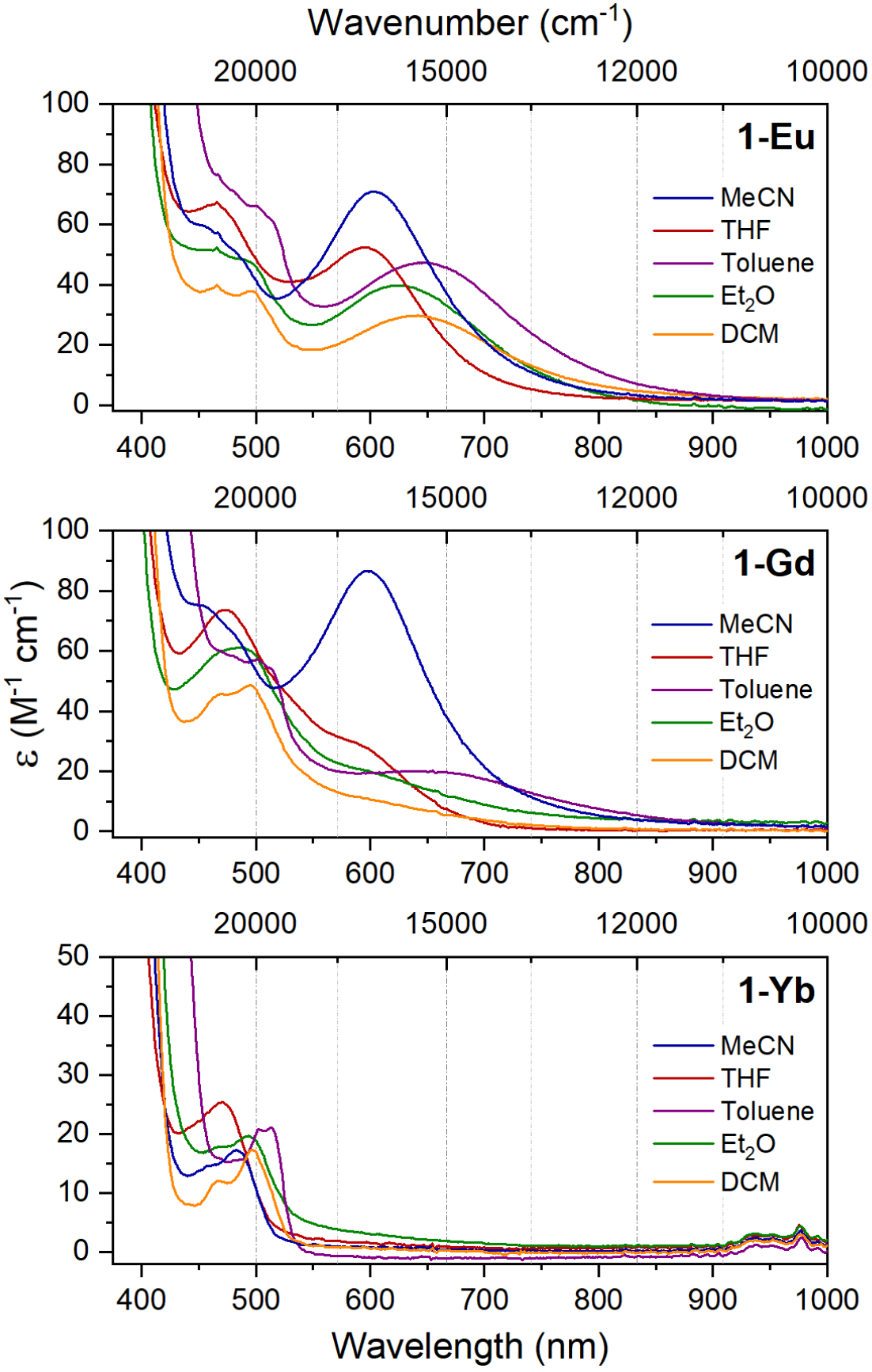

Figure 4.5: Electronic absorption spectra of 1-Ln (Ln = Eu, Gd, Yb), recorded on 2 mM solutions in various solvents.

In solvents of different polarities (and with different coordination properties), **1-Ln** clearly experience a different electronic environment. The excited state energy levels are therefore slightly different in different solvents, resulting in the observed shift in the energy of the electronic transitions. An explanation for these variations may be provided by differences in the solid state molecular structures of **1-Ln** (see Section 2.2.7). In the solid state, pd coordinates to Ln(III) either in a linear (Ln-N-ring angle ≈ 180°) fashion (crystallised from polar solvents, and always for **1-Yb**) or at an angle (crystallised from non-polar solvents, except for **1-Yb**). It is possible that this difference in coordination also occurs in solution, resulting in a different electronic structure for the pd ligand. Alternatively, the observed variations may be due to other interactions between the solvent molecules and the lanthanide ions.

4.4.2 Photoluminescence studies on 1-Ln Ln(hfac)$_3$(*N,N'*-pd) (Ln = Eu, Gd, Tb, Yb)

The photoluminescent properties of **1-Gd** were investigated. The excited states of Gd(III) are too high in energy (in the UV region) to be populated by sensitisation *via* the hfac ligands. Studying the photoluminescent properties of **1-Gd** therefore allows observation of the ligand excited states without energy transfer to the lanthanide. This information may be used to inform other **1-Ln**. The emission spectrum of **1-Gd** is broad, with λ_{max} = 580-587 nm as shown in Figure 4.6, and varies very little when recorded in different solvents, despite the significant variance observed in the absorbance spectra (Figure 4.5). The excitation spectrum of **1-Gd** (also shown in Figure 4.6), on the other hand, had a greater dependence on the solvent. The maximum of the excitation spectrum (with λ_{Em} = 580 nm) ranges from 503 nm in MeCN to 530 nm in toluene. Both excitation and emission are assigned to transitions of the pd ligand, as they are in the same region as absorptions assigned to pd in the electronic spectra of **1-Gd**. From these data the excited states of pd in **1-Gd** are determined to be in the range of 20 000 to 17 000 cm^{-1}. This is very close to the energy of the emissive excited states of Eu(III) ($^5D_0$, *ca* 17 000 cm^{-1}) and particularly overlaps with those of Tb(III) ($^5D_4$, *ca* 18500 cm^{-1}). Back energy transfer from these lanthanides to pd is therefore possible, and could lead to de-excitation of the emissive excited states of Eu(III) and Tb(III).

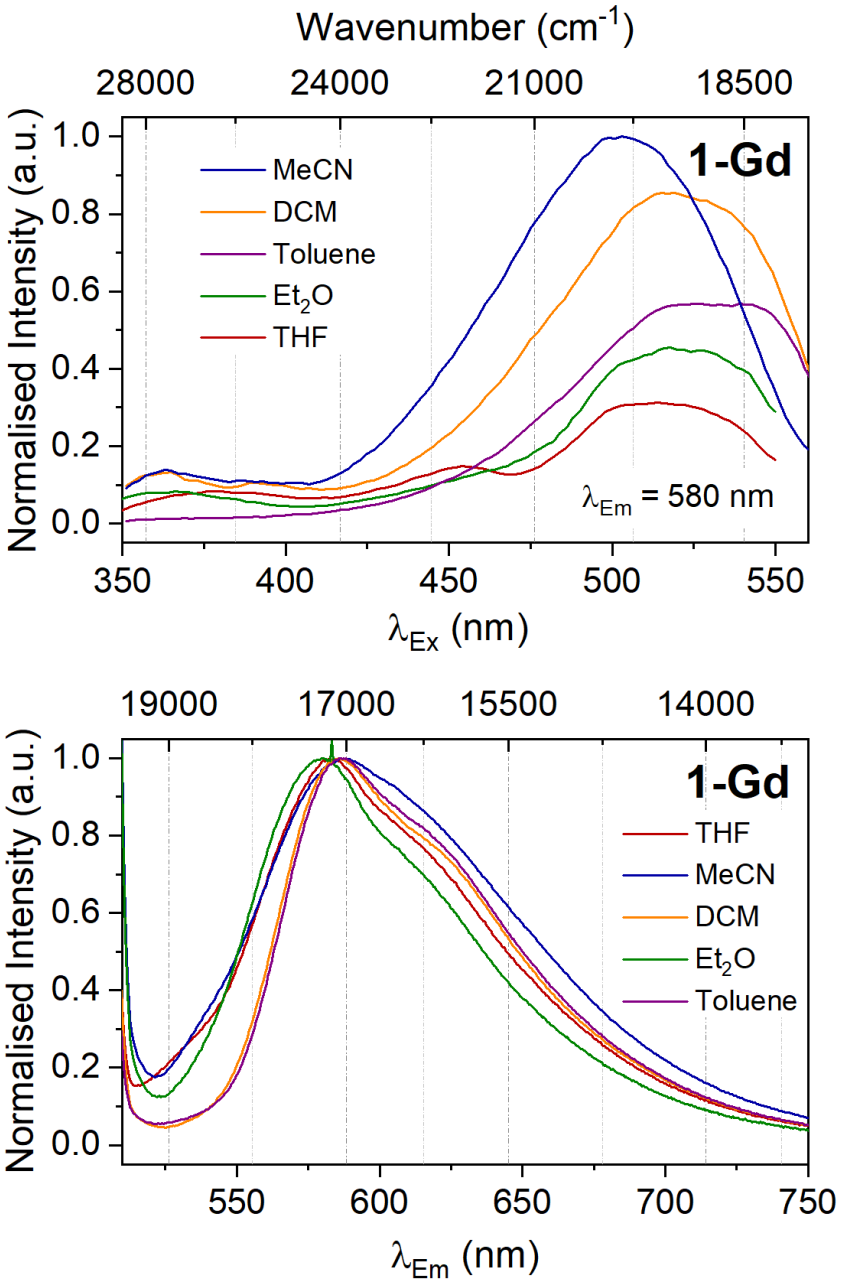

Figure 4.6: Excitation (Top) and Emission (Bottom) spectra of 1-Gd, recorded on 2 mM solutions in various solvents at R.T.

1-Ln (Ln = Eu, Tb, Yb) were investigated by photoluminescence spectroscopy, using dilute (*ca* 40 μM) MeCN solutions. The emission spectrum of **1-Eu** (Figure 4.7) is characteristic of *β*-diketonate complexes of Eu(III), displaying maxima assigned to the $^5D_0 \rightarrow {}^7F_J$ (J = 0-4) transitions. It is also very similar to that of **4-Eu**, being dominated by the hypersensitive $^5D_0 \rightarrow {}^7F_2$ transition at *ca* 610 nm. The excitation spectrum has a maximum at 290 nm, in the region of the absorbance spectrum assigned to the hfac ligands (λ_{max} = 300 nm, see Section 2.2.6, Figure 2.17). Excitation of the absorbance of the pd ligand in the UV region (λ_{max} = 250

nm) did not result in significant emission from Eu(III). As in the case of **4-Eu**, the emission spectrum in MeCN is identical regardless of the excitation wavelength.

The emission spectrum of **1-Tb** was recorded on a dilute MeCN solution (Figure 4.7), and shows a characteristic emission spectrum for Tb(III). The spectrum displays four narrow transitions between 480-615 nm, assigned to the $^5D_4 \rightarrow {}^7F_J$ (J = 6-3) transitions of the Tb(III) ion. As for **1-Eu**, the excitation spectrum (λ_{Em} = 545 nm) has a maximum at 290 nm and does not extend to higher energy. This indicates that as in **1-Eu**, sensitisation of emission from Tb(III) by UV light in **1-Tb** occurs by excitation of the hfac ligands, and not the pd ligand.

The emission spectrum of **1-Yb** was also recorded on a dilute MeCN solution (Figure 4.7), and is characteristic for Yb(III). The spectrum has a sharp line-like transition maximum at 975 nm, and three broader transitions at 940, 1000 and 1030 nm. These transitions are assigned to the vibrational states of the $^2F_{5/2} \rightarrow {}^2F_{7/2}$ transitions of the Yb(III) ion. As for both **1-Eu** and **1-Tb**, the excitation spectrum (λ_{Em} = 975 nm) has a maximum at 290 nm, without extension to higher energy, again indicating that sensitisation by UV light occurs *via* the hfac ligands. No emission from Yb(III) was observed upon excitation of **1-Yb** in the visible region of the spectrum.

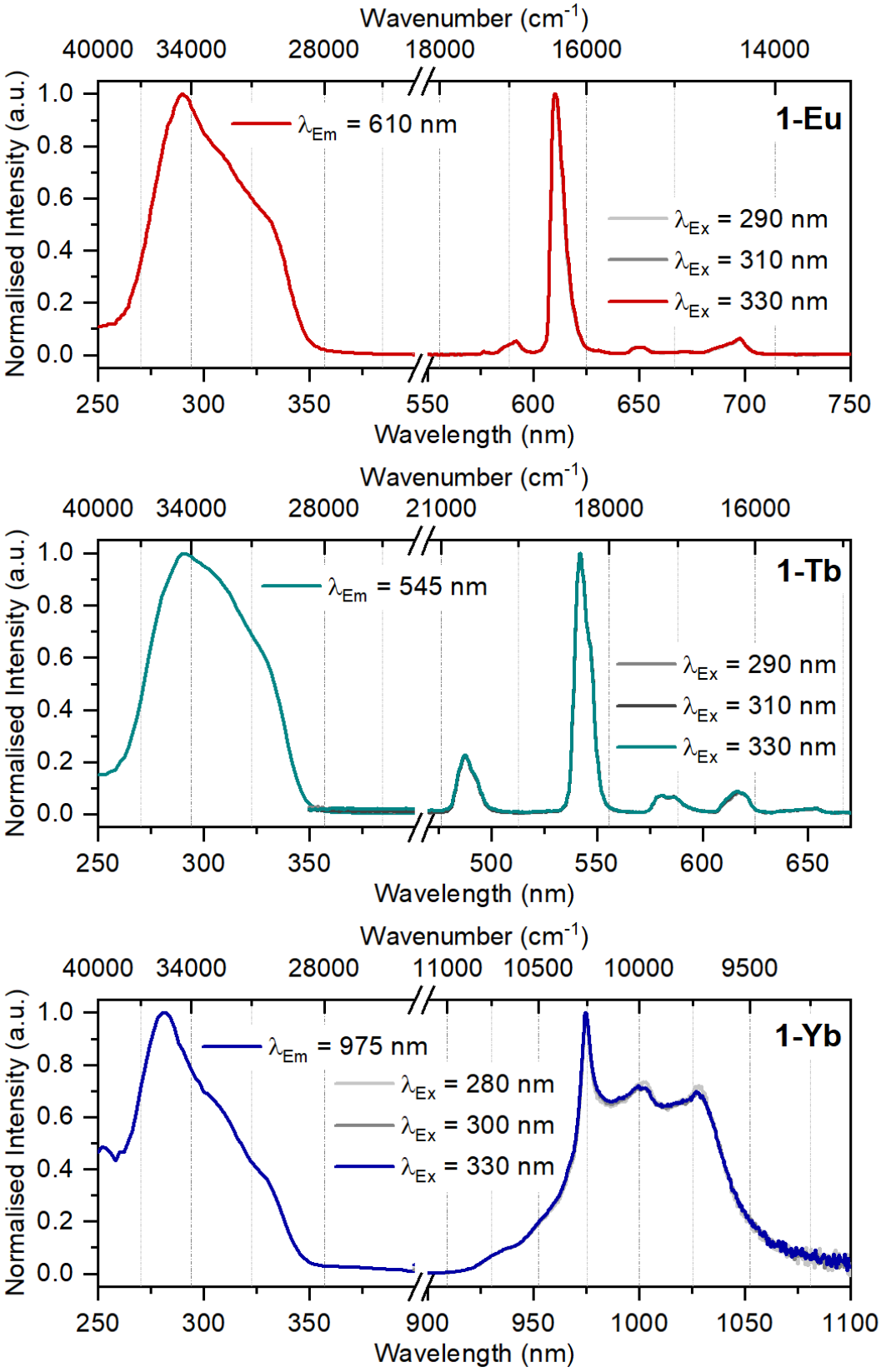

Figure 4.7: Excitation (LHS) and emission (RHS) spectra of 1-Ln (Ln = Eu, Tb, Yb), recorded on dilute (1-Eu, 43 μM; 1-Tb, 30 μM; 1-Yb, 37 μM) MeCN solutions. λ_{Ex} and λ_{Em} are depicted in the figure for each 1-Ln.

Small variations in the emission spectra of **1-Eu** were observed in different solvents, as shown in Figure 4.8. In less-polar, non-coordinating solvents DCM, toluene and Et_2O, the maximum of the hypersensitive $^5D_0 \rightarrow {}^7F_2$ transition occurs at 609 nm, whereas in the polar, coordinating solvents MeCN and THF the transition maximum shifted to 612 and 613 nm respectively. Similarly, the $^5D_0 \rightarrow {}^7F_4$ transition exhibited a different profile in different solvents. In DCM, toluene and Et_2O, the maximum was observed at 700 nm, whereas in THF and MeCN the maximum shifted to higher energy at 693 nm. It is evident that in a similar manner to the absorption spectrum, the polarity and coordination properties of the solvent have an effect on the emission spectrum. It is well documented that the $^5D_0 \rightarrow {}^7F_2$ transition is highly sensitive to ligand field effects.[17] It therefore seems likely that the differences in the emission spectral profile are due to small variations in the solution state ligand environment of **1-Eu** in different solvents.

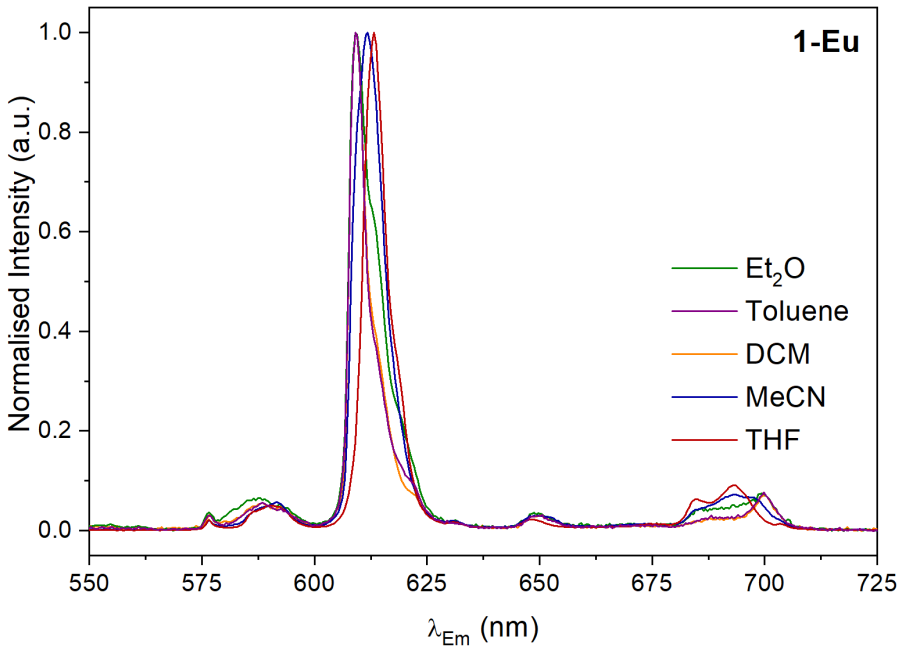

Figure 4.8: Emission spectra of 1-Eu, recorded on 2 mM solutions in various solvents at R.T. and normalised to the height of the $^5D_0 \rightarrow {}^7F_2$ transition.

The emission spectra of **1-Yb** were also recorded in the same set of solvents, shown in Figure 4.9. Unlike that of **1-Eu**, the emission spectrum of **1-Yb** does not vary with the solvent. This is unsurprising, given that the emission spectrum of Yb(III) is generally less dependent on the ligand field than that of Eu(III),[18] and that less variation was observed in the absorption profile of **1-Yb** in different solvents (Figure 4.5).

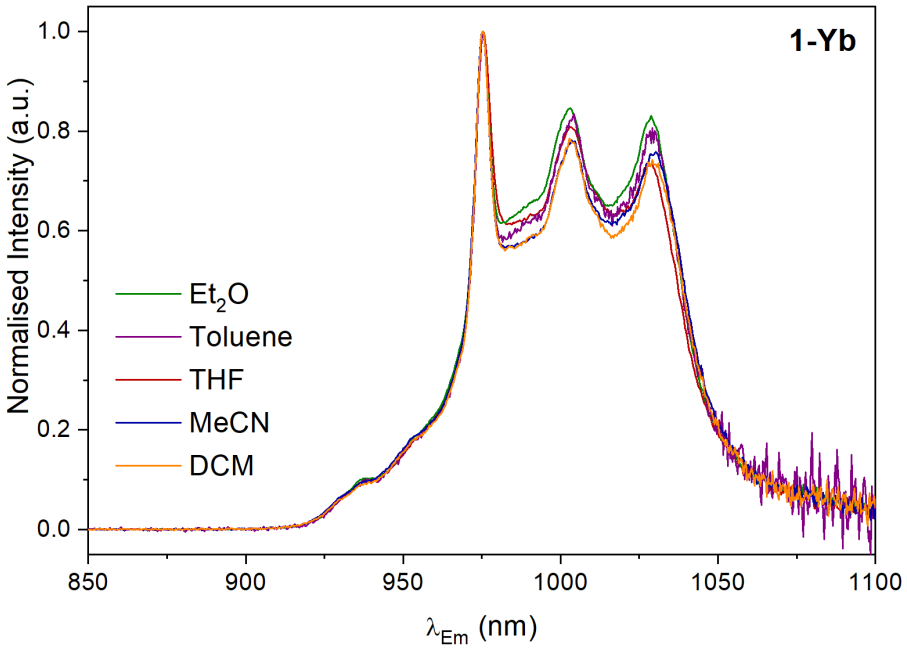

Figure 4.9: Emission spectra of 1-Yb, recorded on 2 mM solutions in various solvents at R.T. and normalised to the height of the $^7F_{5/2} \rightarrow {}^7F_{7/2}$ transition maximum at 975 nm.

4.5 Photoluminescence studies on 5-Ln $[CoCp_2]^+[Ln(hfac)_3(N,N'\text{-pd})]^{-\bullet}$ (Ln = Eu, Yb)

Most lanthanide radical ligand complexes (including lanthanide semiquinone complexes) have been synthesised and investigated for their single-molecule magnet properties.[19-24] Photoluminescence studies on lanthanide compounds where lanthanides are bonded to radical ligands are rare. Radicals are well known to quench luminescence by non-radiative de-excitation.[25-28] Indeed, the introduction of a radical to lanthanide complexes *via* a redox reaction has been used as a "switch-off" luminescent chemical sensor.[29, 30] The examples of lanthanide photoluminescence in complexes containing radical ligands that have been reported typically involve highly stable radicals such as nitronyl and imino nitroxides[31, 32] or tetramethyl piperidinyl oxyl (TEMPO) radicals,[33] which are electronically very different to the semiquinone radicals in **5-Ln**. It was therefore of interest to investigate lanthanide photoluminescence in this unusual environment.

No emission could be detected from **5-Gd**, consistent with the organic radical quenching emission from the pd ligand completely. However, excitation of a dilute solution of **5-Eu** in THF by UV light resulted in characteristic emission from Eu(III) as shown in Figure 4.10. The emission spectrum of **5-Eu** is dominated by the $^5D_0 \rightarrow {}^7F_2$ transition at 609 nm, similarly to **1-Eu** and **4-Eu**. The excitation spectrum has a single maximum at 290 nm, assigned to the hfac ligands as for **1-Ln** and **4-Ln**. Excitation of a dilute solution of **5-Yb** in MeCN resulted in emission characteristic of Yb(III) (Figure 4.10). With a maximum at 975 nm, the emission spectrum is similar to that of **1-Yb** and **4-Yb**. As for other hfac compounds **1-Ln**, **4-Ln** and **5-Eu** the excitation spectrum has a maximum at 290 nm assigned to absorption by the hfac ligands. No sensitisation of emission from **5-Ln** was detected by irradiation in the visible region, despite the significant absorption (ε = 1000-2000 M^{-1} cm^{-1}) which is assigned to an intra-ligand charge transfer transition of the pd radical anion (see Section 3.4.5).

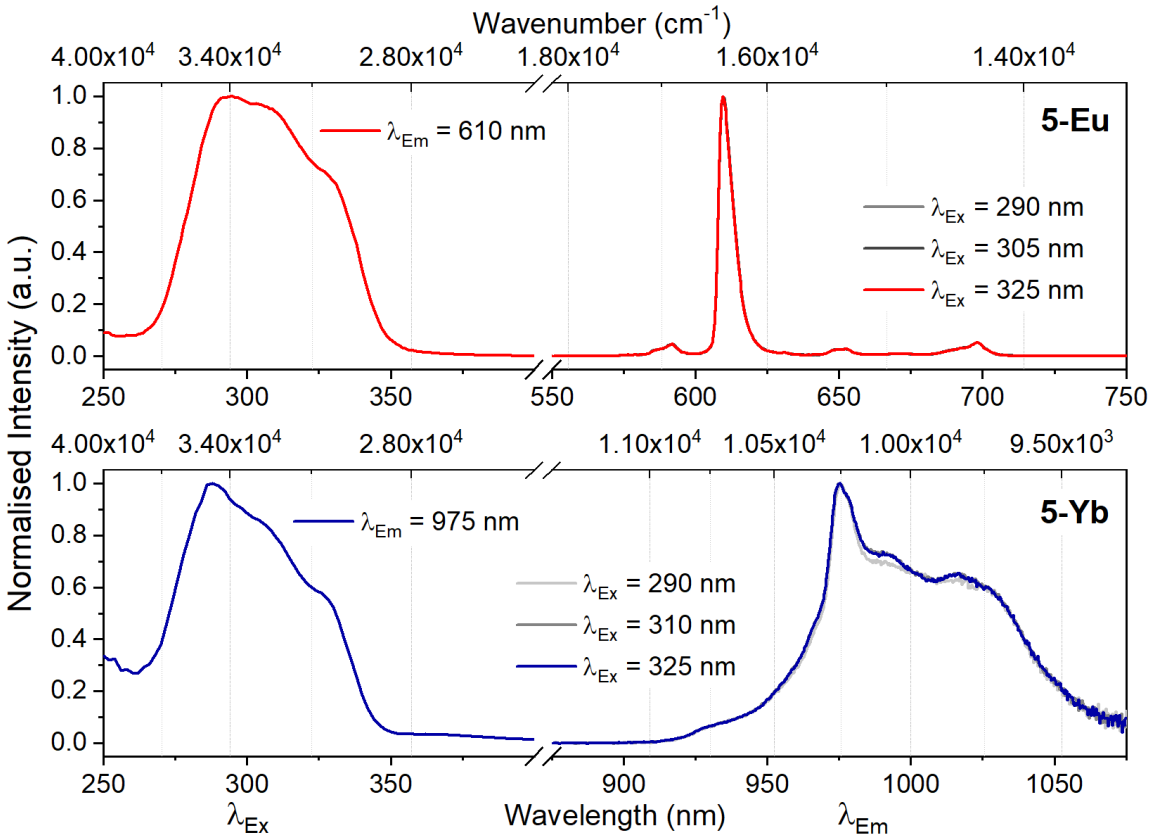

Figure 4.10: Excitation (LHS) and emission (RHS) spectra of 5-Ln (Ln = Eu, Yb) recorded on dilute (5-Eu, 33 μM; 5-Yb, 39 μM) solutions in MeCN (5-Eu) and THF (5-Yb) solutions. λ_{Ex} and λ_{Em} are depicted in the figure for each 5-Ln.

4.6 Photoluminescence lifetime studies on 4-Ln $Ln(hfac)_3(S)_2$, 1-Ln $Ln(hfac)_3(N,N'\text{-pd})$ and 5-Ln $[CoCp_2]^+[Ln(hfac)_3(N,N'\text{-pd})]^{-\bullet}$ (Ln = Eu, Gd)

Time correlated single photon counting (TCSPC) is a method for determining the lifetimes of luminescent states. A pulsed laser is used to excite a sample, which then emits photons which are detected with a picosecond time resolution. This process is repeated to generate a histogram of the intensity of emission at various times following excitation by the laser. The histogram shows a decay proportional to the population of the excited state, from which the lifetime of the excited state may be determined by producing a fit. It is important to note that the lifetime obtained is the lifetime of the emissive excited state, and not the lifetime of the emission process. The lifetime is therefore dependent on the various energy transfer processes which lead to deexcitation of the emissive excited states, and can be used to learn about those processes. TCSPC was used here to perform a methodical analysis of ligand decay dynamics and the various ligand effects on the lanthanide emissive lifetime in **4-Ln**, **1-Ln** and **5-Ln**. This modular system is illustrated in Figure 4.11, and consists of sequential modifications from **4-Ln**. The free coordination sites of **4-Ln** (occupied by solvent molecules in solution) are replaced by the rigid chelating ligand pd in **1-Ln**, which should reduce vibrational quenching of the emissive state of the lanthanide. In **5-Ln**, the pd ligand is oxidised to the radical anion, which will introduce a significant quenching process due to the radical ligand interacting with the lanthanide. The focus of this section is on complexes of Eu(III) due to its typically long lifetimes and bright emission.

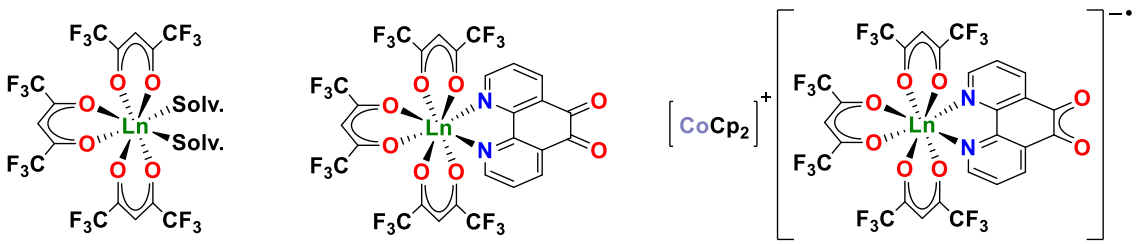

Figure 4.11: The structures of the three components of the modular system studied by TCSPC.

4.6.1 Investigation of the effects of different functional groups on emission from Eu(III)

The modular system comprising **1-Ln**, **4-Ln** and **5-Ln** was used to investigate different deexcitation pathways in THF solutions. The TCSPC emission decay was recorded for **1-Eu**, **4-Eu** and **5-Eu** (with λ_{Em} = 612 nm), and the decays are shown in Figure 4.12. Compared to **1-Eu**, which has the longest lifetime at 589 μs, **4-Eu** exhibited a somewhat shorter lifetime of 460 μs. These lifetimes are within the range commonly observed for Eu(III) complexes of 400-800 μs.[3, 6] It is well-understood that chelating ligands increase the efficiency of lanthanide light emission, by significantly decreasing de-excitation *via* vibrational pathways.[3] For this reason the majority of lanthanide *tris*-diketonate complexes used for light emission are also coordinated by a rigid chelating ligand.[11, 12, 34-39] The shorter lifetime of the Eu(III) emissive excited state in **4-Eu** is therefore consistent with the greater conformational flexibility in **4-Eu** compared to in **1-Eu**.

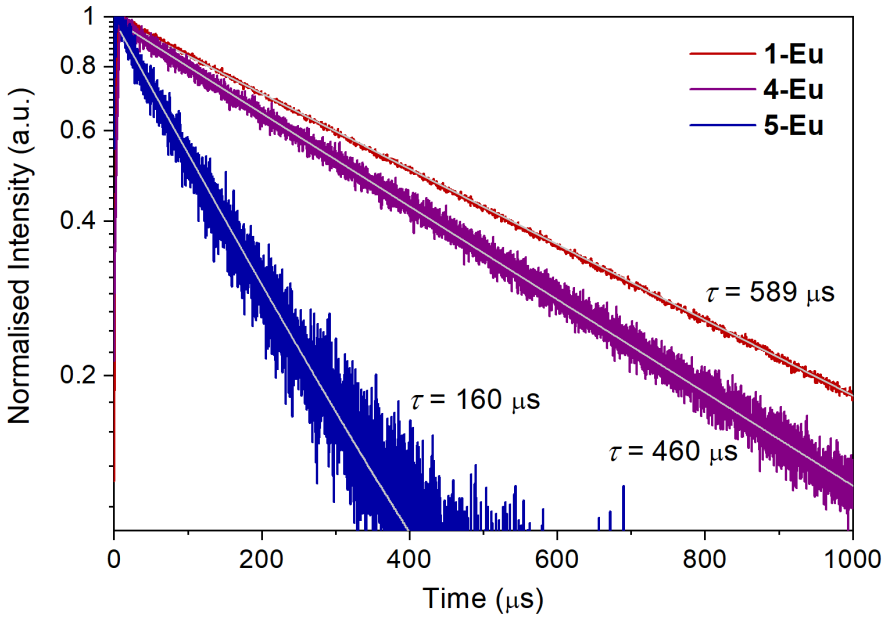

Figure 4.12: Time-correlated emission from 1-Eu (red), 4-Eu (purple) and 5-Eu (blue), all in THF solution. Monitored at λ_{Em} = 612 nm, with λ_{Ex} = 375 nm.

The more dramatic difference in lifetime is between **1-Eu** and **5-Eu**, a reduction from 589 μs to 160 μs. Both **1-Eu** and **5-Eu** are coordinated by three hfac ligands and a diimine chelating ligand. The only difference in the coordination environment of Eu(III) is therefore that the *O,O'* coordination site is changed from a diketone in **1-Eu** to a semiquinone radical in **5-Eu**. As has been mentioned, organic radicals are highly efficient at quenching lanthanide

luminescence.[29-33] However, these studies typically do not describe photoluminescence from the compounds containing organic radicals in detail, in most cases reporting near-complete quenching of luminescence upon introduction of the radical (>95%).[29-31] To the best of our knowledge, the mechanism of this quenching in lanthanide complexes has not been conclusively determined. The radical might interfere with sensitisation by quenching the ligand excited states. Alternatively, it might quench the lanthanide directly. In a recent study, a TEMPO-based radical bimetallic complex exhibited slightly different Tb(III) emission lifetimes in two different binding sites with different proximities to the radical, indicating that the radical was quenching the lanthanide emissive state.[33] Unfortunately, overlap in the emission from Tb(III) in the two sites meant that the photoluminescence decays could not be completely independently determined. In the case of **5-Eu**, introducing the organic radical clearly has a significant impact on the lifetime of Eu(III) photoluminescence. As the lifetime is a measure of the population of the emissive excited state, this indicates that the radical provides a de-excitation pathway for Eu(III). It is however unclear from these data whether the energy transfer process and the ligand excited states are also significantly affected.

4.6.2 Investigation of the dependence of emission from Eu(III) on solvent

As has been demonstrated in section 4.4, the visible absorption spectra of **1-Ln** can exhibit significant variance in different solvents. The photoluminescence emission spectra of **1-Eu** were also slightly different in different solvents, as described in section 4.4.2. It was therefore of interest to determine whether the solvent also had an impact on the energy transfer processes. The photoluminescence lifetime of **1-Eu** (recorded at λ_{Em} = 612 nm) was determined in THF and in toluene, shown in Figure 4.13. In THF, the lifetime was found to be 589 μs, while in toluene it was significantly shorter at 296 μs. These numbers are comparable to the observed lifetimes of a series of similar complexes Eu(dike)$_3$(diimine) (dike = hfac, btfac, tta; diimine = 4,4'-dimethoxy bipyridine, 4,7-dimethyl phenanthroline).[12] In dichloromethane solution, each of Eu(dike)$_3$(diimine) exhibited a lifetime of between 650 μs and 750 μs. Other complexes of europium with diketonates and phenanthroline have generally exhibited similar excited state lifetimes.[36, 37, 39] Notably, the introduction of a single water molecule into the coordination sphere of europium complexes has a significant effect on the observed lifetime. The excited state lifetime of Eu(hfac)$_3$(dmbipy)(H_2O) was much shorter than other Eu(dike)$_3$(diimine) complexes (650-750 μs), at 330 μs.[12] Both O-H and C-H vibrations are

frequently causes of energy loss.[3, 6] However, the effects of other solvents are less well understood, and intermolecular interactions have been shown to have significant influence on photoluminescence.[40, 41]

The observed decrease in excited state lifetime in **1-Eu** in toluene compared to THF solution is of a similar magnitude to that observed upon introduction of a water molecule into the coordination sphere. This major effect indicates that toluene has a particularly strong intermolecular interaction with **1-Eu**. This is perhaps unsurprising given the significant dependence of the absorption spectrum of **1-Ln** on solvent. Interestingly, the difference between the lifetime of Eu(III) emission in **1-Eu** in THF and in toluene (*ca* 300 μs) is greater than the difference between the excited state lifetime of **1-Eu** and **4-Eu** (*ca* 120 μs). Whatever the cause of the lifetime variation of **1-Eu** in different solvents, the effect is greater than the chelating effect of replacing THF molecules with a rigid pd ligand.

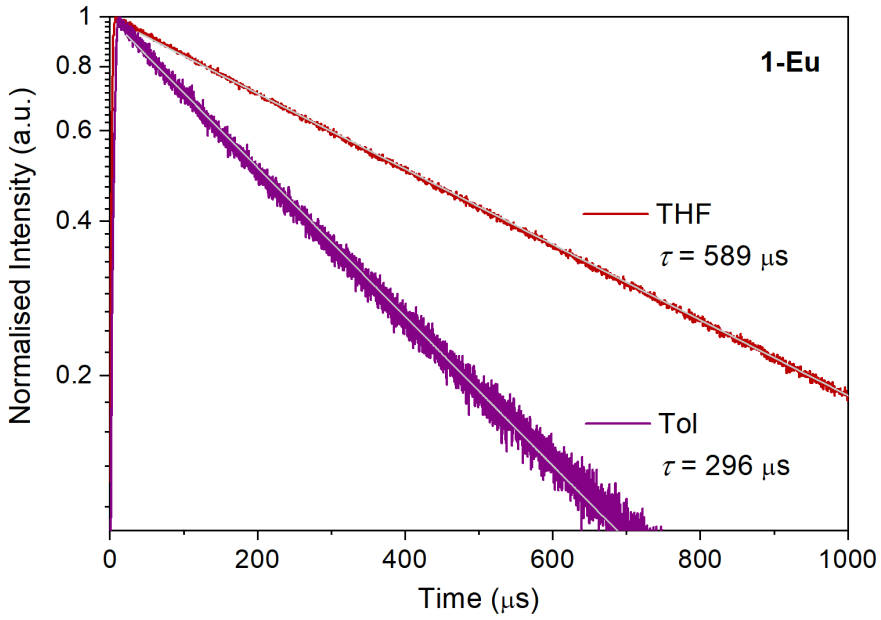

Figure 4.13: Time-correlated emission from 1-Eu in a THF solution (red) and in a toluene solution (purple). Monitored at λ_{Em} = 612 nm, with λ_{Ex} = 375 nm.

4.6.3 Investigation of organic ligand emissive excited states

It is clear from the emission spectroscopy of **1-Eu** and **4-Eu**, lanthanide photoluminescence is the most significant source of light emission from **1-Eu** and **4-Eu**. However, the Eu(III) ions are not the only emissive components of those systems. As demonstrated in Section 4.4.2, emission is also observed from the pd ligand in **1-Gd**. The ligands are integral to the sensitisation process, so the emission from these organic components of the modular system was investigated by TCSPC. Emission was monitored for 10 ns following a laser pulse for **1-Eu**, **1-Gd** and **4-Eu**, to yield the photoluminescence decays shown in Figure 4.14. Due to the very fast timescales and relatively low signal-to-noise ratio precise lifetimes will not be discussed for these decays.

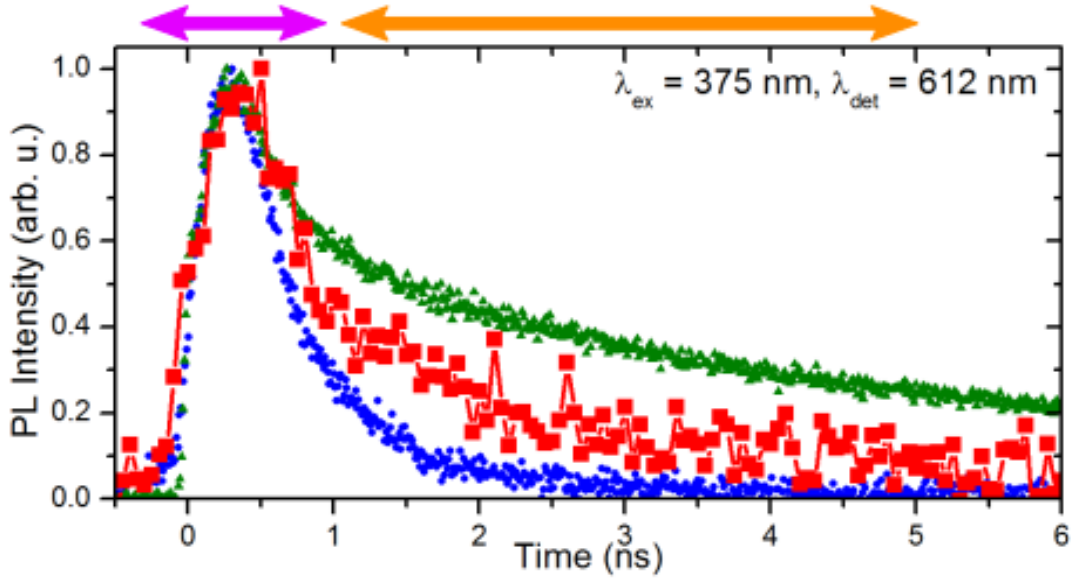

Figure 4.14: Time-correlated emission from 1-Eu (red squares), 1-Gd (green triangles) and 4-Eu (blue circles), all in THF solution. Monitored at λ_{Em} = 612 nm, with λ_{Ex} = 375 nm. Emission from the hfac ligands is highlighted by a purple arrow, emission from pd is highlighted by an orange arrow.

As can be seen in Figure 4.14, **4-Eu** (blue circles) exhibits a single exponential decay, with a lifetime very close to the instrumental accuracy limit, between 0-1 ns. This is assigned to emission from the hfac ligands, as the only ligand present in **4-Eu**. **1-Eu** (red squares) and **1-Gd** (green triangles), on the other hand, both exhibit two separate exponential components to the decay, consistent with emission from two different ligand excited states. In both **1-Eu** and **1-Gd**, a decrease is observed on the same 0-1 ns timescale as for emission from hfac in **4-Eu**. The longer lifetime exponential, of between 2-5 ns, is assigned by process of elimination to emission from the pd ligand in **1-Eu** and **1-Gd**. Notably, the lifetime of this emissive state

appears to be faster in **1-Eu** than in **1-Gd**, consistent with an energy transfer pathway in **1-Eu** from the emissive state of pd, which is not accessible in **1-Gd**. The lowest-lying excited state energy level of Gd(III) is in the UV region (*ca* 300 nm) and is therefore not accessible.[3] Eu(III), however, does have excited states of a comparable energy to the emissive state of the ligand. It is therefore possible that energy transfer is occurring from the excited state of the pd ligand as well as the hfac ligands, to the excited states of Eu(III). The modular system therefore provides an opportunity to observe some of the processes involved in sensitisation *in situ* by monitoring the emissive states of the organic ligands.

4.7 Conclusion

The photoluminescence properties of the modular series of compounds **1-Ln** (Ln = Eu, Gd, Tb, Yb), **4-Ln** (Ln = Eu, Yb) and **5-Ln** (Ln = Eu, Yb) were investigated. Characteristic lanthanide photoluminescence spectra were observed for each complex in the series. Lanthanide light emission was sensitised exclusively by the hfac ligands, absorbing in the UV region at 300 nm, even in the case of NIR-emitting ytterbium compounds. The solvent dependence of the electronic absorption of **1-Ln** (Ln = Eu, Gd, Tb, Yb) was investigated. The solvent had a significant effect on the electronic structure of **1-Ln**, with an absorption at 600 nm being particularly sensitive to the polarity of the solvent.

The modular system was also investigated by TCSPC. The emissive excited state lifetimes of Eu(III) in **1-Eu**, **4-Eu** and **5-Eu** were determined. The effect of the solvent on the lifetime of **1-Eu** was found to be significant, with a lifetime in toluene of 296 μs compared to 589 μs in THF. This effect was greater than the chelating effect of introducing the pd ligand, which increased the lifetime from 460 μs in **4-Eu** to 589 μs in **1-Eu**, both recorded in THF. The impact of the organic radical on the lifetime of photoluminescence was also quantified for the first time in **5-Eu**, which exhibited a very short lifetime for a Eu(III) complex of 160 μs. The fast timescale of TCSPC was also used to observe the emissive excited states of the organic ligands. The emissive excited states of the hfac and pd ligands have been shown to have significantly different lifetimes. Notably, the emissive excited state of the pd ligand exhibited a shorter lifetime in **1-Eu** than in **1-Gd**, indicating that the modular system may provide a rare opportunity to observe energy transfer from the pd ligand to Eu(III) during sensitisation.

4.8 References

1. J.-C. G. Bünzli and C. Piguet, *Chem. Soc. Rev.*, 2005, **34**, 1048-1077.
2. J.-C. G. Bünzli, *Chem. Rev.*, 2010, **110**, 2729-2755.
3. J.-C. G. Bunzli and S. V. Eliseeva, in *Lanthanide Luminescence: Photophysical, Analytical and Biological Aspects*, eds. P. Hanninen and H. Harma, Springer, Berlin, 2011, vol. 7, pp. 1-46.
4. T. Főrster, *Discuss. Faraday Soc.*, 1959, **27**, 7-17.
5. D. L. Dexter, *J. Chem. Phys.*, 1953, **21**, 836-850.
6. D. A. Atwood, ed., *The Rare Earth Elements - Fundamentals and Applications*, Wiley, Chichester, 2012.
7. W. D. Horrocks, J. P. Bolender, W. D. Smith and R. M. Supkowski, *J. Am. Chem. Soc.*, 1997, **119**, 5972-5973.
8. D. Kovacs and K. E. Borbas, *Coord. Chem. Rev.*, 2018, **364**, 1-9.
9. A. N. Swinburne, M. H. L. Paden, T. L. Chan, S. Randall, F. Ortu, A. M. Kenwright and L. S. Natrajan, *Inorganics*, 2016, **4**, 27.
10. S. Cotton, *Lanthanide and Actinide Chemistry*, John Wiley & Sons Ltd., Chichester, 2006.
11. K. Binnemans, in *Handbook on the Physics and Chemistry of Rare Earths*, eds. K. A. Schneider, J.-C. Bunzli and V. K. Pecharsky, Elsevier, 2005, vol. 35, ch. 225, pp. 107-272.
12. C. R. De Silva, J. R. Maeyer, R. Wang, G. S. Nichol and Z. Zheng, *Inorg. Chim. Acta*, 2007, **360**, 3543-3552.
13. N. M. Shavaleev, L. P. Moorcraft, S. J. A. Pope, Z. R. Bell, S. Faulkner and M. D. Ward, *Chem. Commun.*, 2003, **10**, 1134-1135.
14. H.-Y. Wong, W.-S. Lo, W. T. K. Chan and G.-L. Law, *Inorg. Chem.*, 2017, **56**, 5135-5140.
15. P. Hu, F.-P. Xiao, Y. Li, J.-F. Cao, Z.-S. Chen, L.-L. Zhu and W.-P. Huang, *Inorg. Chem. Commun.*, 2017, **84**, 207-211.
16. I. V. Taydakov, V. M. Korshunov, Y. A. Belousov, Y. V. Nelyubina, F. Marchetti, R. Pettinari and C. Pettinari, *Inorg. Chim. Acta*, 2020, **513**, 119922.
17. K. Binnemans, *Coord. Chem. Rev.*, 2015, **295**, 1-45.
18. D. Esteban-Gómez, L. A. Büldt, P. Pérez-Lourido, L. Valencia, M. Seitz and C. Platas-Iglesias, *Inorg. Chem.*, 2019, **58**, 3732-3743.
19. J. D. Rinehart, M. Fang, W. J. Evans and J. R. Long, *J. Am. Chem. Soc.*, 2011, **133**, 14236-14239.
20. J. D. Rinehart, M. Fang, W. J. Evans and J. R. Long, *Nat. Chem.*, 2011, **3**, 538.
21. S. Demir, M. Nippe, M. I. Gonzalez and J. R. Long, *Chem. Sci.*, 2014, **5**, 4701-4711.

22. A. Gould Colin, E. Darago Lucy, I. Gonzalez Miguel, S. Demir and R. Long Jeffrey, *Angew. Chem. Int. Ed.*, 2017, **56**, 10103-10107.

23. A. Caneschi, A. Dei, D. Gatteschi, L. Sorace and K. Vostrikova, *Angew. Chem. Int. Ed.*, 2000, **39**, 246-248.

24. A. Caneschi, A. Dei, D. Gatteschi, S. Poussereau and L. Sorace, *Dalton Trans.*, 2004, 1048-1055.

25. A. P. Darmanyan and A. S. Tatikolov, *J. Photochem.*, 1986, **32**, 157-163.

26. R. E. Belford, G. Seely, D. Gust, T. A. Moore, A. Moore, N. J. Cherepy, S. Ekbundit, J. E. Lewis and S. H. Lin, *J. Photochem. Photobiol A*, 1993, **70**, 125-133.

27. P. Dutta and R. Beaulac, *Chem. Mater.*, 2016, **28**, 1076-1084.

28. P. Dutta, Y. Tang, C. Mi, M. Saniepay, J. A. McGuire and R. Beaulac, *J. Chem. Phys.*, 2019, **151**, 174706.

29. J. K. Molloy, O. Jarjayes, C. Philouze, L. Fedele, D. Imbert and F. Thomas, *Chem. Commun.*, 2017, **53**, 605-608.

30. M. Yano, K. Matsuhira, M. Tatsumi, Y. Kashiwagi, M. Nakamoto, M. Oyama, K. Ohkubo, S. Fukuzumi, H. Misaki and H. Tsukube, *Chem. Commun.*, 2012, **48**, 4082-4084.

31. T. Tsukuda, T. Suzuki and S. Kaizaki, *J. Chem. Soc., Dalton Trans.*, 2002, **8**, 1721-1726.

32. C. Lescop, D. Luneau, P. Rey, G. Bussière and C. Reber, *Inorg. Chem.*, 2002, **41**, 5566-5574.

33. S. G. Reis, M. Briganti, S. Soriano, G. P. Guedes, S. Calancea, C. Tiseanu, M. A. Novak, M. A. del Águila-Sánchez, F. Totti, F. Lopez-Ortiz, M. Andruh and M. G. F. Vaz, *Inorg. Chem.*, 2016, **55**, 11676-11684.

34. Z. Ahmed and K. Iftikhar, *Inorg. Chim. Acta*, 2010, **363**, 2606-2615.

35. R. Marin, G. Brunet and M. Murugesu, *Angew. Chem. Int. Ed.*, 2019, **60**, 1728-1746.

36. K. Misztal, C. Tudisco, A. Sartori, J. M. Malicka, R. Castelli, G. G. Condorelli and E. Dalcanale, *Eur. J. Inorg. Chem.*, 2014, **2014**, 2687-2694.

37. O. Moudam, B. C. Rowan, M. Alamiry, P. Richardson, B. S. Richards, A. C. Jones and N. Robertson, *Chem. Commun.*, 2009, **43**, 6649-6651.

38. A. V. Shurygin, V. V. Korochentsev, A. I. Cherednichenko, A. G. Mirochnik, I. V. Kalinovskaya and V. I. Vovna, *J. Mol. Struct.*, 2018, **1155**, 133-142.

39. J. L. Zhang, B. W. Chen, X. Luo and K. Du, *Chin. Chem. Lett.*, 2012, **23**, 945-948.

40. J. H. Song and M. J. Sailor, *J. Am. Chem. Soc.*, 1997, **119**, 7381-7385.

41. F. Symalla, S. Heidrich, P. Friederich, T. Strunk, T. Neumann, D. Minami, D. Jeong and W. Wenzel, *Adv. Theory Sim.*, 2020, **3**, 1900222.

5 Investigating transmetallation reactivity for the synthesis of lanthanide heterobimetallic compounds of 1,10-phenanthroline-5,6-dione

5.1 Abstract

This chapter details a range of experiments designed to probe the reactivity of **1-Ln**, **3** and **5-Ln** with the goal of synthesis of multimetallic f-block compounds. The reactivities of **3** and **5-Y** with $NiCl_2$ and $[NEt_4]_2[NiCl_4]$ were investigated. The products were highly insoluble and therefore challenging to isolate or characterise. However, the reaction of **3** with $[NEt_4]_2[NiCl_4]$, followed by the addition of **4-Y**, produced a product for which the ATR-IR spectrum was consistent with dissociation of $pd^{-\bullet}$ to a mix of pd^0 and pd^{2-}. This reaction is therefore proposed to form a *d-f* heterometallic species Y(hfac)$_3$(*N,N'-O,O'*-pd)Ni(*N,N'*-pd), where two pd ligands in different oxidation states are bound asymmetrically across the nickel ion.

The organometallic lanthanide compounds **6-Ln** Ln$(Cp^t)_2(OTf)_2K$ (Ln = Y, Yb) (Cp^t = tetramethyl cyclopentadienyl) were synthesised and fully characterised by NMR, ATR-IR and UV-vis spectroscopy, and their solid-state molecular structures were determined. The unusual electronic absorption and photoluminescence properties of **6-Yb** were found to arise from a ligand to metal charge transfer state. The reaction of **6-Y** with **1-Y** was investigated, producing complex product mixtures, and the reaction of **6-Y** with **3** appeared to primarily form coordination polymers which could not be characterised. Additionally, attempts to synthesise Y$(Cp^t)_2$(N") (N" = hexamethyl disilazyl) for further reactivity were made, both by the reaction of **6-Y** with KN" and by the reaction of Y(N")$_3$ with 2 eq. HCp^t. However, Y$(Cp^t)_2$(N") was not successfully isolated by either route.

Finally, the reactions of Ln(Tp*)$_2$(OTf) (Ln = Y, Ce) with **5-Ln** were investigated. The UV-vis, ATR-IR and EPR spectroscopy of the products obtained was consistent with the radical pd ligand in a new coordination environment. However, the only isolable products of the reaction were the result of ligand redistribution reactions. Compounds such as Ln(Tp*)$_2$(hfac) and Ln(Tp*)(hfac)$_2$ were reproducibly crystallised from solutions of the product mixtures. It is proposed that the redistribution of hfac and Tp* ligands is facilitated both by the coordinating solvents in which the reaction was performed, and by the steric bulk of the Tp* ligand. This work provides a baseline from which a new synthesis of lanthanide heterobimetallics is proposed, taking account of and addressing the conditions which favoured redistribution.

5.2 Reaction of 3 and 5-Y with Ni^{2+}

In order to probe the reactivity of **3** $[CoCp_2]^+[pd]^{-\bullet}$ and **5-Y** $[CoCp_2]^+[Y(hfac)_3(N,N'\text{-pd})]^{-\bullet}$, a series of reactions were carried out. The first reaction investigated was the reaction of compounds of the radical anion of pd with nickel complexes. Ni^{2+} is well-known for forming square planar complexes,[1-3] and it was hypothesised that this geometry would allow antiferromagnetic coupling between two pd ligands, thereby stabilising the radicals as shown in Figure 5.1. A range of reactions were therefore carried out between both **3** and **5-Y** and Ni^{2+} compounds $NiCl_2$ and $[NEt_4]_2[NiCl_4]$.

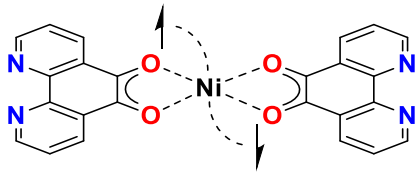

Figure 5.1: Showing the hypothesised stabilisation of pd radical compounds by antiferromagnetic coupling across Ni^{2+}.

All reactions to be discussed here were performed on a small scale in a glovebox. The reaction of $NiCl_2$ with **5-Y** as undertaken in MeCN resulted in no reaction, remaining a dark green solution over blue $NiCl_2$ solid after stirring for several hours. It was apparent that this was due to the highly insoluble nature of the $NiCl_2$ salt in organic solvents, and so the more soluble Ni(II) salt $[NEt_4]_2[NiCl_4]$ was used. A blue solution of $[NEt_4]_2[NiCl_4]$ in MeCN was added to one equivalent of **5-Y** in MeCN at -35°C. Upon stirring, a green precipitate was formed, which was isolated by frit filtration. NMR analysis of the green solid in d_6-DMSO (it was insoluble in both THF and MeCN) under ambient atmospheric conditions showed complex spectra, whose complexity precluded assignment. The resonances observed were consistent with the presence of multiple hfac, pd and $[NEt_4]^+$ environments, consistent with decomposition upon exposure to water and oxygen.

$[NEt_4]^+_2[NiCl_4]^{2-}$ was then dissolved in MeCN and added with stirring to **3**. A brown solid precipitated and was isolated from the pale yellow solution by frit filtration. **4-Y** $Y(hfac)_3(THF)_2$ was dissolved in MeCN and added to the brown solids with stirring. A green solution was obtained and was separated from grey and dark solids by frit filtration. MeCN was removed *in vacuo* and the resulting green solid was analysed by ^1H and ^{19}F NMR in d_3-MeCN. The spectrum showed a mixture of resonances consistent with hfac, $[NEt_4]^+$ and $CoCp_2$, but none

in the region expected for pd, indicating that the pd ligand remained in the insoluble fraction. Due to its bridging nature, insoluble coordination polymers, chains or clusters are not uncommonly observed for the pd ligand,[4-6] and it is likely that Ni-pd coordination polymer(s) formed during this reaction.

The reaction of **3** with $[NEt_4]^+_2[NiCl_4]^{2-}$ was also attempted in THF. Upon stirring the mixture, a red-brown solid precipitated as observed when the reaction was carried out in MeCN. The brown solid was isolated by frit filtration, and was washed with THF and hexane, leaving a purple solid. Some of the solid was removed from the glove-box and was dissolved in d_8-DMSO for analysis by NMR. Despite sonication and heating, very little solid dissolved, and the signal to noise ratio was therefore very low, being dominated by DMSO and H_2O. However, resonances attributable to the pd ligand and to $[CoCp_2]^+$ were present. In a complex containing antiferromagnetically coupled radicals it is expected that unlike for **3** and **5-Ln** the resonances of the pd ligand would be observed. However, it is more likely that decomposition had occurred due to moisture in the solvent.

4-Y was added to the purple solid obtained from the reaction of **3** with $[NEt_4]^+_2[NiCl_4]^{2-}$ in THF with stirring, and a red-brown suspension was obtained. Upon filtration, a maroon solid was obtained, which was washed with hexane. The reaction occurred significantly differently in THF compared to previous reactions in MeCN, attributed to decomposition due to adventitious H_2O in the MeCN solvent. Since decomposition was observed in samples in d_6-DMSO, and the solid was not soluble in the other available deuterated solvents d_3-MeCN or d_8-THF, NMR analysis was not possible. ATR-IR analysis can be informative of the oxidation state and coordination of pd, however, as discussed in previous chapters.[7, 8] The ATR-IR spectrum of the maroon product is shown in Figure 5.2. Absorptions assigned to carbonyl stretching frequencies were observed in the product at 1695, 1653, and 1375 cm^{-1}. The stretching frequency at 1653 cm^{-1} is consistent with that assigned to hfac groups in **1-Ln**, **2-Ln**, **4-Ln** and **5-Ln**.[9, 10] An absorption at 1695 cm^{-1} is consistent with a C=O bond in pd, as observed for pd^0 in **1-Ln** (1697-1699 cm^{-1}), whereas the absorption at 1375 cm^{-1} is a lower energy stretch than was observed for $pd^{-\bullet}$ in **3** and **5-Ln** (1402-1420 cm^{-1}), and similar to that observed for pd^{2-} in **3-Ln** Ln(hfac)$_3$(*N,N'-O,O'*-pd)V(Cp)$_2$ (1373-1381 cm^{-1}).

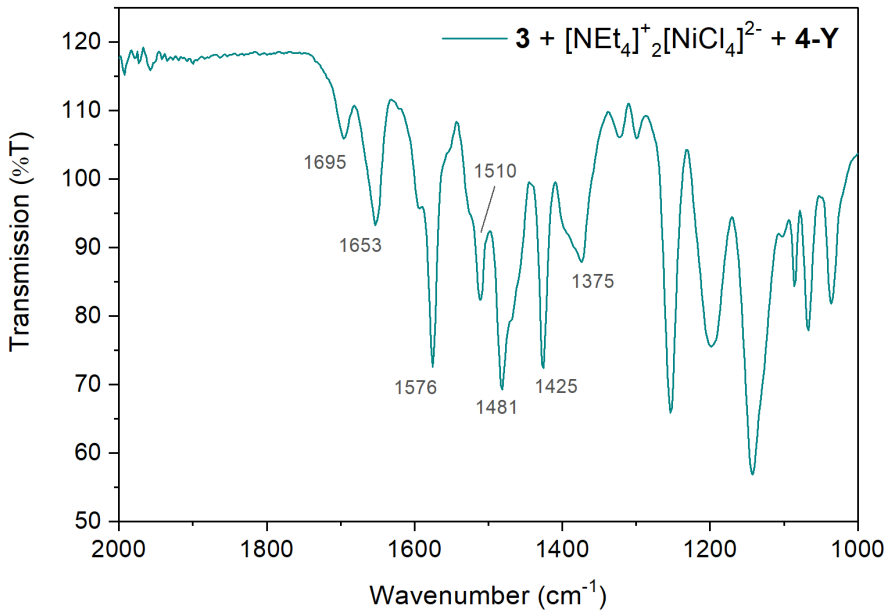

Figure 5.2: ATR-IR spectrum of the product of the reaction between 4-Y, 3 and $[NEt_4]^{+}{}_2[NiCl_4]^{2-}$.

It is therefore proposed that pd is bonded asymmetrically to nickel, undergoing a dissociation reaction from a pair of monoanionic radicals to give one pd ligand in the 2– oxidation state and one in the neutral oxidation state. The proposed structure of this product is Y(hfac)$_3$(*N,N'*-*O,O'*-pd)Ni(*N,N'*-pd), shown in Figure 5.3. However, due to the insoluble nature of the product in our dry glovebox solvents, no solution state characterisation data could be obtained, and nor was a solid-state molecular structure obtained. This bonding mode and oxidation state distribution could not therefore be confirmed by other spectroscopies. Similar chain-like structures have been reported for transition metal complexes of pd^{2-}.[6]

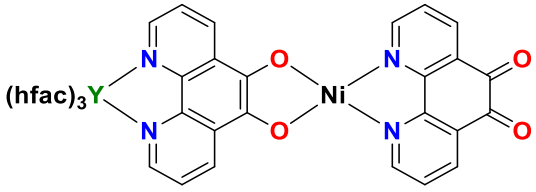

Figure 5.3: The structure of Y(hfac)$_3$(*N,N'*-*O,O'*-pd)Ni(*N,N'*-pd), the proposed product of the reaction between 3 and $[NEt_4]^{+2}[NiCl_4]^{2-}$in THF, followed by addition of 4-Y.

5.3 Synthesis of $Ln(Cp^t)_2(OTf)_2K$ 6-Ln

5.3.1 Literature precedent and starting material choice

A number of groups have explored lanthanide compounds of the Cp^t (Cp^t = tetramethyl cyclopentadienyl) ligand.[11-13] The group of Evans describe the synthesis of several useful lanthanide *bis*-Cp^t compounds, in particular $Y(Cp^t)_2(BPh_4)$, which might be used as a transmetallation reagent. Their synthesis of $Y(Cp^t)_2(BPh_4)$ *via* the alkyl compound $Y(Cp^t)_2(\eta^3\text{-}C_3H_5)$ is restrictive in a number of ways, however. Beginning from the expensive anhydrous lanthanide chloride starting materials (as discussed in chapter 2, high temperature and high vacuum are required to dry lanthanide chlorides), their synthesis also requires access to a glovebox free of coordinating solvents.

It was therefore decided to develop a new synthetic route to *bis*-Cp^t heteroleptics formulated $Ln(Cp^t)_2(OTf)$, using the triflate counter-anion as the leaving group. Relatively few examples of compounds with the general formula $[Ln(Cp^R)_2(OTf)_x]^{(x-1)-}$ (Cp^R = substituted cyclopentadienyl) have been synthesised. Those that are reported vary in coordination structure depending on a number of factors. Reaction of $Yb(OTf)_3$ with 2 eq. NaCp in toluene over 5 days afforded $Yb(Cp)_2(OTf)$, which forms a triflate-bridged dimer in the solid state.[14] This structure type was also observed for $Y(Cp^*)_2(OTf)$ (Cp^* = $C_5Me_5^-$), which was obtained from the reaction of either the hydride-bridged $[(Cp^*)_2Y(\mu\text{-}H)]_2$ or the tuck-over hydride complex $(Cp^*)_2Y(\mu\text{-}H)(\mu\text{-}\eta^1\text{:}\eta^5\text{-}CH_2C_5Me_4)Y(Cp^*)$ with Ag(OTf).[15] Using an extremely sterically encumbering cyclopentadienyl derivative has been found to prevent the formation of these dimeric units, allowing only a single triflate anion to bind to the metal as in $Ce(Cp^{ttt})_2(OTf)$ (Cp^{ttt} = $C_5H_2(^tBu)_3$), the byproduct of the cleavage of a thioester by a cerium hydride complex.[16]

The other structural type that has been observed is the bridged -ate salt, where the triflate anions bridge between the lanthanide and an alkali metal to form multimetallic structures in the solid state. The reaction of $Ln(OTf)_3$ with 2 eq. LiCp'' in THF solution afforded the ladder-like $(Ln(Cp'')_2(\mu\text{-}\kappa^2\text{-}OTf)(\mu_3\text{-}\kappa^3\text{-}OTf)Li(THF)_2)_2$ (Ln = La, Nd; Cp'' = $C_5H_3(SiMe_3)_2$).[17] These bridged dimers could be separated into monomeric complexes in the solid state in a number of ways. Chelating agents such as bipyridine were able to displace the triflate anions from the lanthanide coordination sphere. Alternatively, abstraction of Li using the crown ether 18-

crown-6 (18-c-6), or capping of the complex with TMEDA, produced the monomeric compounds $[Li(18\text{-}c\text{-}6)]^+[Ln(Cp'')_2(OTf)_2]^-$ and $Ln(Cp'')_2(\mu\text{-}OTf)_2Li(TMEDA)$ (TMEDA = tetramethyl ethylene diamine) respectively. A slightly different -ate bridged structure was recently observed upon reaction of $Ln(OTf)_3$ with 2 eq. $K(Cp^{tt})$ in THF solution, which afforded the bridged dimers $(Ln(Cp^{tt})_2(\mu\text{-}OTf)_2K)_2$ (Ln = La, Ce; $Cp^{tt} = C_5H_3(^tBu)_2$).[18] These compounds were then used to synthesise lanthanide alkyl complexes for further reactivity, by reaction with $LiCH_2C_6H_4\text{-}o\text{-}NMe_2$.

5.3.2 Synthesis of 6-Ln $Ln(Cp^t)_2(OTf)_2K$ (Ln = Y, Yb)

The steric properties of the Cp^t ligand are appropriate for reaction with a chelating agent, so the reaction of lanthanide triflate salts with 2 equivalents of $K(Cp^t)$ was performed as shown in Scheme 5.1, affording the triflate salts **6-Ln** $Ln(Cp^t)_2(\mu\text{-}OTf)_2K$ (Ln = Y, Yb).

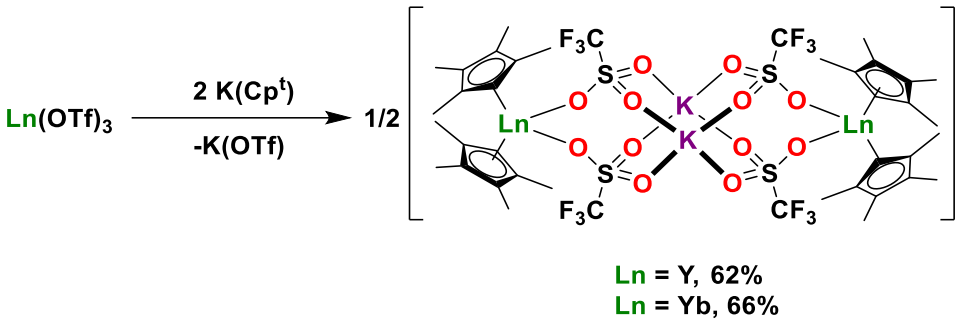

Scheme 5.1: The synthesis of the heteroleptic compounds 6-Ln $Ln(Cp^t)_2(\mu\text{-}OTf)_2K$.

It was found that attempting the synthesis in toluene or Et_2O resulted in a slow reaction with a highly complex NMR spectrum. Gu *et al.* reported that reaction of $Ce(OTf)_3$ with 2 eq. KCp^{tt} in toluene solution afforded *tris*-cyclopentadienyl products.[18] Since Y(III) and Yb(III) are significantly smaller than Ce(III), it would therefore be unlikely for a complex such as $Ln(\eta^5\text{-}Cp^t)_3$ to be formed by this reaction. However, a mixed coordination mode species such as $Ln(\eta^1\text{-}Cp^t)(\eta^5\text{-}Cp^t)_2$ is feasible. Such a complex is likely to have a complex NMR spectrum similar to that observed, due to magnetic inequivalence of the Cp^t-H environments.

Using a coordinating solvent such as THF is likely to improve the efficiency of the metathesis reaction by increasing the lability of the triflate leaving group. While apparently resulting in a more rapid and effective transformation, performing the reaction in THF initially caused challenges in separating the product from K(OTf). However, extraction of the products into a 1:1 mixture of THF and toluene resulted in the effective removal of 1 eq. K(OTf). In the

optimised preparation, a solution of $Ln(OTf)_3$ in THF was added to a solution of 2 eq. $K(Cp^t)$ in THF with stirring. The mixture was stirred for 1 h, then THF was removed *in vacuo*. The solids were washed with toluene, then extracted into a 1:1 mixture of THF:toluene with frit filtration. The solvents were removed *in vacuo* from the solution to obtain **6-Ln** in good yields (Ln = Y, white powder, 62% yield; Ln = Yb, red-brown powder, 66% yield). While solutions of **6-Y** are colourless, **6-Yb** is deep red in solution (See Section 5.3.3). Compounds **6-Ln** are highly sensitive, and form bright yellow decomposition products immediately upon exposure to air.

5.3.3 NMR Spectroscopy of 6-Ln

6-Ln were characterised by ^1H and ^{19}F NMR analysis. **6-Y** exhibits three singlets in the ^1H NMR spectrum recorded in d_8-THF, shown in Figure 5.4, at δ = 1.90, 1.98 and 5.78 ppm, integrating in a 12:12:2 ratio. The resonances at δ = 1.90 and 1.98 ppm have chemical shifts and integration consistent with the methyl groups of Cp^t ligand. That at δ = 5.78 ppm is assigned to the Cp^t aromatic proton by relative integration, and as the chemical shift is consistent with a proton in an aromatic system. Additionally, a single resonance was observed in the ^{19}F NMR spectrum (Figure 5.5) at δ = -78.24 ppm, consistent with the CF_3 group of a bound triflate.

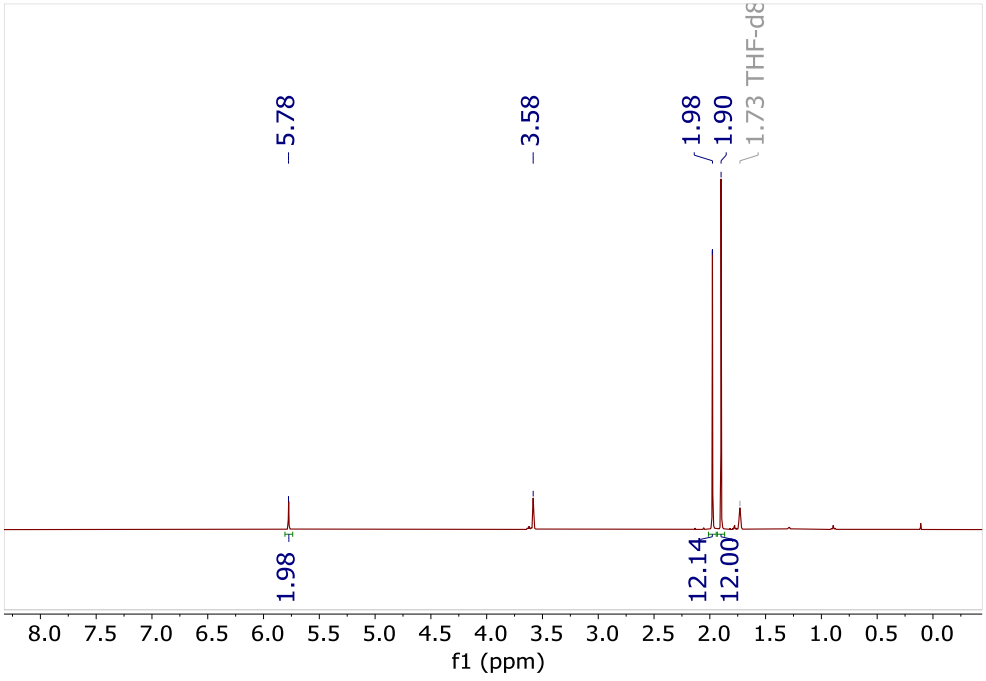

Figure 5.4: ^1H NMR spectrum of 6-Y, recorded in d_8-THF.

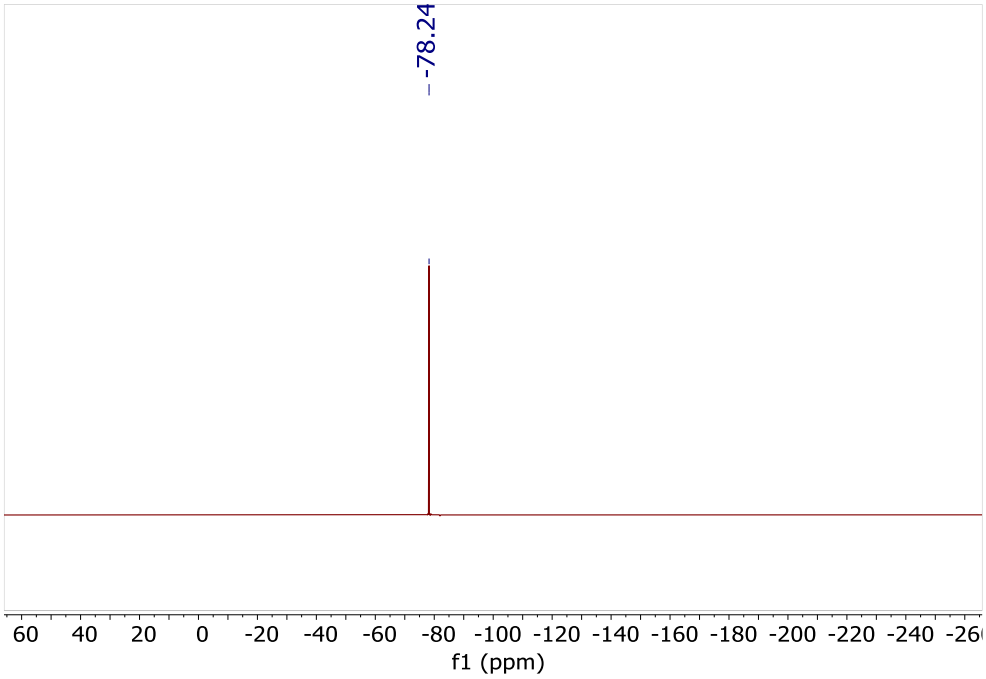

Figure 5.5: $^{19}F\{^{1}H\}$ NMR spectrum of 6-Y, recorded in d_8-THF.

6-Yb likewise exhibited three singlet resonances in the ^{1}H NMR spectrum as recorded in d_8-THF, shown in Figure 5.6, at δ = -72.52, -10.15 and 39.92 ppm, integrating in a 2:12:12 ratio. The resonances at -10.15 and 39.92 ppm integrate to 12 protons each and are therefore assigned by relative integration to the methyl groups on the Cp^t ligands, paramagnetically shifted by proximity to Yb. The resonance at -72.52 ppm integrates to 1.5 protons relative to the methyl resonances, and is therefore assigned by relative integration to the aromatic proton of the Cp^t ligand, with a low integration due to paramagnetic relaxation caused by proximity to the lanthanide. In the ^{19}F NMR spectrum, shown in Figure 5.7, two resonances are observed, one significantly greater than the other. The major resonance at δ = -40.00 ppm is assigned to the CF_3 group of the triflate anion, paramagnetically shifted by proximity to Yb(III). The minor resonance at δ = -79.44 is in the region expected for the CF_3 group of an unbound triflate anion. As triflate is known to be a weakly coordinating anion, the resonance at δ = -79.44 ppm is therefore assigned to a low concentration of free triflate in solution due to partial displacement from the coordination sphere of Yb by the coordinating solvent.

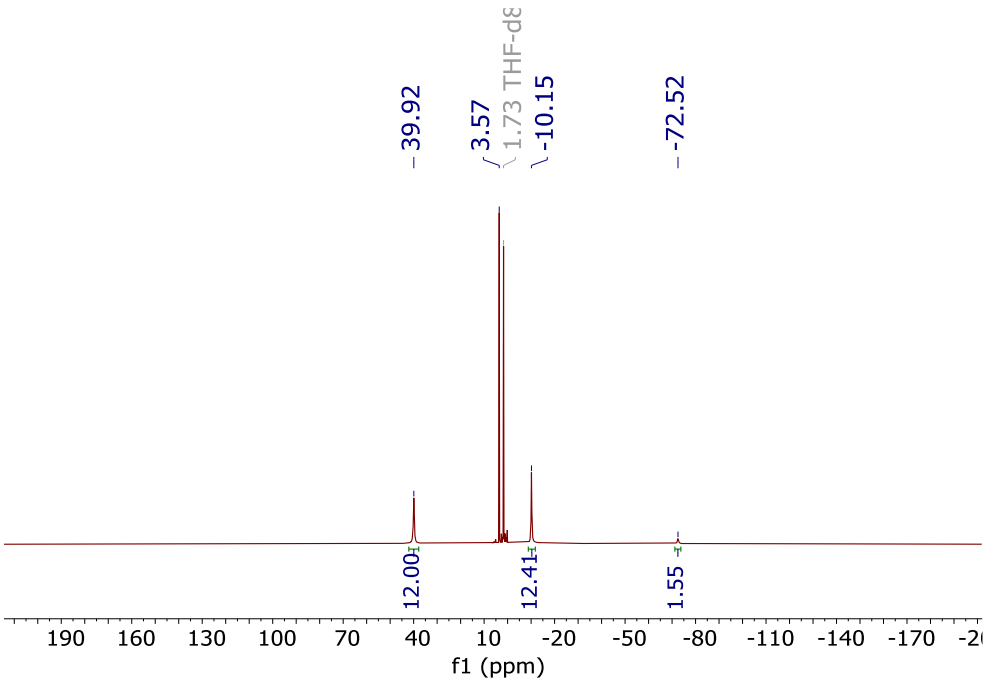

Figure 5.6: ^{1}H NMR spectrum of 6-Yb, recorded in d_8-THF.

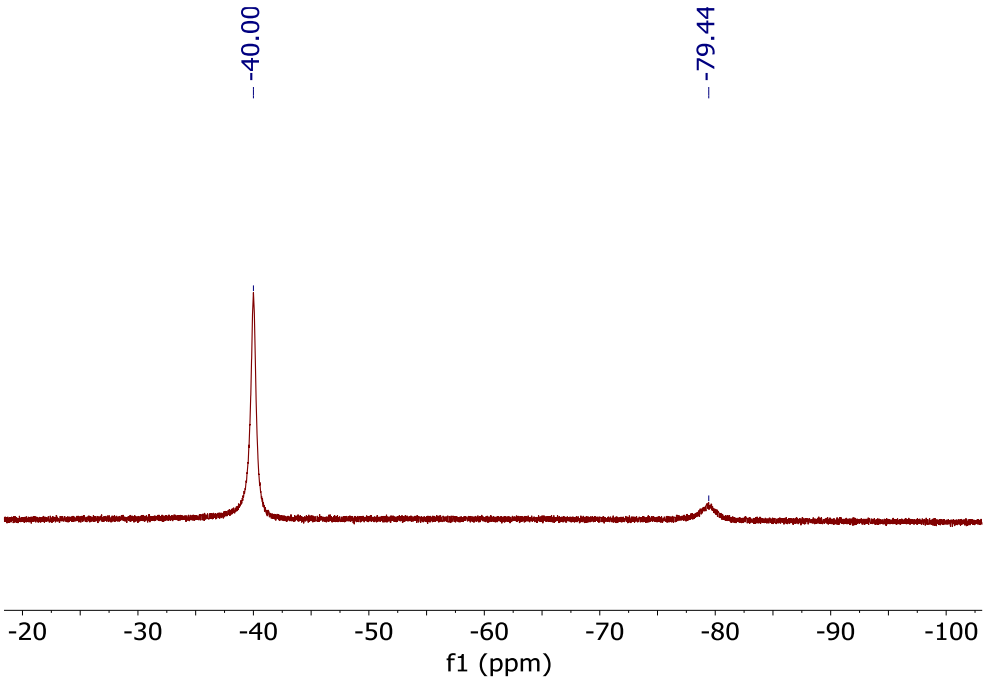

Figure 5.7: ^{19}F{^{1}H} NMR spectrum of 6-Yb, recorded in d_8-THF.

5.3.4 ATR-IR spectroscopy of 6-Ln

The ATR-IR spectra of **6-Ln** were recorded, shown in Figure 5.8. The solids were kept under an inert atmosphere for as long as possible prior to recording the spectra, though the spectra

were recorded under air and therefore some decomposition was unavoidable. It is therefore likely that decomposition by reaction with atmospheric water is responsible for broad absorptions observed in the spectra above 1500 cm^{-1}, preventing analysis of this region of the spectrum. Otherwise, the spectrum is dominated by a group of intensely absorbing frequencies between 1029 and 1324 cm^{-1}, which are almost identical to those observed in the similar compounds $Ln(Cp^{tt})_2(OTf)_2K$ (Ln = La, Ce) (ν = 1030, 1180, 1220, 1240, 1365 cm^{-1}).[18] By comparison to the ATR-IR spectra of $Ln(OTf)_3$ (ν = 1020-1030, 1200-1280 cm^{-1}), an absorption at 1029 cm^{-1}, and absorptions at 1180-1240 cm^{-1} are assigned to the triflate ligands. The absorption at 1324 cm^{-1} is therefore assigned to the C-C stretching frequency of the Cp^t ligands.

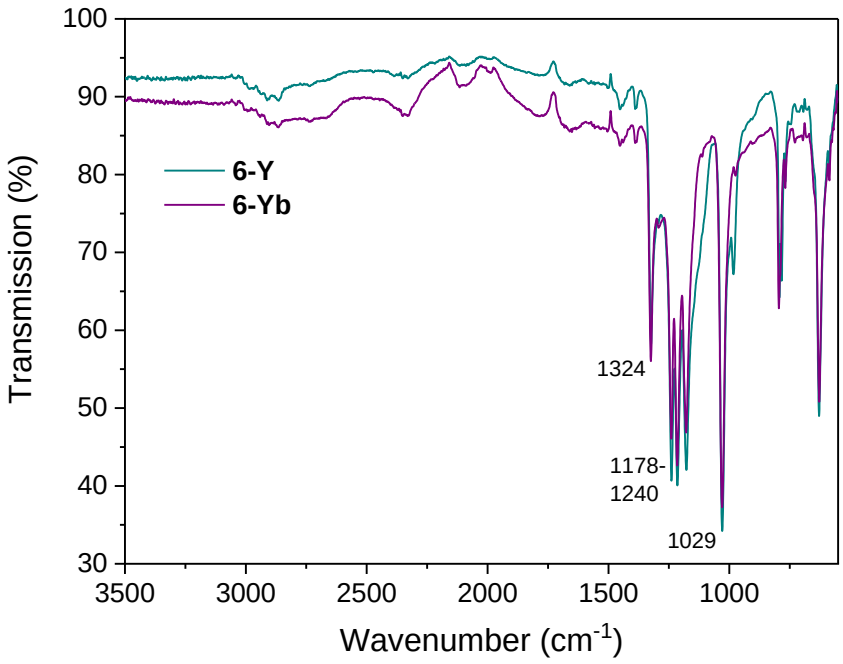

Figure 5.8: ATR-IR spectra of 6-Ln (Ln = Y, Yb).

5.3.5 UV-vis-NIR Spectroscopy of 6-Ln

The colour difference between **6-Ln** (Ln = Y, Yb) is striking, so in order to investigate this phenomenon, their electronic spectra were recorded. With the goal of observing the high-energy UV region absorptions of the ligands, the absorbance spectra of **6-Ln** were recorded in MeCN solution, on dilute samples of 22.7 (**6-Y**) and 24.7 (**6-Yb**) μM. However, the maximum of the absorbance in the ultraviolet region was too close to the instrument detection limit to determine the UV transitions. Small quantities of the stabiliser BHT (butylated

hydroxytoluene) in the THF solvent precluded an attempt to determine the absorptions in the UV region in that solvent.

No absorptions were observed in the visible-NIR region of the electronic spectrum of **6-Y**. However, the vis-NIR absorption spectra of **6-Yb** were spectroscopically rich. The absorption spectra of **6-Yb** recorded at different concentrations in MeCN and in THF are shown in Figure 5.9. It is evident that the more dilute sample as recorded in MeCN has undergone significant decomposition, most likely due to reaction with adventitious moisture in the solvent. However, in the more concentrated MeCN solution a broad maximum is observed in the visible region with λ_{max} = 504 nm, and a molar extinction coefficient of 164 M^{-1} cm^{-1}, consistent with a charge transfer transition.[19] Additionally, a series of transitions are observed in the NIR region between 876 and 987 nm with extinction coefficients of between 3.6 and 52 M^{-1} cm^{-1}, which appear to extend to lower energy, though they are cut off due to the instrument limit. The absorbance spectrum of **6-Yb** as recorded in THF exhibits a single absorption band in the visible region with a maximum at 457 nm and an extinction coefficient of 221 M^{-1} cm^{-1}, consistent with a charge transfer transition. Similarly to those observed in the absorption spectrum recorded in MeCN, a series of transitions are observed between 841-987 nm, with extinction coefficients of between 1.8-33 M^{-1}. The individual transitions in the NIR region occur at different energies in the two solvents.

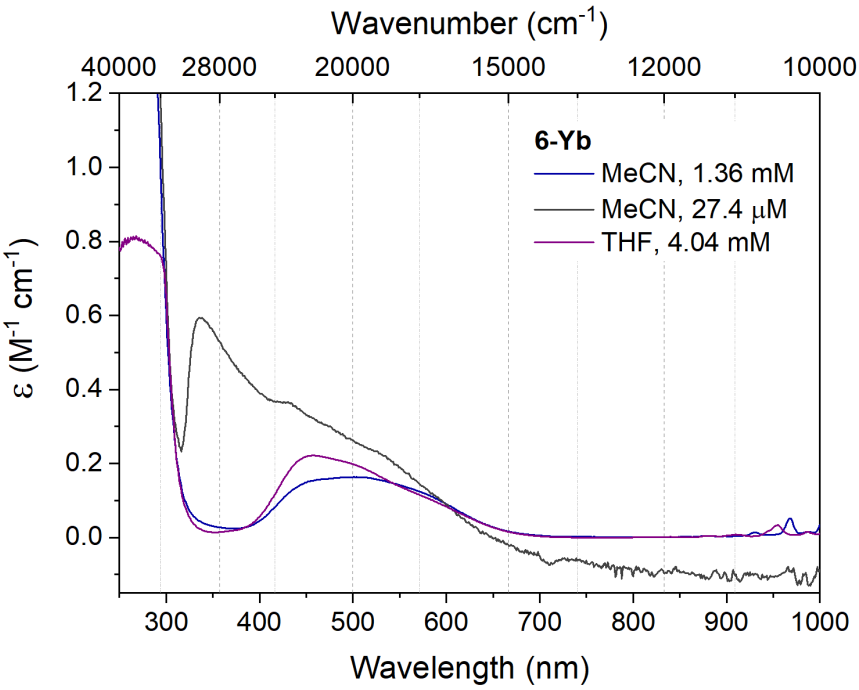

Figure 5.9: Electronic Absorption spectra of 6-Yb, recorded in either MeCN or THF on solutions of varied concentrations at R.T.

Where absorption spectra are reported for ytterbium cyclopentadienyls such as $YbCp_3$, transitions with a similar magnitude to those observed for **6-Yb** are generally seen in the visible spectrum.[20, 21] For example, $YbCp_3$ has a strong green colour due to an absorption with λ_{max} = 660 nm, assigned to the Yb(II)/$Cp^{\bullet}$←Yb(III)/Cp^{-} ligand to metal charge transfer (LMCT) transition. $YbCp_3$ has also previously been studied by DFT in combination with EPR, finding that there was significant spin delocalisation from Yb to the ligand.[22] The transition observed in **6-Yb** with λ_{max} = 457 (THF solution) and 504 nm (MeCN solution) is therefore assigned to the Yb(II)/$Cp^{t\bullet}$←Yb(III)/Cp^{t-} LMCT transition.

The Yb *f-f* transitions in the NIR region (>840 nm) observed in **6-Yb** are of an unusually high intensity for compounds of Yb(III), up to 52 M^{-1} cm^{-1}. An intense set of *f-f* transitions have been observed in $YbCp_3$ however,[20, 21] and in certain other *bis*-cyclopentadienyl compounds. In particular, an electronic structure analysis of $[Ln(Cp^{ttt})_2]^+[B(C_6F_5)_4]^-$ (Ln = Gd, Ho, Er, Tm, Yb, Lu) highlights this unique electronic characteristic of Yb, with similar spectral characteristics observed in the electronic spectrum that were not present for other Ln.[23] Of some note is the observation that these absorptions change significantly in **6-Yb** depending on the solvent in which the compound is dissolved. This indicates that the coordination sphere is significantly different in either THF or in MeCN solutions, and that this has an effect on the electronic

structure of Yb. This property is not limited to **6-Yb**, as spectrometric titrations of $YbCp_3$ with bases also showed major changes in the *f-f* absorptions, presumably due to the covalent bonding of Cp to Yb.[20, 21]

5.3.6 Photoluminescence spectroscopy of 6-Yb

A number of studies have probed the CT sensitisation of Yb photoluminescence in a variety of different systems, from redox-active proteins to *d-f* multimetallics.[24-27] The emission spectra of $YbCp_3$ and various of its adducts upon excitation by the LMCT absorption band has also been investigated.[21] Excitation of a THF solution of **6-Yb** *via* the absorption assigned to LMCT resulted in weak near-infrared emission from Yb. The excitation spectrum of the complex, recorded using λ_{Em} = 985 nm, has a maximum at 415 nm, which is a part of the band in the electronic absorption spectrum assigned to the $Cp^{t\bullet}$/Yb(II)←Cp^{t-}/Yb(III) transition. The emission spectrum observed is atypical for an Yb compound, with at least five transitions apparent at 953, 985, 995, 1030 and 1070 nm. The most striking difference is the presence of two sharp, intense transitions with maxima at 985 and 995 nm, where a typical Yb emission spectrum exhibits a single sharp transition at 975 nm. Emission from "hot" bands (higher energy excited states) of Yb has been previously reported,[28] where up to nine individual transitions were observed in the emission spectrum of an Yb complex with a macrocyclic ligand. In the case of **6-Yb** however, these extra emission lines are due to the unusual electronic structure of ytterbium cyclopentadienyl compounds, as evidenced by the electronic absorption spectroscopy (see Section 5.3.5). There is a recent interest in determining the excited state electronic structure of Yb(III) compounds using electronic absorption and emission spectroscopy.[29] However, for a full analysis of the electronic structure of **6-Yb**, the absorption spectrum would need to be determined to lower energy than was possible on the instrumentation used. Additionally, recording the emission spectrum at low temperature on a solid sample might allow determination of the vibrational states.

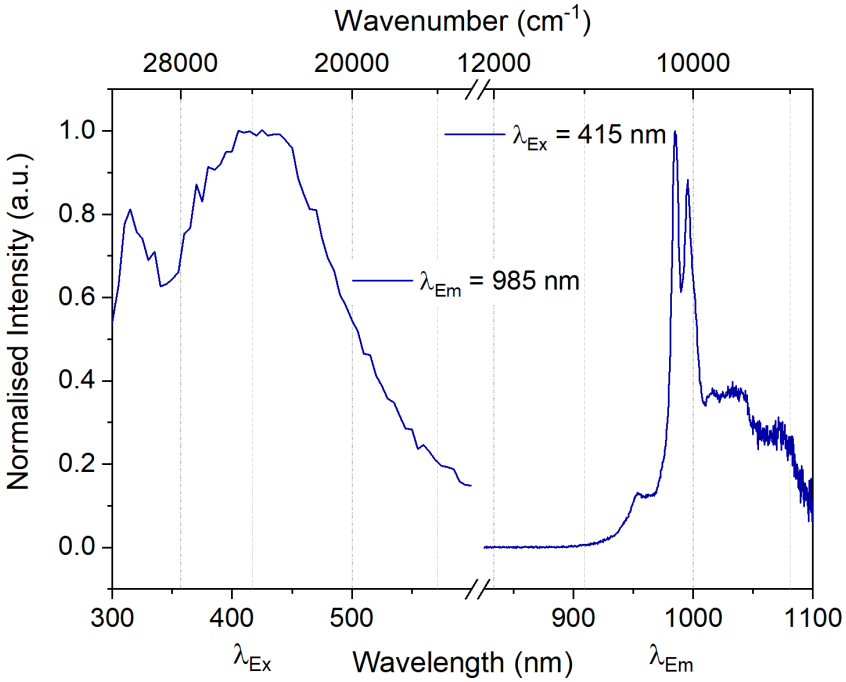

Figure 5.10: Excitation and Emission spectra of 6-Yb, recorded in THF solution at R.T.

As reported for other ligands, sensitisation by charge transfer to Ln(III) is unique to Yb among the lanthanides. This is due to the nature of the excited state electronic structure of the metals. As depicted in Figure 5.11, the $L^{+\bullet}$/Yb(II) state is typically higher in energy than the L/Yb(III)* state, and thus relaxation to the Yb(III) $^2F_{5/2}$ emissive excited state is possible.[24] For Eu, the opposite is true, as the $L^{+\bullet}$/Eu(II) state is most often lower in energy than the L/Eu(III)* $^5D_0$ emissive excited state. In Eu complexes, therefore, LMCT transitions do not result in emission, and can be significant quenching processes. However, this sensitisation (and/or quenching) process, initially described for the Ln(Trp) (Trp = tryptophan) system, does not apply well to $Ln(Cp^R)_x$. In this mechanism, a ligand excited state is accessed, which then undergoes an LMCT transition. However, it appears that the excitation maximum of the $Yb(Cp^R)_x$ compounds corresponds to a transition not present in analogous $Y(Cp^R)_x$ compounds. If this is the case from the ground state of **6-Yb** and $YbCp_3$, absorption of a photon directly induces electron transfer to Yb as shown on the right in Figure 5.11. To the best of our knowledge, this mechanism of sensitisation is unique to $Yb(Cp^R)_x$ compounds.

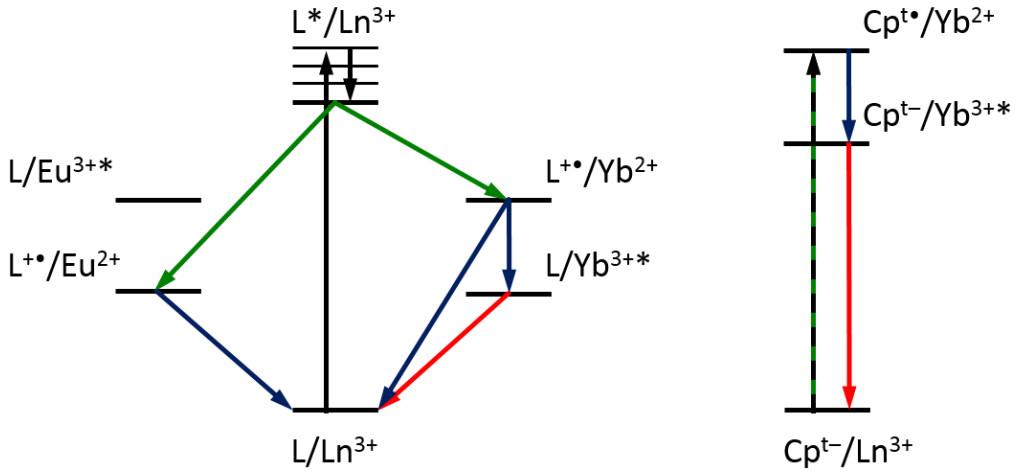

Figure 5.11: Charge transfer processes in sensitisation and quenching of lanthanide luminescence in compounds of Eu and Yb. Diagram on the left adapted from Horrocks et al. 1997.[24] Black arrows depict absorption of a photon, green arrows depict electron transfer, blue depict back electron transfer, and red arrows depict emission of a photon.

5.3.7 Crystallography of 6-Ln

Single crystals of **6-Ln** (Ln = Y, Yb) suitable for X-ray diffraction were obtained by diffusion of a hexane layer into concentrated THF solutions at -35°C overnight. The crystals were large blocks which nevertheless underwent rapid desolvation, visibly losing crystallinity within 10 seconds of removal from the solvent. However despite this, solid-state molecular structures for both solvent-free and solvated structures of **6-Y** were obtained. These show that in the solid state **6-Y** forms a dimeric bridged structure, as shown in Figure 5.12. The Y-Cp^t bond distances in the solvated structure are between 2.571(3)-2.671(3) Å, and those in the desolvated structure are very similar at 2.556(6)-2.702(5) Å, consistent with the Y-Cp^R bonds in $(Y(Cp^*)_2(\mu\text{-OTf}))_2$, of 2.619(3)-2.697(2) Å.[15] However, the Y-O bond distances of 2.287(2) Å and 2.279(4)-2.287(4) Å are significantly shorter than those in the other yttrium *bis*-cyclopentadienyl triflate compound, of 2.339(2)-2.371(2). This is due to the asymmetry and ionic nature of the triflate bridging mode. Rather than bridging two Y centres, the triflate bridges Y and K. This likely results in an increase in electron density on the O atom closest to Y(III) and therefore a shorter Y-O bond. This exact bridging -ate salt structure has been observed in a single previous compound $(Ce(Cp^{tt})_2(\mu\text{-OTf})_2K)_2$, where the Ce atoms were separated by 11.5616(7) Å.[18] This is similar to the separation between Y atoms in these dimeric units of 11.0357(5) and 11.125(1) Å, despite the difference in atomic radii between Ce and Y. It seems likely that this is due to the greater steric encumbrance of the Cp^{tt} ligand

resulting in similar Ln-K-Ln angles despite the increased ionic radius of Ce(III).[30] In the unsolvated structure, a close interaction is observed between K and the Cp ring of the neighbouring dimer, with K-C distances of between 2.988(5)-3.232(5) Å. This interaction is not observed in the solvated structure, where two THF molecules coordinate to K. The significant variation in K-C distances is due to the Cp^t ligand sitting at an angle relative to K.

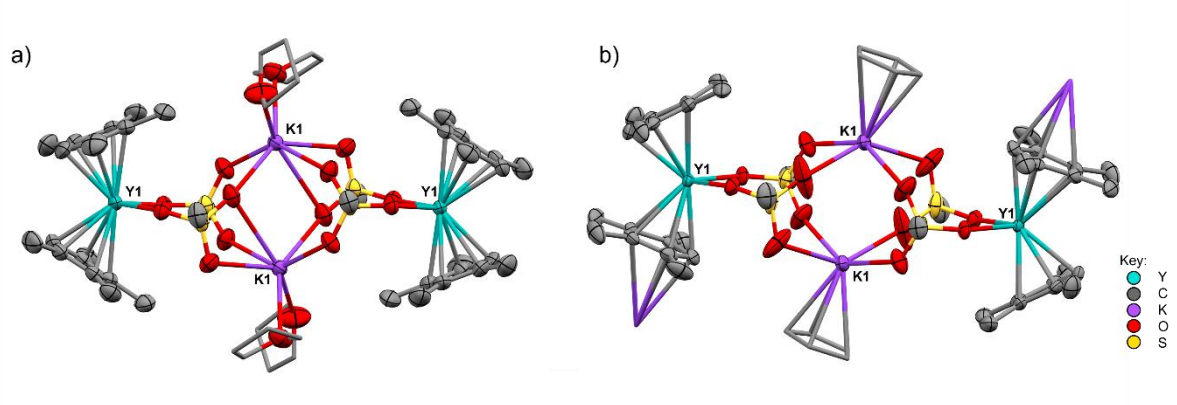

Figure 5.12: The dimeric solid-state molecular structures of 6-Y. a) dimeric $(Y(Cp^t)_2(\mu\text{-}OTf)_2K)_2$ and b) desolvated $\{(Y(Cp^t)_2(\mu\text{-}OTf)_2K(THF)_2)_2\}$(Hex). H and F atoms and the hexane molecule in b) have been omitted for clarity. Close intermolecular interactions and THF molecules (except donor O atoms) are depicted in wireframe. Selected distances (Å): a): Y-C, 2.571(3)-2.671(3); Y-O, 2.287(2); Y-Y, 11.0357(5); K-C, 2.988(5)-3.232(5). b): Y-C, 2.556(6)-2.702(5); Y-O, 2.279(4)-2.287(4); Y-Y, 11.125(1).

For **6-Yb**, the solid-state molecular structure was obtained only for the THF solvate. The structure exhibits a bridging -ate salt structure, as for **6-Y**. The Yb-C distances are not statistically different to those in the Y analogue at 2.543(4)-2.633(3) Å, and are consistent with those in the bridged Yb triflate dimer $(Yb(Cp)_2(\mu\text{-}OTf))_2$ of 2.52(1)-2.59(2) Å.[14] As with the Y analogue, the Yb-O distances of 2.52(2)-2.58(2) are slightly longer than those in $(Yb(Cp)_2(\mu\text{-}OTf))_2$ of 2.24(1) Å. The Yb-Yb separation is 11.0173(3) Å, and unsurprisingly based on the ionic radii,[30] this represents the shortest Ln-Ln distance of the bridged -ate salts, with Y slightly longer, and Ce the longest.

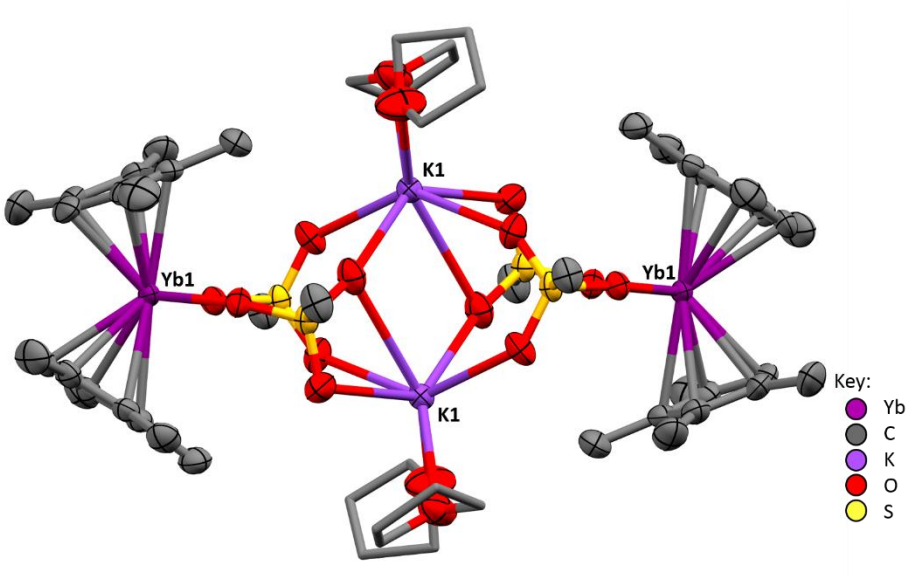

Figure 5.13: The dimeric solid state molecular structure of 6-Yb. Ellipsoids are drawn at 50% probability. H and F atoms have been omitted for clarity, and C atoms of THF molecules are drawn in wireframe for clarity. Selected distances: Yb-C, 2.543(4)-2.633(3); Yb-O, 2.252(2)-2.258(2); Yb-Yb, 11.0172(4).

5.3.8 Conclusions

The synthesis of the lanthanide cyclopentadienyl compounds **6-Ln** (Ln = Y, Yb) was successfully carried out, their full spectroscopic characterisation was undertaken, and they were structurally characterised. **6-Ln** represent a promising metathesis reagent for the synthesis of lanthanide multimetallic compounds. However, they are also of interest in their own right. **6-Yb** displays intriguing *f-f* absorption and emission transitions with unusual energies for Yb(III). The emission arises, at least in part, from a charge transfer process which appears to be unique to ytterbium cyclopentadienyl complexes. However, the data collected was not complete at lower energies, nor was it of a high enough resolution such that a full excited state diagram could be constructed.

5.4 Attempted Synthesis of $Y(Cp^t)_2(N'')$

The dinitrogen bridged dimer $(Y(Cp^t)_2(THF))_2(\eta\text{-}\mu^2\text{:}\mu^2\text{-}N_2)$ ($Y^{Cpt}{}_2N_2$) may be thought of as a Y(II) equivalent, as it readily reacts to reduce substrates by 1 electron, irreversibly releasing ½ eq. N_2 gas in the process.[11] Since equivalent compounds are available for a range of lanthanides, it was targeted as a possible source of Ln for reaction with pd in the synthesis of heterobimetallics. A route to $Y^{Cpt}{}_2N_2$ was therefore sought, beginning from **6-Y** as a starting material. The published procedure uses $Y(Cp^t)_2(BPh_4)$ for the synthesis, but a simple ligand exchange reaction to swap $(OTf)^-$ for $(BPh_4)^-$ by reaction of **6-Y** with $Na(BPh_4)$ was unsuccessful. A route was therefore envisaged *via* the reaction of $Y(Cp^t)_2(N'')$ with $[HNEt_3][BPh_4]$, eliminating HN" and NEt_3 to produce the target compound $Y(Cp^t)_2(BPh_4)$. Additionally, $Y(Cp^t)_2(N'')$ could be used for other protonolysis reactions to introduce other ligands to the complex, and $Y(Cp^t)_2(BPh_4)$ might be used as an alternative transmetallation reagent, making a new route to these compounds synthetically useful.

The compound $Y(Cp^t)_2(N'')$ has previously been synthesised by two routes. The first route was the reaction of the dinitrogen bridged dimer $Y^{Cpt}{}_2N_2$ with $(SiMe_3)N_3$, the second was by the reaction of $Y(Cp^t)_2(BPh_4)$ with KN".[12] As the aim was to use $Y(Cp^t)_2(N'')$ for the synthesis of $Y(Cp^t)_2(BPh_4)$, a key step in the synthesis of $Y^{Cpt}{}_2N_2$, a different route was required. Two synthetic routes were attempted, a salt metathesis route and a protonolysis route, as detailed in Scheme 5.2. A similar compound, with a different silyl amide ligand, $Y(Cp^t)_2(N(SiHMe_2)_2)$ has previously been synthesised by a similar protonolysis route.[13]

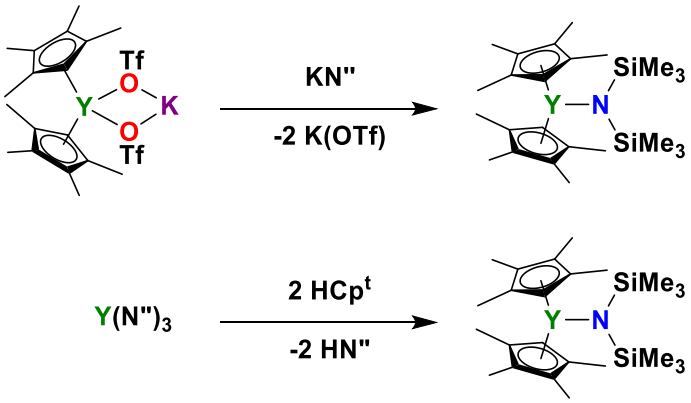

Scheme 5.2: The two synthetic routes explored for the synthesis of $Y(Cp^t)_2(N'')$ from 6-Y

5.4.1 Reaction of 6-Y with KN″

In d_6-benzene, **6-Y** and 1 eq. KN″ were stirred for 5 m, then the mixture was filtered and the colourless solution analysed by ^{1}H and ^{19}F NMR spectroscopy. The ^{1}H NMR spectrum, shown in Figure 5.14, shows a mixture of species. Resonances at δ = 0.10 and 0.14 ppm are assigned to HN″ and KN″ respectively, while that at δ = 0.30 ppm is due to a small amount of grease. By comparison to the ^{1}H NMR spectrum of HCp^{t} starting material in the same solvent, the peaks at δ = 1.93 and 1.96 ppm are assigned to HCp^{t}, which along with HN″ are decomposition products from the reaction of KN″ and **6-Y** with adventitious H_2O. The H_2O was presumably introduced to the reaction either by one of the starting materials or a leak in the Young's tap NMR tube. Also observed are further resonances at δ = 2.06, 2.07 and 5.94 ppm, which have integrals consistent with Cp^{t}. The ^{19}F NMR spectrum exhibits a single resonance at δ = -77.23 ppm, consistent with a triflate group. As potential triflate-containing side-products such as K(OTf), and the starting material **6-Y** are insoluble in benzene, the resonances at δ = 2.06, 2.07 and 5.94 ppm, and the resonance in the ^{19}F NMR spectrum are assigned to Y(Cp^{t})$_2$(OTf) produced after dissociation of K(OTf) from the starting material. Therefore no reaction was observed between **6-Y** and KN″ under these conditions.

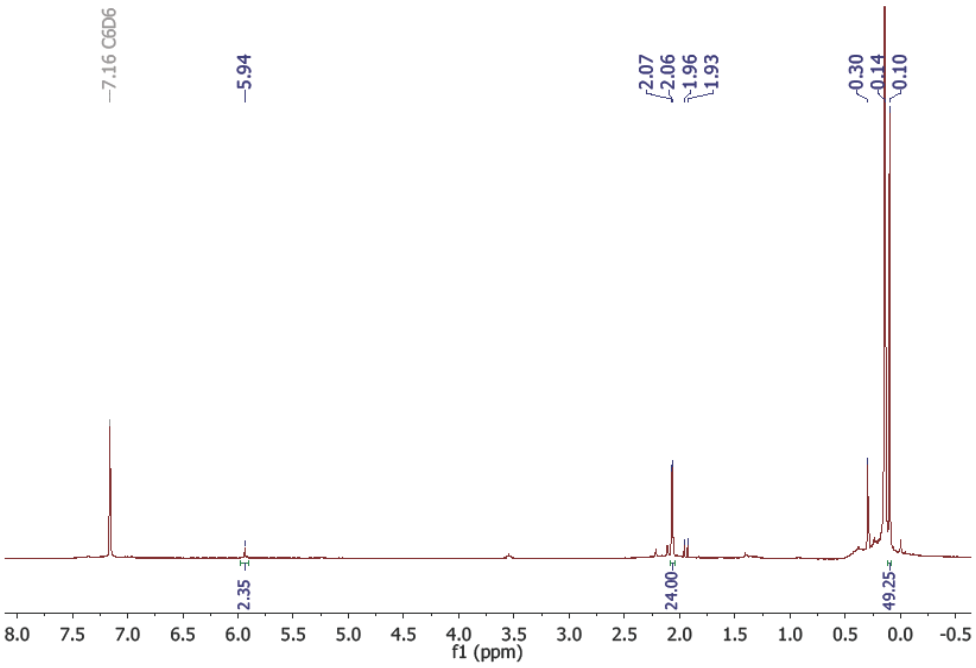

Figure 5.14: The ^{1}H NMR spectrum of the d_6-benzene soluble species from the reaction of 6-Y with KN″.

The reaction was carried out on a slightly larger scale in Et_2O. It was thought that using Et_2O as the solvent would allow dissolution of reagents, while precipitating the K(OTf) byproduct. KN" in Et_2O was added to **6-Y** suspended in Et_2O with stirring. The mixture was stirred vigorously for 15 m, then filtered and Et_2O was removed from the pale yellow suspension *in vacuo*, leaving a beige solid. A small sample was dissolved in C_6D_6 and analysed by ^1H and ^{19}F NMR spectroscopy. The NMR shows that more KN" was consumed, but otherwise shows the same Cp^t-containing product as was obtained by the reaction in d_6-benzene, assigned to $Y(Cp^t)_2(OTf)$. Both HN" and HCp^t are also present, and in greater quantity, indicating that the reagents underwent a reaction with adventitious water in the solvent.

The reaction was performed again in the more polar solvent d_8-THF. To a solution of **6-Y** in d_8-THF was added 1 eq. KN" and the solution was mixed, then the ^1H and ^{19}F NMR spectra were recorded over a 6.5 h period. The ^1H NMR spectra are shown in Figure 5.15. There are some resonances in the spectrum whose chemical shifts appear to change slightly over the course of the reaction. For these resonances the chemical shift is given as a range, from the initial to the final resonance. The spectrum contains two major components which have resonances consistent with the Cp^t ligand. The first of these consists of three singlet resonances at δ = 1.91, 1.99, 5.74 ppm integrating in a 12:12:2 ratio, consistent with **6-Y**. These resonances decrease compared to the other resonances in the spectrum over the course of the experiment (Figure 5.16). The second component (which increases over time) exhibits resonances at δ = 1.95-1.94, 2.01-2.00 and 5.05 ppm, integrating in a 12:12:2 ratio consistent with $[Y(Cp^t)_2]^+$. Another resonance at δ = -0.03-+0.04 ppm is consistent with N" bound to Y(III). However, the relative integrations of these components are not consistent with $Y(Cp^t)_2(N")$ (18:12:12:2), together having an integral ratio of around 25:6:6:1, between the targeted product and $Y(Cp^t)(N")_2$ (36:6:6:1). A number of minor resonances are observed indicating at least one Cp^t-containing side-product is also present. The ^{19}F NMR spectrum (Experimental section, Figure 5.26) did not change over the reaction, displaying a single resonance at δ = -78.83 ppm consistent with a triflate anion displaced from the inner coordination sphere of Y. These NMR data indicate that while a reaction has occurred between **6-Y** and KN", it is very slow and does not cleanly produce the desired product $Y(Cp^t)_2(N")$. Compared to the Cp^t resonances in the product, the N" resonances integrate to more than would be expected in the targeted product $Y(Cp^t)_2(N")$, closer to a product formulated as $Y(Cp^t)(N")_2$.

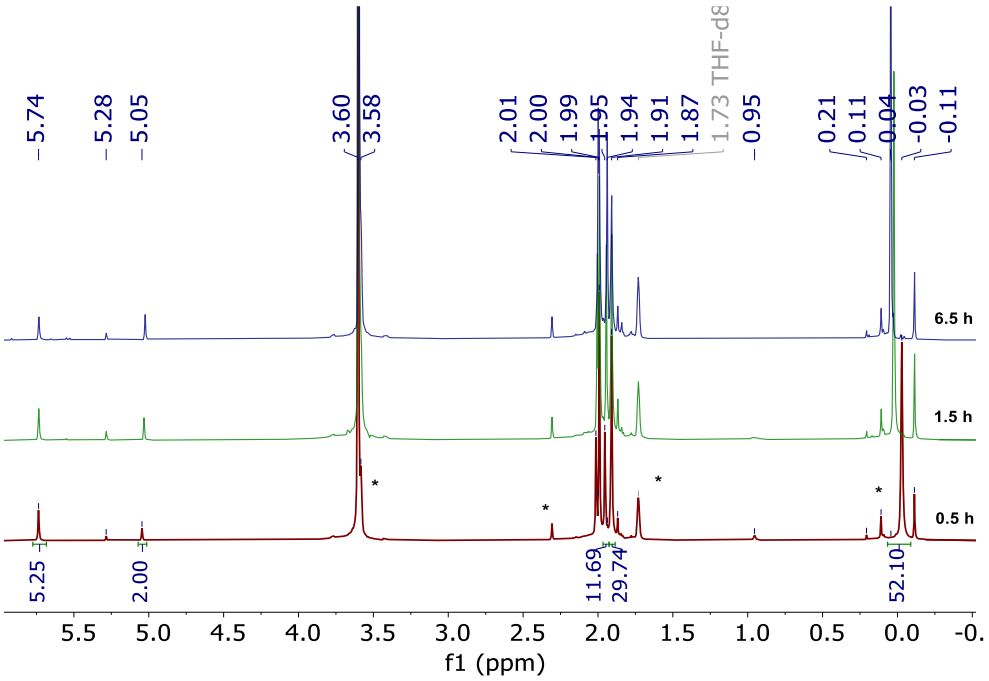

Figure 5.15: The ^{1}H NMR spectrum of the reaction between 6-Y and KN", recorded at intervals over 6.5 h. Resonances assigned to adventitious THF and toluene solvent and silicone grease are denoted by *.

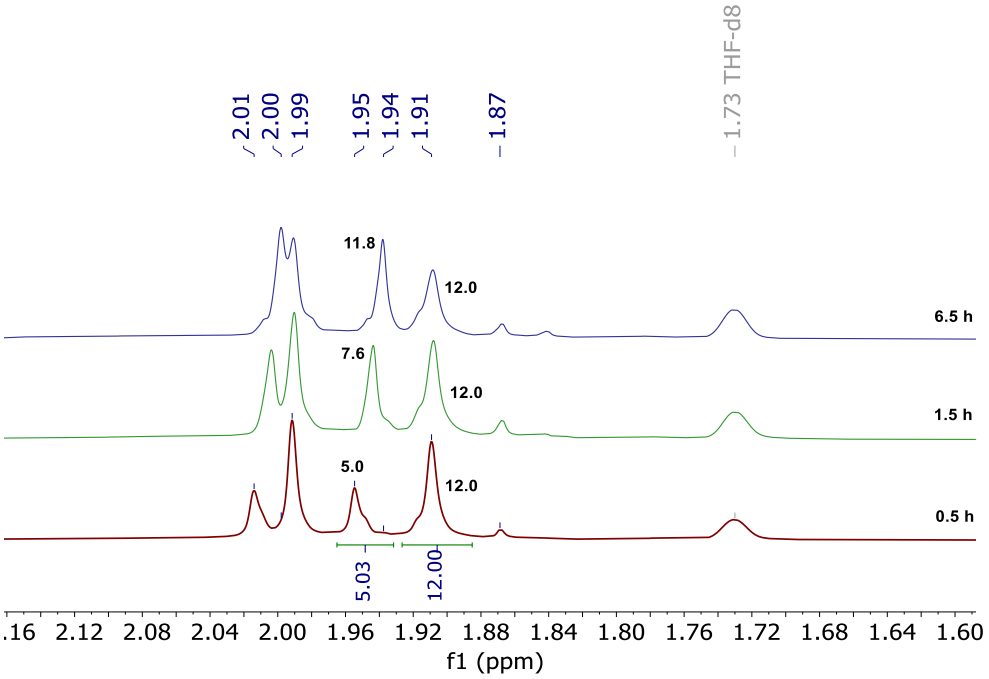

Figure 5.16: An expansion of the part of the ^{1}H NMR spectrum of the reaction between 6-Y and KN" which is assigned to the methyl groups of the Cp^{t} ligands, recorded at intervals over 6.5 h. The numbers next to the resonances at δ = 1.91 and 1.94-1.95 ppm represent the relative integrations of those two resonances. The resonances at δ = 1.99 and 2.00-2.01 ppm are not resolved enough to allow accurate integration.

5.4.2 Reaction of $Y(N'')_3$ with 2 eq. HCp^t

In an alternative preparation, $Y(N'')_3$ was added to a solution of 2 eq. HCp^t in d_6-benzene, and the solution was heated to 60 °C. The ^1H NMR spectrum of the solution was recorded periodically, up to 24 h total heating, shown in Figure 5.17. No reaction was observed, even after 24 h, in contrast to the report of the synthesis of $Y(Cp^t)_2(N(CHMe_2)_2)$.[13] As the related ligand HCp has a relatively acidic pKa value of 16, and HN" is significantly more basic at a pKa of 26, it is reasonable to expect that the thermodynamic force should be sufficient to drive the reaction. That no reaction was observed is therefore likely due to the increased steric bulk of the N" ligand over $(N(CHMe_2)_2)^-$ preventing access to Y and protonolysis.

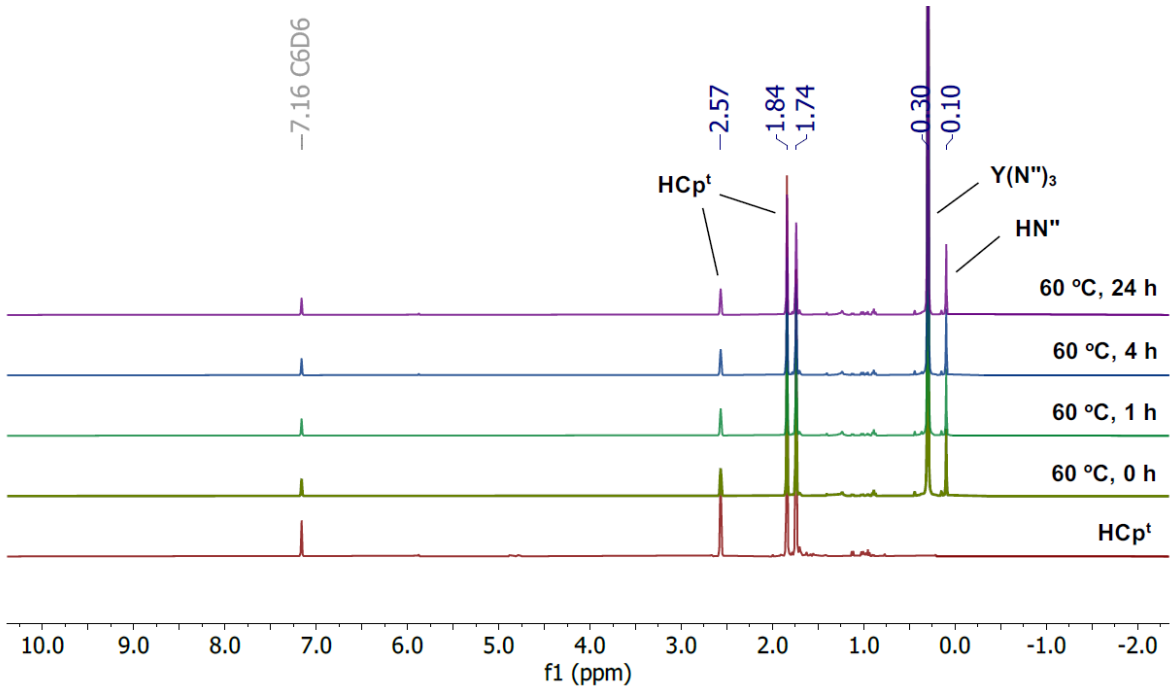

Figure 5.17: ^1H NMR spectra monitoring the reaction of $Y(N'')_3$ with 2 eq. HCp^t at 60 °C.

5.4.3 Conclusions

These reactions showed that the formation of $Y(Cp^t)_2(N'')$ is not favourable under the conditions used, likely due at least in part to the steric encumbrance of the two Cp^t ligands. Particularly in non-coordinating d_6-benzene, no reaction was observed. In d_8-THF, some reaction did occur, producing a product with ^1H NMR resonances consistent with a product containing the Cp^t and N" ligands bound to Y(III). However, the reaction was slow, being nowhere near completion after 6.5 h, and other products were observed in the NMR spectrum, presumably due to the slowness of the target reaction. It was decided not to pursue the isolation of $Y(Cp^t)_2(N'')$ and its reactivity further due to time constraints.

5.5 Reaction of 1-Y with 6-Y

The goal of synthesising **6-Ln** was for use in the synthesis of lanthanide bimetallics, as either a coordination or a metathesis reagent. The reaction of **1-Y** with **6-Y** was therefore carried out in an attempt to synthesise a bimetallic species bridged by pd in the neutral oxidation state, as shown in Scheme 5.3.

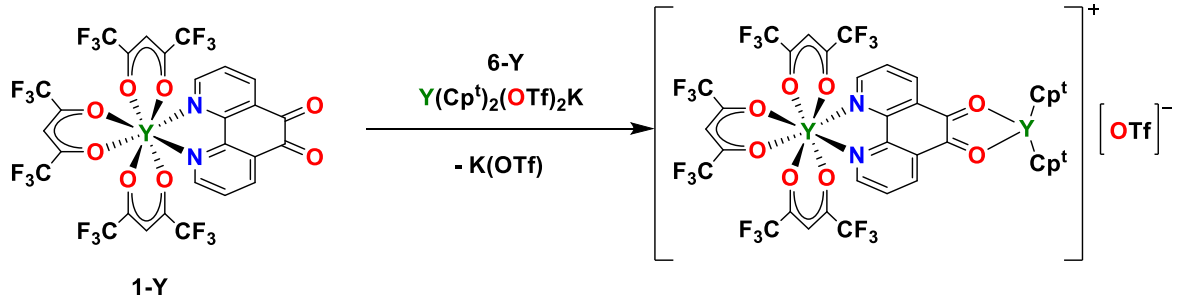

Scheme 5.3: The targeted reaction between [Y(hfac)$_3$(pd)] and [Y(Cp^t)$_2$(OTf)$_2$K] to afford a bimetallic bridged compound.

1-Y was dissolved in Et_2O and was added to **6-Y** suspended in Et_2O. Immediately upon addition, a deep green colour was observed, and this did not change with stirring for 15 m. The mixture was filtered, leaving white and dark green solids, and Et_2O was removed *in vacuo* from the dark green filtrate, leaving a dark green solid. The solid was not soluble in toluene or d_6-benzene. On addition of d_8-THF, the green solid dissolved to afford a reddish solution, and this was analysed by ^{1}H and ^{19}F NMR spectroscopy (Figure 5.18, Figure 5.19). The ^{1}H NMR spectrum shows a single non-solvent peak at δ = 6.30 ppm which could be assigned to either hfac or to the aromatic proton of Cp^t. No signals attributable to pd or to the methyl groups of the Cp^t ligand are visible. The ^{19}F NMR spectrum shows two signals in the region expected for hfac and for OTf. The radical anion of pd does not exhibit any NMR resonances in either **3** or **5-Ln**, and is strongly coloured, consistent with the experimental observations of the reaction of **1-Y** with **6-Y**. If the pd radical anion was generated by an intermolecular redox reaction, its presence could explain the lack of pd resonances. Similarly, if **6-Y** coordinated to the *O,O'* site of the ligand, it is possible that proximity to the organic radical also caused the protons of the Cp^t ligand to not be observable. This intermolecular reaction might be an oxidation of one of the ligands, the solvent, or a intermolecular cyclisation, but as only a single resonance is observed in the ^{1}H NMR spectrum it is not possible to determine which using these data.

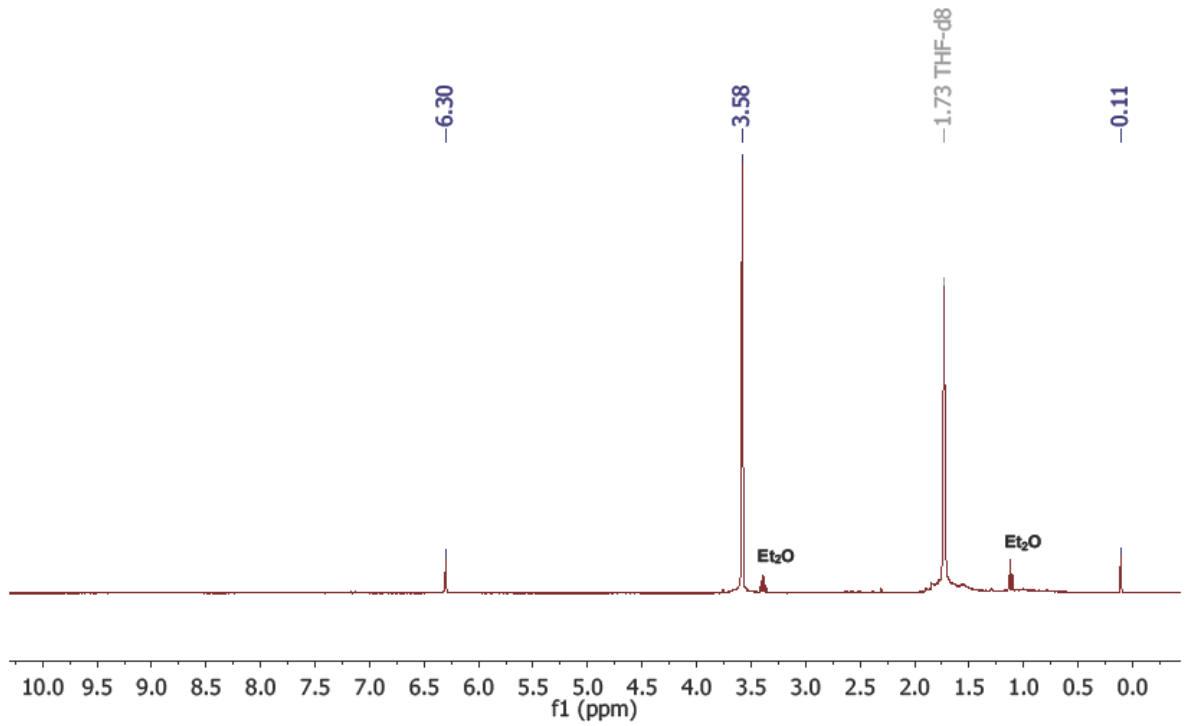

Figure 5.18: 1H NMR spectrum of the product of the reaction between 1-Y and 6-Y, recorded in d_8-THF at 298 K.

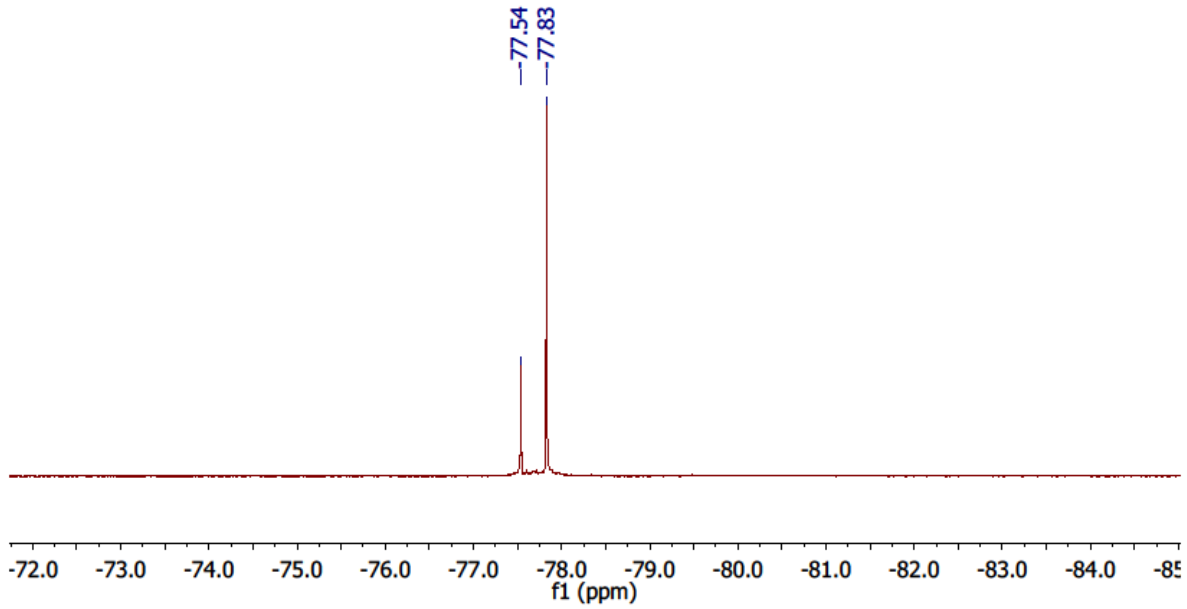

Figure 5.19: ^{19}F NMR spectrum of the product of the reaction between 1-Y and 6-Y, recorded in d_8-THF at 298 K.

Reversible solvatochromic behaviour was observed in the product of the reaction of **1-Y** with **6-Y**. After leaving the initial green solid in the glovebox overnight, it had changed colour to red. When attempting recrystallisation, re-dissolution in Et_2O afforded a green solution, whereas upon dissolution in THF a red solution was again observed. This is consistent with an

intermolecular redox reaction having occurred. The pd ligand and its complexes are not strongly coloured when it is in its neutral oxidation state, but deeper green and red solutions have been observed in solutions of the radical anion[10] (see Chapter 3, Sections 0-5.7 of this chapter and Chapter 6) and the dianion (see Chapter 2).[9] However, the NMR data do not indicate what form this redox reaction might have taken, and no further characterisation data was obtained to identify the product of the reaction.

5.6 Reaction of 3 $[CoCp_2]^+[pd]^{-\bullet}$ with 6-Y

The utility of **6-Ln** as transmetallation reagents was also investigated, targeting the synthesis of bimetallic compounds bridged by the pd radical anion. The transmetallation reaction of **3** $[CoCp_2]^+[pd]^{-\bullet}$ with **6-Ln** was targeted as shown in Scheme 5.4.

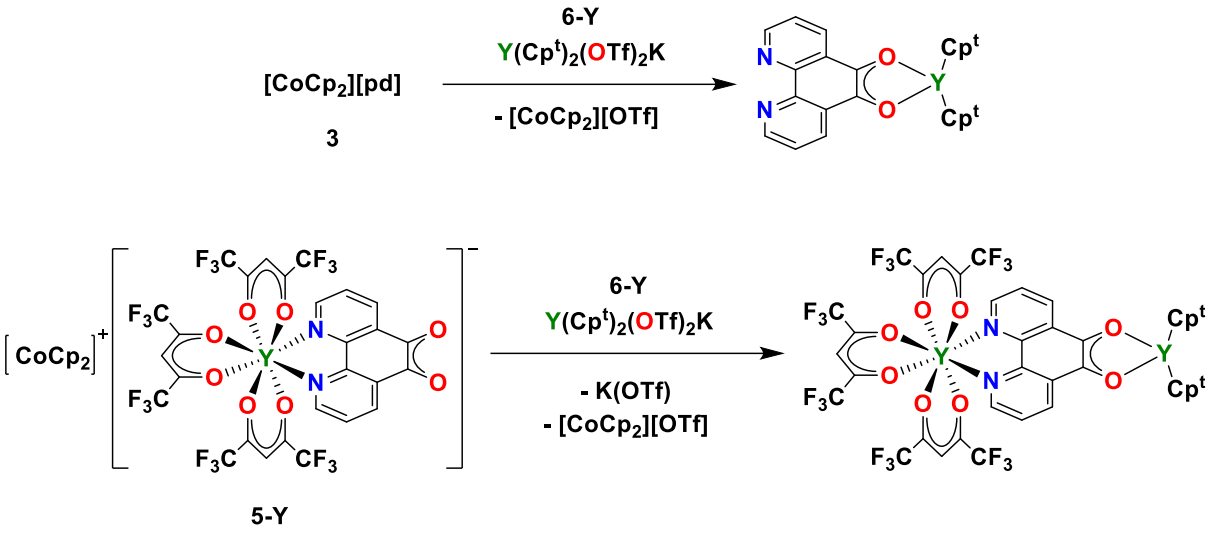

Scheme 5.4: Targeted reactions of 3 and 5-Y with 6-Y to form *O,O'* monometallic or bridged bimetallic compounds.

5.6.1 The reaction of 6-Y with 3

In an NMR tube, **6-Y** was mixed with **3** in d_8-THF, and the ^{1}H and ^{19}F NMR spectra were recorded up to 1 h, during which time no change was observed. The spectrum shows an identical set of resonances to starting material **6-Y** at δ = 1.90, 1.99 and 5.77 ppm, integrating in a 12:12:2 ratio as expected. An additional resonance is also observed at δ = 5.85 ppm, which is assigned to the $[CoCp_2]^+$ cation. Since **3** is not soluble in THF, the presence of this resonance indicates that a transmetallation reaction has occurred, forming the $[CoCp_2][OTf]$ byproduct. Since the Cp^t ligands are still coordinated to a Lewis acidic Y atom in the targeted bimetallic, a significant shift in the resonances of the Cp^t group compared to the starting material is not expected. It is also possible that the Cp^t ^{1}H NMR resonances might be silent due to proximity to the organic radical. To investigate further, the reaction was carried out on a larger scale.

The reaction of **3** with **6-Y** was carried out in THF, then THF was removed *in vacuo* to leave a dark solid. However, the solid was not subsequently soluble in any solvents, indicating that a coordination polymer such as $[Y(Cp^t)_2(N,N'\text{-}O,O'\text{-pd})]_n$ had formed upon removal of the solvent, bridged by $pd^{-\bullet}$. As has been discussed, coordination polymers are relatively common

in pd chemistry due to the bridging nature of the pd ligand if the coordination environment allows it.[4] Similarly, when **3** was reacted with **6-Yb** in MeCN, immediate precipitation of a highly insoluble green solid was observed, even in the presence of DME as a capping ligand to prevent formation of a coordination polymer.

The use of **6-Ln** as a metathesis reagent for the synthesis of lanthanide bimetallic complexes is therefore unlikely to be practical, unless an effective method for prevention of the formation of coordination polymers can be devised. A stronger chelating agent such as a linear tridentate ether or amine might have a sufficiently low dissociation constant, but would be more sterically demanding. Alternatively, a more sterically demanding ligand such as Cp* or indenyl, or even a cross-linked *bis*-cyclopentadienyl ligand could prevent the coordination polymer from forming. Finally, coordination of a second metal to the pd ligand before precipitation could be effective, though this would prevent isolation of the monometallic *O,O'* coordinated complex and its full characterisation.

5.7 Reaction of 5-Y with Ln(Tp*)$_2$(OTf)

5.7.1 Starting material choice and synthesis

Lanthanide triflate salts can be reacted with potassium scorpionates to form heteroleptic lanthanide compounds such as Ln(Tp*)$_2$(OTf) (Ln = La - Nd) or [Ln(Tp*)$_2$]$^+$[OTf]$^-$ (Ln = Y, Sm - Yb) (Tp* = tris(3,5-dimethyl-1-pyrazolyl)borate),[31] and these were identified as possible reagents for metathesis. These complexes were synthesised by a modification of the literature procedures. In THF, Ln(OTf)$_3$ (Ln = Y, Ce) was stirred with Na(Tp*) (2 eq.) for several hours. THF was removed *in vacuo* to leave white solids, and Ln(Tp*)$_2$(OTf) was then extracted into DCM. Analytically pure Ln(Tp*)$_2$(OTf) (Ln = Y, Ce) were obtained by crystallisation from a concentrated MeCN solution at -35 °C.

5.7.2 Reactions of 5-Y with Ln(Tp*)$_2$(OTf)

The metathesis reaction of Ln(Tp*)$_2$(OTf) with **5-Y** was targeted, with the aim of eliminating the stable salt [CoCp$_2$]$^+$[OTf]$^-$ and forming the radical-bridged bimetallic species as shown in Scheme 5.5.

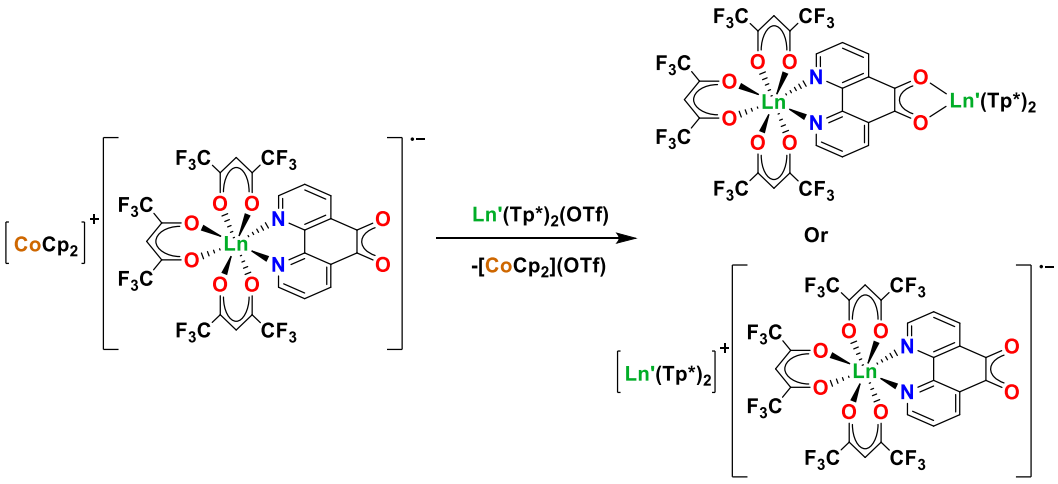

Scheme 5.5: The synthesis of lanthanide bimetallic compounds, as targeted by reaction of 5-Ln with [Ln(Tp*)$_2$(OTf)]

The reactions of **5-Y** with Ln(Tp*)$_2$(OTf) (Ln = Y, Ce) were therefore carried out. Upon stirring **5-Y** with 1 eq. Ln(Tp*)$_2$(OTf) in THF, a colour change from dark green to brown was immediately observed in each case. After removal of THF *in vacuo* from the solution, extraction into either hexane (Ln = Y) or toluene (Ln = Ce) afforded a deep red or orange solution respectively. Removal of the solvent resulted in isolation of moderate yields of red

or orange solids (Ln = Y, 45%; Ce, 62%). NMR analysis was consistent with multiple products in each case, with significant numbers of ^{1}H environments in both the aliphatic and aromatic regions, and as such a full analysis of this data was not possible. Multiple environments were also observed in the ^{19}F and ^{11}B NMR spectra.

5.7.3 ATR-IR spectroscopy of the products of the reaction of 5-Y with Ln(Tp*)$_2$(OTf)

The ATR-IR spectra of the products of the reaction of **5-Y** with Ln(Tp*)$_2$(OTf) are shown in Figure 5.20 and in Figure 5.27 (experimental section). These spectra were used to investigate the oxidation state of pd in the products of the reaction. Consistent with other compounds in this thesis, an intense absorption at 1651 cm^{-1} is assigned to the hfac ligands. Broad absorptions at 2517-2563 cm^{-1} and 2930-2961 cm^{-1} are characteristic of the *tris*-pyrazolyl borate ligands.[31, 32] As discussed in earlier chapters, the diketone group of pd has characteristic stretching frequencies depending on its oxidation state.[7, 8] The products of the reaction between **5-Y** and Ln(Tp*)$_2$(OTf) (Ln = Y, Ce) both exhibit resonances consistent with a semiquinone radical anion at 1418 and 1417 cm^{-1} (1400-1420 cm^{-1} in **3**, 1417-1420 cm^{-1} in **5-Ln**), and no absorptions in the region expected for the neutral pd ligand, indicating that there was no change in the oxidation state of pd during the reaction.

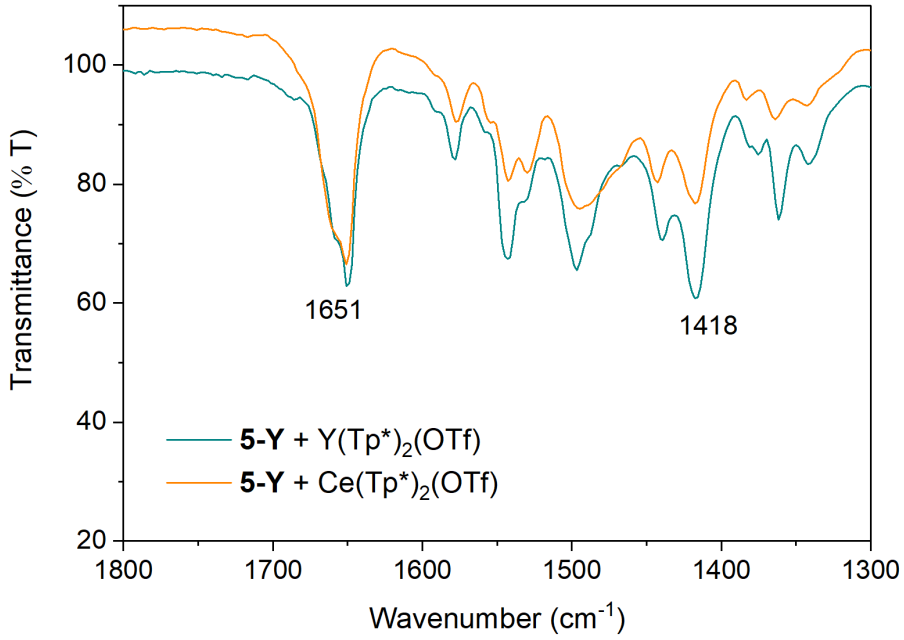

Figure 5.20: An expansion of the ATR-IR spectrum of the hexane-soluble products of the reaction of 5-Y with Ln(Tp*)$_2$(OTf) (Ln = Y, Ce).

5.7.4 Visible absorption spectroscopy of the products of the reaction between 5-Y and Ln(Tp*)$_2$(OTf)

The visible absorption spectra of the products of the reaction between **5-Y** and Ln(Tp*)$_2$(OTf) (shown in Figure 5.21) are likewise consistent with the radical ligand, with absorption maxima of 511 and 468 nm respectively. These absorptions are shifted to higher energy than those in the *N,N'* coordinated compounds **5-Ln**, reflected in the significant colour change. This is consistent with a change in coordination mode of the ligand from *N,N'* in **5-Y** to either *O,O'* or to the bridging *N,N'-O,O'* mode. The intensity of these transition envelopes is similar to the transition observed at 600 nm in **5-Ln**, and they are therefore assigned to the same ILCT transition, shifted by a change in coordination of the pd ligand.

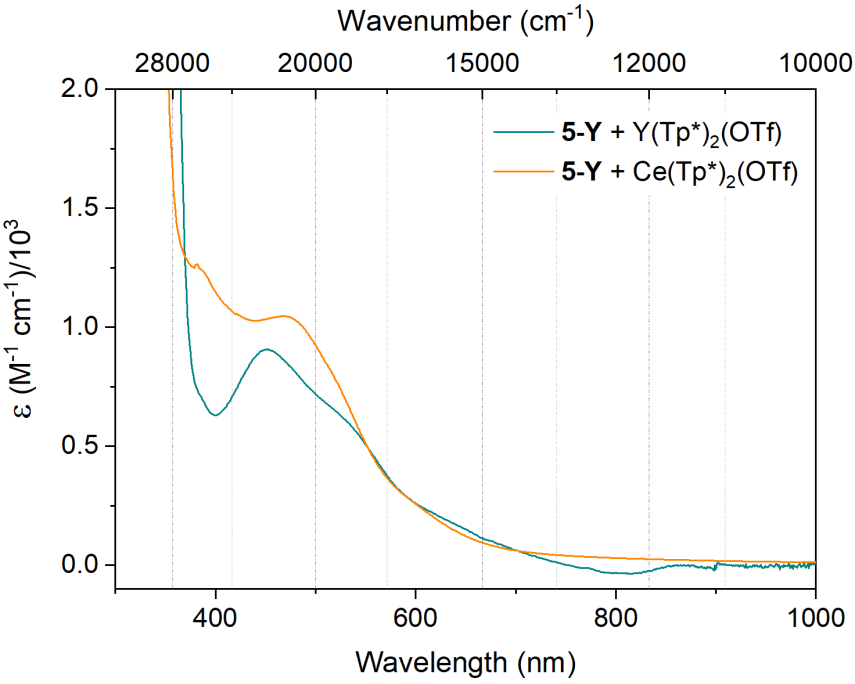

Figure 5.21: The visible absorption spectra of the products of the reaction of 5-Y with Ln(Tp*)$_2$(OTf) (Ln = Y, Ce), recorded in toluene.

5.7.5 EPR spectroscopy of the products of the reaction between 5-Y and Ln(Tp*)$_2$(OTf)

The EPR spectra of the products of the reaction between **5-Y** and Ln(Tp*)$_2$(OTf) were also recorded, and each shows an organic radical with a g-value close to that of a free electron, as shown in Figure 5.22. However, since no structure was available, no simulation was performed and it was not possible to determine whether the coupling was significantly different to that in **5-Y**, as might be expected upon coordination of Y to the *O,O'* binding site of pd.

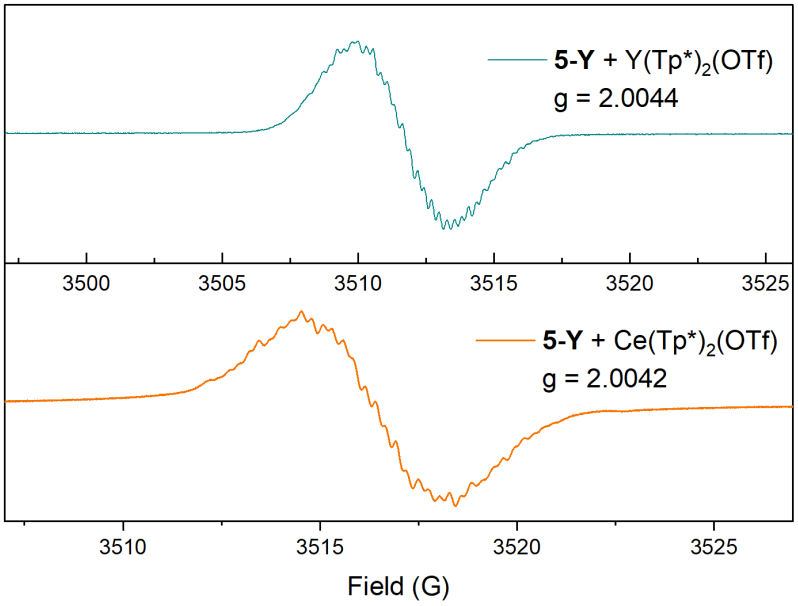

Figure 5.22: The X-band EPR spectra of the products of the reaction of 5-Y with Ln(Tp*)$_2$(OTf) (Ln = Y, Ce), recorded in toluene.

5.7.6 Crystallography of ligand redistribution products

Crystallisation of the products obtained from the reactions of Ln(Tp*)$_2$(OTf) with **5-Y** was attempted under a wide variety of conditions, from toluene, Et$_2$O and hexane solutions, and from mixtures thereof, at -35 °C. However, whenever crystals suitable for X-ray diffraction were obtained from these crystallisations they were products of ligand redistribution reactions. Three such examples are Y(Tp*)$_2$(hfac), Y(Tp*)(hfac)$_2$(THF) and Ce(Tp*)(hfac)$_2$(H-dmpz) (H-dmpz = 1H-dimethylpyrazole).

Single crystals of Y(Tp*)$_2$(hfac) suitable for X-ray diffraction were frequently obtained, and the solid-state molecular structure of Y(Tp*)$_2$(hfac) is shown in Figure 5.23. Several compounds of the general structure Ln(Tp^R)$_2$(*β*-diketonate) (Tp^R = Tp (hydro-*tris*-pyrazolyl borate), Tp*) have been previously synthesised and crystallised, and in some cases studied for their luminescent and magnetic properties.[32-36] However, a search of the CCDC using this structure type for Ln = Y did not yield any results. Examples of *bis*-Tp* compounds of Y have been crystallographically characterised,[37-40] though in each case as the six-coordinate cation [Y(Tp*)$_2$]$^+$ with a non-coordinated anion. Examples of less bulky *bis*-Tp compounds of Y are somewhat more common, and a number of structures of the type Y(Tp)$_2$(L) (L = DTBSQ (3,5-

di-*tert*-butylsemiquinone), tetraoxolene** in various oxidation states, or dithioxalate) have been reported,[1, 41-46] all of which exhibit negatively charged chelating oxygen donor ligands and are therefore useful comparators for the bond data in Y(Tp*)$_2$(hfac). On one occasion, single crystals of Y(Tp*)(hfac)$_2$(THF) suitable for X-ray crystallography were obtained, and the solid-state molecular structure is shown in Figure 5.24. No examples of the Ln(Tp^R)(*β*-diketonate)$_2$ structure were found in a search of the CCDC database.

The Y-N bonds in both Y(Tp*)$_2$(hfac) of 2.453(2)-2.506(2) Å and Y(Tp*)(hfac)$_2$(THF) of 2.412(4)-2.498(4) Å are consistent with each other, though those in the *mono*-Tp* complex are generally shorter, likely due to the decreased steric load due to having one less Tp* ligand. These bond distances are consistent with the Y-N(Tp) bonds of a range of Y(Tp)$_2$(L) compounds,[1, 41-43] despite the increased steric bulk of the Tp* ligands over Tp. The Y-O(hfac) bond distances in Y(Tp*)$_2$(hfac) of 2.384(2) Å and in Y(Tp*)(hfac)$_2$(THF) of 2.303(2)-2.416(4) Å are also consistent with each other, and are very similar to those in **1-Y** of 2.299(3)-2.344(2) Å and in Y(hfac)$_3$(glyme) of 2.32(1)-2.37(1) Å.

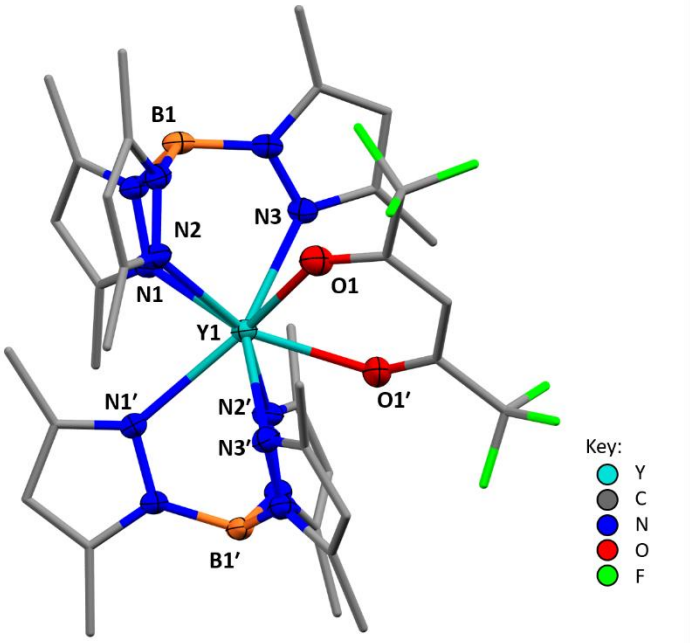

Figure 5.23: Solid-state molecular structure of Y(Tp*)$_2$(hfac). Thermal ellipsoids are drawn at 50% probability. H atoms are omitted, and F and C atoms are shown in wireframe for clarity. Key bond distances: Y-N 2.453(2)-2.506(2), Y-O 2.384(2) Å.

** tetraoxolene: 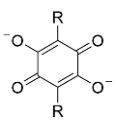

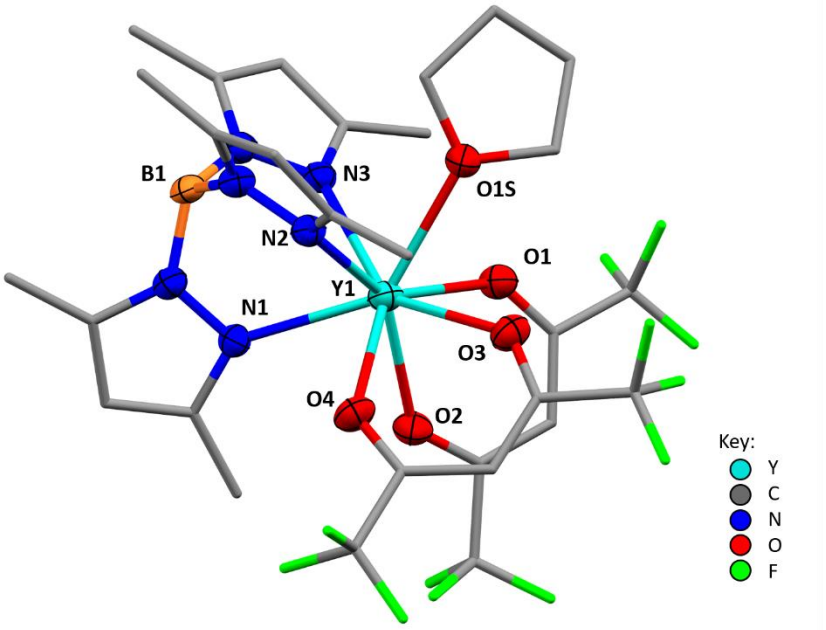

Figure 5.24: Solid-state molecular structure of Y(Tp*)(hfac)$_2$(THF). Thermal ellipsoids are drawn at 50% probability. H atoms are omitted, and C and F atoms are shown in wireframe for clarity. Key bond distances: Y-N 2.412(4)-2.498(4), Y-O(hfac) 2.303(2)-2.416(4), Y-O(THF) 2.501(5) Å.

In the case of Ce(Tp*)(hfac)$_2$(H-dmpz), it is evident that some Tp* ligands have undergone decomposition, likely as the result of a radical-mediated process. However, the NMR data obtained from the products of this reaction are too complex for the relative proportions of products to be determined. The Ce-N bonds in Ce(Tp*)(hfac)$_2$(H-dmpz) of 2.497(5)-2.603(5) Å are consistent with, though slightly shorter than, those observed in the similar Ce(Tp*)$_2$(dmpz) (dmpz = dimethylpyrazolyl) of 2.547(4)-2.667(6) Å.[47] Again, this is unsurprising given the significant decrease in steric bulk in one of the Tp* ligands. The Ce-N(H-dmpz) bond of 2.664(5) Å is significantly longer than the Ce-N(dmpz) bonds in Ce(Tp*)$_2$(dmpz) of 2.385(5)-2.505(5) Å due to the negative charge on dmpz and its chelating bonding to Ce.

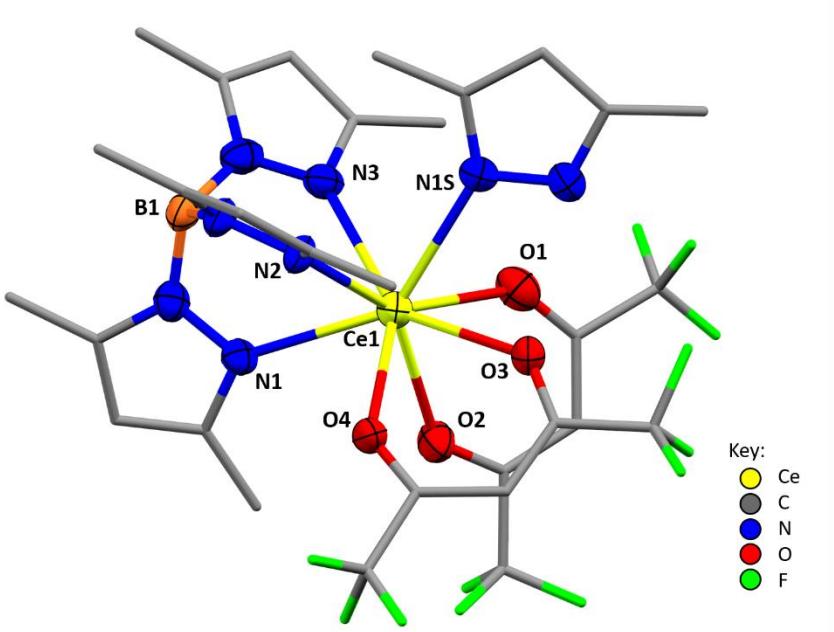

Figure 5.25: Solid-state molecular structure of Ce(Tp*)(hfac)$_2$(dmpz). Thermal ellipsoids are drawn at 50% probability. H atoms are omitted, and C and F atoms are shown in wireframe for clarity. Key bond distances: Ce-N(Tp*) 2.497(5)-2.603(5), Ce-N(dmpz) 2.664(5), Ce-O 2.434(5)-2.467(5) Å.

5.7.7 Conclusions

The ATR-IR, visible absorption and EPR spectroscopy of the products of the reaction between **5-Y** and Ln(Tp*)$_2$(OTf) are consistent both with the pd ligand remaining in the radical anion oxidation state, and with a change in coordination structure as would be expected in the bridged bimetallic target. However, the ^{1}H NMR spectra of the products of the reaction of **5-Y** with Ln(Tp*)$_2$(OTf) indicate that a significant number of Tp* and hfac environments are present. This is reinforced by the range of redistribution products obtained by crystallisation and indicates that ligand redistribution is the primary result of the reaction. However, the mechanism of this redistribution was not determined, nor was the pd-containing, soluble product characterised. Despite the strong interaction between the negatively charged chelating oxygen donor diketonate ligands, it is evident that the ligands have some degree of lability. It has been reported that *β*-diketonate ligands can be labile, particularly in strongly coordinating solvents.[48] The elimination of coordinating solvents from the reaction may therefore prevent or sufficiently reduce the rate of these reactions. It is also possible that the steric bulk of the Tp* ligands is too great to favour coordination of pd *via* the *O,O'* site. However, a number of examples of semiquinone ligands bound to [Ln(Tp)$_2$]$^+$ have been reported, suggesting this might be a more useful ligand environment for the desired *O,O'* coordinated product.[1, 41-46]

5.8 Conclusions

This chapter has described several attempts to synthesise multimetallic lanthanide species, bridged by the pd ligand using metathesis. The reactions of **3** and **5-Y** were investigated with Ni(II) chlorides, a new family of lanthanide cyclopentadienyl triflate compounds **6-Ln**, and with lanthanide scorpionates.

The reaction of $[NEt_4]_2[NiCl_4]$ with **3**, followed by addition of **4-Y** produced insoluble products which could not therefore be characterised by solution methods. However, by ATR-IR spectroscopy the coordination and oxidation states of the pd ligand were investigated, and absorptions consistent with the neutral and dianionic ligand were observed. It is proposed that two monoanionic radical ligands undergo a dissociation reaction to produce one neutral and one dianionic ligand in a product formulated as $Y(hfac)_3(N,N'\text{-}O,O'\text{-}pd^{2-})Ni(N,N'\text{-}pd^{0})$.

The lanthanide cyclopentadienyl triflate salts **6-Ln** $Ln(Cp^t)_2(OTf)_2K$ (Ln = Y, Yb) were synthesised by reaction of lanthanide triflates with $K(Cp^t)$. They were characterised fully by ^1H and ^{19}F NMR, ATR-IR and UV-vis spectroscopy and their solid-state molecular structures were determined by X-ray crystallography. The distinctive red colour of **6-Yb** in solution arose from a transition assigned to charge transfer between the cyclopentadienyl ligand and Yb. Sensitisation of photoluminescence from Yb(III) was observed by excitation of this charge transfer transition. Attempts to use **6-Y** as a metathesis reagent for the synthesis of compounds of the pd radical ligand by reaction with **3** were unsuccessful, producing insoluble coordination polymers.

The reactions of $Ln(Tp^*)_2(OTf)$ (Ln = Y, Ce) with **5-Y** resulted in complex mixtures of products, with UV-vis, ATR-IR and EPR spectroscopy consistent with compounds of the radical pd ligand in a new coordination environment. However, the only compounds obtained from crystallisations of the product mixtures from this reaction were ligand redistribution products containing both hfac and Tp* ligands. It is believed that the steric bulk of the Tp* ligand along with the use of coordinating solvents for the reaction encouraged ligand redistribution, preventing coordination of pd or otherwise causing that reaction to be less favourable than the abstraction of hfac ligands from the other metal. It is suggested that using the non-methylated Tp ligand, in the absence of coordinating solvents, might prevent the ligand redistribution reaction.

5.9 Experimental details for Chapter 5

5.9.1 Starting material synthesis

$NiCl_2$ and $[NEt_4]_2[NiCl_4]$ were dehydrated *in vacuo* and stored under N_2 before use. $K(Cp^t)$ was synthesised as described in Chapter 2. HN" was purchased from Alfa Aesar and freeze-thaw degassed before use. KN" was synthesised by the reaction of KH with HN", and was purified by crystallisation from a concentrated hexane solution at -35 °C. $YN"_3$ was synthesised by the reaction of $Y(OTf)_3$ with 3 eq. KN", then crystallised from a concentrated hexane solution at -35 °C. $Ln(Tp^*)_2(OTf)$ (Ln = Y, Ce) were synthesised by modification of a literature procedure.[31]

5.9.2 Reaction of 5-Y with $NiCl_2$

$NiCl_2$ (2.7 mg, 2.07 $x10^{-2}$ mmol) was suspended in MeCN (2 ml) and **5-Y** (42.4 mg, 3.82 $x10^{-2}$ mmol) was dissolved in MeCN (2 ml). **5-Y** was added to $NiCl_2$ and the mixture was stirred for 24 h. No reaction was observed.

5.9.3 Reaction of 3 with $[NEt_4]_2[NiCl_4]$

$[NEt_4]_2[NiCl_4]$ (15.3 mg, 3.32 $x10^{-3}$ mmol) and **3** (26.7 mg, 6.79 $x10^{-3}$ mmol) were separately dissolved in MeCN (2 ml each) and cooled to -35 °C. $[NEt_4]_2[NiCl_4]$ was added slowly to **3** with stirring and the vial was kept at -35 °C for 16 h. The solution was stirred at R.T. for 2 h, then filtered *via* frit to separate dark solids from a yellow solution. The purple solids were washed with THF (2x 2 ml) and hexane (2x 2 ml), then weighed (16.9 mg).

5.9.4 Reaction of 5-Y with $[NEt_4]_2[NiCl_4]$

5-Y (69.8 mg, 6.20 $x10^{-2}$ mmol) and $[NEt_4]_2[NiCl_4]$ (14.7 mg, 3.19 $x10^{-2}$ mmol) were each dissolved in MeCN and cooled to -35 °C. $[NEt_4]_2[NiCl_4]$ was added dropwise to **5-Y** and the mixture was stirred for 16 h. The mixture was filtered to separate dark green solids from a green solution, and the solids were removed from the glovebox for dissolution in d_6-DMSO and NMR analysis.

5.9.5 Reaction of 3 with $[NEt_4]_2[NiCl_4]$ and 4-Y

$[NEt_4]_2[NiCl_4]$ (23.0 mg, 4.99 $x10^{-2}$ mmol) and **3** (39.6 mg, 9.22 $x10^{-2}$ mmol) were separately suspended in MeCN (3 ml each), and $[NEt_4]_2[NiCl_4]$ was added to **3** with stirring. An immediate colour change from a purple suspension to brown. The mixture was stirred for 1.5 h, then

filtered *via* frit to obtain dark purple solids, which were washed with THF (2x 5 ml) and hexane (2x 5 ml). The solids were dried *in vacuo* and weighed (21.6 mg). A small quantity was removed and analysed by ^{1}H NMR in d_6-DMSO. The remaining solids (20.3 mg) were suspended in THF and cooled to -35 °C and **4-Y** (37.3 mg, 0.0436 mmol) was added with stirring at -35 °C. A colour change from purple to red-brown was observed and the mixture was stirred to R.T. for 1.5 h. The mixture was filtered *via* frit to obtain a maroon solid, which was washed with hexane (2x 5 ml) and weighed (24.5 mg). IR(ATR): 1695 (w), 1653 (m), 1576 (s), 1510 (m), 1481 (s), 1425 (s), 1375 (m) cm^{-1}.

5.9.6 Synthesis of 6-Y Y(Cp^{t})$_2$(OTf)$_2$K

A schlenk tube was charged with Y(OTf)$_3$ (706.1 mg, 1.317 mmol) and K(Cp^{t}) (431.2 mg, 2.690 mmol, 2.04 eq.), and was cooled to -78 °C. THF (20 ml) was added with stirring and the mixture was allowed to warm to room temperature with stirring over 3 h, after which time the suspension had become a yellow solution. THF was removed *in vacuo*, and the solid was then washed with warm toluene (15 ml, then 10 ml, 50 °C). The solids were extracted into Et$_2$O (2x 10 ml), and Et$_2$O was then removed *in vacuo* from the combined filtrates, leaving a white powder, presumed to be Y(Cp^{t})$_2$(OTf)$_2$K. The solid was exposed to air, and immediately formed yellow decomposition products, which were weighed (25 mg, yellow oily solid). Since the yield was low, the solids were again extracted into Et$_2$O (2x 15 ml, with sonication) and Et$_2$O was removed *in vacuo*, affording a bright white powder (38.5 mg). No solubility was observed in DCM. Extraction into a 1:1 mixture of THF and toluene (20 ml) allowed the isolation of a further 508.5 mg, affording a total yield of 547.0 mg (0.818 mmol, 62%). Square, blocky crystals suitable for X-ray diffraction were obtained by layering a concentrated THF solution with hexane at -35 °C overnight. ^{1}H NMR (d_8-THF): δ = 1.90 (s, 12H, Cp^{t}- C**H**$_3$), 1.98 (s, 12H, Cp^{t}-C**H**$_3$), 5.78 (s, 2H, Cp^{t}-**H**) ppm. ^{19}F{^{1}H} NMR (d_8-THF): δ = -78.24 (s, OTf-C**F**$_3$) ppm. IR (ATR)/cm^{-1} (intensity): 1452 (w), 1389 (w), 1324 (m), 1239 (s), 1215 (s), 1177 (s), 1029 (s), 983 (w), 795 (m), 628 (s).

5.9.7 Synthesis of 6-Yb Yb(Cp^{t})$_2$(OTf)$_2$K

Yb(OTf)$_3$ (294.3 mg, 0.475 mmol) was dissolved in THF (10 ml) and added to a suspension of K(Cp^{t}) (152.0 mg, 0.948 mmol) in THF (5 ml). Immediately, a red colour was observed, and the suspension was stirred for 1 h. THF was removed *in vacuo* to give dark solids, which were

washed with toluene (5 ml). The solids were then extracted into a 1:1 mixture of THF and toluene (10 ml), and the mixture was filtered by frit filtration. THF and toluene were then removed from the red solution *in vacuo* to obtain **6-Yb** as a red-brown solid (234.7 mg, 0.312 mmol, 66%). Small, blocky red crystals suitable for X-ray diffraction were obtained by layering a saturated THF solution with hexane (1:3 ratio) at -35 °C overnight. ^{1}H NMR (d_8-THF): δ = -72.52 (s, 2H, Cp^{t}-C**H**), -10.15 (s, 12H, Cp^{t}-C**H**$_3$), 39.92 (s, 12H, Cp^{t}-C**H**$_3$) ppm. ^{19}F{^{1}H} NMR (d_8-THF): δ = -40.00 (s, OTf-C**F**$_3$), -79.44 ppm. ^{1}H NMR (d_3-MeCN): δ = -18.48 (s, 12H, Cp^{t}-C**H**$_3$), 12.44 (s, 1H, Cp^{t}-C**H**) and 17.28 (s, 12H, Cp^{t}-C**H**$_3$) ppm. ^{19}F{^{1}H} NMR (d_3-MeCN): δ = -75.01 (s, OTf-C**F**$_3$) ppm. IR (ATR)/cm^{-1} (intensity): 1452 (w), 1389 (w), 1324 (s), 1240 (s), 1215 (s), 1179 (s), 1030 (s), 974 (w), 795 (m), 628 (s). λ_{max} (MeCN)/nm (ε/M^{-1} cm^{-1}): 504 (164), 876 (4.5), 886 (3.9), 898 (3.6), 931 (14), 968 (52), 987 (16). λ_{max} (THF)/nm (ε/M^{-1}cm^{-1}): 457 (221), 953 (33), 987 (16).

5.9.8 Attempted synthesis of Y(Cp^{t})$_2$(N″)

Synthesis 1 (SH01_377): **6-Y** (8.6 mg, 0.0129 mmol) and 18-crown-6 (3.6 mg, 0.0136 mmol) were stirred in d_8-THF and an NMR spectrum was recorded. KN″ (2.4 mg, 0.0120 mmol) was added to the reaction, after which a slight colour change from colourless to pale pink was observed, and the solution was analysed by ^{1}H and ^{19}F NMR spectroscopy.

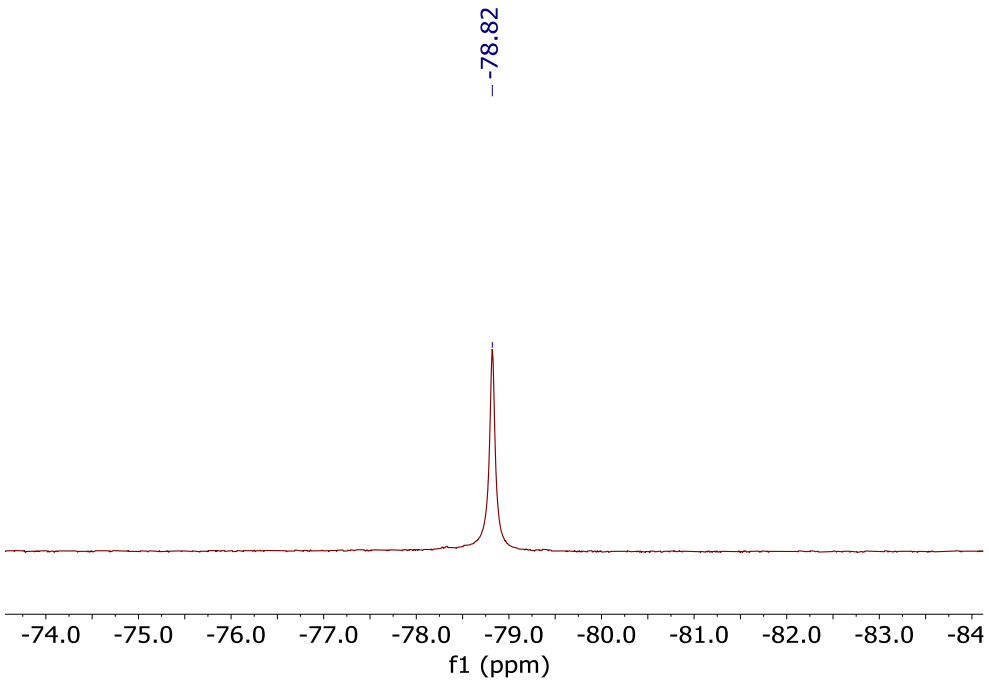

Figure 5.26: A representative ^{19}F NMR spectrum of the reaction between 6-Y and KN".

Synthesis 2: Y(N")$_3$ (15.4 mg, 0.0270 mmol) was added to a solution of HCp^t (6.6 mg, 00540 mmol, 2 eq.) in d_6-benzene. The ^{1}H NMR spectrum was recorded, and the solution was heated to 60 °C. Periodically, the solution was cooled and the ^{1}H NMR spectrum was recorded, up to 24 h.

5.9.9 Reaction of 1-Y with 6-Y

1-Y (71.8 mg, 0.0780 mmol) was dissolved in Et_2O (2 ml) and added to **6-Y** (52.3 mg, 0.0782 mmol) suspended in Et_2O (2 ml) with stirring. An immediate colour change from pale green to dark green was observed. The mixture was filtered *via* frit to obtain a dark green solution and leaving behind white solids.

5.9.10 Reaction of 5-Y with Y(Tp*)$_2$(OTf)

5-Y (266.3 mg, 0.240 mmol) and Y(Tp*)$_2$(OTf) (201.2 mg, 0.240 mmol) were added to a schlenk. At 0 °C, THF (20 ml) was added and the mixture was stirred for 2.5 h, changing colour from green to brown. THF was removed *in vacuo*, leaving dark solids, and the products were extracted into hexane (2x 20 ml) with filtration by filter cannula, giving a deep red solution, and leaving green solids. Hexane was removed *in vacuo* from the filtrate, to give a red solid (172.2 mg, 0.107 mmol, 45% yield). IR (ATR)/cm^{-1} (intensity): 1658 (w), 1651 (s), 1578 (m), 1543 (s), 1530 (w), 1497 (s), 1439 (m), 1418 (s). λ_{max} (Tol)/nm (ε/M^{-1} cm^{-1}): 383, 511 (1194).

5.9.11 Reaction of 5-Y with Ce(Tp*)$_2$(OTf)

5-Y (79.9 mg, 0.0720 mmol) and Ce(Tp*)$_2$(OTf) (63.7 mg, 0.0721 mmol) were dissolved separately in THF and stirred together for 1 h, during which time a colour change to green-brown was observed. The solution was filtered by frit and THF was removed *in vacuo*. The products were extracted into toluene with filtration by frit and toluene was removed *in vacuo* from the orange filtrate to give orange solids (74.4 mg, 0.0450 mmol, 62% yield). IR (ATR)/cm^{-1} (intensity): 1651 (s), 1578 (w), 1543 (m), 1530 (m), 1495 (s), 1443 (m), 1417 (m), 1364 (w). λ_{max} (Tol)/nm (ε/M^{-1} cm^{-1}): 382 (1 266), 468 (1 046).

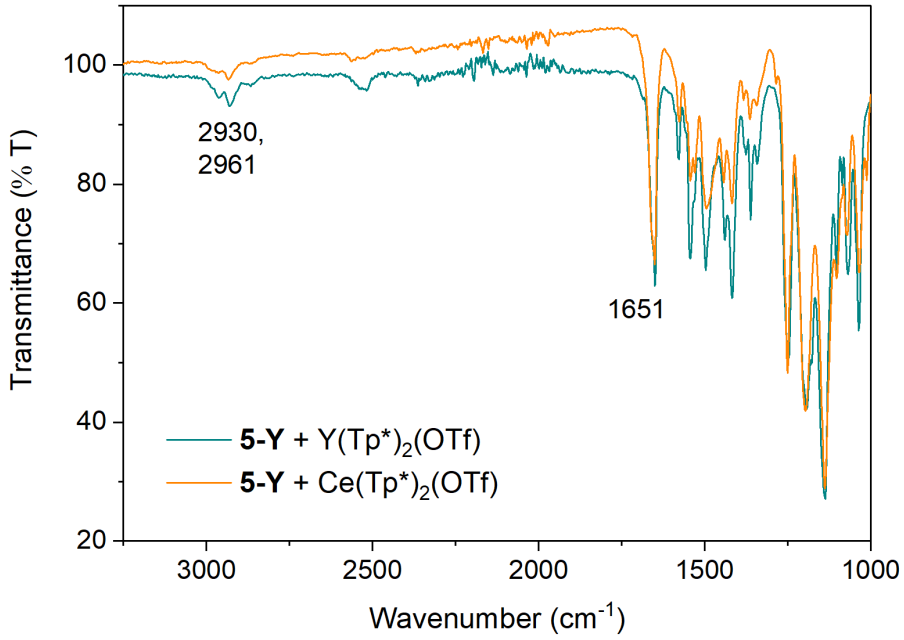

Figure 5.27: The ATR-IR spectra of the products of the reaction between 5-Y and Ln(Tp*)$_2$(OTf) (Ln = Y, Ce).

5.10 References

1. J. McGuire, B. Wilson, J. McAllister, H. N. Miras, C. Wilson, S. Sproules and J. H. Farnaby, *Dalton Trans.*, 2019, **48**, 5491-5495.
2. X. He, Y. Yao, X. Luo, J. Zhang, Y. Liu, L. Zhang and Q. Wu, *Organometallics*, 2003, **22**, 4952-4957.
3. P. Román, A. Luque, J. M. Gutiérrez-Zorilla and J. I. Beitia, *Z. Kristallog.*, 1992, **198**, 213-225.
4. J. R. Hickson, PhD, Imperial College London, 2018.
5. W. Paw and R. Eisenberg, *Inorg. Chem.*, 1997, **36**, 2287-2293.
6. F. Calderazzo, G. Pampaloni and V. Passarelli, *Inorg. Chim. Acta*, 2002, **330**, 136-142.
7. G. A. Fox, S. Bhattacharya and C. G. Pierpont, *Inorg. Chem.*, 1991, **30**, 2895-2899.
8. F. Calderazzo, F. Marchetti, G. Pampaloni and V. Passarelli, *J. Chem. Soc., Dalton Trans.*, 1999, **24**, 4389-4396.
9. J. R. Hickson, S. J. Horsewill, C. Bamforth, J. McGuire, C. Wilson, S. Sproules and J. H. Farnaby, *Dalton Trans.*, 2018, **47**, 10692-10701.
10. J. R. Hickson, S. J. Horsewill, J. McGuire, C. Wilson, S. Sproules and J. H. Farnaby, *Chem. Commun.*, 2018, **54**, 11284-11287.
11. S. Demir, S. E. Lorenz, M. Fang, F. Furche, G. Meyer, J. W. Ziller and W. J. Evans, *J. Am. Chem. Soc.*, 2010, **132**, 11151-11158.
12. S. E. Lorenz, B. M. Schmiege, D. S. Lee, J. W. Ziller and W. J. Evans, *Inorg. Chem.*, 2010, **49**, 6655-6663.
13. M. G. Klimpel, H. W. Görlitzer, M. Tafipolsky, M. Spiegler, W. Scherer and R. Anwander, *J. Organomet. Chem.*, 2002, **647**, 236-244.
14. J. Stehr and R. D. Fischer, *J. Organomet. Chem.*, 1992, **430**, C1-C4.
15. B. M. Schmiege, M. E. Fieser, J. W. Ziller and W. J. Evans, *Organometallics*, 2012, **31**, 5591-5598.
16. E. L. Werkema, L. Castro, L. Maron, O. Eisenstein and R. A. Andersen, *New J. Chem.*, 2013, **37**, 132-142.
17. P. B. Hitchcock, A. G. Hulkes, M. F. Lappert and A. V. Protchenko, *Inorg. Chim. Acta*, 2006, **359**, 2998-3006.
18. D. Gu, C. Yi and W. Ren, *Inorg. Chem.*, 2019, **58**, 9260-9269.
19. P. Atkins, T. Overton, J. Rourke, M. Weller and F. Armstrong, in *Shriver & Atkins: Inorganic Chemistry*, Oxford University Press, Oxford, 4th edn., 2006, ch. *d*-metal complexes: Electronic Structure and Spectra, pp. 459-490.
20. R. Pappalardo and C. K. Jørgensen, *J. Chem. Phys.*, 1967, **46**, 632-638.
21. C. J. Schlesener and A. B. Ellis, *Organometallics*, 1983, **2**, 529-534.

22. R. G. Denning, J. Harmer, J. C. Green and M. Irwin, *J. Am. Chem. Soc.*, 2011, **133**, 20644-20660.

23. C. A. P. Goodwin, D. Reta, F. Ortu, N. F. Chilton and D. P. Mills, *J. Am. Chem. Soc.*, 2017, **139**, 18714-18724.

24. W. D. Horrocks, J. P. Bolender, W. D. Smith and R. M. Supkowski, *J. Am. Chem. Soc.*, 1997, **119**, 5972-5973.

25. A. Beeby, S. Faulkner and J. A. G. Williams, *J. Chem. Soc., Dalton Trans.*, 2002, **9**, 1918-1922.

26. S. Faulkner, B. P. Burton-Pye, T. Khan, L. R. Martin, S. D. Wray and P. J. Skabara, *Chem. Commun.*, 2002, **16**, 1668-1669.

27. T. Lazarides, N. M. Tart, D. Sykes, S. Faulkner, A. Barbieri and M. D. Ward, *Dalton Trans.*, 2009, **20**, 3971-3979.

28. D. Esteban-Gómez, L. A. Büldt, P. Pérez-Lourido, L. Valencia, M. Seitz and C. Platas-Iglesias, *Inorg. Chem.*, 2019, **58**, 3732-3743.

29. N. Kofod, P. Nawrocki, C. Platas-Iglesias and T. J. Sørensen, *Inorg. Chem.*, 2021, **60**, 7453-7464.

30. R. D. Shannon, *Acta Crystallogr. Sect. A*, 1996, **32**, 751-767.

31. S.-Y. Liu, G. H. Maunder, A. Sella, M. Stevenson and D. A. Tocher, *Inorg. Chem.*, 1996, **35**, 76-81.

32. J. L. Galler, S. Goodchild, J. Gould, R. McDonald and A. Sella, *Polyhedron*, 2004, **23**, 253-262.

33. M. A. J. Moss, C. J. Jones and A. J. Edwards, *J. Chem. Soc., Dalton Trans.*, 1989, **7**, 1393-1400.

34. R. G. Lawrence, T. A. Hamor, C. J. Jones, K. Paxton and N. M. Rowley, *J. Chem. Soc., Dalton Trans.*, 2001, **14**, 2121-2126.

35. F. Guégan, F. Riobé, O. Maury, J. Jung, B. Le Guennic, C. Morell and D. Luneau, *Inorg. Chem. Frontiers*, 2018, **5**, 1346-1353.

36. E. A. Mikhalyova, M. Zeller, J. P. Jasinski, R. J. Butcher, L. M. Carrella, A. E. Sedykh, K. S. Gavrilenko, S. S. Smola, M. Frasso, S. C. Cazorla, K. Perera, A. Shi, H. G. Ranjbar, C. Smith, A. Deac, Y. Liu, S. M. McGee, V. P. Dotsenko, M. U. Kumke, K. Müller-Buschbaum, E. Rentschler, A. W. Addison and V. V. Pavlishchuk, *Dalton Trans.*, 2020, **49**, 7774-7789.

37. F. Han, J. Zhang, W. Yi, Z. Zhang, J. Yu, L. Weng and X. Zhou, *Inorg. Chem.*, 2010, **49**, 2793-2798.

38. W. Yi, J. Zhang, F. Zhang, Y. Zhang, Z. Chen and X. Zhou, *Chem. Eur. J.*, 2013, **19**, 11975-11983.

39. F. Zhang, J. Zhang and X. Zhou, *Inorg. Chem.*, 2017, **56**, 2070-2077.

40. F. Zhang, W. Yi, J. Zhang, Q. You, L. Weng and X. Zhou, *Dalton Trans.*, 2019, **48**, 10596-10603.

41. A. Dei, D. Gatteschi, J. Pécaut, S. Poussereau, L. Sorace and K. Vostrikova, *C. R. Acad. Sci. IIC*, 2001, **4**, 135-141.

42. M. A. Dunstan, E. Rousset, M.-E. Boulon, R. W. Gable, L. Sorace and C. Boskovic, *Dalton Trans.*, 2017, **46**, 13756-13767.

43. W. R. Reed, M. A. Dunstan, R. W. Gable, W. Phonsri, K. S. Murray, R. A. Mole and C. Boskovic, *Dalton Trans.*, 2019, **48**, 15635-15645.

44. A. Caneschi, A. Dei, D. Gatteschi, S. Poussereau and L. Sorace, *Dalton Trans.*, 2004, 1048-1055.

45. A. Caneschi, A. Dei, D. Gatteschi, L. Sorace and K. Vostrikova, *Angew. Chem. Int. Ed.*, 2000, **39**, 246-248.

46. P. Zhang, M. Perfetti, M. Kern, P. P. Hallmen, L. Ungur, S. Lenz, M. R. Ringenberg, W. Frey, H. Stoll, G. Rauhut and J. van Slageren, *Chem. Sci.*, 2018, **9**, 1221-1230.

47. F. Ortu, H. Zhu, M.-E. Boulon and D. P. Mills, *Inorganics*, 2015, **3**.

48. K. Binnemans, in *Handbook on the Physics and Chemistry of Rare Earths*, eds. K. A. Schneider, J.-C. Bunzli and V. K. Pecharsky, Elsevier, 2005, vol. 35, ch. 225, pp. 107-272.

6 Synthesis of pd-bridged lanthanide heterobimetallic compounds

6.1 Abstract

A series of heteroleptic transmetallation reagents using the *tris*-pyrazolyl borate ligand $Ln(Tp)_2(OTf)$ **7-Ln** (Ln = Y, Eu, Gd, Yb) were synthesised and fully characterised by multinuclear NMR, UV-vis, photoluminescence and ATR-IR spectroscopies. Solid-state molecular structures of **7-Ln** (Ln = Y, Eu, Yb) have been determined. Both **7-Y** and **7-Eu** exhibited a dimeric structure, bridged by triflate anions. For **7-Yb**, a monomeric THF solvate was observed. The reactivity of **7-Ln** was investigated with the goal of synthesising heterobimetallic lanthanide compounds.

The reaction of **7-Ln** with $[CoCp_2]^+[Ln(hfac)_3(pd)]^{-\bullet}$ **5-Ln** was investigated. In each case, a rapid colour change from the dark green of **5-Ln** to dark red was observed. UV-visible, EPR and ATR-IR spectroscopy of the products obtained were consistent with radical, *O,O'*-coordinated pd. The major product observed by NMR was the ligand redistribution product $Y(Tp)_2(hfac)$, which was obtained from several crystallisations. On two occasions, small, poorly-diffracting red crystals of a supramolecular square compound $\{Ln(hfac)_2(N,N'\text{-}O,O'\text{-pd})\}_4$ were obtained. It is proposed that the reaction produces a mixture of $Ln(Tp)_2(hfac)$ and $\{Ln(hfac)_2(N,N'\text{-}O,O'\text{-pd})\}_4$. Notably, in reactions of **5-Eu** with **7-Yb** and **5-Yb** with **7-Eu**, NMR analysis of the reaction mixtures showed a mixture of both $Eu(Tp)_2(hfac)$ and $Yb(Tp)_2(hfac)$.

A different synthesis was required due to the ligand redistribution. Prior coordination of the lanthanide to pd might reduce this, so **7-Ln** (Ln = Y, Eu, Yb) was reacted with **3** $[CoCp_2]^+[pd]^{-\bullet}$. Electronic absorption spectroscopy of the products indicates that the lanthanide coordinated differently to the radical ligand in the products than in *N,N'*-coordinated **5-Ln**, consistent with $Ln(Tp)_2(O,O'\text{-pd})$. In the case of $Yb(Tp)_2(O,O'\text{-pd})$, sensitisation of photoluminescence from Yb(III) *via* the *O,O'* coordinated radical ligand was observed, unlike in **5-Ln**. Multinuclear NMR spectroscopy of $Ln(Tp)_2(pd)$ was also consistent with *O,O'* coordination, though additionally showing that the metathesis byproduct $[CoCp_2]^+[OTf]^-$ was present in the products.

The heterobimetallic target was predicted to be more soluble and easier to isolate. Therefore, the reaction of **7-Ln** with **3** in toluene was immediately followed by addition of **4-Ln**. Electronic absorption spectroscopy was consistent with *O,O'* coordination of the lanthanide to the radical pd ligand. However, ligand redistribution continued to occur, and products included $Ln(Tp)_2(hfac)$. The reaction was performed at -35 °C and was quickly quenched, minimising redistribution. By this method, solid-state molecular structures were obtained of two

lanthanide heterobimetallic complexes, in which bond lengths were consistent with selective coordination of the lanthanides to the different coordination sites of the ligand. Additionally, the photoluminescent properties of the products were consistent with a selective and asymmetric coordination. The evidence indicates that the reaction of **7-Ln** with **3** and **4-Ln** results in selective synthesis of heterobimetallics, but that ligand redistribution then results in redistribution.

6.2 Synthesis of 7-Ln Ln(Tp)$_2$(OTf)

6.2.1 Literature precedent and synthesis

The previous chapter described attempts to use the lanthanide scorpionate compounds Ln(Tp*)$_2$(OTf) (Tp* = hydrotris-3,5-dimethyl pyrazolyl borate; Ln = Y, Ce) to synthesise lanthanide bimetallics. However, the reactions of Ln(Tp*)$_2$(OTf) with **5-Ln** resulted in uncontrolled ligand redistribution reactions, likely due to the sterics of the supporting ligand environment. The non-methylated scorpionate ligand Tp (Tp = tris-pyrazolyl borate) has been used to synthesise a variety of lanthanide compounds with chelating O-donor ligands.[1-3] The synthesis of metathesis reagents Ln(Tp)$_2$(OTf) **7-Ln** was therefore targeted from the Ln(OTf)$_3$ starting materials. Ln(Tp)$_2$Cl(H$_2$O) (Ln = Y, La, Nd) have been structurally characterised,[4, 5] and the anhydrous compounds Ln(Tp)$_2$(Cl)(Hpz) (Ln = Y, Nd, Sm; Hpz = pyrazole) have also been synthesised.[6, 7] However, these are the only examples of lanthanide *bis*-Tp compounds with an X-type leaving group deposited in the Cambridge Crystallographic Data Centre (CCDC). To the best of our knowledge no anhydrous lanthanide *bis*-Tp triflate metathesis reagent has been previously synthesised and structurally characterised. By modifying the synthesis of Sella's group for Ln(Tp*)$_2$(OTf),[8] the new class of compounds **7-Ln** (Ln = Y, Eu, Gd, Yb) was synthesised by reaction of Ln(OTf)$_3$ with K(Tp), as shown in Scheme 6.1.

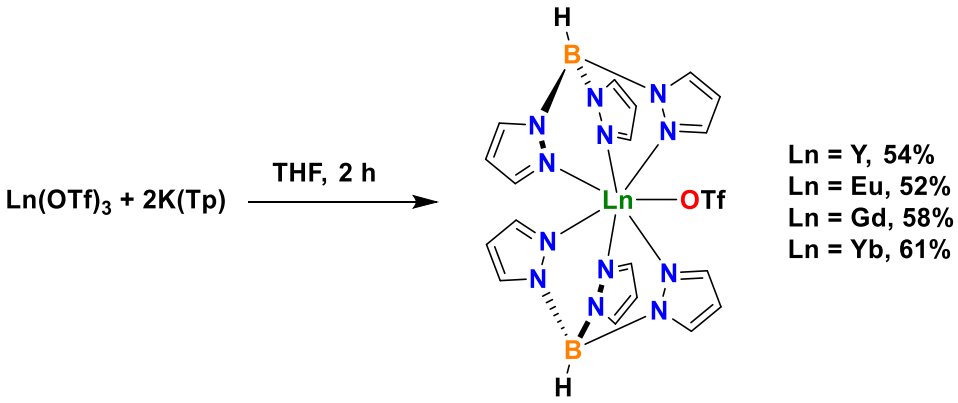

Scheme 6.1: The synthesis of the heteroleptic transmetallation reagents 7-Ln

In a typical preparation, Ln(OTf)$_3$ was stirred with 2 eq. K(Tp) in THF for two hours. THF was then removed *in vacuo* to obtain a white powder, and the product was then extracted into DCM. Stirring the solid in DCM for only minutes in order to extract the product resulted in low yields (ca. 30%). In order to obtain a satisfactory yield, it was necessary to either stir the DCM suspension for up to 15 hours, or to sonicate the reaction mixture for 10 minutes. The

suspension was then filtered slowly *via* filter cannula (a fine suspension was liable to clog the filter), and the solids were extracted twice more with DCM, combining the filtrates. DCM was removed *in vacuo* from the filtrate and the resulting white solid was washed with hexane and dried *in vacuo* to obtain **7-Ln** as analytically pure white solids in good yields.

6.2.2 NMR spectroscopy of 7-Ln

The compounds **7-Ln** were characterised by ^{1}H, ^{19}F and ^{11}B NMR spectroscopy. The ^{1}H NMR spectrum of **7-Y** as recorded in d_3-MeCN, shown in Figure 6.1, exhibits four resonances at δ = 4.72 (2H, br), 6.11 (6H, t, 2.2 Hz), 7.15 (6H, d, 2.1 Hz) and 7.80 (6H, dd, 2.2, 0.7 Hz) ppm. The resonance at δ = 4.72 ppm is assigned to the B-**H** group, and the broad shape is consistent with bonding to the quadrupolar ^{11}B nucleus. The resonances at δ = 6.11, 7.15 and 7.80 ppm are assigned to the three pz-**H**. Both the chemical shifts and the splitting patterns observed are consistent with this assignment and are similar to those in the KTp (δ = 6.06, 7.43, 7.53 ppm in d_3-MeCN). A single resonance is observed in the ^{19}F NMR of **7-Y** as recorded in d_3-MeCN at δ = -79.15 ppm (Figure 6.2), assigned to the OTf-C**F**$_3$ group. This is consistent with other examples of yttrium triflates discussed in this thesis. A single resonance is observed in the ^{11}B NMR at δ = -3.15 (d) ppm (Figure 6.3). This is assigned to the Tp-**B**, as it falls in the region expected for a four-coordinate borate anion such as Tp, and the doublet splitting pattern is consistent with coupling to the B-**H** proton. This signal is observed as a singlet in the ^{11}B{^{1}H} NMR spectrum.

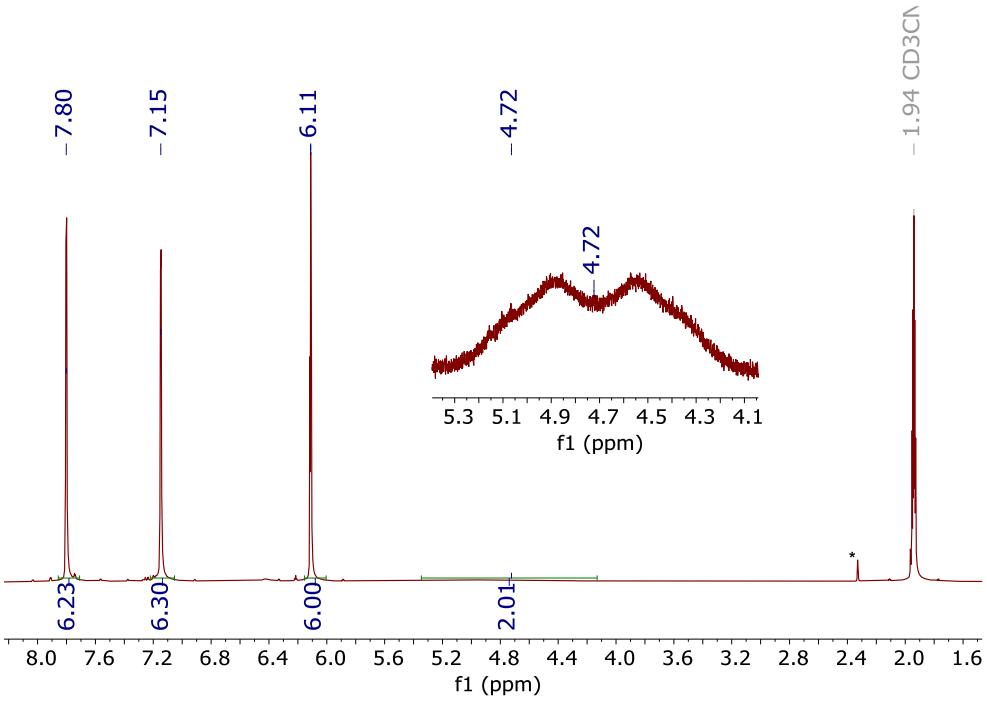

Figure 6.1: ^{1}H NMR spectrum of 7-Y, recorded in d_3-MeCN. The inset shows a zoomed-in view of the broad resonance at δ = 4.72 ppm. Resonances due to a small quantity of adventitious toluene solvent are denoted by *.

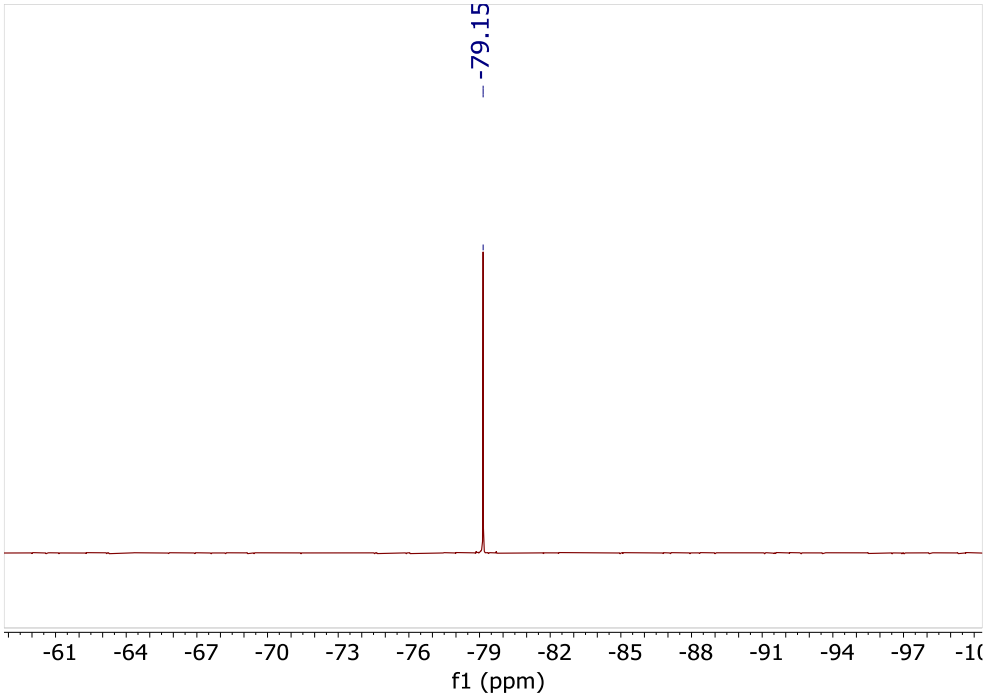

Figure 6.2: The ^{19}F NMR spectrum of 7-Y, recorded in d_3-MeCN.

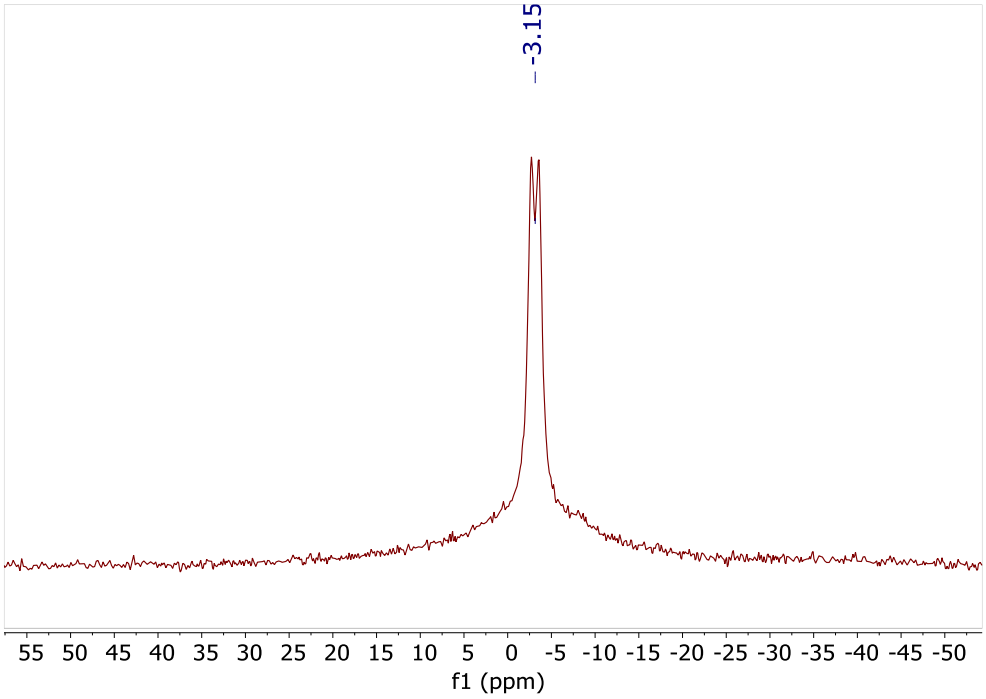

Figure 6.3: The ^{11}B NMR spectrum of 7-Y, recorded in d_3-MeCN.

As has been shown in previous chapters, NMR can be used for the analysis of compounds containing paramagnetic lanthanides. The ^{1}H NMR spectrum of **7-Eu** was recorded in d_3-MeCN solution, shown in Figure 6.4. The spectrum shows four resonances at δ = -1.71 (2H, br), 0.40 (6H, s), 3.02 (6H, s) and 14.05 (6H, s) ppm. The resonance at δ = -1.71 ppm is assigned to the B-**H** group by relative integration and by its broad profile. The resonances at δ = 0.40, 3.02 and 14.05 ppm are assigned to the pz-**H** groups. Each of these resonances experiences a paramagnetic shift from that observed for **7-Y**, consistent with the presence of 4f^6 Eu(III), as is the loss of any multiplicity. In the ^{19}F NMR spectrum of **7-Eu** recorded in the same solution (Figure 6.5), a single resonance is observed at δ = -80.86 ppm. This resonance is assigned to the OTf-C**F**$_3$ group. Likewise, a single resonance is observed in the ^{11}B NMR spectrum as δ = -22.29 ppm, consistent with a Tp ligand paramagnetically shifted by proximity to Eu(III).

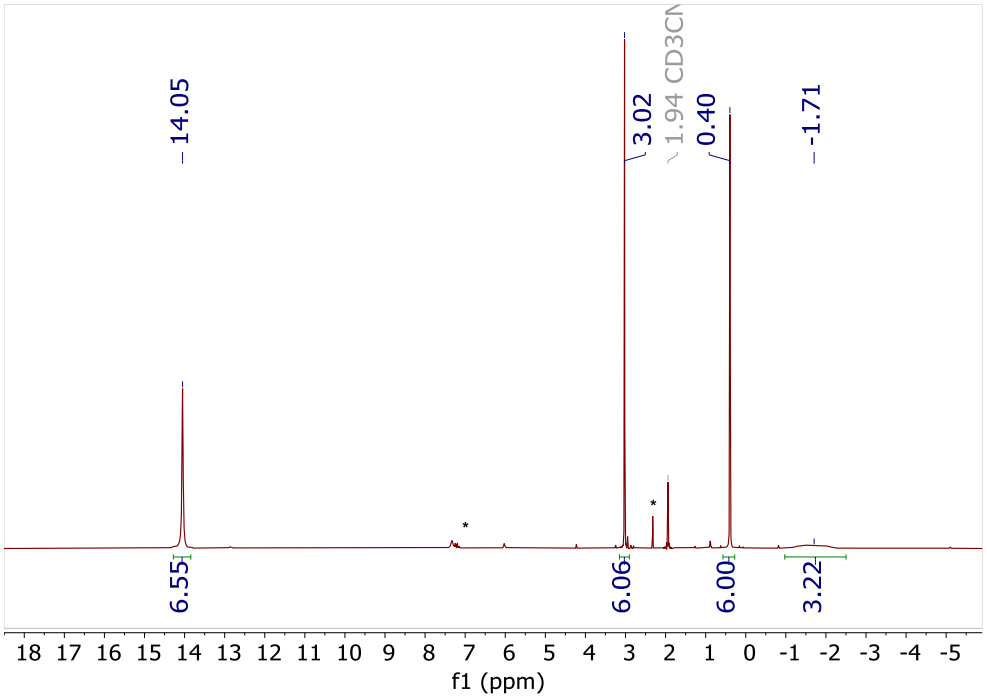

Figure 6.4: The ^{1}H NMR spectrum of 7-Eu, recorded in d_3-MeCN. Resonances due to small quantities of adventitious toluene solvent are denoted by *.

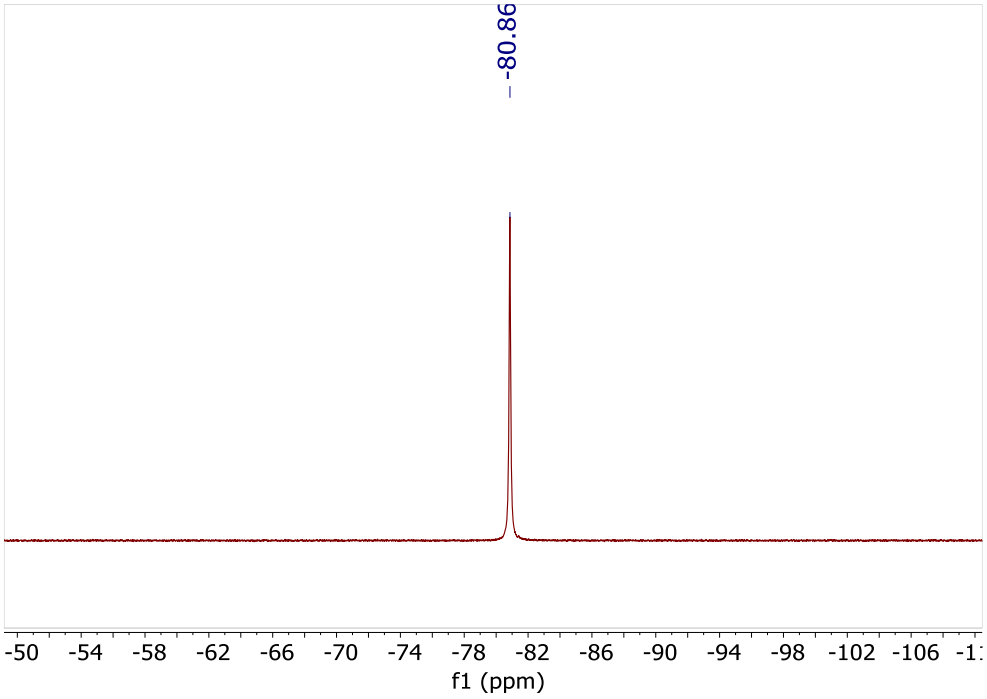

Figure 6.5: The ^{19}F NMR spectrum of 7-Eu, recorded in d_3-MeCN.

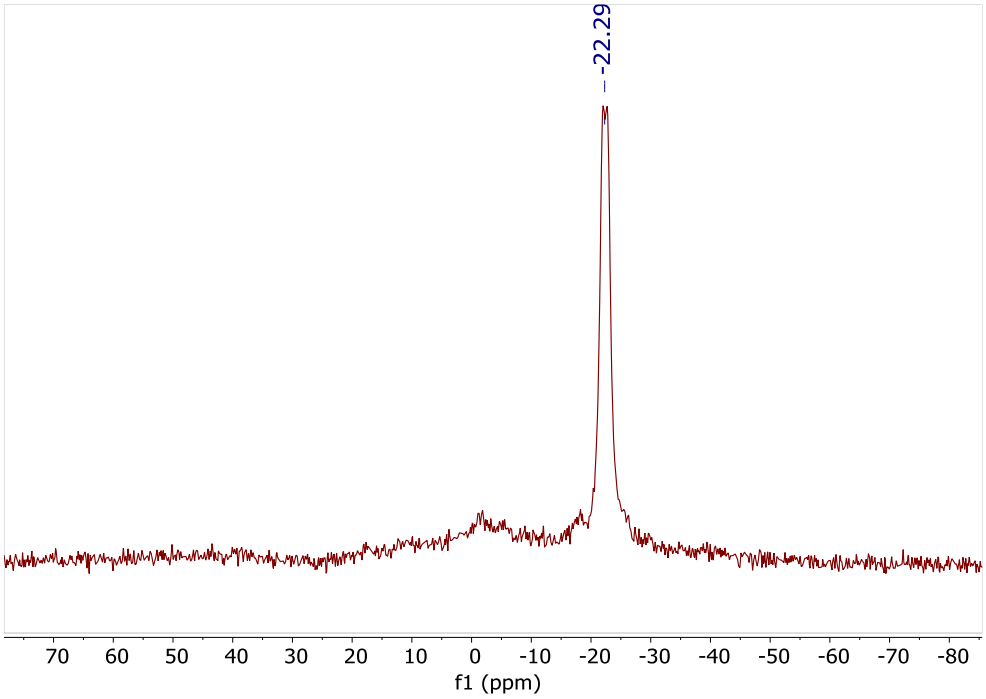

Figure 6.6: The ^{11}B NMR spectrum of 7-Eu, recorded in d_3-MeCN.

The ^{1}H NMR spectrum of **7-Yb** was recorded in d_3-MeCN, shown in Figure 6.7. The spectrum displays four resonances at δ = -22.25 (2H, br), -4.89 (6H, br, s), 6.25 (6H, s), 39.06 (6H, br, s) ppm. The resonance at δ = -22.25 ppm is assigned to the B-**H** group, while the resonances at δ = -4.89, 6.25 and 39.06 ppm are assigned to the pz-**H** groups. The spectral window (a total of 61.31 ppm) is wider than that observed for **7-Eu** in the same solvent (a total of 15.76 ppm), consistent with **1-Ln**, **4-Ln** and **5-Ln** (See Chapters 2 and 3). The ^{19}F NMR spectrum of **7-Yb**, recorded in d_3-MeCN (Figure 6.8) shows a single resonance at δ = -81.37 ppm, assigned to the OTf-C**F**$_3$ group. The ^{11}B NMR spectrum as recorded in d_3-MeCN (Figure 6.9) also shows a single resonance at δ = -68.12 ppm, assigned to the Tp-**B**.

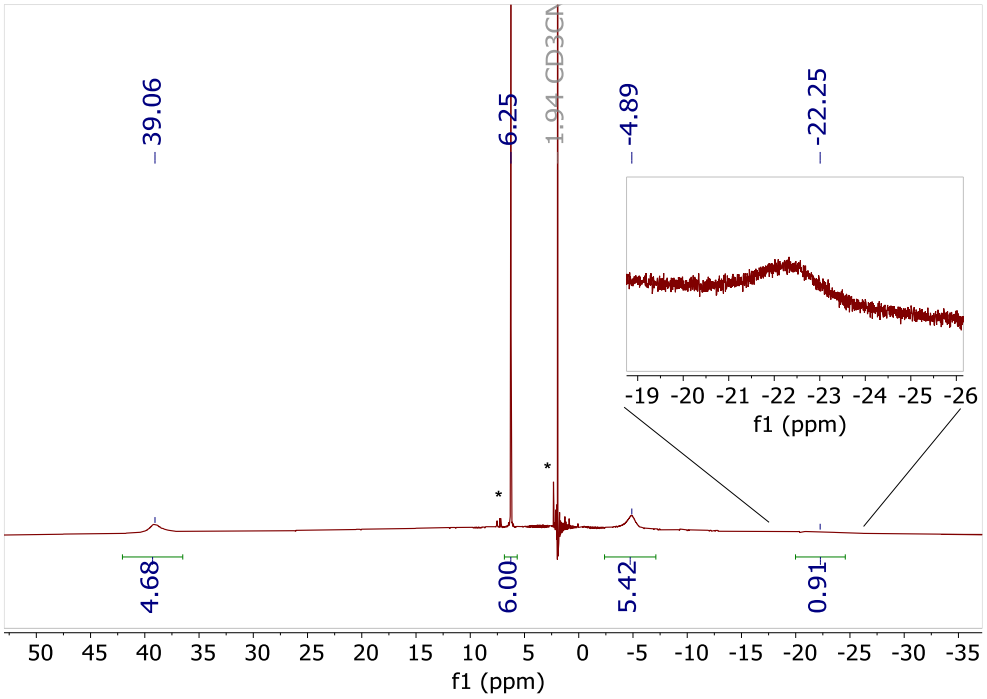

Figure 6.7: The ^{1}H NMR spectrum of 7-Yb, recorded in d_3-MeCN. The inset shows a clearer view of the resonance at δ = -22.25 ppm. Resonances due to a small amount of toluene are denoted by *.

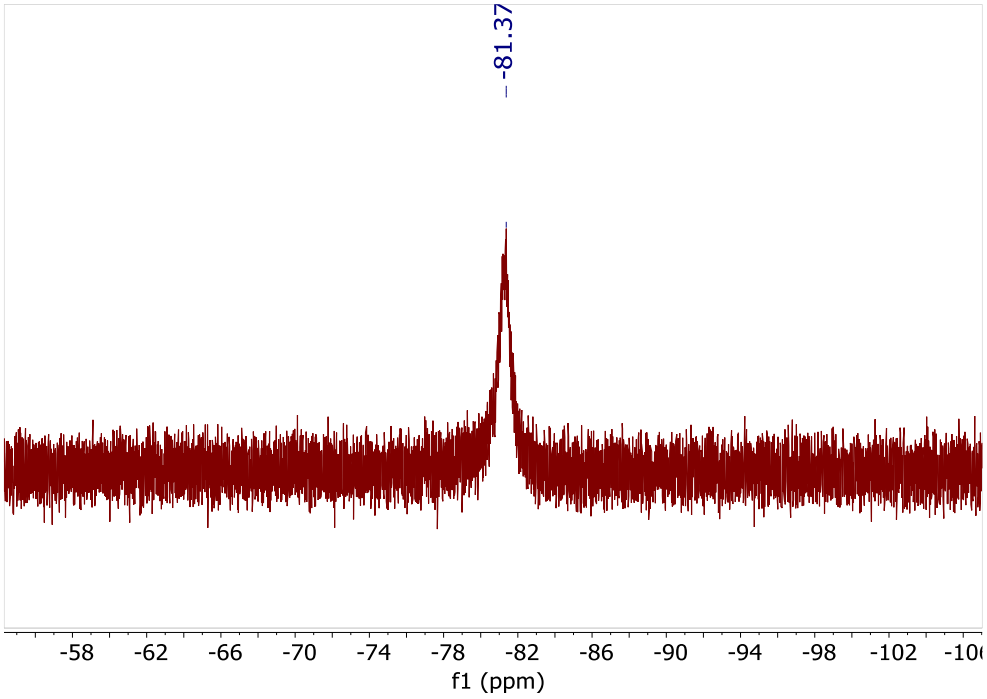

Figure 6.8: The ^{19}F NMR spectrum of 7-Yb, recorded in d_3-MeCN.

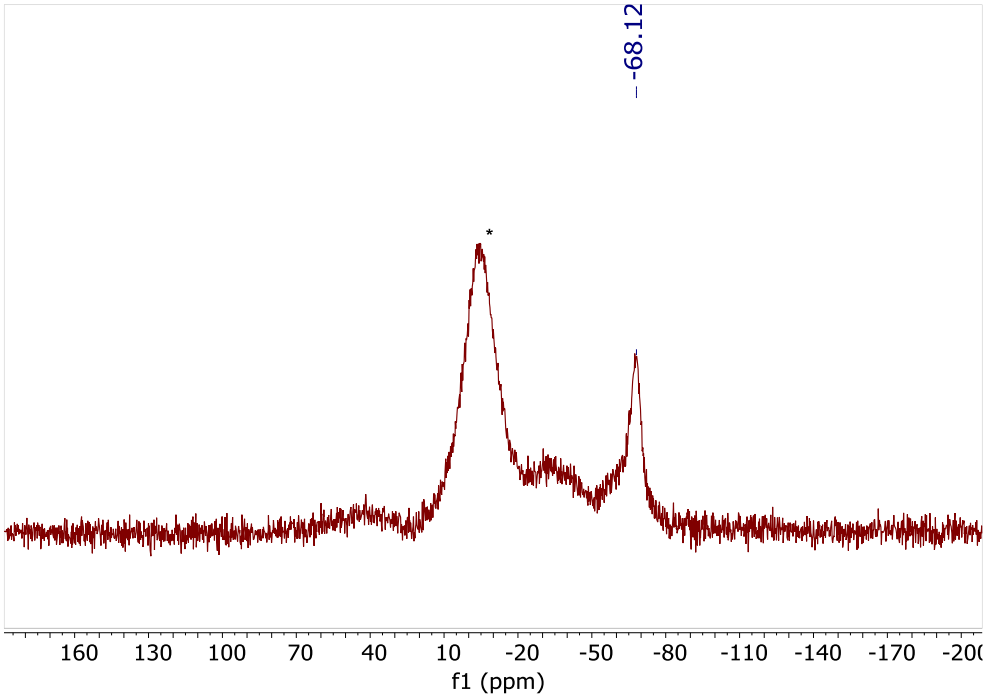

Figure 6.9: The ^{11}B NMR spectrum of 7-Yb, recorded in d_3-MeCN. A resonance due to the ^{11}B present in the borosilicate glass of the NMR tube is denoted by *.

No resonances were observed in the ^{1}H, ^{19}F or ^{11}B NMR spectra of **7-Gd** due to the extremely rapid relaxation caused by the presence of isotropic Gd(III).[9] However, the magnetic moment of **7-Gd** was calculated *via* the Evans' Method to be 7.89-8.21 μ_B, consistent with the expected μ_{SO} value for Gd(III) of 7.94 μ_B. For comparison, in **1-Gd** μ_{eff} = 7.56-7.71.[10]

6.2.3 ATR-IR spectroscopy of 7-Ln

The ATR-IR spectra of **7-Ln** (Ln = Y, Eu, Gd, Yb) were recorded, and are shown in Figure 6.10. In each case, very similar absorptions are seen, and the spectra are nearly superimposable, indicating that the solid-state molecular structures of **7-Ln** are similar. The two absorptions at 2500 and 2350 cm^{-1} are characteristic of *tris*-substituted borohydrides, and are assigned to the B-H stretching frequencies.[4, 5] The resonance observed at 1500 cm^{-1} is assigned to the S=O stretching frequency, being similar to that observed in the similar bridged triflate compound Y(Cp*)$_2$(μ-OTf)].[11]

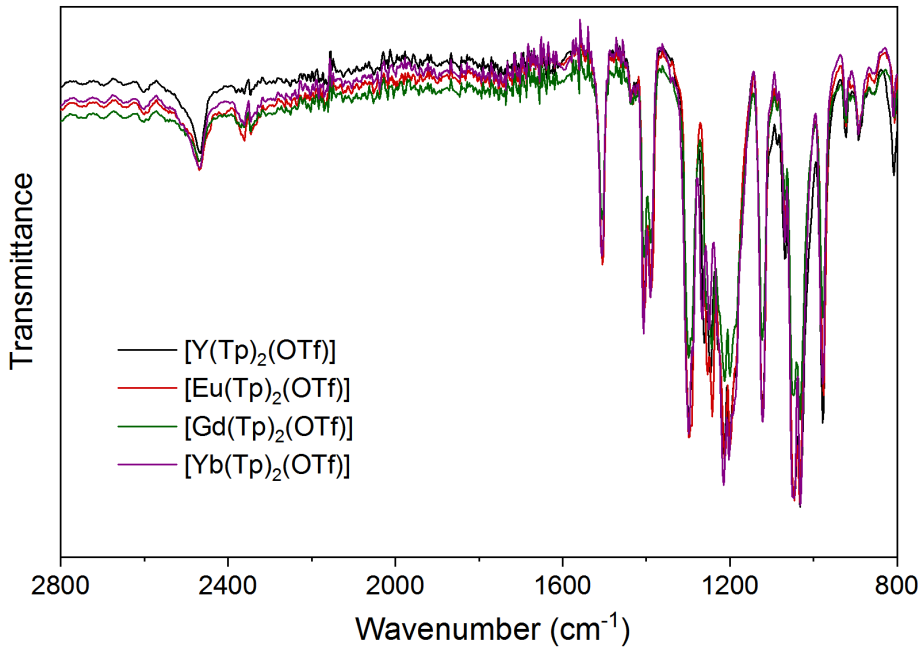

Figure 6.10: The ATR-IR spectra of 7-Ln (Ln = Y, Eu, Gd, Yb), recorded at 298 K.

6.2.4 UV-vis-NIR and photoluminescence spectroscopy of 7-Ln

The electronic absorption spectrum of **7-Eu** was recorded in THF due to very low solubility in MeCN solution, and is shown in Figure 6.11. The concentration of the solution was low due to low solubility, and therefore an absorption at 287 nm is assigned to small quantities of BHT stabiliser in the THF solvent. A low-intensity, narrow absorption is observed with λ_{max} = 394 nm and an extinction coefficient of ε = 6.6 M^{-1} cm^{-1}, consistent with a laporte-forbidden *f-f* transition. This transition is assigned to the $^5L_6 \leftarrow {}^7F_0$ transition of Eu(III), frequently the most intensely absorbing *f-f* transition of Eu(III).[12]

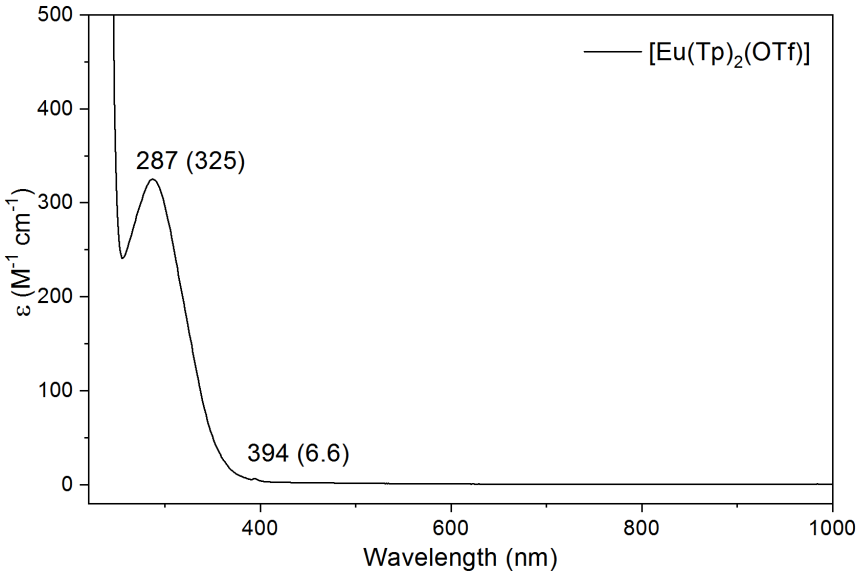

Figure 6.11: Electronic spectrum of 7-Eu, recorded in THF at 298 K on a 2.8 mM solution.

The electronic absorption spectrum of **7-Yb** was recorded in both MeCN and in THF, shown in Figure 6.12. No transition maxima are observed in the UV region in either spectrum. However, a transition is observed in both spectra in the NIR region with λ_{max} = 974 nm (ε = 4.5 M^{-1} cm^{-1}) in MeCN solution, and λ_{max} = 973 nm (ε = 5.9 M^{-1} cm^{-1}) in THF solution. This is a narrow transition whose extinction coefficient is consistent with a laporte-forbidden *f-f* transition, and is assigned to the $^2F_{5/2} \leftarrow {}^2F_{7/2}$ *f-f* transition of Yb(III).

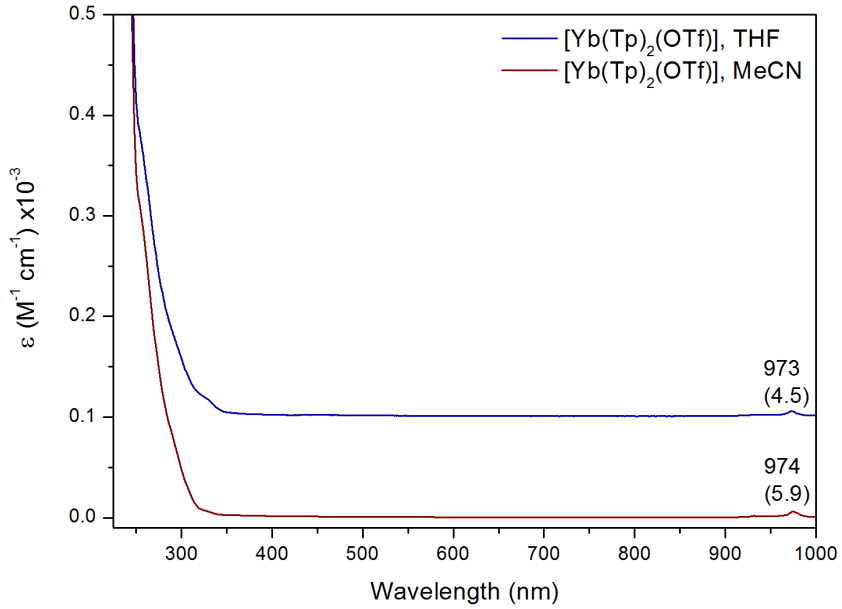

Figure 6.12: Electronic spectrum of 7-Yb, recorded in MeCN (bottom, red) on a 2.7 mM solution and in THF (top, blue) on a 28 mM solution at 298 K. The spectrum as recorded in THF has been offset by 100 M^{-1} cm^{-1} for clarity.

6.2.5 Photoluminescence spectroscopy of 7-Ln

By excitation of a solution of **7-Eu** in THF by UV light, emission was observed from Eu(III), and the excitation and emission spectra are shown in Figure 6.13. The excitation spectrum was recorded by monitoring emission at 612 nm, and shows a maximum at 320 nm, assigned to excitation by energy transfer from the Tp ligand. The emission spectrum was recorded of the complex at various different excitation wavelengths, and these were normalised to the intensity of the $^5D_0 \rightarrow {}^7F_1$ transition (590 nm). Significant variations are observed between these emission profiles, particularly in the intensity of the $^5D_0 \rightarrow {}^7F_2$ transition (612 nm). This is typically due to a change in the coordination environment and symmetry of Eu(III), as this transition is known as a hypersensitive transition.[12] The ratio of the integration of the $^5D_0 \rightarrow {}^7F_1$ (590 nm) and $^5D_0 \rightarrow {}^7F_2$ (612 nm) transitions is often used as a measure of the hypersensitive transition. In **7-Eu** the ratio of those transitions varies from 1:2 for λ_{Ex} = 260 nm to 1:4.5 when λ_{Ex} = 320 nm. In THF solution, it is to be expected that the dimer observed in the solid state will be broken up, and the triflate ligands are somewhat labile. The variations are therefore assigned to dynamic effects in solution.

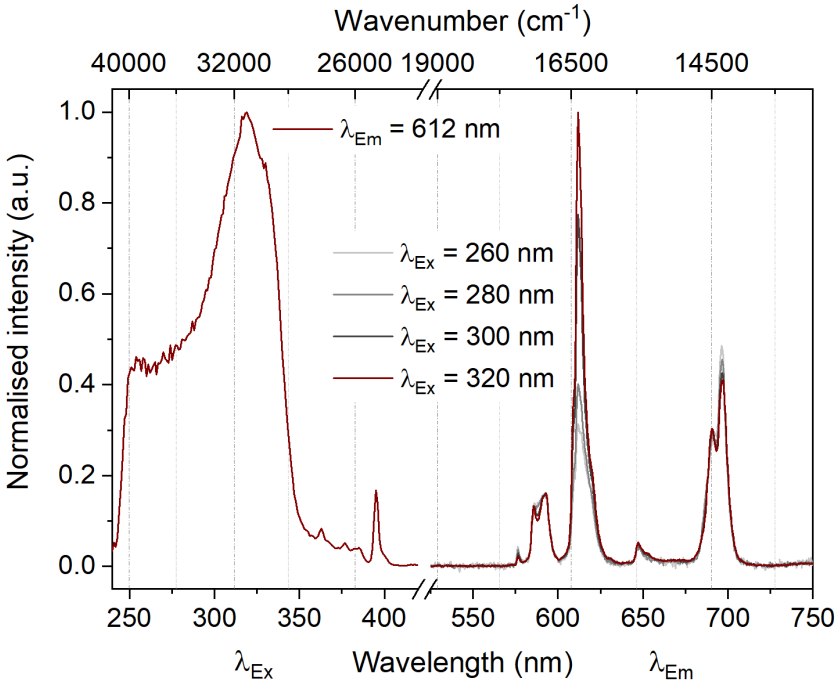

Figure 6.13: Excitation and emission spectra of 7-Eu, recorded in THF at R.T. on a 2.8 mM solution, normalised to the intensity of the $^5D_0 \rightarrow {}^7F_1$ transition (595 nm). The excitation spectrum was recorded based on the $^5D_0 \rightarrow {}^7F_2$ transition (612 nm).

The excitation and emission spectra of **7-Yb** were also recorded, and are shown in Figure 6.15. The excitation spectrum has λ_{max} = 270 nm, assigned to excitation and energy transfer from the Tp ligands. It is of note that there is a large energy gap from the Tp ligand excited states to the Yb(III) excited states (*ca* 27,000 cm^{-1}). The emission spectrum was recorded at a range of excitation wavelengths between 260 nm and 300 nm, and in each case the emission spectrum obtained was identical. The emission spectra show a single maximum at 975 nm, assigned to the $^2F_{7/2} \rightarrow {}^2F_{5/2}$ *f-f* transition of Yb(III). Otherwise, the spectrum has a broad profile with a shoulder at 1020 nm, resulting from relaxation from the $^2F_{7/2}$ excited state to the vibrational excited states of the $^2F_{5/2}$ ground state. This is different from the emission spectra of **1-Yb**, **4-Yb** and **5-Yb**, each of which exhibited three maxima, and from **6-Yb** which exhibited four maxima in the NIR region.

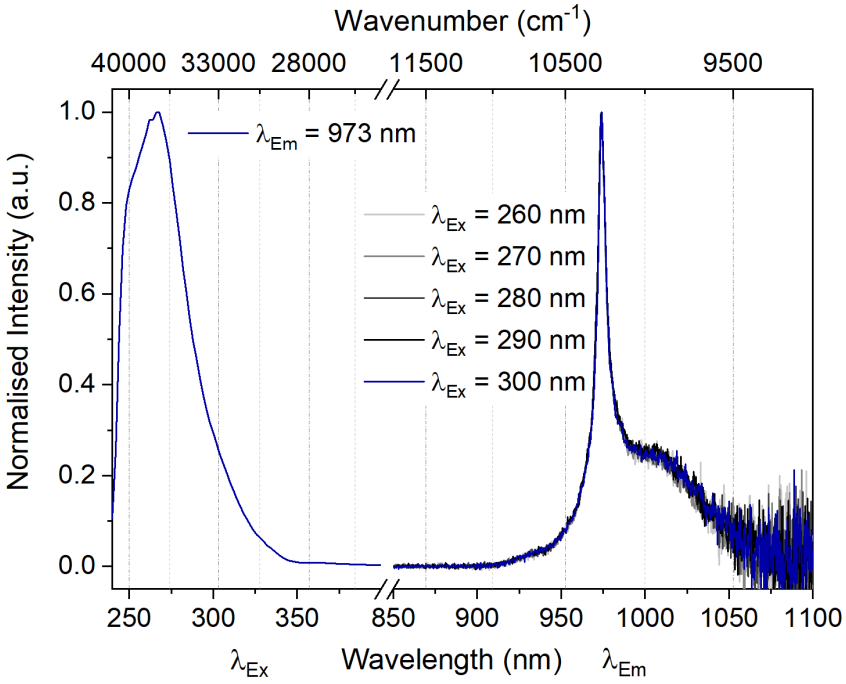

Figure 6.14: Excitation and emission spectra of 7-Yb, recorded in THF at 298 K on a 2.7 mM solution.

6.2.6 Crystallography of 7-Ln

Small, blocky crystals of **7-Y** suitable for X-ray diffraction were obtained by diffusion of a hexane layer into a near-saturated THF solution at -35 °C over several days. The unit cell contains two crystallographically independent dimeric units, each containing two Y ions bridged by two triflate anions, where two oxygen atoms each coordinate to one metal. One of these dimeric units is shown in Figure 6.15. This binding mode of the triflate anion has been observed in three other dimeric yttrium structures lodged in the Cambridge Crystallographic Data Centre (CCDC), two of which have cyclopentadienyl ligands.[11, 13, 14] The separation between the yttrium atoms in the dimers is 6.1678(4)–6.3316(4) Å, comparable to that observed in $\{Y(Cp^*)_2(\mu\text{-OTf})\}_2$ of 6.0298(4) Å and $\{Y(\mu\text{-OTf})(dmcp)\}_2$ (dmcp = 2,6-dimethylcyclopentadienyl pyridine) of 6.103(1) Å.[11, 13] The Y-O(OTf) bonds are likewise similar to literature compounds, falling in the range 2.371(2)–2.435(2) Å. The Y-N(Tp) bond lengths are of the range 2.402(2)–2.540(2) Å, again consistent with literature compounds containing the yttrium *bis*-Tp unit.[2-4, 6]

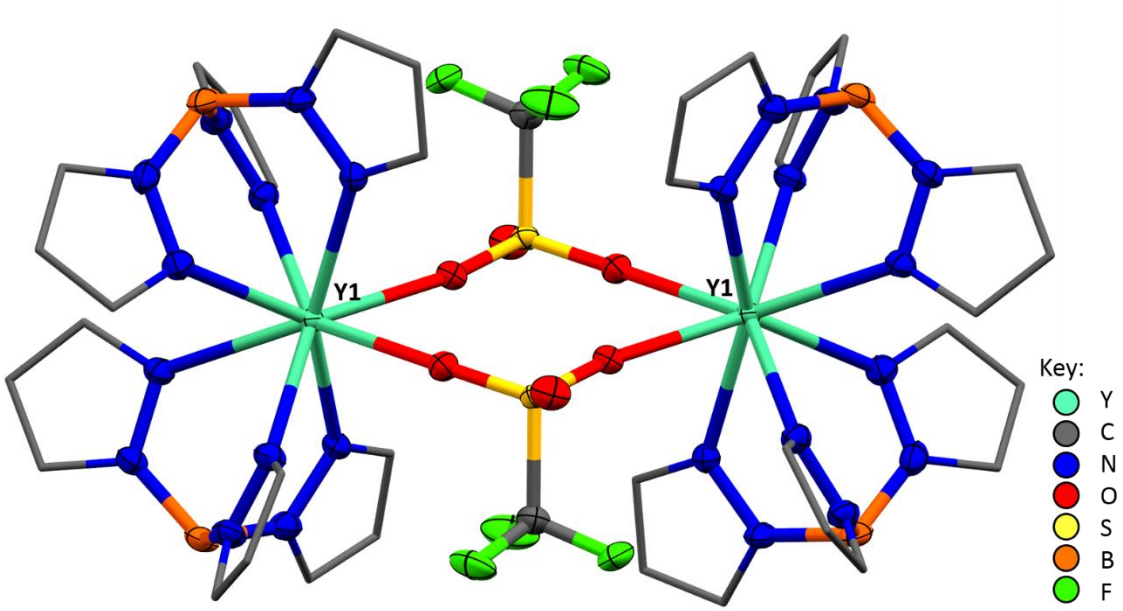

Figure 6.15: The dimeric solid-state molecular structure of 7-Y, showing the $\{Y(Tp)_2(\mu\text{-OTf})\}_2$ dimer. One of two crystallographically independent dimers is shown. C atoms of the pyrazolyl rings on Tp are shown in wireframe and H atoms are omitted for clarity. Thermal ellipsoids are shown at 50% probability. Selected distances (Å): Y-Y, 6.1678(4)-6.3316(4); Y-N, 2.402(2)-2.540(2); Y-O, 2.371(2)-2.435(2).

Similarly, the slow diffusion of a hexane layer into a concentrated THF solution of **7-Eu** afforded blocky, colourless crystals suitable for X-ray diffraction. The solid-state molecular structure was found to be identical to that of $\{Y(Tp)_2(\mu\text{-}OTf)\}_2$, again with two crystallographically independent dimeric units in the unit cell, shown in Figure 6.16. In comparison to the bonds in the solid-state molecular structure of **7-Y**, all Eu-heteroatom bonds are slightly longer, consistent with the larger ionic radius of Eu(III) (1.066 Å) vs. Y(III) (1.019 Å).[15] The distance between Eu atoms in the dimers is 6.1875(4) to 6.3705(4) Å, similar to that between Y atoms in the structural analogue **7-Y**. However, the Eu-Eu distance is significantly longer than that in the only other Eu compound in the CCDC with the same triflate binding mode, an octanuclear Eu cluster with a mixture of bridging oxo and triflate ligands.[16] This is due to the bonding of the Tp ligand, which is relatively linear in **7-Eu**. In the octanuclear cluster the Eu-S-Eu angle is significantly more acute. The Eu-O(OTf) bonds are between 2.425(2) and 2.467(3) Å, which are consistent with those in the triflate bridged Eu cluster, while the Eu-N(Tp) bonds are between 2.452(4) and 2.573(3) Å long, consistent with other Eu(III) complexes of Tp.[17]

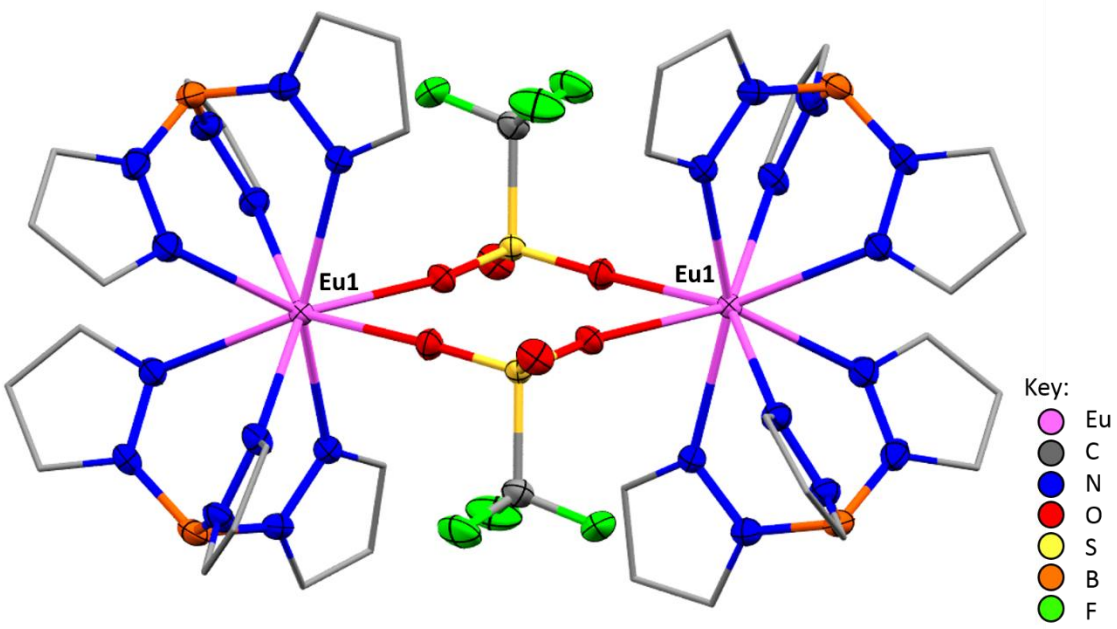

Figure 6.16: The dimeric solid-state molecular structure of 7-Eu, showing the $\{Eu(Tp)_2(\mu\text{-}OTf)\}_2$ dimer. One of two crystallographically independent dimeric units is shown. C atoms of the Tp ligand are shown in wireframe, and H atoms are omitted for clarity. Thermal ellipsoids are shown at 50% probability. Selected distances: Eu-Eu, 6.1875(4)-6.3705(4); Eu-O, 2.425(2)-2.467(3); Eu-N, 2.452(4)-2.573(3) Å.

Single crystals of **7-Yb** suitable for X-ray diffraction were obtained by the slow diffusion of hexane into a concentrated THF solution. The solid-state molecular structure thus obtained is of a monomeric unit of $Yb(Tp)_2(OTf)(THF)$, in contrast to the dimeric bridged structures obtained for **7-Y** and **7-Eu**. The monomeric solid-state structure of **7-Yb** is distinct from the dimeric structures of **7-Y** and **7-Eu** due to the significantly smaller ionic radius of Yb(III) (0.988 Å) compared to Y(III) (1.016 Å) and Eu(III) (1.066 Å).[15] The Yb-N(Tp) bond distances are in the range 2.365(6)-2.489(6) Å, consistent with those in the similar complex $Yb(Tp)_2(NO_3)$, where the Yb-N(Tp) bond distances are in the range 2.353(2)-2.452(2).[18]

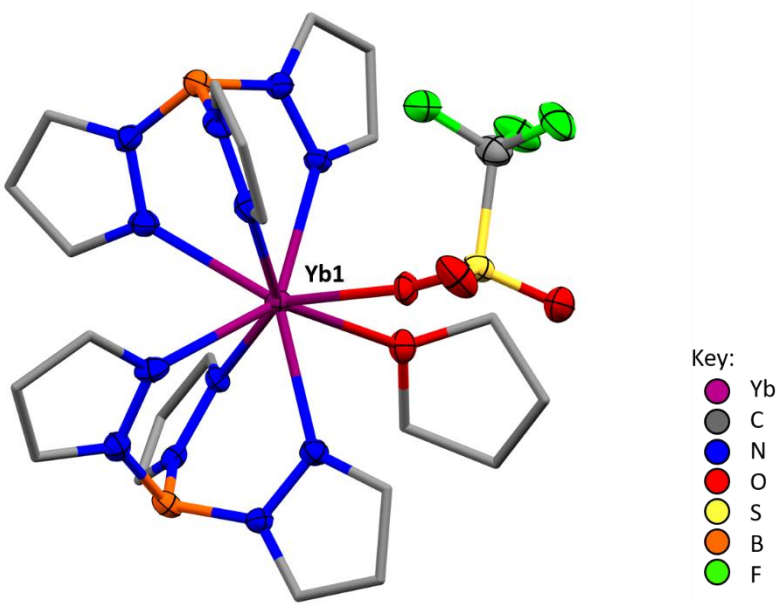

Figure 6.17: The solid-state molecular structure of 7-Yb. C atoms of the Tp and THF ligand are shown in wireframe, and H atoms are omitted for clarity. Thermal ellipsoids are shown at 50% probability. Selected distances: Yb-N 2.365(6)-2.489(6), Yb-O(OTf) 2.296(5), Yb-O(THF) 2.582(5) Å.

6.3 Reaction of $[CoCp_2]^+[Ln(hfac)_3(pd)]^{-\bullet}$ 5-Ln with 7-Ln

Ligand redistribution has been shown to be a significant issue in the reaction of $Ln(Tp^*)_2(OTf)$ with **5-Ln**. However, the less sterically encumbering **7-Ln** might limit the propensity for redistribution by reducing steric strain on the products. It was therefore important to carry out control reactions to investigate this. However, they will not be discussed fully here for brevity, and only the key findings will be presented. Reactions of **7-Ln** (Ln = Y, Yb) were investigated, and in coordinating solvents the product mixture was found to contain an organic radical, indicating that a redox process had occurred. However, in the NMR spectra of the product mixtures, the most significant resonances were assigned to the starting material. No other products of the reaction of **7-Ln** with pd could be assigned based on the data obtained. Reactions of **7-Y** with **1-Y** meanwhile resulted in ligand redistribution and formation of $Y(Tp)_2(hfac)$. Other products of the reaction were not assignable based on the NMR, UV-vis and ATR-IR data collected. It was however clear from colour changes observed during the reaction of **7-Y** with **1-Y** that some changes in the coordination and/or oxidation state of the pd ligand occurred. The reaction of **7-Y** with **1-Y** was observed to be slow, possibly resulting in greater quantities of side-products being obtained. With a driving force such as the formation of an insoluble salt a faster reaction might be expected to reduce side-products somewhat. The reaction of **5-Ln** with **7-Ln** was therefore investigated with the goal of forming a bimetallic bridged species as shown in Scheme 6.2.

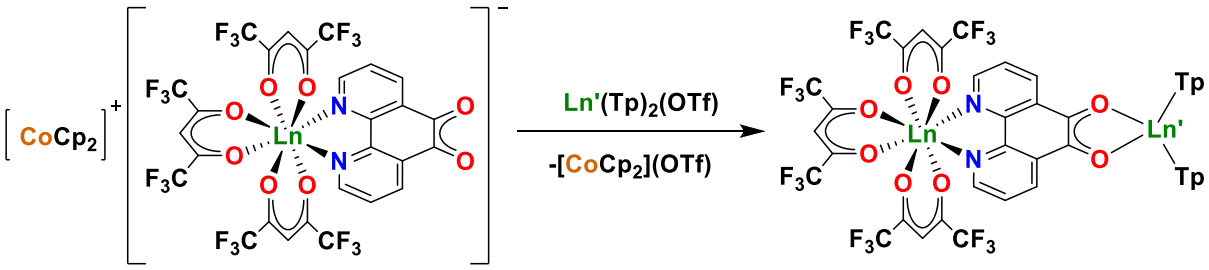

Scheme 6.2: The reaction of 5-Ln with 7-Ln targeting the synthesis of a bimetallic species.

Multiple reactions were carried out, both on an NMR experiment scale and on a slightly larger scale to obtain sufficient material for crystallisations and other characterisation methods. Only a sample of the reactions performed, and selected data will be discussed here for clarity and brevity.

6.3.1 NMR-scale reaction of 7-Y with 5-Y

A Young's tap NMR tube was charged with **7-Ln** and **5-Y** in a 1:1 molar ratio, along with a known quantity of the NMR standard $Si(SiMe_3)_4$, and d_6-benzene was added. A colour change from green to red was observed upon mixing and the sample was sent for multinuclear NMR spectroscopy. Spectra were recorded at intervals from 15 m to 12 h following mixing. The predominant component of the mixture observable by ^{1}H NMR spectroscopy was a set of four resonances at δ = 5.75, 6.46, 7.12 and 7.39 ppm (Figure 6.18), which are assigned by comparison to work carried out by another member of the group to $Y(Tp)_2(hfac)$,[19, 20] the product of a ligand redistribution reaction. The resonances in the ^{19}F NMR spectrum (δ = -76.45 ppm, Figure 6.19) and ^{11}B NMR spectrum (δ = -2.93 ppm, Figure 6.20) are also consistent with $Y(Tp)_2(hfac)$. As $Y(Tp)_2(hfac)$ is diamagnetic, the percentage yield of this species could be determined by relative integration to the NMR standard. The reaction reached 85% conversion to $Y(Tp)_2(hfac)$ over the first 2 hours. As the error of the mass of the NMR standard was around 10%, this represents an essentially quantitative conversion. A number of other resonances observed in the ^{1}H NMR spectrum are of significantly lower intensity and were not assignable based on these data.

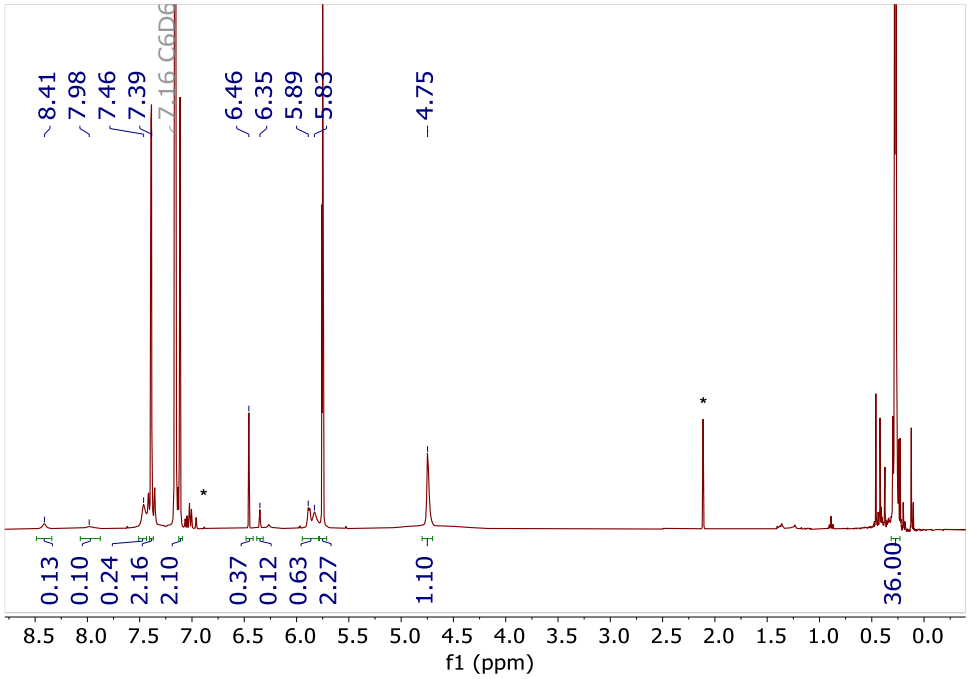

Figure 6.18: The ^{1}H NMR spectrum of the reaction between 5-Y and 7-Y in d_6-benzene, recorded after 15 m. The resonances denoted by * are assigned to adventitious toluene.

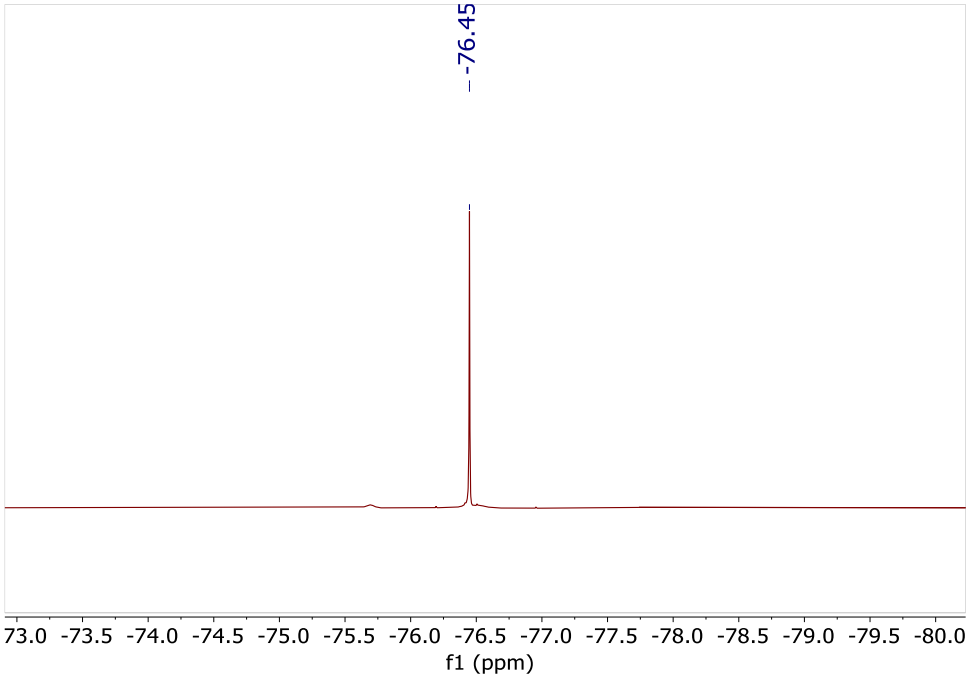

Figure 6.19: The $^{19}F\{^{1}H\}$ NMR spectrum of the reaction between 5-Y and 7-Y in d_6-benzene, recorded after 15 m.

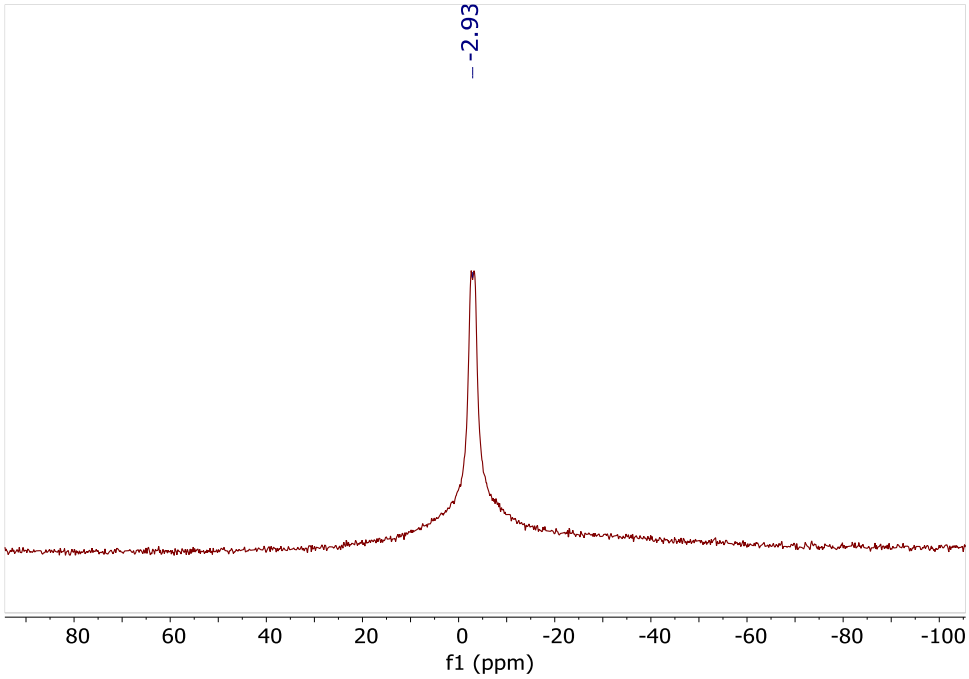

Figure 6.20: The ^{11}B NMR spectrum of the reaction between 5-Y and 7-Y in d_6-benzene, recorded after 15 m.

In order to investigate the reaction further, **5-Eu** was reacted with **7-Yb**, and **5-Yb** was reacted with **7-Eu** in d_6-benzene in a 1:1 ratio in Youngs' tap NMR tubes. Both reactions were performed with a known quantity of NMR standard $Si(SiMe_3)_4$ in the solution. The suspensions were sent for multinuclear NMR analysis after 30 mins (^{1}H NMR spectra in Figure 6.21 and Figure 6.22). In both reactions, resonances consistent with $Yb(Tp)_2(hfac)$ and $Eu(Tp)_2(hfac)$

were identified by comparison to data obtained during another group member's characterisation ($Yb(Tp)_2(hfac)$ δ = -31.23, -1.93, 6.20, 32.76 ppm; $Eu(Tp)_2(hfac)$ δ = 0.06, 1.34, 3.00, 13.12 ppm).[19, 20] No other assignable product resonances were observed in either ^1H NMR spectrum. The ratio of the two products is different in the two reactions, as calculated by relative integration and shown in Table 6.1. In both reactions, the lanthanide in the **7-Ln** starting material made up a greater proportion of the $Ln(Tp)_2(hfac)$ products as might be expected. However, these data clearly show that ligand redistribution was prevalent. Evidently, both the hfac and Tp ligands are somewhat labile under the conditions used for this reaction.

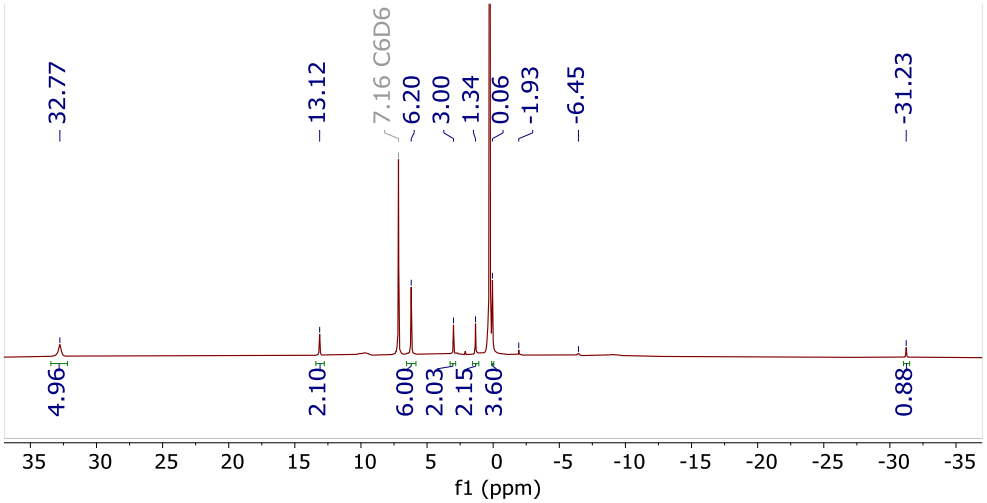

Figure 6.21: The ^1H NMR spectrum of the products of the reaction of 7-Yb with 5-Eu, recorded in d_6-benzene.

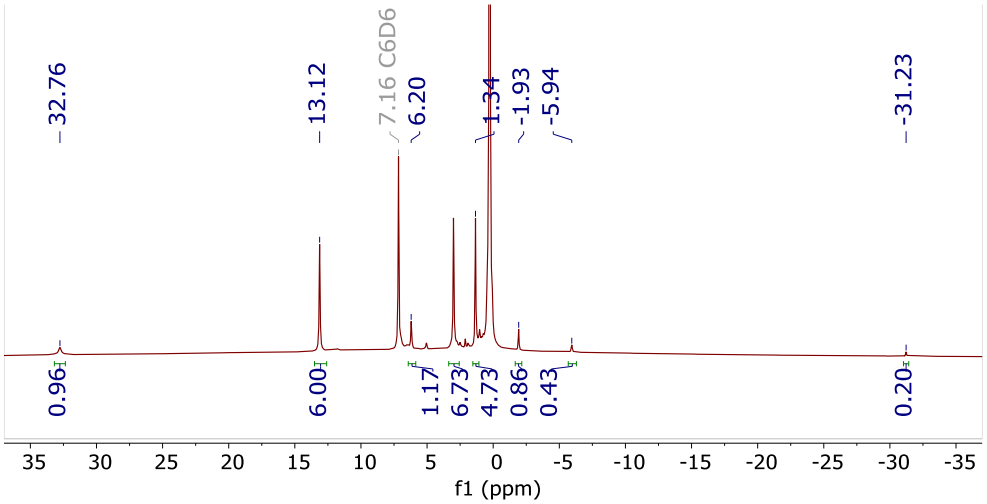

Figure 6.22: The ^1H NMR spectrum of the products of the reaction of 7-Eu with 5-Yb, recorded in d_6-benzene.

Table 6.1: Relative % products of the reaction of 7-Ln with 5-Ln', calculated by relative integration.

Reaction	Relative % products	
	$Yb(Tp)_2(hfac)$	$Eu(Tp)_2(hfac)$
7-Yb + **5-Eu**	86%	14%
7-Eu + **5-Yb**	25%	75%

Despite the high yielding ligand redistribution reactions, in each case the solution retained a red colour over time. However, it is known from isolation of each of the redistribution products $Ln(Tp)_2(hfac)$ (Ln = Y, Eu, Yb) that they do not absorb in the visible region.[19, 20] This indicates that a further species, likely containing the pd ligand, was also present in solution.

6.3.2 UV-vis and EPR spectroscopy of the products of the reaction of 7-Y with 5-Y

In a larger scale reaction, a suspension of **7-Y** in toluene was added to 1 eq. **5-Y**, likewise suspended in toluene, and the mixture was stirred for 45 min. A colour change was observed from green to red over 30 seconds. The mixture was filtered *via* frit and toluene was removed from the filtrate *in vacuo* to obtain a red solid. The products were analysed by multinuclear NMR spectroscopy, which displayed resonances assigned to $Y(Tp)_2(hfac)$, in addition to other minor resonances which were not assignable.

The products of the reaction of **7-Y** with **5-Y** were dissolved in toluene and the UV-vis spectrum of the resulting solution was recorded, shown in Figure 6.23. As is clear from the NMR data, the mixture of products produced by the reaction consists of $Y(Tp)_2(hfac)$ in addition to any pd-containing products, and so extinction coefficients were not determined. The spectrum has a λ_{max} of 484 nm, along with two shoulders at 367 and 385 nm. The profile of the absorption spectrum is similar to that of the uncomplexed radical ligand **3**, which has a lower energy λ_{max} of 558 nm, consistent with the products containing the pd radical anion. Meanwhile **5-Y**, with $Y(hfac)_3$ coordinated to the *N,N'* binding site of the ligand, has a λ_{max} of 650 nm. The λ_{max} of the products of the reaction of **5-Y** with **7-Y** is therefore higher in energy than the starting materials by over 100 nm. This is consistent with a coordination change, as the electronic properties of pd are highly dependent on its coordination state.[21, 22]

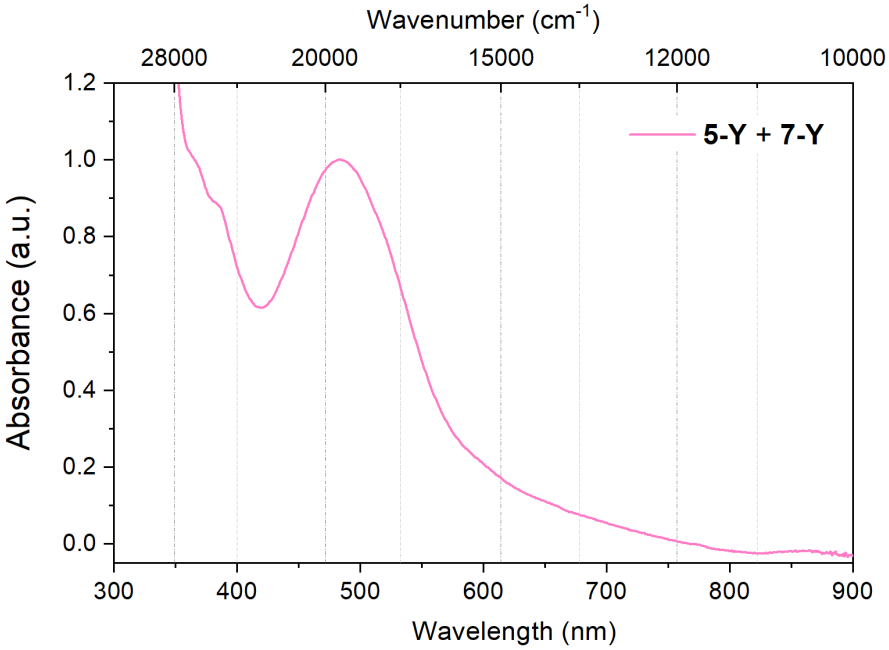

Figure 6.23: The UV-vis spectrum of the products of the reaction of 5-Y with 7-Y, recorded in toluene. The spectrum is normalised to the maximum at 484 nm.

The EPR spectrum of a toluene solution of the products of the reaction of **5-Y** with **7-Y** was recorded, and is shown in Figure 6.24. The spectrum clearly shows an organic radical with g = 2.0016, close to that of a free electron (g = 2.0023).[23] The hyperfine structure indicates that the organic radical is coupled to several other nuclei, similarly to the X-band EPR spectrum of **3** and **5-Y**. This is consistent with the product mixture containing the pd radical anion. However, as the products were not isolated, no simulation was performed and the contributions from different nuclei to the hyperfine coupling were not determined.

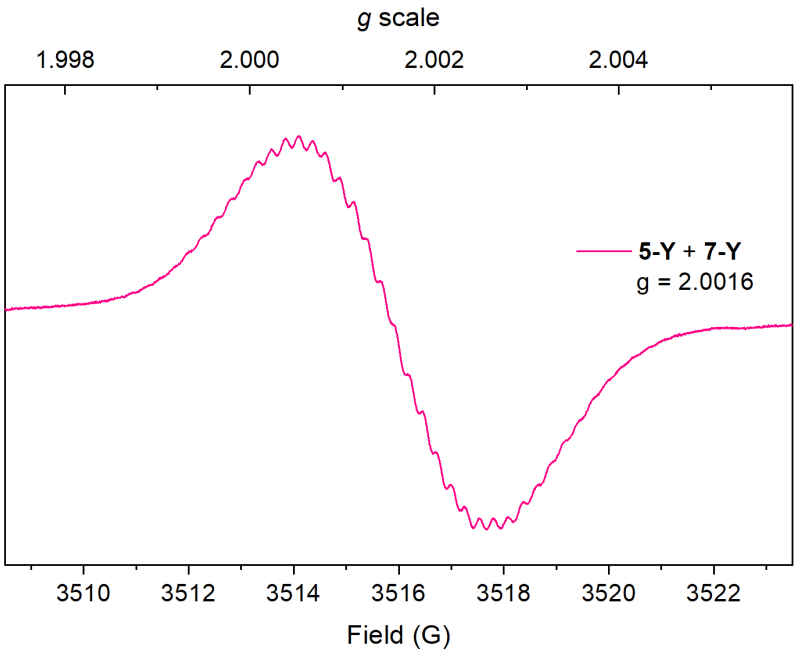

Figure 6.24: X-band EPR spectrum of the products of the reaction of 5-Y with 7-Y, recorded in toluene at 298 K.

6.3.3 X-ray crystallography of the products of the reaction of 5-Y with 7-Y

Single crystals of the side product $Y(Tp)_2(hfac)$ suitable for X-ray diffraction were obtained on multiple occasions, by cooling a concentrated hexane solution of the products to -35 °C overnight. The Y-N(Tp) bonds are in the range 2.435(3)-2.534(3) Å, and are consistent with other examples of the $[Y(Tp)_2]^+$ unit.[2, 3, 24-26]

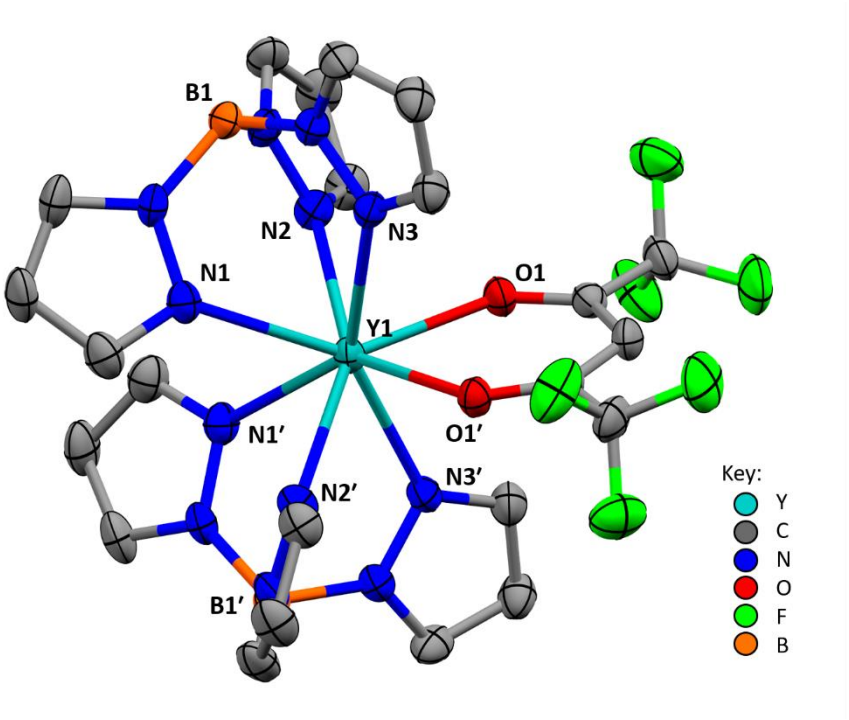

Figure 6.25: The solid-state molecular structure of Y(Tp)$_2$(hfac) as crystallised from the products of the reaction between 5-Y and 7-Y. Thermal ellipsoids are depicted at 50% probability. H atoms are omitted for clarity. Selected bond distances: Y-N(Tp) 2.435(3)-2.534(3), Y-O(hfac) 2.341(2) Å.

On two occasions, the crystals obtained were of the supramolecular square {Y(hfac)$_2$(*N,N'*-*O,O'*-pd)}$_4$, consisting of four yttrium atoms bridged by pd ligands and capped at each corner with two hfac ligands, shown in Figure 6.26. The data were of poor quality due to low crystallinity, and as such only connectivity data is available for this compound. The hfac ligands were particularly disordered, and as such only the oxygen atoms were resolved, though the bridging pd ligand was identifiable. In order to charge balance the complex (assuming that yttrium is in the 3+ oxidation state) the pd ligand must remain in the monoanionic, radical, oxidation state as no non-coordinated counteranions were observed.

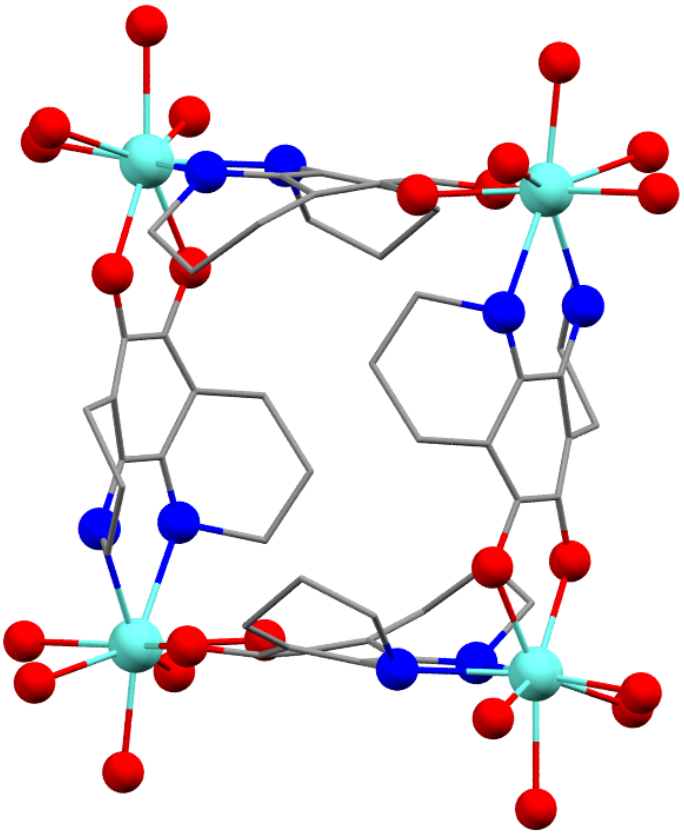

Figure 6.26: The solid-state molecular structure of the supramolecular square {Y(hfac)$_2$(*N,N'-O,O'*-pd)}$_4$. Y, O and N atoms are depicted as ball-and-stick, and C atoms of pd in wireframe for clarity. Only the O atoms of the hfac ligands are depicted, as the C and F atoms of the hfac ligands were not resolved due to high levels of disorder.

6.3.4 Summary

The predominant byproduct observed by NMR was found to be Y(Tp)$_2$(hfac), which was also crystallised on multiple occasions. It is therefore clear that a ligand redistribution reaction occurs upon reaction of **5-Y** with **7-Y**, consisting of one hfac ligand coordinating to [Y(Tp)$_2$]$^+$. The mechanism of this ligand redistribution process is unknown, although lanthanide *β*-diketonate compounds have been found to undergo these types of reactions.[27] This presumably leaves Y(hfac)$_2$(*N,N'*-pd) as a coordinatively unsaturated species (6 coordinate), which self-assembled under the conditions of the crystallisation to form {Y(hfac)$_2$(*N,N'-O,O'*-pd)}$_4$ as depicted in Scheme 6.3. Attempts to isolate {Y(hfac)$_2$(*N,N'-O,O'*-pd)}$_4$ from the reaction mixture were unsuccessful due to its similar solubility to the other components of the reaction. Additionally, deliberate attempts subsequently made to assemble the supramolecular structure resulted in insoluble materials, presumably coordination polymers.

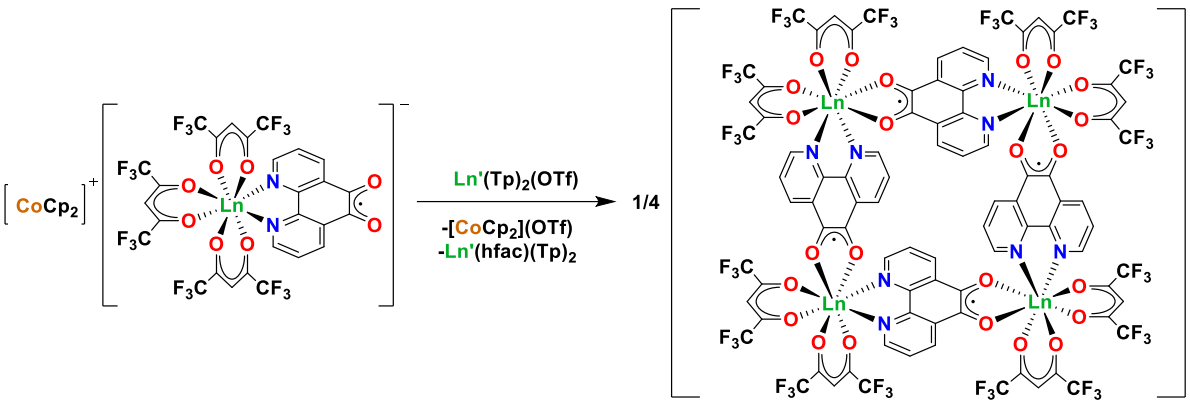

Scheme 6.3: The proposed reaction forming the supramolecular square {Y(hfac)$_2$(N,N'-O,O'-pd)}$_4$.

6.4 Reaction of 3 $[CoCp_2][pd]$ with 7-Ln $Ln(Tp)_2(OTf)$

The reaction of **5-Ln** with **7-Ln** resulted in ligand redistribution, forming $Ln(Tp)_2(hfac)$ and $\{Ln(hfac)_2(N,N'\text{-}O,O'\text{-pd})\}_4$. It was therefore thought that pre-coordination of the $[Ln(Tp)_2]^+$ unit to pd might be a better strategy for the synthesis of heterobimetallics. The reaction of **3** $[CoCp_2]^+[pd]^{-\bullet}$ with **7-Ln** was therefore investigated with the goal of forming the monometallic *O,O'*-coordinated complexes $Ln(Tp)_2(O,O'\text{-pd})$ (**8-Ln**) as shown in Scheme 6.4. A wide range of reactions under various conditions (eg. solvent, temperature, reaction time) were investigated. Selected experiments and key results will be discussed here.

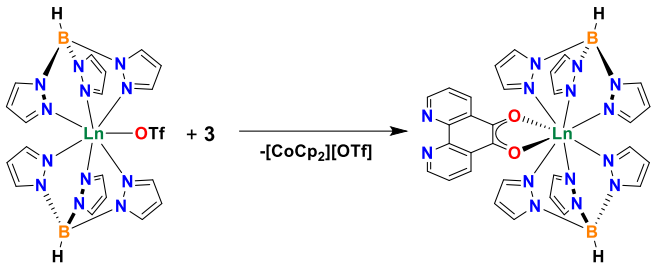

Scheme 6.4: The proposed synthesis of 8-Ln by reaction of 7-Ln with 3.

7-Ln was dissolved in THF (2 ml) and **3** (1 eq.) was suspended in toluene (4 ml). Both were cooled to -35 °C and **7-Ln** was added to **3** with stirring. A colour change from purple to red was observed, and the mixture was stirred for 1 h. The suspension was reduced *in vacuo* by half, removing the majority of the THF, then filtered *via* frit to obtain a red solution. Solvents were removed from the filtrate *in vacuo* and the red solid was weighed and analysed by multinuclear NMR, UV-visible and photoluminescence spectroscopy.

6.4.1 NMR spectroscopy of 8-Yb

The ^1H NMR spectrum of **8-Yb** is shown in Figure 6.27. Three significant resonances at δ = 3.87, 6.40 and 29.03 ppm, each integrating to 6H, are consistent with a the Tp ligand bound to Yb(III). These three resonances are matched by a broad resonance at δ = -2.82 ppm integrating to 2H, which is assigned to the borohydride of the same Tp ligands. For comparison, in the starting material **7-Yb**, resonances are observed at δ = -22.25 (2H, s, br), -4.89 (6H, s, br), 6.25 (6H, s), 39.06 (6H, s, br) ppm. However, a number of other resonances are also present. In particular, a resonance at δ = 5.65 ppm is consistent with $[CoCp_2]^+$,[28] presumably carried through at the filtration step. Meanwhile, three smaller resonances at δ

= -112.20, -107.80 and 27.98 ppm each integrate to 2H. Previously, no resonances have been observed for pd in the radical anion oxidation state due to paramagnetically induced relaxation. However, these resonances are much more shifted than would be expected for Tp ligand bound to Yb(III), and the integration is consistent with the three proton environments of the pd ligand. These resonances are therefore tentatively assigned to the three pd-CH environments. A number of other very minor resonances indicate that there are other, minor products in solution. The $^{19}F\{^{1}H\}$ NMR spectrum, shown in Figure 6.28, displays a single main resonance at δ = -79.33 ppm, consistent with a non-coordinated triflate anion as expected for $[CoCp_2]^+[OTf]^-$, indicating that the metathesis reaction was successful. The $^{11}B\{^{1}H\}$ NMR spectrum, shown in Figure 6.29, contains a single main resonance at δ = -23.68 ppm, consistent with a Tp ligand coordinated to Yb(III), but also displays two resonances of lower intensity at δ = -65.79 and 61.42 ppm, assigned to minor products. The resonance at δ = -65.79 ppm is similar to other examples of Tp ligands bound to Yb(III) in this thesis. The minor resonance at δ = 61.42 ppm is significantly downfield shifted, however and is not consistent with any example of a Tp ligand in this thesis, indicating that in this minor product the Tp ligand may have undergone decomposition. These NMR data are consistent with a successful metathesis reaction to form **8-Yb**. However, the metathesis byproduct $[CoCp_2]^+[OTf]^-$ has not been completely excluded by the extraction, nor have other minor products.

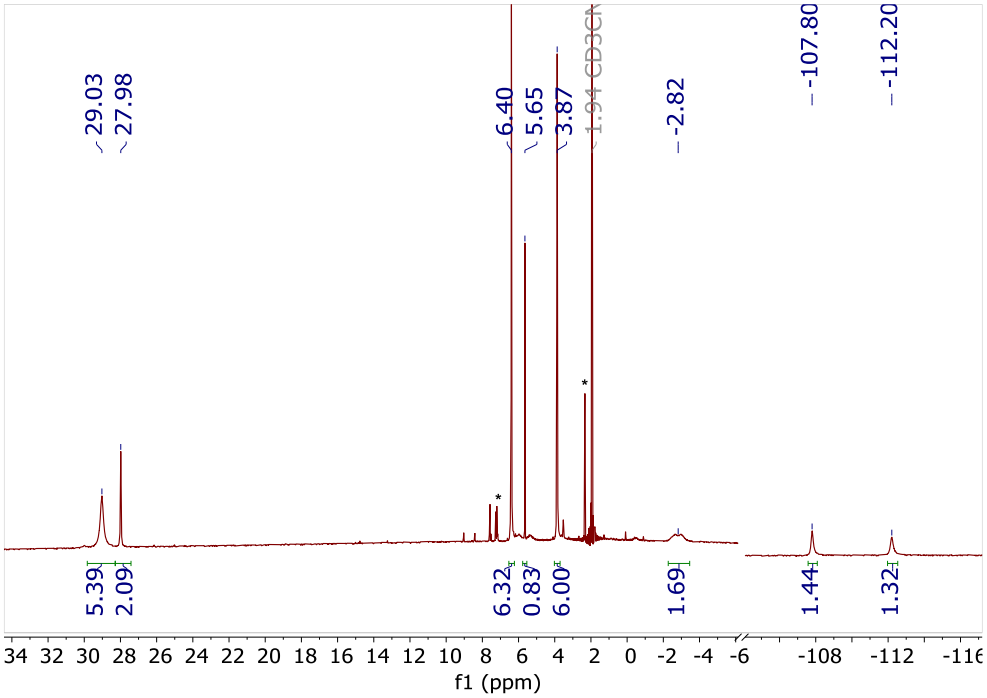

Figure 6.27: The ^{1}H NMR spectrum of the products of the reaction of 7-Yb with 3, recorded in d_3-MeCN. Resonances assigned to toluene solvent are denoted by *.

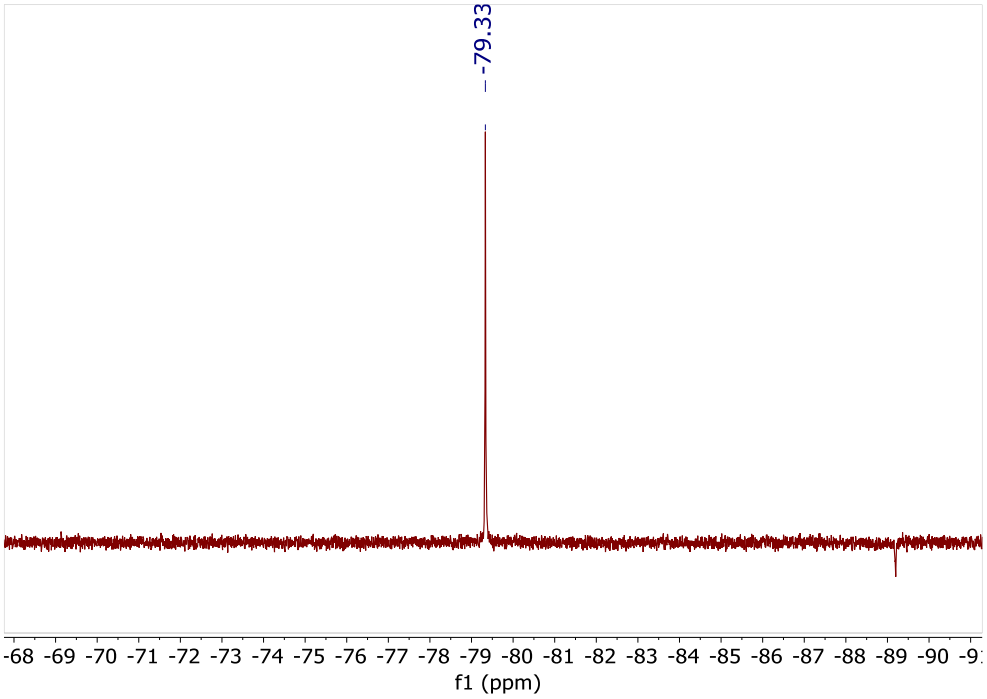

Figure 6.28: The $^{19}F\{^{1}H\}$ NMR spectrum of the products of the reaction of 7-Yb with 3, recorded in d_3-MeCN.

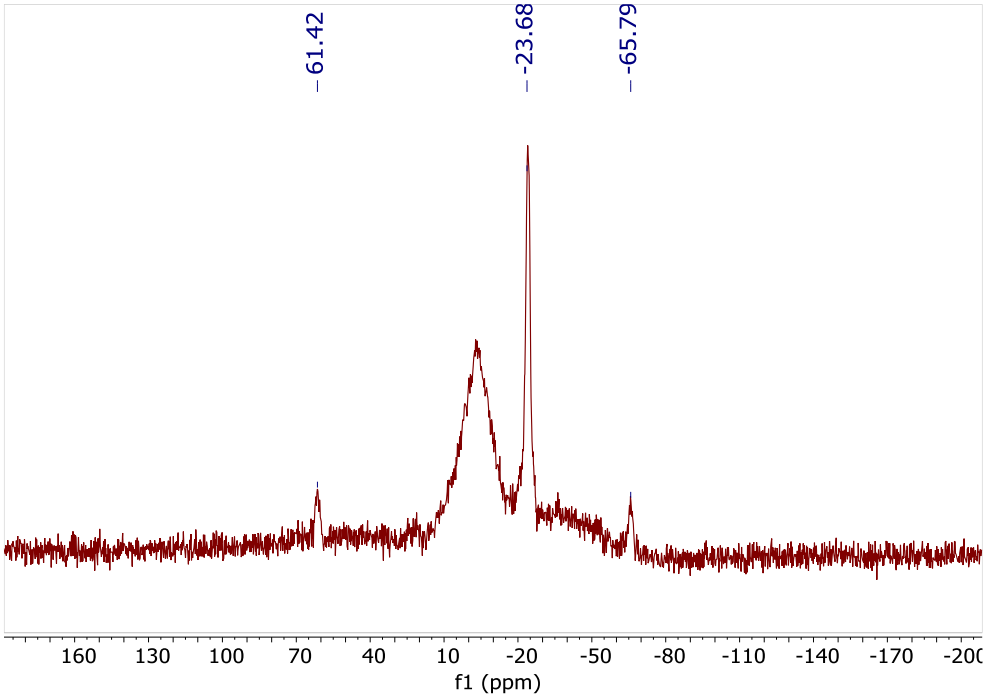

Figure 6.29: The ^{11}B NMR spectrum of the products of the reaction of 7-Yb with 3, recorded in d_3-MeCN.

6.4.2 UV-visible and photoluminescence spectroscopy of 8-Ln

The products of the reaction of **7-Yb** with **3**, including **8-Yb**, were analysed by visible absorption and photoluminescence spectroscopy, recorded in MeCN solution (shown in Figure 6.30). The products are known to contain at least $[CoCp_2]^+[OTf]^-$, so no extinction coefficients were calculated. In the visible region two main transition envelopes are observed, with λ_{max} = 392 and 478 nm. A comparison may be drawn to the absorption spectrum of **3** (also shown in Figure 6.30), which exhibits transitions with λ_{max} = 401 and 558 nm. The most intense absorption of **8-Yb** (λ_{max} = 478 nm) is at a higher energy than the most intense absorption of **3** (λ_{max} = 558 nm) by 80 nm. Meanwhile, in the *N,N'*-coordinated **5-Yb**, the predominant absorption (λ_{max} = 605 nm) is at lower energy than that in **3** by 47 nm. This behaviour is consistent with the electronic structure of the ligand being dependent on the coordination site (*N,N'* or *O,O'*) occupied by the lanthanide. Coordination to the *N,N'* site lowers the energy, while coordination to the *O,O'* site increases the energy of the transition envelope. The products of the reaction of **7-Y** with **5-Y** exhibited a similar spectrum (λ_{max} = 367, 385 and 484 nm, see Section 6.3.2) to that of the products of the reaction of **7-Yb** with **3**. This is a strong indication that **7-Ln** are selective to the *O,O'* coordination site of pd.

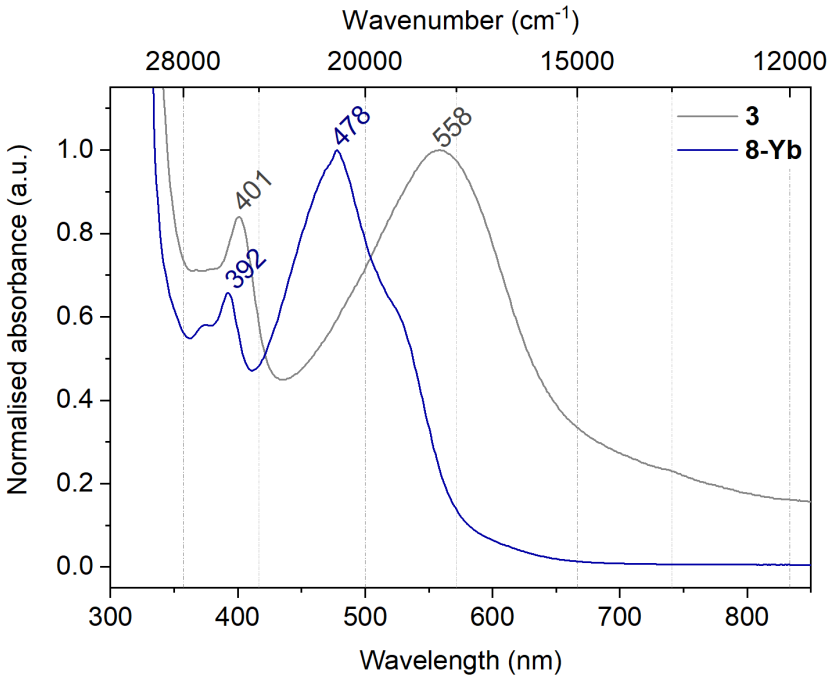

Figure 6.30: The visible absorption spectra of 8-Yb (*ca* 0.18 mM MeCN solution) and 3. Both spectra are normalised for ease of comparison to the maxima at 478 and 558 nm.

The photoluminescence spectra of the products of the reaction between **7-Yb** and **3**, were also recorded in MeCN solution, shown in Figure 6.31. Emission from Yb(III) with λ_{max} = 975 nm was observed following excitation by both UV and visible light. The excitation spectrum displayed several maxima at λ_{Ex} = 275, 315, 390 and 475 nm. Notably, the profile and maxima of the excitation spectrum very closely matched the absorption spectrum of **8-Yb** in the visible region, with maxima at λ_{Ex} = 390 and 475 nm. The emission spectrum was identical irrespective of the excitation wavelength used. Notably, in **8-Yb** photoluminescence from Yb(III) is sensitised by visible light. No emission was observed upon visible light excitation of **1-Yb** or **5-Yb** despite their visible absorptions (see Chapter 4), or **7-Yb**. It is therefore particularly surprising that in **8-Yb** emission from Yb(III) was observed following sensitisation *via* transitions in the visible region which are assigned to the radical ligand, known to quench lanthanide photoluminescence.[29-31] As no such behaviour was observed in *N,N'* coordinated **5-Yb**, it seems that this must be particular to the *O,O'* coordination of Yb(III) to the radical ligand. It is possible either that partial coupling of the radical to the paramagnetic *S* = ½ Yb(III) reduces the quenching, or that in **8-Yb** the *O,O'* coordination allows better electronic contact between the ligand and Yb(III).

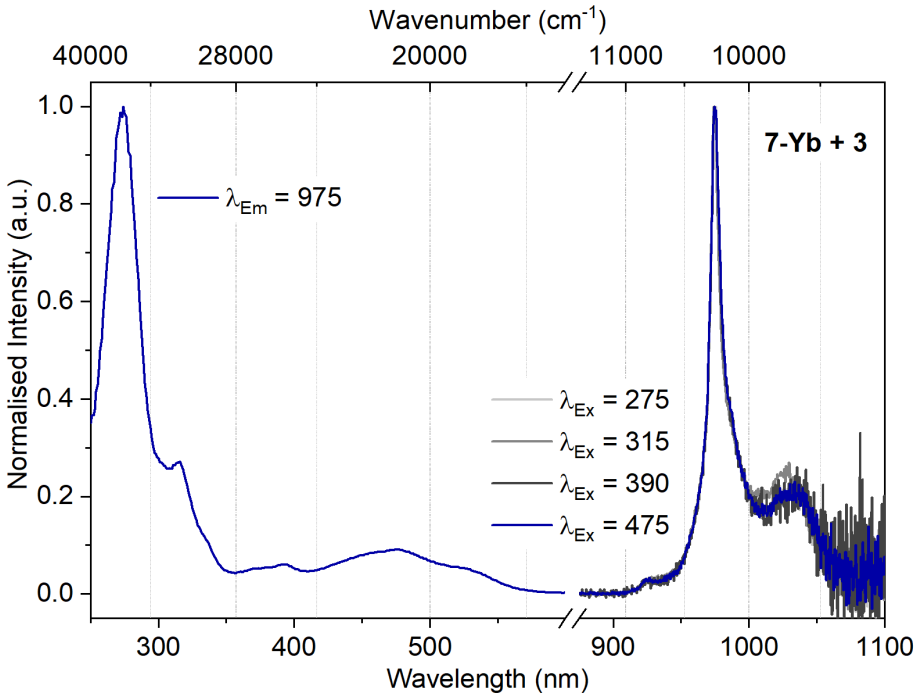

Figure 6.31: The photoluminescence excitation (L) and emission (R) spectra of Yb(Tp)$_2$(*O,O'*-pd), the proposed product of the reaction between 7-Yb and 3.

6.4.3 NMR-scale reaction to synthesise 8-Eu

An NMR-scale reaction of **7-Eu** with **3** was carried out in d_6-benzene to synthesise **8-Eu**. After mixing, a colour change from purple to red was observed as for **8-Yb**. A significantly greater number of resonances were observed in the ^{1}H NMR spectrum (Figure 6.32) than in the case of **8-Yb**, indicating the reaction is significantly less clean in the case of **8-Eu**. Three resonances at δ = 1.36, 4.75 and 24.81 ppm are the most intense observed, and have shifts consistent with Tp ligands bound to Eu(III) (**7-Eu**, δ = 0.40, 3.02, 14.05 ppm). However, there are more resonances in the spectrum than can be assigned. In the ^{19}F NMR spectrum (Figure 6.33) a single resonance is observed at δ = -78.61 ppm, consistent with a triflate anion not coordinated to Eu(III), indicating that the metathesis reaction has occurred as intended. Meanwhile, in the ^{11}B NMR spectrum (Figure 6.34) a single main resonance was observed at δ = -17.95 ppm, consistent with a Tp ligand bound to Eu(III). Some other minor resonances also appear to be present in the baseline of the spectrum.

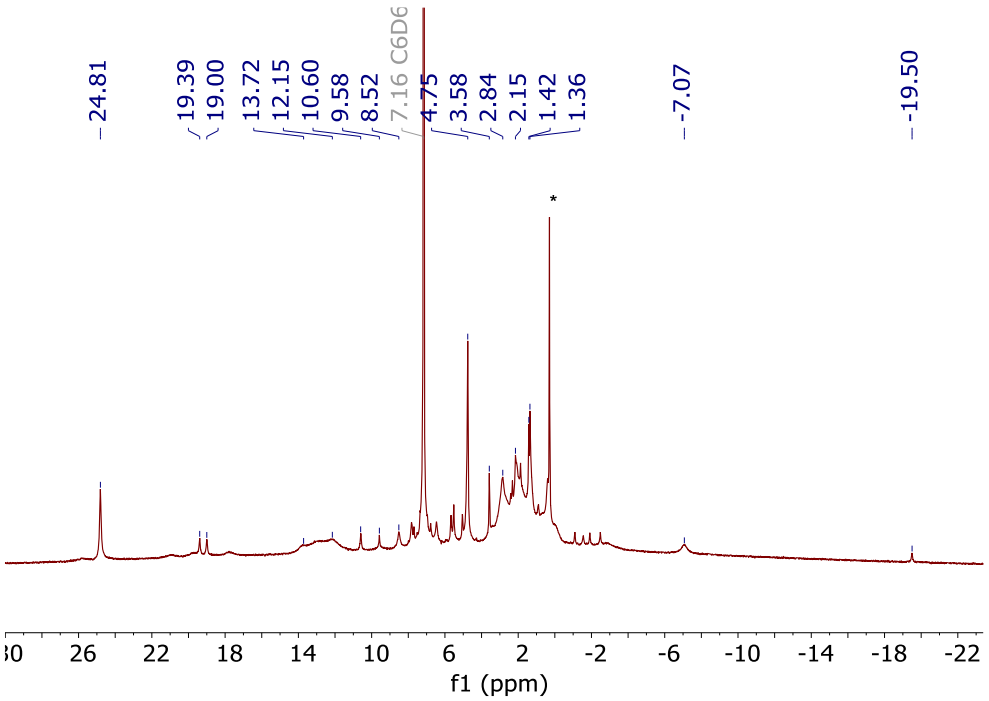

Figure 6.32: The ^{1}H NMR spectrum of the products of the reaction of 7-Eu with 3 in d_6-benzene. A resonance assigned to silicone grease is denoted by *.

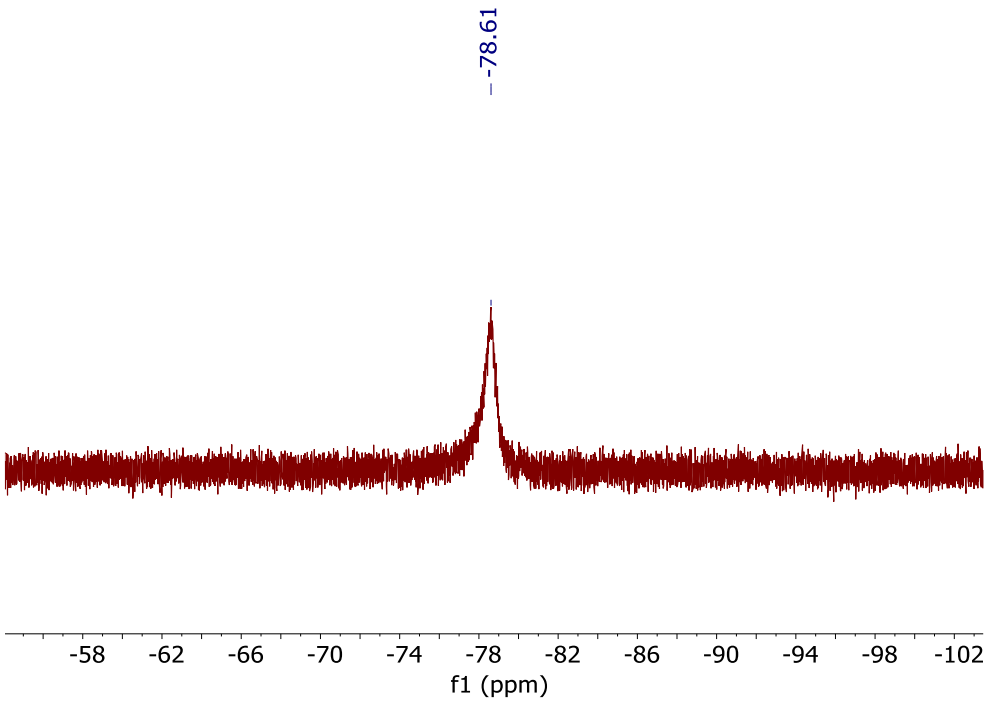

Figure 6.33: The $^{19}F\{^{1}H\}$ NMR spectrum of the products of the reaction of 7-Eu with 3 in d_6-benzene.

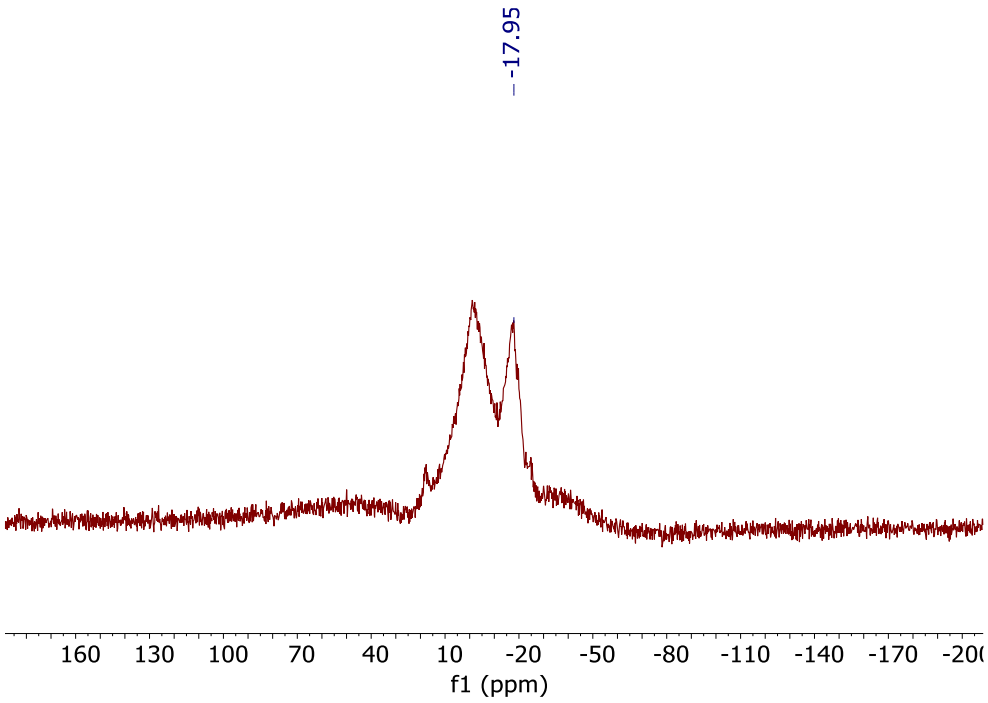

Figure 6.34: The ^{11}B NMR spectrum of the products of the reaction of 7-Eu with 3 in d_6-benzene.

Solvents were removed from the NMR reaction mixture and the products were dissolved in THF, then filtered and diluted to yield a red solution. The electronic absorption spectrum of the solution was then recorded. The red solution exhibited an absorption spectrum nearly identical to that of the products of the reaction of **7-Yb** with **3** as shown in Figure 6.35,

indicating that in **8-Eu** Eu(III) also coordinates to the *O,O* binding site of the ligand. However, the reaction was shown by NMR to be significantly less clean, producing multiple side-products.

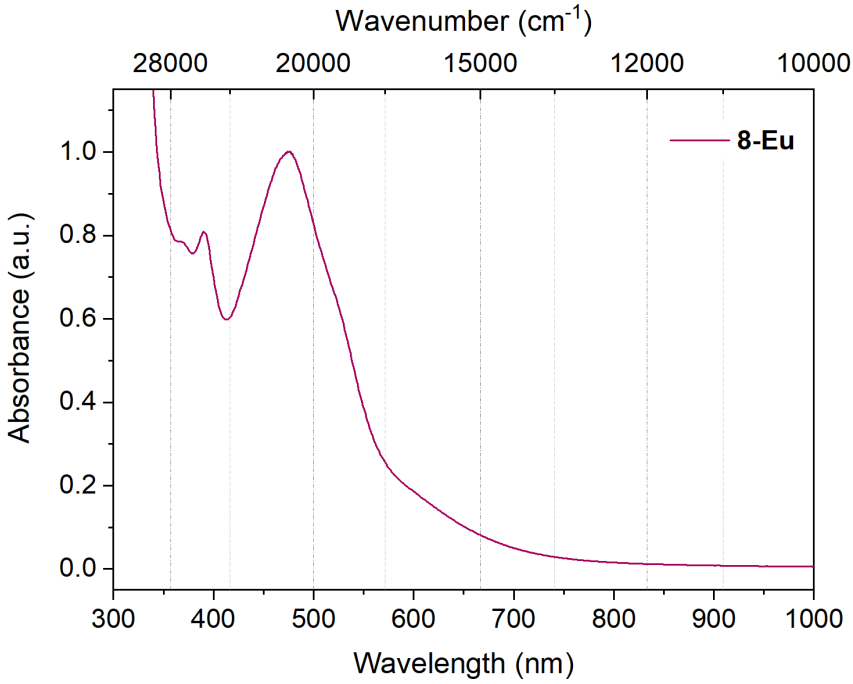

Figure 6.35: The electronic absorption spectrum of the NMR reaction products to synthesise 8-Eu. The spectrum is normalised to the absorption at 490 nm.

6.4.4 Conclusions

Initial results from the reaction of **7-Ln** with **3** are consistent with formation of **8-Ln**. Electronic absorption spectroscopy and photoluminescence spectroscopy of **8-Yb** were consistent with the selective coordination of $[Ln(Tp)_2]^+$ to the *O,O'* binding site of the radical pd ligand. In particular, sensitisation of Yb(III) luminescence *via* the radical ligand was observed in **8-Yb**, which was not observed in **5-Yb**, indicating that the coordination mode is different in the two complexes. However, the solubility properties of **8-Ln** were very similar to the metathesis byproduct $[CoCp_2]^+[OTf]^-$ and **8-Ln** has therefore not yet been fully isolated due to time constraints. A bimetallic species $Ln(hfac)_3$(*N,N'-O,O'*-pd)$Ln(Tp)_2$ should be significantly more soluble due to the influence of the heavily fluorinated hfac ligands. It was therefore decided to react *O,O'*-coordinated **8-Ln** *in situ* with the *N,N'* selective **4-Ln** to synthesise lanthanide heterobimetallics.

6.5 Synthesis of Ln(hfac)$_3$(*N,N'-O,O'*-pd)Ln(Tp)$_2$ 9-LnLn'

The isolation of Ln(Tp)$_2$(*O,O'*-pd) had proven to be challenging due to their solubility properties and those of the byproducts formed in the reaction. However, previous experience had shown that the hfac ligand is highly solubilising for lanthanide compounds of the pd ligand. Therefore, addition of Ln(hfac)$_3$(S)$_2$ **4-Ln** *in situ* was proposed, to form lanthanide heterobimetallics Ln(hfac)$_3$(*N,N'-O,O'*-pd)Ln'(Tp)$_2$ **9-LnLn'** which should be easier to isolate. By pre-coordinating [Ln(Tp)$_2$]$^+$ to pd, rather than introducing **7-Ln** to a hfac-containing complex as in Section 6.3, this should reduce the ligand redistribution seen in previous attempts to synthesise a bimetallic. The synthesis of the bimetallic species **9-LnLn'** was therefore attempted as shown in Scheme 6.5.

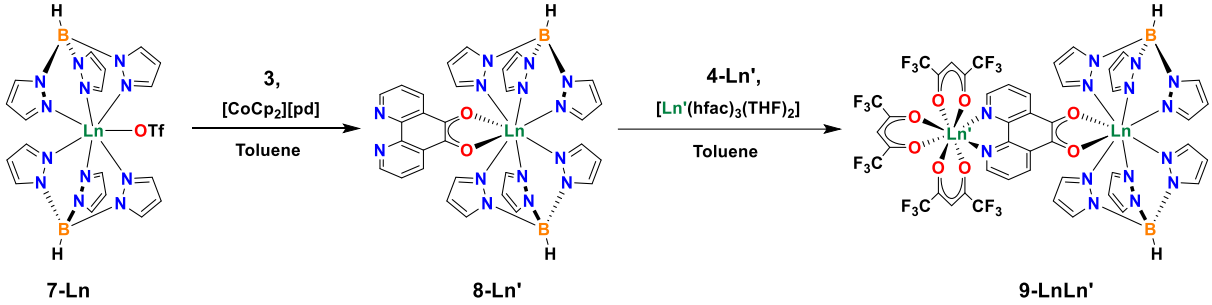

Scheme 6.5: The synthesis of the bimetallic species 9-LnLn' *via* stepwise coordination to the *N,N'* and *O,O'* binding sites of the bridging ligand.

6.5.1 Synthesis and NMR spectroscopy of 9-LnLn'

At -35 °C, **7-Ln'** (Ln' = Y, Eu, Yb) was stirred with 1 eq. **3** in toluene for 30 min, and a colour change was observed from purple to orange-red. Then at -35 °C a solution of 1 eq. **4-Ln** (Ln = Y, Yb, Eu) in toluene was added and the mixture was stirred for 5 min, during which time a colour change from orange-red to dark red was observed. The suspension was filtered *via* frit filtration, and toluene was removed from the dark red filtrate *in vacuo*, to obtain a dark red solid. The solid was extracted into hexane and hexane was removed *in vacuo* to yield a dark red powder. The products were then analysed by multinuclear NMR spectroscopy.

As has been discussed in this thesis, NMR spectroscopy can be useful in the characterisation of paramagnetic complexes. Complexes **1-Ln**, **4-Ln**, **6-Ln** and **7-Ln** were fully assignable by multinuclear NMR. However, there are limits to this application. The pd ligand in **3** and **5-Ln** did not exhibit any NMR resonances, and it is unclear whether incorporation of multiple paramagnetic lanthanide species into a molecule will result in observable NMR resonances.

For the reaction of **7-Y** with **3** and **4-Y** to synthesise **9-YY'**, a single resonance was observed in the $^{19}F\{^{1}H\}$ NMR spectrum of the products (Figure 6.37) at δ = -76.43 ppm. A single resonance was also observed in the ^{11}B NMR spectrum (Figure 6.38) at δ = -2.91 ppm. Both of these resonances are consistent with the ligand redistribution product $Y(Tp)_2(hfac)$.[19, 20] In the ^{1}H NMR spectrum of the products (Figure 6.36), five resonances are observed at δ = 5.74, 6.22, 6.45, 7.11 and 7.38 ppm. Of these, those occurring at δ = 5.74, 6.45, 7.11 and 7.38 ppm are assigned to $Y(Tp)_2(hfac)$. No resonance attributable to $[CoCp_2][OTf]$ is observed. The resonance in the ^{1}H NMR spectrum at δ = 6.22 ppm remains unassigned, though the chemical shift is in the region typically observed for hfac ligands bound to yttrium.[10, 32] While the synthesis resulted in complete elimination of $[CoCp_2][OTf]$ as intended, the ligand redistribution reaction still occurred, with $Y(Tp)_2(hfac)$ being the only assignable component of the products of the reaction of **7-Y** with **3** and **4-Y**.

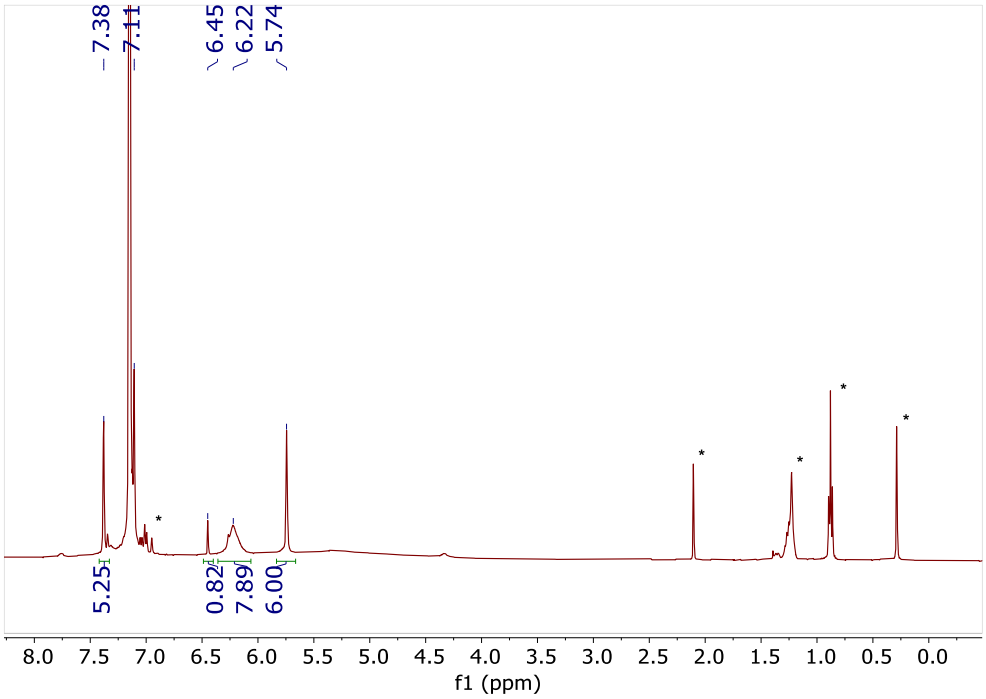

Figure 6.36: The ^{1}H NMR spectrum of the products of the reaction of 7-Y with 3 and 4-Y, recorded in d_6-benzene. Resonances assigned to silicone grease, hexane and toluene are denoted by *.

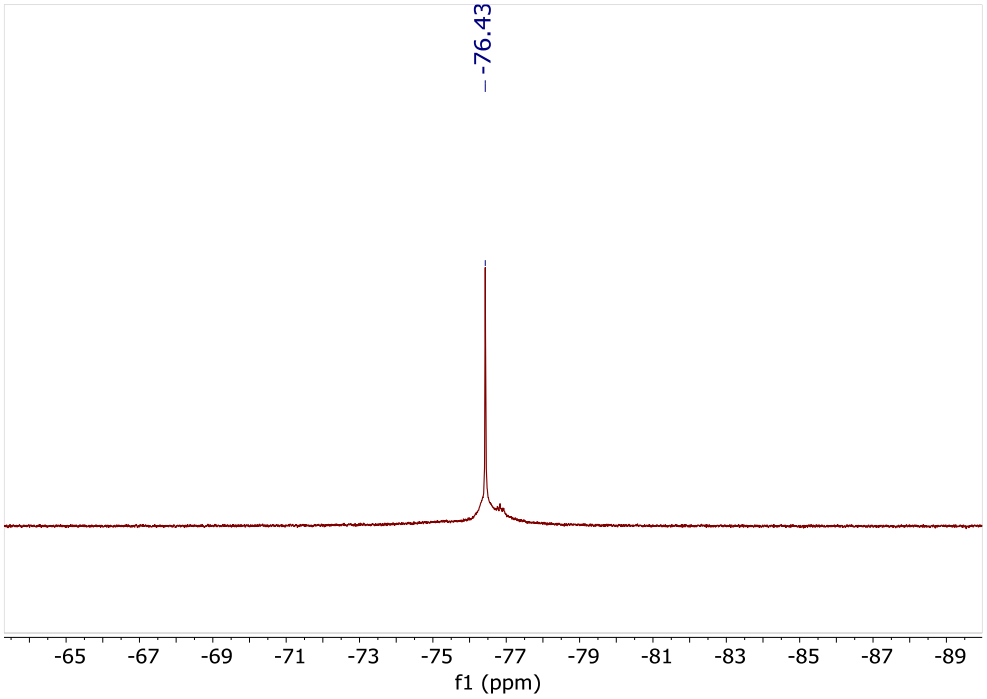

Figure 6.37: The ^{19}F NMR spectrum of the products of the reaction of 7-Y with 3 and 4-Y, recorded in d_6-benzene.

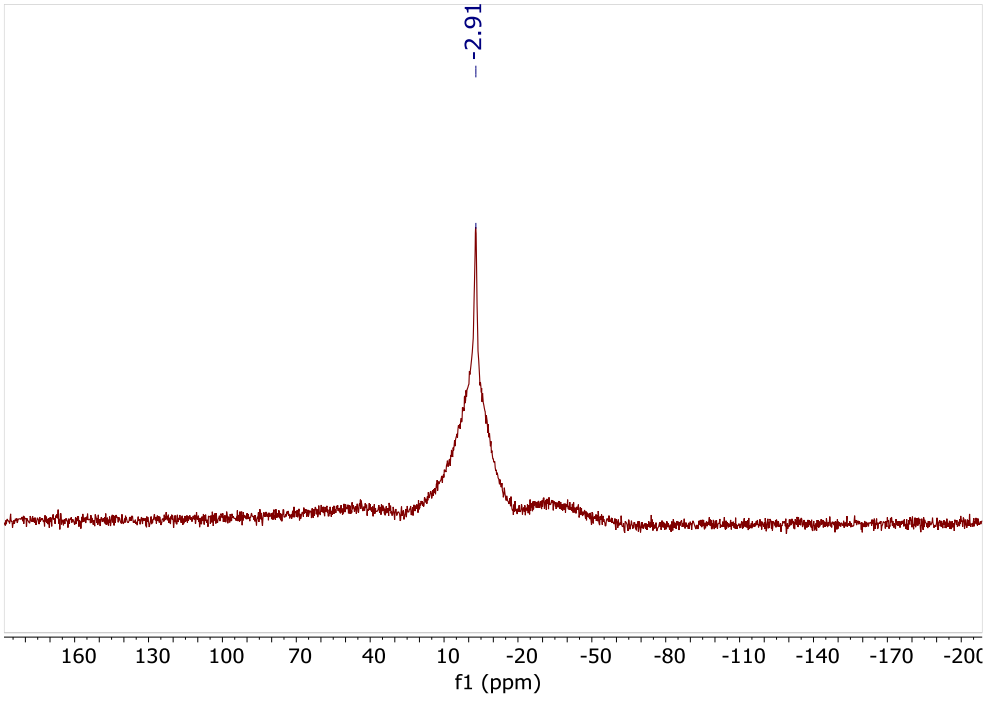

Figure 6.38: The $^{11}B\{^1H\}$ NMR spectrum of the products of the reaction of 7-Y with 3 and 4-Y, recorded in d_6-benzene.

The ^{1}H NMR spectrum of the products of the reaction of **7-Eu** with **3** and **4-Yb** is shown in Figure 6.39, and displays a set of four resonances at δ = -1.91, 1.33, 2.99 and 13.10 ppm. These are assigned to the ligand redistribution product Eu(Tp)$_2$(hfac). In the ^{19}F{^{1}H} NMR spectrum (Figure 6.40), a single resonance is observed at δ = -80.00 ppm, which is assigned to Eu(Tp)$_2$(hfac). Likewise, in the ^{11}B NMR spectrum (Figure 6.41) a single resonance is observed at δ = -18.39 ppm, assigned to Eu(Tp)$_2$(hfac). Unlike in the case of the reaction of **7-Y** with **3** and **4-Y**, no other product resonances are observed in any of these spectra.

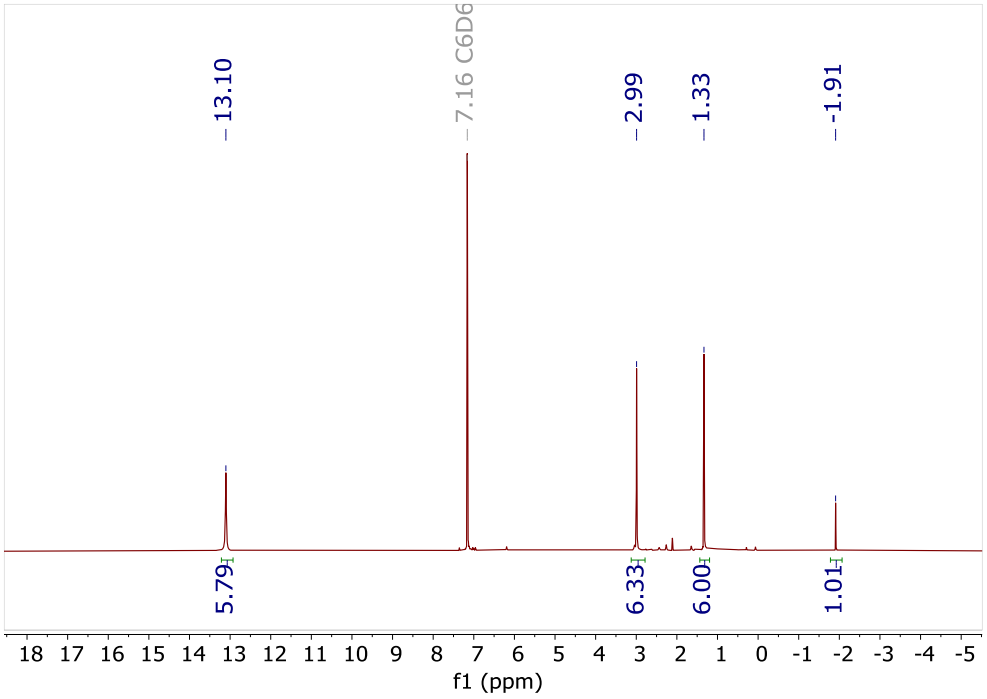

Figure 6.39: The ^{1}H NMR spectrum of the products of the reaction of 7-Eu with 3 and 4-Yb in toluene, recorded in d_6-benzene.

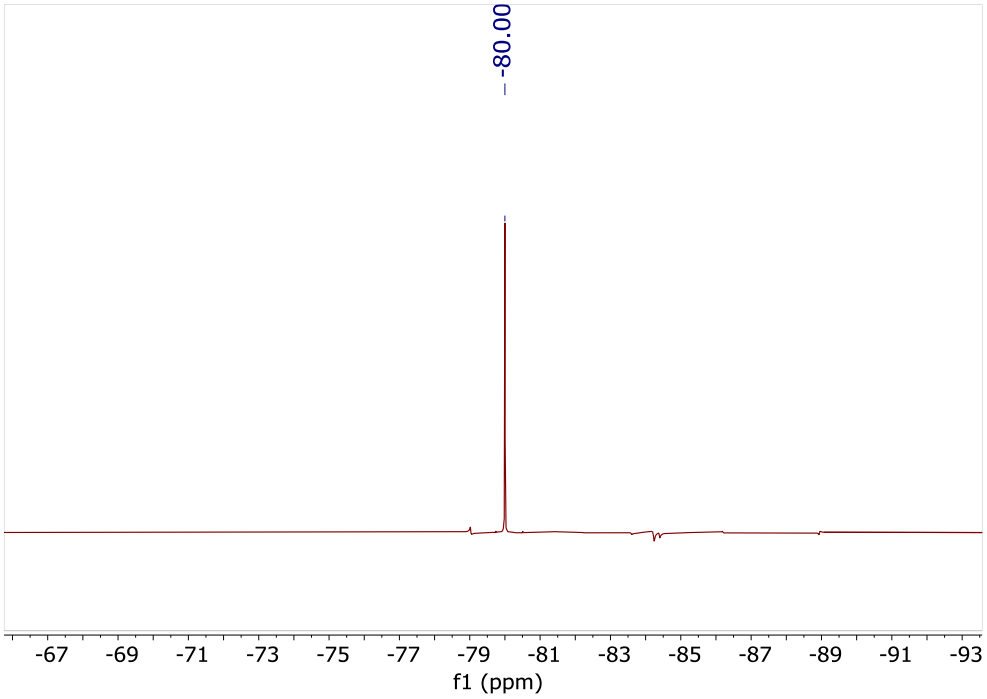

Figure 6.40: The $^{19}F\{^{1}H\}$ NMR spectrum of the products of the reaction of 7-Eu with 3 and 4-Yb in toluene, recorded in d_6-benzene.

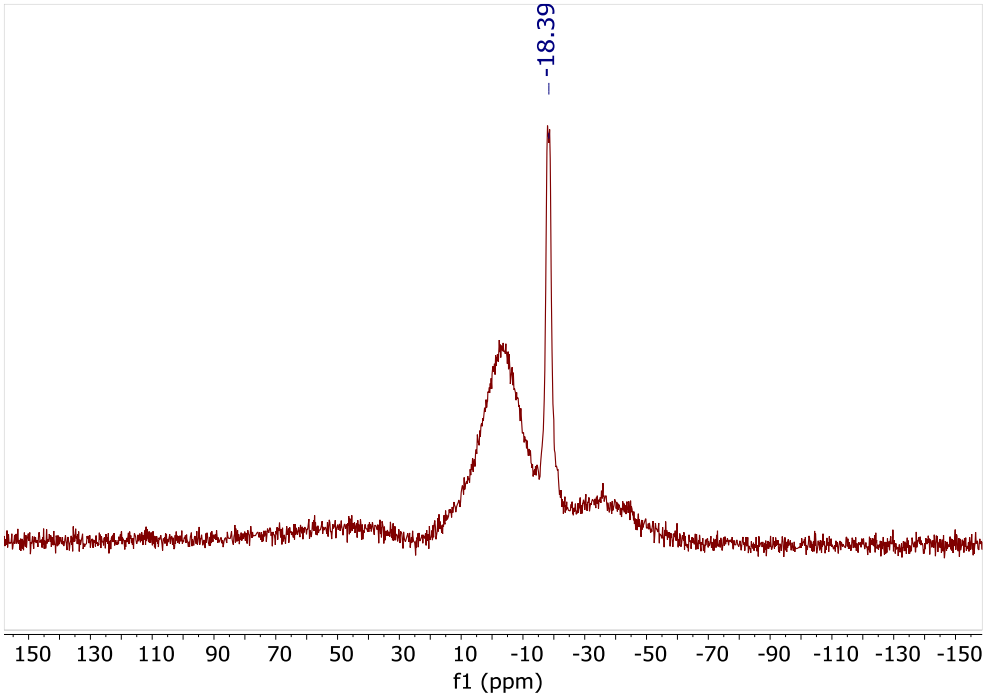

Figure 6.41: The ^{11}B NMR spectrum of the products of the reaction of 7-Eu with 3 and 4-Yb in toluene, recorded in d_6-benzene.

In contrast, the products of the reaction of **7-Yb** with **3** and **4-Eu**, to synthesise **9-EuYb**, exhibit a more complex ^{1}H NMR spectrum as shown in Figure 6.42. Of the resonances observed, none are consistent with the resonances of ligand redistribution product Yb(Tp)$_2$(hfac) (see Table 6.2).[19, 20] However, several environments are present which are consistent with Tp and hfac ligands coordinated to Yb(III) and Eu(III) as observed in other complexes in this thesis (Table 6.2). By relative integration and comparison to other complexes, three resonances at δ = 2.39, 6.22 and 34.02 ppm are proposed to be the resonances of the Tp ligands of a major product. In the ^{1}H NMR spectrum of **8-Yb** (Section 6.4.1) resonances were observed at δ = -112.20, -107.80 and 27.98 ppm, tentatively assigned to the *O,O'*-coordinated pd ligand. Similar resonances are observed in the ^{1}H NMR spectrum of the products of the reaction to synthesise **9-EuYb** at δ = -92.54, -90.21 and 32.75 ppm, which each integrate to *ca* 2H. These could therefore be resonances of the protons of the pd ligand in **9-EuYb**. Several resonances remain unassigned, and of these the resonance at δ = 3.85 ppm is most consistent with other examples of the CH group of hfac ligands bound to Eu(III) (Table 6.2). The ^{19}F NMR spectrum (Figure 6.43) displays several resonances consistent with hfac ligands bound to paramagnetic Yb(III) or Eu(III), with one major product evident at δ = -81.19 ppm, consistent with the CF$_3$ groups of hfac ligands bound to Eu(III) (Table 6.2). These NMR data are consistent with a single major product, which has resonances consistent with the targeted heterobimetallic **9-EuYb**. The minor products are not assigned, but contain resonances consistent with Tp and hfac ligands bound to Eu(III) and Yb(III).

Table 6.2: Chemical shifts of different functional groups in Eu and Yb complexes.

Complex	Chemical shift (/ppm)						
	hfac-C**H**	hfac-C**F**$_3$	Tp-B**H**	Tp-C**H**			Tp-**B**H
1-Eu	3.85	-79.30	-	-	-	-	-
4-Eu	0.08	-81.62	-	-	-	-	-
5-Eu	3.19	-80.50	-	-	-	-	-
7-Yb	-	-	-22.25	-4.89	6.25	39.06	-68.12
8-Yb	-	-	-2.82	3.87	6.40	29.03	-23.68
Yb(Tp)$_2$(hfac)[19, 20]	-31.24	-89.03	-9.20	0.06	6.20	32.72	-36.13

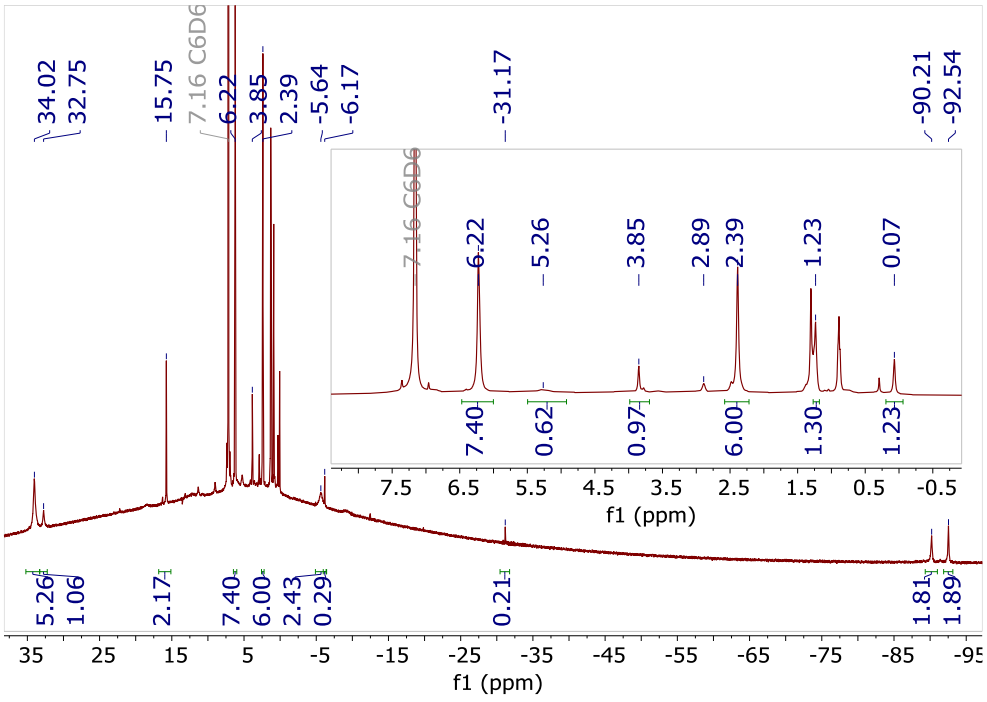

Figure 6.42: The ^{1}H NMR spectrum of the products of the reaction of 7-Yb with 3 and 4-Eu in toluene, recorded in d_6-benzene.

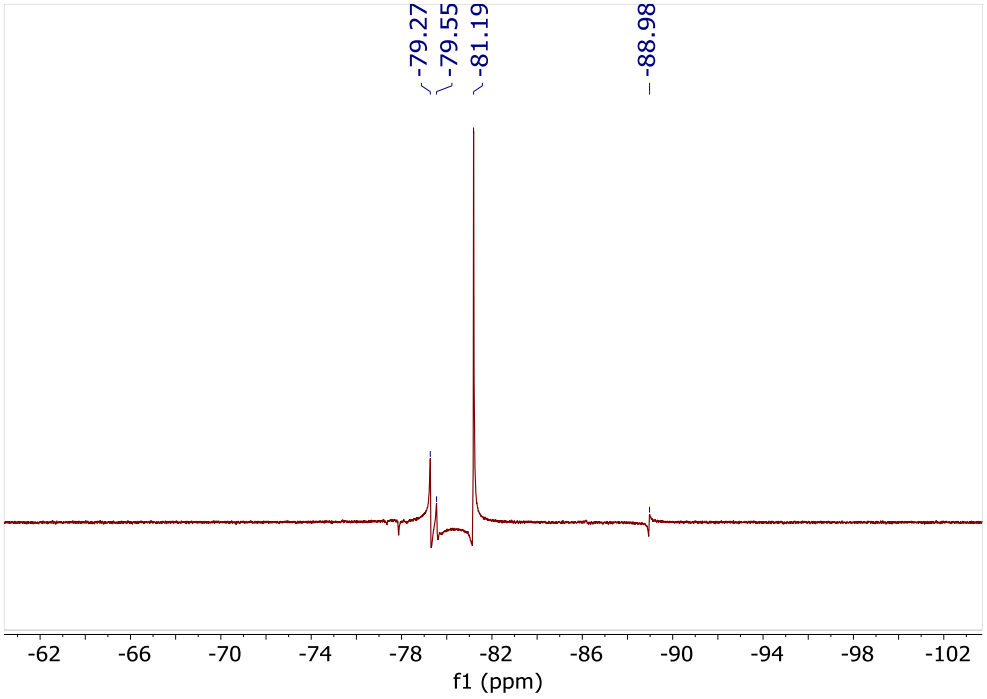

Figure 6.43: The ^{19}F{^{1}H} NMR spectrum of the products of the reaction of 7-Yb with 3 and 4-Eu in toluene, recorded in d_6-benzene.

6.5.2 UV-vis and photoluminescence spectroscopy of 9-LnLn′

The product mixtures containing **9-YbEu** and **9-EuYb** were dissolved in toluene, diluted to *ca* 20 μM concentration (based on an assumed 100% yield of the bimetallic) and their UV-visible absorption spectra were recorded. No extinction coefficients were calculated as the concentration of the mixed species in solution was not known. The toluene solution precluded analysis of the spectrum below the relatively high solvent cut-off at 280 nm. The absorbance spectra each exhibit two transition envelopes with λ_{max} = 292-296 nm and 490-495 nm. The absorbance at 292-296 nm is assigned to the hfac ligands, by comparison to other complexes containing hfac in this thesis (Table 6.3). The absorption at 490-495 nm is similar in energy to transitions in the absorbance spectra of *O,O′*-coordinated products of the reaction of **7-Y** with **5-Y** (λ_{max} = 484 nm) and **8-Yb** (λ_{max} = 475 nm). This is consistent with the products containing the radical pd ligand, coordinated by the *O,O′* binding site to [Ln′(Tp)$_2$]$^+$. Notably, the spectra of **9-YbEu** and **9-EuYb** are near-identical in profile, despite the differences in the species observed in the NMR spectra, indicating that both solutions contain the radical pd ligand in very similar coordination environments. The relative absorbance of the two features in the absorption spectra is also as expected for **9-YbEu** and **9-EuYb** based on the relative extinction coefficients of the hfac absorptions in **1-Ln** and **4-Ln**, and the visible absorption of the radical pd ligand in **3** and **5-Ln** (Table 6.3). The UV-visible absorption spectra are therefore consistent with the heterobimetallic complexes **9-YbEu** and **9-EuYb** in both the energy of the transitions observed and their relative intensities.

Table 6.3: Absorbances assigned to hfac and pd$^{-\bullet}$ in the absorbance spectra of various complexes.

Complex or reaction	λ_{max}/nm (ε/M^{-1} cm^{-1})	
	hfac	pd$^{-\bullet}$
1-Ln (Ln = Eu, Tb, Yb)	300 (26 400-37 800)	-
4-Ln (Ln = Eu, Gd, Yb)	303-304 (23 300-25 900)	-
5-Y	-	642 (2 356)
5-Ln (Ln = Eu, Gd, Yb)	298-301 (39 600-43 200)	600-650 (500-670)
3	-	558 (3 866)

7-Y + 5-Y	-	485
8-Yb	-	475

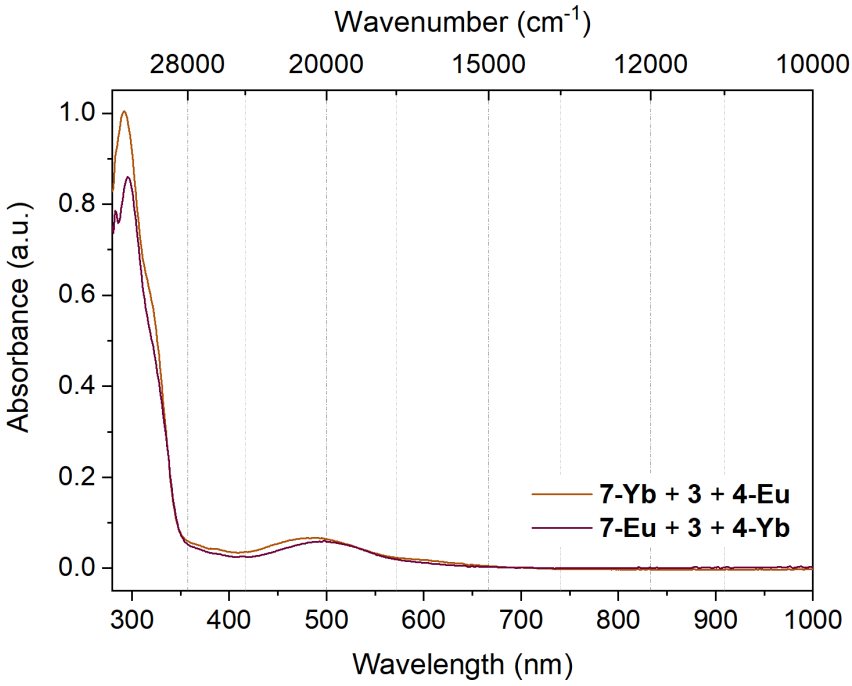

Figure 6.44: The UV-visible absorbance spectra of product mixtures containing 9-EuYb and 9-YbEu, recorded on *ca* 20 μM toluene solutions.

Steady-state photoluminescence spectra were also recorded of the products of the reaction of **7-Ln** (Ln = Eu, Yb) with **3** and **4-Ln'** (Ln' = Eu, Yb). Both product mixtures exhibited characteristic luminescence from both Eu(III) and Yb(III) (see Figure 6.45 and Figure 6.46). In both cases, emission from Yb(III) was observed following irradiation with visible (485-490 nm) light. This is similar to observations of the products of the reaction of **7-Yb** with **3**, which was attributed to sensitisation of Yb(III) in the *O,O'* binding site by the pd radical ligand. The emission from Yb(III) sensitised in this way was qualitatively brighter in **9-EuYb** (Yb in *O,O'* site) than in **9-YbEu** (Yb in *N,N'* site).

It is also notable that the profiles of the Eu(III) and Yb(III) emission spectra are quite different in the products of the two reactions. In the emission spectra of **9-EuYb**, only two maxima are observed in the NIR region for emission from Yb(III), with λ_{max} = 974 and 1025 nm. On the other hand, in the emission spectra of **9-YbEu**, three maxima are observed in the same region with λ_{max} = 975, 1004 and 1030 nm, indicating that the emitting Yb(III) ion is in different

coordination environments in the two complexes. These observations may be compared to the maxima in the emission spectra of other complexes of Yb(III) described previously. The *bis*-Tp coordinated **7-Yb** exhibits two maxima in the emission spectrum at λ_{max} = 975 and 1010 (shoulder) nm (Figure 6.14). Meanwhile, the *tris*-hfac coordinated **5-Yb** exhibits three maxima at λ_{max} = 975, 1000 and 1026 nm (Chapter 4, Figure 4.8). This is indicative that in **9-EuYb** the emissive Yb(III) is in a *bis*-Tp environment, while in **9-YbEu** the emissive Yb(III) ion is in a *tris*-hfac environment.

Differences may also be discerned in the Eu(III) emission spectra. The most salient difference is that the $^5D_0 \rightarrow {}^7F_0$ transition (577 nm) is visible in the spectrum of **9-EuYb** where it is not for **9-YbEu**. This occurrence of this transition is dependent on the symmetry of the site occupied by Eu(III),[12] indicating that in **9-EuYb** and **9-YbEu** the local environment of Eu(III) is different. The ratio of the areas of the $^5D_0 \rightarrow {}^7F_1$ (590 nm) and $^5D_0 \rightarrow {}^7F_2$ (610 nm) transitions is also different in the two products. This ratio has been used as an measure of the coordination environment of Eu(III).[12] The $^5D_0 \rightarrow {}^7F_1$ transition is not hypersensitive, and has very little dependence on the local symmetry or environment. Meanwhile, the $^5D_0 \rightarrow {}^7F_2$ transition is hypersensitive, and therefore varies greatly in intensity depending on the local environment of Eu(III). In **9-YbEu**, the ratio of the $^5D_0 \rightarrow {}^7F_1$ transition to the $^5D_0 \rightarrow {}^7F_2$ transition is around 1:6, while in **9-EuYb**, the ratio of the same two transitions is around 1:12. For reference, the ratio of those transitions in *tris*-hfac, *N,N'* coordinated **5-Eu** is around 1:16 while the ratio of the same transitions in *bis*-Tp **7-Eu** is around 1:4.5.[††] This observation further indicates that the coordination environment of the Eu(III) ions in the two products is different. In **9-YbEu**, the spectrum has greater similarity to **7-Eu** with Eu(III) in a *bis*-Tp environment, while in **9-EuYb** the emission spectrum is closer to **5-Eu** with Eu(III) in an *N,N'*, *tris*-hfac environment.

Together, the differences in the emission spectra of the Eu(III) and Yb(III) ions in **9-EuYb** and **9-YbEu** indicate that the chemical environments of the lanthanide ions remained different in **9-EuYb** and **9-YbEu** over the hours during which the photoluminescence spectra were recorded. This is good evidence for the selective coordination of Eu(III) and Yb(III) in **9-LnLn'**,

[††] Ratio of the $^5D_0 \rightarrow {}^7F_1$ and $^5D_0 \rightarrow {}^7F_2$ transitions determined of the spectrum recorded with λ_{Ex} = 320 nm (see Figure 6.13). The ratio of the same transitions recorded at other λ_{Ex} ranged from 1:3.5 to 1:2.

and also the relative stability of the heterobimetallics in toluene solution at room temperature over that timescale.

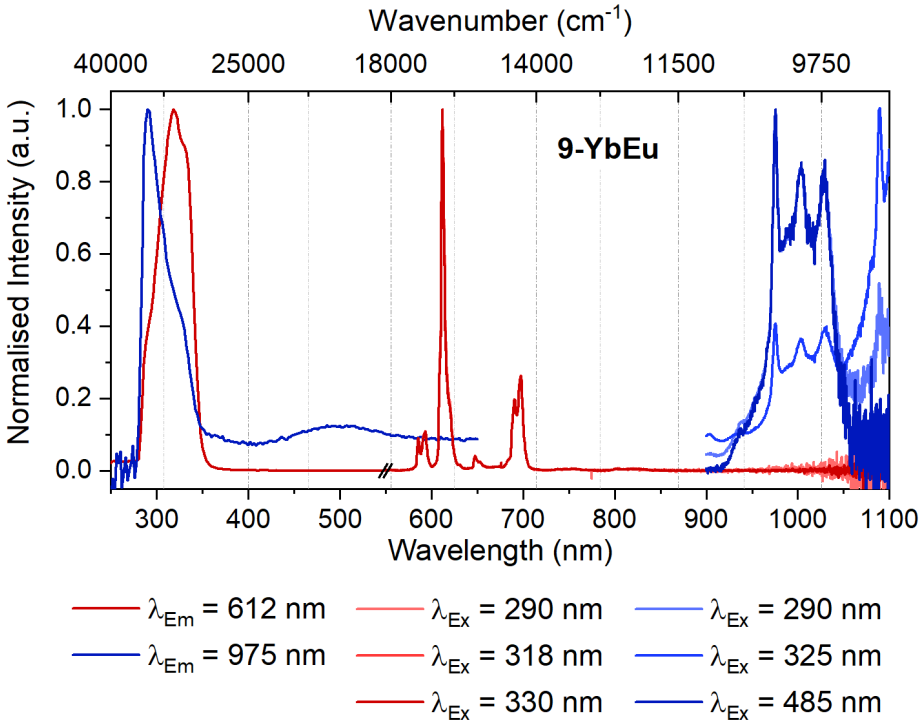

Figure 6.45: Steady-state photoluminescence spectra of 9-YbEu, recorded in *ca* 20 μM toluene solution. Far left, excitation spectra for Eu(III) (λ_{Ex} = 612 nm) and Yb(III) (λ_{Ex} = 975 nm) emission; centre red lines, Eu(III) emission spectra; far right blue lines, Yb(III) emission spectra. All spectra were recorded on the same solution.

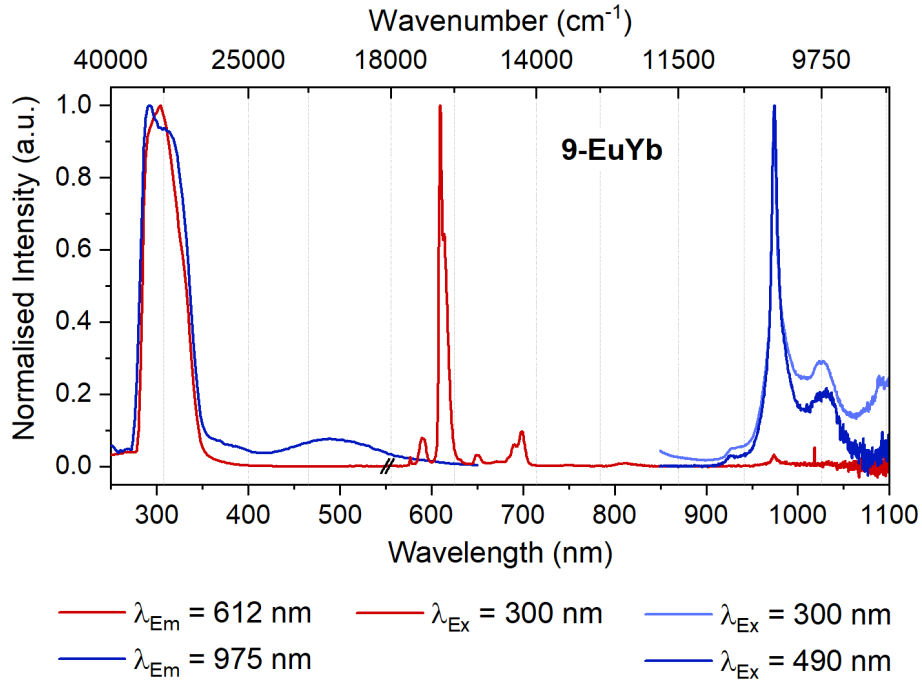

Figure 6.46: Steady-state photoluminescence spectra of 9-EuYb, recorded in *ca* 20 μM toluene solution. Far left, excitation spectra for Eu(III) (λ_{Ex} = 612 nm) and Yb(III) (λ_{Ex} = 975 nm) emission;

centre red line, Eu(III) emission spectrum; far right blue lines, Yb(III) emission spectra. All spectra were recorded on the same solution.

6.5.3 X-ray crystallography of lanthanide heterobimetallics

Single crystals of **9-YY'** and **9-EuYb** suitable for X-ray diffraction were obtained by cooling of the hexane extract from the reactions of **7-Ln'** with **3** and **4-Ln** to -35 °C. In each case, the asymmetric unit comprises two bimetallic molecules, one of which is shown in the figures below. The solid-state molecular structure of **9-YY'** is shown in Figure 6.47, and shows the selective coordination of $[Y(Tp)_2]^+$ to the *O,O'* binding site of pd, while $Y(hfac)_3$ is selectively coordinated to the *N,N'* binding site. The bond lengths of the pd ligand in **9-YY'** are consistent with the ligand being in the radical anion oxidation state. The C-O(pd) bonds of 1.26(2)-1.32(2) Å are consistent with those in **3** of 1.268(4)-1.278(4) Å, and the C5-C6 bonds of 1.42(2)-1.43(2) Å are also similar to that in **3** of 1.456(5) Å.[32] These distances are, as in **3**, consistent with a delocalised electronic structure across the O-C-C-O site. The Y-N(pd) bond distances of 2.491(9)-2.55(1) Å and Y-O(hfac) bond distances of 2.30(1)-2.341(8) Å are consistent with the same metric in **1-Y** (Y-N(pd) 2.501(3)-2.552(3), Y-O(hfac) 2.299(3)-2.344(3) Å).[10] Additionally, the Y-N(Tp) bond distances of 2.42(1)-2.521(8) Å are consistent with those observed in **7-Y** of 2.402(2)-2.540(2) Å. The Y-O(pd) bond distances of 2.328(8)-2.412(8) Å are consistent with the Y-O(CA) bond distances in $(Y(Tp)_2)_2(CA)$ (CA = chloranilate).[2]

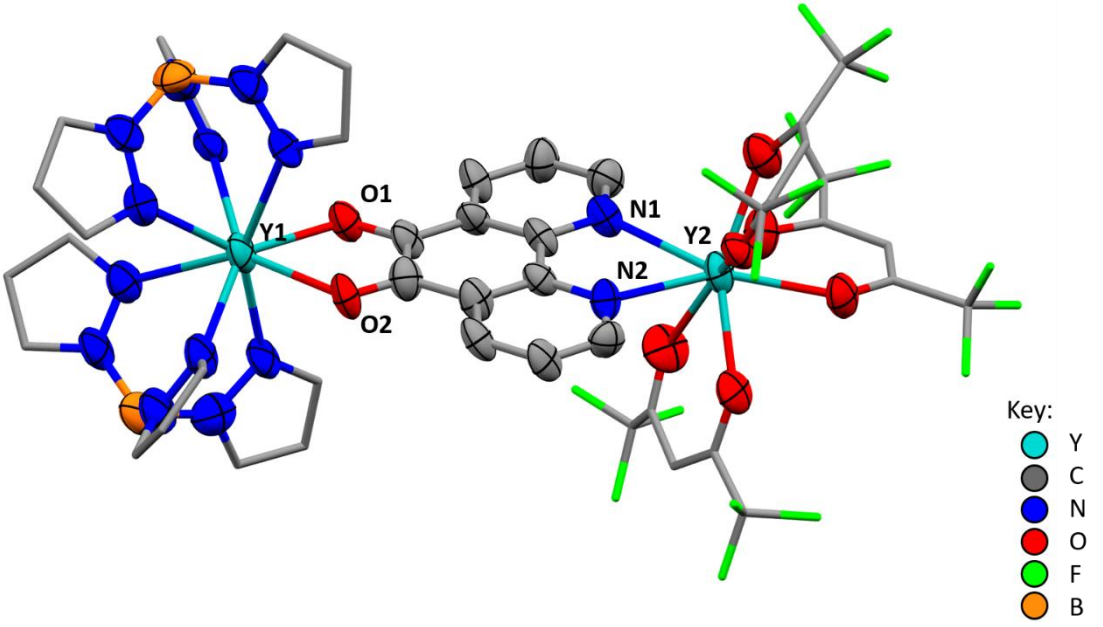

Figure 6.47: The solid-state molecular structure of 9-YY. C and F atoms of the Tp and hfac ligands are drawn in wireframe, and H atoms are omitted for clarity. Thermal ellipsoids are drawn at 50%

probability. Selected distances: C-O(pd) 1.26(2)-1.32(2), C5-C6 1.42(2)-1.43(2), Y-O(pd) 2.328(8)-2.412(8), Y-N(Tp) 2.42(1)-2.521(8), Y-N(pd) 2.491(9)-2.55(1), Y-O(hfac) 2.30(1)-2.341(8) Å.

The solid-state molecular structure of **9-EuYb** is shown in Figure 6.48, and shows the selective coordination of Eu(hfac)$_3$ to the *N,N'* site and [Yb(Tp)$_2$]$^+$ to the *O,O'* site of the pd ligand. Similarly to **9-YY**, the bond distances in the *O,O'* binding site of the pd ligand in **9-EuYb** are consistent with the ligand being in the radical anion oxidation state. The C-O(pd) bond distances are 1.26(1)-1.27(1) Å, while the C5-C6 bonds are in the range 1.42(1)-1.45(1) Å, consistent with the bonds observed in **3** (C-O(pd) 1.268(4)-1.278(4), C5-C6 1.456(5) Å).[32] The Eu-O(hfac) bonds of 2.329(9)-2.412(7) Å and Eu-N(pd) bonds of 2.542(9)-2.592(9) Å are consistent with those observed in **1-Eu** (Eu-O(hfac) 2.354(3)-2.389(3), Eu-N(pd) 2.564(3)-2.569(3) Å). Likewise, the Yb-N(Tp) bonds of 2.390(9)-2.496(9) Å are consistent with those in **7-Yb** (Yb-N(Tp) 2.365(6)-2.489(6) Å). The Yb-O(pd) bond distances of 2.298(6)-2.405(6) Å are consistent with the Yb-O bonds of 2.325(3)-2.334(3) Å in the symmetrically semiquinone-bridged homobimetallic complex {(Tp)$_2$Yb}$_2$(μ-CA) (CA^{2-} = 3,6-dichloro-tetraoxalate).[33]

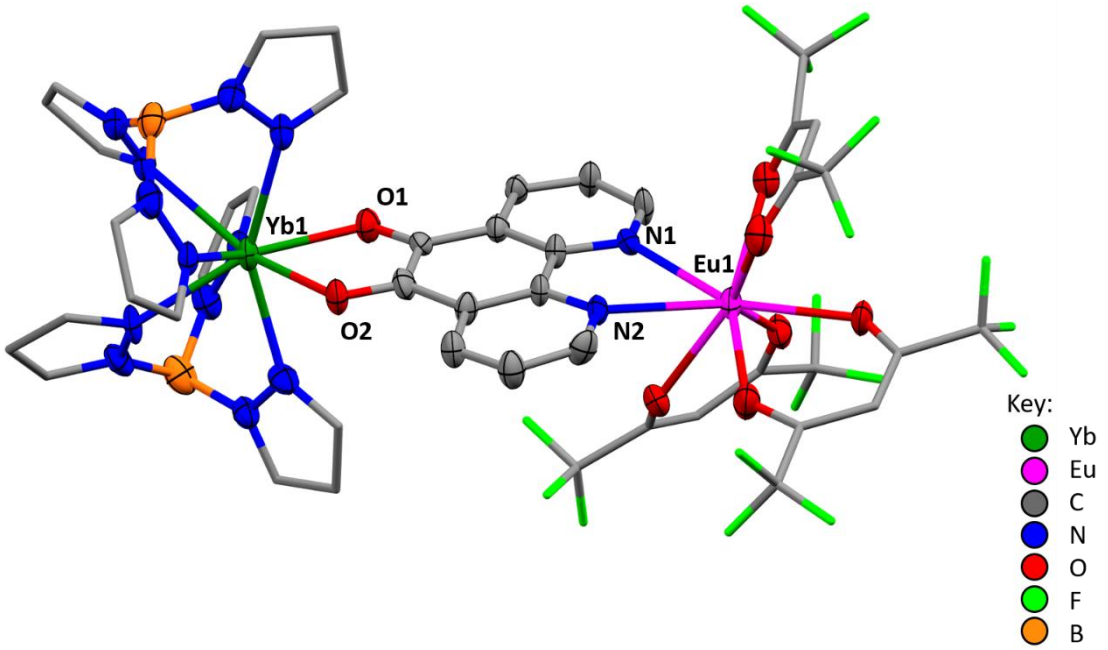

Figure 6.48: The solid-state molecular structure of 9-EuYb. C and F atoms of the Tp and hfac ligands are drawn in wireframe, and H atoms are omitted for clarity. Thermal ellipsoids are drawn at 50% probability. Selected distances: C-O(pd) 1.26(1)-1.27(1), C5-C6 1.42(1)-1.45(1), Yb-O(pd) 2.298(6)-2.405(6), Yb-N(Tp) 2.390(9)-2.496(9), Eu-N(pd) 2.542(9)-2.592(8), Eu-O(hfac) 2.329(9)-2.412(7) Å.

The bond distances of the lanthanides to the ligands may be used as a test to confirm that the lanthanides have not undergone scrambling, due to the significant difference in ionic radii between Eu(III) (1.066 Å) and Yb(III) (0.988 Å).[15] Table 6.4 therefore gives a comparison of selected bond distances in **1-Ln** (Ln = Eu, Yb) and **7-Ln** (Ln = Eu, Yb) to those in **9-EuYb**. It is clear that the bond distances in **9-EuYb** are in much greater agreement with those in **1-Eu** and **7-Yb** than with those in **1-Yb** and **7-Eu**. The close agreement of these bond distances and the relatively small variance of each (generally around 0.02 Å; the difference in ionic radius of 8-coordinate Yb(III) and Eu(III) is 0.081 Å)[15] are strong indicators that the lanthanides have not undergone significant scrambling under the conditions of the crystallisation.

Table 6.4: Comparison of bond distances in 1-Ln (Ln = Eu, Yb), 7-Ln (Ln = Eu, Yb) and 9-EuYb.

Compound	Bond distances (Å)			
	$Ln\text{-}O_{(hfac)}$	$Ln\text{-}N_{(pd)}$	$Ln\text{-}N_{(Tp)}$	$Ln\text{-}O_{(pd)}$
1-Eu	2.354(3)-2.389(3)	2.564(3)-2.539(3)	n/a	n/a
1-Yb	2.268(4)-2.312(2)	2.472(5)-2.492(2)	n/a	n/a
7-Eu	n/a	n/a	2.452(4)-2.573(3)	n/a
7-Yb	n/a	n/a	2.365(6)-2.489(6)	n/a
9-EuYb	2.329(9)-2.412(7)	2.542(9)-2.592(8)	2.390(9)-2.496(9)	2.298(6)-2.405(6)

6.5.4 Fast-timescale reaction of 7-Yb with 3 and 4-Y

It was necessary to further control the reaction and prevent any formation of $Ln(Tp)_2(hfac)$ so that the bimetallic could be isolated in high purity. Since it appeared that the individual stages of the reaction were near-instantaneous at room temperature, it was decided that continuing to perform the reaction at the lowest temperature possible (-35 °C) and minimising the time of reaction might reduce the quantity of byproducts produced. At -35 °C, 1.1 eq. of $Yb(Tp)_2(OTf)$ suspended in toluene was mixed with **3**, also suspended in toluene. A colour change from purple to red was observed. The mixture was stirred for 1 minute or 5 minutes

at -35 °C. **4-Y** in toluene (at -35 °C) was then added and the reaction mixture was stirred for a further 1 minute, then immediately toluene was removed *in vacuo*. Hexane was used to extract the solids with filtration *via* frit, and hexane was removed from the extract *in vacuo*. The solids thus obtained were weighed and NMR spectra were recorded in d_6-benzene. The spectra for t = 1 min and t = 5 min were near identical, so only one will be discussed.

The ^{1}H NMR spectrum (Figure 6.49) contains a significant number of resonances, none of which are attributed to Yb(Tp)$_2$(hfac).[19, 20] A pair of significantly shifted resonances are observed at δ = -93.64 and -93.21 ppm. These are similar to some of the resonances in **9-EuYb** at δ = -92.54 and -90.21 ppm, and echo a pair observed in **8-Yb** at -112.2 and -107.8 ppm. These resonances are therefore assigned to two of the protons of the radical pd ligand, coordinated at the *O,O'* binding site by Yb(III). The resonances with the highest integration are at δ = 0.06 (6H), 6.20 (10H) and 32.76 (6H) ppm, and these are consistent with Tp ligands bound to Yb(III). On the shoulder of the resonance at 6.20 ppm there appears to be a second resonance, with a maximum at δ = 6.18 ppm. The shift of this resonance is consistent with hfac ligands bound to Y(III),[10, 32] and the addition of three protons from the hfac ligands to the six protons of the Tp C-H would explain why this resonance integrates to 10H where the other two main resonances integrate to *ca* 6H. The ^{1}H NMR spectrum is therefore consistent with the formation of a heterobimetallic product **9-YYb**. In addition to the resonances that have been assigned, several others were observed which indicate at least one further product.

The ^{11}B NMR spectrum (Figure 6.51) contains a single predominant resonance at δ = -36.48 ppm, along with a smaller resonance at δ = -32.02 ppm, both of which are consistent with Tp ligands coordinated to Yb(III) as seen previously in this chapter. Meanwhile, the ^{19}F NMR spectrum (Figure 6.50) contains three main resonances, with the most significant at δ = -78.93 ppm and with two less intense resonances at δ = -76.73 and -88.96 ppm. Those at δ = -78.93 and -76.73 ppm are consistent with hfac ligands bound to Y(III).[10, 32] The resonance at δ = -88.96 ppm is more consistent with a hfac ligand bound to Yb(III) (**1-Yb**, -84.42 ppm; **4-Yb**, -90.49 ppm; **5-Yb**, -83.07 ppm), indicating that at least one side-product is the result of a ligand redistribution reaction. As with the ^{1}H NMR data, these data are consistent with a bimetallic product **9-YYb**, in conjunction with a secondary species. The predominance of the single species, with resonances assigned to the heterobimetallic complex, indicates that combining

this synthesis with purification of the products by recrystallisation might be an effective method for obtaining analytically pure heterobimetallics, albeit in low yields.

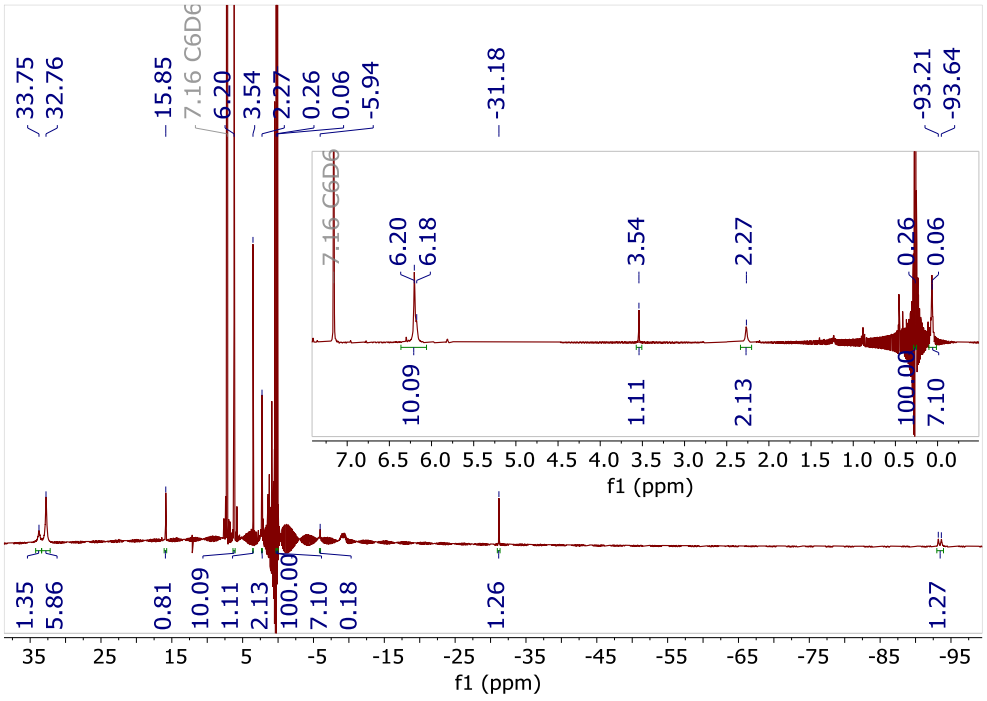

Figure 6.49: The ^{1}H NMR spectrum of the products of the reaction between 7-Yb, 3 and 4-Y in toluene at -35 °C, recorded in d_6-benzene.

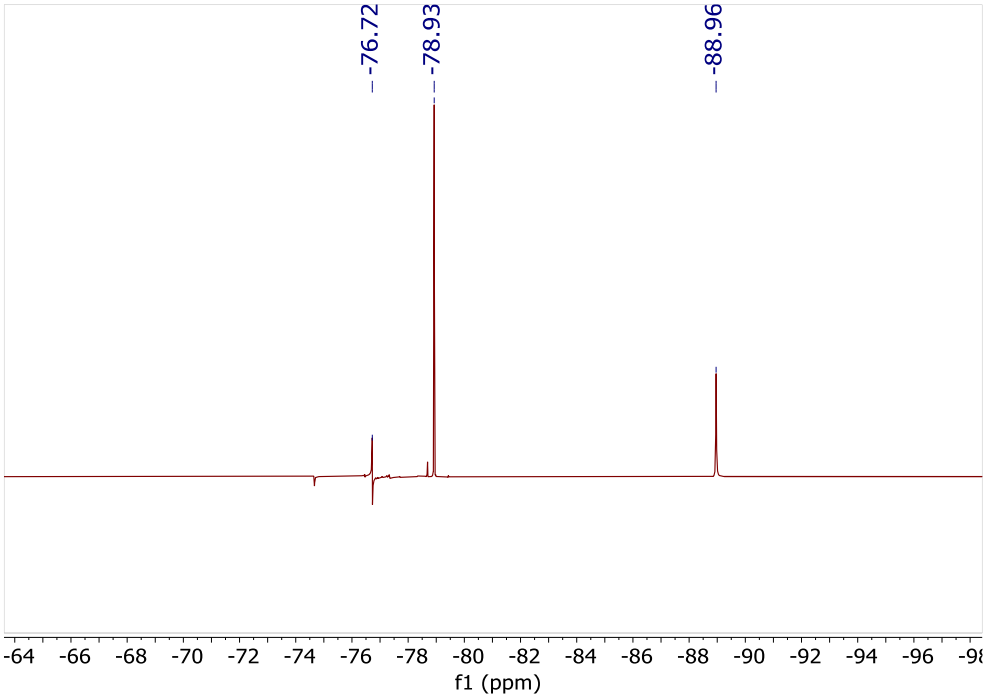

Figure 6.50: The $^{19}F\{^{1}H\}$ NMR spectrum of the products of the reaction between 7-Yb, 3 and 4-Y in toluene at -35 °C, recorded in d_6-benzene.

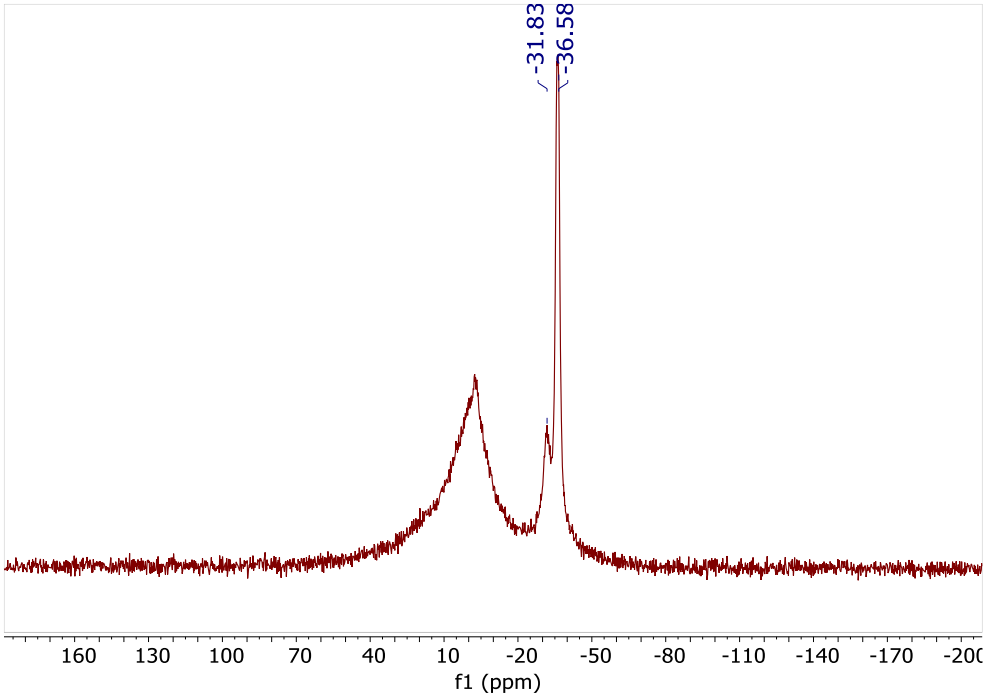

Figure 6.51: The ^{11}B NMR spectrum of the products of the reaction between 7-Yb, 3 and 4-Y in toluene at -35 °C, recorded in d_6-benzene.

6.5.5 Conclusions

The synthesis of lanthanide heterobimetallics has been investigated by the reaction of **7-Ln** with **3** and **4-Ln**, to take advantage of the selective coordination properties of **7-Ln** and **4-Ln**. It is apparent however that ligand redistribution is a significant cause for concern, even when reactions are performed at low temperature in non-coordinating solvents (toluene). Multiple products have been shown by multinuclear NMR spectroscopy to be formed in the reaction, often including $Ln(Tp)_2(hfac)$. NMR analysis of the products is also necessarily limited somewhat, as the multiple paramagnetic centres (Eu(III), Yb(III), organic radical) in the system may render some products NMR silent. However, despite the ligand redistribution observed by NMR spectroscopy, photoluminescence spectroscopy showed that some selectivity was achieved using this synthesis, clearly demonstrating that the products of the reaction of **7-Eu** with **3** and **4-Yb** contained Eu(III) and Yb(III) in different coordination environments than were observed for the products of the reaction of **7-Yb** with **3** and **4-Eu**. Additionally, the solid-state molecular structures of two lanthanide heterobimetallics **9-YY** and **9-EuYb** were successfully obtained. In the case of **9-EuYb**, the Eu-O(hfac) and Eu-N(pd) bond lengths were consistent with, and extremely similar to, similar bonds in **1-Eu**. Similarly, the Yb-N(Tp) bond lengths were extremely similar to those in **7-Yb**, indicating that the complex had not undergone lanthanide scrambling. Severely limiting the time of the reaction to very short (1 min) timescales at low temperatures (-35 °C) appeared to mostly prevent ligand redistribution in the products. This promising result indicates that it might be possible to obtain pure lanthanide heterobimetallics from such a synthesis by a selective crystallisation. However, due to time constraints the lanthanide heterobimetallics **9-LnLn'** have not yet been fully isolated from the reaction mixtures.

6.6 Conclusions

The synthesis of a promising series of lanthanide heteroleptic transmetallation reagents **7-Ln** (Ln = Y, Eu, Gd, Yb) has been presented, along with their full characterisation. Solid state molecular structures have been determined, providing useful bond data. The reactions of **7-Ln** with **5-Ln**, aiming to synthesise lanthanide heterobimetallics, resulted in significant ligand redistribution and lanthanide scrambling in the products, so a different route to the heterobimetallics was sought. The reaction of **7-Ln** with **3** resulted in a selective coordination of **7-Ln** to the *O,O'* binding site of the radical ligand in **8-Ln**. This was evidenced by both electronic spectroscopy and photoluminescence spectroscopy, by comparison to the uncomplexed radical ligand **3** and the *N,N'* coordinated **5-Ln**. In particular, photoluminescence from Yb(III) was sensitised by visible light irradiation of a transition assigned to the radical pd ligand in **8-Yb**, which was not observed in **5-Yb**. **8-Ln** were however challenging to isolate away from the side-product of the metathesis reaction, $[CoCp_2]^+[pd]^-$ due to similar solubilities. **8-Ln** was therefore used *in situ* to synthesise lanthanide heterobimetallics.

The reaction of **7-Ln** with **3** was followed by addition of *N,N'* selective **4-Ln**. There is evidence from the photoluminescence spectra of the products **9-LnLn'** that the lanthanides are selectively bound to the pd ligand and do not undergo redistribution on the timescale of the measurement. Solid-state molecular structures of **9-YY'** and **9-EuYb** were also successfully obtained. The bond lengths in **9-EuYb** are consistent with no lanthanide scrambling having occurred under the conditions of the crystallisation. However, it is clear from multinuclear NMR spectroscopy of the products that ligand redistribution occurred during the reaction in addition to formation of **9-LnLn'**. This redistribution was significantly reduced by ensuring that the reaction was performed on a very short timescale, maintaining the reaction at -35 °C throughout. It is suggested that this reaction could be followed by purification by selective crystallisation to isolate lanthanide heterobimetallics **9-LnLn'**.

6.7 Experimental details for Chapter 6

6.7.1 General synthetic details

$Ln(OTf)_3$, **3** and **5-Ln** were synthesised as described in previous chapters.[10, 32] K(Tp) was synthesised by modification of a literature route.[34]

6.7.2 Synthesis of 7-Y

$Y(OTf)_3$ (520.0 mg, 0.9700 mmol) and K(Tp) (488.9 mg, 1.9391 mmol, 2 eq.) were added dry to a schlenk. THF (20 ml) was added with stirring and the mixture was stirred at room temperature for 1.5 h. THF was removed *in vacuo* and the white powder was extracted into DCM (20 ml) overnight, then washed again with DCM (20 ml). DCM was removed *in vacuo* from the filtrates and the white powder was washed with hexane (2x 15 ml), affording **7-Y** as a white powder (350.9 mg, 0.5284 mmol, 54% yield). Single crystals were grown by slow diffusion of hexane into a concentrated THF solution of **7-Y** over several days. ^{1}H NMR (d_3-MeCN): δ = 6.11 (6H, t; 2.2 Hz, Tp-C**H**), 7.15 (6H, d; 2.1 Hz, Tp-C**H**), 7.80 (6H, dd; 2.2, 0.7 Hz, Tp-C**H**) ppm. ^{19}F{^{1}H} NMR (d_3-MeCN): δ = -79.20 (OTf-C**F**$_3$) ppm. ^{11}B NMR (d_3-MeCN): δ = -3.06 (d; 99.6 Hz, Tp-**B**H) ppm. ^{1}H NMR (d_6-benzene): δ = 4.77 (2H, s, br, Tp-B**H**), 5.79 (6H, d, 2.1 Hz, Tp-C**H**), 7.25 (6H, s, Tp-C**H**), 7.44 (6H, s, Tp-C**H**) ppm. ^{19}F{^{1}H} NMR (d_6-benzene): δ = -76.52 (OTf-C**F**$_3$) ppm. ^{11}B NMR (d_6-benzene): δ = -2.62 (Tp-**B**H) ppm. IR(ATR)/cm^{-1}: 3140 (w), 2469 (m, ν_{BH}), 1506 (m, ν_{SO}), 1406 (s), 1389 (s), 1298 (s), 1213 (s), 1123 (s),1032 (s), 978 (s). Anal. Calcd. for $YC_{19}H_{20}N_{12}O_3B_2SF_3$: C, 34.37%; H, 3.04%; N, 25.31%. Found: C, 34.49-34.64%; H, 3.25-3.30%; N, 23.39-23.71%.

6.7.3 Synthesis of 7-Eu

$Eu(OTf)_3$ (610.6 mg, 1.0191 mmol) and K(Tp) (512.2 mg, 2.031 mmol) were added dry to a schlenk. THF (15 ml) was added with stirring and the mixture was stirred for 2 h, over which time a white precipitate formed. THF was removed *in vacuo* and the solid was extracted into DCM (3x 15 ml), then DCM was removed *in vacuo* from the filtrate. The solid was washed with hexanes (3x 15 ml), then dried *in vacuo* and weighed (232.1 mg, 0.3192 mmol). Due to the low yield, DCM (20 ml) was added to the solid and the mixture was sonicated for 10 m, then the mixture was filtered and the solid washed with DCM (10 ml). DCM was removed *in vacuo* to leave a white powder, which was washed with hexanes (3x 10 ml), dried *in vacuo* and

weighed to give **7-Eu** (154.6 mg, 0.2126 mmol, total 52% yield). Single crystals were grown by slow diffusion of hexane into a concentrated THF solution of **7-Eu** over several days. ^{1}H NMR (d_3-MeCN): δ = -1.71 (2H, br, Tp-B**H**), 0.40 (6H, s, Tp-C**H**), 3.02 (6H, s, Tp-C**H**), 14.05 (6H, s, Tp-C**H**) ppm. ^{19}F NMR (d_3-MeCN): δ = -80.86 (OTf-C**F**$_3$) ppm. ^{11}B NMR (d_3-MeCN): δ = -22.29 (d, Tp-**B**H) ppm. ^{1}H NMR (d_6-benzene): δ = -1.97 (2H, s, Tp-B**H**), 0.01 (6H, s, Tp-C**H**), 2.65 (6H, s, Tp-C**H**), 14.63 (6H, s, Tp-C**H**) ppm. ^{19}F NMR (d_6-benzene): δ = -75.12 (OTf-C**F**$_3$) ppm. ^{11}B NMR (d_6-benzene): -24.94 (Tp-**B**H) ppm. UV-vis (THF) λ_{max}/nm (ε/M^{-1} cm^{-1}): 287 (325, BHT), 394 (6.6). IR(ATR) /cm^{-1}: 3138 (w), 2469 (m, ν_{BH}), 1504 (m, ν_{SO}), 1404 (s), 1298 (s), 1211 (s), 1122 (s), 1033 (s), 976 (s). Anal. Calcd. for $EuC_{19}H_{20}N_{12}O_3B_2SF_3$: C, 31.39%; H, 2.77%; N, 23.12%. Found: C, 32.56-33.16%; H, 2.99-3.04%; N, 22.20-22.51%.

6.7.4 Synthesis of 7-Gd

$Gd(OTf)_3$ (466.4 mg, 0.7716 mmol) and K(Tp) (389.3 mg, 1.544 mmol) were separately slurried in THF (15 ml each), then K(Tp) was added to Gd(OTf) with stirring. The mixture was stirred for 2 h, then THF was removed *in vacuo* from the white suspension. The white solids were extracted into DCM (30 ml, then 15 ml) and DCM was removed from the filtrate *in vacuo*. The solid was washed with hexane (3x 20 ml), affording **7-Gd** as a white powder (326.6 mg, 0.446 mmol, 58% yield). No ^{1}H, ^{19}F or ^{11}B NMR resonances were observed for **7-Gd**. μ_{eff} (Evans' Method) = 7.89-8.21 μ_B. IR(ATR) /cm^{-1}: 3148 (w), 2469 (m, ν_{BH}), 1504 (m, ν_{SO}), 1404 (s), 1298 (s), 1211 (s), 1123 (s), 1032 (s), 978 (s). Anal. Calcd. for $GdC_{19}H_{20}N_{12}O_3B_2SF_3$: C, 31.16%; H, 2.75%; N, 22.95%. Found: C, 31.10-31.14%; 2.74-2.76%; N, 21.63-22.13%.

6.7.5 Synthesis of 7-Yb

$Yb(OTf)_3$ (621.9 mg, 1.003 mmol) was stirred with K(Tp) (505.6 mg, 2.005 mmol) in THF (20 ml) for 2.5 h. THF was removed *in vacuo*, leaving a white powder, which was extracted into DCM (2x 15 ml). DCM was then removed from the filtrate *in vacuo* to afford **7-Yb** as a white powder (457.0 mg, 0.611 mmol, 61%). Single crystals were grown by slow diffusion of hexane into a concentrated THF solution of **7-Yb** over several days. ^{1}H NMR (d_3-MeCN): δ = -22.18 (Tp-B**H**), -4.95 (Tp-C**H**), 6.27 (Tp-C**H**), 39.37 (Tp-C**H**) ppm. ^{19}F NMR (d_3-MeCN): δ = -81.37 (OTf-C**F**$_3$) ppm. ^{11}B NMR (d_3-MeCN): δ = -66.91 (Tp-**B**H) ppm. ^{1}H NMR (d_6-benzene): δ = -24.98 (2H, s, Tp-B**H**), -6.44 (6H, s, Tp-C**H**), 7.40 (6H, s, Tp-C**H**), 53.31 (6H, s, Tp-C**H**) ppm. ^{19}F NMR (d_6-benzene): δ = -100.95 (OTf-C**F**$_3$) ppm. ^{11}B NMR (d_6-benzene): δ = -75.78 (Tp-**B**H) ppm. UV-vis

(MeCN) λ_{max}/nm (ε/M^{-1} cm^{-1}): 974 (5.9). UV-vis (THF) λ_{max}/nm (ε/M^{-1} cm^{-1}): 973 (4.5). IR(ATR)/cm^{-1}: 3144 (w), 2469 (m, ν_{BH}), 1506 (m, ν_{SO}), 1406 (s), 1298 (s), 1215 (s), 1121 (s), 1032 (s), 978 (s). Anal. Calcd. for $YbC_{19}H_{20}N_{12}O_3B_2SF_3$: C, 30.50%; H, 2.69%; N, 22.47%. Found: C, 31.55-33.37%; H, 2.82-2.96%; N, 21.83-23.20%.

6.7.6 Small-scale reaction of 5-Y with 7-Y

A suspension of **7-Y** (46.6 mg, 0.0702 mmol) in toluene (2 ml) was added to a suspension of **5-Y** (77.8 mg, 0.0701 mmol) in toluene (1 ml) with stirring. A colour change from dark green to red was observed, and the reaction was stirred for 45 min. The mixture was filtered *via* frit and toluene was removed from the dark red filtrate *in vacuo* to leave a dark red solid (40.1 mg). Hexane (2x 2 ml) was used to extract the solids with filtration *via* frit, then the hexane solution was placed in the freezer for crystallisation.

6.7.7 NMR-monitoring of the reaction of 5-Y with 7-Y in d_6-benzene

An NMR tube was charged with **5-Y** (11.6 mg, 0.0105 mmol), **7-Y** (7.9 mg, 0.0119 mmol) and $Si(TMS)_4$ (5.6 mg, 0.0175 mmol) and d_6-benzene (0.2 ml) was added (11:45 am). The NMR spectrum was recorded at intervals up to 6 h, after which time a colourless solution was present over a green solid. The intensity of the resonances of $Y(Tp)_2(hfac)$ was determined at each time point relative to that of the standard $Si(TMS)_4$ and was plotted against time.

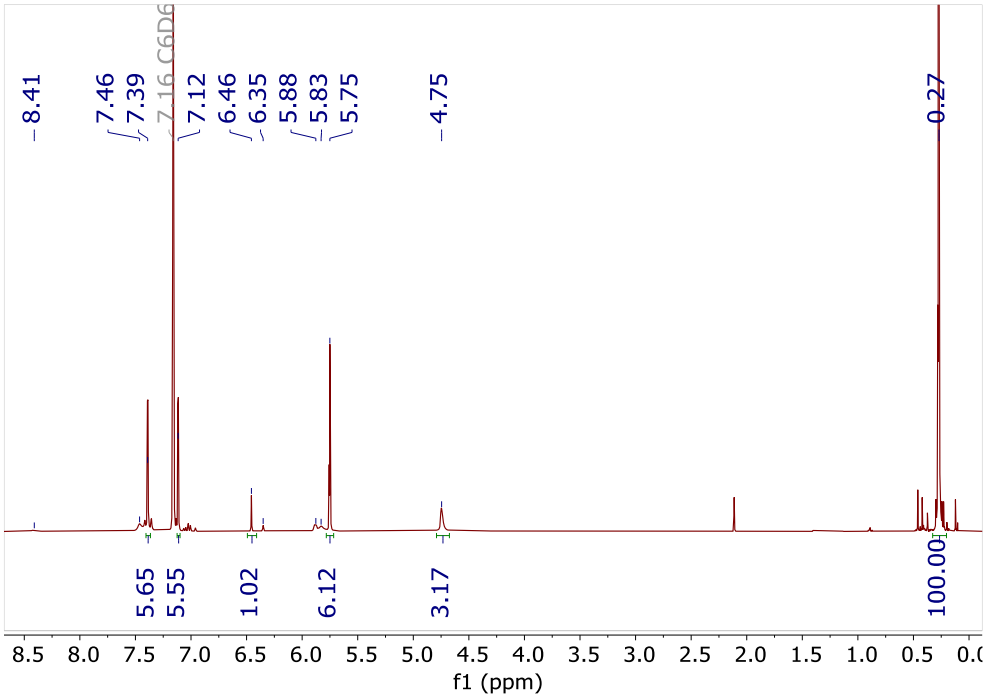

Figure 6.52: The ^{1}H NMR spectrum of the reaction between 5-Y and 7-Y in d_6-benzene, recorded after 10 m.

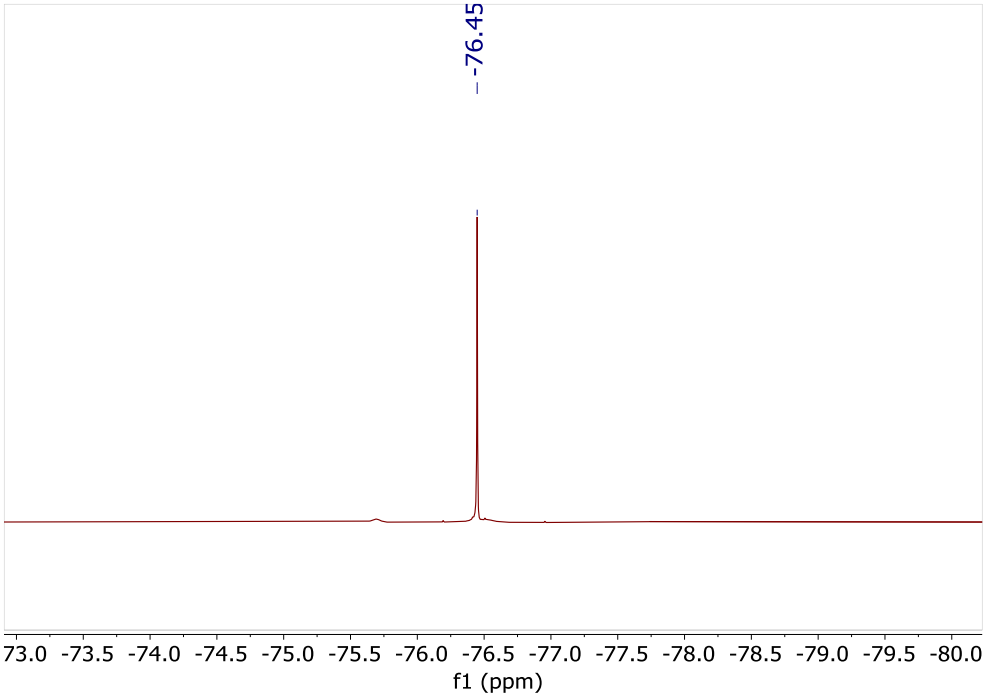

Figure 6.53: The ^{19}F{^{1}H} NMR spectrum of the reaction between 5-Y and 7-Y in d_6-benzene, recorded after 10 m.

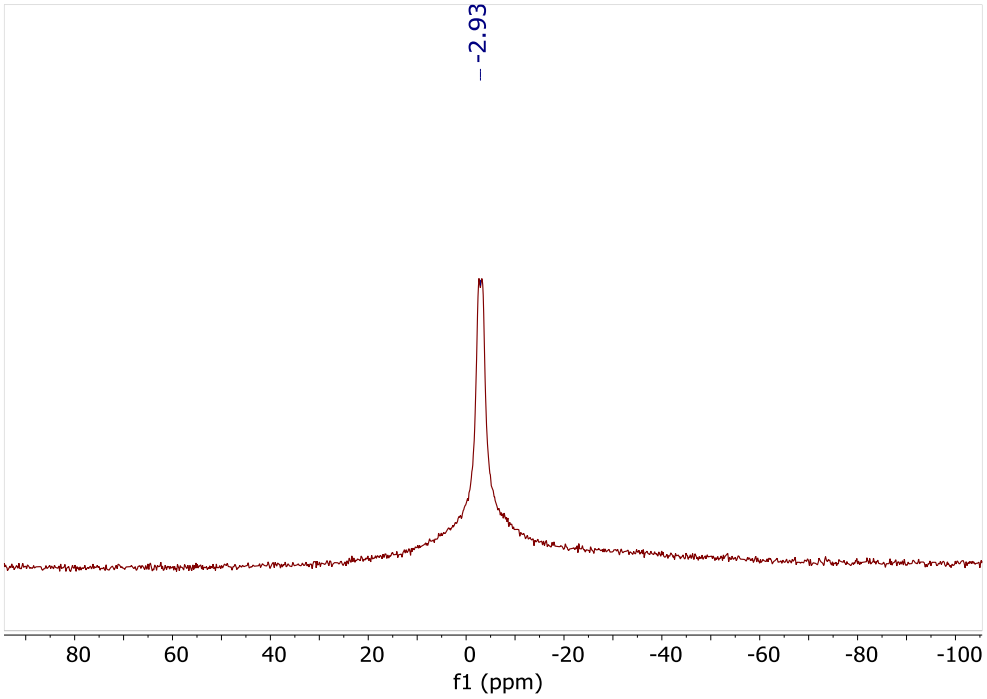

Figure 6.54: The ^{11}B NMR spectrum of the reaction between 5-Y and 7-Y in d_6-benzene, recorded after 10 m.

6.7.8 Reaction of 5-Eu with 7-Yb – SHA_97

5-Eu and **7-Yb** were mixed in d_6-benzene (0.2 ml), and a colour change from green to red was observed. The ^{1}H and ^{19}F{^{1}H} NMR spectrum of the mixture was recorded, though the ^{11}B NMR spectrum was not recorded due to an instrumental issue.

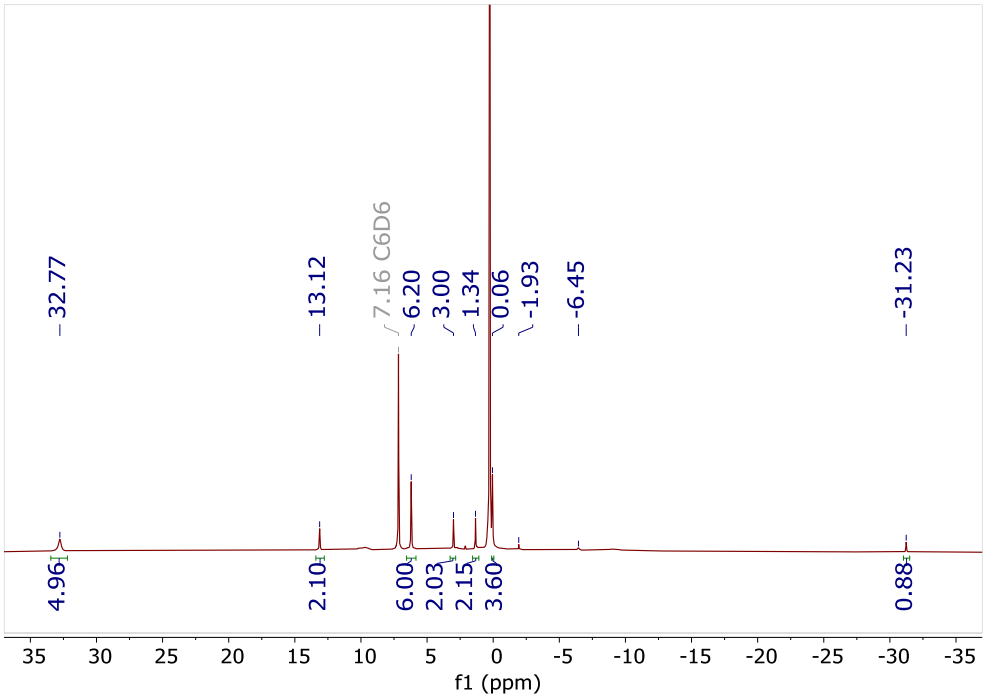

Figure 6.55: The ^{1}H NMR spectrum of the reaction between 5-Eu and 7-Yb in d_6-benzene.

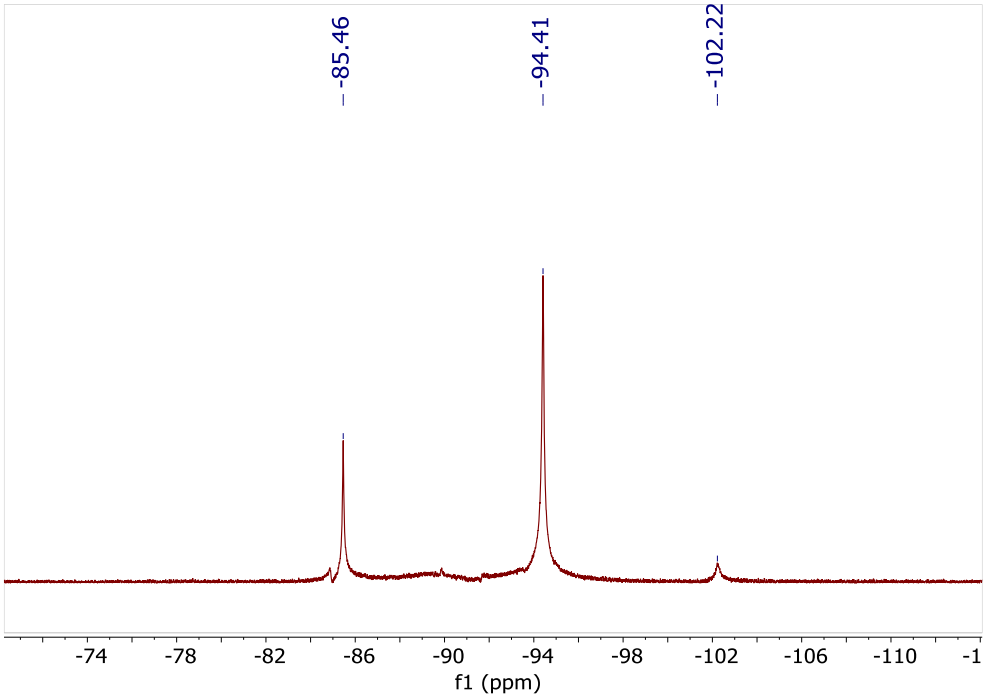

Figure 6.56: The ^{19}F{^{1}H} NMR spectrum of the reaction between 5-Eu and 7-Yb in d_6-benzene.

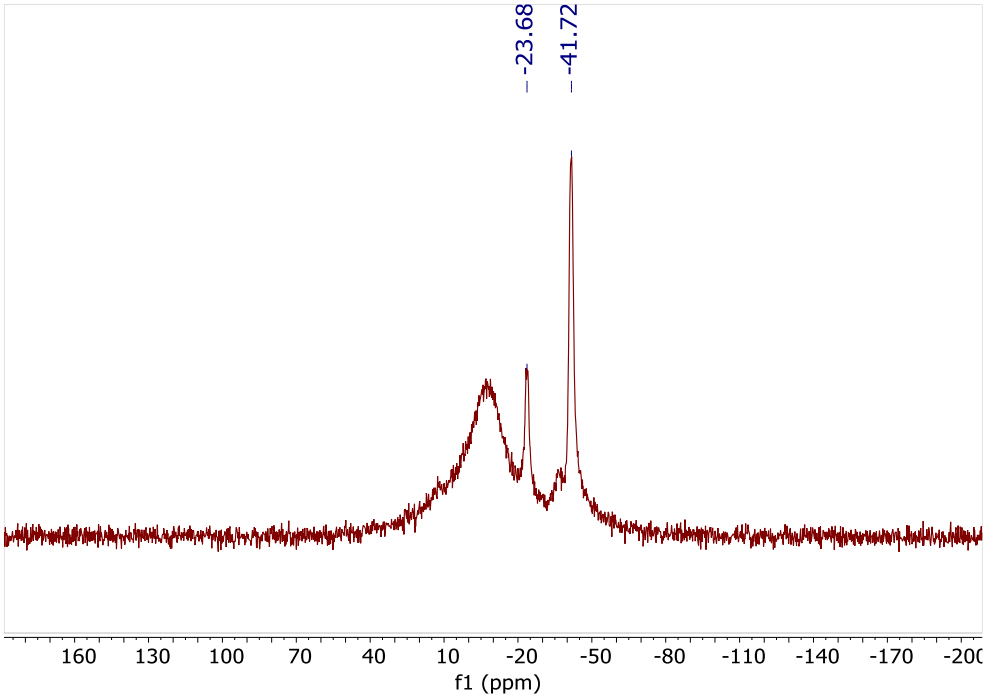

Figure 6.57 The $^{11}B\{^{1}H\}$ NMR spectrum of the reaction between 5-Eu and 7-Yb in d_6-benzene.

6.7.9 Reaction of 5-Yb with 7-Eu – SHA_97

5-Yb and **7-Eu** were mixed in d_6-benzene (0.2 ml), and a colour change from green to red was observed. The ^{1}H and $^{19}F\{^{1}H\}$ NMR spectrum of the mixture was recorded, though the ^{11}B NMR spectrum was not recorded due to an instrumental issue.

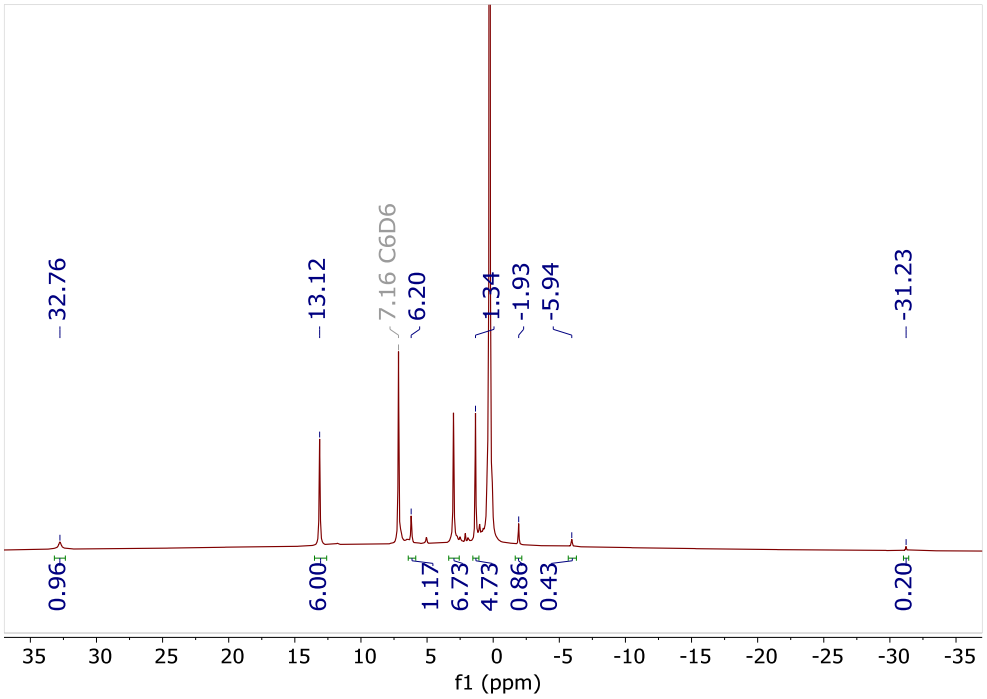

Figure 6.58: The ^{1}H NMR spectrum of the reaction between 7-Eu with 5-Yb.

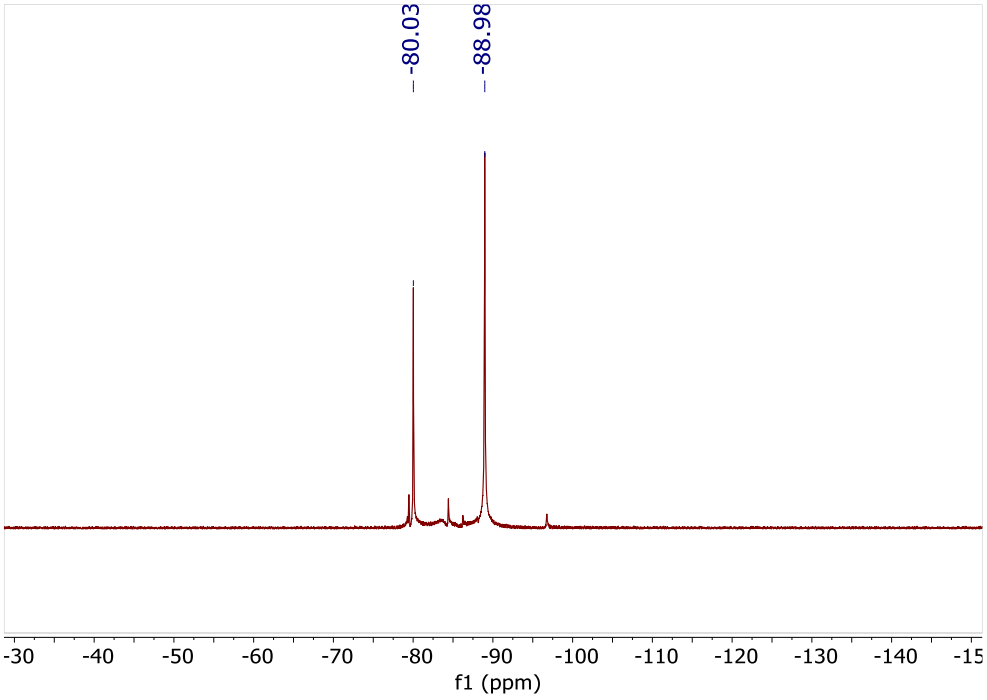

Figure 6.59: The ^{19}F{^{1}H} NMR spectrum of the reaction between 7-Eu with 5-Yb.

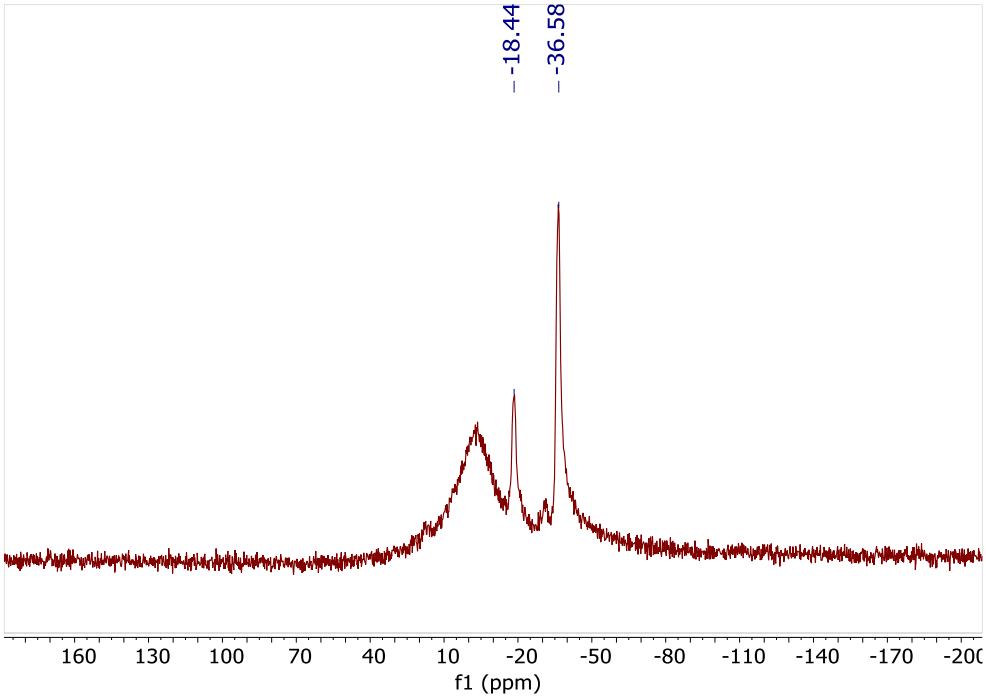

Figure 6.60: The $^{11}B\{^{1}H\}$ NMR spectrum of the reaction between 7-Eu with 5-Yb.

6.7.10 Reaction of 7-Yb with 3

6.7.10.1 Small-scale reaction

7-Yb (72.9 mg, 0.0974 mmol) was dissolved in THF (2 ml) and **3** (38.0 mg, 0.0951 mmol) was suspended in toluene (4 ml). Both were cooled to -35 °C and **7-Yb** was added to **3** with stirring. The reaction was stirred for 1 h, during which time a colour change from purple to red was observed. The solution was reduced by half *in vacuo* and filtered *via* frit to exclude a brown-red precipitate. The solids were washed with toluene (2 ml) and the red filtrates were combined. Toluene was removed *in vacuo* and the red solids were weighed (39.6 mg).

6.7.10.2 Small-scale reactions in toluene

Three separate vials were designated ***1***, ***2*** and ***3***. In each was suspended **3** in toluene (2 ml) at -35 °C, and **7-Yb** suspended in toluene (4 ml) also at -35 °C was added with stirring (see Table 6.5 for all measures for this reaction). The mixtures were stirred at room temperature for 40 min, and a colour change from purple to red was observed in the first 5 min. Over the first 15 min, a brick-coloured precipitate was formed. To each reaction was then added THF, and the mixture was filtered. The solvents were removed *in vacuo* to obtain red solids, which were weighed and analysed by multinuclear NMR spectroscopy.

Table 6.5: Measures of reagents and products obtained from the reaction of 7-Yb with 3.

	Compound	Mass	mMoles (% yield)	THF
1	$[Yb(Tp)_2(OTf)]$	56.7 mg	0.0758	0 ml
	$[CoCp_2][pd]$	30.1 mg	0.0754	
	$[Yb(Tp)_2(pd)]$	4.0 mg	7%	
2	$[Yb(Tp)_2(OTf)]$	51.5 mg	0.0688	0.5 ml
	$[CoCp_2][pd]$	27.4 mg	0.0686	
	$[Yb(Tp)_2(pd)]$	*ca* 6 mg	*ca* 12%	
3	$[Yb(Tp)_2(OTf)]$	56.8 mg	0.0759	2 ml
	$[CoCp_2][pd]$	30.1 mg	0.0754	
	$[Yb(Tp)_2(pd)]$	*ca* 30 mg	*ca* 50%	

6.7.11 Reaction of 7-Eu with 3

7-Eu (9.4 mg, 0.013 mmol) and **3** (5.1 mg, 0.013 mmol) were mixed thoroughly in d_6-benzene. A colour change from purple to red was observed. The mixture was filtered, then sent for multinuclear NMR analysis.

6.7.12 Synthesis of 9-YY

7-Y (143.4 mg, 0.216 mmol) and **3** (85.5 mg, 0.214 mmol) were separately suspended in toluene (2 ml each) and cooled to -35 °C. **7-Y** was added to **3** and the mixture was stirred for 5 min. A colour change from green-dark red was observed. A solution of **4-Y** (184.9 mg, 0.216 mmol) in toluene (2 ml) was added to the suspension at -35 °C and the mixture was stirred for a further 5 min. The mixture was filtered and toluene was removed from the dark red filtrate *in vacuo*. The dark red solid was washed with hexane at -35 °C (3x 5 ml) and dried *in vacuo*, then weighed (160.4 mg). The solid was washed again with cold hexane, then dried *in vacuo* and weighed (135.1 mg). The washings were a dark pink colour, and by cooling the wash solution to -35 °C for several days single crystals suitable for X-ray diffraction were obtained of the bimetallic $Y(hfac)_3(N,N'\text{-}O,O'\text{-pd})Y(Tp)_2$.

6.7.13 Synthesis of 9-YbEu

7-Eu (91.5 mg, 0.125 mmol) and **3** (50.1 mg, 0.125 mmol) were separately suspended in toluene (2 ml each) and cooled to -35 °C. **7-Eu** was added to **3** and the mixture was stirred for 30 min. The mixture was filtered and **4-Yb** (105.4 mg, 0.126 mmol) in toluene (2 ml) at -35 °C was added to the filtrate. The mixture was stirred for 30 min, then was filtered *via* frit and toluene was removed *in vacuo* from the red filtrate. Hexane (3x 2 ml) was used to extract the solid with filtration *via* frit to obtain a red filtrate. Hexane was removed *in vacuo* to obtain a red solid (56.8 mg), which was analysed by multinuclear NMR.

6.7.14 Synthesis of 9-EuYb

7-Yb (64.9 mg, 0.0984 mmol) and **3** (37.2 mg, 0.0932 mmol) were separately suspended in toluene (2 ml each) and cooled to -35 °C. **7-Yb** was added to **3** with stirring and the mixture was stirred for 5 min, and a colour change from purple to orange-red was observed. The suspension was filtered *via* frit and **4-Eu** (85.1 mg, 0.0928 mmol) in toluene (2 ml) at -35 °C was added to the filtrate with stirring. A further colour change from orange-red to pink-red was observed. After stirring for 1 min, toluene was removed *in vacuo* over 30 min, leaving a red solid. The solids were washed with hexane (2x 5 ml) with filtration *via* frit. Hexane was removed *in vacuo* from the filtrate to obtain a red solid, which was analysed by multinuclear NMR in d_6-benzene.

6.7.15 Reaction of 7-Yb with 3 and 4-Y

3 (18.1 mg, 0.0453 mmol, 1 eq.), **7-Yb** (34.6 mg, 0.0462 mmol, 1 eq.) and **4-Y** (38.7 mg, 0.0453 mmol, 1 eq.) were each suspended in toluene (1 ml, 2 ml and 1 ml) and cooled to -35 °C. **7-Yb** was added to **3** and the mixture was stirred for either 1 min or 5 min, then **4-Y** was added and stirred for a further 1 min. Toluene was removed *in vacuo* quickly and hexane (2 ml) was added. The mixture was thoroughly stirred, then filtered *via* frit to obtain a red solution. Hexane was removed *in vacuo* to leave a red solid (19.6 mg).

6.8 References

1. A. Caneschi, A. Dei, D. Gatteschi, L. Sorace and K. Vostrikova, *Angew. Chem. Int. Ed.*, 2000, **39**, 246-248.
2. P. Zhang, M. Perfetti, M. Kern, P. P. Hallmen, L. Ungur, S. Lenz, M. R. Ringenberg, W. Frey, H. Stoll, G. Rauhut and J. van Slageren, *Chem. Sci.*, 2018, **9**, 1221-1230.
3. J. McGuire, B. Wilson, J. McAllister, H. N. Miras, C. Wilson, S. Sproules and J. H. Farnaby, *Dalton Trans.*, 2019, **48**, 5491-5495.
4. D. L. Reger, J. A. Lindeman and L. Lebioda, *Inorg. Chim. Acta*, 1987, **139**, 71-73.
5. S. Chao-De and W. Wing Tak, *Inorg. Chim. Acta*, 1997, **255**, 355-360.
6. D. L. Reger, J. A. Lindeman and L. Lebioda, *Inorg. Chem.*, 1988, **27**, 3923-3929.
7. M. Onishi, N. Nagaoka, K. Hiraki and K. Itoh, *J. Alloys Compd.*, 1996, **236**, 6-12.
8. S.-Y. Liu, G. H. Maunder, A. Sella, M. Stevenson and D. A. Tocher, *Inorg. Chem.*, 1996, **35**, 76-81.
9. M. C. Heffern, L. M. Matosziuk and T. J. Meade, *Chem. Rev.*, 2014, **114**, 4496-4539.
10. J. R. Hickson, S. J. Horsewill, C. Bamforth, J. McGuire, C. Wilson, S. Sproules and J. H. Farnaby, *Dalton Trans.*, 2018, **47**, 10692-10701.
11. B. M. Schmiege, M. E. Fieser, J. W. Ziller and W. J. Evans, *Organometallics*, 2012, **31**, 5591-5598.
12. K. Binnemans, *Coord. Chem. Rev.*, 2015, **295**, 1-45.
13. G. Paolucci, J. Zanon, V. Lucchini, W.-E. Damrau, E. Siebel and R. D. Fischer, *Organometallics*, 2002, **21**, 1088-1094.
14. M. W. Löble, M. Casimiro, D. T. Thielemann, P. Oña-Burgos, I. Fernández, P. W. Roesky and F. Breher, *Chem. Eur. J.*, 2012, **18**, 5325-5334.
15. R. D. Shannon, *Acta Crystallogr. Sect. A*, 1996, **32**, 751-767.
16. A. Babai and A.-V. Mudring, *Z. Anorg. Allg. Chem.*, 2006, **632**, 1956-1958.
17. R. G. Lawrence, T. A. Hamor, C. J. Jones, K. Paxton and N. M. Rowley, *J. Chem. Soc., Dalton Trans.*, 2001, **14**, 2121-2126.
18. F. Guégan, J. Jung, B. Le Guennic, F. Riobé, O. Maury, B. Gillon, J.-F. Jacquot, Y. Guyot, C. Morell and D. Luneau, *Inorg. Chem. Frontiers*, 2019, **6**, 3152-3157.
19. T. Chowdhury, PhD, University of Glasgow, *in progress*.
20. T. Chowdhury, S. J. Horsewill and J. H. Farnaby, *Aust. J. Chem.*, 2021, *Manuscript in preparation*.
21. D. M. Murphy, K. McNamara, P. Richardson, V. Sanchez-Romaguera, R. E. P. Winpenny and L. J. Yellowlees, *Inorg. Chim. Acta*, 2011, **374**, 435-441.
22. J. Yuasa, T. Suenobu and S. Fukuzumi, *J. Phys. Chem. A*, 2005, **109**, 9356-9362.
23. B. Odom, D. Hanneke, B. D'Urso and G. Gabrielse, *Phys. Rev. Lett.*, 2006, **97**, 030801.

24. A. Dei, D. Gatteschi, J. Pécaut, S. Poussereau, L. Sorace and K. Vostrikova, *C. R. Acad. Sci. IIC*, 2001, **4**, 135-141.

25. M. A. Dunstan, E. Rousset, M.-E. Boulon, R. W. Gable, L. Sorace and C. Boskovic, *Dalton Trans.*, 2017, **46**, 13756-13767.

26. W. R. Reed, M. A. Dunstan, R. W. Gable, W. Phonsri, K. S. Murray, R. A. Mole and C. Boskovic, *Dalton Trans.*, 2019, **48**, 15635-15645.

27. K. Binnemans, in *Handbook on the Physics and Chemistry of Rare Earths*, eds. K. A. Schneider, J.-C. Bunzli and V. K. Pecharsky, Elsevier, 2005, vol. 35, ch. 225, pp. 107-272.

28. L. Pauson Peter, *Encyclopedia of Reagents for Organic Synthesis*, 2001.

29. J. K. Molloy, O. Jarjayes, C. Philouze, L. Fedele, D. Imbert and F. Thomas, *Chem. Commun.*, 2017, **53**, 605-608.

30. M. Yano, K. Matsuhira, M. Tatsumi, Y. Kashiwagi, M. Nakamoto, M. Oyama, K. Ohkubo, S. Fukuzumi, H. Misaki and H. Tsukube, *Chem. Commun.*, 2012, **48**, 4082-4084.

31. T. Tsukuda, T. Suzuki and S. Kaizaki, *J. Chem. Soc., Dalton Trans.*, 2002, **8**, 1721-1726.

32. J. R. Hickson, S. J. Horsewill, J. McGuire, C. Wilson, S. Sproules and J. H. Farnaby, *Chem. Commun.*, 2018, **54**, 11284-11287.

33. M. Abdus Subhan, R. Kawahata, H. Nakata, A. Fuyuhiro, T. Tsukuda and S. Kaizaki, *Inorg. Chim. Acta*, 2004, **357**, 3139-3146.

34. S. Trofimenko, J. R. Long, T. Nappier and S. G. Shore, in *Inorg. Synth.*, 1970, pp. 99-109.

7 Conclusions and Outlook

7.1 Conclusions

A thorough review of selectively synthesised lanthanide heterobimetallic complexes in the literature was carried out. The different syntheses were grouped into two categories, based on the method used for speciation control. Thermodynamic control is where the ligands have binding sites which result in the selective binding being the lowest energy state. Kinetic control involves the use of very strongly binding ligands from which the lanthanide ions cannot easily be removed. The advantages and limitations of these two synthetic strategies were identified, and a new protocol was proposed where the coordination properties of lanthanide complexes are tuned to impart selectivity of coordination to the complex as a whole. This would allow the selective coordination to different sites of bridging ligands. The 1,10-phenanthroline-5,6-dione (pd) ligand is presented as such a bridging ligand, which has two rather different binding sites. The pd ligand also has multiple accessible oxidation states, allowing an unprecedented degree of tunability of the electronic structure of its complexes.

A modular system of lanthanide complexes of pd has been developed. The coordination chemistry of the pd ligand with the lanthanides was first investigated. Complexes **1-Ln** Ln(hfac)$_3$(*N,N'*-pd) (Ln = Y, Eu, Gd, Tb, Yb) and *d-f* heterobimetallic complexes **2-Ln** Ln(hfac)$_3$(*N,N'-O,O'*-pd)V(Cp)$_2$ (Ln = Y, Gd) were synthesised and fully characterised (Chapter 2).[1] It was identified that Ln(hfac)$_3$ is selective to the *N,N'* coordination site of pd, and also that some redox processes can be carried out on the pd ligand while coordinated to lanthanides. The first fully characterised, molecular example of the radical anion of pd, **3** $[CoCp_2]^+[pd]^{-\bullet}$ was synthesised, and lanthanide radical compounds **5-Ln** $[CoCp_2]^+[Ln(hfac)_3(N,N'\text{-pd})]^{-\bullet}$ were synthesised by coordination of **4-Ln** Ln(hfac)$_3$(S)$_2$ to **3** (Chapter 3).[2] Again, Ln(hfac)$_3$ was shown to be selective to the *N,N'* coordination site of the radical anion of pd.

The photoluminescence of the modular system (**1-Ln**, **4-Ln**, **5-Ln**) was investigated (Chapter 4). Emission of light from the lanthanides in **1-Ln**, **4-Ln** and **5-Ln** was sensitised almost exclusively by the hfac ligands. TCSPC was used to investigate the energy transfer and de-excitation pathways. The effects of changing the solvent on emission from **1-Eu** were found to be dramatic. Going from THF to toluene solvent reduced the lifetime of the emissive excited state of **1-Eu** by over half. The effect of introducing an organic radical *via* oxidation of

the ligand on the lifetime of the Eu(III) emissive excited state was also quantified for the first time. Finally, determination of the excited state lifetimes of the organic ligands allowed observation of energy transfer from the pd ligand to Eu(III). The excited states of the hfac ligands were too close to the instrument limit for their lifetimes to be determined.

A range of different approaches to the synthesis of lanthanide heteromultimetallics were investigated. Heteroleptic lanthanide complexes **6-Ln** $Ln(Cp^t)_2(OTf)_2K$, $Ln(Tp^*)_2(OTf)$ and **7-Ln** $Ln(Tp)_2(OTf)$ (Cp^t = tetramethyl cyclopentadienyl, Tp = hydro-*tris*-pyrazolyl borate, Tp* = hydro-*tris*-dimethylpyrazolyl borate) were synthesised to this end. **6-Ln** (Ln = Y, Yb) were fully characterised, and their solid-state molecular structures were determined. It was found that **6-Ln** tended to form coordination polymers upon reaction with **3**, presumably due to the Cp^t ligands not having a sufficient steric bulk to prevent the coordination of a second pd radical anion to the lanthanide centre (Chapter 5). Following the reactions of $Ln(Tp^*)_2(OTf)$ with **5-Ln**, ligand redistribution products such as $Ln(Tp^*)_2(hfac)$ and $Ln(Tp^*)(hfac)_2$ were the only identifiable products (Chapter 5).

The most promising reagents were **7-Ln**, which have been fully characterised and solid-state molecular structures have been determined (Chapter 6). The reactions of **7-Ln** with **3** and **5-Ln** were investigated thoroughly. There is strong evidence for the selective coordination of **7-Ln** to the *O,O'* binding site of the radical anion of pd, from differences in electronic spectroscopy to *N,N'* coordinated and uncomplexed radical anion pd compounds. This property has been used to pre-coordinate **7-Ln** to the *O,O'* binding site of **3**, followed by reaction with the *N,N'* selective **4-Ln** to synthesise lanthanide heterobimetallics **8-LnLn'** $Ln(hfac)_3$(*N,N'-O,O'*-pd)$Ln'(Tp)_2$. This synthetic procedure has been partially successful. There is evidence that the lanthanides are selectively bound in the product, and solid-state molecular structures of two lanthanide heterobimetallics (**8-YY'** and **8-EuYb**) have been obtained. However, it is clear from multinuclear NMR spectroscopy that ligand redistribution is an issue and that multiple products are formed during the reaction, from which the lanthanide heterobimetallics have not been successfully isolated except as single crystals.

7.2 Outlook and Future Work

There are two primary avenues of future work following on from this thesis. Firstly, investigation of the energy transfer processes occurring in the modular system. The initial TCSPC results presented in Chapter 4 indicate that it should be possible to observe the process of sensitisation using the modular system. The modular system provides an ideal platform from which to undertake a more in-depth study which will observe the energy transfer processes. A full mapping of the emissive excited states, and their lifetimes, in **4-Ln** (Ln = Gd, Eu) is underway to fully understand the observable energy transfer processes therein. Indeed, emissive excited states of the hfac ligands have already been identified which may play a role in sensitisation. Understanding of the relatively simple **4-Ln** will be applied to the more complex system of **1-Ln**. The modular system will also be extended to new ligands, with complexes such as $Ln(tta)_3(THF)_2$ and $Ln(tta)_3(pd)$ (tta = thenoyl trifluoroacetylacetone). This will provide further control over the electronic properties of the system. The extensive tunability of the modular system will allow a new level of insight into the sensitisation process, which has traditionally been very challenging to observe, and could inform the design of new emissive materials.

The lanthanide heterobimetallic synthesis will also be further developed. It is clear that the main challenge of this synthesis has been ligand redistribution. The most frequent ligand redistribution product which has been observed is $Ln(Tp)_2(hfac)$, apparently formed by the migration of a hfac ligand from $Ln(hfac)_3$ to $[Ln(Tp)_2]^+$. The labile nature of *β*-diketonates such as hfac in coordinating solvents such as H_2O has been remarked upon in the past,[3] and it has been observed here even in the non-coordinating solvent toluene. It therefore seems prudent to direct future efforts away from using this ligand to construct an *N,N'* selective reagent, despite the useful solubilising and sensitising properties for which it was initially selected. However, **7-Ln** showed great promise as an *O,O'* selective reagent and should continue to be used. With this in mind, any alternative *N,N'* selective reagent should be charge neutral, to form an uncharged complex with the putative $Ln(Tp)_2$(*O,O'*-pd), which can be isolated from any other salts such as $[CoCp_2]^+[OTf]^-$. It should also be relatively solubilising, to allow facile dissolution in non-coordinating solvents (which limit any ligand redistribution). Finally, it should satisfy the coordination sphere of the lanthanide ion (with a free coordination site for *N,N'*-pd), and be less labile than lanthanide hfac complexes.

One such ligand might be the tren (*tris*-2-aminoethyl amine) ligand, or a substituted equivalent (Figure 7.1, far left). This ligand is tetradentate and is typically used in the 3- oxidation state, and similar ligands have previously been used for the synthesis of lanthanide heteromultimetallics.[4-6] Functionalisation of the primary amines would allow for tunability of the solubility and electronic properties of its complexes, or for the introduction of useful functionalities such as sensitising antenna groups. As far as I am aware, there are no reported examples of a tren and a phenanthroline ligand coordinated to a lanthanide. Preliminary complexation studies must be carried out to identify whether a lanthanide in this ligand environment is able to coordinate to pd, and whether the ligand environment promotes selective coordination. Alternatively, a ligand such as DO3A (DO3A = 1,4,7,10-tetraazacyclododecane-1,4,7-triacetic acid) might be used. DO3A is a very strongly binding ligand, which has three carboxylic acid functional groups and therefore forms kinetically inert, neutral lanthanide complexes.[7] There are reported examples of DO3A ligands functionalised with a substituted phenanthroline group, which is coordinated by either one or two N atoms to the lanthanide.[8, 9] Such a ligand with the 9,10-phenanthroline oxidised to a 5,6-dione would be ideal for synthesising lanthanide heterobimetallics (Figure 7.1, centre). Otherwise, modification of the pd ligand at the 2,9-sites to increase the denticity of the *N,N'* diimine site could be used to complex the lanthanide more strongly,[10] discouraging ligand redistribution (Figure 7.1, far right). This would also disfavour the formation of coordination polymers, potentially allowing for a greater variety of *O,O'* selective lanthanide reagents.

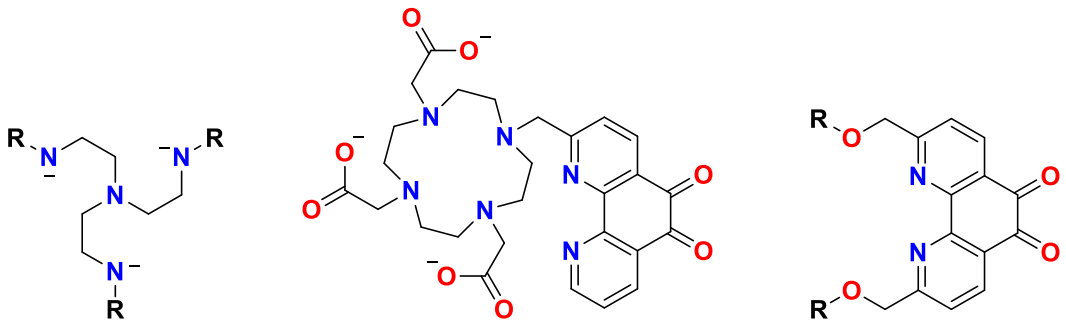

aminofunctionalised tren ***DO3A-appended pd*** ***2,9-functionalised pd***

Figure 7.1: Ligands identified to eliminate the problem of ligand redistribution in the synthesis of lanthanide heterobimetallic complexes.

To conclude, this thesis has developed a modular system of lanthanide complexes (**1-Ln**, **4-Ln**, **5-Ln**) which will provide insight into the sensitisation of lanthanide complexes. A study to this end is ongoing, with promising results already received. The modular system also informed the development of a new synthetic route to lanthanide heterobimetallic complexes. Despite challenges with ligand redistribution, the evidence suggests a selective synthesis of lanthanide heterobimetallic complexes **8-LnLn'** has been achieved. Several strategies have been identified which could be used to address the issue of ligand redistribution and produce selective lanthanide heterobimetallics. This refinement of the hybrid thermodynamic and kinetic control synthesis will allow the facile synthesis of complexes containing an unlimited selection of lanthanide pairs. The environment and bridge is unique among heterometallic lanthanide complexes in that the lanthanides are linked by a partially conjugated bridge, which is redox active. This will be used to investigate the intermolecular lanthanide interactions, and particularly how they change with tuning of the conjugation of the bridge.

7.3 References

1. J. R. Hickson, S. J. Horsewill, C. Bamforth, J. McGuire, C. Wilson, S. Sproules and J. H. Farnaby, *Dalton Trans.*, 2018, **47**, 10692-10701.
2. J. R. Hickson, S. J. Horsewill, J. McGuire, C. Wilson, S. Sproules and J. H. Farnaby, *Chem. Commun.*, 2018, **54**, 11284-11287.
3. K. Binnemans, in *Handbook on the Physics and Chemistry of Rare Earths*, eds. K. A. Schneider, J.-C. Bunzli and V. K. Pecharsky, Elsevier, 2005, vol. 35, ch. 225, pp. 107-272.
4. J.-P. Costes, F. Dahan and F. Nicodème, *Inorg. Chem.*, 2003, **42**, 6556-6563.
5. J.-P. Costes and F. Nicodème, *Chem. Eur. J.*, 2002, **8**, 3442-3447.
6. J. P. Costes, F. Dahan, A. Dupuis, S. Lagrave and J. P. Laurent, *Inorg. Chem.*, 1998, **37**, 153-155.
7. T. J. Sørensen and S. Faulkner, *Acc. Chem. Res.*, 2018, **51**, 2493-2501.
8. G. Bobba, J. C. Frias and D. Parker, *Chem. Commun.*, 2002, **8**, 890-891.
9. S. Quici, G. Marzanni, M. Cavazzini, P. L. Anelli, M. Botta, E. Gianolio, G. Accorsi, N. Armaroli and F. Barigelletti, *Inorg. Chem.*, 2002, **41**, 2777-2784.
10. S. Quici, M. Cavazzini, G. Marzanni, G. Accorsi, N. Armaroli, B. Ventura and F. Barigelletti, *Inorg. Chem.*, 2005, **44**, 529-537.

8 Appendices

8.1 Appendix one: Experimental details

8.1.1 General Details

All air-sensitive manipulations were carried out in an MBraun glovebox (O_2 and H_2O <1 ppm) or by using standard Schlenk techniques under N_2. All glassware was dried at 135 °C overnight prior to use. Filter cannulas were prepared using Whatman 25 mm glass microfiber filters and were pre-dried at 135 °C overnight. Dry solvents were obtained using an Innovative Technology Inc. Pure Solv 400-5-MD solvent purification system (activated alumina columns). Solvents were sparged with N_2 and stored in ampoules over activated molecular sieves under N_2. Deuterated benzene and THF were dried by refluxing over K. Deuterated acetonitrile was dried by refluxing over CaH_2. Dry deuterated solvents were degassed by three freeze–thaw cycles, vacuum distilled, and kept in ampoules in the glovebox under N_2.

8.1.2 Physical Methods

^{1}H NMR data were recorded on a Bruker AVIII 400 MHz spectrometer and were referenced internally to the appropriate residual protio-solvent and are reported relative to tetramethylsilane (δ = 0 ppm). ^{19}F and ^{19}F{^{1}H} NMR spectra were recorded on a Bruker AVIII 400 MHz spectrometer and were referenced to $CFCl_3$ (δ = 0 ppm). All spectra were recorded at a constant temperature of 300 K. Coupling constants (*J*) are reported in hertz (Hz). Standard abbreviations indicating multiplicity were used as follows: m = multiplet, d = doublet, t = triplet, s = singlet. ATR-IR spectra were collected using a Shimadzu IRAffinity-1S, a Shimadzu FTIR 8400S, or a Thermo Scientific NICOLET iS5 FT-IR spectrometer. Elemental analysis was performed at the University of Strathclyde or at London Metropolitan University, and a combustible (tungstic oxide) was used to ensure complete combustion of all complexes. X-band EPR spectra were collected on a Bruker ELEXSYS E500 spectrometer and simulations were performed using Bruker's Xsophe software package. UV/vis/NIR spectra were collected using a Shimadzu UV-3600 UV/vis/NIR or Horiba Duetta™ fluorescence and absorbance spectrometer using anhydrous solvents, which were filtered through Celite® prior to use.

Steady-state fluorescence measurements were collected on a Horiba Duetta™ fluorescence and absorbance spectrometer in anhydrous solvents. TCSPC measurements were collected using a PicoQuant LHD-I Series picosecond pulsed laser of 375 nm. Emitted photons were collected by a lens and passed through a monochromator to be focussed onto a PDM series

single-photon avalanche detector. Measurements were displayed and fitted using software developed in-house by Dr Gordon Hedley.

Crystallographic data for **1-Gd** were collected by the EPSRC UK National Crystallography Service using a CrystalClear-SM Expert 3.1 b27S2 spectrometer and processed with CrysAlis PRO 1.171.38.41. Crystallographic data for **9-YY'** were also collected by the EPSRC UK National Crystallography service using a Rigaku 007HF diffractometer. Crystallographic data for **1-Ln** (Ln = Eu, Tb, Yb), **2a-Gd**, **3**, **4-Ln**, **6-Ln**, **7-Ln**, **9-EuYb**, Y(Tp*)$_2$(hfac), Y(Tp*)(hfac)$_2$(THF), Ce(Tp*)(hfac)$_2$(dmpz), Y(Tp)$_2$(hfac) and {Y(hfac)$_2$(*N,N'-O,O'*-pd)}$_4$ were collected on a Bruker D8 VENTURE diffractometer. All crystallographic data were solved and refined using Olex2 software.

8.2 Appendix two: Calculating magnetic moments

The following formulae were used to determine the expected magnetic moment of Gd(hfac)$_3$(*N,N'-O,O'*-pd)V(Cp)$_2$ **2-Gd** and [CoCp$_2$]$^+$[Gd(hfac)$_3$(*N,N'*-pd)]$^{-\bullet}$ **5-Gd**, each of which contains Gd(III) and a S = 1/2 paramagnet. The assumption is made that the magnetic moment of the complexes is zero. The expected magnetic moment is calculated for three situations: where the paramagnets couple ferromagnetically, couple antiferromagnetically, or do not interact.

Spin-only formula: $\boldsymbol{\mu_{SO} = \sqrt{4S(S+1)}}$

Gd(III) only: 7 unpaired e$^-$, S = 7/2 $\mu_{SO} = \sqrt{4 \times \frac{7}{2} \times (\frac{7}{2} + 1)}$

$$\mu_{SO} = \sqrt{14 \times \frac{9}{2}} = \sqrt{63} = 7.94\ \mu_B$$

Organic radical/V(IV) only: 1 unpaired e$^-$, S = 1/2

$$\mu_{SO} = \sqrt{4 \times \frac{1}{2} \times (\frac{1}{2} + 1)} = \sqrt{3} = 1.73\ \mu_B$$

Ferromagnetic coupling: 8 unpaired e$^-$, S = 8/2

$$\mu_{SO} = \sqrt{4 \times \frac{8}{2} \times (\frac{8}{2} + 1)} = \sqrt{80} = 8.94\ \mu_B$$

Antiferromagnetic coupling: 6 unpaired e$^-$, S = 6/2

$$\mu_{SO} = \sqrt{4 \times \frac{6}{2} \times (\frac{6}{2} + 1)} = \sqrt{48} = 6.92\ \mu_B$$

Formula for non-interacting spins $S_1 \ldots S_n$ where all spins are in the same molecule:

$$\mu_{SO} = \sqrt{4S_1(S_1+1) + \ldots + 4S_n(S_n+1)}$$

No interaction: 7 + 1 unpaired e$^-$, S_1 =7/2, S_2 = 1/2

$$\mu_{SO} = \sqrt{4 \times \frac{7}{2} \times \left(\frac{7}{2} + 1\right) + 4 \times \frac{1}{2} \times \left(\frac{1}{2} + 1\right)}$$

$$\mu_{SO} = \sqrt{14 \times \frac{9}{2} + 2 \times \frac{3}{2}} = \sqrt{66} = 8.12\ \mu_B$$

8.3 Appendix three: Crystallographic tables and full crystallographic data

Crystallographic data for **1-Ln** (Ln = Y, Gd), **2-Y** and **2a-Ln** (Ln = Y, Gd) can be obtained free of charge from the Cambridge Crystallographic Data Centre (CCDC)[‡‡] using CCDC identifiers 1832429–1832434 and 1841191.[1] Crystallographic data for **3** may be obtained using CCDC identifier 1854232.[2] Specific identifier numbers are given in Table 8.1. Crystallographic tables and data for all unpublished compounds in this thesis are given in the sections following.

Table 8.1: CCDC identifier numbers for published compounds described in this thesis

Compound	CCDC Identifier
1(i)-Y Y(hfac)$_3$(*N,N'*-pd).Et$_2$O	1832429
1(ii)-Y Y(hfac)$_3$(*N,N'*-pd).Tol	1832430
1(i)-Gd Gd(hfac)$_3$(*N,N'*-pd).Et$_2$O	1832431
1(ii)-Gd Gd(hfac)$_3$(*N,N'*-pd).Tol	1832432
2-Y Y(hfac)$_3$(*N,N'-O,O'*-pd)V(Cp)$_2$	1832433
2a-Y Y(hfac)$_3$(*N,N'-O,O'*-pd)V(Cp^t)$_2$	1832434
2a-Gd Gd(hfac)$_3$(*N,N'-O,O'*-pd)V(Cp^t)$_2$	1841191
3 [CoCp$_2$]$^+$[pd]$^{-\bullet}$	1854232

[‡‡] https://www.ccdc.cam.ac.uk/structures

1. J. R. Hickson, S. J. Horsewill, C. Bamforth, J. McGuire, C. Wilson, S. Sproules and J. H. Farnaby, *Dalton Trans.*, 2018, 47, 10692-10701.
2. J. R. Hickson, S. J. Horsewill, J. McGuire, C. Wilson, S. Sproules and J. H. Farnaby, *Chem. Commun.,* 2018, 54, 11284-11287.

8.3.1 Crystallographic data for 1-Eu

Crystal data

$C_{27}H_9EuF_{18}N_2O_8 \cdot C_4O$	$F(000)$ = 2024
M_r = 1047.36	D_x = 1.837 Mg m^{-3}
Monoclinic, $P2_1/c$	Mo $K\alpha$ radiation, λ = 0.71073 Å
a = 9.6645 (4) Å	Cell parameters from 9990 reflections
b = 23.0583 (9) Å	θ = 2.6–28.3°
c = 17.1839 (6) Å	μ = 1.80 mm^{-1}
β = 98.634 (2)°	T = 273 K
V = 3786.0 (3) Å^3	Plate, green
Z = 4	0.17 × 0.16 × 0.02 mm

Data collection

Bruker D8 VENTURE diffractometer	9371 independent reflections
Radiation source: microfocus sealed tube, INCOATEC Iμs 3.0	8383 reflections with $I > 2\sigma(I)$
Multilayer mirror optics monochromator	R_{int} = 0.042
Detector resolution: 7.4074 pixels mm^{-1}	θ_{max} = 28.3°, θ_{min} = 2.3°
ϕ and ω scans	h = -12→12
Absorption correction: multi-scan *SADABS2016*/2 (Bruker,2016/2) was used for absorption correction. wR2(int) was 0.0941 before and 0.0637 after correction. The Ratio of minimum to maximum transmission is 0.8491. The λ/2 correction factor is Not present.	k = -30→30
T_{min} = 0.633, T_{max} = 0.746	l = -21→22
44452 measured reflections	

Refinement

Refinement on F^2	Primary atom site location: dual
Least-squares matrix: full	Hydrogen site location: inferred from neighbouring sites
$R[F^2 > 2\sigma(F^2)]$ = 0.043	H-atom parameters constrained
$wR(F^2)$ = 0.109	$w = 1/[\sigma^2(F_o^2) + (0.0459P)^2 + 8.2224P]$ where $P = (F_o^2 + 2F_c^2)/3$
S = 1.10	$(\Delta/\sigma)_{max}$ = 0.001
9371 reflections	$\Delta\rangle_{max}$ = 1.20 e Å^{-3}
541 parameters	$\Delta\rangle_{min}$ = -0.73 e Å^{-3}

0 restraints	

Special details

Geometry. All esds (except the esd in the dihedral angle between two l.s. planes) are estimated using the full covariance matrix. The cell esds are taken into account individually in the estimation of esds in distances, angles and torsion angles; correlations between esds in cell parameters are only used when they are defined by crystal symmetry. An approximate (isotropic) treatment of cell esds is used for estimating esds involving l.s. planes.

Fractional atomic coordinates and isotropic or equivalent isotropic displacement parameters (Å²)

	x	*y*	*z*	U_{iso}*/U_{eq}	Occ. (<1)
Eu1	0.77489 (2)	0.42621 (2)	0.29151 (2)	0.02656 (7)	
O4	0.6787 (3)	0.52019 (11)	0.28188 (16)	0.0363 (6)	
O5	0.6958 (3)	0.43925 (12)	0.41443 (15)	0.0338 (6)	
O8	0.9006 (3)	0.35266 (12)	0.23356 (16)	0.0382 (6)	
O3	0.9392 (3)	0.48917 (12)	0.24624 (16)	0.0357 (6)	
O6	0.9720 (3)	0.41857 (13)	0.39040 (16)	0.0372 (6)	
O7	0.7177 (3)	0.33421 (12)	0.34032 (17)	0.0387 (6)	
F5	0.5774 (3)	0.62209 (14)	0.34035 (17)	0.0623 (8)	
O1	0.3161 (4)	0.43137 (17)	-0.0701 (2)	0.0643 (10)	
N2	0.5107 (3)	0.41567 (14)	0.24541 (19)	0.0327 (6)	
F2	1.1002 (4)	0.53349 (16)	0.1428 (2)	0.0860 (12)	
F10	1.1419 (4)	0.3618 (2)	0.5648 (2)	0.0977 (14)	
C19	0.7449 (4)	0.42205 (18)	0.4820 (2)	0.0376 (8)	
C20	0.8813 (5)	0.4069 (2)	0.5105 (2)	0.0465 (10)	
H20	0.904290	0.395629	0.562766	0.056*	
C11	0.5560 (4)	0.42426 (15)	0.1123 (2)	0.0313 (7)	
F9	0.5171 (4)	0.3999 (3)	0.5052 (2)	0.124 (2)	
F4	0.6487 (5)	0.66807 (14)	0.2485 (3)	0.1071 (16)	
C14	0.9454 (4)	0.54241 (18)	0.2353 (2)	0.0374 (8)	
F7	0.6204 (6)	0.4681 (2)	0.5712 (3)	0.1279 (19)	
F12	1.2079 (4)	0.3680 (2)	0.4572 (2)	0.1013 (15)	
C21	0.9850 (4)	0.40819 (19)	0.4626 (2)	0.0379 (8)	
C4	0.5106 (5)	0.42477 (17)	0.0310 (2)	0.0395 (9)	
F6	0.4914 (4)	0.60345 (18)	0.2235 (2)	0.0897 (13)	
C12	0.4563 (4)	0.41930 (15)	0.1686 (2)	0.0297 (7)	
C26	0.9031 (5)	0.2986 (2)	0.2361 (3)	0.0453 (10)	
F3	1.1906 (4)	0.5481 (3)	0.2584 (3)	0.1217 (18)	

C16	0.7186 (4)	0.56911 (16)	0.2655 (2)	0.0330 (8)	
N1	0.6941 (3)	0.42682 (13)	0.14242 (18)	0.0311 (6)	
O2	0.1303 (4)	0.42462 (17)	0.0350 (2)	0.0641 (10)	
C5	0.3575 (5)	0.4251 (2)	-0.0006 (3)	0.0494 (11)	
C15	0.8472 (5)	0.58410 (18)	0.2444 (2)	0.0408 (9)	
H15	0.867272	0.622895	0.236325	0.049*	
C1	0.7864 (5)	0.42876 (18)	0.0915 (2)	0.0393 (9)	
H1	0.881007	0.431196	0.111678	0.047*	
C25	0.8392 (6)	0.2618 (2)	0.2824 (3)	0.0540 (12)	
H25	0.853494	0.222010	0.279599	0.065*	
C7AA	0.7531 (5)	0.28356 (18)	0.3334 (3)	0.0419 (9)	
F14	0.5537 (6)	0.2446 (3)	0.3756 (4)	0.156 (3)	
C2	0.7489 (6)	0.4274 (2)	0.0104 (3)	0.0482 (11)	
H2	0.816736	0.427343	-0.022631	0.058*	
F8	0.6772 (4)	0.3823 (2)	0.5984 (2)	0.0943 (14)	
C7	0.3121 (4)	0.41696 (18)	0.1439 (3)	0.0399 (9)	
C8	0.2236 (4)	0.4118 (2)	0.1990 (3)	0.0512 (11)	
H8	0.127249	0.410795	0.183363	0.061*	
F11	1.1974 (5)	0.44254 (19)	0.5256 (5)	0.186 (4)	
F1	1.0828 (6)	0.61660 (16)	0.1897 (5)	0.169 (3)	
C6	0.2546 (5)	0.4217 (2)	0.0591 (3)	0.0498 (11)	
F18	0.9769 (7)	0.21607 (18)	0.1696 (3)	0.142 (2)	
C9	0.2783 (4)	0.4081 (3)	0.2772 (3)	0.0548 (12)	
H9	0.220501	0.404062	0.315549	0.066*	
F13	0.7208 (7)	0.2555 (2)	0.4591 (3)	0.159 (3)	
C10	0.4219 (4)	0.4104 (2)	0.2972 (3)	0.0446 (10)	
H10	0.458996	0.408218	0.350234	0.054*	
C22	1.1358 (5)	0.3964 (3)	0.5023 (3)	0.0543 (12)	
C18	0.6378 (5)	0.4183 (3)	0.5393 (3)	0.0582 (14)	
F15	0.7136 (7)	0.18793 (17)	0.3752 (4)	0.164 (3)	
C17	0.6081 (5)	0.61675 (19)	0.2688 (3)	0.0465 (10)	
C3	0.6091 (5)	0.42597 (19)	-0.0199 (2)	0.0467 (10)	
H3	0.580708	0.425833	-0.074024	0.056*	
O1EA	0.3555 (12)	0.3075 (5)	0.0189 (7)	0.086 (3)*	0.5
C13	1.0795 (6)	0.5620 (2)	0.2067 (4)	0.0627 (15)	
F17	0.9763 (9)	0.2970 (3)	0.1122 (3)	0.183 (4)	
F16	1.1250 (6)	0.2784 (3)	0.2040 (4)	0.159 (3)	
C27	0.9924 (8)	0.2710 (3)	0.1787 (4)	0.0763 (19)	
C23	0.6935 (8)	0.2408 (2)	0.3885 (4)	0.0723 (18)	
C3E	0.1955 (17)	0.2920 (6)	-0.0219 (8)	0.070 (3)*	0.5

C2E	0.3912 (8)	0.2560 (3)	0.0674 (4)	0.0856 (19)*	
C4EA	0.120 (3)	0.2851 (12)	-0.0461 (17)	0.156 (9)*	0.5
C1EA	0.5357 (16)	0.2691 (6)	0.1152 (9)	0.069 (3)*	0.5
C4E	0.2293 (16)	0.2680 (7)	-0.0990 (10)	0.087 (4)*	0.5
C3EA	0.251 (2)	0.2991 (9)	-0.0554 (13)	0.114 (6)*	0.5
C1E	0.4928 (18)	0.2733 (7)	0.1336 (10)	0.081 (4)*	0.5
O1E	0.3143 (10)	0.3074 (4)	0.0358 (5)	0.059 (2)*	0.5

Atomic displacement parameters (Å²)

	U^{11}	U^{22}	U^{33}	U^{12}	U^{13}	U^{23}
Eu1	0.02457 (10)	0.03176 (10)	0.02422 (10)	-0.00103 (6)	0.00644 (6)	0.00092 (6)
O4	0.0350 (14)	0.0339 (13)	0.0418 (15)	0.0015 (11)	0.0114 (11)	0.0054 (11)
O5	0.0341 (13)	0.0412 (14)	0.0274 (12)	0.0008 (11)	0.0086 (10)	-0.0016 (10)
O8	0.0406 (15)	0.0408 (15)	0.0357 (14)	0.0084 (12)	0.0138 (12)	0.0037 (11)
O3	0.0315 (13)	0.0395 (14)	0.0382 (14)	-0.0049 (11)	0.0124 (11)	-0.0006 (11)
O6	0.0257 (12)	0.0565 (17)	0.0289 (13)	-0.0022 (11)	0.0024 (10)	0.0024 (12)
O7	0.0400 (15)	0.0339 (14)	0.0458 (16)	-0.0038 (11)	0.0177 (12)	-0.0009 (12)
F5	0.0680 (19)	0.0695 (19)	0.0528 (16)	0.0244 (15)	0.0201 (14)	-0.0046 (14)
O1	0.070 (2)	0.083 (3)	0.0338 (17)	0.0011 (19)	-0.0113 (16)	0.0024 (16)
N2	0.0272 (14)	0.0425 (17)	0.0289 (15)	-0.0006 (12)	0.0062 (12)	0.0008 (13)
F2	0.106 (3)	0.084 (2)	0.086 (2)	-0.003 (2)	0.073 (2)	0.0095 (19)
F10	0.062 (2)	0.157 (4)	0.071 (2)	0.023 (2)	-0.0016 (17)	0.044 (2)
C19	0.037 (2)	0.050 (2)	0.0278 (18)	-0.0043 (16)	0.0105 (15)	-0.0053 (16)
C20	0.040 (2)	0.075 (3)	0.0235 (18)	0.002 (2)	0.0035 (16)	0.0060 (19)
C11	0.0380 (19)	0.0287 (17)	0.0273 (17)	0.0006 (14)	0.0051 (14)	-0.0011 (13)
F9	0.0487 (19)	0.277 (6)	0.0491 (19)	-0.031 (3)	0.0189 (16)	0.015 (3)
F4	0.114 (3)	0.0464 (18)	0.181 (4)	0.0252 (19)	0.086 (3)	0.044 (2)
C14	0.040 (2)	0.043 (2)	0.0323 (19)	-0.0146 (16)	0.0138 (15)	-0.0044 (16)
F7	0.160 (5)	0.120 (4)	0.128 (4)	0.028 (3)	0.101 (4)	-0.019 (3)
F12	0.060 (2)	0.176 (4)	0.066 (2)	0.052 (3)	0.0040 (17)	0.010 (3)
C21	0.0292 (18)	0.051 (2)	0.0319 (19)	-0.0008 (16)	-0.0007 (14)	-0.0015 (17)
C4	0.046 (2)	0.039 (2)	0.0310 (19)	0.0020 (17)	-0.0006 (16)	-0.0026 (16)
F6	0.075 (2)	0.100 (3)	0.081 (2)	0.045 (2)	-0.0307 (19)	-0.022 (2)
C12	0.0279 (17)	0.0299 (17)	0.0308 (17)	0.0009 (13)	0.0029 (13)	0.0002 (13)
C26	0.049 (2)	0.045 (2)	0.044 (2)	0.0147 (19)	0.0157 (19)	-0.0027 (18)
F3	0.049 (2)	0.188 (5)	0.130 (4)	-0.053 (3)	0.021 (2)	-0.024 (4)
C16	0.039 (2)	0.0351 (19)	0.0245 (16)	0.0014 (15)	0.0035 (14)	0.0022 (14)
N1	0.0322 (15)	0.0358 (16)	0.0251 (14)	0.0014 (12)	0.0033 (12)	0.0012 (12)
O2	0.0404 (18)	0.085 (3)	0.061 (2)	0.0050 (17)	-0.0142 (16)	-0.0029 (18)

C5	0.054 (3)	0.054 (3)	0.035 (2)	0.001 (2)	-0.0075 (19)	-0.0039 (19)
C15	0.055 (3)	0.034 (2)	0.036 (2)	-0.0077 (17)	0.0158 (18)	0.0000 (16)
C1	0.040 (2)	0.049 (2)	0.0318 (19)	0.0029 (17)	0.0123 (16)	0.0033 (16)
C25	0.068 (3)	0.035 (2)	0.064 (3)	0.010 (2)	0.026 (3)	0.003 (2)
C7AA	0.045 (2)	0.036 (2)	0.046 (2)	-0.0045 (17)	0.0114 (18)	0.0006 (17)
F14	0.113 (4)	0.139 (5)	0.236 (7)	-0.036 (3)	0.094 (5)	0.044 (5)
C2	0.060 (3)	0.056 (3)	0.032 (2)	0.006 (2)	0.0188 (19)	0.0037 (18)
F8	0.070 (2)	0.161 (4)	0.059 (2)	0.020 (2)	0.0318 (17)	0.047 (2)
C7	0.0322 (19)	0.045 (2)	0.041 (2)	-0.0017 (16)	-0.0011 (16)	0.0011 (17)
C8	0.028 (2)	0.071 (3)	0.054 (3)	-0.0015 (19)	0.0036 (19)	0.002 (2)
F11	0.076 (3)	0.072 (3)	0.364 (10)	-0.010 (2)	-0.118 (5)	-0.012 (4)
F1	0.154 (4)	0.047 (2)	0.355 (9)	-0.027 (2)	0.191 (6)	-0.002 (3)
C6	0.045 (2)	0.054 (3)	0.047 (2)	0.001 (2)	-0.005 (2)	0.001 (2)
F18	0.217 (6)	0.064 (2)	0.181 (5)	0.013 (3)	0.143 (5)	-0.030 (3)
C9	0.031 (2)	0.088 (4)	0.049 (3)	-0.003 (2)	0.0149 (19)	0.001 (2)
F13	0.281 (9)	0.130 (4)	0.070 (3)	-0.099 (5)	0.046 (4)	0.024 (3)
C10	0.0295 (19)	0.072 (3)	0.033 (2)	-0.0029 (19)	0.0074 (15)	0.0007 (19)
C22	0.038 (2)	0.083 (4)	0.039 (2)	0.000 (2)	-0.0041 (18)	0.002 (2)
C18	0.046 (3)	0.100 (4)	0.030 (2)	0.008 (3)	0.0128 (19)	0.002 (2)
F15	0.257 (7)	0.045 (2)	0.234 (6)	0.005 (3)	0.181 (6)	0.030 (3)
C17	0.052 (3)	0.042 (2)	0.047 (2)	0.0081 (19)	0.008 (2)	0.0085 (19)
C3	0.062 (3)	0.052 (3)	0.0250 (18)	0.004 (2)	0.0030 (18)	-0.0012 (17)
C13	0.058 (3)	0.053 (3)	0.086 (4)	-0.022 (2)	0.042 (3)	-0.015 (3)
F17	0.342 (10)	0.142 (5)	0.098 (4)	0.125 (5)	0.140 (5)	0.033 (3)
F16	0.096 (4)	0.166 (5)	0.236 (7)	0.022 (4)	0.099 (4)	-0.053 (5)
C27	0.098 (5)	0.063 (4)	0.079 (4)	0.028 (3)	0.051 (4)	0.000 (3)
C23	0.099 (5)	0.044 (3)	0.086 (4)	-0.011 (3)	0.052 (4)	0.003 (3)

Geometric parameters (Å, º)

Eu1—O4	2.354 (3)	F3—C13	1.326 (8)
Eu1—O5	2.371 (3)	C16—C15	1.390 (6)
Eu1—O8	2.389 (3)	C16—C17	1.538 (6)
Eu1—O3	2.368 (3)	N1—C1	1.341 (5)
Eu1—O6	2.361 (3)	O2—C6	1.213 (6)
Eu1—O7	2.376 (3)	C5—C6	1.534 (8)
Eu1—N2	2.569 (3)	C15—H15	0.9300
Eu1—N1	2.564 (3)	C1—H1	0.9300
O4—C16	1.238 (4)	C1—C2	1.385 (6)
O5—C19	1.251 (5)	C25—H25	0.9300

O8—C26	1.247 (5)	C25—C7AA	1.389 (6)
O3—C14	1.245 (5)	C7AA—C23	1.538 (7)
O6—C21	1.251 (5)	F14—C23	1.338 (9)
O7—C7AA	1.228 (5)	C2—H2	0.9300
F5—C17	1.313 (5)	C2—C3	1.374 (7)
O1—C5	1.211 (5)	F8—C18	1.323 (6)
N2—C12	1.348 (5)	C7—C8	1.374 (6)
N2—C10	1.331 (5)	C7—C6	1.483 (6)
F2—C13	1.322 (6)	C8—H8	0.9300
F10—C22	1.333 (6)	C8—C9	1.371 (6)
C19—C20	1.381 (6)	F11—C22	1.255 (7)
C19—C18	1.535 (6)	F1—C13	1.293 (7)
C20—H20	0.9300	F18—C27	1.282 (7)
C20—C21	1.389 (6)	C9—H9	0.9300
C11—C4	1.399 (5)	C9—C10	1.379 (6)
C11—C12	1.469 (5)	F13—C23	1.250 (8)
C11—N1	1.359 (5)	C10—H10	0.9300
F9—C18	1.296 (6)	F15—C23	1.261 (7)
F4—C17	1.310 (5)	C3—H3	0.9300
C14—C15	1.376 (6)	O1EA—C3E	1.638 (19)
C14—C13	1.521 (6)	O1EA—C2E	1.461 (13)
F7—C18	1.292 (7)	F17—C27	1.279 (8)
F12—C22	1.295 (6)	F16—C27	1.301 (9)
C21—C22	1.537 (6)	C3E—C4E	1.51 (2)
C4—C5	1.498 (6)	C2E—C1EA	1.540 (16)
C4—C3	1.386 (7)	C2E—C1E	1.443 (17)
F6—C17	1.307 (6)	C2E—O1E	1.460 (11)
C12—C7	1.395 (5)	C4EA—C3EA	1.34 (3)
C26—C25	1.372 (7)	C3EA—O1E	1.61 (2)
C26—C27	1.543 (6)		
O4—Eu1—O5	76.65 (9)	N1—C1—H1	118.1
O4—Eu1—O8	147.60 (9)	N1—C1—C2	123.8 (4)
O4—Eu1—O3	71.92 (9)	C2—C1—H1	118.1
O4—Eu1—O6	112.75 (10)	C26—C25—H25	119.8
O4—Eu1—O7	137.42 (9)	C26—C25—C7AA	120.4 (4)
O4—Eu1—N2	72.65 (10)	C7AA—C25—H25	119.8
O4—Eu1—N1	82.35 (10)	O7—C7AA—C25	127.4 (4)
O5—Eu1—O8	135.53 (9)	O7—C7AA—C23	114.5 (4)
O5—Eu1—O7	71.08 (9)	C25—C7AA—C23	118.1 (4)

O5—Eu1—N2	81.27 (10)	C1—C2—H2	120.8
O5—Eu1—N1	143.04 (10)	C3—C2—C1	118.4 (4)
O8—Eu1—N2	110.39 (10)	C3—C2—H2	120.8
O8—Eu1—N1	71.63 (10)	C12—C7—C6	120.4 (4)
O3—Eu1—O5	122.47 (9)	C8—C7—C12	119.3 (4)
O3—Eu1—O8	83.69 (10)	C8—C7—C6	120.2 (4)
O3—Eu1—O7	150.02 (9)	C7—C8—H8	120.2
O3—Eu1—N2	129.89 (10)	C9—C8—C7	119.6 (4)
O3—Eu1—N1	77.70 (10)	C9—C8—H8	120.2
O6—Eu1—O5	72.65 (9)	O2—C6—C5	118.6 (4)
O6—Eu1—O8	80.86 (10)	O2—C6—C7	123.0 (5)
O6—Eu1—O3	76.91 (9)	C7—C6—C5	118.4 (4)
O6—Eu1—O7	83.38 (10)	C8—C9—H9	121.1
O6—Eu1—N2	150.71 (10)	C8—C9—C10	117.8 (4)
O6—Eu1—N1	144.21 (10)	C10—C9—H9	121.1
O7—Eu1—O8	70.92 (9)	N2—C10—C9	124.3 (4)
O7—Eu1—N2	75.61 (10)	N2—C10—H10	117.9
O7—Eu1—N1	107.79 (10)	C9—C10—H10	117.9
N1—Eu1—N2	63.44 (10)	F10—C22—C21	112.9 (4)
C16—O4—Eu1	136.2 (3)	F12—C22—F10	102.5 (5)
C19—O5—Eu1	131.2 (3)	F12—C22—C21	112.5 (4)
C26—O8—Eu1	134.7 (3)	F11—C22—F10	106.8 (5)
C14—O3—Eu1	134.8 (3)	F11—C22—F12	110.3 (6)
C21—O6—Eu1	132.7 (3)	F11—C22—C21	111.4 (5)
C7AA—O7—Eu1	137.0 (3)	F9—C18—C19	112.0 (4)
C12—N2—Eu1	121.3 (2)	F9—C18—F8	106.1 (5)
C10—N2—Eu1	120.9 (3)	F7—C18—C19	111.5 (5)
C10—N2—C12	117.6 (3)	F7—C18—F9	108.5 (5)
O5—C19—C20	128.2 (4)	F7—C18—F8	105.9 (5)
O5—C19—C18	114.5 (4)	F8—C18—C19	112.5 (4)
C20—C19—C18	117.3 (4)	F5—C17—C16	110.9 (3)
C19—C20—H20	119.3	F4—C17—F5	106.4 (4)
C19—C20—C21	121.4 (4)	F4—C17—C16	113.5 (4)
C21—C20—H20	119.3	F6—C17—F5	106.4 (4)
C4—C11—C12	121.3 (4)	F6—C17—F4	108.6 (4)
N1—C11—C4	121.5 (4)	F6—C17—C16	110.6 (4)
N1—C11—C12	117.2 (3)	C4—C3—H3	120.3
O3—C14—C15	128.5 (4)	C2—C3—C4	119.4 (4)
O3—C14—C13	113.9 (4)	C2—C3—H3	120.3
C15—C14—C13	117.6 (4)	C2E—O1EA—C3E	101.2 (9)

O6—C21—C20	128.1 (4)	F2—C13—C14	111.3 (4)
O6—C21—C22	114.9 (4)	F2—C13—F3	103.1 (5)
C20—C21—C22	117.0 (4)	F3—C13—C14	110.8 (5)
C11—C4—C5	120.4 (4)	F1—C13—F2	106.5 (5)
C3—C4—C11	119.2 (4)	F1—C13—C14	114.4 (5)
C3—C4—C5	120.3 (4)	F1—C13—F3	110.0 (6)
N2—C12—C11	116.8 (3)	F18—C27—C26	114.8 (5)
N2—C12—C7	121.4 (4)	F18—C27—F16	105.2 (6)
C7—C12—C11	121.7 (3)	F17—C27—C26	111.9 (5)
O8—C26—C25	129.1 (4)	F17—C27—F18	111.0 (7)
O8—C26—C27	113.6 (4)	F17—C27—F16	102.7 (7)
C25—C26—C27	117.3 (4)	F16—C27—C26	110.4 (6)
O4—C16—C15	127.4 (4)	F14—C23—C7AA	108.6 (6)
O4—C16—C17	113.6 (4)	F13—C23—C7AA	112.3 (5)
C15—C16—C17	119.0 (4)	F13—C23—F14	101.7 (6)
C11—N1—Eu1	121.0 (2)	F13—C23—F15	115.0 (7)
C1—N1—Eu1	121.4 (3)	F15—C23—C7AA	115.2 (5)
C1—N1—C11	117.7 (3)	F15—C23—F14	102.3 (6)
O1—C5—C4	121.4 (5)	C4E—C3E—O1EA	98.1 (12)
O1—C5—C6	120.9 (5)	O1EA—C2E—C1EA	105.2 (8)
C4—C5—C6	117.5 (4)	C1E—C2E—O1E	108.5 (9)
C14—C15—C16	121.0 (4)	C4EA—C3EA—O1E	98 (2)
C14—C15—H15	119.5	C2E—O1E—C3EA	111.2 (10)
C16—C15—H15	119.5		

8.3.2 Crystallographic data for 1-Tb

Crystal data

$C_{27}H_9F_{18}N_2O_8Tb \cdot C_7H_8$	$F(000)$ = 2104
M_r = 1082.42	D_x = 1.877 Mg m^{-3}
Monoclinic, $P2_1/c$	Mo $K\alpha$ radiation, λ = 0.71073 Å
a = 12.9679 (8) Å	Cell parameters from 9895 reflections
b = 16.6975 (11) Å	θ = 2.4–28.0°
c = 18.1571 (10) Å	μ = 1.99 mm^{-1}
β = 103.078 (2)°	T = 150 K
V = 3829.6 (4) Å^3	Rod, yellow
Z = 4	0.23 × 0.05 × 0.04 mm

Data collection

Bruker D8 VENTURE diffractometer	9523 independent reflections
Radiation source: microfocus sealed tube, INCOATEC Iμs 3.0	6650 reflections with $I > 2\sigma(I)$
Multilayer mirror optics monochromator	$R_{int} = 0.053$
Detector resolution: 7.4074 pixels mm^{-1}	$\theta_{max} = 28.3°$, $\theta_{min} = 2.4°$
ϕ and ω scans	$h = -17 \rightarrow 16$
Absorption correction: multi-scan *SADABS2016*/2 (Bruker,2016/2) was used for absorption correction. wR2(int) was 0.1067 before and 0.0648 after correction. The Ratio of minimum to maximum transmission is 0.8792. The λ/2 correction factor is Not present.	$k = -21 \rightarrow 22$
$T_{min} = 0.656$, $T_{max} = 0.746$	$l = -24 \rightarrow 23$
39063 measured reflections	

Refinement

Refinement on F^2	861 restraints
Least-squares matrix: full	Hydrogen site location: inferred from neighbouring sites
$R[F^2 > 2\sigma(F^2)] = 0.046$	H-atom parameters constrained
$wR(F^2) = 0.119$	$w = 1/[\sigma^2(F_o^2) + (0.0526P)^2 + 4.3934P]$ where $P = (F_o^2 + 2F_c^2)/3$
$S = 1.03$	$(\Delta/\sigma)_{max} = 0.002$
9523 reflections	$\Delta\rangle_{max} = 1.29$ e Å^{-3}
691 parameters	$\Delta\rangle_{min} = -0.56$ e Å^{-3}

Special details

Geometry. All esds (except the esd in the dihedral angle between two l.s. planes) are estimated using the full covariance matrix. The cell esds are taken into account individually in the estimation of esds in distances, angles and torsion angles; correlations between esds in cell parameters are only used when they are defined by crystal symmetry. An approximate (isotropic) treatment of cell esds is used for estimating esds involving l.s. planes.

Fractional atomic coordinates and isotropic or equivalent isotropic displacement parameters (Å²)

	x	*y*	*z*	U_{iso}*/U_{eq}	Occ. (<1)
Tb1	0.31723 (2)	0.76783 (2)	0.26150 (2)	0.04010 (9)	

F1	0.0760 (12)	0.6008 (7)	0.3878 (7)	0.135 (4)	0.5
F2	0.1046 (15)	0.7022 (14)	0.4530 (9)	0.106 (6)	0.5
F3	-0.0426 (17)	0.7015 (19)	0.3860 (18)	0.136 (10)	0.5
F4	-0.038 (2)	0.7373 (12)	0.0749 (11)	0.138 (8)	0.5
F5	-0.0086 (13)	0.8589 (13)	0.0917 (8)	0.128 (5)	0.5
F6	-0.1245 (19)	0.811 (2)	0.138 (2)	0.135 (10)	0.5
O3	0.1958 (3)	0.7246 (2)	0.33263 (18)	0.0494 (8)	
O4	0.1441 (3)	0.7795 (2)	0.18518 (17)	0.0504 (9)	
C13	0.0541 (14)	0.6777 (13)	0.3848 (10)	0.067 (3)	0.5
C14	0.0978 (4)	0.7262 (4)	0.3235 (3)	0.0594 (14)	
C15	0.0230 (4)	0.7507 (4)	0.2610 (3)	0.0693 (18)	
H15	-0.049736	0.750909	0.262643	0.083*	
C16	0.0525 (4)	0.7749 (3)	0.1963 (3)	0.0526 (13)	
C17	-0.028 (3)	0.792 (2)	0.128 (2)	0.086 (6)	0.5
F1A	0.0551 (10)	0.7784 (8)	0.4364 (6)	0.128 (4)	0.5
F5A	-0.0294 (14)	0.8874 (10)	0.1275 (8)	0.123 (5)	0.5
F6A	-0.1265 (17)	0.781 (2)	0.1342 (18)	0.124 (9)	0.5
C01H	-0.037 (2)	0.811 (2)	0.1274 (19)	0.070 (4)	0.5
F3A	-0.0353 (17)	0.6679 (18)	0.3752 (16)	0.127 (8)	0.5
C0AA	0.0597 (15)	0.7158 (14)	0.3977 (12)	0.084 (4)	0.5
F2A	0.1208 (15)	0.6655 (12)	0.4390 (9)	0.099 (5)	0.5
F4A	-0.0190 (12)	0.7807 (13)	0.0656 (8)	0.106 (6)	0.5
F7	0.1310 (3)	0.9667 (2)	0.3745 (2)	0.0941 (13)	
F8	0.2754 (4)	1.0343 (2)	0.3885 (2)	0.0879 (11)	
F9	0.1390 (3)	1.0686 (2)	0.3042 (2)	0.0898 (12)	
F10	0.1761 (7)	0.9895 (14)	0.0464 (5)	0.122 (8)	0.66 (3)
F11	0.3273 (17)	1.0372 (7)	0.0909 (5)	0.122 (7)	0.66 (3)
F12	0.3088 (15)	0.9269 (6)	0.0375 (6)	0.103 (5)	0.66 (3)
O5	0.2640 (3)	0.8850 (2)	0.31054 (17)	0.0496 (8)	
O6	0.3180 (3)	0.8684 (2)	0.17006 (17)	0.0483 (8)	
C18	0.1918 (5)	1.0059 (4)	0.3375 (3)	0.0663 (15)	
C19	0.2317 (4)	0.9511 (3)	0.2830 (3)	0.0497 (11)	
C20	0.2296 (4)	0.9783 (3)	0.2100 (3)	0.0573 (13)	
H20	0.196705	1.028106	0.193993	0.069*	
C21	0.2738 (4)	0.9349 (3)	0.1605 (3)	0.0485 (11)	
C22	0.2717 (5)	0.9739 (4)	0.0828 (3)	0.0617 (13)	
F13	0.5545 (6)	0.7870 (3)	0.5283 (3)	0.0973 (18)	0.9
F14	0.6567 (4)	0.6912 (4)	0.5137 (2)	0.0992 (16)	0.9
F15	0.4969 (5)	0.6696 (4)	0.5155 (3)	0.1067 (17)	0.9
F16	0.6710 (3)	0.7702 (3)	0.1967 (2)	0.0852 (11)	

F17	0.7532 (2)	0.6931 (3)	0.28554 (19)	0.0784 (10)	
F18	0.6298 (3)	0.6461 (3)	0.1966 (2)	0.0861 (11)	
O7	0.4301 (3)	0.7523 (2)	0.38352 (19)	0.0462 (8)	
O8	0.4879 (3)	0.7460 (2)	0.24410 (18)	0.0474 (8)	
C23	0.5610 (4)	0.7216 (4)	0.4920 (3)	0.0615 (14)	
C24	0.5252 (4)	0.7337 (3)	0.4067 (3)	0.0489 (11)	
C25	0.6000 (4)	0.7195 (3)	0.3631 (3)	0.0561 (14)	
H25	0.669645	0.703822	0.387755	0.067*	
C26	0.5753 (4)	0.7275 (3)	0.2856 (3)	0.0474 (11)	
C27	0.6588 (4)	0.7088 (4)	0.2406 (3)	0.0608 (14)	
O1	0.5148 (4)	0.3970 (2)	0.1916 (3)	0.0793 (12)	
O2	0.4409 (4)	0.4496 (3)	0.0476 (2)	0.0832 (13)	
N1	0.3480 (3)	0.6170 (2)	0.2828 (2)	0.0465 (9)	
N2	0.3117 (3)	0.6831 (3)	0.1448 (2)	0.0449 (9)	
C1	0.3576 (4)	0.5828 (3)	0.3498 (3)	0.0540 (12)	
H1	0.335339	0.612086	0.388342	0.065*	
C2	0.3986 (5)	0.5062 (4)	0.3668 (3)	0.0653 (15)	
H2	0.401820	0.482970	0.415037	0.078*	
C3	0.4342 (5)	0.4650 (3)	0.3117 (3)	0.0635 (14)	
H3	0.465708	0.413661	0.322094	0.076*	
C4	0.4237 (4)	0.4992 (3)	0.2409 (3)	0.0502 (11)	
C5	0.4589 (5)	0.4569 (3)	0.1802 (3)	0.0582 (13)	
C6	0.4268 (4)	0.4905 (3)	0.0997 (3)	0.0577 (13)	
C7	0.3786 (4)	0.5702 (3)	0.0899 (3)	0.0489 (11)	
C8	0.3512 (4)	0.6054 (3)	0.0193 (3)	0.0547 (12)	
H8	0.367186	0.579244	-0.023240	0.066*	
C9	0.3013 (4)	0.6778 (4)	0.0106 (3)	0.0573 (13)	
H9	0.279708	0.701946	-0.037770	0.069*	
C10	0.2830 (4)	0.7150 (3)	0.0748 (3)	0.0530 (13)	
H10	0.248583	0.765555	0.069177	0.064*	
C11	0.3776 (4)	0.5749 (3)	0.2273 (3)	0.0459 (10)	
C12	0.3563 (3)	0.6114 (3)	0.1516 (3)	0.0442 (10)	
C1S	0.1576 (10)	0.4288 (7)	0.0911 (7)	0.072 (3)*	0.639 (12)
C2S	0.1226 (10)	0.5020 (8)	0.0641 (8)	0.077 (4)*	0.639 (12)
H2S	0.113689	0.516200	0.012399	0.093*	0.639 (12)
C3S	0.1011 (10)	0.5537 (8)	0.1167 (8)	0.088 (4)*	0.639 (12)
H3S	0.076344	0.605770	0.100604	0.106*	0.639 (12)
C4S	0.1135 (12)	0.5342 (10)	0.1941 (9)	0.109 (5)*	0.639 (12)
H4S	0.097695	0.571677	0.229293	0.130*	0.639 (12)
C5S	0.1504 (14)	0.4565 (10)	0.2165 (8)	0.108 (5)*	0.639 (12)

H5S	0.161023	0.440277	0.267854	0.129*	0.639 (12)
C6S	0.1705 (11)	0.4052 (8)	0.1631 (8)	0.082 (3)*	0.639 (12)
H6S	0.193873	0.352274	0.176999	0.099*	0.639 (12)
C7S	0.1768 (10)	0.3739 (8)	0.0312 (7)	0.108 (5)*	0.639 (12)
H7SA	0.130942	0.388971	-0.017493	0.162*	0.639 (12)
H7SB	0.161101	0.318745	0.043572	0.162*	0.639 (12)
H7SC	0.251065	0.377727	0.027957	0.162*	0.639 (12)
C1T	0.1278 (14)	0.4931 (12)	0.2122 (9)	0.058 (4)*	0.361 (12)
C2T	0.1039 (14)	0.5487 (10)	0.1538 (10)	0.059 (4)*	0.361 (12)
H2T	0.081427	0.601767	0.160906	0.071*	0.361 (12)
C3T	0.1154 (16)	0.5205 (13)	0.0846 (11)	0.064 (5)*	0.361 (12)
H3T	0.096270	0.557558	0.044068	0.077*	0.361 (12)
C4T	0.151 (2)	0.4453 (16)	0.0641 (17)	0.113 (10)*	0.361 (12)
H4T	0.152575	0.431074	0.013686	0.136*	0.361 (12)
C5T	0.184 (2)	0.3943 (18)	0.1258 (15)	0.126 (10)*	0.361 (12)
H5T	0.218625	0.345008	0.120886	0.151*	0.361 (12)
C6T	0.165 (2)	0.4187 (13)	0.1956 (15)	0.098 (8)*	0.361 (12)
H6T	0.178630	0.380451	0.235333	0.117*	0.361 (12)
C7T	0.103 (3)	0.5090 (18)	0.2856 (14)	0.171 (15)*	0.361 (12)
H7TA	0.100768	0.566999	0.293600	0.257*	0.361 (12)
H7TB	0.157236	0.484965	0.325834	0.257*	0.361 (12)
H7TC	0.033667	0.485801	0.286425	0.257*	0.361 (12)
F14A	0.654 (2)	0.756 (2)	0.518 (2)	0.075 (9)	0.1
F15A	0.577 (5)	0.6471 (12)	0.510 (2)	0.083 (9)	0.1
F13A	0.506 (4)	0.750 (3)	0.537 (2)	0.086 (12)	0.1
F10A	0.217 (2)	1.0429 (11)	0.0714 (11)	0.093 (8)	0.34 (3)
F11A	0.230 (3)	0.9263 (13)	0.0317 (10)	0.115 (12)	0.34 (3)
F12A	0.3647 (13)	0.992 (2)	0.0728 (14)	0.115 (11)	0.34 (3)

Atomic displacement parameters (Å²)

	U^{11}	U^{22}	U^{33}	U^{12}	U^{13}	U^{23}
Tb1	0.03922 (13)	0.04922 (15)	0.03293 (12)	0.00772 (10)	0.01040 (8)	0.00105 (10)
F1	0.199 (12)	0.102 (7)	0.123 (8)	-0.029 (7)	0.077 (8)	0.028 (6)
F2	0.088 (10)	0.195 (17)	0.039 (5)	-0.047 (11)	0.025 (5)	-0.004 (8)
F3	0.052 (7)	0.28 (3)	0.091 (11)	0.028 (11)	0.043 (7)	0.059 (15)
F4	0.131 (14)	0.199 (17)	0.067 (9)	0.019 (11)	-0.014 (7)	-0.011 (10)
F5	0.101 (8)	0.184 (16)	0.086 (11)	0.027 (11)	-0.004 (8)	0.062 (10)
F6	0.060 (9)	0.27 (3)	0.079 (9)	0.077 (12)	0.017 (8)	0.035 (13)
O3	0.0426 (17)	0.066 (2)	0.0404 (17)	0.0063 (16)	0.0118 (14)	0.0074 (15)

O4	0.0388 (17)	0.075 (3)	0.0369 (16)	0.0107 (16)	0.0084 (13)	0.0059 (15)
C13	0.041 (6)	0.105 (9)	0.054 (7)	-0.024 (6)	0.006 (5)	0.002 (6)
C14	0.044 (3)	0.092 (4)	0.044 (3)	0.004 (3)	0.015 (2)	0.007 (3)
C15	0.042 (3)	0.120 (6)	0.051 (3)	0.012 (3)	0.020 (2)	0.014 (3)
C16	0.035 (2)	0.077 (4)	0.043 (2)	0.013 (2)	0.0043 (18)	0.000 (2)
C17	0.046 (7)	0.149 (16)	0.062 (7)	0.038 (9)	0.007 (6)	0.022 (8)
F1A	0.152 (10)	0.183 (10)	0.072 (6)	0.025 (8)	0.074 (6)	0.011 (6)
F5A	0.120 (11)	0.120 (8)	0.110 (11)	0.046 (7)	-0.012 (9)	0.037 (8)
F6A	0.042 (7)	0.25 (2)	0.071 (9)	-0.011 (11)	-0.004 (6)	0.053 (12)
C01H	0.040 (7)	0.123 (10)	0.047 (6)	0.028 (8)	0.009 (6)	0.017 (8)
F3A	0.070 (10)	0.23 (2)	0.078 (10)	-0.053 (12)	0.004 (8)	0.055 (11)
C0AA	0.053 (7)	0.153 (12)	0.049 (8)	0.001 (7)	0.018 (6)	0.022 (7)
F2A	0.075 (6)	0.161 (14)	0.069 (10)	0.009 (8)	0.029 (7)	0.050 (8)
F4A	0.064 (6)	0.215 (19)	0.034 (4)	0.025 (11)	0.002 (4)	-0.005 (9)
F7	0.118 (3)	0.079 (3)	0.110 (3)	0.031 (2)	0.077 (3)	0.020 (2)
F8	0.134 (3)	0.065 (2)	0.066 (2)	0.009 (2)	0.023 (2)	-0.0095 (18)
F9	0.119 (3)	0.071 (2)	0.090 (2)	0.043 (2)	0.045 (2)	0.016 (2)
F10	0.083 (5)	0.22 (2)	0.062 (5)	0.023 (7)	0.003 (4)	0.054 (9)
F11	0.210 (17)	0.098 (8)	0.060 (4)	-0.079 (10)	0.034 (6)	0.005 (4)
F12	0.175 (13)	0.095 (6)	0.056 (5)	0.026 (7)	0.062 (7)	0.017 (4)
O5	0.061 (2)	0.049 (2)	0.0420 (17)	0.0095 (16)	0.0172 (15)	0.0028 (15)
O6	0.0509 (19)	0.055 (2)	0.0394 (16)	-0.0004 (16)	0.0122 (14)	0.0051 (15)
C18	0.083 (4)	0.053 (4)	0.068 (3)	0.019 (3)	0.027 (3)	0.008 (3)
C19	0.049 (3)	0.049 (3)	0.051 (3)	0.006 (2)	0.012 (2)	-0.002 (2)
C20	0.065 (3)	0.054 (3)	0.053 (3)	0.006 (3)	0.012 (2)	0.009 (2)
C21	0.049 (3)	0.052 (3)	0.042 (2)	-0.007 (2)	0.006 (2)	0.006 (2)
C22	0.077 (4)	0.062 (3)	0.044 (3)	-0.003 (3)	0.008 (2)	0.010 (2)
F13	0.151 (6)	0.089 (4)	0.044 (2)	0.024 (3)	0.004 (3)	-0.002 (2)
F14	0.076 (3)	0.153 (5)	0.058 (2)	0.046 (3)	-0.006 (2)	0.018 (3)
F15	0.118 (4)	0.131 (5)	0.063 (3)	-0.028 (3)	0.004 (3)	0.046 (3)
F16	0.067 (2)	0.110 (3)	0.088 (3)	0.005 (2)	0.0389 (19)	0.021 (2)
F17	0.0408 (17)	0.109 (3)	0.081 (2)	0.0131 (18)	0.0060 (15)	-0.003 (2)
F18	0.066 (2)	0.102 (3)	0.091 (2)	0.007 (2)	0.0201 (19)	-0.034 (2)
O7	0.0436 (17)	0.050 (2)	0.0449 (18)	0.0047 (14)	0.0095 (14)	0.0036 (14)
O8	0.0377 (17)	0.060 (2)	0.0439 (17)	-0.0009 (14)	0.0086 (13)	-0.0006 (15)
C23	0.063 (3)	0.067 (4)	0.051 (3)	0.010 (3)	0.005 (2)	0.014 (2)
C24	0.048 (3)	0.048 (3)	0.050 (2)	0.005 (2)	0.007 (2)	0.009 (2)
C25	0.045 (3)	0.071 (4)	0.049 (3)	0.010 (2)	0.004 (2)	0.008 (2)
C26	0.043 (2)	0.050 (3)	0.049 (2)	-0.003 (2)	0.0092 (19)	0.001 (2)
C27	0.052 (3)	0.072 (4)	0.060 (3)	0.007 (3)	0.015 (2)	-0.005 (3)

O1	0.089 (3)	0.049 (2)	0.098 (3)	0.013 (2)	0.016 (2)	-0.008 (2)
O2	0.099 (3)	0.074 (3)	0.084 (3)	0.019 (3)	0.036 (3)	-0.019 (2)
N1	0.043 (2)	0.046 (2)	0.052 (2)	0.0025 (18)	0.0132 (17)	0.0031 (18)
N2	0.040 (2)	0.053 (3)	0.0420 (19)	0.0012 (18)	0.0096 (16)	-0.0050 (17)
C1	0.052 (3)	0.056 (3)	0.055 (3)	-0.004 (2)	0.013 (2)	0.006 (2)
C2	0.074 (4)	0.059 (4)	0.062 (3)	0.000 (3)	0.015 (3)	0.017 (3)
C3	0.075 (4)	0.043 (3)	0.070 (3)	0.002 (3)	0.012 (3)	0.008 (3)
C4	0.043 (3)	0.044 (3)	0.063 (3)	-0.005 (2)	0.011 (2)	0.002 (2)
C5	0.062 (3)	0.039 (3)	0.075 (3)	-0.001 (2)	0.020 (3)	-0.007 (2)
C6	0.051 (3)	0.055 (3)	0.070 (3)	-0.001 (2)	0.019 (2)	-0.014 (2)
C7	0.039 (2)	0.052 (3)	0.059 (3)	-0.004 (2)	0.017 (2)	-0.007 (2)
C8	0.050 (3)	0.064 (3)	0.055 (3)	-0.001 (2)	0.022 (2)	-0.004 (2)
C9	0.061 (3)	0.070 (4)	0.043 (3)	0.004 (3)	0.016 (2)	-0.002 (2)
C10	0.059 (3)	0.058 (4)	0.043 (2)	0.002 (2)	0.013 (2)	-0.004 (2)
C11	0.037 (2)	0.043 (3)	0.058 (3)	-0.002 (2)	0.011 (2)	-0.002 (2)
C12	0.028 (2)	0.053 (3)	0.052 (2)	-0.0033 (19)	0.0097 (19)	-0.005 (2)
F14A	0.068 (12)	0.080 (19)	0.063 (17)	0.004 (12)	-0.015 (12)	0.027 (18)
F15A	0.11 (3)	0.067 (10)	0.062 (19)	0.019 (11)	0.01 (2)	0.023 (13)
F13A	0.10 (2)	0.10 (3)	0.065 (15)	0.04 (2)	0.028 (18)	0.03 (2)
F10A	0.118 (17)	0.077 (10)	0.080 (10)	0.023 (10)	0.013 (12)	0.038 (8)
F11A	0.18 (3)	0.102 (10)	0.046 (6)	-0.037 (14)	-0.015 (11)	0.004 (6)
F12A	0.086 (8)	0.18 (3)	0.081 (15)	-0.011 (9)	0.024 (7)	0.052 (17)

Geometric parameters (Å, º)

Tb1—O3	2.364 (3)	C24—C25	1.404 (7)
Tb1—O4	2.364 (3)	C25—H25	0.9500
Tb1—O5	2.318 (3)	C25—C26	1.376 (7)
Tb1—O6	2.363 (3)	C26—C27	1.529 (7)
Tb1—O7	2.377 (3)	O1—C5	1.225 (6)
Tb1—O8	2.335 (3)	O2—C6	1.214 (6)
Tb1—O1^{i}	3.046 (4)	N1—C1	1.324 (6)
Tb1—N1	2.566 (4)	N1—C11	1.353 (6)
Tb1—N2	2.536 (4)	N2—C10	1.351 (6)
F1—C13	1.31 (2)	N2—C12	1.322 (6)
F2—C13	1.33 (2)	C1—H1	0.9500
F3—C13	1.32 (3)	C1—C2	1.393 (8)
F4—C17	1.32 (4)	C2—H2	0.9500
F5—C17	1.35 (4)	C2—C3	1.378 (8)
F6—C17	1.33 (4)	C3—H3	0.9500

O3—C14	1.244 (6)	C3—C4	1.385 (7)
O4—C16	1.252 (6)	C4—C5	1.467 (7)
C13—C14	1.58 (2)	C4—C11	1.396 (7)
C14—C15	1.378 (8)	C5—C6	1.532 (8)
C14—C0AA	1.55 (2)	C6—C7	1.462 (8)
C15—H15	0.9500	C7—C8	1.382 (7)
C15—C16	1.375 (7)	C7—C12	1.400 (6)
C16—C17	1.46 (3)	C8—H8	0.9500
C16—C01H	1.62 (3)	C8—C9	1.363 (8)
F1A—C0AA	1.27 (3)	C9—H9	0.9500
F5A—C01H	1.28 (3)	C9—C10	1.387 (7)
F6A—C01H	1.29 (4)	C10—H10	0.9500
C01H—F4A	1.30 (3)	C11—C12	1.472 (7)
F3A—C0AA	1.45 (3)	C1S—C2S	1.357 (14)
C0AA—F2A	1.28 (3)	C1S—C6S	1.338 (14)
F7—C18	1.319 (7)	C1S—C7S	1.486 (13)
F8—C18	1.344 (7)	C2S—H2S	0.9500
F9—C18	1.320 (6)	C2S—C3S	1.362 (14)
F10—C22	1.293 (9)	C3S—H3S	0.9500
F11—C22	1.270 (10)	C3S—C4S	1.415 (14)
F12—C22	1.305 (9)	C4S—H4S	0.9500
O5—C19	1.245 (6)	C4S—C5S	1.410 (16)
O6—C21	1.243 (6)	C5S—H5S	0.9500
C18—C19	1.521 (7)	C5S—C6S	1.364 (15)
C19—C20	1.396 (7)	C6S—H6S	0.9500
C20—H20	0.9500	C7S—H7SA	0.9800
C20—C21	1.377 (7)	C7S—H7SB	0.9800
C21—C22	1.548 (7)	C7S—H7SC	0.9800
C22—F10A	1.341 (15)	C1T—C2T	1.392 (17)
C22—F11A	1.246 (16)	C1T—C6T	1.390 (18)
C22—F12A	1.297 (17)	C1T—C7T	1.464 (18)
F13—C23	1.289 (7)	C2T—H2T	0.9500
F14—C23	1.315 (6)	C2T—C3T	1.382 (17)
F15—C23	1.336 (7)	C3T—H3T	0.9500
F16—C27	1.331 (7)	C3T—C4T	1.417 (18)
F17—C27	1.334 (6)	C4T—H4T	0.9500
F18—C27	1.318 (7)	C4T—C5T	1.395 (19)
O7—C24	1.248 (6)	C5T—H5T	0.9500
O8—C26	1.249 (6)	C5T—C6T	1.406 (18)
C23—C24	1.527 (7)	C6T—H6T	0.9500

C23—F14A	1.326 (16)	C7T—H7TA	0.9800
C23—F15A	1.289 (15)	C7T—H7TB	0.9800
C23—F13A	1.295 (16)	C7T—H7TC	0.9800
O3—Tb1—O4	71.57 (11)	F15—C23—C24	110.0 (5)
O3—Tb1—O7	78.65 (11)	F14A—C23—C24	110.7 (17)
O3—Tb1—O1^{i}	125.87 (12)	F15A—C23—C24	112.1 (18)
O3—Tb1—N1	73.60 (12)	F15A—C23—F14A	104 (3)
O3—Tb1—N2	112.94 (12)	F15A—C23—F13A	106 (3)
O4—Tb1—O7	149.08 (11)	F13A—C23—C24	121 (2)
O4—Tb1—O1^{i}	129.03 (12)	F13A—C23—F14A	102 (3)
O4—Tb1—N1	105.28 (13)	O7—C24—C23	115.2 (5)
O4—Tb1—N2	73.29 (12)	O7—C24—C25	127.5 (5)
O5—Tb1—O3	75.79 (12)	C25—C24—C23	117.3 (5)
O5—Tb1—O4	80.20 (12)	C24—C25—H25	119.0
O5—Tb1—O6	73.70 (11)	C26—C25—C24	121.9 (5)
O5—Tb1—O7	84.74 (11)	C26—C25—H25	119.0
O5—Tb1—O8	123.93 (12)	O8—C26—C25	127.6 (5)
O5—Tb1—O1^{i}	63.37 (13)	O8—C26—C27	112.5 (4)
O5—Tb1—N1	145.07 (12)	C25—C26—C27	119.8 (5)
O5—Tb1—N2	146.86 (12)	F16—C27—C26	110.9 (5)
O6—Tb1—O3	135.24 (11)	F17—C27—C26	112.1 (4)
O6—Tb1—O4	71.60 (12)	F18—C27—F16	107.7 (5)
O6—Tb1—O7	129.26 (11)	F18—C27—C26	110.3 (5)
O6—Tb1—O1^{i}	64.98 (11)	C1—N1—Tb1	122.8 (3)
O6—Tb1—N1	141.11 (12)	C1—N1—C11	118.5 (5)
O6—Tb1—N2	79.24 (13)	C11—N1—Tb1	117.2 (3)
O7—Tb1—O1^{i}	64.30 (11)	C10—N2—Tb1	121.1 (3)
O7—Tb1—N1	73.16 (12)	C12—N2—Tb1	119.8 (3)
O7—Tb1—N2	127.81 (12)	C12—N2—C10	117.8 (4)
O8—Tb1—O3	142.68 (12)	N1—C1—H1	118.3
O8—Tb1—O4	137.50 (11)	N1—C1—C2	123.5 (5)
O8—Tb1—O6	82.02 (12)	C2—C1—H1	118.3
O8—Tb1—O7	72.93 (11)	C1—C2—H2	120.9
O8—Tb1—O1^{i}	60.57 (12)	C3—C2—C1	118.1 (5)
O8—Tb1—N1	75.36 (12)	C3—C2—H2	120.9
O8—Tb1—N2	69.39 (12)	C2—C3—H3	120.3
N1—Tb1—O1^{i}	125.16 (12)	C2—C3—C4	119.3 (5)
N2—Tb1—O1^{i}	120.79 (13)	C4—C3—H3	120.3
N2—Tb1—N1	63.40 (13)	C3—C4—C5	121.1 (5)

C14—O3—Tb1	135.0 (3)	C3—C4—C11	119.0 (5)
C16—O4—Tb1	135.2 (3)	C11—C4—C5	119.9 (5)
F1—C13—F2	102 (2)	O1—C5—C4	122.6 (5)
F1—C13—F3	119 (2)	O1—C5—C6	119.0 (5)
F1—C13—C14	114.9 (13)	C4—C5—C6	118.4 (5)
F2—C13—C14	108.5 (15)	O2—C6—C5	118.6 (5)
F3—C13—F2	99 (2)	O2—C6—C7	123.5 (5)
F3—C13—C14	111 (2)	C7—C6—C5	117.8 (5)
O3—C14—C13	114.4 (8)	C8—C7—C6	120.9 (5)
O3—C14—C15	128.6 (5)	C8—C7—C12	118.4 (5)
O3—C14—C0AA	113.6 (8)	C12—C7—C6	120.6 (5)
C15—C14—C13	115.7 (8)	C7—C8—H8	120.0
C15—C14—C0AA	116.5 (9)	C9—C8—C7	120.0 (5)
C14—C15—H15	119.7	C9—C8—H8	120.0
C16—C15—C14	120.7 (5)	C8—C9—H9	121.1
C16—C15—H15	119.7	C8—C9—C10	117.9 (5)
O4—C16—C15	127.8 (5)	C10—C9—H9	121.1
O4—C16—C17	112.1 (17)	N2—C10—C9	123.4 (5)
O4—C16—C01H	113.2 (13)	N2—C10—H10	118.3
C15—C16—C17	119.9 (17)	C9—C10—H10	118.3
C15—C16—C01H	118.6 (13)	N1—C11—C4	121.4 (5)
F4—C17—F5	102 (3)	N1—C11—C12	117.2 (4)
F4—C17—F6	109 (4)	C4—C11—C12	121.4 (4)
F4—C17—C16	115 (2)	N2—C12—C7	122.4 (5)
F5—C17—C16	114 (3)	N2—C12—C11	116.6 (4)
F6—C17—F5	99 (2)	C7—C12—C11	121.0 (5)
F6—C17—C16	116 (3)	C2S—C1S—C7S	112.9 (13)
F5A—C01H—C16	109 (2)	C6S—C1S—C2S	125.1 (12)
F5A—C01H—F6A	117 (3)	C6S—C1S—C7S	121.9 (13)
F5A—C01H—F4A	111 (3)	C1S—C2S—H2S	122.5
F6A—C01H—C16	107 (3)	C1S—C2S—C3S	115.0 (12)
F6A—C01H—F4A	106 (3)	C3S—C2S—H2S	122.5
F4A—C01H—C16	106.4 (19)	C2S—C3S—H3S	118.2
F1A—C0AA—C14	117.1 (16)	C2S—C3S—C4S	123.7 (12)
F1A—C0AA—F3A	118 (2)	C4S—C3S—H3S	118.2
F1A—C0AA—F2A	109 (2)	C3S—C4S—H4S	121.5
F3A—C0AA—C14	103.7 (19)	C5S—C4S—C3S	117.0 (13)
F2A—C0AA—C14	107.9 (16)	C5S—C4S—H4S	121.5
F2A—C0AA—F3A	100 (2)	C4S—C5S—H5S	120.7
C19—O5—Tb1	134.1 (3)	C6S—C5S—C4S	118.6 (13)

C21—O6—Tb1	131.1 (3)	C6S—C5S—H5S	120.7
F7—C18—F8	107.8 (5)	C1S—C6S—C5S	120.6 (12)
F7—C18—F9	108.6 (5)	C1S—C6S—H6S	119.7
F7—C18—C19	111.3 (5)	C5S—C6S—H6S	119.7
F8—C18—C19	108.7 (5)	C1S—C7S—H7SA	109.5
F9—C18—F8	106.8 (5)	C1S—C7S—H7SB	109.5
F9—C18—C19	113.4 (5)	C1S—C7S—H7SC	109.5
O5—C19—C18	113.9 (4)	H7SA—C7S—H7SB	109.5
O5—C19—C20	127.0 (5)	H7SA—C7S—H7SC	109.5
C20—C19—C18	119.0 (5)	H7SB—C7S—H7SC	109.5
C19—C20—H20	119.1	C2T—C1T—C7T	121.0 (14)
C21—C20—C19	121.8 (5)	C6T—C1T—C2T	117.3 (16)
C21—C20—H20	119.1	C6T—C1T—C7T	121.3 (15)
O6—C21—C20	128.7 (5)	C1T—C2T—H2T	122.8
O6—C21—C22	114.5 (5)	C3T—C2T—C1T	114.5 (15)
C20—C21—C22	116.7 (5)	C3T—C2T—H2T	122.8
F10—C22—F12	104.3 (8)	C2T—C3T—H3T	114.7
F10—C22—C21	111.5 (6)	C2T—C3T—C4T	131 (2)
F11—C22—F10	110.1 (10)	C4T—C3T—H3T	114.7
F11—C22—F12	107.0 (8)	C3T—C4T—H4T	123.5
F11—C22—C21	110.7 (6)	C5T—C4T—C3T	113 (2)
F12—C22—C21	112.9 (6)	C5T—C4T—H4T	123.5
F10A—C22—C21	113.7 (8)	C4T—C5T—H5T	121.2
F11A—C22—C21	109.0 (10)	C4T—C5T—C6T	118 (3)
F11A—C22—F10A	108.0 (13)	C6T—C5T—H5T	121.2
F11A—C22—F12A	107.8 (15)	C1T—C6T—C5T	127 (2)
F12A—C22—C21	113.8 (9)	C1T—C6T—H6T	116.7
F12A—C22—F10A	104.2 (13)	C5T—C6T—H6T	116.7
C24—O7—Tb1	133.9 (3)	C1T—C7T—H7TA	109.5
C26—O8—Tb1	135.7 (3)	C1T—C7T—H7TB	109.5
F13—C23—F14	109.8 (6)	C1T—C7T—H7TC	109.5
F13—C23—F15	105.6 (6)	H7TA—C7T—H7TB	109.5
F13—C23—C24	111.6 (5)	H7TA—C7T—H7TC	109.5
F14—C23—F15	105.5 (5)	H7TB—C7T—H7TC	109.5
F14—C23—C24	113.9 (5)		

Symmetry code: (i) -*x*+1, *y*+1/2, -*z*+1/2.

8.3.3 Crystallographic data for 1(i)-Yb

Crystal data

$C_{27}H_9F_{18}N_2O_8Yb \cdot C_4H_{10}O$	$F(000) = 2092$
$M_r = 1078.52$	$D_x = 1.932$ Mg m^{-3}
Monoclinic, $P2_1/c$	Mo $K\alpha$ radiation, $\lambda = 0.71073$ Å
$a = 9.6652$ (4) Å	Cell parameters from 9965 reflections
$b = 22.8397$ (10) Å	$\theta = 2.4$–$28.3°$
$c = 17.0144$ (7) Å	$\mu = 2.67$ mm^{-1}
$\beta = 99.138$ (1)°	$T = 150$ K
$V = 3708.3$ (3) Å^3	Block, yellow green
$Z = 4$	0.27 × 0.1 × 0.07 mm

Data collection

Bruker D8 VENTURE diffractometer	9198 independent reflections
Radiation source: microfocus sealed tube, INCOATEC Iμs 3.0	8263 reflections with $I > 2\sigma(I)$
Multilayer mirror optics monochromator	$R_{int} = 0.041$
Detector resolution: 7.4074 pixels mm^{-1}	$\theta_{max} = 28.3°$, $\theta_{min} = 2.3°$
ϕ and ω scans	$h = -12 \rightarrow 12$
Absorption correction: multi-scan *SADABS2016*/2 (Bruker,2016/2) was used for absorption correction. wR2(int) was 0.0947 before and 0.0527 after correction. The Ratio of minimum to maximum transmission is 0.8261. The λ/2 correction factor is Not present.	$k = -30 \rightarrow 30$
$T_{min} = 0.616$, $T_{max} = 0.746$	$l = -22 \rightarrow 22$
58669 measured reflections	

Refinement

Refinement on F^2	Primary atom site location: dual
Least-squares matrix: full	Hydrogen site location: inferred from neighbouring sites
$R[F^2 > 2\sigma(F^2)] = 0.026$	H-atom parameters constrained
$wR(F^2) = 0.061$	$w = 1/[\sigma^2(F_o^2) + (0.0221P)^2 + 5.748P]$ where $P = (F_o^2 + 2F_c^2)/3$
$S = 1.04$	$(\Delta/\sigma)_{max} = 0.003$
9198 reflections	$\Delta\rangle_{max} = 0.77$ e Å^{-3}

584 parameters	$\Delta\rangle_{min}$ = -0.51 e Å^{-3}
39 restraints	

Special details

Geometry. All esds (except the esd in the dihedral angle between two l.s. planes) are estimated using the full covariance matrix. The cell esds are taken into account individually in the estimation of esds in distances, angles and torsion angles; correlations between esds in cell parameters are only used when they are defined by crystal symmetry. An approximate (isotropic) treatment of cell esds is used for estimating esds involving l.s. planes.

Fractional atomic coordinates and isotropic or equivalent isotropic displacement parameters (Å²)

	x	*y*	*z*	U_{iso}*/U_{eq}	Occ. (<1)
Yb1	0.77317 (2)	0.42380 (2)	0.28883 (2)	0.01846 (4)	
F1	0.7153 (4)	0.18544 (10)	0.3722 (2)	0.0893 (15)	0.892 (6)
F2	0.7221 (6)	0.25374 (16)	0.45721 (17)	0.1020 (18)	0.892 (6)
F3	0.5479 (3)	0.24334 (16)	0.3680 (3)	0.1004 (15)	0.892 (6)
F4	0.9683 (4)	0.21617 (11)	0.1615 (2)	0.1015 (12)	
F5	1.1230 (3)	0.27695 (16)	0.2023 (3)	0.1226 (14)	
F6	0.9757 (5)	0.29978 (15)	0.10798 (18)	0.1406 (18)	
F7	1.2073 (2)	0.36594 (12)	0.45106 (13)	0.0674 (7)	
F8	1.1419 (2)	0.36096 (11)	0.56218 (12)	0.0600 (6)	
F9	1.1965 (3)	0.44345 (11)	0.5197 (2)	0.1085 (13)	
F10	0.6771 (2)	0.38319 (11)	0.59519 (12)	0.0588 (6)	
F11	0.5139 (2)	0.40052 (15)	0.49868 (13)	0.0783 (9)	
F12	0.6193 (3)	0.47074 (11)	0.56505 (16)	0.0767 (8)	
F13	1.1939 (2)	0.54013 (13)	0.26859 (16)	0.0762 (8)	
F14	1.1026 (2)	0.53159 (10)	0.14739 (13)	0.0582 (6)	
F15	1.0939 (3)	0.61416 (10)	0.2048 (3)	0.1151 (14)	
F16	0.4923 (2)	0.60109 (11)	0.22592 (14)	0.0698 (7)	
F17	0.5794 (2)	0.61641 (9)	0.34601 (11)	0.0450 (5)	
F18	0.6525 (3)	0.66576 (9)	0.25615 (19)	0.0807 (9)	
O1	0.3229 (3)	0.43192 (11)	-0.07564 (13)	0.0463 (6)	
O2	0.1358 (2)	0.42586 (10)	0.02970 (15)	0.0442 (6)	
O3	0.71679 (19)	0.33495 (8)	0.33727 (11)	0.0270 (4)	
O4	0.89748 (19)	0.35350 (8)	0.23152 (11)	0.0265 (4)	
O5	0.96788 (19)	0.41537 (9)	0.38420 (11)	0.0271 (4)	
O6	0.69570 (19)	0.43849 (8)	0.40802 (10)	0.0239 (4)	

O7	0.93662 (18)	0.48367 (8)	0.24780 (11)	0.0254 (4)	
O8	0.67780 (19)	0.51497 (8)	0.28051 (11)	0.0266 (4)	
N1	0.6994 (2)	0.42660 (9)	0.14171 (13)	0.0223 (4)	
N2	0.5165 (2)	0.41232 (10)	0.24372 (13)	0.0245 (4)	
C1	0.7926 (3)	0.42899 (12)	0.09146 (16)	0.0275 (5)	
H1	0.889228	0.431300	0.113355	0.033*	
C2	0.7565 (3)	0.42828 (13)	0.00936 (17)	0.0336 (6)	
H2	0.826548	0.428721	-0.023986	0.040*	
C3	0.6163 (3)	0.42692 (13)	-0.02276 (17)	0.0337 (6)	
H3	0.588120	0.426825	-0.078857	0.040*	
C4	0.5168 (3)	0.42570 (11)	0.02765 (16)	0.0271 (5)	
C5	0.3649 (3)	0.42632 (13)	-0.00503 (18)	0.0333 (6)	
C6	0.2601 (3)	0.42284 (12)	0.05402 (18)	0.0332 (6)	
C7	0.3174 (3)	0.41648 (12)	0.13989 (17)	0.0276 (6)	
C8	0.2279 (3)	0.40906 (15)	0.19484 (19)	0.0353 (7)	
H8	0.129360	0.408201	0.178185	0.042*	
C9	0.2834 (3)	0.40294 (16)	0.27393 (19)	0.0391 (7)	
H9	0.224172	0.397496	0.312854	0.047*	
C10	0.4274 (3)	0.40487 (14)	0.29561 (17)	0.0335 (6)	
H10	0.465251	0.400687	0.350363	0.040*	
C11	0.4615 (3)	0.41825 (11)	0.16644 (15)	0.0223 (5)	
C12	0.5622 (3)	0.42440 (10)	0.10993 (15)	0.0216 (5)	
C13	0.6877 (4)	0.24086 (14)	0.3827 (2)	0.0501 (9)	
C14	0.7503 (3)	0.28238 (11)	0.32960 (16)	0.0282 (6)	
C15	0.8358 (3)	0.26093 (12)	0.27837 (18)	0.0344 (6)	
H15	0.850107	0.219917	0.274914	0.041*	
C16	0.9008 (3)	0.29877 (12)	0.23200 (16)	0.0282 (6)	
C17	0.9893 (4)	0.27152 (15)	0.1745 (2)	0.0524 (9)	
C18	1.1343 (3)	0.39471 (14)	0.49748 (17)	0.0363 (7)	
C19	0.9823 (3)	0.40563 (12)	0.45742 (16)	0.0263 (5)	
C20	0.8804 (3)	0.40470 (14)	0.50620 (16)	0.0318 (6)	
H20	0.904151	0.392700	0.560119	0.038*	
C21	0.7430 (3)	0.42131 (12)	0.47651 (16)	0.0262 (5)	
C22	0.6367 (3)	0.41876 (15)	0.53453 (17)	0.0381 (7)	
C23	1.0850 (4)	0.55741 (14)	0.2154 (2)	0.0454 (8)	
C24	0.9473 (3)	0.53815 (12)	0.24056 (15)	0.0261 (5)	
C25	0.8499 (3)	0.58086 (12)	0.25076 (17)	0.0287 (6)	
H25	0.872339	0.621038	0.245677	0.034*	
C26	0.7199 (3)	0.56502 (11)	0.26835 (15)	0.0250 (5)	
C27	0.6106 (3)	0.61309 (13)	0.27366 (17)	0.0336 (6)	

O1S	0.3356 (3)	0.30625 (11)	0.02110 (19)	0.0717 (9)	
C1S	0.5137 (5)	0.26943 (18)	0.1202 (3)	0.0708 (13)	
H1SA	0.484188	0.291104	0.164369	0.106*	
H1SB	0.578721	0.293488	0.095272	0.106*	
H1SC	0.560615	0.233142	0.140348	0.106*	
C2S	0.3903 (4)	0.25524 (16)	0.0609 (3)	0.0575 (10)	
H2SA	0.416861	0.226928	0.021883	0.069*	
H2SB	0.317670	0.236806	0.087802	0.069*	
C3S	0.2634 (10)	0.2930 (4)	-0.0593 (5)	0.060 (2)	0.5
H3SA	0.303719	0.257613	-0.080445	0.072*	0.5
H3SB	0.271789	0.326188	-0.095658	0.072*	0.5
C4S	0.1145 (10)	0.2831 (4)	-0.0512 (6)	0.068 (3)	0.5
H4SA	0.061965	0.270742	-0.102586	0.101*	0.5
H4SB	0.074226	0.319417	-0.034173	0.101*	0.5
H4SC	0.108879	0.252432	-0.011461	0.101*	0.5
C5S	0.1948 (9)	0.2914 (4)	-0.0274 (5)	0.0502 (18)	0.5
H5SA	0.148598	0.259762	-0.001406	0.060*	0.5
H5SB	0.132915	0.326185	-0.033074	0.060*	0.5
C6S	0.2243 (10)	0.2721 (5)	-0.1059 (5)	0.072 (3)	0.5
H6SA	0.278163	0.302408	-0.128408	0.108*	0.5
H6SB	0.135728	0.265421	-0.141647	0.108*	0.5
H6SC	0.278468	0.235666	-0.099743	0.108*	0.5
F1A	0.8086 (18)	0.2083 (10)	0.4309 (12)	0.056 (7)*	0.108 (6)
F3A	0.622 (3)	0.1994 (12)	0.3522 (14)	0.081 (9)*	0.108 (6)
F2A	0.639 (2)	0.2644 (10)	0.4365 (16)	0.063 (8)*	0.108 (6)

Atomic displacement parameters (Å²)

	U^{11}	U^{22}	U^{33}	U^{12}	U^{13}	U^{23}
Yb1	0.01829 (5)	0.02047 (6)	0.01709 (6)	-0.00053 (4)	0.00424 (4)	0.00091 (4)
F1	0.132 (3)	0.0230 (12)	0.136 (3)	0.0046 (15)	0.090 (3)	0.0171 (15)
F2	0.178 (5)	0.087 (3)	0.0443 (18)	-0.059 (3)	0.028 (2)	0.0180 (17)
F3	0.0590 (19)	0.091 (3)	0.163 (4)	-0.0207 (17)	0.055 (2)	0.035 (2)
F4	0.150 (3)	0.0444 (14)	0.136 (3)	-0.0039 (16)	0.102 (2)	-0.0340 (15)
F5	0.0657 (18)	0.129 (3)	0.190 (4)	0.0072 (18)	0.072 (2)	-0.053 (3)
F6	0.275 (5)	0.100 (2)	0.075 (2)	0.098 (3)	0.113 (3)	0.0291 (17)
F7	0.0414 (11)	0.116 (2)	0.0451 (12)	0.0358 (12)	0.0084 (9)	0.0119 (13)
F8	0.0427 (11)	0.0933 (18)	0.0421 (11)	0.0175 (11)	0.0007 (9)	0.0248 (11)
F9	0.0499 (14)	0.0495 (14)	0.201 (4)	-0.0106 (12)	-0.0590 (18)	-0.0014 (19)

F10	0.0486 (11)	0.0937 (18)	0.0387 (11)	0.0116 (11)	0.0206 (9)	0.0265 (11)
F11	0.0342 (10)	0.170 (3)	0.0331 (11)	-0.0259 (14)	0.0108 (9)	0.0051 (14)
F12	0.0964 (19)	0.0737 (17)	0.0732 (17)	0.0214 (15)	0.0539 (15)	-0.0077 (13)
F13	0.0321 (11)	0.111 (2)	0.0860 (18)	-0.0275 (12)	0.0106 (11)	-0.0224 (16)
F14	0.0715 (14)	0.0589 (13)	0.0560 (13)	-0.0008 (11)	0.0460 (11)	0.0073 (10)
F15	0.105 (2)	0.0318 (12)	0.240 (4)	-0.0210 (13)	0.124 (3)	-0.0070 (18)
F16	0.0602 (14)	0.0815 (17)	0.0562 (14)	0.0419 (13)	-0.0258 (11)	-0.0194 (12)
F17	0.0454 (10)	0.0546 (12)	0.0376 (10)	0.0164 (9)	0.0144 (8)	-0.0042 (9)
F18	0.0924 (18)	0.0302 (11)	0.137 (2)	0.0217 (11)	0.0719 (18)	0.0301 (13)
O1	0.0530 (14)	0.0567 (15)	0.0233 (11)	0.0036 (11)	-0.0120 (10)	0.0002 (10)
O2	0.0310 (11)	0.0503 (14)	0.0453 (13)	0.0026 (9)	-0.0120 (10)	0.0014 (10)
O3	0.0298 (9)	0.0231 (9)	0.0303 (10)	-0.0020 (7)	0.0111 (8)	0.0008 (8)
O4	0.0301 (9)	0.0258 (10)	0.0250 (9)	0.0041 (7)	0.0094 (7)	0.0013 (7)
O5	0.0214 (8)	0.0381 (11)	0.0214 (9)	-0.0019 (7)	0.0025 (7)	0.0011 (8)
O6	0.0260 (9)	0.0268 (9)	0.0192 (9)	0.0008 (7)	0.0049 (7)	-0.0012 (7)
O7	0.0254 (9)	0.0241 (9)	0.0285 (10)	-0.0029 (7)	0.0097 (7)	0.0002 (7)
O8	0.0262 (9)	0.0235 (9)	0.0316 (10)	0.0017 (7)	0.0090 (8)	0.0036 (8)
N1	0.0255 (10)	0.0223 (10)	0.0194 (10)	0.0007 (8)	0.0046 (8)	0.0013 (8)
N2	0.0225 (10)	0.0308 (12)	0.0203 (10)	-0.0028 (9)	0.0042 (8)	0.0004 (9)
C1	0.0298 (13)	0.0304 (14)	0.0234 (13)	0.0010 (11)	0.0072 (11)	0.0026 (10)
C2	0.0442 (16)	0.0356 (16)	0.0233 (13)	0.0032 (13)	0.0122 (12)	0.0005 (11)
C3	0.0497 (18)	0.0324 (15)	0.0185 (13)	0.0013 (13)	0.0038 (12)	0.0010 (11)
C4	0.0353 (14)	0.0220 (13)	0.0225 (13)	0.0018 (10)	-0.0002 (11)	-0.0004 (10)
C5	0.0401 (16)	0.0295 (15)	0.0267 (14)	0.0020 (12)	-0.0056 (12)	-0.0022 (11)
C6	0.0339 (15)	0.0281 (14)	0.0339 (15)	0.0015 (11)	-0.0060 (12)	-0.0015 (12)
C7	0.0257 (13)	0.0249 (13)	0.0306 (14)	-0.0005 (10)	-0.0009 (11)	-0.0001 (11)
C8	0.0199 (12)	0.0450 (18)	0.0395 (17)	-0.0009 (11)	-0.0003 (11)	0.0010 (13)
C9	0.0239 (13)	0.060 (2)	0.0341 (16)	-0.0031 (13)	0.0079 (12)	0.0035 (14)
C10	0.0253 (13)	0.0518 (18)	0.0235 (14)	-0.0044 (12)	0.0049 (11)	0.0019 (12)
C11	0.0240 (12)	0.0201 (12)	0.0221 (12)	-0.0004 (9)	0.0022 (9)	-0.0002 (9)
C12	0.0272 (12)	0.0180 (11)	0.0193 (12)	-0.0002 (9)	0.0024 (9)	-0.0003 (9)
C13	0.067 (2)	0.0290 (17)	0.062 (2)	-0.0079 (16)	0.032 (2)	0.0004 (16)
C14	0.0279 (13)	0.0251 (14)	0.0314 (14)	-0.0026 (10)	0.0042 (11)	0.0021 (11)
C15	0.0408 (16)	0.0223 (14)	0.0419 (17)	0.0050 (12)	0.0124 (13)	0.0015 (12)
C16	0.0305 (13)	0.0280 (14)	0.0266 (13)	0.0062 (11)	0.0058 (11)	-0.0007 (11)
C17	0.073 (3)	0.0374 (18)	0.055 (2)	0.0175 (18)	0.037 (2)	0.0027 (16)
C18	0.0281 (14)	0.0482 (19)	0.0309 (15)	-0.0004 (13)	-0.0004 (12)	0.0030 (13)
C19	0.0229 (12)	0.0301 (13)	0.0249 (13)	-0.0013 (10)	0.0004 (10)	-0.0009 (10)
C20	0.0288 (13)	0.0468 (17)	0.0194 (13)	0.0009 (12)	0.0028 (10)	0.0029 (12)
C21	0.0280 (13)	0.0317 (14)	0.0195 (12)	-0.0020 (11)	0.0060 (10)	-0.0021 (10)

C22	0.0321 (15)	0.060 (2)	0.0229 (14)	0.0042 (14)	0.0080 (12)	0.0020 (13)
C23	0.0450 (18)	0.0332 (16)	0.065 (2)	-0.0135 (14)	0.0313 (17)	-0.0080 (16)
C24	0.0291 (13)	0.0292 (14)	0.0210 (12)	-0.0079 (11)	0.0074 (10)	-0.0033 (10)
C25	0.0397 (15)	0.0211 (13)	0.0271 (13)	-0.0042 (11)	0.0108 (11)	-0.0007 (10)
C26	0.0316 (13)	0.0256 (13)	0.0176 (12)	0.0026 (10)	0.0031 (10)	0.0013 (9)
C27	0.0405 (16)	0.0298 (15)	0.0317 (15)	0.0084 (12)	0.0092 (12)	0.0044 (12)
O1S	0.087 (2)	0.0338 (14)	0.079 (2)	-0.0018 (13)	-0.0339 (17)	0.0009 (13)
C1S	0.085 (3)	0.038 (2)	0.078 (3)	-0.007 (2)	-0.024 (2)	0.006 (2)
C2S	0.058 (2)	0.0379 (19)	0.073 (3)	-0.0029 (17)	0.000 (2)	0.0039 (18)
C3S	0.084 (6)	0.056 (5)	0.045 (5)	-0.026 (5)	0.025 (5)	-0.018 (4)
C4S	0.066 (6)	0.063 (6)	0.065 (6)	-0.004 (5)	-0.015 (5)	-0.012 (4)
C5S	0.043 (4)	0.053 (5)	0.052 (5)	-0.005 (4)	0.002 (4)	-0.008 (4)
C6S	0.065 (5)	0.099 (8)	0.048 (5)	-0.011 (5)	0.003 (4)	-0.007 (5)

Geometric parameters (Å, º)

Yb1—O3	2.2884 (18)	C7—C8	1.381 (4)
Yb1—O4	2.3118 (18)	C7—C11	1.395 (4)
Yb1—O5	2.2894 (18)	C8—H8	0.9500
Yb1—O6	2.2952 (17)	C8—C9	1.374 (4)
Yb1—O7	2.2811 (17)	C9—H9	0.9500
Yb1—O8	2.2725 (18)	C9—C10	1.383 (4)
Yb1—N1	2.492 (2)	C10—H10	0.9500
Yb1—N2	2.492 (2)	C11—C12	1.479 (4)
F1—C13	1.312 (4)	C13—C14	1.502 (4)
F2—C13	1.292 (5)	C13—F1A	1.512 (18)
F3—C13	1.336 (5)	C13—F3A	1.21 (2)
F4—C17	1.294 (4)	C13—F2A	1.22 (2)
F5—C17	1.310 (5)	C14—C15	1.382 (4)
F6—C17	1.291 (4)	C15—H15	0.9500
F7—C18	1.315 (4)	C15—C16	1.386 (4)
F8—C18	1.336 (3)	C16—C17	1.530 (4)
F9—C18	1.293 (4)	C18—C19	1.538 (4)
F10—C22	1.323 (3)	C19—C20	1.385 (4)
F11—C22	1.314 (4)	C20—H20	0.9500
F12—C22	1.318 (4)	C20—C21	1.396 (4)
F13—C23	1.335 (4)	C21—C22	1.535 (4)
F14—C23	1.333 (4)	C23—C24	1.526 (4)
F15—C23	1.313 (4)	C24—C25	1.385 (4)

F16—C27	1.321 (3)	C25—H25	0.9500
F17—C27	1.315 (3)	C25—C26	1.385 (4)
F18—C27	1.319 (3)	C26—C27	1.537 (4)
O1—C5	1.212 (4)	O1S—C2S	1.408 (4)
O2—C6	1.209 (4)	O1S—C3S	1.464 (8)
O3—C14	1.256 (3)	O1S—C5S	1.513 (8)
O4—C16	1.251 (3)	C1S—H1SA	0.9800
O5—C19	1.251 (3)	C1S—H1SB	0.9800
O6—C21	1.246 (3)	C1S—H1SC	0.9800
O7—C24	1.256 (3)	C1S—C2S	1.471 (5)
O8—C26	1.242 (3)	C2S—H2SA	0.9900
N1—C1	1.338 (3)	C2S—H2SB	0.9900
N1—C12	1.351 (3)	C3S—H3SA	0.9900
N2—C10	1.338 (3)	C3S—H3SB	0.9900
N2—C11	1.344 (3)	C3S—C4S	1.485 (11)
C1—H1	0.9500	C4S—H4SA	0.9800
C1—C2	1.385 (4)	C4S—H4SB	0.9800
C2—H2	0.9500	C4S—H4SC	0.9800
C2—C3	1.379 (4)	C5S—H5SA	0.9900
C3—H3	0.9500	C5S—H5SB	0.9900
C3—C4	1.387 (4)	C5S—C6S	1.477 (10)
C4—C5	1.486 (4)	C6S—H6SA	0.9800
C4—C12	1.399 (4)	C6S—H6SB	0.9800
C5—C6	1.538 (5)	C6S—H6SC	0.9800
C6—C7	1.485 (4)		
O3—Yb1—O4	72.87 (6)	C14—C15—C16	120.5 (3)
O3—Yb1—O5	83.46 (7)	C16—C15—H15	119.7
O3—Yb1—O6	71.44 (6)	O4—C16—C15	127.9 (3)
O3—Yb1—N1	109.76 (7)	O4—C16—C17	114.8 (3)
O3—Yb1—N2	74.65 (7)	C15—C16—C17	117.4 (3)
O4—Yb1—N1	71.28 (7)	F4—C17—F5	105.8 (3)
O4—Yb1—N2	110.84 (7)	F4—C17—C16	114.7 (3)
O5—Yb1—O4	79.44 (7)	F5—C17—C16	110.5 (3)
O5—Yb1—O6	74.51 (6)	F6—C17—F4	110.3 (4)
O5—Yb1—N1	141.79 (7)	F6—C17—F5	103.1 (4)
O5—Yb1—N2	151.13 (7)	F6—C17—C16	111.6 (3)
O6—Yb1—O4	137.61 (6)	F7—C18—F8	104.0 (3)
O6—Yb1—N1	143.35 (7)	F7—C18—C19	112.3 (2)
O6—Yb1—N2	80.73 (7)	F8—C18—C19	112.5 (2)

O7—Yb1—O3	149.08 (6)	F9—C18—F7	109.7 (3)
O7—Yb1—O4	81.70 (7)	F9—C18—F8	107.1 (3)
O7—Yb1—O5	74.70 (7)	F9—C18—C19	110.9 (3)
O7—Yb1—O6	121.45 (6)	O5—C19—C18	114.7 (2)
O7—Yb1—N1	77.21 (7)	O5—C19—C20	128.4 (3)
O7—Yb1—N2	132.29 (7)	C20—C19—C18	116.9 (2)
O8—Yb1—O3	135.85 (6)	C19—C20—H20	119.8
O8—Yb1—O4	147.45 (6)	C19—C20—C21	120.3 (3)
O8—Yb1—O5	113.63 (7)	C21—C20—H20	119.8
O8—Yb1—O6	74.64 (7)	O6—C21—C20	127.7 (2)
O8—Yb1—O7	74.06 (6)	O6—C21—C22	115.5 (2)
O8—Yb1—N1	82.27 (7)	C20—C21—C22	116.9 (2)
O8—Yb1—N2	72.72 (7)	F10—C22—C21	112.4 (2)
N2—Yb1—N1	65.25 (7)	F11—C22—F10	107.5 (3)
C14—O3—Yb1	136.90 (17)	F11—C22—F12	107.8 (3)
C16—O4—Yb1	134.91 (17)	F11—C22—C21	111.2 (2)
C19—O5—Yb1	132.05 (17)	F12—C22—F10	106.6 (3)
C21—O6—Yb1	131.11 (17)	F12—C22—C21	111.1 (3)
C24—O7—Yb1	134.05 (17)	F13—C23—C24	110.7 (3)
C26—O8—Yb1	135.50 (17)	F14—C23—F13	105.2 (3)
C1—N1—Yb1	121.92 (18)	F14—C23—C24	110.7 (3)
C1—N1—C12	117.6 (2)	F15—C23—F13	108.8 (3)
C12—N1—Yb1	120.46 (16)	F15—C23—F14	107.3 (3)
C10—N2—Yb1	121.55 (18)	F15—C23—C24	113.7 (3)
C10—N2—C11	117.6 (2)	O7—C24—C23	113.7 (2)
C11—N2—Yb1	120.67 (16)	O7—C24—C25	128.1 (2)
N1—C1—H1	118.1	C25—C24—C23	118.2 (2)
N1—C1—C2	123.8 (3)	C24—C25—H25	120.0
C2—C1—H1	118.1	C26—C25—C24	120.0 (2)
C1—C2—H2	120.8	C26—C25—H25	120.0
C3—C2—C1	118.3 (3)	O8—C26—C25	127.5 (2)
C3—C2—H2	120.8	O8—C26—C27	113.6 (2)
C2—C3—H3	120.3	C25—C26—C27	118.8 (2)
C2—C3—C4	119.3 (3)	F16—C27—C26	110.6 (2)
C4—C3—H3	120.3	F17—C27—F16	106.4 (3)
C3—C4—C5	120.6 (3)	F17—C27—F18	106.5 (3)
C3—C4—C12	118.8 (3)	F17—C27—C26	111.0 (2)
C12—C4—C5	120.6 (3)	F18—C27—F16	108.5 (3)
O1—C5—C4	121.8 (3)	F18—C27—C26	113.5 (2)
O1—C5—C6	120.1 (3)	C2S—O1S—C3S	111.4 (4)

C4—C5—C6	118.0 (2)	C2S—O1S—C5S	108.3 (4)
O2—C6—C5	119.7 (3)	H1SA—C1S—H1SB	109.5
O2—C6—C7	122.5 (3)	H1SA—C1S—H1SC	109.5
C7—C6—C5	117.8 (2)	H1SB—C1S—H1SC	109.5
C8—C7—C6	120.1 (3)	C2S—C1S—H1SA	109.5
C8—C7—C11	119.0 (3)	C2S—C1S—H1SB	109.5
C11—C7—C6	120.9 (3)	C2S—C1S—H1SC	109.5
C7—C8—H8	120.5	O1S—C2S—C1S	110.4 (3)
C9—C8—C7	119.1 (3)	O1S—C2S—H2SA	109.6
C9—C8—H8	120.5	O1S—C2S—H2SB	109.6
C8—C9—H9	120.7	C1S—C2S—H2SA	109.6
C8—C9—C10	118.5 (3)	C1S—C2S—H2SB	109.6
C10—C9—H9	120.7	H2SA—C2S—H2SB	108.1
N2—C10—C9	123.6 (3)	O1S—C3S—H3SA	110.6
N2—C10—H10	118.2	O1S—C3S—H3SB	110.6
C9—C10—H10	118.2	O1S—C3S—C4S	105.7 (7)
N2—C11—C7	122.2 (2)	H3SA—C3S—H3SB	108.7
N2—C11—C12	116.5 (2)	C4S—C3S—H3SA	110.6
C7—C11—C12	121.2 (2)	C4S—C3S—H3SB	110.6
N1—C12—C4	122.1 (2)	C3S—C4S—H4SA	109.5
N1—C12—C11	116.7 (2)	C3S—C4S—H4SB	109.5
C4—C12—C11	121.2 (2)	C3S—C4S—H4SC	109.5
F1—C13—F3	103.7 (3)	H4SA—C4S—H4SB	109.5
F1—C13—C14	114.7 (3)	H4SA—C4S—H4SC	109.5
F2—C13—F1	109.1 (4)	H4SB—C4S—H4SC	109.5
F2—C13—F3	105.6 (4)	O1S—C5S—H5SA	110.6
F2—C13—C14	112.4 (3)	O1S—C5S—H5SB	110.6
F3—C13—C14	110.7 (3)	H5SA—C5S—H5SB	108.7
C14—C13—F1A	106.6 (8)	C6S—C5S—O1S	105.9 (7)
F3A—C13—C14	118.1 (14)	C6S—C5S—H5SA	110.6
F3A—C13—F1A	99.0 (13)	C6S—C5S—H5SB	110.6
F3A—C13—F2A	115.3 (16)	C5S—C6S—H6SA	109.5
F2A—C13—C14	114.5 (13)	C5S—C6S—H6SB	109.5
F2A—C13—F1A	99.6 (12)	C5S—C6S—H6SC	109.5
O3—C14—C13	113.9 (2)	H6SA—C6S—H6SB	109.5
O3—C14—C15	126.5 (3)	H6SA—C6S—H6SC	109.5
C15—C14—C13	119.6 (3)	H6SB—C6S—H6SC	109.5
C14—C15—H15	119.7		

8.3.4 Crystallographic data for 1(ii)-Yb

Crystal data

$C_{27}H_9F_{18}N_2O_8Yb \cdot C_7H_8$	D_x = 1.837 Mg m^{-3}
M_r = 1096.54	Mo $K\alpha$ radiation, λ = 0.71073 Å
Orthorhombic, $P2_12_12_1$	Cell parameters from 9977 reflections
a = 9.5091 (7) Å	θ = 2.3–28.3°
b = 19.5821 (13) Å	μ = 2.50 mm^{-1}
c = 21.2876 (13) Å	T = 150 K
V = 3963.9 (5) Å^3	Block, green
Z = 4	0.16 × 0.05 × 0.01 mm
F(000) = 2124	

Data collection

Bruker D8 VENTURE diffractometer	9813 independent reflections
Radiation source: microfocus sealed tube, INCOATEC Iμs 3.0	8934 reflections with $I > 2\sigma(I)$
Multilayer mirror optics monochromator	R_{int} = 0.053
Detector resolution: 7.4074 pixels mm^{-1}	θ_{max} = 28.3°, θ_{min} = 2.3°
ϕ and ω scans	h = -12→12
Absorption correction: multi-scan *SADABS2016*/2 (Bruker,2016/2) was used for absorption correction. wR2(int) was 0.1423 before and 0.0981 after correction. The Ratio of minimum to maximum transmission is 0.7980. The λ/2 correction factor is Not present.	k = -26→17
T_{min} = 0.595, T_{max} = 0.746	l = -28→27
29748 measured reflections	

Refinement

Refinement on F^2	Hydrogen site location: inferred from neighbouring sites
Least-squares matrix: full	H-atom parameters constrained
$R[F^2 > 2\sigma(F^2)]$ = 0.038	$w = 1/[\sigma^2(F_o^2) + (0.0419P)^2 + 1.1599P]$ where $P = (F_o^2 + 2F_c^2)/3$
$wR(F^2)$ = 0.092	$(\Delta/\sigma)_{max}$ = 0.001
S = 1.03	$\Delta\rangle_{max}$ = 0.84 e Å^{-3}

9813 reflections	$\Delta\rangle_{min}$ = -0.71 e Å^{-3}
563 parameters	Absolute structure: Refined as an inversion twin.
744 restraints	Absolute structure parameter: 0.021 (12)

Special details

Geometry. All esds (except the esd in the dihedral angle between two l.s. planes) are estimated using the full covariance matrix. The cell esds are taken into account individually in the estimation of esds in distances, angles and torsion angles; correlations between esds in cell parameters are only used when they are defined by crystal symmetry. An approximate (isotropic) treatment of cell esds is used for estimating esds involving l.s. planes.
Refinement. Refined as a 2-component inversion twin.

Fractional atomic coordinates and isotropic or equivalent isotropic displacement parameters (Å²)

	x	*y*	*z*	U_{iso}*/U_{eq}	Occ. (<1)
Yb1	0.20067 (3)	0.46041 (2)	0.31255 (2)	0.02685 (8)	
F1	0.3229 (7)	0.6393 (3)	0.1120 (3)	0.0802 (18)	
F2	0.3910 (16)	0.6700 (7)	0.2027 (6)	0.058 (3)*	0.4
F3	0.4836 (16)	0.5851 (7)	0.1618 (6)	0.060 (3)*	0.4
F4	-0.1991 (6)	0.6132 (3)	0.2538 (3)	0.0685 (14)	
F5	-0.2264 (5)	0.5214 (3)	0.2001 (3)	0.0686 (15)	
F6	-0.1588 (6)	0.6130 (4)	0.1541 (3)	0.092 (2)	
F7	0.5324 (15)	0.3126 (7)	0.2133 (6)	0.072 (3)*	0.5
F8	0.3967 (7)	0.2287 (3)	0.1843 (4)	0.091 (2)	
F9	0.4205 (15)	0.3182 (6)	0.1332 (5)	0.069 (3)*	0.5
F10	-0.0942 (10)	0.2523 (4)	0.3271 (3)	0.114 (3)	
F11	-0.0858 (7)	0.2236 (3)	0.2307 (3)	0.0825 (19)	
F12	-0.1971 (8)	0.3119 (3)	0.2586 (5)	0.120 (3)	
F13	0.3297 (15)	0.2316 (6)	0.3850 (5)	0.082 (4)*	0.6
F14	0.4496 (14)	0.2924 (7)	0.4461 (7)	0.097 (4)*	0.6
F15	0.2884 (16)	0.2461 (6)	0.4878 (5)	0.100 (4)*	0.6
F16	-0.0841 (6)	0.3910 (3)	0.5365 (2)	0.0680 (15)	
F17	-0.1050 (7)	0.4893 (3)	0.4930 (3)	0.0829 (19)	
F18	-0.2107 (6)	0.4026 (3)	0.4555 (2)	0.0705 (15)	
O1	0.7715 (6)	0.6444 (3)	0.4291 (3)	0.0574 (16)	
O2	0.5527 (6)	0.7156 (3)	0.4778 (3)	0.0564 (15)	
O3	0.2973 (6)	0.5314 (3)	0.2402 (2)	0.0410 (11)	
O4	0.0195 (5)	0.5196 (2)	0.2695 (2)	0.0341 (10)	

O5	0.3099 (6)	0.3894 (2)	0.2425 (2)	0.0389 (10)	
O6	0.0374 (5)	0.3789 (2)	0.2854 (2)	0.0372 (11)	
O7	0.2794 (6)	0.3701 (2)	0.3715 (2)	0.0393 (11)	
O8	0.0522 (5)	0.4529 (2)	0.3969 (2)	0.0333 (10)	
N1	0.4457 (6)	0.4849 (3)	0.3431 (3)	0.0308 (11)	
N2	0.2325 (6)	0.5669 (3)	0.3747 (3)	0.0292 (11)	
C1	0.5516 (7)	0.4437 (4)	0.3247 (3)	0.0396 (16)	
H1	0.528531	0.401494	0.305280	0.047*	
C2	0.6933 (7)	0.4599 (4)	0.3327 (3)	0.0419 (14)	
H2	0.765402	0.430463	0.317922	0.050*	
C3	0.7245 (7)	0.5200 (4)	0.3627 (4)	0.0412 (16)	
H3	0.819925	0.532728	0.368853	0.049*	
C4	0.6185 (7)	0.5621 (3)	0.3839 (3)	0.0303 (13)	
C5	0.6518 (8)	0.6250 (4)	0.4193 (3)	0.0381 (15)	
C6	0.5281 (8)	0.6674 (3)	0.4450 (4)	0.0384 (15)	
C7	0.3856 (8)	0.6470 (3)	0.4274 (3)	0.0331 (14)	
C8	0.2693 (8)	0.6850 (4)	0.4449 (4)	0.0423 (17)	
H8	0.281280	0.725545	0.468862	0.051*	
C9	0.1362 (8)	0.6643 (4)	0.4278 (4)	0.0435 (18)	
H9	0.055762	0.689577	0.440455	0.052*	
C10	0.1224 (7)	0.6058 (3)	0.3919 (3)	0.0334 (14)	
H10	0.030962	0.592594	0.378651	0.040*	
C11	0.4796 (6)	0.5434 (3)	0.3723 (3)	0.0270 (11)	
C12	0.3619 (7)	0.5869 (3)	0.3914 (3)	0.0269 (12)	
C13	0.3650 (10)	0.6057 (5)	0.1613 (4)	0.063 (2)	
C14	0.2510 (8)	0.5703 (4)	0.1987 (3)	0.0373 (15)	
C15	0.1125 (8)	0.5819 (4)	0.1842 (4)	0.0434 (16)	
H15	0.089757	0.607932	0.147961	0.052*	
C16	0.0064 (8)	0.5567 (3)	0.2209 (3)	0.0356 (14)	
C17	-0.1465 (9)	0.5759 (4)	0.2071 (4)	0.0506 (19)	
C18	0.4141 (11)	0.2932 (5)	0.1945 (5)	0.080 (3)	
C19	0.2885 (10)	0.3282 (4)	0.2267 (4)	0.0437 (16)	
C20	0.1664 (9)	0.2909 (4)	0.2352 (4)	0.051 (2)	
H20	0.164092	0.244333	0.222558	0.062*	
C21	0.0476 (8)	0.3197 (4)	0.2616 (4)	0.0411 (16)	
C22	-0.0834 (10)	0.2769 (4)	0.2687 (4)	0.056 (2)	
C23	0.3152 (13)	0.2726 (5)	0.4320 (4)	0.077 (3)	
C24	0.2307 (9)	0.3366 (4)	0.4160 (4)	0.0425 (18)	
C25	0.1122 (10)	0.3506 (4)	0.4503 (4)	0.0471 (18)	
H25	0.083643	0.319773	0.482292	0.056*	

C26	0.0336 (8)	0.4084 (4)	0.4392 (3)	0.0360 (14)	
C27	-0.0917 (9)	0.4231 (4)	0.4822 (4)	0.0526 (19)	
F2A	0.4462 (13)	0.6398 (6)	0.1953 (6)	0.086 (3)*	0.6
F3A	0.4552 (10)	0.5555 (5)	0.1370 (4)	0.061 (2)*	0.6
F7A	0.5161 (13)	0.2885 (6)	0.2408 (5)	0.060 (3)*	0.5
F8A	0.477 (2)	0.3310 (9)	0.1552 (9)	0.112 (6)*	0.5
F13A	0.388 (2)	0.2478 (9)	0.3864 (7)	0.074 (5)*	0.4
F14A	0.397 (2)	0.2833 (9)	0.4804 (8)	0.090 (5)*	0.4
F15A	0.2265 (14)	0.2217 (6)	0.4560 (6)	0.059 (3)*	0.4
C1S	0.5327 (12)	0.5770 (6)	0.5793 (4)	0.074 (3)	
C2S	0.5575 (13)	0.5184 (6)	0.5464 (5)	0.080 (3)	
H2S	0.651876	0.504614	0.539059	0.097*	
C3S	0.4508 (16)	0.4791 (6)	0.5236 (5)	0.098 (4)	
H3S	0.471847	0.438252	0.501549	0.117*	
C4S	0.3147 (17)	0.4979 (7)	0.5322 (6)	0.112 (4)	
H4S	0.239830	0.470719	0.516468	0.134*	
C5S	0.2891 (13)	0.5563 (7)	0.5639 (6)	0.097 (4)	
H5S	0.194368	0.570410	0.569763	0.117*	
C6S	0.3946 (13)	0.5960 (6)	0.5879 (5)	0.090 (3)	
H6S	0.372651	0.636532	0.610435	0.108*	
C7S	0.653 (2)	0.6183 (10)	0.6056 (8)	0.157 (8)	
H7SA	0.628668	0.666939	0.603805	0.236*	
H7SB	0.737474	0.609886	0.580675	0.236*	
H7SC	0.669431	0.604949	0.649284	0.236*	

Atomic displacement parameters (Å²)

	U^{11}	U^{22}	U^{33}	U^{12}	U^{13}	U^{23}
Yb1	0.01923 (11)	0.02662 (12)	0.03471 (12)	0.00024 (11)	-0.00118 (11)	0.00056 (12)
F1	0.074 (4)	0.095 (4)	0.072 (3)	0.001 (4)	0.017 (3)	0.040 (3)
F4	0.048 (3)	0.062 (3)	0.095 (3)	0.027 (3)	0.009 (3)	0.013 (3)
F5	0.039 (3)	0.081 (4)	0.086 (4)	-0.006 (2)	-0.020 (2)	0.006 (3)
F6	0.059 (4)	0.126 (5)	0.092 (4)	0.021 (4)	-0.011 (3)	0.058 (4)
F8	0.072 (4)	0.074 (4)	0.126 (5)	0.009 (3)	0.011 (5)	-0.051 (4)
F10	0.143 (7)	0.107 (5)	0.091 (4)	-0.072 (5)	0.028 (5)	-0.016 (4)
F11	0.077 (4)	0.062 (3)	0.108 (5)	-0.024 (3)	-0.001 (4)	-0.034 (3)
F12	0.037 (3)	0.068 (4)	0.256 (10)	-0.012 (3)	-0.009 (5)	-0.033 (5)
F16	0.058 (3)	0.104 (4)	0.042 (2)	-0.009 (3)	0.007 (2)	0.015 (3)
F17	0.088 (4)	0.064 (3)	0.097 (4)	0.000 (3)	0.055 (4)	-0.010 (3)

F18	0.035 (3)	0.111 (4)	0.065 (3)	-0.009 (3)	-0.001 (2)	0.020 (3)
O1	0.029 (3)	0.051 (3)	0.092 (4)	-0.010 (2)	-0.014 (3)	-0.010 (3)
O2	0.044 (3)	0.047 (3)	0.077 (4)	-0.008 (3)	-0.013 (3)	-0.022 (3)
O3	0.028 (2)	0.054 (3)	0.041 (2)	-0.003 (3)	0.005 (2)	0.010 (2)
O4	0.023 (2)	0.036 (3)	0.043 (2)	0.0029 (19)	-0.0025 (19)	0.0054 (19)
O5	0.032 (3)	0.040 (2)	0.045 (2)	0.004 (2)	-0.001 (2)	-0.009 (2)
O6	0.028 (2)	0.031 (2)	0.053 (3)	-0.004 (2)	-0.006 (2)	-0.005 (2)
O7	0.035 (3)	0.034 (2)	0.049 (2)	0.010 (2)	-0.003 (2)	0.006 (2)
O8	0.026 (2)	0.032 (2)	0.042 (2)	0.000 (2)	0.0026 (17)	0.001 (2)
N1	0.021 (3)	0.035 (3)	0.036 (3)	0.003 (2)	0.000 (2)	-0.005 (2)
N2	0.022 (3)	0.029 (3)	0.037 (3)	-0.003 (2)	0.000 (2)	-0.001 (2)
C1	0.025 (3)	0.041 (4)	0.053 (4)	0.007 (3)	-0.003 (3)	-0.009 (3)
C2	0.024 (3)	0.047 (4)	0.055 (3)	0.010 (4)	0.003 (3)	-0.007 (3)
C3	0.020 (3)	0.049 (4)	0.054 (4)	0.001 (3)	-0.002 (3)	0.003 (3)
C4	0.020 (3)	0.036 (3)	0.035 (3)	-0.003 (2)	-0.004 (2)	0.002 (2)
C5	0.026 (3)	0.035 (3)	0.053 (4)	-0.004 (3)	-0.007 (3)	0.004 (3)
C6	0.029 (3)	0.032 (3)	0.054 (4)	-0.010 (3)	-0.002 (3)	-0.004 (3)
C7	0.028 (3)	0.024 (3)	0.047 (4)	-0.002 (3)	-0.001 (3)	0.000 (3)
C8	0.037 (4)	0.032 (3)	0.058 (4)	0.000 (3)	0.004 (3)	-0.011 (3)
C9	0.026 (3)	0.037 (4)	0.067 (5)	0.007 (3)	0.004 (3)	-0.011 (4)
C10	0.020 (3)	0.031 (3)	0.049 (4)	-0.002 (3)	0.000 (3)	-0.003 (3)
C11	0.018 (3)	0.030 (3)	0.033 (3)	0.000 (2)	0.001 (2)	0.005 (3)
C12	0.023 (3)	0.026 (3)	0.032 (3)	-0.001 (2)	0.002 (2)	0.001 (2)
C13	0.049 (5)	0.076 (7)	0.063 (5)	-0.010 (5)	0.003 (4)	0.019 (5)
C14	0.039 (3)	0.039 (4)	0.034 (3)	-0.002 (3)	0.005 (2)	0.001 (3)
C15	0.045 (4)	0.043 (4)	0.042 (3)	0.004 (3)	-0.002 (3)	0.012 (4)
C16	0.032 (3)	0.035 (4)	0.039 (3)	0.002 (3)	-0.004 (3)	-0.001 (3)
C17	0.036 (4)	0.060 (5)	0.055 (4)	0.011 (3)	-0.003 (3)	0.023 (4)
C18	0.055 (6)	0.070 (6)	0.116 (9)	0.008 (5)	0.011 (6)	-0.048 (7)
C19	0.038 (4)	0.047 (4)	0.046 (4)	0.005 (3)	-0.006 (3)	-0.014 (3)
C20	0.038 (4)	0.042 (4)	0.074 (5)	0.004 (3)	-0.010 (3)	-0.022 (4)
C21	0.036 (4)	0.038 (4)	0.049 (4)	0.001 (3)	-0.007 (3)	-0.003 (3)
C22	0.047 (5)	0.039 (4)	0.082 (5)	-0.010 (3)	0.002 (4)	-0.007 (4)
C23	0.099 (9)	0.066 (6)	0.065 (6)	0.030 (7)	-0.003 (7)	0.015 (5)
C24	0.055 (5)	0.027 (3)	0.046 (4)	0.006 (3)	-0.010 (3)	0.005 (3)
C25	0.052 (5)	0.042 (4)	0.048 (4)	0.001 (4)	0.003 (3)	0.008 (3)
C26	0.035 (4)	0.036 (3)	0.037 (3)	-0.006 (3)	-0.002 (3)	-0.001 (3)
C27	0.048 (5)	0.061 (5)	0.049 (4)	-0.009 (4)	0.010 (3)	0.005 (4)
C1S	0.079 (7)	0.093 (7)	0.050 (5)	-0.021 (6)	-0.001 (5)	0.003 (5)
C2S	0.080 (7)	0.100 (8)	0.062 (6)	0.008 (6)	0.023 (5)	0.011 (5)

C3S	0.160 (11)	0.079 (8)	0.053 (6)	-0.018 (8)	-0.002 (7)	-0.002 (5)
C4S	0.136 (10)	0.127 (10)	0.073 (7)	-0.048 (10)	-0.041 (8)	0.042 (6)
C5S	0.055 (6)	0.139 (11)	0.099 (8)	-0.006 (7)	0.000 (6)	0.044 (7)
C6S	0.103 (8)	0.096 (9)	0.070 (6)	0.000 (7)	0.022 (6)	-0.003 (6)
C7S	0.160 (16)	0.196 (16)	0.116 (11)	-0.096 (14)	-0.067 (12)	0.047 (11)

Geometric parameters (Å, º)

Yb1—O3	2.270 (5)	C6—C7	1.462 (10)
Yb1—O4	2.269 (4)	C7—C8	1.385 (10)
Yb1—O5	2.288 (5)	C7—C12	1.422 (9)
Yb1—O6	2.301 (5)	C8—H8	0.9500
Yb1—O7	2.294 (5)	C8—C9	1.378 (10)
Yb1—O8	2.289 (4)	C9—H9	0.9500
Yb1—N1	2.466 (5)	C9—C10	1.383 (10)
Yb1—N2	2.487 (5)	C10—H10	0.9500
F1—C13	1.303 (9)	C11—C12	1.464 (9)
F2—C13	1.556 (16)	C13—C14	1.513 (11)
F3—C13	1.197 (17)	C13—F2A	1.251 (12)
F4—C17	1.331 (9)	C13—F3A	1.403 (11)
F5—C17	1.319 (9)	C14—C15	1.372 (11)
F6—C17	1.345 (8)	C15—H15	0.9500
F7—C18	1.253 (17)	C15—C16	1.368 (10)
F8—C18	1.294 (10)	C16—C17	1.530 (11)
F9—C18	1.394 (13)	C18—C19	1.538 (13)
F10—C22	1.337 (10)	C18—F7A	1.385 (13)
F11—C22	1.322 (9)	C18—F8A	1.265 (15)
F12—C22	1.298 (10)	C19—C20	1.384 (12)
F13—C23	1.290 (12)	C20—H20	0.9500
F14—C23	1.369 (14)	C20—C21	1.382 (11)
F15—C23	1.322 (12)	C21—C22	1.509 (11)
F16—C27	1.318 (8)	C23—C24	1.526 (12)
F17—C27	1.323 (9)	C23—F13A	1.290 (14)
F18—C27	1.329 (9)	C23—F14A	1.308 (15)
O1—C5	1.218 (8)	C23—F15A	1.403 (13)
O2—C6	1.196 (9)	C24—C25	1.369 (12)
O3—C14	1.247 (8)	C25—H25	0.9500
O4—C16	1.269 (8)	C25—C26	1.376 (11)
O5—C19	1.261 (9)	C26—C27	1.529 (11)
O6—C21	1.267 (9)	C1S—C2S	1.366 (10)

O7—C24	1.243 (9)	C1S—C6S	1.378 (11)
O8—C26	1.266 (8)	C1S—C7S	1.505 (18)
N1—C1	1.348 (8)	C2S—H2S	0.9500
N1—C11	1.343 (9)	C2S—C3S	1.361 (11)
N2—C10	1.346 (8)	C3S—H3S	0.9500
N2—C12	1.340 (8)	C3S—C4S	1.358 (12)
C1—H1	0.9500	C4S—H4S	0.9500
C1—C2	1.395 (10)	C4S—C5S	1.351 (11)
C2—H2	0.9500	C5S—H5S	0.9500
C2—C3	1.371 (10)	C5S—C6S	1.368 (11)
C3—H3	0.9500	C6S—H6S	0.9500
C3—C4	1.378 (10)	C7S—H7SA	0.9800
C4—C5	1.478 (10)	C7S—H7SB	0.9800
C4—C11	1.393 (8)	C7S—H7SC	0.9800
C5—C6	1.541 (10)		
O3—Yb1—O5	75.28 (17)	C14—C15—H15	119.3
O3—Yb1—O6	121.86 (18)	C16—C15—C14	121.3 (7)
O3—Yb1—O7	135.3 (2)	C16—C15—H15	119.3
O3—Yb1—O8	145.25 (18)	O4—C16—C15	126.8 (7)
O3—Yb1—N1	71.16 (19)	O4—C16—C17	113.0 (6)
O3—Yb1—N2	78.38 (18)	C15—C16—C17	120.1 (6)
O4—Yb1—O3	73.77 (18)	F4—C17—F6	107.3 (7)
O4—Yb1—O5	113.04 (17)	F4—C17—C16	110.4 (7)
O4—Yb1—O6	74.97 (18)	F5—C17—F4	108.1 (7)
O4—Yb1—O7	149.57 (18)	F5—C17—F6	107.0 (7)
O4—Yb1—O8	83.19 (16)	F5—C17—C16	111.7 (6)
O4—Yb1—N1	136.42 (18)	F6—C17—C16	112.1 (7)
O4—Yb1—N2	83.08 (17)	F7—C18—F8	117.7 (11)
O5—Yb1—O6	73.79 (19)	F7—C18—F9	98.8 (12)
O5—Yb1—O7	74.93 (17)	F7—C18—C19	114.8 (9)
O5—Yb1—O8	138.80 (17)	F8—C18—F9	101.1 (9)
O5—Yb1—N1	82.00 (19)	F8—C18—C19	114.3 (9)
O5—Yb1—N2	143.19 (18)	F8—C18—F7A	98.2 (9)
O6—Yb1—N1	146.99 (18)	F9—C18—C19	107.1 (9)
O6—Yb1—N2	142.88 (18)	F7A—C18—C19	104.9 (9)
O7—Yb1—O6	79.78 (18)	F8A—C18—F8	121.3 (12)
O7—Yb1—N1	72.38 (19)	F8A—C18—C19	113.5 (12)
O7—Yb1—N2	108.37 (17)	F8A—C18—F7A	100.4 (13)
O8—Yb1—O6	74.72 (17)	O5—C19—C18	114.6 (8)

O8—Yb1—O7	73.90 (18)	O5—C19—C20	127.1 (8)
O8—Yb1—N1	112.87 (17)	C20—C19—C18	118.3 (7)
O8—Yb1—N2	73.23 (17)	C19—C20—H20	119.3
N1—Yb1—N2	65.29 (17)	C21—C20—C19	121.4 (7)
C14—O3—Yb1	135.4 (5)	C21—C20—H20	119.3
C16—O4—Yb1	134.1 (4)	O6—C21—C20	126.8 (7)
C19—O5—Yb1	132.7 (6)	O6—C21—C22	113.8 (7)
C21—O6—Yb1	133.0 (5)	C20—C21—C22	119.2 (7)
C24—O7—Yb1	134.7 (5)	F10—C22—C21	110.9 (8)
C26—O8—Yb1	133.5 (4)	F11—C22—F10	106.4 (7)
C1—N1—Yb1	120.9 (4)	F11—C22—C21	113.1 (8)
C11—N1—Yb1	121.0 (4)	F12—C22—F10	106.2 (9)
C11—N1—C1	117.7 (6)	F12—C22—F11	107.5 (8)
C10—N2—Yb1	121.7 (4)	F12—C22—C21	112.2 (7)
C12—N2—Yb1	119.9 (4)	F13—C23—F14	104.3 (11)
C12—N2—C10	118.5 (5)	F13—C23—F15	118.1 (10)
N1—C1—H1	118.3	F13—C23—C24	113.3 (9)
N1—C1—C2	123.4 (7)	F14—C23—C24	107.9 (9)
C2—C1—H1	118.3	F15—C23—F14	95.4 (11)
C1—C2—H2	121.3	F15—C23—C24	115.0 (10)
C3—C2—C1	117.5 (6)	F13A—C23—C24	115.2 (10)
C3—C2—H2	121.3	F13A—C23—F14A	109.5 (15)
C2—C3—H3	119.8	F13A—C23—F15A	109.2 (12)
C2—C3—C4	120.5 (6)	F14A—C23—C24	111.0 (11)
C4—C3—H3	119.8	F14A—C23—F15A	100.5 (12)
C3—C4—C5	120.6 (6)	F15A—C23—C24	110.4 (10)
C3—C4—C11	118.6 (6)	O7—C24—C23	114.0 (8)
C11—C4—C5	120.8 (6)	O7—C24—C25	127.4 (7)
O1—C5—C4	123.2 (7)	C25—C24—C23	118.6 (7)
O1—C5—C6	118.9 (7)	C24—C25—H25	119.3
C4—C5—C6	117.9 (6)	C24—C25—C26	121.3 (7)
O2—C6—C5	118.9 (7)	C26—C25—H25	119.3
O2—C6—C7	123.1 (7)	O8—C26—C25	127.8 (7)
C7—C6—C5	117.9 (6)	O8—C26—C27	113.9 (6)
C8—C7—C6	121.6 (6)	C25—C26—C27	118.4 (7)
C8—C7—C12	117.6 (7)	F16—C27—F17	108.7 (7)
C12—C7—C6	120.8 (6)	F16—C27—F18	106.1 (7)
C7—C8—H8	119.9	F16—C27—C26	113.1 (7)
C9—C8—C7	120.3 (7)	F17—C27—F18	106.8 (8)
C9—C8—H8	119.9	F17—C27—C26	111.3 (7)

C8—C9—H9	120.8	F18—C27—C26	110.6 (6)
C8—C9—C10	118.5 (7)	C2S—C1S—C6S	117.4 (11)
C10—C9—H9	120.8	C2S—C1S—C7S	120.8 (13)
N2—C10—C9	123.1 (6)	C6S—C1S—C7S	121.8 (13)
N2—C10—H10	118.5	C1S—C2S—H2S	119.1
C9—C10—H10	118.5	C3S—C2S—C1S	121.9 (11)
N1—C11—C4	122.3 (6)	C3S—C2S—H2S	119.1
N1—C11—C12	116.2 (5)	C2S—C3S—H3S	119.7
C4—C11—C12	121.5 (6)	C4S—C3S—C2S	120.7 (13)
N2—C12—C7	122.0 (6)	C4S—C3S—H3S	119.7
N2—C12—C11	117.3 (5)	C3S—C4S—H4S	121.0
C7—C12—C11	120.7 (6)	C5S—C4S—C3S	117.9 (14)
F1—C13—F2	95.5 (8)	C5S—C4S—H4S	121.0
F1—C13—C14	115.8 (8)	C4S—C5S—H5S	118.8
F1—C13—F3A	104.2 (8)	C4S—C5S—C6S	122.4 (14)
F3—C13—F1	117.9 (10)	C6S—C5S—H5S	118.8
F3—C13—F2	96.8 (11)	C1S—C6S—H6S	120.1
F3—C13—C14	121.0 (10)	C5S—C6S—C1S	119.7 (11)
C14—C13—F2	100.8 (8)	C5S—C6S—H6S	120.1
F2A—C13—F1	112.8 (10)	C1S—C7S—H7SA	109.5
F2A—C13—C14	112.5 (9)	C1S—C7S—H7SB	109.5
F2A—C13—F3A	102.1 (9)	C1S—C7S—H7SC	109.5
F3A—C13—C14	108.1 (8)	H7SA—C7S—H7SB	109.5
O3—C14—C13	113.5 (7)	H7SA—C7S—H7SC	109.5
O3—C14—C15	126.8 (7)	H7SB—C7S—H7SC	109.5
C15—C14—C13	119.6 (7)		

8.3.5 Crystallographic data for 4-Eu

Crystal data

$C_{19}H_9EuF_{18}N_2O_6$	$F(000)$ = 3280
M_r = 855.24	D_x = 1.961 Mg m^{-3}
Monoclinic, $P2_1/c$	Mo $K\alpha$ radiation, λ = 0.71073 Å
a = 22.4196 (7) Å	Cell parameters from 9919 reflections
b = 14.1520 (4) Å	θ = 53.6–5.6°
c = 18.3091 (7) Å	μ = 2.32 mm^{-1}
β = 94.059 (1)°	T = 150 K
V = 5794.6 (3) Å^3	Block, colourless

Z = 8	0.16 × 0.1 × 0.04 mm

Data collection

Bruker D8 VENTURE diffractometer	14311 independent reflections
Radiation source: microfocus sealed tube, INCOATEC Iμs 3.0	10741 reflections with $I > 2\sigma(I)$
Multilayer mirror optics monochromator	R_{int} = 0.045
Detector resolution: 7.4074 pixels mm^{-1}	θ_{max} = 28.3°, θ_{min} = 2.2°
ϕ and ω scans	h = -29→29
Absorption correction: multi-scan *SADABS2016*/2 (Bruker,2016/2) was used for absorption correction. wR2(int) was 0.1212 before and 0.0545 after correction. The Ratio of minimum to maximum transmission is 0.8652. The λ/2 correction factor is Not present.	k = -16→18
T_{min} = 0.645, T_{max} = 0.746	l = -24→24
43678 measured reflections	

Refinement

Refinement on F^2	Primary atom site location: dual
Least-squares matrix: full	Hydrogen site location: inferred from neighbouring sites
$R[F^2 > 2\sigma(F^2)]$ = 0.045	H-atom parameters constrained
$wR(F^2)$ = 0.113	$w = 1/[\sigma^2(F_o^2) + (0.051P)^2 + 6.9265P]$ where $P = (F_o^2 + 2F_c^2)/3$
S = 1.02	$(\Delta/\sigma)_{max}$ = 0.002
14311 reflections	$\Delta\rangle_{max}$ = 1.39 e Å^{-3}
889 parameters	$\Delta\rangle_{min}$ = -0.72 e Å^{-3}
1309 restraints	

Special details

Geometry. All esds (except the esd in the dihedral angle between two l.s. planes) are estimated using the full covariance matrix. The cell esds are taken into account individually in the estimation of esds in distances, angles and torsion angles; correlations between esds in cell parameters are only used when they are defined by crystal symmetry. An approximate (isotropic) treatment of cell esds is used for estimating esds involving l.s. planes.

Fractional atomic coordinates and isotropic or equivalent isotropic displacement parameters (Å²)

	x	*y*	*z*	U_{iso}*/U_{eq}	Occ. (<1)
Eu1	0.58122 (2)	0.30368 (2)	0.37678 (2)	0.02995 (7)	
F1	0.46036 (17)	0.5627 (4)	0.2584 (3)	0.127 (2)	
F2	0.4045 (3)	0.4472 (5)	0.2460 (4)	0.162 (3)	
F3	0.3837 (2)	0.5513 (5)	0.3163 (4)	0.169 (3)	
F4	0.3895 (3)	0.4090 (4)	0.5498 (3)	0.147 (2)	
F5	0.4680 (3)	0.3575 (5)	0.5991 (3)	0.141 (2)	
F6	0.4133 (3)	0.2683 (3)	0.5383 (3)	0.154 (3)	
F7	0.7211 (2)	0.4820 (4)	0.2509 (3)	0.1155 (18)	
F8	0.7258 (3)	0.5871 (4)	0.3251 (3)	0.132 (2)	
F9	0.79345 (19)	0.4871 (6)	0.3340 (4)	0.182 (3)	
F10	0.78402 (18)	0.3401 (5)	0.5672 (3)	0.143 (2)	
F11	0.7059 (2)	0.2821 (3)	0.6029 (3)	0.1157 (19)	
F12	0.71915 (19)	0.4288 (3)	0.6070 (2)	0.0872 (13)	
F13	0.7802 (2)	0.0609 (4)	0.3240 (5)	0.172 (3)	
F14	0.7582 (2)	0.1746 (5)	0.2557 (3)	0.150 (3)	
F15	0.79646 (17)	0.1955 (4)	0.3593 (3)	0.1146 (19)	
F16	0.6252 (2)	-0.0901 (3)	0.4315 (4)	0.129 (2)	
F17	0.53839 (17)	-0.0323 (3)	0.4128 (3)	0.0998 (15)	
F18	0.5874 (2)	-0.0107 (3)	0.5127 (3)	0.1130 (16)	
O1	0.51566 (14)	0.4265 (2)	0.33624 (19)	0.0406 (8)	
O2	0.51532 (14)	0.3317 (2)	0.46996 (18)	0.0386 (7)	
O3	0.64714 (14)	0.4257 (2)	0.34742 (19)	0.0428 (8)	
O4	0.64399 (14)	0.3352 (2)	0.48266 (18)	0.0417 (8)	
O5	0.67321 (14)	0.2315 (2)	0.34668 (19)	0.0412 (8)	
O6	0.58525 (14)	0.1468 (2)	0.4212 (2)	0.0412 (8)	
N1A	0.57890 (19)	0.2955 (3)	0.2399 (2)	0.0475 (11)	
N2A	0.48390 (18)	0.2187 (3)	0.3326 (2)	0.0449 (10)	
C1	0.4299 (3)	0.5094 (5)	0.2952 (5)	0.089 (2)	
C1A	0.5785 (2)	0.3020 (4)	0.1785 (3)	0.0458 (12)	
C2	0.4653 (2)	0.4512 (3)	0.3541 (3)	0.0455 (12)	
C2A	0.5786 (3)	0.3117 (5)	0.0984 (3)	0.0698 (19)	
H2AA	0.538996	0.332015	0.078471	0.105*	
H2AB	0.588563	0.250801	0.076959	0.105*	
H2AC	0.608478	0.358928	0.086631	0.105*	
C3	0.4381 (2)	0.4298 (4)	0.4176 (3)	0.0479 (13)	
H3	0.399719	0.455163	0.424770	0.058*	
C3A	0.4489 (2)	0.1653 (4)	0.3129 (3)	0.0509 (14)	
C4	0.4656 (2)	0.3725 (3)	0.4705 (3)	0.0395 (10)	
C4A	0.4059 (3)	0.0946 (5)	0.2866 (5)	0.097 (3)	

H4AA	0.380793	0.120197	0.245306	0.146*	
H4AB	0.380782	0.077038	0.326095	0.146*	
H4AC	0.427149	0.038544	0.270555	0.146*	
C5	0.4319 (3)	0.3517 (4)	0.5383 (4)	0.0641 (16)	
C6	0.7369 (3)	0.4951 (5)	0.3199 (4)	0.080 (2)	
C7	0.7002 (2)	0.4403 (4)	0.3717 (3)	0.0483 (12)	
C8	0.7273 (2)	0.4143 (4)	0.4388 (3)	0.0529 (13)	
H8	0.768296	0.429079	0.450001	0.063*	
C9	0.6960 (2)	0.3675 (4)	0.4900 (3)	0.0443 (11)	
C10	0.7269 (2)	0.3543 (5)	0.5677 (3)	0.0621 (15)	
C11	0.7571 (2)	0.1444 (5)	0.3211 (3)	0.0598 (15)	
C12	0.6957 (2)	0.1521 (4)	0.3508 (3)	0.0382 (10)	
C13	0.6709 (2)	0.0713 (4)	0.3798 (3)	0.0452 (12)	
H13	0.691229	0.012652	0.377481	0.054*	
C14	0.6171 (2)	0.0756 (3)	0.4120 (3)	0.0414 (11)	
C15	0.5917 (3)	-0.0157 (4)	0.4416 (4)	0.0670 (17)	
Eu2	0.08421 (2)	0.17924 (2)	0.35393 (2)	0.03285 (7)	
F19	-0.0910 (3)	0.3274 (4)	0.4564 (3)	0.133 (2)	
F20	-0.04089 (18)	0.2911 (3)	0.5539 (3)	0.0907 (14)	
F21	-0.1191 (2)	0.2186 (4)	0.5234 (3)	0.126 (2)	
F25	0.2238 (2)	0.3444 (3)	0.5243 (2)	0.0927 (13)	
F26	0.18607 (16)	0.2615 (3)	0.6058 (2)	0.0774 (11)	
F27	0.27385 (16)	0.2310 (3)	0.5747 (2)	0.0911 (14)	
F28	0.2243 (2)	-0.1013 (3)	0.4796 (2)	0.0854 (12)	
F29	0.21058 (14)	-0.1029 (2)	0.36457 (19)	0.0631 (9)	
F30	0.28826 (14)	-0.0381 (3)	0.4158 (3)	0.0833 (13)	
F31	0.0955 (3)	0.5245 (3)	0.4202 (3)	0.134 (2)	
F32	0.04153 (17)	0.5176 (3)	0.3212 (3)	0.1140 (18)	
F33	0.12791 (16)	0.5748 (2)	0.3221 (2)	0.0777 (11)	
O7	0.01429 (14)	0.2210 (2)	0.4390 (2)	0.0425 (8)	
O8	0.02015 (13)	0.0467 (2)	0.36735 (19)	0.0383 (7)	
O9	0.14245 (14)	0.2206 (3)	0.4620 (2)	0.0449 (8)	
O10	0.14920 (14)	0.0499 (2)	0.38460 (19)	0.0401 (8)	
O11	0.08243 (13)	0.3444 (2)	0.3455 (2)	0.0438 (8)	
O12	0.17770 (13)	0.2307 (2)	0.3133 (2)	0.0402 (8)	
N3A	-0.01196 (18)	0.2292 (3)	0.2790 (2)	0.0443 (10)	
N4A	0.08792 (18)	0.1167 (3)	0.2238 (3)	0.0490 (11)	
C5A	-0.0513 (2)	0.2694 (4)	0.2532 (3)	0.0461 (12)	
C6A	-0.1018 (3)	0.3220 (5)	0.2194 (4)	0.084 (2)	
H6AA	-0.131948	0.330689	0.254991	0.125*	

H6AB	-0.119323	0.286848	0.177005	0.125*	
H6AC	-0.088061	0.383872	0.203329	0.125*	
C7A	0.0850 (2)	0.1016 (4)	0.1631 (3)	0.0508 (13)	
C8A	0.0803 (3)	0.0821 (6)	0.0846 (4)	0.081 (2)	
H8AA	0.113949	0.042300	0.072251	0.121*	
H8AB	0.081288	0.141719	0.057459	0.121*	
H8AC	0.042653	0.049186	0.071359	0.121*	
C16	-0.0722 (2)	0.2560 (4)	0.4976 (4)	0.0628 (16)	
C17	-0.0351 (2)	0.1884 (3)	0.4535 (3)	0.0405 (11)	
C18	-0.0593 (2)	0.1009 (4)	0.4346 (3)	0.0454 (12)	
H18	-0.097596	0.084897	0.449881	0.055*	
C19	-0.0292 (2)	0.0364 (3)	0.3942 (3)	0.0367 (10)	
C20	-0.0590 (2)	-0.0586 (4)	0.3790 (3)	0.0469 (12)	
C21	0.2200 (2)	0.2574 (4)	0.5494 (3)	0.0602 (15)	
C22	0.1916 (2)	0.1911 (4)	0.4898 (3)	0.0466 (12)	
C23	0.2207 (2)	0.1095 (4)	0.4738 (3)	0.0465 (12)	
H23	0.258993	0.097805	0.497584	0.056*	
C24	0.1967 (2)	0.0430 (3)	0.4242 (3)	0.0379 (10)	
C25	0.2303 (2)	-0.0519 (4)	0.4165 (3)	0.0468 (12)	
C26	0.0965 (2)	0.5066 (4)	0.3509 (4)	0.0595 (15)	
C27	0.1205 (2)	0.4076 (3)	0.3390 (3)	0.0400 (11)	
C28	0.1796 (2)	0.3980 (3)	0.3249 (3)	0.0439 (12)	
H28	0.204245	0.452382	0.322866	0.053*	
C29	0.2033 (2)	0.3090 (3)	0.3137 (3)	0.0396 (11)	
C30	0.2699 (3)	0.3045 (4)	0.3009 (4)	0.0645 (16)	
F22	-0.0814 (6)	-0.0928 (6)	0.4390 (4)	0.087 (3)	0.640 (19)
F23	-0.1029 (6)	-0.0516 (6)	0.3309 (7)	0.097 (5)	0.640 (19)
F24	-0.0209 (5)	-0.1221 (6)	0.3623 (10)	0.122 (6)	0.640 (19)
F34	0.2945 (4)	0.2231 (8)	0.3272 (12)	0.124 (9)	0.52 (2)
F35	0.3020 (4)	0.3674 (10)	0.3349 (9)	0.097 (6)	0.52 (2)
F36	0.2815 (5)	0.3069 (19)	0.2346 (6)	0.143 (10)	0.52 (2)
F22A	-0.1128 (7)	-0.0686 (12)	0.3991 (18)	0.114 (10)	0.360 (19)
F23A	-0.0634 (11)	-0.0813 (11)	0.3079 (6)	0.083 (6)	0.360 (19)
F24A	-0.0286 (9)	-0.1299 (10)	0.4038 (12)	0.095 (7)	0.360 (19)
F34A	0.3011 (5)	0.297 (2)	0.3612 (7)	0.150 (12)	0.48 (2)
F35A	0.2876 (8)	0.3824 (9)	0.2650 (16)	0.155 (11)	0.48 (2)
F36A	0.2817 (6)	0.2387 (9)	0.2554 (8)	0.084 (5)	0.48 (2)

Atomic displacement parameters (Å²)

	U^{11}	U^{22}	U^{33}	U^{12}	U^{13}	U^{23}
Eu1	0.02881 (12)	0.03281 (12)	0.02828 (13)	0.00120 (9)	0.00247 (8)	-0.00300 (9)
F1	0.058 (2)	0.141 (4)	0.184 (5)	0.015 (2)	0.020 (3)	0.124 (4)
F2	0.126 (5)	0.182 (6)	0.165 (6)	-0.024 (4)	-0.077 (4)	0.083 (4)
F3	0.103 (4)	0.216 (6)	0.197 (6)	0.111 (4)	0.076 (4)	0.142 (5)
F4	0.167 (5)	0.143 (5)	0.148 (5)	0.082 (4)	0.122 (4)	0.041 (4)
F5	0.137 (4)	0.237 (7)	0.054 (3)	-0.015 (4)	0.041 (3)	0.000 (4)
F6	0.233 (6)	0.077 (3)	0.171 (6)	-0.062 (4)	0.152 (5)	-0.017 (3)
F7	0.099 (3)	0.172 (5)	0.080 (3)	-0.059 (3)	0.038 (3)	-0.024 (3)
F8	0.197 (5)	0.094 (3)	0.103 (4)	-0.066 (3)	-0.003 (4)	0.020 (3)
F9	0.050 (2)	0.281 (8)	0.216 (7)	-0.038 (4)	0.017 (3)	0.141 (6)
F10	0.053 (2)	0.295 (8)	0.076 (3)	0.056 (3)	-0.023 (2)	-0.034 (4)
F11	0.140 (4)	0.103 (3)	0.093 (3)	-0.027 (3)	-0.070 (3)	0.029 (3)
F12	0.114 (3)	0.085 (3)	0.059 (2)	0.015 (2)	-0.016 (2)	-0.031 (2)
F13	0.102 (4)	0.095 (4)	0.335 (9)	0.043 (3)	0.121 (5)	0.009 (4)
F14	0.069 (3)	0.325 (9)	0.061 (3)	0.057 (4)	0.031 (2)	0.029 (4)
F15	0.041 (2)	0.181 (5)	0.122 (4)	-0.012 (3)	0.008 (2)	-0.044 (4)
F16	0.091 (3)	0.043 (2)	0.258 (7)	0.013 (2)	0.054 (4)	0.032 (3)
F17	0.068 (2)	0.072 (3)	0.156 (4)	-0.032 (2)	-0.016 (3)	0.028 (3)
F18	0.145 (4)	0.093 (3)	0.101 (3)	-0.035 (3)	0.011 (3)	0.043 (3)
O1	0.0346 (16)	0.0414 (18)	0.046 (2)	0.0016 (14)	0.0065 (14)	0.0077 (15)
O2	0.0374 (17)	0.0482 (19)	0.0310 (18)	0.0053 (14)	0.0073 (14)	-0.0031 (14)
O3	0.0364 (17)	0.0419 (18)	0.050 (2)	-0.0058 (14)	0.0006 (15)	-0.0003 (15)
O4	0.0360 (17)	0.054 (2)	0.0342 (19)	0.0009 (15)	-0.0024 (14)	-0.0083 (15)
O5	0.0392 (18)	0.0426 (18)	0.043 (2)	0.0042 (15)	0.0137 (15)	-0.0042 (15)
O6	0.0353 (17)	0.0358 (17)	0.053 (2)	0.0033 (14)	0.0043 (15)	0.0014 (15)
N1A	0.047 (2)	0.065 (3)	0.031 (2)	-0.003 (2)	0.0052 (18)	-0.012 (2)
N2A	0.038 (2)	0.045 (2)	0.051 (3)	-0.0018 (18)	-0.0011 (19)	-0.008 (2)
C1	0.035 (3)	0.091 (5)	0.139 (7)	0.008 (3)	0.005 (3)	0.062 (4)
C1A	0.048 (3)	0.053 (3)	0.037 (3)	-0.002 (2)	0.004 (2)	-0.015 (2)
C2	0.031 (2)	0.039 (3)	0.067 (3)	0.004 (2)	0.008 (2)	0.011 (2)
C2A	0.080 (4)	0.096 (5)	0.033 (3)	0.004 (4)	0.002 (3)	-0.008 (3)
C3	0.029 (2)	0.045 (3)	0.072 (4)	0.005 (2)	0.015 (2)	0.007 (2)
C3A	0.037 (3)	0.051 (3)	0.065 (4)	0.001 (2)	0.005 (2)	-0.014 (3)
C4	0.039 (2)	0.036 (2)	0.046 (3)	-0.0052 (19)	0.014 (2)	-0.007 (2)
C4A	0.057 (4)	0.085 (5)	0.149 (8)	-0.018 (4)	0.004 (5)	-0.048 (5)
C5	0.070 (4)	0.068 (4)	0.059 (4)	0.005 (3)	0.033 (3)	0.002 (3)
C6	0.063 (4)	0.098 (5)	0.080 (4)	-0.049 (4)	0.003 (3)	0.001 (4)
C7	0.040 (3)	0.042 (3)	0.064 (3)	-0.006 (2)	0.008 (2)	-0.013 (2)
C8	0.032 (3)	0.057 (3)	0.068 (4)	-0.004 (2)	-0.004 (2)	-0.017 (3)

C9	0.035 (2)	0.046 (3)	0.050 (3)	0.008 (2)	-0.008 (2)	-0.019 (2)
C10	0.045 (3)	0.078 (4)	0.060 (4)	0.002 (3)	-0.016 (3)	-0.021 (3)
C11	0.040 (3)	0.084 (4)	0.057 (4)	0.016 (3)	0.010 (3)	-0.011 (3)
C12	0.029 (2)	0.049 (3)	0.035 (3)	0.0058 (19)	-0.0023 (18)	-0.014 (2)
C13	0.040 (2)	0.040 (2)	0.054 (3)	0.007 (2)	-0.007 (2)	-0.009 (2)
C14	0.035 (2)	0.037 (2)	0.051 (3)	0.0028 (19)	-0.009 (2)	0.000 (2)
C15	0.052 (3)	0.046 (3)	0.102 (5)	-0.001 (3)	-0.001 (3)	0.014 (3)
Eu2	0.02491 (11)	0.03202 (12)	0.04177 (15)	-0.00185 (9)	0.00338 (9)	-0.00209 (9)
F19	0.168 (5)	0.112 (4)	0.125 (4)	0.100 (4)	0.045 (4)	0.011 (3)
F20	0.077 (3)	0.098 (3)	0.098 (3)	0.011 (2)	0.015 (2)	-0.053 (3)
F21	0.082 (3)	0.124 (4)	0.183 (6)	-0.030 (3)	0.084 (3)	-0.078 (4)
F25	0.112 (3)	0.072 (2)	0.091 (3)	-0.032 (2)	-0.014 (3)	-0.018 (2)
F26	0.074 (2)	0.101 (3)	0.057 (2)	0.000 (2)	0.0009 (18)	-0.031 (2)
F27	0.057 (2)	0.118 (3)	0.095 (3)	0.007 (2)	-0.026 (2)	-0.055 (3)
F28	0.126 (3)	0.064 (2)	0.065 (3)	0.017 (2)	-0.003 (2)	0.0168 (19)
F29	0.058 (2)	0.0557 (19)	0.072 (2)	0.0135 (16)	-0.0196 (17)	-0.0182 (16)
F30	0.0354 (17)	0.065 (2)	0.148 (4)	0.0069 (16)	-0.005 (2)	-0.025 (2)
F31	0.256 (7)	0.063 (3)	0.091 (3)	0.051 (3)	0.061 (4)	-0.014 (2)
F32	0.054 (2)	0.057 (2)	0.230 (6)	0.0228 (19)	0.004 (3)	0.000 (3)
F33	0.076 (2)	0.0360 (17)	0.121 (3)	-0.0010 (16)	0.010 (2)	0.0081 (19)
O7	0.0339 (17)	0.0432 (18)	0.052 (2)	-0.0007 (14)	0.0112 (15)	-0.0102 (16)
O8	0.0331 (16)	0.0352 (17)	0.047 (2)	-0.0017 (13)	0.0070 (14)	-0.0013 (14)
O9	0.0358 (17)	0.053 (2)	0.046 (2)	0.0014 (16)	0.0001 (15)	-0.0115 (16)
O10	0.0331 (16)	0.0392 (17)	0.047 (2)	-0.0019 (14)	-0.0046 (14)	-0.0008 (14)
O11	0.0292 (16)	0.0340 (17)	0.069 (3)	0.0020 (13)	0.0078 (16)	-0.0005 (16)
O12	0.0314 (16)	0.0354 (16)	0.055 (2)	0.0005 (13)	0.0112 (15)	-0.0061 (15)
N3A	0.034 (2)	0.048 (2)	0.049 (3)	0.0027 (18)	-0.0053 (18)	0.0020 (19)
N4A	0.034 (2)	0.062 (3)	0.051 (3)	-0.004 (2)	0.004 (2)	-0.011 (2)
C5A	0.038 (3)	0.048 (3)	0.052 (3)	0.000 (2)	0.002 (2)	0.003 (2)
C6A	0.056 (4)	0.105 (6)	0.088 (6)	0.029 (4)	-0.002 (4)	0.021 (4)
C7A	0.029 (2)	0.066 (4)	0.057 (3)	-0.004 (2)	0.005 (2)	-0.014 (3)
C8A	0.056 (4)	0.130 (7)	0.056 (4)	0.001 (4)	0.002 (3)	-0.029 (4)
C16	0.047 (3)	0.057 (3)	0.086 (5)	0.005 (3)	0.018 (3)	-0.020 (3)
C17	0.033 (2)	0.044 (3)	0.046 (3)	0.0015 (19)	0.007 (2)	-0.003 (2)
C18	0.032 (2)	0.049 (3)	0.057 (3)	-0.006 (2)	0.015 (2)	-0.005 (2)
C19	0.032 (2)	0.040 (2)	0.038 (3)	-0.0027 (18)	0.0022 (19)	0.0039 (19)
C20	0.046 (3)	0.042 (3)	0.053 (3)	-0.010 (2)	0.011 (2)	0.001 (2)
C21	0.049 (3)	0.072 (4)	0.059 (4)	0.003 (3)	-0.003 (3)	-0.024 (3)
C22	0.035 (2)	0.060 (3)	0.044 (3)	-0.004 (2)	0.001 (2)	-0.007 (2)
C23	0.035 (3)	0.057 (3)	0.045 (3)	0.000 (2)	-0.006 (2)	-0.006 (2)

C24	0.030 (2)	0.043 (2)	0.040 (3)	-0.0030 (19)	0.0014 (19)	0.004 (2)
C25	0.041 (3)	0.046 (3)	0.053 (3)	0.004 (2)	-0.004 (2)	-0.002 (2)
C26	0.053 (3)	0.039 (3)	0.088 (4)	0.005 (2)	0.014 (3)	-0.004 (3)
C27	0.040 (2)	0.033 (2)	0.046 (3)	-0.0012 (18)	-0.002 (2)	-0.002 (2)
C28	0.036 (2)	0.036 (2)	0.061 (3)	-0.008 (2)	0.006 (2)	-0.007 (2)
C29	0.031 (2)	0.044 (2)	0.044 (3)	-0.0073 (19)	0.007 (2)	-0.010 (2)
C30	0.039 (3)	0.063 (3)	0.094 (5)	-0.009 (2)	0.022 (3)	-0.022 (3)
F22	0.120 (8)	0.072 (5)	0.072 (5)	-0.049 (5)	0.026 (4)	0.010 (4)
F23	0.115 (8)	0.065 (5)	0.101 (7)	-0.026 (5)	-0.059 (7)	-0.004 (5)
F24	0.085 (6)	0.044 (4)	0.248 (17)	-0.018 (3)	0.085 (8)	-0.036 (7)
F34	0.036 (5)	0.087 (6)	0.25 (3)	0.019 (5)	0.032 (9)	0.029 (9)
F35	0.027 (4)	0.109 (8)	0.158 (14)	-0.032 (5)	0.020 (6)	-0.058 (9)
F36	0.060 (6)	0.29 (3)	0.086 (6)	-0.024 (14)	0.040 (5)	-0.028 (9)
F22A	0.071 (8)	0.077 (11)	0.20 (2)	-0.040 (7)	0.066 (12)	-0.051 (14)
F23A	0.126 (15)	0.061 (9)	0.060 (6)	-0.043 (9)	-0.017 (6)	-0.009 (5)
F24A	0.102 (13)	0.047 (6)	0.127 (15)	-0.017 (7)	-0.062 (10)	0.027 (8)
F34A	0.036 (5)	0.29 (4)	0.116 (8)	-0.012 (13)	-0.017 (5)	-0.042 (11)
F35A	0.103 (11)	0.073 (7)	0.31 (3)	0.007 (7)	0.143 (16)	0.034 (11)
F36A	0.052 (5)	0.094 (8)	0.109 (11)	0.008 (6)	0.038 (7)	-0.033 (7)

Geometric parameters (Å, º)

Eu1—O1	2.361 (3)	Eu2—O10	2.381 (3)
Eu1—O2	2.368 (3)	Eu2—O11	2.343 (3)
Eu1—O3	2.359 (3)	Eu2—O12	2.387 (3)
Eu1—O4	2.356 (3)	Eu2—N3A	2.572 (4)
Eu1—O5	2.400 (3)	Eu2—N4A	2.548 (5)
Eu1—O6	2.363 (3)	F19—C16	1.312 (7)
Eu1—N1A	2.506 (4)	F20—C16	1.303 (7)
Eu1—N2A	2.571 (4)	F21—C16	1.296 (6)
F1—C1	1.246 (7)	F25—C21	1.319 (7)
F2—C1	1.357 (9)	F26—C21	1.325 (6)
F3—C1	1.277 (7)	F27—C21	1.316 (6)
F4—C5	1.278 (6)	F28—C25	1.365 (6)
F5—C5	1.332 (7)	F29—C25	1.250 (6)
F6—C5	1.252 (7)	F30—C25	1.314 (5)
F7—C6	1.301 (7)	F31—C26	1.294 (7)
F8—C6	1.329 (8)	F32—C26	1.320 (6)
F9—C6	1.281 (7)	F33—C26	1.327 (6)
F10—C10	1.296 (6)	O7—C17	1.245 (6)

F11—C10	1.315 (7)	O8—C19	1.251 (5)
F12—C10	1.295 (6)	O9—C22	1.252 (6)
F13—C11	1.290 (7)	O10—C24	1.248 (5)
F14—C11	1.272 (7)	O11—C27	1.247 (5)
F15—C11	1.307 (7)	O12—C29	1.248 (5)
F16—C15	1.314 (6)	N3A—C5A	1.124 (6)
F17—C15	1.294 (6)	N4A—C7A	1.129 (7)
F18—C15	1.313 (7)	C5A—C6A	1.457 (7)
O1—C2	1.248 (6)	C6A—H6AA	0.9800
O2—C4	1.256 (5)	C6A—H6AB	0.9800
O3—C7	1.258 (6)	C6A—H6AC	0.9800
O4—C9	1.251 (6)	C7A—C8A	1.461 (8)
O5—C12	1.231 (6)	C8A—H8AA	0.9800
O6—C14	1.253 (5)	C8A—H8AB	0.9800
N1A—C1A	1.127 (7)	C8A—H8AC	0.9800
N2A—C3A	1.129 (6)	C16—C17	1.534 (7)
C1—C2	1.532 (8)	C17—C18	1.386 (7)
C1A—C2A	1.472 (8)	C18—H18	0.9500
C2—C3	1.384 (7)	C18—C19	1.380 (7)
C2A—H2AA	0.9800	C19—C20	1.517 (7)
C2A—H2AB	0.9800	C20—F22	1.331 (7)
C2A—H2AC	0.9800	C20—F23	1.278 (7)
C3—H3	0.9500	C20—F24	1.292 (8)
C3—C4	1.375 (7)	C20—F22A	1.295 (10)
C3A—C4A	1.449 (8)	C20—F23A	1.339 (10)
C4—C5	1.528 (8)	C20—F24A	1.282 (11)
C4A—H4AA	0.9800	C21—C22	1.542 (7)
C4A—H4AB	0.9800	C22—C23	1.368 (7)
C4A—H4AC	0.9800	C23—H23	0.9500
C6—C7	1.512 (9)	C23—C24	1.389 (7)
C7—C8	1.382 (8)	C24—C25	1.553 (7)
C8—H8	0.9500	C26—C27	1.522 (7)
C8—C9	1.380 (8)	C27—C28	1.374 (7)
C9—C10	1.548 (8)	C28—H28	0.9500
C11—C12	1.520 (7)	C28—C29	1.389 (7)
C12—C13	1.393 (7)	C29—C30	1.528 (7)
C13—H13	0.9500	C30—F34	1.351 (9)
C13—C14	1.381 (7)	C30—F35	1.278 (9)
C14—C15	1.526 (8)	C30—F36	1.261 (10)
Eu2—O7	2.362 (3)	C30—F34A	1.268 (11)

Eu2—O8	2.385 (3)	C30—F35A	1.357 (10)
Eu2—O9	2.366 (3)	C30—F36A	1.289 (10)
O1—Eu1—O2	72.35 (11)	O8—Eu2—O12	145.11 (11)
O1—Eu1—O5	140.06 (12)	O8—Eu2—N3A	77.45 (12)
O1—Eu1—O6	143.81 (11)	O8—Eu2—N4A	83.27 (13)
O1—Eu1—N1A	75.60 (13)	O9—Eu2—O8	114.13 (12)
O1—Eu1—N2A	75.51 (12)	O9—Eu2—O10	72.57 (11)
O2—Eu1—O5	145.77 (11)	O9—Eu2—O12	74.98 (12)
O2—Eu1—N1A	139.33 (13)	O9—Eu2—N3A	140.42 (13)
O2—Eu1—N2A	75.32 (13)	O9—Eu2—N4A	144.61 (12)
O3—Eu1—O1	77.05 (11)	O10—Eu2—O8	74.60 (11)
O3—Eu1—O2	118.31 (12)	O10—Eu2—O12	76.81 (11)
O3—Eu1—O5	72.34 (11)	O10—Eu2—N3A	144.38 (12)
O3—Eu1—O6	139.13 (11)	O10—Eu2—N4A	83.89 (13)
O3—Eu1—N1A	76.99 (13)	O11—Eu2—O7	77.58 (12)
O3—Eu1—N2A	143.29 (13)	O11—Eu2—O8	141.59 (10)
O4—Eu1—O1	116.20 (12)	O11—Eu2—O9	79.29 (12)
O4—Eu1—O2	75.07 (11)	O11—Eu2—O10	142.14 (10)
O4—Eu1—O3	72.64 (12)	O11—Eu2—O12	71.73 (11)
O4—Eu1—O5	78.26 (12)	O11—Eu2—N3A	71.40 (12)
O4—Eu1—O6	83.60 (12)	O11—Eu2—N4A	106.66 (14)
O4—Eu1—N1A	143.18 (13)	O12—Eu2—N3A	118.11 (13)
O4—Eu1—N2A	142.34 (14)	O12—Eu2—N4A	74.15 (12)
O5—Eu1—N1A	73.02 (13)	N4A—Eu2—N3A	71.22 (14)
O5—Eu1—N2A	116.90 (12)	C17—O7—Eu2	133.6 (3)
O6—Eu1—O2	85.43 (12)	C19—O8—Eu2	133.5 (3)
O6—Eu1—O5	70.53 (11)	C22—O9—Eu2	132.5 (3)
O6—Eu1—N1A	107.35 (14)	C24—O10—Eu2	132.8 (3)
O6—Eu1—N2A	71.35 (12)	C27—O11—Eu2	135.5 (3)
N1A—Eu1—N2A	72.93 (14)	C29—O12—Eu2	133.1 (3)
C2—O1—Eu1	132.7 (3)	C5A—N3A—Eu2	164.9 (4)
C4—O2—Eu1	133.0 (3)	C7A—N4A—Eu2	169.2 (5)
C7—O3—Eu1	129.2 (3)	N3A—C5A—C6A	179.4 (7)
C9—O4—Eu1	131.0 (3)	C5A—C6A—H6AA	109.5
C12—O5—Eu1	136.7 (3)	C5A—C6A—H6AB	109.5
C14—O6—Eu1	135.9 (3)	C5A—C6A—H6AC	109.5
C1A—N1A—Eu1	172.7 (4)	H6AA—C6A—H6AB	109.5
C3A—N2A—Eu1	165.4 (4)	H6AA—C6A—H6AC	109.5
F1—C1—F2	104.7 (8)	H6AB—C6A—H6AC	109.5

F1—C1—F3	111.6 (6)	N4A—C7A—C8A	179.3 (6)
F1—C1—C2	115.5 (5)	C7A—C8A—H8AA	109.5
F2—C1—C2	106.9 (5)	C7A—C8A—H8AB	109.5
F3—C1—F2	101.0 (7)	C7A—C8A—H8AC	109.5
F3—C1—C2	115.3 (7)	H8AA—C8A—H8AB	109.5
N1A—C1A—C2A	179.1 (7)	H8AA—C8A—H8AC	109.5
O1—C2—C1	113.5 (5)	H8AB—C8A—H8AC	109.5
O1—C2—C3	128.3 (5)	F19—C16—C17	110.1 (5)
C3—C2—C1	118.2 (5)	F20—C16—F19	107.2 (6)
C1A—C2A—H2AA	109.5	F20—C16—C17	111.9 (5)
C1A—C2A—H2AB	109.5	F21—C16—F19	106.6 (6)
C1A—C2A—H2AC	109.5	F21—C16—F20	105.8 (6)
H2AA—C2A—H2AB	109.5	F21—C16—C17	114.9 (5)
H2AA—C2A—H2AC	109.5	O7—C17—C16	113.9 (4)
H2AB—C2A—H2AC	109.5	O7—C17—C18	128.0 (5)
C2—C3—H3	119.4	C18—C17—C16	118.1 (4)
C4—C3—C2	121.2 (5)	C17—C18—H18	119.1
C4—C3—H3	119.4	C19—C18—C17	121.9 (4)
N2A—C3A—C4A	177.7 (6)	C19—C18—H18	119.1
O2—C4—C3	128.3 (5)	O8—C19—C18	127.7 (4)
O2—C4—C5	114.1 (5)	O8—C19—C20	114.9 (4)
C3—C4—C5	117.6 (5)	C18—C19—C20	117.3 (4)
C3A—C4A—H4AA	109.5	F22—C20—C19	111.0 (5)
C3A—C4A—H4AB	109.5	F23—C20—C19	111.4 (5)
C3A—C4A—H4AC	109.5	F23—C20—F22	106.2 (7)
H4AA—C4A—H4AB	109.5	F23—C20—F24	112.4 (9)
H4AA—C4A—H4AC	109.5	F24—C20—C19	111.8 (6)
H4AB—C4A—H4AC	109.5	F24—C20—F22	103.6 (7)
F4—C5—F5	103.8 (6)	F22A—C20—C19	116.9 (7)
F4—C5—C4	115.3 (5)	F22A—C20—F23A	104.1 (12)
F5—C5—C4	111.2 (5)	F23A—C20—C19	113.1 (6)
F6—C5—F4	110.3 (6)	F24A—C20—C19	114.7 (9)
F6—C5—F5	103.9 (7)	F24A—C20—F22A	107.1 (13)
F6—C5—C4	111.4 (5)	F24A—C20—F23A	99.0 (11)
F7—C6—F8	99.8 (6)	F25—C21—F26	106.6 (5)
F7—C6—C7	114.4 (5)	F25—C21—C22	110.7 (5)
F8—C6—C7	110.2 (6)	F26—C21—C22	110.3 (5)
F9—C6—F7	112.4 (7)	F27—C21—F25	107.9 (5)
F9—C6—F8	105.0 (6)	F27—C21—F26	107.6 (5)
F9—C6—C7	113.7 (6)	F27—C21—C22	113.5 (5)

O3—C7—C6	113.9 (5)	O9—C22—C21	113.1 (5)
O3—C7—C8	128.0 (5)	O9—C22—C23	127.8 (5)
C8—C7—C6	118.1 (5)	C23—C22—C21	119.1 (5)
C7—C8—H8	119.3	C22—C23—H23	118.5
C9—C8—C7	121.3 (5)	C22—C23—C24	122.9 (5)
C9—C8—H8	119.3	C24—C23—H23	118.5
O4—C9—C8	128.1 (5)	O10—C24—C23	127.0 (5)
O4—C9—C10	114.1 (5)	O10—C24—C25	114.5 (4)
C8—C9—C10	117.7 (5)	C23—C24—C25	118.5 (4)
F10—C10—F11	105.8 (6)	F28—C25—C24	106.8 (4)
F10—C10—C9	113.0 (5)	F29—C25—F28	107.3 (5)
F11—C10—C9	113.0 (5)	F29—C25—F30	112.1 (5)
F12—C10—F10	107.6 (5)	F29—C25—C24	114.8 (4)
F12—C10—F11	106.9 (6)	F30—C25—F28	104.0 (4)
F12—C10—C9	110.1 (5)	F30—C25—C24	111.1 (4)
F13—C11—F15	103.3 (6)	F31—C26—F32	107.5 (6)
F13—C11—C12	115.0 (5)	F31—C26—F33	107.0 (5)
F14—C11—F13	108.2 (6)	F31—C26—C27	110.5 (5)
F14—C11—F15	105.1 (6)	F32—C26—F33	104.8 (5)
F14—C11—C12	113.0 (5)	F32—C26—C27	112.3 (5)
F15—C11—C12	111.3 (5)	F33—C26—C27	114.2 (5)
O5—C12—C11	114.8 (5)	O11—C27—C26	113.2 (4)
O5—C12—C13	126.9 (5)	O11—C27—C28	128.5 (4)
C13—C12—C11	118.3 (5)	C28—C27—C26	118.3 (4)
C12—C13—H13	119.6	C27—C28—H28	119.9
C14—C13—C12	120.8 (4)	C27—C28—C29	120.2 (4)
C14—C13—H13	119.6	C29—C28—H28	119.9
O6—C14—C13	127.9 (5)	O12—C29—C28	128.7 (4)
O6—C14—C15	113.8 (5)	O12—C29—C30	114.6 (4)
C13—C14—C15	118.3 (5)	C28—C29—C30	116.7 (4)
F16—C15—C14	113.4 (5)	F34—C30—C29	111.1 (6)
F17—C15—F16	108.5 (6)	F35—C30—C29	114.7 (7)
F17—C15—F18	106.4 (6)	F35—C30—F34	102.6 (9)
F17—C15—C14	111.5 (5)	F36—C30—C29	114.6 (8)
F18—C15—F16	105.4 (6)	F36—C30—F34	105.1 (11)
F18—C15—C14	111.3 (5)	F36—C30—F35	107.7 (10)
O7—Eu2—O8	72.30 (11)	F34A—C30—C29	110.7 (8)
O7—Eu2—O9	74.89 (12)	F34A—C30—F35A	109.2 (13)
O7—Eu2—O10	117.41 (12)	F34A—C30—F36A	112.0 (12)
O7—Eu2—O12	140.17 (11)	F35A—C30—C29	111.3 (8)

O7—Eu2—N3A	73.30 (13)	F36A—C30—C29	112.1 (7)
O7—Eu2—N4A	140.39 (12)	F36A—C30—F35A	101.2 (10)

8.3.6 Crystallographic data for 4-Gd

Crystal data

$C_{32}H_9F_{36}Gd_2NO_{12}\cdot 0.5(C_7H_8)$	$F(000)$ = 6248
M_r = 1643.97	D_x = 2.007 Mg m^{-3}
Monoclinic, *C*2/*c*	Mo *K*α radiation, λ = 0.71073 Å
a = 42.092 (2) Å	Cell parameters from 9871 reflections
b = 12.2296 (6) Å	θ = 2.3–28.1°
c = 22.3919 (10) Å	μ = 2.59 mm^{-1}
β = 109.292 (2)°	*T* = 150 K
V = 10879.5 (9) Å^3	Plate, colourless
Z = 8	0.21 × 0.2 × 0.03 mm

Data collection

Bruker D8 Venture diffractometer	13491 independent reflections
Radiation source: microfocus sealed tube, INCOATEC Iμs 3.0	10290 reflections with $I > 2\sigma(I)$
Multilayer mirror optics monochromator	R_{int} = 0.043
Detector resolution: 7.4074 pixels mm^{-1}	θ_{max} = 28.3°, θ_{min} = 2.3°
ϕ and ω scans	*h* = -56→56
Absorption correction: multi-scan *SADABS2016*/2 (Bruker,2016/2) was used for absorption correction. wR2(int) was 0.1368 before and 0.0662 after correction. The Ratio of minimum to maximum transmission is 0.7912. The λ/2 correction factor is Not present.	*k* = -16→16
T_{min} = 0.590, T_{max} = 0.746	*l* = -28→29
57629 measured reflections	

Refinement

Refinement on F^2	Primary atom site location: dual
Least-squares matrix: full	Hydrogen site location: inferred from neighbouring sites
$R[F^2 > 2\sigma(F^2)]$ = 0.043	H-atom parameters constrained

$wR(F^2)$ = 0.115	$w = 1/[\sigma^2(F_o^2) + (0.0546P)^2 + 28.632P]$ where $P = (F_o^2 + 2F_c^2)/3$
S = 1.05	$(\Delta/\sigma)_{max}$ = 0.003
13491 reflections	$\Delta\rangle_{max}$ = 1.24 e Å^{-3}
912 parameters	$\Delta\rangle_{min}$ = -0.64 e Å^{-3}
1089 restraints	

Special details

Geometry. All esds (except the esd in the dihedral angle between two l.s. planes) are estimated using the full covariance matrix. The cell esds are taken into account individually in the estimation of esds in distances, angles and torsion angles; correlations between esds in cell parameters are only used when they are defined by crystal symmetry. An approximate (isotropic) treatment of cell esds is used for estimating esds involving l.s. planes.

Fractional atomic coordinates and isotropic or equivalent isotropic displacement parameters (Å²)

	x	*y*	*z*	U_{iso}*/U_{eq}	Occ. (<1)
Gd1	0.64320 (2)	0.39574 (2)	0.79480 (2)	0.03804 (7)	
Gd2	0.61891 (2)	0.15581 (2)	0.68728 (2)	0.04077 (7)	
F1	0.67791 (16)	0.6858 (5)	0.9557 (4)	0.184 (3)	
F2	0.7238 (2)	0.6171 (5)	1.0148 (2)	0.210 (4)	
F3	0.71868 (15)	0.6798 (4)	0.9264 (3)	0.1296 (19)	
F4	0.71887 (14)	0.2384 (4)	1.03958 (19)	0.1298 (19)	
F5	0.67063 (13)	0.1772 (5)	0.9918 (3)	0.1253 (19)	
F6	0.71121 (14)	0.1412 (4)	0.9591 (2)	0.1110 (16)	
F7	0.7057 (3)	0.6023 (15)	0.6876 (7)	0.130 (5)*	0.4
F8	0.6603 (6)	0.6677 (17)	0.6050 (11)	0.192 (12)*	0.4
F9	0.6847 (6)	0.5188 (15)	0.6034 (9)	0.167 (7)*	0.4
F10	0.55453 (12)	0.4907 (4)	0.5548 (2)	0.1256 (19)	
F11	0.54833 (11)	0.3345 (3)	0.5858 (3)	0.125 (2)	
F12	0.54525 (12)	0.4673 (7)	0.6398 (3)	0.164 (3)	
F13	0.5551 (3)	0.4745 (10)	0.9042 (7)	0.102 (4)	0.6
F14	0.6041 (2)	0.4771 (8)	0.9655 (4)	0.105 (3)	0.6
F15	0.5737 (4)	0.3435 (7)	0.9693 (5)	0.122 (4)	0.6
F16	0.57031 (13)	0.0272 (3)	0.8459 (3)	0.1161 (18)	
F17	0.58921 (10)	0.0196 (2)	0.76876 (17)	0.0713 (9)	
F18	0.62209 (12)	0.0149 (3)	0.86495 (18)	0.0929 (13)	
F19	0.72814 (11)	0.3329 (4)	0.7405 (2)	0.1002 (14)	
F20	0.71693 (8)	0.3825 (3)	0.82291 (17)	0.0698 (9)	

F21	0.75527 (9)	0.2631 (4)	0.8301 (2)	0.1125 (16)	
F22	0.6811 (5)	-0.1713 (9)	0.7859 (9)	0.189 (9)	0.624 (17)
F23	0.6885 (4)	-0.0939 (11)	0.8746 (6)	0.150 (6)	0.624 (17)
F24	0.7276 (2)	-0.1056 (11)	0.8380 (7)	0.124 (5)	0.624 (17)
F25	0.72627 (16)	0.1360 (8)	0.6376 (4)	0.229 (5)	
F26	0.70687 (16)	0.0591 (7)	0.5475 (3)	0.172 (3)	
F27	0.7084 (2)	-0.0232 (8)	0.6278 (4)	0.204 (4)	
F28	0.6014 (2)	0.1955 (6)	0.4260 (2)	0.187 (3)	
F29	0.5747 (3)	0.2991 (5)	0.4689 (2)	0.215 (4)	
F30	0.5637 (2)	0.1365 (6)	0.4581 (3)	0.180 (3)	
F31	0.5913 (8)	-0.2309 (17)	0.6214 (9)	0.160 (8)	0.5
F32	0.5988 (7)	-0.1601 (19)	0.5413 (12)	0.188 (10)	0.5
F33	0.5470 (5)	-0.192 (2)	0.5390 (13)	0.207 (11)	0.5
F34	0.4771 (4)	0.0723 (17)	0.5914 (7)	0.123 (6)	0.5
F35	0.4994 (5)	0.1008 (14)	0.6880 (6)	0.128 (5)	0.5
F36	0.4963 (4)	0.2232 (12)	0.6202 (10)	0.136 (5)	0.5
O1	0.67434 (9)	0.5185 (3)	0.87029 (16)	0.0520 (8)	
O2	0.67070 (9)	0.2944 (3)	0.88407 (15)	0.0517 (8)	
O3	0.66602 (9)	0.4832 (3)	0.72232 (18)	0.0579 (9)	
O4	0.60748 (8)	0.3540 (2)	0.68796 (14)	0.0387 (7)	
O5	0.60596 (10)	0.4167 (3)	0.85154 (16)	0.0486 (8)	
O6	0.61111 (8)	0.2231 (2)	0.78771 (14)	0.0387 (7)	
O7	0.66845 (8)	0.2470 (3)	0.75621 (15)	0.0443 (7)	
O8	0.65287 (10)	0.0258 (3)	0.76020 (18)	0.0566 (9)	
O9	0.66405 (11)	0.1191 (3)	0.65147 (19)	0.0664 (11)	
O10	0.60408 (12)	0.2039 (3)	0.58199 (17)	0.0681 (11)	
O11	0.60236 (12)	-0.0128 (3)	0.63974 (19)	0.0700 (11)	
O12	0.56085 (10)	0.1453 (3)	0.6628 (2)	0.0646 (10)	
N1	0.61169 (12)	0.5714 (3)	0.76277 (19)	0.0504 (10)	
C1	0.70315 (17)	0.6228 (6)	0.9576 (3)	0.091 (2)	
C2	0.69105 (14)	0.5123 (5)	0.9277 (3)	0.0558 (13)	
C3	0.69902 (16)	0.4199 (5)	0.9648 (3)	0.0671 (15)	
H3	0.712208	0.426659	1.008162	0.081*	
C4	0.68831 (14)	0.3177 (5)	0.9404 (2)	0.0553 (12)	
C5	0.69757 (15)	0.2187 (5)	0.9829 (2)	0.0743 (16)	
C6	0.67596 (19)	0.5873 (6)	0.6425 (3)	0.096 (2)	
C7	0.65286 (15)	0.5155 (5)	0.6671 (3)	0.0583 (13)	
C8	0.61954 (14)	0.4975 (4)	0.6279 (2)	0.0543 (12)	
H8	0.611157	0.538313	0.589829	0.065*	
C9	0.59880 (13)	0.4248 (4)	0.6420 (2)	0.0435 (10)	

C10	0.56209 (14)	0.4291 (4)	0.6050 (2)	0.0608 (13)	
C11	0.58006 (15)	0.4095 (4)	0.9287 (2)	0.0681 (15)	
C12	0.59270 (14)	0.3541 (4)	0.8794 (2)	0.0475 (11)	
C13	0.58890 (16)	0.2419 (4)	0.8719 (3)	0.0555 (13)	
H13	0.579662	0.202643	0.898892	0.067*	
C14	0.59795 (13)	0.1850 (4)	0.8271 (2)	0.0464 (11)	
C15	0.59413 (14)	0.0613 (4)	0.8261 (3)	0.0666 (15)	
C16	0.72529 (13)	0.2965 (5)	0.7943 (3)	0.0674 (15)	
C17	0.69832 (13)	0.2087 (5)	0.7819 (2)	0.0523 (11)	
C18	0.70718 (15)	0.1038 (5)	0.7978 (3)	0.0638 (14)	
H18	0.730391	0.086086	0.815423	0.077*	
C19	0.68326 (17)	0.0200 (5)	0.7894 (3)	0.0630 (14)	
C20	0.69550 (18)	-0.0889 (6)	0.8213 (4)	0.094 (2)	
C21	0.7018 (2)	0.0744 (9)	0.6016 (4)	0.130 (3)	
C22	0.6680 (2)	0.1119 (5)	0.5983 (3)	0.0757 (17)	
C23	0.6448 (2)	0.1370 (6)	0.5407 (3)	0.0840 (19)	
H23	0.649840	0.123156	0.503105	0.101*	
C24	0.6146 (2)	0.1813 (5)	0.5370 (3)	0.0759 (17)	
C25	0.5889 (2)	0.2055 (6)	0.4725 (3)	0.110 (3)	
C26	0.5778 (3)	-0.1600 (6)	0.5748 (4)	0.125 (3)	
C27	0.5746 (2)	-0.0527 (5)	0.6087 (3)	0.0802 (18)	
C28	0.5431 (2)	-0.0122 (6)	0.6008 (3)	0.092 (2)	
H28	0.524009	-0.050688	0.574497	0.110*	
C29	0.53849 (16)	0.0829 (6)	0.6299 (3)	0.0784 (17)	
C30	0.5043 (3)	0.1180 (15)	0.6325 (8)	0.095 (4)	0.5
C31	0.60191 (16)	0.6570 (4)	0.7638 (2)	0.0566 (14)	
C32	0.5895 (2)	0.7672 (6)	0.7648 (4)	0.104 (3)	
H32A	0.566170	0.764434	0.764367	0.156*	
H32B	0.590474	0.806981	0.727420	0.156*	
H32C	0.603478	0.804678	0.803127	0.156*	
F7A	0.6798 (3)	0.6847 (6)	0.6701 (6)	0.142 (4)	0.6
F8A	0.6618 (2)	0.6135 (10)	0.5818 (4)	0.128 (4)	0.6
F9A	0.7042 (2)	0.5408 (8)	0.6480 (6)	0.115 (3)	0.6
F13A	0.5687 (5)	0.5066 (11)	0.9085 (13)	0.107 (6)	0.4
F14A	0.6033 (4)	0.4005 (18)	0.9833 (5)	0.134 (6)	0.4
F15A	0.5516 (3)	0.3630 (13)	0.9317 (8)	0.108 (4)	0.4
F22A	0.6714 (3)	-0.1567 (13)	0.8205 (13)	0.119 (7)	0.376 (17)
F23A	0.7192 (8)	-0.0792 (18)	0.8771 (10)	0.187 (12)	0.376 (17)
F24A	0.7081 (7)	-0.1452 (14)	0.7839 (11)	0.138 (8)	0.376 (17)
F31A	0.6012 (8)	-0.229 (2)	0.6068 (10)	0.179 (9)	0.5

F32A	0.5864 (4)	-0.1304 (16)	0.5254 (8)	0.113 (4)	0.5
F33A	0.5509 (5)	-0.223 (2)	0.5586 (14)	0.185 (9)	0.5
F34A	0.4840 (6)	0.0288 (17)	0.5963 (15)	0.198 (12)	0.5
F35A	0.4988 (4)	0.166 (2)	0.6605 (12)	0.193 (9)	0.5
F36A	0.4958 (4)	0.1804 (17)	0.5612 (11)	0.212 (8)	0.5
C30A	0.5021 (3)	0.1170 (17)	0.6108 (11)	0.142 (7)	0.5
C1S	0.500000	0.4909 (13)	0.750000	0.186 (9)	
H1SA	0.505058	0.464224	0.793416	0.278*	0.5
H1SB	0.477812	0.464224	0.723855	0.278*	0.5
H1SC	0.517130	0.464224	0.732729	0.278*	0.5
C2S	0.500000	0.6152 (10)	0.750000	0.116 (4)	
C3S	0.4935 (3)	0.6726 (8)	0.6939 (4)	0.124 (3)	
H3S	0.489015	0.634355	0.655080	0.149*	
C4S	0.4934 (2)	0.7853 (8)	0.6945 (5)	0.130 (4)	
H4S	0.488786	0.824535	0.655936	0.155*	
C5S	0.500000	0.8407 (12)	0.750000	0.126 (5)	
H5S	0.500001	0.918368	0.749999	0.152*	

Atomic displacement parameters (Å²)

	U^{11}	U^{22}	U^{33}	U^{12}	U^{13}	U^{23}
Gd1	0.04528 (14)	0.02892 (10)	0.03877 (12)	-0.00268 (9)	0.01235 (10)	-0.00041 (8)
Gd2	0.04461 (14)	0.03366 (11)	0.04335 (13)	0.00108 (9)	0.01358 (10)	-0.00474 (8)
F1	0.139 (5)	0.129 (5)	0.293 (9)	-0.026 (4)	0.082 (5)	-0.148 (5)
F2	0.330 (10)	0.108 (4)	0.091 (3)	-0.069 (5)	-0.066 (5)	-0.026 (3)
F3	0.148 (5)	0.081 (3)	0.152 (4)	-0.054 (3)	0.040 (4)	-0.028 (3)
F4	0.154 (5)	0.124 (4)	0.070 (2)	0.003 (3)	-0.019 (3)	0.038 (2)
F5	0.105 (4)	0.138 (4)	0.136 (4)	0.006 (3)	0.044 (3)	0.079 (3)
F6	0.142 (4)	0.085 (3)	0.104 (3)	0.052 (3)	0.039 (3)	0.038 (2)
F10	0.092 (3)	0.132 (4)	0.114 (3)	-0.010 (3)	-0.018 (3)	0.077 (3)
F11	0.065 (3)	0.075 (3)	0.184 (5)	-0.008 (2)	-0.028 (3)	0.023 (3)
F12	0.066 (3)	0.299 (9)	0.116 (4)	0.055 (4)	0.014 (3)	-0.053 (5)
F13	0.107 (7)	0.130 (9)	0.083 (5)	0.046 (7)	0.048 (6)	-0.003 (6)
F14	0.123 (6)	0.124 (7)	0.074 (5)	-0.010 (5)	0.041 (4)	-0.050 (5)
F15	0.233 (12)	0.084 (5)	0.103 (7)	0.020 (7)	0.128 (8)	0.015 (5)
F16	0.153 (4)	0.047 (2)	0.204 (5)	-0.024 (2)	0.135 (4)	-0.007 (2)
F17	0.091 (3)	0.0341 (14)	0.091 (2)	-0.0057 (16)	0.033 (2)	-0.0103 (15)
F18	0.138 (4)	0.0506 (19)	0.090 (3)	0.027 (2)	0.036 (2)	0.0239 (18)
F19	0.083 (3)	0.133 (4)	0.104 (3)	-0.042 (3)	0.056 (3)	-0.031 (3)

F20	0.0500 (19)	0.072 (2)	0.082 (2)	-0.0054 (16)	0.0153 (17)	-0.0160 (17)
F21	0.042 (2)	0.112 (3)	0.155 (4)	0.013 (2)	-0.007 (2)	-0.037 (3)
F22	0.200 (15)	0.064 (5)	0.242 (15)	0.047 (8)	-0.010 (12)	0.002 (8)
F23	0.187 (13)	0.136 (9)	0.164 (9)	0.100 (9)	0.109 (10)	0.099 (8)
F24	0.099 (5)	0.128 (9)	0.151 (10)	0.075 (6)	0.050 (6)	0.072 (8)
F25	0.101 (4)	0.357 (11)	0.259 (9)	-0.061 (6)	0.099 (5)	-0.205 (9)
F26	0.161 (5)	0.236 (7)	0.172 (5)	-0.041 (5)	0.126 (5)	-0.100 (5)
F27	0.159 (6)	0.240 (8)	0.252 (9)	0.104 (6)	0.121 (6)	0.026 (7)
F28	0.290 (9)	0.217 (7)	0.049 (3)	0.006 (6)	0.052 (4)	-0.003 (3)
F29	0.417 (12)	0.112 (4)	0.065 (3)	0.100 (6)	0.008 (5)	0.011 (3)
F30	0.193 (7)	0.186 (6)	0.094 (4)	-0.032 (5)	-0.045 (4)	0.021 (4)
F31	0.34 (2)	0.039 (5)	0.127 (10)	0.000 (9)	0.109 (10)	-0.028 (6)
F32	0.37 (3)	0.078 (12)	0.175 (19)	-0.008 (14)	0.17 (2)	-0.035 (10)
F33	0.316 (15)	0.133 (18)	0.133 (14)	-0.128 (13)	0.024 (11)	-0.079 (12)
F34	0.049 (6)	0.196 (15)	0.103 (7)	-0.040 (9)	-0.002 (5)	0.006 (8)
F35	0.093 (9)	0.185 (15)	0.105 (7)	0.005 (10)	0.032 (6)	0.024 (7)
F36	0.058 (7)	0.129 (8)	0.225 (17)	0.005 (6)	0.053 (11)	0.047 (9)
O1	0.057 (2)	0.0421 (17)	0.0502 (18)	-0.0071 (16)	0.0090 (16)	-0.0079 (14)
O2	0.058 (2)	0.0442 (18)	0.0450 (17)	0.0033 (16)	0.0070 (16)	0.0067 (14)
O3	0.053 (2)	0.059 (2)	0.063 (2)	-0.0136 (18)	0.0200 (18)	0.0068 (17)
O4	0.0436 (18)	0.0323 (14)	0.0404 (15)	-0.0006 (13)	0.0143 (13)	0.0037 (11)
O5	0.069 (2)	0.0343 (15)	0.0489 (18)	0.0012 (15)	0.0273 (17)	0.0021 (13)
O6	0.0453 (18)	0.0309 (14)	0.0443 (16)	-0.0026 (13)	0.0205 (14)	0.0008 (12)
O7	0.0365 (17)	0.0487 (18)	0.0459 (17)	0.0059 (14)	0.0112 (14)	-0.0030 (14)
O8	0.063 (2)	0.0448 (19)	0.063 (2)	0.0154 (17)	0.0224 (19)	0.0087 (16)
O9	0.071 (3)	0.075 (3)	0.064 (2)	-0.001 (2)	0.037 (2)	-0.0175 (19)
O10	0.103 (3)	0.054 (2)	0.0441 (19)	0.004 (2)	0.019 (2)	-0.0068 (16)
O11	0.097 (3)	0.0414 (19)	0.064 (2)	-0.005 (2)	0.017 (2)	-0.0128 (17)
O12	0.045 (2)	0.057 (2)	0.083 (3)	-0.0113 (17)	0.0084 (19)	0.0027 (19)
N1	0.069 (3)	0.0328 (18)	0.048 (2)	0.0010 (19)	0.017 (2)	0.0029 (16)
C1	0.108 (6)	0.079 (4)	0.077 (4)	-0.025 (4)	0.018 (4)	-0.036 (4)
C2	0.055 (3)	0.057 (3)	0.051 (3)	-0.005 (2)	0.011 (2)	-0.014 (2)
C3	0.072 (4)	0.078 (3)	0.044 (3)	-0.001 (3)	0.008 (3)	-0.006 (2)
C4	0.053 (3)	0.062 (3)	0.048 (3)	0.008 (3)	0.013 (2)	0.010 (2)
C5	0.076 (4)	0.078 (4)	0.060 (3)	0.013 (3)	0.010 (3)	0.022 (3)
C6	0.099 (5)	0.101 (5)	0.097 (5)	-0.023 (4)	0.045 (5)	0.019 (4)
C7	0.064 (3)	0.060 (3)	0.063 (3)	-0.008 (3)	0.037 (3)	0.009 (2)
C8	0.065 (3)	0.054 (3)	0.049 (3)	-0.004 (3)	0.024 (2)	0.015 (2)
C9	0.051 (3)	0.038 (2)	0.042 (2)	0.003 (2)	0.018 (2)	0.0018 (17)
C10	0.056 (3)	0.063 (3)	0.056 (3)	0.011 (3)	0.007 (2)	0.009 (2)

C11	0.107 (5)	0.052 (3)	0.060 (3)	0.002 (3)	0.047 (3)	-0.007 (2)
C12	0.063 (3)	0.039 (2)	0.044 (2)	0.006 (2)	0.023 (2)	0.0017 (18)
C13	0.084 (4)	0.038 (2)	0.060 (3)	0.000 (2)	0.045 (3)	0.007 (2)
C14	0.057 (3)	0.032 (2)	0.056 (3)	0.001 (2)	0.027 (2)	0.0026 (18)
C15	0.088 (4)	0.040 (3)	0.090 (4)	0.002 (3)	0.054 (3)	0.008 (3)
C16	0.036 (3)	0.089 (4)	0.074 (3)	0.003 (3)	0.013 (3)	-0.015 (3)
C17	0.041 (3)	0.068 (3)	0.047 (3)	0.007 (2)	0.014 (2)	-0.009 (2)
C18	0.047 (3)	0.076 (3)	0.065 (3)	0.022 (3)	0.014 (3)	0.005 (3)
C19	0.065 (3)	0.061 (3)	0.067 (3)	0.026 (3)	0.028 (3)	0.009 (3)
C20	0.092 (5)	0.073 (4)	0.114 (5)	0.037 (4)	0.029 (4)	0.029 (4)
C21	0.107 (6)	0.172 (8)	0.133 (7)	-0.005 (6)	0.071 (6)	-0.071 (6)
C22	0.098 (5)	0.066 (4)	0.083 (4)	-0.017 (3)	0.057 (3)	-0.029 (3)
C23	0.138 (6)	0.065 (4)	0.067 (3)	-0.017 (4)	0.060 (4)	-0.018 (3)
C24	0.139 (5)	0.041 (3)	0.050 (3)	-0.008 (3)	0.034 (3)	-0.009 (2)
C25	0.203 (8)	0.067 (4)	0.046 (3)	0.003 (5)	0.023 (4)	-0.007 (3)
C26	0.216 (9)	0.057 (4)	0.104 (6)	-0.048 (5)	0.055 (5)	-0.038 (3)
C27	0.132 (5)	0.047 (3)	0.053 (3)	-0.027 (3)	0.018 (4)	-0.008 (2)
C28	0.100 (5)	0.081 (4)	0.072 (4)	-0.046 (4)	-0.002 (4)	-0.003 (3)
C29	0.059 (3)	0.075 (4)	0.085 (4)	-0.024 (3)	0.002 (3)	0.016 (3)
C30	0.045 (7)	0.125 (10)	0.095 (8)	-0.027 (7)	-0.006 (6)	0.026 (9)
C31	0.080 (4)	0.039 (2)	0.047 (3)	0.004 (2)	0.016 (3)	0.002 (2)
C32	0.161 (8)	0.053 (4)	0.099 (5)	0.033 (4)	0.043 (6)	-0.001 (4)
F7A	0.187 (9)	0.081 (5)	0.214 (9)	-0.079 (6)	0.141 (8)	-0.020 (5)
F8A	0.134 (7)	0.160 (9)	0.109 (5)	-0.046 (6)	0.067 (5)	0.064 (6)
F9A	0.081 (5)	0.128 (7)	0.171 (8)	-0.015 (4)	0.088 (6)	0.040 (6)
F13A	0.164 (15)	0.060 (6)	0.142 (12)	0.030 (8)	0.111 (13)	0.005 (7)
F14A	0.179 (11)	0.164 (15)	0.053 (5)	0.025 (11)	0.031 (6)	-0.034 (8)
F15A	0.151 (10)	0.098 (9)	0.121 (11)	-0.025 (9)	0.107 (9)	-0.034 (8)
F22A	0.100 (9)	0.074 (10)	0.20 (2)	0.039 (6)	0.064 (10)	0.076 (11)
F23A	0.18 (2)	0.140 (15)	0.165 (13)	0.048 (15)	-0.041 (14)	0.058 (12)
F24A	0.153 (18)	0.081 (10)	0.218 (16)	0.063 (12)	0.112 (15)	0.041 (11)
F31A	0.334 (19)	0.070 (9)	0.127 (11)	0.035 (12)	0.068 (14)	-0.037 (8)
F32A	0.164 (11)	0.078 (11)	0.104 (7)	-0.009 (8)	0.055 (8)	-0.036 (6)
F33A	0.289 (13)	0.106 (13)	0.21 (2)	-0.119 (11)	0.145 (15)	-0.095 (14)
F34A	0.073 (11)	0.148 (14)	0.35 (3)	-0.052 (11)	0.030 (13)	-0.011 (13)
F35A	0.046 (7)	0.23 (3)	0.29 (2)	0.020 (15)	0.041 (16)	-0.038 (16)
F36A	0.080 (9)	0.212 (17)	0.29 (2)	0.033 (10)	-0.008 (12)	0.103 (16)
C30A	0.054 (8)	0.120 (13)	0.209 (19)	-0.022 (8)	-0.017 (11)	0.008 (11)
C1S	0.33 (3)	0.110 (8)	0.095 (10)	0.000	0.043 (13)	0.000
C2S	0.145 (12)	0.099 (7)	0.083 (7)	0.000	0.011 (8)	0.000

C3S	0.145 (9)	0.122 (6)	0.080 (5)	-0.034 (7)	0.005 (5)	0.003 (4)
C4S	0.108 (7)	0.125 (6)	0.117 (7)	-0.030 (6)	-0.015 (6)	0.029 (5)
C5S	0.082 (9)	0.106 (9)	0.145 (10)	0.000	-0.025 (9)	0.000

Geometric parameters (Å, º)

Gd1—O1	2.316 (3)	O5—C12	1.231 (6)
Gd1—O2	2.311 (3)	O6—C14	1.275 (5)
Gd1—O3	2.394 (3)	O7—C17	1.286 (6)
Gd1—O4	2.422 (3)	O8—C19	1.232 (7)
Gd1—O5	2.335 (3)	O9—C22	1.257 (7)
Gd1—O6	2.483 (3)	O10—C24	1.258 (7)
Gd1—O7	2.407 (3)	O11—C27	1.245 (8)
Gd1—N1	2.502 (4)	O12—C29	1.246 (7)
Gd2—O4	2.473 (3)	N1—C31	1.128 (6)
Gd2—O6	2.516 (3)	C1—C2	1.519 (8)
Gd2—O7	2.418 (3)	C2—C3	1.377 (8)
Gd2—O8	2.386 (3)	C3—C4	1.378 (8)
Gd2—O9	2.337 (4)	C4—C5	1.509 (8)
Gd2—O10	2.307 (4)	C6—C7	1.541 (8)
Gd2—O11	2.319 (4)	C6—F7A	1.328 (7)
Gd2—O12	2.325 (4)	C6—F8A	1.330 (7)
F1—C1	1.302 (6)	C6—F9A	1.285 (7)
F2—C1	1.290 (6)	C7—C8	1.404 (8)
F3—C1	1.305 (6)	C8—C9	1.354 (7)
F4—C5	1.311 (6)	C9—C10	1.494 (7)
F5—C5	1.316 (6)	C11—C12	1.533 (7)
F6—C5	1.310 (6)	C11—F13A	1.304 (8)
F7—C6	1.335 (8)	C11—F14A	1.294 (8)
F8—C6	1.320 (8)	C11—F15A	1.347 (8)
F9—C6	1.346 (8)	C12—C13	1.385 (7)
F10—C10	1.302 (5)	C13—C14	1.374 (7)
F11—C10	1.302 (6)	C14—C15	1.521 (7)
F12—C10	1.302 (6)	C16—C17	1.520 (8)
F13—C11	1.287 (8)	C17—C18	1.351 (8)
F14—C11	1.354 (7)	C18—C19	1.405 (9)
F15—C11	1.307 (7)	C19—C20	1.518 (9)
F16—C15	1.292 (5)	C20—F22A	1.307 (9)
F17—C15	1.333 (5)	C20—F23A	1.323 (9)

F18—C15	1.337 (6)	C20—F24A	1.323 (9)
F19—C16	1.326 (6)	C21—C22	1.474 (11)
F20—C16	1.338 (6)	C22—C23	1.370 (11)
F21—C16	1.317 (6)	C23—C24	1.358 (11)
F22—C20	1.300 (9)	C24—C25	1.520 (10)
F23—C20	1.321 (8)	C26—C27	1.544 (10)
F24—C20	1.295 (8)	C26—F31A	1.309 (16)
F25—C21	1.316 (7)	C26—F32A	1.323 (15)
F26—C21	1.313 (7)	C26—F33A	1.321 (16)
F27—C21	1.318 (8)	C27—C28	1.369 (11)
F28—C25	1.320 (7)	C28—C29	1.379 (11)
F29—C25	1.281 (7)	C29—C30	1.520 (9)
F30—C25	1.309 (7)	C29—C30A	1.507 (10)
F31—C26	1.329 (10)	C31—C32	1.448 (8)
F32—C26	1.333 (10)	F34A—C30A	1.298 (17)
F33—C26	1.342 (10)	F35A—C30A	1.309 (17)
F34—C30	1.332 (15)	F36A—C30A	1.307 (17)
F35—C30	1.341 (15)	C1S—C2S	1.520 (19)
F36—C30	1.336 (16)	C2S—C3S^{i}	1.385 (9)
O1—C2	1.248 (6)	C2S—C3S	1.385 (9)
O2—C4	1.267 (6)	C3S—C4S	1.378 (11)
O3—C7	1.240 (6)	C4S—C5S	1.361 (10)
O4—C9	1.301 (5)		
O1—Gd1—O3	87.03 (13)	F11—C10—F12	104.2 (6)
O1—Gd1—O4	150.95 (11)	F11—C10—C9	114.7 (4)
O1—Gd1—O5	81.47 (13)	F12—C10—C9	110.4 (4)
O1—Gd1—O6	139.69 (11)	F13—C11—F14	102.9 (9)
O1—Gd1—O7	122.77 (12)	F13—C11—F15	110.6 (9)
O1—Gd1—N1	76.79 (13)	F13—C11—C12	113.2 (8)
O2—Gd1—O1	73.46 (12)	F14—C11—C12	109.9 (6)
O2—Gd1—O3	128.85 (13)	F15—C11—F14	103.8 (8)
O2—Gd1—O4	135.35 (11)	F15—C11—C12	115.3 (6)
O2—Gd1—O5	79.80 (12)	F13A—C11—C12	109.0 (11)
O2—Gd1—O6	72.90 (11)	F13A—C11—F15A	100.0 (12)
O2—Gd1—O7	75.57 (12)	F14A—C11—C12	108.0 (8)
O2—Gd1—N1	140.80 (13)	F14A—C11—F13A	118.8 (15)
O3—Gd1—O4	71.44 (11)	F14A—C11—F15A	109.0 (12)
O3—Gd1—O6	131.92 (11)	F15A—C11—C12	112.0 (7)
O3—Gd1—O7	76.73 (12)	O5—C12—C11	114.5 (4)

O3—Gd1—N1	73.47 (14)	O5—C12—C13	127.4 (5)
O4—Gd1—O6	67.09 (10)	C13—C12—C11	118.1 (4)
O4—Gd1—N1	78.48 (12)	C14—C13—C12	122.8 (5)
O5—Gd1—O3	144.27 (12)	O6—C14—C13	127.5 (4)
O5—Gd1—O4	104.55 (12)	O6—C14—C15	115.0 (4)
O5—Gd1—O6	71.29 (10)	C13—C14—C15	117.4 (4)
O5—Gd1—O7	137.20 (11)	F16—C15—F17	108.4 (5)
O5—Gd1—N1	70.99 (13)	F16—C15—F18	104.8 (5)
O6—Gd1—N1	119.08 (13)	F16—C15—C14	114.0 (4)
O7—Gd1—O4	71.93 (10)	F17—C15—F18	106.7 (4)
O7—Gd1—O6	68.27 (11)	F17—C15—C14	112.1 (4)
O7—Gd1—N1	143.24 (12)	F18—C15—C14	110.3 (5)
O4—Gd2—O6	65.83 (9)	F19—C16—F20	106.8 (5)
O7—Gd2—O4	70.89 (10)	F19—C16—C17	110.9 (4)
O7—Gd2—O6	67.56 (10)	F20—C16—C17	110.1 (4)
O8—Gd2—O4	136.28 (12)	F21—C16—F19	107.5 (5)
O8—Gd2—O6	80.32 (11)	F21—C16—F20	107.7 (5)
O8—Gd2—O7	71.04 (12)	F21—C16—C17	113.5 (5)
O9—Gd2—O4	111.86 (13)	O7—C17—C16	112.7 (5)
O9—Gd2—O6	136.92 (12)	O7—C17—C18	127.4 (5)
O9—Gd2—O7	71.34 (12)	C18—C17—C16	119.9 (5)
O9—Gd2—O8	74.68 (14)	C17—C18—C19	122.3 (5)
O10—Gd2—O4	76.63 (12)	O8—C19—C18	127.0 (5)
O10—Gd2—O6	139.36 (12)	O8—C19—C20	115.6 (6)
O10—Gd2—O7	114.83 (14)	C18—C19—C20	117.4 (6)
O10—Gd2—O8	140.16 (13)	F22—C20—F23	108.5 (13)
O10—Gd2—O9	71.00 (16)	F22—C20—C19	112.1 (9)
O10—Gd2—O11	79.56 (14)	F23—C20—C19	108.9 (6)
O10—Gd2—O12	82.21 (16)	F24—C20—F22	106.7 (11)
O11—Gd2—O4	147.66 (13)	F24—C20—F23	104.7 (9)
O11—Gd2—O6	126.38 (13)	F24—C20—C19	115.7 (8)
O11—Gd2—O7	140.14 (14)	F22A—C20—C19	114.1 (9)
O11—Gd2—O8	75.11 (14)	F22A—C20—F23A	114.2 (17)
O11—Gd2—O9	80.02 (16)	F22A—C20—F24A	97.8 (13)
O11—Gd2—O12	73.13 (16)	F23A—C20—C19	113.5 (11)
O12—Gd2—O4	82.18 (12)	F23A—C20—F24A	108.0 (18)
O12—Gd2—O6	77.97 (13)	F24A—C20—C19	107.6 (10)
O12—Gd2—O7	142.54 (13)	F25—C21—F27	103.7 (10)
O12—Gd2—O8	118.04 (14)	F25—C21—C22	113.6 (7)
O12—Gd2—O9	144.98 (15)	F26—C21—F25	108.2 (7)

C2—O1—Gd1	134.7 (3)	F26—C21—F27	101.9 (8)
C4—O2—Gd1	134.6 (3)	F26—C21—C22	116.6 (8)
C7—O3—Gd1	132.1 (4)	F27—C21—C22	111.4 (7)
C9—O4—Gd1	124.2 (3)	O9—C22—C21	113.6 (7)
C9—O4—Gd2	130.6 (3)	O9—C22—C23	126.9 (7)
C12—O5—Gd1	134.9 (3)	C23—C22—C21	119.5 (6)
C14—O6—Gd1	128.2 (3)	C24—C23—C22	120.6 (6)
C14—O6—Gd2	135.5 (3)	O10—C24—C23	127.4 (6)
C17—O7—Gd1	126.7 (3)	O10—C24—C25	113.0 (7)
C17—O7—Gd2	128.9 (3)	C23—C24—C25	119.6 (6)
C19—O8—Gd2	133.2 (4)	F28—C25—C24	112.7 (7)
C22—O9—Gd2	135.5 (5)	F29—C25—F28	109.5 (7)
C24—O10—Gd2	135.6 (4)	F29—C25—F30	103.8 (9)
C27—O11—Gd2	133.5 (5)	F29—C25—C24	113.8 (6)
C29—O12—Gd2	134.7 (5)	F30—C25—F28	104.3 (7)
C31—N1—Gd1	162.4 (4)	F30—C25—C24	111.9 (6)
F1—C1—F3	102.4 (7)	F31—C26—F32	104.5 (16)
F1—C1—C2	111.1 (5)	F31—C26—F33	111 (2)
F2—C1—F1	109.8 (7)	F31—C26—C27	104.7 (11)
F2—C1—F3	105.6 (7)	F32—C26—F33	111 (2)
F2—C1—C2	114.0 (6)	F32—C26—C27	117.3 (12)
F3—C1—C2	113.2 (5)	F33—C26—C27	108.5 (14)
O1—C2—C1	113.2 (5)	F31A—C26—C27	116.6 (14)
O1—C2—C3	127.8 (5)	F31A—C26—F32A	105.7 (16)
C3—C2—C1	119.1 (5)	F31A—C26—F33A	101 (2)
C2—C3—C4	121.6 (5)	F32A—C26—C27	105.7 (10)
O2—C4—C3	127.2 (5)	F33A—C26—C27	115.3 (15)
O2—C4—C5	113.1 (5)	F33A—C26—F32A	112.1 (17)
C3—C4—C5	119.7 (5)	O11—C27—C26	112.9 (8)
F4—C5—F5	105.8 (6)	O11—C27—C28	128.3 (6)
F4—C5—C4	114.5 (5)	C28—C27—C26	118.8 (7)
F5—C5—C4	110.4 (5)	C27—C28—C29	121.7 (6)
F6—C5—F4	106.0 (5)	O12—C29—C28	126.8 (7)
F6—C5—F5	107.3 (6)	O12—C29—C30	110.1 (9)
F6—C5—C4	112.4 (5)	O12—C29—C30A	119.7 (10)
F7—C6—F9	100.9 (12)	C28—C29—C30	122.7 (9)
F7—C6—C7	110.6 (9)	C28—C29—C30A	112.9 (10)
F8—C6—F7	121.7 (15)	F34—C30—F35	102.3 (15)
F8—C6—F9	103.7 (15)	F34—C30—F36	99.3 (15)
F8—C6—C7	114.2 (14)	F34—C30—C29	117.7 (15)

F9—C6—C7	102.6 (11)	F35—C30—C29	115.3 (13)
F7A—C6—C7	109.7 (6)	F36—C30—F35	103.6 (14)
F7A—C6—F8A	101.8 (9)	F36—C30—C29	116.2 (13)
F8A—C6—C7	112.4 (6)	N1—C31—C32	179.5 (8)
F9A—C6—C7	112.7 (6)	F34A—C30A—C29	107.3 (17)
F9A—C6—F7A	112.7 (9)	F34A—C30A—F35A	112 (2)
F9A—C6—F8A	107.0 (9)	F34A—C30A—F36A	110 (2)
O3—C7—C6	114.3 (5)	F35A—C30A—C29	105.6 (14)
O3—C7—C8	126.7 (5)	F36A—C30A—C29	107.9 (14)
C8—C7—C6	118.9 (5)	F36A—C30A—F35A	114 (2)
C9—C8—C7	123.0 (5)	C3S^{i}—C2S—C1S	120.5 (6)
O4—C9—C8	125.9 (5)	C3S—C2S—C1S	120.5 (6)
O4—C9—C10	115.5 (4)	C3S—C2S—C3S^{i}	119.1 (13)
C8—C9—C10	118.4 (4)	C4S—C3S—C2S	119.9 (10)
F10—C10—F12	106.5 (6)	C5S—C4S—C3S	120.4 (11)
F10—C10—C9	114.4 (5)	C4S—C5S—C4S^{i}	120.3 (14)
F11—C10—F10	105.9 (5)		

Symmetry code: (i) -*x*+1, *y*, -*z*+3/2.

8.3.7 Crystallographic data for 6-Y (solv.)

Abstract

Chemical context

Structural commentary

Supra-molecular features

Database survey

Synthesis and crystallization

Refinement

Crystal data, data collection and structure refinement details are summarized in Table 1.

Computing details

Data collection: *APEX3* Ver. 2016.9-0 (Bruker-AXS, 2016); cell refinement: *SAINT* V8.37A (Bruker-AXS, 2016); data reduction: *APEX3* Ver. 2016.9-0 (Bruker-AXS, 2016); program(s) used to solve structure: XT (Sheldrick, 2015); program(s) used to refine structure: *SHELXL* (Sheldrick, 2015); molecular graphics: Olex2 (Dolomanov *et al.*, 2009); software used to prepare material for publication: Olex2 (Dolomanov *et al.*, 2009).

References

Dolomanov, O. V., Bourhis, L. J., Gildea, R. J., Howard, J. A. K. & Puschmann, H. (2009). *J. Appl. Cryst.* **42**, 339–341.

Sheldrick, G. M. (2015). *Acta Cryst.* A**71**, 3–8.

Sheldrick, G. M. (2015). *Acta Cryst.* C**71**, 3–8.

(mo_sh01_335_r1_150k_0m)

Crystal data

$C_{28}H_{42}F_6KO_8S_2Y \cdot C_6H_{14}$	$Z = 2$
$M_r = 898.91$	$F(000) = 936$
Triclinic, $P\bar{1}$	$D_x = 1.382$ Mg m^{-3}
$a = 12.2707$ (6) Å	Mo $K\alpha$ radiation, $\lambda = 0.71073$ Å
$b = 13.5440$ (6) Å	Cell parameters from 9886 reflections
$c = 13.9340$ (6) Å	$\theta = 2.3$–$28.1°$
$\alpha = 68.992$ (2)°	$\mu = 1.61$ mm^{-1}
$\beta = 89.689$ (2)°	$T = 150$ K
$\gamma = 88.097$ (2)°	Block, colourless
$V = 2160.58$ (17) Å^3	0.3 × 0.24 × 0.08 mm

Data collection

Bruker D8 VENTURE diffractometer	10646 independent reflections
Radiation source: microfocus sealed tube, INCOATEC Iμs 3.0	8223 reflections with $I > 2\sigma(I)$
Multilayer mirror optics monochromator	$R_{int} = 0.043$
Detector resolution: 7.4074 pixels mm^{-1}	$\theta_{max} = 28.3°$, $\theta_{min} = 2.3°$
ϕ and ω scans	$h = -16 \rightarrow 16$
Absorption correction: multi-scan *SADABS2016*/2 (Bruker,2016/2) was used for absorption correction. wR2(int) was 0.0894 before and 0.0620 after correction. The Ratio of	$k = -17 \rightarrow 18$

minimum to maximum transmission is 0.7995. The λ/2 correction factor is Not present.	
T_{min} = 0.596, T_{max} = 0.746	l = -18→17
27678 measured reflections	

Refinement

Refinement on F^2	Primary atom site location: dual
Least-squares matrix: full	Hydrogen site location: inferred from neighbouring sites
$R[F^2 > 2\sigma(F^2)]$ = 0.045	H-atom parameters constrained
$wR(F^2)$ = 0.120	$w = 1/[\sigma^2(F_o^2) + (0.0597P)^2 + 0.4608P]$ where $P = (F_o^2 + 2F_c^2)/3$
S = 1.02	$(\Delta/\sigma)_{max}$ = 0.002
10646 reflections	$\Delta\rangle_{max}$ = 0.48 e Å^{-3}
498 parameters	$\Delta\rangle_{min}$ = -0.42 e Å^{-3}
162 restraints	

Special details

Geometry. All esds (except the esd in the dihedral angle between two l.s. planes) are estimated using the full covariance matrix. The cell esds are taken into account individually in the estimation of esds in distances, angles and torsion angles; correlations between esds in cell parameters are only used when they are defined by crystal symmetry. An approximate (isotropic) treatment of cell esds is used for estimating esds involving l.s. planes.

Fractional atomic coordinates and isotropic or equivalent isotropic displacement parameters (Å²)

	x	*y*	*z*	U_{iso}*/U_{eq}	Occ. (<1)
Y1	0.73661 (2)	0.75612 (2)	0.84369 (2)	0.03038 (8)	
K1	0.57100 (5)	0.90347 (4)	0.42299 (4)	0.03397 (13)	
S1	0.46986 (5)	0.82499 (5)	0.72122 (5)	0.03552 (15)	
S2	0.73532 (5)	0.98856 (5)	0.61293 (5)	0.03356 (15)	
F1	0.34760 (19)	0.68912 (18)	0.85442 (15)	0.0825 (7)	
F2	0.3967 (2)	0.64357 (17)	0.72910 (18)	0.0808 (7)	
F3	0.27400 (17)	0.76525 (19)	0.70675 (19)	0.0856 (7)	
F4	0.85934 (17)	1.12039 (15)	0.65462 (16)	0.0650 (5)	
F5	0.82787 (19)	1.15816 (17)	0.49494 (16)	0.0819 (7)	
F6	0.94000 (15)	1.03088 (17)	0.57541 (17)	0.0693 (6)	
O1	0.56213 (15)	0.76605 (14)	0.78328 (14)	0.0406 (4)	

O2	0.42622 (17)	0.90745 (15)	0.75226 (16)	0.0496 (5)	
O3	0.48507 (17)	0.85206 (17)	0.61352 (14)	0.0507 (5)	
O4	0.77163 (15)	0.90940 (14)	0.71046 (13)	0.0390 (4)	
O5	0.64299 (16)	1.05084 (16)	0.62257 (16)	0.0477 (5)	
O6	0.73361 (17)	0.95009 (17)	0.53040 (15)	0.0488 (5)	
O7	0.5140 (2)	0.7120 (2)	0.4306 (3)	0.0872 (9)	
O8	0.73150 (19)	0.85611 (19)	0.31049 (17)	0.0600 (6)	
C1	0.8140 (2)	0.7470 (2)	1.0190 (2)	0.0428 (6)	
H1	0.878812	0.707595	1.039917	0.051*	
C2	0.7083 (3)	0.7076 (2)	1.04224 (19)	0.0421 (6)	
C3	0.6338 (2)	0.7924 (2)	0.99715 (19)	0.0384 (6)	
C4	0.6931 (2)	0.8842 (2)	0.94555 (19)	0.0356 (6)	
C5	0.8056 (2)	0.8555 (2)	0.95926 (19)	0.0386 (6)	
C6	0.6797 (3)	0.5970 (3)	1.1110 (2)	0.0638 (10)	
H6A	0.618073	0.574805	1.082671	0.096*	
H6B	0.661946	0.596757	1.178334	0.096*	
H6C	0.740765	0.549342	1.115808	0.096*	
C7	0.5114 (3)	0.7877 (3)	1.0101 (2)	0.0516 (8)	
H7A	0.476743	0.842492	0.953171	0.077*	
H7B	0.491917	0.797736	1.072936	0.077*	
H7C	0.487807	0.719999	1.012568	0.077*	
C8	0.6449 (3)	0.9940 (2)	0.8920 (2)	0.0516 (8)	
H8A	0.696189	1.035808	0.843236	0.077*	
H8B	0.628561	1.026192	0.941779	0.077*	
H8C	0.579093	0.989991	0.856726	0.077*	
C9	0.8985 (3)	0.9281 (3)	0.9198 (2)	0.0554 (8)	
H9A	0.962977	0.887361	0.916573	0.083*	
H9B	0.911119	0.965683	0.965284	0.083*	
H9C	0.880817	0.977743	0.852389	0.083*	
C10	0.8289 (3)	0.5708 (2)	0.8993 (2)	0.0510 (8)	
H10	0.833042	0.534128	0.969835	0.061*	
C11	0.9095 (3)	0.6386 (2)	0.8395 (2)	0.0486 (7)	
C12	0.8727 (3)	0.6770 (2)	0.7372 (2)	0.0444 (7)	
C13	0.7691 (3)	0.6339 (2)	0.7343 (2)	0.0447 (7)	
C14	0.7433 (3)	0.5679 (2)	0.8361 (2)	0.0473 (7)	
C15	1.0195 (3)	0.6587 (3)	0.8763 (3)	0.0709 (11)	
H15A	1.030166	0.733562	0.852760	0.106*	
H15B	1.075891	0.625440	0.849286	0.106*	
H15C	1.022209	0.630025	0.950018	0.106*	
C16	0.9359 (3)	0.7458 (3)	0.6464 (3)	0.0631 (9)	

H16A	0.886157	0.789479	0.594363	0.095*	
H16B	0.979524	0.701965	0.619040	0.095*	
H16C	0.982464	0.789790	0.667710	0.095*	
C17	0.7040 (3)	0.6502 (3)	0.6388 (3)	0.0613 (9)	
H17A	0.628427	0.639132	0.656166	0.092*	
H17B	0.729513	0.600758	0.607991	0.092*	
H17C	0.712386	0.721048	0.591190	0.092*	
C18	0.6422 (3)	0.5038 (3)	0.8691 (3)	0.0710 (11)	
H18A	0.635368	0.480776	0.942425	0.106*	
H18B	0.647836	0.443277	0.848640	0.106*	
H18C	0.579250	0.546704	0.837047	0.106*	
C19	0.3657 (3)	0.7249 (3)	0.7546 (2)	0.0549 (8)	
C20	0.8477 (3)	1.0790 (2)	0.5835 (2)	0.0470 (7)	
C21	0.4083 (4)	0.6784 (4)	0.4633 (4)	0.0961 (15)	
H21C	0.367235	0.730516	0.482976	0.115*	0.673 (13)
H21D	0.410095	0.611124	0.520217	0.115*	0.673 (13)
H21A	0.360957	0.739112	0.457498	0.115*	0.327 (13)
H21B	0.410339	0.631594	0.534742	0.115*	0.327 (13)
C22	0.3627 (10)	0.6685 (10)	0.3689 (8)	0.124 (4)	0.673 (13)
H22A	0.340285	0.736869	0.318951	0.149*	0.673 (13)
H22B	0.301597	0.621849	0.384244	0.149*	0.673 (13)
C23	0.4655 (8)	0.6186 (9)	0.3307 (8)	0.113 (3)	0.673 (13)
H23A	0.462477	0.542142	0.353773	0.136*	0.673 (13)
H23B	0.471193	0.647231	0.256393	0.136*	0.673 (13)
C24	0.5557 (7)	0.6512 (7)	0.3797 (9)	0.098 (3)	0.673 (13)
H24A	0.594086	0.589368	0.427224	0.117*	0.673 (13)
H24B	0.606804	0.690960	0.328057	0.117*	0.673 (13)
C25	0.7177 (3)	0.8957 (4)	0.2009 (3)	0.0742 (11)	
H25A	0.642577	0.918891	0.182366	0.089*	
H25B	0.737190	0.841150	0.173365	0.089*	
C26	0.7914 (4)	0.9864 (4)	0.1600 (3)	0.0959 (15)	
H26C	0.749672	1.051315	0.124656	0.115*	0.739 (14)
H26D	0.843023	0.974163	0.112106	0.115*	0.739 (14)
H26A	0.809028	1.001818	0.088232	0.115*	0.261 (14)
H26B	0.762121	1.049708	0.169322	0.115*	0.261 (14)
C27	0.8510 (6)	0.9940 (7)	0.2527 (5)	0.086 (3)	0.739 (14)
H27A	0.927171	1.009804	0.237942	0.103*	0.739 (14)
H27B	0.816759	1.046744	0.276158	0.103*	0.739 (14)
C28	0.8380 (3)	0.8833 (4)	0.3296 (3)	0.0713 (11)	
H28C	0.892555	0.834785	0.319059	0.086*	0.739 (14)

H28D	0.844511	0.882066	0.399366	0.086*	0.739 (14)
H28A	0.881619	0.820277	0.366958	0.086*	0.261 (14)
H28B	0.834572	0.929007	0.369614	0.086*	0.261 (14)
C22A	0.365 (2)	0.622 (2)	0.3986 (12)	0.114 (5)	0.327 (13)
H22C	0.286124	0.627934	0.393658	0.137*	0.327 (13)
H22D	0.388523	0.548088	0.423458	0.137*	0.327 (13)
C23A	0.4180 (18)	0.684 (2)	0.2986 (13)	0.120 (5)	0.327 (13)
H23C	0.422202	0.643835	0.253270	0.143*	0.327 (13)
H23D	0.378616	0.750545	0.263914	0.143*	0.327 (13)
C24A	0.5266 (18)	0.701 (2)	0.3309 (13)	0.112 (5)	0.327 (13)
H24C	0.575757	0.642069	0.336105	0.135*	0.327 (13)
H24D	0.556080	0.765169	0.281544	0.135*	0.327 (13)
C27A	0.8848 (11)	0.9384 (19)	0.2286 (10)	0.085 (6)	0.261 (14)
H27C	0.925564	0.889075	0.204848	0.102*	0.261 (14)
H27D	0.933272	0.992445	0.231406	0.102*	0.261 (14)
C1S	0.8162 (5)	0.2422 (5)	0.9028 (5)	0.124 (2)*	
H1SA	0.757871	0.268530	0.934243	0.187*	0.529 (9)
H1SB	0.787664	0.195814	0.871509	0.187*	0.529 (9)
H1SC	0.869268	0.204129	0.954247	0.187*	0.529 (9)
H1SD	0.796075	0.169530	0.929247	0.187*	0.471 (9)
H1SE	0.840355	0.262433	0.958391	0.187*	0.471 (9)
H1SF	0.754261	0.286120	0.869573	0.187*	0.471 (9)
C2S	0.8679 (8)	0.3316 (8)	0.8239 (7)	0.094 (3)*	0.529 (9)
H2SA	0.890577	0.377942	0.858833	0.113*	0.529 (9)
H2SB	0.809827	0.369714	0.776960	0.113*	0.529 (9)
C3S	0.9604 (8)	0.3242 (8)	0.7586 (8)	0.103 (3)*	0.529 (9)
H3SA	1.013061	0.273867	0.803268	0.124*	0.529 (9)
H3SB	0.933252	0.292023	0.711768	0.124*	0.529 (9)
C4S	1.0157 (6)	0.4076 (6)	0.7020 (6)	0.160 (3)*	
H4SA	1.032657	0.442988	0.749272	0.192*	0.529 (9)
H4SB	0.961651	0.453276	0.654790	0.192*	0.529 (9)
H4SC	1.069582	0.350244	0.714600	0.192*	0.471 (9)
H4SD	0.975471	0.409281	0.641680	0.192*	0.471 (9)
C5S	1.1151 (12)	0.4183 (12)	0.6389 (12)	0.186 (7)*	0.529 (9)
H5SA	1.171490	0.372114	0.682312	0.224*	0.529 (9)
H5SB	1.099457	0.390842	0.585190	0.224*	0.529 (9)
C6S	1.1607 (7)	0.5198 (7)	0.5906 (6)	0.173 (3)*	
H6SA	1.224402	0.512955	0.552885	0.260*	0.529 (9)
H6SB	1.107927	0.566702	0.544402	0.260*	0.529 (9)
H6SC	1.180382	0.547863	0.642094	0.260*	0.529 (9)

H6SD	1.185022	0.588366	0.584561	0.260*	0.471 (9)
H6SE	1.220541	0.469091	0.612080	0.260*	0.471 (9)
H6SF	1.133626	0.522206	0.525257	0.260*	0.471 (9)
C2T	0.9002 (11)	0.2548 (10)	0.8321 (10)	0.130 (5)*	0.471 (9)
H2TA	0.875997	0.233138	0.776717	0.156*	0.471 (9)
H2TB	0.962160	0.209432	0.865607	0.156*	0.471 (9)
C3T	0.9335 (9)	0.3628 (7)	0.7901 (8)	0.078 (3)*	0.471 (9)
H3TA	0.961554	0.378702	0.847660	0.094*	0.471 (9)
H3TB	0.866941	0.405597	0.768035	0.094*	0.471 (9)
C5T	1.0710 (12)	0.4878 (12)	0.6690 (12)	0.150 (6)*	0.471 (9)
H5TA	1.102872	0.493309	0.730373	0.180*	0.471 (9)
H5TB	1.017262	0.545627	0.644853	0.180*	0.471 (9)

Atomic displacement parameters (Å²)

	U^{11}	U^{22}	U^{33}	U^{12}	U^{13}	U^{23}
Y1	0.03621 (15)	0.02953 (13)	0.02417 (12)	0.00458 (10)	-0.00146 (9)	-0.00861 (9)
K1	0.0341 (3)	0.0370 (3)	0.0322 (3)	-0.0004 (2)	0.0001 (2)	-0.0142 (2)
S1	0.0325 (4)	0.0370 (3)	0.0311 (3)	-0.0045 (3)	0.0012 (3)	-0.0047 (2)
S2	0.0307 (3)	0.0373 (3)	0.0288 (3)	-0.0060 (3)	-0.0006 (2)	-0.0067 (2)
F1	0.0908 (17)	0.0931 (16)	0.0491 (11)	-0.0485 (13)	0.0191 (11)	-0.0045 (10)
F2	0.0974 (18)	0.0601 (13)	0.0886 (16)	-0.0322 (12)	0.0011 (13)	-0.0287 (11)
F3	0.0453 (12)	0.0997 (17)	0.0915 (17)	-0.0228 (11)	-0.0161 (11)	-0.0075 (13)
F4	0.0690 (13)	0.0624 (12)	0.0754 (13)	-0.0227 (10)	-0.0002 (10)	-0.0371 (10)
F5	0.0833 (16)	0.0710 (14)	0.0613 (12)	-0.0345 (12)	0.0023 (11)	0.0155 (10)
F6	0.0355 (10)	0.0881 (15)	0.0922 (15)	-0.0149 (10)	0.0148 (10)	-0.0410 (12)
O1	0.0398 (11)	0.0386 (10)	0.0418 (10)	0.0012 (8)	-0.0057 (8)	-0.0126 (8)
O2	0.0462 (12)	0.0410 (11)	0.0564 (13)	0.0062 (9)	0.0039 (10)	-0.0120 (9)
O3	0.0491 (13)	0.0624 (13)	0.0319 (10)	-0.0101 (10)	0.0033 (9)	-0.0056 (9)
O4	0.0439 (11)	0.0369 (10)	0.0311 (9)	-0.0006 (8)	-0.0006 (8)	-0.0062 (7)
O5	0.0335 (11)	0.0481 (11)	0.0530 (12)	0.0030 (9)	0.0013 (9)	-0.0082 (9)
O6	0.0501 (13)	0.0621 (13)	0.0365 (10)	-0.0126 (10)	-0.0040 (9)	-0.0196 (9)
O7	0.083 (2)	0.0771 (19)	0.126 (3)	-0.0204 (16)	0.0159 (18)	-0.0646 (19)
O8	0.0558 (14)	0.0786 (16)	0.0529 (13)	-0.0066 (12)	0.0130 (11)	-0.0322 (12)
C1	0.0455 (17)	0.0541 (17)	0.0286 (13)	0.0102 (13)	-0.0084 (12)	-0.0155 (11)
C2	0.0562 (19)	0.0423 (15)	0.0261 (12)	0.0013 (13)	0.0032 (12)	-0.0104 (10)
C3	0.0428 (16)	0.0478 (15)	0.0280 (12)	-0.0042 (12)	0.0058 (11)	-0.0173 (11)
C4	0.0442 (16)	0.0366 (13)	0.0304 (12)	0.0012 (11)	0.0016 (11)	-0.0176 (10)
C5	0.0416 (16)	0.0493 (16)	0.0295 (12)	-0.0045 (12)	-0.0003 (11)	-0.0192 (11)

C6	0.095 (3)	0.0515 (19)	0.0360 (16)	-0.0035 (18)	0.0115 (17)	-0.0047 (13)
C7	0.0486 (19)	0.065 (2)	0.0444 (16)	-0.0061 (15)	0.0147 (14)	-0.0226 (14)
C8	0.065 (2)	0.0416 (16)	0.0522 (17)	0.0031 (14)	0.0038 (15)	-0.0215 (13)
C9	0.0490 (19)	0.075 (2)	0.0497 (18)	-0.0153 (16)	0.0036 (15)	-0.0307 (16)
C10	0.072 (2)	0.0340 (15)	0.0403 (15)	0.0214 (14)	-0.0019 (15)	-0.0075 (12)
C11	0.0505 (18)	0.0487 (17)	0.0472 (16)	0.0235 (14)	-0.0089 (14)	-0.0200 (13)
C12	0.0507 (18)	0.0462 (16)	0.0372 (14)	0.0174 (13)	0.0018 (13)	-0.0177 (12)
C13	0.0552 (19)	0.0415 (15)	0.0416 (15)	0.0133 (13)	-0.0033 (13)	-0.0213 (12)
C14	0.064 (2)	0.0305 (14)	0.0474 (16)	0.0084 (13)	0.0009 (15)	-0.0146 (12)
C15	0.051 (2)	0.089 (3)	0.076 (3)	0.0314 (19)	-0.0175 (18)	-0.035 (2)
C16	0.062 (2)	0.070 (2)	0.0526 (19)	0.0151 (18)	0.0173 (17)	-0.0179 (16)
C17	0.077 (2)	0.065 (2)	0.056 (2)	0.0114 (18)	-0.0124 (18)	-0.0400 (17)
C18	0.088 (3)	0.0402 (18)	0.084 (3)	-0.0068 (18)	0.012 (2)	-0.0201 (17)
C19	0.051 (2)	0.0554 (19)	0.0488 (18)	-0.0174 (15)	-0.0011 (15)	-0.0051 (14)
C20	0.0410 (17)	0.0525 (17)	0.0434 (16)	-0.0134 (14)	0.0016 (13)	-0.0112 (13)
C21	0.113 (4)	0.071 (3)	0.114 (4)	-0.020 (3)	0.023 (3)	-0.044 (3)
C22	0.118 (6)	0.149 (8)	0.090 (6)	-0.033 (7)	-0.017 (5)	-0.021 (6)
C23	0.159 (7)	0.126 (6)	0.082 (5)	-0.053 (5)	0.025 (5)	-0.067 (5)
C24	0.103 (6)	0.060 (4)	0.152 (8)	-0.013 (4)	0.038 (6)	-0.064 (5)
C25	0.069 (3)	0.116 (3)	0.057 (2)	0.007 (2)	-0.0004 (19)	-0.056 (2)
C26	0.099 (4)	0.130 (4)	0.048 (2)	-0.008 (3)	0.019 (2)	-0.019 (2)
C27	0.057 (4)	0.108 (6)	0.083 (4)	-0.023 (4)	0.010 (3)	-0.023 (4)
C28	0.051 (2)	0.111 (3)	0.054 (2)	0.006 (2)	0.0020 (17)	-0.032 (2)
C22A	0.123 (9)	0.141 (10)	0.081 (8)	-0.074 (8)	0.005 (7)	-0.037 (8)
C23A	0.136 (10)	0.152 (10)	0.067 (8)	-0.007 (9)	0.009 (8)	-0.034 (8)
C24A	0.129 (10)	0.123 (11)	0.101 (9)	-0.037 (9)	0.024 (9)	-0.058 (8)
C27A	0.060 (10)	0.106 (13)	0.095 (11)	-0.018 (9)	0.021 (8)	-0.043 (10)

Geometric parameters (Å, º)

Y1—O1	2.2869 (19)	C18—H18A	0.9600
Y1—O4	2.2865 (17)	C18—H18B	0.9600
Y1—C1	2.586 (3)	C18—H18C	0.9600
Y1—C2	2.628 (3)	C21—H21C	0.9700
Y1—C3	2.662 (3)	C21—H21D	0.9700
Y1—C4	2.646 (2)	C21—H21A	0.9700
Y1—C5	2.602 (3)	C21—H21B	0.9700
Y1—C10	2.571 (3)	C21—C22	1.482 (9)
Y1—C11	2.622 (3)	C21—C22A	1.482 (13)

Y1—C12	2.672 (3)	C22—H22A	0.9700
Y1—C13	2.642 (3)	C22—H22B	0.9700
Y1—C14	2.587 (3)	C22—C23	1.589 (11)
K1—K1^{i}	4.2613 (11)	C23—H23A	0.9700
K1—S1^{i}	3.5220 (8)	C23—H23B	0.9700
K1—O2^{i}	2.836 (2)	C23—C24	1.463 (9)
K1—O3^{i}	3.216 (2)	C24—H24A	0.9700
K1—O3	2.709 (2)	C24—H24B	0.9700
K1—O5^{i}	2.704 (2)	C25—H25A	0.9700
K1—O6	2.723 (2)	C25—H25B	0.9700
K1—O7	2.674 (3)	C25—C26	1.489 (6)
K1—O8	2.711 (2)	C26—H26C	0.9700
K1—C24A	3.47 (2)	C26—H26D	0.9700
S1—O1	1.4569 (19)	C26—H26A	0.9700
S1—O2	1.423 (2)	C26—H26B	0.9700
S1—O3	1.424 (2)	C26—C27	1.525 (7)
S1—C19	1.829 (3)	C26—C27A	1.472 (12)
S2—O4	1.4577 (18)	C27—H27A	0.9700
S2—O5	1.425 (2)	C27—H27B	0.9700
S2—O6	1.423 (2)	C27—C28	1.510 (7)
S2—C20	1.821 (3)	C28—H28C	0.9700
F1—C19	1.319 (4)	C28—H28D	0.9700
F2—C19	1.318 (4)	C28—H28A	0.9700
F3—C19	1.309 (4)	C28—H28B	0.9700
F4—C20	1.312 (3)	C28—C27A	1.460 (12)
F5—C20	1.330 (3)	C22A—H22C	0.9700
F6—C20	1.313 (4)	C22A—H22D	0.9700
O7—C21	1.408 (5)	C22A—C23A	1.502 (13)
O7—C24	1.354 (7)	C23A—H23C	0.9700
O7—C24A	1.455 (12)	C23A—H23D	0.9700
O8—C25	1.434 (4)	C23A—C24A	1.462 (13)
O8—C28	1.421 (4)	C24A—H24C	0.9700
C1—H1	0.9300	C24A—H24D	0.9700
C1—C2	1.411 (4)	C27A—H27C	0.9700
C1—C5	1.406 (4)	C27A—H27D	0.9700
C2—C3	1.402 (4)	C1S—H1SA	0.9600
C2—C6	1.512 (4)	C1S—H1SB	0.9600
C3—C4	1.416 (4)	C1S—H1SC	0.9600
C3—C7	1.513 (4)	C1S—H1SD	0.9600
C4—C5	1.416 (4)	C1S—H1SE	0.9600

C4—C8	1.507 (4)	C1S—H1SF	0.9600
C5—C9	1.499 (4)	C1S—C2S	1.472 (9)
C6—H6A	0.9600	C1S—C2T	1.394 (11)
C6—H6B	0.9600	C2S—H2SA	0.9700
C6—H6C	0.9600	C2S—H2SB	0.9700
C7—H7A	0.9600	C2S—C3S	1.474 (11)
C7—H7B	0.9600	C3S—H3SA	0.9700
C7—H7C	0.9600	C3S—H3SB	0.9700
C8—H8A	0.9600	C3S—C4S	1.330 (9)
C8—H8B	0.9600	C4S—H4SA	0.9700
C8—H8C	0.9600	C4S—H4SB	0.9700
C9—H9A	0.9600	C4S—H4SC	0.9700
C9—H9B	0.9600	C4S—H4SD	0.9700
C9—H9C	0.9600	C4S—C5S	1.480 (12)
C10—H10	0.9300	C4S—C3T	1.545 (12)
C10—C11	1.419 (5)	C4S—C5T	1.239 (12)
C10—C14	1.385 (4)	C5S—H5SA	0.9700
C11—C12	1.403 (4)	C5S—H5SB	0.9700
C11—C15	1.514 (5)	C5S—C6S	1.427 (12)
C12—C13	1.423 (4)	C6S—H6SA	0.9600
C12—C16	1.504 (4)	C6S—H6SB	0.9600
C13—C14	1.420 (4)	C6S—H6SC	0.9600
C13—C17	1.498 (4)	C6S—H6SD	0.9600
C14—C18	1.511 (5)	C6S—H6SE	0.9600
C15—H15A	0.9600	C6S—H6SF	0.9600
C15—H15B	0.9600	C6S—C5T	1.508 (12)
C15—H15C	0.9600	C2T—H2TA	0.9700
C16—H16A	0.9600	C2T—H2TB	0.9700
C16—H16B	0.9600	C2T—C3T	1.439 (13)
C16—H16C	0.9600	C3T—H3TA	0.9700
C17—H17A	0.9600	C3T—H3TB	0.9700
C17—H17B	0.9600	C5T—H5TA	0.9700
C17—H17C	0.9600	C5T—H5TB	0.9700
O1—Y1—C1	132.18 (8)	C12—C13—Y1	75.63 (15)
O1—Y1—C2	102.75 (8)	C12—C13—C17	125.2 (3)
O1—Y1—C3	81.87 (8)	C14—C13—Y1	72.14 (16)
O1—Y1—C4	93.92 (8)	C14—C13—C12	107.8 (3)
O1—Y1—C5	125.20 (8)	C14—C13—C17	126.8 (3)
O1—Y1—C10	114.64 (9)	C17—C13—Y1	121.45 (19)

O1—Y1—C11	133.33 (9)	C10—C14—Y1	73.76 (16)
O1—Y1—C12	110.35 (8)	C10—C14—C13	107.6 (3)
O1—Y1—C13	82.68 (8)	C10—C14—C18	126.2 (3)
O1—Y1—C14	84.99 (9)	C13—C14—Y1	76.37 (16)
O4—Y1—O1	89.13 (7)	C13—C14—C18	126.2 (3)
O4—Y1—C1	114.19 (8)	C18—C14—Y1	117.1 (2)
O4—Y1—C2	134.02 (8)	C11—C15—H15A	109.5
O4—Y1—C3	112.10 (8)	C11—C15—H15B	109.5
O4—Y1—C4	83.98 (7)	C11—C15—H15C	109.5
O4—Y1—C5	84.75 (8)	H15A—C15—H15B	109.5
O4—Y1—C10	131.33 (9)	H15A—C15—H15C	109.5
O4—Y1—C11	101.23 (9)	H15B—C15—H15C	109.5
O4—Y1—C12	81.19 (8)	C12—C16—H16A	109.5
O4—Y1—C13	94.48 (8)	C12—C16—H16B	109.5
O4—Y1—C14	125.97 (8)	C12—C16—H16C	109.5
C1—Y1—C2	31.38 (9)	H16A—C16—H16B	109.5
C1—Y1—C3	51.17 (9)	H16A—C16—H16C	109.5
C1—Y1—C4	51.50 (9)	H16B—C16—H16C	109.5
C1—Y1—C5	31.46 (9)	C13—C17—H17A	109.5
C1—Y1—C11	84.53 (9)	C13—C17—H17B	109.5
C1—Y1—C12	113.98 (9)	C13—C17—H17C	109.5
C1—Y1—C13	132.10 (9)	H17A—C17—H17B	109.5
C1—Y1—C14	108.96 (9)	H17A—C17—H17C	109.5
C2—Y1—C3	30.74 (9)	H17B—C17—H17C	109.5
C2—Y1—C4	51.39 (8)	C14—C18—H18A	109.5
C2—Y1—C12	131.94 (9)	C14—C18—H18B	109.5
C2—Y1—C13	130.74 (9)	C14—C18—H18C	109.5
C3—Y1—C12	162.65 (9)	H18A—C18—H18B	109.5
C4—Y1—C3	30.94 (8)	H18A—C18—H18C	109.5
C4—Y1—C12	151.18 (10)	H18B—C18—H18C	109.5
C5—Y1—C2	52.01 (9)	F1—C19—S1	110.7 (2)
C5—Y1—C3	51.52 (9)	F2—C19—S1	111.0 (2)
C5—Y1—C4	31.30 (8)	F2—C19—F1	107.6 (3)
C5—Y1—C11	101.16 (9)	F3—C19—S1	110.3 (2)
C5—Y1—C12	122.20 (10)	F3—C19—F1	108.5 (3)
C5—Y1—C13	152.02 (10)	F3—C19—F2	108.6 (3)
C10—Y1—C1	81.52 (10)	F4—C20—S2	111.3 (2)
C10—Y1—C2	83.66 (9)	F4—C20—F5	107.5 (3)
C10—Y1—C3	112.88 (9)	F4—C20—F6	108.4 (2)
C10—Y1—C4	131.83 (9)	F5—C20—S2	109.7 (2)

C10—Y1—C5	109.70 (10)	F6—C20—S2	111.3 (2)
C10—Y1—C11	31.70 (10)	F6—C20—F5	108.4 (3)
C10—Y1—C12	51.35 (9)	O7—C21—H21C	111.5
C10—Y1—C13	51.45 (9)	O7—C21—H21D	111.5
C10—Y1—C14	31.15 (10)	O7—C21—H21A	109.8
C11—Y1—C2	101.83 (9)	O7—C21—H21B	109.8
C11—Y1—C3	132.15 (9)	O7—C21—C22	101.1 (6)
C11—Y1—C4	132.13 (9)	O7—C21—C22A	109.4 (10)
C11—Y1—C12	30.71 (9)	H21C—C21—H21D	109.4
C11—Y1—C13	51.46 (9)	H21A—C21—H21B	108.2
C13—Y1—C3	148.88 (9)	C22—C21—H21C	111.5
C13—Y1—C4	176.30 (8)	C22—C21—H21D	111.5
C13—Y1—C12	31.07 (10)	C22A—C21—H21A	109.8
C14—Y1—C2	99.48 (9)	C22A—C21—H21B	109.8
C14—Y1—C3	120.00 (9)	C21—C22—H22A	111.7
C14—Y1—C4	149.95 (9)	C21—C22—H22B	111.7
C14—Y1—C5	139.56 (9)	C21—C22—C23	100.5 (7)
C14—Y1—C11	52.11 (10)	H22A—C22—H22B	109.4
C14—Y1—C12	51.76 (10)	C23—C22—H22A	111.7
C14—Y1—C13	31.49 (9)	C23—C22—H22B	111.7
S1^{i}—K1—K1^{i}	62.714 (17)	C22—C23—H23A	111.4
O2^{i}—K1—K1^{i}	85.47 (4)	C22—C23—H23B	111.4
O2^{i}—K1—S1^{i}	22.75 (4)	H23A—C23—H23B	109.3
O2^{i}—K1—O3^{i}	46.42 (5)	C24—C23—C22	101.9 (7)
O2^{i}—K1—C24A	106.0 (4)	C24—C23—H23A	111.4
O3^{i}—K1—K1^{i}	39.45 (4)	C24—C23—H23B	111.4
O3—K1—K1^{i}	48.97 (5)	O7—C24—C23	108.3 (7)
O3—K1—S1^{i}	111.38 (5)	O7—C24—H24A	110.0
O3^{i}—K1—S1^{i}	23.85 (4)	O7—C24—H24B	110.0
O3—K1—O2^{i}	133.94 (7)	C23—C24—H24A	110.0
O3—K1—O3^{i}	88.42 (6)	C23—C24—H24B	110.0
O3—K1—O6	77.40 (6)	H24A—C24—H24B	108.4
O3—K1—O8	144.73 (7)	O8—C25—H25A	110.5
O3^{i}—K1—C24A	144.1 (5)	O8—C25—H25B	110.5
O3—K1—C24A	109.3 (3)	O8—C25—C26	106.2 (3)
O5^{i}—K1—K1^{i}	67.42 (5)	H25A—C25—H25B	108.7
O5^{i}—K1—S1^{i}	69.82 (4)	C26—C25—H25A	110.5
O5^{i}—K1—O2^{i}	76.94 (6)	C26—C25—H25B	110.5
O5^{i}—K1—O3	78.94 (6)	C25—C26—H26C	110.5
O5^{i}—K1—O3^{i}	69.68 (6)	C25—C26—H26D	110.5

O5^{i}—K1—O6	140.17 (7)	C25—C26—H26A	112.3
O5^{i}—K1—O8	129.50 (7)	C25—C26—H26B	112.3
O5^{i}—K1—C24A	83.0 (4)	C25—C26—C27	106.3 (4)
O6—K1—K1^{i}	72.86 (5)	H26C—C26—H26D	108.7
O6—K1—S1^{i}	89.76 (5)	H26A—C26—H26B	109.9
O6—K1—O2^{i}	97.47 (6)	C27—C26—H26C	110.5
O6—K1—O3^{i}	78.06 (6)	C27—C26—H26D	110.5
O6—K1—C24A	135.2 (4)	C27A—C26—C25	97.2 (8)
O7—K1—K1^{i}	128.87 (7)	C27A—C26—H26A	112.3
O7—K1—S1^{i}	142.07 (8)	C27A—C26—H26B	112.3
O7—K1—O2^{i}	127.45 (9)	C26—C27—H27A	111.6
O7—K1—O3^{i}	151.80 (8)	C26—C27—H27B	111.6
O7—K1—O3	86.62 (9)	H27A—C27—H27B	109.4
O7—K1—O5^{i}	82.12 (8)	C28—C27—C26	100.6 (5)
O7—K1—O6	127.50 (9)	C28—C27—H27A	111.6
O7—K1—O8	78.83 (8)	C28—C27—H27B	111.6
O7—K1—C24A	23.0 (3)	O8—C28—C27	104.5 (3)
O8—K1—K1^{i}	151.88 (6)	O8—C28—H28C	110.9
O8—K1—S1^{i}	99.45 (6)	O8—C28—H28D	110.9
O8—K1—O2^{i}	78.64 (7)	O8—C28—H28A	110.6
O8—K1—O3^{i}	118.75 (7)	O8—C28—H28B	110.6
O8—K1—O6	86.29 (7)	O8—C28—C27A	105.8 (7)
O8—K1—C24A	62.5 (3)	C27—C28—H28C	110.9
C24A—K1—K1^{i}	145.2 (3)	C27—C28—H28D	110.9
C24A—K1—S1^{i}	124.6 (4)	H28C—C28—H28D	108.9
O1—S1—K1^{i}	131.34 (8)	H28A—C28—H28B	108.7
O1—S1—C19	101.63 (13)	C27A—C28—H28A	110.6
O2—S1—K1^{i}	50.43 (9)	C27A—C28—H28B	110.6
O2—S1—O1	114.05 (12)	C21—C22A—H22C	112.0
O2—S1—O3	115.68 (13)	C21—C22A—H22D	112.0
O2—S1—C19	105.13 (15)	C21—C22A—C23A	99.1 (13)
O3—S1—K1^{i}	65.92 (9)	H22C—C22A—H22D	109.6
O3—S1—O1	113.74 (12)	C23A—C22A—H22C	112.0
O3—S1—C19	104.60 (14)	C23A—C22A—H22D	112.0
C19—S1—K1^{i}	126.26 (12)	C22A—C23A—H23C	111.2
O4—S2—C20	101.37 (13)	C22A—C23A—H23D	111.2
O5—S2—O4	113.33 (12)	H23C—C23A—H23D	109.1
O5—S2—C20	104.57 (14)	C24A—C23A—C22A	102.8 (16)
O6—S2—O4	113.74 (12)	C24A—C23A—H23C	111.2
O6—S2—O5	116.90 (13)	C24A—C23A—H23D	111.2

O6—S2—C20	104.70 (13)	K1—C24A—H24C	127.1
S1—O1—Y1	151.58 (12)	K1—C24A—H24D	64.5
S1—O2—K1^{i}	106.82 (11)	O7—C24A—K1	45.9 (7)
K1—O3—K1^{i}	91.58 (6)	O7—C24A—C23A	106.6 (14)
S1—O3—K1^{i}	90.23 (10)	O7—C24A—H24C	110.4
S1—O3—K1	164.55 (13)	O7—C24A—H24D	110.4
S2—O4—Y1	147.72 (12)	C23A—C24A—K1	121.3 (15)
S2—O5—K1^{i}	144.99 (13)	C23A—C24A—H24C	110.4
S2—O6—K1	133.75 (13)	C23A—C24A—H24D	110.4
C21—O7—K1	118.8 (2)	H24C—C24A—H24D	108.6
C21—O7—C24A	105.6 (8)	C26—C27A—H27C	110.6
C24—O7—K1	129.7 (4)	C26—C27A—H27D	110.6
C24—O7—C21	108.2 (4)	C28—C27A—C26	105.6 (9)
C24A—O7—K1	111.1 (10)	C28—C27A—H27C	110.6
C25—O8—K1	117.4 (2)	C28—C27A—H27D	110.6
C28—O8—K1	115.2 (2)	H27C—C27A—H27D	108.7
C28—O8—C25	106.2 (3)	H1SA—C1S—H1SB	109.5
Y1—C1—H1	115.7	H1SA—C1S—H1SC	109.5
C2—C1—Y1	75.96 (15)	H1SB—C1S—H1SC	109.5
C2—C1—H1	125.5	H1SD—C1S—H1SE	109.5
C5—C1—Y1	74.87 (15)	H1SD—C1S—H1SF	109.5
C5—C1—H1	125.5	H1SE—C1S—H1SF	109.5
C5—C1—C2	109.0 (3)	C2S—C1S—H1SA	109.5
C1—C2—Y1	72.67 (14)	C2S—C1S—H1SB	109.5
C1—C2—C6	126.6 (3)	C2S—C1S—H1SC	109.5
C3—C2—Y1	75.96 (15)	C2T—C1S—H1SD	109.5
C3—C2—C1	107.4 (2)	C2T—C1S—H1SE	109.5
C3—C2—C6	125.8 (3)	C2T—C1S—H1SF	109.5
C6—C2—Y1	121.3 (2)	C1S—C2S—H2SA	105.8
C2—C3—Y1	73.31 (15)	C1S—C2S—H2SB	105.8
C2—C3—C4	108.5 (2)	C1S—C2S—C3S	126.1 (8)
C2—C3—C7	125.2 (3)	H2SA—C2S—H2SB	106.2
C4—C3—Y1	73.91 (14)	C3S—C2S—H2SA	105.8
C4—C3—C7	126.1 (3)	C3S—C2S—H2SB	105.8
C7—C3—Y1	123.00 (18)	C2S—C3S—H3SA	106.6
C3—C4—Y1	75.15 (14)	C2S—C3S—H3SB	106.6
C3—C4—C5	107.8 (2)	H3SA—C3S—H3SB	106.5
C3—C4—C8	125.9 (3)	C4S—C3S—C2S	123.0 (10)
C5—C4—Y1	72.62 (14)	C4S—C3S—H3SA	106.6
C5—C4—C8	126.2 (3)	C4S—C3S—H3SB	106.6

C8—C4—Y1	121.21 (18)	C3S—C4S—H4SA	104.1
C1—C5—Y1	73.67 (15)	C3S—C4S—H4SB	104.1
C1—C5—C4	107.3 (2)	C3S—C4S—C5S	132.5 (10)
C1—C5—C9	126.3 (3)	H4SA—C4S—H4SB	105.5
C4—C5—Y1	76.09 (14)	H4SC—C4S—H4SD	105.2
C4—C5—C9	126.3 (3)	C5S—C4S—H4SA	104.1
C9—C5—Y1	117.34 (18)	C5S—C4S—H4SB	104.1
C2—C6—H6A	109.5	C3T—C4S—H4SC	103.2
C2—C6—H6B	109.5	C3T—C4S—H4SD	103.2
C2—C6—H6C	109.5	C5T—C4S—H4SC	103.2
H6A—C6—H6B	109.5	C5T—C4S—H4SD	103.2
H6A—C6—H6C	109.5	C5T—C4S—C3T	135.8 (11)
H6B—C6—H6C	109.5	C4S—C5S—H5SA	107.3
C3—C7—H7A	109.5	C4S—C5S—H5SB	107.3
C3—C7—H7B	109.5	H5SA—C5S—H5SB	106.9
C3—C7—H7C	109.5	C6S—C5S—C4S	120.0 (12)
H7A—C7—H7B	109.5	C6S—C5S—H5SA	107.3
H7A—C7—H7C	109.5	C6S—C5S—H5SB	107.3
H7B—C7—H7C	109.5	C5S—C6S—H6SA	109.5
C4—C8—H8A	109.5	C5S—C6S—H6SB	109.5
C4—C8—H8B	109.5	C5S—C6S—H6SC	109.5
C4—C8—H8C	109.5	H6SA—C6S—H6SB	109.5
H8A—C8—H8B	109.5	H6SA—C6S—H6SC	109.5
H8A—C8—H8C	109.5	H6SB—C6S—H6SC	109.5
H8B—C8—H8C	109.5	H6SD—C6S—H6SE	109.5
C5—C9—H9A	109.5	H6SD—C6S—H6SF	109.5
C5—C9—H9B	109.5	H6SE—C6S—H6SF	109.5
C5—C9—H9C	109.5	C5T—C6S—H6SD	109.5
H9A—C9—H9B	109.5	C5T—C6S—H6SE	109.5
H9A—C9—H9C	109.5	C5T—C6S—H6SF	109.5
H9B—C9—H9C	109.5	C1S—C2T—H2TA	109.3
Y1—C10—H10	115.4	C1S—C2T—H2TB	109.3
C11—C10—Y1	76.16 (16)	C1S—C2T—C3T	111.7 (11)
C11—C10—H10	125.3	H2TA—C2T—H2TB	107.9
C14—C10—Y1	75.09 (16)	C3T—C2T—H2TA	109.3
C14—C10—H10	125.3	C3T—C2T—H2TB	109.3
C14—C10—C11	109.4 (3)	C4S—C3T—H3TA	105.9
C10—C11—Y1	72.14 (16)	C4S—C3T—H3TB	105.9
C10—C11—C15	127.0 (3)	C2T—C3T—C4S	125.8 (10)
C12—C11—Y1	76.58 (16)	C2T—C3T—H3TA	105.9

C12—C11—C10	107.3 (3)	C2T—C3T—H3TB	105.9
C12—C11—C15	125.5 (3)	H3TA—C3T—H3TB	106.2
C15—C11—Y1	121.2 (2)	C4S—C5T—C6S	132.6 (13)
C11—C12—Y1	72.70 (16)	C4S—C5T—H5TA	104.1
C11—C12—C13	107.9 (3)	C4S—C5T—H5TB	104.1
C11—C12—C16	125.4 (3)	C6S—C5T—H5TA	104.1
C13—C12—Y1	73.31 (15)	C6S—C5T—H5TB	104.1
C13—C12—C16	126.5 (3)	H5TA—C5T—H5TB	105.5
C16—C12—Y1	122.7 (2)		

Symmetry code: (i) -*x*+1, -*y*+2, -*z*+1.

8.3.8 Crystallographic data for 6-Y (desolv.)

Crystal data

$C_{20}H_{26}F_6KO_6S_2Y$	Z = 2
M_r = 668.54	F(000) = 676
Triclinic, $P\bar{1}$	D_x = 1.652 Mg m^{-3}
a = 9.8418 (15) Å	Mo $K\alpha$ radiation, λ = 0.71073 Å
b = 11.3441 (16) Å	Cell parameters from 2574 reflections
c = 12.2787 (19) Å	θ = 2.3–24.9°
α = 98.495 (5)°	μ = 2.55 mm^{-1}
β = 96.617 (5)°	T = 150 K
γ = 92.557 (5)°	Plate, yellow
V = 1344.1 (3) Å^3	0.15 × 0.11 × 0.01 mm

Data collection

Bruker D8 VENTURE diffractometer	6556 independent reflections
Radiation source: microfocus sealed tube, INCOATEC Iμs 3.0	3745 reflections with $I > 2\sigma(I)$
Multilayer mirror optics monochromator	R_{int} = 0.059
Detector resolution: 7.4074 pixels mm^{-1}	θ_{max} = 28.3°, θ_{min} = 2.3°
ϕ and ω scans	h = -12→13
Absorption correction: multi-scan *SADABS2016*/2 (Bruker,2016/2) was used for absorption correction. wR2(int) was 0.0869 before and 0.0592 after correction. The Ratio of minimum to maximum transmission is 0.8156. The λ/2 correction factor is Not present.	k = -15→12

T_{min} = 0.608, T_{max} = 0.746	l = -16→15
11896 measured reflections	

Refinement

Refinement on F^2	Primary atom site location: dual
Least-squares matrix: full	Hydrogen site location: inferred from neighbouring sites
$R[F^2 > 2\sigma(F^2)]$ = 0.071	H-atom parameters constrained
$wR(F^2)$ = 0.151	$w = 1/[\sigma^2(F_o^2) + (0.0605P)^2]$ where $P = (F_o^2 + 2F_c^2)/3$
S = 1.01	$(\Delta/\sigma)_{max}$ = 0.006
6556 reflections	$\Delta\rangle_{max}$ = 0.84 e Å^{-3}
346 parameters	$\Delta\rangle_{min}$ = -0.62 e Å^{-3}
9 restraints	

Special details

Geometry. All esds (except the esd in the dihedral angle between two l.s. planes) are estimated using the full covariance matrix. The cell esds are taken into account individually in the estimation of esds in distances, angles and torsion angles; correlations between esds in cell parameters are only used when they are defined by crystal symmetry. An approximate (isotropic) treatment of cell esds is used for estimating esds involving l.s. planes.

Fractional atomic coordinates and isotropic or equivalent isotropic displacement parameters (Å²)

	x	*y*	*z*	U_{iso}*/U_{eq}	Occ. (<1)
Y1	0.65968 (5)	0.76045 (5)	0.76314 (4)	0.02196 (16)	
K1	1.17255 (12)	0.59785 (11)	0.57963 (11)	0.0346 (3)	
S2	0.85188 (16)	0.75221 (13)	0.52887 (12)	0.0319 (4)	
S1	0.85240 (19)	0.49906 (15)	0.71657 (14)	0.0444 (5)	
O4	0.7640 (4)	0.7926 (3)	0.6129 (3)	0.0315 (9)	
O1	0.7858 (4)	0.5972 (3)	0.7743 (3)	0.0327 (10)	
O6	0.9939 (4)	0.7711 (4)	0.5669 (4)	0.0505 (13)	
F4	0.6925 (4)	0.8448 (4)	0.3835 (3)	0.0723 (14)	
F6	0.8419 (4)	0.9682 (3)	0.4825 (4)	0.0697 (13)	
F5	0.9021 (4)	0.8429 (4)	0.3546 (3)	0.0772 (14)	
F1	0.7918 (8)	0.3873 (7)	0.8763 (6)	0.082 (3)	0.868 (12)
F3	0.9356 (9)	0.3047 (6)	0.7820 (7)	0.082 (3)	0.868 (12)
O5	0.8058 (5)	0.6403 (4)	0.4662 (4)	0.0627 (14)	

C1	0.6440 (6)	0.9094 (5)	0.9383 (5)	0.0321 (14)	
H1	0.555064	0.913737	0.961000	0.038*	
C13	0.4021 (5)	0.6872 (5)	0.7894 (5)	0.0313 (14)	
C11	0.4364 (5)	0.7509 (5)	0.6242 (5)	0.0270 (13)	
C5	0.7428 (6)	0.8320 (5)	0.9718 (5)	0.0329 (14)	
C3	0.8327 (6)	0.9452 (5)	0.8540 (5)	0.0297 (13)	
C4	0.8595 (6)	0.8539 (5)	0.9186 (5)	0.0301 (13)	
O2	0.7599 (7)	0.4202 (5)	0.6345 (4)	0.0853 (19)	
C2	0.6980 (6)	0.9801 (5)	0.8652 (5)	0.0318 (14)	
C12	0.3889 (5)	0.7852 (5)	0.7280 (5)	0.0293 (13)	
C14	0.4552 (6)	0.5938 (5)	0.7222 (6)	0.0369 (15)	
C8	0.9940 (6)	0.7970 (6)	0.9315 (5)	0.0454 (17)	
H8A	0.981952	0.723194	0.962850	0.068*	
H8B	1.061254	0.852189	0.981358	0.068*	
H8C	1.026672	0.778590	0.858855	0.068*	
C10	0.4780 (5)	0.6313 (5)	0.6215 (5)	0.0349 (15)	
H10	0.514749	0.585298	0.561924	0.042*	
C9	0.7279 (6)	0.7453 (6)	1.0512 (5)	0.0471 (18)	
H9A	0.631438	0.735616	1.062813	0.071*	
H9B	0.783220	0.775715	1.122254	0.071*	
H9C	0.759384	0.668002	1.020651	0.071*	
F2	0.9950 (7)	0.4654 (5)	0.8940 (5)	0.106 (3)	0.868 (12)
C16	0.3183 (6)	0.8985 (5)	0.7603 (5)	0.0455 (17)	
H16A	0.331150	0.920178	0.841231	0.068*	
H16B	0.220178	0.885579	0.733894	0.068*	
H16C	0.357834	0.963095	0.726662	0.068*	
C15	0.4315 (6)	0.8232 (6)	0.5311 (5)	0.0456 (18)	
H15A	0.480320	0.901198	0.557559	0.068*	
H15B	0.335855	0.834519	0.504718	0.068*	
H15C	0.475197	0.781137	0.470051	0.068*	
C6	0.6320 (7)	1.0799 (6)	0.8162 (6)	0.0522 (19)	
H6A	0.626791	1.063439	0.735112	0.078*	
H6B	0.686549	1.154960	0.843836	0.078*	
H6C	0.539349	1.086656	0.837464	0.078*	
C20	0.8197 (7)	0.8592 (6)	0.4319 (5)	0.0430 (17)	
C7	0.9332 (6)	1.0017 (6)	0.7904 (5)	0.0444 (17)	
H7A	0.979884	0.939178	0.748071	0.067*	
H7B	1.000938	1.054171	0.842432	0.067*	
H7C	0.884134	1.048619	0.739389	0.067*	
C19	0.8931 (8)	0.4067 (6)	0.8225 (7)	0.055 (2)	

C17	0.3539 (6)	0.6803 (7)	0.9002 (5)	0.054 (2)	
H17A	0.411668	0.628325	0.939949	0.082*	
H17B	0.258548	0.647632	0.889163	0.082*	
H17C	0.359902	0.760449	0.943784	0.082*	
C18	0.4731 (7)	0.4698 (6)	0.7531 (7)	0.060 (2)	
H18A	0.518631	0.421747	0.696620	0.090*	
H18B	0.383105	0.431349	0.757160	0.090*	
H18C	0.529193	0.476619	0.825314	0.090*	
O3	0.9747 (6)	0.5297 (5)	0.6824 (6)	0.114 (3)	
F1A	0.781 (4)	0.333 (3)	0.773 (4)	0.12 (2)*	0.132 (12)
F3A	0.991 (3)	0.333 (3)	0.802 (4)	0.056 (15)*	0.132 (12)
F2A	0.832 (6)	0.438 (5)	0.912 (4)	0.11 (3)*	0.132 (12)

Atomic displacement parameters (Å²)

	U^{11}	U^{22}	U^{33}	U^{12}	U^{13}	U^{23}
Y1	0.0219 (3)	0.0232 (3)	0.0206 (3)	0.0071 (2)	0.0045 (2)	-0.0001 (2)
K1	0.0241 (7)	0.0351 (8)	0.0419 (8)	0.0057 (6)	0.0048 (6)	-0.0049 (6)
S2	0.0443 (9)	0.0251 (8)	0.0304 (9)	0.0117 (7)	0.0144 (7)	0.0076 (7)
S1	0.0629 (12)	0.0366 (10)	0.0450 (11)	0.0280 (9)	0.0285 (9)	0.0185 (9)
O4	0.034 (2)	0.043 (2)	0.021 (2)	0.0065 (19)	0.0125 (17)	0.0069 (18)
O1	0.036 (2)	0.026 (2)	0.037 (2)	0.0128 (18)	0.0039 (18)	0.0017 (18)
O6	0.035 (3)	0.065 (3)	0.061 (3)	0.023 (2)	0.014 (2)	0.027 (3)
F4	0.063 (3)	0.101 (4)	0.061 (3)	0.005 (3)	-0.004 (2)	0.045 (3)
F6	0.096 (3)	0.034 (2)	0.083 (3)	0.009 (2)	0.011 (3)	0.019 (2)
F5	0.092 (3)	0.107 (4)	0.051 (3)	0.028 (3)	0.045 (2)	0.040 (3)
F1	0.119 (6)	0.083 (6)	0.071 (5)	0.042 (5)	0.064 (5)	0.054 (5)
F3	0.102 (6)	0.045 (4)	0.110 (6)	0.047 (5)	0.025 (5)	0.030 (4)
O5	0.107 (4)	0.031 (3)	0.052 (3)	0.005 (3)	0.026 (3)	-0.001 (2)
C1	0.030 (3)	0.037 (3)	0.027 (3)	0.006 (3)	0.009 (3)	-0.007 (3)
C13	0.019 (3)	0.045 (4)	0.031 (3)	-0.005 (3)	0.002 (2)	0.010 (3)
C11	0.018 (3)	0.033 (3)	0.029 (3)	0.003 (2)	-0.002 (2)	0.005 (3)
C5	0.034 (3)	0.036 (4)	0.023 (3)	0.001 (3)	-0.001 (3)	-0.005 (3)
C3	0.027 (3)	0.028 (3)	0.030 (3)	-0.006 (3)	0.009 (3)	-0.009 (3)
C4	0.032 (3)	0.029 (3)	0.025 (3)	0.000 (3)	0.003 (3)	-0.006 (3)
O2	0.147 (6)	0.058 (3)	0.043 (3)	0.039 (4)	-0.006 (3)	-0.017 (3)
C2	0.035 (3)	0.023 (3)	0.032 (3)	0.004 (3)	0.001 (3)	-0.009 (3)
C12	0.023 (3)	0.030 (3)	0.034 (4)	0.004 (2)	0.001 (3)	0.003 (3)
C14	0.024 (3)	0.033 (4)	0.051 (4)	-0.001 (3)	-0.002 (3)	0.004 (3)

C8	0.031 (4)	0.065 (5)	0.033 (4)	0.005 (3)	-0.005 (3)	-0.009 (3)
C10	0.020 (3)	0.041 (4)	0.041 (4)	0.007 (3)	0.004 (3)	-0.003 (3)
C9	0.044 (4)	0.076 (5)	0.025 (4)	0.004 (4)	0.009 (3)	0.018 (4)
F2	0.119 (6)	0.088 (5)	0.100 (5)	0.016 (4)	-0.063 (4)	0.029 (4)
C16	0.030 (3)	0.051 (4)	0.050 (4)	0.016 (3)	-0.003 (3)	-0.008 (3)
C15	0.041 (4)	0.063 (5)	0.035 (4)	0.009 (3)	0.001 (3)	0.017 (4)
C6	0.062 (5)	0.036 (4)	0.060 (5)	0.015 (3)	0.016 (4)	0.006 (4)
C20	0.052 (4)	0.047 (4)	0.038 (4)	0.009 (4)	0.013 (3)	0.024 (4)
C7	0.040 (4)	0.044 (4)	0.044 (4)	-0.011 (3)	0.009 (3)	-0.007 (3)
C19	0.059 (5)	0.048 (5)	0.066 (6)	0.026 (4)	0.016 (5)	0.022 (4)
C17	0.039 (4)	0.094 (6)	0.036 (4)	0.005 (4)	0.011 (3)	0.022 (4)
C18	0.042 (4)	0.039 (4)	0.102 (6)	-0.008 (3)	-0.004 (4)	0.028 (4)
O3	0.106 (5)	0.082 (4)	0.201 (7)	0.058 (4)	0.116 (5)	0.085 (5)

Geometric parameters (Å, º)

Y1—O4	2.279 (4)	C11—C12	1.415 (8)
Y1—O1	2.287 (3)	C11—C10	1.431 (7)
Y1—C1	2.555 (5)	C11—C15	1.501 (7)
Y1—C13	2.702 (5)	C5—C4	1.415 (8)
Y1—C11	2.610 (5)	C5—C9	1.498 (8)
Y1—C5	2.595 (6)	C3—C4	1.411 (7)
Y1—C3	2.663 (6)	C3—C2	1.416 (7)
Y1—C4	2.643 (6)	C3—C7	1.506 (8)
Y1—C2	2.608 (5)	C4—C8	1.501 (7)
Y1—C12	2.684 (5)	C2—C6	1.499 (7)
Y1—C14	2.650 (6)	C12—C16	1.511 (7)
Y1—C10	2.581 (6)	C14—C10	1.404 (8)
K1—K1^{i}	4.099 (3)	C14—C18	1.522 (8)
K1—S2	3.7117 (18)	C8—H8A	0.9800
K1—S1^{i}	3.617 (2)	C8—H8B	0.9800
K1—O6	2.704 (4)	C8—H8C	0.9800
K1—O5^{i}	2.700 (4)	C10—H10	0.9500
K1—C13^{ii}	3.233 (6)	C9—H9A	0.9800
K1—C11^{ii}	3.008 (5)	C9—H9B	0.9800
K1—O2^{i}	2.766 (5)	C9—H9C	0.9800
K1—C12^{ii}	3.151 (6)	F2—C19	1.336 (9)
K1—C14^{ii}	3.117 (6)	C16—H16A	0.9800
K1—C10^{ii}	2.989 (5)	C16—H16B	0.9800

K1—O3	2.589 (5)	C16—H16C	0.9800
S2—O4	1.457 (4)	C15—H15A	0.9800
S2—O6	1.418 (4)	C15—H15B	0.9800
S2—O5	1.410 (5)	C15—H15C	0.9800
S2—C20	1.834 (6)	C6—H6A	0.9800
S1—O1	1.452 (4)	C6—H6B	0.9800
S1—O2	1.447 (6)	C6—H6C	0.9800
S1—C19	1.809 (7)	C7—H7A	0.9800
S1—O3	1.367 (5)	C7—H7B	0.9800
F4—C20	1.315 (7)	C7—H7C	0.9800
F6—C20	1.296 (7)	C19—F1A	1.374 (19)
F5—C20	1.316 (7)	C19—F3A	1.322 (19)
F1—C19	1.285 (8)	C19—F2A	1.32 (2)
F3—C19	1.297 (8)	C17—H17A	0.9800
C1—H1	0.9500	C17—H17B	0.9800
C1—C5	1.406 (7)	C17—H17C	0.9800
C1—C2	1.420 (8)	C18—H18A	0.9800
C13—C12	1.435 (7)	C18—H18B	0.9800
C13—C14	1.403 (8)	C18—H18C	0.9800
C13—C17	1.503 (8)		
O4—Y1—O1	88.39 (13)	S2—O4—Y1	149.7 (2)
O4—Y1—C1	127.27 (17)	S1—O1—Y1	147.9 (2)
O4—Y1—C13	133.56 (15)	S2—O6—K1	125.5 (3)
O4—Y1—C11	83.34 (15)	S2—O5—K1^{i}	150.1 (3)
O4—Y1—C5	128.57 (17)	Y1—C1—H1	114.9
O4—Y1—C3	79.82 (16)	C5—C1—Y1	75.7 (3)
O4—Y1—C4	97.80 (16)	C5—C1—H1	125.3
O4—Y1—C2	95.71 (17)	C5—C1—C2	109.3 (5)
O4—Y1—C12	111.32 (15)	C2—C1—Y1	76.1 (3)
O4—Y1—C14	115.15 (18)	C2—C1—H1	125.3
O4—Y1—C10	85.56 (17)	Y1—C13—K1^{iii}	121.8 (2)
O1—Y1—C1	119.57 (15)	C12—C13—Y1	73.9 (3)
O1—Y1—C13	105.29 (16)	C12—C13—K1^{iii}	73.8 (3)
O1—Y1—C11	121.52 (16)	C12—C13—C17	126.5 (6)
O1—Y1—C5	88.17 (16)	C14—C13—Y1	72.8 (3)
O1—Y1—C3	104.40 (15)	C14—C13—K1^{iii}	72.7 (3)
O1—Y1—C4	80.10 (15)	C14—C13—C12	107.5 (5)
O1—Y1—C2	131.76 (16)	C14—C13—C17	125.8 (6)
O1—Y1—C12	132.44 (16)	C17—C13—Y1	123.9 (4)

O1—Y1—C14	81.68 (15)	C17—C13—K1^{iii}	114.2 (4)
O1—Y1—C10	89.79 (16)	Y1—C11—K1^{iii}	135.0 (2)
C1—Y1—C13	84.31 (19)	C12—C11—Y1	77.4 (3)
C1—Y1—C11	110.86 (18)	C12—C11—K1^{iii}	82.4 (3)
C1—Y1—C5	31.66 (16)	C12—C11—C10	107.3 (5)
C1—Y1—C3	51.69 (18)	C12—C11—C15	125.8 (5)
C1—Y1—C4	51.71 (18)	C10—C11—Y1	72.9 (3)
C1—Y1—C2	31.89 (17)	C10—C11—K1^{iii}	75.5 (3)
C1—Y1—C12	83.04 (18)	C10—C11—C15	126.7 (5)
C1—Y1—C14	112.7 (2)	C15—C11—Y1	119.6 (4)
C1—Y1—C10	133.06 (18)	C15—C11—K1^{iii}	104.8 (3)
C11—Y1—C13	51.44 (17)	C1—C5—Y1	72.6 (3)
C11—Y1—C3	130.32 (17)	C1—C5—C4	107.0 (5)
C11—Y1—C4	158.37 (17)	C1—C5—C9	126.2 (5)
C11—Y1—C12	30.97 (16)	C4—C5—Y1	76.2 (3)
C11—Y1—C14	51.74 (17)	C4—C5—C9	126.7 (5)
C5—Y1—C13	96.59 (19)	C9—C5—Y1	118.1 (4)
C5—Y1—C11	139.08 (18)	C4—C3—Y1	73.8 (3)
C5—Y1—C3	51.73 (18)	C4—C3—C2	108.2 (5)
C5—Y1—C4	31.34 (17)	C4—C3—C7	125.9 (5)
C5—Y1—C2	52.57 (18)	C2—C3—Y1	72.3 (3)
C5—Y1—C12	108.39 (18)	C2—C3—C7	125.8 (5)
C5—Y1—C14	115.0 (2)	C7—C3—Y1	122.9 (4)
C3—Y1—C13	135.12 (18)	C5—C4—Y1	72.5 (3)
C3—Y1—C12	121.07 (17)	C5—C4—C8	127.2 (5)
C4—Y1—C13	127.92 (18)	C3—C4—Y1	75.4 (3)
C4—Y1—C3	30.83 (16)	C3—C4—C5	108.6 (5)
C4—Y1—C12	134.74 (17)	C3—C4—C8	124.1 (5)
C4—Y1—C14	141.63 (19)	C8—C4—Y1	121.1 (4)
C2—Y1—C13	105.97 (19)	S1—O2—K1^{i}	114.6 (3)
C2—Y1—C11	106.67 (17)	C1—C2—Y1	72.0 (3)
C2—Y1—C3	31.13 (16)	C1—C2—C6	127.3 (5)
C2—Y1—C4	51.70 (17)	C3—C2—Y1	76.6 (3)
C2—Y1—C12	90.38 (17)	C3—C2—C1	106.9 (5)
C2—Y1—C14	136.28 (19)	C3—C2—C6	125.6 (6)
C12—Y1—C13	30.89 (16)	C6—C2—Y1	120.9 (4)
C14—Y1—C13	30.37 (18)	Y1—C12—K1^{iii}	125.5 (2)
C14—Y1—C3	164.30 (19)	C13—C12—Y1	75.2 (3)
C14—Y1—C12	50.79 (17)	C13—C12—K1^{iii}	80.2 (3)
C10—Y1—C13	51.21 (19)	C13—C12—C16	126.4 (5)

C10—Y1—C11	32.00 (16)	C11—C12—Y1	71.6 (3)
C10—Y1—C5	145.7 (2)	C11—C12—K1^{iii}	71.1 (3)
C10—Y1—C3	159.20 (18)	C11—C12—C13	108.1 (5)
C10—Y1—C4	169.22 (17)	C11—C12—C16	125.0 (5)
C10—Y1—C2	138.41 (17)	C16—C12—Y1	125.5 (4)
C10—Y1—C12	51.57 (18)	C16—C12—K1^{iii}	108.3 (3)
C10—Y1—C14	31.11 (18)	Y1—C14—K1^{iii}	128.2 (2)
S2—K1—K1^{i}	61.12 (4)	C13—C14—Y1	76.9 (3)
S1^{i}—K1—K1^{i}	60.92 (4)	C13—C14—K1^{iii}	81.9 (3)
S1^{i}—K1—S2	87.95 (4)	C13—C14—C10	109.0 (5)
O6—K1—K1^{i}	79.09 (11)	C13—C14—C18	124.0 (6)
O6—K1—S2	18.12 (10)	C10—C14—Y1	71.8 (3)
O6—K1—S1^{i}	95.48 (10)	C10—C14—K1^{iii}	71.6 (3)
O6—K1—C13^{ii}	107.74 (15)	C10—C14—C18	126.8 (6)
O6—K1—C11^{ii}	99.14 (14)	C18—C14—Y1	121.4 (4)
O6—K1—O2^{i}	97.66 (14)	C18—C14—K1^{iii}	109.7 (4)
O6—K1—C12^{ii}	89.63 (14)	C4—C8—H8A	109.5
O6—K1—C14^{ii}	131.69 (16)	C4—C8—H8B	109.5
O6—K1—C10^{ii}	126.76 (15)	C4—C8—H8C	109.5
O5^{i}—K1—K1^{i}	64.01 (12)	H8A—C8—H8B	109.5
O5^{i}—K1—S2	124.95 (12)	H8A—C8—H8C	109.5
O5^{i}—K1—S1^{i}	69.16 (10)	H8B—C8—H8C	109.5
O5^{i}—K1—O6	143.05 (15)	Y1—C10—K1^{iii}	137.4 (2)
O5^{i}—K1—C13^{ii}	104.93 (15)	Y1—C10—H10	114.1
O5^{i}—K1—C11^{ii}	116.56 (16)	K1^{iii}—C10—H10	108.2
O5^{i}—K1—O2^{i}	80.00 (15)	C11—C10—Y1	75.1 (3)
O5^{i}—K1—C12^{ii}	126.66 (15)	C11—C10—K1^{iii}	76.9 (3)
O5^{i}—K1—C14^{ii}	83.87 (16)	C11—C10—H10	126.0
O5^{i}—K1—C10^{ii}	89.27 (16)	C14—C10—Y1	77.1 (3)
C13^{ii}—K1—K1^{i}	154.18 (11)	C14—C10—K1^{iii}	81.9 (3)
C13^{ii}—K1—S2	122.62 (11)	C14—C10—C11	108.1 (5)
C13^{ii}—K1—S1^{i}	139.82 (11)	C14—C10—H10	126.0
C11^{ii}—K1—K1^{i}	162.28 (12)	C5—C9—H9A	109.5
C11^{ii}—K1—S2	116.91 (11)	C5—C9—H9B	109.5
C11^{ii}—K1—S1^{i}	102.01 (12)	C5—C9—H9C	109.5
C11^{ii}—K1—C13^{ii}	43.20 (14)	H9A—C9—H9B	109.5
C11^{ii}—K1—C12^{ii}	26.44 (14)	H9A—C9—H9C	109.5
C11^{ii}—K1—C14^{ii}	43.97 (15)	H9B—C9—H9C	109.5
O2^{i}—K1—K1^{i}	82.04 (14)	C12—C16—H16A	109.5
O2^{i}—K1—S2	96.42 (12)	C12—C16—H16B	109.5

O2^{i}—K1—S1^{i}	21.33 (13)	C12—C16—H16C	109.5
O2^{i}—K1—C13^{ii}	120.43 (17)	H16A—C16—H16B	109.5
O2^{i}—K1—C11^{ii}	80.72 (17)	H16A—C16—H16C	109.5
O2^{i}—K1—C12^{ii}	106.45 (17)	H16B—C16—H16C	109.5
O2^{i}—K1—C14^{ii}	103.22 (18)	C11—C15—H15A	109.5
O2^{i}—K1—C10^{ii}	78.69 (18)	C11—C15—H15B	109.5
C12^{ii}—K1—K1^{i}	166.82 (11)	C11—C15—H15C	109.5
C12^{ii}—K1—S2	107.22 (10)	H15A—C15—H15B	109.5
C12^{ii}—K1—S1^{i}	127.74 (12)	H15A—C15—H15C	109.5
C12^{ii}—K1—C13^{ii}	25.93 (13)	H15B—C15—H15C	109.5
C14^{ii}—K1—K1^{i}	146.28 (12)	C2—C6—H6A	109.5
C14^{ii}—K1—S2	147.83 (13)	C2—C6—H6B	109.5
C14^{ii}—K1—S1^{i}	118.55 (13)	C2—C6—H6C	109.5
C14^{ii}—K1—C13^{ii}	25.44 (15)	H6A—C6—H6B	109.5
C14^{ii}—K1—C12^{ii}	42.81 (14)	H6A—C6—H6C	109.5
C10^{ii}—K1—K1^{i}	149.42 (13)	H6B—C6—H6C	109.5
C10^{ii}—K1—S2	144.41 (12)	F4—C20—S2	110.8 (4)
C10^{ii}—K1—S1^{i}	96.96 (13)	F4—C20—F5	108.4 (5)
C10^{ii}—K1—C13^{ii}	42.89 (16)	F6—C20—S2	111.1 (4)
C10^{ii}—K1—C11^{ii}	27.61 (14)	F6—C20—F4	108.7 (5)
C10^{ii}—K1—C12^{ii}	43.75 (15)	F6—C20—F5	108.0 (5)
C10^{ii}—K1—C14^{ii}	26.48 (15)	F5—C20—S2	109.8 (4)
O3—K1—K1^{i}	56.88 (19)	C3—C7—H7A	109.5
O3—K1—S2	65.61 (12)	C3—C7—H7B	109.5
O3—K1—S1^{i}	117.73 (19)	C3—C7—H7C	109.5
O3—K1—O6	76.36 (14)	H7A—C7—H7B	109.5
O3—K1—O5^{i}	81.60 (17)	H7A—C7—H7C	109.5
O3—K1—C13^{ii}	99.7 (2)	H7B—C7—H7C	109.5
O3—K1—C11^{ii}	140.2 (2)	F1—C19—S1	113.1 (5)
O3—K1—O2^{i}	138.9 (2)	F1—C19—F3	108.6 (8)
O3—K1—C12^{ii}	114.0 (2)	F1—C19—F2	108.3 (8)
O3—K1—C14^{ii}	110.9 (2)	F3—C19—S1	112.0 (6)
O3—K1—C10^{ii}	137.4 (2)	F3—C19—F2	108.0 (8)
O4—S2—K1	125.10 (15)	F2—C19—S1	106.8 (5)
O4—S2—C20	101.4 (3)	F1A—C19—S1	87 (2)
O6—S2—K1	36.38 (18)	F3A—C19—S1	114 (2)
O6—S2—O4	113.8 (3)	F3A—C19—F1A	99 (3)
O6—S2—C20	104.4 (3)	F3A—C19—F2A	132 (4)
O5—S2—K1	82.5 (2)	F2A—C19—S1	113 (3)
O5—S2—O4	113.0 (3)	F2A—C19—F1A	92 (4)

O5—S2—O6	117.4 (3)	C13—C17—H17A	109.5
O5—S2—C20	104.5 (3)	C13—C17—H17B	109.5
C20—S2—K1	126.3 (2)	C13—C17—H17C	109.5
O1—S1—K1^{i}	127.53 (17)	H17A—C17—H17B	109.5
O1—S1—C19	103.1 (3)	H17A—C17—H17C	109.5
O2—S1—K1^{i}	44.0 (2)	H17B—C17—H17C	109.5
O2—S1—O1	113.4 (3)	C14—C18—H18A	109.5
O2—S1—C19	102.5 (3)	C14—C18—H18B	109.5
C19—S1—K1^{i}	125.7 (3)	C14—C18—H18C	109.5
O3—S1—K1^{i}	72.1 (4)	H18A—C18—H18B	109.5
O3—S1—O1	115.2 (3)	H18A—C18—H18C	109.5
O3—S1—O2	114.8 (4)	H18B—C18—H18C	109.5
O3—S1—C19	105.7 (4)	S1—O3—K1	167.3 (5)

Symmetry codes: (i) -*x*+2, -*y*+1, -*z*+1; (ii) *x*+1, *y*, *z*; (iii) *x*-1, *y*, *z*.

8.3.9 Crystallographic data for 6-Yb

Crystal data

$C_{28}H_{42}F_6KO_8S_2Yb \cdot C_6H_{14}$	Z = 2
M_r = 983.04	F(000) = 998
Triclinic, $P\bar{1}$	D_x = 1.523 Mg m^{-3}
a = 12.2538 (4) Å	Mo $K\alpha$ radiation, λ = 0.71073 Å
b = 13.4960 (5) Å	Cell parameters from 9859 reflections
c = 13.8859 (4) Å	θ = 2.3–28.2°
α = 69.044 (1)°	μ = 2.45 mm^{-1}
β = 89.690 (1)°	T = 150 K
γ = 87.910 (1)°	Block, red
V = 2143.02 (12) Å^3	0.48 × 0.23 × 0.22 mm

Data collection

Bruker D8 VENTURE diffractometer	10599 independent reflections
Radiation source: microfocus sealed tube, INCOATEC Iμs 3.0	9929 reflections with $I > 2\sigma(I)$
Multilayer mirror optics monochromator	R_{int} = 0.051
Detector resolution: 7.4074 pixels mm^{-1}	θ_{max} = 28.3°, θ_{min} = 2.3°
ϕ and ω scans	h = -16→16

Absorption correction: multi-scan *SADABS2016*/2 (Bruker,2016/2) was used for absorption correction. wR2(int) was 0.0981 before and 0.0626 after correction. The Ratio of minimum to maximum transmission is 0.6623. The λ/2 correction factor is Not present.	k = -17→17
T_{min} = 0.494, T_{max} = 0.746	l = -17→18
48446 measured reflections	

Refinement

Refinement on F^2	Primary atom site location: dual
Least-squares matrix: full	Hydrogen site location: inferred from neighbouring sites
$R[F^2 > 2\sigma(F^2)]$ = 0.027	H-atom parameters constrained
$wR(F^2)$ = 0.070	$w = 1/[\sigma^2(F_o^2) + (0.0241P)^2 + 2.5891P]$ where $P = (F_o^2 + 2F_c^2)/3$
S = 1.04	$(\Delta/\sigma)_{max}$ = 0.002
10599 reflections	$\Delta\rangle_{max}$ = 0.90 e Å^{-3}
470 parameters	$\Delta\rangle_{min}$ = -0.80 e Å^{-3}
207 restraints	

Special details

Geometry. All esds (except the esd in the dihedral angle between two l.s. planes) are estimated using the full covariance matrix. The cell esds are taken into account individually in the estimation of esds in distances, angles and torsion angles; correlations between esds in cell parameters are only used when they are defined by crystal symmetry. An approximate (isotropic) treatment of cell esds is used for estimating esds involving l.s. planes.

Fractional atomic coordinates and isotropic or equivalent isotropic displacement parameters (Å²)

	x	*y*	*z*	U_{iso}*/U_{eq}	Occ. (<1)
Yb1	0.26301 (2)	0.74406 (2)	0.65554 (2)	0.02736 (4)	
K1	0.42872 (5)	0.59718 (4)	1.07706 (4)	0.03033 (11)	
S1	0.26458 (5)	0.51313 (5)	0.88585 (5)	0.03010 (13)	
S2	0.52812 (5)	0.67393 (5)	0.77769 (5)	0.03150 (13)	
O4	0.43560 (16)	0.73326 (15)	0.71541 (15)	0.0360 (4)	
F3	0.14075 (18)	0.38091 (17)	0.84335 (18)	0.0593 (5)	
O6	0.51330 (18)	0.64628 (18)	0.88603 (15)	0.0448 (5)	
O3	0.35695 (17)	0.44945 (17)	0.87692 (17)	0.0432 (5)	

O1	0.22901 (16)	0.59305 (15)	0.78759 (14)	0.0345 (4)	
O5	0.57244 (18)	0.59144 (17)	0.74599 (17)	0.0437 (5)	
F1	0.05890 (15)	0.47182 (19)	0.92150 (19)	0.0645 (6)	
O2	0.26608 (18)	0.55166 (18)	0.96887 (16)	0.0433 (5)	
F4	0.6009 (2)	0.85569 (18)	0.7713 (2)	0.0720 (7)	
F5	0.6503 (2)	0.8109 (2)	0.64447 (16)	0.0749 (7)	
F6	0.72454 (18)	0.7338 (2)	0.7927 (2)	0.0770 (7)	
O7	0.2687 (2)	0.6462 (2)	1.18968 (19)	0.0555 (6)	
F2	0.1704 (2)	0.34420 (19)	1.00410 (18)	0.0738 (7)	
O8	0.4868 (3)	0.7896 (2)	1.0676 (3)	0.0782 (9)	
C14	0.2913 (3)	0.7933 (2)	0.4586 (2)	0.0383 (6)	
C13	0.3660 (2)	0.7078 (2)	0.5041 (2)	0.0346 (6)	
C4	0.1286 (3)	0.8214 (3)	0.7614 (2)	0.0421 (7)	
C3	0.2326 (3)	0.8640 (2)	0.7647 (2)	0.0420 (7)	
C5	0.0916 (3)	0.8605 (3)	0.6584 (2)	0.0458 (7)	
C10	0.1854 (3)	0.7538 (3)	0.4824 (2)	0.0400 (6)	
H10	0.120429	0.793546	0.461701	0.048*	
C12	0.3062 (2)	0.6163 (2)	0.5565 (2)	0.0333 (5)	
C19	0.1517 (3)	0.4228 (3)	0.9154 (2)	0.0425 (7)	
C2	0.2589 (3)	0.9308 (2)	0.6626 (3)	0.0449 (7)	
C11	0.1937 (2)	0.6451 (2)	0.5424 (2)	0.0362 (6)	
C1	0.1718 (3)	0.9283 (2)	0.5985 (2)	0.0481 (8)	
H1	0.167450	0.965363	0.527772	0.058*	
C7	0.2978 (3)	0.8477 (3)	0.8608 (3)	0.0553 (9)	
H7A	0.289934	0.776443	0.908367	0.083*	
H7B	0.271781	0.896999	0.891962	0.083*	
H7C	0.373435	0.859096	0.843468	0.083*	
C17	0.4874 (3)	0.7120 (3)	0.4904 (2)	0.0456 (7)	
H17A	0.510914	0.780751	0.485505	0.068*	
H17B	0.506499	0.699584	0.428406	0.068*	
H17C	0.522622	0.658535	0.548401	0.068*	
C16	0.3551 (3)	0.5057 (2)	0.6102 (3)	0.0445 (7)	
H16A	0.421067	0.509681	0.645420	0.067*	
H16B	0.371396	0.473486	0.560061	0.067*	
H16C	0.303956	0.463739	0.659096	0.067*	
C18	0.3190 (4)	0.9034 (3)	0.3884 (3)	0.0577 (9)	
H18A	0.257002	0.950963	0.382019	0.086*	
H18B	0.337883	0.902232	0.321575	0.086*	
H18C	0.379696	0.927127	0.416702	0.086*	
C15	0.1005 (3)	0.5726 (3)	0.5821 (3)	0.0499 (8)	

H15A	0.115512	0.527007	0.652020	0.075*	
H15B	0.091874	0.530264	0.540067	0.075*	
H15C	0.034623	0.614170	0.579570	0.075*	
C8	0.0650 (3)	0.7536 (3)	0.8526 (3)	0.0582 (9)	
H8A	0.017377	0.710252	0.831302	0.087*	
H8B	0.022460	0.798342	0.880071	0.087*	
H8C	0.114663	0.708991	0.904634	0.087*	
C21	0.2828 (4)	0.6072 (4)	1.2996 (3)	0.0693 (12)	
H21A	0.262289	0.661874	1.327050	0.083*	
H21B	0.358301	0.584700	1.318174	0.083*	
C20	0.6321 (3)	0.7743 (3)	0.7447 (3)	0.0486 (8)	
C6	0.3599 (4)	0.9944 (3)	0.6298 (3)	0.0659 (11)	
H6A	0.423057	0.950656	0.660672	0.099*	
H6B	0.355113	1.054315	0.651724	0.099*	
H6C	0.365772	1.018890	0.556071	0.099*	
C9	-0.0190 (3)	0.8414 (4)	0.6222 (3)	0.0670 (11)	
H9A	-0.021183	0.867720	0.548167	0.101*	
H9B	-0.074623	0.877640	0.647308	0.101*	
H9C	-0.031391	0.766610	0.648026	0.101*	
C24	0.1621 (3)	0.6177 (4)	1.1702 (3)	0.0676 (11)	
H24A	0.156060	0.618566	1.100296	0.081*	0.75
H24B	0.106576	0.665881	1.180605	0.081*	0.75
H24C	0.166452	0.574371	1.127548	0.081*	0.25
H24D	0.116798	0.680694	1.135162	0.081*	0.25
C22	0.2101 (4)	0.5153 (5)	1.3407 (3)	0.0870 (15)	
H22A	0.158035	0.527171	1.388669	0.104*	0.75
H22B	0.252783	0.450581	1.376264	0.104*	0.75
H22C	0.242196	0.451491	1.333645	0.104*	0.25
H22D	0.191276	0.501168	1.412214	0.104*	0.25
C25	0.5933 (4)	0.8217 (4)	1.0359 (4)	0.0844 (13)	
H25A	0.591376	0.892376	0.983550	0.101*	0.5
H25B	0.629342	0.772999	1.007702	0.101*	0.5
H25C	0.593313	0.874512	0.966693	0.101*	0.5
H25D	0.640874	0.761794	1.038305	0.101*	0.5
C34	0.1861 (6)	1.2590 (5)	0.5970 (5)	0.115 (2)*	
H34A	0.243860	1.233498	0.563966	0.173*	0.5
H34B	0.133629	1.300483	0.546160	0.173*	0.5
H34C	0.215786	1.302181	0.631658	0.173*	0.5
H34D	0.206148	1.331875	0.570095	0.173*	0.5
H34E	0.247706	1.215145	0.631990	0.173*	0.5

H34F	0.163472	1.237785	0.541389	0.173*	0.5
C23	0.1510 (5)	0.5068 (6)	1.2476 (5)	0.0788 (18)	0.75
H23A	0.186393	0.454106	1.224217	0.095*	0.75
H23B	0.075047	0.489896	1.262571	0.095*	0.75
C26A	0.6511 (9)	0.8208 (11)	1.1286 (8)	0.089 (3)*	0.5
H26A	0.688245	0.752973	1.164698	0.107*	0.5
H26B	0.702474	0.877286	1.113222	0.107*	0.5
C27	0.5290 (9)	0.8963 (10)	1.1658 (10)	0.089 (3)*	0.5
H27A	0.542734	0.887093	1.237234	0.107*	0.5
H27B	0.500698	0.967967	1.128647	0.107*	0.5
C28A	0.4460 (7)	0.8567 (7)	1.1132 (8)	0.064 (2)*	0.5
H28A	0.380633	0.831727	1.152832	0.077*	0.5
H28B	0.434507	0.929066	1.065570	0.077*	0.5
C33	0.1313 (8)	1.1662 (7)	0.6743 (7)	0.076 (2)*	0.5
H33A	0.107596	1.123139	0.635858	0.091*	0.5
H33B	0.188867	1.124818	0.720434	0.091*	0.5
C31	-0.0184 (12)	1.0699 (11)	0.7997 (12)	0.106 (4)*	0.5
H31A	-0.042535	1.038706	0.750781	0.127*	0.5
H31B	0.033742	1.020170	0.846307	0.127*	0.5
C32	0.0377 (9)	1.1712 (9)	0.7420 (9)	0.088 (3)*	0.5
H32A	-0.016721	1.221792	0.699563	0.105*	0.5
H32B	0.063892	1.199805	0.792163	0.105*	0.5
C33A	0.0987 (11)	1.2473 (10)	0.6675 (11)	0.125 (5)*	0.5
H33C	0.036434	1.292021	0.632694	0.150*	0.5
H33D	0.120891	1.269321	0.723535	0.150*	0.5
C30	-0.1132 (14)	1.0851 (12)	0.8594 (15)	0.169 (7)*	0.5
H30A	-0.090628	1.114184	0.910413	0.203*	0.5
H30B	-0.167161	1.133741	0.814089	0.203*	0.5
C29	-0.1590 (8)	0.9810 (8)	0.9098 (8)	0.165 (4)*	
H29A	-0.181438	0.953406	0.858514	0.247*	0.5
H29B	-0.220907	0.987528	0.950056	0.247*	0.5
H29C	-0.104676	0.933607	0.954049	0.247*	0.5
H29D	-0.211068	1.038424	0.901448	0.247*	0.5
H29E	-0.125435	0.959862	0.976818	0.247*	0.5
H29F	-0.195431	0.921988	0.903188	0.247*	0.5
C32A	0.0683 (9)	1.1370 (7)	0.7083 (8)	0.075 (2)*	0.5
H32C	0.133805	1.092549	0.732440	0.090*	0.5
H32D	0.037300	1.119088	0.652743	0.090*	0.5
C30A	-0.0740 (14)	1.0162 (13)	0.8295 (14)	0.154 (7)*	0.5
H30C	-0.019232	0.958648	0.849124	0.185*	0.5

H30D	-0.108493	1.014385	0.767480	0.185*	0.5
C22A	0.1166 (10)	0.5575 (16)	1.2717 (10)	0.072 (5)	0.25
H22E	0.070486	0.603559	1.296000	0.086*	0.25
H22F	0.073345	0.500273	1.267771	0.086*	0.25
C27A	0.5565 (9)	0.8394 (13)	1.1852 (10)	0.115 (4)*	0.5
H27C	0.566785	0.901834	1.202782	0.138*	0.5
H27D	0.548533	0.779072	1.248736	0.138*	0.5
C28	0.4604 (10)	0.8191 (10)	1.1561 (10)	0.096 (3)*	0.5
H28C	0.385351	0.846161	1.149822	0.116*	0.5
H28D	0.466421	0.756356	1.218242	0.116*	0.5
C26	0.6272 (11)	0.8685 (13)	1.1154 (11)	0.115 (4)*	0.5
H26C	0.673864	0.817378	1.167248	0.138*	0.5
H26D	0.668376	0.931579	1.082134	0.138*	0.5
C31A	-0.0121 (14)	1.1118 (13)	0.7949 (13)	0.126 (6)*	0.5
H31C	0.027618	1.113055	0.854719	0.151*	0.5
H31D	-0.064981	1.170964	0.776661	0.151*	0.5

Atomic displacement parameters (Å²)

	U^{11}	U^{22}	U^{33}	U^{12}	U^{13}	U^{23}
Yb1	0.03398 (7)	0.02622 (6)	0.02065 (6)	0.00560 (4)	-0.00146 (4)	-0.00748 (4)
K1	0.0317 (3)	0.0323 (3)	0.0280 (3)	-0.0003 (2)	-0.0007 (2)	-0.0121 (2)
S1	0.0276 (3)	0.0335 (3)	0.0255 (3)	-0.0053 (2)	-0.0007 (2)	-0.0055 (2)
S2	0.0305 (3)	0.0313 (3)	0.0273 (3)	-0.0044 (2)	0.0012 (2)	-0.0037 (2)
O4	0.0356 (10)	0.0337 (10)	0.0362 (10)	0.0021 (8)	-0.0053 (8)	-0.0097 (8)
F3	0.0627 (13)	0.0599 (12)	0.0664 (13)	-0.0222 (10)	0.0030 (10)	-0.0340 (11)
O6	0.0446 (12)	0.0540 (13)	0.0277 (10)	-0.0090 (10)	0.0028 (8)	-0.0040 (9)
O3	0.0325 (10)	0.0425 (11)	0.0467 (12)	0.0027 (9)	-0.0009 (9)	-0.0065 (9)
O1	0.0401 (10)	0.0335 (10)	0.0261 (9)	-0.0003 (8)	0.0010 (8)	-0.0060 (8)
O5	0.0418 (11)	0.0384 (11)	0.0475 (12)	0.0039 (9)	0.0033 (9)	-0.0117 (9)
F1	0.0318 (10)	0.0840 (16)	0.0866 (16)	-0.0136 (10)	0.0136 (10)	-0.0405 (13)
O2	0.0459 (12)	0.0556 (13)	0.0310 (10)	-0.0118 (10)	-0.0024 (9)	-0.0178 (9)
F4	0.0890 (17)	0.0531 (13)	0.0781 (16)	-0.0287 (12)	0.0004 (13)	-0.0262 (12)
F5	0.0830 (17)	0.0846 (16)	0.0448 (11)	-0.0455 (14)	0.0186 (11)	-0.0044 (11)
F6	0.0433 (12)	0.0893 (17)	0.0816 (17)	-0.0223 (11)	-0.0133 (11)	-0.0080 (14)
O7	0.0519 (14)	0.0716 (16)	0.0500 (13)	-0.0058 (12)	0.0110 (11)	-0.0303 (13)
F2	0.0766 (15)	0.0664 (14)	0.0535 (12)	-0.0337 (12)	0.0014 (11)	0.0118 (11)
O8	0.0745 (19)	0.0689 (18)	0.114 (3)	-0.0148 (15)	0.0129 (18)	-0.0593 (19)
C14	0.0527 (17)	0.0382 (14)	0.0219 (12)	0.0013 (13)	0.0027 (11)	-0.0086 (11)

C13	0.0433 (15)	0.0386 (14)	0.0259 (12)	-0.0017 (12)	0.0052 (11)	-0.0167 (11)
C4	0.0458 (16)	0.0443 (16)	0.0369 (15)	0.0160 (13)	0.0016 (12)	-0.0170 (13)
C3	0.0576 (19)	0.0362 (15)	0.0363 (15)	0.0141 (13)	-0.0031 (13)	-0.0196 (12)
C5	0.0499 (18)	0.0457 (17)	0.0412 (16)	0.0246 (14)	-0.0089 (13)	-0.0171 (14)
C10	0.0454 (16)	0.0505 (17)	0.0236 (12)	0.0092 (13)	-0.0075 (11)	-0.0137 (12)
C12	0.0402 (14)	0.0363 (14)	0.0270 (12)	-0.0005 (11)	0.0039 (10)	-0.0157 (11)
C19	0.0383 (15)	0.0448 (16)	0.0408 (15)	-0.0127 (13)	0.0014 (12)	-0.0098 (13)
C2	0.063 (2)	0.0270 (13)	0.0452 (17)	0.0100 (13)	0.0008 (15)	-0.0146 (12)
C11	0.0401 (15)	0.0457 (15)	0.0259 (12)	-0.0026 (12)	0.0003 (11)	-0.0166 (11)
C1	0.072 (2)	0.0317 (14)	0.0355 (15)	0.0222 (14)	-0.0030 (15)	-0.0078 (12)
C7	0.069 (2)	0.061 (2)	0.0468 (18)	0.0133 (18)	-0.0117 (17)	-0.0339 (17)
C17	0.0419 (16)	0.0578 (19)	0.0387 (15)	-0.0045 (14)	0.0116 (13)	-0.0191 (14)
C16	0.0559 (19)	0.0365 (15)	0.0447 (16)	0.0045 (13)	0.0017 (14)	-0.0195 (13)
C18	0.086 (3)	0.0443 (18)	0.0328 (16)	-0.0004 (18)	0.0108 (16)	-0.0021 (14)
C15	0.0446 (17)	0.068 (2)	0.0434 (17)	-0.0136 (16)	0.0031 (14)	-0.0264 (16)
C8	0.055 (2)	0.069 (2)	0.0447 (18)	0.0172 (18)	0.0130 (16)	-0.0159 (17)
C21	0.066 (2)	0.105 (3)	0.055 (2)	0.008 (2)	-0.0039 (19)	-0.051 (2)
C20	0.0493 (18)	0.0508 (18)	0.0387 (16)	-0.0177 (15)	0.0013 (13)	-0.0061 (14)
C6	0.091 (3)	0.0342 (17)	0.072 (3)	-0.0093 (18)	0.007 (2)	-0.0174 (17)
C9	0.049 (2)	0.090 (3)	0.067 (2)	0.032 (2)	-0.0185 (18)	-0.036 (2)
C24	0.046 (2)	0.107 (3)	0.053 (2)	0.008 (2)	0.0005 (16)	-0.033 (2)
C22	0.087 (3)	0.117 (4)	0.047 (2)	-0.007 (3)	0.017 (2)	-0.017 (3)
C25	0.096 (3)	0.064 (3)	0.104 (3)	-0.019 (2)	0.019 (3)	-0.041 (2)
C23	0.053 (3)	0.099 (5)	0.076 (4)	-0.016 (3)	0.013 (3)	-0.020 (4)
C22A	0.034 (7)	0.095 (12)	0.085 (11)	-0.007 (7)	0.022 (7)	-0.030 (9)

Geometric parameters (Å, º)

Yb1—O4	2.2572 (19)	C6—H6B	0.9600
Yb1—O1	2.2516 (18)	C6—H6C	0.9600
Yb1—C14	2.597 (3)	C9—H9A	0.9600
Yb1—C13	2.630 (3)	C9—H9B	0.9600
Yb1—C4	2.629 (3)	C9—H9C	0.9600
Yb1—C3	2.601 (3)	C24—H24A	0.9700
Yb1—C5	2.586 (3)	C24—H24B	0.9700
Yb1—C10	2.547 (3)	C24—H24C	0.9700
Yb1—C12	2.601 (3)	C24—H24D	0.9700
Yb1—C2	2.556 (3)	C24—C23	1.509 (7)
Yb1—C11	2.564 (3)	C24—C22A	1.470 (11)

Yb1—C1	2.541 (3)	C22—H22A	0.9700
K1—K1^{i}	4.2607 (11)	C22—H22B	0.9700
K1—S2^{i}	3.5110 (9)	C22—H22C	0.9700
K1—O6^{i}	3.193 (2)	C22—H22D	0.9700
K1—O6	2.704 (2)	C22—C23	1.527 (7)
K1—O3^{i}	2.704 (2)	C22—C22A	1.460 (12)
K1—O5^{i}	2.837 (2)	C25—H25A	0.9700
K1—O2	2.718 (2)	C25—H25B	0.9700
K1—O7	2.710 (2)	C25—H25C	0.9700
K1—O8	2.676 (3)	C25—H25D	0.9700
S1—O3	1.428 (2)	C25—C26A	1.468 (10)
S1—O1	1.4610 (19)	C25—C26	1.521 (11)
S1—O2	1.425 (2)	C34—H34A	0.9600
S1—C19	1.824 (3)	C34—H34B	0.9600
S2—O4	1.457 (2)	C34—H34C	0.9600
S2—O6	1.427 (2)	C34—H34D	0.9600
S2—O5	1.425 (2)	C34—H34E	0.9600
S2—C20	1.828 (3)	C34—H34F	0.9600
F3—C19	1.323 (4)	C34—C33	1.504 (9)
F1—C19	1.312 (4)	C34—C33A	1.422 (11)
F4—C20	1.322 (4)	C23—H23A	0.9700
F5—C20	1.320 (4)	C23—H23B	0.9700
F6—C20	1.315 (4)	C26A—H26A	0.9700
O7—C21	1.434 (4)	C26A—H26B	0.9700
O7—C24	1.429 (5)	C26A—C27A	1.461 (12)
F2—C19	1.322 (4)	C27—H27A	0.9700
O8—C25	1.408 (5)	C27—H27B	0.9700
O8—C28A	1.357 (8)	C27—C28	1.405 (11)
O8—C28	1.452 (10)	C27—C26	1.492 (12)
C14—C13	1.406 (4)	C28A—H28A	0.9700
C14—C10	1.414 (4)	C28A—H28B	0.9700
C14—C18	1.507 (4)	C28A—C27A	1.646 (11)
C13—C12	1.417 (4)	C33—H33A	0.9700
C13—C17	1.500 (4)	C33—H33B	0.9700
C4—C3	1.425 (5)	C33—C32	1.494 (10)
C4—C5	1.407 (4)	C31—H31A	0.9700
C4—C8	1.503 (5)	C31—H31B	0.9700
C3—C2	1.424 (4)	C31—C32	1.505 (11)
C3—C7	1.501 (4)	C31—C30	1.474 (12)
C5—C1	1.418 (5)	C32—H32A	0.9700

C5—C9	1.510 (5)	C32—H32B	0.9700
C10—H10	0.9300	C33A—H33C	0.9700
C10—C11	1.405 (4)	C33A—H33D	0.9700
C12—C11	1.414 (4)	C33A—C32A	1.452 (11)
C12—C16	1.512 (4)	C30—H30A	0.9700
C2—C1	1.402 (5)	C30—H30B	0.9700
C2—C6	1.506 (5)	C30—C29	1.459 (12)
C11—C15	1.501 (4)	C29—H29A	0.9600
C1—H1	0.9300	C29—H29B	0.9600
C7—H7A	0.9600	C29—H29C	0.9600
C7—H7B	0.9600	C29—H29D	0.9600
C7—H7C	0.9600	C29—H29E	0.9600
C17—H17A	0.9600	C29—H29F	0.9600
C17—H17B	0.9600	C29—C30A	1.482 (11)
C17—H17C	0.9600	C32A—H32C	0.9700
C16—H16A	0.9600	C32A—H32D	0.9700
C16—H16B	0.9600	C32A—C31A	1.501 (11)
C16—H16C	0.9600	C30A—H30C	0.9700
C18—H18A	0.9600	C30A—H30D	0.9700
C18—H18B	0.9600	C30A—C31A	1.448 (12)
C18—H18C	0.9600	C22A—H22E	0.9700
C15—H15A	0.9600	C22A—H22F	0.9700
C15—H15B	0.9600	C27A—H27C	0.9700
C15—H15C	0.9600	C27A—H27D	0.9700
C8—H8A	0.9600	C28—H28C	0.9700
C8—H8B	0.9600	C28—H28D	0.9700
C8—H8C	0.9600	C26—H26C	0.9700
C21—H21A	0.9700	C26—H26D	0.9700
C21—H21B	0.9700	C31A—H31C	0.9700
C21—C22	1.492 (6)	C31A—H31D	0.9700
C6—H6A	0.9600		
O4—Yb1—C14	102.57 (9)	C13—C17—H17C	109.5
O4—Yb1—C13	81.34 (8)	H17A—C17—H17B	109.5
O4—Yb1—C4	110.53 (9)	H17A—C17—H17C	109.5
O4—Yb1—C3	82.34 (9)	H17B—C17—H17C	109.5
O4—Yb1—C5	133.93 (9)	C12—C16—H16A	109.5
O4—Yb1—C10	132.46 (9)	C12—C16—H16B	109.5
O4—Yb1—C12	93.54 (8)	C12—C16—H16C	109.5
O4—Yb1—C2	84.55 (9)	H16A—C16—H16B	109.5

O4—Yb1—C11	125.29 (8)	H16A—C16—H16C	109.5
O4—Yb1—C1	114.94 (10)	H16B—C16—H16C	109.5
O1—Yb1—O4	88.84 (7)	C14—C18—H18A	109.5
O1—Yb1—C14	134.67 (8)	C14—C18—H18B	109.5
O1—Yb1—C13	112.24 (8)	C14—C18—H18C	109.5
O1—Yb1—C4	80.72 (9)	H18A—C18—H18B	109.5
O1—Yb1—C3	94.03 (9)	H18A—C18—H18C	109.5
O1—Yb1—C5	101.30 (9)	H18B—C18—H18C	109.5
O1—Yb1—C10	114.48 (9)	C11—C15—H15A	109.5
O1—Yb1—C12	83.75 (8)	C11—C15—H15B	109.5
O1—Yb1—C2	126.07 (9)	C11—C15—H15C	109.5
O1—Yb1—C11	84.61 (8)	H15A—C15—H15B	109.5
O1—Yb1—C1	131.76 (9)	H15A—C15—H15C	109.5
C14—Yb1—C13	31.20 (9)	H15B—C15—H15C	109.5
C14—Yb1—C4	132.00 (10)	C4—C8—H8A	109.5
C14—Yb1—C3	130.66 (10)	C4—C8—H8B	109.5
C14—Yb1—C12	52.23 (9)	C4—C8—H8C	109.5
C4—Yb1—C13	163.18 (10)	H8A—C8—H8B	109.5
C3—Yb1—C13	148.59 (10)	H8A—C8—H8C	109.5
C3—Yb1—C4	31.62 (11)	H8B—C8—H8C	109.5
C3—Yb1—C12	175.38 (9)	O7—C21—H21A	110.5
C5—Yb1—C14	101.35 (10)	O7—C21—H21B	110.5
C5—Yb1—C13	132.10 (10)	O7—C21—C22	106.0 (3)
C5—Yb1—C4	31.29 (10)	H21A—C21—H21B	108.7
C5—Yb1—C3	52.45 (10)	C22—C21—H21A	110.5
C5—Yb1—C12	131.95 (10)	C22—C21—H21B	110.5
C10—Yb1—C14	31.89 (10)	F4—C20—S2	111.0 (2)
C10—Yb1—C13	51.96 (9)	F5—C20—S2	110.8 (2)
C10—Yb1—C4	113.67 (10)	F5—C20—F4	107.8 (3)
C10—Yb1—C3	132.29 (10)	F6—C20—S2	110.5 (2)
C10—Yb1—C5	83.70 (10)	F6—C20—F4	108.2 (3)
C10—Yb1—C12	52.27 (9)	F6—C20—F5	108.3 (3)
C10—Yb1—C2	108.88 (10)	C2—C6—H6A	109.5
C10—Yb1—C11	31.90 (10)	C2—C6—H6B	109.5
C12—Yb1—C13	31.42 (8)	C2—C6—H6C	109.5
C12—Yb1—C4	150.89 (10)	H6A—C6—H6B	109.5
C2—Yb1—C14	98.85 (10)	H6A—C6—H6C	109.5
C2—Yb1—C13	119.40 (10)	H6B—C6—H6C	109.5
C2—Yb1—C4	52.75 (11)	C5—C9—H9A	109.5
C2—Yb1—C3	32.04 (10)	C5—C9—H9B	109.5

C2—Yb1—C5	53.14 (11)	C5—C9—H9C	109.5
C2—Yb1—C12	149.97 (10)	H9A—C9—H9B	109.5
C2—Yb1—C11	139.98 (10)	H9A—C9—H9C	109.5
C11—Yb1—C14	52.88 (9)	H9B—C9—H9C	109.5
C11—Yb1—C13	52.34 (9)	O7—C24—H24A	110.9
C11—Yb1—C4	121.69 (10)	O7—C24—H24B	110.9
C11—Yb1—C3	152.21 (10)	O7—C24—H24C	110.5
C11—Yb1—C5	100.51 (10)	O7—C24—H24D	110.5
C11—Yb1—C12	31.76 (9)	O7—C24—C23	104.1 (4)
C1—Yb1—C14	82.77 (10)	O7—C24—C22A	106.1 (6)
C1—Yb1—C13	112.45 (10)	H24A—C24—H24B	108.9
C1—Yb1—C4	52.25 (10)	H24C—C24—H24D	108.7
C1—Yb1—C3	52.49 (10)	C23—C24—H24A	110.9
C1—Yb1—C5	32.09 (11)	C23—C24—H24B	110.9
C1—Yb1—C10	80.70 (10)	C22A—C24—H24C	110.5
C1—Yb1—C12	131.74 (10)	C22A—C24—H24D	110.5
C1—Yb1—C2	31.93 (11)	C21—C22—H22A	110.5
C1—Yb1—C11	109.34 (11)	C21—C22—H22B	110.5
$S2^{i}$—K1—$K1^{i}$	62.780 (18)	C21—C22—H22C	112.0
O6—K1—$K1^{i}$	48.49 (5)	C21—C22—H22D	112.0
$O6^{i}$—K1—$K1^{i}$	39.36 (4)	C21—C22—C23	106.3 (4)
O6—K1—$S2^{i}$	110.98 (5)	H22A—C22—H22B	108.7
$O6^{i}$—K1—$S2^{i}$	23.98 (4)	H22C—C22—H22D	109.6
O6—K1—$O6^{i}$	87.85 (6)	C23—C22—H22A	110.5
O6—K1—$O5^{i}$	133.75 (7)	C23—C22—H22B	110.5
O6—K1—O2	76.72 (7)	C22A—C22—C21	99.0 (8)
O6—K1—O7	144.76 (8)	C22A—C22—H22C	112.0
$O3^{i}$—K1—$K1^{i}$	67.34 (5)	C22A—C22—H22D	112.0
$O3^{i}$—K1—$S2^{i}$	69.29 (5)	O8—C25—H25A	110.5
$O3^{i}$—K1—$O6^{i}$	69.14 (6)	O8—C25—H25B	110.5
$O3^{i}$—K1—O6	79.25 (7)	O8—C25—H25C	111.4
$O3^{i}$—K1—$O5^{i}$	76.49 (7)	O8—C25—H25D	111.4
$O3^{i}$—K1—O2	140.25 (7)	O8—C25—C26A	106.0 (6)
$O3^{i}$—K1—O7	129.34 (8)	O8—C25—C26	101.9 (6)
$O5^{i}$—K1—$K1^{i}$	85.73 (5)	H25A—C25—H25B	108.7
$O5^{i}$—K1—$S2^{i}$	22.95 (5)	H25C—C25—H25D	109.2
$O5^{i}$—K1—$O6^{i}$	46.75 (6)	C26A—C25—H25A	110.5
O2—K1—$K1^{i}$	73.00 (5)	C26A—C25—H25B	110.5
O2—K1—$S2^{i}$	90.51 (5)	C26—C25—H25C	111.4
O2—K1—$O6^{i}$	78.72 (7)	C26—C25—H25D	111.4

O2—K1—O5^{i}	98.30 (7)	H34A—C34—H34B	109.5
O7—K1—K1^{i}	152.24 (6)	H34A—C34—H34C	109.5
O7—K1—S2^{i}	99.79 (6)	H34B—C34—H34C	109.5
O7—K1—O6^{i}	119.28 (7)	H34D—C34—H34E	109.5
O7—K1—O5^{i}	78.76 (7)	H34D—C34—H34F	109.5
O7—K1—O2	86.52 (7)	H34E—C34—H34F	109.5
O8—K1—K1^{i}	128.30 (7)	C33—C34—H34A	109.5
O8—K1—S2^{i}	141.80 (8)	C33—C34—H34B	109.5
O8—K1—O6	86.70 (9)	C33—C34—H34C	109.5
O8—K1—O6^{i}	151.14 (9)	C33A—C34—H34D	109.5
O8—K1—O3^{i}	81.99 (9)	C33A—C34—H34E	109.5
O8—K1—O5^{i}	127.30 (9)	C33A—C34—H34F	109.5
O8—K1—O2	127.16 (10)	C24—C23—C22	100.9 (5)
O8—K1—O7	79.04 (9)	C24—C23—H23A	111.6
O3—S1—O1	113.43 (12)	C24—C23—H23B	111.6
O3—S1—C19	104.34 (14)	C22—C23—H23A	111.6
O1—S1—C19	101.78 (13)	C22—C23—H23B	111.6
O2—S1—O3	116.84 (14)	H23A—C23—H23B	109.4
O2—S1—O1	113.78 (13)	C25—C26A—H26A	112.1
O2—S1—C19	104.45 (14)	C25—C26A—H26B	112.1
O4—S2—K1^{i}	131.83 (8)	H26A—C26A—H26B	109.8
O4—S2—C20	101.59 (14)	C27A—C26A—C25	98.1 (8)
O6—S2—K1^{i}	65.40 (10)	C27A—C26A—H26A	112.1
O6—S2—O4	114.01 (13)	C27A—C26A—H26B	112.1
O6—S2—C20	104.46 (14)	H27A—C27—H27B	109.8
O5—S2—K1^{i}	50.90 (9)	C28—C27—H27A	112.2
O5—S2—O4	114.04 (13)	C28—C27—H27B	112.2
O5—S2—O6	115.66 (14)	C28—C27—C26	97.6 (10)
O5—S2—C20	105.01 (16)	C26—C27—H27A	112.2
C20—S2—K1^{i}	125.87 (12)	C26—C27—H27B	112.2
S2—O4—Yb1	151.75 (12)	O8—C28A—H28A	113.3
K1—O6—K1^{i}	92.15 (6)	O8—C28A—H28B	113.3
S2—O6—K1^{i}	90.62 (11)	O8—C28A—C27A	91.7 (7)
S2—O6—K1	164.77 (14)	H28A—C28A—H28B	110.7
S1—O3—K1^{i}	144.92 (14)	C27A—C28A—H28A	113.3
S1—O1—Yb1	148.40 (12)	C27A—C28A—H28B	113.3
S2—O5—K1^{i}	106.15 (11)	C34—C33—H33A	105.7
S1—O2—K1	133.63 (13)	C34—C33—H33B	105.7
C21—O7—K1	117.4 (2)	H33A—C33—H33B	106.1
C24—O7—K1	114.3 (2)	C32—C33—C34	126.5 (8)

C24—O7—C21	106.5 (3)	C32—C33—H33A	105.7
C25—O8—K1	118.8 (2)	C32—C33—H33B	105.7
C25—O8—C28	108.3 (5)	H31A—C31—H31B	107.7
C28A—O8—K1	132.1 (5)	C32—C31—H31A	108.9
C28A—O8—C25	106.5 (5)	C32—C31—H31B	108.9
C28—O8—K1	116.8 (5)	C30—C31—H31A	108.9
C13—C14—Yb1	75.69 (15)	C30—C31—H31B	108.9
C13—C14—C10	107.2 (3)	C30—C31—C32	113.4 (12)
C13—C14—C18	126.2 (3)	C33—C32—C31	118.0 (10)
C10—C14—Yb1	72.11 (15)	C33—C32—H32A	107.8
C10—C14—C18	126.3 (3)	C33—C32—H32B	107.8
C18—C14—Yb1	122.6 (2)	C31—C32—H32A	107.8
C14—C13—Yb1	73.11 (15)	C31—C32—H32B	107.8
C14—C13—C12	108.3 (3)	H32A—C32—H32B	107.1
C14—C13—C17	125.0 (3)	C34—C33A—H33C	109.8
C12—C13—Yb1	73.15 (15)	C34—C33A—H33D	109.8
C12—C13—C17	126.5 (3)	C34—C33A—C32A	109.5 (10)
C17—C13—Yb1	123.88 (19)	H33C—C33A—H33D	108.2
C3—C4—Yb1	73.12 (16)	C32A—C33A—H33C	109.8
C3—C4—C8	126.2 (3)	C32A—C33A—H33D	109.8
C5—C4—Yb1	72.68 (17)	C31—C30—H30A	110.3
C5—C4—C3	108.1 (3)	C31—C30—H30B	110.3
C5—C4—C8	125.6 (3)	H30A—C30—H30B	108.6
C8—C4—Yb1	123.6 (2)	C29—C30—C31	106.9 (11)
C4—C3—Yb1	75.26 (16)	C29—C30—H30A	110.3
C4—C3—C7	125.4 (3)	C29—C30—H30B	110.3
C2—C3—Yb1	72.23 (16)	C30—C29—H29A	109.5
C2—C3—C4	107.9 (3)	C30—C29—H29B	109.5
C2—C3—C7	126.5 (3)	C30—C29—H29C	109.5
C7—C3—Yb1	122.1 (2)	H29A—C29—H29B	109.5
C4—C5—Yb1	76.03 (17)	H29A—C29—H29C	109.5
C4—C5—C1	107.5 (3)	H29B—C29—H29C	109.5
C4—C5—C9	125.2 (3)	H29D—C29—H29E	109.5
C1—C5—Yb1	72.22 (17)	H29D—C29—H29F	109.5
C1—C5—C9	127.0 (3)	H29E—C29—H29F	109.5
C9—C5—Yb1	122.2 (2)	C30A—C29—H29D	109.5
Yb1—C10—H10	115.9	C30A—C29—H29E	109.5
C14—C10—Yb1	76.00 (16)	C30A—C29—H29F	109.5
C14—C10—H10	125.4	C33A—C32A—H32C	108.7
C11—C10—Yb1	74.70 (15)	C33A—C32A—H32D	108.7

C11—C10—C14	109.2 (3)	C33A—C32A—C31A	114.3 (10)
C11—C10—H10	125.4	H32C—C32A—H32D	107.6
C13—C12—Yb1	75.43 (15)	C31A—C32A—H32C	108.7
C13—C12—C16	125.4 (3)	C31A—C32A—H32D	108.7
C11—C12—Yb1	72.68 (15)	C29—C30A—H30C	104.6
C11—C12—C13	108.1 (3)	C29—C30A—H30D	104.6
C11—C12—C16	126.3 (3)	H30C—C30A—H30D	105.7
C16—C12—Yb1	121.79 (18)	C31A—C30A—C29	130.6 (14)
F3—C19—S1	110.9 (2)	C31A—C30A—H30C	104.6
F1—C19—S1	111.5 (2)	C31A—C30A—H30D	104.6
F1—C19—F3	107.9 (3)	C24—C22A—H22E	110.5
F1—C19—F2	108.7 (3)	C24—C22A—H22F	110.5
F2—C19—S1	109.9 (2)	C22—C22A—C24	106.0 (8)
F2—C19—F3	107.8 (3)	C22—C22A—H22E	110.5
C3—C2—Yb1	75.72 (16)	C22—C22A—H22F	110.5
C3—C2—C6	126.5 (3)	H22E—C22A—H22F	108.7
C1—C2—Yb1	73.46 (17)	C26A—C27A—C28A	109.3 (9)
C1—C2—C3	107.2 (3)	C26A—C27A—H27C	109.8
C1—C2—C6	126.3 (3)	C26A—C27A—H27D	109.8
C6—C2—Yb1	117.7 (2)	C28A—C27A—H27C	109.8
C10—C11—Yb1	73.39 (16)	C28A—C27A—H27D	109.8
C10—C11—C12	107.2 (3)	H27C—C27A—H27D	108.3
C10—C11—C15	126.3 (3)	O8—C28—H28C	109.0
C12—C11—Yb1	75.56 (15)	O8—C28—H28D	109.0
C12—C11—C15	126.5 (3)	C27—C28—O8	112.8 (9)
C15—C11—Yb1	117.69 (19)	C27—C28—H28C	109.0
Yb1—C1—H1	116.3	C27—C28—H28D	109.0
C5—C1—Yb1	75.69 (17)	H28C—C28—H28D	107.8
C5—C1—H1	125.3	C25—C26—H26C	109.6
C2—C1—Yb1	74.61 (17)	C25—C26—H26D	109.6
C2—C1—C5	109.3 (3)	C27—C26—C25	110.3 (9)
C2—C1—H1	125.3	C27—C26—H26C	109.6
C3—C7—H7A	109.5	C27—C26—H26D	109.6
C3—C7—H7B	109.5	H26C—C26—H26D	108.1
C3—C7—H7C	109.5	C32A—C31A—H31C	106.5
H7A—C7—H7B	109.5	C32A—C31A—H31D	106.5
H7A—C7—H7C	109.5	C30A—C31A—C32A	123.5 (13)
H7B—C7—H7C	109.5	C30A—C31A—H31C	106.5
C13—C17—H17A	109.5	C30A—C31A—H31D	106.5
C13—C17—H17B	109.5	H31C—C31A—H31D	106.5

Symmetry code: (i) -*x*+1, -*y*+1, -*z*+2.

8.3.10 Crystallographic data for 7-Y

Crystal data

$C_{19}H_{20}B_2F_3N_{12}O_3SY$	$Z = 4$
$M_r = 664.06$	$F(000) = 1336$
Triclinic, $P\bar{1}$	$D_x = 1.651$ Mg m^{-3}
$a = 11.9549$ (6) Å	Mo $K\alpha$ radiation, $\lambda = 0.71073$ Å
$b = 12.3329$ (7) Å	Cell parameters from 9937 reflections
$c = 18.2724$ (9) Å	$\theta = 2.4$–$27.8°$
$\alpha = 96.912$ (2)°	$\mu = 2.33$ mm^{-1}
$\beta = 91.681$ (2)°	$T = 150$ K
$\gamma = 91.478$ (2)°	Block, colourless
$V = 2672.2$ (2) Å^3	0.17 × 0.12 × 0.05 mm

Data collection

Bruker D8 VENTURE diffractometer	13277 independent reflections
Radiation source: microfocus sealed tube, INCOATEC Iμs 3.0	9931 reflections with $I > 2\sigma(I)$
Multilayer mirror optics monochromator	$R_{int} = 0.077$
Detector resolution: 7.4074 pixels mm^{-1}	$\theta_{max} = 28.3°$, $\theta_{min} = 2.3°$
ϕ and ω scans	$h = -15 \rightarrow 15$
Absorption correction: multi-scan *SADABS2016*/2 (Bruker,2016/2) was used for absorption correction. wR2(int) was 0.0910 before and 0.0670 after correction. The Ratio of minimum to maximum transmission is 0.7865. The λ/2 correction factor is Not present.	$k = -16 \rightarrow 16$
$T_{min} = 0.587$, $T_{max} = 0.746$	$l = -24 \rightarrow 24$
63730 measured reflections	

Refinement

Refinement on F^2	Primary atom site location: dual
Least-squares matrix: full	Hydrogen site location: inferred from neighbouring sites
$R[F^2 > 2\sigma(F^2)] = 0.048$	H-atom parameters constrained

$wR(F^2)$ = 0.119	$w = 1/[\sigma^2(F_o^2) + (0.0574P)^2 + 1.3452P]$ where $P = (F_o^2 + 2F_c^2)/3$
S = 1.02	$(\Delta/\sigma)_{max}$ = 0.002
13277 reflections	$\Delta\rangle_{max}$ = 1.28 e Å^{-3}
752 parameters	$\Delta\rangle_{min}$ = -0.67 e Å^{-3}
9 restraints	

Special details

Geometry. All esds (except the esd in the dihedral angle between two l.s. planes) are estimated using the full covariance matrix. The cell esds are taken into account individually in the estimation of esds in distances, angles and torsion angles; correlations between esds in cell parameters are only used when they are defined by crystal symmetry. An approximate (isotropic) treatment of cell esds is used for estimating esds involving l.s. planes.

Fractional atomic coordinates and isotropic or equivalent isotropic displacement parameters (Å²)

	x	*y*	*z*	U_{iso}*/U_{eq}	Occ. (<1)
Y1	0.84426 (2)	0.30353 (2)	0.02072 (2)	0.01846 (8)	
S1	0.84978 (7)	0.60387 (7)	-0.00448 (4)	0.02042 (17)	
F1	0.7856 (3)	0.5380 (3)	-0.14217 (14)	0.0581 (12)	0.843 (6)
F2	0.8328 (4)	0.7041 (4)	-0.1234 (2)	0.098 (2)	0.843 (6)
F3	0.6763 (2)	0.6471 (4)	-0.08546 (18)	0.0567 (11)	0.843 (6)
O1	0.8506 (2)	0.48712 (19)	-0.00837 (13)	0.0308 (6)	
O2	0.96060 (18)	0.65254 (18)	-0.00556 (12)	0.0240 (5)	
O3	0.7812 (2)	0.6564 (2)	0.05036 (14)	0.0389 (6)	
N1	0.8968 (2)	0.3699 (2)	0.20672 (14)	0.0241 (6)	
N2	0.9075 (2)	0.4109 (2)	0.14121 (14)	0.0227 (6)	
N3	0.7280 (2)	0.2487 (2)	0.17793 (14)	0.0255 (6)	
N4	0.6996 (2)	0.2847 (2)	0.11182 (14)	0.0254 (6)	
N5	0.9236 (2)	0.1733 (2)	0.16439 (14)	0.0253 (6)	
N6	0.9432 (2)	0.1834 (2)	0.09226 (14)	0.0244 (6)	
N7	0.6239 (2)	0.2572 (3)	-0.10267 (15)	0.0288 (7)	
N8	0.6706 (2)	0.3327 (2)	-0.04901 (14)	0.0254 (6)	
N9	0.6912 (2)	0.0809 (2)	-0.06616 (16)	0.0307 (7)	
N10	0.7558 (2)	0.1137 (2)	-0.00436 (15)	0.0284 (6)	
N11	0.7981 (2)	0.1788 (2)	-0.15534 (14)	0.0249 (6)	
N12	0.8824 (2)	0.2282 (2)	-0.10874 (14)	0.0231 (6)	
C1	0.9420 (3)	0.4407 (3)	0.26183 (17)	0.0269 (7)	
H1	0.944272	0.430449	0.312553	0.032*	

C2	0.9841 (3)	0.5298 (3)	0.23319 (18)	0.0311 (8)	
H2	1.021011	0.592848	0.258885	0.037*	
C3	0.9604 (3)	0.5072 (3)	0.15726 (18)	0.0256 (7)	
H3	0.979748	0.554440	0.121924	0.031*	
C4	0.6352 (3)	0.2179 (3)	0.21036 (19)	0.0302 (8)	
H4	0.633104	0.189781	0.256500	0.036*	
C5	0.5438 (3)	0.2334 (3)	0.1661 (2)	0.0333 (8)	
H5	0.467282	0.219529	0.175249	0.040*	
C6	0.5878 (3)	0.2740 (3)	0.10526 (19)	0.0291 (8)	
H6	0.544431	0.291801	0.064230	0.035*	
C7	0.9859 (4)	0.0930 (3)	0.1855 (2)	0.0368 (9)	
H7	0.987362	0.069739	0.233171	0.044*	
C8	1.0472 (4)	0.0497 (3)	0.1271 (2)	0.0414 (10)	
H8	1.098843	-0.007731	0.126278	0.050*	
C9	1.0174 (3)	0.1080 (3)	0.0699 (2)	0.0317 (8)	
H9	1.045442	0.096167	0.021534	0.038*	
C10	0.5295 (3)	0.2952 (4)	-0.1298 (2)	0.0417 (10)	
H10	0.481916	0.257497	-0.167603	0.050*	
C11	0.5126 (3)	0.3972 (4)	-0.0943 (2)	0.0460 (11)	
H11	0.452910	0.444168	-0.102415	0.055*	
C12	0.6021 (3)	0.4169 (3)	-0.0439 (2)	0.0324 (8)	
H12	0.613062	0.481537	-0.010215	0.039*	
C13	0.6406 (4)	-0.0160 (3)	-0.0596 (2)	0.0480 (11)	
H13	0.590606	-0.055487	-0.095166	0.058*	
C14	0.6725 (4)	-0.0482 (4)	0.0064 (2)	0.0519 (12)	
H14	0.650640	-0.113374	0.025783	0.062*	
C15	0.7442 (4)	0.0351 (3)	0.0389 (2)	0.0388 (9)	
H15	0.780215	0.035986	0.086016	0.047*	
C16	0.8372 (3)	0.1548 (3)	-0.22347 (17)	0.0278 (8)	
H16	0.794883	0.120869	-0.265227	0.033*	
C17	0.9471 (3)	0.1870 (3)	-0.22303 (18)	0.0278 (8)	
H17	0.996035	0.180305	-0.263286	0.033*	
C18	0.9720 (3)	0.2317 (3)	-0.15075 (17)	0.0249 (7)	
H18	1.043462	0.260944	-0.133349	0.030*	
C37	0.7817 (3)	0.6288 (3)	-0.0929 (2)	0.0339 (8)	
B1	0.8490 (3)	0.2545 (3)	0.2095 (2)	0.0264 (8)	
H1A	0.849109	0.238327	0.261860	0.032*	
B2	0.6811 (3)	0.1507 (3)	-0.1292 (2)	0.0291 (9)	
H2A	0.635980	0.109768	-0.171011	0.035*	
F1A	0.8360 (14)	0.6112 (16)	-0.1470 (8)	0.045 (5)*	0.157 (6)

F2A	0.7625 (14)	0.7390 (10)	-0.0802 (9)	0.042 (5)*	0.157 (6)
F3A	0.6841 (15)	0.583 (2)	-0.1047 (13)	0.070 (7)*	0.157 (6)
Y2	0.34448 (2)	0.20384 (2)	0.52763 (2)	0.01525 (8)	
S2	0.56020 (6)	0.06478 (6)	0.40400 (4)	0.01621 (15)	
F4	0.5236 (2)	-0.0628 (2)	0.28165 (12)	0.0532 (7)	
F5	0.44219 (18)	0.09017 (17)	0.28567 (11)	0.0357 (5)	
F6	0.37786 (18)	-0.03393 (19)	0.34569 (12)	0.0431 (6)	
O4	0.48662 (18)	0.13507 (18)	0.44840 (11)	0.0223 (5)	
O5	0.59117 (18)	-0.03144 (17)	0.43659 (11)	0.0210 (5)	
O6	0.65106 (19)	0.12169 (19)	0.37523 (12)	0.0260 (5)	
N13	0.3602 (2)	0.4491 (2)	0.63239 (16)	0.0265 (6)	
N14	0.3486 (2)	0.4065 (2)	0.55966 (15)	0.0235 (6)	
N15	0.3238 (2)	0.2921 (2)	0.70753 (14)	0.0254 (6)	
N16	0.2949 (2)	0.2076 (2)	0.65497 (14)	0.0224 (6)	
N17	0.5163 (2)	0.3326 (2)	0.66439 (14)	0.0233 (6)	
N18	0.5186 (2)	0.2654 (2)	0.59924 (14)	0.0205 (6)	
N19	0.0792 (2)	0.2758 (2)	0.47523 (14)	0.0207 (6)	
N20	0.1475 (2)	0.2758 (2)	0.53576 (14)	0.0209 (6)	
N21	0.2112 (2)	0.2585 (2)	0.37023 (14)	0.0234 (6)	
N22	0.3112 (2)	0.2687 (2)	0.40869 (14)	0.0220 (6)	
N23	0.1264 (2)	0.0901 (2)	0.41764 (14)	0.0226 (6)	
N24	0.2060 (2)	0.0648 (2)	0.46827 (14)	0.0194 (5)	
C19	0.3340 (3)	0.5550 (3)	0.6400 (2)	0.0335 (9)	
H19	0.335125	0.602351	0.685047	0.040*	
C20	0.3050 (3)	0.5834 (3)	0.5716 (2)	0.0368 (9)	
H20	0.282974	0.652834	0.559686	0.044*	
C21	0.3153 (3)	0.4886 (3)	0.5240 (2)	0.0308 (8)	
H21	0.300374	0.482704	0.472309	0.037*	
C22	0.2804 (3)	0.2718 (4)	0.77216 (18)	0.0358 (9)	
H22	0.287248	0.319066	0.817242	0.043*	
C23	0.2249 (3)	0.1725 (4)	0.7623 (2)	0.0377 (9)	
H23	0.187274	0.136726	0.798175	0.045*	
C24	0.2359 (3)	0.1356 (3)	0.68803 (19)	0.0293 (8)	
H24	0.205418	0.068179	0.664094	0.035*	
C25	0.6212 (3)	0.3554 (3)	0.6911 (2)	0.0296 (8)	
H25	0.641221	0.400390	0.735734	0.036*	
C26	0.6950 (3)	0.3028 (3)	0.6434 (2)	0.0307 (8)	
H26	0.774413	0.303690	0.647728	0.037*	
C27	0.6265 (3)	0.2481 (3)	0.58748 (18)	0.0256 (7)	
H27	0.653324	0.203839	0.545873	0.031*	

C28	-0.0097 (3)	0.3385 (3)	0.49131 (19)	0.0272 (7)	
H28	-0.068642	0.351585	0.457808	0.033*	
C29	-0.0002 (3)	0.3800 (3)	0.56420 (19)	0.0281 (8)	
H29	-0.050411	0.426703	0.591270	0.034*	
C30	0.0984 (3)	0.3392 (3)	0.58991 (19)	0.0245 (7)	
H30	0.127382	0.353991	0.639161	0.029*	
C31	0.2211 (3)	0.3027 (3)	0.30652 (18)	0.0318 (8)	
H31	0.163240	0.305534	0.270114	0.038*	
C32	0.3284 (3)	0.3426 (3)	0.3031 (2)	0.0346 (9)	
H32	0.359498	0.378691	0.265009	0.042*	
C33	0.3820 (3)	0.3191 (3)	0.36748 (19)	0.0274 (7)	
H33	0.458462	0.336305	0.380504	0.033*	
C34	0.0589 (3)	0.0031 (3)	0.39733 (18)	0.0267 (7)	
H34	-0.002812	0.000587	0.363164	0.032*	
C35	0.0927 (3)	-0.0820 (3)	0.43356 (19)	0.0284 (8)	
H35	0.060969	-0.153980	0.429835	0.034*	
C36	0.1838 (3)	-0.0390 (3)	0.47677 (18)	0.0230 (7)	
H36	0.225650	-0.078967	0.508850	0.028*	
C38	0.4706 (3)	0.0114 (3)	0.32456 (17)	0.0237 (7)	
B3	0.4071 (3)	0.3836 (3)	0.6924 (2)	0.0285 (9)	
H3A	0.423318	0.433733	0.738936	0.034*	
B4	0.1070 (3)	0.2079 (3)	0.4015 (2)	0.0229 (8)	
H4A	0.042368	0.208310	0.365586	0.028*	

Atomic displacement parameters (Å²)

	U^{11}	U^{22}	U^{33}	U^{12}	U^{13}	U^{23}
Y1	0.01878 (16)	0.02356 (16)	0.01264 (14)	0.00194 (12)	-0.00048 (11)	0.00051 (11)
S1	0.0186 (4)	0.0271 (4)	0.0154 (4)	0.0026 (3)	-0.0015 (3)	0.0020 (3)
F1	0.067 (2)	0.084 (3)	0.0205 (14)	0.015 (2)	-0.0144 (13)	-0.0059 (15)
F2	0.094 (3)	0.131 (4)	0.078 (3)	-0.079 (3)	-0.063 (3)	0.085 (3)
F3	0.0332 (17)	0.092 (3)	0.0463 (18)	0.0307 (17)	-0.0147 (13)	0.0124 (19)
O1	0.0344 (14)	0.0326 (13)	0.0258 (12)	-0.0009 (11)	-0.0080 (10)	0.0077 (10)
O2	0.0188 (11)	0.0328 (13)	0.0200 (11)	-0.0022 (10)	-0.0021 (9)	0.0030 (10)
O3	0.0285 (14)	0.0569 (17)	0.0301 (14)	0.0113 (13)	0.0060 (11)	-0.0028 (12)
N1	0.0295 (15)	0.0293 (15)	0.0129 (13)	0.0012 (12)	-0.0005 (11)	0.0003 (11)
N2	0.0261 (15)	0.0273 (15)	0.0148 (13)	0.0019 (12)	0.0008 (11)	0.0021 (11)
N3	0.0298 (16)	0.0325 (16)	0.0141 (13)	-0.0009 (13)	0.0020 (11)	0.0026 (11)
N4	0.0256 (15)	0.0331 (16)	0.0183 (13)	0.0021 (12)	0.0021 (11)	0.0051 (12)

N5	0.0326 (16)	0.0275 (15)	0.0158 (13)	0.0008 (12)	-0.0029 (11)	0.0037 (11)
N6	0.0286 (15)	0.0260 (15)	0.0183 (13)	0.0052 (12)	-0.0004 (11)	0.0008 (11)
N7	0.0190 (14)	0.0461 (19)	0.0194 (14)	0.0035 (13)	-0.0034 (11)	-0.0035 (13)
N8	0.0209 (14)	0.0366 (16)	0.0176 (13)	0.0013 (12)	-0.0012 (11)	-0.0007 (12)
N9	0.0296 (16)	0.0338 (17)	0.0265 (15)	-0.0042 (13)	-0.0035 (12)	-0.0033 (13)
N10	0.0319 (16)	0.0290 (16)	0.0228 (15)	-0.0049 (13)	-0.0051 (12)	-0.0010 (12)
N11	0.0210 (14)	0.0341 (16)	0.0175 (13)	0.0046 (12)	-0.0052 (11)	-0.0049 (12)
N12	0.0197 (14)	0.0292 (15)	0.0185 (13)	0.0023 (12)	-0.0037 (11)	-0.0042 (11)
C1	0.035 (2)	0.0303 (18)	0.0138 (15)	-0.0004 (15)	-0.0011 (13)	-0.0038 (13)
C2	0.041 (2)	0.0309 (19)	0.0197 (17)	-0.0025 (16)	-0.0035 (15)	-0.0045 (14)
C3	0.0291 (18)	0.0275 (18)	0.0199 (16)	-0.0004 (15)	-0.0018 (13)	0.0021 (13)
C4	0.036 (2)	0.0314 (19)	0.0219 (17)	-0.0072 (16)	0.0073 (15)	0.0001 (14)
C5	0.029 (2)	0.039 (2)	0.033 (2)	-0.0039 (16)	0.0101 (16)	0.0036 (16)
C6	0.0219 (18)	0.036 (2)	0.0302 (19)	-0.0006 (15)	0.0021 (14)	0.0056 (15)
C7	0.054 (3)	0.032 (2)	0.0263 (19)	0.0071 (18)	-0.0056 (17)	0.0102 (16)
C8	0.052 (3)	0.032 (2)	0.041 (2)	0.0182 (19)	-0.0040 (19)	0.0047 (17)
C9	0.035 (2)	0.0302 (19)	0.0297 (19)	0.0097 (16)	-0.0008 (15)	0.0004 (15)
C10	0.0240 (19)	0.069 (3)	0.028 (2)	0.0114 (19)	-0.0094 (15)	-0.0090 (19)
C11	0.032 (2)	0.072 (3)	0.033 (2)	0.025 (2)	-0.0062 (17)	-0.005 (2)
C12	0.0278 (19)	0.042 (2)	0.0278 (18)	0.0101 (16)	0.0025 (15)	0.0019 (16)
C13	0.051 (3)	0.043 (2)	0.045 (3)	-0.020 (2)	-0.007 (2)	-0.004 (2)
C14	0.066 (3)	0.039 (2)	0.049 (3)	-0.020 (2)	-0.003 (2)	0.009 (2)
C15	0.049 (3)	0.034 (2)	0.034 (2)	-0.0063 (18)	0.0007 (18)	0.0076 (17)
C16	0.0315 (19)	0.0355 (19)	0.0148 (15)	0.0036 (15)	-0.0057 (13)	-0.0025 (14)
C17	0.0287 (19)	0.0349 (19)	0.0191 (16)	0.0021 (15)	0.0045 (14)	0.0000 (14)
C18	0.0233 (17)	0.0270 (17)	0.0230 (17)	0.0002 (14)	0.0016 (13)	-0.0030 (13)
C37	0.029 (2)	0.041 (2)	0.033 (2)	-0.0013 (17)	-0.0088 (16)	0.0142 (17)
B1	0.034 (2)	0.031 (2)	0.0138 (17)	-0.0007 (17)	-0.0001 (15)	0.0033 (15)
B2	0.023 (2)	0.039 (2)	0.0222 (19)	-0.0020 (17)	-0.0055 (15)	-0.0052 (17)
Y2	0.01490 (15)	0.01803 (15)	0.01247 (14)	0.00145 (11)	-0.00049 (10)	0.00040 (11)
S2	0.0173 (4)	0.0200 (4)	0.0115 (3)	0.0018 (3)	0.0010 (3)	0.0026 (3)
F4	0.0536 (15)	0.0658 (16)	0.0320 (12)	0.0295 (13)	-0.0184 (11)	-0.0291 (11)
F5	0.0423 (13)	0.0394 (12)	0.0268 (11)	-0.0022 (10)	-0.0141 (9)	0.0144 (9)
F6	0.0361 (13)	0.0571 (15)	0.0363 (12)	-0.0223 (11)	-0.0118 (10)	0.0146 (11)
O4	0.0229 (12)	0.0264 (12)	0.0178 (11)	0.0054 (9)	0.0024 (9)	0.0019 (9)
O5	0.0219 (12)	0.0220 (11)	0.0191 (11)	0.0031 (9)	-0.0028 (9)	0.0023 (9)
O6	0.0218 (12)	0.0346 (13)	0.0227 (12)	-0.0048 (10)	0.0038 (9)	0.0086 (10)
N13	0.0194 (14)	0.0259 (15)	0.0317 (16)	0.0048 (12)	0.0000 (12)	-0.0080 (12)
N14	0.0229 (14)	0.0211 (14)	0.0252 (14)	0.0007 (11)	-0.0028 (11)	-0.0017 (11)

N15	0.0202 (14)	0.0388 (17)	0.0158 (13)	0.0066 (12)	0.0009 (11)	-0.0038 (12)
N16	0.0193 (14)	0.0298 (15)	0.0176 (13)	0.0042 (12)	0.0018 (11)	-0.0005 (11)
N17	0.0195 (14)	0.0292 (15)	0.0192 (13)	0.0005 (12)	-0.0043 (11)	-0.0043 (11)
N18	0.0188 (14)	0.0213 (14)	0.0206 (13)	0.0035 (11)	-0.0006 (10)	-0.0007 (11)
N19	0.0166 (13)	0.0256 (14)	0.0203 (13)	0.0017 (11)	-0.0021 (10)	0.0055 (11)
N20	0.0162 (13)	0.0257 (14)	0.0198 (13)	0.0007 (11)	-0.0028 (10)	-0.0005 (11)
N21	0.0240 (15)	0.0308 (15)	0.0163 (13)	0.0042 (12)	-0.0021 (11)	0.0065 (11)
N22	0.0180 (14)	0.0308 (15)	0.0175 (13)	0.0025 (11)	-0.0007 (10)	0.0040 (11)
N23	0.0189 (14)	0.0288 (15)	0.0193 (13)	0.0009 (11)	-0.0014 (11)	0.0000 (11)
N24	0.0165 (13)	0.0218 (14)	0.0193 (13)	0.0017 (11)	-0.0026 (10)	0.0000 (11)
C19	0.0224 (18)	0.0249 (18)	0.049 (2)	0.0038 (15)	0.0009 (16)	-0.0131 (16)
C20	0.0268 (19)	0.0214 (18)	0.062 (3)	0.0042 (15)	-0.0004 (18)	0.0031 (17)
C21	0.0263 (19)	0.0266 (19)	0.040 (2)	0.0013 (15)	-0.0031 (15)	0.0069 (16)
C22	0.0243 (19)	0.067 (3)	0.0152 (16)	0.0125 (18)	0.0041 (14)	-0.0017 (17)
C23	0.0237 (19)	0.064 (3)	0.0279 (19)	0.0032 (19)	0.0106 (15)	0.0125 (18)
C24	0.0242 (18)	0.040 (2)	0.0255 (18)	0.0023 (15)	0.0056 (14)	0.0081 (15)
C25	0.0267 (19)	0.0307 (19)	0.0292 (18)	-0.0032 (15)	-0.0078 (14)	-0.0026 (15)
C26	0.0173 (17)	0.037 (2)	0.037 (2)	-0.0022 (15)	-0.0041 (14)	0.0025 (16)
C27	0.0204 (17)	0.0294 (18)	0.0260 (17)	0.0039 (14)	0.0024 (13)	-0.0014 (14)
C28	0.0212 (17)	0.0275 (18)	0.0341 (19)	0.0061 (14)	-0.0013 (14)	0.0078 (15)
C29	0.0236 (18)	0.0265 (18)	0.0345 (19)	0.0059 (14)	0.0071 (15)	0.0029 (15)
C30	0.0234 (17)	0.0234 (17)	0.0252 (17)	0.0014 (14)	0.0047 (13)	-0.0041 (13)
C31	0.035 (2)	0.044 (2)	0.0188 (17)	0.0091 (17)	0.0013 (14)	0.0133 (15)
C32	0.040 (2)	0.041 (2)	0.0269 (19)	0.0087 (17)	0.0087 (16)	0.0159 (16)
C33	0.0267 (18)	0.0301 (18)	0.0273 (18)	0.0015 (15)	0.0045 (14)	0.0106 (15)
C34	0.0210 (17)	0.0321 (19)	0.0240 (17)	-0.0068 (14)	-0.0039 (13)	-0.0056 (14)
C35	0.0265 (18)	0.0264 (18)	0.0294 (18)	-0.0056 (15)	-0.0013 (14)	-0.0059 (14)
C36	0.0211 (16)	0.0202 (16)	0.0268 (17)	0.0026 (13)	-0.0012 (13)	-0.0011 (13)
C38	0.0264 (18)	0.0259 (17)	0.0186 (16)	0.0025 (14)	-0.0026 (13)	0.0028 (13)
B3	0.023 (2)	0.036 (2)	0.0218 (19)	0.0038 (17)	-0.0066 (15)	-0.0114 (16)
B4	0.0180 (18)	0.034 (2)	0.0174 (17)	0.0025 (15)	-0.0049 (14)	0.0044 (15)

Geometric parameters (Å, º)

Y1—O1	2.387 (2)	B2—H2A	1.0000
Y1—O2^{i}	2.413 (2)	Y2—O4	2.372 (2)
Y1—N2	2.514 (3)	Y2—O5^{ii}	2.435 (2)
Y1—N4	2.462 (3)	Y2—N14	2.496 (3)
Y1—N6	2.402 (3)	Y2—N16	2.413 (2)

Y1—N8	2.461 (3)	Y2—N18	2.478 (3)
Y1—N10	2.529 (3)	Y2—N20	2.540 (3)
Y1—N12	2.495 (3)	Y2—N22	2.430 (3)
S1—O1	1.433 (3)	Y2—N24	2.481 (3)
S1—O2	1.442 (2)	S2—O4	1.448 (2)
S1—O3	1.420 (2)	S2—O5	1.442 (2)
S1—C37	1.851 (4)	S2—O6	1.425 (2)
F1—C37	1.352 (5)	S2—C38	1.825 (3)
F2—C37	1.289 (5)	F4—C38	1.319 (4)
F3—C37	1.293 (4)	F5—C38	1.317 (4)
N1—N2	1.362 (4)	F6—C38	1.317 (4)
N1—C1	1.342 (4)	N13—N14	1.371 (4)
N1—B1	1.528 (5)	N13—C19	1.343 (4)
N2—C3	1.328 (4)	N13—B3	1.540 (5)
N3—N4	1.373 (4)	N14—C21	1.332 (4)
N3—C4	1.341 (4)	N15—N16	1.360 (4)
N3—B1	1.538 (5)	N15—C22	1.352 (4)
N4—C6	1.339 (4)	N15—B3	1.540 (5)
N5—N6	1.365 (4)	N16—C24	1.332 (4)
N5—C7	1.340 (4)	N17—N18	1.368 (4)
N5—B1	1.539 (5)	N17—C25	1.342 (4)
N6—C9	1.338 (4)	N17—B3	1.539 (5)
N7—N8	1.364 (4)	N18—C27	1.333 (4)
N7—C10	1.339 (5)	N19—N20	1.355 (4)
N7—B2	1.529 (5)	N19—C28	1.348 (4)
N8—C12	1.336 (4)	N19—B4	1.548 (4)
N9—N10	1.363 (4)	N20—C30	1.344 (4)
N9—C13	1.346 (5)	N21—N22	1.364 (4)
N9—B2	1.522 (5)	N21—C31	1.351 (4)
N10—C15	1.329 (5)	N21—B4	1.534 (4)
N11—N12	1.381 (4)	N22—C33	1.338 (4)
N11—C16	1.344 (4)	N23—N24	1.376 (4)
N11—B2	1.536 (5)	N23—C34	1.335 (4)
N12—C18	1.338 (4)	N23—B4	1.539 (5)
C1—H1	0.9500	N24—C36	1.329 (4)
C1—C2	1.364 (5)	C19—H19	0.9500
C2—H2	0.9500	C19—C20	1.375 (6)
C2—C3	1.401 (5)	C20—H20	0.9500
C3—H3	0.9500	C20—C21	1.381 (5)
C4—H4	0.9500	C21—H21	0.9500

C4—C5	1.371 (5)	C22—H22	0.9500
C5—H5	0.9500	C22—C23	1.368 (6)
C5—C6	1.385 (5)	C23—H23	0.9500
C6—H6	0.9500	C23—C24	1.390 (5)
C7—H7	0.9500	C24—H24	0.9500
C7—C8	1.375 (5)	C25—H25	0.9500
C8—H8	0.9500	C25—C26	1.379 (5)
C8—C9	1.382 (5)	C26—H26	0.9500
C9—H9	0.9500	C26—C27	1.387 (5)
C10—H10	0.9500	C27—H27	0.9500
C10—C11	1.366 (6)	C28—H28	0.9500
C11—H11	0.9500	C28—C29	1.368 (5)
C11—C12	1.389 (5)	C29—H29	0.9500
C12—H12	0.9500	C29—C30	1.386 (5)
C13—H13	0.9500	C30—H30	0.9500
C13—C14	1.361 (6)	C31—H31	0.9500
C14—H14	0.9500	C31—C32	1.368 (5)
C14—C15	1.386 (6)	C32—H32	0.9500
C15—H15	0.9500	C32—C33	1.387 (5)
C16—H16	0.9500	C33—H33	0.9500
C16—C17	1.363 (5)	C34—H34	0.9500
C17—H17	0.9500	C34—C35	1.370 (5)
C17—C18	1.389 (5)	C35—H35	0.9500
C18—H18	0.9500	C35—C36	1.382 (5)
C37—F1A	1.199 (13)	C36—H36	0.9500
C37—F2A	1.378 (12)	B3—H3A	1.0000
C37—F3A	1.282 (15)	B4—H4A	1.0000
B1—H1A	1.0000		
O1—Y1—O2^{i}	74.27 (8)	N9—B2—N11	109.8 (3)
O1—Y1—N2	77.20 (8)	N9—B2—H2A	109.6
O1—Y1—N4	109.28 (9)	N11—B2—H2A	109.6
O1—Y1—N6	141.07 (9)	O4—Y2—O5^{ii}	70.05 (7)
O1—Y1—N8	72.21 (9)	O4—Y2—N14	115.23 (8)
O1—Y1—N10	147.87 (9)	O4—Y2—N16	139.08 (8)
O1—Y1—N12	92.28 (9)	O4—Y2—N18	77.21 (8)
O2^{i}—Y1—N2	75.32 (8)	O4—Y2—N20	146.05 (8)
O2^{i}—Y1—N4	144.40 (8)	O4—Y2—N22	72.25 (8)
O2^{i}—Y1—N8	133.97 (8)	O4—Y2—N24	91.71 (8)
O2^{i}—Y1—N10	124.74 (9)	O5^{ii}—Y2—N14	145.36 (8)

O2^{i}—Y1—N12	75.02 (8)	O5^{ii}—Y2—N18	79.03 (8)
N2—Y1—N10	129.62 (9)	O5^{ii}—Y2—N20	127.18 (8)
N4—Y1—N2	71.30 (9)	O5^{ii}—Y2—N24	75.44 (8)
N4—Y1—N10	71.42 (9)	N14—Y2—N20	69.00 (9)
N4—Y1—N12	138.13 (9)	N16—Y2—O5^{ii}	75.37 (8)
N6—Y1—O2^{i}	75.47 (9)	N16—Y2—N14	82.45 (9)
N6—Y1—N2	71.87 (9)	N16—Y2—N18	75.30 (9)
N6—Y1—N4	82.65 (9)	N16—Y2—N20	73.78 (9)
N6—Y1—N8	146.08 (10)	N16—Y2—N22	148.39 (9)
N6—Y1—N10	70.85 (10)	N16—Y2—N24	100.27 (9)
N6—Y1—N12	102.95 (9)	N18—Y2—N14	69.71 (9)
N8—Y1—N2	125.18 (9)	N18—Y2—N20	130.74 (8)
N8—Y1—N4	77.42 (9)	N18—Y2—N24	154.35 (9)
N8—Y1—N10	76.87 (10)	N22—Y2—O5^{ii}	132.90 (8)
N8—Y1—N12	75.74 (9)	N22—Y2—N14	77.24 (9)
N12—Y1—N2	150.23 (9)	N22—Y2—N18	118.55 (9)
N12—Y1—N10	71.58 (9)	N22—Y2—N20	76.42 (8)
O1—S1—O2	112.65 (14)	N22—Y2—N24	78.55 (9)
O1—S1—C37	104.06 (16)	N24—Y2—N14	135.47 (9)
O2—S1—C37	104.77 (15)	N24—Y2—N20	69.29 (8)
O3—S1—O1	115.21 (16)	O4—S2—C38	102.99 (14)
O3—S1—O2	114.11 (15)	O5—S2—O4	113.91 (12)
O3—S1—C37	104.52 (17)	O5—S2—C38	103.87 (14)
S1—O1—Y1	164.17 (15)	O6—S2—O4	113.88 (14)
S1—O2—Y1^{i}	167.77 (15)	O6—S2—O5	114.60 (14)
N2—N1—B1	120.9 (3)	O6—S2—C38	105.95 (14)
C1—N1—N2	110.0 (3)	S2—O4—Y2	164.33 (14)
C1—N1—B1	128.8 (3)	S2—O5—Y2^{ii}	170.79 (13)
N1—N2—Y1	121.9 (2)	N14—N13—B3	122.7 (3)
C3—N2—Y1	132.2 (2)	C19—N13—N14	109.7 (3)
C3—N2—N1	105.8 (3)	C19—N13—B3	127.4 (3)
N4—N3—B1	122.6 (3)	N13—N14—Y2	118.8 (2)
C4—N3—N4	109.6 (3)	C21—N14—Y2	133.5 (2)
C4—N3—B1	127.6 (3)	C21—N14—N13	105.5 (3)
N3—N4—Y1	119.7 (2)	N16—N15—B3	121.6 (2)
C6—N4—Y1	132.1 (2)	C22—N15—N16	108.8 (3)
C6—N4—N3	105.6 (3)	C22—N15—B3	129.0 (3)
N6—N5—B1	120.6 (3)	N15—N16—Y2	123.1 (2)
C7—N5—N6	108.8 (3)	C24—N16—Y2	130.2 (2)
C7—N5—B1	130.4 (3)	C24—N16—N15	106.8 (3)

N5—N6—Y1	124.2 (2)	N18—N17—B3	121.5 (3)
C9—N6—Y1	128.7 (2)	C25—N17—N18	109.8 (3)
C9—N6—N5	106.8 (3)	C25—N17—B3	128.1 (3)
N8—N7—B2	122.3 (3)	N17—N18—Y2	121.60 (19)
C10—N7—N8	109.8 (3)	C27—N18—Y2	132.9 (2)
C10—N7—B2	127.7 (3)	C27—N18—N17	105.5 (3)
N7—N8—Y1	123.4 (2)	N20—N19—B4	120.6 (2)
C12—N8—Y1	130.8 (2)	C28—N19—N20	110.3 (3)
C12—N8—N7	105.8 (3)	C28—N19—B4	129.1 (3)
N10—N9—B2	121.7 (3)	N19—N20—Y2	121.96 (18)
C13—N9—N10	109.5 (3)	C30—N20—Y2	130.9 (2)
C13—N9—B2	128.8 (3)	C30—N20—N19	105.6 (3)
N9—N10—Y1	122.2 (2)	N22—N21—B4	121.5 (2)
C15—N10—Y1	131.1 (2)	C31—N21—N22	109.5 (3)
C15—N10—N9	105.8 (3)	C31—N21—B4	129.0 (3)
N12—N11—B2	123.2 (3)	N21—N22—Y2	124.43 (19)
C16—N11—N12	109.6 (3)	C33—N22—Y2	129.4 (2)
C16—N11—B2	127.1 (3)	C33—N22—N21	106.1 (3)
N11—N12—Y1	121.05 (19)	N24—N23—B4	122.6 (3)
C18—N12—Y1	133.6 (2)	C34—N23—N24	109.7 (3)
C18—N12—N11	105.1 (3)	C34—N23—B4	126.5 (3)
N1—C1—H1	125.5	N23—N24—Y2	121.68 (19)
N1—C1—C2	108.9 (3)	C36—N24—Y2	133.4 (2)
C2—C1—H1	125.5	C36—N24—N23	104.9 (3)
C1—C2—H2	127.9	N13—C19—H19	125.7
C1—C2—C3	104.3 (3)	N13—C19—C20	108.6 (3)
C3—C2—H2	127.9	C20—C19—H19	125.7
N2—C3—C2	111.0 (3)	C19—C20—H20	127.7
N2—C3—H3	124.5	C19—C20—C21	104.6 (3)
C2—C3—H3	124.5	C21—C20—H20	127.7
N3—C4—H4	125.5	N14—C21—C20	111.6 (3)
N3—C4—C5	109.0 (3)	N14—C21—H21	124.2
C5—C4—H4	125.5	C20—C21—H21	124.2
C4—C5—H5	127.6	N15—C22—H22	125.4
C4—C5—C6	104.7 (3)	N15—C22—C23	109.2 (3)
C6—C5—H5	127.6	C23—C22—H22	125.4
N4—C6—C5	111.1 (3)	C22—C23—H23	127.8
N4—C6—H6	124.4	C22—C23—C24	104.5 (3)
C5—C6—H6	124.4	C24—C23—H23	127.8
N5—C7—H7	125.4	N16—C24—C23	110.8 (3)

N5—C7—C8	109.2 (3)	N16—C24—H24	124.6
C8—C7—H7	125.4	C23—C24—H24	124.6
C7—C8—H8	127.6	N17—C25—H25	125.6
C7—C8—C9	104.8 (3)	N17—C25—C26	108.9 (3)
C9—C8—H8	127.6	C26—C25—H25	125.6
N6—C9—C8	110.3 (3)	C25—C26—H26	128.0
N6—C9—H9	124.9	C25—C26—C27	104.0 (3)
C8—C9—H9	124.9	C27—C26—H26	128.0
N7—C10—H10	125.5	N18—C27—C26	111.8 (3)
N7—C10—C11	108.9 (3)	N18—C27—H27	124.1
C11—C10—H10	125.5	C26—C27—H27	124.1
C10—C11—H11	127.7	N19—C28—H28	125.9
C10—C11—C12	104.7 (3)	N19—C28—C29	108.3 (3)
C12—C11—H11	127.7	C29—C28—H28	125.9
N8—C12—C11	110.8 (3)	C28—C29—H29	127.5
N8—C12—H12	124.6	C28—C29—C30	105.0 (3)
C11—C12—H12	124.6	C30—C29—H29	127.5
N9—C13—H13	125.6	N20—C30—C29	110.9 (3)
N9—C13—C14	108.9 (4)	N20—C30—H30	124.6
C14—C13—H13	125.6	C29—C30—H30	124.6
C13—C14—H14	127.7	N21—C31—H31	125.7
C13—C14—C15	104.6 (4)	N21—C31—C32	108.6 (3)
C15—C14—H14	127.7	C32—C31—H31	125.7
N10—C15—C14	111.2 (4)	C31—C32—H32	127.5
N10—C15—H15	124.4	C31—C32—C33	105.0 (3)
C14—C15—H15	124.4	C33—C32—H32	127.5
N11—C16—H16	125.5	N22—C33—C32	110.7 (3)
N11—C16—C17	109.1 (3)	N22—C33—H33	124.6
C17—C16—H16	125.5	C32—C33—H33	124.6
C16—C17—H17	127.6	N23—C34—H34	125.4
C16—C17—C18	104.8 (3)	N23—C34—C35	109.2 (3)
C18—C17—H17	127.6	C35—C34—H34	125.4
N12—C18—C17	111.4 (3)	C34—C35—H35	128.0
N12—C18—H18	124.3	C34—C35—C36	103.9 (3)
C17—C18—H18	124.3	C36—C35—H35	128.0
F1—C37—S1	109.7 (3)	N24—C36—C35	112.2 (3)
F2—C37—S1	112.7 (3)	N24—C36—H36	123.9
F2—C37—F1	105.0 (4)	C35—C36—H36	123.9
F2—C37—F3	112.3 (4)	F4—C38—S2	110.1 (2)
F3—C37—S1	111.3 (3)	F5—C38—S2	110.8 (2)

F3—C37—F1	105.3 (4)	F5—C38—F4	108.5 (3)
F1A—C37—S1	116.5 (8)	F5—C38—F6	107.8 (3)
F1A—C37—F2A	109.1 (11)	F6—C38—S2	110.9 (2)
F1A—C37—F3A	109.9 (14)	F6—C38—F4	108.6 (3)
F2A—C37—S1	101.5 (7)	N13—B3—N15	111.1 (3)
F3A—C37—S1	113.9 (10)	N13—B3—H3A	109.6
F3A—C37—F2A	104.8 (13)	N15—B3—H3A	109.6
N1—B1—N3	108.3 (3)	N17—B3—N13	107.5 (3)
N1—B1—N5	108.3 (3)	N17—B3—N15	109.3 (3)
N1—B1—H1A	109.5	N17—B3—H3A	109.6
N3—B1—N5	111.7 (3)	N19—B4—H4A	109.5
N3—B1—H1A	109.5	N21—B4—N19	109.2 (3)
N5—B1—H1A	109.5	N21—B4—N23	111.7 (3)
N7—B2—N11	108.6 (3)	N21—B4—H4A	109.5
N7—B2—H2A	109.6	N23—B4—N19	107.5 (3)
N9—B2—N7	109.7 (3)	N23—B4—H4A	109.5

Symmetry codes: (i) -*x*+2, -*y*+1, -*z*; (ii) -*x*+1, -*y*, -*z*+1.

8.3.11 Crystallographic data for 7-Eu

Crystal data

$C_{19}H_{20}B_2EuF_3N_{12}O_3S$	$Z = 4$
$M_r = 727.11$	$F(000) = 1432$
Triclinic, $P\bar{1}$	$D_x = 1.791$ Mg m^{-3}
$a = 11.9525$ (5) Å	Mo $K\alpha$ radiation, $\lambda = 0.71073$ Å
$b = 12.3640$ (5) Å	Cell parameters from 9759 reflections
$c = 18.3912$ (8) Å	$\theta = 2.3$–$28.3°$
$\alpha = 96.930$ (2)°	$\mu = 2.47$ mm^{-1}
$\beta = 91.524$ (2)°	$T = 150$ K
$\gamma = 91.531$ (2)°	Block, clear colourless
$V = 2695.8$ (2) Å^3	0.28 × 0.15 × 0.14 mm

Data collection

Bruker D8 VENTURE diffractometer	13388 independent reflections
Radiation source: microfocus sealed tube, INCOATEC Iμs 3.0	11221 reflections with $I > 2\sigma(I)$

Multilayer mirror optics monochromator	R_{int} = 0.046
Detector resolution: 7.4074 pixels mm^{-1}	θ_{max} = 28.3°, θ_{min} = 2.3°
ϕ and ω scans	h = -15→15
Absorption correction: multi-scan *SADABS2016*/2 (Bruker,2016/2) was used for absorption correction. wR2(int) was 0.1481 before and 0.0528 after correction. The Ratio of minimum to maximum transmission is 0.7975. The $\lambda/2$ correction factor is Not present.	k = -16→16
T_{min} = 0.595, T_{max} = 0.746	l = -24→24
63865 measured reflections	

Refinement

Refinement on F^2	Primary atom site location: dual
Least-squares matrix: full	Hydrogen site location: inferred from neighbouring sites
$R[F^2 > 2\sigma(F^2)]$ = 0.034	H-atom parameters constrained
$wR(F^2)$ = 0.077	$w = 1/[\sigma^2(F_o^2) + (0.0178P)^2 + 9.5828P]$ where $P = (F_o^2 + 2F_c^2)/3$
S = 1.06	$(\Delta/\sigma)_{max}$ = 0.002
13388 reflections	$\Delta\rangle_{max}$ = 2.44 e Å^{-3}
767 parameters	$\Delta\rangle_{min}$ = -2.81 e Å^{-3}
72 restraints	

Special details

Geometry. All esds (except the esd in the dihedral angle between two l.s. planes) are estimated using the full covariance matrix. The cell esds are taken into account individually in the estimation of esds in distances, angles and torsion angles; correlations between esds in cell parameters are only used when they are defined by crystal symmetry. An approximate (isotropic) treatment of cell esds is used for estimating esds involving l.s. planes.

Fractional atomic coordinates and isotropic or equivalent isotropic displacement parameters (Å²)

	x	y	z	U_{iso}*/U_{eq}	Occ. (<1)
Eu1	0.65560 (2)	0.79464 (2)	0.47344 (2)	0.01462 (5)	
S1	0.43591 (7)	0.93501 (7)	0.59635 (4)	0.01630 (16)	
F1	0.4770 (3)	1.0659 (3)	0.71576 (15)	0.0544 (9)	
F2	0.5542 (2)	0.9114 (2)	0.71408 (13)	0.0364 (6)	
F3	0.6214 (2)	1.0300 (2)	0.65153 (15)	0.0438 (7)	

O1	0.5074 (2)	0.8615 (2)	0.55286 (13)	0.0218 (5)	
O2	0.4085 (2)	1.0305 (2)	0.56190 (13)	0.0208 (5)	
O3	0.3433 (2)	0.8822 (2)	0.62639 (15)	0.0264 (6)	
N1	0.6387 (3)	0.5467 (3)	0.36871 (19)	0.0266 (7)	
N2	0.6500 (3)	0.5894 (3)	0.44034 (18)	0.0242 (7)	
N3	0.4835 (3)	0.6629 (3)	0.33483 (17)	0.0243 (7)	
N4	0.4797 (3)	0.7314 (2)	0.39888 (17)	0.0207 (6)	
N5	0.6772 (3)	0.7020 (3)	0.29263 (17)	0.0261 (7)	
N6	0.7057 (3)	0.7877 (3)	0.34413 (17)	0.0228 (7)	
N7	0.7943 (3)	0.7427 (3)	0.63121 (17)	0.0232 (7)	
N8	0.6936 (3)	0.7311 (3)	0.59458 (17)	0.0224 (7)	
N9	0.9244 (3)	0.7236 (3)	0.52547 (17)	0.0212 (6)	
N10	0.8550 (3)	0.7215 (2)	0.46556 (17)	0.0202 (6)	
N11	0.8790 (3)	0.9096 (3)	0.58229 (16)	0.0211 (6)	
N12	0.7984 (3)	0.9348 (2)	0.53329 (17)	0.0207 (6)	
C1	0.6633 (3)	0.4403 (3)	0.3621 (3)	0.0351 (10)	
H1	0.661973	0.392612	0.317483	0.042*	
C2	0.6903 (4)	0.4123 (3)	0.4295 (3)	0.0380 (11)	
H2	0.710718	0.342758	0.441597	0.046*	
C3	0.6814 (3)	0.5080 (3)	0.4768 (3)	0.0317 (9)	
H3A	0.695778	0.514420	0.528168	0.038*	
C4	0.3791 (3)	0.6409 (3)	0.3070 (2)	0.0300 (9)	
H4A	0.359682	0.595204	0.262942	0.036*	
C5	0.3054 (3)	0.6956 (3)	0.3530 (2)	0.0308 (9)	
H5	0.226156	0.695838	0.347532	0.037*	
C6	0.3719 (3)	0.7504 (3)	0.4089 (2)	0.0262 (8)	
H6	0.344122	0.795864	0.449389	0.031*	
C7	0.7213 (4)	0.7203 (4)	0.2282 (2)	0.0365 (11)	
H7	0.714507	0.672183	0.183843	0.044*	
C8	0.7770 (4)	0.8188 (4)	0.2371 (2)	0.0389 (11)	
H8	0.815378	0.853114	0.201073	0.047*	
C9	0.7652 (3)	0.8580 (4)	0.3104 (2)	0.0298 (9)	
H9	0.795462	0.925857	0.333306	0.036*	
C10	0.7863 (4)	0.7009 (4)	0.6949 (2)	0.0310 (9)	
H10	0.845359	0.699282	0.730365	0.037*	
C11	0.6793 (4)	0.6611 (4)	0.7007 (2)	0.0337 (10)	
H11	0.649351	0.626714	0.739694	0.040*	
C12	0.6246 (4)	0.6824 (3)	0.6366 (2)	0.0289 (9)	
H12	0.548011	0.664479	0.624496	0.035*	
C13	1.0137 (3)	0.6616 (3)	0.5089 (2)	0.0279 (9)	

H13	1.073732	0.650102	0.541784	0.033*	
C14	1.0033 (3)	0.6183 (3)	0.4371 (2)	0.0289 (9)	
H14	1.053424	0.571581	0.410118	0.035*	
C15	0.9031 (3)	0.6576 (3)	0.4120 (2)	0.0241 (8)	
H15	0.872990	0.641254	0.363425	0.029*	
C16	0.9456 (3)	0.9966 (3)	0.6029 (2)	0.0273 (8)	
H16	1.007374	0.999056	0.636671	0.033*	
C17	0.9110 (3)	1.0819 (3)	0.5678 (2)	0.0283 (9)	
H17	0.942455	1.153851	0.572049	0.034*	
C18	0.8201 (3)	1.0396 (3)	0.5250 (2)	0.0243 (8)	
H18	0.777936	1.079687	0.493478	0.029*	
C19	0.5276 (3)	0.9889 (3)	0.6745 (2)	0.0250 (8)	
B1	0.5933 (4)	0.6108 (4)	0.3082 (2)	0.0272 (10)	
H1A	0.577633	0.559982	0.262281	0.033*	
B2	0.8986 (4)	0.7917 (4)	0.5982 (2)	0.0242 (9)	
H2A	0.964005	0.791308	0.633217	0.029*	
Eu2	1.15709 (2)	0.69640 (2)	0.97980 (2)	0.02065 (5)	
S2	0.84725 (8)	0.60688 (8)	0.99743 (5)	0.02346 (19)	
F4	0.7913 (7)	0.5524 (8)	0.8596 (3)	0.066 (3)	0.675 (17)
F5	0.6714 (5)	0.6425 (8)	0.9184 (5)	0.054 (2)	0.675 (17)
F6	0.8165 (9)	0.7230 (9)	0.8880 (6)	0.098 (5)	0.675 (17)
O4	0.9589 (2)	0.6519 (2)	0.99560 (15)	0.0285 (6)	
O5	0.8449 (3)	0.4917 (3)	0.99146 (17)	0.0370 (7)	
O6	0.7806 (3)	0.6593 (3)	1.05344 (18)	0.0488 (9)	
N13	1.1041 (3)	0.6302 (3)	0.79251 (17)	0.0256 (7)	
N14	1.0928 (3)	0.5889 (3)	0.85756 (17)	0.0245 (7)	
N15	1.0783 (3)	0.8262 (3)	0.83438 (18)	0.0294 (8)	
N16	1.0570 (3)	0.8173 (3)	0.90592 (18)	0.0284 (7)	
N17	1.2736 (3)	0.7509 (3)	0.82095 (17)	0.0278 (7)	
N18	1.3028 (3)	0.7163 (3)	0.88636 (18)	0.0283 (7)	
N19	1.3800 (3)	0.7476 (3)	1.10377 (18)	0.0297 (8)	
N20	1.3353 (3)	0.6715 (3)	1.05022 (18)	0.0269 (7)	
N21	1.3100 (3)	0.9223 (3)	1.0662 (2)	0.0346 (8)	
N22	1.2457 (3)	0.8881 (3)	1.00491 (19)	0.0325 (8)	
N23	1.2047 (3)	0.8243 (3)	1.15636 (18)	0.0279 (7)	
N24	1.1213 (3)	0.7733 (3)	1.11111 (18)	0.0272 (7)	
C20	1.0595 (4)	0.5593 (3)	0.7375 (2)	0.0298 (9)	
H20	1.057300	0.569553	0.687083	0.036*	
C21	1.0177 (4)	0.4699 (4)	0.7662 (2)	0.0337 (10)	
H21	0.981503	0.406514	0.740688	0.040*	

C22	1.0404 (4)	0.4930 (3)	0.8414 (2)	0.0288 (9)	
H22	1.020670	0.445953	0.876499	0.035*	
C23	1.0177 (4)	0.9078 (4)	0.8128 (3)	0.0414 (12)	
H23	1.017407	0.930905	0.765384	0.050*	
C24	0.9567 (5)	0.9517 (4)	0.8704 (3)	0.0470 (13)	
H24	0.906298	1.009882	0.871004	0.056*	
C25	0.9840 (4)	0.8935 (4)	0.9275 (2)	0.0359 (10)	
H25	0.954891	0.905851	0.975226	0.043*	
C26	1.3661 (4)	0.7828 (3)	0.7881 (2)	0.0331 (10)	
H26	1.367710	0.810492	0.742152	0.040*	
C27	1.4576 (4)	0.7686 (4)	0.8321 (2)	0.0363 (10)	
H27	1.534010	0.783654	0.822981	0.044*	
C28	1.4143 (4)	0.7274 (4)	0.8929 (2)	0.0332 (9)	
H28	1.457831	0.709675	0.933555	0.040*	
C29	1.4748 (4)	0.7118 (5)	1.1302 (3)	0.0445 (12)	
H29	1.521473	0.750195	1.167917	0.053*	
C30	1.4945 (4)	0.6109 (5)	1.0947 (3)	0.0479 (13)	
H30	1.555824	0.565777	1.102150	0.058*	
C31	1.4049 (3)	0.5891 (4)	1.0451 (2)	0.0327 (9)	
H31	1.394668	0.524122	1.012106	0.039*	
C32	1.3609 (5)	1.0178 (4)	1.0591 (3)	0.0523 (14)	
H32	1.410755	1.057661	1.094234	0.063*	
C33	1.3293 (5)	1.0488 (4)	0.9926 (3)	0.0581 (15)	
H33	1.351556	1.113311	0.972868	0.070*	
C34	1.2584 (4)	0.9661 (4)	0.9606 (3)	0.0419 (11)	
H34	1.223179	0.964322	0.913507	0.050*	
C35	1.1668 (4)	0.8479 (4)	1.2245 (2)	0.0304 (9)	
H35	1.209225	0.883083	1.265484	0.036*	
C36	1.0580 (4)	0.8135 (4)	1.2253 (2)	0.0327 (9)	
H36	1.009970	0.819023	1.265875	0.039*	
C37	1.0325 (3)	0.7682 (3)	1.1536 (2)	0.0276 (8)	
H37	0.961269	0.737670	1.136881	0.033*	
C38	0.7786 (3)	0.6362 (4)	0.9114 (2)	0.0364 (10)	
B3	1.1527 (4)	0.7442 (4)	0.7893 (2)	0.0286 (10)	
H3	1.152812	0.759950	0.737280	0.034*	
B4	1.3210 (4)	0.8534 (4)	1.1294 (3)	0.0311 (10)	
H4	1.365871	0.895390	1.170655	0.037*	
F4A	0.8386 (13)	0.6203 (19)	0.8561 (5)	0.062 (5)	0.325 (17)
F5A	0.7617 (17)	0.7426 (10)	0.9236 (10)	0.078 (5)	0.325 (17)
F6A	0.6794 (13)	0.593 (2)	0.9003 (14)	0.079 (6)	0.325 (17)

Atomic displacement parameters (Å²)

	U^{11}	U^{22}	U^{33}	U^{12}	U^{13}	U^{23}
Eu1	0.01451 (8)	0.01500 (8)	0.01427 (8)	0.00170 (6)	-0.00062 (6)	0.00141 (6)
S1	0.0181 (4)	0.0176 (4)	0.0137 (4)	0.0026 (3)	0.0014 (3)	0.0032 (3)
F1	0.0575 (19)	0.0623 (19)	0.0357 (15)	0.0321 (15)	-0.0208 (13)	-0.0270 (14)
F2	0.0458 (15)	0.0371 (14)	0.0281 (13)	0.0003 (12)	-0.0132 (11)	0.0150 (11)
F3	0.0383 (15)	0.0533 (17)	0.0403 (15)	-0.0205 (13)	-0.0121 (12)	0.0155 (13)
O1	0.0254 (14)	0.0224 (13)	0.0182 (12)	0.0074 (11)	0.0029 (10)	0.0027 (10)
O2	0.0245 (13)	0.0196 (13)	0.0191 (12)	0.0038 (10)	-0.0019 (10)	0.0059 (10)
O3	0.0238 (14)	0.0314 (15)	0.0254 (14)	-0.0021 (11)	0.0039 (11)	0.0095 (12)
N1	0.0202 (16)	0.0219 (16)	0.0351 (19)	0.0012 (13)	-0.0021 (14)	-0.0071 (14)
N2	0.0228 (16)	0.0213 (16)	0.0281 (17)	0.0012 (13)	-0.0033 (13)	0.0017 (13)
N3	0.0214 (16)	0.0253 (17)	0.0242 (16)	0.0016 (13)	-0.0037 (13)	-0.0040 (13)
N4	0.0192 (15)	0.0199 (15)	0.0218 (15)	0.0028 (12)	-0.0019 (12)	-0.0016 (12)
N5	0.0234 (17)	0.0362 (19)	0.0172 (15)	0.0061 (14)	0.0003 (13)	-0.0034 (13)
N6	0.0218 (16)	0.0279 (17)	0.0185 (15)	0.0035 (13)	0.0009 (12)	0.0009 (13)
N7	0.0235 (16)	0.0296 (17)	0.0181 (15)	0.0046 (13)	-0.0019 (12)	0.0085 (13)
N8	0.0191 (15)	0.0275 (17)	0.0220 (16)	0.0029 (13)	0.0001 (12)	0.0080 (13)
N9	0.0166 (15)	0.0239 (16)	0.0238 (16)	0.0039 (12)	-0.0019 (12)	0.0057 (13)
N10	0.0186 (15)	0.0191 (15)	0.0229 (15)	0.0012 (12)	-0.0018 (12)	0.0026 (12)
N11	0.0206 (16)	0.0245 (16)	0.0177 (15)	-0.0011 (12)	-0.0032 (12)	0.0012 (12)
N12	0.0194 (15)	0.0198 (15)	0.0222 (15)	0.0024 (12)	-0.0024 (12)	0.0005 (12)
C1	0.025 (2)	0.020 (2)	0.056 (3)	0.0030 (16)	0.002 (2)	-0.0120 (19)
C2	0.029 (2)	0.019 (2)	0.065 (3)	0.0059 (17)	0.000 (2)	0.001 (2)
C3	0.026 (2)	0.021 (2)	0.048 (3)	0.0013 (16)	-0.0021 (19)	0.0072 (18)
C4	0.026 (2)	0.029 (2)	0.033 (2)	-0.0016 (17)	-0.0087 (17)	-0.0010 (17)
C5	0.0187 (19)	0.034 (2)	0.040 (2)	-0.0003 (16)	-0.0051 (17)	0.0044 (18)
C6	0.0216 (19)	0.028 (2)	0.029 (2)	0.0029 (16)	0.0014 (16)	0.0029 (16)
C7	0.026 (2)	0.064 (3)	0.0185 (19)	0.011 (2)	0.0029 (16)	-0.003 (2)
C8	0.027 (2)	0.066 (3)	0.027 (2)	0.008 (2)	0.0085 (18)	0.014 (2)
C9	0.0208 (19)	0.039 (2)	0.031 (2)	0.0042 (17)	0.0049 (16)	0.0087 (18)
C10	0.034 (2)	0.040 (2)	0.0209 (19)	0.0080 (19)	-0.0022 (17)	0.0122 (17)
C11	0.037 (2)	0.038 (2)	0.030 (2)	0.0072 (19)	0.0080 (18)	0.0173 (19)
C12	0.027 (2)	0.031 (2)	0.031 (2)	0.0027 (17)	0.0052 (17)	0.0118 (17)
C13	0.0185 (19)	0.032 (2)	0.036 (2)	0.0070 (16)	0.0036 (16)	0.0115 (18)
C14	0.023 (2)	0.023 (2)	0.041 (2)	0.0063 (16)	0.0064 (17)	0.0034 (17)
C15	0.0219 (19)	0.0230 (19)	0.0264 (19)	0.0011 (15)	0.0033 (15)	-0.0015 (15)
C16	0.024 (2)	0.032 (2)	0.0233 (19)	-0.0056 (16)	-0.0034 (15)	-0.0052 (16)

C17	0.030 (2)	0.023 (2)	0.030 (2)	-0.0068 (16)	0.0038 (17)	-0.0020 (16)
C18	0.0242 (19)	0.0187 (18)	0.029 (2)	0.0025 (15)	0.0014 (16)	-0.0006 (15)
C19	0.031 (2)	0.0248 (19)	0.0195 (18)	0.0036 (16)	-0.0038 (15)	0.0032 (15)
B1	0.023 (2)	0.032 (2)	0.023 (2)	0.0046 (18)	-0.0050 (17)	-0.0089 (18)
B2	0.019 (2)	0.032 (2)	0.022 (2)	0.0032 (17)	-0.0064 (16)	0.0036 (18)
Eu2	0.01987 (10)	0.02650 (10)	0.01556 (9)	0.00402 (7)	-0.00055 (7)	0.00191 (7)
S2	0.0189 (4)	0.0316 (5)	0.0202 (4)	0.0037 (4)	-0.0010 (3)	0.0043 (4)
F4	0.069 (5)	0.106 (6)	0.021 (2)	0.030 (4)	-0.011 (3)	-0.007 (3)
F5	0.028 (3)	0.082 (6)	0.056 (4)	0.019 (3)	-0.010 (2)	0.020 (4)
F6	0.094 (7)	0.107 (7)	0.105 (7)	-0.067 (6)	-0.066 (5)	0.088 (6)
O4	0.0215 (14)	0.0404 (17)	0.0238 (14)	-0.0019 (12)	-0.0024 (11)	0.0057 (12)
O5	0.0307 (16)	0.0427 (18)	0.0392 (17)	-0.0027 (14)	-0.0132 (13)	0.0152 (14)
O6	0.0329 (18)	0.077 (3)	0.0354 (18)	0.0169 (17)	0.0077 (14)	-0.0016 (17)
N13	0.0282 (18)	0.0310 (18)	0.0176 (15)	0.0052 (14)	0.0000 (13)	0.0018 (13)
N14	0.0269 (17)	0.0288 (17)	0.0182 (15)	0.0018 (14)	0.0003 (13)	0.0040 (13)
N15	0.039 (2)	0.0287 (18)	0.0213 (16)	0.0065 (15)	-0.0032 (14)	0.0051 (14)
N16	0.0323 (19)	0.0309 (18)	0.0219 (16)	0.0080 (15)	-0.0024 (14)	0.0019 (14)
N17	0.0351 (19)	0.0302 (18)	0.0184 (15)	0.0012 (15)	0.0029 (14)	0.0042 (13)
N18	0.0276 (18)	0.037 (2)	0.0210 (16)	0.0028 (15)	0.0020 (14)	0.0073 (14)
N19	0.0235 (17)	0.038 (2)	0.0255 (17)	0.0035 (15)	-0.0040 (14)	-0.0021 (15)
N20	0.0224 (17)	0.0327 (18)	0.0253 (17)	0.0022 (14)	-0.0009 (13)	0.0023 (14)
N21	0.033 (2)	0.035 (2)	0.034 (2)	-0.0027 (16)	-0.0044 (16)	0.0001 (16)
N22	0.040 (2)	0.0299 (19)	0.0271 (18)	0.0005 (16)	-0.0009 (15)	0.0009 (15)
N23	0.0259 (18)	0.0326 (19)	0.0237 (17)	0.0060 (14)	-0.0047 (14)	-0.0028 (14)
N24	0.0226 (17)	0.0338 (19)	0.0236 (17)	0.0039 (14)	-0.0033 (13)	-0.0029 (14)
C20	0.036 (2)	0.035 (2)	0.0178 (18)	0.0053 (18)	0.0004 (16)	-0.0003 (16)
C21	0.038 (2)	0.036 (2)	0.025 (2)	0.0020 (19)	-0.0024 (18)	-0.0032 (18)
C22	0.032 (2)	0.032 (2)	0.0225 (19)	0.0044 (17)	-0.0007 (16)	0.0033 (16)
C23	0.062 (3)	0.033 (2)	0.030 (2)	0.015 (2)	-0.009 (2)	0.0073 (19)
C24	0.061 (3)	0.036 (3)	0.045 (3)	0.025 (2)	-0.006 (2)	0.008 (2)
C25	0.043 (3)	0.030 (2)	0.033 (2)	0.0127 (19)	-0.0017 (19)	-0.0025 (18)
C26	0.042 (3)	0.031 (2)	0.027 (2)	-0.0034 (19)	0.0089 (19)	0.0039 (17)
C27	0.037 (2)	0.039 (2)	0.034 (2)	-0.006 (2)	0.0114 (19)	0.0048 (19)
C28	0.026 (2)	0.042 (3)	0.032 (2)	0.0000 (18)	0.0020 (17)	0.0034 (19)
C29	0.027 (2)	0.066 (3)	0.037 (3)	0.013 (2)	-0.0102 (19)	-0.008 (2)
C30	0.031 (2)	0.066 (4)	0.044 (3)	0.023 (2)	-0.008 (2)	-0.009 (2)
C31	0.026 (2)	0.041 (2)	0.032 (2)	0.0124 (18)	-0.0002 (17)	0.0017 (19)
C32	0.057 (3)	0.043 (3)	0.053 (3)	-0.021 (3)	-0.011 (3)	-0.001 (2)
C33	0.081 (4)	0.039 (3)	0.054 (3)	-0.020 (3)	-0.005 (3)	0.011 (3)
C34	0.050 (3)	0.037 (3)	0.040 (3)	-0.006 (2)	-0.001 (2)	0.011 (2)

C35	0.033 (2)	0.039 (2)	0.0177 (18)	0.0069 (18)	-0.0061 (16)	-0.0031 (17)
C36	0.033 (2)	0.041 (2)	0.023 (2)	0.0033 (19)	0.0037 (17)	0.0000 (18)
C37	0.026 (2)	0.030 (2)	0.026 (2)	0.0019 (16)	0.0009 (16)	-0.0032 (16)
C38	0.024 (2)	0.048 (3)	0.038 (2)	0.0021 (19)	-0.0107 (19)	0.014 (2)
B3	0.041 (3)	0.028 (2)	0.017 (2)	0.002 (2)	0.0022 (19)	0.0058 (18)
B4	0.027 (2)	0.037 (3)	0.026 (2)	0.001 (2)	-0.0069 (19)	-0.006 (2)
F4A	0.052 (8)	0.114 (14)	0.026 (5)	0.039 (8)	0.003 (5)	0.028 (7)
F5A	0.096 (12)	0.061 (8)	0.080 (10)	0.041 (8)	-0.025 (8)	0.019 (7)
F6A	0.052 (9)	0.102 (14)	0.086 (13)	-0.022 (9)	-0.050 (8)	0.041 (11)

Geometric parameters (Å, º)

Eu1—O1	2.425 (2)	Eu2—N14	2.558 (3)
Eu1—O2^{i}	2.466 (2)	Eu2—N16	2.452 (3)
Eu1—N2	2.535 (3)	Eu2—N18	2.508 (3)
Eu1—N4	2.532 (3)	Eu2—N20	2.509 (3)
Eu1—N6	2.460 (3)	Eu2—N22	2.556 (4)
Eu1—N8	2.485 (3)	Eu2—N24	2.538 (3)
Eu1—N10	2.574 (3)	S2—O4	1.434 (3)
Eu1—N12	2.532 (3)	S2—O5	1.415 (3)
S1—O1	1.448 (3)	S2—O6	1.423 (3)
S1—O2	1.447 (2)	S2—C38	1.842 (4)
S1—O3	1.427 (3)	F4—C38	1.334 (7)
S1—C19	1.832 (4)	F5—C38	1.294 (7)
F1—C19	1.315 (4)	F6—C38	1.280 (6)
F2—C19	1.312 (4)	N13—N14	1.365 (4)
F3—C19	1.319 (5)	N13—C20	1.345 (5)
N1—N2	1.361 (5)	N13—B3	1.519 (6)
N1—C1	1.347 (5)	N14—C22	1.323 (5)
N1—B1	1.539 (6)	N15—N16	1.363 (5)
N2—C3	1.332 (5)	N15—C23	1.349 (5)
N3—N4	1.367 (4)	N15—B3	1.546 (6)
N3—C4	1.344 (5)	N16—C25	1.334 (5)
N3—B1	1.543 (5)	N17—N18	1.364 (4)
N4—C6	1.330 (5)	N17—C26	1.347 (5)
N5—N6	1.363 (4)	N17—B3	1.539 (6)
N5—C7	1.350 (5)	N18—C28	1.336 (5)
N5—B1	1.546 (6)	N19—N20	1.364 (5)
N6—C9	1.330 (5)	N19—C29	1.329 (5)

N7—N8	1.360 (4)	N19—B4	1.533 (6)
N7—C10	1.341 (5)	N20—C31	1.329 (5)
N7—B2	1.542 (5)	N21—N22	1.363 (5)
N8—C12	1.326 (5)	N21—C32	1.336 (6)
N9—N10	1.358 (4)	N21—B4	1.528 (6)
N9—C13	1.351 (5)	N22—C34	1.344 (6)
N9—B2	1.536 (5)	N23—N24	1.370 (5)
N10—C15	1.339 (5)	N23—C35	1.346 (5)
N11—N12	1.369 (4)	N23—B4	1.537 (6)
N11—C16	1.332 (5)	N24—C37	1.339 (5)
N11—B2	1.544 (5)	C20—H20	0.9500
N12—C18	1.342 (5)	C20—C21	1.370 (6)
C1—H1	0.9500	C21—H21	0.9500
C1—C2	1.361 (7)	C21—C22	1.397 (6)
C2—H2	0.9500	C22—H22	0.9500
C2—C3	1.389 (6)	C23—H23	0.9500
C3—H3A	0.9500	C23—C24	1.369 (7)
C4—H4A	0.9500	C24—H24	0.9500
C4—C5	1.372 (6)	C24—C25	1.379 (6)
C5—H5	0.9500	C25—H25	0.9500
C5—C6	1.381 (6)	C26—H26	0.9500
C6—H6	0.9500	C26—C27	1.370 (7)
C7—H7	0.9500	C27—H27	0.9500
C7—C8	1.363 (7)	C27—C28	1.391 (6)
C8—H8	0.9500	C28—H28	0.9500
C8—C9	1.389 (6)	C29—H29	0.9500
C9—H9	0.9500	C29—C30	1.366 (7)
C10—H10	0.9500	C30—H30	0.9500
C10—C11	1.369 (6)	C30—C31	1.386 (6)
C11—H11	0.9500	C31—H31	0.9500
C11—C12	1.390 (6)	C32—H32	0.9500
C12—H12	0.9500	C32—C33	1.372 (8)
C13—H13	0.9500	C33—H33	0.9500
C13—C14	1.367 (6)	C33—C34	1.375 (7)
C14—H14	0.9500	C34—H34	0.9500
C14—C15	1.393 (5)	C35—H35	0.9500
C15—H15	0.9500	C35—C36	1.358 (6)
C16—H16	0.9500	C36—H36	0.9500
C16—C17	1.368 (6)	C36—C37	1.393 (6)
C17—H17	0.9500	C37—H37	0.9500

C17—C18	1.378 (6)	C38—F4A	1.259 (9)
C18—H18	0.9500	C38—F5A	1.330 (11)
B1—H1A	1.0000	C38—F6A	1.287 (12)
B2—H2A	1.0000	B3—H3	1.0000
Eu2—O4	2.451 (3)	B4—H4	1.0000
Eu2—O5^{ii}	2.446 (3)		
O1—Eu1—O2^{i}	70.49 (8)	O4—Eu2—N20	134.73 (10)
O1—Eu1—N2	114.05 (10)	O4—Eu2—N22	124.50 (11)
O1—Eu1—N4	77.05 (9)	O4—Eu2—N24	75.78 (10)
O1—Eu1—N6	139.06 (9)	O5^{ii}—Eu2—O4	75.56 (10)
O1—Eu1—N8	73.04 (9)	O5^{ii}—Eu2—N14	77.66 (10)
O1—Eu1—N10	146.49 (9)	O5^{ii}—Eu2—N16	141.61 (11)
O1—Eu1—N12	93.45 (9)	O5^{ii}—Eu2—N18	108.43 (11)
O2^{i}—Eu1—N2	145.28 (9)	O5^{ii}—Eu2—N20	72.61 (10)
O2^{i}—Eu1—N4	79.41 (9)	O5^{ii}—Eu2—N22	147.35 (11)
O2^{i}—Eu1—N8	132.31 (9)	O5^{ii}—Eu2—N24	93.02 (11)
O2^{i}—Eu1—N10	127.20 (9)	N16—Eu2—N14	70.81 (11)
O2^{i}—Eu1—N12	75.52 (9)	N16—Eu2—N18	81.42 (11)
N2—Eu1—N10	69.24 (10)	N16—Eu2—N20	144.82 (12)
N4—Eu1—N2	68.99 (10)	N16—Eu2—N22	70.98 (12)
N4—Eu1—N10	130.02 (9)	N16—Eu2—N24	104.12 (11)
N4—Eu1—N12	154.91 (10)	N18—Eu2—N14	70.66 (11)
N6—Eu1—O2^{i}	76.27 (9)	N18—Eu2—N20	77.65 (11)
N6—Eu1—N2	81.35 (11)	N18—Eu2—N22	71.58 (12)
N6—Eu1—N4	73.89 (10)	N18—Eu2—N24	137.71 (11)
N6—Eu1—N8	147.50 (10)	N20—Eu2—N14	126.22 (11)
N6—Eu1—N10	73.84 (10)	N20—Eu2—N22	75.69 (12)
N6—Eu1—N12	100.83 (10)	N20—Eu2—N24	74.65 (11)
N8—Eu1—N2	78.35 (11)	N22—Eu2—N14	129.15 (11)
N8—Eu1—N4	120.65 (10)	N24—Eu2—N14	151.24 (11)
N8—Eu1—N10	75.33 (10)	N24—Eu2—N22	71.01 (11)
N8—Eu1—N12	77.10 (10)	O4—S2—C38	104.88 (18)
N12—Eu1—N2	135.36 (10)	O5—S2—O4	112.25 (18)
N12—Eu1—N10	68.76 (10)	O5—S2—O6	115.3 (2)
O1—S1—C19	102.96 (17)	O5—S2—C38	103.8 (2)
O2—S1—O1	113.32 (15)	O6—S2—O4	114.7 (2)
O2—S1—C19	103.84 (16)	O6—S2—C38	104.4 (2)
O3—S1—O1	114.11 (16)	S2—O4—Eu2	169.47 (19)
O3—S1—O2	114.96 (16)	S2—O5—Eu2^{ii}	163.2 (2)

O3—S1—C19	105.99 (17)	N14—N13—B3	121.4 (3)
S1—O1—Eu1	161.25 (17)	C20—N13—N14	109.9 (3)
S1—O2—Eu1^{i}	168.58 (16)	C20—N13—B3	128.5 (3)
N2—N1—B1	123.2 (3)	N13—N14—Eu2	122.1 (2)
C1—N1—N2	109.4 (4)	C22—N14—Eu2	132.0 (3)
C1—N1—B1	127.1 (4)	C22—N14—N13	105.8 (3)
N1—N2—Eu1	119.4 (2)	N16—N15—B3	121.3 (3)
C3—N2—Eu1	132.6 (3)	C23—N15—N16	108.6 (3)
C3—N2—N1	106.0 (3)	C23—N15—B3	129.8 (4)
N4—N3—B1	121.8 (3)	N15—N16—Eu2	123.9 (2)
C4—N3—N4	109.7 (3)	C25—N16—Eu2	128.7 (3)
C4—N3—B1	128.0 (3)	C25—N16—N15	107.1 (3)
N3—N4—Eu1	121.7 (2)	N18—N17—B3	123.2 (3)
C6—N4—Eu1	132.6 (3)	C26—N17—N18	109.6 (3)
C6—N4—N3	105.7 (3)	C26—N17—B3	127.0 (4)
N6—N5—B1	121.8 (3)	N17—N18—Eu2	120.0 (2)
C7—N5—N6	109.0 (4)	C28—N18—Eu2	131.3 (3)
C7—N5—B1	128.7 (4)	C28—N18—N17	106.2 (3)
N5—N6—Eu1	123.2 (2)	N20—N19—B4	122.4 (3)
C9—N6—Eu1	130.2 (3)	C29—N19—N20	109.6 (4)
C9—N6—N5	106.5 (3)	C29—N19—B4	128.0 (4)
N8—N7—B2	122.1 (3)	N19—N20—Eu2	123.5 (2)
C10—N7—N8	109.3 (3)	C31—N20—Eu2	130.4 (3)
C10—N7—B2	128.5 (3)	C31—N20—N19	106.0 (3)
N7—N8—Eu1	124.3 (2)	N22—N21—B4	121.8 (4)
C12—N8—Eu1	129.3 (3)	C32—N21—N22	109.9 (4)
C12—N8—N7	106.4 (3)	C32—N21—B4	128.3 (4)
N10—N9—B2	121.3 (3)	N21—N22—Eu2	122.8 (3)
C13—N9—N10	109.9 (3)	C34—N22—Eu2	130.5 (3)
C13—N9—B2	128.7 (3)	C34—N22—N21	105.7 (4)
N9—N10—Eu1	122.2 (2)	N24—N23—B4	123.1 (3)
C15—N10—Eu1	130.4 (3)	C35—N23—N24	109.9 (3)
C15—N10—N9	106.0 (3)	C35—N23—B4	126.9 (4)
N12—N11—B2	122.6 (3)	N23—N24—Eu2	121.8 (2)
C16—N11—N12	109.9 (3)	C37—N24—Eu2	132.9 (3)
C16—N11—B2	126.6 (3)	C37—N24—N23	105.1 (3)
N11—N12—Eu1	122.2 (2)	N13—C20—H20	125.7
C18—N12—Eu1	132.8 (3)	N13—C20—C21	108.6 (4)
C18—N12—N11	104.9 (3)	C21—C20—H20	125.7
N1—C1—H1	125.5	C20—C21—H21	127.9

N1—C1—C2	109.0 (4)	C20—C21—C22	104.3 (4)
C2—C1—H1	125.5	C22—C21—H21	127.9
C1—C2—H2	127.7	N14—C22—C21	111.4 (4)
C1—C2—C3	104.6 (4)	N14—C22—H22	124.3
C3—C2—H2	127.7	C21—C22—H22	124.3
N2—C3—C2	110.9 (4)	N15—C23—H23	125.6
N2—C3—H3A	124.5	N15—C23—C24	108.8 (4)
C2—C3—H3A	124.5	C24—C23—H23	125.6
N3—C4—H4A	125.8	C23—C24—H24	127.3
N3—C4—C5	108.5 (4)	C23—C24—C25	105.3 (4)
C5—C4—H4A	125.8	C25—C24—H24	127.3
C4—C5—H5	127.6	N16—C25—C24	110.2 (4)
C4—C5—C6	104.8 (4)	N16—C25—H25	124.9
C6—C5—H5	127.6	C24—C25—H25	124.9
N4—C6—C5	111.4 (4)	N17—C26—H26	125.7
N4—C6—H6	124.3	N17—C26—C27	108.6 (4)
C5—C6—H6	124.3	C27—C26—H26	125.7
N5—C7—H7	125.5	C26—C27—H27	127.5
N5—C7—C8	109.0 (4)	C26—C27—C28	104.9 (4)
C8—C7—H7	125.5	C28—C27—H27	127.5
C7—C8—H8	127.6	N18—C28—C27	110.6 (4)
C7—C8—C9	104.7 (4)	N18—C28—H28	124.7
C9—C8—H8	127.6	C27—C28—H28	124.7
N6—C9—C8	110.8 (4)	N19—C29—H29	125.4
N6—C9—H9	124.6	N19—C29—C30	109.1 (4)
C8—C9—H9	124.6	C30—C29—H29	125.4
N7—C10—H10	125.5	C29—C30—H30	127.7
N7—C10—C11	109.0 (4)	C29—C30—C31	104.5 (4)
C11—C10—H10	125.5	C31—C30—H30	127.7
C10—C11—H11	127.8	N20—C31—C30	110.7 (4)
C10—C11—C12	104.3 (4)	N20—C31—H31	124.6
C12—C11—H11	127.8	C30—C31—H31	124.6
N8—C12—C11	110.9 (4)	N21—C32—H32	125.7
N8—C12—H12	124.6	N21—C32—C33	108.6 (5)
C11—C12—H12	124.6	C33—C32—H32	125.7
N9—C13—H13	125.7	C32—C33—H33	127.5
N9—C13—C14	108.5 (4)	C32—C33—C34	105.1 (5)
C14—C13—H13	125.7	C34—C33—H33	127.5
C13—C14—H14	127.6	N22—C34—C33	110.8 (5)
C13—C14—C15	104.8 (3)	N22—C34—H34	124.6

C15—C14—H14	127.6	C33—C34—H34	124.6
N10—C15—C14	110.7 (4)	N23—C35—H35	125.5
N10—C15—H15	124.6	N23—C35—C36	109.0 (4)
C14—C15—H15	124.6	C36—C35—H35	125.5
N11—C16—H16	125.3	C35—C36—H36	127.7
N11—C16—C17	109.3 (4)	C35—C36—C37	104.7 (4)
C17—C16—H16	125.3	C37—C36—H36	127.7
C16—C17—H17	127.9	N24—C37—C36	111.3 (4)
C16—C17—C18	104.2 (3)	N24—C37—H37	124.4
C18—C17—H17	127.9	C36—C37—H37	124.4
N12—C18—C17	111.7 (4)	F4—C38—S2	109.3 (4)
N12—C18—H18	124.2	F5—C38—S2	110.8 (5)
C17—C18—H18	124.2	F5—C38—F4	104.8 (5)
F1—C19—S1	109.9 (3)	F6—C38—S2	113.8 (4)
F1—C19—F3	108.9 (3)	F6—C38—F4	108.4 (7)
F2—C19—S1	110.8 (3)	F6—C38—F5	109.2 (7)
F2—C19—F1	109.1 (3)	F4A—C38—S2	114.3 (5)
F2—C19—F3	107.7 (3)	F4A—C38—F5A	107.4 (10)
F3—C19—S1	110.4 (3)	F4A—C38—F6A	112.9 (13)
N1—B1—N3	107.7 (3)	F5A—C38—S2	103.2 (7)
N1—B1—N5	111.3 (3)	F6A—C38—S2	113.8 (10)
N1—B1—H1A	109.6	F6A—C38—F5A	104.0 (12)
N3—B1—N5	109.0 (3)	N13—B3—N15	108.2 (3)
N3—B1—H1A	109.6	N13—B3—N17	109.0 (3)
N5—B1—H1A	109.6	N13—B3—H3	109.5
N7—B2—N11	111.2 (3)	N15—B3—H3	109.5
N7—B2—H2A	109.4	N17—B3—N15	111.0 (3)
N9—B2—N7	109.6 (3)	N17—B3—H3	109.5
N9—B2—N11	107.8 (3)	N19—B4—N23	108.7 (4)
N9—B2—H2A	109.4	N19—B4—H4	109.4
N11—B2—H2A	109.4	N21—B4—N19	109.8 (4)
O4—Eu2—N14	75.54 (10)	N21—B4—N23	110.2 (4)
O4—Eu2—N16	75.81 (11)	N21—B4—H4	109.4
O4—Eu2—N18	143.91 (10)	N23—B4—H4	109.4

Symmetry codes: (i) -*x*+1, -*y*+2, -*z*+1; (ii) -*x*+2, -*y*+1, -*z*+2.

8.3.12 Crystallographic data for 7-Yb

Crystal data

$C_{23}H_{28}B_2F_3N_{12}O_4SYb$	D_x = 1.782 Mg m^{-3}
M_r = 820.29	Mo $K\alpha$ radiation, λ = 0.71073 Å
Orthorhombic, *Pbca*	Cell parameters from 9285 reflections
a = 18.6229 (14) Å	θ = 2.6–28.3°
b = 15.4376 (10) Å	μ = 3.20 mm^{-1}
c = 21.2684 (14) Å	T = 150 K
V = 6114.5 (7) Å^3	Needle, colourless
Z = 8	0.29 × 0.16 × 0.14 mm
F(000) = 3240	

Data collection

Bruker APEX-II CCD diffractometer	7594 measured reflections
ϕ and ω scans	7594 independent reflections
Absorption correction: multi-scan TWINABS-2012/1 (Bruker,2012) was used for absorption correction. Final HKLF 4 output contains 68215 reflections, Rint = 0.1099 (35291 with I > 3sig(I), Rint = 0.0842)	6287 reflections with $I > 2\sigma(I)$
	θ_{max} = 28.4°, θ_{min} = 2.6°

Refinement

Refinement on F^2	Primary atom site location: dual
Least-squares matrix: full	Hydrogen site location: inferred from neighbouring sites
$R[F^2 > 2\sigma(F^2)]$ = 0.057	H-atom parameters constrained
$wR(F^2)$ = 0.147	$w = 1/[\sigma^2(F_o^2) + (0.0469P)^2 + 122.0251P]$ where $P = (F_o^2 + 2F_c^2)/3$
S = 1.03	$(\Delta/\sigma)_{max}$ = 0.001
7594 reflections	$\Delta\rangle_{max}$ = 2.44 e Å^{-3}
415 parameters	$\Delta\rangle_{min}$ = -1.85 e Å^{-3}
0 restraints	

Special details

Geometry. All esds (except the esd in the dihedral angle between two l.s. planes) are estimated using the full covariance matrix. The cell esds are taken into account individually in the estimation of esds in distances, angles and torsion angles; correlations between esds in cell parameters are only used when they are defined by crystal symmetry. An approximate (isotropic) treatment of cell esds is used for estimating esds involving l.s. planes.

Fractional atomic coordinates and isotropic or equivalent isotropic displacement parameters (Å²)

	x	*y*	*z*	U_{iso}*/U_{eq}
Yb1	0.68626 (2)	0.71137 (2)	0.34550 (2)	0.01557 (10)
S1	0.70967 (11)	0.58208 (12)	0.49325 (8)	0.0229 (4)
O4	0.8014 (3)	0.7761 (3)	0.3943 (2)	0.0225 (10)
F3	0.6417 (3)	0.5999 (4)	0.5995 (2)	0.0393 (12)
O1	0.7094 (3)	0.6346 (3)	0.4357 (2)	0.0224 (10)
F2	0.6743 (3)	0.7203 (3)	0.5577 (2)	0.0399 (12)
F1	0.5844 (3)	0.6508 (4)	0.5200 (2)	0.0406 (12)
O2	0.7767 (3)	0.5853 (4)	0.5259 (3)	0.0330 (13)
N3	0.5264 (3)	0.8118 (4)	0.3136 (3)	0.0204 (12)
N12	0.7457 (3)	0.7943 (4)	0.2678 (3)	0.0174 (11)
N1	0.5639 (3)	0.8296 (4)	0.4240 (3)	0.0188 (11)
N4	0.5925 (3)	0.7960 (4)	0.2891 (3)	0.0218 (12)
N11	0.7726 (3)	0.7612 (4)	0.2127 (3)	0.0168 (11)
N8	0.7840 (3)	0.6162 (4)	0.3142 (3)	0.0192 (12)
N7	0.8091 (3)	0.6137 (4)	0.2532 (3)	0.0182 (11)
O3	0.6767 (4)	0.4987 (4)	0.4855 (3)	0.0373 (15)
N2	0.6362 (3)	0.8215 (4)	0.4164 (3)	0.0178 (11)
N5	0.5136 (3)	0.6858 (4)	0.3875 (3)	0.0237 (13)
N6	0.5758 (3)	0.6436 (4)	0.3749 (3)	0.0226 (12)
N9	0.6919 (3)	0.6316 (4)	0.1972 (3)	0.0204 (12)
N10	0.6497 (3)	0.6306 (4)	0.2502 (3)	0.0219 (12)
C23	0.8681 (4)	0.7895 (5)	0.3603 (4)	0.0296 (17)
H23A	0.873918	0.851456	0.349592	0.036*
H23B	0.868145	0.755407	0.320904	0.036*
C3	0.6662 (4)	0.8822 (5)	0.4525 (3)	0.0211 (14)
H3	0.716454	0.890703	0.456971	0.025*
C20	0.8220 (4)	0.7762 (5)	0.4601 (4)	0.0284 (17)
H20A	0.785165	0.747104	0.486143	0.034*
H20B	0.828511	0.836202	0.475599	0.034*
C18	0.7553 (4)	0.8805 (5)	0.2632 (4)	0.0228 (14)
H18	0.742846	0.920893	0.295075	0.027*
C6	0.5909 (4)	0.8266 (5)	0.2302 (3)	0.0221 (14)
H6	0.629704	0.823106	0.201354	0.026*
C10	0.8674 (4)	0.5626 (5)	0.2502 (4)	0.0249 (15)
H10	0.894020	0.549972	0.213198	0.030*

C4	0.4855 (4)	0.8530 (5)	0.2713 (4)	0.0273 (16)
H4	0.437347	0.871432	0.277594	0.033*
C11	0.8820 (4)	0.5315 (5)	0.3094 (4)	0.0251 (15)
H11	0.919932	0.493926	0.321563	0.030*
C12	0.8293 (4)	0.5672 (5)	0.3476 (3)	0.0202 (13)
H12	0.825835	0.558026	0.391697	0.024*
C21	0.8919 (5)	0.7272 (5)	0.4621 (4)	0.0329 (18)
H21A	0.884006	0.663826	0.460429	0.039*
H21B	0.920017	0.741633	0.500230	0.039*
C16	0.7959 (4)	0.8257 (5)	0.1755 (4)	0.0228 (15)
H16	0.816067	0.819072	0.134708	0.027*
C5	0.5249 (4)	0.8642 (5)	0.2171 (4)	0.0278 (16)
H5	0.510200	0.891595	0.179168	0.033*
C2	0.6145 (4)	0.9309 (5)	0.4826 (4)	0.0248 (15)
H2	0.621896	0.978618	0.510046	0.030*
C15	0.5848 (4)	0.6039 (5)	0.2302 (4)	0.0272 (16)
H15	0.544263	0.596117	0.256731	0.033*
B2	0.7699 (5)	0.6617 (5)	0.1998 (4)	0.0200 (15)
H2A	0.793970	0.648857	0.158868	0.024*
C1	0.5504 (4)	0.8958 (5)	0.4643 (4)	0.0244 (15)
H1	0.504234	0.914633	0.477564	0.029*
C17	0.7857 (4)	0.9026 (5)	0.2063 (4)	0.0288 (17)
H17	0.797088	0.959102	0.191658	0.035*
C13	0.6533 (4)	0.6082 (5)	0.1467 (3)	0.0250 (15)
H13	0.670548	0.605301	0.104671	0.030*
C9	0.5627 (5)	0.5595 (5)	0.3870 (4)	0.0302 (17)
H9	0.596632	0.514038	0.382288	0.036*
C14	0.5847 (4)	0.5892 (5)	0.1660 (4)	0.0285 (17)
H14	0.545713	0.570046	0.140783	0.034*
C7	0.4627 (5)	0.6294 (6)	0.4071 (4)	0.0325 (18)
H7	0.414817	0.643448	0.418677	0.039*
C19	0.6490 (4)	0.6424 (5)	0.5451 (4)	0.0287 (16)
C8	0.4926 (5)	0.5487 (6)	0.4073 (4)	0.035 (2)
H8	0.469919	0.495903	0.418993	0.043*
B1	0.5082 (4)	0.7857 (5)	0.3807 (4)	0.0218 (16)
H1A	0.458671	0.805583	0.391777	0.026*
C22	0.9286 (5)	0.7601 (8)	0.4027 (5)	0.050 (3)
H22A	0.961194	0.808997	0.412554	0.060*
H22B	0.956792	0.713395	0.382530	0.060*

Atomic displacement parameters (Å²)

	U^{11}	U^{22}	U^{33}	U^{12}	U^{13}	U^{23}
Yb1	0.01583 (15)	0.01425 (14)	0.01663 (15)	0.00014 (10)	0.00122 (10)	0.00013 (10)
S1	0.0302 (9)	0.0198 (8)	0.0189 (8)	0.0041 (7)	0.0045 (7)	0.0015 (7)
O4	0.025 (3)	0.022 (2)	0.021 (3)	-0.002 (2)	-0.003 (2)	0.003 (2)
F3	0.045 (3)	0.052 (3)	0.021 (2)	-0.006 (2)	0.008 (2)	0.001 (2)
O1	0.025 (3)	0.026 (3)	0.016 (2)	0.001 (2)	-0.003 (2)	0.007 (2)
F2	0.057 (3)	0.026 (2)	0.036 (3)	-0.006 (2)	0.012 (2)	-0.012 (2)
F1	0.030 (3)	0.058 (3)	0.034 (3)	0.009 (2)	0.002 (2)	-0.011 (2)
O2	0.035 (3)	0.039 (3)	0.026 (3)	0.011 (3)	-0.003 (2)	0.004 (2)
N3	0.015 (3)	0.022 (3)	0.024 (3)	0.001 (2)	-0.002 (2)	-0.001 (2)
N12	0.017 (3)	0.023 (3)	0.013 (2)	0.001 (2)	0.001 (2)	0.002 (2)
N1	0.016 (3)	0.019 (3)	0.021 (3)	-0.001 (2)	0.000 (2)	-0.004 (2)
N4	0.019 (3)	0.025 (3)	0.022 (3)	0.000 (2)	0.003 (2)	-0.003 (2)
N11	0.012 (2)	0.017 (3)	0.021 (3)	0.001 (2)	0.000 (2)	0.004 (2)
N8	0.022 (3)	0.017 (3)	0.019 (3)	0.002 (2)	0.001 (2)	0.000 (2)
N7	0.017 (3)	0.018 (3)	0.019 (3)	0.002 (2)	0.001 (2)	-0.001 (2)
O3	0.068 (5)	0.019 (3)	0.024 (3)	-0.002 (3)	0.006 (3)	0.000 (2)
N2	0.018 (3)	0.017 (3)	0.018 (3)	0.002 (2)	0.001 (2)	-0.004 (2)
N5	0.018 (3)	0.032 (3)	0.021 (3)	-0.010 (3)	0.004 (2)	-0.001 (3)
N6	0.024 (3)	0.024 (3)	0.020 (3)	-0.003 (2)	0.000 (2)	0.001 (2)
N9	0.025 (3)	0.016 (3)	0.020 (3)	0.003 (2)	-0.002 (2)	0.001 (2)
N10	0.015 (3)	0.021 (3)	0.030 (3)	-0.001 (2)	0.004 (2)	-0.002 (3)
C23	0.019 (3)	0.030 (4)	0.040 (5)	-0.001 (3)	0.001 (3)	0.000 (3)
C3	0.019 (3)	0.023 (3)	0.021 (3)	-0.003 (3)	-0.005 (3)	-0.002 (3)
C20	0.035 (4)	0.017 (3)	0.033 (4)	0.000 (3)	-0.012 (3)	-0.004 (3)
C18	0.015 (3)	0.018 (3)	0.035 (4)	-0.002 (3)	-0.001 (3)	-0.003 (3)
C6	0.022 (4)	0.027 (4)	0.017 (3)	-0.003 (3)	0.001 (3)	0.004 (3)
C10	0.019 (3)	0.024 (4)	0.031 (4)	0.000 (3)	0.003 (3)	-0.004 (3)
C4	0.020 (4)	0.035 (4)	0.027 (4)	0.002 (3)	-0.003 (3)	0.004 (3)
C11	0.019 (3)	0.023 (3)	0.033 (4)	0.009 (3)	-0.004 (3)	0.000 (3)
C12	0.023 (3)	0.020 (3)	0.017 (3)	0.002 (3)	-0.004 (3)	0.000 (3)
C21	0.040 (5)	0.023 (4)	0.035 (4)	0.002 (3)	-0.010 (4)	0.001 (3)
C16	0.015 (3)	0.028 (4)	0.025 (3)	-0.001 (3)	0.001 (3)	0.010 (3)
C5	0.023 (4)	0.034 (4)	0.027 (4)	0.002 (3)	-0.008 (3)	0.004 (3)
C2	0.031 (4)	0.018 (3)	0.025 (4)	-0.001 (3)	-0.003 (3)	-0.001 (3)
C15	0.023 (4)	0.028 (4)	0.031 (4)	-0.003 (3)	-0.003 (3)	-0.003 (3)
B2	0.027 (4)	0.018 (3)	0.015 (3)	0.000 (3)	0.004 (3)	0.000 (3)

C1	0.025 (4)	0.023 (3)	0.026 (4)	0.002 (3)	0.009 (3)	-0.004 (3)
C17	0.023 (4)	0.019 (3)	0.045 (5)	-0.004 (3)	0.000 (3)	0.011 (3)
C13	0.031 (4)	0.023 (3)	0.021 (4)	0.001 (3)	-0.005 (3)	-0.002 (3)
C9	0.041 (5)	0.021 (3)	0.030 (4)	-0.013 (3)	0.002 (3)	-0.001 (3)
C14	0.026 (4)	0.030 (4)	0.030 (4)	-0.004 (3)	-0.013 (3)	-0.003 (3)
C7	0.027 (4)	0.042 (5)	0.029 (4)	-0.019 (4)	0.004 (3)	-0.009 (4)
C19	0.026 (4)	0.032 (4)	0.029 (4)	-0.005 (3)	0.005 (3)	-0.003 (3)
C8	0.042 (5)	0.031 (4)	0.033 (4)	-0.022 (4)	0.005 (4)	-0.007 (3)
B1	0.020 (4)	0.026 (4)	0.020 (4)	0.001 (3)	0.001 (3)	-0.004 (3)
C22	0.023 (4)	0.068 (7)	0.059 (6)	-0.001 (4)	-0.009 (4)	0.015 (6)

Geometric parameters (Å, º)

Yb1—O4	2.582 (5)	C23—H23B	0.9900
Yb1—O1	2.296 (5)	C23—C22	1.513 (12)
Yb1—N12	2.365 (6)	C3—H3	0.9500
Yb1—N4	2.489 (6)	C3—C2	1.378 (10)
Yb1—N8	2.433 (6)	C20—H20A	0.9900
Yb1—N2	2.456 (6)	C20—H20B	0.9900
Yb1—N6	2.391 (6)	C20—C21	1.507 (11)
Yb1—N10	2.476 (6)	C18—H18	0.9500
S1—O1	1.468 (5)	C18—C17	1.378 (11)
S1—O2	1.429 (6)	C6—H6	0.9500
S1—O3	1.435 (6)	C6—C5	1.388 (10)
S1—C19	1.832 (8)	C10—H10	0.9500
O4—C23	1.452 (9)	C10—C11	1.376 (11)
O4—C20	1.452 (9)	C4—H4	0.9500
F3—C19	1.337 (9)	C4—C5	1.378 (11)
F2—C19	1.321 (9)	C11—H11	0.9500
F1—C19	1.322 (9)	C11—C12	1.388 (10)
N3—N4	1.359 (8)	C12—H12	0.9500
N3—C4	1.339 (9)	C21—H21A	0.9900
N3—B1	1.522 (10)	C21—H21B	0.9900
N12—N11	1.373 (8)	C21—C22	1.524 (13)
N12—C18	1.346 (9)	C16—H16	0.9500
N1—N2	1.363 (8)	C16—C17	1.370 (11)
N1—C1	1.358 (9)	C5—H5	0.9500
N1—B1	1.544 (10)	C2—H2	0.9500
N4—C6	1.339 (9)	C2—C1	1.368 (11)

N11—C16	1.345 (9)	C15—H15	0.9500
N11—B2	1.560 (9)	C15—C14	1.384 (11)
N8—N7	1.379 (8)	B2—H2A	1.0000
N8—C12	1.337 (9)	C1—H1	0.9500
N7—C10	1.343 (9)	C17—H17	0.9500
N7—B2	1.540 (10)	C13—H13	0.9500
N2—C3	1.334 (9)	C13—C14	1.374 (11)
N5—N6	1.354 (9)	C9—H9	0.9500
N5—C7	1.354 (9)	C9—C8	1.385 (12)
N5—B1	1.552 (10)	C14—H14	0.9500
N6—C9	1.347 (9)	C7—H7	0.9500
N9—N10	1.374 (8)	C7—C8	1.364 (13)
N9—B2	1.526 (10)	C8—H8	0.9500
N9—C13	1.342 (9)	B1—H1A	1.0000
N10—C15	1.345 (9)	C22—H22A	0.9900
C23—H23A	0.9900	C22—H22B	0.9900
O1—Yb1—O4	73.04 (17)	O4—C20—C21	104.8 (7)
O1—Yb1—N12	140.86 (19)	H20A—C20—H20B	108.9
O1—Yb1—N4	143.61 (19)	C21—C20—H20A	110.8
O1—Yb1—N8	77.10 (19)	C21—C20—H20B	110.8
O1—Yb1—N2	85.10 (19)	N12—C18—H18	124.3
O1—Yb1—N6	73.6 (2)	N12—C18—C17	111.3 (7)
O1—Yb1—N10	118.5 (2)	C17—C18—H18	124.3
N12—Yb1—O4	71.50 (18)	N4—C6—H6	124.6
N12—Yb1—N4	73.00 (19)	N4—C6—C5	110.9 (7)
N12—Yb1—N8	77.6 (2)	C5—C6—H6	124.6
N12—Yb1—N2	103.4 (2)	N7—C10—H10	125.7
N12—Yb1—N6	145.3 (2)	N7—C10—C11	108.7 (7)
N12—Yb1—N10	80.2 (2)	C11—C10—H10	125.7
N4—Yb1—O4	124.96 (18)	N3—C4—H4	125.7
N8—Yb1—O4	73.87 (18)	N3—C4—C5	108.6 (7)
N8—Yb1—N4	135.28 (19)	C5—C4—H4	125.7
N8—Yb1—N2	150.4 (2)	C10—C11—H11	127.5
N8—Yb1—N10	71.2 (2)	C10—C11—C12	104.9 (6)
N2—Yb1—O4	78.49 (18)	C12—C11—H11	127.5
N2—Yb1—N4	70.53 (19)	N8—C12—C11	111.0 (6)
N2—Yb1—N10	138.33 (19)	N8—C12—H12	124.5
N6—Yb1—O4	141.10 (18)	C11—C12—H12	124.5
N6—Yb1—N4	75.6 (2)	C20—C21—H21A	111.5

N6—Yb1—N8	116.8 (2)	C20—C21—H21B	111.5
N6—Yb1—N2	79.4 (2)	C20—C21—C22	101.3 (7)
N6—Yb1—N10	76.0 (2)	H21A—C21—H21B	109.3
N10—Yb1—O4	138.78 (18)	C22—C21—H21A	111.5
N10—Yb1—N4	71.1 (2)	C22—C21—H21B	111.5
O1—S1—C19	102.6 (3)	N11—C16—H16	125.8
O2—S1—O1	112.9 (3)	N11—C16—C17	108.3 (7)
O2—S1—O3	117.4 (4)	C17—C16—H16	125.8
O2—S1—C19	103.2 (4)	C6—C5—H5	127.8
O3—S1—O1	113.4 (3)	C4—C5—C6	104.5 (7)
O3—S1—C19	105.1 (4)	C4—C5—H5	127.8
C23—O4—Yb1	124.5 (4)	C3—C2—H2	127.4
C23—O4—C20	104.6 (6)	C1—C2—C3	105.2 (6)
C20—O4—Yb1	127.4 (4)	C1—C2—H2	127.4
S1—O1—Yb1	169.3 (3)	N10—C15—H15	124.4
N4—N3—B1	120.9 (6)	N10—C15—C14	111.3 (7)
C4—N3—N4	110.1 (6)	C14—C15—H15	124.4
C4—N3—B1	129.0 (6)	N11—B2—H2A	109.5
N11—N12—Yb1	124.4 (4)	N7—B2—N11	109.2 (6)
C18—N12—Yb1	130.4 (5)	N7—B2—H2A	109.5
C18—N12—N11	104.9 (6)	N9—B2—N11	109.7 (6)
N2—N1—B1	123.6 (6)	N9—B2—N7	109.4 (6)
C1—N1—N2	109.1 (6)	N9—B2—H2A	109.5
C1—N1—B1	125.7 (6)	N1—C1—C2	108.4 (6)
N3—N4—Yb1	123.1 (4)	N1—C1—H1	125.8
C6—N4—Yb1	130.7 (5)	C2—C1—H1	125.8
C6—N4—N3	106.0 (6)	C18—C17—H17	127.4
N12—N11—B2	120.3 (5)	C16—C17—C18	105.2 (6)
C16—N11—N12	110.2 (6)	C16—C17—H17	127.4
C16—N11—B2	129.5 (6)	N9—C13—H13	125.8
N7—N8—Yb1	121.8 (4)	N9—C13—C14	108.4 (7)
C12—N8—Yb1	131.9 (5)	C14—C13—H13	125.8
C12—N8—N7	105.7 (6)	N6—C9—H9	124.9
N8—N7—B2	121.3 (5)	N6—C9—C8	110.3 (8)
C10—N7—N8	109.6 (6)	C8—C9—H9	124.9
C10—N7—B2	129.1 (6)	C15—C14—H14	127.5
N1—N2—Yb1	120.8 (4)	C13—C14—C15	105.0 (7)
C3—N2—Yb1	133.0 (5)	C13—C14—H14	127.5
C3—N2—N1	106.3 (5)	N5—C7—H7	126.2
N6—N5—B1	121.0 (6)	N5—C7—C8	107.6 (8)

C7—N5—N6	110.5 (7)	C8—C7—H7	126.2
C7—N5—B1	128.5 (7)	F3—C19—S1	109.5 (6)
N5—N6—Yb1	125.2 (5)	F2—C19—S1	111.4 (5)
C9—N6—Yb1	128.9 (6)	F2—C19—F3	107.8 (7)
C9—N6—N5	105.7 (6)	F2—C19—F1	108.5 (7)
N10—N9—B2	121.2 (6)	F1—C19—S1	111.7 (5)
C13—N9—N10	110.3 (6)	F1—C19—F3	107.7 (6)
C13—N9—B2	128.4 (6)	C9—C8—H8	127.1
N9—N10—Yb1	120.6 (4)	C7—C8—C9	105.8 (7)
C15—N10—Yb1	131.3 (5)	C7—C8—H8	127.1
C15—N10—N9	105.0 (6)	N3—B1—N1	107.0 (6)
O4—C23—H23A	110.2	N3—B1—N5	109.7 (6)
O4—C23—H23B	110.2	N3—B1—H1A	110.1
O4—C23—C22	107.4 (7)	N1—B1—N5	109.7 (6)
H23A—C23—H23B	108.5	N1—B1—H1A	110.1
C22—C23—H23A	110.2	N5—B1—H1A	110.1
C22—C23—H23B	110.2	C23—C22—C21	105.0 (7)
N2—C3—H3	124.5	C23—C22—H22A	110.7
N2—C3—C2	111.0 (6)	C23—C22—H22B	110.7
C2—C3—H3	124.5	C21—C22—H22A	110.7
O4—C20—H20A	110.8	C21—C22—H22B	110.7
O4—C20—H20B	110.8	H22A—C22—H22B	108.8
Yb1—O4—C23—C22	-136.7 (6)	N6—C9—C8—C7	0.2 (10)
Yb1—O4—C20—C21	119.6 (6)	N9—N10—C15—C14	-0.9 (9)
Yb1—N12—N11—C16	173.1 (4)	N9—C13—C14—C15	0.9 (9)
Yb1—N12—N11—B2	-4.4 (8)	N10—N9—B2—N11	-69.0 (8)
Yb1—N12—C18—C17	-172.7 (5)	N10—N9—B2—N7	50.8 (8)
Yb1—N4—C6—C5	175.0 (5)	N10—N9—C13—C14	-1.5 (8)
Yb1—N8—N7—C10	173.9 (5)	N10—C15—C14—C13	0.0 (9)
Yb1—N8—N7—B2	-8.5 (8)	C23—O4—C20—C21	-39.8 (7)
Yb1—N8—C12—C11	-172.9 (5)	C3—C2—C1—N1	-1.0 (8)
Yb1—N2—C3—C2	177.9 (5)	C20—O4—C23—C22	23.5 (8)
Yb1—N6—C9—C8	175.2 (5)	C20—C21—C22—C23	-24.4 (10)
Yb1—N10—C15—C14	158.5 (5)	C18—N12—N11—C16	-1.6 (7)
O4—C23—C22—C21	1.4 (10)	C18—N12—N11—B2	-179.1 (6)

O4—C20—C21—C22	39.6 (8)	C10—N7—B2—N11	-118.8 (7)
O1—S1—C19—F3	177.7 (5)	C10—N7—B2—N9	121.1 (7)
O1—S1—C19—F2	-63.0 (6)	C10—C11—C12—N8	0.9 (9)
O1—S1—C19—F1	58.5 (6)	C4—N3—N4—Yb1	-175.4 (5)
O2—S1—O1—Yb1	-171.1 (17)	C4—N3—N4—C6	-1.4 (8)
O2—S1—C19—F3	-64.7 (6)	C4—N3—B1—N1	-121.6 (8)
O2—S1—C19—F2	54.5 (7)	C4—N3—B1—N5	119.5 (8)
O2—S1—C19—F1	176.1 (6)	C12—N8—N7—C10	1.4 (8)
N3—N4—C6—C5	1.6 (8)	C12—N8—N7—B2	178.9 (6)
N3—C4—C5—C6	0.4 (9)	C16—N11—B2—N7	126.0 (7)
N12—N11—C16—C17	1.0 (8)	C16—N11—B2—N9	-114.2 (8)
N12—N11—B2—N7	-57.1 (8)	B2—N11—C16—C17	178.2 (7)
N12—N11—B2—N9	62.8 (8)	B2—N7—C10—C11	-178.1 (7)
N12—C18—C17—C16	-1.0 (9)	B2—N9—N10—Yb1	15.8 (8)
N1—N2—C3—C2	-1.2 (8)	B2—N9—N10—C15	177.9 (6)
N4—N3—C4—C5	0.6 (9)	B2—N9—C13—C14	-177.6 (7)
N4—N3—B1—N1	56.6 (8)	C1—N1—N2—Yb1	-178.7 (5)
N4—N3—B1—N5	-62.3 (8)	C1—N1—N2—C3	0.5 (8)
N4—C6—C5—C4	-1.3 (9)	C1—N1—B1—N3	109.8 (8)
N11—N12—C18—C17	1.6 (8)	C1—N1—B1—N5	-131.3 (7)
N11—C16—C17—C18	0.0 (8)	C13—N9—N10—Yb1	-160.7 (5)
N8—N7—C10—C11	-0.8 (8)	C13—N9—N10—C15	1.4 (8)
N8—N7—B2—N11	64.1 (8)	C13—N9—B2—N11	106.8 (8)
N8—N7—B2—N9	-55.9 (8)	C13—N9—B2—N7	-133.4 (7)
N7—N8—C12—C11	-1.4 (8)	C7—N5—N6—Yb1	-175.5 (5)
N7—C10—C11—C12	-0.1 (8)	C7—N5—N6—C9	0.0 (8)
O3—S1—O1—Yb1	52.2 (19)	C7—N5—B1—N3	-123.4 (8)
O3—S1—C19—F3	58.9 (6)	C7—N5—B1—N1	119.3 (8)
O3—S1—C19—F2	178.1 (6)	C19—S1—O1—Yb1	-60.7 (19)
O3—S1—C19—F1	-60.3 (7)	B1—N3—N4—Yb1	6.1 (8)
N2—N1—C1—C2	0.3 (8)	B1—N3—N4—C6	-179.9 (6)
N2—N1—B1—N3	-54.0 (9)	B1—N3—C4—C5	178.9 (7)
N2—N1—B1—N5	65.0 (8)	B1—N1—N2—Yb1	-12.6 (8)
N2—C3—C2—C1	1.4 (9)	B1—N1—N2—C3	166.6 (6)
N5—N6—C9—C8	-0.1 (9)	B1—N1—C1—C2	-165.4 (7)
N5—C7—C8—C9	-0.2 (9)	B1—N5—N6—Yb1	2.8 (9)
N6—N5—C7—C8	0.1 (9)	B1—N5—N6—C9	178.4 (6)

N6—N5—B1—N3	58.5 (8)	B1—N5—C7—C8	-178.1 (7)
N6—N5—B1—N1	-58.8 (8)		

8.3.13 Crystallographic data for 9-YY′

Crystal data

$C_{45}H_{29}B_2F_{18}N_{14}O_8Y_2 \cdot 0.75(C_6H_{14})$	$F(000)$ = 11976
M_r = 1499.89	D_x = 1.607 Mg m^{-3}
Monoclinic, *C*2/*c*	Cu *K*α radiation, λ = 1.54178 Å
a = 30.4551 (13) Å	Cell parameters from 8959 reflections
b = 28.9932 (13) Å	θ = 4.4–67.3°
c = 29.9247 (8) Å	μ = 3.55 mm^{-1}
β = 110.225 (4)°	*T* = 100 K
V = 24794.0 (18) Å^3	Plate, red
Z = 16	0.07 × 0.06 × 0.01 mm

Data collection

Rigaku 007HF equipped with Varimax confocal mirrors and an AFC11 goniometer and HyPix 6000 detector diffractometer	13807 independent reflections
Radiation source: Rotating anode, Rigaku 007 HF	8465 reflections with $I > 2\sigma(I)$
Mirror monochromator	R_{int} = 0.171
Detector resolution: 10 pixels mm^{-1}	θ_{max} = 51.9°, θ_{min} = 3.0°
profile data from ω–scans	*h* = -28→31
Absorption correction: multi-scan *CrysAlis PRO* 1.171.40.82a (Rigaku Oxford Diffraction, 2020) Empirical absorption correction using spherical harmonics, implemented in SCALE3 ABSPACK scaling algorithm.	*k* = -29→29
T_{min} = 0.725, T_{max} = 1.000	*l* = -30→29
75599 measured reflections	

Refinement

Refinement on F^2	350 restraints
Least-squares matrix: full	Hydrogen site location: mixed
$R[F^2 > 2\sigma(F^2)]$ = 0.089	H-atom parameters constrained

$wR(F^2)$ = 0.250	$w = 1/[\sigma^2(F_o^2) + (0.1397P)^2 + 63.5134P]$ where $P = (F_o^2 + 2F_c^2)/3$
S = 1.07	$(\Delta/\sigma)_{max}$ = 0.005
13807 reflections	$\Delta\rangle_{max}$ = 1.48 e Å^{-3}
1701 parameters	$\Delta\rangle_{min}$ = -0.62 e Å^{-3}

Special details

Geometry. All esds (except the esd in the dihedral angle between two l.s. planes) are estimated using the full covariance matrix. The cell esds are taken into account individually in the estimation of esds in distances, angles and torsion angles; correlations between esds in cell parameters are only used when they are defined by crystal symmetry. An approximate (isotropic) treatment of cell esds is used for estimating esds involving l.s. planes.

Fractional atomic coordinates and isotropic or equivalent isotropic displacement parameters (Å²)

	x	*y*	*z*	U_{iso}*/U_{eq}	Occ. (<1)
Y2A	0.86140 (4)	0.55612 (4)	0.63859 (4)	0.0495 (4)	
Y1B	0.17385 (4)	0.67751 (4)	0.13421 (3)	0.0480 (4)	
Y1A	0.69011 (4)	0.59469 (4)	0.82224 (4)	0.0499 (4)	
Y2B	0.38362 (4)	0.63141 (4)	0.41893 (4)	0.0538 (4)	
O3B	0.3614 (3)	0.5559 (3)	0.4288 (3)	0.058 (2)	
O1B	0.2352 (3)	0.6313 (3)	0.1810 (3)	0.052 (2)	
F1A	0.7698 (3)	0.6611 (3)	0.5128 (3)	0.073 (2)	
O2A	0.7389 (3)	0.5433 (3)	0.7992 (3)	0.051 (2)	
O7A	0.8977 (3)	0.6279 (3)	0.6502 (3)	0.058 (2)	
O2B	0.2189 (3)	0.7161 (3)	0.2071 (3)	0.049 (2)	
F6B	0.2209 (3)	0.6547 (3)	0.4165 (3)	0.078 (2)	
O3A	0.8101 (3)	0.5933 (3)	0.5721 (3)	0.050 (2)	
O6A	0.9042 (3)	0.4880 (4)	0.6575 (3)	0.069 (3)	
O1A	0.7188 (3)	0.6295 (3)	0.7672 (3)	0.053 (2)	
O7B	0.4422 (4)	0.5882 (4)	0.4042 (3)	0.072 (3)	
F13A	0.9039 (3)	0.7201 (3)	0.6421 (3)	0.084 (2)	
F2A	0.7124 (3)	0.6148 (3)	0.5028 (3)	0.083 (3)	
O6B	0.3774 (3)	0.6878 (3)	0.4714 (3)	0.061 (2)	
F11A	0.9671 (4)	0.3948 (3)	0.6385 (3)	0.097 (3)	
O4B	0.3061 (3)	0.6313 (3)	0.4129 (3)	0.060 (2)	
N13B	0.2428 (4)	0.7030 (3)	0.1147 (3)	0.045 (3)	
F4B	0.2182 (3)	0.6455 (3)	0.3437 (3)	0.095 (3)	
F11B	0.3415 (4)	0.7468 (3)	0.5185 (3)	0.088 (3)	

F9B	0.5239 (3)	0.6387 (3)	0.6014 (3)	0.090 (3)	
O5A	0.9114 (3)	0.5559 (3)	0.5954 (3)	0.057 (2)	
F3A	0.7491 (3)	0.6155 (3)	0.4535 (2)	0.086 (3)	
F6A	0.7900 (3)	0.4580 (3)	0.4658 (3)	0.087 (3)	
F5B	0.1913 (3)	0.5933 (3)	0.3778 (3)	0.084 (2)	
N5A	0.6658 (4)	0.5170 (4)	0.8342 (4)	0.053 (3)	
O8B	0.4408 (4)	0.6831 (3)	0.4181 (3)	0.069 (3)	
N11B	0.1586 (4)	0.7585 (4)	0.1144 (3)	0.057 (3)	
F7B	0.5281 (3)	0.5963 (4)	0.5452 (3)	0.113 (4)	
O5B	0.4377 (3)	0.6129 (3)	0.4928 (3)	0.066 (3)	
N1A	0.8062 (3)	0.6079 (4)	0.6627 (3)	0.047 (3)	
O4A	0.8249 (3)	0.5006 (3)	0.5823 (3)	0.062 (2)	
N2B	0.3390 (4)	0.6937 (4)	0.3608 (3)	0.049 (3)	
F10A	0.9649 (4)	0.4173 (4)	0.7049 (3)	0.107 (3)	
N2A	0.8213 (4)	0.5191 (4)	0.6906 (3)	0.050 (3)	
N13A	0.6894 (4)	0.6763 (4)	0.8381 (4)	0.055 (3)	
F10B	0.3990 (3)	0.7813 (4)	0.5077 (4)	0.096 (3)	
O8A	0.9077 (4)	0.5628 (4)	0.7191 (3)	0.082 (3)	
F14A	0.9642 (4)	0.7199 (4)	0.7058 (3)	0.127 (4)	
N14B	0.2375 (4)	0.7333 (4)	0.0776 (3)	0.051 (3)	
N12B	0.1673 (4)	0.7789 (4)	0.0771 (3)	0.049 (3)	
F5A	0.7802 (4)	0.4253 (3)	0.5239 (3)	0.112 (4)	
N4B	0.1005 (4)	0.6243 (4)	0.1824 (3)	0.053 (3)	
F8A	0.9337 (4)	0.5438 (4)	0.5104 (3)	0.107 (3)	
N3B	0.1371 (4)	0.6548 (4)	0.1930 (3)	0.053 (3)	
N10A	0.7046 (4)	0.6291 (4)	0.9353 (4)	0.058 (3)	
N10B	0.1591 (4)	0.7118 (4)	0.0224 (3)	0.051 (3)	
F12A	0.9027 (4)	0.3944 (4)	0.6504 (4)	0.105 (3)	
N14A	0.7079 (4)	0.6952 (4)	0.8837 (4)	0.064 (3)	
N1B	0.3494 (4)	0.6052 (4)	0.3347 (3)	0.048 (3)	
F8B	0.4859 (4)	0.5755 (4)	0.5849 (3)	0.108 (3)	
N7A	0.6084 (4)	0.6101 (4)	0.8177 (4)	0.061 (3)	
N9A	0.6878 (4)	0.5939 (4)	0.9052 (4)	0.054 (3)	
F9A	0.9993 (4)	0.5182 (4)	0.5546 (3)	0.113 (4)	
N3A	0.6338 (4)	0.5702 (4)	0.7421 (3)	0.054 (3)	
N5B	0.1541 (4)	0.5958 (4)	0.1165 (3)	0.060 (3)	
F12B	0.4070 (5)	0.7514 (4)	0.5759 (3)	0.143 (5)	
C4B	0.2939 (4)	0.6168 (4)	0.2558 (4)	0.043 (3)	
N4A	0.5960 (4)	0.5434 (4)	0.7389 (4)	0.058 (3)	
F15A	0.9664 (4)	0.6886 (4)	0.6438 (4)	0.117 (3)	

N12A	0.7769 (5)	0.6419 (4)	0.9150 (4)	0.066 (3)	
N11A	0.7696 (4)	0.6125 (4)	0.8764 (3)	0.057 (3)	
F4A	0.8486 (4)	0.4385 (4)	0.5248 (4)	0.125 (4)	
F7A	0.9783 (4)	0.5865 (4)	0.5623 (4)	0.109 (3)	
N6B	0.1146 (4)	0.5760 (5)	0.1182 (4)	0.066 (3)	
C5B	0.2589 (5)	0.6464 (4)	0.2220 (4)	0.045 (3)	
N7B	0.0878 (4)	0.6795 (5)	0.0959 (3)	0.068 (3)	
N9B	0.1552 (4)	0.6735 (4)	0.0462 (4)	0.057 (3)	
C7A	0.7821 (4)	0.5284 (4)	0.7486 (4)	0.042 (3)	
C14A	0.7875 (5)	0.5820 (5)	0.5307 (5)	0.054 (3)	
C8B	0.2724 (5)	0.7519 (5)	0.2997 (4)	0.052 (3)	
H8B	0.249496	0.771115	0.279881	0.063*	
C4A	0.7619 (5)	0.6206 (5)	0.7139 (4)	0.049 (3)	
C11A	0.7977 (4)	0.5456 (5)	0.7114 (4)	0.045 (3)	
N8A	0.5752 (4)	0.5772 (4)	0.8044 (3)	0.060 (3)	
N6A	0.6211 (4)	0.5014 (4)	0.8172 (4)	0.059 (3)	
C6A	0.7546 (4)	0.5581 (5)	0.7666 (4)	0.047 (3)	
C1A	0.7981 (4)	0.6509 (5)	0.6480 (4)	0.049 (3)	
H1A	0.810796	0.661635	0.625837	0.058*	
C12B	0.3182 (4)	0.6325 (5)	0.3023 (4)	0.041 (3)	
C3A	0.7520 (4)	0.6662 (5)	0.6962 (4)	0.052 (4)	
H3A	0.732839	0.685444	0.706188	0.063*	
C16B	0.2741 (5)	0.6025 (6)	0.4022 (4)	0.050 (3)	
C38B	0.1137 (5)	0.6634 (6)	-0.0307 (4)	0.063 (4)	
H38B	0.094879	0.650142	-0.059181	0.075*	
C15A	0.7869 (5)	0.5394 (5)	0.5102 (4)	0.054 (4)	
H15A	0.772947	0.536322	0.477330	0.065*	
C13A	0.7542 (6)	0.6194 (6)	0.4997 (4)	0.059 (4)	
C45B	0.2799 (5)	0.7397 (5)	0.0735 (5)	0.051 (3)	
H45B	0.285743	0.758851	0.051291	0.061*	
N8B	0.0596 (4)	0.6437 (5)	0.0968 (4)	0.071 (4)	
C3B	0.3032 (5)	0.5722 (5)	0.2437 (4)	0.051 (3)	
H3B	0.288256	0.561324	0.212938	0.061*	
C43B	0.2882 (5)	0.6933 (5)	0.1313 (5)	0.056 (4)	
H43B	0.301979	0.674183	0.157309	0.067*	
C10A	0.8322 (5)	0.4754 (5)	0.7074 (5)	0.058 (4)	
H10A	0.848897	0.456905	0.693564	0.070*	
C12A	0.7875 (4)	0.5924 (4)	0.6952 (4)	0.042 (3)	
C11B	0.3113 (4)	0.6788 (5)	0.3161 (4)	0.044 (3)	
C37B	0.1275 (5)	0.6441 (5)	0.0147 (4)	0.054 (4)	

H37B	0.118702	0.615072	0.021941	0.065*	
C31A	0.6910 (5)	0.4829 (5)	0.8629 (4)	0.058 (4)	
H31A	0.723149	0.483669	0.878741	0.070*	
C7B	0.2786 (4)	0.7083 (5)	0.2844 (4)	0.045 (3)	
C8A	0.7941 (5)	0.4842 (5)	0.7640 (4)	0.056 (4)	
H8A	0.784994	0.472465	0.788322	0.068*	
C39B	0.1335 (5)	0.7050 (6)	-0.0243 (4)	0.055 (4)	
H39B	0.130174	0.726464	-0.048380	0.066*	
C2A	0.7716 (4)	0.6808 (5)	0.6640 (4)	0.049 (3)	
H2A	0.766983	0.710994	0.652783	0.059*	
C44A	0.6668 (6)	0.7122 (6)	0.8108 (5)	0.072 (4)	
H44A	0.651381	0.710284	0.778063	0.086*	
C9B	0.2997 (5)	0.7670 (5)	0.3439 (5)	0.061 (4)	
H9B	0.296445	0.796542	0.354342	0.073*	
C40A	0.6866 (6)	0.6275 (6)	0.9706 (5)	0.073 (5)	
H40A	0.692421	0.648532	0.995523	0.087*	
C42B	0.1533 (5)	0.8224 (6)	0.0734 (4)	0.064 (4)	
H42B	0.156001	0.843429	0.050956	0.077*	
C9A	0.8193 (5)	0.4571 (5)	0.7443 (5)	0.059 (4)	
H9A	0.827744	0.427188	0.755219	0.071*	
C10B	0.3327 (6)	0.7362 (6)	0.3727 (5)	0.061 (4)	
H10B	0.351730	0.746546	0.402493	0.073*	
C31B	0.1784 (5)	0.5626 (6)	0.1042 (4)	0.058 (4)	
H31B	0.206949	0.566707	0.099986	0.070*	
C21B	0.4043 (6)	0.7011 (5)	0.5131 (5)	0.064 (4)	
C16A	0.8065 (5)	0.5014 (5)	0.5371 (5)	0.057 (4)	
C5A	0.7429 (5)	0.6044 (5)	0.7499 (4)	0.053 (4)	
C15B	0.2784 (6)	0.5548 (6)	0.4029 (4)	0.064 (4)	
H15B	0.251948	0.536174	0.393435	0.077*	
C30A	0.5738 (5)	0.5334 (5)	0.6925 (5)	0.071 (4)	
H30A	0.546509	0.516178	0.680740	0.086*	
F16B	0.4881 (5)	0.7589 (5)	0.4249 (6)	0.152 (5)	
C45A	0.6692 (6)	0.7517 (6)	0.8369 (6)	0.078 (5)	
H45A	0.655349	0.780109	0.826201	0.093*	
C39A	0.6584 (5)	0.5898 (6)	0.9634 (4)	0.063 (4)	
H39A	0.641814	0.579786	0.982498	0.076*	
C20B	0.4429 (5)	0.6780 (6)	0.5426 (5)	0.068 (4)	
H20B	0.459731	0.690966	0.571936	0.082*	
C6B	0.2508 (5)	0.6914 (5)	0.2364 (5)	0.051 (3)	
C1B	0.3557 (5)	0.5631 (5)	0.3223 (4)	0.051 (3)	

H1B	0.376108	0.544267	0.345370	0.061*	
C2B	0.3338 (5)	0.5444 (5)	0.2767 (4)	0.055 (4)	
H2B	0.339965	0.514521	0.269396	0.066*	
C44B	0.3126 (5)	0.7142 (5)	0.1065 (5)	0.059 (4)	
H44B	0.344351	0.711593	0.111105	0.071*	
C33B	0.1147 (7)	0.5309 (7)	0.1076 (5)	0.077 (5)	
H33B	0.091443	0.509715	0.106546	0.092*	
C22A	0.9421 (5)	0.4180 (6)	0.6582 (5)	0.069 (5)	
C40B	0.1391 (5)	0.7912 (6)	0.1323 (5)	0.066 (4)	
H40B	0.129937	0.786840	0.158591	0.079*	
C41B	0.1340 (5)	0.8319 (6)	0.1082 (5)	0.077 (5)	
H41B	0.120728	0.859271	0.113717	0.092*	
C29A	0.5964 (5)	0.5518 (5)	0.6656 (5)	0.065 (4)	
H29A	0.589401	0.548290	0.633002	0.078*	
C38A	0.6594 (5)	0.5697 (5)	0.9227 (4)	0.059 (4)	
H38A	0.642999	0.543306	0.908949	0.071*	
C19A	0.9390 (5)	0.5267 (6)	0.5884 (4)	0.062 (4)	
C35A	0.5882 (6)	0.6443 (6)	0.8340 (5)	0.070 (4)	
H35A	0.603197	0.671745	0.846526	0.084*	
C20A	0.9498 (5)	0.4841 (5)	0.6083 (4)	0.060 (4)	
H20A	0.970771	0.465858	0.599859	0.072*	
C17A	0.8072 (6)	0.4561 (6)	0.5138 (6)	0.068 (4)	
C22B	0.3878 (7)	0.7451 (7)	0.5288 (5)	0.077 (5)	
C18A	0.9629 (6)	0.5428 (7)	0.5536 (5)	0.072 (5)	
C34A	0.6183 (6)	0.4604 (6)	0.8353 (5)	0.071 (4)	
H34A	0.590965	0.443252	0.828962	0.085*	
C41A	0.8133 (5)	0.6023 (5)	0.8783 (5)	0.063 (4)	
H41A	0.819680	0.584076	0.855715	0.075*	
C18B	0.5001 (6)	0.6126 (7)	0.5661 (5)	0.076 (5)	
C19B	0.4574 (5)	0.6371 (6)	0.5307 (5)	0.067 (4)	
C26B	0.4828 (7)	0.6773 (7)	0.4234 (5)	0.070 (4)	
C37A	0.5356 (6)	0.5907 (7)	0.8112 (6)	0.078 (5)	
H37A	0.508020	0.573990	0.804361	0.094*	
C46A	0.6964 (6)	0.7398 (6)	0.8822 (5)	0.075 (5)	
H46A	0.705617	0.759755	0.908154	0.090*	
C30B	0.0847 (5)	0.6206 (6)	0.2191 (5)	0.071 (4)	
H30B	0.059654	0.602688	0.219831	0.086*	
C21A	0.9309 (5)	0.4669 (5)	0.6405 (4)	0.056 (4)	
C23A	0.9384 (5)	0.6950 (5)	0.6704 (5)	0.084 (4)	
F17B	0.5384 (6)	0.7237 (5)	0.4050 (6)	0.168 (6)	

C43A	0.8224 (7)	0.6464 (6)	0.9384 (5)	0.076 (5)	
H43A	0.835492	0.664121	0.965665	0.092*	
C28A	0.6327 (5)	0.5772 (5)	0.6971 (4)	0.062 (4)	
H28A	0.658917	0.573031	0.693123	0.074*	
C32B	0.1548 (7)	0.5216 (6)	0.0988 (5)	0.073 (4)	
H32B	0.164156	0.493193	0.090739	0.088*	
C24A	0.9228 (6)	0.6506 (5)	0.6845 (5)	0.076 (3)	
C24B	0.4848 (6)	0.5953 (7)	0.4151 (6)	0.085 (5)	
F18B	0.5417 (6)	0.7244 (5)	0.4738 (5)	0.185 (7)	
C17B	0.2244 (6)	0.6235 (6)	0.3852 (5)	0.073 (4)	
C33A	0.6618 (6)	0.4468 (6)	0.8650 (5)	0.068 (4)	
H33A	0.669939	0.419694	0.882586	0.082*	
B2B	0.1898 (6)	0.7521 (5)	0.0466 (5)	0.050 (4)	
H2BA	0.193856	0.772623	0.022253	0.059*	
C28B	0.1437 (5)	0.6679 (5)	0.2377 (4)	0.064 (4)	
H28B	0.166856	0.688357	0.254939	0.077*	
C36A	0.5443 (6)	0.6343 (7)	0.8303 (5)	0.079 (5)	
H36A	0.523724	0.653101	0.838894	0.095*	
C25B	0.5080 (7)	0.6374 (8)	0.4252 (6)	0.093 (6)	
H25B	0.540285	0.638604	0.433067	0.111*	
C29B	0.1122 (5)	0.6478 (5)	0.2550 (5)	0.064 (4)	
H29B	0.110083	0.651791	0.284985	0.077*	
C34B	0.0613 (6)	0.7075 (7)	0.0622 (6)	0.082 (5)	
H34B	0.071420	0.735535	0.054195	0.098*	
C42A	0.8474 (6)	0.6212 (6)	0.9165 (5)	0.079 (5)	
H42A	0.879621	0.617798	0.925532	0.094*	
C35B	0.0165 (6)	0.6898 (8)	0.0401 (6)	0.092 (6)	
H35B	-0.007973	0.702983	0.015502	0.110*	
C36B	0.0162 (6)	0.6492 (8)	0.0624 (6)	0.094 (6)	
H36B	-0.008797	0.628681	0.055566	0.113*	
C26A	0.9297 (7)	0.5918 (7)	0.7454 (5)	0.103 (4)	
B2A	0.7356 (7)	0.6658 (6)	0.9258 (5)	0.068 (5)	
H2AA	0.748272	0.685416	0.954070	0.082*	
B1A	0.5820 (5)	0.5321 (6)	0.7814 (6)	0.060 (5)	
H1AA	0.552491	0.514939	0.770709	0.072*	
B1B	0.0778 (7)	0.6032 (7)	0.1301 (6)	0.074 (6)	
H1BA	0.051766	0.582823	0.128989	0.089*	
C27B	0.5107 (7)	0.7211 (9)	0.4293 (8)	0.104 (7)	
C25A	0.9391 (7)	0.6358 (7)	0.7299 (5)	0.101 (4)	
H25A	0.957808	0.655899	0.752800	0.121*	

C8S	0.4977 (12)	0.7664 (12)	0.6921 (12)	0.202 (13)*	
H8SA	0.490688	0.799078	0.691671	0.242*	
H8SB	0.468581	0.749424	0.679092	0.242*	
C7S	0.5306 (10)	0.7563 (10)	0.6636 (10)	0.170 (10)*	
H7SA	0.547445	0.728235	0.674960	0.255*	
H7SB	0.552301	0.781303	0.667761	0.255*	
H7SC	0.512300	0.753152	0.630420	0.255*	
C9S	0.5236 (10)	0.7513 (11)	0.7394 (11)	0.182 (11)*	
H9SA	0.547906	0.772901	0.756431	0.219*	
H9SB	0.536868	0.720782	0.739981	0.219*	
F18A	0.9365 (10)	0.5485 (8)	0.8126 (6)	0.103 (5)	0.5
F16A	0.9500 (9)	0.6233 (8)	0.8282 (6)	0.131 (6)	0.5
F2B	0.2853 (6)	0.4620 (7)	0.4120 (7)	0.088 (7)	0.56 (2)
C4S	0.4035 (10)	0.6975 (9)	0.2586 (10)	0.197 (13)*	
H4SA	0.371990	0.685643	0.250885	0.237*	
H4SB	0.407254	0.705933	0.228748	0.237*	
C2S	0.3771 (13)	0.7828 (12)	0.2717 (13)	0.249 (18)*	
H2SA	0.345067	0.772137	0.263335	0.299*	
H2SB	0.380772	0.792850	0.242281	0.299*	
C6S	0.4389 (17)	0.6133 (14)	0.2579 (18)	0.34 (3)*	
H6SA	0.463578	0.595091	0.279366	0.512*	
H6SB	0.409626	0.597577	0.251215	0.512*	
H6SC	0.444982	0.617849	0.228745	0.512*	
F17A	0.9714 (10)	0.5589 (10)	0.8134 (8)	0.130 (6)	0.5
F1	0.9030 (9)	0.5690 (9)	0.8104 (6)	0.125 (7)	0.5
C27A	0.9368 (10)	0.5889 (12)	0.7992 (8)	0.114 (5)	0.5
C13B	0.3261 (5)	0.4840 (5)	0.4250 (5)	0.082 (5)	
C14B	0.3226 (6)	0.5355 (5)	0.4180 (4)	0.055 (3)	
F1B	0.3537 (10)	0.4612 (7)	0.4089 (13)	0.145 (11)	0.56 (2)
F3B	0.3427 (9)	0.4746 (7)	0.4730 (5)	0.127 (10)	0.56 (2)
F15B	0.5555 (5)	0.5508 (8)	0.4410 (7)	0.110 (7)*	0.5
F14B	0.4919 (7)	0.5126 (6)	0.4134 (8)	0.112 (7)*	0.5
F2	0.9885 (8)	0.6005 (9)	0.8233 (6)	0.114 (5)	0.5
F13B	0.5132 (7)	0.5537 (8)	0.3656 (6)	0.120 (7)*	0.5
F1AA	0.3681 (7)	0.4665 (10)	0.4440 (10)	0.106 (12)	0.44 (2)
F9	0.3152 (11)	0.4665 (8)	0.3787 (6)	0.109 (10)	0.44 (2)
F14	0.2973 (11)	0.4629 (11)	0.4402 (13)	0.125 (12)	0.44 (2)
C23B	0.5118 (4)	0.5525 (6)	0.4105 (6)	0.156 (12)	
F3	0.5020 (11)	0.5250 (12)	0.3736 (10)	0.212 (17)*	0.5
F4	0.5573 (6)	0.5647 (9)	0.4209 (9)	0.130 (9)*	0.5

F5	0.5116 (12)	0.5257 (12)	0.4475 (11)	0.216 (15)*	0.5
F6	0.9916 (9)	0.5358 (9)	0.7897 (7)	0.127 (6)	0.5
C1	0.9612 (14)	0.5688 (14)	0.7912 (10)	0.113 (5)	0.5
C1S	0.3811 (17)	0.8269 (14)	0.3024 (17)	0.34 (3)*	
H1SA	0.358094	0.848986	0.284896	0.504*	
H1SB	0.375738	0.818962	0.331283	0.504*	
H1SC	0.411766	0.839863	0.310038	0.504*	
C3S	0.4069 (10)	0.7420 (8)	0.2874 (10)	0.179 (11)*	
H3SA	0.403703	0.732615	0.317292	0.215*	
H3SB	0.438816	0.752805	0.295270	0.215*	
C5S	0.4369 (13)	0.6581 (12)	0.2797 (14)	0.263 (19)*	
H5SA	0.467970	0.671171	0.287586	0.316*	
H5SB	0.433021	0.651132	0.309797	0.316*	

Atomic displacement parameters (Å²)

	U^{11}	U^{22}	U^{33}	U^{12}	U^{13}	U^{23}
Y2A	0.0645 (8)	0.0592 (9)	0.0294 (6)	0.0058 (6)	0.0222 (5)	0.0041 (5)
Y1B	0.0641 (7)	0.0537 (8)	0.0271 (6)	-0.0017 (6)	0.0169 (5)	0.0026 (5)
Y1A	0.0685 (8)	0.0570 (8)	0.0296 (6)	-0.0001 (6)	0.0239 (5)	-0.0015 (5)
Y2B	0.0681 (8)	0.0635 (9)	0.0290 (6)	-0.0011 (7)	0.0159 (5)	-0.0006 (6)
O3B	0.073 (6)	0.060 (7)	0.042 (5)	0.000 (5)	0.023 (5)	-0.002 (4)
O1B	0.072 (6)	0.062 (6)	0.020 (5)	-0.006 (5)	0.013 (4)	-0.003 (4)
F1A	0.095 (6)	0.059 (6)	0.054 (5)	0.008 (5)	0.013 (4)	0.011 (4)
O2A	0.069 (5)	0.053 (6)	0.035 (5)	0.005 (4)	0.023 (4)	-0.002 (4)
O7A	0.073 (5)	0.077 (6)	0.024 (4)	-0.001 (5)	0.015 (4)	0.004 (4)
O2B	0.064 (5)	0.053 (6)	0.033 (5)	0.001 (5)	0.019 (4)	0.002 (4)
F6B	0.090 (6)	0.069 (6)	0.079 (6)	0.003 (5)	0.034 (5)	0.003 (5)
O3A	0.070 (6)	0.051 (6)	0.031 (5)	-0.005 (5)	0.020 (4)	-0.006 (4)
O6A	0.076 (6)	0.089 (8)	0.052 (5)	0.013 (6)	0.034 (5)	0.013 (5)
O1A	0.076 (6)	0.057 (6)	0.032 (4)	0.016 (5)	0.028 (4)	0.002 (4)
O7B	0.068 (7)	0.099 (9)	0.046 (5)	0.010 (6)	0.015 (5)	-0.013 (5)
F13A	0.095 (6)	0.072 (6)	0.071 (5)	0.001 (5)	0.011 (5)	0.006 (4)
F2A	0.075 (6)	0.091 (7)	0.085 (6)	0.006 (5)	0.029 (5)	0.025 (5)
O6B	0.072 (6)	0.080 (7)	0.028 (5)	-0.003 (5)	0.015 (4)	-0.002 (4)
F11A	0.136 (8)	0.080 (7)	0.102 (7)	0.023 (6)	0.077 (7)	0.027 (5)
O4B	0.075 (6)	0.067 (7)	0.043 (5)	-0.002 (6)	0.028 (5)	0.010 (5)
N13B	0.068 (8)	0.040 (7)	0.029 (5)	-0.010 (6)	0.018 (5)	-0.002 (5)
F4B	0.093 (6)	0.123 (8)	0.059 (5)	0.010 (6)	0.014 (4)	0.034 (5)

F11B	0.100 (7)	0.099 (7)	0.069 (6)	0.007 (6)	0.037 (5)	-0.014 (5)
F9B	0.086 (6)	0.120 (8)	0.045 (5)	0.009 (5)	-0.001 (4)	-0.014 (5)
O5A	0.079 (6)	0.060 (6)	0.042 (5)	0.004 (5)	0.034 (5)	0.008 (4)
F3A	0.134 (7)	0.089 (6)	0.033 (4)	0.030 (5)	0.025 (4)	0.014 (4)
F6A	0.147 (8)	0.065 (6)	0.048 (5)	0.004 (5)	0.035 (5)	-0.011 (4)
F5B	0.071 (5)	0.097 (7)	0.079 (6)	-0.018 (5)	0.018 (4)	-0.001 (5)
N5A	0.084 (9)	0.043 (7)	0.037 (6)	-0.010 (7)	0.029 (6)	-0.010 (6)
O8B	0.075 (7)	0.090 (8)	0.044 (5)	-0.017 (6)	0.023 (5)	-0.007 (5)
N11B	0.085 (8)	0.058 (8)	0.038 (6)	0.016 (6)	0.036 (6)	0.001 (6)
F7B	0.105 (7)	0.145 (10)	0.076 (6)	0.041 (7)	0.013 (6)	-0.027 (6)
O5B	0.081 (6)	0.074 (7)	0.042 (5)	0.008 (5)	0.021 (5)	0.000 (5)
N1A	0.059 (6)	0.058 (8)	0.027 (5)	0.004 (6)	0.020 (5)	0.010 (5)
O4A	0.085 (6)	0.058 (7)	0.047 (6)	0.008 (5)	0.027 (5)	0.004 (5)
N2B	0.076 (7)	0.044 (8)	0.027 (6)	-0.006 (6)	0.019 (5)	-0.006 (5)
F10A	0.146 (8)	0.114 (8)	0.053 (6)	0.034 (7)	0.024 (6)	0.033 (5)
N2A	0.066 (7)	0.042 (8)	0.040 (6)	0.013 (6)	0.019 (5)	0.001 (5)
N13A	0.085 (8)	0.052 (8)	0.036 (6)	0.005 (6)	0.031 (6)	0.008 (6)
F10B	0.106 (7)	0.072 (7)	0.098 (7)	0.008 (6)	0.021 (6)	0.001 (6)
O8A	0.103 (7)	0.114 (8)	0.020 (4)	-0.020 (6)	0.009 (4)	0.007 (5)
F14A	0.160 (9)	0.098 (7)	0.074 (6)	-0.055 (7)	-0.021 (6)	0.020 (5)
N14B	0.080 (8)	0.048 (7)	0.030 (6)	-0.009 (6)	0.024 (5)	-0.002 (5)
N12B	0.071 (7)	0.033 (7)	0.046 (6)	0.002 (6)	0.024 (5)	0.002 (5)
F5A	0.198 (11)	0.075 (7)	0.081 (6)	-0.046 (7)	0.073 (7)	-0.026 (5)
N4B	0.066 (7)	0.067 (8)	0.031 (6)	0.002 (6)	0.025 (5)	0.014 (5)
F8A	0.132 (8)	0.152 (10)	0.051 (6)	0.020 (7)	0.049 (6)	0.029 (6)
N3B	0.065 (7)	0.058 (8)	0.037 (6)	-0.010 (6)	0.020 (5)	-0.005 (5)
N10A	0.094 (8)	0.053 (8)	0.033 (6)	-0.001 (7)	0.030 (6)	-0.001 (6)
N10B	0.076 (7)	0.056 (8)	0.022 (6)	-0.006 (6)	0.020 (5)	0.002 (5)
F12A	0.090 (7)	0.112 (8)	0.115 (8)	0.011 (6)	0.041 (6)	0.040 (6)
N14A	0.101 (9)	0.060 (9)	0.039 (7)	0.001 (7)	0.035 (6)	0.008 (6)
N1B	0.076 (7)	0.041 (8)	0.030 (6)	-0.002 (6)	0.022 (6)	-0.006 (5)
F8B	0.125 (8)	0.103 (8)	0.065 (6)	0.016 (7)	-0.006 (5)	0.010 (6)
N7A	0.071 (8)	0.071 (9)	0.050 (7)	-0.003 (8)	0.031 (6)	-0.009 (6)
N9A	0.073 (7)	0.054 (8)	0.039 (6)	0.005 (6)	0.022 (6)	0.007 (6)
F9A	0.118 (8)	0.147 (10)	0.102 (7)	0.063 (7)	0.074 (6)	0.061 (7)
N3A	0.068 (7)	0.072 (8)	0.020 (6)	-0.007 (7)	0.012 (5)	-0.010 (5)
N5B	0.061 (7)	0.080 (10)	0.036 (6)	-0.007 (7)	0.014 (5)	0.011 (6)
F12B	0.209 (12)	0.131 (9)	0.048 (6)	0.079 (9)	-0.008 (6)	-0.028 (6)
C4B	0.058 (8)	0.041 (9)	0.031 (7)	-0.003 (7)	0.017 (6)	-0.002 (6)
N4A	0.074 (8)	0.063 (8)	0.035 (7)	-0.003 (7)	0.015 (6)	-0.008 (5)

F15A	0.123 (8)	0.124 (8)	0.117 (8)	-0.017 (6)	0.055 (6)	0.013 (6)
N12A	0.070 (9)	0.073 (9)	0.048 (7)	-0.008 (7)	0.012 (7)	0.014 (7)
N11A	0.090 (9)	0.059 (8)	0.027 (6)	-0.007 (6)	0.028 (6)	-0.003 (5)
F4A	0.107 (8)	0.125 (10)	0.113 (8)	0.037 (7)	0.002 (6)	-0.062 (7)
F7A	0.132 (9)	0.110 (9)	0.112 (8)	-0.015 (7)	0.075 (7)	0.017 (7)
N6B	0.081 (9)	0.087 (11)	0.034 (6)	-0.020 (8)	0.025 (6)	-0.008 (6)
C5B	0.074 (9)	0.045 (9)	0.023 (7)	0.003 (7)	0.025 (7)	0.010 (6)
N7B	0.052 (7)	0.115 (11)	0.029 (6)	0.009 (8)	0.005 (5)	0.026 (7)
N9B	0.071 (7)	0.050 (8)	0.045 (6)	-0.007 (6)	0.014 (6)	-0.010 (6)
C7A	0.066 (8)	0.026 (8)	0.036 (7)	-0.001 (7)	0.021 (6)	0.003 (6)
C14A	0.070 (9)	0.042 (10)	0.055 (10)	0.005 (8)	0.030 (8)	-0.001 (8)
C8B	0.081 (9)	0.052 (10)	0.025 (7)	0.009 (8)	0.021 (7)	0.008 (7)
C4A	0.070 (9)	0.048 (10)	0.033 (7)	0.010 (7)	0.020 (6)	0.011 (6)
C11A	0.054 (8)	0.047 (10)	0.033 (7)	0.010 (7)	0.014 (6)	-0.008 (6)
N8A	0.061 (8)	0.077 (9)	0.037 (6)	-0.007 (7)	0.013 (5)	-0.017 (6)
N6A	0.083 (9)	0.046 (8)	0.053 (7)	-0.019 (7)	0.031 (7)	-0.003 (6)
C6A	0.071 (8)	0.050 (10)	0.022 (6)	0.001 (7)	0.019 (6)	0.001 (6)
C1A	0.057 (8)	0.048 (10)	0.043 (7)	-0.008 (7)	0.019 (6)	0.009 (7)
C12B	0.053 (7)	0.051 (9)	0.023 (7)	-0.003 (7)	0.017 (6)	0.006 (7)
C3A	0.072 (9)	0.054 (10)	0.028 (7)	0.016 (7)	0.015 (6)	-0.002 (6)
C16B	0.064 (9)	0.059 (11)	0.027 (6)	-0.007 (8)	0.016 (6)	0.000 (6)
C38B	0.077 (10)	0.089 (13)	0.018 (7)	-0.010 (9)	0.011 (6)	-0.002 (7)
C15A	0.077 (9)	0.067 (11)	0.021 (6)	0.007 (8)	0.019 (6)	0.003 (7)
C13A	0.082 (11)	0.063 (12)	0.031 (8)	0.005 (9)	0.022 (7)	-0.001 (7)
C45B	0.056 (9)	0.050 (9)	0.052 (8)	-0.014 (7)	0.023 (7)	-0.009 (7)
N8B	0.058 (8)	0.113 (12)	0.046 (7)	-0.008 (8)	0.022 (7)	0.021 (7)
C3B	0.071 (9)	0.045 (10)	0.035 (7)	-0.002 (7)	0.018 (7)	-0.011 (7)
C43B	0.053 (9)	0.065 (10)	0.045 (8)	-0.016 (8)	0.012 (7)	-0.014 (7)
C10A	0.070 (9)	0.059 (11)	0.056 (9)	-0.002 (8)	0.035 (7)	-0.004 (8)
C12A	0.050 (7)	0.042 (9)	0.030 (6)	0.002 (7)	0.009 (6)	-0.003 (6)
C11B	0.068 (8)	0.050 (10)	0.020 (7)	-0.002 (7)	0.021 (6)	0.005 (6)
C37B	0.073 (9)	0.050 (9)	0.039 (8)	-0.021 (8)	0.019 (7)	0.001 (7)
C31A	0.080 (10)	0.069 (11)	0.032 (7)	0.003 (9)	0.027 (7)	0.003 (7)
C7B	0.069 (8)	0.051 (10)	0.020 (7)	-0.002 (7)	0.021 (6)	-0.001 (6)
C8A	0.078 (9)	0.070 (11)	0.031 (7)	0.007 (8)	0.030 (7)	-0.003 (7)
C39B	0.068 (9)	0.064 (11)	0.034 (8)	0.010 (8)	0.018 (7)	0.010 (7)
C2A	0.077 (9)	0.048 (9)	0.024 (6)	0.008 (7)	0.019 (6)	0.010 (6)
C44A	0.108 (12)	0.065 (11)	0.057 (9)	0.023 (10)	0.047 (9)	0.013 (9)
C9B	0.097 (11)	0.044 (9)	0.045 (9)	-0.023 (9)	0.027 (8)	-0.028 (8)
C40A	0.098 (12)	0.094 (14)	0.040 (8)	0.009 (11)	0.040 (8)	0.008 (8)

C42B	0.090 (10)	0.067 (12)	0.036 (8)	0.011 (9)	0.022 (7)	0.006 (7)
C9A	0.075 (9)	0.056 (10)	0.055 (8)	0.008 (8)	0.033 (8)	0.012 (7)
C10B	0.097 (11)	0.056 (11)	0.033 (8)	-0.015 (9)	0.027 (8)	-0.015 (8)
C31B	0.079 (10)	0.069 (12)	0.022 (7)	0.001 (10)	0.010 (6)	-0.003 (7)
C21B	0.089 (11)	0.071 (11)	0.039 (9)	0.018 (9)	0.033 (9)	0.009 (8)
C16A	0.073 (9)	0.059 (11)	0.042 (9)	-0.002 (8)	0.025 (7)	-0.002 (8)
C5A	0.060 (8)	0.064 (11)	0.037 (7)	0.008 (8)	0.020 (7)	0.006 (7)
C15B	0.079 (10)	0.078 (12)	0.036 (7)	-0.015 (9)	0.021 (7)	-0.010 (7)
C30A	0.069 (10)	0.074 (12)	0.061 (11)	0.018 (8)	0.010 (9)	-0.013 (9)
F16B	0.150 (11)	0.109 (11)	0.215 (15)	-0.025 (9)	0.087 (11)	-0.012 (10)
C45A	0.126 (13)	0.055 (11)	0.072 (11)	0.037 (10)	0.061 (10)	0.017 (9)
C39A	0.081 (10)	0.086 (12)	0.032 (8)	-0.001 (10)	0.032 (7)	0.002 (7)
C20B	0.085 (11)	0.066 (11)	0.043 (8)	0.010 (9)	0.008 (8)	-0.020 (8)
C6B	0.060 (9)	0.048 (10)	0.050 (9)	0.006 (7)	0.025 (7)	0.013 (8)
C1B	0.073 (9)	0.051 (10)	0.029 (7)	0.011 (7)	0.018 (6)	-0.003 (7)
C2B	0.066 (9)	0.053 (10)	0.043 (8)	0.007 (8)	0.016 (7)	-0.008 (7)
C44B	0.047 (8)	0.077 (11)	0.055 (9)	0.003 (8)	0.022 (8)	-0.010 (8)
C33B	0.114 (14)	0.078 (14)	0.035 (8)	-0.047 (11)	0.023 (8)	-0.007 (8)
C22A	0.054 (9)	0.112 (15)	0.055 (10)	0.012 (10)	0.035 (8)	0.022 (9)
C40B	0.076 (10)	0.077 (12)	0.037 (8)	0.015 (9)	0.010 (7)	0.002 (9)
C41B	0.094 (11)	0.078 (13)	0.052 (9)	0.039 (10)	0.017 (8)	-0.014 (9)
C29A	0.084 (10)	0.079 (11)	0.029 (7)	0.008 (9)	0.015 (8)	-0.008 (7)
C38A	0.074 (9)	0.070 (10)	0.043 (8)	-0.003 (8)	0.033 (7)	0.004 (7)
C19A	0.061 (9)	0.106 (14)	0.026 (7)	0.024 (9)	0.025 (6)	0.009 (8)
C35A	0.081 (12)	0.071 (12)	0.073 (10)	0.034 (9)	0.044 (9)	0.010 (8)
C20A	0.069 (9)	0.077 (12)	0.044 (8)	0.020 (8)	0.031 (7)	0.016 (8)
C17A	0.083 (12)	0.056 (12)	0.068 (11)	-0.011 (10)	0.031 (9)	-0.008 (9)
C22B	0.096 (14)	0.081 (14)	0.039 (9)	0.033 (11)	0.004 (8)	-0.014 (9)
C18A	0.076 (11)	0.101 (16)	0.050 (10)	0.013 (11)	0.037 (9)	0.014 (9)
C34A	0.078 (12)	0.077 (13)	0.061 (10)	-0.023 (10)	0.027 (9)	-0.010 (9)
C41A	0.075 (10)	0.083 (12)	0.044 (9)	-0.005 (9)	0.038 (8)	0.014 (8)
C18B	0.092 (12)	0.088 (14)	0.041 (9)	0.026 (11)	0.015 (9)	-0.002 (10)
C19B	0.072 (10)	0.076 (12)	0.049 (9)	0.000 (9)	0.016 (8)	-0.002 (9)
C26B	0.067 (12)	0.097 (15)	0.045 (8)	-0.028 (12)	0.017 (8)	-0.014 (8)
C37A	0.069 (11)	0.095 (15)	0.073 (10)	0.010 (10)	0.028 (8)	-0.017 (10)
C46A	0.136 (14)	0.041 (11)	0.051 (10)	0.001 (10)	0.037 (10)	0.006 (8)
C30B	0.068 (9)	0.110 (14)	0.042 (8)	-0.001 (9)	0.026 (8)	0.002 (9)
C21A	0.066 (9)	0.052 (10)	0.046 (8)	0.024 (8)	0.015 (7)	0.019 (7)
C23A	0.108 (8)	0.089 (8)	0.048 (6)	-0.019 (7)	0.018 (6)	0.006 (6)
F17B	0.209 (14)	0.139 (11)	0.204 (14)	-0.076 (10)	0.133 (13)	-0.034 (10)

C43A	0.118 (16)	0.073 (12)	0.044 (9)	-0.023 (11)	0.035 (11)	0.009 (8)
C28A	0.070 (9)	0.077 (11)	0.033 (8)	0.020 (8)	0.010 (7)	-0.004 (7)
C32B	0.119 (14)	0.058 (12)	0.045 (9)	-0.014 (11)	0.032 (9)	-0.019 (7)
C24A	0.095 (6)	0.089 (7)	0.039 (5)	-0.015 (6)	0.017 (5)	0.013 (5)
C24B	0.045 (11)	0.123 (18)	0.084 (11)	0.028 (12)	0.020 (9)	-0.013 (11)
F18B	0.245 (16)	0.155 (13)	0.105 (10)	-0.104 (12)	-0.002 (10)	-0.017 (9)
C17B	0.082 (11)	0.077 (12)	0.046 (9)	-0.017 (10)	0.006 (8)	0.013 (9)
C33A	0.089 (12)	0.070 (12)	0.049 (9)	-0.009 (10)	0.029 (9)	0.014 (8)
B2B	0.087 (12)	0.031 (10)	0.034 (8)	0.004 (9)	0.025 (8)	0.005 (7)
C28B	0.077 (10)	0.080 (11)	0.031 (8)	-0.012 (8)	0.013 (7)	-0.008 (7)
C36A	0.073 (12)	0.117 (17)	0.061 (10)	0.001 (10)	0.041 (8)	-0.019 (10)
C25B	0.067 (11)	0.109 (17)	0.092 (13)	-0.039 (14)	0.015 (9)	-0.036 (12)
C29B	0.081 (10)	0.080 (11)	0.042 (8)	-0.013 (9)	0.035 (8)	0.006 (8)
C34B	0.058 (10)	0.126 (16)	0.062 (10)	0.005 (10)	0.023 (8)	0.018 (11)
C42A	0.075 (11)	0.099 (14)	0.051 (9)	-0.031 (10)	0.008 (9)	0.009 (9)
C35B	0.070 (12)	0.144 (18)	0.053 (9)	0.004 (11)	0.012 (8)	0.036 (11)
C36B	0.077 (13)	0.145 (19)	0.063 (11)	-0.022 (12)	0.028 (10)	-0.006 (12)
C26A	0.126 (7)	0.122 (8)	0.035 (5)	-0.030 (6)	-0.005 (5)	0.012 (6)
B2A	0.110 (15)	0.063 (13)	0.030 (9)	-0.014 (11)	0.022 (9)	0.009 (8)
B1A	0.047 (9)	0.073 (13)	0.055 (10)	-0.023 (9)	0.011 (8)	-0.007 (9)
B1B	0.077 (12)	0.103 (16)	0.044 (10)	-0.028 (11)	0.024 (9)	0.003 (10)
C27B	0.081 (14)	0.12 (2)	0.126 (18)	-0.014 (14)	0.060 (14)	-0.037 (15)
C25A	0.124 (8)	0.111 (8)	0.042 (6)	-0.027 (7)	-0.004 (6)	0.010 (6)
F18A	0.122 (12)	0.136 (11)	0.031 (7)	-0.031 (10)	0.000 (9)	0.037 (8)
F16A	0.181 (15)	0.148 (14)	0.032 (8)	-0.042 (12)	-0.004 (10)	0.011 (9)
F2B	0.117 (14)	0.064 (12)	0.061 (13)	-0.009 (10)	0.002 (11)	0.020 (11)
F17A	0.156 (12)	0.146 (11)	0.049 (8)	-0.020 (10)	-0.013 (10)	0.018 (9)
F1	0.150 (14)	0.169 (15)	0.031 (8)	-0.042 (13)	0.001 (11)	0.011 (10)
C27A	0.140 (9)	0.134 (9)	0.036 (7)	-0.031 (8)	-0.009 (7)	0.015 (7)
C13B	0.096 (13)	0.084 (13)	0.069 (11)	-0.016 (11)	0.033 (10)	-0.002 (10)
C14B	0.087 (11)	0.047 (9)	0.037 (7)	-0.011 (9)	0.029 (7)	-0.002 (6)
F1B	0.18 (3)	0.070 (15)	0.25 (3)	0.013 (19)	0.15 (2)	0.01 (2)
F3B	0.19 (2)	0.079 (14)	0.079 (14)	-0.017 (14)	-0.001 (15)	0.033 (11)
F2	0.147 (12)	0.134 (12)	0.028 (7)	-0.041 (10)	-0.013 (8)	0.021 (8)
F1AA	0.13 (2)	0.070 (17)	0.08 (2)	0.031 (15)	-0.014 (17)	0.001 (16)
F9	0.15 (2)	0.054 (15)	0.13 (2)	0.033 (16)	0.048 (18)	0.018 (14)
F14	0.16 (3)	0.12 (2)	0.14 (3)	0.00 (2)	0.10 (2)	0.04 (2)
C23B	0.027 (10)	0.29 (4)	0.13 (2)	0.030 (15)	0.004 (11)	0.07 (2)
F6	0.148 (13)	0.150 (14)	0.065 (10)	0.006 (12)	0.014 (10)	0.038 (10)
C1	0.136 (9)	0.132 (9)	0.041 (7)	-0.024 (8)	-0.010 (8)	0.019 (7)

Geometric parameters (Å, º)

Y2A—O7A	2.325 (9)	C45B—H45B	0.9300
Y2A—O3A	2.328 (8)	C45B—C44B	1.354 (18)
Y2A—O6A	2.325 (10)	N8B—C36B	1.38 (2)
Y2A—O5A	2.314 (8)	N8B—B1B	1.52 (2)
Y2A—N1A	2.536 (10)	C3B—H3B	0.9300
Y2A—O4A	2.317 (9)	C3B—C2B	1.362 (18)
Y2A—N2A	2.528 (10)	C43B—H43B	0.9300
Y2A—O8A	2.342 (9)	C43B—C44B	1.361 (18)
Y1B—O1B	2.331 (8)	C10A—H10A	0.9300
Y1B—O2B	2.413 (8)	C10A—C9A	1.399 (18)
Y1B—N13B	2.477 (10)	C11B—C7B	1.404 (17)
Y1B—N11B	2.427 (11)	C37B—H37B	0.9300
Y1B—N3B	2.477 (10)	C31A—H31A	0.9300
Y1B—N5B	2.456 (13)	C31A—C33A	1.389 (19)
Y1B—N7B	2.472 (11)	C7B—C6B	1.478 (18)
Y1B—N9B	2.499 (10)	C8A—H8A	0.9300
Y1A—O2A	2.369 (8)	C8A—C9A	1.367 (17)
Y1A—O1A	2.344 (8)	C39B—H39B	0.9300
Y1A—N5A	2.435 (11)	C2A—H2A	0.9300
Y1A—N13A	2.416 (11)	C44A—H44A	0.9300
Y1A—N7A	2.486 (11)	C44A—C45A	1.37 (2)
Y1A—N9A	2.509 (10)	C9B—H9B	0.9300
Y1A—N3A	2.521 (10)	C9B—C10B	1.40 (2)
Y1A—N11A	2.458 (12)	C40A—H40A	0.9300
Y2B—O3B	2.339 (10)	C40A—C39A	1.36 (2)
Y2B—O7B	2.342 (10)	C42B—H42B	0.9300
Y2B—O6B	2.319 (9)	C42B—C41B	1.391 (19)
Y2B—O4B	2.304 (10)	C9A—H9A	0.9300
Y2B—O8B	2.304 (10)	C10B—H10B	0.9300
Y2B—O5B	2.317 (9)	C31B—H31B	0.9300
Y2B—N2B	2.549 (10)	C31B—C32B	1.37 (2)
Y2B—N1B	2.489 (9)	C21B—C20B	1.38 (2)
O3B—C14B	1.261 (16)	C21B—C22B	1.51 (2)
O1B—C5B	1.267 (14)	C16A—C17A	1.49 (2)
F1A—C13A	1.310 (16)	C15B—H15B	0.9300
O2A—C6A	1.299 (13)	C15B—C14B	1.38 (2)
O7A—C24A	1.237 (16)	C30A—H30A	0.9300

O2B—C6B	1.281 (15)	C30A—C29A	1.33 (2)
F6B—C17B	1.333 (18)	F16B—C27B	1.28 (2)
O3A—C14A	1.234 (15)	C45A—H45A	0.9300
O6A—C21A	1.257 (15)	C45A—C46A	1.37 (2)
O1A—C5A	1.265 (14)	C39A—H39A	0.9300
O7B—C24B	1.243 (18)	C39A—C38A	1.360 (18)
F13A—C23A	1.318 (14)	C20B—H20B	0.9300
F2A—C13A	1.313 (16)	C20B—C19B	1.35 (2)
O6B—C21B	1.291 (16)	C1B—H1B	0.9300
F11A—C22A	1.302 (16)	C1B—C2B	1.404 (18)
O4B—C16B	1.239 (15)	C2B—H2B	0.9300
N13B—N14B	1.380 (13)	C44B—H44B	0.9300
N13B—C43B	1.329 (16)	C33B—H33B	0.9300
F4B—C17B	1.350 (16)	C33B—C32B	1.36 (2)
F11B—C22B	1.335 (18)	C22A—C21A	1.51 (2)
F9B—C18B	1.297 (18)	C40B—H40B	0.9300
O5A—C19A	1.259 (15)	C40B—C41B	1.36 (2)
F3A—C13A	1.341 (14)	C41B—H41B	0.9300
F6A—C17A	1.348 (17)	C29A—H29A	0.9300
F5B—C17B	1.296 (17)	C29A—C28A	1.388 (19)
N5A—N6A	1.357 (15)	C38A—H38A	0.9300
N5A—C31A	1.358 (17)	C19A—C20A	1.363 (19)
O8B—C26B	1.243 (19)	C19A—C18A	1.537 (19)
N11B—N12B	1.371 (13)	C35A—H35A	0.9300
N11B—C40B	1.325 (17)	C35A—C36A	1.34 (2)
F7B—C18B	1.309 (17)	C20A—H20A	0.9300
O5B—C19B	1.292 (17)	C20A—C21A	1.373 (18)
N1A—C1A	1.319 (15)	C34A—H34A	0.9300
N1A—C12A	1.362 (14)	C34A—C33A	1.37 (2)
O4A—C16A	1.273 (15)	C41A—H41A	0.9300
N2B—C11B	1.381 (15)	C41A—C42A	1.37 (2)
N2B—C10B	1.314 (16)	C18B—C19B	1.54 (2)
F10A—C22A	1.327 (16)	C26B—C25B	1.38 (2)
N2A—C11A	1.341 (14)	C26B—C27B	1.51 (3)
N2A—C10A	1.359 (16)	C37A—H37A	0.9300
N13A—N14A	1.396 (15)	C37A—C36A	1.37 (2)
N13A—C44A	1.354 (17)	C46A—H46A	0.9300
F10B—C22B	1.33 (2)	C30B—H30B	0.9300
O8A—C26A	1.187 (19)	C30B—C29B	1.36 (2)
F14A—C23A	1.297 (13)	C23A—C24A	1.484 (15)

N14B—C45B	1.351 (15)	F17B—C27B	1.292 (19)
N14B—B2B	1.530 (19)	C43A—H43A	0.9300
N12B—C42B	1.323 (17)	C43A—C42A	1.37 (2)
N12B—B2B	1.530 (17)	C28A—H28A	0.8551
F5A—C17A	1.319 (16)	C32B—H32B	0.9300
N4B—N3B	1.371 (14)	C24A—C25A	1.34 (2)
N4B—C30B	1.346 (15)	C24B—C25B	1.39 (2)
N4B—B1B	1.60 (2)	C24B—C23B	1.520 (16)
F8A—C18A	1.291 (17)	F18B—C27B	1.34 (2)
N3B—C28B	1.339 (15)	C33A—H33A	0.9300
N10A—N9A	1.338 (14)	B2B—H2BA	0.9800
N10A—C40A	1.350 (16)	C28B—H28B	0.9300
N10A—B2A	1.52 (2)	C28B—C29B	1.367 (18)
N10B—N9B	1.344 (14)	C36A—H36A	0.9300
N10B—C39B	1.360 (16)	C25B—H25B	0.9300
N10B—B2B	1.515 (18)	C29B—H29B	0.9300
F12A—C22A	1.329 (17)	C34B—H34B	0.9300
N14A—C46A	1.336 (17)	C34B—C35B	1.39 (2)
N14A—B2A	1.51 (2)	C42A—H42A	0.9300
N1B—C12B	1.354 (15)	C35B—H35B	0.9300
N1B—C1B	1.307 (15)	C35B—C36B	1.35 (2)
F8B—C18B	1.353 (19)	C36B—H36B	0.9300
N7A—N8A	1.347 (15)	C26A—C25A	1.42 (2)
N7A—C35A	1.344 (17)	C26A—C27A	1.551 (19)
N9A—C38A	1.350 (16)	C26A—C1	1.528 (19)
F9A—C18A	1.308 (17)	B2A—H2AA	0.9800
N3A—N4A	1.364 (14)	B1A—H1AA	0.9800
N3A—C28A	1.351 (15)	B1B—H1BA	0.9800
N5B—N6B	1.352 (15)	C25A—H25A	0.9300
N5B—C31B	1.340 (17)	C8S—H8SA	0.9700
F12B—C22B	1.339 (16)	C8S—H8SB	0.9700
C4B—C5B	1.466 (17)	C8S—C7S	1.55 (4)
C4B—C12B	1.406 (16)	C8S—C9S	1.43 (4)
C4B—C3B	1.399 (17)	C7S—H7SA	0.9600
N4A—C30A	1.349 (17)	C7S—H7SB	0.9600
N4A—B1A	1.511 (19)	C7S—H7SC	0.9600
F15A—C23A	1.367 (14)	C9S—C9S^{i}	1.76 (5)
N12A—N11A	1.390 (15)	C9S—H9SA	0.9700
N12A—C43A	1.324 (19)	C9S—H9SB	0.9700
N12A—B2A	1.56 (2)	F18A—C1	1.29 (5)

N11A—C41A	1.345 (17)	F16A—C27A	1.29 (4)
F4A—C17A	1.294 (17)	F2B—C13B	1.330 (13)
F7A—C18A	1.344 (19)	C4S—H4SA	0.9700
N6B—C33B	1.345 (19)	C4S—H4SB	0.9700
N6B—B1B	1.51 (2)	C4S—C3S	1.536 (17)
C5B—C6B	1.423 (18)	C4S—C5S	1.512 (19)
N7B—N8B	1.354 (16)	C2S—H2SA	0.9700
N7B—C34B	1.328 (18)	C2S—H2SB	0.9700
N9B—C37B	1.334 (16)	C2S—C1S	1.553 (19)
C7A—C11A	1.441 (16)	C2S—C3S	1.467 (18)
C7A—C6A	1.432 (17)	C6S—H6SA	0.9600
C7A—C8A	1.367 (17)	C6S—H6SB	0.9600
C14A—C15A	1.378 (18)	C6S—H6SC	0.9600
C14A—C13A	1.55 (2)	C6S—C5S	1.466 (19)
C8B—H8B	0.9300	F17A—C27A	1.32 (2)
C8B—C7B	1.378 (17)	F1—C27A	1.320 (19)
C8B—C9B	1.367 (18)	C13B—C14B	1.505 (15)
C4A—C3A	1.415 (17)	C13B—F1B	1.288 (13)
C4A—C12A	1.374 (16)	C13B—F3B	1.376 (13)
C4A—C5A	1.465 (17)	C13B—F1AA	1.311 (17)
C11A—C12A	1.441 (17)	C13B—F9	1.402 (16)
N8A—C37A	1.349 (17)	C13B—F14	1.275 (17)
N8A—B1A	1.52 (2)	F15B—C23B	1.328 (13)
N6A—C34A	1.323 (18)	F14B—C23B	1.322 (13)
N6A—B1A	1.57 (2)	F2—C1	1.38 (5)
C6A—C5A	1.434 (18)	F13B—C23B	1.361 (13)
C1A—H1A	0.9300	C23B—F3	1.310 (14)
C1A—C2A	1.377 (17)	C23B—F4	1.358 (16)
C12B—C11B	1.442 (17)	C23B—F5	1.356 (18)
C3A—H3A	0.9300	F6—C1	1.34 (2)
C3A—C2A	1.364 (16)	C1S—H1SA	0.9600
C16B—C15B	1.39 (2)	C1S—H1SB	0.9600
C16B—C17B	1.54 (2)	C1S—H1SC	0.9600
C38B—H38B	0.9300	C3S—H3SA	0.9700
C38B—C37B	1.393 (17)	C3S—H3SB	0.9700
C38B—C39B	1.333 (19)	C5S—H5SA	0.9700
C15A—H15A	0.9300	C5S—H5SB	0.9700
C15A—C16A	1.373 (18)		
O7A—Y2A—O3A	81.8 (3)	C10A—C9A—H9A	120.9

O7A—Y2A—N1A	75.9 (3)	C8A—C9A—C10A	118.2 (13)
O7A—Y2A—N2A	126.5 (3)	C8A—C9A—H9A	120.9
O7A—Y2A—O8A	71.7 (3)	N2B—C10B—C9B	125.0 (12)
O3A—Y2A—N1A	69.8 (3)	N2B—C10B—H10B	117.5
O3A—Y2A—N2A	113.5 (3)	C9B—C10B—H10B	117.5
O3A—Y2A—O8A	146.0 (4)	N5B—C31B—H31B	125.0
O6A—Y2A—O7A	121.7 (3)	N5B—C31B—C32B	109.9 (14)
O6A—Y2A—O3A	139.1 (3)	C32B—C31B—H31B	125.0
O6A—Y2A—N1A	143.5 (3)	O6B—C21B—C20B	126.2 (13)
O6A—Y2A—N2A	80.7 (3)	O6B—C21B—C22B	112.7 (13)
O6A—Y2A—O8A	74.5 (4)	C20B—C21B—C22B	121.1 (14)
O5A—Y2A—O7A	73.4 (3)	O4A—C16A—C15A	125.5 (13)
O5A—Y2A—O3A	84.3 (3)	O4A—C16A—C17A	114.0 (13)
O5A—Y2A—O6A	73.3 (3)	C15A—C16A—C17A	120.5 (13)
O5A—Y2A—N1A	142.1 (3)	O1A—C5A—C4A	123.3 (13)
O5A—Y2A—O4A	80.5 (3)	O1A—C5A—C6A	120.3 (11)
O5A—Y2A—N2A	153.5 (3)	C6A—C5A—C4A	116.3 (12)
O5A—Y2A—O8A	107.2 (3)	C16B—C15B—H15B	120.4
O4A—Y2A—O7A	144.4 (3)	C14B—C15B—C16B	119.1 (14)
O4A—Y2A—O3A	71.8 (3)	C14B—C15B—H15B	120.4
O4A—Y2A—O6A	71.0 (3)	N4A—C30A—H30A	124.6
O4A—Y2A—N1A	114.8 (3)	C29A—C30A—N4A	110.8 (14)
O4A—Y2A—N2A	86.6 (3)	C29A—C30A—H30A	124.6
O4A—Y2A—O8A	140.6 (4)	C44A—C45A—H45A	127.8
N2A—Y2A—N1A	64.3 (3)	C46A—C45A—C44A	104.4 (14)
O8A—Y2A—N1A	83.2 (3)	C46A—C45A—H45A	127.8
O8A—Y2A—N2A	69.4 (3)	C40A—C39A—H39A	126.9
O1B—Y1B—O2B	68.7 (3)	C38A—C39A—C40A	106.1 (12)
O1B—Y1B—N13B	75.2 (3)	C38A—C39A—H39A	126.9
O1B—Y1B—N11B	138.4 (3)	C21B—C20B—H20B	118.6
O1B—Y1B—N3B	83.5 (3)	C19B—C20B—C21B	122.8 (14)
O1B—Y1B—N5B	70.2 (3)	C19B—C20B—H20B	118.6
O1B—Y1B—N7B	142.5 (4)	O2B—C6B—C5B	118.5 (12)
O1B—Y1B—N9B	116.7 (3)	O2B—C6B—C7B	121.6 (12)
O2B—Y1B—N13B	79.1 (3)	C5B—C6B—C7B	119.9 (12)
O2B—Y1B—N11B	76.8 (3)	N1B—C1B—H1B	117.7
O2B—Y1B—N3B	74.8 (3)	N1B—C1B—C2B	124.7 (12)
O2B—Y1B—N5B	131.5 (3)	C2B—C1B—H1B	117.7
O2B—Y1B—N7B	126.1 (3)	C3B—C2B—C1B	116.9 (12)
O2B—Y1B—N9B	145.6 (3)	C3B—C2B—H2B	121.5

N13B—Y1B—N9B	70.6 (3)	C1B—C2B—H2B	121.5
N11B—Y1B—N13B	76.1 (3)	C45B—C44B—C43B	103.6 (12)
N11B—Y1B—N3B	109.6 (3)	C45B—C44B—H44B	128.2
N11B—Y1B—N5B	150.3 (4)	C43B—C44B—H44B	128.2
N11B—Y1B—N7B	77.4 (4)	N6B—C33B—H33B	125.8
N11B—Y1B—N9B	80.4 (4)	N6B—C33B—C32B	108.3 (14)
N3B—Y1B—N13B	150.9 (3)	C32B—C33B—H33B	125.8
N3B—Y1B—N9B	137.9 (4)	F11A—C22A—F10A	107.1 (12)
N5B—Y1B—N13B	113.6 (4)	F11A—C22A—F12A	106.7 (15)
N5B—Y1B—N3B	76.1 (4)	F11A—C22A—C21A	115.0 (11)
N5B—Y1B—N7B	77.4 (4)	F10A—C22A—F12A	106.8 (11)
N5B—Y1B—N9B	77.2 (4)	F10A—C22A—C21A	111.0 (14)
N7B—Y1B—N13B	137.1 (3)	F12A—C22A—C21A	109.8 (12)
N7B—Y1B—N3B	70.7 (3)	N11B—C40B—H40B	123.5
N7B—Y1B—N9B	72.2 (3)	N11B—C40B—C41B	113.1 (13)
O2A—Y1A—N5A	73.4 (3)	C41B—C40B—H40B	123.5
O2A—Y1A—N13A	136.3 (3)	C42B—C41B—H41B	128.5
O2A—Y1A—N7A	144.5 (4)	C40B—C41B—C42B	103.0 (13)
O2A—Y1A—N9A	121.2 (3)	C40B—C41B—H41B	128.5
O2A—Y1A—N3A	80.5 (3)	C30A—C29A—H29A	127.5
O2A—Y1A—N11A	75.5 (3)	C30A—C29A—C28A	105.0 (12)
O1A—Y1A—O2A	69.1 (3)	C28A—C29A—H29A	127.5
O1A—Y1A—N5A	135.1 (3)	N9A—C38A—C39A	109.9 (13)
O1A—Y1A—N13A	75.3 (3)	N9A—C38A—H38A	125.0
O1A—Y1A—N7A	119.6 (3)	C39A—C38A—H38A	125.0
O1A—Y1A—N9A	147.6 (3)	O5A—C19A—C20A	127.7 (11)
O1A—Y1A—N3A	75.4 (3)	O5A—C19A—C18A	114.2 (15)
O1A—Y1A—N11A	81.4 (3)	C20A—C19A—C18A	118.2 (13)
N5A—Y1A—N7A	79.9 (4)	N7A—C35A—H35A	123.8
N5A—Y1A—N9A	74.4 (3)	C36A—C35A—N7A	112.4 (16)
N5A—Y1A—N3A	74.8 (4)	C36A—C35A—H35A	123.8
N5A—Y1A—N11A	112.2 (4)	C19A—C20A—H20A	118.7
N13A—Y1A—N5A	148.6 (3)	C19A—C20A—C21A	122.6 (12)
N13A—Y1A—N7A	76.0 (4)	C21A—C20A—H20A	118.7
N13A—Y1A—N9A	79.0 (3)	F6A—C17A—C16A	113.5 (13)
N13A—Y1A—N3A	114.4 (4)	F5A—C17A—F6A	103.1 (12)
N13A—Y1A—N11A	74.8 (4)	F5A—C17A—C16A	112.3 (12)
N7A—Y1A—N9A	71.7 (3)	F4A—C17A—F6A	105.9 (12)
N7A—Y1A—N3A	70.1 (3)	F4A—C17A—F5A	107.7 (15)
N9A—Y1A—N3A	134.1 (4)	F4A—C17A—C16A	113.7 (13)

N11A—Y1A—N7A	137.5 (4)	F11B—C22B—F12B	106.2 (14)
N11A—Y1A—N9A	73.0 (3)	F11B—C22B—C21B	113.5 (16)
N11A—Y1A—N3A	151.4 (3)	F10B—C22B—F11B	106.6 (13)
O3B—Y2B—O7B	78.2 (3)	F10B—C22B—F12B	107.6 (16)
O3B—Y2B—N2B	129.8 (3)	F10B—C22B—C21B	110.7 (14)
O3B—Y2B—N1B	78.6 (3)	F12B—C22B—C21B	111.9 (13)
O7B—Y2B—N2B	120.7 (3)	F8A—C18A—F9A	108.8 (13)
O7B—Y2B—N1B	74.1 (3)	F8A—C18A—F7A	104.3 (14)
O6B—Y2B—O3B	118.7 (3)	F8A—C18A—C19A	111.2 (13)
O6B—Y2B—O7B	138.6 (3)	F9A—C18A—F7A	106.0 (14)
O6B—Y2B—N2B	79.3 (3)	F9A—C18A—C19A	114.5 (14)
O6B—Y2B—N1B	142.8 (3)	F7A—C18A—C19A	111.5 (14)
O4B—Y2B—O3B	71.1 (3)	N6A—C34A—H34A	125.1
O4B—Y2B—O7B	144.1 (4)	N6A—C34A—C33A	109.8 (14)
O4B—Y2B—O6B	74.6 (3)	C33A—C34A—H34A	125.1
O4B—Y2B—O5B	116.5 (3)	N11A—C41A—H41A	123.2
O4B—Y2B—N2B	70.0 (3)	N11A—C41A—C42A	113.7 (14)
O4B—Y2B—N1B	82.0 (3)	C42A—C41A—H41A	123.2
O8B—Y2B—O3B	149.6 (4)	F9B—C18B—F7B	109.2 (15)
O8B—Y2B—O7B	73.6 (4)	F9B—C18B—F8B	107.1 (13)
O8B—Y2B—O6B	77.7 (3)	F9B—C18B—C19B	113.1 (15)
O8B—Y2B—O4B	139.3 (4)	F7B—C18B—F8B	105.4 (15)
O8B—Y2B—O5B	82.5 (3)	F7B—C18B—C19B	111.9 (13)
O8B—Y2B—N2B	76.0 (3)	F8B—C18B—C19B	109.7 (14)
O8B—Y2B—N1B	104.0 (3)	O5B—C19B—C20B	127.7 (14)
O5B—Y2B—O3B	78.7 (3)	O5B—C19B—C18B	112.3 (14)
O5B—Y2B—O7B	73.7 (3)	C20B—C19B—C18B	119.9 (15)
O5B—Y2B—O6B	73.4 (3)	O8B—C26B—C25B	130.6 (17)
O5B—Y2B—N2B	148.2 (3)	O8B—C26B—C27B	114.7 (19)
O5B—Y2B—N1B	143.7 (4)	C25B—C26B—C27B	114.7 (18)
N1B—Y2B—N2B	65.7 (3)	N8A—C37A—H37A	126.9
C14B—O3B—Y2B	133.9 (9)	N8A—C37A—C36A	106.1 (14)
C5B—O1B—Y1B	117.0 (8)	C36A—C37A—H37A	126.9
C6A—O2A—Y1A	116.2 (8)	N14A—C46A—C45A	109.9 (14)
C24A—O7A—Y2A	136.5 (8)	N14A—C46A—H46A	125.1
C6B—O2B—Y1B	114.7 (8)	C45A—C46A—H46A	125.1
C14A—O3A—Y2A	135.4 (8)	N4B—C30B—H30B	126.2
C21A—O6A—Y2A	134.5 (8)	N4B—C30B—C29B	107.5 (13)
C5A—O1A—Y1A	116.8 (8)	C29B—C30B—H30B	126.2
C24B—O7B—Y2B	131.1 (10)	O6A—C21A—C22A	114.4 (11)

C21B—O6B—Y2B	133.7 (9)	O6A—C21A—C20A	126.5 (13)
C16B—O4B—Y2B	135.6 (9)	C20A—C21A—C22A	119.1 (13)
N14B—N13B—Y1B	120.5 (8)	F13A—C23A—F15A	102.6 (11)
C43B—N13B—Y1B	135.0 (8)	F13A—C23A—C24A	113.6 (13)
C43B—N13B—N14B	104.4 (10)	F14A—C23A—F13A	110.0 (12)
C19A—O5A—Y2A	134.4 (8)	F14A—C23A—F15A	103.1 (13)
N6A—N5A—Y1A	124.8 (9)	F14A—C23A—C24A	114.5 (12)
N6A—N5A—C31A	105.6 (11)	F15A—C23A—C24A	112.0 (13)
C31A—N5A—Y1A	129.2 (10)	N12A—C43A—H43A	124.9
C26B—O8B—Y2B	131.2 (11)	N12A—C43A—C42A	110.2 (15)
N12B—N11B—Y1B	122.9 (7)	C42A—C43A—H43A	124.9
C40B—N11B—Y1B	132.0 (9)	N3A—C28A—C29A	109.6 (13)
C40B—N11B—N12B	105.0 (11)	N3A—C28A—H28A	114.5
C19B—O5B—Y2B	132.3 (9)	C29A—C28A—H28A	113.3
C1A—N1A—Y2A	122.2 (7)	C31B—C32B—H32B	127.1
C1A—N1A—C12A	118.1 (10)	C33B—C32B—C31B	105.9 (15)
C12A—N1A—Y2A	119.4 (8)	C33B—C32B—H32B	127.1
C16A—O4A—Y2A	133.2 (9)	O7A—C24A—C23A	113.0 (12)
C11B—N2B—Y2B	116.2 (8)	O7A—C24A—C25A	125.2 (15)
C10B—N2B—Y2B	125.0 (9)	C25A—C24A—C23A	121.4 (15)
C10B—N2B—C11B	117.2 (11)	O7B—C24B—C25B	127.5 (16)
C11A—N2A—Y2A	119.5 (8)	O7B—C24B—C23B	113.0 (16)
C11A—N2A—C10A	117.6 (10)	C25B—C24B—C23B	119.1 (17)
C10A—N2A—Y2A	120.9 (7)	F6B—C17B—F4B	107.8 (14)
N14A—N13A—Y1A	123.2 (8)	F6B—C17B—C16B	110.1 (12)
C44A—N13A—Y1A	132.1 (10)	F4B—C17B—C16B	107.4 (12)
C44A—N13A—N14A	103.8 (11)	F5B—C17B—F6B	109.3 (14)
C26A—O8A—Y2A	137.8 (10)	F5B—C17B—F4B	108.0 (12)
N13B—N14B—B2B	122.5 (10)	F5B—C17B—C16B	114.0 (14)
C45B—N14B—N13B	108.2 (11)	C31A—C33A—H33A	128.0
C45B—N14B—B2B	129.2 (10)	C34A—C33A—C31A	104.1 (14)
N11B—N12B—B2B	121.3 (10)	C34A—C33A—H33A	128.0
C42B—N12B—N11B	109.4 (10)	N14B—B2B—H2BA	109.3
C42B—N12B—B2B	129.2 (10)	N12B—B2B—N14B	110.2 (10)
N3B—N4B—B1B	120.9 (9)	N12B—B2B—H2BA	109.3
C30B—N4B—N3B	110.8 (11)	N10B—B2B—N14B	108.3 (11)
C30B—N4B—B1B	127.8 (12)	N10B—B2B—N12B	110.3 (11)
N4B—N3B—Y1B	122.7 (7)	N10B—B2B—H2BA	109.3
C28B—N3B—Y1B	133.3 (9)	N3B—C28B—H28B	124.0
C28B—N3B—N4B	103.9 (10)	N3B—C28B—C29B	112.1 (13)

N9A—N10A—C40A	109.7 (12)	C29B—C28B—H28B	124.0
N9A—N10A—B2A	121.9 (10)	C35A—C36A—C37A	106.0 (14)
C40A—N10A—B2A	128.2 (14)	C35A—C36A—H36A	127.0
N9B—N10B—C39B	107.5 (11)	C37A—C36A—H36A	127.0
N9B—N10B—B2B	122.5 (10)	C26B—C25B—C24B	119.7 (17)
C39B—N10B—B2B	129.8 (12)	C26B—C25B—H25B	120.2
N13A—N14A—B2A	120.9 (12)	C24B—C25B—H25B	120.2
C46A—N14A—N13A	109.5 (11)	C30B—C29B—C28B	105.6 (12)
C46A—N14A—B2A	129.6 (13)	C30B—C29B—H29B	127.2
C12B—N1B—Y2B	119.4 (8)	C28B—C29B—H29B	127.2
C1B—N1B—Y2B	121.4 (8)	N7B—C34B—H34B	124.0
C1B—N1B—C12B	118.5 (10)	N7B—C34B—C35B	111.9 (16)
N8A—N7A—Y1A	121.6 (9)	C35B—C34B—H34B	124.0
C35A—N7A—Y1A	133.4 (11)	C41A—C42A—C43A	103.1 (15)
C35A—N7A—N8A	103.8 (12)	C41A—C42A—H42A	128.4
N10A—N9A—Y1A	121.5 (7)	C43A—C42A—H42A	128.4
N10A—N9A—C38A	106.4 (10)	C34B—C35B—H35B	127.5
C38A—N9A—Y1A	129.0 (9)	C36B—C35B—C34B	105.1 (15)
N4A—N3A—Y1A	120.4 (7)	C36B—C35B—H35B	127.5
C28A—N3A—Y1A	132.9 (10)	N8B—C36B—H36B	126.3
C28A—N3A—N4A	106.6 (10)	C35B—C36B—N8B	107.4 (15)
N6B—N5B—Y1B	123.8 (10)	C35B—C36B—H36B	126.3
C31B—N5B—Y1B	129.5 (10)	O8A—C26A—C25A	123.5 (13)
C31B—N5B—N6B	106.6 (12)	O8A—C26A—C27A	119 (2)
C12B—C4B—C5B	120.2 (12)	O8A—C26A—C1	109 (2)
C3B—C4B—C5B	121.7 (11)	C25A—C26A—C27A	115 (2)
C3B—C4B—C12B	118.1 (12)	C25A—C26A—C1	123 (2)
N3A—N4A—B1A	122.8 (10)	N10A—B2A—N12A	109.0 (13)
C30A—N4A—N3A	107.7 (11)	N10A—B2A—H2AA	109.3
C30A—N4A—B1A	129.4 (13)	N14A—B2A—N10A	110.2 (13)
N11A—N12A—B2A	122.3 (12)	N14A—B2A—N12A	109.6 (11)
C43A—N12A—N11A	109.7 (13)	N14A—B2A—H2AA	109.3
C43A—N12A—B2A	128.0 (14)	N12A—B2A—H2AA	109.3
N12A—N11A—Y1A	121.0 (9)	N4A—B1A—N8A	108.4 (12)
C41A—N11A—Y1A	135.7 (9)	N4A—B1A—N6A	109.2 (11)
C41A—N11A—N12A	103.2 (11)	N4A—B1A—H1AA	109.2
N5B—N6B—B1B	122.0 (14)	N8A—B1A—N6A	111.6 (11)
C33B—N6B—N5B	109.2 (13)	N8A—B1A—H1AA	109.2
C33B—N6B—B1B	128.7 (14)	N6A—B1A—H1AA	109.2
O1B—C5B—C4B	120.2 (11)	N4B—B1B—H1BA	109.6

O1B—C5B—C6B	120.6 (11)	N6B—B1B—N4B	109.1 (13)
C6B—C5B—C4B	119.2 (11)	N6B—B1B—N8B	112.5 (11)
N8B—N7B—Y1B	123.4 (9)	N6B—B1B—H1BA	109.6
C34B—N7B—Y1B	129.5 (11)	N8B—B1B—N4B	106.4 (14)
C34B—N7B—N8B	105.1 (12)	N8B—B1B—H1BA	109.6
N10B—N9B—Y1B	119.3 (7)	F16B—C27B—C26B	116.6 (18)
C37B—N9B—Y1B	129.2 (9)	F16B—C27B—F17B	109 (2)
C37B—N9B—N10B	107.8 (10)	F16B—C27B—F18B	102.1 (19)
C6A—C7A—C11A	118.4 (11)	F17B—C27B—C26B	115.9 (18)
C8A—C7A—C11A	117.5 (11)	F17B—C27B—F18B	100.5 (17)
C8A—C7A—C6A	124.1 (10)	F18B—C27B—C26B	111 (2)
O3A—C14A—C15A	127.0 (13)	C24A—C25A—C26A	124.8 (16)
O3A—C14A—C13A	116.0 (12)	C24A—C25A—H25A	117.6
C15A—C14A—C13A	116.9 (13)	C26A—C25A—H25A	117.6
C7B—C8B—H8B	119.8	H8SA—C8S—H8SB	108.9
C9B—C8B—H8B	119.8	C7S—C8S—H8SA	110.9
C9B—C8B—C7B	120.5 (13)	C7S—C8S—H8SB	110.9
C3A—C4A—C5A	119.1 (11)	C9S—C8S—H8SA	110.9
C12A—C4A—C3A	118.7 (11)	C9S—C8S—H8SB	110.9
C12A—C4A—C5A	122.1 (12)	C9S—C8S—C7S	104 (3)
N2A—C11A—C7A	122.2 (12)	C8S—C7S—H7SA	109.5
N2A—C11A—C12A	118.2 (10)	C8S—C7S—H7SB	109.5
C12A—C11A—C7A	119.7 (10)	C8S—C7S—H7SC	109.5
N7A—N8A—C37A	111.6 (12)	H7SA—C7S—H7SB	109.5
N7A—N8A—B1A	122.3 (11)	H7SA—C7S—H7SC	109.5
C37A—N8A—B1A	126.0 (13)	H7SB—C7S—H7SC	109.5
N5A—N6A—B1A	119.4 (11)	C8S—C9S—C9S^{i}	97 (3)
C34A—N6A—N5A	110.1 (12)	C8S—C9S—H9SA	112.4
C34A—N6A—B1A	130.4 (13)	C8S—C9S—H9SB	112.4
O2A—C6A—C7A	119.9 (11)	C9S^{i}—C9S—H9SA	112.4
O2A—C6A—C5A	117.5 (11)	C9S^{i}—C9S—H9SB	112.4
C7A—C6A—C5A	122.6 (10)	H9SA—C9S—H9SB	110.0
N1A—C1A—H1A	118.5	H4SA—C4S—H4SB	106.9
N1A—C1A—C2A	123.1 (11)	C3S—C4S—H4SA	107.4
C2A—C1A—H1A	118.5	C3S—C4S—H4SB	107.4
N1B—C12B—C4B	121.3 (12)	C5S—C4S—H4SA	107.4
N1B—C12B—C11B	118.4 (10)	C5S—C4S—H4SB	107.4
C4B—C12B—C11B	120.3 (11)	C5S—C4S—C3S	120 (2)
C4A—C3A—H3A	121.1	H2SA—C2S—H2SB	106.4
C2A—C3A—C4A	117.8 (11)	C1S—C2S—H2SA	106.3

C2A—C3A—H3A	121.1	C1S—C2S—H2SB	106.3
O4B—C16B—C15B	127.2 (13)	C3S—C2S—H2SA	106.3
O4B—C16B—C17B	114.4 (14)	C3S—C2S—H2SB	106.3
C15B—C16B—C17B	118.4 (14)	C3S—C2S—C1S	124 (3)
C37B—C38B—H38B	127.6	H6SA—C6S—H6SB	109.5
C39B—C38B—H38B	127.6	H6SA—C6S—H6SC	109.5
C39B—C38B—C37B	104.8 (12)	H6SB—C6S—H6SC	109.5
C14A—C15A—H15A	119.3	C5S—C6S—H6SA	109.5
C16A—C15A—C14A	121.4 (12)	C5S—C6S—H6SB	109.5
C16A—C15A—H15A	119.3	C5S—C6S—H6SC	109.5
F1A—C13A—F2A	109.3 (12)	F16A—C27A—C26A	124 (3)
F1A—C13A—F3A	106.6 (12)	F16A—C27A—F17A	105.3 (18)
F1A—C13A—C14A	111.7 (12)	F16A—C27A—F1	104.7 (17)
F2A—C13A—F3A	107.3 (12)	F17A—C27A—C26A	100.4 (19)
F2A—C13A—C14A	109.6 (12)	F17A—C27A—F1	104 (2)
F3A—C13A—C14A	112.1 (12)	F1—C27A—C26A	117 (2)
N14B—C45B—H45B	124.9	F2B—C13B—C14B	114.9 (15)
N14B—C45B—C44B	110.1 (12)	F2B—C13B—F3B	100.3 (11)
C44B—C45B—H45B	124.9	F1B—C13B—F2B	108.0 (13)
N7B—N8B—C36B	110.4 (13)	F1B—C13B—C14B	118.8 (15)
N7B—N8B—B1B	121.1 (12)	F1B—C13B—F3B	103.7 (14)
C36B—N8B—B1B	128.3 (15)	F3B—C13B—C14B	108.9 (13)
C4B—C3B—H3B	119.8	F1AA—C13B—C14B	117.0 (18)
C2B—C3B—C4B	120.5 (12)	F1AA—C13B—F9	98.8 (13)
C2B—C3B—H3B	119.8	F9—C13B—C14B	103.9 (14)
N13B—C43B—H43B	123.3	F14—C13B—C14B	120.2 (19)
N13B—C43B—C44B	113.5 (13)	F14—C13B—F1AA	110.3 (16)
C44B—C43B—H43B	123.3	F14—C13B—F9	102.8 (15)
N2A—C10A—H10A	118.4	O3B—C14B—C15B	127.9 (13)
N2A—C10A—C9A	123.1 (12)	O3B—C14B—C13B	114.6 (13)
C9A—C10A—H10A	118.4	C15B—C14B—C13B	117.5 (14)
N1A—C12A—C4A	122.1 (12)	F15B—C23B—C24B	114.3 (17)
N1A—C12A—C11A	117.1 (10)	F15B—C23B—F13B	108.3 (13)
C4A—C12A—C11A	120.8 (10)	F14B—C23B—C24B	115.6 (16)
N2B—C11B—C12B	117.9 (11)	F14B—C23B—F15B	107.2 (14)
N2B—C11B—C7B	121.1 (12)	F14B—C23B—F13B	105.0 (14)
C7B—C11B—C12B	120.9 (11)	F13B—C23B—C24B	105.8 (16)
N9B—C37B—C38B	109.5 (12)	F3—C23B—C24B	127 (2)
N9B—C37B—H37B	125.2	F3—C23B—F4	105.7 (16)
C38B—C37B—H37B	125.2	F3—C23B—F5	105.9 (17)

N5A—C31A—H31A	124.8	F4—C23B—C24B	107.9 (17)
N5A—C31A—C33A	110.4 (14)	F5—C23B—C24B	104 (2)
C33A—C31A—H31A	124.8	F5—C23B—F4	104.8 (15)
C8B—C7B—C11B	118.8 (11)	F18A—C1—C26A	111 (3)
C8B—C7B—C6B	122.0 (12)	F18A—C1—F2	106 (3)
C11B—C7B—C6B	119.3 (12)	F18A—C1—F6	103 (3)
C7A—C8A—H8A	119.4	F2—C1—C26A	112 (3)
C9A—C8A—C7A	121.3 (11)	F6—C1—C26A	121 (3)
C9A—C8A—H8A	119.4	F6—C1—F2	104 (3)
N10B—C39B—H39B	124.8	C2S—C1S—H1SA	109.5
C38B—C39B—N10B	110.3 (12)	C2S—C1S—H1SB	109.5
C38B—C39B—H39B	124.8	C2S—C1S—H1SC	109.5
C1A—C2A—H2A	120.0	H1SA—C1S—H1SB	109.5
C3A—C2A—C1A	120.0 (12)	H1SA—C1S—H1SC	109.5
C3A—C2A—H2A	120.0	H1SB—C1S—H1SC	109.5
N13A—C44A—H44A	123.8	C4S—C3S—H3SA	105.9
N13A—C44A—C45A	112.4 (14)	C4S—C3S—H3SB	105.9
C45A—C44A—H44A	123.8	C2S—C3S—C4S	126 (3)
C8B—C9B—H9B	121.3	C2S—C3S—H3SA	105.9
C8B—C9B—C10B	117.3 (13)	C2S—C3S—H3SB	105.9
C10B—C9B—H9B	121.3	H3SA—C3S—H3SB	106.2
N10A—C40A—H40A	126.1	C4S—C5S—H5SA	105.4
N10A—C40A—C39A	107.9 (14)	C4S—C5S—H5SB	105.4
C39A—C40A—H40A	126.1	C6S—C5S—C4S	128 (3)
N12B—C42B—H42B	125.3	C6S—C5S—H5SA	105.4
N12B—C42B—C41B	109.5 (13)	C6S—C5S—H5SB	105.4
C41B—C42B—H42B	125.3	H5SA—C5S—H5SB	106.0
Y2A—O7A—C24A—C23A	177.1 (9)	N7B—N8B—C36B—C35B	-1.8 (18)
Y2A—O7A—C24A—C25A	4 (3)	N7B—N8B—B1B—N4B	54.0 (16)
Y2A—O3A—C14A—C15A	-1 (2)	N7B—N8B—B1B—N6B	-65.4 (18)
Y2A—O3A—C14A—C13A	175.4 (8)	N7B—C34B—C35B—C36B	0.6 (19)
Y2A—O6A—C21A—C22A	-166.7 (10)	N9B—N10B—C39B—C38B	-0.4 (15)
Y2A—O6A—C21A—C20A	13 (2)	N9B—N10B—B2B—N14B	47.0 (15)
Y2A—O5A—C19A—C20A	-4 (2)	N9B—N10B—B2B—N12B	-73.7 (15)

Y2A—O5A—C19A—C18A	176.6 (10)	C7A—C11A—C12A—N1A	175.0 (10)
Y2A—N1A—C1A—C2A	-174.0 (9)	C7A—C11A—C12A—C4A	-1.6 (17)
Y2A—N1A—C12A—C4A	172.1 (9)	C7A—C6A—C5A—O1A	-179.5 (12)
Y2A—N1A—C12A—C11A	-4.5 (13)	C7A—C6A—C5A—C4A	-1.7 (18)
Y2A—O4A—C16A—C15A	-27.5 (19)	C7A—C8A—C9A—C10A	-1 (2)
Y2A—O4A—C16A—C17A	152.8 (10)	C14A—C15A—C16A—O4A	3 (2)
Y2A—N2A—C11A—C7A	-167.4 (9)	C14A—C15A—C16A—C17A	-177.4 (13)
Y2A—N2A—C11A—C12A	13.5 (14)	C8B—C7B—C6B—O2B	-1.5 (17)
Y2A—N2A—C10A—C9A	165.1 (10)	C8B—C7B—C6B—C5B	179.1 (11)
Y2A—O8A—C26A—C25A	-9 (3)	C8B—C9B—C10B—N2B	-1 (2)
Y2A—O8A—C26A—C27A	152.1 (15)	C4A—C3A—C2A—C1A	3.0 (18)
Y2A—O8A—C26A—C1	-166.2 (18)	C11A—N2A—C10A—C9A	1.0 (19)
Y1B—O1B—C5B—C4B	171.9 (8)	C11A—C7A—C6A—O2A	178.2 (11)
Y1B—O1B—C5B—C6B	-5.9 (13)	C11A—C7A—C6A—C5A	-1.3 (18)
Y1B—O2B—C6B—C5B	5.1 (13)	C11A—C7A—C8A—C9A	-1.1 (19)
Y1B—O2B—C6B—C7B	-174.4 (8)	N8A—N7A—C35A—C36A	-1.5 (15)
Y1B—N13B—N14B—C45B	-177.4 (7)	N8A—C37A—C36A—C35A	-0.3 (17)
Y1B—N13B—N14B—B2B	-0.7 (13)	N6A—N5A—C31A—C33A	-2.1 (13)
Y1B—N13B—C43B—C44B	175.8 (8)	N6A—C34A—C33A—C31A	-0.5 (16)
Y1B—N11B—N12B—C42B	176.7 (9)	C6A—C7A—C11A—N2A	-176.0 (11)
Y1B—N11B—N12B—B2B	-3.1 (15)	C6A—C7A—C11A—C12A	3.1 (17)
Y1B—N11B—C40B—C41B	-175.2 (10)	C6A—C7A—C8A—C9A	178.0 (13)
Y1B—N3B—C28B—C29B	175.5 (10)	C1A—N1A—C12A—C4A	-2.1 (17)
Y1B—N5B—N6B—C33B	-178.7 (8)	C1A—N1A—C12A—C11A	-178.7 (10)

Y1B—N5B—N6B—B1B	1.6 (15)	C12B—N1B—C1B—C2B	2.7 (18)
Y1B—N5B—C31B—C32B	178.5 (8)	C12B—C4B—C5B—O1B	-176.2 (10)
Y1B—N7B—N8B—C36B	-163.0 (10)	C12B—C4B—C5B—C6B	1.5 (16)
Y1B—N7B—N8B—B1B	12.8 (16)	C12B—C4B—C3B—C2B	2.0 (17)
Y1B—N7B—C34B—C35B	162.2 (11)	C12B—C11B—C7B—C8B	178.3 (10)
Y1B—N9B—C37B—C38B	158.6 (9)	C12B—C11B—C7B—C6B	0.3 (16)
Y1A—O2A—C6A—C7A	-176.4 (8)	C3A—C4A—C12A—N1A	4.6 (18)
Y1A—O2A—C6A—C5A	3.2 (14)	C3A—C4A—C12A—C11A	-178.9 (11)
Y1A—O1A—C5A—C4A	177.8 (9)	C3A—C4A—C5A—O1A	-1.8 (19)
Y1A—O1A—C5A—C6A	-4.6 (15)	C3A—C4A—C5A—C6A	-179.5 (11)
Y1A—N5A—N6A—C34A	-170.9 (8)	C16B—C15B—C14B—O3B	-5.2 (19)
Y1A—N5A—N6A—B1A	8.6 (14)	C16B—C15B—C14B—C13B	171.5 (11)
Y1A—N5A—C31A—C33A	170.2 (8)	C15A—C14A—C13A—F1A	-153.6 (11)
Y1A—N13A—N14A—C46A	-171.0 (9)	C15A—C14A—C13A—F2A	85.0 (14)
Y1A—N13A—N14A—B2A	8.4 (16)	C15A—C14A—C13A—F3A	-34.0 (18)
Y1A—N13A—C44A—C45A	167.9 (10)	C15A—C16A—C17A—F6A	4 (2)
Y1A—N7A—N8A—C37A	170.7 (9)	C15A—C16A—C17A—F5A	-112.6 (15)
Y1A—N7A—N8A—B1A	-13.2 (15)	C15A—C16A—C17A—F4A	124.8 (15)
Y1A—N7A—C35A—C36A	-169.1 (10)	C13A—C14A—C15A—C16A	-165.1 (12)
Y1A—N9A—C38A—C39A	-159.7 (9)	C45B—N14B—B2B—N12B	-123.8 (13)
Y1A—N3A—N4A—C30A	-176.5 (8)	C45B—N14B—B2B—N10B	115.5 (13)
Y1A—N3A—N4A—B1A	8.3 (16)	N8B—N7B—C34B—C35B	-1.6 (17)
Y1A—N3A—C28A—C29A	173.4 (9)	C3B—C4B—C5B—O1B	1.8 (17)
Y1A—N11A—C41A—C42A	179.5 (10)	C3B—C4B—C5B—C6B	179.5 (11)

Y2B—O3B—C14B—C15B	-12.2 (19)	C3B—C4B—C12B—N1B	-0.8 (16)
Y2B—O3B—C14B—C13B	171.1 (7)	C3B—C4B—C12B—C11B	177.7 (10)
Y2B—O7B—C24B—C25B	-23 (3)	C43B—N13B—N14B—C45B	0.8 (12)
Y2B—O7B—C24B—C23B	164.1 (9)	C43B—N13B—N14B—B2B	177.4 (11)
Y2B—O6B—C21B—C20B	-13 (2)	C10A—N2A—C11A—C7A	-3.1 (17)
Y2B—O6B—C21B—C22B	170.0 (11)	C10A—N2A—C11A—C12A	177.8 (11)
Y2B—O4B—C16B—C15B	20.3 (18)	C12A—N1A—C1A—C2A	0.0 (17)
Y2B—O4B—C16B—C17B	-157.9 (9)	C12A—C4A—C3A—C2A	-5.0 (18)
Y2B—O8B—C26B—C25B	10 (2)	C12A—C4A—C5A—O1A	-179.0 (12)
Y2B—O8B—C26B—C27B	-169.4 (11)	C12A—C4A—C5A—C6A	3.3 (18)
Y2B—O5B—C19B—C20B	19 (2)	C11B—N2B—C10B—C9B	1.2 (18)
Y2B—O5B—C19B—C18B	-165.3 (10)	C11B—C7B—C6B—O2B	176.5 (10)
Y2B—N2B—C11B—C12B	-14.5 (12)	C11B—C7B—C6B—C5B	-3.0 (16)
Y2B—N2B—C11B—C7B	167.7 (8)	C37B—C38B—C39B—N10B	1.0 (15)
Y2B—N2B—C10B—C9B	-163.9 (10)	C31A—N5A—N6A—C34A	1.8 (13)
Y2B—N1B—C12B—C4B	-172.4 (8)	C31A—N5A—N6A—B1A	-178.7 (11)
Y2B—N1B—C12B—C11B	9.1 (13)	C7B—C8B—C9B—C10B	-1.6 (18)
Y2B—N1B—C1B—C2B	173.4 (9)	C8A—C7A—C11A—N2A	3.2 (18)
O1B—C5B—C6B—O2B	0.3 (16)	C8A—C7A—C11A—C12A	-177.7 (11)
O1B—C5B—C6B—C7B	179.8 (10)	C8A—C7A—C6A—O2A	-1.0 (19)
O2A—C6A—C5A—O1A	0.9 (18)	C8A—C7A—C6A—C5A	179.5 (12)
O2A—C6A—C5A—C4A	178.7 (11)	C39B—N10B—N9B—Y1B	-160.6 (8)
O7A—C24A—C25A—C26A	0 (3)	C39B—N10B—N9B—C37B	-0.4 (13)
O3A—C14A—C15A—C16A	11 (2)	C39B—N10B—B2B—N14B	-129.1 (13)

O3A—C14A—C13A—F1A	29.6 (16)	C39B—N10B—B2B—N12B	110.2 (13)
O3A—C14A—C13A—F2A	-91.7 (15)	C39B—C38B—C37B—N9B	-1.2 (15)
O3A—C14A—C13A—F3A	149.3 (13)	C44A—N13A—N14A—C46A	-0.3 (14)
O7B—C24B—C25B—C26B	0 (3)	C44A—N13A—N14A—B2A	179.1 (13)
O7B—C24B—C23B—F15B	-149.1 (15)	C44A—C45A—C46A—N14A	-2.8 (18)
O7B—C24B—C23B—F14B	-24 (2)	C9B—C8B—C7B—C11B	4.0 (17)
O7B—C24B—C23B—F13B	91.8 (17)	C9B—C8B—C7B—C6B	-178.0 (11)
O7B—C24B—C23B—F3	50 (3)	C40A—N10A—N9A—Y1A	160.8 (9)
O7B—C24B—C23B—F4	177.1 (16)	C40A—N10A—N9A—C38A	-0.9 (14)
O7B—C24B—C23B—F5	-72 (2)	C40A—N10A—B2A—N14A	-105.4 (16)
F13A—C23A—C24A—O7A	51.6 (18)	C40A—N10A—B2A—N12A	134.3 (14)
F13A—C23A—C24A—C25A	-134.8 (17)	C40A—C39A—C38A—N9A	0.6 (16)
O6B—C21B—C20B—C19B	0 (2)	C42B—N12B—B2B—N14B	121.8 (14)
O6B—C21B—C22B—F11B	41.8 (19)	C42B—N12B—B2B—N10B	-118.6 (14)
O6B—C21B—C22B—F10B	-78.1 (17)	C10B—N2B—C11B—C12B	179.2 (10)
O6B—C21B—C22B—F12B	162.0 (15)	C10B—N2B—C11B—C7B	1.4 (16)
F11A—C22A—C21A—O6A	175.6 (13)	C31B—N5B—N6B—C33B	0.7 (13)
F11A—C22A—C21A—C20A	-4 (2)	C31B—N5B—N6B—B1B	-178.9 (11)
O4B—C16B—C15B—C14B	1.7 (19)	C21B—C20B—C19B—O5B	-3 (3)
O4B—C16B—C17B—F6B	-51.5 (15)	C21B—C20B—C19B—C18B	-178.4 (15)
O4B—C16B—C17B—F4B	65.7 (16)	C5A—C4A—C3A—C2A	177.7 (12)
O4B—C16B—C17B—F5B	-174.7 (11)	C5A—C4A—C12A—N1A	-178.1 (11)
N13B—N14B—C45B—C44B	0.6 (14)	C5A—C4A—C12A—C11A	-1.6 (18)
N13B—N14B—B2B—N12B	60.4 (14)	C15B—C16B—C17B—F6B	130.1 (13)

N13B—N14B—B2B—N10B	-60.4 (13)	C15B—C16B—C17B—F4B	-112.7 (14)
N13B—C43B—C44B—C45B	2.3 (15)	C15B—C16B—C17B—F5B	6.9 (17)
F9B—C18B—C19B—O5B	171.5 (13)	C30A—N4A—B1A—N8A	-118.3 (15)
F9B—C18B—C19B—C20B	-12 (2)	C30A—N4A—B1A—N6A	119.8 (15)
O5A—C19A—C20A—C21A	0 (2)	C30A—C29A—C28A—N3A	5.6 (16)
O5A—C19A—C18A—F8A	-71.8 (19)	C20B—C21B—C22B—F11B	-135.3 (15)
O5A—C19A—C18A—F9A	164.4 (14)	C20B—C21B—C22B—F10B	104.8 (15)
O5A—C19A—C18A—F7A	44.1 (18)	C20B—C21B—C22B—F12B	-15 (3)
N5A—N6A—C34A—C33A	-0.8 (15)	C1B—N1B—C12B—C4B	-1.5 (16)
N5A—N6A—B1A—N4A	56.3 (15)	C1B—N1B—C12B—C11B	179.9 (10)
N5A—N6A—B1A—N8A	-63.5 (14)	C33B—N6B—B1B—N4B	119.5 (14)
N5A—C31A—C33A—C34A	1.6 (15)	C33B—N6B—B1B—N8B	-122.7 (15)
O8B—C26B—C25B—C24B	7 (3)	C40B—N11B—N12B—C42B	0.1 (14)
O8B—C26B—C27B—F16B	-5 (3)	C40B—N11B—N12B—B2B	-179.7 (12)
O8B—C26B—C27B—F17B	-135.2 (19)	C19A—C20A—C21A—O6A	-4 (2)
O8B—C26B—C27B—F18B	111.3 (19)	C19A—C20A—C21A—C22A	175.7 (14)
N11B—N12B—C42B—C41B	-1.0 (16)	C35A—N7A—N8A—C37A	1.3 (14)
N11B—N12B—B2B—N14B	-58.5 (15)	C35A—N7A—N8A—B1A	177.4 (12)
N11B—N12B—B2B—N10B	61.1 (15)	C20A—C19A—C18A—F8A	109.0 (17)
N11B—C40B—C41B—C42B	-1.5 (17)	C20A—C19A—C18A—F9A	-15 (2)
F7B—C18B—C19B—O5B	48 (2)	C20A—C19A—C18A—F7A	-135.1 (15)
F7B—C18B—C19B—C20B	-136.3 (16)	C22B—C21B—C20B—C19B	176.5 (16)
N1A—C1A—C2A—C3A	-0.5 (19)	C18A—C19A—C20A—C21A	178.9 (14)
O4A—C16A—C17A—F6A	-176.4 (12)	C34A—N6A—B1A—N4A	-124.3 (14)

O4A—C16A—C17A—F5A	67.1 (17)	C34A—N6A—B1A—N8A	115.9 (15)
O4A—C16A—C17A—F4A	-55.4 (18)	C37A—N8A—B1A—N4A	121.9 (14)
N2B—C11B—C7B—C8B	-4.0 (16)	C37A—N8A—B1A—N6A	-117.8 (14)
N2B—C11B—C7B—C6B	178.0 (10)	C46A—N14A—B2A—N10A	114.0 (17)
F10A—C22A—C21A—O6A	-62.6 (16)	C46A—N14A—B2A—N12A	-126.1 (15)
F10A—C22A—C21A—C20A	117.4 (14)	C30B—N4B—N3B—Y1B	-175.2 (9)
N2A—C11A—C12A—N1A	-5.9 (16)	C30B—N4B—N3B—C28B	1.9 (14)
N2A—C11A—C12A—C4A	177.5 (11)	C30B—N4B—B1B—N6B	-127.3 (15)
N2A—C10A—C9A—C8A	1 (2)	C30B—N4B—B1B—N8B	111.1 (15)
N13A—N14A—C46A—C45A	2.1 (17)	C23A—C24A—C25A—C26A	-173.1 (18)
N13A—N14A—B2A—N10A	-65.3 (16)	C43A—N12A—N11A—Y1A	-179.4 (8)
N13A—N14A—B2A—N12A	54.6 (17)	C43A—N12A—N11A—C41A	-2.2 (14)
N13A—C44A—C45A—C46A	2.7 (18)	C43A—N12A—B2A—N10A	-120.5 (15)
O8A—C26A—C25A—C24A	3 (3)	C43A—N12A—B2A—N14A	118.9 (15)
O8A—C26A—C27A—F16A	-163 (2)	C28A—N3A—N4A—C30A	1.9 (14)
O8A—C26A—C27A—F17A	81 (3)	C28A—N3A—N4A—B1A	-173.4 (13)
O8A—C26A—C27A—F1	-30 (3)	C17B—C16B—C15B—C14B	179.9 (11)
O8A—C26A—C1—F18A	-63 (3)	B2B—N14B—C45B—C44B	-175.7 (12)
O8A—C26A—C1—F2	179 (2)	B2B—N12B—C42B—C41B	178.8 (13)
O8A—C26A—C1—F6	56 (4)	B2B—N10B—N9B—Y1B	22.5 (14)
F14A—C23A—C24A—O7A	179.1 (14)	B2B—N10B—N9B—C37B	-177.3 (11)
F14A—C23A—C24A—C25A	-7 (2)	B2B—N10B—C39B—C38B	176.2 (13)
N14B—N13B—C43B—C44B	-1.9 (14)	C25B—C26B—C27B—F16B	175.7 (18)
N14B—C45B—C44B—C43B	-1.7 (14)	C25B—C26B—C27B—F17B	45 (3)

N12B—N11B—C40B—C41B	0.9 (16)	C25B—C26B—C27B—F18B	-68 (2)
N12B—C42B—C41B—C40B	1.5 (16)	C25B—C24B—C23B—F15B	38 (2)
N4B—N3B—C28B—C29B	-1.2 (15)	C25B—C24B—C23B—F14B	163.0 (16)
N4B—C30B—C29B—C28B	1.1 (17)	C25B—C24B—C23B—F13B	-81.4 (18)
N3B—N4B—C30B—C29B	-1.9 (16)	C25B—C24B—C23B—F3	-123 (2)
N3B—N4B—B1B—N6B	61.3 (17)	C25B—C24B—C23B—F4	4 (2)
N3B—N4B—B1B—N8B	-60.3 (16)	C25B—C24B—C23B—F5	115 (2)
N3B—C28B—C29B—C30B	0.1 (17)	C34B—N7B—N8B—C36B	2.1 (16)
N10A—N9A—C38A—C39A	0.1 (15)	C34B—N7B—N8B—B1B	177.9 (13)
N10A—C40A—C39A—C38A	-1.2 (17)	C34B—C35B—C36B—N8B	0.7 (19)
N10B—N9B—C37B—C38B	1.0 (15)	C36B—N8B—B1B—N4B	-130.9 (15)
F12A—C22A—C21A—O6A	55.3 (16)	C36B—N8B—B1B—N6B	109.7 (17)
F12A—C22A—C21A—C20A	-124.7 (14)	B2A—N10A—N9A—Y1A	-14.5 (16)
N14A—N13A—C44A—C45A	-1.5 (15)	B2A—N10A—N9A—C38A	-176.2 (13)
N1B—C12B—C11B—N2B	4.0 (15)	B2A—N10A—C40A—C39A	176.2 (14)
N1B—C12B—C11B—C7B	-178.2 (10)	B2A—N14A—C46A—C45A	-177.3 (14)
N1B—C1B—C2B—C3B	-1.5 (19)	B2A—N12A—N11A—Y1A	-1.2 (15)
F8B—C18B—C19B—O5B	-68.9 (16)	B2A—N12A—N11A—C41A	176.0 (11)
F8B—C18B—C19B—C20B	107.1 (17)	B2A—N12A—C43A—C42A	-177.3 (13)
N7A—N8A—C37A—C36A	-0.7 (16)	B1A—N4A—C30A—C29A	176.5 (14)
N7A—N8A—B1A—N4A	-53.6 (16)	B1A—N8A—C37A—C36A	-176.6 (13)
N7A—N8A—B1A—N6A	66.7 (15)	B1A—N6A—C34A—C33A	179.7 (13)
N7A—C35A—C36A—C37A	1.1 (18)	B1B—N4B—N3B—Y1B	-2.6 (16)
N9A—N10A—C40A—C39A	1.3 (16)	B1B—N4B—N3B—C28B	174.6 (13)

N9A—N10A—B2A—N14A	68.9 (17)	B1B—N4B—C30B—C29B	-173.9 (14)
N9A—N10A—B2A—N12A	-51.4 (16)	B1B—N6B—C33B—C32B	179.3 (13)
N3A—N4A—C30A—C29A	1.6 (16)	B1B—N8B—C36B—C35B	-177.3 (15)
N3A—N4A—B1A—N8A	55.8 (16)	C27B—C26B—C25B—C24B	-173.1 (16)
N3A—N4A—B1A—N6A	-66.0 (16)	C25A—C26A—C27A—F16A	0 (3)
N5B—N6B—C33B—C32B	-0.3 (15)	C25A—C26A—C27A—F17A	-116 (2)
N5B—N6B—B1B—N4B	-61.0 (16)	C25A—C26A—C27A—F1	133 (3)
N5B—N6B—B1B—N8B	56.8 (17)	C25A—C26A—C1—F18A	140 (3)
N5B—C31B—C32B—C33B	0.7 (15)	C25A—C26A—C1—F2	22 (4)
C4B—C5B—C6B—O2B	-177.4 (10)	C25A—C26A—C1—F6	-101 (4)
C4B—C5B—C6B—C7B	2.0 (16)	C7S—C8S—C9S—C9S^{i}	-166 (2)
C4B—C12B—C11B—N2B	-174.5 (10)	F2B—C13B—C14B—O3B	-177.7 (13)
C4B—C12B—C11B—C7B	3.3 (16)	F2B—C13B—C14B—C15B	5.2 (18)
C4B—C3B—C2B—C1B	-1.0 (18)	C27A—C26A—C25A—C24A	-159 (2)
N4A—N3A—C28A—C29A	-4.7 (15)	F1B—C13B—C14B—O3B	-48 (2)
N4A—C30A—C29A—C28A	-4.4 (16)	F1B—C13B—C14B—C15B	135 (2)
F15A—C23A—C24A—O7A	-64.1 (18)	F3B—C13B—C14B—O3B	70.7 (17)
F15A—C23A—C24A—C25A	109.5 (18)	F3B—C13B—C14B—C15B	-106.4 (18)
N12A—N11A—C41A—C42A	3.0 (15)	F1AA—C13B—C14B—O3B	4 (2)
N12A—C43A—C42A—C41A	1.0 (16)	F1AA—C13B—C14B—C15B	-172.9 (18)
N11A—N12A—C43A—C42A	0.8 (16)	F9—C13B—C14B—O3B	-103.4 (17)
N11A—N12A—B2A—N10A	61.7 (15)	F9—C13B—C14B—C15B	79.5 (18)
N11A—N12A—B2A—N14A	-59.0 (17)	F14—C13B—C14B—O3B	142 (2)
N11A—C41A—C42A—C43A	-2.6 (16)	F14—C13B—C14B—C15B	-35 (3)

N6B—N5B—C31B—C32B	-0.9 (13)	C23B—C24B—C25B—C26B	171.8 (15)
N6B—C33B—C32B—C31B	-0.3 (15)	C1—C26A—C25A—C24A	157 (2)
C5B—C4B—C12B—N1B	177.3 (10)	C1S—C2S—C3S—C4S	179 (4)
C5B—C4B—C12B—C11B	-4.2 (16)	C3S—C4S—C5S—C6S	180 (4)
C5B—C4B—C3B—C2B	-176.0 (11)	C5S—C4S—C3S—C2S	180 (4)

Symmetry code: (i) -*x*+1, *y*, -*z*+3/2.

8.3.14 Crystallographic data for 9-EuYb

Crystal data

$0.5(C_{45}H_{27}B_2EuF_{18}N_{14}O_8Yb)\cdot0.5(C_{45}H_{31}B_2EuF_{18}N_{14}O_8Yb)\cdot0.5(C_7H_8)\cdot0.25(C_6H_{14})$	$F(000)$ = 6428
M_r = 1650.05	D_x = 1.612 Mg m^{-3}
Monoclinic, $P2_1/n$	Mo $K\alpha$ radiation, λ = 0.71073 Å
a = 21.2729 (14) Å	Cell parameters from 9848 reflections
b = 28.6357 (16) Å	θ = 2.3–25.5°
c = 22.3529 (15) Å	μ = 2.39 mm^{-1}
β = 93.020 (3)°	T = 273 K
V = 13597.7 (15) Å^3	Rod, orange
Z = 8	0.23 × 0.02 × 0.02 mm

Data collection

Bruker D8 VENTURE diffractometer	16901 reflections with $I > 2\sigma(I)$
Radiation source: microfocus sealed tube, INCOATEC Iμs 3.0	R_{int} = 0.192
Multilayer mirror optics monochromator	θ_{max} = 26.5°, θ_{min} = 1.2°
Detector resolution: 7.4074 pixels mm^{-1}	h = -26→26
ϕ and ω scans	k = -35→35
225078 measured reflections	l = -27→27
27925 independent reflections	

Refinement

Refinement on F^2	Primary atom site location: dual
Least-squares matrix: full	Hydrogen site location: inferred from neighbouring sites
$R[F^2 > 2\sigma(F^2)] = 0.074$	H-atom parameters constrained
$wR(F^2) = 0.204$	$w = 1/[\sigma^2(F_o^2) + (0.0862P)^2 + 63.6974P]$ where $P = (F_o^2 + 2F_c^2)/3$
$S = 1.08$	$(\Delta/\sigma)_{max} = 0.007$
27925 reflections	$\Delta\rangle_{max} = 2.15$ e Å^{-3}
1784 parameters	$\Delta\rangle_{min} = -0.95$ e Å^{-3}
183 restraints	

Special details

Geometry. All esds (except the esd in the dihedral angle between two l.s. planes) are estimated using the full covariance matrix. The cell esds are taken into account individually in the estimation of esds in distances, angles and torsion angles; correlations between esds in cell parameters are only used when they are defined by crystal symmetry. An approximate (isotropic) treatment of cell esds is used for estimating esds involving l.s. planes.

Fractional atomic coordinates and isotropic or equivalent isotropic displacement parameters (Å²)

	x	*y*	*z*	U_{iso}*/U_{eq}	Occ. (<1)
Yb01	0.24328 (2)	0.56721 (2)	0.08500 (2)	0.02656 (12)	
Yb02	0.10287 (2)	0.83718 (2)	0.20257 (2)	0.02590 (12)	
Eu03	0.51311 (3)	0.81521 (2)	0.28926 (3)	0.02829 (14)	
Eu04	0.26088 (3)	0.61693 (2)	0.47565 (3)	0.03157 (15)	
O005	0.2578 (3)	0.5285 (2)	0.1802 (3)	0.0299 (17)	
O006	0.1907 (3)	0.7883 (2)	0.2011 (3)	0.0309 (17)	
O007	0.5501 (4)	0.8907 (3)	0.2650 (3)	0.0343 (18)	
O008	0.2166 (3)	0.6151 (2)	0.1621 (3)	0.0296 (17)	
F009	0.7466 (3)	0.8313 (3)	0.3381 (4)	0.062 (2)	
O00A	0.1914 (3)	0.8743 (2)	0.2472 (3)	0.0307 (17)	
F00B	0.4667 (4)	0.6570 (2)	0.3283 (3)	0.054 (2)	
O00C	0.5290 (4)	0.7537 (3)	0.3602 (4)	0.038 (2)	
F00D	0.4678 (4)	0.5947 (2)	0.3814 (4)	0.057 (2)	
O00E	0.6244 (3)	0.8112 (3)	0.3112 (4)	0.0358 (19)	
O00F	0.5129 (3)	0.8471 (2)	0.3871 (3)	0.0311 (18)	
O00G	0.3234 (4)	0.5619 (3)	0.5316 (4)	0.045 (2)	
F00H	0.5172 (4)	0.9112 (3)	0.4718 (3)	0.063 (2)	
O00I	0.5532 (4)	0.7572 (3)	0.2283 (4)	0.041 (2)	

F00J	0.5298 (4)	0.6751 (3)	0.4438 (5)	0.076 (3)	
O00K	0.2987 (4)	0.6958 (3)	0.4696 (4)	0.038 (2)	
F00L	0.5587 (4)	0.8640 (3)	0.5347 (3)	0.066 (2)	
F00M	0.3973 (4)	0.6039 (3)	0.3106 (4)	0.068 (3)	
O00N	0.1660 (4)	0.6575 (3)	0.4908 (4)	0.047 (2)	
N00O	0.0631 (4)	0.7833 (3)	0.3316 (4)	0.034 (2)	
O00P	0.4696 (4)	0.8366 (3)	0.1913 (3)	0.0366 (19)	
O00Q	0.3572 (4)	0.6173 (3)	0.4266 (4)	0.0344 (18)	
O00R	0.2587 (4)	0.6354 (3)	0.5790 (4)	0.047 (2)	
N00S	0.4110 (4)	0.8603 (3)	0.3024 (4)	0.027 (2)	
F00T	0.4602 (4)	0.8598 (3)	0.5116 (4)	0.073 (3)	
N00U	0.1283 (4)	0.8882 (3)	0.0697 (4)	0.031 (2)	
N00V	0.0638 (4)	0.7586 (3)	0.1991 (4)	0.029 (2)	
N00W	0.1086 (4)	0.8130 (3)	0.3102 (4)	0.032 (2)	
O00X	0.1853 (4)	0.5617 (3)	0.4994 (4)	0.051 (2)	
N00Y	0.0145 (5)	0.8725 (3)	0.0816 (4)	0.033 (2)	
F00Z	0.3787 (10)	0.7893 (9)	0.4084 (8)	0.046 (5)	0.56 (2)
N010	0.2556 (5)	0.6476 (3)	0.0542 (4)	0.036 (2)	
N011	0.0217 (5)	0.7411 (3)	0.2383 (4)	0.036 (2)	
N012	0.2582 (4)	0.5536 (3)	0.3935 (4)	0.028 (2)	
F013	0.7741 (4)	0.7624 (3)	0.3184 (5)	0.079 (3)	
N014	0.3111 (5)	0.5588 (3)	-0.0003 (4)	0.038 (2)	
N015	0.0999 (4)	0.5163 (3)	0.0688 (4)	0.030 (2)	
N016	0.1873 (4)	0.4655 (3)	0.0327 (4)	0.031 (2)	
N017	0.2382 (4)	0.4850 (3)	0.0618 (4)	0.031 (2)	
F018	0.2625 (5)	0.6750 (4)	0.6938 (4)	0.087 (3)	
N019	0.2195 (4)	0.6429 (3)	0.3723 (4)	0.033 (2)	
N01A	0.1558 (5)	0.8576 (3)	0.1110 (4)	0.032 (2)	
F01B	0.4275 (5)	0.8988 (4)	0.0675 (4)	0.108 (4)	
F01C	0.7185 (4)	0.7771 (4)	0.3934 (4)	0.092 (3)	
N01D	0.0673 (5)	0.9390 (3)	0.1362 (4)	0.036 (2)	
N01E	0.3516 (5)	0.5950 (4)	-0.0156 (5)	0.042 (3)	
N01F	0.4102 (4)	0.7709 (3)	0.2593 (4)	0.0243 (19)	
F01G	0.2442 (5)	0.6072 (4)	0.7294 (4)	0.080 (3)	
F01H	0.6064 (5)	0.7079 (3)	0.4872 (5)	0.100 (4)	
N01I	0.0848 (4)	0.9190 (3)	0.1898 (4)	0.033 (2)	
N01J	-0.0307 (4)	0.8145 (3)	0.2743 (4)	0.034 (2)	
N01K	0.3090 (5)	0.6660 (3)	0.0343 (4)	0.038 (2)	
F01L	0.5716 (6)	0.7029 (4)	0.1332 (5)	0.099 (4)	
N01M	-0.0022 (4)	0.8489 (3)	0.2440 (4)	0.030 (2)	

N01N	0.1340 (4)	0.5463 (3)	0.1053 (4)	0.029 (2)	
F01O	0.5666 (6)	0.9955 (3)	0.1907 (5)	0.109 (4)	
F01P	0.6111 (6)	0.6870 (4)	0.3969 (6)	0.115 (5)	
C01Q	0.2495 (5)	0.5668 (4)	0.3351 (4)	0.023 (2)	
N01R	0.3514 (4)	0.5863 (3)	0.1216 (4)	0.033 (2)	
C01S	0.2416 (5)	0.8046 (4)	0.2248 (5)	0.029 (2)	
N01T	0.0228 (4)	0.8357 (3)	0.1198 (4)	0.033 (2)	
N01U	0.3890 (5)	0.6152 (3)	0.0892 (5)	0.038 (2)	
F01V	0.5629 (6)	0.9852 (3)	0.2820 (5)	0.100 (4)	
N01W	0.1448 (4)	0.5334 (3)	-0.0289 (4)	0.030 (2)	
N01X	0.1778 (4)	0.5719 (3)	-0.0082 (4)	0.032 (2)	
C01Y	0.2251 (5)	0.6003 (4)	0.2151 (5)	0.025 (2)	
C01Z	0.2417 (5)	0.8508 (4)	0.2510 (4)	0.022 (2)	
C020	0.2577 (5)	0.5371 (4)	0.2868 (5)	0.026 (2)	
C021	0.2280 (5)	0.6153 (4)	0.3243 (5)	0.025 (2)	
C022	0.2475 (5)	0.5541 (4)	0.2256 (5)	0.026 (2)	
C023	0.3019 (5)	0.9147 (4)	0.3043 (5)	0.026 (2)	
H023	0.265677	0.932826	0.305226	0.031*	
F024	0.6359 (4)	0.9571 (4)	0.2406 (7)	0.117 (5)	
C025	0.3853 (5)	0.5750 (4)	0.1712 (5)	0.036 (3)	
H025	0.371573	0.556281	0.201866	0.043*	
F026	0.5691 (6)	0.6594 (3)	0.2059 (5)	0.101 (4)	
C027	0.2135 (5)	0.6304 (4)	0.2662 (5)	0.027 (2)	
C028	0.1290 (6)	0.5386 (4)	-0.0876 (6)	0.042 (3)	
H028	0.107160	0.516788	-0.111453	0.050*	
C029	0.3009 (5)	0.7781 (4)	0.2263 (5)	0.026 (2)	
C02A	0.5273 (5)	0.8328 (4)	0.4393 (5)	0.033 (3)	
C02B	0.4111 (5)	0.9036 (4)	0.3252 (5)	0.034 (3)	
H02B	0.449105	0.915776	0.340566	0.041*	
C02C	0.2756 (5)	0.4910 (4)	0.2997 (5)	0.034 (3)	
H02C	0.283296	0.470241	0.268895	0.040*	
F02D	0.3992 (7)	0.8334 (4)	0.0923 (5)	0.131 (6)	
C02E	0.2994 (5)	0.8691 (4)	0.2787 (5)	0.025 (2)	
C02F	0.6653 (5)	0.7816 (4)	0.2989 (5)	0.035 (3)	
F02G	0.0483 (6)	0.5177 (4)	0.5570 (6)	0.114 (4)	
F02H	0.1415 (7)	0.4923 (5)	0.5737 (9)	0.153 (7)	
C02I	0.3035 (5)	0.7332 (4)	0.2000 (5)	0.032 (3)	
H02I	0.267992	0.720484	0.180160	0.039*	
C02J	0.3578 (5)	0.9311 (4)	0.3273 (5)	0.031 (3)	
H02J	0.360290	0.960662	0.344464	0.037*	

C02K	0.1961 (5)	0.6854 (4)	0.3632 (6)	0.036 (3)	
H02K	0.190724	0.704354	0.396377	0.043*	
C02L	0.2734 (5)	0.5096 (4)	0.4037 (5)	0.029 (3)	
H02L	0.279004	0.499936	0.443356	0.035*	
C02M	0.1874 (5)	0.6754 (4)	0.2582 (5)	0.033 (3)	
H02M	0.175943	0.686081	0.219901	0.039*	
C02N	0.3054 (6)	0.5314 (4)	-0.0477 (6)	0.041 (3)	
H02N	0.281039	0.504424	-0.049650	0.049*	
C02O	0.1503 (5)	0.8188 (4)	0.3564 (5)	0.034 (3)	
H02O	0.186275	0.837076	0.355207	0.041*	
C02P	0.3590 (5)	0.7087 (4)	0.2039 (5)	0.035 (3)	
H02P	0.362041	0.679253	0.186674	0.042*	
C02Q	0.0330 (6)	0.6875 (4)	0.1684 (6)	0.043 (3)	
H02A	0.002654	0.682024	0.135188	0.052*	
H02D	0.058577	0.659661	0.174643	0.052*	
C02R	0.2147 (6)	0.6819 (4)	0.0555 (5)	0.040 (3)	
H02R	0.173596	0.678811	0.067342	0.047*	
C02S	0.4458 (6)	0.6205 (5)	0.1190 (6)	0.045 (3)	
H02S	0.479350	0.638194	0.106448	0.055*	
F02T	0.1756 (5)	0.6384 (5)	0.6702 (4)	0.114 (4)	
F46	0.0630 (12)	0.6850 (8)	0.5958 (7)	0.103 (7)	0.658 (17)
C02V	0.0782 (6)	0.7722 (4)	0.3885 (5)	0.043 (3)	
H02V	0.055113	0.752775	0.412505	0.051*	
C02W	0.5491 (6)	0.7889 (4)	0.4547 (6)	0.039 (3)	
H02W	0.565025	0.783578	0.493641	0.046*	
C02X	0.4108 (5)	0.7291 (4)	0.2346 (5)	0.031 (3)	
H02X	0.448138	0.712203	0.237895	0.037*	
C02Y	0.2803 (6)	0.4521 (4)	0.0697 (5)	0.035 (3)	
H02Y	0.320086	0.456655	0.088043	0.042*	
C02Z	0.1994 (6)	0.4199 (4)	0.0242 (6)	0.040 (3)	
H02Z	0.171911	0.398465	0.005525	0.048*	
C030	0.0616 (6)	0.9939 (4)	0.2055 (6)	0.045 (3)	
H030	0.054959	1.022210	0.224633	0.054*	
C031	0.6608 (6)	0.7445 (5)	0.2593 (6)	0.045 (3)	
H031	0.695588	0.725403	0.254546	0.054*	
C032	-0.0420 (6)	0.8716 (4)	0.0513 (6)	0.046 (3)	
H032	-0.057268	0.893287	0.023123	0.055*	
F033	0.3610 (5)	0.8895 (6)	0.1333 (6)	0.147 (6)	
C034	-0.0442 (5)	0.8833 (4)	0.2374 (5)	0.035 (3)	
H034	-0.037343	0.911429	0.217887	0.043*	

C035	0.0820 (5)	0.9528 (4)	0.2310 (6)	0.035 (3)	
H035	0.092515	0.948816	0.271600	0.043*	
C036	0.0945 (6)	0.5614 (4)	0.1451 (6)	0.037 (3)	
H036	0.105161	0.582772	0.175282	0.044*	
C037	0.1501 (6)	0.5809 (4)	-0.1066 (6)	0.043 (3)	
H037	0.145070	0.594094	-0.144622	0.052*	
C038	0.1333 (6)	0.7943 (4)	0.4057 (5)	0.040 (3)	
H038	0.154753	0.792963	0.443014	0.048*	
C039	0.3551 (5)	0.8426 (4)	0.2803 (5)	0.027 (2)	
C03A	0.4449 (6)	0.5957 (4)	0.1700 (6)	0.046 (3)	
H03A	0.477677	0.592792	0.198999	0.055*	
C03B	0.5482 (6)	0.7530 (4)	0.4146 (6)	0.036 (3)	
F03C	0.6562 (5)	0.6773 (5)	0.1727 (7)	0.156 (7)	
C03D	0.3000 (7)	0.7119 (4)	0.0243 (6)	0.044 (3)	
H03D	0.330282	0.732173	0.010694	0.053*	
C03E	-0.0300 (6)	0.8108 (4)	0.1137 (6)	0.041 (3)	
H03E	-0.037760	0.783444	0.134545	0.049*	
C03F	0.1789 (6)	0.7032 (4)	0.3063 (5)	0.036 (3)	
H03F	0.162187	0.733061	0.301652	0.044*	
C03G	0.0704 (6)	0.7262 (4)	0.1575 (5)	0.040 (3)	
H03G	0.096442	0.728962	0.125470	0.047*	
C03H	0.0400 (6)	0.5121 (4)	0.0873 (6)	0.041 (3)	
C03I	0.6045 (6)	0.7356 (5)	0.2264 (6)	0.042 (3)	
C03J	0.5781 (7)	0.9641 (5)	0.2314 (6)	0.047 (3)	
C03K	0.2207 (6)	0.8693 (5)	0.0367 (6)	0.044 (3)	
H03K	0.255691	0.867563	0.013588	0.053*	
C03L	0.0532 (6)	0.9843 (4)	0.1456 (6)	0.047 (3)	
H03L	0.039945	1.005543	0.116108	0.056*	
C03M	0.1813 (6)	0.5998 (4)	-0.0550 (5)	0.040 (3)	
H03M	0.201807	0.628513	-0.053930	0.048*	
C03N	0.0342 (6)	0.5409 (5)	0.1358 (6)	0.046 (3)	
C03O	0.2120 (6)	0.8472 (4)	0.0903 (5)	0.039 (3)	
H03O	0.241353	0.827610	0.109684	0.047*	
C03P	0.2589 (6)	0.4103 (4)	0.0475 (6)	0.038 (3)	
H03P	0.279819	0.381765	0.048158	0.046*	
C03Q	0.5388 (6)	0.9194 (4)	0.2243 (5)	0.039 (3)	
C03R	-0.0890 (5)	0.8282 (5)	0.2859 (6)	0.041 (3)	
H03R	-0.118005	0.810781	0.306158	0.049*	
C03S	0.3789 (6)	0.6954 (4)	0.3994 (5)	0.037 (3)	
H03S	0.402983	0.714081	0.375455	0.045*	

F03T	0.4060 (16)	0.5126 (11)	0.6492 (18)	0.086 (8)	0.5
C03U	0.0030 (6)	0.6991 (4)	0.2199 (6)	0.046 (3)	
H03U	-0.025732	0.680396	0.238574	0.055*	
C03V	0.2818 (5)	0.4768 (4)	0.3589 (5)	0.035 (3)	
H03V	0.291251	0.445898	0.368618	0.043*	
C03W	0.1223 (6)	0.6481 (5)	0.5211 (6)	0.051 (4)	
C03X	0.4642 (6)	0.8747 (5)	0.1632 (5)	0.039 (3)	
F03Y	0.0984 (7)	0.4915 (5)	0.4853 (7)	0.157 (7)	
C03Z	0.3555 (5)	0.7964 (4)	0.2551 (5)	0.028 (2)	
C040	-0.0732 (6)	0.8319 (5)	0.0705 (6)	0.049 (3)	
H04A	-0.082792	0.810826	0.037291	0.058*	
H04E	-0.112089	0.840278	0.088602	0.058*	
C041	0.3852 (6)	0.6476 (4)	0.3975 (5)	0.035 (3)	
F042	0.4230 (17)	0.5126 (8)	0.5579 (15)	0.086 (7)	0.5
F043	0.3480 (15)	0.4691 (12)	0.5833 (15)	0.095 (7)	0.5
C044	0.4358 (6)	0.4730 (6)	0.0227 (8)	0.059 (4)	
H044	0.424246	0.496757	-0.004123	0.070*	
C045	0.3373 (6)	0.7157 (4)	0.4365 (5)	0.036 (3)	
C046	0.4970 (6)	0.9152 (5)	0.1746 (6)	0.046 (3)	
H046	0.491166	0.940428	0.148643	0.055*	
C047	0.1670 (7)	0.8943 (4)	0.0247 (6)	0.048 (3)	
H047	0.158571	0.912657	-0.009096	0.058*	
C048	0.5158 (6)	0.8670 (5)	0.4895 (6)	0.043 (3)	
B049	0.0038 (6)	0.7703 (5)	0.2940 (6)	0.035 (3)	
H049	-0.023691	0.751535	0.318420	0.042*	
C04A	0.7276 (6)	0.7871 (5)	0.3376 (7)	0.050 (4)	
C04B	0.3396 (7)	0.5473 (5)	-0.0939 (7)	0.056 (4)	
H04B	0.342010	0.534180	-0.131788	0.067*	
B04C	0.1289 (6)	0.4943 (4)	0.0134 (6)	0.030 (3)	
H04C	0.097685	0.473681	-0.006775	0.036*	
C04D	0.3693 (7)	0.5864 (5)	-0.0723 (6)	0.058 (4)	
H04D	0.397351	0.604406	-0.093053	0.070*	
C04E	0.5749 (7)	0.7048 (5)	0.4356 (7)	0.052 (4)	
F04F	0.3500 (13)	0.7836 (6)	0.4968 (6)	0.079 (6)	0.56 (2)
C04G	-0.0986 (6)	0.8714 (5)	0.2631 (7)	0.053 (4)	
H04G	-0.134859	0.889399	0.264716	0.064*	
C04H	0.2668 (6)	0.6118 (5)	0.6260 (6)	0.045 (3)	
F04I	0.2804 (8)	0.7881 (8)	0.4235 (15)	0.094 (6)	0.56 (2)
C04J	0.4303 (7)	0.6264 (4)	0.3547 (7)	0.048 (3)	
C04K	0.3354 (5)	0.7689 (4)	0.4408 (5)	0.055 (4)	

C04L	0.1332 (7)	0.5637 (5)	0.5232 (6)	0.057 (4)	
C04M	0.4598 (8)	0.4860 (7)	0.0785 (10)	0.074 (5)	
H04M	0.464977	0.517225	0.088966	0.089*	
C04N	0.1020 (7)	0.6033 (6)	0.5383 (7)	0.066 (5)	
H04N	0.066446	0.600689	0.560520	0.079*	
C04O	0.6020 (7)	0.6941 (5)	0.1845 (9)	0.062 (4)	
C04P	0.2416 (7)	0.7242 (4)	0.0365 (6)	0.050 (4)	
H04P	0.223026	0.753529	0.033367	0.060*	
C04Q	0.3276 (7)	0.5502 (5)	0.5855 (6)	0.054 (4)	
F44	0.1130 (11)	0.7301 (6)	0.5359 (12)	0.126 (8)	0.658 (17)
C04S	0.2991 (8)	0.5719 (5)	0.6330 (6)	0.061 (4)	
H04S	0.302622	0.558124	0.670698	0.073*	
B04T	0.0637 (7)	0.9115 (5)	0.0780 (7)	0.041 (4)	
H04T	0.052652	0.932235	0.044193	0.050*	
B04U	0.3683 (7)	0.6346 (6)	0.0265 (7)	0.046 (4)	
H04U	0.402356	0.653217	0.010742	0.055*	
C04V	0.4011 (9)	0.4175 (8)	-0.0562 (9)	0.103 (7)	
H04F	0.392400	0.445843	-0.077985	0.155*	
H04H	0.430670	0.399040	-0.076953	0.155*	
H04I	0.362774	0.400187	-0.052919	0.155*	
C04W	0.0834 (8)	0.6893 (6)	0.5408 (6)	0.083 (5)	
C04X	0.4132 (7)	0.8748 (6)	0.1126 (7)	0.061 (4)	
C04Y	0.1053 (11)	0.5156 (7)	0.5374 (10)	0.089 (6)	
C04Z	0.4277 (8)	0.4288 (7)	0.0039 (9)	0.071 (5)	
F45	0.0364 (9)	0.6977 (8)	0.4994 (8)	0.123 (7)	0.658 (17)
C051	0.2364 (8)	0.6341 (7)	0.6804 (7)	0.067 (5)	
C052	0.3763 (19)	0.5099 (14)	0.5954 (17)	0.085 (7)	0.5
C053	0.4679 (10)	0.4054 (10)	0.1000 (13)	0.113 (10)	
H053	0.478666	0.381136	0.126222	0.136*	
C054	0.4758 (8)	0.4510 (11)	0.1180 (9)	0.094 (7)	
H054	0.491833	0.457919	0.156515	0.113*	
C055	0.4440 (9)	0.3958 (7)	0.0433 (12)	0.085 (6)	
H055	0.438936	0.364705	0.031954	0.103*	
C1	0.015 (2)	0.5997 (16)	0.360 (2)	0.110 (15)*	0.5
H1A	0.036392	0.594874	0.399331	0.132*	0.5
H1B	-0.010032	0.571819	0.354385	0.132*	0.5
C3	0.0857 (15)	0.5438 (11)	0.3223 (14)	0.067 (9)*	0.5
H3A	0.102703	0.530685	0.359195	0.100*	0.5
H3B	0.119090	0.549163	0.295862	0.100*	0.5
H3C	0.055732	0.522464	0.303783	0.100*	0.5

C5	0.0548 (18)	0.5875 (12)	0.3343 (17)	0.075 (10)*	0.5
H5A	0.089422	0.607063	0.349227	0.091*	0.5
H5B	0.043795	0.599267	0.294397	0.091*	0.5
C10	-0.116 (2)	0.6817 (16)	0.427 (2)	0.116 (15)*	0.5
H10A	-0.103674	0.708953	0.405650	0.174*	0.5
H10B	-0.110865	0.687282	0.469329	0.174*	0.5
H10C	-0.159369	0.674670	0.416572	0.174*	0.5
C11	-0.028 (3)	0.6252 (18)	0.379 (2)	0.127 (17)*	0.5
H11A	-0.051345	0.627327	0.339976	0.152*	0.5
H11B	-0.003797	0.653708	0.380374	0.152*	0.5
C14	-0.078 (2)	0.6429 (15)	0.411 (2)	0.104 (13)*	0.5
H14A	-0.063085	0.632859	0.451166	0.125*	0.5
H14B	-0.110250	0.620686	0.399538	0.125*	0.5
F13	0.1203 (14)	0.7088 (12)	0.5847 (15)	0.124 (8)	0.342 (17)
F14	0.0323 (16)	0.6837 (18)	0.572 (2)	0.113 (9)	0.342 (17)
F25	0.080 (3)	0.7285 (12)	0.509 (2)	0.121 (9)	0.342 (17)
F1	0.3000 (15)	0.7866 (7)	0.4824 (13)	0.082 (6)	0.44 (2)
F6	0.2961 (12)	0.7817 (10)	0.3940 (10)	0.077 (7)	0.44 (2)
F18	0.3878 (12)	0.7925 (13)	0.4320 (14)	0.065 (8)	0.44 (2)
F17	0.4078 (17)	0.4935 (8)	0.5644 (14)	0.082 (6)	0.5
F20	0.3832 (17)	0.5001 (11)	0.6567 (17)	0.088 (8)	0.5
F35	0.3200 (15)	0.4700 (13)	0.5957 (16)	0.097 (7)	0.5
C18	0.3617 (18)	0.5050 (15)	0.6000 (16)	0.084 (7)	0.5

Atomic displacement parameters (Å²)

	U^{11}	U^{22}	U^{33}	U^{12}	U^{13}	U^{23}
Yb01	0.0216 (3)	0.0274 (2)	0.0301 (3)	-0.00022 (19)	-0.00344 (19)	0.0013 (2)
Yb02	0.0170 (2)	0.0264 (2)	0.0335 (3)	0.00041 (19)	-0.00611 (19)	0.0000 (2)
Eu03	0.0166 (3)	0.0327 (3)	0.0350 (3)	0.0006 (2)	-0.0038 (2)	-0.0012 (2)
Eu04	0.0264 (3)	0.0355 (3)	0.0324 (3)	-0.0021 (2)	-0.0022 (2)	-0.0015 (2)
O005	0.027 (4)	0.029 (4)	0.033 (4)	0.005 (3)	-0.006 (3)	-0.003 (3)
O006	0.018 (4)	0.031 (4)	0.043 (5)	0.000 (3)	-0.008 (3)	-0.007 (3)
O007	0.024 (4)	0.043 (5)	0.035 (5)	-0.002 (3)	-0.008 (3)	0.004 (4)
O008	0.029 (4)	0.030 (4)	0.029 (4)	0.003 (3)	-0.002 (3)	-0.003 (3)
F009	0.031 (4)	0.069 (6)	0.083 (6)	-0.007 (4)	-0.023 (4)	-0.021 (4)
O00A	0.021 (4)	0.033 (4)	0.038 (5)	0.004 (3)	-0.005 (3)	-0.002 (3)
F00B	0.059 (5)	0.045 (4)	0.062 (5)	-0.007 (4)	0.023 (4)	-0.002 (4)

O00C	0.028 (5)	0.032 (4)	0.054 (6)	-0.004 (3)	-0.002 (4)	0.003 (4)
F00D	0.040 (5)	0.035 (4)	0.097 (6)	0.007 (3)	0.022 (4)	0.001 (4)
O00E	0.015 (4)	0.047 (5)	0.045 (5)	0.002 (3)	-0.003 (3)	-0.010 (4)
O00F	0.026 (4)	0.028 (4)	0.039 (5)	-0.001 (3)	-0.005 (3)	0.002 (3)
O00G	0.035 (5)	0.051 (5)	0.048 (6)	0.004 (4)	-0.007 (4)	-0.004 (4)
F00H	0.091 (7)	0.043 (5)	0.054 (5)	-0.003 (4)	0.006 (5)	-0.006 (4)
O00I	0.023 (5)	0.050 (5)	0.048 (5)	0.000 (4)	-0.002 (4)	-0.012 (4)
F00J	0.067 (6)	0.044 (5)	0.114 (8)	-0.014 (4)	-0.016 (5)	0.030 (5)
O00K	0.031 (5)	0.044 (5)	0.038 (5)	0.006 (4)	0.001 (4)	-0.008 (4)
F00L	0.072 (6)	0.081 (6)	0.043 (5)	0.008 (5)	-0.028 (4)	-0.013 (4)
F00M	0.068 (6)	0.078 (6)	0.060 (5)	-0.020 (5)	0.013 (5)	-0.038 (4)
O00N	0.022 (5)	0.072 (6)	0.048 (6)	0.001 (4)	0.010 (4)	-0.001 (5)
N00O	0.026 (5)	0.036 (5)	0.039 (6)	-0.001 (4)	0.000 (4)	0.008 (4)
O00P	0.027 (4)	0.052 (5)	0.029 (4)	-0.002 (4)	-0.008 (3)	-0.005 (4)
O00Q	0.026 (4)	0.035 (4)	0.043 (5)	-0.006 (3)	0.004 (4)	-0.001 (4)
O00R	0.041 (6)	0.061 (6)	0.038 (5)	0.001 (4)	-0.005 (4)	-0.011 (4)
N00S	0.020 (5)	0.041 (5)	0.019 (5)	0.002 (4)	-0.005 (4)	-0.002 (4)
F00T	0.047 (5)	0.084 (6)	0.091 (7)	-0.018 (5)	0.028 (5)	-0.026 (5)
N00U	0.028 (5)	0.032 (5)	0.032 (5)	-0.005 (4)	-0.005 (4)	0.001 (4)
N00V	0.015 (5)	0.034 (5)	0.038 (6)	-0.001 (4)	-0.006 (4)	-0.004 (4)
N00W	0.020 (5)	0.035 (5)	0.041 (6)	-0.002 (4)	-0.007 (4)	0.005 (4)
O00X	0.044 (6)	0.059 (6)	0.050 (6)	-0.014 (4)	0.013 (5)	-0.017 (4)
N00Y	0.035 (6)	0.034 (5)	0.029 (5)	0.011 (4)	-0.011 (4)	-0.005 (4)
F00Z	0.075 (11)	0.029 (8)	0.034 (10)	-0.022 (7)	0.008 (9)	-0.010 (9)
N010	0.030 (6)	0.033 (5)	0.044 (6)	0.006 (4)	0.005 (5)	-0.003 (4)
N011	0.032 (6)	0.033 (5)	0.044 (6)	-0.014 (4)	-0.006 (5)	0.003 (4)
N012	0.028 (5)	0.027 (5)	0.029 (5)	-0.001 (4)	-0.004 (4)	-0.001 (4)
F013	0.022 (4)	0.094 (7)	0.117 (8)	0.017 (4)	-0.013 (5)	-0.031 (6)
N014	0.026 (6)	0.047 (6)	0.039 (6)	0.009 (4)	0.005 (4)	0.003 (5)
N015	0.020 (5)	0.029 (5)	0.040 (6)	0.000 (4)	-0.008 (4)	0.010 (4)
N016	0.020 (5)	0.034 (5)	0.038 (6)	0.000 (4)	-0.007 (4)	-0.002 (4)
N017	0.028 (5)	0.040 (6)	0.026 (5)	-0.002 (4)	-0.005 (4)	0.006 (4)
F018	0.108 (9)	0.082 (7)	0.070 (7)	-0.002 (6)	0.008 (6)	-0.032 (5)
N019	0.028 (5)	0.033 (5)	0.039 (6)	0.003 (4)	-0.002 (4)	-0.001 (4)
N01A	0.037 (6)	0.032 (5)	0.027 (5)	-0.006 (4)	-0.004 (4)	0.006 (4)
F01B	0.112 (9)	0.143 (10)	0.064 (6)	-0.048 (7)	-0.052 (6)	0.052 (7)
F01C	0.046 (6)	0.175 (11)	0.053 (6)	0.001 (6)	-0.011 (4)	0.038 (6)
N01D	0.034 (6)	0.032 (5)	0.041 (6)	0.003 (4)	-0.010 (5)	-0.002 (4)
N01E	0.028 (6)	0.047 (6)	0.052 (7)	-0.005 (5)	0.002 (5)	0.009 (5)
N01F	0.016 (4)	0.030 (5)	0.027 (5)	0.002 (4)	-0.005 (4)	0.003 (4)

F01G	0.075 (7)	0.114 (8)	0.052 (6)	-0.015 (6)	-0.002 (5)	0.003 (5)
F01H	0.116 (9)	0.049 (5)	0.126 (9)	-0.003 (5)	-0.080 (7)	0.019 (5)
N01I	0.020 (5)	0.042 (6)	0.038 (6)	-0.003 (4)	-0.004 (4)	0.000 (4)
N01J	0.020 (5)	0.045 (6)	0.036 (6)	-0.002 (4)	-0.003 (4)	-0.005 (4)
N01K	0.038 (6)	0.032 (5)	0.044 (6)	-0.009 (5)	-0.002 (5)	0.008 (4)
F01L	0.120 (10)	0.094 (8)	0.082 (8)	0.002 (7)	-0.006 (7)	-0.039 (6)
N01M	0.020 (5)	0.033 (5)	0.036 (6)	0.000 (4)	-0.006 (4)	0.003 (4)
N01N	0.017 (5)	0.027 (5)	0.045 (6)	-0.006 (4)	0.001 (4)	0.011 (4)
F01O	0.157 (11)	0.072 (7)	0.093 (8)	-0.056 (7)	-0.057 (7)	0.042 (6)
F01P	0.116 (9)	0.100 (8)	0.136 (10)	0.080 (7)	0.063 (8)	0.060 (7)
C01Q	0.016 (5)	0.029 (6)	0.024 (5)	-0.004 (4)	-0.005 (4)	0.004 (4)
N01R	0.024 (5)	0.032 (5)	0.044 (6)	-0.013 (4)	-0.002 (4)	0.008 (4)
C01S	0.024 (6)	0.035 (6)	0.028 (6)	-0.001 (5)	-0.008 (5)	0.006 (5)
N01T	0.017 (5)	0.036 (5)	0.045 (6)	0.002 (4)	-0.015 (4)	-0.002 (4)
N01U	0.031 (6)	0.037 (6)	0.047 (6)	-0.002 (4)	0.004 (5)	0.002 (5)
F01V	0.153 (11)	0.063 (6)	0.085 (7)	-0.040 (6)	0.015 (7)	-0.018 (5)
N01W	0.024 (5)	0.033 (5)	0.032 (5)	0.000 (4)	-0.010 (4)	-0.001 (4)
N01X	0.028 (5)	0.034 (5)	0.033 (5)	-0.001 (4)	-0.007 (4)	0.001 (4)
C01Y	0.014 (5)	0.026 (6)	0.035 (6)	-0.002 (4)	-0.005 (4)	0.004 (5)
C01Z	0.019 (5)	0.030 (6)	0.017 (5)	-0.001 (4)	-0.001 (4)	0.001 (4)
C020	0.020 (6)	0.033 (6)	0.024 (6)	0.002 (4)	-0.002 (4)	-0.002 (4)
C021	0.010 (5)	0.032 (6)	0.031 (6)	-0.002 (4)	-0.005 (4)	-0.005 (5)
C022	0.022 (6)	0.027 (6)	0.028 (6)	0.000 (4)	0.003 (5)	-0.002 (4)
C023	0.017 (5)	0.028 (6)	0.032 (6)	0.004 (4)	-0.003 (4)	-0.006 (4)
F024	0.034 (6)	0.071 (7)	0.243 (15)	-0.016 (5)	-0.004 (7)	0.011 (8)
C025	0.028 (7)	0.046 (7)	0.033 (7)	0.000 (5)	-0.005 (5)	0.004 (5)
F026	0.116 (10)	0.056 (6)	0.128 (10)	-0.019 (6)	-0.004 (7)	-0.022 (6)
C027	0.026 (6)	0.028 (6)	0.026 (6)	0.002 (5)	-0.003 (5)	-0.005 (4)
C028	0.039 (8)	0.043 (8)	0.043 (8)	0.003 (6)	-0.002 (6)	-0.007 (6)
C029	0.019 (6)	0.023 (5)	0.036 (6)	0.004 (4)	-0.002 (5)	-0.002 (4)
C02A	0.022 (6)	0.044 (7)	0.033 (7)	-0.002 (5)	-0.003 (5)	0.002 (5)
C02B	0.015 (6)	0.037 (7)	0.049 (7)	0.000 (5)	-0.009 (5)	-0.014 (5)
C02C	0.032 (7)	0.021 (6)	0.048 (8)	0.003 (5)	-0.008 (5)	-0.006 (5)
F02D	0.187 (14)	0.087 (8)	0.107 (9)	-0.048 (8)	-0.104 (9)	0.016 (6)
C02E	0.019 (6)	0.030 (6)	0.027 (6)	0.000 (4)	-0.001 (4)	0.003 (4)
C02F	0.024 (6)	0.042 (7)	0.040 (7)	-0.005 (5)	0.002 (5)	0.007 (5)
F02G	0.095 (9)	0.114 (9)	0.141 (10)	-0.057 (7)	0.071 (8)	-0.035 (7)
F02H	0.111 (12)	0.096 (10)	0.26 (2)	-0.010 (8)	0.052 (12)	0.074 (12)
C02I	0.022 (6)	0.029 (6)	0.044 (7)	-0.002 (5)	-0.006 (5)	0.000 (5)
C02J	0.017 (6)	0.030 (6)	0.045 (7)	0.001 (5)	-0.004 (5)	-0.010 (5)

C02K	0.032 (7)	0.028 (6)	0.047 (8)	0.009 (5)	-0.002 (6)	-0.006 (5)
C02L	0.027 (6)	0.032 (6)	0.028 (6)	-0.002 (5)	-0.011 (5)	0.002 (5)
C02M	0.031 (7)	0.042 (7)	0.025 (6)	0.003 (5)	-0.002 (5)	0.008 (5)
C02N	0.035 (7)	0.042 (7)	0.048 (8)	0.012 (6)	0.013 (6)	-0.003 (6)
C02O	0.018 (6)	0.051 (7)	0.032 (7)	0.004 (5)	-0.007 (5)	-0.011 (5)
C02P	0.028 (7)	0.027 (6)	0.047 (7)	0.003 (5)	-0.006 (5)	-0.004 (5)
C02Q	0.043 (8)	0.029 (7)	0.056 (9)	0.002 (6)	-0.014 (7)	-0.001 (6)
C02R	0.040 (8)	0.050 (8)	0.028 (7)	-0.001 (6)	0.000 (5)	-0.005 (5)
C02S	0.022 (7)	0.049 (8)	0.065 (9)	-0.002 (6)	-0.004 (6)	0.007 (7)
F02T	0.062 (7)	0.217 (14)	0.063 (7)	0.029 (8)	0.000 (5)	-0.032 (7)
F46	0.144 (16)	0.095 (10)	0.077 (11)	0.062 (12)	0.074 (11)	0.032 (10)
C02V	0.046 (8)	0.052 (8)	0.031 (7)	-0.001 (6)	-0.003 (6)	0.006 (6)
C02W	0.032 (7)	0.042 (7)	0.041 (7)	0.003 (5)	-0.013 (6)	0.007 (6)
C02X	0.025 (6)	0.020 (6)	0.047 (7)	0.007 (4)	0.005 (5)	-0.004 (5)
C02Y	0.028 (6)	0.043 (7)	0.032 (7)	0.010 (5)	-0.006 (5)	0.004 (5)
C02Z	0.041 (8)	0.028 (6)	0.051 (8)	0.002 (5)	-0.005 (6)	0.002 (5)
C030	0.042 (8)	0.025 (6)	0.066 (9)	0.003 (5)	-0.007 (7)	-0.015 (6)
C031	0.027 (7)	0.051 (8)	0.057 (9)	0.003 (6)	0.003 (6)	-0.009 (6)
C032	0.050 (9)	0.031 (7)	0.054 (9)	0.007 (6)	-0.020 (7)	-0.003 (6)
F033	0.049 (7)	0.29 (2)	0.099 (9)	0.032 (9)	-0.036 (7)	-0.029 (10)
C034	0.019 (6)	0.038 (7)	0.050 (8)	0.008 (5)	0.002 (5)	0.008 (5)
C035	0.023 (6)	0.038 (7)	0.044 (7)	0.006 (5)	-0.009 (5)	-0.009 (5)
C036	0.031 (7)	0.037 (7)	0.043 (7)	0.000 (5)	0.004 (6)	0.007 (5)
C037	0.045 (8)	0.045 (8)	0.039 (7)	0.010 (6)	-0.003 (6)	0.007 (6)
C038	0.040 (8)	0.052 (8)	0.025 (6)	0.012 (6)	-0.013 (5)	0.001 (5)
C039	0.015 (5)	0.030 (6)	0.036 (6)	-0.001 (4)	-0.005 (4)	0.000 (5)
C03A	0.024 (7)	0.049 (8)	0.063 (9)	-0.002 (6)	-0.020 (6)	-0.007 (7)
C03B	0.028 (7)	0.034 (7)	0.045 (8)	0.007 (5)	-0.002 (6)	0.016 (6)
F03C	0.046 (7)	0.168 (12)	0.252 (17)	0.005 (7)	0.006 (8)	-0.164 (12)
C03D	0.055 (9)	0.026 (6)	0.051 (8)	-0.015 (6)	-0.005 (7)	0.006 (5)
C03E	0.029 (7)	0.036 (7)	0.056 (8)	0.000 (5)	-0.013 (6)	0.002 (6)
C03F	0.034 (7)	0.037 (7)	0.038 (7)	0.006 (5)	0.001 (5)	-0.003 (5)
C03G	0.035 (7)	0.046 (8)	0.036 (7)	0.013 (6)	-0.006 (6)	0.000 (6)
C03H	0.025 (7)	0.046 (8)	0.051 (8)	0.001 (5)	-0.010 (6)	0.013 (6)
C03I	0.021 (7)	0.056 (8)	0.049 (8)	0.000 (6)	0.004 (6)	-0.009 (6)
C03J	0.042 (9)	0.047 (8)	0.051 (9)	-0.004 (6)	-0.005 (7)	-0.004 (7)
C03K	0.040 (8)	0.052 (8)	0.041 (8)	-0.015 (6)	0.009 (6)	-0.005 (6)
C03L	0.050 (9)	0.027 (7)	0.061 (9)	0.002 (6)	-0.013 (7)	0.004 (6)
C03M	0.035 (7)	0.047 (8)	0.037 (7)	-0.007 (6)	-0.008 (6)	0.001 (6)
C03N	0.034 (8)	0.047 (8)	0.056 (9)	0.009 (6)	-0.005 (6)	-0.003 (6)

C03O	0.024 (7)	0.052 (8)	0.040 (7)	-0.009 (5)	-0.003 (5)	0.002 (6)
C03P	0.033 (7)	0.025 (6)	0.057 (8)	0.004 (5)	-0.003 (6)	-0.005 (5)
C03Q	0.028 (7)	0.053 (8)	0.035 (7)	0.003 (6)	0.004 (5)	0.007 (6)
C03R	0.019 (6)	0.055 (8)	0.049 (8)	-0.005 (5)	-0.001 (5)	-0.006 (6)
C03S	0.033 (7)	0.047 (8)	0.032 (7)	-0.001 (6)	0.002 (5)	0.005 (5)
F03T	0.102 (18)	0.070 (13)	0.080 (11)	0.018 (11)	-0.039 (12)	-0.009 (11)
C03U	0.042 (8)	0.025 (6)	0.069 (10)	-0.011 (5)	-0.007 (7)	-0.009 (6)
C03V	0.030 (7)	0.027 (6)	0.047 (8)	0.006 (5)	-0.012 (6)	0.000 (5)
C03W	0.033 (8)	0.074 (10)	0.046 (8)	-0.001 (7)	-0.003 (6)	-0.015 (7)
C03X	0.026 (7)	0.059 (9)	0.031 (7)	0.002 (6)	-0.002 (5)	0.003 (6)
F03Y	0.177 (15)	0.133 (11)	0.169 (14)	-0.103 (11)	0.085 (12)	-0.082 (10)
C03Z	0.014 (5)	0.036 (6)	0.032 (6)	-0.006 (4)	-0.003 (5)	-0.001 (5)
C040	0.025 (7)	0.070 (10)	0.050 (8)	0.004 (6)	-0.005 (6)	-0.015 (7)
C041	0.033 (7)	0.038 (7)	0.033 (7)	0.000 (5)	-0.002 (5)	-0.009 (5)
F042	0.102 (16)	0.061 (12)	0.094 (11)	0.038 (12)	-0.019 (11)	-0.005 (12)
F043	0.118 (17)	0.063 (9)	0.102 (12)	0.028 (12)	-0.012 (12)	-0.014 (9)
C044	0.026 (8)	0.070 (11)	0.081 (12)	0.010 (7)	0.014 (8)	0.011 (9)
C045	0.031 (7)	0.040 (7)	0.035 (7)	-0.002 (5)	-0.012 (5)	0.001 (5)
C046	0.040 (8)	0.061 (9)	0.037 (7)	-0.009 (6)	-0.011 (6)	0.003 (6)
C047	0.056 (9)	0.038 (7)	0.051 (9)	-0.010 (7)	0.001 (7)	0.002 (6)
C048	0.041 (8)	0.049 (8)	0.036 (7)	-0.010 (6)	-0.008 (6)	0.001 (6)
B049	0.025 (7)	0.035 (7)	0.046 (9)	-0.008 (6)	0.002 (6)	0.010 (6)
C04A	0.026 (7)	0.066 (10)	0.057 (9)	0.007 (7)	-0.002 (6)	0.012 (7)
C04B	0.047 (9)	0.070 (10)	0.052 (9)	-0.004 (8)	0.010 (7)	-0.013 (7)
B04C	0.022 (7)	0.021 (6)	0.047 (8)	-0.004 (5)	-0.011 (6)	0.001 (5)
C04D	0.052 (9)	0.074 (10)	0.051 (9)	0.012 (8)	0.036 (8)	0.022 (8)
C04E	0.048 (9)	0.042 (8)	0.066 (10)	0.004 (7)	-0.009 (8)	0.015 (7)
F04F	0.136 (17)	0.039 (8)	0.066 (10)	-0.019 (11)	0.028 (11)	-0.022 (7)
C04G	0.027 (7)	0.058 (9)	0.075 (11)	-0.003 (6)	-0.002 (7)	-0.010 (7)
C04H	0.024 (7)	0.064 (9)	0.045 (8)	-0.005 (6)	-0.003 (6)	-0.011 (7)
F04I	0.059 (11)	0.048 (9)	0.174 (17)	0.018 (8)	0.013 (12)	-0.009 (13)
C04J	0.043 (8)	0.033 (7)	0.069 (10)	-0.011 (6)	0.011 (7)	-0.001 (6)
C04K	0.042 (9)	0.044 (8)	0.077 (11)	0.005 (7)	-0.005 (8)	-0.003 (8)
C04L	0.059 (10)	0.062 (10)	0.051 (9)	-0.025 (8)	0.019 (8)	-0.014 (7)
C04M	0.042 (10)	0.080 (13)	0.102 (15)	-0.009 (9)	0.032 (10)	-0.019 (11)
C04N	0.046 (9)	0.091 (13)	0.063 (10)	-0.018 (9)	0.025 (8)	-0.022 (9)
C04O	0.033 (8)	0.054 (10)	0.097 (14)	0.010 (7)	-0.005 (8)	-0.027 (9)
C04P	0.071 (11)	0.022 (6)	0.057 (9)	-0.001 (6)	-0.002 (8)	0.001 (6)
C04Q	0.070 (11)	0.056 (9)	0.035 (8)	-0.003 (7)	-0.019 (7)	0.001 (6)
F44	0.166 (18)	0.094 (11)	0.127 (16)	0.057 (12)	0.084 (13)	0.019 (10)

C04S	0.093 (13)	0.051 (9)	0.037 (8)	-0.007 (8)	-0.014 (8)	0.010 (7)
B04T	0.047 (9)	0.032 (8)	0.044 (9)	0.004 (6)	-0.012 (7)	0.007 (6)
B04U	0.027 (8)	0.058 (10)	0.054 (10)	-0.006 (7)	0.009 (7)	0.012 (8)
C04V	0.065 (13)	0.139 (19)	0.107 (17)	-0.008 (12)	0.015 (12)	-0.042 (14)
C04W	0.068 (14)	0.096 (15)	0.085 (15)	0.007 (11)	-0.001 (11)	-0.004 (12)
C04X	0.035 (9)	0.091 (12)	0.056 (10)	-0.010 (8)	-0.011 (7)	0.026 (9)
C04Y	0.091 (17)	0.083 (14)	0.097 (16)	-0.026 (12)	0.037 (13)	-0.034 (12)
C04Z	0.048 (10)	0.080 (13)	0.088 (14)	0.006 (9)	0.036 (9)	-0.016 (11)
F45	0.137 (16)	0.127 (13)	0.107 (12)	0.071 (11)	0.039 (12)	0.038 (11)
C051	0.050 (10)	0.104 (14)	0.047 (10)	0.013 (9)	-0.014 (8)	-0.012 (9)
C052	0.108 (16)	0.060 (10)	0.083 (10)	0.026 (11)	-0.024 (11)	-0.004 (9)
C053	0.058 (13)	0.15 (2)	0.14 (2)	0.020 (14)	0.042 (14)	0.10 (2)
C054	0.039 (10)	0.17 (2)	0.073 (14)	-0.026 (14)	0.015 (9)	0.009 (16)
C055	0.054 (12)	0.070 (13)	0.13 (2)	-0.010 (9)	0.026 (13)	0.003 (13)
F13	0.161 (18)	0.101 (14)	0.114 (16)	0.080 (14)	0.055 (16)	0.007 (13)
F14	0.136 (18)	0.108 (14)	0.102 (16)	0.053 (15)	0.075 (15)	0.043 (14)
F25	0.15 (2)	0.110 (15)	0.108 (17)	0.063 (15)	0.060 (16)	0.038 (14)
F1	0.112 (15)	0.037 (9)	0.102 (13)	0.002 (12)	0.047 (13)	-0.012 (10)
F6	0.045 (13)	0.044 (11)	0.14 (2)	0.017 (9)	0.006 (13)	-0.013 (14)
F18	0.066 (12)	0.033 (9)	0.094 (19)	-0.016 (9)	-0.005 (14)	-0.037 (15)
F17	0.101 (16)	0.056 (11)	0.086 (11)	0.025 (11)	-0.019 (10)	0.000 (11)
F20	0.117 (19)	0.068 (12)	0.073 (11)	0.024 (12)	-0.039 (13)	0.007 (10)
F35	0.118 (18)	0.067 (9)	0.105 (12)	0.023 (13)	0.003 (13)	-0.010 (10)
C18	0.108 (16)	0.058 (10)	0.082 (10)	0.025 (11)	-0.024 (11)	-0.008 (9)

Geometric parameters (Å, º)

Yb01—O005	2.405 (7)	C02M—C03F	1.357 (16)
Yb01—O008	2.296 (7)	C02N—H02N	0.9300
Yb01—N010	2.420 (9)	C02N—C04B	1.371 (18)
Yb01—N014	2.463 (10)	C02O—H02O	0.9300
Yb01—N017	2.412 (9)	C02O—C038	1.371 (17)
Yb01—N01N	2.465 (8)	C02P—H02P	0.9300
Yb01—N01R	2.461 (9)	C02P—C02X	1.396 (15)
Yb01—N01X	2.448 (9)	C02Q—H02A	0.9700
Yb01—C01Y	3.102 (11)	C02Q—H02D	0.9700
Yb01—C022	3.162 (11)	C02Q—C03G	1.395 (17)
Yb02—O006	2.336 (7)	C02Q—C03U	1.385 (18)
Yb02—O00A	2.340 (7)	C02R—H02R	0.9300

Yb02—N00V	2.399 (9)	C02R—C04P	1.414 (17)
Yb02—N00W	2.500 (9)	C02S—H02S	0.9300
Yb02—N01A	2.459 (9)	C02S—C03A	1.344 (18)
Yb02—N01I	2.389 (10)	F02T—C051	1.306 (17)
Yb02—N01M	2.487 (9)	F46—C04W	1.331 (10)
Yb02—C01S	3.110 (11)	F46—F13	1.43 (4)
Yb02—N01T	2.449 (9)	F46—F14	0.82 (5)
Yb02—C01Z	3.116 (10)	C02V—H02V	0.9300
Eu03—O007	2.373 (8)	C02V—C038	1.370 (17)
Eu03—O00C	2.382 (8)	C02W—H02W	0.9300
Eu03—O00E	2.395 (7)	C02W—C03B	1.363 (17)
Eu03—O00F	2.370 (8)	C02X—H02X	0.9300
Eu03—O00I	2.338 (8)	C02Y—H02Y	0.9300
Eu03—O00P	2.412 (8)	C02Y—C03P	1.366 (16)
Eu03—N00S	2.557 (9)	C02Z—H02Z	0.9300
Eu03—N01F	2.588 (8)	C02Z—C03P	1.371 (16)
Eu04—O00G	2.374 (9)	C030—H030	0.9300
Eu04—O00K	2.402 (8)	C030—C035	1.370 (17)
Eu04—O00N	2.369 (8)	C030—C03L	1.370 (18)
Eu04—O00Q	2.374 (8)	C031—H031	0.9300
Eu04—O00R	2.372 (8)	C031—C03I	1.397 (17)
Eu04—O00X	2.336 (9)	C032—H032	0.9300
Eu04—N012	2.578 (9)	C032—C040	1.396 (18)
Eu04—N019	2.540 (9)	F033—C04X	1.296 (19)
O005—C022	1.280 (12)	C034—H034	0.9300
O006—C01S	1.269 (12)	C034—C04G	1.363 (17)
O007—C03Q	1.240 (14)	C035—H035	0.9300
O008—C01Y	1.262 (12)	C036—H036	0.9300
F009—C04A	1.330 (16)	C036—C03N	1.417 (17)
O00A—C01Z	1.264 (12)	C037—H037	0.9300
F00B—C04J	1.328 (14)	C037—C03M	1.409 (17)
O00C—C03B	1.263 (14)	C038—H038	0.9300
F00D—C04J	1.328 (15)	C039—C03Z	1.438 (15)
O00E—C02F	1.254 (14)	C03A—H03A	0.9300
O00F—C02A	1.259 (13)	C03B—C04E	1.556 (17)
O00G—C04Q	1.250 (15)	F03C—C04O	1.290 (16)
F00H—C048	1.327 (14)	C03D—H03D	0.9300
O00I—C03I	1.258 (14)	C03D—C04P	1.334 (19)
F00J—C04E	1.303 (16)	C03E—H03E	0.9300
O00K—C045	1.270 (14)	C03E—C040	1.431 (17)

F00L—C048	1.328 (14)	C03F—H03F	0.9300
F00M—C04J	1.344 (15)	C03G—H03G	0.9300
O00N—C03W	1.208 (16)	C03H—C03N	1.374 (18)
N00O—N00W	1.393 (12)	C03I—C04O	1.513 (19)
N00O—C02V	1.334 (14)	C03J—C03Q	1.533 (18)
N00O—B049	1.525 (16)	C03K—H03K	0.9300
O00P—C03X	1.259 (14)	C03K—C03O	1.377 (17)
O00Q—C041	1.252 (14)	C03K—C047	1.361 (19)
O00R—C04H	1.253 (16)	C03L—H03L	0.9300
N00S—C02B	1.339 (14)	C03M—H03M	0.9300
N00S—C039	1.362 (13)	C03O—H03O	0.9300
F00T—C048	1.321 (15)	C03P—H03P	0.9300
N00U—N01A	1.380 (12)	C03Q—C046	1.390 (16)
N00U—C047	1.344 (16)	C03R—H03R	0.9300
N00U—B04T	1.548 (18)	C03R—C04G	1.350 (19)
N00V—N011	1.378 (13)	C03S—H03S	0.9300
N00V—C03G	1.327 (14)	C03S—C041	1.377 (16)
N00W—C02O	1.335 (13)	C03S—C045	1.374 (17)
O00X—C04L	1.255 (16)	F03T—C052	1.331 (10)
N00Y—N01T	1.362 (13)	F03T—F20	0.63 (5)
N00Y—C032	1.350 (15)	F03T—C18	1.43 (7)
N00Y—B04T	1.535 (18)	C03U—H03U	0.9300
F00Z—C04K	1.335 (7)	C03V—H03V	0.9300
F00Z—F18	0.56 (3)	C03W—C04N	1.41 (2)
N010—N01K	1.350 (13)	C03W—C04W	1.52 (2)
N010—C02R	1.315 (15)	C03X—C046	1.373 (18)
N011—C03U	1.324 (14)	C03X—C04X	1.524 (18)
N011—B049	1.565 (17)	F03Y—C04Y	1.36 (2)
N012—C01Q	1.364 (13)	C040—H04A	0.9700
N012—C02L	1.317 (13)	C040—H04E	0.9700
F013—C04A	1.306 (15)	C041—C04J	1.517 (18)
N014—N01E	1.402 (14)	F042—C052	1.335 (10)
N014—C02N	1.319 (15)	F042—F17	0.66 (4)
N015—N01N	1.368 (12)	F042—C18	1.66 (7)
N015—C03H	1.364 (15)	F043—C052	1.334 (10)
N015—B04C	1.545 (17)	F043—F17	1.53 (5)
N016—N017	1.354 (12)	F043—F35	0.67 (5)
N016—C02Z	1.347 (14)	F043—C18	1.13 (7)
N016—B04C	1.534 (15)	C044—H044	0.9300
N017—C02Y	1.305 (14)	C044—C04M	1.37 (2)

F018—C051	1.32 (2)	C044—C04Z	1.34 (2)
N019—C021	1.353 (13)	C045—C04K	1.525 (16)
N019—C02K	1.327 (14)	C046—H046	0.9300
N01A—C03O	1.336 (15)	C047—H047	0.9300
F01B—C04X	1.272 (16)	B049—H049	0.9800
F01C—C04A	1.305 (15)	C04B—H04B	0.9300
N01D—N01I	1.362 (13)	C04B—C04D	1.36 (2)
N01D—C03L	1.349 (15)	B04C—H04C	0.9800
N01D—B04T	1.519 (17)	C04D—H04D	0.9300
N01E—C04D	1.365 (16)	F04F—C04K	1.340 (7)
N01E—B04U	1.502 (19)	F04F—F1	1.10 (3)
N01F—C02X	1.318 (13)	F04F—F18	1.71 (3)
N01F—C03Z	1.373 (13)	C04G—H04G	0.9300
F01G—C051	1.344 (19)	C04H—C04S	1.339 (19)
F01H—C04E	1.305 (16)	C04H—C051	1.54 (2)
N01I—C035	1.339 (14)	F04I—C04K	1.334 (7)
N01J—N01M	1.356 (13)	F04I—F1	1.36 (3)
N01J—C03R	1.339 (14)	F04I—F6	0.78 (3)
N01J—B049	1.517 (16)	C04K—F1	1.328 (10)
N01K—C03D	1.344 (15)	C04K—F6	1.356 (10)
N01K—B04U	1.567 (18)	C04K—F18	1.328 (10)
F01L—C04O	1.310 (18)	C04L—C04N	1.37 (2)
N01M—C034	1.333 (14)	C04L—C04Y	1.54 (2)
N01N—C036	1.328 (14)	C04M—H04M	0.9300
F01O—C03J	1.294 (16)	C04M—C054	1.37 (3)
F01P—C04E	1.294 (17)	C04N—H04N	0.9300
C01Q—C020	1.392 (14)	C04P—H04P	0.9300
C01Q—C021	1.476 (14)	C04Q—C04S	1.39 (2)
N01R—N01U	1.382 (13)	C04Q—C052	1.56 (5)
N01R—C025	1.329 (14)	C04Q—C18	1.51 (5)
C01S—C01Z	1.448 (15)	F44—C04W	1.336 (10)
C01S—C029	1.471 (14)	F44—F13	1.25 (4)
N01T—C03E	1.331 (14)	F44—F25	0.90 (6)
N01U—C02S	1.358 (15)	C04S—H04S	0.9300
N01U—B04U	1.550 (18)	B04T—H04T	0.9800
F01V—C03J	1.334 (16)	B04U—H04U	0.9800
N01W—N01X	1.373 (12)	C04V—H04F	0.9600
N01W—C028	1.345 (15)	C04V—H04H	0.9600
N01W—B04C	1.517 (15)	C04V—H04I	0.9600
N01X—C03M	1.322 (15)	C04V—C04Z	1.46 (3)

C01Y—C022	1.421 (14)	C04W—F45	1.346 (10)
C01Y—C027	1.461 (15)	C04W—F13	1.347 (10)
C01Z—C02E	1.444 (14)	C04W—F14	1.330 (10)
C020—C022	1.458 (14)	C04W—F25	1.332 (10)
C020—C02C	1.400 (15)	C04Z—C055	1.33 (3)
C021—C027	1.387 (14)	F45—F14	1.68 (4)
C023—H023	0.9300	F45—F25	1.29 (6)
C023—C02E	1.424 (14)	C052—F17	1.09 (6)
C023—C02J	1.355 (14)	C052—F20	1.40 (7)
F024—C03J	1.252 (16)	C052—F35	1.65 (7)
C025—H025	0.9300	C053—H053	0.9300
C025—C03A	1.402 (17)	C053—C054	1.37 (3)
F026—C04O	1.318 (19)	C053—C055	1.37 (3)
C027—C02M	1.413 (15)	C054—H054	0.9300
C028—H028	0.9300	C055—H055	0.9300
C028—C037	1.369 (17)	C1—H1A	0.9700
C029—C02I	1.415 (15)	C1—H1B	0.9700
C029—C03Z	1.400 (14)	C1—C5	1.10 (5)
C02A—C02W	1.378 (16)	C1—C11	1.27 (6)
C02A—C048	1.519 (17)	C3—H3A	0.9600
C02B—H02B	0.9300	C3—H3B	0.9600
C02B—C02J	1.384 (15)	C3—H3C	0.9600
C02C—H02C	0.9300	C3—C5	1.45 (4)
C02C—C03V	1.386 (16)	C5—H5A	0.9700
F02D—C04X	1.297 (19)	C5—H5B	0.9700
C02E—C039	1.405 (14)	C10—H10A	0.9600
C02F—C031	1.384 (17)	C10—H10B	0.9600
C02F—C04A	1.552 (17)	C10—H10C	0.9600
F02G—C04Y	1.31 (2)	C10—C14	1.43 (5)
F02H—C04Y	1.28 (3)	C11—H11A	0.9700
C02I—H02I	0.9300	C11—H11B	0.9700
C02I—C02P	1.373 (15)	C11—C14	1.40 (6)
C02J—H02J	0.9300	C14—H14A	0.9700
C02K—H02K	0.9300	C14—H14B	0.9700
C02K—C03F	1.401 (16)	F17—C18	1.335 (10)
C02L—H02L	0.9300	F20—C18	1.332 (10)
C02L—C03V	1.392 (15)	F35—C18	1.339 (10)
C02M—H02M	0.9300		
O005—Yb01—N010	132.7 (3)	N00S—C039—C02E	121.8 (10)

O005—Yb01—N014	126.0 (3)	N00S—C039—C03Z	117.4 (9)
O005—Yb01—N017	75.1 (3)	C02E—C039—C03Z	120.6 (9)
O005—Yb01—N01N	78.7 (3)	C025—C03A—H03A	126.5
O005—Yb01—N01R	74.6 (3)	C02S—C03A—C025	107.0 (11)
O005—Yb01—N01X	145.0 (3)	C02S—C03A—H03A	126.5
O005—Yb01—C01Y	47.7 (3)	O00C—C03B—C02W	128.0 (10)
O005—Yb01—C022	21.6 (2)	O00C—C03B—C04E	113.6 (11)
O008—Yb01—O005	68.6 (2)	C02W—C03B—C04E	118.5 (11)
O008—Yb01—N010	71.4 (3)	N01K—C03D—H03D	124.8
O008—Yb01—N014	144.8 (3)	C04P—C03D—N01K	110.5 (11)
O008—Yb01—N017	137.2 (3)	C04P—C03D—H03D	124.8
O008—Yb01—N01N	74.6 (3)	N01T—C03E—H03E	124.7
O008—Yb01—N01R	83.2 (3)	N01T—C03E—C040	110.6 (11)
O008—Yb01—N01X	117.0 (3)	C040—C03E—H03E	124.7
O008—Yb01—C01Y	21.0 (3)	C02K—C03F—H03F	121.1
O008—Yb01—C022	47.1 (3)	C02M—C03F—C02K	117.9 (11)
N010—Yb01—N014	78.2 (3)	C02M—C03F—H03F	121.1
N010—Yb01—N01N	113.6 (3)	N00V—C03G—C02Q	110.5 (11)
N010—Yb01—N01R	76.7 (3)	N00V—C03G—H03G	124.8
N010—Yb01—N01X	76.8 (3)	C02Q—C03G—H03G	124.8
N010—Yb01—C01Y	89.8 (3)	N015—C03H—C03N	108.2 (11)
N010—Yb01—C022	113.4 (3)	O00I—C03I—C031	127.9 (12)
N014—Yb01—N01N	135.6 (3)	O00I—C03I—C04O	113.9 (11)
N014—Yb01—C01Y	149.6 (3)	C031—C03I—C04O	118.1 (11)
N014—Yb01—C022	140.4 (3)	F01O—C03J—F01V	103.7 (13)
N017—Yb01—N010	150.6 (3)	F01O—C03J—C03Q	115.1 (11)
N017—Yb01—N014	76.1 (3)	F01V—C03J—C03Q	108.1 (11)
N017—Yb01—N01N	76.7 (3)	F024—C03J—F01O	112.0 (14)
N017—Yb01—N01R	108.6 (3)	F024—C03J—F01V	102.3 (13)
N017—Yb01—N01X	81.6 (3)	F024—C03J—C03Q	114.1 (12)
N017—Yb01—C01Y	119.6 (3)	C03O—C03K—H03K	127.4
N017—Yb01—C022	95.5 (3)	C047—C03K—H03K	127.4
N01N—Yb01—C01Y	74.8 (3)	C047—C03K—C03O	105.3 (12)
N01N—Yb01—C022	76.5 (3)	N01D—C03L—C030	109.1 (11)
N01R—Yb01—N014	72.8 (3)	N01D—C03L—H03L	125.5
N01R—Yb01—N01N	150.0 (3)	C030—C03L—H03L	125.5
N01R—Yb01—C01Y	77.3 (3)	N01X—C03M—C037	111.9 (11)
N01R—Yb01—C022	73.6 (3)	N01X—C03M—H03M	124.1
N01X—Yb01—N014	71.1 (3)	C037—C03M—H03M	124.1

N01X—Yb01—N01N	70.7 (3)	C03H—C03N—C036	104.2 (11)
N01X—Yb01—N01R	138.6 (3)	N01A—C03O—C03K	111.2 (11)
N01X—Yb01—C01Y	133.5 (3)	N01A—C03O—H03O	124.4
N01X—Yb01—C022	146.9 (3)	C03K—C03O—H03O	124.4
C01Y—Yb01—C022	26.2 (3)	C02Y—C03P—C02Z	104.2 (10)
O006—Yb02—O00A	69.7 (2)	C02Y—C03P—H03P	127.9
O006—Yb02—N00V	73.4 (3)	C02Z—C03P—H03P	127.9
O006—Yb02—N00W	81.3 (3)	O007—C03Q—C03J	113.2 (11)
O006—Yb02—N01A	74.3 (3)	O007—C03Q—C046	128.3 (12)
O006—Yb02—N01I	135.3 (3)	C046—C03Q—C03J	118.5 (11)
O006—Yb02—N01M	145.2 (3)	N01J—C03R—H03R	125.7
O006—Yb02—C01S	21.5 (3)	N01J—C03R—C04G	108.6 (12)
O006—Yb02—N01T	120.2 (3)	C04G—C03R—H03R	125.7
O006—Yb02—C01Z	48.4 (3)	C041—C03S—H03S	119.8
O00A—Yb02—N00V	135.2 (3)	C045—C03S—H03S	119.8
O00A—Yb02—N00W	73.6 (3)	C045—C03S—C041	120.4 (11)
O00A—Yb02—N01A	81.6 (3)	C052—F03T—C18	14 (3)
O00A—Yb02—N01I	74.1 (3)	F20—F03T—C052	83 (7)
O00A—Yb02—N01M	119.9 (3)	F20—F03T—C18	69 (6)
O00A—Yb02—C01S	48.2 (3)	N011—C03U—C02Q	109.5 (12)
O00A—Yb02—N01T	147.4 (3)	N011—C03U—H03U	125.2
O00A—Yb02—C01Z	21.3 (2)	C02Q—C03U—H03U	125.2
N00V—Yb02—N00W	76.7 (3)	C02C—C03V—C02L	118.7 (10)
N00V—Yb02—N01A	111.7 (3)	C02C—C03V—H03V	120.7
N00V—Yb02—N01M	79.8 (3)	C02L—C03V—H03V	120.7
N00V—Yb02—C01S	92.8 (3)	O00N—C03W—C04N	127.4 (14)
N00V—Yb02—N01T	74.5 (3)	O00N—C03W—C04W	116.0 (13)
N00V—Yb02—C01Z	116.7 (3)	C04N—C03W—C04W	116.5 (13)
N00W—Yb02—C01S	76.5 (3)	O00P—C03X—C046	127.4 (11)
N00W—Yb02—C01Z	72.7 (3)	O00P—C03X—C04X	114.4 (12)
N01A—Yb02—N00W	150.0 (3)	C046—C03X—C04X	118.1 (12)
N01A—Yb02—N01M	137.6 (3)	N01F—C03Z—C029	120.7 (10)
N01A—Yb02—C01S	74.4 (3)	N01F—C03Z—C039	119.0 (9)
N01A—Yb02—C01Z	78.0 (3)	C029—C03Z—C039	120.2 (9)
N01I—Yb02—N00V	149.6 (3)	C032—C040—C03E	104.7 (11)
N01I—Yb02—N00W	112.7 (3)	C032—C040—H04A	110.8
N01I—Yb02—N01A	75.2 (3)	C032—C040—H04E	110.8
N01I—Yb02—N01M	76.7 (3)	C03E—C040—H04A	110.8

N01I—Yb02—C01S	117.3 (3)	C03E—C040—H04E	110.8
N01I—Yb02—N01T	80.0 (3)	H04A—C040—H04E	108.9
N01I—Yb02—C01Z	93.6 (3)	O00Q—C041—C03S	128.5 (11)
N01M—Yb02—N00W	71.2 (3)	O00Q—C041—C04J	112.6 (10)
N01M—Yb02—C01S	147.7 (3)	C03S—C041—C04J	118.9 (11)
N01M—Yb02—C01Z	135.0 (3)	C052—F042—C18	6 (2)
C01S—Yb02—C01Z	26.9 (3)	F17—F042—C052	55 (5)
N01T—Yb02—N00W	135.9 (3)	F17—F042—C18	50 (5)
N01T—Yb02—N01A	72.9 (3)	C052—F043—F17	44 (3)
N01T—Yb02—N01M	71.4 (3)	F35—F043—C052	107 (6)
N01T—Yb02—C01S	137.0 (3)	F35—F043—F17	150 (6)
N01T—Yb02—C01Z	150.9 (3)	F35—F043—C18	93 (5)
O007—Eu03—O00C	142.1 (3)	C18—F043—C052	14 (3)
O007—Eu03—O00E	75.8 (3)	C18—F043—F17	58 (2)
O007—Eu03—O00P	71.1 (3)	C04M—C044—H044	117.5
O007—Eu03—N00S	81.9 (3)	C04Z—C044—H044	117.5
O007—Eu03—N01F	132.3 (3)	C04Z—C044—C04M	125.0 (17)
O00C—Eu03—O00E	74.0 (3)	O00K—C045—C03S	128.2 (12)
O00C—Eu03—O00P	145.7 (3)	O00K—C045—C04K	113.2 (10)
O00C—Eu03—N00S	112.9 (3)	C03S—C045—C04K	118.7 (11)
O00C—Eu03—N01F	84.1 (3)	C03Q—C046—H046	119.4
O00E—Eu03—O00P	121.8 (3)	C03X—C046—C03Q	121.3 (12)
O00E—Eu03—N00S	146.9 (3)	C03X—C046—H046	119.4
O00E—Eu03—N01F	147.5 (3)	N00U—C047—C03K	109.0 (12)
O00F—Eu03—O007	82.9 (3)	N00U—C047—H047	125.5
O00F—Eu03—O00C	71.2 (3)	C03K—C047—H047	125.5
O00F—Eu03—O00E	83.1 (3)	F00H—C048—F00L	105.3 (10)
O00F—Eu03—O00P	136.1 (3)	F00H—C048—C02A	112.8 (10)
O00F—Eu03—N00S	69.9 (3)	F00L—C048—C02A	113.0 (11)
O00F—Eu03—N01F	112.6 (3)	F00T—C048—F00H	107.2 (11)
O00I—Eu03—O007	112.3 (3)	F00T—C048—F00L	107.4 (11)
O00I—Eu03—O00C	79.5 (3)	F00T—C048—C02A	110.9 (10)
O00I—Eu03—O00E	72.4 (3)	N00O—B049—N011	109.8 (10)
O00I—Eu03—O00F	146.1 (3)	N00O—B049—H049	109.1
O00I—Eu03—O00P	77.7 (3)	N011—B049—H049	109.1
O00I—Eu03—N00S	139.8 (3)	N01J—B049—N00O	109.3 (10)
O00I—Eu03—N01F	80.2 (3)	N01J—B049—N011	110.4 (10)
O00P—Eu03—N00S	71.8 (3)	N01J—B049—H049	109.1
O00P—Eu03—N01F	67.1 (3)	F009—C04A—C02F	110.5 (10)
N00S—Eu03—N01F	64.2 (3)	F013—C04A—F009	106.4 (11)

O00G—Eu04—O00K	118.2 (3)	F013—C04A—C02F	113.7 (12)
O00G—Eu04—N012	84.2 (3)	F01C—C04A—F009	105.1 (13)
O00G—Eu04—N019	146.2 (3)	F01C—C04A—F013	110.4 (12)
O00K—Eu04—N012	128.0 (3)	F01C—C04A—C02F	110.2 (11)
O00K—Eu04—N019	77.0 (3)	C02N—C04B—H04B	127.4
O00N—Eu04—O00G	135.0 (3)	C04D—C04B—C02N	105.1 (13)
O00N—Eu04—O00K	80.7 (3)	C04D—C04B—H04B	127.4
O00N—Eu04—O00Q	145.7 (3)	N015—B04C—H04C	109.0
O00N—Eu04—O00R	72.0 (3)	N016—B04C—N015	110.2 (9)
O00N—Eu04—N012	117.3 (3)	N016—B04C—H04C	109.0
O00N—Eu04—N019	74.3 (3)	N01W—B04C—N015	108.0 (9)
O00Q—Eu04—O00G	76.9 (3)	N01W—B04C—N016	111.6 (10)
O00Q—Eu04—O00K	70.7 (3)	N01W—B04C—H04C	109.0
O00Q—Eu04—N012	70.3 (3)	N01E—C04D—H04D	125.3
O00Q—Eu04—N019	81.0 (3)	C04B—C04D—N01E	109.4 (12)
O00R—Eu04—O00G	71.0 (3)	C04B—C04D—H04D	125.3
O00R—Eu04—O00K	82.5 (3)	F00J—C04E—F01H	105.5 (12)
O00R—Eu04—O00Q	120.7 (3)	F00J—C04E—C03B	111.2 (12)
O00R—Eu04—N012	148.1 (3)	F01H—C04E—C03B	111.7 (12)
O00R—Eu04—N019	142.8 (3)	F01P—C04E—F00J	107.8 (13)
O00X—Eu04—O00G	78.7 (3)	F01P—C04E—F01H	108.8 (13)
O00X—Eu04—O00K	152.3 (3)	F01P—C04E—C03B	111.6 (12)
O00X—Eu04—O00N	72.4 (3)	C04K—F04F—F18	49.8 (8)
O00X—Eu04—O00Q	136.8 (3)	F1—F04F—C04K	65.1 (9)
O00X—Eu04—O00R	83.1 (3)	F1—F04F—F18	103.4 (18)
O00X—Eu04—N012	72.3 (3)	C034—C04G—H04G	127.1
O00X—Eu04—N019	101.3 (3)	C03R—C04G—C034	105.9 (12)
N019—Eu04—N012	64.2 (3)	C03R—C04G—H04G	127.1
C022—O005—Yb01	114.8 (6)	O00R—C04H—C04S	127.2 (13)
C01S—O006—Yb02	116.0 (7)	O00R—C04H—C051	113.1 (13)
C03Q—O007—Eu03	135.9 (8)	C04S—C04H—C051	119.7 (14)
C01Y—O008—Yb01	118.4 (7)	C04K—F04I—F1	59.1 (9)
C01Z—O00A—Yb02	116.5 (6)	F6—F04I—C04K	74.8 (11)
C03B—O00C—Eu03	132.8 (7)	F6—F04I—F1	133.6 (15)
C02F—O00E—Eu03	132.6 (7)	F00B—C04J—F00M	106.4 (11)
C02A—O00F—Eu03	135.8 (7)	F00B—C04J—C041	114.8 (11)
C04Q—O00G—Eu04	134.1 (9)	F00D—C04J—F00B	107.6 (11)
C03I—O00I—Eu03	135.5 (8)	F00D—C04J—F00M	106.3 (11)
C045—O00K—Eu04	133.2 (7)	F00D—C04J—C041	112.1 (12)
C03W—O00N—Eu04	131.2 (10)	F00M—C04J—C041	109.3 (11)

N00W—N00O—B049	122.0 (9)	F00Z—C04K—C045	112.5 (15)
C02V—N00O—N00W	109.7 (10)	F00Z—C04K—F04F	103.7 (13)
C02V—N00O—B049	128.2 (10)	F00Z—C04K—F6	82.9 (17)
C03X—O00P—Eu03	133.9 (8)	F04F—C04K—C045	111.5 (11)
C041—O00Q—Eu04	133.5 (8)	F04F—C04K—F6	137.6 (17)
C04H—O00R—Eu04	133.5 (9)	F04I—C04K—F00Z	106 (2)
C02B—N00S—Eu03	121.8 (7)	F04I—C04K—C045	114.8 (14)
C02B—N00S—C039	117.7 (9)	F04I—C04K—F04F	107.3 (17)
C039—N00S—Eu03	120.1 (7)	F04I—C04K—F6	33.6 (13)
N01A—N00U—B04T	122.8 (10)	F1—C04K—F00Z	130.2 (18)
C047—N00U—N01A	109.1 (10)	F1—C04K—C045	116.3 (13)
C047—N00U—B04T	128.1 (11)	F1—C04K—F04F	48.6 (14)
N011—N00V—Yb02	123.8 (7)	F1—C04K—F04I	61.5 (16)
C03G—N00V—Yb02	128.9 (8)	F1—C04K—F6	95.0 (18)
C03G—N00V—N011	106.8 (9)	F6—C04K—C045	103.8 (15)
N00O—N00W—Yb02	120.0 (6)	F18—C04K—F00Z	24.3 (15)
C02O—N00W—Yb02	135.0 (8)	F18—C04K—C045	118 (2)
C02O—N00W—N00O	104.8 (9)	F18—C04K—F04F	79.8 (15)
C04L—O00X—Eu04	134.4 (9)	F18—C04K—F04I	119 (2)
N01T—N00Y—B04T	122.1 (9)	F18—C04K—F1	114.9 (19)
C032—N00Y—N01T	112.5 (10)	F18—C04K—F6	104 (2)
C032—N00Y—B04T	125.3 (10)	O00X—C04L—C04N	126.4 (13)
F18—F00Z—C04K	77.2 (15)	O00X—C04L—C04Y	114.0 (14)
N01K—N010—Yb01	124.8 (7)	C04N—C04L—C04Y	119.6 (15)
C02R—N010—Yb01	128.5 (8)	C044—C04M—H04M	121.4
C02R—N010—N01K	106.6 (10)	C054—C04M—C044	117.2 (18)
N00V—N011—B049	120.4 (9)	C054—C04M—H04M	121.4
C03U—N011—N00V	109.0 (10)	C03W—C04N—H04N	119.1
C03U—N011—B049	130.6 (11)	C04L—C04N—C03W	121.9 (14)
C01Q—N012—Eu04	118.9 (7)	C04L—C04N—H04N	119.1
C02L—N012—Eu04	123.6 (7)	F01L—C04O—F026	102.5 (13)
C02L—N012—C01Q	116.8 (9)	F01L—C04O—C03I	112.9 (13)
N01E—N014—Yb01	120.6 (7)	F026—C04O—C03I	111.7 (14)
C02N—N014—Yb01	130.4 (8)	F03C—C04O—F01L	107.5 (16)
C02N—N014—N01E	106.0 (10)	F03C—C04O—F026	106.9 (15)
N01N—N015—B04C	120.8 (9)	F03C—C04O—C03I	114.6 (12)
C03H—N015—N01N	110.4 (10)	C02R—C04P—H04P	128.3
C03H—N015—B04C	128.7 (10)	C03D—C04P—C02R	103.4 (11)
N017—N016—B04C	122.0 (9)	C03D—C04P—H04P	128.3
C02Z—N016—N017	108.4 (9)	O00G—C04Q—C04S	127.1 (14)

C02Z—N016—B04C	129.7 (9)	O00G—C04Q—C052	110.4 (18)
N016—N017—Yb01	122.1 (7)	O00G—C04Q—C18	116.4 (18)
C02Y—N017—Yb01	130.7 (8)	C04S—C04Q—C052	122.3 (17)
C02Y—N017—N016	107.0 (9)	C04S—C04Q—C18	116.2 (17)
C021—N019—Eu04	119.7 (7)	C18—C04Q—C052	13 (3)
C02K—N019—Eu04	121.1 (8)	F13—F44—C04W	62.7 (11)
C02K—N019—C021	118.8 (10)	F25—F44—C04W	69.9 (16)
N00U—N01A—Yb02	120.7 (7)	F25—F44—F13	128 (3)
C03O—N01A—Yb02	133.7 (8)	C04H—C04S—C04Q	122.2 (13)
C03O—N01A—N00U	105.4 (9)	C04H—C04S—H04S	118.9
N01I—N01D—B04T	122.3 (9)	C04Q—C04S—H04S	118.9
C03L—N01D—N01I	108.7 (10)	N00U—B04T—H04T	110.2
C03L—N01D—B04T	129.0 (11)	N00Y—B04T—N00U	107.7 (10)
N014—N01E—B04U	122.2 (10)	N00Y—B04T—H04T	110.2
C04D—N01E—N014	107.2 (11)	N01D—B04T—N00U	108.7 (10)
C04D—N01E—B04U	130.6 (12)	N01D—B04T—N00Y	109.7 (11)
C02X—N01F—Eu03	121.7 (7)	N01D—B04T—H04T	110.2
C02X—N01F—C03Z	118.8 (9)	N01E—B04U—N01K	109.7 (11)
C03Z—N01F—Eu03	117.4 (6)	N01E—B04U—N01U	110.1 (11)
N01D—N01I—Yb02	123.6 (7)	N01E—B04U—H04U	109.9
C035—N01I—Yb02	129.7 (8)	N01K—B04U—H04U	109.9
C035—N01I—N01D	106.3 (9)	N01U—B04U—N01K	107.3 (11)
N01M—N01J—B049	122.0 (9)	N01U—B04U—H04U	109.9
C03R—N01J—N01M	109.1 (10)	H04F—C04V—H04H	109.5
C03R—N01J—B049	128.7 (11)	H04F—C04V—H04I	109.5
N010—N01K—B04U	120.6 (9)	H04H—C04V—H04I	109.5
C03D—N01K—N010	108.8 (10)	C04Z—C04V—H04F	109.5
C03D—N01K—B04U	130.6 (11)	C04Z—C04V—H04H	109.5
N01J—N01M—Yb02	121.5 (7)	C04Z—C04V—H04I	109.5
C034—N01M—Yb02	132.0 (8)	F46—C04W—C03W	113.9 (15)
C034—N01M—N01J	106.1 (9)	F46—C04W—F44	109.5 (18)
N015—N01N—Yb01	121.3 (7)	F46—C04W—F45	112.7 (19)
C036—N01N—Yb01	132.8 (8)	F46—C04W—F13	65 (2)
C036—N01N—N015	105.6 (9)	F46—C04W—F25	124 (3)
N012—C01Q—C020	123.8 (9)	F44—C04W—C03W	112.9 (15)
N012—C01Q—C021	116.3 (9)	F44—C04W—F45	97.1 (19)
C020—C01Q—C021	119.9 (9)	F44—C04W—F13	55.6 (19)
N01U—N01R—Yb01	121.0 (7)	F45—C04W—C03W	109.6 (14)
C025—N01R—Yb01	132.8 (8)	F45—C04W—F13	144 (2)
C025—N01R—N01U	106.1 (9)	F13—C04W—C03W	103.1 (18)

O006—C01S—Yb02	42.5 (5)	F14—C04W—F46	36 (2)
O006—C01S—C01Z	119.3 (10)	F14—C04W—C03W	122 (3)
O006—C01S—C029	122.1 (10)	F14—C04W—F44	123 (3)
C01Z—C01S—Yb02	76.8 (6)	F14—C04W—F45	78 (2)
C01Z—C01S—C029	118.6 (9)	F14—C04W—F13	97 (3)
C029—C01S—Yb02	164.6 (7)	F14—C04W—F25	111 (3)
N00Y—N01T—Yb02	121.4 (7)	F25—C04W—C03W	121 (2)
C03E—N01T—Yb02	129.6 (8)	F25—C04W—F44	40 (3)
C03E—N01T—N00Y	105.7 (9)	F25—C04W—F45	58 (3)
N01R—N01U—B04U	122.9 (10)	F25—C04W—F13	93 (3)
C02S—N01U—N01R	109.6 (10)	F01B—C04X—F02D	106.0 (15)
C02S—N01U—B04U	127.3 (11)	F01B—C04X—F033	110.5 (15)
N01X—N01W—B04C	120.7 (9)	F01B—C04X—C03X	113.5 (12)
C028—N01W—N01X	109.7 (9)	F02D—C04X—C03X	113.6 (13)
C028—N01W—B04C	129.5 (10)	F033—C04X—F02D	103.7 (15)
N01W—N01X—Yb01	120.0 (6)	F033—C04X—C03X	109.1 (14)
C03M—N01X—Yb01	130.8 (8)	F02G—C04Y—F03Y	104.6 (17)
C03M—N01X—N01W	105.6 (9)	F02G—C04Y—C04L	113.6 (17)
O008—C01Y—Yb01	40.6 (5)	F02H—C04Y—F02G	110 (2)
O008—C01Y—C022	119.8 (10)	F02H—C04Y—F03Y	108 (2)
O008—C01Y—C027	121.0 (9)	F02H—C04Y—C04L	111.8 (18)
C022—C01Y—Yb01	79.3 (6)	F03Y—C04Y—C04L	107.7 (17)
C022—C01Y—C027	119.1 (10)	C044—C04Z—C04V	122 (2)
C027—C01Y—Yb01	161.3 (7)	C055—C04Z—C044	116.1 (19)
O00A—C01Z—Yb02	42.2 (5)	C055—C04Z—C04V	122 (2)
O00A—C01Z—C01S	118.5 (9)	C04W—F45—F14	50.8 (12)
O00A—C01Z—C02E	122.2 (9)	F25—F45—C04W	60.7 (14)
C01S—C01Z—Yb02	76.3 (6)	F25—F45—F14	95 (3)
C02E—C01Z—Yb02	164.4 (7)	F018—C051—F01G	106.9 (12)
C02E—C01Z—C01S	119.3 (9)	F018—C051—C04H	110.8 (14)
C01Q—C020—C022	120.2 (9)	F01G—C051—C04H	111.4 (14)
C01Q—C020—C02C	117.5 (10)	F02T—C051—F018	110.8 (16)
C02C—C020—C022	122.2 (10)	F02T—C051—F01G	106.0 (15)
N019—C021—C01Q	118.3 (9)	F02T—C051—C04H	110.8 (12)
N019—C021—C027	121.8 (10)	F03T—C052—F042	103 (3)
C027—C021—C01Q	119.8 (9)	F03T—C052—F043	115 (3)
O005—C022—Yb01	43.7 (5)	F03T—C052—C04Q	111 (3)
O005—C022—C01Y	118.1 (10)	F03T—C052—F20	27 (2)
O005—C022—C020	122.0 (9)	F03T—C052—F35	110 (3)

C01Y—C022—Yb01	74.5 (6)	F042—C052—C04Q	112 (3)
C01Y—C022—C020	119.9 (9)	F042—C052—F20	126 (4)
C020—C022—Yb01	165.4 (7)	F042—C052—F35	127 (3)
C02E—C023—H023	120.6	F043—C052—F042	106 (3)
C02J—C023—H023	120.6	F043—C052—C04Q	109 (3)
C02J—C023—C02E	118.9 (10)	F043—C052—F20	93 (3)
N01R—C025—H025	125.2	F043—C052—F35	22.8 (17)
N01R—C025—C03A	109.5 (11)	C04Q—C052—F35	92 (2)
C03A—C025—H025	125.2	F17—C052—F03T	109 (4)
C021—C027—C01Y	120.7 (9)	F17—C052—F042	29.3 (19)
C021—C027—C02M	118.0 (10)	F17—C052—F043	77 (3)
C02M—C027—C01Y	121.4 (10)	F17—C052—C04Q	131 (4)
N01W—C028—H028	125.3	F17—C052—F20	120 (5)
N01W—C028—C037	109.4 (11)	F17—C052—F35	100 (3)
C037—C028—H028	125.3	F20—C052—C04Q	109 (3)
C02I—C029—C01S	120.8 (10)	F20—C052—F35	84 (3)
C03Z—C029—C01S	120.4 (10)	C054—C053—H053	120.1
C03Z—C029—C02I	118.8 (9)	C055—C053—H053	120.1
O00F—C02A—C02W	126.2 (11)	C055—C053—C054	119.8 (19)
O00F—C02A—C048	115.8 (10)	C04M—C054—C053	119 (2)
C02W—C02A—C048	117.9 (11)	C04M—C054—H054	120.5
N00S—C02B—H02B	118.1	C053—C054—H054	120.5
N00S—C02B—C02J	123.7 (10)	C04Z—C055—C053	123 (2)
C02J—C02B—H02B	118.1	C04Z—C055—H055	118.5
C020—C02C—H02C	120.5	C053—C055—H055	118.5
C03V—C02C—C020	118.9 (10)	H1A—C1—H1B	103.3
C03V—C02C—H02C	120.5	C5—C1—H1A	95.9
C023—C02E—C01Z	121.2 (9)	C5—C1—H1B	95.9
C039—C02E—C01Z	120.7 (9)	C5—C1—C11	161 (6)
C039—C02E—C023	118.2 (9)	C11—C1—H1A	95.9
O00E—C02F—C031	129.3 (11)	C11—C1—H1B	95.9
O00E—C02F—C04A	113.1 (11)	H3A—C3—H3B	109.5
C031—C02F—C04A	117.5 (11)	H3A—C3—H3C	109.5
C029—C02I—H02I	120.3	H3B—C3—H3C	109.5
C02P—C02I—C029	119.4 (10)	C5—C3—H3A	109.5
C02P—C02I—H02I	120.3	C5—C3—H3B	109.5
C023—C02J—C02B	119.6 (10)	C5—C3—H3C	109.5
C023—C02J—H02J	120.2	C1—C5—C3	138 (4)
C02B—C02J—H02J	120.2	C1—C5—H5A	102.7
N019—C02K—H02K	118.3	C1—C5—H5B	102.7

N019—C02K—C03F	123.3 (11)	C3—C5—H5A	102.7
C03F—C02K—H02K	118.3	C3—C5—H5B	102.7
N012—C02L—H02L	117.9	H5A—C5—H5B	105.0
N012—C02L—C03V	124.2 (10)	H10A—C10—H10B	109.5
C03V—C02L—H02L	117.9	H10A—C10—H10C	109.5
C027—C02M—H02M	119.9	H10B—C10—H10C	109.5
C03F—C02M—C027	120.2 (10)	C14—C10—H10A	109.5
C03F—C02M—H02M	119.9	C14—C10—H10B	109.5
N014—C02N—H02N	123.9	C14—C10—H10C	109.5
N014—C02N—C04B	112.2 (13)	C1—C11—H11A	95.2
C04B—C02N—H02N	123.9	C1—C11—H11B	95.2
N00W—C02O—H02O	124.2	C1—C11—C14	163 (6)
N00W—C02O—C038	111.5 (11)	H11A—C11—H11B	103.2
C038—C02O—H02O	124.2	C14—C11—H11A	95.2
C02I—C02P—H02P	121.0	C14—C11—H11B	95.2
C02I—C02P—C02X	118.1 (10)	C10—C14—H14A	99.4
C02X—C02P—H02P	121.0	C10—C14—H14B	99.4
H02A—C02Q—H02D	108.9	C11—C14—C10	149 (5)
C03G—C02Q—H02A	110.9	C11—C14—H14A	99.4
C03G—C02Q—H02D	110.9	C11—C14—H14B	99.4
C03U—C02Q—H02A	110.9	H14A—C14—H14B	104.0
C03U—C02Q—H02D	110.9	F44—F13—F46	108.4 (18)
C03U—C02Q—C03G	104.2 (11)	F44—F13—C04W	61.7 (11)
N010—C02R—H02R	124.6	C04W—F13—F46	57.2 (11)
N010—C02R—C04P	110.7 (12)	F46—F14—C04W	72.1 (15)
C04P—C02R—H02R	124.6	F46—F14—F45	123 (2)
N01U—C02S—H02S	126.2	C04W—F14—F45	51.7 (13)
C03A—C02S—N01U	107.7 (11)	F44—F25—C04W	70.4 (16)
C03A—C02S—H02S	126.2	F44—F25—F45	132.1 (16)
C04W—F46—F13	58.3 (11)	F45—F25—C04W	61.8 (15)
F14—F46—C04W	71.9 (14)	F04F—F1—F04I	121.9 (15)
F14—F46—F13	124 (3)	F04F—F1—C04K	66.3 (9)
N00O—C02V—H02V	125.8	C04K—F1—F04I	59.5 (9)
N00O—C02V—C038	108.5 (11)	F04I—F6—C04K	71.6 (11)
C038—C02V—H02V	125.8	F00Z—F18—F04F	128 (2)
C02A—C02W—H02W	119.0	F00Z—F18—C04K	78.6 (15)
C03B—C02W—C02A	122.0 (11)	C04K—F18—F04F	50.4 (8)
C03B—C02W—H02W	119.0	F042—F17—F043	150 (6)

N01F—C02X—C02P	124.2 (10)	F042—F17—C052	96 (5)
N01F—C02X—H02X	117.9	F042—F17—C18	108 (6)
C02P—C02X—H02X	117.9	C052—F17—F043	58 (2)
N017—C02Y—H02Y	124.1	C052—F17—C18	13 (3)
N017—C02Y—C03P	111.7 (11)	C18—F17—F043	46 (3)
C03P—C02Y—H02Y	124.1	F03T—F20—C052	71 (6)
N016—C02Z—H02Z	125.7	F03T—F20—C18	85 (7)
N016—C02Z—C03P	108.6 (11)	C18—F20—C052	15 (3)
C03P—C02Z—H02Z	125.7	F043—F35—C052	51 (5)
C035—C030—H030	127.6	F043—F35—C18	57 (6)
C03L—C030—H030	127.6	C18—F35—C052	7 (3)
C03L—C030—C035	104.8 (11)	F03T—C18—F042	85 (3)
C02F—C031—H031	119.8	F03T—C18—C04Q	109 (3)
C02F—C031—C03I	120.4 (12)	F043—C18—F03T	123 (5)
C03I—C031—H031	119.8	F043—C18—F042	97 (3)
N00Y—C032—H032	126.7	F043—C18—C04Q	127 (4)
N00Y—C032—C040	106.6 (11)	F043—C18—F17	76 (3)
C040—C032—H032	126.7	F043—C18—F20	107 (4)
N01M—C034—H034	124.8	F043—C18—F35	30 (2)
N01M—C034—C04G	110.3 (11)	C04Q—C18—F042	99 (3)
C04G—C034—H034	124.8	F17—C18—F03T	91 (3)
N01I—C035—C030	111.1 (11)	F17—C18—F042	22.1 (15)
N01I—C035—H035	124.4	F17—C18—C04Q	116 (3)
C030—C035—H035	124.4	F17—C18—F35	106 (3)
N01N—C036—H036	124.2	F20—C18—F03T	26 (2)
N01N—C036—C03N	111.5 (11)	F20—C18—F042	108 (3)
C03N—C036—H036	124.2	F20—C18—C04Q	116 (3)
C028—C037—H037	128.3	F20—C18—F17	108 (3)
C028—C037—C03M	103.5 (11)	F20—C18—F35	100 (3)
C03M—C037—H037	128.3	F35—C18—F03T	125 (4)
C02O—C038—H038	127.2	F35—C18—F042	126 (3)
C02V—C038—C02O	105.6 (10)	F35—C18—C04Q	108 (3)
C02V—C038—H038	127.2		
Yb01—O005—C022—C01Y	4.2 (12)	C03W—C04W—F14—F45	-106 (2)
Yb01—O005—C022—C020	-176.3 (8)	C03W—C04W—F25—F44	-89 (4)
Yb01—O008—C01Y—C022	-3.4 (12)	C03W—C04W—F25—F45	95 (3)
Yb01—O008—	175.4 (7)	C03Z—N01F—	0.2 (17)

C01Y—C027		C02X—C02P	
Yb01—N010—N01K—C03D	-176.8 (8)	C03Z—C029—C02I—C02P	0.8 (17)
Yb01—N010—N01K—B04U	3.1 (15)	C041—C03S—C045—O00K	-4.0 (19)
Yb01—N010—C02R—C04P	176.8 (8)	C041—C03S—C045—C04K	175.4 (10)
Yb01—N014—N01E—C04D	-163.5 (8)	F042—C052—F17—F043	-164 (6)
Yb01—N014—N01E—B04U	15.8 (14)	F042—C052—F17—C18	-161 (17)
Yb01—N014—C02N—C04B	159.6 (9)	F042—C052—F20—F03T	37 (7)
Yb01—N017—C02Y—C03P	-177.2 (8)	F042—C052—F20—C18	-155 (15)
Yb01—N01N—C036—C03N	175.3 (8)	F042—C052—F35—F043	20 (8)
Yb01—N01R—N01U—C02S	179.5 (8)	F042—C052—F35—C18	-169 (31)
Yb01—N01R—N01U—B04U	-4.5 (15)	F042—F17—C18—F03T	-73 (6)
Yb01—N01R—C025—C03A	-179.5 (8)	F042—F17—C18—F043	163 (7)
Yb01—N01X—C03M—C037	158.9 (8)	F042—F17—C18—C04Q	39 (6)
Yb01—C01Y—C022—O005	-3.0 (8)	F042—F17—C18—F20	-93 (6)
Yb01—C01Y—C022—C020	177.5 (9)	F042—F17—C18—F35	160 (6)
Yb01—C01Y—C027—C021	-165.3 (17)	F043—C052—F17—F042	164 (6)
Yb01—C01Y—C027—C02M	15 (3)	F043—C052—F17—C18	3 (17)
Yb02—O006—C01S—C01Z	0.7 (12)	F043—C052—F20—F03T	148 (6)
Yb02—O006—C01S—C029	-179.0 (8)	F043—C052—F20—C18	-44 (11)
Yb02—O00A—C01Z—C01S	3.4 (12)	F043—C052—F35—C18	171 (28)
Yb02—O00A—C01Z—C02E	-178.6 (7)	F043—F17—C18—F03T	124 (5)
Yb02—N00V—N011—C03U	171.7 (8)	F043—F17—C18—F042	-163 (7)
Yb02—N00V—N011—B049	-8.6 (13)	F043—F17—C18—C04Q	-124 (4)
Yb02—N00V—C03G—C02Q	-171.6 (8)	F043—F17—C18—F20	103 (4)

Yb02—N00W—C02O—C038	-174.1 (8)	F043—F17—C18—F35	-4 (3)
Yb02—N01A—C03O—C03K	-177.4 (8)	F043—F35—C18—F03T	-96 (7)
Yb02—N01I—C035—C030	-171.2 (8)	F043—F35—C18—F042	17 (7)
Yb02—N01M—C034—C04G	172.4 (8)	F043—F35—C18—C04Q	133 (7)
Yb02—C01S—C01Z—O00A	-2.4 (8)	F043—F35—C18—F17	7 (6)
Yb02—C01S—C01Z—C02E	179.6 (9)	F043—F35—C18—F20	-105 (7)
Yb02—C01S—C029—C02I	-1 (3)	C044—C04M—C054—C053	1 (2)
Yb02—C01S—C029—C03Z	-180 (2)	C044—C04Z—C055—C053	0 (3)
Yb02—N01T—C03E—C040	159.2 (8)	C045—C03S—C041—O00Q	0 (2)
Yb02—C01Z—C02E—C023	-2 (3)	C045—C03S—C041—C04J	178.4 (11)
Yb02—C01Z—C02E—C039	179 (2)	C045—C04K—F1—F04F	96.4 (18)
Eu03—O007—C03Q—C03J	-180.0 (8)	C045—C04K—F1—F04I	-105.3 (17)
Eu03—O007—C03Q—C046	-1 (2)	C045—C04K—F6—F04I	114 (4)
Eu03—O00C—C03B—C02W	20.7 (19)	C045—C04K—F18—F00Z	82 (8)
Eu03—O00C—C03B—C04E	-157.7 (8)	C045—C04K—F18—F04F	-109.1 (14)
Eu03—O00E—C02F—C031	12.2 (19)	C046—C03X—C04X—F01B	38 (2)
Eu03—O00E—C02F—C04A	-163.8 (8)	C046—C03X—C04X—F02D	159.0 (14)
Eu03—O00F—C02A—C02W	-0.8 (18)	C046—C03X—C04X—F033	-85.9 (17)
Eu03—O00F—C02A—C048	-177.4 (7)	C047—N00U—N01A—Yb02	178.7 (7)
Eu03—O00I—C03I—C031	-9 (2)	C047—N00U—N01A—C03O	1.9 (12)
Eu03—O00I—C03I—C04O	168.7 (10)	C047—N00U—B04T—N00Y	121.6 (12)
Eu03—O00P—C03X—C046	19 (2)	C047—N00U—B04T—N01D	-119.6 (12)
Eu03—O00P—C03X—C04X	-158.7 (9)	C047—C03K—C03O—N01A	0.1 (14)
Eu03—N00S—C02B—C02J	173.0 (9)	C048—C02A—C02W—C03B	165.8 (11)

Eu03—N00S—C039—C02E	-170.5 (8)	B049—N00O—N00W—Yb02	-9.3 (13)
Eu03—N00S—C039—C03Z	5.8 (13)	B049—N00O—N00W—C02O	175.6 (10)
Eu03—N01F—C02X—C02P	-162.9 (9)	B049—N00O—C02V—C038	-175.1 (11)
Eu03—N01F—C03Z—C029	165.2 (8)	B049—N011—C03U—C02Q	-178.8 (11)
Eu03—N01F—C03Z—C039	-14.2 (12)	B049—N01J—N01M—Yb02	10.9 (13)
Eu04—O00G—C04Q—C04S	-8 (2)	B049—N01J—N01M—C034	-176.1 (10)
Eu04—O00G—C04Q—C052	177.8 (15)	B049—N01J—C03R—C04G	175.5 (12)
Eu04—O00G—C04Q—C18	164.8 (18)	C04A—C02F—C031—C03I	175.3 (12)
Eu04—O00K—C045—C03S	-12.9 (18)	B04C—N015—N01N—Yb01	0.2 (12)
Eu04—O00K—C045—C04K	167.7 (7)	B04C—N015—N01N—C036	175.3 (9)
Eu04—O00N—C03W—C04N	-27 (2)	B04C—N015—C03H—C03N	-175.0 (11)
Eu04—O00N—C03W—C04W	155.4 (10)	B04C—N016—N017—Yb01	-1.1 (13)
Eu04—O00Q—C041—C03S	22.2 (19)	B04C—N016—N017—C02Y	-177.5 (10)
Eu04—O00Q—C041—C04J	-156.7 (8)	B04C—N016—C02Z—C03P	177.8 (12)
Eu04—O00R—C04H—C04S	24 (2)	B04C—N01W—N01X—Yb01	21.8 (12)
Eu04—O00R—C04H—C051	-157.9 (10)	B04C—N01W—N01X—C03M	-177.3 (10)
Eu04—O00X—C04L—C04N	6 (3)	B04C—N01W—C028—C037	176.0 (11)
Eu04—O00X—C04L—C04Y	-171.6 (12)	C04D—N01E—B04U—N01K	110.6 (15)
Eu04—N012—C01Q—C020	168.7 (8)	C04D—N01E—B04U—N01U	-131.6 (14)
Eu04—N012—C01Q—C021	-13.4 (11)	F04F—C04K—F1—F04I	158 (2)
Eu04—N012—C02L—C03V	-169.5 (8)	F04F—C04K—F6—F04I	-32 (5)
Eu04—N019—C021—C01Q	12.2 (12)	F04F—C04K—F18—F00Z	-169 (7)
Eu04—N019—C021—C027	-171.7 (8)	F04I—C04K—F1—F04F	-158 (2)
Eu04—N019—C02K—C03F	173.0 (9)	F04I—C04K—F18—F00Z	-65 (8)

O006—C01S—C01Z—Yb02	-0.5 (9)	F04I—C04K—F18—F04F	104 (2)
O006—C01S—C01Z—O00A	-2.8 (15)	C04K—F00Z—F18—F04F	-11 (7)
O006—C01S—C01Z—C02E	179.2 (9)	C04K—F04F—F1—F04I	-22 (2)
O006—C01S—C029—C02I	1.3 (17)	C04K—F04F—F18—F00Z	14 (9)
O006—C01S—C029—C03Z	-177.2 (10)	C04K—F04I—F1—F04F	23 (2)
O007—C03Q—C046—C03X	-4 (2)	C04M—C044—C04Z—C04V	179.3 (15)
O008—C01Y—C022—Yb01	2.2 (8)	C04M—C044—C04Z—C055	1 (2)
O008—C01Y—C022—O005	-0.8 (15)	C04N—C03W—C04W—F46	39 (2)
O008—C01Y—C022—C020	179.7 (9)	C04N—C03W—C04W—F44	164.8 (18)
O008—C01Y—C027—C021	-174.5 (10)	C04N—C03W—C04W—F45	-88.1 (18)
O008—C01Y—C027—C02M	5.4 (16)	C04N—C03W—C04W—F13	107 (2)
O00A—C01Z—C02E—C023	1.3 (16)	C04N—C03W—C04W—F14	-1 (4)
O00A—C01Z—C02E—C039	-177.9 (10)	C04N—C03W—C04W—F25	-151 (4)
O00C—C03B—C04E—F00J	-76.3 (16)	C04N—C04L—C04Y—F02G	8 (3)
O00C—C03B—C04E—F01H	166.1 (12)	C04N—C04L—C04Y—F02H	-118 (2)
O00C—C03B—C04E—F01P	44.0 (17)	C04N—C04L—C04Y—F03Y	123.3 (19)
O00E—C02F—C031—C03I	-1 (2)	C04Q—C052—F17—F042	59 (8)
O00E—C02F—C04A—F009	-48.7 (15)	C04Q—C052—F17—F043	-105 (4)
O00E—C02F—C04A—F013	-168.3 (11)	C04Q—C052—F17—C18	-102 (20)
O00E—C02F—C04A—F01C	67.1 (15)	C04Q—C052—F20—F03T	-101 (7)
O00F—C02A—C02W—C03B	-11 (2)	C04Q—C052—F20—C18	67 (12)
O00F—C02A—C048—F00H	-25.9 (15)	C04Q—C052—F35—F043	140 (6)
O00F—C02A—C048—F00L	-145.1 (11)	C04Q—C052—F35—C18	-49 (27)
O00F—C02A—C048—F00T	94.3 (13)	F44—C04W—F45—F14	-123 (3)

O00G—C04Q—C04S—C04H	-6 (3)	F44—C04W—F45—F25	3 (3)
O00G—C04Q—C052—F03T	147 (2)	F44—C04W—F13—F46	141 (2)
O00G—C04Q—C052—F042	32 (3)	F44—C04W—F14—F46	-77 (5)
O00G—C04Q—C052—F043	-84 (3)	F44—C04W—F14—F45	90 (3)
O00G—C04Q—C052—F17	5 (5)	F44—C04W—F25—F45	-176 (5)
O00G—C04Q—C052—F20	176 (3)	C04S—C04H—C051—F018	115.4 (16)
O00G—C04Q—C052—F35	-100 (2)	C04S—C04H—C051—F01G	-4 (2)
O00G—C04Q—C18—F03T	132 (3)	C04S—C04H—C051—F02T	-121.3 (17)
O00G—C04Q—C18—F042	45 (3)	C04S—C04Q—C052—F03T	-27 (3)
O00G—C04Q—C18—F043	-61 (5)	C04S—C04Q—C052—F042	-142 (2)
O00G—C04Q—C18—F17	31 (3)	C04S—C04Q—C052—F043	101 (3)
O00G—C04Q—C18—F20	160 (2)	C04S—C04Q—C052—F17	-169 (4)
O00G—C04Q—C18—F35	-88 (3)	C04S—C04Q—C052—F20	2 (4)
O00I—C03I—C04O—F01L	43.4 (19)	C04S—C04Q—C052—F35	86 (3)
O00I—C03I—C04O—F026	-71.4 (17)	C04S—C04Q—C18—F03T	-54 (4)
O00I—C03I—C04O—F03C	166.9 (16)	C04S—C04Q—C18—F042	-141 (2)
O00K—C045—C04K—F00Z	176.5 (14)	C04S—C04Q—C18—F043	113 (4)
O00K—C045—C04K—F04F	60.4 (16)	C04S—C04Q—C18—F17	-155 (2)
O00K—C045—C04K—F04I	-62 (2)	C04S—C04Q—C18—F20	-26 (3)
O00K—C045—C04K—F1	7 (2)	C04S—C04Q—C18—F35	86 (3)
O00K—C045—C04K—F6	-95.6 (17)	B04T—N00U—N01A—Yb02	0.3 (13)
O00K—C045—C04K—F18	150.3 (19)	B04T—N00U—N01A—C03O	-176.4 (10)
O00N—C03W—C04N—C04L	3 (3)	B04T—N00U—C047—C03K	176.3 (11)
O00N—C03W—C04W—F46	-143.2 (19)	B04T—N00Y—N01T—Yb02	15.0 (14)

O00N—C03W—C04W—F44	-18 (2)	B04T—N00Y—N01T—C03E	176.2 (11)
O00N—C03W—C04W—F45	89.5 (18)	B04T—N00Y—C032—C040	-176.1 (11)
O00N—C03W—C04W—F13	-75 (2)	B04T—N01D—N01I—Yb02	-5.9 (14)
O00N—C03W—C04W—F14	177 (3)	B04T—N01D—N01I—C035	-179.2 (11)
O00N—C03W—C04W—F25	26 (4)	B04T—N01D—C03L—C030	178.1 (12)
N00O—N00W—C02O—C038	-0.1 (13)	B04U—N01E—C04D—C04B	-176.9 (13)
N00O—C02V—C038—C02O	-0.2 (14)	B04U—N01K—C03D—C04P	179.5 (13)
O00P—C03X—C046—C03Q	-5 (2)	B04U—N01U—C02S—C03A	-176.1 (12)
O00P—C03X—C04X—F01B	-144.6 (15)	C04V—C04Z—C055—C053	-178.8 (17)
O00P—C03X—C04X—F02D	-23.3 (19)	C04W—F46—F13—F44	36.1 (17)
O00P—C03X—C04X—F033	91.7 (17)	C04W—F46—F14—F45	-12 (4)
O00Q—C041—C04J—F00B	-172.2 (11)	C04W—C03W—C04N—C04L	179.9 (15)
O00Q—C041—C04J—F00D	-49.1 (14)	C04W—F44—F13—F46	-34.2 (16)
O00Q—C041—C04J—F00M	68.4 (14)	C04W—F44—F25—F45	5 (6)
O00R—C04H—C04S—C04Q	-2 (2)	C04W—F45—F14—F46	14 (5)
O00R—C04H—C051—F018	-63.3 (16)	C04W—F45—F25—F44	-5 (6)
O00R—C04H—C051—F01G	177.9 (12)	C04X—C03X—C046—C03Q	172.3 (13)
O00R—C04H—C051—F02T	60.1 (19)	C04Y—C04L—C04N—C03W	-173.7 (16)
N00S—C02B—C02J—C023	-1.3 (19)	C04Z—C044—C04M—C054	-1 (2)
N00S—C039—C03Z—N01F	5.8 (15)	F45—C04W—F13—F46	94 (4)
N00S—C039—C03Z—C029	-173.5 (10)	F45—C04W—F13—F44	-47 (4)
N00U—N01A—C03O—C03K	-1.2 (13)	F45—C04W—F14—F46	-167 (5)
N00V—N011—C03U—C02Q	0.9 (14)	F45—C04W—F25—F44	176 (5)
N00V—N011—B049—N00O	-55.8 (13)	C051—C04H—C04S—C04Q	180.0 (14)

N00V—N011—B049—N01J	64.8 (13)	C052—F03T—F20—C18	-3 (3)
N00W—N00O—C02V—C038	0.1 (14)	C052—F03T—C18—F042	14 (11)
N00W—N00O—B049—N011	65.6 (13)	C052—F03T—C18—F043	110 (13)
N00W—N00O—B049—N01J	-55.6 (14)	C052—F03T—C18—C04Q	-83 (13)
N00W—C02O—C038—C02V	0.2 (14)	C052—F03T—C18—F17	35 (11)
O00X—C04L—C04N—C03W	9 (3)	C052—F03T—C18—F20	167 (14)
O00X—C04L—C04Y—F02G	-174.1 (16)	C052—F03T—C18—F35	146 (15)
O00X—C04L—C04Y—F02H	60 (2)	C052—F042—F17—F043	29 (10)
O00X—C04L—C04Y—F03Y	-59 (2)	C052—F042—F17—C18	4 (4)
N00Y—N01T—C03E—C040	0.2 (14)	C052—F042—C18—F03T	-37 (31)
N00Y—C032—C040—C03E	0.1 (14)	C052—F042—C18—F043	-159 (35)
F00Z—C04K—F1—F04F	-71 (3)	C052—F042—C18—C04Q	72 (33)
F00Z—C04K—F1—F04I	88 (3)	C052—F042—C18—F17	-143 (33)
F00Z—C04K—F6—F04I	-134 (4)	C052—F042—C18—F20	-49 (31)
F00Z—C04K—F18—F04F	169 (7)	C052—F042—C18—F35	-168 (36)
N010—N01K—C03D—C04P	-0.6 (15)	C052—F043—F17—F042	-34 (12)
N010—N01K—B04U—N01E	57.5 (15)	C052—F043—F17—C18	-1 (5)
N010—N01K—B04U—N01U	-62.0 (14)	C052—F043—F35—C18	-1 (4)
N010—C02R—C04P—C03D	0.1 (15)	C052—F043—C18—F03T	-80 (15)
N011—N00V—C03G—C02Q	0.3 (13)	C052—F043—C18—F042	9 (14)
N012—C01Q—C020—C022	-179.8 (9)	C052—F043—C18—C04Q	115 (18)
N012—C01Q—C020—C02C	0.4 (16)	C052—F043—C18—F17	2 (16)
N012—C01Q—C021—N019	1.0 (14)	C052—F043—C18—F20	-103 (17)
N012—C01Q—C021—C027	-175.2 (9)	C052—F043—C18—F35	175 (15)

N012—C02L—C03V—C02C	2.0 (18)	C052—C04Q—C04S—C04H	167 (2)
N014—N01E—C04D—C04B	2.4 (15)	C052—C04Q—C18—F03T	66 (10)
N014—N01E—B04U—N01K	-68.6 (14)	C052—C04Q—C18—F042	-21 (9)
N014—N01E—B04U—N01U	49.2 (15)	C052—C04Q—C18—F043	-127 (13)
N014—C02N—C04B—C04D	1.6 (17)	C052—C04Q—C18—F17	-35 (9)
N015—N01N—C036—C03N	1.0 (13)	C052—C04Q—C18—F20	94 (11)
N015—C03H—C03N—C036	-1.0 (13)	C052—C04Q—C18—F35	-154 (12)
N016—N017—C02Y—C03P	-1.2 (13)	C052—F17—C18—F03T	-53 (17)
N016—C02Z—C03P—C02Y	-0.1 (14)	C052—F17—C18—F042	20 (18)
N017—N016—C02Z—C03P	-0.6 (14)	C052—F17—C18—F043	-177 (21)
N017—N016—B04C—N015	-60.4 (13)	C052—F17—C18—C04Q	59 (18)
N017—N016—B04C—N01W	59.6 (14)	C052—F17—C18—F20	-73 (17)
N017—C02Y—C03P—C02Z	0.8 (14)	C052—F17—C18—F35	179 (100)
N019—C021—C027—C01Y	177.9 (10)	C052—F20—C18—F03T	-12 (13)
N019—C021—C027—C02M	-2.1 (16)	C052—F20—C18—F042	17 (10)
N019—C02K—C03F—C02M	-0.6 (18)	C052—F20—C18—F043	121 (13)
N01A—N00U—C047—C03K	-1.9 (13)	C052—F20—C18—C04Q	-93 (13)
N01A—N00U—B04T—N00Y	-60.5 (13)	C052—F20—C18—F17	40 (11)
N01A—N00U—B04T—N01D	58.3 (14)	C052—F20—C18—F35	151 (14)
N01D—N01I—C035—C030	1.5 (13)	C052—F35—C18—F03T	-104 (29)
N01E—N014—C02N—C04B	-0.2 (14)	C052—F35—C18—F042	9 (25)
N01I—N01D—C03L—C030	0.2 (14)	C052—F35—C18—F043	-8 (26)
N01I—N01D—B04T—N00U	-55.9 (15)	C052—F35—C18—C04Q	125 (29)
N01I—N01D—B04T—N00Y	61.7 (14)	C052—F35—C18—F17	-1 (26)

N01J—N01M—C034—C04G	0.4 (14)	C052—F35—C18—F20	-113 (29)
N01J—C03R—C04G—C034	0.1 (15)	C054—C053—C055—C04Z	0 (3)
N01K—N010—C02R—C04P	-0.5 (13)	C055—C053—C054—C04M	0 (3)
N01K—C03D—C04P—C02R	0.3 (15)	C1—C11—C14—C10	162 (16)
N01M—N01J—C03R—C04G	0.1 (14)	C5—C1—C11—C14	-175 (15)
N01M—N01J—B049—N00O	55.2 (14)	C11—C1—C5—C3	-162 (15)
N01M—N01J—B049—N011	-65.7 (13)	F13—F46—C04W—C03W	94 (2)
N01M—C034—C04G—C03R	-0.3 (15)	F13—F46—C04W—F44	-34 (2)
N01N—N015—C03H—C03N	1.6 (13)	F13—F46—C04W—F45	-141 (2)
N01N—N015—B04C—N016	59.9 (12)	F13—F46—C04W—F14	-154 (5)
N01N—N015—B04C—N01W	-62.3 (12)	F13—F46—C04W—F25	-75 (4)
N01N—C036—C03N—C03H	0.0 (14)	F13—F46—F14—C04W	27 (5)
F01O—C03J—C03Q—O007	-178.3 (13)	F13—F46—F14—F45	15 (9)
F01O—C03J—C03Q—C046	2.7 (19)	F13—F44—C04W—F46	37 (2)
C01Q—N012—C02L—C03V	0.8 (16)	F13—F44—C04W—C03W	-91 (2)
C01Q—C020—C022—Yb01	166 (2)	F13—F44—C04W—F45	155 (2)
C01Q—C020—C022—O005	176.4 (10)	F13—F44—C04W—F14	75 (4)
C01Q—C020—C022—C01Y	-4.2 (15)	F13—F44—C04W—F25	158 (5)
C01Q—C020—C02C—C03V	2.6 (16)	F13—F44—F25—C04W	-25 (5)
C01Q—C021—C027—C01Y	-6.1 (15)	F13—F44—F25—F45	-20 (10)
C01Q—C021—C027—C02M	174.0 (10)	F13—C04W—F45—F14	-86 (5)
N01R—N01U—C02S—C03A	-0.3 (15)	F13—C04W—F45—F25	40 (5)
N01R—N01U—B04U—N01E	-56.6 (15)	F13—C04W—F14—F46	-23 (5)
N01R—N01U—B04U—N01K	62.7 (15)	F13—C04W—F14—F45	144 (2)

N01R—C025—C03A—C02S	1.2 (15)	F13—C04W—F25—F44	18 (4)
C01S—C01Z—C02E—C023	179.2 (10)	F13—C04W—F25—F45	-158 (2)
C01S—C01Z—C02E—C039	0.0 (15)	F14—F46—C04W—C03W	-112 (5)
C01S—C029—C02I—C02P	-177.7 (11)	F14—F46—C04W—F44	120 (5)
C01S—C029—C03Z—N01F	176.8 (10)	F14—F46—C04W—F45	13 (5)
C01S—C029—C03Z—C039	-3.9 (16)	F14—F46—C04W—F13	154 (5)
N01T—N00Y—C032—C040	0.0 (14)	F14—F46—C04W—F25	79 (6)
N01T—N00Y—B04T—N00U	51.2 (14)	F14—F46—F13—F44	6 (7)
N01T—N00Y—B04T—N01D	-66.9 (14)	F14—F46—F13—C04W	-30 (6)
N01T—C03E—C040—C032	-0.2 (15)	F14—C04W—F45—F25	125 (4)
N01U—N01R—C025—C03A	-1.3 (13)	F14—C04W—F13—F46	15 (3)
N01U—C02S—C03A—C025	-0.5 (15)	F14—C04W—F13—F44	-126 (3)
F01V—C03J—C03Q—O007	-62.9 (15)	F14—C04W—F25—F44	117 (4)
F01V—C03J—C03Q—C046	118.1 (14)	F14—C04W—F25—F45	-59 (4)
N01W—N01X—C03M—C037	0.9 (14)	F14—F45—F25—F44	34 (8)
N01W—C028—C037—C03M	1.7 (14)	F14—F45—F25—C04W	39 (2)
N01X—N01W—C028—C037	-1.3 (14)	F25—F44—C04W—F46	-120 (4)
N01X—N01W—B04C—N015	49.1 (13)	F25—F44—C04W—C03W	112 (4)
N01X—N01W—B04C—N016	-72.2 (13)	F25—F44—C04W—F45	-3 (4)
C01Y—C027—C02M—C03F	-177.9 (10)	F25—F44—C04W—F13	-158 (5)
C01Z—C01S—C029—C02I	-178.4 (10)	F25—F44—C04W—F14	-83 (5)
C01Z—C01S—C029—C03Z	3.1 (16)	F25—F44—F13—F46	-8 (6)
C01Z—C02E—C039—N00S	175.3 (10)	F25—F44—F13—C04W	27 (5)
C01Z—C02E—C039—C03Z	-0.8 (16)	F25—C04W—F45—F14	-125 (4)

C020—C01Q—C021—N019	179.0 (9)	F25—C04W—F13—F46	127 (3)
C020—C01Q—C021—C027	2.8 (15)	F25—C04W—F13—F44	-14 (3)
C020—C02C—C03V—C02L	-3.7 (17)	F25—C04W—F14—F46	-120 (5)
C021—N019—C02K—C03F	0.6 (17)	F25—C04W—F14—F45	48 (4)
C021—C01Q—C020—C022	2.4 (15)	F25—F45—F14—F46	-31 (7)
C021—C01Q—C020—C02C	-177.4 (10)	F25—F45—F14—C04W	-46 (3)
C021—C027—C02M—C03F	2.0 (17)	F1—F04F—C04K—F00Z	132 (2)
C022—C01Y—C027—C021	4.3 (15)	F1—F04F—C04K—C045	-106.6 (18)
C022—C01Y—C027—C02M	-175.8 (10)	F1—F04F—C04K—F04I	20 (2)
C022—C020—C02C—C03V	-177.2 (10)	F1—F04F—C04K—F6	38 (3)
C023—C02E—C039—N00S	-3.8 (16)	F1—F04F—C04K—F18	137 (3)
C023—C02E—C039—C03Z	180.0 (10)	F1—F04F—F18—F00Z	-26 (11)
F024—C03J—C03Q—O007	50.1 (17)	F1—F04F—F18—C04K	-40 (2)
F024—C03J—C03Q—C046	-128.8 (15)	F1—F04I—C04K—F00Z	-127.3 (18)
C025—N01R—N01U—C02S	1.0 (13)	F1—F04I—C04K—C045	107.7 (16)
C025—N01R—N01U—B04U	177.0 (11)	F1—F04I—C04K—F04F	-16.8 (18)
C027—C01Y—C022—Yb01	-176.6 (9)	F1—F04I—C04K—F6	-175 (4)
C027—C01Y—C022—O005	-179.6 (9)	F1—F04I—C04K—F18	-104 (2)
C027—C01Y—C022—C020	0.9 (15)	F1—F04I—F6—C04K	6 (5)
C027—C02M—C03F—C02K	-0.8 (17)	F1—C04K—F6—F04I	-4 (4)
C028—N01W—N01X—Yb01	-160.6 (7)	F1—C04K—F18—F00Z	-134 (7)
C028—N01W—N01X—C03M	0.2 (12)	F1—C04K—F18—F04F	35 (2)
C028—N01W—B04C—N015	-127.8 (12)	F6—F04I—C04K—F00Z	48 (4)
C028—N01W—B04C—N016	110.9 (13)	F6—F04I—C04K—C045	-77 (4)

C028—C037—C03M—N01X	-1.6 (15)	F6—F04I—C04K—F04F	158 (4)
C029—C01S—C01Z—Yb02	179.2 (10)	F6—F04I—C04K—F1	175 (4)
C029—C01S—C01Z—O00A	176.9 (9)	F6—F04I—C04K—F18	71 (4)
C029—C01S—C01Z—C02E	-1.1 (15)	F6—F04I—F1—F04F	17 (8)
C029—C02I—C02P—C02X	0.6 (17)	F6—F04I—F1—C04K	-7 (6)
C02A—C02W—C03B—O00C	1 (2)	F6—C04K—F1—F04F	-156 (2)
C02A—C02W—C03B—C04E	178.9 (12)	F6—C04K—F1—F04I	3 (2)
C02B—N00S—C039—C02E	2.9 (16)	F6—C04K—F18—F00Z	-32 (8)
C02B—N00S—C039—C03Z	179.2 (10)	F6—C04K—F18—F04F	136.8 (17)
C02C—C020—C022—Yb01	-14 (4)	F18—F00Z—C04K—C045	-110 (7)
C02C—C020—C022—O005	-3.8 (16)	F18—F00Z—C04K—F04F	11 (8)
C02C—C020—C022—C01Y	175.6 (10)	F18—F00Z—C04K—F04I	124 (7)
C02E—C023—C02J—C02B	0.3 (17)	F18—F00Z—C04K—F1	58 (8)
C02E—C039—C03Z—N01F	-177.9 (10)	F18—F00Z—C04K—F6	148 (7)
C02E—C039—C03Z—C029	2.8 (16)	F18—F04F—C04K—F00Z	-5 (3)
C02F—C031—C03I—O00I	-2 (2)	F18—F04F—C04K—C045	117 (2)
C02F—C031—C03I—C04O	-178.9 (13)	F18—F04F—C04K—F04I	-117 (3)
C02I—C029—C03Z—N01F	-1.7 (16)	F18—F04F—C04K—F1	-137 (3)
C02I—C029—C03Z—C039	177.6 (10)	F18—F04F—C04K—F6	-99 (3)
C02I—C02P—C02X—N01F	-1.2 (18)	F18—F04F—F1—F04I	11 (3)
C02J—C023—C02E—C01Z	-177.1 (10)	F18—F04F—F1—C04K	32.6 (16)
C02J—C023—C02E—C039	2.1 (16)	F18—C04K—F1—F04F	-48 (3)
C02K—N019—C021—C01Q	-175.3 (10)	F18—C04K—F1—F04I	110 (3)
C02K—N019—C021—C027	0.8 (16)	F18—C04K—F6—F04I	-122 (4)

C02L—N012—C01Q—C020	-2.1 (15)	F17—F042—C052—F03T	105 (7)
C02L—N012—C01Q—C021	175.8 (9)	F17—F042—C052—F043	-17 (6)
C02N—N014—N01E—C04D	-1.3 (13)	F17—F042—C052—C04Q	-135 (7)
C02N—N014—N01E—B04U	178.1 (11)	F17—F042—C052—F20	88 (7)
C02N—C04B—C04D—N01E	-2.4 (17)	F17—F042—C052—F35	-24 (6)
C02R—N010—N01K—C03D	0.7 (13)	F17—F042—C18—F03T	106 (6)
C02R—N010—N01K—B04U	-179.5 (11)	F17—F042—C18—F043	-16 (7)
C02S—N01U—B04U—N01E	118.7 (13)	F17—F042—C18—C04Q	-145 (6)
C02S—N01U—B04U—N01K	-122.0 (13)	F17—F042—C18—F20	94 (7)
F46—C04W—F45—F14	-8 (3)	F17—F042—C18—F35	-25 (7)
F46—C04W—F45—F25	117 (3)	F17—F043—C052—F03T	-105 (5)
F46—C04W—F13—F44	-141 (2)	F17—F043—C052—F042	8 (3)
F46—C04W—F14—F45	167 (5)	F17—F043—C052—C04Q	129 (4)
F46—C04W—F25—F44	79 (5)	F17—F043—C052—F20	-120 (5)
F46—C04W—F25—F45	-97 (4)	F17—F043—C052—F35	172 (8)
C02V—N00O—N00W—Yb02	175.1 (8)	F17—F043—F35—C052	-11 (11)
C02V—N00O—N00W—C02O	0.0 (12)	F17—F043—F35—C18	-12 (11)
C02V—N00O—B049—N011	-119.7 (13)	F17—F043—C18—F03T	-82 (5)
C02V—N00O—B049—N01J	119.0 (13)	F17—F043—C18—F042	6 (3)
C02W—C02A—C048—F00H	157.2 (11)	F17—F043—C18—C04Q	113 (4)
C02W—C02A—C048—F00L	38.0 (16)	F17—F043—C18—F20	-105 (3)
C02W—C02A—C048—F00T	-82.6 (14)	F17—F043—C18—F35	173 (6)
C02W—C03B—C04E—F00J	105.1 (14)	F17—C052—F20—F03T	71 (7)
C02W—C03B—C04E—F01H	-12.5 (19)	F17—C052—F20—C18	-121 (14)

C02W—C03B—C04E—F01P	-134.6 (14)	F17—C052—F35—F043	8 (8)
C02X—N01F—C03Z—C029	1.3 (15)	F17—C052—F35—C18	179 (100)
C02X—N01F—C03Z—C039	-178.1 (10)	F20—F03T—C052—F042	-150 (6)
C02Z—N016—N017—Yb01	177.5 (7)	F20—F03T—C052—F043	-36 (7)
C02Z—N016—N017—C02Y	1.1 (12)	F20—F03T—C052—C04Q	89 (7)
C02Z—N016—B04C—N015	121.3 (12)	F20—F03T—C052—F17	-120 (7)
C02Z—N016—B04C—N01W	-118.7 (12)	F20—F03T—C052—F35	-11 (7)
C031—C02F—C04A—F009	134.8 (12)	F20—F03T—C18—F042	-153 (6)
C031—C02F—C04A—F013	15.1 (17)	F20—F03T—C18—F043	-58 (9)
C031—C02F—C04A—F01C	-109.5 (14)	F20—F03T—C18—C04Q	109 (6)
C031—C03I—C04O—F01L	-138.9 (14)	F20—F03T—C18—F17	-132 (7)
C031—C03I—C04O—F026	106.2 (15)	F20—F03T—C18—F35	-21 (8)
C031—C03I—C04O—F03C	-16 (2)	F20—C052—F17—F042	-111 (6)
C032—N00Y—N01T—Yb02	-161.3 (8)	F20—C052—F17—F043	86 (4)
C032—N00Y—N01T—C03E	-0.1 (13)	F20—C052—F17—C18	88 (18)
C032—N00Y—B04T—N00U	-133.0 (12)	F20—C052—F35—F043	-112 (7)
C032—N00Y—B04T—N01D	108.9 (13)	F20—C052—F35—C18	60 (27)
C035—C030—C03L—N01D	0.8 (15)	F35—F043—C052—F03T	83 (7)
C039—N00S—C02B—C02J	-0.3 (17)	F35—F043—C052—F042	-164 (7)
C03D—N01K—B04U—N01E	-122.6 (13)	F35—F043—C052—C04Q	-43 (7)
C03D—N01K—B04U—N01U	117.8 (13)	F35—F043—C052—F17	-172 (8)
C03G—N00V—N011—C03U	-0.7 (12)	F35—F043—C052—F20	68 (7)
C03G—N00V—N011—B049	179.0 (10)	F35—F043—F17—F042	-19 (23)
C03G—C02Q—C03U—N011	-0.6 (15)	F35—F043—F17—C052	15 (15)

C03H—N015—N01N—Yb01	-176.8 (7)	F35—F043—F17—C18	15 (13)
C03H—N015—N01N—C036	-1.6 (11)	F35—F043—C18—F03T	105 (6)
C03H—N015—B04C—N016	-123.8 (11)	F35—F043—C18—F042	-167 (5)
C03H—N015—B04C—N01W	114.1 (12)	F35—F043—C18—C04Q	-60 (8)
C03J—C03Q—C046—C03X	174.8 (12)	F35—F043—C18—F17	-173 (6)
C03L—N01D—N01I—Yb02	172.3 (8)	F35—F043—C18—F20	82 (6)
C03L—N01D—N01I—C035	-1.0 (13)	F35—C052—F17—F042	161 (5)
C03L—N01D—B04T—N00U	126.4 (13)	F35—C052—F17—F043	-3 (3)
C03L—N01D—B04T—N00Y	-116.1 (13)	F35—C052—F17—C18	0 (16)
C03L—C030—C035—N01I	-1.4 (15)	F35—C052—F20—F03T	169 (6)
C03O—C03K—C047—N00U	1.1 (14)	F35—C052—F20—C18	-23 (11)
C03R—N01J—N01M—Yb02	-173.3 (7)	C18—F03T—C052—F042	-162 (15)
C03R—N01J—N01M—C034	-0.3 (12)	C18—F03T—C052—F043	-47 (11)
C03R—N01J—B049—N00O	-119.6 (12)	C18—F03T—C052—C04Q	78 (13)
C03R—N01J—B049—N011	119.5 (12)	C18—F03T—C052—F17	-132 (15)
C03S—C041—C04J—F00B	8.8 (18)	C18—F03T—C052—F20	-12 (13)
C03S—C041—C04J—F00D	131.9 (11)	C18—F03T—C052—F35	-23 (11)
C03S—C041—C04J—F00M	-110.6 (12)	C18—F03T—F20—C052	3 (3)
C03S—C045—C04K—F00Z	-3.0 (18)	C18—F042—C052—F03T	139 (34)
C03S—C045—C04K—F04F	-119.0 (16)	C18—F042—C052—F043	18 (31)
C03S—C045—C04K—F04I	118.7 (19)	C18—F042—C052—C04Q	-101 (33)
C03S—C045—C04K—F1	-172 (2)	C18—F042—C052—F17	34 (31)
C03S—C045—C04K—F6	84.9 (18)	C18—F042—C052—F20	123 (35)
C03S—C045—C04K—F18	-29 (2)	C18—F042—C052—F35	10 (29)

F03T—C052—F17—F042	-84 (6)	C18—F042—F17—F043	25 (10)
F03T—C052—F17—F043	112 (4)	C18—F042—F17—C052	-4 (4)
F03T—C052—F17—C18	115 (19)	C18—F043—C052—F03T	78 (15)
F03T—C052—F20—C18	168 (13)	C18—F043—C052—F042	-169 (18)
F03T—C052—F35—F043	-106 (7)	C18—F043—C052—C04Q	-48 (15)
F03T—C052—F35—C18	65 (26)	C18—F043—C052—F17	-177 (19)
F03T—F20—C18—F042	28 (7)	C18—F043—C052—F20	63 (15)
F03T—F20—C18—F043	132 (7)	C18—F043—C052—F35	-5 (16)
F03T—F20—C18—C04Q	-81 (7)	C18—F043—F17—F042	-33 (14)
F03T—F20—C18—F17	51 (7)	C18—F043—F17—C052	1 (5)
F03T—F20—C18—F35	162 (7)	C18—F043—F35—C052	1 (4)
C03U—N011—B049—N00O	123.8 (13)	C18—C04Q—C04S—C04H	-179 (2)
C03U—N011—B049—N01J	-115.6 (13)	C18—C04Q—C052—F03T	-93 (11)
C03U—C02Q—C03G—N00V	0.2 (14)	C18—C04Q—C052—F042	152 (12)
C03W—C04W—F45—F14	120 (3)	C18—C04Q—C052—F043	35 (9)
C03W—C04W—F45—F25	-115 (3)	C18—C04Q—C052—F17	125 (13)
C03W—C04W—F13—F46	-110.5 (15)	C18—C04Q—C052—F20	-65 (10)
C03W—C04W—F13—F44	108.9 (17)	C18—C04Q—C052—F35	20 (9)
C03W—C04W—F14—F46	87 (5)		

8.3.15 Crystallographic data for $Y(Tp^*)_2(hfac)$

Crystal data

$C_{35}H_{45}B_2F_6N_{12}O_2Y$	D_x = 1.391 Mg m^{-3}
M_r = 890.36	Mo $K\alpha$ radiation, λ = 0.71073 Å
Orthorhombic, *Fddd*	Cell parameters from 4637 reflections

a = 21.3779 (15) Å	θ = 2.3–26.2°
b = 24.9537 (14) Å	μ = 1.44 mm^{-1}
c = 31.8785 (19) Å	T = 150 K
V = 17005.8 (18) $Å^3$	Block, pink
Z = 16	0.3 × 0.12 × 0.1 mm
F(000) = 7328	

Data collection

Bruker APEX-II CCD diffractometer	5116 independent reflections
Radiation source: microfocus sealed tube, INCOATEC Iμs 3.0	3508 reflections with $I > 2\sigma(I)$
Multilayer mirror optics monochromator	R_{int} = 0.120
Detector resolution: 7.4074 pixels mm^{-1}	θ_{max} = 28.9°, θ_{min} = 2.3°
ϕ and ω scans	h = -27→28
Absorption correction: multi-scan *SADABS2016*/2 (Bruker,2016/2) was used for absorption correction. wR2(int) was 0.1141 before and 0.0913 after correction. The Ratio of minimum to maximum transmission is 0.7522. The λ/2 correction factor is Not present.	k = -33→33
T_{min} = 0.561, T_{max} = 0.746	l = -36→38
28721 measured reflections	

Refinement

Refinement on F^2	Primary atom site location: dual
Least-squares matrix: full	Hydrogen site location: inferred from neighbouring sites
$R[F^2 > 2\sigma(F^2)]$ = 0.052	H-atom parameters constrained
$wR(F^2)$ = 0.124	$w = 1/[\sigma^2(F_o^2) + (0.0455P)^2 + 45.6142P]$ where $P = (F_o^2 + 2F_c^2)/3$
S = 1.02	$(\Delta/\sigma)_{max}$ = 0.005
5116 reflections	$\Delta\rangle_{max}$ = 0.41 e $Å^{-3}$
281 parameters	$\Delta\rangle_{min}$ = -0.56 e $Å^{-3}$
6 restraints	

Special details

Geometry. All esds (except the esd in the dihedral angle between two l.s. planes) are estimated using the full covariance matrix. The cell esds are taken into account individually in the estimation

of esds in distances, angles and torsion angles; correlations between esds in cell parameters are only used when they are defined by crystal symmetry. An approximate (isotropic) treatment of cell esds is used for estimating esds involving l.s. planes.

Fractional atomic coordinates and isotropic or equivalent isotropic displacement parameters (Å²)

	x	*y*	*z*	U_{iso}*/U_{eq}	Occ. (<1)
Y1	0.625000	0.34329 (2)	0.625000	0.02003 (12)	
F1	0.6629 (2)	0.54942 (18)	0.69806 (17)	0.1040 (16)	0.75
F2	0.74772 (18)	0.5135 (3)	0.68147 (15)	0.0949 (16)	0.75
F3	0.6899 (3)	0.47785 (19)	0.72714 (11)	0.1074 (18)	0.75
O1	0.66579 (10)	0.42129 (8)	0.65842 (7)	0.0310 (5)	
C1	0.6911 (2)	0.50271 (16)	0.68988 (15)	0.0581 (11)	
C2	0.65763 (16)	0.47064 (13)	0.65544 (11)	0.0388 (8)	
C3	0.625000	0.49791 (19)	0.625000	0.0463 (13)	
H3	0.625000	0.535983	0.624999	0.056*	
N1T	0.69657 (11)	0.37393 (9)	0.56780 (7)	0.0244 (5)	
N2T	0.66741 (11)	0.36625 (9)	0.52963 (7)	0.0241 (5)	
N3T	0.66491 (12)	0.26454 (9)	0.58420 (7)	0.0253 (5)	
N4T	0.65567 (11)	0.26703 (9)	0.54130 (7)	0.0234 (5)	
N5T	0.54190 (11)	0.31861 (10)	0.57559 (7)	0.0250 (5)	
N6T	0.55815 (11)	0.32306 (9)	0.53390 (7)	0.0237 (5)	
C1T	0.77665 (16)	0.43602 (14)	0.59701 (11)	0.0396 (8)	
H1TA	0.766522	0.417666	0.623324	0.059*	
H1TB	0.771033	0.474723	0.600604	0.059*	
H1TC	0.820190	0.428532	0.589375	0.059*	
C2T	0.73411 (14)	0.41632 (12)	0.56290 (10)	0.0283 (7)	
C3T	0.72860 (16)	0.43669 (13)	0.52247 (10)	0.0345 (8)	
H3T	0.750086	0.466658	0.511061	0.041*	
C4T	0.68603 (15)	0.40486 (12)	0.50250 (10)	0.0299 (7)	
C5T	0.66078 (17)	0.40941 (15)	0.45889 (11)	0.0429 (9)	
H5TA	0.669784	0.376372	0.443411	0.064*	
H5TB	0.680574	0.439815	0.444660	0.064*	
H5TC	0.615445	0.415036	0.460033	0.064*	
C6T	0.70689 (18)	0.19693 (13)	0.63479 (10)	0.0405 (8)	
H6TA	0.704073	0.226710	0.654734	0.061*	
H6TB	0.749701	0.182895	0.634547	0.061*	
H6TC	0.677916	0.168454	0.643203	0.061*	
C7T	0.69007 (15)	0.21632 (12)	0.59190 (10)	0.0303 (7)	

C8T	0.69715 (15)	0.18812 (12)	0.55440 (10)	0.0316 (7)	
H8T	0.713904	0.153112	0.551095	0.038*	
C9T	0.67517 (14)	0.22090 (12)	0.52336 (10)	0.0273 (7)	
C10T	0.67233 (17)	0.21001 (13)	0.47748 (10)	0.0367 (8)	
H10A	0.628736	0.211538	0.468048	0.055*	
H10B	0.689450	0.174323	0.471766	0.055*	
H10C	0.696926	0.237013	0.462441	0.055*	
C11T	0.44433 (16)	0.30876 (15)	0.61656 (11)	0.0413 (9)	
H11A	0.429053	0.271749	0.617380	0.062*	
H11B	0.408794	0.333480	0.618188	0.062*	
H11C	0.472387	0.315010	0.640380	0.062*	
C12T	0.47895 (14)	0.31795 (12)	0.57664 (10)	0.0288 (7)	
C13T	0.45490 (15)	0.32313 (13)	0.53680 (10)	0.0331 (7)	
H13T	0.411963	0.324269	0.529171	0.040*	
C14T	0.50567 (14)	0.32632 (12)	0.51011 (10)	0.0294 (7)	
C15T	0.50601 (17)	0.33222 (15)	0.46332 (11)	0.0429 (9)	
H15A	0.521078	0.368056	0.455844	0.064*	
H15B	0.463489	0.327305	0.452507	0.064*	
H15C	0.533702	0.305142	0.451031	0.064*	
B1T	0.62684 (16)	0.31654 (13)	0.51980 (10)	0.0235 (7)	
H1T	0.627379	0.310519	0.488788	0.028*	
F2A	0.7127 (9)	0.5476 (6)	0.6706 (5)	0.116 (5)*	0.25
F3A	0.7438 (7)	0.4800 (6)	0.7002 (5)	0.099 (5)*	0.25
F1A	0.6580 (7)	0.5137 (8)	0.7193 (5)	0.101 (5)*	0.25

Atomic displacement parameters (Å²)

	U^{11}	U^{22}	U^{33}	U^{12}	U^{13}	U^{23}
Y1	0.0234 (2)	0.02162 (19)	0.0151 (2)	0.000	0.00055 (17)	0.000
F1	0.113 (4)	0.072 (3)	0.126 (4)	0.014 (3)	-0.031 (3)	-0.071 (3)
F2	0.052 (2)	0.145 (4)	0.088 (3)	-0.049 (3)	0.012 (2)	-0.064 (3)
F3	0.184 (5)	0.094 (3)	0.045 (2)	-0.080 (3)	-0.035 (3)	-0.004 (2)
O1	0.0357 (12)	0.0294 (11)	0.0279 (12)	-0.0077 (9)	0.0019 (10)	-0.0019 (9)
C1	0.062 (3)	0.041 (2)	0.072 (3)	-0.020 (2)	0.003 (2)	-0.018 (2)
C2	0.040 (2)	0.0335 (18)	0.043 (2)	-0.0105 (15)	0.0060 (16)	-0.0091 (16)
C3	0.057 (3)	0.026 (2)	0.056 (3)	0.000	-0.001 (3)	0.000
N1T	0.0249 (12)	0.0277 (12)	0.0204 (13)	0.0007 (11)	-0.0006 (10)	0.0020 (10)
N2T	0.0250 (12)	0.0293 (13)	0.0180 (13)	0.0035 (10)	0.0027 (10)	0.0021 (10)
N3T	0.0339 (14)	0.0240 (12)	0.0181 (13)	0.0050 (10)	0.0009 (11)	0.0021 (10)

N4T	0.0280 (13)	0.0264 (12)	0.0158 (13)	0.0036 (10)	0.0000 (10)	-0.0006 (10)
N5T	0.0235 (13)	0.0322 (13)	0.0191 (14)	0.0006 (10)	0.0014 (10)	-0.0026 (10)
N6T	0.0271 (13)	0.0240 (12)	0.0199 (13)	0.0021 (10)	-0.0013 (10)	-0.0008 (10)
C1T	0.0335 (19)	0.050 (2)	0.036 (2)	-0.0125 (15)	-0.0018 (15)	0.0071 (16)
C2T	0.0241 (15)	0.0326 (16)	0.0282 (17)	-0.0019 (12)	0.0041 (13)	0.0034 (13)
C3T	0.0361 (18)	0.0356 (18)	0.0317 (19)	-0.0055 (14)	0.0048 (15)	0.0109 (14)
C4T	0.0310 (16)	0.0329 (16)	0.0259 (17)	0.0020 (13)	0.0058 (13)	0.0090 (13)
C5T	0.046 (2)	0.050 (2)	0.033 (2)	-0.0047 (17)	-0.0042 (16)	0.0188 (16)
C6T	0.057 (2)	0.0329 (17)	0.032 (2)	0.0140 (16)	-0.0067 (16)	0.0022 (14)
C7T	0.0356 (18)	0.0261 (15)	0.0293 (17)	0.0079 (13)	-0.0026 (14)	0.0020 (13)
C8T	0.0382 (18)	0.0243 (15)	0.0323 (19)	0.0081 (13)	0.0002 (14)	-0.0038 (13)
C9T	0.0265 (15)	0.0286 (15)	0.0267 (17)	0.0026 (12)	0.0015 (13)	-0.0054 (13)
C10T	0.044 (2)	0.0370 (18)	0.0294 (19)	0.0054 (15)	0.0030 (15)	-0.0120 (15)
C11T	0.0291 (18)	0.056 (2)	0.038 (2)	-0.0083 (16)	0.0072 (15)	-0.0071 (16)
C12T	0.0232 (15)	0.0318 (16)	0.0314 (18)	-0.0034 (12)	-0.0001 (13)	-0.0078 (13)
C13T	0.0222 (15)	0.0403 (18)	0.0367 (19)	-0.0008 (13)	-0.0070 (14)	-0.0051 (15)
C14T	0.0311 (17)	0.0287 (15)	0.0285 (18)	0.0028 (13)	-0.0079 (14)	-0.0025 (13)
C15T	0.041 (2)	0.057 (2)	0.031 (2)	0.0000 (17)	-0.0109 (16)	0.0075 (16)
B1T	0.0269 (17)	0.0287 (16)	0.0151 (16)	0.0057 (14)	0.0021 (14)	0.0012 (13)

Geometric parameters (Å, º)

Y1—O1^{i}	2.384 (2)	C1T—H1TC	0.9800
Y1—O1	2.384 (2)	C1T—C2T	1.500 (4)
Y1—N1T	2.500 (2)	C2T—C3T	1.390 (4)
Y1—N1T^{i}	2.500 (2)	C3T—H3T	0.9500
Y1—N3T	2.506 (2)	C3T—C4T	1.365 (5)
Y1—N3T^{i}	2.506 (2)	C4T—C5T	1.495 (4)
Y1—N5T^{i}	2.453 (2)	C5T—H5TA	0.9800
Y1—N5T	2.453 (2)	C5T—H5TB	0.9800
F1—C1	1.338 (6)	C5T—H5TC	0.9800
F2—C1	1.268 (5)	C6T—H6TA	0.9800
F3—C1	1.340 (6)	C6T—H6TB	0.9800
O1—C2	1.247 (4)	C6T—H6TC	0.9800
C1—C2	1.536 (5)	C6T—C7T	1.494 (4)
C1—F2A	1.359 (13)	C7T—C8T	1.395 (4)
C1—F3A	1.304 (13)	C8T—H8T	0.9500
C1—F1A	1.206 (13)	C8T—C9T	1.367 (4)
C2—C3	1.375 (4)	C9T—C10T	1.489 (4)

C3—H3	0.9500	C10T—H10A	0.9800
N1T—N2T	1.380 (3)	C10T—H10B	0.9800
N1T—C2T	1.337 (4)	C10T—H10C	0.9800
N2T—C4T	1.355 (4)	C11T—H11A	0.9800
N2T—B1T	1.546 (4)	C11T—H11B	0.9800
N3T—N4T	1.383 (3)	C11T—H11C	0.9800
N3T—C7T	1.340 (4)	C11T—C12T	1.490 (4)
N4T—C9T	1.351 (4)	C12T—C13T	1.376 (4)
N4T—B1T	1.541 (4)	C13T—H13T	0.9500
N5T—N6T	1.378 (3)	C13T—C14T	1.381 (5)
N5T—C12T	1.346 (4)	C14T—C15T	1.499 (4)
N6T—C14T	1.357 (4)	C15T—H15A	0.9800
N6T—B1T	1.544 (4)	C15T—H15B	0.9800
C1T—H1TA	0.9800	C15T—H15C	0.9800
C1T—H1TB	0.9800	B1T—H1T	1.0000
O1^{i}—Y1—O1	70.55 (10)	H1TB—C1T—H1TC	109.5
O1^{i}—Y1—N1T	69.41 (8)	C2T—C1T—H1TA	109.5
O1—Y1—N1T	81.51 (7)	C2T—C1T—H1TB	109.5
O1—Y1—N1T^{i}	69.41 (8)	C2T—C1T—H1TC	109.5
O1^{i}—Y1—N1T^{i}	81.51 (7)	N1T—C2T—C1T	122.6 (3)
O1^{i}—Y1—N3T	122.19 (7)	N1T—C2T—C3T	110.3 (3)
O1^{i}—Y1—N3T^{i}	138.37 (8)	C3T—C2T—C1T	127.1 (3)
O1—Y1—N3T^{i}	122.19 (7)	C2T—C3T—H3T	127.0
O1—Y1—N3T	138.38 (8)	C4T—C3T—C2T	106.0 (3)
O1—Y1—N5T^{i}	69.70 (8)	C4T—C3T—H3T	127.0
O1^{i}—Y1—N5T	69.70 (8)	N2T—C4T—C3T	108.2 (3)
O1^{i}—Y1—N5T^{i}	139.19 (8)	N2T—C4T—C5T	122.8 (3)
O1—Y1—N5T	139.19 (8)	C3T—C4T—C5T	129.0 (3)
N1T^{i}—Y1—N1T	144.39 (11)	C4T—C5T—H5TA	109.5
N1T^{i}—Y1—N3T^{i}	69.70 (8)	C4T—C5T—H5TB	109.5
N1T—Y1—N3T^{i}	145.75 (8)	C4T—C5T—H5TC	109.5
N1T—Y1—N3T	69.69 (8)	H5TA—C5T—H5TB	109.5
N1T^{i}—Y1—N3T	145.75 (8)	H5TA—C5T—H5TC	109.5
N3T^{i}—Y1—N3T	76.72 (11)	H5TB—C5T—H5TC	109.5
N5T^{i}—Y1—N1T	95.84 (8)	H6TA—C6T—H6TB	109.5
N5T—Y1—N1T	92.96 (8)	H6TA—C6T—H6TC	109.5
N5T—Y1—N1T^{i}	95.84 (8)	H6TB—C6T—H6TC	109.5
N5T^{i}—Y1—N1T^{i}	92.97 (8)	C7T—C6T—H6TA	109.5
N5T^{i}—Y1—N3T^{i}	73.53 (8)	C7T—C6T—H6TB	109.5

N5T—Y1—N3T^{i}	83.67 (8)	C7T—C6T—H6TC	109.5
N5T^{i}—Y1—N3T	83.67 (8)	N3T—C7T—C6T	123.7 (3)
N5T—Y1—N3T	73.53 (8)	N3T—C7T—C8T	109.8 (3)
N5T^{i}—Y1—N5T	150.92 (11)	C8T—C7T—C6T	126.5 (3)
C2—O1—Y1	136.1 (2)	C7T—C8T—H8T	126.8
F1—C1—F3	102.8 (5)	C9T—C8T—C7T	106.3 (3)
F1—C1—C2	112.5 (4)	C9T—C8T—H8T	126.8
F2—C1—F1	106.6 (4)	N4T—C9T—C8T	108.0 (3)
F2—C1—F3	107.7 (5)	N4T—C9T—C10T	124.0 (3)
F2—C1—C2	113.8 (4)	C8T—C9T—C10T	128.0 (3)
F3—C1—C2	112.5 (3)	C9T—C10T—H10A	109.5
F2A—C1—C2	105.4 (8)	C9T—C10T—H10B	109.5
F3A—C1—C2	110.9 (8)	C9T—C10T—H10C	109.5
F3A—C1—F2A	100.4 (11)	H10A—C10T—H10B	109.5
F1A—C1—C2	113.6 (9)	H10A—C10T—H10C	109.5
F1A—C1—F2A	111.3 (12)	H10B—C10T—H10C	109.5
F1A—C1—F3A	114.2 (12)	H11A—C11T—H11B	109.5
O1—C2—C1	113.3 (3)	H11A—C11T—H11C	109.5
O1—C2—C3	127.8 (3)	H11B—C11T—H11C	109.5
C3—C2—C1	118.9 (3)	C12T—C11T—H11A	109.5
C2—C3—C2^{i}	120.7 (4)	C12T—C11T—H11B	109.5
C2^{i}—C3—H3	119.7	C12T—C11T—H11C	109.5
C2—C3—H3	119.7	N5T—C12T—C11T	121.3 (3)
N2T—N1T—Y1	108.90 (16)	N5T—C12T—C13T	110.5 (3)
C2T—N1T—Y1	134.0 (2)	C13T—C12T—C11T	128.1 (3)
C2T—N1T—N2T	106.1 (2)	C12T—C13T—H13T	126.9
N1T—N2T—B1T	122.9 (2)	C12T—C13T—C14T	106.3 (3)
C4T—N2T—N1T	109.3 (2)	C14T—C13T—H13T	126.9
C4T—N2T—B1T	127.3 (3)	N6T—C14T—C13T	107.6 (3)
N4T—N3T—Y1	115.41 (16)	N6T—C14T—C15T	123.9 (3)
C7T—N3T—Y1	138.2 (2)	C13T—C14T—C15T	128.5 (3)
C7T—N3T—N4T	106.2 (2)	C14T—C15T—H15A	109.5
N3T—N4T—B1T	122.2 (2)	C14T—C15T—H15B	109.5
C9T—N4T—N3T	109.6 (2)	C14T—C15T—H15C	109.5
C9T—N4T—B1T	128.2 (2)	H15A—C15T—H15B	109.5
N6T—N5T—Y1	114.60 (17)	H15A—C15T—H15C	109.5
C12T—N5T—Y1	135.3 (2)	H15B—C15T—H15C	109.5
C12T—N5T—N6T	106.1 (2)	N2T—B1T—H1T	108.3
N5T—N6T—B1T	120.8 (2)	N4T—B1T—N2T	109.2 (2)
C14T—N6T—N5T	109.6 (2)	N4T—B1T—N6T	109.6 (2)

C14T—N6T—B1T	129.0 (3)	N4T—B1T—H1T	108.3
H1TA—C1T—H1TB	109.5	N6T—B1T—N2T	112.9 (2)
H1TA—C1T—H1TC	109.5	N6T—B1T—H1T	108.3

Symmetry code: (i) -*x*+5/4, *y*, -*z*+5/4.

8.3.16 Crystallographic data for Y(Tp*)(hfac)$_2$(THF)

Crystal data

$C_{29}H_{32}BF_{12}N_6O_5Y$	Z = 2
M_r = 872.32	F(000) = 880
Triclinic, $P\bar{1}$	D_x = 1.641 Mg m^{-3}
a = 8.2157 (6) Å	Mo $K\alpha$ radiation, λ = 0.71073 Å
b = 11.2286 (16) Å	Cell parameters from 1800 reflections
c = 20.006 (3) Å	θ = 2.4–23.9°
α = 74.493 (3)°	μ = 1.76 mm^{-1}
β = 85.766 (3)°	T = 150 K
γ = 83.772 (2)°	Tablet, pink
V = 1765.9 (4) Å^3	0.29 × 0.27 × 0.07 mm

Data collection

Bruker D8 VENTURE diffractometer	5811 independent reflections
Radiation source: microfocus sealed tube, INCOATEC Iμs 3.0	3709 reflections with $I > 2\sigma(I)$
Multilayer mirror optics monochromator	R_{int} = 0.081
Detector resolution: 7.4074 pixels mm^{-1}	θ_{max} = 25.4°, θ_{min} = 2.4°
ϕ and ω scans	h = -9→8
Absorption correction: multi-scan *SADABS2016*/2 (Bruker,2016/2) was used for absorption correction. wR2(int) was 0.0603 before and 0.0482 after correction. The Ratio of minimum to maximum transmission is 0.9083. The λ/2 correction factor is Not present.	k = -13→13
T_{min} = 0.610, T_{max} = 0.745	l = -24→24
10471 measured reflections	

Refinement

Refinement on F^2	Primary atom site location: dual

Least-squares matrix: full	Hydrogen site location: inferred from neighbouring sites
$R[F^2 > 2\sigma(F^2)] = 0.058$	H-atom parameters constrained
$wR(F^2) = 0.151$	$w = 1/[\sigma^2(F_o^2) + (0.0483P)^2]$ where $P = (F_o^2 + 2F_c^2)/3$
$S = 1.05$	$(\Delta/\sigma)_{max} < 0.001$
5811 reflections	$\Delta\rangle_{max} = 0.50$ e Å^{-3}
493 parameters	$\Delta\rangle_{min} = -0.60$ e Å^{-3}
0 restraints	

Special details

Geometry. All esds (except the esd in the dihedral angle between two l.s. planes) are estimated using the full covariance matrix. The cell esds are taken into account individually in the estimation of esds in distances, angles and torsion angles; correlations between esds in cell parameters are only used when they are defined by crystal symmetry. An approximate (isotropic) treatment of cell esds is used for estimating esds involving l.s. planes.

Fractional atomic coordinates and isotropic or equivalent isotropic displacement parameters (Å²)

	x	*y*	*z*	U_{iso}*/U_{eq}
Y1	0.63273 (6)	0.58368 (5)	0.24407 (3)	0.02838 (18)
F1	0.9901 (5)	0.9574 (4)	0.2055 (3)	0.0865 (16)
F2	0.8443 (7)	1.0530 (4)	0.1198 (3)	0.0943 (17)
F3	0.7342 (4)	1.0005 (3)	0.2219 (2)	0.0542 (10)
F4	1.0522 (5)	0.6055 (4)	0.0340 (2)	0.0756 (14)
F5	0.9375 (6)	0.7764 (4)	-0.0226 (2)	0.0874 (15)
F6	0.8101 (5)	0.6121 (5)	0.0033 (2)	0.0823 (15)
F7	0.3505 (5)	1.0506 (3)	0.2753 (2)	0.0756 (14)
F8	0.2138 (4)	0.9074 (4)	0.3387 (2)	0.0596 (11)
F9	0.4629 (5)	0.9125 (4)	0.3589 (2)	0.0734 (13)
F10	0.2410 (5)	0.7913 (5)	0.0606 (2)	0.0904 (17)
F11	0.4695 (5)	0.8621 (4)	0.0243 (2)	0.0702 (13)
F12	0.2760 (6)	0.9786 (4)	0.0565 (2)	0.0908 (16)
O1	0.7687 (4)	0.7621 (4)	0.2226 (2)	0.0342 (10)
O1F	0.5231 (4)	0.4517 (4)	0.1782 (2)	0.0348 (10)
O2	0.7979 (4)	0.6063 (4)	0.1401 (2)	0.0346 (10)
O3	0.4729 (4)	0.7407 (4)	0.2895 (2)	0.0363 (10)
O4	0.4772 (4)	0.7108 (4)	0.1571 (2)	0.0376 (10)
N1T	0.4170 (5)	0.4767 (4)	0.3161 (2)	0.0290 (11)

N2T	0.4555 (5)	0.3706 (4)	0.3672 (2)	0.0324 (11)
N3T	0.7920 (5)	0.3757 (4)	0.2764 (2)	0.0303 (11)
N4T	0.7542 (5)	0.2992 (4)	0.3411 (2)	0.0333 (12)
N5T	0.7331 (5)	0.5571 (4)	0.3621 (2)	0.0285 (11)
N6T	0.6912 (5)	0.4510 (4)	0.4125 (2)	0.0311 (11)
C1	0.8453 (8)	0.9637 (6)	0.1784 (4)	0.0482 (17)
C1F	0.4927 (8)	0.4866 (6)	0.1052 (3)	0.0425 (16)
H1FA	0.560136	0.551466	0.080096	0.051*
H1FB	0.378310	0.515840	0.097620	0.051*
C1T	0.1680 (7)	0.5832 (6)	0.2556 (3)	0.0436 (17)
H1TA	0.181534	0.661549	0.264245	0.065*
H1TB	0.053541	0.571055	0.258825	0.065*
H1TC	0.212349	0.582628	0.209894	0.065*
C2	0.8175 (6)	0.8380 (5)	0.1679 (3)	0.0335 (14)
C2F	0.5373 (8)	0.3697 (7)	0.0827 (3)	0.0518 (18)
H2FA	0.654660	0.357066	0.073494	0.062*
H2FB	0.481385	0.371566	0.041313	0.062*
C2T	0.2556 (6)	0.4819 (5)	0.3078 (3)	0.0313 (13)
C3	0.8523 (7)	0.8170 (6)	0.1042 (3)	0.0371 (15)
H3	0.880198	0.881405	0.066447	0.045*
C3F	0.4801 (10)	0.2698 (7)	0.1441 (3)	0.064 (2)
H3FA	0.370001	0.251662	0.138322	0.077*
H3FB	0.552914	0.194088	0.149921	0.077*
C3T	0.1915 (7)	0.3788 (6)	0.3535 (3)	0.0389 (15)
H3T	0.082772	0.360614	0.358453	0.047*
C4	0.8457 (7)	0.6980 (6)	0.0960 (3)	0.0361 (15)
C4F	0.4838 (8)	0.3233 (6)	0.2056 (3)	0.0433 (16)
H4FA	0.378061	0.320523	0.230720	0.052*
H4FB	0.566215	0.276236	0.237035	0.052*
C4T	0.3204 (7)	0.3096 (6)	0.3897 (3)	0.0373 (15)
C5	0.9093 (8)	0.6752 (7)	0.0264 (4)	0.0470 (17)
C5T	0.3220 (8)	0.1904 (6)	0.4447 (3)	0.0521 (18)
H5TA	0.390288	0.127328	0.428954	0.078*
H5TB	0.212460	0.166140	0.454563	0.078*
H5TC	0.364413	0.200722	0.486033	0.078*
C6	0.3609 (8)	0.9305 (6)	0.3082 (4)	0.0486 (18)
C6T	0.9738 (7)	0.3541 (6)	0.1738 (3)	0.0472 (17)
H6TA	0.887542	0.390585	0.142714	0.071*
H6TB	1.033196	0.286368	0.159050	0.071*
H6TC	1.046953	0.415479	0.173319	0.071*

C7	0.4116 (7)	0.8470 (6)	0.2601 (4)	0.0404 (16)
C7T	0.9026 (7)	0.3079 (6)	0.2448 (3)	0.0354 (15)
C8	0.3774 (7)	0.8934 (6)	0.1898 (3)	0.0389 (16)
H8	0.334297	0.975301	0.173204	0.047*
C8T	0.9321 (7)	0.1900 (6)	0.2882 (4)	0.0454 (17)
H8T	1.002211	0.125330	0.278452	0.054*
C9	0.4075 (6)	0.8183 (6)	0.1453 (3)	0.0379 (16)
C9T	0.8391 (7)	0.1863 (5)	0.3477 (3)	0.0380 (15)
C10	0.3482 (8)	0.8651 (6)	0.0711 (4)	0.0510 (18)
C10T	0.8263 (9)	0.0807 (6)	0.4121 (4)	0.062 (2)
H10A	0.902565	0.011965	0.407446	0.093*
H10B	0.716957	0.055629	0.418187	0.093*
H10C	0.851272	0.107153	0.451715	0.093*
C11T	0.8580 (7)	0.7508 (6)	0.3636 (3)	0.0456 (17)
H11A	0.945656	0.742207	0.330277	0.068*
H11B	0.897252	0.783094	0.398681	0.068*
H11C	0.770136	0.806676	0.340771	0.068*
C12T	0.7971 (6)	0.6262 (5)	0.3968 (3)	0.0323 (14)
C13T	0.7974 (7)	0.5688 (6)	0.4667 (3)	0.0402 (15)
H13T	0.834825	0.598806	0.501294	0.048*
C14T	0.7314 (7)	0.4584 (6)	0.4752 (3)	0.0395 (15)
C15T	0.6980 (9)	0.3612 (7)	0.5414 (3)	0.0561 (19)
H15A	0.583245	0.349511	0.546458	0.084*
H15B	0.729253	0.387501	0.580099	0.084*
H15C	0.760153	0.284345	0.539886	0.084*
B1T	0.6315 (8)	0.3399 (6)	0.3946 (4)	0.0337 (16)
H1T	0.629162	0.271463	0.436930	0.040*

Atomic displacement parameters (Å²)

	U^{11}	U^{22}	U^{33}	U^{12}	U^{13}	U^{23}
Y1	0.0288 (3)	0.0228 (3)	0.0336 (3)	-0.0015 (2)	-0.0035 (2)	-0.0073 (2)
F1	0.042 (2)	0.081 (3)	0.164 (5)	-0.018 (2)	0.000 (2)	-0.076 (3)
F2	0.167 (5)	0.034 (3)	0.077 (3)	-0.032 (3)	0.032 (3)	-0.008 (2)
F3	0.051 (2)	0.039 (2)	0.078 (3)	-0.0059 (17)	0.0119 (19)	-0.026 (2)
F4	0.054 (2)	0.096 (4)	0.086 (3)	0.003 (2)	0.016 (2)	-0.047 (3)
F5	0.142 (4)	0.059 (3)	0.055 (3)	-0.013 (3)	0.034 (3)	-0.012 (2)
F6	0.077 (3)	0.129 (5)	0.065 (3)	-0.047 (3)	0.021 (2)	-0.058 (3)
F7	0.105 (3)	0.022 (2)	0.090 (3)	-0.004 (2)	0.039 (3)	-0.012 (2)

F8	0.048 (2)	0.049 (3)	0.077 (3)	-0.0013 (18)	0.022 (2)	-0.016 (2)
F9	0.065 (3)	0.072 (3)	0.101 (4)	0.011 (2)	-0.017 (2)	-0.057 (3)
F10	0.082 (3)	0.103 (4)	0.080 (3)	-0.034 (3)	-0.042 (3)	0.008 (3)
F11	0.072 (3)	0.082 (3)	0.044 (3)	0.001 (2)	-0.005 (2)	0.004 (2)
F12	0.109 (4)	0.066 (3)	0.073 (3)	0.041 (3)	-0.024 (3)	0.010 (3)
O1	0.033 (2)	0.033 (2)	0.040 (3)	-0.0084 (18)	-0.0020 (18)	-0.012 (2)
O1F	0.044 (2)	0.030 (2)	0.032 (2)	-0.0074 (18)	-0.0059 (18)	-0.0077 (19)
O2	0.036 (2)	0.030 (2)	0.039 (3)	-0.0040 (18)	0.0015 (18)	-0.011 (2)
O3	0.034 (2)	0.027 (2)	0.045 (3)	0.0025 (18)	-0.0034 (18)	-0.005 (2)
O4	0.037 (2)	0.030 (3)	0.042 (3)	0.0001 (19)	-0.0061 (18)	-0.004 (2)
N1T	0.029 (3)	0.025 (3)	0.033 (3)	-0.002 (2)	-0.0036 (19)	-0.008 (2)
N2T	0.038 (3)	0.025 (3)	0.034 (3)	-0.002 (2)	-0.002 (2)	-0.008 (2)
N3T	0.035 (3)	0.025 (3)	0.031 (3)	0.003 (2)	-0.008 (2)	-0.009 (2)
N4T	0.040 (3)	0.024 (3)	0.037 (3)	0.000 (2)	-0.011 (2)	-0.008 (2)
N5T	0.030 (2)	0.027 (3)	0.029 (3)	0.000 (2)	-0.005 (2)	-0.007 (2)
N6T	0.036 (3)	0.024 (3)	0.033 (3)	0.000 (2)	-0.005 (2)	-0.006 (2)
C1	0.046 (4)	0.037 (4)	0.063 (5)	-0.013 (3)	0.011 (3)	-0.014 (4)
C1F	0.056 (4)	0.047 (4)	0.026 (4)	-0.011 (3)	-0.012 (3)	-0.006 (3)
C1T	0.029 (3)	0.047 (4)	0.053 (4)	-0.002 (3)	-0.004 (3)	-0.009 (3)
C2	0.026 (3)	0.028 (3)	0.044 (4)	-0.004 (2)	-0.004 (3)	-0.005 (3)
C2F	0.058 (4)	0.062 (5)	0.040 (4)	-0.011 (4)	-0.002 (3)	-0.018 (4)
C2T	0.036 (3)	0.028 (3)	0.034 (4)	-0.009 (3)	-0.001 (3)	-0.011 (3)
C3	0.041 (3)	0.036 (4)	0.034 (4)	-0.005 (3)	0.005 (3)	-0.010 (3)
C3F	0.101 (6)	0.049 (5)	0.041 (4)	0.005 (4)	-0.001 (4)	-0.015 (4)
C3T	0.033 (3)	0.043 (4)	0.045 (4)	-0.018 (3)	0.002 (3)	-0.014 (3)
C4	0.032 (3)	0.037 (4)	0.040 (4)	-0.001 (3)	0.003 (3)	-0.012 (3)
C4F	0.055 (4)	0.035 (4)	0.043 (4)	-0.013 (3)	-0.006 (3)	-0.012 (3)
C4T	0.045 (4)	0.034 (4)	0.035 (4)	-0.021 (3)	0.006 (3)	-0.008 (3)
C5	0.045 (4)	0.048 (5)	0.052 (5)	-0.015 (3)	0.008 (3)	-0.020 (4)
C5T	0.062 (4)	0.043 (4)	0.049 (4)	-0.019 (3)	0.003 (3)	-0.003 (4)
C6	0.041 (4)	0.037 (4)	0.064 (5)	-0.001 (3)	0.006 (3)	-0.010 (4)
C6T	0.053 (4)	0.045 (4)	0.048 (4)	0.014 (3)	0.002 (3)	-0.029 (4)
C7	0.027 (3)	0.029 (4)	0.062 (5)	-0.003 (3)	0.009 (3)	-0.011 (3)
C7T	0.034 (3)	0.029 (4)	0.048 (4)	0.010 (3)	-0.012 (3)	-0.020 (3)
C8	0.032 (3)	0.020 (3)	0.058 (5)	0.001 (2)	-0.003 (3)	0.000 (3)
C8T	0.043 (4)	0.036 (4)	0.063 (5)	0.011 (3)	-0.013 (3)	-0.026 (4)
C9	0.022 (3)	0.029 (4)	0.053 (4)	-0.005 (3)	0.000 (3)	0.005 (3)
C9T	0.048 (4)	0.020 (3)	0.050 (4)	0.006 (3)	-0.019 (3)	-0.015 (3)
C10	0.050 (4)	0.040 (4)	0.052 (5)	-0.004 (3)	-0.004 (3)	0.008 (4)
C10T	0.075 (5)	0.024 (4)	0.081 (6)	0.010 (3)	-0.016 (4)	-0.006 (4)

C11T	0.052 (4)	0.042 (4)	0.050 (4)	-0.014 (3)	-0.006 (3)	-0.019 (3)
C12T	0.030 (3)	0.034 (4)	0.034 (4)	0.001 (3)	-0.008 (3)	-0.011 (3)
C13T	0.046 (4)	0.039 (4)	0.042 (4)	-0.002 (3)	-0.010 (3)	-0.021 (3)
C14T	0.047 (4)	0.043 (4)	0.028 (4)	0.006 (3)	-0.010 (3)	-0.010 (3)
C15T	0.084 (5)	0.052 (5)	0.032 (4)	0.000 (4)	-0.016 (4)	-0.010 (4)
B1T	0.045 (4)	0.019 (4)	0.037 (4)	-0.006 (3)	-0.007 (3)	-0.003 (3)

Geometric parameters (Å, º)

Y1—O1	2.324 (4)	C2F—H2FA	0.9700
Y1—O1F	2.501 (4)	C2F—H2FB	0.9700
Y1—O2	2.368 (4)	C2F—C3F	1.511 (9)
Y1—O3	2.417 (4)	C2T—C3T	1.396 (8)
Y1—O4	2.302 (4)	C3—H3	0.9300
Y1—N1T	2.412 (4)	C3—C4	1.396 (8)
Y1—N3T	2.498 (4)	C3F—H3FA	0.9700
Y1—N5T	2.491 (4)	C3F—H3FB	0.9700
F1—C1	1.331 (7)	C3F—C4F	1.509 (9)
F2—C1	1.324 (8)	C3T—H3T	0.9300
F3—C1	1.325 (7)	C3T—C4T	1.373 (8)
F4—C5	1.333 (7)	C4—C5	1.527 (9)
F5—C5	1.316 (8)	C4F—H4FA	0.9700
F6—C5	1.317 (7)	C4F—H4FB	0.9700
F7—C6	1.330 (7)	C4T—C5T	1.487 (8)
F8—C6	1.332 (7)	C5T—H5TA	0.9600
F9—C6	1.324 (8)	C5T—H5TB	0.9600
F10—C10	1.336 (8)	C5T—H5TC	0.9600
F11—C10	1.321 (8)	C6—C7	1.523 (9)
F12—C10	1.313 (8)	C6T—H6TA	0.9600
O1—C2	1.263 (7)	C6T—H6TB	0.9600
O1F—C1F	1.440 (6)	C6T—H6TC	0.9600
O1F—C4F	1.461 (7)	C6T—C7T	1.477 (8)
O2—C4	1.243 (7)	C7—C8	1.401 (9)
O3—C7	1.249 (7)	C7T—C8T	1.383 (8)
O4—C9	1.248 (7)	C8—H8	0.9300
N1T—N2T	1.371 (6)	C8—C9	1.375 (9)
N1T—C2T	1.342 (7)	C8T—H8T	0.9300
N2T—C4T	1.353 (7)	C8T—C9T	1.360 (9)
N2T—B1T	1.555 (8)	C9—C10	1.533 (9)

N3T—N4T	1.384 (6)	C9T—C10T	1.505 (9)
N3T—C7T	1.351 (7)	C10T—H10A	0.9600
N4T—C9T	1.358 (7)	C10T—H10B	0.9600
N4T—B1T	1.541 (8)	C10T—H10C	0.9600
N5T—N6T	1.396 (6)	C11T—H11A	0.9600
N5T—C12T	1.338 (7)	C11T—H11B	0.9600
N6T—C14T	1.346 (7)	C11T—H11C	0.9600
N6T—B1T	1.524 (8)	C11T—C12T	1.501 (8)
C1—C2	1.524 (9)	C12T—C13T	1.375 (8)
C1F—H1FA	0.9700	C13T—H13T	0.9300
C1F—H1FB	0.9700	C13T—C14T	1.371 (9)
C1F—C2F	1.500 (9)	C14T—C15T	1.503 (8)
C1T—H1TA	0.9600	C15T—H15A	0.9600
C1T—H1TB	0.9600	C15T—H15B	0.9600
C1T—H1TC	0.9600	C15T—H15C	0.9600
C1T—C2T	1.483 (8)	B1T—H1T	0.9800
C2—C3	1.362 (8)		
O1—Y1—O1F	139.20 (13)	C4T—C3T—H3T	126.7
O1—Y1—O2	69.95 (13)	O2—C4—C3	127.1 (6)
O1—Y1—O3	69.09 (13)	O2—C4—C5	115.6 (6)
O1—Y1—N1T	142.59 (15)	C3—C4—C5	117.3 (6)
O1—Y1—N3T	119.60 (14)	O1F—C4F—C3F	106.9 (5)
O1—Y1—N5T	80.88 (14)	O1F—C4F—H4FA	110.3
O2—Y1—O1F	73.91 (13)	O1F—C4F—H4FB	110.3
O2—Y1—O3	129.36 (13)	C3F—C4F—H4FA	110.3
O2—Y1—N1T	146.24 (15)	C3F—C4F—H4FB	110.3
O2—Y1—N3T	82.83 (14)	H4FA—C4F—H4FB	108.6
O2—Y1—N5T	125.84 (13)	N2T—C4T—C3T	107.3 (5)
O3—Y1—O1F	125.45 (13)	N2T—C4T—C5T	123.3 (5)
O3—Y1—N3T	144.34 (15)	C3T—C4T—C5T	129.4 (5)
O3—Y1—N5T	74.53 (14)	F4—C5—C4	109.8 (6)
O4—Y1—O1	80.56 (14)	F5—C5—F4	105.6 (5)
O4—Y1—O1F	71.58 (14)	F5—C5—F6	108.9 (6)
O4—Y1—O2	73.70 (13)	F5—C5—C4	114.6 (6)
O4—Y1—O3	71.38 (14)	F6—C5—F4	105.7 (6)
O4—Y1—N1T	98.94 (14)	F6—C5—C4	111.7 (5)
O4—Y1—N3T	141.50 (15)	C4T—C5T—H5TA	109.5
O4—Y1—N5T	145.17 (15)	C4T—C5T—H5TB	109.5
N1T—Y1—O1F	72.54 (14)	C4T—C5T—H5TC	109.5

N1T—Y1—O3	75.30 (14)	H5TA—C5T—H5TB	109.5
N1T—Y1—N3T	83.87 (15)	H5TA—C5T—H5TC	109.5
N1T—Y1—N5T	78.93 (15)	H5TB—C5T—H5TC	109.5
N3T—Y1—O1F	72.82 (14)	F7—C6—F8	106.4 (5)
N5T—Y1—O1F	137.38 (14)	F7—C6—C7	113.1 (6)
N5T—Y1—N3T	73.25 (15)	F8—C6—C7	110.8 (6)
C2—O1—Y1	133.8 (4)	F9—C6—F7	107.6 (6)
C1F—O1F—Y1	126.3 (3)	F9—C6—F8	106.3 (6)
C1F—O1F—C4F	107.0 (4)	F9—C6—C7	112.3 (5)
C4F—O1F—Y1	126.7 (3)	H6TA—C6T—H6TB	109.5
C4—O2—Y1	133.1 (4)	H6TA—C6T—H6TC	109.5
C7—O3—Y1	131.4 (4)	H6TB—C6T—H6TC	109.5
C9—O4—Y1	135.7 (4)	C7T—C6T—H6TA	109.5
N2T—N1T—Y1	119.8 (3)	C7T—C6T—H6TB	109.5
C2T—N1T—Y1	131.9 (4)	C7T—C6T—H6TC	109.5
C2T—N1T—N2T	106.4 (4)	O3—C7—C6	114.8 (6)
N1T—N2T—B1T	120.5 (4)	O3—C7—C8	127.3 (6)
C4T—N2T—N1T	110.2 (4)	C8—C7—C6	117.8 (6)
C4T—N2T—B1T	129.1 (5)	N3T—C7T—C6T	124.0 (5)
N4T—N3T—Y1	116.6 (3)	N3T—C7T—C8T	109.5 (6)
C7T—N3T—Y1	136.9 (4)	C8T—C7T—C6T	126.4 (6)
C7T—N3T—N4T	106.2 (4)	C7—C8—H8	119.9
N3T—N4T—B1T	123.5 (4)	C9—C8—C7	120.2 (6)
C9T—N4T—N3T	109.2 (5)	C9—C8—H8	119.9
C9T—N4T—B1T	127.3 (5)	C7T—C8T—H8T	126.5
N6T—N5T—Y1	116.0 (3)	C9T—C8T—C7T	107.1 (6)
C12T—N5T—Y1	137.6 (4)	C9T—C8T—H8T	126.5
C12T—N5T—N6T	105.3 (4)	O4—C9—C8	128.3 (6)
N5T—N6T—B1T	122.9 (5)	O4—C9—C10	112.4 (6)
C14T—N6T—N5T	109.3 (5)	C8—C9—C10	119.3 (6)
C14T—N6T—B1T	127.3 (5)	N4T—C9T—C8T	108.0 (6)
F1—C1—C2	110.0 (5)	N4T—C9T—C10T	123.0 (6)
F2—C1—F1	107.3 (6)	C8T—C9T—C10T	129.0 (6)
F2—C1—F3	107.1 (6)	F10—C10—C9	110.0 (5)
F2—C1—C2	112.9 (6)	F11—C10—F10	105.9 (6)
F3—C1—F1	106.5 (6)	F11—C10—C9	111.8 (5)
F3—C1—C2	112.8 (5)	F12—C10—F10	107.3 (6)
O1F—C1F—H1FA	110.9	F12—C10—F11	107.4 (6)
O1F—C1F—H1FB	110.9	F12—C10—C9	114.0 (6)
O1F—C1F—C2F	104.4 (5)	C9T—C10T—H10A	109.5

H1FA—C1F—H1FB	108.9	C9T—C10T—H10B	109.5
C2F—C1F—H1FA	110.9	C9T—C10T—H10C	109.5
C2F—C1F—H1FB	110.9	H10A—C10T—H10B	109.5
H1TA—C1T—H1TB	109.5	H10A—C10T—H10C	109.5
H1TA—C1T—H1TC	109.5	H10B—C10T—H10C	109.5
H1TB—C1T—H1TC	109.5	H11A—C11T—H11B	109.5
C2T—C1T—H1TA	109.5	H11A—C11T—H11C	109.5
C2T—C1T—H1TB	109.5	H11B—C11T—H11C	109.5
C2T—C1T—H1TC	109.5	C12T—C11T—H11A	109.5
O1—C2—C1	113.6 (6)	C12T—C11T—H11B	109.5
O1—C2—C3	127.2 (6)	C12T—C11T—H11C	109.5
C3—C2—C1	119.1 (6)	N5T—C12T—C11T	124.3 (5)
C1F—C2F—H2FA	111.1	N5T—C12T—C13T	111.0 (5)
C1F—C2F—H2FB	111.1	C13T—C12T—C11T	124.7 (5)
C1F—C2F—C3F	103.3 (5)	C12T—C13T—H13T	126.9
H2FA—C2F—H2FB	109.1	C14T—C13T—C12T	106.1 (5)
C3F—C2F—H2FA	111.1	C14T—C13T—H13T	126.9
C3F—C2F—H2FB	111.1	N6T—C14T—C13T	108.2 (5)
N1T—C2T—C1T	122.5 (5)	N6T—C14T—C15T	123.2 (6)
N1T—C2T—C3T	109.5 (5)	C13T—C14T—C15T	128.5 (6)
C3T—C2T—C1T	128.0 (5)	C14T—C15T—H15A	109.5
C2—C3—H3	120.2	C14T—C15T—H15B	109.5
C2—C3—C4	119.5 (6)	C14T—C15T—H15C	109.5
C4—C3—H3	120.2	H15A—C15T—H15B	109.5
C2F—C3F—H3FA	110.8	H15A—C15T—H15C	109.5
C2F—C3F—H3FB	110.8	H15B—C15T—H15C	109.5
H3FA—C3F—H3FB	108.9	N2T—B1T—H1T	108.4
C4F—C3F—C2F	104.7 (6)	N4T—B1T—N2T	111.5 (5)
C4F—C3F—H3FA	110.8	N4T—B1T—H1T	108.4
C4F—C3F—H3FB	110.8	N6T—B1T—N2T	111.3 (5)
C2T—C3T—H3T	126.7	N6T—B1T—N4T	108.9 (5)
C4T—C3T—C2T	106.5 (5)	N6T—B1T—H1T	108.4

8.3.17 Crystallographic data for Ce(Tp*)(hfac)$_2$(dmpz)

Crystal data

$C_{30}H_{32}BCeF_{12}N_8O_4$	$F(000)$ = 1884
M_r = 947.56	D_x = 1.628 Mg m^{-3}
Monoclinic, $P2_1/n$	Mo $K\alpha$ radiation, λ = 0.71073 Å

a = 13.4458 (6) Å	Cell parameters from 7065 reflections
b = 18.3918 (10) Å	θ = 2.4–27.3°
c = 15.7973 (9) Å	μ = 1.28 mm^{-1}
β = 98.247 (2)°	T = 150 K
V = 3866.2 (4) $Å^3$	Block, orange
Z = 4	0.44 × 0.28 × 0.12 mm

Data collection

Four-circle diffractometer	9152 independent reflections
Radiation source: microfocus sealed tube, INCOATEC Iμs 3.0	6014 reflections with $I > 2\sigma(I)$
Multilayer mirror optics monochromator	R_{int} = 0.073
Detector resolution: 7.4074 pixels mm^{-1}	θ_{max} = 29.7°, θ_{min} = 2.2°
ϕ and ω scans	h = -18→16
Absorption correction: multi-scan *SADABS2016*/2 (Bruker,2016/2) was used for absorption correction. wR2(int) was 0.0920 before and 0.0692 after correction. The Ratio of minimum to maximum transmission is 0.8360. The λ/2 correction factor is Not present.	k = -21→23
T_{min} = 0.624, T_{max} = 0.746	l = -22→21
26357 measured reflections	

Refinement

Refinement on F^2	Primary atom site location: dual
Least-squares matrix: full	Hydrogen site location: inferred from neighbouring sites
$R[F^2 > 2\sigma(F^2)]$ = 0.067	H-atom parameters constrained
$wR(F^2)$ = 0.212	$w = 1/[\sigma^2(F_o^2) + (0.1013P)^2 + 14.0737P]$ where $P = (F_o^2 + 2F_c^2)/3$
S = 1.04	$(\Delta/\sigma)_{max}$ = 0.001
9152 reflections	$\Delta\rangle_{max}$ = 1.39 e $Å^{-3}$
538 parameters	$\Delta\rangle_{min}$ = -1.66 e $Å^{-3}$
0 restraints	

Special details

Geometry. All esds (except the esd in the dihedral angle between two l.s. planes) are estimated using the full covariance matrix. The cell esds are taken into account individually in the estimation

of esds in distances, angles and torsion angles; correlations between esds in cell parameters are only used when they are defined by crystal symmetry. An approximate (isotropic) treatment of cell esds is used for estimating esds involving l.s. planes.

Fractional atomic coordinates and isotropic or equivalent isotropic displacement parameters (Å²)

	x	*y*	*z*	U_{iso}*/U_{eq}	Occ. (<1)
Ce1	0.56260 (3)	0.36273 (2)	0.32990 (2)	0.03521 (15)	
F1AA	0.607 (3)	0.407 (2)	0.021 (3)	0.055 (10)*	0.146 (13)
F1	0.7582 (5)	0.4896 (5)	0.1409 (4)	0.120 (3)	
F3AA	0.650 (6)	0.318 (4)	-0.010 (6)	0.08 (2)*	0.146 (13)
F2	0.7830 (6)	0.5799 (4)	0.2246 (6)	0.119 (3)	
F2AA	0.528 (4)	0.313 (3)	0.004 (4)	0.061 (14)*	0.146 (13)
F3	0.8996 (4)	0.5051 (4)	0.2202 (5)	0.096 (2)	
F4	0.9562 (5)	0.4298 (5)	0.5100 (5)	0.135 (3)	
F4AA	0.901 (2)	0.2679 (18)	0.3324 (18)	0.033 (7)*	0.146 (13)
F5	0.8357 (6)	0.4313 (4)	0.5790 (4)	0.106 (2)	
F5AA	0.919 (3)	0.265 (2)	0.203 (2)	0.055 (10)*	0.146 (13)
F6	0.8763 (5)	0.3320 (3)	0.5259 (4)	0.097 (2)	
F6AA	0.848 (3)	0.1801 (19)	0.267 (2)	0.062 (11)*	0.146 (13)
F7	0.5365 (7)	0.2814 (7)	0.0042 (5)	0.083 (3)	0.854 (13)
F8	0.5481 (9)	0.3960 (5)	0.0207 (4)	0.093 (3)	0.854 (13)
F9	0.6777 (8)	0.3321 (9)	-0.0087 (6)	0.102 (4)	0.854 (13)
F10	0.8994 (5)	0.2127 (5)	0.2144 (4)	0.082 (3)	0.854 (13)
F11	0.9265 (5)	0.3036 (6)	0.2969 (10)	0.143 (6)	0.854 (13)
F12	0.8708 (6)	0.2107 (7)	0.3410 (5)	0.126 (5)	0.854 (13)
O1	0.6717 (3)	0.4509 (3)	0.2742 (3)	0.0442 (11)	
O2	0.7069 (4)	0.3955 (3)	0.4346 (3)	0.0475 (12)	
O3	0.5648 (3)	0.3410 (3)	0.1761 (3)	0.0360 (10)	
O4	0.7112 (3)	0.2932 (2)	0.3064 (3)	0.0335 (9)	
N1P	0.5903 (4)	0.2508 (3)	0.4377 (3)	0.0386 (12)	
N1T	0.4508 (4)	0.3924 (3)	0.4428 (3)	0.0392 (12)	
N2P	0.6886 (4)	0.2309 (3)	0.4612 (4)	0.0430 (13)	
H2P	0.739072	0.250254	0.439348	0.052*	
N2T	0.3480 (5)	0.3859 (3)	0.4230 (4)	0.0415 (13)	
N3T	0.4203 (4)	0.4484 (3)	0.2592 (3)	0.0333 (11)	
N4T	0.3229 (4)	0.4364 (3)	0.2735 (4)	0.0364 (12)	
N5T	0.4156 (4)	0.2814 (3)	0.2856 (4)	0.0342 (12)	
N6T	0.3184 (4)	0.3001 (3)	0.2948 (4)	0.0371 (12)	

C1	0.8009 (7)	0.5097 (6)	0.2175 (7)	0.075 (3)	
C1P	0.4287 (6)	0.2123 (5)	0.4810 (6)	0.058 (2)	
H1PA	0.409361	0.261614	0.495695	0.087*	
H1PB	0.406803	0.177590	0.521618	0.087*	
H1PC	0.396734	0.200367	0.422985	0.087*	
C1T	0.5741 (7)	0.4121 (5)	0.5744 (5)	0.058 (2)	
H1TA	0.612630	0.367867	0.567366	0.087*	
H1TB	0.571205	0.420179	0.635355	0.087*	
H1TC	0.606769	0.453754	0.551169	0.087*	
C2	0.7625 (5)	0.4670 (4)	0.2896 (5)	0.0492 (18)	
C2P	0.5389 (6)	0.2084 (4)	0.4851 (4)	0.0456 (17)	
C2T	0.4705 (6)	0.4039 (4)	0.5280 (5)	0.0492 (18)	
C3	0.8286 (6)	0.4522 (4)	0.3639 (6)	0.058 (2)	
H3	0.897295	0.465711	0.368227	0.070*	
C3P	0.6053 (7)	0.1630 (5)	0.5367 (5)	0.064 (2)	
H3P	0.587659	0.127520	0.575653	0.077*	
C3T	0.3798 (7)	0.4055 (4)	0.5620 (5)	0.055 (2)	
H3T	0.372102	0.413672	0.620071	0.066*	
C4	0.7932 (6)	0.4180 (4)	0.4307 (5)	0.0486 (18)	
C4P	0.6994 (7)	0.1787 (5)	0.5212 (5)	0.059 (2)	
C4T	0.3050 (7)	0.3932 (4)	0.4961 (6)	0.055 (2)	
C5	0.8693 (7)	0.4024 (5)	0.5115 (7)	0.073 (3)	
C5P	0.8029 (7)	0.1479 (5)	0.5484 (9)	0.101 (5)	
H5PA	0.834725	0.137623	0.497630	0.152*	
H5PB	0.797579	0.102808	0.580505	0.152*	
H5PC	0.843600	0.183189	0.584693	0.152*	
C5T	0.1950 (7)	0.3858 (5)	0.4967 (7)	0.073 (3)	
H5TA	0.159969	0.426786	0.465834	0.109*	
H5TB	0.181026	0.385714	0.555934	0.109*	
H5TC	0.171355	0.340174	0.468816	0.109*	
C6	0.5990 (8)	0.3356 (6)	0.0352 (5)	0.065 (2)	
C6T	0.5062 (6)	0.5367 (4)	0.1736 (5)	0.054 (2)	
H6TA	0.554736	0.551783	0.222735	0.080*	
H6TB	0.486290	0.578944	0.137316	0.080*	
H6TC	0.536989	0.500083	0.140467	0.080*	
C7	0.6309 (5)	0.3244 (4)	0.1323 (4)	0.0424 (16)	
C7T	0.4165 (5)	0.5053 (4)	0.2042 (4)	0.0369 (14)	
C8	0.7255 (5)	0.2945 (5)	0.1589 (5)	0.0482 (18)	
H8	0.767729	0.282437	0.117586	0.058*	
C8T	0.3168 (6)	0.5284 (4)	0.1842 (4)	0.0432 (16)	

H8T	0.292846	0.567431	0.147423	0.052*	
C9	0.7586 (5)	0.2821 (4)	0.2449 (5)	0.0394 (15)	
C9T	0.2610 (5)	0.4843 (4)	0.2277 (4)	0.0405 (16)	
C10	0.8645 (6)	0.2512 (6)	0.2700 (6)	0.062 (2)	
C10T	0.1488 (6)	0.4860 (4)	0.2279 (6)	0.056 (2)	
H10A	0.119691	0.439228	0.207763	0.084*	
H10B	0.119077	0.524910	0.190043	0.084*	
H10C	0.134776	0.495106	0.286213	0.084*	
C11T	0.5031 (5)	0.1763 (4)	0.2323 (5)	0.0461 (18)	
H11A	0.521504	0.194643	0.178390	0.069*	
H11B	0.489903	0.124004	0.227356	0.069*	
H11C	0.558428	0.185253	0.278687	0.069*	
C12T	0.4108 (5)	0.2147 (3)	0.2514 (4)	0.0362 (14)	
C13T	0.3122 (5)	0.1901 (4)	0.2383 (5)	0.0428 (16)	
H13T	0.288319	0.145015	0.214016	0.051*	
C14T	0.2568 (5)	0.2444 (4)	0.2676 (5)	0.0435 (17)	
C15T	0.1451 (5)	0.2472 (5)	0.2685 (7)	0.060 (2)	
H15A	0.131578	0.265262	0.324068	0.090*	
H15B	0.116761	0.198306	0.258775	0.090*	
H15C	0.114132	0.279844	0.223153	0.090*	
B1T	0.2947 (6)	0.3755 (4)	0.3317 (5)	0.0393 (17)	
H1T	0.220620	0.378137	0.332984	0.047*	

Atomic displacement parameters (Å²)

	U^{11}	U^{22}	U^{33}	U^{12}	U^{13}	U^{23}
Ce1	0.0317 (2)	0.0389 (2)	0.0349 (2)	0.00062 (15)	0.00447 (14)	0.00313 (15)
F1	0.105 (5)	0.183 (8)	0.073 (4)	-0.078 (5)	0.011 (4)	0.043 (4)
F2	0.105 (5)	0.071 (4)	0.189 (8)	-0.007 (4)	0.046 (5)	0.057 (5)
F3	0.060 (3)	0.113 (5)	0.120 (5)	-0.013 (3)	0.033 (3)	0.030 (4)
F4	0.083 (4)	0.154 (7)	0.143 (7)	-0.047 (5)	-0.069 (5)	0.047 (5)
F5	0.148 (6)	0.090 (5)	0.063 (4)	-0.008 (4)	-0.040 (4)	-0.005 (3)
F6	0.099 (4)	0.060 (3)	0.110 (5)	0.005 (3)	-0.061 (4)	0.005 (3)
F7	0.086 (5)	0.112 (8)	0.044 (4)	0.001 (6)	-0.017 (3)	-0.023 (5)
F8	0.132 (9)	0.111 (6)	0.035 (3)	0.043 (6)	0.006 (4)	0.016 (3)
F9	0.075 (6)	0.201 (12)	0.033 (3)	-0.011 (7)	0.018 (4)	0.013 (5)
F10	0.052 (4)	0.109 (7)	0.081 (5)	0.037 (4)	-0.003 (3)	-0.038 (5)
F11	0.031 (3)	0.096 (7)	0.290 (15)	0.007 (4)	-0.022 (5)	-0.089 (9)
F12	0.089 (6)	0.200 (12)	0.087 (6)	0.086 (7)	0.008 (4)	0.039 (6)

O1	0.034 (2)	0.045 (3)	0.052 (3)	-0.008 (2)	-0.002 (2)	0.010 (2)
O2	0.057 (3)	0.043 (3)	0.040 (3)	-0.002 (2)	-0.002 (2)	-0.003 (2)
O3	0.031 (2)	0.045 (3)	0.032 (2)	-0.001 (2)	0.0040 (18)	0.0038 (19)
O4	0.029 (2)	0.036 (2)	0.036 (2)	0.0029 (18)	0.0018 (17)	-0.0001 (18)
N1P	0.039 (3)	0.041 (3)	0.036 (3)	0.000 (2)	0.006 (2)	0.008 (2)
N1T	0.047 (3)	0.039 (3)	0.033 (3)	0.007 (3)	0.012 (2)	0.005 (2)
N2P	0.039 (3)	0.046 (3)	0.042 (3)	0.004 (3)	0.002 (2)	0.010 (3)
N2T	0.050 (3)	0.035 (3)	0.043 (3)	0.006 (3)	0.019 (3)	0.004 (2)
N3T	0.037 (3)	0.027 (3)	0.036 (3)	0.002 (2)	0.006 (2)	0.002 (2)
N4T	0.036 (3)	0.031 (3)	0.042 (3)	0.004 (2)	0.005 (2)	-0.001 (2)
N5T	0.023 (2)	0.033 (3)	0.048 (3)	0.000 (2)	0.009 (2)	0.001 (2)
N6T	0.026 (2)	0.034 (3)	0.053 (3)	0.004 (2)	0.012 (2)	0.005 (2)
C1	0.052 (5)	0.082 (7)	0.091 (8)	-0.014 (5)	0.010 (5)	0.018 (6)
C1P	0.059 (5)	0.052 (5)	0.070 (5)	0.008 (4)	0.030 (4)	0.023 (4)
C1T	0.083 (6)	0.060 (5)	0.029 (3)	0.023 (5)	0.001 (4)	-0.001 (3)
C2	0.039 (4)	0.043 (4)	0.065 (5)	-0.011 (3)	0.007 (3)	0.000 (4)
C2P	0.056 (4)	0.046 (4)	0.037 (4)	-0.004 (3)	0.014 (3)	0.011 (3)
C2T	0.072 (5)	0.042 (4)	0.035 (4)	0.014 (4)	0.016 (3)	0.006 (3)
C3	0.036 (4)	0.052 (5)	0.079 (6)	-0.007 (4)	-0.017 (4)	-0.004 (4)
C3P	0.079 (6)	0.062 (5)	0.050 (5)	-0.001 (5)	0.005 (4)	0.028 (4)
C3T	0.090 (6)	0.046 (4)	0.035 (4)	0.018 (4)	0.029 (4)	0.003 (3)
C4	0.053 (4)	0.036 (4)	0.052 (4)	-0.002 (3)	-0.010 (3)	-0.004 (3)
C4P	0.064 (5)	0.055 (5)	0.056 (5)	0.002 (4)	-0.003 (4)	0.026 (4)
C4T	0.068 (5)	0.039 (4)	0.065 (5)	0.012 (4)	0.038 (4)	0.011 (4)
C5	0.065 (6)	0.065 (6)	0.077 (7)	-0.020 (5)	-0.030 (5)	0.004 (5)
C5P	0.053 (5)	0.064 (6)	0.173 (13)	0.000 (5)	-0.034 (6)	0.073 (7)
C5T	0.077 (6)	0.063 (5)	0.093 (7)	0.006 (5)	0.062 (6)	0.005 (5)
C6	0.072 (6)	0.094 (7)	0.030 (4)	0.008 (6)	0.010 (4)	0.004 (4)
C6T	0.054 (4)	0.055 (5)	0.050 (4)	-0.004 (4)	0.003 (3)	0.025 (4)
C7	0.049 (4)	0.054 (4)	0.024 (3)	-0.005 (3)	0.005 (3)	0.005 (3)
C7T	0.044 (4)	0.036 (3)	0.031 (3)	0.002 (3)	0.004 (3)	0.001 (3)
C8	0.038 (4)	0.070 (5)	0.040 (4)	0.002 (4)	0.016 (3)	-0.006 (3)
C8T	0.051 (4)	0.036 (4)	0.040 (4)	0.010 (3)	-0.003 (3)	0.005 (3)
C9	0.030 (3)	0.042 (4)	0.045 (4)	-0.002 (3)	0.001 (3)	-0.003 (3)
C9T	0.040 (4)	0.030 (3)	0.048 (4)	0.008 (3)	-0.004 (3)	-0.005 (3)
C10	0.034 (4)	0.084 (6)	0.064 (5)	0.014 (4)	-0.001 (4)	-0.020 (5)
C10T	0.041 (4)	0.048 (4)	0.076 (6)	0.019 (4)	0.001 (4)	-0.004 (4)
C11T	0.026 (3)	0.035 (4)	0.076 (5)	0.005 (3)	0.004 (3)	-0.009 (3)
C12T	0.028 (3)	0.029 (3)	0.051 (4)	-0.002 (3)	0.006 (3)	-0.001 (3)
C13T	0.032 (3)	0.029 (3)	0.067 (5)	-0.002 (3)	0.007 (3)	0.002 (3)

C14T	0.028 (3)	0.035 (4)	0.066 (5)	-0.004 (3)	0.004 (3)	0.005 (3)
C15T	0.028 (3)	0.051 (5)	0.102 (7)	-0.007 (3)	0.014 (4)	0.000 (4)
B1T	0.030 (4)	0.040 (4)	0.050 (4)	0.005 (3)	0.011 (3)	0.001 (3)

Geometric parameters (Å, º) for

Ce1—O1	2.435 (5)	N2P—C4P	1.342 (9)
Ce1—O2	2.437 (5)	N2T—C4T	1.369 (9)
Ce1—O3	2.467 (4)	N2T—B1T	1.527 (10)
Ce1—O4	2.444 (4)	N3T—N4T	1.377 (7)
Ce1—N1P	2.664 (5)	N3T—C7T	1.357 (8)
Ce1—N1T	2.551 (5)	N4T—C9T	1.350 (8)
Ce1—N3T	2.604 (5)	N4T—B1T	1.532 (10)
Ce1—N5T	2.498 (5)	N5T—N6T	1.379 (7)
F1AA—C6	1.33 (4)	N5T—C12T	1.338 (8)
F1—C1	1.316 (12)	N6T—C14T	1.348 (9)
F3AA—F2AA	1.69 (9)	N6T—B1T	1.554 (9)
F3AA—C6	1.10 (8)	C1—C2	1.534 (12)
F2—C1	1.320 (13)	C1P—C2P	1.475 (11)
F2AA—C6	1.09 (6)	C1T—C2T	1.486 (12)
F3—C1	1.324 (11)	C2—C3	1.393 (11)
F4—C5	1.275 (11)	C2P—C3P	1.397 (11)
F4AA—C10	1.08 (3)	C2T—C3T	1.401 (11)
F5—C5	1.328 (13)	C3—C4	1.371 (12)
F5AA—C10	1.40 (4)	C3P—C4P	1.354 (13)
F6—C5	1.315 (11)	C3T—C4T	1.359 (13)
F6AA—C10	1.33 (4)	C4—C5	1.544 (11)
F7—C6	1.350 (14)	C4P—C5P	1.507 (12)
F8—C6	1.307 (13)	C4T—C5T	1.487 (12)
F9—C6	1.347 (15)	C6—C7	1.547 (10)
F10—C10	1.270 (10)	C6T—C7T	1.479 (10)
F11—C10	1.304 (12)	C7—C8	1.395 (10)
F12—C10	1.339 (13)	C7T—C8T	1.399 (9)
O1—C2	1.245 (8)	C8—C9	1.387 (10)
O2—C4	1.242 (9)	C8T—C9T	1.356 (10)
O3—C7	1.239 (8)	C9—C10	1.531 (10)
O4—C9	1.254 (8)	C9T—C10T	1.510 (10)
N1P—N2P	1.369 (8)	C11T—C12T	1.496 (9)
N1P—C2P	1.340 (9)	C12T—C13T	1.388 (9)

N1T—N2T	1.379 (8)	C13T—C14T	1.366 (10)
N1T—C2T	1.351 (9)	C14T—C15T	1.505 (9)
O1—Ce1—O2	67.56 (16)	N1T—C2T—C3T	109.2 (7)
O1—Ce1—O3	70.04 (16)	C3T—C2T—C1T	127.9 (7)
O1—Ce1—O4	75.28 (16)	C4—C3—C2	119.2 (7)
O1—Ce1—N1P	135.21 (16)	C4P—C3P—C2P	107.6 (7)
O1—Ce1—N1T	123.77 (18)	C4T—C3T—C2T	107.0 (7)
O1—Ce1—N3T	83.43 (16)	O2—C4—C3	128.3 (7)
O1—Ce1—N5T	142.32 (17)	O2—C4—C5	114.2 (8)
O2—Ce1—O3	125.96 (16)	C3—C4—C5	117.4 (8)
O2—Ce1—O4	69.15 (16)	N2P—C4P—C3P	105.7 (7)
O2—Ce1—N1P	74.50 (17)	N2P—C4P—C5P	118.2 (8)
O2—Ce1—N1T	87.94 (18)	C3P—C4P—C5P	135.8 (8)
O2—Ce1—N3T	127.28 (16)	N2T—C4T—C5T	122.5 (8)
O2—Ce1—N5T	149.22 (18)	C3T—C4T—N2T	107.9 (7)
O3—Ce1—N1P	118.97 (16)	C3T—C4T—C5T	129.6 (8)
O3—Ce1—N1T	144.59 (16)	F4—C5—F5	106.0 (8)
O3—Ce1—N3T	77.74 (16)	F4—C5—F6	110.4 (9)
O3—Ce1—N5T	75.41 (16)	F4—C5—C4	114.2 (9)
O4—Ce1—O3	68.92 (14)	F5—C5—C4	109.1 (8)
O4—Ce1—N1P	69.52 (16)	F6—C5—F5	106.3 (9)
O4—Ce1—N1T	142.58 (16)	F6—C5—C4	110.4 (7)
O4—Ce1—N3T	144.88 (15)	F1AA—C6—C7	106.1 (18)
O4—Ce1—N5T	105.98 (15)	F3AA—C6—F1AA	96 (4)
N1T—Ce1—N1P	76.18 (17)	F3AA—C6—C7	120 (4)
N1T—Ce1—N3T	72.53 (17)	F2AA—C6—F1AA	112 (3)
N3T—Ce1—N1P	140.25 (17)	F2AA—C6—F3AA	100 (5)
N5T—Ce1—N1P	75.45 (17)	F2AA—C6—C7	120 (3)
N5T—Ce1—N1T	78.59 (18)	F7—C6—C7	109.3 (8)
N5T—Ce1—N3T	74.86 (17)	F8—C6—F7	106.3 (10)
C6—F3AA—F2AA	40 (3)	F8—C6—F9	112.4 (10)
C6—F2AA—F3AA	40 (4)	F8—C6—C7	110.5 (8)
C2—O1—Ce1	135.4 (5)	F9—C6—F7	105.8 (11)
C4—O2—Ce1	135.1 (5)	F9—C6—C7	112.2 (8)
C7—O3—Ce1	134.4 (4)	O3—C7—C6	113.7 (7)
C9—O4—Ce1	136.1 (4)	O3—C7—C8	128.8 (6)
N2P—N1P—Ce1	114.9 (4)	C8—C7—C6	117.5 (7)
C2P—N1P—Ce1	140.4 (5)	N3T—C7T—C6T	123.6 (6)
C2P—N1P—N2P	104.4 (5)	N3T—C7T—C8T	109.0 (6)

N2T—N1T—Ce1	119.7 (4)	C8T—C7T—C6T	127.4 (6)
C2T—N1T—Ce1	132.8 (5)	C9—C8—C7	120.7 (6)
C2T—N1T—N2T	106.7 (6)	C9T—C8T—C7T	106.6 (6)
C4P—N2P—N1P	112.6 (6)	O4—C9—C8	127.3 (6)
N1T—N2T—B1T	123.0 (5)	O4—C9—C10	114.6 (6)
C4T—N2T—N1T	109.3 (6)	C8—C9—C10	118.1 (7)
C4T—N2T—B1T	127.6 (7)	N4T—C9T—C8T	108.6 (6)
N4T—N3T—Ce1	119.3 (4)	N4T—C9T—C10T	123.5 (7)
C7T—N3T—Ce1	134.4 (4)	C8T—C9T—C10T	127.9 (6)
C7T—N3T—N4T	106.2 (5)	F4AA—C10—F5AA	115 (2)
N3T—N4T—B1T	122.6 (5)	F4AA—C10—F6AA	112 (2)
C9T—N4T—N3T	109.6 (5)	F4AA—C10—C9	114.7 (17)
C9T—N4T—B1T	127.8 (6)	F5AA—C10—C9	107.7 (16)
N6T—N5T—Ce1	123.0 (4)	F6AA—C10—F5AA	105 (2)
C12T—N5T—Ce1	130.7 (4)	F6AA—C10—C9	102.0 (16)
C12T—N5T—N6T	106.3 (5)	F10—C10—F11	110.8 (9)
N5T—N6T—B1T	120.7 (5)	F10—C10—F12	106.5 (9)
C14T—N6T—N5T	108.9 (5)	F10—C10—C9	116.7 (7)
C14T—N6T—B1T	130.4 (6)	F11—C10—F12	100.2 (10)
F1—C1—F2	107.0 (10)	F11—C10—C9	109.7 (8)
F1—C1—F3	108.3 (10)	F12—C10—C9	111.6 (7)
F1—C1—C2	113.0 (8)	N5T—C12T—C11T	121.4 (6)
F2—C1—F3	104.7 (8)	N5T—C12T—C13T	110.4 (6)
F2—C1—C2	110.7 (9)	C13T—C12T—C11T	128.2 (6)
F3—C1—C2	112.7 (8)	C14T—C13T—C12T	105.5 (6)
O1—C2—C1	113.7 (7)	N6T—C14T—C13T	108.9 (6)
O1—C2—C3	127.4 (8)	N6T—C14T—C15T	122.6 (6)
C3—C2—C1	118.9 (7)	C13T—C14T—C15T	128.4 (7)
N1P—C2P—C1P	122.9 (6)	N2T—B1T—N4T	110.6 (6)
N1P—C2P—C3P	109.6 (7)	N2T—B1T—N6T	111.9 (6)
C3P—C2P—C1P	127.5 (7)	N4T—B1T—N6T	110.2 (6)
N1T—C2T—C1T	122.9 (7)		

8.3.18 Crystallographic data for $Y(Tp)_2(hfac)$

Crystal data

$C_{23}H_{21}B_2F_6N_{12}O_2Y$	$F(000) = 1448$
$M_r = 722.05$	$D_x = 1.643$ Mg m^{-3}
Monoclinic, $C2/c$	Mo $K\alpha$ radiation, $\lambda = 0.71073$ Å

a = 14.570 (3) Å	Cell parameters from 2156 reflections
b = 12.770 (3) Å	θ = 2.4–22.5°
c = 15.716 (3) Å	μ = 2.08 mm^{-1}
β = 93.383 (7)°	T = 150 K
V = 2919.2 (10) $Å^3$	Column
Z = 4	0.25 × 0.02 × 0.01 mm

Data collection

Bruker APEX-II CCD diffractometer	3586 independent reflections
Radiation source: microfocus sealed tube, INCOATEC Iμs 3.0	2362 reflections with $I > 2\sigma(I)$
Multilayer mirror optics monochromator	R_{int} = 0.073
Detector resolution: 7.4074 pixels mm^{-1}	θ_{max} = 28.3°, θ_{min} = 2.4°
ϕ and ω scans	h = -19→19
Absorption correction: multi-scan *SADABS2016*/2 (Bruker,2016/2) was used for absorption correction. wR2(int) was 0.1228 before and 0.0544 after correction. The Ratio of minimum to maximum transmission is 0.8219. The λ/2 correction factor is Not present.	k = -13→17
T_{min} = 0.613, T_{max} = 0.746	l = -18→20
10916 measured reflections	

Refinement

Refinement on F^2	Primary atom site location: dual
Least-squares matrix: full	Hydrogen site location: mixed
$R[F^2 > 2\sigma(F^2)]$ = 0.057	H atoms treated by a mixture of independent and constrained refinement
$wR(F^2)$ = 0.107	$w = 1/[\sigma^2(F_o^2) + (0.030P)^2 + 5.5643P]$ where $P = (F_o^2 + 2F_c^2)/3$
S = 1.02	$(\Delta/\sigma)_{max}$ = 0.001
3586 reflections	$\Delta\rangle_{max}$ = 0.70 e $Å^{-3}$
211 parameters	$\Delta\rangle_{min}$ = -0.51 e $Å^{-3}$
0 restraints	

Special details

Geometry. All esds (except the esd in the dihedral angle between two l.s. planes) are estimated using the full covariance matrix. The cell esds are taken into account individually in the estimation

of esds in distances, angles and torsion angles; correlations between esds in cell parameters are only used when they are defined by crystal symmetry. An approximate (isotropic) treatment of cell esds is used for estimating esds involving l.s. planes.

Fractional atomic coordinates and isotropic or equivalent isotropic displacement parameters (Å²)

	x	*y*	*z*	U_{iso}*/U_{eq}
Y1	0.500000	0.42286 (4)	0.250000	0.02181 (15)
O1	0.52109 (16)	0.27456 (19)	0.16578 (16)	0.0272 (6)
F2	0.47696 (17)	0.1574 (2)	0.02764 (16)	0.0527 (7)
F3	0.61305 (16)	0.1137 (2)	0.07170 (16)	0.0503 (7)
F1	0.49860 (17)	0.01568 (18)	0.09904 (16)	0.0518 (7)
N4T	0.3339 (2)	0.6078 (2)	0.20412 (19)	0.0264 (7)
N2T	0.3084 (2)	0.5102 (2)	0.3411 (2)	0.0279 (7)
N1T	0.3940 (2)	0.4697 (2)	0.3579 (2)	0.0280 (7)
N5T	0.34361 (19)	0.3715 (2)	0.1839 (2)	0.0251 (7)
N3T	0.4221 (2)	0.5805 (2)	0.18719 (19)	0.0277 (7)
N6T	0.26644 (19)	0.4281 (2)	0.19853 (19)	0.0260 (7)
C7T	0.3140 (3)	0.2936 (3)	0.1327 (3)	0.0327 (10)
H7T	0.352943	0.241346	0.111183	0.039*
C3	0.500000	0.1240 (5)	0.250000	0.0321 (14)
C2	0.5155 (2)	0.1774 (3)	0.1744 (2)	0.0262 (9)
C3T	0.2643 (3)	0.5157 (3)	0.4130 (3)	0.0352 (10)
H3T	0.203397	0.540979	0.417407	0.042*
C8T	0.2205 (3)	0.2978 (3)	0.1146 (3)	0.0348 (10)
H8T	0.183679	0.251090	0.080166	0.042*
C6T	0.3160 (3)	0.7049 (3)	0.1743 (3)	0.0358 (10)
H6T	0.259548	0.741310	0.178339	0.043*
C1T	0.3997 (3)	0.4503 (3)	0.4412 (3)	0.0342 (10)
H1T	0.451960	0.420086	0.470864	0.041*
C2T	0.3205 (3)	0.4793 (3)	0.4795 (3)	0.0382 (11)
H2T	0.307967	0.474990	0.537997	0.046*
C9T	0.1925 (3)	0.3843 (3)	0.1571 (3)	0.0324 (10)
H9T	0.131162	0.409361	0.157409	0.039*
C4T	0.4563 (3)	0.6628 (3)	0.1478 (3)	0.0354 (10)
H4T	0.517045	0.666624	0.129172	0.043*
C5T	0.3914 (3)	0.7426 (3)	0.1376 (3)	0.0399 (11)
H5T	0.398285	0.808637	0.110952	0.048*
C1	0.5270 (3)	0.1148 (3)	0.0932 (3)	0.0357 (10)

B1T	0.2710 (3)	0.5311 (3)	0.2487 (3)	0.0262 (10)
H1TA	0.207879	0.561715	0.249449	0.031*
H3	0.500000	0.053 (4)	0.250000	0.018 (14)*

Atomic displacement parameters (Å²)

	U^{11}	U^{22}	U^{33}	U^{12}	U^{13}	U^{23}
Y1	0.0272 (3)	0.0178 (3)	0.0207 (3)	0.000	0.0028 (2)	0.000
O1	0.0334 (14)	0.0217 (14)	0.0267 (16)	0.0008 (11)	0.0047 (12)	-0.0020 (12)
F2	0.0690 (17)	0.0512 (17)	0.0356 (16)	0.0228 (13)	-0.0141 (14)	-0.0128 (13)
F3	0.0448 (14)	0.0598 (18)	0.0476 (17)	0.0054 (12)	0.0135 (13)	-0.0134 (13)
F1	0.0744 (18)	0.0281 (14)	0.0534 (18)	-0.0054 (12)	0.0090 (14)	-0.0165 (12)
N4T	0.0357 (18)	0.0180 (16)	0.0256 (19)	0.0050 (13)	0.0020 (15)	0.0002 (13)
N2T	0.0323 (17)	0.0237 (17)	0.028 (2)	0.0066 (14)	0.0071 (15)	-0.0006 (14)
N1T	0.0323 (17)	0.0304 (18)	0.0214 (19)	0.0038 (14)	0.0025 (15)	0.0006 (14)
N5T	0.0269 (16)	0.0220 (17)	0.0266 (19)	0.0034 (13)	0.0021 (14)	0.0009 (14)
N3T	0.0345 (16)	0.0240 (16)	0.0246 (18)	-0.0001 (15)	0.0007 (14)	0.0033 (15)
N6T	0.0283 (15)	0.0240 (16)	0.0259 (18)	0.0024 (15)	0.0020 (13)	0.0000 (16)
C7T	0.037 (2)	0.025 (2)	0.036 (3)	-0.0007 (17)	0.000 (2)	-0.0019 (18)
C3	0.034 (3)	0.018 (3)	0.045 (4)	0.000	0.003 (3)	0.000
C2	0.0242 (19)	0.025 (2)	0.029 (2)	0.0021 (16)	0.0002 (17)	-0.0024 (17)
C3T	0.040 (2)	0.035 (2)	0.032 (3)	0.0079 (19)	0.016 (2)	0.0012 (19)
C8T	0.035 (2)	0.029 (2)	0.039 (3)	-0.0030 (18)	-0.008 (2)	-0.0019 (19)
C6T	0.054 (3)	0.022 (2)	0.032 (3)	0.0111 (19)	0.002 (2)	-0.0017 (18)
C1T	0.041 (2)	0.037 (3)	0.024 (2)	0.0028 (18)	0.0009 (19)	-0.0012 (19)
C2T	0.052 (3)	0.041 (3)	0.022 (2)	0.007 (2)	0.009 (2)	0.000 (2)
C9T	0.0248 (19)	0.033 (2)	0.038 (3)	-0.0006 (17)	-0.0068 (18)	0.0078 (19)
C4T	0.044 (2)	0.033 (2)	0.030 (3)	-0.0045 (19)	0.004 (2)	0.0043 (19)
C5T	0.064 (3)	0.022 (2)	0.034 (3)	0.001 (2)	0.010 (2)	0.0072 (19)
C1	0.039 (2)	0.025 (2)	0.043 (3)	0.0063 (18)	0.000 (2)	-0.009 (2)
B1T	0.025 (2)	0.025 (2)	0.028 (3)	0.0025 (18)	0.000 (2)	0.0050 (19)

Geometric parameters (Å, º)

Y1—O1	2.341 (2)	N6T—C9T	1.347 (4)
Y1—O1^{i}	2.341 (2)	N6T—B1T	1.533 (5)
Y1—N1T^{i}	2.435 (3)	C7T—H7T	0.9500
Y1—N1T	2.435 (3)	C7T—C8T	1.376 (5)
Y1—N5T	2.534 (3)	C3—C2^{i}	1.400 (5)

Y1—N5T^{i}	2.534 (3)	C3—C2	1.400 (5)
Y1—N3T	2.487 (3)	C3—H3	0.90 (5)
Y1—N3T^{i}	2.487 (3)	C2—C1	1.523 (5)
O1—C2	1.251 (4)	C3T—H3T	0.9500
F2—C1	1.342 (5)	C3T—C2T	1.370 (5)
F3—C1	1.318 (4)	C8T—H8T	0.9500
F1—C1	1.336 (4)	C8T—C9T	1.365 (5)
N4T—N3T	1.372 (4)	C6T—H6T	0.9500
N4T—C6T	1.346 (4)	C6T—C5T	1.359 (5)
N4T—B1T	1.538 (5)	C1T—H1T	0.9500
N2T—N1T	1.361 (4)	C1T—C2T	1.384 (5)
N2T—C3T	1.334 (5)	C2T—H2T	0.9500
N2T—B1T	1.544 (5)	C9T—H9T	0.9500
N1T—C1T	1.331 (5)	C4T—H4T	0.9500
N5T—N6T	1.367 (4)	C4T—C5T	1.393 (5)
N5T—C7T	1.336 (5)	C5T—H5T	0.9500
N3T—C4T	1.331 (5)	B1T—H1TA	1.0000
O1—Y1—O1^{i}	72.02 (12)	C9T—N6T—B1T	127.9 (3)
O1^{i}—Y1—N1T^{i}	134.62 (9)	N5T—C7T—H7T	124.0
O1^{i}—Y1—N1T	72.26 (9)	N5T—C7T—C8T	112.0 (4)
O1—Y1—N1T^{i}	72.26 (9)	C8T—C7T—H7T	124.0
O1—Y1—N1T	134.62 (9)	C2^{i}—C3—C2	121.6 (5)
O1—Y1—N5T^{i}	82.95 (9)	C2—C3—H3	119.2 (3)
O1—Y1—N5T	72.77 (9)	C2^{i}—C3—H3	119.2 (3)
O1^{i}—Y1—N5T^{i}	72.77 (9)	O1—C2—C3	126.2 (4)
O1^{i}—Y1—N5T	82.95 (9)	O1—C2—C1	114.7 (3)
O1—Y1—N3T	120.17 (9)	C3—C2—C1	119.1 (4)
O1^{i}—Y1—N3T^{i}	120.17 (9)	N2T—C3T—H3T	125.3
O1^{i}—Y1—N3T	143.83 (9)	N2T—C3T—C2T	109.4 (4)
O1—Y1—N3T^{i}	143.83 (9)	C2T—C3T—H3T	125.3
N1T^{i}—Y1—N1T	151.54 (15)	C7T—C8T—H8T	127.7
N1T^{i}—Y1—N5T	111.76 (10)	C9T—C8T—C7T	104.6 (4)
N1T—Y1—N5T	75.92 (10)	C9T—C8T—H8T	127.7
N1T^{i}—Y1—N5T^{i}	75.92 (10)	N4T—C6T—H6T	125.4
N1T—Y1—N5T^{i}	111.76 (10)	N4T—C6T—C5T	109.2 (4)
N1T—Y1—N3T^{i}	79.52 (10)	C5T—C6T—H6T	125.4
N1T—Y1—N3T	77.52 (10)	N1T—C1T—H1T	124.1
N1T^{i}—Y1—N3T	79.52 (10)	N1T—C1T—C2T	111.8 (4)
N1T^{i}—Y1—N3T^{i}	77.52 (10)	C2T—C1T—H1T	124.1

N5T^{i}—Y1—N5T	149.98 (13)	C3T—C2T—C1T	103.7 (4)
N3T^{i}—Y1—N5T^{i}	70.66 (10)	C3T—C2T—H2T	128.2
N3T^{i}—Y1—N5T	138.64 (10)	C1T—C2T—H2T	128.2
N3T—Y1—N5T	70.66 (10)	N6T—C9T—C8T	108.6 (3)
N3T—Y1—N5T^{i}	138.64 (10)	N6T—C9T—H9T	125.7
N3T^{i}—Y1—N3T	71.88 (14)	C8T—C9T—H9T	125.7
C2—O1—Y1	136.8 (2)	N3T—C4T—H4T	124.4
N3T—N4T—B1T	121.1 (3)	N3T—C4T—C5T	111.1 (4)
C6T—N4T—N3T	109.3 (3)	C5T—C4T—H4T	124.4
C6T—N4T—B1T	129.5 (3)	C6T—C5T—C4T	104.6 (4)
N1T—N2T—B1T	121.1 (3)	C6T—C5T—H5T	127.7
C3T—N2T—N1T	109.7 (3)	C4T—C5T—H5T	127.7
C3T—N2T—B1T	128.8 (3)	F2—C1—C2	110.4 (3)
N2T—N1T—Y1	124.8 (2)	F3—C1—F2	106.8 (4)
C1T—N1T—Y1	129.3 (3)	F3—C1—F1	108.1 (3)
C1T—N1T—N2T	105.4 (3)	F3—C1—C2	112.0 (3)
N6T—N5T—Y1	121.5 (2)	F1—C1—F2	106.3 (3)
C7T—N5T—Y1	133.7 (2)	F1—C1—C2	113.0 (4)
C7T—N5T—N6T	104.8 (3)	N4T—B1T—N2T	110.6 (3)
N4T—N3T—Y1	122.6 (2)	N4T—B1T—H1TA	109.3
C4T—N3T—Y1	130.5 (3)	N2T—B1T—H1TA	109.3
C4T—N3T—N4T	105.7 (3)	N6T—B1T—N4T	108.7 (3)
N5T—N6T—B1T	121.9 (3)	N6T—B1T—N2T	109.8 (3)
C9T—N6T—N5T	110.0 (3)	N6T—B1T—H1TA	109.3

Symmetry code: (i) -*x*+1, *y*, -*z*+1/2.

8.3.19 Crystallographic data for {Y(hfac)$_2$(*N,N'-O,O'*-pd)}$_4$

Crystal data

0.25($C_{48}F_4N_8O_{24}Y_4$)·8(F)·0.5(C_2F_2)	D_x = 0.362 Mg m^{-3}
M_r = 238.42	Mo *K*α radiation, λ = 0.71073 Å
Tetragonal, *I*4/*m*	Cell parameters from 1841 reflections
a = 23.428 (3) Å	θ = 2.3–24.8°
c = 15.937 (3) Å	μ = 0.45 mm^{-1}
V = 8748 (2) Å^3	*T* = 273 K
Z = 8	Block, red
F(000) = 929.608	0.47 × 0.32 × 0.14 mm

Data collection

Bruker APEX-II CCD diffractometer	R_{int} = 0.182
ϕ and ω scans	θ_{max} = 25.4°, θ_{min} = 2.3°
9327 measured reflections	h = -16→28
3937 independent reflections	k = -24→28
901 reflections with $I \geq 2u(I)$	l = -16→19

Refinement

Refinement on F^2	0 restraints
Least-squares matrix: full	0 constraints
$R[F^2 > 2\sigma(F^2)]$ = 0.354	Primary atom site location: dual
$wR(F^2)$ = 0.663	$w = 1/[\sigma^2(F_o^2) + (0.1P)^2]$ where $P = (F_o^2 + 2F_c^2)/3$
S = 2.37	$(\Delta/\sigma)_{max}$ = 0.040
3937 reflections	$\Delta\rangle_{max}$ = 10.06 e Å^{-3}
82 parameters	$\Delta\rangle_{min}$ = -2.87 e Å^{-3}

Fractional atomic coordinates and isotropic or equivalent isotropic displacement parameters (Å²)

	x	*y*	*z*	U_{iso}*/U_{eq}	Occ. (<1)
Y001	0.45997 (19)	0.2362 (2)	0.5	0.090 (2)*	
O002	0.3854 (14)	0.1699 (14)	0.5	0.142 (12)*	
O003	0.5199 (12)	0.1497 (13)	0.5	0.112 (10)*	
O1	0.4558 (11)	0.1973 (11)	0.3591 (15)	0.175 (11)*	
C009	0.3242 (14)	0.4235 (14)	0.4604 (14)	0.104 (12)*	
O2	0.4150 (14)	0.3086 (14)	0.4217 (17)	0.207 (13)*	
C00F	0.3623 (19)	0.389 (2)	0.418 (3)	0.156 (16)*	
N3	0.2920 (17)	0.4652 (17)	0.420 (2)	0.199 (16)*	
F3	0.606 (2)	0.083 (2)	0.5	0.30 (2)*	
F7	0.273 (2)	0.120 (2)	0.5	0.27 (2)*	
C1	0.3803 (14)	0.3472 (16)	0.4600 (16)	0.115 (13)*	
F1	0.4914 (13)	0.1780 (13)	0.2096 (16)	0.245 (13)*	
F9	0.5617 (19)	0.020 (2)	0.5	0.257 (19)*	
F30	0.4224 (17)	0.1455 (16)	0.224 (2)	0.324 (18)*	
F5	0.338 (3)	0.065 (3)	0.5	0.37 (3)*	
F19	0.4877 (16)	0.1070 (17)	0.231 (2)	0.307 (16)*	

C12	0.363 (3)	0.065 (3)	0.418 (4)	0.13 (2)*	0.500000
C29	0.536 (2)	0.042 (2)	0.579 (3)	0.072 (18)*	0.500000
C18	0.374 (3)	0.475 (3)	0.310 (4)	0.13 (2)*	0.500000
C26	0.320 (3)	0.503 (3)	0.341 (4)	0.13 (2)*	0.500000
C35	0.375 (3)	0.405 (3)	0.321 (4)	0.28 (3)*	
C30	0.512 (4)	0.106 (4)	0.581 (5)	0.19 (4)*	0.500000

Geometric parameters (Å, º)

Y001—O002	2.34 (3)	O2—C1	1.36 (4)
Y001—O003	2.46 (3)	C00F—C1	1.25 (4)
Y001—O1	2.43 (2)	C00F—C35	1.63 (5)
Y001—O1^{i}	2.43 (2)	N3—C26	1.68 (6)
Y001—O2	2.36 (3)	C1—C1^{i}	1.28 (5)
Y001—O2^{i}	2.36 (3)	F1—F19	1.70 (4)
Y001—N3^{ii}	2.53 (4)	F9—C29	1.49 (5)
Y001—N3^{iii}	2.53 (4)	F9—C29^{i}	1.49 (5)
O003—C30^{i}	1.65 (9)	F5—C12^{i}	1.44 (6)
O003—C30	1.65 (9)	F5—C12	1.44 (6)
C009—C009^{i}	1.26 (5)	C29—C30	1.61 (9)
C009—C00F	1.38 (4)	C18—C26	1.51 (8)
C009—N3	1.39 (4)	C18—C35	1.65 (8)
O003—Y001—O002	83.1 (11)	N3^{ii}—Y001—O2^{i}	70.8 (12)
O1—Y001—O002	73.8 (7)	N3^{iii}—Y001—O2	70.8 (12)
O1^{i}—Y001—O002	73.8 (7)	N3^{ii}—Y001—N3^{iii}	60.3 (17)
O1—Y001—O003	73.4 (6)	C30^{i}—O003—Y001	116 (3)
O1^{i}—Y001—O003	73.4 (6)	C30—O003—Y001	116 (3)
O1—Y001—O1^{i}	135.6 (13)	C30^{i}—O003—C30	103 (6)
O2—Y001—O002	98.3 (10)	N3—C009—C00F	123 (3)
O2^{i}—Y001—O002	98.3 (10)	C1—O2—Y001^{i}	121 (2)
O2^{i}—Y001—O003	147.9 (8)	C1—C00F—C009	115 (4)
O2—Y001—O003	147.9 (8)	C35—C00F—C009	116 (4)
O2^{i}—Y001—O1^{i}	76.2 (10)	C35—C00F—C1	129 (5)
O2—Y001—O1	76.2 (10)	C009—N3—Y001^{iv}	122 (2)
O2^{i}—Y001—O1	138.0 (10)	C26—N3—Y001^{iv}	102 (3)
O2—Y001—O1^{i}	138.0 (10)	C26—N3—C009	121 (4)
O2—Y001—O2^{i}	64.0 (15)	C00F—C1—O2	119 (3)
N3^{ii}—Y001—O002	149.5 (8)	C1^{i}—C1—O2	117 (2)

N3^{iii}—Y001—O002	149.5 (8)	C1^{i}—C1—C00F	122 (3)
N3^{ii}—Y001—O003	91.7 (11)	C29^{i}—F9—C29	116 (5)
N3^{iii}—Y001—O003	91.7 (11)	C12—F5—C12^{i}	131 (8)
N3^{ii}—Y001—O1^{i}	75.9 (10)	C30—C29—F9	118 (5)
N3^{iii}—Y001—O1^{i}	133.4 (11)	C35—C18—C26	115 (6)
N3^{iii}—Y001—O1	75.9 (10)	C18—C26—N3	110 (5)
N3^{ii}—Y001—O1	133.4 (11)	C18—C35—C00F	109 (5)
N3^{iii}—Y001—O2^{i}	101.8 (11)	C29—C30—O003	122 (6)
N3^{ii}—Y001—O2	101.8 (11)		
Y001—O003—C30—C29	165 (4)	C009^{i}—C009—C00F—C1	22.4 (16)
Y001—O003—C30^{i}—C29^{i}	-165 (4)	C009^{i}—C009—C00F—C35	-161 (3)
Y001—O2—C1—C00F	172 (3)	C009^{i}—C009—N3—C26	133 (3)
Y001^{i}—O2—C1—C00F	172 (3)	C009—C00F—C1—O2	176 (4)
Y001—O2—C1—C1^{i}	10 (3)	C009—C00F—C1—C1^{i}	-23 (5)
Y001—O2^{i}—C1^{i}—C1	-10 (3)	C009—C00F—C35—C18	36 (5)
Y001^{v}—N3—C009—C009^{i}	1 (3)	C009—N3—C26—C18	14 (4)
Y001^{iv}—N3—C009—C009^{i}	1 (3)	O2—C1—C00F—C35	-0 (5)
Y001^{v}—N3—C009—C00F	-169 (3)	O2—C1—C1^{i}—O2^{i}	0 (5)
Y001^{iv}—N3—C009—C00F	-169 (3)	O2—C1—C1^{i}—C00F^{i}	162 (3)
Y001^{iv}—N3—C26—C18	154 (4)	C00F—C1—C1^{i}—C00F^{i}	-0 (7)
Y001^{v}—N3—C26—C18	154 (4)	C00F—C35—C18—C26	-55 (5)
O003—C30—C29—F9	-5 (8)	N3—C26—C18—C35	30 (5)
O003^{i}—C30—C29—F9	-5 (8)		

Symmetry codes: (i) *x*, *y*, -*z*+1; (ii) -*y*+1, *x*, -*z*+1; (iii) -*y*+1, *x*, *z*; (iv) *y*, -*x*+1, -*z*+1; (v) *y*, -*x*+1, *z*.

8.4 Appendix Four: List of Figures

8.5 Appendix Five: List of Tables